OCS Study
MMS 95-0038

Gulf of Mexico Air Quality Study, Final Report

Volume I: Summary of Data Analysis and Modeling

Prepared by

Systems Applications International
101 Lucas Valley Road
San Rafael, California 94903

Sonoma Technology, Inc.
5510 Skylane Boulevard, Suite 101
Santa Rosa, California 95403

Earth Tech
196 Baker Avenue
Concord, Massachusetts 01742

Alpine Geophysics
P. O. Box 17344
Covington, Kentucky 41017

A.T. Kearney
225 Reinekers Lane
Alexandria, Virginia 22313

Prepared under MMS Contract
14-35-0001-30604
by
Systems Applications International
101 Lucas Valley Road
San Rafael, California 94903

Published by

U.S. Department of the Interior
Minerals Management Service
Gulf of Mexico OCS Region

New Orleans
August 1995

DISCLAIMER

This report was prepared under contract between the Minerals Management Service (MMS) and Systems Applications International (SAI). This report has been technically reviewed by the MMS and approved for publication. Approval does not signify that the contents necessarily reflect the views and policies of the Service, nor does mention of trade names or commercial products constitute endorsement of recommendations for use. It is, however, exempt from review and compliance with MMS editorial standards.

REPORT AVAILABILITY

Extra copies of the report may be obtained from the Public Information Unit (Mail Stop 5034) at the following address:

U.S. Department of the Interior
Minerals Management Service
Gulf of Mexico OCS Region
Public Information Unit (MS 5034)
1201 Elmwood Park Boulevard
New Orleans, Louisiana 70123-2394

Telephone Number: (504) 736-2519 or 1-800-200-GULF

SUGGESTED CITATION

Systems Applications International, Sonoma Technology Inc., Earth Tech, Alpine Geophysics, and A. T. Kearney. 1995. Gulf of Mexico air quality study, final report. Volume I: Summary of data analysis and modeling. OCS Study MMS-95-0038. U.S. Department of the Interior, Minerals Management Service, Gulf of Mexico OCS Region, New Orleans, La. 654 pp.

AUTHORS

Systems Applications International (SAI)

Jay L. Haney
Nina K. Lolk
Thomas C. Myers
Marianne C. Causley
Cyntia K. Steiner
LuAnn Gardner
Gary Z. Whitten
Sharon G. Douglas
C. Shepherd Burton

Sonoma Technology Inc. (STI)

Paul C. Roberts
Timothy S. Dye
Marcelo E. Korc
Charles G. Lindsey
Hilary H. Main
Scott E. Ray

CONTENTS

List of Figures xi
List of Tables xxvii
Acronyms and Abbreviations xxxi
Executive Summary xxxiii
Acknowledgments xlv
List of Supporting Documentation xlix

1 INTRODUCTION 1-1
1.1 Background 1-1
Legislation 1-1
Air quality background 1-3
1.2 Goals and objectives of the study 1-3
1.3 Project elements and chronology 1-4
Overview of the field study (April–October 1993) 1-5
Overview of data analyses 1-8
Overview of emissions inventory development 1-9
Overview of meteorological modeling 1-11
Overview of photochemical modeling 1-11
1.4 The GMAQS participants 1-12

2 OVERVIEW OF THE GMAQS FIELD STUDY 2-1
2.1 Description of the field study 2-1
Field study objectives and technical approach 2-1
Field study management, measurement components, and participating organizations 2-3
Forecasting criteria and decision-making process 2-4
GMAQS monitoring sites 2-6
GMAQS aircraft operations 2-6
Quality assurance activities 2-12
Data archival and management activities 2-14
2.2 Summary of the GMAQS field study results 2-16
General statistics 2-16
Ozone episodes captured 2-19

3 DATA ANALYSIS 3-1
3.1 Data analysis objectives 3-1
3.2 Data availability and data validation 3-1
Description of data sources 3-1

Data validation procedures and results 3-3
VOC data 3-5
Comparison of ozone concentration measurements among aircraft 3-6
Comparison of upper-air and surface ozone measurements . . . 3-7
3.3 Climatology and representativeness 3-8
3.4 Descriptive analyses of the GMAQS data 3-12
Description of ozone air quality 3-12
Description of synoptic meteorology during ozone episodes . . . 3-15
Analyses of surface and upper-air meteorological conditions . . 3-16
Analyses of mixing depths and boundary layer development . . 3-22
Analyses of hydrocarbon and carbonyl compound data 3-26
Investigation of high NMHC concentrations during the August episode at Clinton 3-33
3.5 Case studies of ozone episodes 3-36
Case study of the 17–20 August 1993 ozone episode 3-36
Case study of the 10 August 1993 ozone episode 3-41
Case study of the 7–11 September 1993 ozone episode in southeast Texas 3-45
Case study of the 17–19 August 1993 ozone episode in Baton Rouge 3-50
3.6 Analysis of transport processes and onshore–offshore flux 3-54
Analyses of ventilation and recirculation 3-54
Analyses of pollutant transport using trajectories 3-58
Results of onshore–offshore pollutant flux calculations 3-62
3.7 Data analysis conclusions, conceptual model of ozone exceedances, and assessment of OCSPD contributions 3-70
Conclusions and conceptual model 3-70
Assessment of OCSPD emission contributions to ozone exceedances in southeast Texas and Baton Rouge 3-78

4 BASE YEAR MODELING ANALYSIS 4-1
4.1 Introduction 4-1
4.2 Overview of UAM-V 4-1
4.3 Specification of the GMAQS modeling domain 4-2
4.4 Selection of historical episodes (1987–1990) 4-3
4.5 Simulation of the 1988 modeling episode 4-4
4.6 Selection of the 1993 episodes 4-5
4.7 UAM-V base case-input preparation for the 1993 episodes 4-6
Emission inventory development 4-6
Meteorological inputs 4-26
Air quality inputs 4-55
Land-use inputs 4-57
Other inputs 4-57
4.8 Diagnostic and sensitivity analysis 4-57
Analysis of the 17–20 August 1993 episode 4-58
Analysis of the 6–11 September 1993 episode 4-64
Summary of diagnostic and sensitivity analysis results 4-66

4.9 Base-case simulations: 1993 episodes 4-67
August episode 4-67
Comparison of UAM-V simulated concentrations with aircraft measurements 4-72
September episodes 4-73
4.10 Summary of and interpretation of the results of the UAM-V performance evaluation for the August and September episodes 4-78
Summary of the UAM-V performance for the August episode . 4-79
Summary of the UAM-V performance for the September episode 4-80
Recommendations regarding use of the modeling system for estimating the impacts of OCSPD emissions 4-81

5 OCSPD IMPACT ANALYSIS FOR 1993 AND 1999 5-1
5.1 Methodology for Assessing Ozone Impacts from OCSPD Emission Sources Using the UAM-V 5-1
5.2 Summary of the Base-Year (1993) OCSPD Impact Simulations 5-3
Summary of OCSPD Emissions for 1993 5-3
OCSPD Impact Simulation Results for 1993 5-9
5.3 Emission Projections—1990 to 1999 5-23
Offshore Region 5-30
Onshore Region 5-32
Results of Emissions Processing for the 1999 Inventories 5-36
5.4 Summary of Future-Year UAM-V Simulation Results for 1999 5-37
1999 OCSPD Emission Scenario Simulation Results 5-39

6 SUMMARY AND CONCLUSIONS 6-1
6.1 Summary of the OCSPD Impact Analysis 6-1
6.2 Goals and objectives of the GMAQS 6-2
6.3 Summary of results of GMAQS activities 6-4
Results of the field study design and implementation 6-4
Results of the data analyses 6-5
Emission inventory preparation 6-7
Results of the meteorological modeling 6-8
Results of the photochemical modeling 6-9
6.4 Concluding remarks 6-13

7 RECOMMENDATIONS FOR FUTURE GULF OF MEXICO MEASUREMENT AND MODELING PROGRAMS 7-1
Additional field measurements 7-1
Data analyses 7-4
Emission inventory 7-4
Meteorological and photochemical modeling 7-5

REFERENCES R-1

VOLUME 2: DATA ANALYSIS APPENDICES A-M

Appendix A: List of Surface and Upper-Air Sites and the Parameters Measured at These Sites

Appendix B: Surface Hydrocarbon and Carbonyl Compound Species Lists and Data

Appendix C: Comparisons Between Surface and Aircraft Ozone Measurements During the August 17-21, 1993 Episode

Appendix D: List of Sites that Exceeded the National Ambient Air Quality Standard (NAAQS) for Ozone During 1993 Episodes

Appendix E: Analyses of Pressure Gradients and Onshore-Offshore Winds in Southeast Texas and Louisiana

Appendix F: Analyses of Hourly Surface Ozone Concentrations, Onshore-Offshore Velocity Components, and Surface Winds in Southeast Texas on August 19, 1993 and September 8, 1993

Appendix G: Plots of Mixing Depth Derived from C_n^2 and Virtual Temperature Data

Appendix H: Aircraft Hydrocarbon and Carbonyl Compound Data

Appendix I: Comparisons of Surface and Aircraft Hydrocarbon and Carbonyl Compound Data

Appendix J: Analyses of Integral Transport Quantities for the Radar Profiler Stations in Southeast Texas and Louisiana

Appendix K: Trajectory Analyses

Appendix L: Profile Plots of Ozone and NO_x Concentrations, Southwesterly Component of the Wind Speed, and Ozone and NO_x Flux at Galveston on August 10, 1993

Appendix M: Time Series Plots of Surface Ozone and NO_x Concentrations, Surface Southwesterly Component of the Wind Speed, and Ozone and NO_x Fluxes for Galveston, Gilchrist, Seabrook, Smith Point, and HRM Site 7 for August 17-21 and September 7-11, 1993

VOLUME 3: INVENTORY PREPARATION APPENDICES N-P

Appendix N: Offshore Emissions Inventory Preparation

Appendix O: Spatial Surrogates

Appendix P: Spatial Density Plots by Major Source Category for August 17,1993

LIST OF FIGURES

1-1	The MMS GMAQS modeling domain and existing ozone nonattainment areas	1-2
1-2	Locations of supplemental meteorological and air quality measurement systems for the 1993 MMS GMAQS field program	1-6
2-1	Example of a typical morning flight performed in the Texas sampling area during the 1993 MMS Gulf of Mexico Air Quality Study	2-8
2-2	Example of a typical afternoon flight performed in the Texas sampling area during the 1993 MMS Gulf of Mexico Air Quality Study	2-9
2-3	Example of a typical morning flight performed in the Louisiana sampling area during the 1993 MMS Gulf of Mexico Air Quality Study	2-10
2-4	Example of a typical afternoon flight performed in the Louisiana sampling area during the 1993 MMS Gulf of Mexico Air Quality Study	2-11
2-5	Daily maximum ozone concentration and number of exceedances of the NAAQS in southeast Texas from July 15, 1993 to September 30, 1993	2-20
2-6	Daily maximum ozone concentration and number of exceedances of the NAAQS in Louisiana from July 15, 1993 to September 30, 1993	2-21
3-1	Locations of surface air quality sites and volatile organic compound samplers, surface and upper-air meteorological sensors, and locations of aircraft spirals in the southeast Texas region	3-81
3-2	Locations of surface air quality sites and volatile organic compound samplers, surface and upper-air meteorological sensors, and locations of aircraft spirals in the Louisiana region	3-84
3-3	Examples of questionable data identified during the data validation	3-87
3-4	Comparison between aircraft ozone concentration profiles at Beaumont for the early morning flight on August 10, 1993	3-88

3-5 Scatter plot comparisons of 6670Y and 9PW, 9862F, and 85585 aircraft ozone mixed-layer averages for all the spirals over Beaumont during the summer of 1993 3-89

3-6 Comparison between surface ozone concentrations at the Swiss& Monroe surface site and mixed-layer averages and lowest-altitude averages at Houston Hobby Airport during the 17-20 August 1993 episode 3-90

3-7 Cumulative distribution functions for ozone exceedances in the GMAQS region 3-91

3-8 Probability distribution functions for meteorological variables in the GMAQS region for the historical period and for 1993 for all days in the summer 3-92

3-9 Maximum ozone concentrations in the Houston region for the 1982-1992 exceedance days and for the 1993 episode days plotted versus surface meteorological variables observed at Intercontinental Airport, and 850 mb temperature observed at Municipal Airport in Lake Charles 3-93

3-10 Box plot presentations of daily maximum ozone concentrations over the monitoring networks in the Houston, Baton Rouge, and New Orleans regions 3-94

3-11 Contour of maximum ozone concentrations in the southeast Texas region on August 9, 1993, August 10, 1993, and August 11, 1993 3-95

3-12 Contour of maximum ozone concentrations in the southeast Texas region on August 17, 18, 19, 20, and 21, 1993 3-98

3-13 Contour of maximum ozone concentrations in the southeast Texas region on September 7, 8, 9, 10, and 11, 1993 3-103

3-14 Contour of maximum ozone concentrations in the Baton Rouge region on August 17, 18, and 19, 1993 3-108

3-15 Daily weather map for August 10, 1993 at 0600 CST 3-111

3-16 Daily weather map for August 19, 1993 at 0600 CST 3-112

3-17 Daily weather map for September 8, 1993 at 0600 CST 3-113

3-18 Time series of meteorological and air quality measurements at the Galveston radar profiler site for the period July 18-September 15, 1993 and at the Gilchrist, Texas surface monitoring site for the period August 9-14, 1993 3-114

3-19 Maximum ozone concentrations observed in southeast Texas during the GMAQS project 3-116

3-20 Sea-level pressure differences across the Gulf of Mexico between the High Island and Ship Shoal Platform radar profiler sites, and the component of the surface wind perpendicular to the coastline at Galveston for the period 18 July–15 September 1993 3-117

3-21 Onshore-offshore sea-level pressure differences and temperature differences between the Southeast Houston and High Island Platform radar profiler sites, and the component of the surface wind perpendicular to the coastline at Galveston for the period 17–21 August 1993 3-118

3-22 The component of the surface wind perpendicular to the coastline at the Southeast Houston, Galveston, and High Island Platform radar profiler sites for the period 17–21 August 1993 3-119

3-23 Wind profiles measured by the 915 MHz radar profiler at Galveston, 10 August 1993 3-120

3-24 Wind profiles measured by the 915 MHz radar profiler at High Island Platform 19 August 1993 3-121

3-25 Conceptual model of the six stages of the onshore-offshore-onshore flow reversal in southeast Texas on episode days 3-122

3-26 Sea-level pressure differences across the Gulf of Mexico between the High Island and Ship Shoal Platform radar profiler sites, and the component of the surface wind perpendicular to the coastline at Cocodrie, LA, for the period 18 July–15 September 1993 3-123

3-27 Onshore-offshore sea-level pressure differences between the Louisiana State University and Ship Shoal Platform radar profiler sites, and the component of the surface wind perpendicular to the coastline at LSU, for the period 17–21 August 1993 3-124

3-28 Wind profiles measured by the 915 MHz radar profilers at Cocodrie, LA and Louisiana State University on 19 August 1993 . . . 3-125

3-29 Scatter plot of C_n^2-derived mixing depths and mixing depths estimated from aircraft profiles of pollutant concentrations, turbulence, and temperature 3-126

3-30 Time series plot of mixing depths estimated from C_n^2 and virtual temperature data for profiler sites in southeast Texas and offshore on 19 August 1993 3-127

3-31 Mixing depth estimated on August 19, 1993 computed from aircraft and RASS virtual temperature data for the period 0500-0800 CST and aircraft and C_n^2 data for the period 1100-1300 CST 3-128

3-32 Example of mixing depth analysis during an ozone episode in southeast Texas using radar profiler data from 10 August 1993 3-129

3-33 Offshore-to-onshore cross section of normalized C_n^2 and winds aloft measured at radar profiler sites on 19 August 1993 3-130

3-34 Average concentrations of abundant hydrocarbons and carbonyl compounds by time of day at Gilchrist, Texas 3-131

3-35 Average concentrations of abundant hydrocarbons and carbonyl compounds by time of day at Cocodrie, Louisiana 3-132

3-36 Median concentrations of abundant hydrocarbons by time of day at Clinton, Texas 3-133

3-37 Diurnal plots of C5 paraffins at Clinton, Texas for 17–21 August 1993 and all of August 1993 3-134

3-38 Diurnal plots of acetylene and isoprene at Clinton, Texas on 17–21 August 1993 3-135

3-39 Diurnal plots of NMHC/NO_x ratios at Clinton, Texas during 20–21 August 1993 and all of August 1993 3-136

3-40 Average concentrations of abundant hydrocarbons and carbonyl compounds by sampling time collected by aircraft at lower altitudes during intensive sampling days 3-137

3-41 Concentrations of abundant hydrocarbons and carbonyl compounds aloft over High Island Platform and at the surface at Gilchrist on the morning of 20 August 1993 3-138

3-42 Weight percent of NMOC of abundant hydrocarbons and carbonyl compounds aloft over High Island Platform and at the surface at Gilchrist on the morning of 20 August 1993 3-139

3-43 Concentrations of abundant hydrocarbons and carbonyl compounds aloft over High Island Platform and at the surface at Gilchrist midday on 20 August 1993 3-140

3-44 Concentrations of abundant hydrocarbons and carbonyl compounds aloft over Ship Shoal Platform and at the surface at Cocodrie on the morning of 19 August 1993 3-141

3-45 Temperature and NO, NO_x, and ozone concentrations measured by aircraft during a spiral over Baytown on the mornings of 20 August and 16 August 1993 3-142

3-46 Concentrations of abundant hydrocarbons aloft over Baytown and at the surface at Clinton in the morning and midday on 20 August 1993 3-143

3-47 Normalized weight percent of NMHC of one California Air Resources Board and three EPA emission profiles 3-144

3-48 Isopleths of ozone concentrations, onshore-offshore component of the surface wind perpendicular to the shoreline, and surface winds on 19 August 1993 3-145

3-49 Time-height cross sections of winds from the Southeast Houston, Galveston, and High Island Platform radar profilers on 19 and 20 August 1993 3-146

3-50 Time series of hourly averaged surface winds, temperature, ozone, NO_x, and NO measured at Aldine on 19 August 1993 3-147

3-51 Early morning aircraft measurements of temperature, ozone, and oxides of nitrogen on 10 August 1993 over Baytown and Houston Hobby Airport, and on 19 August 1993 over Houston Hobby and Andrau 3-148

3-52 Hourly ozone concentrations at Northwest Harris, Lang, Houston Regional Monitoring Site 1, and Monroe on 10 August 1993 3-149

3-53 Aircraft measurements of temperature, ozone and oxides of nitrogen on 10 August 1993 over High Island Platform, Galveston Airport, and Houston Hobby Airport 3-150

3-54 Time-height cross sections of winds from the High Island Platform, Galveston, and Southeast Houston profilers on 10–11 August 1993 . . 3-151

3-55 Time-height cross sections of C_n^2 from High Island Platform, Galveston, and Southeast Houston profilers on 10-11 August 1993 . . . 3-152

3-56 Hourly ozone concentrations on 10 September 1993 at Galveston, Texas City, Seabrook, and Houston 3-153

3-57 Plots of surface winds and ozone concentrations in the southeast Texas region 3-154

3-58 Time series plots of ozone concentrations and surface winds at Seabrook, Smith Point, and Gilchrist for 8–11 September 1993 3-159

3-59 Time-height cross sections of winds from the Southeast Houston, Galveston, and High Island Platform profilers on 9-10 September 1993 3-160

3-60 Surface winds and ozone concentrations at 0800 CST and 1400 CST on August 17, 18, and 19, 1993 3-161

3-61 Aloft winds from the radar profiler sites in Baton Rouge, Cocodrie, and Ship Shoal Platform on 18–19 August 1993 3-164

3-62 Surface ozone, NO, and NO_x concentrations and winds measured at the Cocodrie site for the period 17–19 August 1993 3-165

3-63 Ozone, NO, and NO_x concentrations and temperature measured during a descending aircraft spiral over Baton Rouge at 1010 CDT on 19 August 1993 3-166

3-64 Vector-integrated transport distances, resultant wind directions, and recirculation factors calculated from radar profiler data for the period 0600–1700 CDT on 16 August 1993 in southeast Texas 3-167

3-65 Vector-integrated transport distances, resultant wind directions, and recirculation factors calculated from radar profiler data for the period 0600–1700 CDT on 19 August 1993 in southeast Texas 3-168

3-66 Vector-integrated transport distances, resultant wind directions, and recirculation factors calculated from radar profiler data for the period 0600–1700 CDT on 19 August 1993 in Louisiana 3-169

3-67 Time-height cross section of recirculation factor, vector-integrated transport distance, and resultant wind directions collected from radar profiler data for the period 18 July–15 September 1993 3-170

3-68 Map showing the modeling domain used by the surface and aloft wind fields, as well as the trajectory generation program 3-171

3-69 300-m backward trajectory starting from Aldine, Texas, at 1600 CST on 19 August 1993 3-172

3-70 300-m forward trajectory starting from Baytown, Texas, at 0800 CST on 19 August 1993 3-173

3-71 300-m backward trajectory starting from Ascension Parish, Louisiana, at 1400 CST on 19 August 1993 3-174

3-72 300-m forward trajectories from Galveston, Texas, at all hours on 18 August and 19 August 1993 3-175

3-73 100-m backward trajectories from Gilchrist, Texas City, Seabrook, and Smith Point at 1400 CST, on 8 September 1993 3-176

3-74 100-m forward trajectories from Baytown, Seabrook, and Clinton at 0200 CST, on 8 September 1993 3-177

3-75 100-m forward trajectories from Galveston and Gilchrist at 0200 CST, on 8 September 1993 3-178

3-76 100-m backward trajectory from Texas City at 1200 CST, Gilchrist at 1400 CST, and Galveston at 1400 CST, on 10 September 1993 3-179

3-77 100-m backward trajectory from Gilchrist at 1400 CST, on 10 September 1993 3-180

3-78 100-m backward trajectory from Galveston at 1400 and 1900 CST, on 10 September 1993 3-181

3-79 100-m forward trajectory from Galveston and Gilchrist at 0200 CST, on 10 September 1993 3-182

3-80 Five northeast-southwest flux planes specific to five surface monitoring sites: Galveston, Gilchrist, Seabrook, Smith Point, and Houston Regional Monitoring Site 7 3-183

3-81 Vertical profiles of ozone concentration, southeasterly component of the wind speed, and estimated ozone flux at Gilchrist on 10 August 1993 3-184

3-82 Vertical profiles of NO_x concentration, southeasterly component of the wind speed, and estimated NO_x flux at Gilchrist on 10 August, 1993 3-185

3-83 Ozone concentration, southeasterly component of the wind speed, and estimated relative ozone flux at Galveston, Gilchrist, Seabrook, Smith Point, and Houston Regional Monitoring Site 7 for 9–11 August 1993 3-186

3-84 NO_x concentration and estimated relative NO_x flux at Galveston, Gilchrist, Seabrook, Smith Point, and Houston Regional Monitoring Site 7 for 9–11 August 1993 3-187

4-1 Backward particle paths for the Houston region on 29 July 1988 culminating at 1000 and 1600 CST 4-82

4-2 Ozone nonattainment status by county for the MMS GMAQS modeling domain. 4-83

4-3 Data sources for onshore point source, onshore area source, nonroad mobile source, and onroad motor vehicle emissions 4-84

4-4 Subregions used for EPS 2.0 emissions processing 4-87

4-5 Spatial density of baseline low level anthropogenic NO_x, VOC, and CO emissions for August 17, 1993 4-88

4-6 Spatial distribution of baseline elevated NO_x, VOC, and CO emissions for August 17, 1993 4-91

4-7 Emissions density of biogenic VOC and NO_x emissions for August 17, 1993 4-94

4-8 MMS GMAQS meteorological modeling domains 4-96

4-9 Locations of meteorological monitoring sites 4-97

4-10 Objective analysis of surface wind observations and spatial weighting coefficients 4-99

4-11 SAIMM wind fields for the coarse-grid domain on 19 August 1993 at 1000 CST 4-100

4-12 SAIMM wind fields for the coarse-grid domain on 19 August 1993 at 1600 CST 4-103

4-13 SAIMM wind fields for the fine-grid domain on 19 August 1993 at 1000 CST 4-106

4-14 SAIMM wind fields for the fine-grid domain on 19 August 1993 at 1600 CST 4-109

4-15 Twenty-four-hour backward particle paths ending at 1600 CST on 19 August 1993 4-112

4-16 Vertical cross sections of wind and potential temperature for the fine-grid domain along west-east grid cell number 20 from south-north grid cells 2 to 40 on 19 August 4-113

4-17 SAIMM surface-level temperature fields for the coarse-grid domain on 19 August 1993 4-117

4-18 SAIMM surface-level temperature fields for the fine-grid domain on 19 August 1993 4-119

4-19 SAIMM surface-level specific humidity fields for the coarse-grid domain on 19 August 1993 4-121

4-20 SAIMM surface-level specific humidity fields for the fine-grid domain on 19 August 1993 4-123

4-21 UAM-V-ready vertical turbulent exchange coefficients for the coarse-grid domain on 19 August 1993 4-125

4-22 Comparison of midday observed and simulated wind profiles for Galveston on 18 August 1993 4-131

4-23 Comparison of midday observed and simulated wind profiles for Houston on 18 August 1993 4-133

4-24 Comparison of midday observed and simulated wind profiles for Galveston on 19 August 1993 4-135

4-25 Comparison of midday observed and simulated wind profiles for Houston on 19 August 1993 4-137

4-26 Layer 1 concentrations of emission tracers HOU and HOUPT on 18 August 1993 at 1000 CST 4-139

4-27 Layer 1 concentrations of emission tracers TEX and TEXPT on 18 August 1993 at 1000 CST 4-141

4-28 Layer 1 concentrations of emission tracers HOU and HOUPT on 19 August 1993 at 1000 CST 4-143

4-29 Layer 1 concentrations of emission tracers SHP and SHPPT on 19 August 1993 at 1000 CST 4-145

4-30 SAIMM wind fields for the coarse-grid domain on 8 September 1993 at 1000 CST 4-147

4-31 SAIMM wind fields for the coarse-grid domain on 8 September 1993 at 1600 CST 4-150

4-32 Twenty-four-hour forward particle paths for the surface layer on 8 September 1993 4-153

4-33 SAIMM wind fields for the fine-grid domain on 8 September 1993 at 1000 CST 4-155

4-34 SAIMM wind fields for the fine-grid domain on 8 September 1993 at 1600 CST 4-158

4-35 Vertical cross section of wind and potential temperature for the fine-grid domain along west-east grid cell number 20 from south-north grid cells 2 to 40 on 8 September 1993 4-161

4-36 Twenty-four-hour backward particle paths for the surface layer ending at 1400 CST on 8 September 1993 4-165

4-37 SAIMM wind fields for the coarse-grid domain on 9 September 1993 at 1000 CST 4-166

4-38 SAIMM wind fields for the coarse-grid domain on 9 September 1993 at 1600 CST 4-169

4-39 Twenty-four-hour forward particle paths for the surface layer on 9 September 1993 4-172

4-40 SAIMM wind fields for the fine-grid domain on 9 September 1993 at 1000 CST 4-174

4-41 SAIMM wind fields for the fine-grid domain on 9 September 1993 at 1600 CST 4-177

4-42 Twenty-four-hour backward particle path for the surface layer ending at 1500 CST on 9 September 1993 4-180

4-43 Vertical cross section of wind and potential temperature for the fine-grid domain along west-east grid cell number 20 from south-north grid cells 2 to 40 on 9 September 1993 4-181

4-44 SAIMM surface-level temperature fields for the coarse-grid domain on 8 September 1993 4-185

4-45 SAIMM surface-level temperature fields for the fine-grid domain on 8 September 1993 4-187

4-46 SAIMM surface-level temperature fields for the coarse-grid domain on 9 September 1993 4-189

4-47 SAIMM surface-level temperature fields for the fine-grid domain on 9 September 1993 4-191

4-48 SAIMM surface-level specific humidity fields for the coarse-grid domain on 8 September 1993 4-193

4-49 SAIMM surface-level specific humidity fields for the fine-grid domain on 8 September 1993 4-195

4-50 SAIMM surface-level specific humidity fields for the coarse-grid domain on 9 September 1993 4-197

4-51 SAIMM surface-level specific humidity fields for the fine-grid domain on 9 September 1993 4-199

4-52 UAM-V-ready vertical turbulent exchange coefficients for the coarse-grid domain on 8 September 1993 at 1600 CST 4-201

4-53 UAM-V-ready vertical turbulent exchange coefficients for the coarse-grid domain on 9 September 1993 at 1600 CST 4-207

4-54 Comparison of midday observed and simulated wind profiles for Galveston on 8 September 1993 4-213

4-55 Comparison of midday observed and simulated wind profiles for Houston on 8 September 1993 4-215

4-56 Comparison of midday observed and simulated wind profiles for Galveston on 9 September 1993 4-217

4-57 Comparison of midday observed and simulated wind profiles for Houston on 9 September 1993 4-219

4-58 Layer 1 concentrations of emission tracers HOU and HOUPT on 8 September 1993 at 1000 CST 4-221

4-59 Layer 1 concentrations of emission tracers SHP and SHPPT on 8 September 1993 at 1000 CST 4-223

4-60 Layer 1 concentrations of emission tracers HOU and HOUPT on 8 September 1993 at 1600 CST 4-225

4-61 Layer 1 concentrations of emission tracers SHP and SHPPT on 8 September 1993 at 1600 CST 4-227

4-62 Layer 1 concentrations of emission tracers HOU and HOUPT on 9 September 1993 at 1000 CST 4-229

4-63 Layer 1 concentrations of emission tracers SHP and SHPPT on 9 September 1993 at 1000 CST 4-231

4-64 Layer 1 concentrations of emission tracers HOU and HOUPT on 9 September 1993 at 1600 CST 4-233

4-65 Layer 1 concentrations of emission tracers SHP and SHPPT on 9 September 1993 at 1600 CST 4-235

4-66 Subdomains used to develop background concentration for the modeling domain 4-237

4-67 Initial UAM concentrations of ozone and NO_2 in the modeling domain on 17 August 1993 4-238

4-68 Fractional coverage of the urban, water, and forest land-use categories in the GMAQS domain 4-240

4-69 Percent contribution of 19th elevated NO_x tracer at 1200 EST, 19 August 1993 4-243

4-70 Percent contribution of 19th low-level NO_x tracer at 1200 EST, 19 August 1993 4-244

4-71 Interpolated observations of daily maximum ozone on 19 August 4-245

4-72 Back trajectories using UAM-V wind field from four of the highest ozone observation sites starting at the time that the 231 ppb observation occurred on 19 August 4-246

4-73 Midday NMHC concentration observed near the ship channel for 17–19 August 1993 4-247

4-74 Flight route used on the early afternoon of 19 August 4-248

4-75 Contour plot of UAM-V simulated ozone for 19 August without HC spill on ship channel 4-249

4-76 Contour plot of UAM-V simulated ozone for 19 August with HC spill on ship channel 4-250

4-77 3-D plot of Figure 4-76 looking to the northwest 4-251

4-78 Grid cells of the Houston ship channel that were set to zero for one of the September sensitivity tests 4-252

4-79 Changes in maximum simulated ozone for 8 September when 50 tons of ship channel NO_x emissions located as shown in Figure 4-78 are set to zero 4-253

4-80 Changes in maximum simulated ozone for 9 September when 50 tons of ship channel NO_x emissions located as shown in Figure 4-78 are set to zero 4-254

4-81 Changes in maximum simulated ozone for 8 September when 50 tons of point NO_x emissions located near Texas City are set to zero 4-255

4-82 Changes in maximum simulated ozone for 9 September when 50 tons of point NO_x emissions located near Texas City are set to zero 4-256

4-83 Locations of selected ozone monitoring sites in the Houston subdomain 4-257

4-84 Maximum simulated ozone concentrations in the Houston area on 17 August 1993 for the base-case simulation 4-258

4-85 Maximum simulated ozone concentrations in the GMAQS domain on 17 August 1993 for the base-case simulation 4-259

4-86 Maximum simulated ozone concentrations in the Houston area on 18 August 1993 for the base-case simulation 4-260

4-87 Maximum simulated ozone concentrations in the GMAQS domain on 18 August 1993 for the base-case simulation 4-261

4-88 Maximum simulated ozone concentrations in the Houston area on 19 August 1993 for the base-case simulation 4-262

4-89 Maximum simulated ozone concentrations in the GMAQS domain on 19 August 1993 for the base-case simulation 4-263

4-90 Maximum simulated ozone concentrations in the Houston area on 20 August 1993 for the base-case simulation 4-264

4-91 Maximum simulated ozone concentrations in the GMAQS domain on 20 August 1993 for the base-case simulation 4-265

4-92 Time-series plots comparing simulated and observed ozone concentrations for selected monitoring sites within the Houston subdomain for the 17–20 August 1993 period 4-266

4-93 Time-series plots comparing simulated and observed ozone concentrations for selected monitoring sites in the Beaumont/Port Arthur/Lake Charles area for the 17–20 August 1993 period 4-268

4-94 Time-series plots comparing simulated and observed ozone concentrations for selected monitoring sites within the Baton Rouge area for the 17–20 August 1993 period 4-269

4-95 Comparison of upper-air simulated and observed ozone and NO_x concentrations HPY aircraft spiral location on 18 August 1993 at 0545–0553 CST for the base-case simulation 4-270

4-96 Comparison of upper-air simulated and observed ozone and NO_x concentrations for the HOU aircraft spiral location on 19 August 1993 at 0616–0640 CST for the base-case simulation 4-272

4-97 Comparison of upper-air simulated and observed ozone, NO_x, and RHC concentrations for the CRY aircraft spiral location on 19 August 1993 at 1248–1257 CST for the base-case simulation 4-274

4-98 Maximum simulated ozone concentrations in the Houston area on 6 September 1993 for the base-case simulation 4-277

4-99 Maximum simulated ozone concentrations in the GMAQS domain on 6 September 1993 for the base-case simulation 4-278

4-100 Maximum simulated ozone concentrations in the Houston area on 7 September 1993 for the base-case simulation 4-279

4-101 Maximum simulated ozone concentrations in the GMAQS domain on 7 September 1993 for the base-case simulation 4-280

4-102 Maximum simulated ozone concentrations in the Houston area on 8 September 1993 for the base-case simulation 4-281

4-103 Maximum simulated ozone concentrations in the GMAQS domain on 8 September 1993 for the base-case simulation 4-282

4-104 Maximum simulated ozone concentrations in the Houston area on 9 September 1993 for the base-case simulation 4-283

4-105 Maximum simulated ozone concentrations in the GMAQS domain on 9 September 1993 for the base-case simulation 4-284

4-106 Maximum simulated ozone concentrations in the Houston area on 10 September 1993 for the base-case simulation 4-285

4-107 Maximum simulated ozone concentrations in the GMAQS domain on 10 September 1993 for the base-case simulation 4-286

4-108 Maximum simulated ozone concentrations in the Houston area on 11 September 1993 for the base-case simulation 4-287

4-109 Maximum simulated ozone concentrations in the GMAQS domain on 11 September 1993 for the base-case simulation 4-288

4-110 Time-series plots comparing simulated and observed ozone concentrations for monitoring sites south and east of the Houston area and within the Houston area for 6–11 September 1993 4-289

4-111 Time-series plots comparing simulated and observed ozone concentrations for selected monitoring sites located within the Beaumont/Port Arthur/Lake Charles area for 6–11 September 1993 4-291

4-112 Time-series plots comparing simulated and observed ozone concentrations for selected monitoring sites located within the Baton Rouge area for 6–11 September 1993 4-292

4-113 Time-series plots comparing simulated and observed ozone concentrations for selected monitoring sites located along the Texas gulf coast for 6–11 September 1993 4-293

5-1 Depiction of nonattainment areas in the GMAQS domain for which daily ozone impacts from OCSPD emissions have been tabulated . . . 5-4

5-2 OCSPD NO_x emission totals for 17 August 1993 for the Texas portion of the GMAQS domain 5-5

5-3 OCSPD RHC emission totals for 17 August 1993 for the Texas portion of the GMAQS domain 5-6

5-4 OCSPD NO_x emission totals for 17 August 1993 for the Louisiana portion of the GMAQS domain 5-7

5-5 OCSPD RHC emission totals for 17 August 1993 for the Louisiana portion of the GMAQS domain 5-8

5-6 UAM-V simulated ozone impacts from OCSPD emissions for the Houston and Louisiana subdomains for 1700 CST 18 August 1993 . . 5-12

5-7 UAM-V calculated ozone impacts from OCSPD emissions for the Houston and Louisiana subdomains for 1700 CST 19 August 1993 . . 5-14

5-8 UAM-V calculated ozone impacts from OCSPD emissions for the Houston and Louisiana subdomains for 1600 CST 8 September 1993 . 5-17

5-9 UAM-V simulated ozone impacts from OCSPD emissions for the Houston and Louisiana subdomains for 1600 CST 9 September 1993 . 5-19

5-10 UAM-V simulated ozone impacts from OCSPD emissions for the Houston and Louisiana subdomains for 1500 CST 10 September 1993 5-21

5-11 UAM-V calculated ozone impacts from onroad mobile emissions for the Houston and Louisiana subdomains for 1600 CST 8 September 1993 . 5-24

5-12 UAM-V simulated impacts from onroad mobile emissions for the Houston and Louisiana subdomains for 1600 CST 9 September 1993 . 5-26

5-13 UAM-V simulated ozone impacts from onroad mobile emissions for the Houston and Louisiana subdomains for 1600 CST 10 September 1993 5-28

5-14 UAM-V calculated ozone impacts for 1999 from OCSPD emissions for the Houston and Louisiana subdomains for 1700 CST 19 August 5-43

5-15 UAM-V calculated ozone impacts for 1999 from double OCSPD emissions for the Houston and Louisiana subdomains for 1700 CST 19 August 5-45

5-16 UAM-V calculated ozone impacts for 1999 from OCSPD emissions for the Houston and Louisiana subdomains for 1500 CST 10 September 5-51

5-17 UAM-V calculated ozone impacts for 1999 from double OCSPD emissions for the Houston and Louisiana subdomains for 1500 CST 10 September 5-53

LIST OF TABLES

2-1	Major GMAQS field study events	2-2
2-2	Summary of GMAQS sites, locations, sampling equipment, and site operator	2-6
2-3	GMAQS resources expended during the 1993 field program operating periods	2-16
2-4	Summary of the 1993 COAST and GMAQS field program intensive sampling days	2-17
2-5	Data capture rate for the 1993 GMAQS surface air quality and meteorological measurements	2-18
2-6	Data capture rate for the 1993 GMAQS VOC and carbonyl compound samples	2-18
2-7	Data capture rate for the 1993 GMAQS and COAST upper-air meteorological measurements	2-18
3-1	Distances between aircraft locations and the corresponding nearby surface sites, and lowest altitudes reached by the aircraft near the corresponding surface sites for all flights during summer of 1993	3-8
3-2	Differences between mixed-layer averages and surface ozone concentrations and between lowest-altitude averages and surface ozone concentrations for all flights during summer of 1993	3-9
3-3	Episode dates, maximum ozone concentrations, and number of exceedances in the southeast Texas region	3-13
3-4	Episode dates, maximum ozone concentrations, and number of exceedances in the Baton Rouge region	3-13
3-5	Relative reactivity estimates	3-32
3-6	C3+ carbonyl compound concentrations and the contribution of these species to total NMOC and carbonyl compounds measured at the surface during the 1993 GMAQS, 1994 Northeast Air Quality Study, and the 1987 Southern California Air Quality Study	3-33

3-7 Maximum temperature, solar radiation, and ozone concentration observed in the Houston area during August 1993 3-34

3-8 Dates and times during which the continuous GC samples had high NMHC concentrations, C4 and C5 alkane concentrations, total reactivity estimate, and weight percent of unidentified carbon 3-35

3-9 Average ozone and NO_x concentration and southeasterly component of the wind speed at Gilchrist and Galveston, and the average ozone and NO_x flux and mass flow rate across the Gilchrist and Galveston imaginary planes during 10 August 1993 3-66

3-10 Maximum ozone fluxes at Galveston, Gilchrist, Seabrook, Smith Point, and Houston Regional Monitoring Site 7 and the corresponding southeasterly component of wind speed and ozone concentration for 10 August, 19 August, and 9 September 1993 3-68

3-11 Maximum NO_x fluxes at Galveston, Gilchrist, Seabrook, Smith Point, and Houston Regional Monitoring Site 7 and the corresponding southeasterly component of wind speed and NO_x concentration for 10 August, 19 August, and 9 September 1993 3-69

4-1 1993 offshore emissions: August episode, weekday 4-9

4-2 Data variables from the EPA's 1990 interim point source inventory . . 4-10

4-3 Adjustment factors applied to the Houston/Galveston area onroad mobile emissions 4-12

4-4 Biogenic emission totals for the MMS domain 4-13

4-5 Special and EPS 2.0 default spatial allocation surrogate assignments . . 4-18

4-6 Baseline 1993 anthropogenic emissions by subregion and data source for the August 1993 episode 4-21

4-7 1993 baseline emission totals by major source category for the 17–20 August 1993 modeling episode 4-22

4-8 1993 baseline emission totals by major source category for the 6–11 September 1993 modeling episode 4-23

4-9 Uncertainties associated with the OCS production-related emissions inventory 4-25

4-10 Vertical structure of the SAIMM modeling domain for application to the GMAQS study area 4-29

4-11 Land-use categories and surface characteristics used in the application of the SAIMM to the Texas–Louisiana Gulf Coast region . 4-30

4-12 Input parameters for application of the SAIMM to the Texas–Louisiana Gulf Coast region 4-31

4-13 Meteorological surface and upper-air sites used in the application of the SAIMM to the Texas–Louisiana Gulf Coast region 4-32

4-14 Comparison of observed and estimated air temperature using observed virtual temperature profiles and surface temperature and humidity data for 19 August 1993 4-37

4-15 Comparison of observed and estimated air temperature using observed virtual temperature profiles and surface temperature and humidity data for 8 September 1993 4-38

4-16 Comparison of observed and estimated air temperature using observed virtual temperature profiles and surface temperature and humidity data for 9 September 1993 4-39

4-17 Marine air concentrations 4-55

4-18 EPA default boundary concentrations 4-56

4-19 Average surface concentrations for north, east and west boundaries . . 4-56

4-20 Selected model performance statistics for the August 1993 episode (Houston subdomain) 4-69

4-21 Selected model performance statistics for the August 1993 episode (Beaumont/Port Arthur/Lake Charles subdomain) 4-71

4-22 Selected model performance statistics for the August 1993 episode (Baton Rouge subdomain) 4-71

4-23 Selected model performance statistics for the August 1993 episode (full modeling domain) 4-72

4-24 Selected model performance statistics for the September 1993 episode (Houston subdomain) 4-76

4-25 Selected model performance statistics for the September 1993 episode (Beaumont/Port Arthur/Lake Charles subdomain) 4-77

4-26 Selected model performance statistics for the September 1993 episode (Baton Rouge subdomain) 4-77

4-27 Selected model performance statistics for the September 1993 episode (full modeling domain) 4-78

5-1 Emissions summary for OCSPD sources in the OCS western and Beaumont/Port Arthur subregions, 17 August 1993 5-10

5-2 Future year projection factors for OCSPD emission sources 5-30

5-3 Offshore emissions comparisons: 1999 vs. 1993 for the August episode, weekday 5-31

5-4 Baseline emissions for 1999 including OCS, August 17–20 5-37

5-5 Baseline emissions for 1999 including OCS, September 6–10 5-38

5-6 MMS GMAQS 1999 UAM-V simulations for the August and September episodes 5-39

5-7 Maximum simulated ozone concentrations for the Houston/Galveston, Beaumont/Port Arthur, Lake Charles, and Baton Rouge subdomains for 1993 and 1999 for the August episode 5-41

5-8 UAM-V simulated maximum ozone impacts for 1999 for the August episode due to OCSPD emissions 5-48

5-9 Maximum simulated ozone concentrations for the Houston/Galveston, Beaumont/Port Arthur, Lake Charles, and Baton Rouge subdomains for 1993 and 1999 for the September episode 5-49

5-10 UAM-V simulated maximum ozone impacts for 1999 for the September episode due to OCSPD emissions 5-56

ACRONYMS AND ABBREVIATIONS

AFS	AIRS Facility Subsystem
AG	Alpine Geophysics
AIRS	Aerometric Information Retrieval System
AMS	Area and Mobile Source
ARB	California Air Resources Board
ASC	Area Source Category
AtmAA	Atmospheric Assessment Associates
ATP	Antitampering Program
AV	AeroVironment
BEIS	Biogenic Emission Inventory System
BPA/LC	Beaumont/Port Arthur/Lake Charles
CAAA	Clean Air Act Amendments
CART	Classification and Regression Tree
CB-IV	Carbon-Bond Chemical Mechanism
CBL	Convective Boundary Layer
CDF	Cumulative Distribution Function
COAST	Coastal Oxidant Assessment for Southeast Texas
COTR	Contract Officer's Technical Representative
CST	Central Standard time
CSUMM	Colorado State University Mesoscale Model
DAS	Doppler Acoustic Sounder
DIAL	Differential Absorption Lidar
DNPH	2,4-dinitrophenylhydrazine
DRI	Desert Research Institute
DWM	Diagnostic Wind Model
EPS	Emissions Preprocessing System
ESE	Environmental Science and Engineering, Inc.
FAA	Federal Aviation Administration
FDDA	Four-Dimensional Data Assimilation
GC-FID	Gas Chromatography with Flame Ionization Detection
GMAQS	Gulf of Mexico Air Quality Study
HPMS	Highway Performance and Monitoring Survey
HRM	Houston Regional Monitoring
I/M	Inspection and Maintenance
IOP	Intensive Observation Period
LAA	Lowest-altitude Average
LATEX	Texas-Louisiana Shelf Circulation Program
LCL	Lifting Condensation Level

LDEQ	Louisiana Department of Environmental Quality
LOOP	Louisiana Offshore Oil Port
MIR	Maximum Incremental Reactivity
MLA	Mixed Layer Average
MMS	Minerals Management Service
NAAQS	National Ambient Air Quality Standard
NBL	Nocturnal Boundary Layer
NCDC	National Climatic Data Center
NMHC	Nonmethane Hydrocarbons
NMOC	Nonmethane Organic Compounds (includes carbonyls)
NWS	National Weather Service
OAQPS	Office of Air Quality Planning and Standards
OCS	Outer Continental Shelf
OCSPD	Outer Continental Shelf Petroleum Development
OPIS	OCS Platform Inventory System
PAMS	Photochemical Assessment Monitoring Stations
PBL	Planetary Boundary Layer
P-i-G	Plume-in-Grid
QA	Quality Assurance
RASS	Radio Acoustic Sounding Systems
RCS	Revision Control System
RMSE	Root-Mean-Square Error
ROG	Reactive Organic Gases
SAI	Systems Applications International
SAIMM	SAI Mesoscale Model
SCAQS	Southern California Air Quality Study
SETRPC	Southeast Texas Regional Planning Commission
STI	Sonoma Technology
TKE	Turbulent Kinetic Energy
TNRCC	Texas Natural Resource Conservation Commission
TRG	Technical Review Group
UAM	Urban Airshed Model
UAM-V	UAM Version V
USGS	U.S. Geological Survey
VMT	Vehicle Miles Traveled
VOC	Volatile Organic Compounds

EXECUTIVE SUMMARY

The design, implementation, and results of the data collection, data analysis, and air quality modeling analyses conducted as part of the Gulf of Mexico Air Quality Study (GMAQS) are detailed in this report. This effort, sponsored by the U.S. Department of the Interior's Minerals Management Service (MMS), was performed in response to a mandate written into the Clean Air Act Amendments of 1990 (CAAA Title VIII, Sec 801(b)). The study was undertaken to assess the potential impacts of emissions from oil and gas exploration, development, and production in the Outer Continental Shelf (OCS) regions of the Gulf of Mexico on ozone concentrations in the onshore areas of Texas and Louisiana that are designated by the EPA as nonattainment of the National Ambient Air Quality Standard (NAAQS) for one-hour average ozone, 0.12 parts per million (ppm). The nonattainment areas in Louisiana include the six-parish area around Baton Rouge (designated a "serious" area) and the Lake Charles/Calcasieu Parish "marginal" area, and those in Texas include the Houston/Galveston "severe-17" area, the Beaumont/Port Arthur "serious" area, and the Victoria County "incomplete data" ozone nonattainment area. The scope of the GMAQS, which was performed from May 1992 to August 1995, entailed (1) collection of air quality, meteorological, and emission inventory data during the summer of 1993, (2) analysis of the data, and (3) application of computer simulation models, one to simulate the meteorological conditions and one that uses the meteorological conditions and emission inventory information to simulate the formation and transport of photochemical pollutants, such as ozone, and quantify the impacts of emissions from OCS petroleum development (OCSPD) sources.

AIR QUALITY BACKGROUND

Ozone is a secondary pollutant formed in the presence of sunlight from the reaction of volatile organic compounds (VOC) and oxides of nitrogen (NO_x). VOCs are emitted from natural (e.g., vegetation) and anthropogenic sources such as automobiles and industrial sources (paints, solvents, etc.). NO_x is emitted in the combustion of fossil fuel (e.g., by power plants, automobiles, industrial boilers). Historically, most exceedances of the NAAQS for ozone in the study area occur near major urban and industrial source regions (Baton Rouge, New Orleans, Lake Charles, Houston, Galveston, Beaumont, Port Arthur, and Victoria County, Texas). Exceedances occur during all seasons, but about 85 percent of the exceedance days occur from April through October and are usually associated with generally stagnant or weak synoptic-scale wind conditions, subsidence (high pressure), low humidity, suppressed convection (little cloudiness), and ample solar radiation. Local meteorological conditions, especially the land/gulf breeze circulation in the Houston and Beaumont areas, are prominently

associated with elevated ozone levels or exceedances of the ozone NAAQS. Since 1980, ozone concentrations in excess of 0.12 ppm (the national standard) and as high as 0.34 ppm have been observed at shoreline and inland locations that could potentially be influenced by emission sources in the Gulf of Mexico.

Many episodes, including those that occurred during the 1993 field program, are 2 to 5 days in length, suggesting very consistent weather patterns from day to day and the potential for buildup of pollutant concentrations at the surface and aloft over several days. Conditions like this can lead to increasingly complex and diverse ozone patterns on each successive day of multiday ozone episodes.

GOALS AND OBJECTIVES OF THE STUDY

The overall goal of this study was to assess, through computer simulation modeling (meteorological and photochemical), the effects of current and future OCS development in the Gulf of Mexico on ozone nonattainment areas in Texas and Louisiana. The meteorological modeling used the SAI Mesoscale Model (SAIMM), a data-assimilating prognostic meteorological model similar to those used by the National Weather Service to forecast weather, and the photochemical modeling used an updated, variable-grid version of the Urban Airshed Model, referred to as the UAM-V.

The GMAQS had six specific objectives which addressed both near-term and longer-term requirements. The study had two short-term objectives:

- Analyses of historical data, supplemented by recent meteorological measurements, that describe the conditions and likelihood of OCSPD emissions reaching coastal areas under conditions conducive to ozone formation

- Preliminary meteorological and photochemical modeling of historical episodes of high onshore ozone concentrations to estimate OCSPD contributions to onshore ozone for historical high ozone episodes.

The study had four longer-term objectives:

- Collection of extensive meteorological and air quality data during the summer ozone season

- Extension, refinement, evaluation, and application of meteorological and photochemical modeling techniques using the data collected during the field study

- Evaluation of the sources of uncertainty in estimates of impacts

- Recommendation of future monitoring and modeling efforts to address these uncertainties.

PROJECT ELEMENTS AND CHRONOLOGY

The project was divided into nine major tasks conducted in the following sequence:

1. Identification of representative historical ozone episodes.

2. Development of emissions inventories for these historical episodes (including OCS and onshore emissions, and growth/control in future years of interest).

3. Preliminary meteorological and photochemical modeling of selected historical episodes.

4. Design and execution of a field study to collect appropriate meteorological and air quality data during the summer of 1993.

5. Development of emission inventories for the 1993 ozone episodes and projection of future-year emission inventories.

6. Data analysis using both historical and 1993 data.

7. Meteorological and photochemical modeling of 1993 ozone episodes; assessment of the ozone impacts of alternative OCS future development scenarios in the Gulf Coast area on the onshore ozone nonattainment areas.

8. Characterization of the uncertainty in the model estimations.

9. Evaluation of the needs for future research or data collection efforts to improve understanding of the OCSPD-related effects on ambient ozone onshore.

The principal elements of the GMAQS were the field study, data analyses, emissions inventory development, meteorological modeling, and photochemical modeling. An overview of the results of each of these elements is provided below.

OVERVIEW OF THE FIELD STUDY (APRIL–OCTOBER 1993)

The field program was planned in late 1992 and early 1993. Three offshore platforms and five onshore sites were selected for the installation of supplemental (to those already operating in the area) air quality and/or meteorological measurement systems for the study. These sites are shown in Figure 1-2, in the body of the report. The equipment was installed and began operating by mid-April 1993. These sites include the following:

Offshore:

- Texaco High Island 199A
- ARCO Ship Shoal 178
- Chevron Garden Banks 236

Onshore:

- Gilchrist, Texas
- LUMCON (Cocodrie, LA)
- Southeast Houston (Hobby Airport)
- Galveston, Texas
- Louisiana State University - Baton Rouge, LA

The intensive measurement portion of the field study ran from 18 July to 28 August 1993. During this time, two highly instrumented twin engine aircraft were on alert in Beaumont to fly when conditions were favorable for ozone exceedances. The National Weather Service, which collects twice daily measurements of wind, temperature, and humidity aloft, provided one additional upper-air meteorological measurement daily as needed from Slidell and Lake Charles, Louisiana. Either two or three soundings were made from the Garden Banks platform to measure meteorological variables aloft at an offshore location. In addition, VOC and carbonyl samples were collected at shore locations in Texas and Louisiana.

The 1993 GMAQS field study was uncommonly successful: the occurrence of ozone conducive conditions coincided with the availability of comprehensive observational systems. Several high-ozone episodes were captured, including those with peak ozone concentrations approximating historically high levels throughout the study area. Four episodes (29-31 July, 10-13 August, 18-21 August, and 7-11 September) occurred during the summer of 1993. The days 9-11 August, 17-21 August, and 7-11 September were selected for analysis, and from these the days 17-20 August and 7-11 September were selected for modeling. High data recovery rates were achieved, even in the challenging offshore operating environment. Ozone episode forecasts for intensive monitoring deployments were very successful; few high events were missed, few false alarms were forecast, and intensive monitoring resources were almost fully spent by the end of the intensive measurement period window.

The 1993 GMAQS field program ran concurrently with the Texas Natural Resource Conservation Commission's (TNRCC) Coastal Oxidant Assessment for Southeast Texas (COAST) field program. The forecasting of intensive measurement periods and the deployment of the GMAQS and COAST monitoring resources were closely coordinated. In addition, MMS and TNRCC agreed to freely share data collected in the two studies. Much of the COAST data (all those released in time) were used in this study along with data collected during the 1993 GMAQS.

RESULTS OF THE DATA ANALYSES

Historical data and data collected during the 1993 field program were analyzed. Historically available data routinely collected for monitoring sites within the GMAQS modeling domain were acquired and analyzed to provide information for selection of historical episodes for modeling and for the development of an episode forecasting methodology for the 1993 field program.

Descriptions and displays of air quality and meteorological data (objective data analysis) collected during the 1993 field program were prepared and apparent relationships between parameters were identified. Summary statistics and visual displays were prepared to characterize important features of the air quality and meteorological conditions in the Gulf Coast region. The key findings of the data analysis include the following:

- Ozone exceedance days in the southeast Texas portion of the GMAQS study are associated with a distinct flow reversal. The strength and duration of the land breeze (which occurs mainly during the nighttime hours), and corresponding stagnation during transition during the day to onshore flow (gulf breeze) is an important mechanism that causes a recirculation of precursor emissions and contributes to observed hourly ozone concentrations exceeding 0.12 ppm. Detailed analysis of the observed wind data for 10 exceedance days in 1993 suggests that the land breeze "front" typically traveled 75 to 100 km offshore before the winds reversed and began blowing onshore again. No exceedance events occurred in this area during 1993 without the observed flow reversal.

- Maximum ozone concentrations occurred during the period when southerly winds accompanying the onshore component of the flow reversal were present. The ozone "cloud" (or "plume") of pollutants that was transported offshore with the land breeze was then pushed northward (inland) with the gulf breeze, with the highest ozone concentrations usually observed north of Houston. After the passage of the gulf-breeze front and establishment of steady onshore flow (gulf breeze), ozone concentrations measured at coastal locations dropped dramatically.

- In Louisiana, the same general pattern of the onshore-offshore-onshore flow reversal was observed on a number of study days, including 18–19 August, when the NAAQS for ozone was exceeded in Baton Rouge.

- Calculated air parcel trajectories for each episode examined indicated that marine air coming onshore (from potential OCSPD source areas) on the day of an ozone exceedance did not reach the areas where maximum ozone concentrations were observed until several hours after the highest ozone concentrations had occurred.

- Air parcel trajectory analysis using a simple diagnostic wind field model (involving the interpolation of observed wind data) was performed to assess the potential transport of pollutants from offshore source areas to onshore nonattainment areas. Although no direct measurements of the transport using inert tracers were made during the 1993 GMAQS field program, the transport analysis using the interpolated wind fields indicated that direct, same-day transport of offshore OCSPD emissions from source regions in the Gulf of Mexico (south and east of Louisiana) to exceedance sites near Baton Rouge did not occur during the August and September episodes.

A range of data analysis methods were used to examine the potential for OCSPD emissions to contribute to ozone exceedances in the southeast Texas and Baton Rouge nonattainment areas. Shoreline flux estimates, calculated for both the August and

September episodes, indicated that the amount of NO_x emissions transported into the Houston area from OCSPD sources is small compared to that from onshore sources. Similarly, for ozone, the flux calculations indicate that the amount of ozone transported onshore is small compared to that produced in the Houston area. For example, the NO_x mass flow rate passing through an imaginary plane about 600 m deep across 50 km of shoreline during midday onshore flow conditions was estimated through the analysis of the data to be about 2 mg/min, which corresponds to be less than 5 ten-millionths of 1 percent of typical surface emission rates in the Houston Ship Channel area.

OVERVIEW OF EMISSION INVENTORY PREPARATION

Emission inventory information was provided by the MMS and the states of Louisiana and Texas. Using these data, gridded, hourly emissions inventories were prepared for the entire study area, for both historical and 1993 ozone episodes, and for future-year emissions scenarios. These inventories cover an area of nearly one million square kilometers, encompassing the western and central portions of the Gulf of Mexico and onshore ozone nonattainment areas (Houston/Galveston, Beaumont/Port Arthur, Calcasieu Parish/Lake Charles, and Baton Rouge).

Air pollutants inventoried included NO, NO_2, speciated VOC, and CO. The modeling emission inventories included emissions from both onshore and offshore sources and those specifically associated with OCSPD-related emissions. Relevant emissions from anthropogenic and biogenic sources were inventoried, with special attention focused on offshore anthropogenic sources.

- OCSPD emissions in offshore lease tracts adjacent to the Houston and Beaumont/Port Arthur areas represent less than 2 percent of the total anthropogenic NO_x emissions and less than 1 percent of the total VOC emissions in the Houston and Beaumont/Port Arthur onshore nonattainment areas.

- OCSPD emissions in the western and central Gulf of Mexico comprise approximately 5 percent of the total anthropogenic NO_x emissions and less than 2 percent of the total anthropogenic VOC emissions within the entire GMAQS modeling domain.

Initial simulation results using the baseline modeling emission inventory suggested that VOC emissions were understated relative to NO_x emissions in the Houston area. The data analysis results support this inference.

- An anthropogenic emission-based VOC-to-NO_x ratio of approximately 2.5 is not consistent with measurement-derived estimates of 10 or greater.

The use of the inventory in the modeling analysis also indicated that uncertainties in the day-specific emission estimates, especially for mobile and industrial sources, may have affected model performance for both episodes.

- Based on the results of numerous diagnostic and sensitivity simulations performed using the UAM-V, modeling emission inventories for the Houston area were adjusted such that the NO_x emissions from elevated point sources were reduced by 50 percent, VOC emissions from stationary sources (including area, nonroad, and point sources) were increased by 50 percent, and VOC emissions for mobile sources were increased by a factor of 2 for both episodes. With these adjustments, the performance of the model in replicating the observed ozone concentrations improved significantly.

- Based on an analysis of hydrocarbon data for the Clinton site and information obtained from county records, VOC emissions for the 19 August base-case analysis were modified to incorporate the effects of a petroleum product spill in the Houston Ship Channel area. Emissions from this assumed accidental occurrence were included in the base-case performance evaluation simulations only; additional simulations for this day performed to assess OCSPD emission impacts, however, did not include these emissions.

It is anticipated that more refined emission inventory information collected as part of the 1993 COAST program (not available in time for use in the GMAQS) for anthropogenic and biogenic sources could be used to improve the GMAQS inventory and base-case modeling results.

RESULTS OF THE METEOROLOGICAL MODELING

Meteorological fields for application of the UAM-V to the GMAQS modeling domain were prepared using the SAI Mesoscale Model (SAIMM). For this application, the model was exercised using a one-way nested-grid approach with 16-km horizontal resolution for the coarse grid or outer domain and 4-km resolution for the inner domain. Routine and supplementary meteorological data collected during the GMAQS and COAST field programs were incorporated into the SAIMM simulations using four-dimensional data assimilation (FDDA). This procedure involves the introduction of real data into the solution of the prognostic model to aid in replicating the observed meteorological features.

The evaluation of the model using data collected during each of the episodes showed that the model provided a reasonable representation of the observed regional-scale flow patterns and the temporal and spatial features of the gulf breeze and associated airflow patterns.

- Good agreement between the simulated and observed winds aloft for both episodes indicates that the SAIMM was able to simulate the day-to-day variations in the regional-scale meteorological conditions (and, thus, the regional-scale transport patterns) associated with anticyclonic flow aloft during the August episode and northerly winds aloft during the September episode.

- The simulated vertical and temporal evolution of the gulf breeze (as illustrated by vertical cross-section plots) demonstrates the ability of the model to realistically represent the complex, three-dimensional circulation patterns associated with the development of the gulf breeze including the transition from weak offshore-directed flow to steady onshore flow, the inland propagation of the gulf breeze front, and the vertical development of the gulf-breeze layer.

- A comparison with the data analysis results for both episodes indicates that the fine-grid SAIMM-simulated airflow patterns conform to the conceptual models of offshore-onshore flow reversal suggested by the data. The various stages of flow reversal were identified in the simulated wind fields.

UAM-V simulations of inert material (not physical tracers) were used to evaluate the three-dimensional meteorological fields with respect to the data analysis results. In these simulations, inert pollutant material is tracked as it is advected and dispersed within the grid; no chemistry takes place in these simulations.

- Tracer simulation results for the August episode support the general conclusions from the data analysis that northeastward transport of pollutants occurred during this episode and that carryover (recirculation) of ozone and precursor pollutants was unlikely.

- Results for the September episode show that the simulated wind fields represent carryover/recirculation of pollutants from onshore sources that was determined, through data analysis, to have occurred during this episode. On 8 and 9 September, the simulated tracers are advected approximately 32 km offshore; the data analysis results suggest that this distance is somewhere between 10 and 50 km.

RESULTS OF THE PHOTOCHEMICAL MODELING ANALYSES

An advanced photochemical air quality model, the variable-grid version of the Urban Airshed Model (UAM-V), was applied for the GMAQS domain to provide simulations of the chemical and physical mechanisms affecting observed ozone concentrations within the study domain and to provide quantitative estimates of the impacts of OCSPD emissions on ozone concentrations within the onshore nonattainment areas. The primary focus of the photochemical modeling analysis was the Houston area. Three multiday ozone episodes were simulated: 27–28 July 1988, 17–20 August 1993, and 6–11 September 1993. Supplemental air quality meteorological data were available for the 1993 episodes.

- The objective of the modeling effort for the 1988 episode was to test whether the GMAQS modeling system (consisting of the Emissions Preprocessing System (EPS 2.0), SAIMM, and UAM-V) was capable of simulating ozone formation and transport in the Gulf of Mexico area. It provided an opportunity to test and refine input preparation methodologies and to identify deficiencies in the available meteorological and air quality databases for consideration in designing the 1993 field study.

- The 1993 modeling episodes were selected based on the magnitude and extent of observed high ozone concentrations within the onshore ozone nonattainment areas and the estimated potential for OCS emissions to contribute to the onshore concentrations.

- Analysis of historical ozone episodes indicated that the 1993 GMAQS episodes were representative of the period 1982–1992 and that the meteorological variables monitored during the 1993 episodes were within the ranges of distributions for ozone exceedance days during this historical period.

Numerous diagnostic and sensitivity tests were carried out to examine the response of the UAM-V to uncertainties in inputs to assess whether the model was able to perform reasonably well in replicating the temporal and spatial characteristics of the observed ozone concentration patterns.

- The diagnostic and sensitivity simulations showed that either lower localized NO_x or higher VOC emissions in the Houston/Galveston Bay area or some combination of the two provided a better simulation of ozone for all the high ozone days.

- The simulation results also indicated that some of the isolated (in space and time) high observed ozone concentrations in the Houston area may have been the result of localized fluctuations in emissions combined with adverse meteorological conditions or synergistic interactions of the local, diverse emissions.

- The modeling emission inventories were adjusted within considered ranges of uncertainty to enable the UAM-V to reasonably depict the air quality characteristics of the ozone episodes. The adjustments included a 50 percent decrease in elevated point-source NO_x emissions, a 50 percent increase in stationary source VOC emissions, and 100 percent increase in mobile-source VOC emissions. VOC emissions corresponding to a petroleum product spill were also included for the simulation of 19 August for the base-case model evaluation.

Evaluation of UAM-V model performance, based on the adjusted inventory for the Houston area, was completed using available air quality measurements and a variety of graphical and statistical analysis techniques. The performance evaluation was conducted to determine whether the modeling database could reliably be used to "predict" future air quality levels.

- The assessment of model performance for the August and September episodes indicated that the modeling system provided a reasonable simulation of each of the episodes. The simulation results were generally consistent with the conceptual models of the episodes developed through analysis of the air quality and meteorological data, and the statistical measures were generally within the ranges provided by the EPA for acceptable photochemical model performance.

- Uncertainty in the model inputs, however, adversely affected model performance, and the results of the model performance evaluation indicated that use of the

modeling system to assess the impacts of OCSPD emissions on ozone concentrations within the GMAQS region should consider these uncertainties.

SUMMARY OF OCSPD IMPACT ANALYSIS

OCSPD Impact Analysis for 1993

To assess the incremental impacts of OCSPD emissions relative to the ozone standard of 0.12 ppm, two simulations of UAM-V were run; one simulation included OCSPD emissions and the other did not. The incremental impacts due to OCSPD emissions were derived by subtracting the ozone concentrations in the simulation without OCSPD emissions from those in the simulation that included OCSPD emissions. Modeling of OCSPD impacts for 1993 for the August and September episodes revealed:

- The maximum incremental increases to peak hourly ozone concentrations due to OCSPD emissions for both episodes were approximately 25-35 ppb, in locations over the central Gulf of Mexico region, more than 120 km south of the Louisiana coastline (near the area of highest OCSPD emission density). Peak simulated ozone concentrations in this area (with OCSPD emissions) ranged from 70 to 80 ppb. The maximum simulated onshore incremental impacts due to OCSPD emissions were greatest during the nighttime hours for all episode days. These maximum simulated onshore incremental impacts occurred at coastal and inland locations throughout the GMAQS domain, when observed and simulated ozone concentrations were relatively low.

- Maximum ozone impacts due to OCSPD operations for both episodes in the Houston and Beaumont/Port Arthur area were estimated to be 6-8 ppb at a time when the hourly average ozone concentrations calculated from all other emission sources were approximately 50 ppb. During periods and at locations where ozone concentrations were simulated to equal or exceed 120 ppb, the incremental ozone impacts due to OCSPD emissions were simulated to be less than 2 ppb.

- For the Baton Rouge nonattainment area, the maximum simulated incremental impacts from OCSPD emissions for the August episode, during the time when simulated ozone concentrations were equal to or above 120 ppb, were less than 2 ppb. Larger impacts from OCSPD emissions are simulated during other hours, and at locations along the Louisiana coastline and over the Gulf, well south of the Baton Rouge nonattainment area.

OCSPD Impact Analysis for 1999

The meteorological and air quality inputs were fixed and the model was used as a forecasting tool to provide likely future ozone concentration estimates ("predictions") for a number of future-year (1999) onshore and OCSPD emission scenarios to assess the simulated impacts of OCSPD sources on the onshore nonattainment areas. The future-year (1999) modeling indicated:

- Maximum incremental increases to peak hourly ozone concentrations due to OCSPD emissions for 1999 for both episodes were approximately 25-35 ppb, in locations over the central Gulf of Mexico region, more than 120 km south of the Louisiana coastline (near the area of highest OCSPD emission density). Peak simulated ozone concentrations in this area (with OCSPD emissions) ranged from 70 to 80 ppb. The maximum simulated onshore hourly incremental impacts due to OCSPD emissions were greatest during the nighttime hours for all episode days. These maximum simulated onshore incremental impacts occurred at coastal and inland locations throughout the GMAQS domain, when observed and simulated ozone concentrations were relatively low.

- The maximum simulated ozone impacts for both episodes due to estimated 1999 OCSPD operations in the Houston, Beaumont-Port Arthur, Lake Charles, and Baton Rouge areas were 10-20 ppb. These impacts occurred during hours when the maximum simulated concentrations were in the range of 30-80 ppb.

- During periods and at locations where ozone concentrations were simulated to exceed 124 ppb, the incremental ozone impacts due to OCSPD emissions, for both episodes in all nonattainment areas, were simulated to be 2-6 ppb.

- To assess the sensitivity of the model and to bracket the uncertainty in the future-year OCSPD emission estimates, simulations were performed for scenarios that assumed a doubling and a 50 percent decrease in OCSPD emissions. When the OCSPD emissions were doubled for the August episode, the maximum simulated hourly incremental impacts increased to 18-20 ppb in the Houston area, 14-16 ppb in the Beaumont area, 10-12 ppb in the Lake Charles area, and 14-16 ppb in the Baton Rouge area. When the OCSPD emissions were doubled for the September episode, the maximum simulated hourly incremental impacts increased to 16-18 ppb in the Houston area, 10-12 ppb in the Beaumont area, 10-12 ppb in the Lake Charles area, and 16-18 ppb in the Baton Rouge area.

- The maximum simulated incremental impacts for the August and September episodes occurred at times and locations when simulated ozone concentrations were less than 124 ppb.

- The magnitudes of the simulated incremental OCSPD ozone impacts for either episode, based on numerous sensitivity tests, do not appear to be sensitive to uncertainties in the base inventories used for the Houston subdomain. Regardless of which future-year inventory is used (baseline or adjusted), the simulated incremental impacts from OCSPD operations are very similar.

- Uncertainties exist in the modeling inputs, especially the emission inventory, and although the magnitude of the simulated incremental impacts are smaller than the model uncertainties, the impacts should not be interpreted as being meaningless. The UAM-V is most accurate when used to estimate relative impacts, and we believe that they are considerably more accurate than what is suggested by the estimated standard deviations of the simulation results.

RECOMMENDATIONS FOR FUTURE WORK

Recommendations are provided for four categories: field measurements, emission inventory, meteorological, and photochemical modeling. The recommendations follow from the insights gained during this study concerning the mechanisms that influence ozone formation and transport in the area, and are meant to complement and extend the analyses performed to date.

The recommendations include:

1. Make additional field measurements of meteorological and air quality parameters both at the surface and aloft, in onshore and offshore areas. The measurements should cover a longer period to capture more episodes over a larger geographical area.

2. Improve the emission inventory by identifying uninventoried sources, providing speciated hydrocarbon emissions estimates, updating biogenic emissions, providing better estimates for fugitive emissions, providing more refined estimates of mobile source emissions, and quantifying day-specific emissions of unusual events.

3. Improve the meteorological modeling analysis by using an increased horizontal resolution and applying a prognostic meteorological model with added capabilities (e.g., true nested grid formulation, improved data-assimilation procedures, cloud physics, nonhydrostatic model dynamics) for improved characterization of the three-dimensional airflow patterns and pollutant transport associated with gulf breeze circulations.

4. Improve the photochemical modeling analysis by using increased vertical resolution to allow better representation of the distribution of point-source emissions and meteorological features. Address the effects of performance and impacts of using alternative chemical mechanisms, particularly mechanisms that consider alternative aromatic chemistry, long-chain alkanes, and terpenes.

Acknowledgments

A Technical Review Group (TRG) was formed at the beginning of the study that consisted of interested parties, including other government agencies and industry. The members of the TRG were:

Mr. William Steorts (TRG Chairperson)
Minerals Management Service—New Orleans

Mr. Dick Karp
Texas Natural Resource Conservation Commission

Mr. Jim Yarbrough
U.S. Environmental Protection Agency, Region VI

Mr. Gus Von Bodungen
Louisiana Department of Environmental Quality

Mr. James Magee
Louisiana Department of Environmental Quality

Dr. Richard Scheffe
U.S. Environmental Protection Agency, Office of Air Quality Planning and Standards

Mr. Dirk Herkhof
Minerals Management Service — Headquarters, Herndon, VA

Mr. Brian Shannon
ARCO

Dr. Stephen Ziman
Chevron

Mr. David Scalfano
Chevron

Dr. S. A. Hsu
Louisiana State University (LSU)

The contributions of these TRG members' time and the insights and opinions they freely offered were extremely valuable and are greatly appreciated.

Special recognition is given to Chevron, Texaco, ARCO, LSU, and LUMCON for providing monitoring sites. Chevron, Texaco, and ARCO in particular, not only provided space and power to their offshore platforms for monitoring equipment, but also donated logistical and other support for offshore field operations. In particular, the following individuals from these organizations are recognized for their contributions to the 1993 GMAQS field program:

Paul Versowsky - Chevron
Jose Abadin - Texaco
Mike Park, Mike Pawelek - ARCO
Brian Blanchard, Jeremy Champagne - LSU
Steve Rabalais, Robert Highes, Chuck Guidry - LUMCON

List of Contractor Participants

The individuals who participated in the MMS GMAQS from each of the contracting organizations include the following:

AeroVironment, Inc.

Alexander N. Barnett
William C. Brick
Kurt Bumiller
David H. Bush
Barbara J. McMurray
Marc Q. Moritsch
David V. Pankratz
Steven R. Peterson

Alpine Geophysics

Dennis E. McNally
Thomas W. Tesche

Earth Tech/Sigma Research

Joseph C. Chang
Steven R. Hanna
John (Xiaoming) Zhang

Environmental Science & Engineering

Michael Dybevick
Sandy Grenville
Mike Jackson
Anna Karmazyn
Mark Kimball
Joey Landreneau
Carl Nagle

Evans-Hamilton, Inc.

Charles E. Abbott
Barbara E. Allen
Robert C. Hamilton

A. T. Kearney

Garry Brown
Emily MacDonald
Barbara Wallace

Atmospheric Assessment Associates (AtmAA, Inc.)

Kochy Fung

Oregon Graduate Institute

Rei Rasmussen

Radian Corporation

Larry Best
Mike Gatewood
Robert Hernandez
John Neuschaefer
Carlton Schneider
David Vik
Gary Zeigler

Ed Roy, Ltd.

Jim Bedore
Eduardo Bosch
George Harvey
Bob Moore
Gene Snyder

T & B Systems

Nancy L. Alexander

TRC Environmental

John Koos

Weather Modification, Inc.

Denise Banaszewski
Tim DeForest

Sonoma Technology, Inc. (STI)

Jerry A. Anderson
Mark Arthur
Donald L. Blumenthal
James M. Crowdus
Timothy S. Dye
Dennis Haase
Don H. Hern
Marcelo E. Korc
Charles G. Lindsey
Hilary H. Main
Jeff D. Prouty
Scott E Ray
Paul T. Roberts
Jesse Rosen
Bastian M. Schoell
Mark W. Stoelting
David B. Wright

STI Production Staff
Barbara A. Austin
Sandra Borger
Carolee A. Dewitt
Sue Z. Hymek

Systems Applications International

C. Shepherd Burton
Marianne C. Causley
Sharon G. Douglas
Christopher A. Emery
LuAnn Gardner
Paul D. Guthrie
Jay L. Haney
A. Belle Hudischewskyj
Robert G. Jackson
Michele M. Jimenez
Robert C. Kessler (deceased)
Dirk Kleinhesselink
Mary P. Ligocki
Nina K. Lolk
Richard E. Looker
Gary W. Lundberg
Gerard E. Mansell
Julie K. Morgan
Ralph E. Morris
Thomas C. Myers
Eric M. Neri
Steven B. Reid
Stella B. Shepard
Cyntia K. Steiner
Hedy Tunggal
Steve D. Vu
Yi Hua Wei
Gary Z. Whitten
Gary M. Wilson
Shiang Wu
Mark A. Yocke

SAI Production Staff
Andrew L. Alden, Technical Editor
Rita L. Beacock
Cristi-Ann Jackson
Jo Ann Moennighoff
Max Jungbauer
Sandra Christensen

Special recognition is given to the memory of Robert C. Kessler, and his pioneering role in the development of prognostic meteorological modeling techniques, some of which were utilized in this study.

LIST OF SUPPORTING DOCUMENTATION PREPARED FOR THE MMS GULF OF MEXICO AIR QUALITY STUDY

"Gulf of Mexico Air Quality Study Field Plan," by P. Roberts, D. Blumenthal, C. Lindsey, J. Anderson, M. Yocke, A. Barnett, R. Hamilton, M. Dybevick, and G. Zeigler. Working draft no. 2 prepared for the Minerals Management Service by Sonoma Technology, Inc., Santa Rosa, CA (STI-92040-1212-WD2, Contract No. 1435000130604). 1992.

"Gulf of Mexico Air Quality Study Forecasting and Decision-Making Protocol," by P. T. Roberts and T. S. Dye. Draft report prepared for Systems Applications International and Minerals Management Service by Sonoma Technology, Inc., Santa Rosa, CA (STI-92040-1361-DP, Contract No. 1435000130604). 1993.

"Gulf of Mexico Air Quality Study Data Archival Protocol," by Systems Applications International (SYSAPP-93/076). Draft report prepared for Minerals Management Service. 1993.

"Quality assurance report for the Western and Central Gulf of Mexico Air Quality Study," by AeroVironment, Inc. (AV-FR-94/6012). Final report prepared for Systems Applications International. 1994.

"Data collected by the STI aircraft during the 1993 Gulf of Mexico Air Quality Study (GMAQS)," by J. A. Anderson, D. H. Hern, P. T. Roberts, J. D. Prouty, and B. M. Schoell. Data volume prepared for Systems Applications International and Minerals Management Service by Sonoma Technology, Inc., Santa Rosa, CA, STI-92070-1403-DV. 1994.

"The airborne air quality sampling program performed during the 1993 Gulf of Mexico Air Quality Study (GMAQS)," by J. A. Anderson and P. T. Roberts. Draft final report prepared for Systems Applications International and Minerals Management Service by Sonoma Technology, Inc., Santa Rosa, CA, STI-92070-1412-DFR. 1994.

"Upper Air Data Collected by 915 MHz Radar Wind Profilers and Radio Acoustic Sounding Systems During the 1993 Gulf of Mexico Air Quality Study and the Coastal Oxidant Assessment in Southeast Texas Study," by T. S. Dye, C. G. Lindsey, B. M. Schoell, J. N. Rosen, and C. M. Jones. Data volume prepared for Systems Applications International, Minerals Management Service and Texas Natural Resource Conservation Commission by Sonoma Technology, Inc., Santa Rosa, CA, STI-92084/93320-1408-DV. 1994.

"A Description of the Gulf of Mexico Air Quality Study Data Archive Files," by Systems Applications International. Prepared for Minerals Management Service OCS Study MMS 94-0046 (SYSAPP-94/085). 1994.

"Upper Air Data Collected by STI on Chevron's Garden Banks 236A Platform During the 2993 Gulf of Mexico Air Quality Study," by B. M. Schoell, C. G. Lindsey, T. S. Dye, J. D. Prouty, and J. N. Rosen. Data volume prepared for Systems Applications International and Minerals Management Service by Sonoma Technology, Inc., Santa Rosa, CA (STI-92064-1407-DV). 1994.

"Data Collected by a Network of Surface Meteorological Monitoring Stations During the 1993 Gulf of Mexico Air Quality Study," by B. M. Schoell, C. G. Lindsey, T. S. Dye, J. N. Rosen, J. D. Prouty, and M. W. Stoelting. Data volume prepared for Systems Applications International and Minerals Management Service by Sonoma Technology, Inc., Santa Rosa, CA (STI-92084-1409-DV). 1994.

"Representativeness of 1993 GMAQS ozone episodes and relations between ozone episodes and meteorological variables in the Gulf of Mexico," by J. C. Chang and S. R. Hanna. Report prepared for Systems Applications International by Earth Tech, Concord, MA, No. 1246. 1995.

1 INTRODUCTION

This report describes the design, implementation, and results of the data collection, data analysis, and air quality modeling analyses conducted as part of the Gulf of Mexico Air Quality Study (GMAQS). This effort, sponsored by the U.S. Department of the Interior's Minerals Management Service (MMS), entailed the collection of supplemental air quality, meteorological, and emission inventory data during the summer of 1993, a detailed analysis of the data, and the application of a meteorological/photochemical modeling system to assess the potential ozone impacts that offshore petroleum development sources in the Gulf of Mexico may have upon the onshore nonattainment areas of Texas and Louisiana.

1.1 BACKGROUND

LEGISLATION

The Clean Air Act Amendments of 1990 (CAAA Title VIII, Sec 801(b)) specifically mandate that the MMS conduct a research study to assess the potential for onshore impacts of certain types of air pollutant emissions from offshore oil and gas exploration, development, and production in the Outer Continental Shelf (OCS) regions of the Gulf of Mexico. Furthermore, the study results will form the basis for consultations between the Department of the Interior and the U.S. Environmental Protection Agency regarding any needed changes in the regulations for emission sources related to OCS petroleum development (OCSPD). This mandate grew out of widely expressed concerns regarding the cumulative onshore impacts of air pollutant emissions from more than three thousand offshore facilities in the central and western Gulf of Mexico. The impacts of greatest concern are ozone concentrations in onshore areas not attaining the National Ambient Air Quality Standard (NAAQS) for one-hour average ozone 0.12 parts per million (ppm). These nonattainment areas, classified by the EPA, include, in Louisiana, the six-parish area around Baton Rouge (designated a "serious" area) and the Lake Charles/Calcasieu Parish "marginal" area, and, in Texas, the Houston/Galveston "severe-17" area, the Beaumont/Port Arthur "serious" area, and the Victoria County "incomplete data" ozone nonattainment area. The GMAQS study area and these nonattainment areas are depicted in Figure 1-1.

Accordingly, MMS undertook sponsorship of the Gulf of Mexico Air Quality Study, which is intended to evaluate the effects of the development of OCS petroleum resources on onshore ozone concentrations. The first stages of this three-year project began in May 1992.

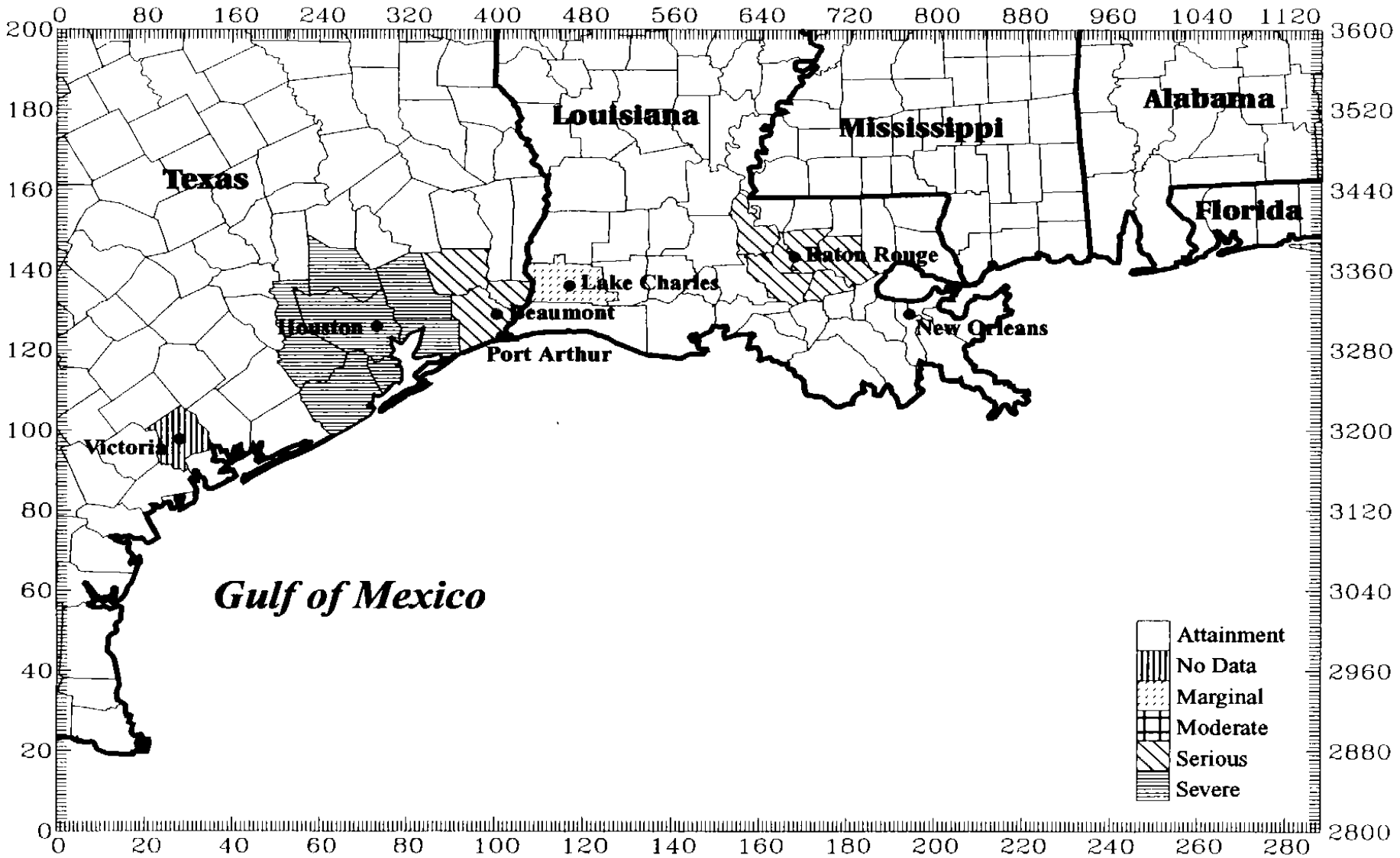

Figure 1-1. The MMS GMAQS modeling domain and existing ozone nonattainment areas.

AIR QUALITY BACKGROUND

Historically, most ozone exceedances in the study area occur near major urban and industrial regions (Baton Rouge, New Orleans, Lake Charles, Houston, Galveston, Beaumont, Port Arthur, and Victoria County, Texas) with a few exceedances occurring in rural areas. Recently most rural areas have had no exceedances, although in the past, very few monitors have actually been located in exclusively rural portions of the Gulf Coast area. Exceedances occur during all seasons, but about 85 percent of the exceedance days occur from April through October. Exceedances are almost always associated with generally stagnant or weak wind conditions at the large (synoptic) scale. During summer ozone episodes, especially in the Houston/Beaumont area, the local land/sea breeze circulation is superimposed on these generally weak or disorganized synoptic flow patterns. Local meteorological patterns appear to play a prominent role in determining ozone levels. Episodes are also associated with atmospheric conditions that include subsidence, low humidity, suppressed convection, and ample solar radiation. During the past 12 years, ozone concentrations in excess of 0.12 ppm (the national standard) and as high as 0.34 ppm have been observed at shoreline and inland locations that could potentially be influenced by emission sources in the Gulf of Mexico.

In some parts of the study region, transport of ozone and ozone precursors from one urban/industrial area to another is suggested in the historical patterns. In particular, transport from Houston to Beaumont and Lake Charles is likely. The transported air pollutants can combine with those emitted locally to exacerbate local ozone levels.

Many episodes are 2 to 5 days in length, suggesting very consistent weather patterns from day to day and the potential for buildup of pollutant concentrations, at the surface and aloft, over several days. Conditions like this can lead to increasing complexity and diversity of ozone patterns on each successive day of ozone episodes. Analyzing and accurately simulating the relevant physical and chemical processes for such episodes requires the application of advanced techniques of analysis and air quality modeling.

Current information on air pollutant emissions from both onshore and offshore sources in the region is highly uncertain. Different sources of information for the two ozone precursor species, nitrogen oxides (NO_x) and reactive organic gases (ROG), differ by factors of 2 or more. The impacts of OCS emissions on onshore ozone and the development of effective ozone control strategies are critically sensitive to the NO_x and ROG emission levels and their ratio, ROG/NO_x.

1.2 GOALS AND OBJECTIVES OF THE STUDY

The overall goal of this study was to quantitatively determine through modeling (meteorological and photochemical) the effects of current and future OCS development in the Gulf of Mexico on ozone nonattainment areas in Texas and Louisiana. The meteorological modeling employed the SAI Mesoscale Model (SAIMM), a data-assimilating prognostic meteorological model, and a variable-grid version of the Urban Airshed Model, referred to as UAM-V, for the photochemical model.

The GMAQS had six specific objectives, which addressed both near-term and longer-term requirements. The study had two short-term objectives:

- Analyses of historical data, supplemented by recent meteorological measurements, that describe the conditions and likelihood of OCSPD emissions reaching coastal areas under conditions conducive to ozone formation.

- Preliminary meteorological and photochemical modeling of historical episodes of high onshore ozone concentrations to estimate OCSPD contributions to onshore ozone for those episodes.

The study had four longer-term objectives:

- Collection of extensive meteorological and air quality data during the summer ozone season.

- Extension, refinement, evaluation, and application of meteorological and photochemical modeling techniques using the data collected during the field study.

- Evaluation of the sources of uncertainty in estimates of impacts.

- Recommendation of future monitoring and modeling efforts that can address these uncertainties.

1.3 PROJECT ELEMENTS AND CHRONOLOGY

The project was divided into nine major tasks conducted in the following sequence:

1. Identification of representative historical ozone episodes.

2. Development of emissions inventories for those historical episodes (including OCS and onshore emissions, and growth/control in calendar years of interest).

3. Preliminary meteorological and photochemical modeling of selected historical episodes.

4. Design and conduct of a field study to collect appropriate meteorological and air quality data during the summer of 1993.

5. Development of emission inventories for any 1993 ozone episodes and projection of future-year emission inventories.

6. Data analysis using both historical and 1993 data.

7. Meteorological and photochemical modeling of ozone episodes selected from the 1993 field study, and assessment of the ozone impacts of alternative OCS future development scenarios on the onshore ozone nonattainment areas.

8. Characterization of the uncertainty in the model estimations.

9. Evaluation of the needs for future research or data collection efforts to improve understanding of the OCS effects on ambient ozone onshore.

The principal elements of the GMAQS were the field study, data analyses, emissions inventory development, meteorological modeling, and photochemical modeling. An overview of each of these elements is provided below.

OVERVIEW OF THE FIELD STUDY (APRIL–OCTOBER 1993)

Three offshore platforms and five onshore sites were selected for the installation of supplemental air quality and meteorological measurement systems for the study. These sites are shown in Figure 1-2. The equipment was installed and began operating by mid-April 1993. These sites include the following:

- Texaco High Island 199A—offshore, hourly upper-air and surface meteorological measurements employing Radar Profiler/Radio Acoustic Sounding Systems (RASS) and surface meteorological instruments for six months.

- ARCO Ship Shoal 178—offshore, hourly upper-air and surface meteorological measurements employing Radar Profiler/RASS and surface meteorological instruments for six months.

- Chevron Garden Banks 236—offshore, upper-air soundings, two or three times per day during the six-week summer intensive period.

- Gilchrist, Texas—onshore, hourly surface air quality (NO, NO_x, ozone) and meteorological measurements for a six-month period and grab samples for volatile organic compound (VOC) and carbonyl analyses during intensive measurement periods.

- LUMCON (Cocodrie, Louisiana)—onshore, hourly surface air quality (NO, NO_x, ozone) measurements for a six-month period and grab samples for VOC and carbonyl analyses during intensives; continuous upper-air and surface meteorological measurements employing Radar Profiler/RASS and surface meteorological instruments for six months.

- Southeast Houston (Hobby Airport)—onshore, hourly upper-air and surface meteorological measurements employing Radar Profiler/RASS and surface meteorological instruments for six months.

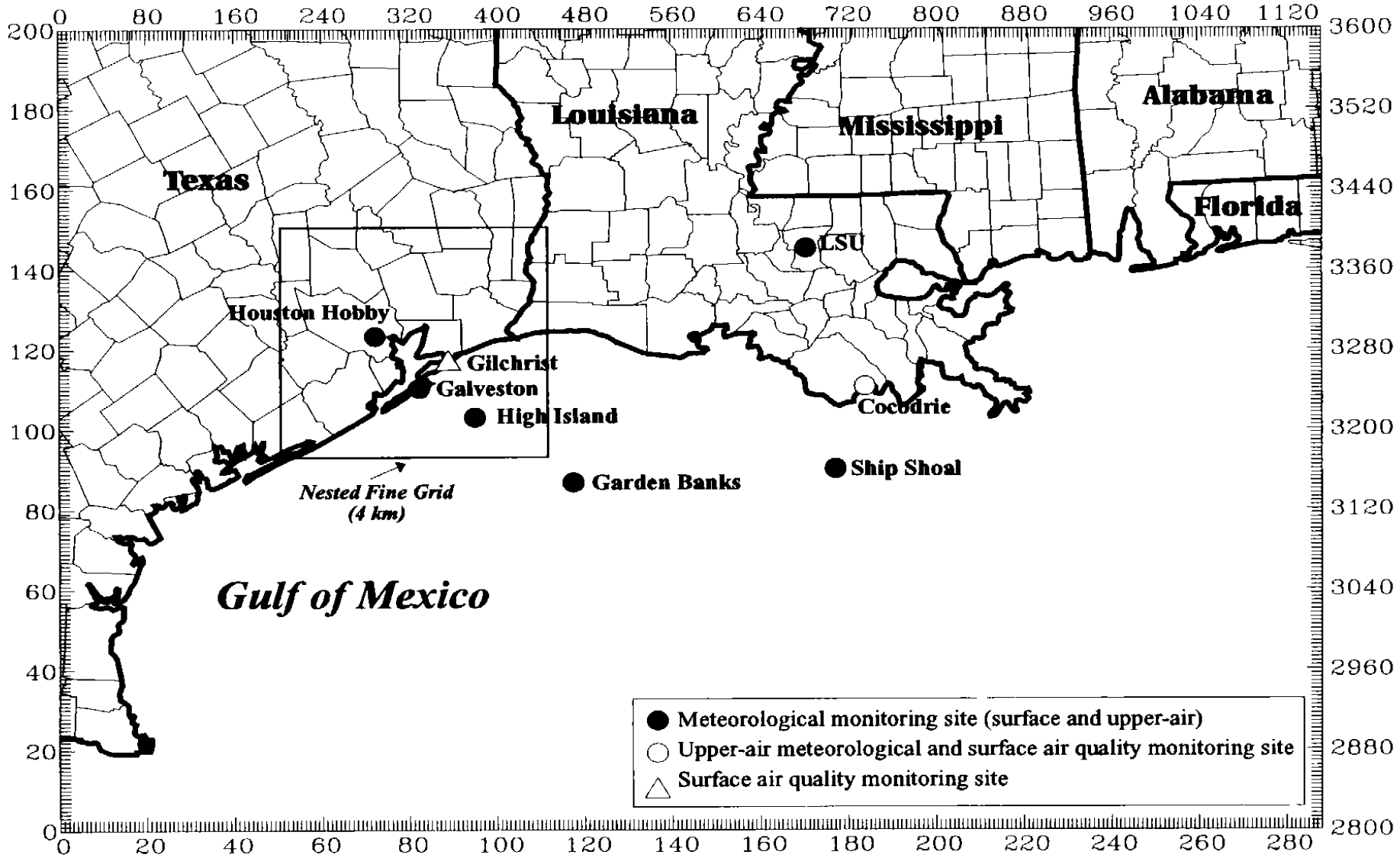

Figure 1-2. Locations of supplemental meteorological and air quality measurement systems for the 1993 MMS GMAQS field program including location of the UAM-V 4-km nested fine grid for Houston.

- Galveston, Texas—onshore, hourly upper-air and surface meteorological measurements employing Radar Profiler/RASS and surface meteorological instruments for six months.

- Louisiana State University (near Baton Rouge)—onshore, hourly upper-air and surface meteorological measurements employing Radar Profiler/RASS and surface meteorological instruments for six months.

The intensive measurement portion of the field study ran from 18 July to 28 August 1993. During this time, two highly instrumented twin-engine aircraft were on alert in Beaumont to fly when conditions were favorable for ozone exceedances. In addition, the National Weather Service (NWS) provided one additional upper-air meteorological measurement daily as needed from Slidell and Lake Charles, Louisiana. During this intensive period, a conference call was held each afternoon to decide whether meteorological conditions looked conducive to ozone exceedances for the next 24- to 48-hour period and to determine a go/no-go decision regarding conducting an intensive operating period the next day. Weather forecast and air quality data were transmitted daily to key personnel, allowing a decision to be reached by each member and discussed during the conference call. If a go decision was reached, aircraft were deployed at 6:00 a.m. the following day on predetermined flight paths, the NWS launched an additional upper-air sounding, an additional upper-air sounding was taken at the Garden Banks platform, and field personnel gathered VOC and carbonyl samples from the Gulf Coast area. Additional conference calls were held on each flight day to discuss whether the afternoon flights should be conducted.

The 1993 GMAQS field study was uncommonly successful. Several high-ozone episodes were captured, including peak ozone concentrations at approximately the same level as air quality planning design values throughout the study area. High rates of data recovery were achieved, even in the challenging offshore operating environment. Ozone episode forecasts for intensive monitoring deployments were unusually successful; few high events were missed, few false alarms were forecast, and intensive monitoring resources were almost fully spent by the end of the intensive measurement period.

It should be noted that the Texas Natural Resource Conservation Commission (TNRCC) planned and fielded its own special monitoring study, the Coastal Oxidant Assessment for Southeast Texas (COAST) (Lawson et al., 1995), to run concurrently with and to supplement the GMAQS study. The COAST data collection efforts focused on the Houston and Beaumont areas. The COAST study included additional instrumented aircraft flights and an additional instrumented aircraft, extra surface-level air quality sites, extra surface VOC grab samples, and additional onshore upper-level meteorological measurements. The forecasting of intensive measurement periods and the deployment of the GMAQS and COAST monitoring resources were closely coordinated. In addition, the MMS and TNRCC agreed to freely share the data collected in the two studies. Much of the COAST data (all those released in time) were used in this study along with data collected during the 1993 GMAQS.

OVERVIEW OF DATA ANALYSES

Data analysis tasks included (1) analyses of data collected during historical ozone episodes and (2) analyses of data collected during the 1993 field study.

Historical Data Analyses

The focus of the historical data analyses was on the following four areas: selection of historical episodes for modeling; acquisition, processing, and analysis of the historical meteorological and air quality data; evaluation of the representativeness of the 1993 episodes; and the development of an episode forecasting methodology. In selecting historical ozone episodes for modeling, air quality and meteorological data for the period 1987–1991 were examined. Ozone exceedance days within the three regions (Houston/Beaumont/Port Arthur, Lake Charles, and Baton Rouge) were identified and the potential for onshore transport of OCS emissions assessed. The determination of onshore transport included examination of daily surface weather maps (and pressure gradients), hourly surface winds at selected locations, and upper-air winds at nearby NWS radiosonde sites as well as the calculation of surface-layer particle paths. Based on this analysis, six candidate historical modeling episodes were selected, including four primary episodes and two alternates. The 28–29 July 1988 period was chosen for further analysis and as the episode to be simulated with the meteorological and photochemical models.

A major focus of this task was the preparation of a comprehensive meteorological and air quality database for the historical modeling episodes. The data were used in the preparation of gridded wind and temperature fields for the calculation of biogenic emissions using the Biogenic Emission Inventory System (BEIS) (EPA, 1992b), and the preparation of inputs for the photochemical and meteorological models.

In addition, ozone and meteorological data for 1982–1992 were analyzed to determine whether the 1993 GMAQS episodes selected for analysis and modeling were representative of those occurring in the region in the past.

Additional analysis of the historical meteorological and air quality data provided information for the development and refinement of the forecasting plan. This included application of the Classification and Regression Tree (CART) software using air quality and meteorological data collected during July and August of 1988 to 1991. The objective was to identify those measured and predicted variables that are most useful in forecasting ozone events in the Houston and the Baton Rouge areas.

Analyses of the 1993 Field Data

The accuracy, precision, and validity of the historical and 1993 field measurements for modeling activities were evaluated. All suspicious values in the data set were evaluated, flagged, and reconciled.

Descriptions and displays of air quality and meteorological data (objective data analysis) were prepared and apparent relationships between parameters were identified. Summary statistics and visual displays were prepared to characterize the important features of the air quality and meteorological conditions in the Gulf Coast region. Analysis subtasks included the following:

- Description and display of continuous air quality data, synoptic meteorology, surface and upper-air meteorological data, three-dimensional air quality data, and speciated VOC and carbonyl data.
- Computation of the frequency of episodes to compare 1993 air quality and meteorology with past years.
- Comparison of air quality data measured at the surface and aloft.
- Characterization of land and sea breezes.
- Identification and quantification of relationships between air quality and meteorological processes.
- Estimation of the depth of the mixed layer, as a function of space and time, and characterization and evaluation of the importance of mixing of pollutants from aloft into the mixed layer.
- Description, display, and evaluation of wind flow patterns and trajectories for important source and receptor areas.
- Estimation of pollutant fluxes at the shoreline from offshore sources.
- Description and display of meteorological and air quality conditions during each intensive monitoring period.
- Description of the important atmospheric processes that influence the formation and transport of ozone and ozone precursors that may be the result of emissions from OCS sources.
- Reconciliation of modeled air quality and meteorological parameters with measured values.

OVERVIEW OF EMISSIONS INVENTORY DEVELOPMENT

Gridded, hourly emission inventories were prepared for the entire study area, for both historical and 1993 ozone episodes, and for future-year emissions scenarios. These inventories cover an area of nearly one million square kilometers, encompassing the western and central portions of the Gulf of Mexico and onshore ozone nonattainment areas (Houston, Beaumont, Lake Charles, and Baton Rouge).

Air pollutants inventoried include NO, NO_2, speciated VOC, and CO. These inventories were converted to formats suitable for input to the photochemical model using the Emissions Preprocessing System (EPS 2.0) (EPA, 1992d). Quality assurance guidelines and procedures were developed, applied, and documented throughout the emissions inventory process to assure traceable emissions processing with minimal errors.

The emission inventories prepared included both onshore and offshore emissions and OCSPD-related emissions. Relevant emissions from anthropogenic and natural (i.e., biogenic) sources were considered, with special attention focused on offshore anthropogenic sources. The following sources were addressed in this effort:

Offshore anthropogenic sources:

- Oil and gas production facilities in the OCS and state waters
- Crew and supply boats/helicopters serving OCS facilities
- Recreational and commercial shipping
- Pipeline vessels
- Exploratory vessels
- Military vessels
- Intercoastal barges
- The Louisiana Offshore Oil Port (LOOP)

Onshore anthropogenic sources (EPA's 1990 Interim State Implementation Plan (SIP) data, LDEQ data, and TNRCC data):

- Point sources
- Area sources
- Nonroad mobile sources
- Mobile sources

Natural sources:

- Biogenic sources

A special survey was conducted to inventory offshore emissions sources. In conjunction with MMS, three survey forms were designed to solicit the information needed to estimate emissions from OCS production platforms, crew/supply boats and crew/supply helicopters. The survey responses for crew and supply boats and helicopters were entered by MMS into database files and later translated to spreadsheets to calculate emissions. The survey responses for production platforms were entered by MMS into database files for input to the OCS Platform Inventory System (OPIS). The OPIS was designed for this study to estimate platform emissions by accessing the MMS database, assigning quality assurance tracking codes, making quality control checks and data corrections, calculating emissions, and preparing the emissions data files in the format required by EPS 2.0. The emission calculations performed by the OPIS reflect recent updates to the methodology given in the EPA's *Compilation of Air Pollutant Emission Factors* (AP-42, Supplement E).

Fugitive emissions were estimated outside of OPIS using a FORTRAN program. These estimates were based on a recent MMS Pacific OCS Study (DOI, 1992) and not data from the American Petroleum Institute, as was originally intended. Based on the MMS Pacific Study, a methodology for estimating platform fugitive emissions was developed.

Emission methodologies were developed for several other OCS sources, including pipeline and military vessels and helicopters. The helicopter data used for emissions estimations were obtained from the survey, the military vessel data from the Navy, and the pipeline vessel data from MMS. Actual facility locations were used for point source locations. Where required to spatially distribute the OCS area emissions, special surrogates for OCS region were set up by lease block area, platform-weighted area by lease block, and state waters. Commercial shipping emissions were allocated uniformly along existing shipping lanes.

In order to process the data through EPS 2.0, four subregions were defined and gridded. The entire region inventory was gridded into 4-km grids. The 1990 base-year EPA Interim Inventory was used for the onshore domain and was interfaced with the LDEQ and the TNRCC 1990 inventory data. Estimates for motor vehicles were generated using the EPA 1990 Vehicle Miles Traveled data.

Future-year projections were built up from the base-year inventories using a variety of projection factors (population, economic, transportation, industry-specific, etc.) supplied by Louisiana, Texas, MMS, and the EPA.

OVERVIEW OF METEOROLOGICAL MODELING

Meteorological fields for application of the UAM-V photochemical model to the GMAQS modeling domain were prepared using the SAI Mesoscale Model (SAIMM). The SAIMM is a prognostic meteorological model that simulates the response of the atmosphere to differential surface heating and terrain irregularities. For this application, the model was exercised using a one-way nested-grid approach with 16-km horizontal resolution for the coarse grid or outer domain and 4-km resolution for the inner domain. Routine and supplementary meteorological data collected during the GMAQS and COAST field programs were incorporated into the SAIMM simulations using four-dimensional data assimilation (FDDA).

OVERVIEW OF PHOTOCHEMICAL MODELING

An advanced photochemical air quality model, the variable-grid version of the Urban Airshed Model (UAM-V), was applied for the GMAQS domain to provide simulations of the chemical and physical mechanisms affecting observed ozone concentrations within the study domain. The UAM-V is a three-dimensional photochemical grid model that numerically simulates the emissions, transport, dispersion, chemical reaction, and deposition mechanisms that affect ozone production in the lower atmosphere. Three multiday ozone episodes were simulated including 27-28 July 1988 and the 17-20 August and 6-11 September 1993 periods, in connection with which supplemental air

quality and meteorological data were collected during the summer of 1993. The nested-grid feature of the UAM-V was employed: the modeling domain structure consisted of an outer coarse grid (with 8-km resolution) covering the large domain and an inner nested grid (4-km resolution) encompassing the Houston, Beaumont, and Port Arthur areas (Figure 1-2). For this application, seven fixed vertical layers with varying thickness were used.

Available meteorological, air quality, and anthropogenic and biogenic emission data for each of the episodes were used to develop the required inputs to the model. The model's performance for these episodes was evaluated using available air quality measurements, and numerous diagnostic and sensitivity tests were carried out to examine the model's responses to uncertainties in inputs to assess whether the model was able to perform reasonably well in replicating, in time and space, the observed ozone concentration patterns. Once the performance of the model was deemed acceptable in replicating the complex chemical and physical processes observed during each of the episodes, the base-case meteorological inputs were fixed and the model was used as a forecasting tool to provide likely future ozone concentration estimates for a number of future-year (1999) onshore and OCSPD emission scenarios to assess the simulated impacts of OCSPD sources on the onshore nonattainment areas.

1.4 THE GMAQS PARTICIPANTS

A team was assembled to carry out the study. The project team members and their particular areas of responsibility are listed below.

Systems Applications International (SAI)	Overall project management; emission inventory development; meteorological and photochemical modeling; data archiving, quality assurance, and data analyses; and recommendations for future efforts
Sonoma Technology, Inc. (STI)	Field program design, field management, air quality aircraft measurements, surface meteorological measurements at radar profiler sites, upper-air meteorological data collection and processing, field program data analyses, and recommendations for future efforts
Alpine Geophysics (AG)	Assistance in photochemical modeling
AeroVironment (AV)	Field auditing and quality assurance of field monitoring program
Earth Tech/Sigma Research	Climatological/air quality analyses
Environmental Science and Engineering (ESE)	Surface air quality and meteorological measurements

Oregon Graduate Institute	Laboratory analysis of VOC species
Atmospheric Assessment Associates (AtmA)	Laboratory analysis of carbonyl species
Ed Roy, Limited	Meteorological forecasting assistance
A.T. Kearney	Compilation and preparation of 1992 emissions estimates for each of the principal offshore emissions sources not related to OCS petroleum development, for inclusion in the overall emissions inventory prepared by SAI
Radian Corporation	Manufacture, installation, and maintenance of radar profilers/RASS systems for continuous upper level wind and temperature measurements
Evans-Hamilton, Inc.	Offshore logistical support

The project team was directed by Mr. William Steorts of MMS—New Orleans. Since May 1995, Mr. Dirk Herkhof of MMS—Herndon, VA served as project director. Katherine Valltos was the MMS Contracting Officer.

2 OVERVIEW OF THE GMAQS FIELD STUDY

This section provides a general summary of the GMAQS field study—its objectives and technical approach, management and measurement components, participating organizations, intensive forecasting and decision-making process, monitoring sites, aircraft operations, quality assurance, and data management. Additional details are provided in various reports and data volumes, which are listed below, and in a Field Study Plan prepared in late 1992 (Roberts et al., 1992), although some specifics were changed before the measurements started.

The second part of this section summarizes the results of the field study.

2.1 DESCRIPTION OF THE FIELD STUDY

FIELD STUDY OBJECTIVES AND TECHNICAL APPROACH

The GMAQS includes a meteorological and air quality field measurement program that took place in the summer of 1993. The objectives of the field program were to provide data to be used

- as initial-condition and boundary-condition input for the application of the UAM-V for the 1993 episodes,
- to develop wind fields for the 1993 modeling,
- to evaluate the results of both the historical (pre-1993) and 1993 modeling,
- to assess the uncertainties of the model results,
- to characterize the meteorology and air quality of the offshore and coastal regions in the vicinity of the Louisiana and Texas nonattainment areas under meteorological conditions associated with high ozone concentrations and potential transport of offshore emissions to coastal areas and beyond,
- to fill in some known gaps in our understanding of pollutant transport and distribution in the coastal areas, and
- to develop recommendations for a subsequent field and modeling program to improve the predictive capabilities of the models.

The field program included the following components:

- Continuous routine upper-air meteorological measurements (six sites), surface meteorological measurements (seven sites), and continuous ozone and nitrogen oxides air quality measurements (two sites) for 6 months for the period 19 April–16 October 1993.

- Two upper-air meteorological soundings on an offshore platform every day for 6 weeks for the period 16 July–28 August, plus a third sounding on Intensive Operating Period (IOP) days. A third sounding was also performed at NWS stations in Lake Charles and Slidell, Louisiana on IOP days.

- Two-hour grab samples for ROG and carbonyl species at two shoreline sites on intensive days during the 6-week period.

- Air quality and meteorological data collected aloft using two instrumented aircraft.

Additional measurements were taken during a coordinated program sponsored by the Texas Natural Resource Conservation Commission (TNRCC), called the Coastal Oxidant Assessment for Southeast Texas (COAST) (Lawson et al., 1995). COAST included routine measurements of surface air quality and meteorology, routine measurements of upper-air meteorology, intensive measurements of ROG and carbonyl compounds, and additional aircraft measurements aloft.

In addition, air quality and meteorological data were obtained for the GMAQS study period from existing sources. The measurement program also included a forecasting and field management function, as well as data management and quality assurance efforts. Table 2-1 provides a schedule of major GMAQS field study events.

Table 2-1. Major GMAQS field study events.

Activity	Date (1993)
Begin routine monitoring	April 19
Perform audits of routine operations	April 26–May 24
Present problems from audits to field manager	by May 24
Begin informal IOP forecasting, 2 weeks (to develop criteria further)	mid-June
Begin forecasting for IOPs (for practice)	July 12
Review performance during practice period	July 16
Begin forecasting for IOPs	July 16
Start intensive field study	July 18
End intensive field study	August 28
End routine operations	October 16

The routine measurements were made to assess the representativeness of the intensive study days, to provide information on the meteorology and air quality conditions on the days leading up to the episodes, and to assess the meteorological regimes and transport patterns that lead to ozone episodes. The intensive study components and the continuous monitoring data were made to improve our understanding of the causes of pollutant episodes in the study region and to provide data for input to the models and for model evaluation.

FIELD STUDY MANAGEMENT, MEASUREMENT COMPONENTS, AND PARTICIPATING ORGANIZATIONS

Under subcontract to SAI, Sonoma Technology, Inc. (STI) managed the field study operations, coordinated the site-selection process, and was responsible for ensuring that the field measurements met the field objectives. STI also led the development of the forecasting protocol and the daily decision process to select IOP days (see Roberts and Dye, 1993).

GMAQS measurement components are listed below, along with the organizations responsible, their responsibilities, and references to their reports and data volumes.

Surface air quality and meteorological measurements at two shoreline sites, Gilchrist, Texas and Cocodrie, Louisiana: Environmental Science and Engineering (ESE) provided ozone and NO/NO_x monitoring equipment, surface meteorological monitoring equipment for wind speed, wind direction, temperature, humidity, and data acquisition equipment; set up and operated monitoring sites; on IOP days, collected grab samples for later laboratory analysis for ROG and carbonyl compounds; validated data; and delivered data to the GMAQS data manager. ESE also collected integrated traffic counts along Texas Highway 87.

ROG analysis of samples collected at surface sites and from aircraft: Oregon Graduate Institute provided ROG sampling equipment for both surface and aircraft operations, performed laboratory analyses of collected samples, validated data, and delivered data to the GMAQS data manager.

Carbonyl compound analysis of samples collected at surface sites and from aircraft: Atmospheric Assessment Associates (AtmAA, Inc., 1993) provided carbonyl compound sampling equipment for both surface and aircraft operations, performed laboratory analyses of collected samples, validated data, and delivered data to the GMAQS data manager.

Upper-air and surface meteorological measurements: STI (Dye et al., 1994; Schoell et al., 1994a, 1994b) managed the radar profiler and rawinsonde upper-air meteorological measurements and associated surface meteorological measurements; coordinated site selection, logistical support, and operations; performed daily review of the data and data processing; and delivered the data to the GMAQS and COAST data managers. STI also performed the offshore rawinsonde operations from the Garden Banks Platform. Radian Corporation was responsible for operation of the radar profilers; STI checked the data

daily and processed the data. Evans-Hamilton, Inc., provided logistical support for the offshore operations of both radar profilers and rawinsondes. Note that Radian also installed and operated the radar profiler at Jefferson County Airport for COAST; STI also reviewed these data on a daily basis, processed the data, and delivered the data to the GMAQS and COAST data managers. At the radar profiler sites, wind speed, wind direction, and virtual temperature were measured every hour as a function of altitude, and surface wind speed, wind direction, temperature, humidity, and rain were measured every hour. At the rawinsonde site, wind speed, wind direction, temperature, and humidity were measured as a function of altitude twice each day during 18 July–28 August, with a third sounding on IOP days.

Aircraft: STI (Anderson and Roberts, 1994b; Anderson et al., 1994) prepared the two aircraft for field sampling, performed the aircraft sampling flights on intensive days, processed and validated the data, and delivered the data to the GMAQS and COAST data managers. One of these two aircraft was shared with COAST; in addition, STI operated a third aircraft for COAST. All three aircraft were twin-engine aircraft; one was a Piper Aztec, the other two were Cessna 340s. All three aircraft measured ozone, NO, NO_x, temperature, and location every second and collected grab samples for later laboratory analyses for ROG and carbonyl compounds; one of the aircraft also measured humidity, solar radiation, and turbulence.

Quality Assurance: AeroVironment (AeroVironment Inc., 1994) prepared an audit plan, performed systems and performance audits, recommended solutions to problems, documented the audit results, and estimated accuracy and precision of each measurement system. In addition, intercomparison samples for later laboratory analysis for ROG and carbonyl compounds were collected at the Clinton Drive site during the COAST intercomparison (18 August 1993).

Data Management: Systems Applications International (SAI, 1994) prepared a data management plan, collected GMAQS and COAST data and combined them into a common format, collected supplemental data from other sources, and distributed the data to the modeling and data analysis contractors and to the COAST data manager (Desert Research Institute).

FORECASTING CRITERIA AND DECISION-MAKING PROCESS

A forecasting and decision-making protocol was developed and used to determine when high ozone concentrations were likely to occur and to decide whether or not to conduct or continue an Intensive Observation Period (IOP) (see Roberts and Dye, 1993). The daily decision process was a joint one between the GMAQS and COAST studies.

Intensive sampling for the GMAQS was conducted on 13 days during the 6-week intensive period 18 July–28 August 1993. Intensive observation periods were conducted in the Texas area, the Louisiana area, or both areas on selected days when onshore ozone concentrations were forecasted to exceed the NAAQS for ozone ($\geq$125 ppb) and when conditions were favorable for potential OCSPD emission contribution.

To develop the decision-making protocol, Roberts and Dye (1993) reviewed historical data and discussed the characteristics of high ozone episodes with researchers familiar with Gulf Coast meteorology and air quality. They analyzed the characteristics of historical high ozone episodes by reviewing 9 years of air quality and meteorological data for the Houston and Baton Rouge regions. These analyses examined the average number of exceedances per week and per day, the average length (in days) of the episodes, whether or not Baton Rouge exceedances coincided with Houston exceedances, the typical number of exceedances to expect during the July and August field study, and the frequency of exceedances as a function of wind direction.

Based on this analysis, Roberts and Dye (1993) developed a conceptual model of the conditions that produce high ozone in the Baton Rouge and Houston regions. In addition, they described several meteorological scenarios associated with potential OCSPD emission contributions to onshore ozone exceedances.

The "go/no-go" decision to start or continue an IOP was made each afternoon for the following day, and a preliminary decision was made for the day after so that aircraft and instrument operators had sufficient time to prepare for sampling. The decision to call a go/no-go for an IOP depended on four major criteria:

- Current and forecasted meteorological conditions
- Current and forecasted air quality conditions
- Potential for OCSPD emission contribution to high ozone concentrations onshore
- Performance in each region to date

In addition, the decision depended on the ongoing coordination of joint resources between the GMAQS and the COAST programs.

Several organizations participated in the forecasting and decision-making process. Ed Roy, Ltd. provided meteorological forecasts for the Gulf Coast region and air quality forecasts for the Baton Rouge area. This information was sent to STI, SAI, and the MMS COTR (Contract Officer's Technical Representative) via fax each afternoon. The field contractors provided the operational status of their equipment to the STI field manager on a daily basis. The LDEQ, the TNRCC, and Environmental Science and Engineering (ESE) provided the previous and the current day's maximum ozone concentrations for the sites that they operated. Before and during a conference call each afternoon at 3:00 p.m. CDT, the participants used this information to decide whether or not an IOP was to be conducted the next day.

The GMAQS was originally planned as a stand-alone study. However, during late 1992 and early 1993, as plans for the COAST were being developed, several participants of both studies (especially TNRCC and STI representatives) helped coordinate plans for both studies. Coordination between the two studies resulted in a joint forecasting and decision-making conference call for both the GMAQS and the COAST programs every afternoon at 3:00 p.m. CDT. The conference call included representatives from the sponsors of both studies (MMS and TNRCC), SAI, STI, DRI, and Ed Roy, Ltd., plus participation by others as needed. During the conference call each afternoon, the discussion led to a decision on whether or not to perform intensive sampling. This

decision was communicated directly to GMAQS field personnel and posted on a message machine that was available to all GMAQS participants. If intensive sampling was being performed on a particular day, another conference call was held at 11:00 a.m. CDT on that day to decide if sampling was to continue during that afternoon.

GMAQS MONITORING SITES

Table 2-2 provides a list of GMAQS sites, including location and the general measurements performed at each site. The radar profilers measured upper-air wind speed and direction, and virtual temperature as a function of altitude. The rawinsonde system measured upper-air wind speed and direction, temperature, and relative humidity as a function of altitude. The surface meteorological systems measured wind speed and direction, temperature, relative humidity, solar radiation, and rainfall. The surface air quality systems measured ozone, NO, and NO_x, and collected grab samples for later laboratory analyses for ROG and carbonyl compounds.

Table 2-2. Summary of GMAQS sites, locations, sampling equipment, and site operator.

Site Name	Lat/Long	UTM_N	UTM_W	Radar Profiler	Rawin-sonde	Surface Meteor-ology	Surface Air Quality
Southeast Houston	29.64/95.29	3281.8	277.9	×		×	
Galveston	29.23/94.92	3235.0	312.7	×		×	
High Island 199	29.15/94.19	3225.4	383.7	×		×	
Gilchrist	29.52/94.46	3266.6	358.5			×	×
Garden Banks 236A	27.76/93.14	3070.4	486.1		×		
LSU	30.36/91.17	3359.9	675.1	×		×	
Cocodrie	29.25/90.65	3238.2	728.0	×		×	×
Ship Shoal 178A	28.59/91.20	3164.7	675.4	×		×	

GMAQS AIRCRAFT OPERATIONS

Each flight consisted of a series of sequential events including spirals, traverses, dolphins, and ferry operations. Spirals were flown to document the vertical structure of the atmosphere. A spiral (or vertical profile) consisted of sampling while the aircraft ascended or descended over a fixed surface location. Traverses were flown to document spatial distributions of pollutants. A traverse consisted of sampling at a constant altitude (typically less than about 600 m msl) as the aircraft moved in a straight line from one sampling location to another. Sampling as the aircraft varied its altitude (up and down repeatedly) while moving in a straight line from one location to another was called a dolphin. Thus, both vertical and horizontal information was collected during dolphins. Normally, the maximum altitude sampled was about 600 m msl. There were always some segments of a flight during which the aircraft was positioning itself (to start a

spiral, traverse, or dolphin), in a holding pattern at the FAA's request, or enroute to another sampling location; these events were called ferry operations. Data were collected and reported for all sampling events.

Typical sampling flight paths are shown in Figures 2-1, 2-2, 2-3, and 2-4. Sampling flights for the GMAQS were performed in either the Texas or Louisiana coastal regions. Morning flights typically started about 0545-0615 CDT; afternoon flights started about 1200 CDT. Morning flights were performed to document air quality conditions aloft before daytime chemical and meteorological processes begin to occur. Afternoon flights were performed to document air quality conditions aloft during periods of peak ozone concentration and to quantify pollutant fluxes near the coast.

An example of a typical morning sampling route flown in the Texas area is shown in Figure 2-1. The flight pattern began with an upward spiral at the Beaumont Airport (BMT). The flight continued with spirals at Sabine (SAB) and Gilchrist (GIL) with ferry segments between locations. After the Gilchrist spiral, the aircraft climbed enroute (a modified dolphin) to High Island Platform 199 (HIP) and spiraled at the platform. A dolphin (climb) to a location (halfway between the platform and Galveston Airport) called Overwater 1 (OW1) was followed by a spiral at this location. The flight continued with a dolphin (climb) to, and spiral at, the Galveston Airport (GLS). The remainder of the flight consisted of spirals at the Houston Gulf (SPX), Chambers County (TOO), and Beaumont municipal airports with ferry segments between.

An example of a typical afternoon sampling route for the Texas area is shown in Figure 2-2. The takeoff spiral at Beaumont was followed by ferry to, and spiral at, Gilchrist. A dolphin (climb to spiral altitude) to the platform, a spiral at the platform, a dolphin (climb to spiral altitude) to the Galveston Airport, and a spiral at Galveston followed. The ferry to Matagorda Peninsula (MAT) was followed by a spiral at that location. The dolphin leg from Matagorda to Sabine was flown between about 60 and 600 m minimum and maximum altitudes. After a Sabine spiral, ferry to Kountze/Silsbee Airport (45R), spiral at Silsbee, and ferry to Beaumont, the aircraft ended its sampling with a spiral into the airport.

A typical morning flight in the Louisiana area followed the route indicated in Figure 2-3. After takeoff the aircraft flew a dolphin pattern first to North Point (NPT) and then to Ship Shoal Platform 178A (SSP). After a spiral at the platform, the aircraft flew a dolphin pattern to, and spiral at, Cocodrie (COC), Houma-Terrebonne (HUM), and a private airport called Cane (CAN). A traverse from Cane to the Baton Rouge VOR (BRV) was followed by a traverse to Zachary (ZAC). After ferry to Baton Rouge Airport (BTR), a spiral to landing was performed.

A typical afternoon flight in the Louisiana area is shown in Figure 2-4. A spiral at Baton Rouge Airport, ferry to Zachary, traverse to the VOR and then to Cane was followed by a spiral at Cane. The flight continued with a dolphin to, and spiral at, Cocodrie; a dolphin to, and spiral at, the platform; and a dolphin to the Leeville VOR (LEV). At Leeville, the aircraft turned westward and flew a dolphin pattern back to Beaumont.

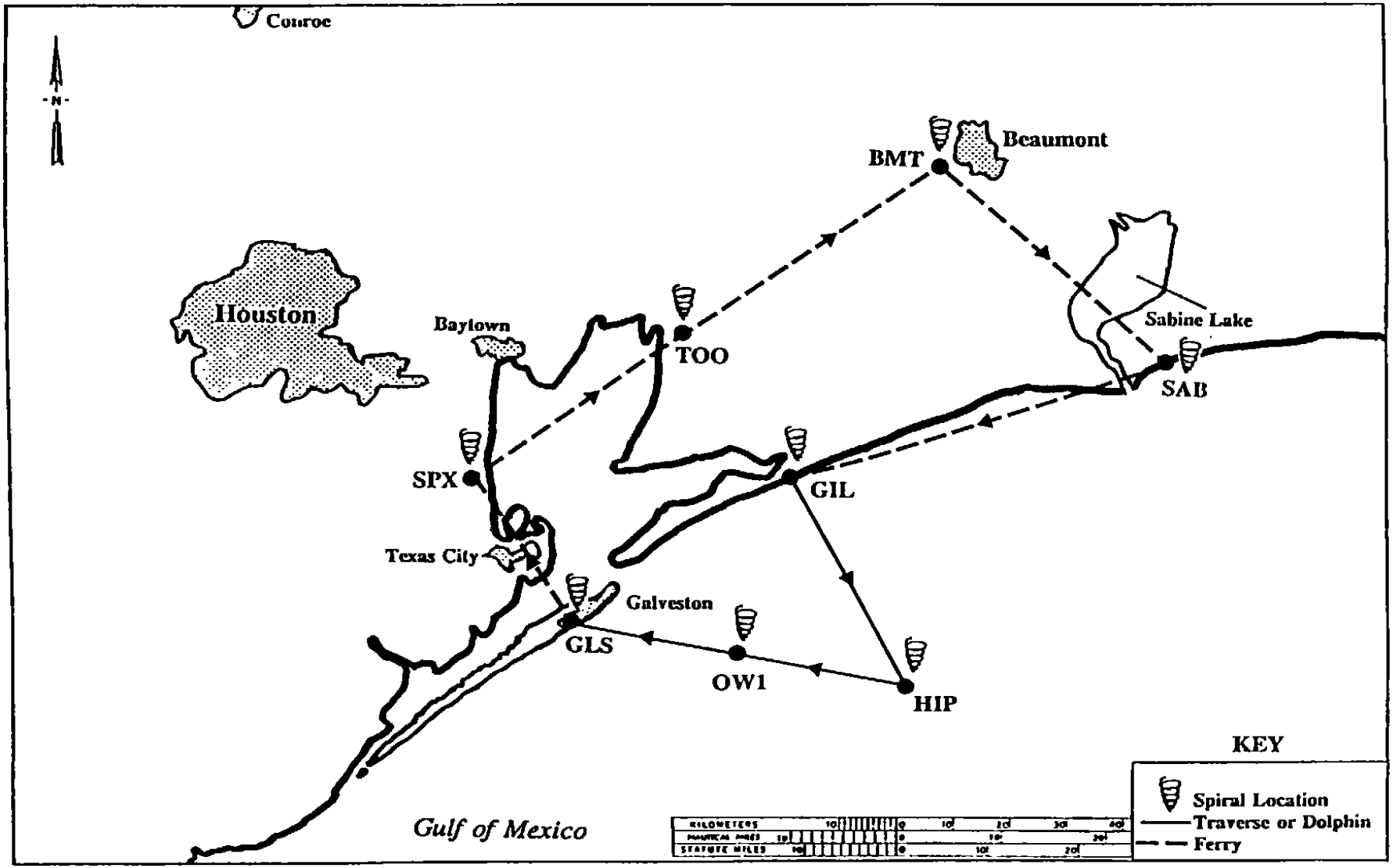

Figure 2-1. Example of a typical morning flight performed in the Texas sampling area during the 1993 MMS Gulf of Mexico Air Quality Study.

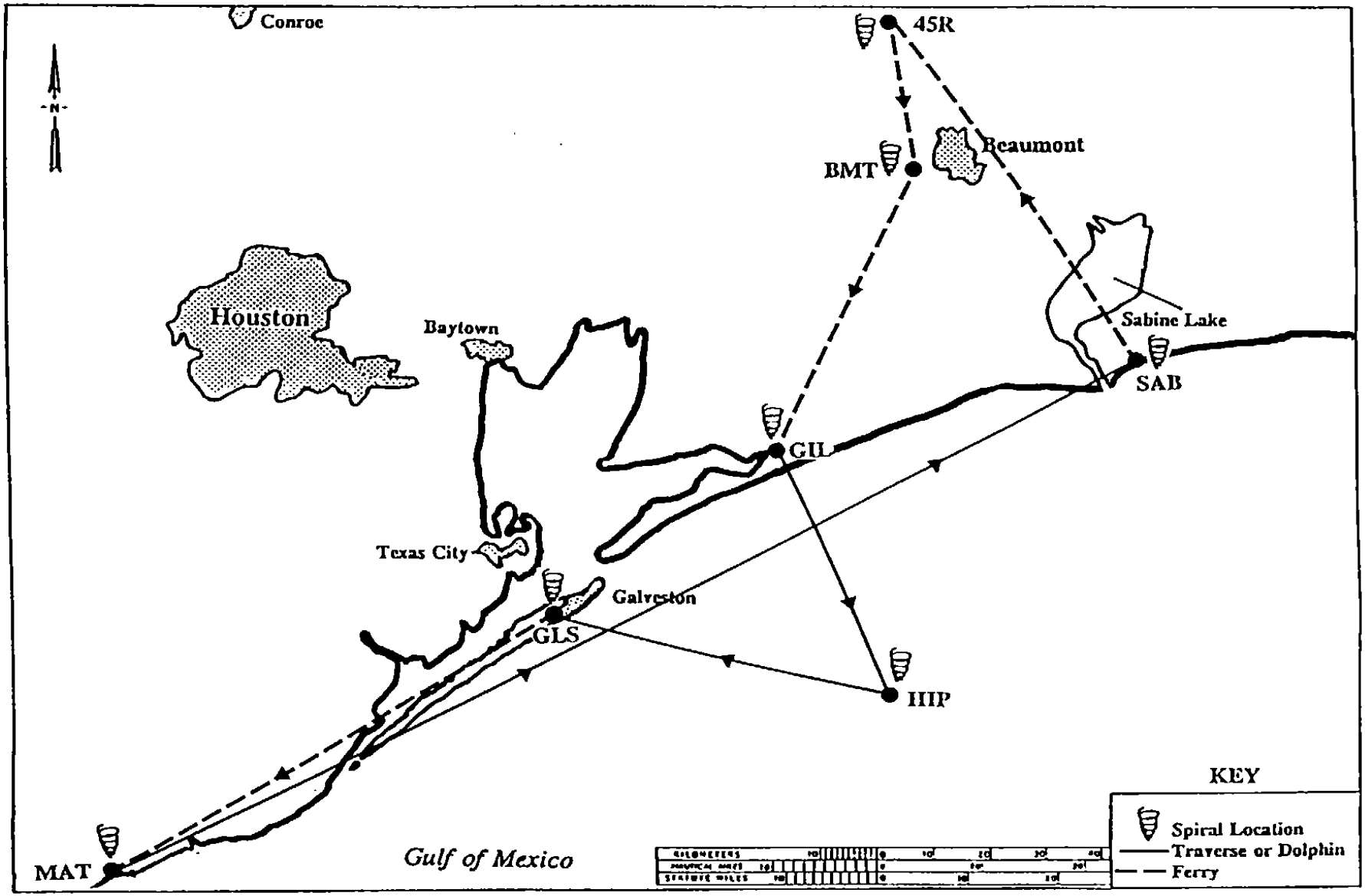

Figure 2-2. Example of a typical afternoon flight performed in the Texas sampling area during the 1993 MMS Gulf of Mexico Air Quality Study.

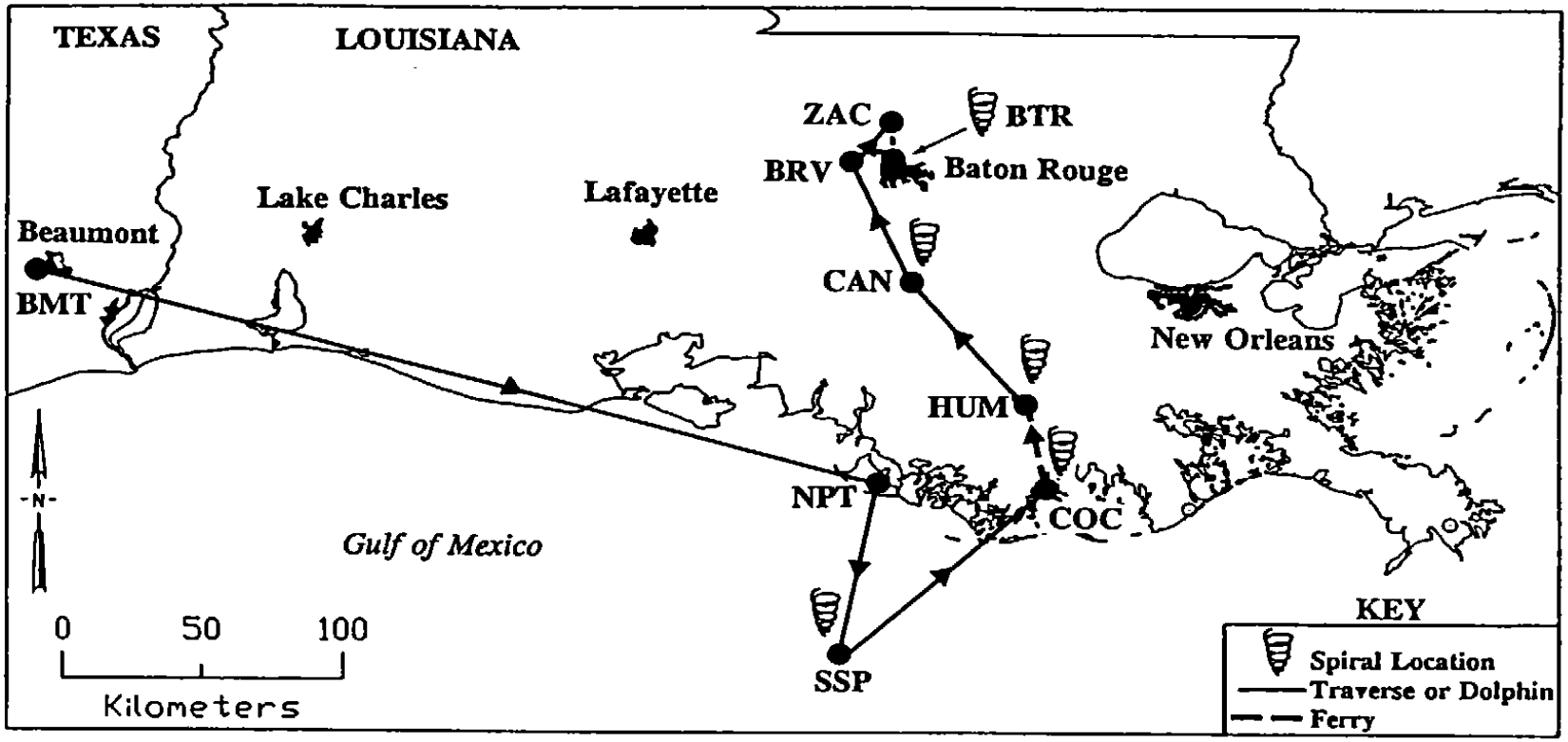

Figure 2-3. Example of a typical morning flight performed in the Louisiana sampling area during the 1993 MMS Gulf of Mexico Air Quality Study.

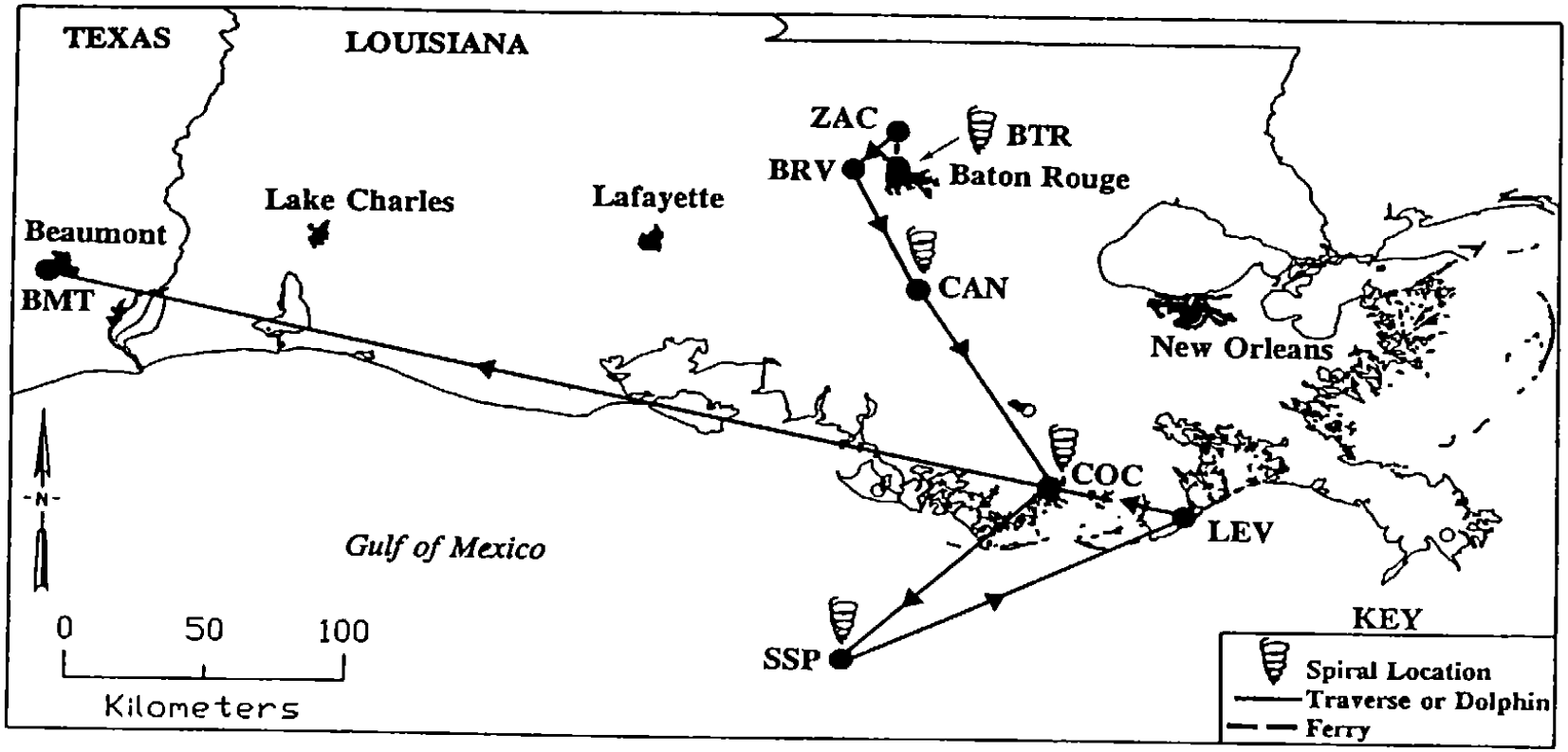

Figure 2-4. Example of a typical afternoon flight performed in the Louisiana sampling area during the 1993 MMS Gulf of Mexico Air Quality Study.

Some minor modifications were made to these typical routes during sampling on several days, due to modified sampling objectives, weather, or FAA requests (see individual sampling summary tables and flight route maps in the data volume, Anderson et al., 1994). In addition, inland sampling in Texas (sponsored by the TNRCC) was frequently performed on the same days on which these typical routes were flown (see details in the COAST aircraft data volume, Anderson et al., 1993; and the COAST aircraft report, Anderson and Roberts, 1994a).

QUALITY ASSURANCE ACTIVITIES

Quality assurance (QA) activities were designed to ensure that the field measurements met specified accuracy and precision objectives. QA for the GMAQS was performed by AeroVironment, Inc. (AV). During the planning and organization phase of this study, the QA officer met with SAI and STI to develop data quality objectives addressing monitoring and data processing, with specific consideration of the manner in which data were to be used in analysis and modeling. The GMAQS monitoring program was designed to meet those objectives.

The QA activities are reported by AeroVironment Inc. (1994) and summarized below:

- Conducted site surveys of 44 existing surface air quality and meteorological monitoring sites, including sites operated by state and local agencies, contractors (for industrial organizations), and the National Weather Service.

- Reviewed standard operating procedures (SOPs) and other QA-related material for GMAQS field and laboratory measurements and data processing.

- Performed system and performance audits of GMAQS measurement systems. These GMAQS measurement systems included those listed in Table 2-2, plus the air quality aircraft operated for both the GMAQS and COAST.

- Participated in and reviewed the results of an interlaboratory comparison for analysis of hydrocarbons for the GMAQS and COAST (see Fujita et al., 1994a).

- Performed data processing audits of the contractors who processed the surface air quality, the surface and upper-air meteorological, and aircraft data. In addition, a data processing audit was also performed of the GMAQS data manager.

The purpose of the surveys of existing sites was to characterize the spatial representativeness of the air quality and meteorological data being collected and to make a best estimate of the quality of the data collected at each site. The results of the surveys were used to determine which data sets to include in the GMAQS database, and to prioritize network improvements. As a result of these surveys, new meteorological measurement systems were installed at several Texas sites by about July 15.

The reviews of SOPs and other QA-related materials included the following elements:

- Stated accuracies and precisions were compared with the requirements of the data analysis and of the models.

- Adequacy of the measurement methods in terms of the intended use of the data was assessed and potential problems for obtaining adequate results were determined.

- Plans for instrument calibrations were reviewed, with the emphasis on ensuring traceability to acceptable reference standards.

- Review of the SOPs ensured that they were complete and that they contained adequate provisions for quality control and data validation.

System and performance audits were conducted of the air quality and meteorological measurement systems at the surface sites and in the aircraft. The procedures and criteria for these audits were based on those set forth in 40 CFR 58, Appendix A and the EPA Quality Assurance Handbook for Air Pollution Systems (Volumes I, II, and IV) and AV's experience with aircraft measurements.

The audits of the rawinsonde operations on one offshore platform were conducted with an emphasis on reviewing operational procedures used by platform personnel, though some aspects of the system performance were checked concurrently.

The radar profilers were audited once. These system and performance audits were conducted in accordance with EPA-recommended guidelines. An AV Doppler Acoustic Sounder (DAS) Model 2000 was set up at each radar profiler site and collected wind speed and wind direction data at 30-m intervals up to 750 m simultaneously with the radar profiler.

System and performance audits of the Radio Acoustic Sounding Systems (RASS) were conducted concurrently with the audits of the radar profilers. The performance audit of the RASS was done by releasing two A.I.R. PTH free-flight airsondes and comparing the temperature soundings from these airsondes with the temperature profiles collected by the RASS during the same time frames.

Audits of all data processing operations were performed. These verified that the data validation procedures were being followed and that the results of data validation activities were documented properly in the databases. They also checked the accuracy and traceability of all data processing and dissemination, and included hand calculations of values starting with data from the original data sources.

Within 24 hours of each audit the STI project manager and the manager of the monitoring components were informed of problems noted during the audit so that, if necessary, immediate action to correct the problems could be taken. A written report summarizing the audit results was submitted to the SAI and STI project managers within 2 weeks of the audits (AeroVironment Inc., 1994).

The audit equipment and standards were maintained by AV's QA Department and certified in AV's standards laboratory by a qualified technician. Certification protocols were in accordance with applicable EPA guidelines.

All audit results are included in a summary report (AeroVironment, 1994). In general, performance audits demonstrated that all measurements met the specified accuracy and precision objectives; systems audits demonstrated that SOPs were being followed.

DATA ARCHIVAL AND MANAGEMENT ACTIVITIES

Before the data from the GMAQS field program began to arrive, SAI developed a data archival protocol to address issues relating to archiving and managing data collected during the 1993 field program (SAI, 1993). The protocol defined procedures for transmittal of data collected during the field program to the location of a centralized data archive (SAI), the procedures for identifying and recording the data archived, the archival process, and the necessary tasks in support of the archive. The primary goal of this protocol was to maintain the integrity of the data collected during the field program.

Data collected during the GMAQS field program include surface air quality and meteorological data, upper-air meteorological data, air quality measurements taken aloft from aircraft, and hydrocarbon samples collected during the study by ESE and STI. The data collected and methodology used are summarized above. In addition to data from the GMAQS, the data archive files contain other data obtained to augment the data from the study. The other data include routine surface and upper-air measurements, buoy data, and C-MAN data from the National Climatic Data Center (NCDC); surface air quality and meteorological data from the TNRCC; surface air quality data from the LDEQ; surface air quality data for portions of Alabama, Mississippi, and Florida from the USEPA; surface air quality data from the Southeast Texas Regional Planning Commission (SETRPC); offshore meteorological data from the Texas-Louisiana Shelf Circulation Program (LATEX); and surface air quality and meteorological data from the COAST and HRM programs obtained from Desert Research Institute (DRI). This section presents a summary of the procedures followed in handling the data and the general content and structure of the archive.

Data collected as part of GMAQS, with the exception of logs, tables, and some documentation, were transmitted on magnetic media to SAI for archiving. Data obtained from other agencies were on magnetic media in most cases. However, some hard copy data were entered at SAI, and some data were obtained via the Internet.

A data log was maintained to track receipt and storage of the data transmitted for archiving ("raw data"), to track storage of working copies of data received, and to track and document system backups. A logbook was set up with specific forms to record these events. Each form contained a column titled "SAI ID" in which a unique identification number was assigned in sequence and affixed to the physical storage item (tape, floppy, or cassette). Regardless of the media used for transmittal of data to SAI, working copies of all files were made on a disk drive connected to one of SAI's

Multiflow computers and then copied to 8-mm Exabyte tape for long-term storage. Logs were also used to record processing of data, database file names, summaries of analyses performed, and other pertinent information. All data processing files and software development files utilized at SAI were stored on a disk drive connected to one of SAI's Multiflow computers. Multiple MMS project tape backups of this disk have been made during the course of this project. In addition, SAI system backups have been performed daily.

Each database file has been given a unique name. The file names are in the format 'typMMMYY.vsn' where:

typ	= type of data file format
	hr = hourly
	sd = sounding
MMM	= month (jan, feb,...)
YY	= year (93,94,...)
vsn	= version number (1.1, 1.2,...)

In addition to the surface and upper-air files, aircraft data and surface VOC samples collected during the study have been maintained in the format received from the monitoring contractor.

Separate database files have been maintained for each month of the field program. This design provides comparatively small files that allow portions of the database to be used on IBM-compatible PCs and on other systems with relatively limited disk space. The database files were the source for any data used in modeling, analysis, or distribution to third parties. Database files have been recorded on long-term storage media (8-mm cassette tape).

To allow for revisions and corrections to the data that have occasionally been necessary, the Revision Control System (RCS), which is available on many Unix-based systems including both our Multiflow and SGI systems, has been used to access the database files. RCS has been used to track changes to the database, to log comments regarding changes, and to limit access to the files when necessary. Using RCS prevents loss of data since any prior revision of the database can be retrieved from the RCS file. In addition, RCS automatically records the version and creation date of the database file internally in the file. Since a file retrieved from the RCS file is just a text file, it has been possible to develop simple Unix scripts for retrieval of portions of the data. The text file is also used as the export format for the databases because it is readily transportable to a variety of computer systems.

The data archive files are of several types. All hourly surface data are organized into a single file for each month of the study. Similarly, all upper-air meteorological data are organized into a single file for each month of the study. A site file provides the location and identifying information for each site. A parameter codes file and a unit codes file list the identifiers for the variables and the units in the data files. The aircraft data files contain measurements of NO_x, ozone, VOCs, and other species in addition to some meteorological parameters collected during flights in the Houston area, along the coast,

and in Louisiana. Summaries of the analyses of VOC samples collected during the GMAQS are in the form of text files produced from spreadsheets. The formats and content of these files have been documented in the GMAQS data archive report (SAI, 1994).

2.2 SUMMARY OF THE GMAQS FIELD STUDY RESULTS

GENERAL STATISTICS

Table 2-3 lists the resources expended during the intensive operating periods in both Texas and Louisiana. In general, about 80 to 90 percent of the budgeted resources were used; thus, if another ozone episode had been forecasted after the 18–21 August 1993 episode, resources would have been available.

Table 2-3. GMAQS resources expended during the 1993 field program operating periods.

Resource	Amount Expended (%)
Aircraft flights	89
Aircraft VOC and carbonyl compound samples	91
Surface VOC and carbonyl compound sample	
Gilchrist, Texas	83
Cocodrie, Louisiana	58
Third rawinsonde soundings on Garden Banks Platform	80
Third rawinsonde soundings at NWS sites	72

Table 2-4 provides a list of days on which intensive sampling was conducted in either Texas or Louisiana for the GMAQS and for COAST. Note that during many of the intensive sampling days, including the high ozone episodes on 31 July–1 August, 9–11 August, and 18–20 August, intensive sampling was being performed for both the COAST and GMAQS studies. This provides an enhanced data set for data analysis and modeling.

Tables 2-5, 2-6, and 2-7 provide data capture rates for the surface air quality and meteorological measurements, the VOC and carbonyl compound samples, and the upper-air meteorological measurements. Excellent data capture rates were achieved for all measurement components.

Table 2-4. Summary of the 1993 COAST and GMAQS field program intensive sampling days.[a]

Date	COAST Sampling Dates in Texas	GMAQS Sampling Dates in Texas	GMAQS Sampling Dates in Louisiana
28 July	●		
31 July	●	●	●
1 August	●	●	●
2 August			●
9 August	●	●[b]	
10 August		●	
11 August	●	●[c]	●
12 August	●	●	
13 August	●		
14 August	●		
15 August	●	●[b]	
16 August	●		
18 August	●		
19 August	●	●[d]	●
20 August	●	●	
24 August			●
25 August	●	●[e]	
26 August	●[b]		
28 August		●[f]	●[d]

[a] On GMAQS sampling days, the following were performed, unless otherwise noted: morning and afternoon aircraft flights, surface ROG and carbonyl compound samples collected, and a third upper-air meteorological sounding at Garden Banks. On COAST sampling days, the following were performed, unless otherwise noted: morning and afternoon aircraft flights, and surface ROG and carbonyl compound samples collected.

[b] Morning aircraft flight only.

[c] Afternoon aircraft flight only.

[d] Surface ROG and carbonyl compound samples only, no aircraft flights.

[e] No midday sounding at Garden Banks.

[f] No surface ROG or carbonyl compound samples.

Table 2-5. Data capture rate (percent of possible hours, excluding planned down time) for the 1993 GMAQS surface air quality and meteorological measurements.

Site Name	Data Capture Rate for Parameter (%)									
	WS	WD	T	P	RH	SR	Pcp	O_3	NO	NO_x
Cocodrie, LA	100	100	100	100	100	100	100	99	98	98
Louisiana State University, LA	100	100	100	100	84	100	100	—	—	—
Ship Shoal 178A Platform	100	100	84	100	100	100	100	—	—	—
Galveston, TX	100	100	100	100	100	100	100	—	—	—
Gilchrist, TX	84	84	99	—	—	—	—	98	97	97
High Island 199 Platform	100	100	100	100	100	100	100	—	—	—
Southeast Houston, TX	100	100	100	100	100	100	100	—	—	—

Table 2-6. Data capture rate for the 1993 GMAQS VOC and carbonyl compound samples.

Site	VOC Samples Collected	Carbonyl Compound Samples Collected
Gilchrist, TX	30 of 30 (100%)	29 of 30 (97%)[a]
Aircraft in Texas	221 of 230 (96%)[b]	222 of 234 (95%)[c]
Cocodrie, LA	23 of 23 (100%)	19 of 23 (83%)[d]
Aircraft in Louisiana	57 of 59 (97%)[e]	58 of 59 (98%)[f]

[a] 1 sample invalidated due to double exposure.
[b] 9 samples invalidated or missing.
[c] 12 samples invalidated for one of the following reasons: double exposure, cartridge/canister number matching problems, missing, or voided by laboratory.
[d] 4 samples not exposed.
[e] 2 samples missing.
[f] 1 sample with cartridge/canister number matching problem.

Table 2-7. Data capture rate for the 1993 GMAQS and COAST upper-air meteorological measurements.

Site Name	Data Capture Rate (% of possible hours)
Cocodrie, LA	99
Louisiana State University, LA	100
Ship Shoal 178A Platform	100
Galveston, TX	100
High Island 199 Platform	98
Jefferson County Airport, TX	96
Southeast Houston, TX	100
Garden Banks Platform	97[a]

[a] Rawinsonde sounding site; data capture rate calculation based on percentage of scheduled soundings completed.

OZONE EPISODES CAPTURED

Figures 2-5 and 2-6 provide information on the ozone episodes that occurred in Texas and Louisiana respectively during the intensive operating period, and indicate the days when intensive measurements were taken. Note that all three major ozone episodes in Texas were captured with intensive measurements by GMAQS, COAST, or both. It was more difficult to forecast ozone episodes in the Baton Rouge, Louisiana, area since the episodes occurred infrequently and were typically only one day in duration. However, some intensive measurements were collected on the only multiday ozone episode in Baton Rouge. Case studies of the major ozone episodes are included in Section 3.5.

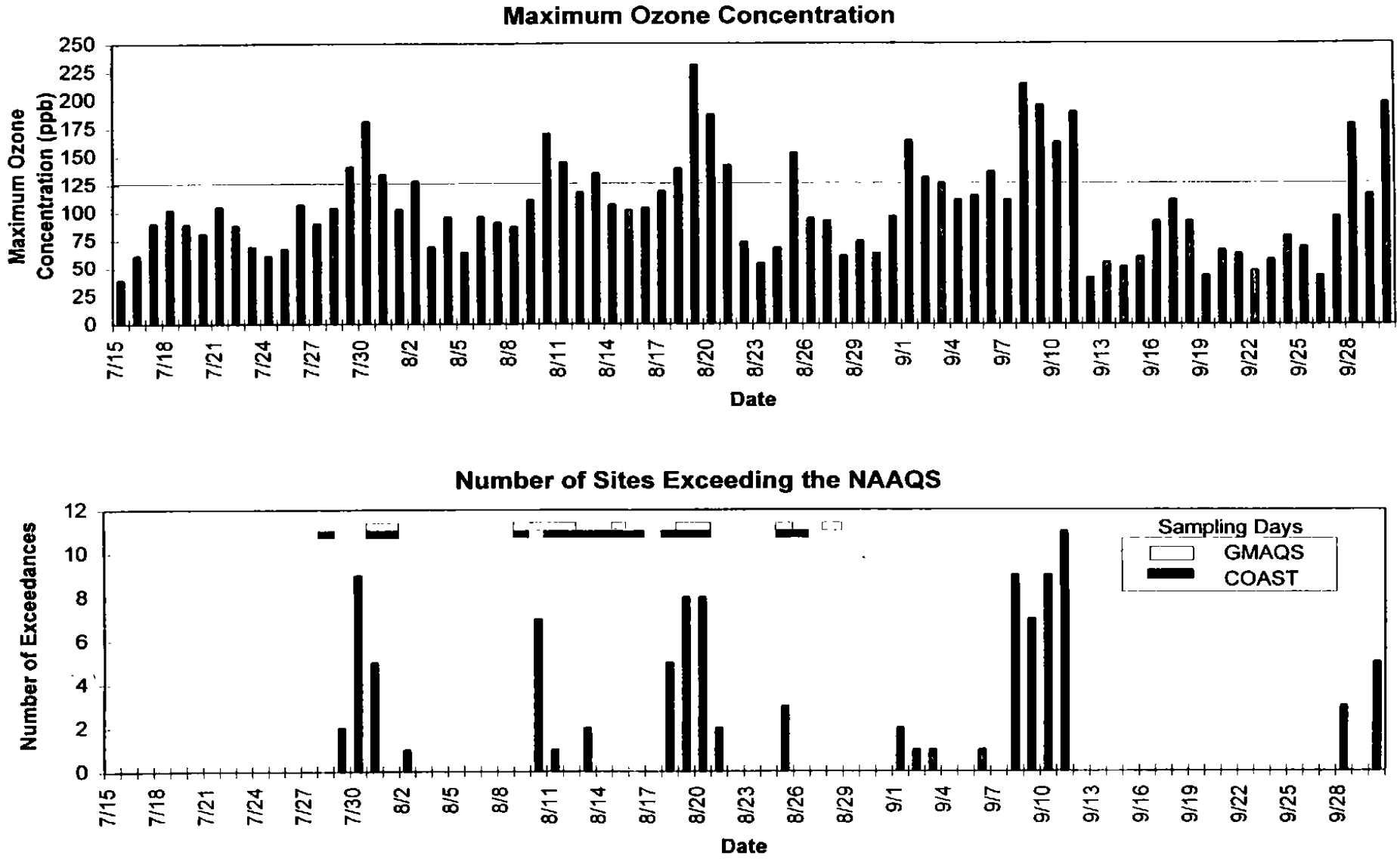

Figure 2-5. Daily maximum ozone concentration (top panel) and number of exceedances of the NAAQS (bottom panel) in southeast Texas from July 15, 1993 to September 30, 1993. Bars denote days when intensive measurements were taken.

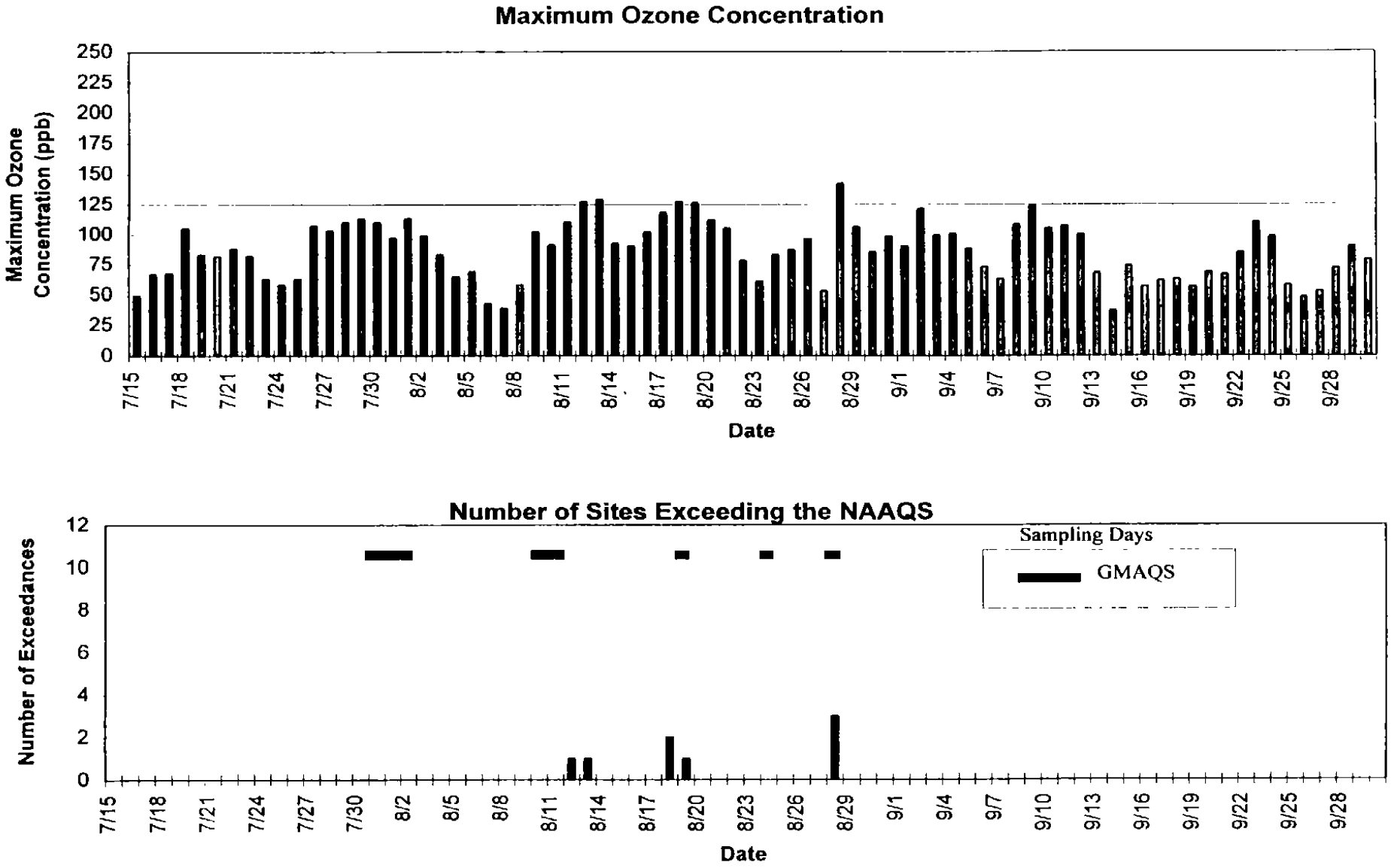

Figure 2-6. Daily maximum ozone concentration (top panel) and number of exceedances of the NAAQS (bottom panel) in Louisiana from July 15, 1993 to September 30, 1993. Bars denote days when intensive measurements were taken.

3 DATA ANALYSIS

3.1 DATA ANALYSIS OBJECTIVES

There were four objectives of the data analysis effort:

- To ensure that the GMAQS modeling database is consistent and quality-assured
- To characterize the air quality and meteorological processes that influence the formation and transport of ozone and ozone precursors in the Gulf Coast region
- To recommend specifications for the modeling system that adequately describe those processes
- To provide information on the appropriate boundary and initial conditions to use during the meteorological and photochemical modeling

The data analysis efforts required to achieve these objectives naturally fell into three general categories: (1) evaluating the data set and preparing it for subsequent analyses and modeling, (2) describing and displaying the data set, and (3) performing interpretative data analyses. The major purpose of the first part of the effort was to assess the accuracy, precision, and validity of the data set. The second part involved tasks designed to summarize the data, to make the data useful to other tasks, and to illustrate specific ozone formation and transport processes at work in the region. The third part, interpretative data analyses, integrated large amounts of information to describe the evolution of pollutant concentrations in the region and the relevant physical and chemical processes influencing ozone concentrations.

3.2 DATA AVAILABILITY AND DATA VALIDATION

DESCRIPTION OF DATA SOURCES

The extensive data collected during the 1993 GMAQS field study include continuous surface and aloft monitoring of air quality and meteorological conditions in southeast Texas, southern Louisiana, and the northern Gulf of Mexico. The Coastal Oxidant Assessment in Southeast Texas (COAST) study was also performed along with the

GMAQS, and data collected during both studies were jointly shared. These programs included air quality and meteorological measurements made as part of routine measurement systems and during intensive sampling periods. The data included measurements made at year-round monitoring sites operated by state air quality agencies and by the National Weather Service (NWS). In addition, the GMAQS contractors operated two air quality surface sites and a network of surface and upper-air meteorological sensors from mid-April to mid-October 1993. During the period 15 July–28 August 1993, additional sampling platforms were deployed on specific intensive operation period (IOP) days when high ozone concentrations were expected (see Table 2-4 for a listing of IOP days). The additional measurements included midday upper-air measurements made by rawinsondes, measurements of volatile organic compounds (VOC) and carbonyl compounds at two sites, and sampling of air quality and meteorological conditions aloft by aircraft.

This section summarizes the databases available for data analyses and includes a summary of the surface and aloft measurements made during the GMAQS and COAST programs, as well as the sampling locations and the variables measured at each site. In addition to the data discussed in this section, other useful data sources included visible satellite images of the southeast Texas and southern Louisiana regions and maps of NWS surface, upper-air, and radar analyses.

The GMAQS surface data set consisted of routine hourly measurements made at existing sites and sites installed for the GMAQS and COAST projects. The GMAQS routine data were collected for a 6-month period starting in mid-April 1993. Appendix A (in Volume 2) lists the air quality and meteorological parameters measured at each site. The general types of measurements made at these sites are summarized below.

- Surface air quality measurements were made at the existing monitoring sites in Texas and Louisiana and at coastline sites at Gilchrist, Texas and Cocodrie, Louisiana deployed specifically for the GMAQS. Figure 3-1a and 3-2a show the locations of these surface air quality sites in the southeast Texas and Louisiana regions. (Figures for this section begin on page 3-81.) Air quality variables included concentrations of ozone and NO/NO_x, although NO/NO_x was not measured at all sites.

- Samples of surface VOC and carbonyl compounds were collected at the two coastline sites (Gilchrist and Cocodrie) on IOP days. Samples of VOC and carbonyl compounds were also collected as part of the COAST project at six sites, although the data are not yet available for analysis. Sample collection and laboratory analyses are discussed later in this section.

- Surface meteorological measurements were made at some air quality monitoring sites, at NWS stations, at the two air quality sites at Gilchrist and Cocodrie, and at six upper-air sites. Figures 3-1b and 3-2b show the locations of these surface meteorological sites. The meteorological variables measured at these sites included wind speed, wind direction, temperature, dewpoint temperature, relative humidity, pressure, precipitation, and solar radiation.

Meteorological measurements taken aloft were made by several types of upper-air instruments. The locations of these sensors are shown in Figures 3-1b and 3-2b. Continuous upper-air wind measurements were made by a network of seven radar profilers and Radio Acoustic Sounding Systems (RASS) from mid-April to mid-October 1993. The profilers measured hourly wind speed, wind direction, and vertical velocity from about 140 m to 4000 m above ground level (agl). The RASS measured virtual temperature from 140 m to about 1500 m agl. Six of these profilers were equipped with surface meteorological stations. Two of the radar profilers were located on oil platforms in the Gulf of Mexico. Details about the radar profiler and RASS data can be found in Dye et al. (1994). To monitor conditions in the middle of the Gulf, a rawinsonde system was located on an oil platform about 200 km offshore in the Gulf of Mexico. Two soundings were made at 0600 and 1800 CST each day during the period 18 July–28 August 1993. An additional sounding was launched at 1200 CST on IOP days (details about these data are provided in Schoell et al., 1994a). In addition to the routine twice-per-day soundings made at NWS stations in Lake Charles and Slidell, Louisiana, a sounding was launched at 1200 CST on IOP days to monitor daytime conditions onshore. The rawinsonde data consisted of wind speed, wind direction, pressure, temperature, and dewpoint from the ground to at least 5000 m agl. Four sodars were deployed in the southeast Texas region to provide hourly wind speed and wind direction measurements from about 50 to 500 m agl.

To characterize the structure of pollutants aloft during the GMAQS and COAST programs, one to three aircraft, equipped with air quality and meteorological monitors, were flown on IOP days; the GMAQS and COAST projects sponsored one plane each; and a third plane was jointly shared between the studies. The aircraft flew only on IOP days and typically made two flights per day. These flights included descending spirals at the locations shown in Figures 3-1c and 3-2c, as well as transects between these spiral locations. All three planes made continuous measurements of ozone, NO/NO_x, and temperature. In addition to these variables, the third plane measured turbulence, dewpoint temperature, and light scattering. Grab samples of hydrocarbon and carbonyl compounds were also collected at preplanned locations and altitudes. Additional details about the aircraft data can be found in Anderson et al. (1993, 1994). A fourth plane, equipped with a downward-looking UV DIAL lidar, was flown on IOP days and measured ozone concentrations aloft in the southeast Texas region; these data were not available for the analyses.

DATA VALIDATION PROCEDURES AND RESULTS

Data validation is the process of determining the quality of the data and identifying their validity. It was a necessary component of this project because it identified errors, biases, and physically unrealistic values before they were used for analyses or modeling. The objectives of the data validation process were to produce a database with values that are validated and of a known quality; to evaluate the internal, spatial, temporal, and physical consistency of the data; and to intercompare data to identify errors, biases, or outliers.

Before discussing the actual procedures for data validation, it is useful to define some terminology. Outliers are defined as data that are physically, spatially, or temporally inconsistent. To identify outliers, errors, or biases, data validation was performed in several stages or levels:

- Level 1 data validation means that observations have received quantitative and qualitative reviews for accuracy, completeness, and internal consistency. Level 1 data validation was performed by those who collected the data and the GMAQS and COAST data managers.

- Level 2 data validation means that observations have been compared for external consistency against other independent data sets (e.g., comparing surface ozone concentrations from nearby sites, or intercomparing rawinsonde and radar profiler winds).

- Level 3 data validation means that observations have been determined to be physically, spatially, and temporally consistent during interpretive data analyses.

All three levels of data validation were performed on the data set. The procedures for data validation were similar for the different types of data: surface air quality and meteorological data, air quality and meteorological data aloft, VOC data, and aircraft data. The procedures used for Level 2 data validation were to compare data at adjacent times, compare data at nearby sites, and intercompare data collected by different instruments. The findings of the Level 2 and Level 3 data validations are described below.

In general, the Level 1 validation performed before the data were delivered for data analysis was sufficient to identify most outliers in the surface air quality and meteorological data. A few problems were identified in the surface meteorological data during the Level 2 review. For example, Figure 3-3a shows wind directions at the Cocodrie site that were constant for 57 hours from 31 July to 2 August 1993; winds at nearby sites varied during this time period. These winds were invalid and not used for data analysis. Other questionable winds were found at an automated weather station at Grand Isle in southeastern Louisiana, as shown in Figure 3-3b. Wind speeds measured at this site were 13.5 m/s and were considered suspect based on comparison of nearby winds.

No significant problems were identified during the Level 2 review of the upper-air meteorological database.

Ozone concentrations were measured aloft by in situ monitors aboard the three aircraft and by a UV DIAL lidar remote sensing system aboard a fourth aircraft. No significant problems were identified in the air quality data collected by in situ sensors, although ozone concentrations were discovered to be too low during one flight due to an improper altitude correction factor. Because they were unavailable in time for this analysis, DIAL ozone data were not used for data analysis.

Data validation efforts for several subsets of data, including VOC, carbonyl, and aircraft, were nonroutine and are described separately below.

VOC DATA

Collection and Analysis of Surface Hydrocarbon and Carbonyl Compound Data

On intensive sampling days, hydrocarbon samples were collected in stainless steel canisters at Cocodrie, Louisiana and Gilchrist, Texas. Two-hour samples were collected beginning at 0700, 1200, and 1700 CDT. Analyses were performed by Biospherics Research Corp. using gas chromatography with flame ionization detection (GC-FID). The 71 target compounds (listed in Appendix B) were reported with detection limits of 0.1 parts-per-billion-carbon (ppbC). Hydrocarbon species reported below the detection limit were assigned 0.0 ppbC. On average, 82 percent of the detected nonmethane hydrocarbon (NMHC) compounds in the surface samples were identified by species name.

Carbonyl compound samples were collected using C-18 cartridges coated with 2,4-dinitro phenylhydrazine (DNPH). Aldehydes and ketones react with DNPH to form hydrocarbons that are detected by high-performance liquid chromatography. Carbonyl compound samples were collected on the same schedule as the hydrocarbon samples. Atmospheric Assessment Associates (AtmAA, Inc.) extracted and analyzed the carbonyl cartridges and reported concentrations for 10 carbonyl compounds. Detection limits varied by species but were below 1 ppbC for all species. Carbonyl compounds below the detection limit were assigned 0.0 ppbC.

Hourly hydrocarbon concentrations were measured by continuous gas chromatograph (GC) at the Clinton and Galleria, Texas sites during the summer of 1993. Carbonyl compound samples were not collected at these sites. Data were processed by Radian, and Level 1 data validation was performed by Desert Research Institute (DRI). Additional data validation tasks were performed at STI on the data from Clinton including inspecting summary statistics, preparing scatter and line plots, and investigating outliers. NO_x concentration data were added to this database. The 54 target compounds (listed in Appendix B) were reported with detection limits of 0.1 ppbC. Hydrocarbon species reported below the detection limit were assigned 0.0 ppbC. On average, 70 percent of the detected NMHCs in the surface samples were identified by species name; this is less than the 85–95 percent typically identified in canister samples.

Collection and Analysis of Aircraft Hydrocarbon and Carbonyl Compound Data

Hydrocarbon and carbonyl compound samples were collected aloft during vertical spirals performed on the morning and midday/afternoon of each intensive day. Most of the samples were collected between 150 and 350 meters above mean sea level (m msl). Several samples were collected above 3000 m msl at Houston, and a few samples were collected above 3000 m msl at Beaumont and Baton Rouge. The hydrocarbon samples were collected in the same types of canisters used at the surface. However, unlike the surface samples, which were filled slowly over 2 hours, the aircraft samples were grab samples that were filled within about 2 minutes. On average, about 70 percent of the total NMHC was identified in the aircraft samples. To measure carbonyl compounds aloft, air was collected in Tedlar bags at the same locations and altitudes as for the

canisters. The bags filled in 2 to 3 minutes. Once at the surface, the air in the bags was pumped through DNPH cartridges. Sampling locations are shown in Figures 3-1c and 3-2c. Additional sampling and analysis details are provided by Anderson and Roberts (1994a, 1994b), Anderson et al. (1993, 1994), AtmAA Inc. (1993), Fung (1990), and Rasmussen (1994).

Validation of Surface and Aircraft Hydrocarbon and Carbonyl Compound Data

The hydrocarbon and carbonyl compound data collected in the aircraft or at the surface were merged by matching canister and cartridge numbers. The sampling times, durations, locations, and sample numbers were checked. In some cases, samples were invalidated by the laboratory or data analyst because of suspected contamination, the cartridge or canister was unexposed or lost, or the cartridge or canister numbers were invalid. For the surface data, the average NO_x concentration during the sampling period was added to the database. For the aircraft data, the average air quality (e.g., ozone, NO, NO_x concentrations) was calculated for each canister based on the beginning and ending times and added to the database. Adding air quality concentrations to the database allowed an evaluation of representativeness for group samples aloft and allowed calculation of the ratios NMHC/NO_x and NMOC/NO_x (nonmethane organic compunds versus NO_x). In most cases, the carbonyl compound sample bags were filled over the same time period, plus or minus about 10 percent.

Data validation of the surface and aircraft data included review of line plots of species concentrations and weight fractions for every sample; review of scatter plots; review of summary statistics stratified by date, time of day, and site; and identification and examination of potential outliers. Samples were flagged as having unusually high fractions of selected species if the carbon fraction of a particular species exceeded about 20 percent of the total NMHC or the total unidentified NMHC exceeded 50 percent on a carbon basis. Finally, a summary code was assigned separately to the hydrocarbon and carbonyl compound data that describes the data as valid, suspect, or invalid. A list of the suspect and invalid samples is provided in Appendix B.

COMPARISON OF OZONE CONCENTRATION MEASUREMENTS AMONG AIRCRAFT

As mentioned previously, three aircraft were operated during the study; however, due to mechanical problems with one of the aircraft, a fourth aircraft was operated for several flights as a replacement. The four aircraft were called 9PW, 9862F, 85585, and 6670Y. Measurements made by the first three aircraft were compared to the measurements made by the 6670Y aircraft. Because the 6670Y aircraft flew the greatest number of flights, it was considered the reference aircraft. Aircraft measurements were compared for spirals over Beaumont shortly after takeoff from and/or shortly before landing at Beaumont Airport. The 6670Y aircraft measurements were made fairly close in time (within 5 to 45 minutes) to the 9PW, 9862F, and 85585 measurements.

Ozone concentrations measured by the aircraft were first averaged into 30-second bins, and the concentration profiles were compared. Figure 3-4 shows an example of the comparisons made. The figure shows that the ozone concentrations measured by the 9862F and 6670Y aircraft during the early morning on 10 August 1993 were in excellent agreement (within 10 ppb).

The ozone concentrations measured by the aircraft were then averaged to represent a mixed-layer average (MLA). The MLA was computed by averaging the ozone concentrations below the subsidence inversion, which was typically located between 1300 and 1700 m agl. Figure 3-5 shows a scatter plot that compares the MLA ozone concentrations measured by the 6670Y aircraft with those measured by the 9PW, 9862F, and 85585 aircraft for all the spirals flown over Beaumont during the summer of 1993. The figure shows that the MLA ozone concentrations measured by the 6670Y aircraft were in excellent agreement with those measured by the other three aircraft, with r^2 of 0.94.

Similar comparisons were made for the NO_x concentrations measured by the four aircraft; results were also excellent.

COMPARISON OF UPPER-AIR AND SURFACE OZONE MEASUREMENTS

Ozone measurements made aloft at spiral locations were compared to measurements made at nearby surface sites. In some cases, measurements aloft at a particular location were made by more than one aircraft. However, because of the excellent agreement among the aircraft, the comparisons shown here are not specific for each aircraft but rather for each spiral location.

Ozone measurements made aloft were compared to surface measurements at 10 locations. Table 3-1 lists the surface sites and the aircraft spiral locations used for the comparisons, the average and range of the lowest altitudes reached by the aircraft at each location, and the horizontal distances between the spiral locations and the corresponding nearby surface sites. Note that the aircraft spirals were typically about 3 km in diameter.

As with the comparison among aircraft described above, the ozone concentrations aloft were averaged to represent a MLA. In addition, the concentrations aloft were averaged to represent a lowest-altitude average (LAA). The LAA was computed by averaging the ozone concentrations over 30 seconds in the lowest section of the aircraft spiral, which was typically between 25 and 100 m agl (see Table 3-1). Our analyses indicate that, in general, the MLA concentrations were very similar to the LAA concentrations during the early afternoon periods. This agreement suggests that the boundary layer was well mixed. (During the early morning period, however, the two concentrations tended to differ.)

Figure 3-6 shows the comparisons between surface ozone measurements made at the Swiss&Monroe surface site and aircraft ozone measurements made over Houston Hobby Airport during the 17–21 August 1993 episode. These locations are about 4 km apart (see Table 3-1). The figure shows that the surface data and data aloft were usually in very good agreement. These results suggest that during the morning at Houston Hobby

Table 3-1. Distances between aircraft locations and the corresponding nearby surface sites, and lowest altitudes reached by the aircraft near the corresponding surface sites for all flights during summer of 1993.

Aircraft Location	Surface Site	Distance (km)	Lowest Altitude (m agl)	
			Range	Average
Baton Rouge Airport	Highway 1	6.4	27–62	35
Cocodrie/LUMCON	Cocodrie	2.6	29–125	82
Galveston Airport	Galveston	0.8	15–356	52
Gilchrist	Gilchrist	1.0	49–164	70
Houston Gulf Airport	Seabrook	7.6	23–42	30
Houston Hobby Airport	Swiss&Monroe	3.9	10–71	27
Houston Southwest	Croquet	11.2	13–44	27
Kountze/Silsbee Airport	Kountze C85	4.4	17–58	33
Lake Houston (near Crosby)	Crosby	5.8	37–115	70
May	NW Harris C26	1.5	13–47	24

Airport the aircraft penetrated the nocturnal inversion. In the afternoon, concentrations aloft were between 10 and 20 ppb higher than the surface concentrations. Comparisons for all the locations during the 17–21 August 1993 episode are shown in Appendix C.

Table 3-2 shows the average and standard deviation of the differences between MLA and surface ozone concentrations and LAA and surface ozone concentrations. Because the number of flights performed only during intensive episodes is small, the statistics were calculated for all the flights performed during the summer. The MLAs were computed for the afternoon flights, and the LAAs were computed for the morning and afternoon flights. The table shows that the aircraft and surface observations agreed very well: on average the differences between aircraft and surface ozone concentrations were less than 10 ppb with standard deviations of less than 12 ppb. These results are very different from the results of the comparison analyses performed in the Southern California Air Quality Study (SCAQS), in which the low-altitude ozone concentrations were consistently higher than the surface concentrations by about 25 ppb (Roberts and Main, 1992). The SCAQS comparisons were for urban sites, whereas the GMAQS comparisons are for a mix of urban, industrial, and rural sites.

3.3 CLIMATOLOGY AND REPRESENTATIVENESS

Four 1993 episode periods (29–31 July, 10–13 August, 18–21 August, and 8–11 September) have been selected for use in data analysis and as candidates for possible modeling analysis, and thus eventually in making regulatory decisions regarding source attribution and control strategies. In the U.S. EPA's (1991a) *Guideline for Regulatory*

Table 3-2. Differences between mixed-layer averages (MLAs) and surface ozone concentrations and between lowest-altitude averages (LAAs) and surface ozone concentrations for all flights during summer of 1993.

Aircraft Location	MLA − Surface*		LAA − Surface	
	Average (ppb)	Standard Deviation (ppb)	Average (ppb)	Standard Deviation (ppb)
Baton Rouge Airport	−5	4	3	8
Cocodrie/LUMCON	−3	4	7	9
Galveston Airport	−1	6	3	7
Gilchrist	−2	4	6	7
Houston Gulf Airport			3	2
Houston Hobby Airport	9	6	9	6
Houston Southwest			7	5
Kountze/Silsbee Airport	3	7	−2	4
Lake Houston (near Crosby)	2	9	6	10
May	1	12	5	8

* MLAs computed for the afternoon flights only.

Application of the Urban Airshed Model, criteria were set up to ensure that UAM applications would use episodes "representative" of those that have occurred in the past. Episodes that are candidates for modeling should have meteorological conditions and temporal and spatial patterns of ozone observations that are similar to those in the historical record.

The primary objective of this analysis was to determine whether the four 1993 GMAQS episodes were representative of those occurring in the region in the past. A secondary objective was to determine fundamental relationships between ozone observations and meteorological observations. For the purposes of this analysis, representativeness was determined on the basis of similarity to typical (e.g., the median and range of values for key parameters) historical ozone-conducive conditions.

The ozone problem along the Gulf of Mexico coast from Victoria to Houston to New Orleans has been recognized and studied for more than 20 years. The scoping study by STI (Blumenthal et al., 1993) reviews the published literature and carries out further analysis of the data during the period 1982-1990; this document was used for planning the summer 1993 GMAQS field study.

The representativeness analysis carried out as part of the GMAQS is summarized here and reported in more detail in Chang and Hanna (1995), who analyzed ozone and meteorological data for 1982-1992 to address the objectives listed above. It was assumed in the analysis that the 17 continuously operating (during the period 1982-1993) ozone monitoring stations in the GMAQS region provided sufficient spatial coverage in the areas of high ozone concentrations. It was necessary to limit the analysis to those 17

sites in order to avoid biases associated with incomplete data, even though other less-continuous sites may have recorded higher ozone concentrations. The data analyses involved various statistical comparisons between data for 1993 and the 1982–1992 period, including numbers of ozone exceedance days, cumulative distributions of exceedance days, duration and spatial coverage of exceedances, and probability distribution functions of ozone and meteorological variables for summer periods and for ozone episodes only. The analysis also involved an investigation of relationships between ozone and meteorological variables, including trends, ozone roses, scatter plots, correlations, and cluster and factor analysis.

The following general conclusions can be drawn from the analyses:

- High ozone concentrations in the Houston, Baton Rouge, and New Orleans regions are generally associated with summertime stagnation conditions, where the region is under the influence of a broad high-pressure system and when sea/land breeze recirculations are present. Long-range transport from upwind source regions probably plays a less important role in determining the magnitude of local ozone concentrations.

- The 1993 GMAQS ozone episodes and exceedances are representative of episodes and exceedances during the historical period (1982–1992). That is, the meteorological conditions during the 1993 ozone episodes are similar to those during ozone episodes in the historical period.

- When all summer (July, August, and September) days are considered, ozone concentrations in the GMAQS region are not strongly correlated with maximum daily temperatures. This is contrary to the Lake Michigan and NJ-NY-CT regions, where a strong correlation between ozone and temperature exists. This is because summer days in the GMAQS region are nearly always warm and humid, with very few intrusions of cool, clean air associated with cold frontal passages.

- There appears to be a downward trend in the number of ozone exceedance days during the period 1982–1993 in the Houston region. This downward trend exists even in the presence of an upward trend in temperatures for most years.

Moreover, it is possible to make the following specific conclusions based on individual statistical analyses:

Representativeness

- The tabulations of the numbers and magnitudes of ozone exceedances during the period 1982–1993 suggest that there is much year-to-year variability (the maximum ozone concentration varies from 161 to 340 ppb and number of exceedance days varies from 6 to 38 for the 12-year period). The 1993 observations fall well within these historical ranges (the 1993 maximum is 231 ppb, and the 1993 number of exceedance days is 16).

- The cumulative distribution functions (CDFs) for the 1993 ozone exceedances and episodes are within the range of the 11 individual CDFs during the period 1982–1992 (see Figure 3-7). The CDFs are defined by the daily maximum 1-hour ozone concentration anywhere in the GMAQS region. The 11-year data set can be approximated by the exponential relation: $(1 - \text{CDF}) = 0.0714 \exp(-0.0318(C - 120))$, where C is ozone concentration in ppb. The CDFs for the Houston region for 1993 also fall within the range of the 11 individual CDFs for 1982–1992; however, the number of exceedances in the Baton Rouge area are too few to make the comparison valid.

- About 18 percent of all time periods with GMAQS ozone exceedances in 1982–1992 had durations of 3 days or longer. None of the 1993 ozone episodes lasted for more than 3 days. However, the 1993 durations were within the normal year-to-year range.

- Distributions of meteorological variables for the entire summer (July-August-September) were similar in 1993 and in the 1982–1992 historical period. The median surface and 850-mb temperatures were about 1°C above normal in the summer of 1993 (see Figure 3-8).

- Distributions of meteorological variables (wind speed, maximum temperature, 850-mb temperature, and cloud cover) during the 1993 ozone exceedance days were within the ranges of distributions for the ozone exceedance days in the 1982–1992 historical record (see Figure 3-9).

- The ozone roses for 1982–1992 show that most Houston ozone exceedances occur with southeasterly to northeasterly winds. These same relations are also found in 1993.

- The diurnal variations of hourly averaged ozone concentrations on exceedance days in 1993 were similar to those in 1982–1992 for the entire GMAQS region (see Figure 3-10). In both the 1982–1992 and 1993 data sets, minimum ozone concentrations were observed from 5:00 to 6:00 a.m., and maximum ozone concentrations were observed from noon to 3:00 p.m. The historical data set shows a median ozone concentration exceeding 80 ppb for hours between 10:00 a.m. and 5:00 p.m. in the GMAQS region.

General Relations Between Ozone Observations and Meteorological Variables Based on the Historical Data

- A comparison of wind roses and ozone episode roses for 1982–1992 suggests that winds from the northeast to southeast generally enhance ozone concentrations in Houston, and that winds from the northwest to north and from the south generally enhance ozone concentrations in Baton Rouge.

- When the CDFs of meteorological variables during ozone episodes are compared with CDFs during the entire summer for 1982–1992, maximum surface

temperatures are similar for normal and episode days in Houston. On the average, maximum surface temperatures are 1 to 2°C higher than normal during episode days in Baton Rouge and New Orleans. The 850-mb temperatures are similar for normal and episode days. Cloud cover is about 10 percent less during episodes. Wind speed is about 1 m/s less than normal during episodes.

- A significant correlation between the peak daily ozone concentration and the maximum temperature was not found in the GMAQS region, contrary to findings in more northern regions of the United States. Correlations between ozone and temperature range from 0.18 to 0.37 (i.e., only 3 to 14 percent of the variance is explained) in Houston, Baton Rouge, and New Orleans. Similarly, weak correlations with ozone are found for wind speed, relative humidity, and cloud cover.

3.4 DESCRIPTIVE ANALYSES OF THE GMAQS DATA

DESCRIPTION OF OZONE AIR QUALITY

This section provides an overview of ozone concentrations measured during several episodes in the southeast Texas and Baton Rouge regions. An ozone episode is a period (one or more days) when ozone concentrations at one or more sites exceed the National Ambient Air Quality Standard (NAAQS) for ozone of 125 ppb. As discussed in Section 2, numerous ozone episodes occurred during the summer of 1993. Four of these episodes were selected to examine the air quality and meteorological conditions in greater detail. These episodes were chosen because it was during these periods that the highest ozone concentrations and the greater number of exceedances of the NAAQS in the summer of 1993 were observed. Because of the lower ozone concentration measured and the unavailability of supplemental data, the 29–31 July 1993 episode was not analyzed further.

For each episode, the preceding day (also referred to as the buildup day) was included so that conditions leading to the high concentrations could be studied. The ozone episodes analyzed in the southeast Texas region were 9–11 August 1993, 17–21 August 1993, and 7–11 September 1993. In the Baton Rouge area, the 17–19 August 1993 episode was studied. Tables 3-3 and 3-4 list the maximum ozone concentrations and number of exceedances for these episodes in each region. Appendix D lists the locations of all exceedances measured during these episodes. The remainder of this section provides a brief synopsis of the maximum ozone concentrations measured during these episodes.

During the 9–11 August episode in southeast Texas, ozone concentrations exceeded the NAAQS on 10 August and 11 August. Daily maximum ozone concentrations during this three-day period are shown in Figure 3-11. On the buildup day (9 August), ozone concentrations ranged from 60 to 111 ppb, with highest concentrations measured at urban sites in Houston and Beaumont. On 10 August, ozone concentrations at seven sites exceeded the NAAQS as shown in Figure 3-11b. These exceedances occurred from the industrial-urban regions of Houston to the rural regions northwest of the city; an urban and an industrial site in the Houston region each measured a maximum concentration of 170 ppb on this day. On 11 August, one exceedance occurred at a rural

Table 3-3. Episode dates, maximum ozone concentrations, and number of exceedances in the southeast Texas region.

Episode Day (1993)	Maximum Ozone Concentration (ppb)	Number of Ozone Exceedances
9 August	111	0
10 August	170	7
11 August	145	1
17 August	119	0
18 August	139	5
19 August	231	9
20 August	187	8
21 August	142	3
7 September	111	0
8 September	214	10
9 September	195	7
10 September	162	11
11 September	189	11

Table 3-4. Episode dates, maximum ozone concentrations, and number of exceedances in the Baton Rouge region.

Episode Day (1993)	Maximum Ozone Concentration (ppb)	Number of Ozone Exceedances
17 August	118	0
18 August	127	2
19 August	126	1

site northwest of Houston. Maximum ozone concentrations at the coastal sites at Galveston and Gilchrist remained below about 80 ppb throughout this episode.

The highest ozone concentration measured during the summer (231 ppb) was measured during the 17–21 August episode in the Houston region. In addition, this episode had 25 exceedances of the NAAQS, which was the second highest of the summer (the 7–11 September episode had 39 exceedances). Plots of the maximum ozone concentration are shown in Figure 3-12. On 17 August 1993, ozone concentrations were characteristic of a buildup day and mostly ranged from 40 to 80 ppb with several sites to the east of the urban-industrial regions of Houston measuring ozone concentrations greater than 100 ppb. By 18 August, five ozone exceedances occurred from the urban region into the

rural regions to the east and northeast of Houston. The peak day occurred on 19 August, when nine sites exceeded the NAAQS, with highest ozone concentrations observed to the north and east of the ship channel and at a rural site northwest of Houston. The highest concentration of 231 ppb was measured on this day at Aldine, an urban site north of the ship channel. Ozone concentrations remained high on 20 August, when eight sites extending from the urban-industrial areas of Houston to northeast of the city exceeded the NAAQS. By 21 August, ozone concentrations decreased to generally below 100 ppb throughout the southeast Texas region except for the sites east of Houston, where two ozone exceedances were measured. Maximum ozone concentrations at the Galveston site remained below 80 ppb throughout the episode. Ozone levels at Gilchrist were below 80 ppb on all days except on 20 August, when a maximum of 115 ppb was measured.

The 7-11 September episode in southeast Texas was substantially different from the August episodes because the highest ozone concentrations were observed closer to the coastline. In fact, five of the six exceedances measured at the Galveston and Gilchrist sites in the summer of 1993 occurred during this episode. As shown in Figure 3-13, the highest ozone concentrations occurred near the coastline and at sites surrounding Galveston Bay. On 7 September, maximum ozone concentrations of 80 to 111 ppb were measured at sites south of Houston. The peak day of this episode occurred on 8 September, when two sites measured ozone concentrations above 200 ppb. On this day, 10 exceedances occurred between the ship channel and the coastline. By 9 September, the exceedance region moved further south with the highest ozone concentrations measured at sites near Galveston Bay and within 20 km of the coast. On 10 September, ozone exceedances still occurred along the coast, but also extended northward into the urban regions of Houston and into the Beaumont/Port Arthur area. Ozone concentrations at 11 sites exceeded the NAAQS on this day, with the maximum ozone of 162 ppb measured at the Galveston site along the coastline. By 11 September, the region of exceedances shifted further northward into the Houston area, where 11 sites exceeded the NAAQS. Maximum ozone levels along the coast decreased to about 100 ppb, or less.

The 17-19 August episode in the Baton Rouge, Louisiana, area was the only multiday episode observed in this region during the summer of 1993. As shown in Figure 3-14, ozone concentrations on the buildup day (17 August) were generally above 100 ppb just south of Baton Rouge. Ozone concentrations in the rural regions ranged from 70 to 90 ppb. Ozone concentrations at the rural coastline site in Cocodrie, Louisiana peaked at 98 ppb (this high concentration occurred during persistent northerly flow). On 18 August, two exceedances of the NAAQS occurred. One exceedance occurred in East Baton Rouge Parish (Highway 964) while the second exceedance occurred in Dutchtown about 25 km southeast of the city. Maximum concentrations at other sites ranged from 90 to 120 ppb and were located within 10 to 20 km of Baton Rouge. On 19 August, one site exceeded the NAAQS. Ozone concentrations greater than 100 ppb were measured at sites located 25 to 50 km southeast of Baton Rouge, while concentrations at sites in northern Baton Rouge remained about 80 ppb. Maximum ozone concentrations at Cocodrie were 71 ppb on both 18 and 19 August.

The air quality and meteorological conditions during these episodes are discussed in greater detail in Section 3.5, Case Studies of Ozone Episodes.

DESCRIPTION OF SYNOPTIC METEOROLOGY DURING OZONE EPISODES

Synoptic-scale meteorology was examined to understand the large-scale weather conditions associated with high ozone concentrations in the southeast Texas and Baton Rouge regions. To examine these conditions, several data sets were used. These included surface meteorological observations from the National Weather Service (NWS), objectively analyzed surface and upper-air maps (850, 700, and 500 mb), and daily weather maps depicting surface and upper-air conditions at 0600 CST. Historical weather conditions are summarized first followed by a description of the synoptic meteorology during the 9–11 August, 17–21 August, and 7–11 September 1993 episodes.

The general synoptic-scale meteorology during the summer in the Gulf Coast region was characterized by onshore (i.e., southeasterly to southwesterly) winds, associated with clockwise (anticyclonic) flow around the Bermuda high-pressure system, the center of which was usually located east of the study region. Days were generally sunny, warm, and humid, and convective showers occurred on some days. Data collected during the GMAQS demonstrated that the general meteorological conditions occurring during the 1993 study were consistent with these climatological features, and thus 1993 was a representative year with respect to the meteorological conditions observed.

Blumenthal et al. (1993) investigated synoptic conditions associated with high ozone episodes in the southeast Texas and Baton Rouge regions from 1987 to 1990. Synoptic weather conditions on days with high ozone were found to differ from the general meteorological conditions described above. During ozone episodes, the region was dominated by a surface high-pressure system and weak surface pressure gradients. This weak synoptic forcing allowed diurnally varying onshore and offshore flows to form. Conditions aloft were characterized by a high-pressure ridge over the central to western United States, with weak to moderate easterly to northerly winds.

Synoptic meteorological conditions during the 9–11 August episode were characterized by a broad ridge of high pressure located over the southern United States. At the surface, a high-pressure system moved southwestward into the southeast Texas region as shown by the daily weather map in Figure 3-15. Pressure gradients throughout the region weakened, and the diurnally varying onshore-offshore flow formed. At 500 mb, a ridge of high pressure moved westward into New Mexico by 10 August, which produced easterly and northeasterly winds aloft. Synoptic weather conditions observed during this episode were consistent with historical conditions during ozone episodes identified by Blumenthal et al. (1993).

The surface and upper-air weather patterns of the 17–21 August episode were similar to the 9–11 August episode. The 17–21 August episode started when an extension of the Bermuda high-pressure system moved westward into the Gulf of Mexico. On the exceedance days, this extended high-pressure system was located over southern Louisiana and southeast Texas. As shown by the daily weather maps for 19 August in Figure 3-16, the synoptic forcing produced weak surface pressure gradients, and in response the synoptic wind speeds decreased. Diurnally varying onshore and offshore flows similar to those observed in the historical data set were observed on these days and are explained in more detail in the next section. A ridge of high pressure at 500 mb

extended over most of the United States. This weather pattern produced easterly to northeasterly winds aloft and subsidence over the region. The subsiding air produced clear skies and suppressed convective showers and thunderstorms. Synoptic meteorological conditions observed during this episode were representative of those observed during historical episodes.

Meteorological conditions during the 7-11 September episode were substantially different from those observed during the August episodes. As shown by the daily weather map in Figure 3-17, the differences include prevailing wind directions aloft, location and origin of the high-pressure systems, and the 500-mb pattern. During this episode the Bermuda high remained off the Atlantic coast and a series of three weak fronts followed by continental high-pressure systems moved southeastward through the region between 6 and 11 September. The weak fronts produced some clouds, but little or no precipitation. Continental high-pressure systems moved southeastward into the region behind (i.e., north of) the fronts whereas the subtropical high-pressure systems observed in the August episodes had moved into the region from the east. Northerly flow behind these continental high-pressure systems brought drier air into the region, which produced sunnier skies over land and offshore. The pattern at 500 mb showed a trough over the eastern United States with westerly to northerly winds aloft. Synoptic weather conditions during this episode were observed in the historical database, but not as frequently as the conditions in the August episodes.

ANALYSES OF SURFACE AND UPPER-AIR METEOROLOGICAL CONDITIONS

Figure 3-18 shows a time series (hourly averages) of surface winds, temperature, dewpoint, solar radiation, relative humidity, and precipitation measured by the 10-m surface meteorological station located at the Galveston radar profiler site. The data shown in Figure 3-18 cover the period from mid-July through mid-September 1993, which encompasses the IOP portion of the GMAQS and extends through the period of the September ozone episodes described previously. The wind data are shown as vectors in the "bristle brush" plot at the top of the figure, with north to the top. As summarized in the preceding section, the typical summertime synoptic-scale meteorology in southeast Texas is characterized by onshore (i.e., southeasterly to southwesterly) winds, associated with clockwise flow around the Bermuda high-pressure system, the center of which is usually located east of the study region. Using the Galveston data as representative of the conditions observed during the GMAQS in southeast Texas, the data shown in Figure 3-18 indicate that the historical summertime meteorological conditions observed during the 1993 study were consistent with these features.

On many days, the prevailing flow at Galveston was from the south throughout the day. Figure 3-18b shows hourly ozone, NO_x, and meteorological data for an example period of persistent southerly flow. When onshore flow persisted for several days at a time, the ozone concentration at the shoreline slowly and steadily dropped from typically about 60 to 80 ppb on the first day to 20 to 40 ppb after several days. NO_x concentrations also dropped from about 4 to 6 ppb to less than 2 ppb during steady onshore flow conditions.

In addition, NO concentrations during persistent onshore flow were typically zero (less than 0.5 ppb). These data indicate that offshore emissions alone did not produce ozone exceedances in the southeast Texas and Baton Rouge nonattainment areas during persistent onshore flow conditions.

The wind data presented in Figure 3-18 show that on most days the prevailing flow at Galveston was from the south throughout the day. On occasion the winds reversed direction and blew offshore. Time-series plots of the surface observations collected onshore at Southeast Houston and offshore at the High Island Platform radar profiler sites show a similar pattern of generally persistent onshore winds occasionally interrupted by periods of offshore winds (Schoell et al., 1994b). Likewise, the radar profiler data collected at the Texas stations show patterns of generally persistent southerly winds throughout the full diurnal cycle, which were periodically interrupted by periods of offshore winds on the same days shown in Figure 3-18 (Dye et al., 1994; see the following section on analyses of transport processes for more information on the characteristics of the winds aloft over the region as revealed by the profiler data). Although it is not immediately obvious from the wind vector plot shown in Figure 3-18, closer examination of the surface data shows that the northerly winds typically began in the early morning hours (e.g., 0400–0600 CST) and persisted until midmorning or early afternoon (e.g., 1000–1300 CST).

The significance of the flow reversal to ozone episodes in southeast Texas is indicated by the analysis presented in Figure 3-19, which is a time-series plot of the daily maximum ozone concentration observed in the Houston region on each day of the study for the period 17 July–15 September 1993. Days on which the flow reversal occurred are indicated by the dark bars. The presence of the flow reversal was determined by examining time series plots like the one shown in Figure 3-18, and by examining the radar profiler data, which showed the presence of the flow reversal aloft (see below for more information on the aloft characteristics of the flow reversal). As shown in Figure 3-19, every ozone exceedance observed in the southeast Texas region during the 1993 field study coincided with the occurrence of the flow reversal. Days with flow reversals occurred that were not exceedance days, but they were usually associated with a buildup to, or ramp-down from, a multiday episode. The timing of the flow reversal was also potentially significant: it occurred during the morning hours, when morning rush hour emissions were potentially highest and photochemical activity was beginning. When steady onshore flow persisted for the full diurnal cycle and the flow reversal did not occur, no ozone exceedances were observed in southeast Texas.

An explanation for the development of the flow reversal was sought by examining the synoptic-scale and mesoscale sea-level pressure gradients that developed across the region. As explained in most meteorological texts (e.g., Hess, 1959), the geostrophic wind is the horizontal wind velocity that occurs when horizontal pressure gradient forces are balanced by the Coriolis force (produced by the rotation of the earth), and frictional effects are ignored. Southerly geostrophic winds develop in response to a positive east-west synoptic pressure gradient (pressure higher to the east). Northerly geostrophic winds develop in response to a negative east-west pressure gradient (pressure higher to the west). Likewise, the westerly component of the geostrophic wind is driven by the north-south component of the synoptic pressure gradient. In other words, as air moves

from higher to lower pressure in response to pressure gradient forces, the effect of the rotation of the earth is to turn the wind parallel to lines of constant pressure (isobars). In the northern hemisphere, the winds turn clockwise (anticyclonically) with time, with low pressure to the left. The time required to achieve geostrophic balance at the latitude of southeast Texas is roughly 12 hours.

Figure 3-20 analyzes the differences in sea-level pressure (mb) measured between the Ship Shoal and High Island platforms for the period 18 July–15 September 1993. Also shown in the figure is the onshore-offshore component of the surface wind normal (perpendicular) to the coastline (V_n), which was computed from the wind data measured by the surface station located at the Galveston radar profiler site. To minimize diurnal influences in the pressure gradient analysis, the sea-level pressure differences were subjected to a 24-hour running average filter. Pressure differences greater than 0 mb indicate that the pressure was higher over the eastern side of the Gulf compared to the Texas side of the Gulf. Conversely, pressure differences less than 0 mb indicate that pressures were higher over the Texas portion of the Gulf, compared to the Louisiana side. To emphasize any diurnal cycle that might exist in the velocity data, a 12-hour running average filter was applied to the onshore-offshore velocity components measured by the Galveston surface station. An onshore-offshore velocity component greater than 0 indicates onshore (southeasterly) winds. Conversely, values of V_n less than 0 indicate offshore (northwesterly) winds.

Applying the geostrophic relationship to the analysis presented in Figure 3-20, and using the sea-level pressure difference between the Ship Shoal and High Island platforms as a surrogate for the east-west synoptic-scale pressure gradient across the Gulf, onshore (southeasterly) winds would be expected when the pressure at Ship Shoal Platform is greater than the pressure at High Island Platform. Likewise, offshore winds would be expected when the pressure gradient is negative, that is, the pressure at Ship Shoal Platform is less than the pressure at High Island Platform. The onshore-offshore component of the wind at Galveston shown in Figure 3-20 does indeed show onshore flow ($V_n > 0$) when the synoptic-scale pressure gradient across the Gulf would be expected to produce onshore geostrophic flows. A 0.25 mb average pressure difference between Ship Shoal and High Island would produce an average southerly geostrophic wind component of approximately 5 m/s. This value is generally in good agreement with the pressure differences presented in Figure 3-20 and the wind velocities shown in Figure 3-18, given that frictional effects have been ignored.

The periods when the offshore winds of the flow reversal ($V_n < 0$) occurred also coincided with periods when the synoptic-scale pressure gradient across the Gulf reversed. In addition, the analyses of the Galveston wind data presented in Figure 3-20 show a pronounced diurnal signal, with velocities generally higher during the day than at night. Likewise, V_n tends to reach a minimum (or reverses entirely during a flow reversal and indicates offshore winds) during the nighttime or early morning hours. This pattern suggests the formation of a mesoscale sea/land breeze circulation.

A sea breeze develops when the land being heated by the sun becomes warmer than the adjacent waters during the day. This temperature difference produces a onshore pressure

gradient (pressure higher over the water than over the land), which in turn produces onshore winds. At night, this pattern reverses, with the land becoming cooler than the water and the development of an offshore-directed pressure gradient that would, at least theoretically, produce the offshore winds of a land breeze. The duration of a diurnal sea/land breeze circulation is usually not long enough for these winds to come into balance with the Coriolis force, which explains why these mesoscale flows do not behave like geostrophic winds and blow perpendicular to the pressure gradient. Even so, a clockwise turning of the winds with time is evident in the Galveston wind data.

A figure similar to Figure 3-20 showing an analysis of the pressure differences between the Southeast Houston and High Island radar profiler sites, as well as the analysis of the across-Gulf pressure gradient, is given in Appendix E. The Southeast Houston-to-High Island Platform pressure difference was used as an indicator of the mesoscale pressure gradient that developed as a result of the diurnal heating and cooling of the land relative to the water. The diurnal signal in the onshore-offshore velocity components observed at Galveston was also evident in the onshore-offshore sea-level pressure gradient, which supports the conclusion that mesoscale conditions in the region favor the development of the sea/land breeze circulation. In the rest of this report, the local version of the sea breeze will be called the "gulf breeze" to distinguish it from the general case.

The structure of the gulf/land breeze circulation is examined in more detail in Figure 3-21, an analysis of the diurnal cycles of the mesoscale pressure and temperature gradients between the Southeast Houston and High Island radar profiler sites, as well as the onshore-offshore velocity component (V_n) at Galveston, during the ozone episode of 17-21 August 1993. The figure shows a near-textbook case of the development of a diurnal sea/land breeze circulation. During the day, the air over the land became warmer than the air over the Gulf, which in turn produced an onshore-directed pressure gradient and subsequently onshore winds ($V_n > 0$). At night, the land became cooler than the water, the pressure gradient reversed, and an offshore wind ($V_n < 0$) developed.

The results presented in Figure 3-21 indicate that the maximum (minimum) mesoscale pressure gradient coincided closely with the minimum (maximum) temperature difference (occurring within approximately 1 to 2 hours of each other). Similarly, the maximum onshore velocity of the gulf breeze also coincided closely with the minimum (onshore-directed) pressure gradient. Note that the start of the gulf breeze at Galveston coincided almost exactly with the reversal of the temperature and pressure gradients. However, the maximum offshore wind velocities in the flow reversal lagged the maximum (offshore-directed) pressure gradient by a few hours. This is consistent with the earlier observation that the flow reversal typically began late at night or early in the morning, and persisted into the late morning or early afternoon hours. Interestingly, the start of the flow reversal (first time V_n became less than 0) coincided with the time when the temperature difference between the Southeast Houston and the High Island Platform sites was at its greatest (coolest onshore temperatures).

The timing of the gulf breeze and flow reversal offshore was different from that at the onshore stations. Figure 3-22 shows an analysis of the onshore-offshore velocity components normal to the shoreline (V_n) calculated from the surface winds measured at the Southeast Houston, Galveston, and High Island radar profiler sites during the 17-21

August 1993 ozone episode. Generally, the start of the gulf breeze and the time of its maximum velocity were observed first at the shoreline (Galveston), followed 1 to 3 hours later inland at the Southeast Houston site. Offshore, the start of the gulf breeze was delayed a few hours relative to when it was first observed at the shoreline. The flow reversal (land breeze) was usually observed first at Galveston and Southeast Houston, and several hours later offshore at High Island Platform. The maximum winds of the flow reversal did not occur offshore at High Island until about 1100 CST, and the onshore winds of the gulf breeze ($V_n > 0$) did not develop until about 1500 CST.

The gulf breeze and flow reversal were not limited to the surface layer. They were observed in the radar profiler data collected at all the Texas sites, including the offshore High Island Platform. Figure 3-23 shows an example of 24 hours of hourly averaged upper-air wind data measured by the radar profiler at Galveston on 10 August 1993, one of the days that the ozone standard was exceeded in the region (other examples of the structure of the flow reversal aloft and the gulf breeze are given in Dye et al., 1994). The upper-air data show onshore flow from midnight until about 0500 CST (0600 CDT in the figure), which is the continuation of the gulf breeze that began on 9 August. Offshore winds then occurred during the period 0500–0930 CST (0600–1030 CDT) through a layer that was about 500 to 600 m deep. Finally, the gulf breeze arrived again at about 1000 CST (1100 CDT). The depth of the gulf breeze inflow layer (600 to 700 m agl) was somewhat greater than the depth of the layer of offshore winds.

Figure 3-24 shows upper-air wind data measured offshore by the High Island radar profiler site on 19 August 1993, the day on which the highest ozone concentration of the study was observed. The flow reversal began at High Island about 0900 CST (1000 CDT), and it persisted until about 1400 CST (1500 CDT), at which time the gulf breeze was re-established. The depth of the flow reversal and the gulf breeze that followed was approximately 1200 m agl, which was much deeper than the conditions observed during the 10 August episode. This pattern of onshore-offshore-onshore flow through a layer a few hundred meters deep, with the flow reversal occurring in the morning hours, was very consistent during the study period.

Given the results presented above, the following conclusions can be drawn about the cause of the flow reversal that accompanies ozone episodes in southeast Texas. During the daytime on most study days, the synoptic-scale pressure gradient and the mesoscale pressure gradient, which is produced by the differential heating of the land relative to the water, combine to produce onshore (southerly) flows. At night on most days, the cooling of the land relative to the water produces an offshore-directed mesoscale pressure gradient, but the onshore-directed synoptic pressure gradient is stronger than the offshore mesoscale pressure gradient, resulting in the winds in the region continuing to blow onshore, but at lower wind speeds. However, on some days the synoptic-scale pressure gradient weakens or reverses. As explained in the preceding section describing the synoptic meteorology of the ozone episodes that occurred in 1993, this is likely due to the Bermuda high shifting westward over the Gulf region. At night on these days, the land breeze forms, and the winds in the region reverse and blow offshore, augmented perhaps by the offshore-directed pressure gradient. During the day, an onshore-directed mesoscale pressure gradient forms as the air over the land becomes warmer than the air

over the Gulf, which once again produces a gulf breeze and southerly winds. Thus, the flow reversal appears to be a land breeze that is produced by the interactions between the synoptic-scale environment and locally produced mesoscale conditions.

Based on analyses of the surface and upper-air wind data collected during ozone episodes in southeast Texas in 1993, a conceptual model of the development of stages of the gulf/land breeze circulation and the flow reversal is shown in Figure 3-25 (examples of the analyses that were used to develop this conceptual model are presented in Section 3.5 for the 19 August episode, and in Appendix F). There were six stages in the development of this onshore-offshore-onshore flow reversal pattern:

- Stage 1 commenced with the development of the gulf breeze on the day preceding an exceedance day, and was characterized by steady onshore flow at virtually all observing stations. Stage 1 flows typically persisted from the afternoon/early evening preceding an exceedance day to 0400–0500 CST on the exceedance day.

- Stage 2 occurred during the early morning hours (0500–0700 CST), and was characterized by the development of offshore winds at inland sites and at the shoreline, but onshore winds continued at the offshore stations, out to distances of at least 120 to 150 km, producing a convergence zone near the shoreline.

- Stage 3 occurred during the morning daylight hours (0700–1000 CST), and was characterized by steady offshore winds at all stations, including those offshore. Offshore winds were observed out to at least 125 to 150 km into the Gulf.

- Stage 4 occurred during the late morning-early afternoon (1100–1300 CST), and marked the start of the gulf breeze. The gulf breeze was first observed at the shoreline sites. Offshore (northerly) winds continued at stations farther inland, producing a convergence zone onshore as the gulf breeze front propagated inland; offshore winds also continued at High Island Platform and buoys located in the Gulf, producing a divergence zone offshore.

- Stage 5 occurred during early afternoon (1300–1500 CST), and was characterized by steady onshore flow behind the gulf breeze at the inland stations, but offshore winds persisted at the offshore stations, maintaining the divergence zone offshore.

- Stage 6 was characterized by the development of steady onshore flow accompanying the gulf breeze at all stations, including those offshore. It was first observed in the middle of the afternoon, and persisted the rest of the night. Stage 6 represented the start of the Stage 1 flow pattern for the next day.

Finally, the general surface and meteorological conditions aloft that were observed in the Louisiana portion of the study area were similar in many respects to the conditions observed in southeast Texas (time-series plots of surface observations are available in Schoell et al., 1994b; time-height cross sections of the Louisiana radar profiler data are available in Dye et al., 1994). Figure 3-26 shows an analysis of the north-south velocity component (V_n) calculated from the surface wind data measured at the Cocodrie radar profiler site, along with the analysis of the across-Gulf pressure gradient shown

previously in Figure 3-20. The same 12-hour and 24-hour running average filters that were applied to the data shown in Figure 3-20 were applied to the wind velocity and pressure difference data shown in Figure 3-26. According to these analyses, the gulf/land breeze circulation also occurred along the Louisiana coastline, and the correlation with the orientation of the synoptic-scale pressure gradient was also evident, although perhaps not as strongly as was the case for southeast Texas. As was seen offshore in southeast Texas, the gulf/land breeze circulation was also observed offshore at the Ship Shoal radar profiler site (Schoell et al., 1994a).

The same type of analysis as that presented in Figure 3-26 was performed to examine the north-south component of the winds measured at the Louisiana State University radar profiler site in Baton Rouge, and is shown in Figure 3-27. Again, a diurnal north-south circulation was frequently observed. At Louisiana State University, the relationship between the development of a north-south flow reversal and the orientation of the synoptic pressure gradient was not as strong as that seen at Cocodrie or in southeast Texas. Instead, the winds appeared to be more in quasi-geostrophic balance. The flow reversal occurred most often when the synoptic-scale pressure gradient was weak (less than approximately 0.1 mb). Additional analyses of the meteorological conditions observed onshore and offshore in Louisiana, similar to the ones presented in this section for southeast Texas, are given in Appendix E.

Figure 3-28 shows the upper-air data measured at the Cocodrie and Louisiana State University radar profiler sites on 19 August 1993, which was a day when ozone concentrations in Baton Rouge exceeded the NAAQS. The offshore winds of the flow reversal were first observed at Cocodrie at 0600 CST (0700 CDT); they persisted until about 1600 CST (1700 CDT), when the southerly winds of the gulf breeze were first observed. At Louisiana State University, a similar pattern was evident: northerly to northwesterly winds began about 0600 CST (0700 CDT) and persisted until approximately 1600 CST (1700 CDT). Southwesterly winds were first observed at Louisiana State University at about 1800 CST (1900 CDT). Given the distance from the coast to the Louisiana State University site, it is not clear that the flow reversal is a true sea/land breeze circulation. Rather, the winds may simply have been responding to the region-wide reversal in the mesoscale pressure gradient produced by the diurnal cycle of heating and cooling, in the same manner a "true" sea/land breeze was produced at the shoreline.

ANALYSES OF MIXING DEPTHS AND BOUNDARY LAYER DEVELOPMENT

Mixing depth is defined as the altitude above the surface through which vigorous vertical mixing occurs (Holzworth, 1972). During the daytime, the mixing depth is defined as the altitude of a stable layer or a temperature inversion capping a well-mixed convective boundary layer (CBL). At night, identification of the top of the mixed layer is more complicated because often several stratified layers exist with weak vertical mixing confining surface-based pollutants to the lowest several hundred meters in the nocturnal boundary layer (NBL). At present, there is no overall accepted definition of mixing depth at night (Beyrich and Weill, 1993).

The depth of the mixed layer is a critical parameter for understanding the formation, dispersion, and transport of ozone and ozone precursors that lead to pollution episodes. This section describes how mixing depths were estimated during the GMAQS using data collected by the network of 915-MHz radar profilers and Radio Acoustic Sounding Systems (RASS) deployed in southeast Texas and Louisiana. To evaluate the quality of these mixing depth estimates, they were compared to subjectively analyzed mixing depths from aircraft data collected during spirals, and the results are presented in this section. In addition, several examples of the evolution and structure of the atmospheric boundary layer (ABL) at inland, shoreline, and offshore sites during ozone episodes are presented.

As discussed in an earlier section, seven 915-MHz radar profilers and RASS were deployed to monitor winds and virtual temperatures (T_v) aloft. Besides measuring winds and temperature, the refractive index structure parameter (C_n^2) can be computed from the radar's reflectivity measurements. This parameter measures the variations in the refractive index of the atmosphere, which are produced when turbulence creates gradients in humidity. Theoretical work by Wyngaard and LeMone (1980) showed that maximum values of C_n^2 occur at the top of the mixed layer, where warm drier air above the inversion mixes with cooler moist air below (i.e., strong humidity gradients). Recently, White (1993) estimated mixing depths using C_n^2 data from 915-MHz radar profilers and demonstrated that C_n^2-derived mixing depths compare well with mixing depths inferred from rawinsonde data collected during the daytime in a CBL.

Mixing depths were estimated using C_n^2 data during the day and T_v data at night and during the early morning. Daytime mixing depths were estimated from C_n^2 data using an algorithm developed by Dye et al. (1995) as part of this project. The algorithm processed 30-second data and computed a median profile of C_n^2 data for 30- and 60-minute periods. The maximum value of C_n^2 in each median profile was classified as the mixed layer depth for that period. An advantage of this approach is that C_n^2 can be computed from 140 m to about 4000 m agl, whereas the altitude coverage for T_v was typically between 140 and 1000 m agl. Consequently, during the daytime, C_n^2 was used to resolve deep boundary layers. One limitation of this technique was that C_n^2 could not fully resolve shallow, surface-based mixed layers below about 300 m msl.

To identify the height of the NBL at night, T_v profiles measured by RASS were combined with T_v measured at surface monitors. The height of the NBL was identified as the altitude where the temperature lapse rate changed from subadiabatic (i.e., stable) to adiabatic. Virtual temperature profiles were also used to monitor the initial growth of the CBL during the morning. The depth of the morning CBL was estimated using an algorithm developed by Holzworth (1972), which has historically been applied to twice-per-day NWS rawinsonde data to estimate mixing depths. With this approach, the mixing depth was estimated as the altitude at which a surface air parcel, if lifted adiabatically, would intersect the temperature sounding (i.e., the altitude where the air parcel became cooler than the ambient air). At offshore profiler sites a marine boundary layer (MBL) was commonly observed. Both C_n^2 and T_v data were used to identify the capping inversion or stable layer associated with the top of the MBL.

To evaluate the quality of the C_n^2-derived mixing depths, they were compared to mixing depths estimated from aircraft profiles of pollutant concentrations, turbulence, and temperature. Aircraft made morning and midday spirals near the profilers. Figure 3-29 shows a comparison of mixing depths during the midday spirals (typically between 1000 and 1300 CST). The agreement is quite good, except for one outlier, which can be explained by the difficulty in identifying one mixing depth using aircraft data when several layers were observed. As expected, comparisons made during the mornings showed that shallow mixed layers (typically less than 200 m agl) were not resolved by the C_n^2 data. However, these shallow mixing depths were resolved in the surface and aloft T_v data. Comparisons between the T_v-derived and the aircraft-estimated mixing depths were comparable to those shown in Figure 3-29.

The combined C_n^2- and T_v-derived mixing depths provided 24-hour estimates of the mixing depth at the profiler sites during this study. Mixing depth estimates were computed at each radar profiler site during the ozone episodes selected for analysis and are contained in Appendix G. In addition, mixing depths during each of the ozone episodes are described in greater detail in Section 3.5.

Significant differences between the structure and evolution of the inland and offshore mixing depths were observed due to the temperature differences between the land and waters of the Gulf. To illustrate these different types of boundary layer evolutions, Figure 3-30 shows time-series plots of mixing depth for 19 August 1993 at the four profiler sites in southeast Texas. Mixing depths were estimated from both the C_n^2 and T_v data using the techniques discussed above. Mixing at inland sites at Houston and Port Arthur showed large diurnal changes from shallow mixing in the NBL at night to deep mixing in the CBL during the day. At night, the depths of the NBL were typically less than 300 m msl, and the reflectivity data identified a layer aloft at about 500 m msl associated with the top of the marine air that flowed onshore during the gulf breeze. Shortly after sunrise, the CBL grew as thermals vertically mixed heat, moisture, momentum, and pollutants upward. By afternoon, the depth of the CBL ranged from 1500 to 2000 msl. At sunset these thermals decayed and the stable conditions of the NBL returned.

As illustrated in Figure 3-30d, the marine layer offshore showed modest diurnal variations with depths ranging from 500 to 1000 m msl. The marine layer typically deepened to about 1000 m msl during the period of offshore flow associated with the land breeze, which usually lasted from 0700 to 1200 CST. This deepening was likely due to increased levels of turbulence associated with air that had a fetch over land. After about 1200 CST, the marine layer lowered due to subsiding air associated with the return flow of the developing sea breeze circulation. At Galveston (Figure 3-30c), the boundary layer had characteristics of the convective and marine boundary layers depending upon wind direction. During the morning (0600–1100 CST), offshore winds created a CBL typical of inland locations and the mixing depth increased rapidly. This growing CBL was undercut by the gulf breeze that passed at 1200 CST, which brought cooler, stable marine air from the Gulf.

The spatial extent of mixing was also examined by plotting mixing depths computed from the profiler-based and aircraft data. Figure 3-31 shows morning and midday

mixing depths in the southeast Texas region estimated from these data for 19 August 1993. During the morning, the mixing was confined to the lowest 300 m msl over most inland locations. By midday, there was a relatively strong north-south gradient of mixing over the region, with the deepest development over urban areas. This observation is consistent with urban heat island effects and previous studies of mixed layer development in urban versus rural areas.

Cross sections of mixing depth using C_n^2 were used to diagnose the structure and evolution of the mixed layer during the 9–11 August 1993 episode. An example of this type of analysis is shown in Figure 3-32. The figure shows an analysis of the mixed layer in an approximate southeast-northwest cross section extending from the offshore High Island Platform radar profiler site (to the left in the figure) onshore to the Southeast Houston radar profiler site (to the right in the figure). The figure shows contours of normalized C_n^2 ($C_n^2/C_{n\,max}^2$) computed from the radar profiler data collected on 10 August 1993 at approximately 1300 CST (1400 CDT in the figure). The radar reflectivity data were normalized by the maximum value of C_n^2 observed by each profiler to account for differences in computed C_n^2 values due to different instrument configurations. The top of the mixed layer is indicated by values of $C_n^2/C_{n\,max}^2$ close to one. Note that the $C_n^2/C_{n\,max}^2$ data are calculated between stations by simple interpolation, so some features shown may not be real. The vertical wind profiles measured by the profilers are also shown in Figure 3-32. In addition, below the cross section the vertical profiles of ozone measured by one of the GMAQS aircraft as it spiraled at each of the profiler sites are plotted, as well as the vertical profiles of C_n^2. Note the good agreement between the profiler-based estimates of the top of the mixed layer and the aircraft observations of ozone concentrations.

This analysis shows that the northerly component of the flow reversal was still present both offshore at High Island and onshore at Southeast Houston, but that the gulf breeze had begun at Galveston by 1300 CST (1400 CDT). This pattern was characteristic of Stage 4 flows in the conceptual model presented in the previous section. The mixed layer over Houston was quite deep, approximately 2300 m agl, and the aircraft data showed that indeed ozone was being mixed to these altitudes. At the shoreline at Galveston, the marine layer had undercut the convective boundary layer, so that the mixed layer was only about 500 m deep. Interestingly, the mixed layer was somewhat deeper offshore at High Island, which was likely the result of somewhat greater levels of turbulence associated with the offshore flow.

An analysis of the development of the mixed layer during the 19 August 1993 ozone episode in southeast Texas, similar to the one shown in Figure 3-32, is presented in Figure 3-33. The figure presents offshore-onshore cross sections of normalized C_n^2 and vertical wind profiles measured at the profiler sites at three different times: 0500 CST (0600 CDT in the figure), 1000 CST (1100 CDT), and 1500 CST (1600 CDT). The first panel also shows contours of virtual potential temperature along the cross section, which were analyzed from the RASS measurements made at each profiler site. As indicated by the analyses presented in Figures 3-32 and 3-33, a relatively strong onshore-offshore gradient in mixing depth developed over the region as the day progressed, with the deepest mixed layers observed inland over the urban area of Southeast Houston.

At 0500 CST, the southerly to southwesterly winds of the gulf breeze were observed at all three sites (Stage 1). The mixed layer was approximately 800 to 900 m deep and was relatively uniform along the cross section, indicating the presence of the top of the marine layer over the region. As indicated by the vertical lapse rate of virtual potential temperature, the C_n^2 analysis at this time did not detect the top of the NBL, which was shallower and at an altitude that the C_n^2 analysis was unable to resolve fully.

At 1000 CST (1100 CDT), a growing CBL was evident over Southeast Houston, with the top of the mixed layer at approximately 1200 m (Stage 3). Offshore at High Island, the mixed layer appeared to have deepened to approximately 1000 m, which may have reflected increased turbulence in the offshore winds of the flow reversal. However, at the shoreline, the top of the mixed layer was at about the same altitude as it was at 0500 CST (0600 CDT), although increased C_n^2 values indicated mixing was occurring over a layer from approximately 200 m agl (roughly the first altitude at which C_n^2 was computed) up to approximately 1200 m agl.

By 1500 CST (1600 CDT), the southeasterly winds of the gulf breeze were again observed at all three stations (Stage 5). With the inland push of marine air from the Gulf, the top of the mixed layer (really the top of the marine layer) offshore at High Island and at the shoreline at Galveston was uniform and relatively shallow (approximately 500 m). At about 1200 m msl, the remnants of a developing daytime CBL were evident at the shoreline, which had been undercut and capped off by the penetration of the marine air accompanying the passage of the gulf breeze. Farther inland, the CBL had deepened to approximately 1900 m msl.

Boundary layer evolution on most episode days was similar to that shown in these examples. However, day-to-day variability in the depth of the mixed layer was caused by other meteorological events such as widespread clouds, fronts, and thunderstorms.

ANALYSES OF HYDROCARBON AND CARBONYL COMPOUND DATA

Surface NMOC Composition

Figure 3-34 shows the average composition of the abundant hydrocarbon species and the carbonyl compounds by time of day at Gilchrist. In the morning, the NMHC concentrations were as much as 5 times higher than later in the day, while most of the carbonyl compound concentrations were about 25 percent lower. The highest concentrations at Gilchrist occurred on the morning when winds were offshore. This is consistent with lower mixing heights in the morning and transport of hydrocarbons emitted in the Houston urban/industrial area to Gilchrist. The composition of the morning samples also differed from the composition later in the day (when winds were typically onshore). For example, olefins and aromatic hydrocarbons were more abundant in the morning and the relative contributions of hexane and other C6 paraffins to the total NMHC were lower later in the day. At midday, concentrations of isoprene and most carbonyl compounds were generally highest.

At Cocodrie (Figure 3-35), the composition remained relatively unchanged during the day. Hydrocarbon concentrations were lowest midday and highest in the morning while carbonyl compound concentrations were highest midday and lowest in the morning. The average composition at Cocodrie was similar to the Gilchrist midday and afternoon composition. However, the average hydrocarbon concentrations at Cocodrie were two to three times higher all day than the Gilchrist midday and afternoon concentrations.

Figure 3-36 shows the median concentrations of the abundant hydrocarbon species at Clinton for the morning, midday, and afternoon hours, which correspond to the canister sampling times at the other sites. The median was chosen because there were a large number of outliers in the data set at this site and these values tended to skew the average. The concentrations of most species were highest in the early morning except for *i*-butane, *n*-butane, 2- and 3-methyl pentanes, and *n*-hexane, which were highest during the period 1600–1800 CST, possibly due to evaporative emissions. Concentrations were typically lowest at midday, probably because of the higher mixing height at this time compared to the other two sampling periods.

Hourly statistics for August 1993 were plotted for all species measured by continuous GC including the minimum, maximum, average, and 25th, 50th, 75th, and 90th percentiles. These plots were useful for showing the typical diurnal profiles and for investigating species outliers. Diurnal plots were also prepared for the 17–21 August intensive sampling period. By comparing these sets of plots, the intensive period may be placed in perspective with the rest of the month. Appendix B shows the plots for all the species and species groups that were prepared. Figure 3-37a shows that C5 paraffin concentrations appeared to be relatively high on 19 August 1993 (200 ppbC at 1300 CST). However, this outlier was lower than other outliers observed during the month of August (see Figure 3-37b). The high NMHC concentration observed on 19 August is discussed further at the end of Section 3.4.

Figure 3-38 shows diurnal profiles of acetylene (associated with motor vehicle exhaust) and isoprene (associated with biogenic emissions) for the August episode. Acetylene concentrations peaked during the commute period (0500–0800 CST). Isoprene concentrations rose rapidly near sunrise and declined rapidly at sunset; concentrations were highest during the late afternoon. These profiles are representative of the monthly averages and are consistent with the emission sources of these species.

Investigation of the remainder of the species measured by the Clinton continuous GC showed the following: most species had many outliers with very high concentrations; most species had peak concentrations during the period 0500–0700 CST; and most species had a second peak in concentration in the afternoon/evening (1500–2100 CST). Olefins typically had higher concentrations in the afternoon than in the morning (particularly C4 and C5 olefins). These species are present from primary emissions. For the August episode, there were significant deviations from the typical diurnal profiles described above. For example, high concentrations of propane and C4 paraffins were observed during the period 0100–0400 CST on 17, 18, 19, and 20 August. High toluene concentrations were observed during the period 2000–2200 CST on 18 and 19 August.

These large variations in species concentrations at Clinton might be due to variations in meteorological parameters (including wind speed, wind direction, and mixing height) at the sources or along the transport route, or to variations in emissions, or to variations in chemical reaction rates.

Surface NMOC/NO_x and NMHC/NO_x Ratios

At the Gilchrist shoreline site, 24 of the 29 NMOC/NO_x ratios were above 10. Of the five exceptions, three were observed during the 1600–1800 CST sampling period and two were observed during the morning. Four of the samples had similar NMHC, total carbonyl compound, and NO_x concentrations. The other sample, collected at 0500–0700 CST on 1 August, had NMHC and NO_x concentrations about 2 to 3 times higher than the other samples; in addition, 16 of the 29 ratios were above 20. At Cocodrie, all 19 of the ratios were above 10, while 13 of the 19 ratios were above 20.

Figure 3-39 shows the diurnal variation of NMHC/NO_x ratios at Clinton for the August episode and statistics for the month of August (NO_x data were unavailable for 17, 18, and 19 August). The median ratios during August exceeded 10 for most of the day except during the morning (0500–0900 CST), when the ratios varied between 5 and 10. The ratios were highest in the afternoon and evening. On 20 and 21 August, NMHC/NO_x ratios were below 10 during the period 0300–1200 CST on both days and also dropped to 10 or below on 21 August after about 1800 CST. The NMHC/NO_x ratio in this source-rich area was seldom above 20.

Aircraft NMOC Composition

Hydrocarbon and carbonyl compound samples were collected during aircraft flights at two average altitudes, 220 and 3100 m msl, to characterize the mixed layer and top boundary, respectively. Plots were prepared of the average composition of the abundant hydrocarbon species and the carbonyl compounds for the morning and midday flights at these altitudes. For the lower altitude flights (Figure 3-40), higher concentrations of isoprene and carbonyl compounds and lower concentrations of ethene, propene, and aromatic hydrocarbons were observed at midday than in the morning. For the higher altitude samples, the average concentrations were very low (less than 2 ppbC per species), contained no isoprene and few olefins, and changed little with time of day (see Appendix H). Carbonyl compound concentrations measured at the higher altitudes, on the other hand, were similar to concentrations measured at the lower altitudes.

Aircraft NMOC/NO_x Ratios

Almost all (209 of 215) NMOC/NO_x ratios collected aloft in Texas were greater than 10. Of the six exceptions, three occurred in the morning and three in the midday/afternoon. The morning samples with lower ratios were observed at Beaumont and Houston (18 August) and Baytown (28 July). Ozone concentrations in these samples

were below 12 ppb. NO concentrations were 7 to 11 ppb, and NO_x concentrations were 17 to 28 ppb. The NMOC concentrations in these samples varied from 153 to 209 ppbC. In the afternoon, all the ratios below 10 were observed at Baytown (11, 13, and 25 August). The ozone concentrations varied from 41 to 61 ppb in these samples, higher than the morning samples with NMOC/NO_x ratios below 10. However, the NO and NO_x concentrations varied over the same range as the morning samples with ratios below 10. About 75 percent of the ratios were over 20.

In Louisiana, 53 of the 55 NMOC/NO_x ratios collected aloft were greater than 10. The two exceptions were Baton Rouge (11 August, 1100 CST) and Houma-Terrabonne (19 August, 0800 CST). Ozone (48, 59 ppb), NO (3, 5 ppb), NO_x (11, 12 ppb), and NMOC (110, 116 ppbC) concentrations were very similar in these two samples. The composition of these samples was similar to that of other samples collected at that location. In addition, 50 of the 55 ratios were over 20.

Surface and Aircraft NMOC Comparison

Comparisons were made of hydrocarbon and carbonyl compound concentrations in samples collected at the surface and at nearby or offshore aloft locations. Grab samples collected aloft were matched with the 1- or 2-hour surface samples during which grab samples were collected. Three such comparisons are discussed here. Samples collected aloft over Baytown and surface samples at Clinton were compared to investigate a suspected hydrocarbon-rich source region. Samples collected aloft over Ship Shoal and High Island platforms and surface samples at Cocodrie and Gilchrist were compared to investigate the differences and similarities between the offshore and shoreline NMOC.

Figure 3-41 shows the concentrations of the abundant NMHC species and carbonyl compounds at Gilchrist and aloft near High Island Platform on the morning of 20 August. Winds were offshore at Gilchrist and NMHC concentrations were high, indicating influence from the Houston urban/industrial area emissions. Carbonyl compound concentrations were higher at Gilchrist than offshore, except for acetone and C5 carbonyl compounds. The weight fractions of NMOC show that the hydrocarbon composition in the morning at Gilchrist differed significantly from the composition offshore (Figure 3-42). Specifically, ethene, propene, and C3–C6 paraffins were relatively more abundant at Gilchrist than at High Island Platform. The offshore samples showed significantly higher fractions of 2,3-dimethyl pentane and 2,4,4-trimethyl-1-pentene than the shoreline sample. The EPA's emission profile data indicate that these species are most abundant in gasoline exhaust profiles. However, these species consistently appear in higher proportions in the offshore aloft samples than in the onshore.

By midday of 20 August, the winds were onshore and the NMHC concentrations at the two locations were more similar (Figure 3-43) than in the morning. Concentrations were still higher at Gilchrist than aloft over High Island Platform; however, the two samples had very similar weight fractions for most species. Trajectory analyses (see Section 3.6) showed that air parcels originating near the shoreline could have been carried offshore as far as High Island Platform prior to the transition at midday to onshore flow. Considering all matches of the data, formaldehyde, acetaldehyde, and C4 carbonyl

compounds were nearly always present at higher concentrations at the shoreline than offshore, whereas acetone, C6, and C7 carbonyl compounds were nearly always present at higher concentrations offshore than at the shoreline (see Appendix I).

Figure 3-44 shows the concentrations of the abundant NMHC species and carbonyl compounds at Cocodrie and aloft near Ship Shoal Platform on the morning of 19 August. Hydrocarbon concentrations were very similar at both sites, although the offshore sample had somewhat higher concentrations. The acetone and C5–C7 carbonyl compound concentrations were higher offshore than at the shoreline. In the afternoon, the composition and concentration at the shoreline and aloft offshore were similar. In general, acetone, C6, and C7 carbonyl compound concentrations were nearly always higher offshore than at the shoreline. Trajectory analyses showed that air parcels originating near the shoreline could be carried offshore, although it is unclear how far offshore.

Eighteen matches of Clinton surface samples and samples collected aloft near Baytown were investigated. Although these sites are 29 km apart, the NMHC concentrations showed good agreement between the surface and aloft except for six samples. These samples had NMHC concentrations of 200 ppbC or less at Baytown but over 450 ppbC at Clinton. Five of these samples were collected in the early morning. An investigation of the air quality data collected during the spiral showed that these aircraft samples were collected above the surface layer and, therefore, one might expect the surface sample to have a higher concentration. However, on other mornings, surface and aircraft hydrocarbon concentrations were similar when the aircraft sampled above the surface layer.

Figure 3-45a shows the ozone, NO, and NO_x concentrations measured during the spiral over Baytown on the morning of 20 August (an example in which the NMHC concentration aloft did not match the surface NMHC). A layer was present between about 400 and 480 m msl with relatively high NO_x (40 ppb) and depleted ozone concentrations. (The hydrocarbon and carbonyl compound samples were collected between 460 and 60 m msl.) This layer appears to be relatively fresh. A layer aloft with high NO_x and low ozone concentrations was observed frequently in the morning flights and occasionally in the afternoon flights. Figure 3-45b shows an air quality profile on a morning when the surface and aircraft NMHC matched well. This spiral showed several layers aloft as well.

The sample species-by-species comparisons for Baytown/Clinton typically showed one of the following three results: the aircraft concentrations were greater than the surface concentrations for all species and the profiles were different, the C2–C4 species had higher concentrations in the aircraft but the rest of the species concentrations were higher at the surface, or most of the species concentrations at the surface exceeded the concentrations aloft and the profiles were similar. Figure 3-46 shows the comparison of the surface data and data collected aloft on 20 August. In the morning, the surface concentrations were higher than concentrations measured aloft. In the midday, however, the aircraft C2–C4 species were present in higher concentrations and in different proportions than at the surface. The emission sources that affected the midday sample aloft appeared to be different from those affecting the surface sample. The frequent differences between the NMHC composition at the surface and aloft and the presence of

NO_x layers aloft over Baytown may indicate that the aircraft often flew through air parcels associated with a particular source (one with an elevated plume rise) that differed from the source(s) influencing the surface NMHC composition.

Relative Reactivity of NMHC

A comparison was made of the relative reactivity of the offshore emission profiles with the reactivity of the average composition of samples collected at the surface at Cocodrie and Gilchrist and aloft at Ship Shoal and High Island platforms. The emission profiles used to represent offshore emissions included natural gas seeps (California Air Resources Board no. 550), oil and gas production-fugitives-unclassified (EPA no. 1010), fixed roof tank-crude oil production (EPA no. 0296), and fixed roof tank-crude oil refinery (EPA no. 0297). These profiles are shown in Figure 3-47; note that the profiles lump many hydrocarbons together, such as isomers of hexane. The four profiles are composed nearly entirely of paraffins.

The maximum incremental reactivity (MIR) scale developed by Carter (1991) was used to characterize the NMOC reactivity of the samples. The MIR scale provides an estimate of moles ozone formed per mole carbon of each organic species measured, where the ozone formation estimates are intended to be used in a relative rather than absolute manner. The reactivity of each compound is estimated by multiplication of its mole percent by its MIR factor, and the reactivity of the sample is estimated by summing the reactivity of its constituents. The average ambient data were normalized without unidentified mass, which was a significant contributor to the total carbon (up to 30 percent). The carbonyl compounds were not considered for this comparison because MIR factors have not yet been assigned to most of the C4+ carbonyl compounds. The estimated total MIR values are provided in Table 3-5. The samples collected at the shoreline (Cocodrie and Gilchrist) have total reactivities that are similar to or higher than those of the emission profiles on a composition basis. In comparison, the offshore aircraft data have up to 50 percent more reactive composition than the shoreline data or up to twice emission profile reactivity. The offshore aircraft data have higher weight percent ethene, C6+ alkanes, and 2,4,4-trimethyl-1-pentene, with ethene as the most important species on a weight-percent basis.

Surface and Aircraft NMOC Analyses—Conclusions

- NMHC species distributions were highly variable both at the surface (Clinton) and aloft (all spiral locations).

- Almost all (209 of 215) NMOC/NO_x ratios measured aloft in Texas were greater than 10; 159 of 215 were greater than 20. Similarly, at the Gilchrist shoreline site, 23 of the 29 NMOC/NO_x ratios were above 10; 16 of 29 were above 20.

- In Louisiana, 53 of the 55 NMOC/NO_x ratios measured aloft were greater than 10; 50 of 55 were greater than 20. At the Cocodrie shoreline site, all 19 NMOC/NO_x ratios were above 10; 13 of 19 were above 20.

Table 3-5. Relative reactivity estimates (mol ozone/mol carbon), based on Carter (1991) MIR.

Data	Total MIR*
EPA profile 1010[a]	.19
EPA profile 0296[b]	.15
EPA profile 0297[c]	.18
ARB profile 550[d]	.14
Cocodrie 0700–0900[e]	.19
Cocodrie 1200–1400	.22
Cocodrie 1700–1900	.19
Gilchrist 0700–0900	.23
Gilchrist 1200–1400	.23
Gilchrist 1700–1900	.22
High Island Platform (all samples)	.29
Ship Shoal Platform (all samples)	.31
Reference compounds:	
Ethane	.05
Propane	.1
n-Butane	.19
i-Butane	.21
n-Cyclohexane	.34
Toluene	.51
Ethylene	1.6

* Unidentified compounds excluded.
[a] Oil and gas production - fugitives - unclassified
[b] Fixed roof tank - crude oil production
[c] Fixed roof tank - crude oil refinery
[d] California Air Resources Board - natural gas seeps
[e] CDT

- The shoreline hydrocarbon composition was similar to the aircraft hydrocarbon composition measured near offshore platforms under onshore flow conditions. Trajectory analyses showed that air parcels originating near the shoreline could be carried offshore in the morning as far as High Island Platform prior to the wind shift to onshore flow later in the day.

- Average hydrocarbon profiles observed aloft near platforms were dominated by paraffins and toluene; however, when considered on a weight-percent basis, a significant portion of the composition was attributed to ethene and 2,4,4-trimethyl-1-pentene to make the relative reactivity of the offshore samples higher than the average shoreline samples. The average NMHC composition both offshore and at the shoreline was relatively more reactive (up to twice) than the ARB and EPA emission profiles.

- Carbonyl compounds accounted for a large fraction of the carbon, often more than 50 weight percent, in the aloft samples and an average of 35 percent at the shoreline surface sites.

- C3+ carbonyl compounds accounted for about a quarter of the total carbon and more than half of the total carbonyl compounds on average at the surface. However, current PAMS (Photochemical Assessment Monitoring Stations) guidelines call for collection and analysis of carbonyl compounds for only formaldehyde, acetaldehyde, and acetone. Studies in other parts of the country also indicate the significance of the higher carbon number carbonyl species (see Table 3-6).

Table 3-6. C3+ carbonyl compound concentrations and the contribution of these species to total NMOC and carbonyl compounds measured at the surface during the 1993 GMAQS (this work), 1994 Northeast Air Quality Study (Blumenthal et al., 1995), and the 1987 Southern California Air Quality Study (Lurmann et al., 1992).

Surface Data	C3+ Carbonyl Compound Concentration (ppbC)	Contribution to NMOC (wt %)	Contribution to Total Carbonyl Compounds (wt %)
GMAQS 1993	21	22	62
NEAQS 1994	51	33	72
SCAQS 1987	60	9	53

INVESTIGATION OF HIGH NMHC CONCENTRATIONS DURING THE AUGUST EPISODE AT CLINTON

As discussed above, a high NMHC concentration was observed at Clinton during the period 1300-1400 CST on 19 August 1993. Apparently, the high NMHC concentration was principally due to high C4 and C5 alkane concentrations, possibly resulting from increased emissions from a fuel spill. Documentation showed that there was a petroleum product spill on 19 August in the ship channel area. The emission inventory was adjusted for the base-case modeling runs to account for the observed hydrocarbon concentration increase on 19 August. In this analysis, the Clinton data were used to independently investigate whether or not the high NMHC concentration on 19 August might have had a significant effect on ozone concentrations that day. The continuous GC data at Clinton for August were first screened to find days on which the ozone production capability was similar to that of 19 August; i.e., clear, sunny days, with similar maximum solar radiation and peak temperature. Next, the hydrocarbon data were investigated on the resulting days to determine if there were high (outlier) concentrations during the period 0900-1300 CST. NMHC and C4 and C5 alkane data were considered outliers if concentrations were at or above the August 90th percentile for that hour. The 90th percentile concentrations were about 500 ppbC NMHC, 30 ppbC C4 alkanes, and 90 ppbC C5 alkanes.

Table 3-7 shows the six days (including 19 August) that were clear and sunny and had NMHC, C4, and C5 concentrations above the 90th percentile. Table 3-8 summarizes the total NMHC and C4 and C5 alkane concentrations, total reactivity estimate, and the percent unidentified carbon in these samples. The C5 alkane concentrations are further split into the more-reactive iso- and cyclopentanes, which were quantified together, and the less-reactive *n*-pentane. On 10, 11, and 19 August, the ozone concentrations exceeded the NAAQS. On these days, the NMHC concentrations ranged between 531 and 932 ppbC, the C4 alkane concentrations ranged between 53 and 136 ppbC, C5 alkane concentrations ranged between 144 and 220 ppbC, and the iso- and cyclopentane concentrations were greater than the *n*-pentane concentrations by a factor of two or more. The total reactivity of the samples during the selected hours on these days ranged from 166 moles ozone on 19 August at 1300–1400 CST to 354 moles ozone on 10 August at 1100–1200 CST. On 5 and 16 August, peak ozone concentrations were lower than those observed on the exceedance days (64 and 104 ppb), and the C5 alkane

Table 3-7. Maximum temperature, solar radiation, and ozone concentration observed in the Houston area during August 1993.

Day	Max. Temperature (°C)	Max. Solar Radiation (W/m^2)	Max. Ozone (ppb)
5 August	34.5	837	64
10 August	34.3	859	170
11 August	33.9	840	145
16 August	33.9	878	104
19 August	35.4	907	231
24 August	34.6	860	68

composition was different from that observed on the exceedance days, with much higher proportions of *n*-pentane. Note, however, that while the C4 alkane concentrations were lower on these two days, the total NMHC concentrations were above 900 ppbC and total reactivity was above 340 moles ozone. On 24 August, the NMHC concentrations were 430 ppbC, and the C4 and C5 alkane concentrations were above the 90th percentile (47 and 104 ppbC, respectively). The C5 alkane composition was also similar to the composition on the exceedance days. The total reactivity of 156 moles ozone was within 10 percent of the reactivity of the 19 August sample. However, on this day the peak ozone concentration in the region did not exceed 70 ppb.

Thus, the peak ozone concentrations exceeded the NAAQS on several clear, sunny days during August with similar maximum temperature and solar radiation (conducive to ozone production); with high concentrations of NMHC, C4 alkanes, and C5 alkanes; and with a ratio of iso- and cyclopentanes to *n*-pentane of more than 2. However, on at least one day that met all the aforementioned criteria (24 August), ozone concentrations did not rise above 70 ppb. Furthermore, the estimated total reactivity on 24 August was within 10 percent of the total reactivity of the 19 August sample. Finally, the total reactivity of the 5 August sample was one of the highest of the samples investigated;

Table 3-8. Dates and times during which the continuous GC samples had high NMHC concentrations, C4 and C5 alkane concentrations, total reactivity estimate, and weight percent of unidentified carbon.

Day	Time of Day (Hour, CST)	NMHC (ppbC)	C4 Alkanes (ppbC)	C5 Alkanes (ppbC)			Total Reactivity Σ(MIR[a] ppbC) (moles ozone)	Weight Percent Unidentified
				iso- and Cyclopentane	*n*-Pentane	Total		
5 August	11	962	2	15	381	396	341	31
10 August	09	531	53	99	54	154	185	19
	10	728	95	145	76	220	250	14
	11	952	136	123	56	179	354	15
	12	721	121	125	56	181	235	14
11 August	09	595	52	106	39	144	275	20
16 August	12	914	4	25	347	372	483	24
19 August	13	538	57	146	59	205	166	14
24 August	13	430	47	76	28	104	156	22

[a] MIR = maximum incremental reactivity. Species concentrations in ppbC multiplied by the Carter reactivity in maximum moles ozone/mole carbon. Values are summed to obtain an estimate of the total reactivity. Note that the unidentified carbon is not included in the reactivity estimate.

however, on this day the peak ozone concentration in the Houston area was less than 70 ppb. This investigation illustrates that an unusually high NMHC or C5 concentration itself does not necessarily produce an unusually high regional ozone concentration maximum, and that other factors such as mesoscale meteorological conditions likely dominate the production of ozone in the Houston area.

3.5 CASE STUDIES OF OZONE EPISODES

CASE STUDY OF THE 17-20 AUGUST 1993 OZONE EPISODE

During the period 17-20 August 1993 the NAAQS for ozone was exceeded at a number of monitoring sites in the Houston area. The highest ozone concentration observed during the GMAQS occurred during this episode, when 231 ppb of ozone was measured at the Aldine site in Harris County, north-northeast of downtown Houston, at 1600 CST on 19 August. As was shown in Figure 3-12, this episode consisted of buildup days on 17 and 18 August, with no exceedances on 17 August, but with ozone concentrations reaching 100 ppb at several sites east of Houston. On 18 August, five exceedances of the NAAQS for ozone were recorded in the Houston area. On 19 August, nine sites exceeded the NAAQS for ozone. Other than the 231 ppb recorded at Aldine, maximum ozone concentrations at the other exceedance sites ranged from 141 to 177 ppb, with all but one concentration in the range 160 to 177 ppb. On 20 August, eight sites exceeded the NAAQS for ozone; the highest concentration observed was 187 ppb at the HRM 11 site east of Houston and north of Galveston Bay. Maximum ozone concentrations at the remaining exceedance sites ranged from 129 to 185 ppb.

The pattern of the exceedance region shown in Figure 3-12 suggests transport of ozone from urban regions to downwind receptors. Figure 3-48 shows an objective analysis of hourly ozone concentrations, surface winds, and contours of the onshore-offshore component of the surface wind (component perpendicular to the shoreline) for six times on 19 August. The times of the analyses were chosen to represent air quality and meteorological conditions during the six stages of the onshore-offshore-onshore flow reversal, which was presented in an earlier section. Conditions during Stage 1 (steady onshore flow), Stage 2 (start of the land breeze), and Stage 3 (steady offshore flow of the land breeze) are reflected in Figures 3-48a through 3-48c, which show the analyses for 19 August 1993 at 0400 CST, 0600 CST, and 0900 CST, respectively. Conditions during Stage 4 (land breeze inland and offshore; start of the gulf breeze at the shoreline), Stage 5 (gulf breeze onshore; land breeze offshore), and Stage 6 (steady onshore flow of the gulf breeze) are shown in Figures 3-48d through 3-48f, which present the analyses for 19 August 1993 at 1100 CST, 1400 CST, and 1600 CST, respectively.

On 19 August, the onshore winds of the gulf breeze during Stage 1 were generally southwesterly, which reflects the clockwise turning of the winds with time produced by the Coriolis force since the development of the gulf breeze on the preceding day. Note that the buoy data near 28°N latitude also showed generally southerly winds. At the shoreline, ozone concentrations were low (10 to 30 ppb), and NO_x concentrations (not shown) were 1 to 2 ppb. At the inland stations, ozone concentrations were near zero as

a result of titration of ozone overnight by fresh NO emissions (NO_x concentrations observed at the inland stations were 10 to 30 ppb). As the land breeze formed during Stage 2, ozone concentrations near the shoreline decreased to a few ppb, while NO_x concentrations near the coastline (not shown) increased to 10 to 20 ppb, which indicated transport of fresh emissions from urban-industrial sources southward and offshore by the land breeze. By 0900 CST, the steady offshore winds of the land breeze (Stage 3) were present at all the stations, including offshore at the High Island Platform radar profiler site. The surface winds shown in Figure 3-48c indicated that emissions from the Houston area were being transported to the southeast, toward Galveston Bay.

The normal buildup of ozone precursors during the morning hours occurred during Stage 4 (Figure 3-48d), as the northwesterly winds of the land breeze continued to transport precursors from Houston to the southeast side of the city. The highest ozone concentrations during Stage 4 were observed southeast of Houston. At 1100 CST, the onshore winds of the gulf breeze were reported at the stations nearest the shoreline. Emissions from onshore sources that had been carried offshore by the land breeze were likely beginning to be transported back onshore about the time ozone concentrations were beginning to increase onshore. Likewise, there was evidence of a local sea breeze (a "bay breeze") off Galveston Bay at the stations along the western shoreline of the bay. Farther inland, and offshore at the High Island Platform, the northerly winds of the land breeze were still observed.

As shown in Figure 3-48e, by 1400 CST, the onshore winds accompanying the gulf breeze (Stage 5) were reported at virtually all sites except the offshore stations and the buoys located near 28°N latitude. Several exceedances of the NAAQS for ozone had occurred by 1400 CST, with maximum ozone concentrations of 125 to 145 ppb reported by air quality stations east and northeast of downtown Houston. Near the coastline, ozone concentrations were generally in the range of 70 to 80 ppb; one site, Texas City, reported 104 ppb of ozone. This was the highest concentration observed near the shoreline on 19 August 1993. Surface winds, which were generally southeasterly, had reversed nearly 180 degrees from the winds of the land breeze earlier in the day. The high ozone concentration observed at Texas City may have been the result of ozone produced near the shoreline or offshore during the land breeze, which was then transported back onshore by the gulf breeze.

A similar situation likely occurred on 20 August, when the air quality station at Gilchrist reported 114 ppb of ozone at 1200 CST, during the hour when the land breeze ended and the gulf breeze began at Gilchrist. At 1300 CST on 20 August, the ozone concentration at Gilchrist was still 115 ppb in the onshore winds of the gulf breeze. Ozone concentrations at Gilchrist continued to decline, until by 1600 CST they were 65 ppb. These results suggest that ozone produced onshore was transported offshore by the land breeze, and/or that there may have been some production of ozone offshore in the land breeze. The winds of the gulf breeze then transported this ozone back onshore.

The maximum ozone concentrations observed on 19 August occurred at 1600 CST, at the beginning of the steady onshore flows (Stage 6) of the gulf breeze. As shown in Figure 3-48f, the area of maximum concentrations had moved northwestward, farther inland, and was located northeast and north of downtown Houston. As the gulf breeze

pushed through the area, ozone concentrations near the coast and along the shoreline of Galveston Bay decreased to 50 to 60 ppb. North of Galveston Bay, several sites exceeding the NAAQS for ozone earlier during Stage 5 reported ozone concentrations of 100 ppb or less. For example, the site at HRM 11 reported 140 ppb of ozone at 1500 CST. By 1600 CST, ozone at HRM 11 had decreased to 101 ppb; by 1700 CST (not shown), the ozone concentration had further declined to only 60 ppb.

In conjunction with the analyses presented above, the upper-air data measured at the radar profiler sites and high-resolution satellite imagery were used to estimate the seaward extent of the land breeze and to examine the timing of the maximum ozone concentrations relative to the development of the onshore winds of the gulf breeze. The three panels in Figure 3-49 show time-height cross sections of the upper-air winds measured by the profilers located at Southeast Houston, Galveston, and High Island. Surface winds measured by the collocated 10-m towers at each site are also shown in each panel. The heavy dark lines are approximate estimates of the top of the boundary layer at each site, as determined from analyses of C_n^2 and RASS temperature profiles.

According to the surface data collected at Galveston, the first offshore winds of the land breeze on 19 August occurred at 0600 CST (0700 CDT in the figure). The upper-air data showed that the land breeze appeared aloft about 1 hour later, and that the depth of the land breeze layer increased over the next few hours. This pattern is similar to that observed during the passage of a weather front. Offshore at High Island, the surface data indicated that on 19 August the offshore winds of the flow reversal first occurred at approximately 0800 CST (0900 CDT), or about 2 hours after the flow reversal was first observed at Galveston. Aloft, the winds were still southerly. As at Galveston, the first upper-air observations of the flow reversal at High Island occurred 1 to 2 hours later, and the depth of the flow reversal layer increased over the next few hours, again suggesting the passage of a front.

The average wind speeds of the land breeze observed at Galveston and High Island were approximately 2.5 m/s, or about 5 knots. Assuming that these wind speeds were representative of the airflows between Galveston and High Island, onshore air that crossed the shoreline was only transported about 18 km offshore during the 2 hours that elapsed between the first appearance of the flow reversal at Galveston and at High Island. Thus, it is very unlikely that the first appearance of the flow reversal at High Island coincided with the arrival of air that had originated onshore. Instead, the initial appearance of the flow reversal at High Island appeared to be due to the general reversal of the mesoscale onshore-offshore pressure gradient over the region, in a manner similar to that observed in Louisiana. As shown in Figure 3-48d, the northerly winds of the flow reversal were observed at the offshore buoys located near 28°N latitude as early as 1100 CST (no data from these stations were available for previous hours). Given the wind speeds observed over the region, it is extremely unlikely that these offshore winds were the "land breeze" per se. That is, the air moving southward past the buoys at 1100 CST did not originate over the land, but rather originated somewhere between the shoreline and the buoys. In a similar manner, the air passing the High Island profiler site in the first few hours of the flow reversal originated somewhere between the shoreline and the platform.

High-resolution visible satellite imagery showed that a narrow line of cumulus clouds had developed about 10 to 15 km off the southeast Texas coast by 0730 CST (0830 CDT), or about 90 minutes after the land breeze first appeared at Galveston. This cloud line was roughly parallel to the shoreline, and the imagery showed that it propagated southward toward the High Island site as the morning progressed. According to the satellite imagery, the rapid growth of the mixed layer at High Island during the period 1000-1100 CST (1100-1200 CDT), shown in Figure 3-49c, and the rapid decrease during the period 1100-1200 CST (1200-1300 CDT), coincided with the arrival and passage of the line of cumulus clouds. The increase in the mixed layer was likely due to increased turbulence associated with cumulus convection. Likewise, the decrease in the mixed layer was likely produced by subsidence behind the line of cumulus clouds; indeed, the satellite imagery showed skies completely free of clouds from behind the cloud line to the coast. It appears as though the clouds formed behind the leading edge of the land breeze "front." The cloud line was likely produced by the land breeze front wedging under the still landward-directed winds aloft; this in turn produced vertical mixing of air parcels to the lifting condensation level (LCL), where clouds developed. It therefore appears that the line of cumulus clouds served as a marker for the movement of the "real" land breeze (air that originated onshore and was being transported offshore). Likewise, the upper-air data collected at High Island showed when air that had originated onshore passed the platform site.

The offshore winds of the land breeze continued for approximately another 3 hours at High Island on 19 August. Given that the average wind speeds in the land breeze remained about 2.5 m/s, air that originated onshore likely was transported only another 20 to 30 km offshore beyond the High Island site before the gulf breeze developed and transported air back toward shore.

The satellite imagery was also helpful in identifying the inland propagation of the gulf breeze. The visible imagery showed a line of cumulus clouds along the leading edge of the gulf breeze "front," and clearing behind the front. As was the case for the land breeze, the reversal of the winds from offshore to onshore occurred over a wide area within a short period of time, in response to the reversal of the mesoscale pressure gradient. The gulf breeze "front" marked the leading edge of the marine air moving inland, that is, air that had originated offshore. The surface wind data and the satellite imagery showed that the maximum ozone concentrations observed on each day of this episode preceded the passage of the gulf breeze front. Prior to the passage of the front, ozone concentrations increased at a station as the southerly winds of the onshore component of the flow reversal transported ozone that had been produced upwind (to the south) into downwind receptor areas. Once the front passed, ozone concentrations declined. Thus, the passage of the gulf breeze "front" at a station usually marked the time when ozone concentrations stopped increasing at that station.

To illustrate the discussion just presented, Figure 3-50 shows a time-series plot of ozone, NO_x, NO, surface winds, and temperature at Aldine (TN10) on 19 August 1993. The land breeze was last observed at Aldine at 0900 CST, and the first winds of the onshore component of the flow reversal were observed at 1000 CST. From 1000 CST until the time of the maximum ozone concentration at 1600 CST, the winds at Aldine were generally southerly to southeasterly at approximately 2 to 3 m/s. Ozone concentrations

remained less than 100 ppb through 1300 CST. As shown in Figure 3-48, however, ozone concentrations were increasing at stations southeast of Aldine. During the period 1400–1600 CST, the ozone concentration at Aldine increased rapidly from 111 to 231 ppb. During the period 1600–1700 CST, the surface winds were southeasterly, with wind speeds about 3 m/s. During this period, the ozone concentration at Aldine decreased to about 100 ppb. The wind shift during the period 1800–1900 CST marked the passage of the gulf breeze front. The rapid buildup of ozone at Aldine preceded the arrival of the gulf breeze front. Ozone concentrations began to decrease prior to the arrival of the gulf breeze front, although NO_x concentrations remained elevated. Once the gulf breeze front passed, ozone and NO_x concentrations decreased.

The peak day of the 17–20 August ozone episode occurred on 19 August. A number of exceedances occurred on 20 August, but none were as high as the 231 ppb observed at Aldine on 19 August. Analyses of the surface meteorological data collected on 19 and 20 August did not reveal any significant differences in the development of the flow reversal or the movement of pollutants through the region that might explain why 19 August was the peak day. However, the upper-air data presented in Figure 3-49 for 20 August do indicate some important differences. The mixing depth analysis performed using the Southeast Houston radar profiler data showed that there was a rapid increase in mixing depth at Southeast Houston on 20 August during the period 1200–1300 CST (1300–1400 CDT in the figure), a time when maximum ozone production was likely occurring. The maximum ozone concentration observed on 20 August (187 ppb) occurred at 1400 CST. No such rapid growth of the mixed layer was observed on 19 August, and the maximum ozone concentration on the 19th was not observed until 1600 CST, 2 hours later than on 20 August. On 20 August, in the course of one hour, the depth of the mixed layer nearly doubled from about 1200 to 2400 m. The increased mixing and dilution that accompanied this event may explain why ozone concentrations stopped increasing after 1400 CST and did not reach higher values on 20 August.

Additional information on the air quality conditions and the mixed layer aloft was obtained from aircraft flights performed on 18 and 19 August. Figure 3-51 shows the vertical profiles of ozone, NO_x, NO, and temperature measured during the morning spirals on 18 August at Houston Hobby Airport (HOU; Figure 3-51a) and Baytown (HPY; Figure 3-51b), and on 19 August at Houston Hobby Airport (Figure 3-51c) and Andrau (AAP; Figure 3-51d). The data presented in Figure 3-51 are generally representative of the observations collected during all the aircraft spirals on the mornings of 18 and 19 August (refer to Anderson et al., 1993 and 1994 for a summary of aircraft operations and the data collected during the sampling flights).

On 18 August (Figures 3-51a and 3-51b), a shallow nocturnal boundary layer (NBL) extended from the surface to 200 to 400 m msl, and was characterized by high values of NO_x and NO, which represented plumes aloft and fresh emissions of NO_x emitted near the surface that had not been well mixed in the stable NBL. Above the NBL, a layer of relatively clean air (20 ppb of ozone and 1 to 2 ppb NO_x) extended to approximately 800 m msl. As indicated by the upper-air data shown in Figure 3-49, this layer coincided with the gulf breeze inflow layer. At Southeast Houston (Figure 3-49a), the winds in the gulf breeze inflow layer were southwesterly veering to westerly as the

morning progressed, turning in response to the Coriolis force. The wind data aloft and the C_n^2 analysis showed that the top of the gulf breeze inflow layer was near the top of the layer of clean air observed in the spiral at Houston.

Above the gulf breeze inflow layer, there was a layer of aged pollutants (60 to 90 ppb ozone, 5 ppb NO_x, minimal NO) that extended to approximately 1400 m msl. In this layer, the winds aloft were easterly to southeasterly. This layer was likely a carryover, or residual, layer from the previous day, and represented the remnants of the convective boundary layer (CBL) that developed on 17 August. The winds in this layer were consistent with synoptic-scale flows around the Bermuda high, which had retrograded westward from its position on 17 August. Ozone produced on 17 August had been initially transported eastward by westerly winds aloft on 17 August (see Dye et al., 1994). As the high-pressure system moved westward, winds aloft in the lower troposphere shifted easterly to southeasterly. It was likely that the carryover of pollutants observed on 18 August was the result of the transport of pollutants produced on 17 August eastward, and then recirculated back into the area on 18 August. A layer of 60 to 90 ppb of ozone 400 m thick, when mixed into the 1200 to 2000-m-deep mixed layer observed on 18 August, would add at most about 10 to 20 ppb of ozone to the total ozone observed on this day (this estimate ignores factors that might have lessened the contribution of carryover ozone, such as transport and photochemistry processes). Thus, the potential contribution of these aged pollutants to ozone concentrations on 18 August was likely not too significant, even though the maximum ozone concentrations observed on 18 August were in the range of 130 to 140 ppb.

The data for 19 August shown in Figure 3-51 do not indicate any such carryover of pollutants from 18 August to 19 August. The stable NBL was again present on 19 August, as indicated by the high concentrations of NO_x and NO from the surface to approximately 200 m msl observed in the spirals at Houston and Andrau. The gulf breeze inflow layer was again present, and some fresh emissions were present in this layer at Houston. No fresh emissions were evident in the gulf breeze inflow layer at Andrau, which was upwind of the Houston urban center. Above the top of the gulf breeze inflow layer, there was relatively clean air (60 to 70 ppb ozone), with no evidence of any significant carryover of pollutants from 18 August. Winds aloft in the gulf breeze layer overnight were 5 to 7.5 m/s. It was likely that these strong flows during Stage 6 of the flow reversal were effective at ventilating the area and transporting pollutants out of the region. This issue is addressed in more detail in a following section that discusses transport processes aloft. Regardless, it is postulated based on this analysis that the high ozone concentrations observed on 19 August cannot be fully explained by carryover of ozone from 18 August to 19 August, nor by the transport of ozone into the region from possible emission areas upwind.

CASE STUDY OF THE 10 AUGUST 1993 OZONE EPISODE

During the period 9–11 August 1993 the NAAQS for ozone was exceeded at a number of monitoring sites in the Houston area. The highest ozone concentrations of this episode were observed on August 10, when nine sites exceeded the NAAQS for ozone of 125 ppb. As was shown in Figure 3-11, the exceedances occurred along a 40-km-wide

swath extending from Houston to northwest Harris County. The highest ozone concentration of 172 ppb was measured at the Galleria site (west of Houston). Maximum ozone concentrations were lower south of Houston and along the coastline. Lower ozone concentrations were measured on 9 and 11 August, with only one exceedance of 145 ppb on 11 August.

The pattern of the exceedance region shown in Figure 3-11 suggests transport of ozone from urban regions to downwind receptors. Figure 3-52 shows a time series of hourly ozone concentrations from four sites along the axis of exceedances. The southern sites (Monroe and Houston Regional Monitoring Site 1) located near the source region peaked earliest, while northern sites (Lang and Northwest Harris) peaked several hours later, implying downwind transport. Note that ozone concentrations at the Monroe site stopped increasing at 1300 CST (1400 CDT in the figure). As discussed below, this is the result of a bay breeze off Galveston Bay passing through the area.

Figure 3-53 shows the vertical profiles of temperature, ozone, and NO_x measured on 10 August during the morning and afternoon aircraft spirals performed near the High Island Platform, Galveston, and Southeast Houston radar profiler sites (Southeast Houston was located next to the spiral point at the Houston Hobby Airport). All the morning spirals showed relatively clean air, with ozone concentrations ranging from 30 to 50 ppb. The morning spirals at Galveston and Houston Hobby showed the influence of local sources, indicated by plumes of NO_x aloft in the Houston Hobby spiral and higher NO_x concentrations in the lowest 150 m of the Galveston spiral.

By afternoon, air quality conditions aloft at the urban site (Houston Hobby) differed substantially from the conditions observed near the coast and offshore. Ozone and NO_x concentrations over the High Island and Galveston profiler sites were basically similar and indicated relatively clean air. The spiral at Houston Hobby, on the other hand, showed very polluted air from the surface to 2300 m msl. Ozone and NO_x were nearly constant from the surface to 900 m. Above 900 m, ozone and NO_x concentrations slowly decreased with altitude, but pollutant concentrations were still significantly higher than those observed a few hours earlier.

The synoptic-scale meteorological conditions on 9–11 August 1993 were characterized by a broad high-pressure ridge over the southern United States. The 500-mb ridge retrograded westward and was centered over eastern New Mexico by 10 August. The 850-mb high retrograded southwestward from western Tennessee on 9 August to southeast Texas on 10 August. Air quality conditions on 10 August were characterized by weak winds, which increased insolation and reduced clouds and thunderstorms.

Figure 3-54 shows the winds measured aloft by the GMAQS profilers on 10 and 11 August. These data indicate that the winds above about 1000 m were generally consistent over the region; they show easterly winds aloft, characteristic of clockwise flow around the southern portion of the high that had shifted westward. However, below 1000 m the winds changed in response to diurnal forcing (e.g., the sea/land breeze circulation). As stated earlier, the development of the flow reversal coincided with a period when the synoptic-scale pressure gradient across the Gulf reversed as the

center of the Bermuda high shifted westward. This allowed the diurnally forced, onshore-offshore pressure gradient to produce a sea/land breeze circulation.

A gulf breeze occurred on all three episode days, although with different onset times and depths. The solid lines in Figures 3-54b and 3-54c denote the gulf breeze. On 10 August, the gulf breeze arrived 3 hours later at Galveston and 7 hours later at Southeast Houston than on 11 August. Also, the gulf breeze was 150 to 200 m shallower on 10 August than on 11 August. The top of the gulf breeze front was typically characterized by wind shears of 20 to 30 degrees; the RASS temperature profiles (Dye et al., 1994) showed increased stability across the front. On 10 August, the easterly winds at Southeast Houston from 1400–1500 CST (1500–1600 CDT in the figure) suggested that a bay breeze off Galveston Bay arrived about 2 hours ahead of the gulf breeze front. The occurrence of a bay breeze was supported by satellite imagery, which showed clearing behind the front. The bay breeze front is indicated in Figure 3-54c by the solid line preceding the gulf breeze. Onshore flow generally persisted well into the night and early morning. At Houston and Galveston on 10 and 11 August, the onshore flow continued from midnight until about 0400 CST (0500 CDT).

The northerly winds of the early morning flow reversal were evident in all three profiler data sets. At Galveston, the land breeze started by 0400 CST (0500 CDT) on both days, but persisted much longer on 10 August (until 1100 CDT). The duration of the land breeze at Galveston was 6 hours on 10 August, but only about 2 hours on 11 August. At Southeast Houston, the land breeze lasted 4 hours longer on 10 August than on 11 August. The combination of the onshore flow of the gulf breeze and the development of the northeasterly winds of the land breeze produced a convergence zone, which is shown by the thick dashed line in Figures 3-54b and 3-54c.

The structure of the marine layer and the development of the convective boundary layer during this episode were examined using three parameters measured by the radar profilers: vertical velocity, virtual temperature (T_v), and the refractive index structure parameter (C_n^2). Figure 3-55 shows objectively analyzed time-height cross sections of C_n^2 measured at the High Island, Galveston, and Southeast Houston radar profiler sites, with annotations to indicate vertical motions, the location of the gulf breeze front, and the estimated top of the mixed layer. The purpose of the discussion that follows is to use the 10 August episode to demonstrate the general characteristics of the development of the boundary layer offshore, at the shoreline, and inland during an ozone episode.

The top of the marine boundary layer offshore at High Island (dotted line in Figure 3-55a) showed little diurnal variation. The depth of the marine layer increased from 600 m on 10 August to 800 m on 11 August. Vertical velocities (not shown) at High Island were generally less than ± 0.5 m/s and generally near zero on both days. Evolution of the boundary layer near the coastline at Galveston (Figure 3-55b) showed more diurnal variation. Between midnight and 0400 CST (0500 CDT in the figure) on both days, the onshore flow accompanying the land breeze was capped by a weak inversion from 600 to 800 m. A surface-based radiation inversion limited vertical mixing to the lowest 100 m during the night, but by 0700 CST (0800 CDT) a convective boundary layer (CBL) was developing. By 0800 CST (0900 CDT), stronger vertical motion (e.g., +1 m/s) increased the depth of the CBL. Ahead of the gulf breeze, low-

level convergence resulted in deep updrafts extending to 1600 m. In and above these updrafts, C_n^2 was very high, indicating scattering from strong turbulence and large cloud droplets. On 10 August, the CBL was undercut by the gulf breeze. In response to the marine air moving onshore, the boundary layer top lowered from 900 m at 1000 CST (1100 CDT) to 450 m at 1300 CST (1400 CDT). Development of the boundary layer on 11 August was similar to that of 10 August, but with weaker updrafts along the gulf breeze front and a deeper afternoon mixed layer.

Boundary layer evolution in Houston (Figure 3-55c) was more characteristic of an inland CBL. From midnight until 0500 CST (0600 CDT) on both days, the boundary layer was 500 to 600 m deep, which is explained by the inland penetration of marine air during this period. Passage of the convergence zone at 0500 CST (0600 CDT) on 10 August and 11 August was indicated by very high radar reflectivity and updrafts extending from 100 to 2200 m. On 10 August, the CBL grew from 700 to 1600 m during the period 0700–1300 CST (0800–1400 CDT). Large vertical velocities during the period 0900–1300 CST (1000–1400 CDT) contributed to the growth of the CBL. Deep updrafts ahead of the bay breeze produced strong radar reflectivities, suggesting strong turbulence and cloud development. As the gulf breeze passed, the profiler measured another deep updraft. Behind the gulf breeze, strong downward motion (-1 m/s) occurred during the period 1500–1600 CST (1600–1700 CDT). On 11 August, the vertical development of the CBL was more rapid and extended higher than on 10 August. In addition, strong vertical motion occurred even after the gulf breeze passed, suggesting that the marine air was destabilized and significantly modified as it moved inland.

The remaining discussion in this section links air quality and meteorological observations to provide a conceptual model of the 9–11 August ozone episode. Differences between mesoscale and synoptic-scale processes on 10 August are compared to 9 and 11 August to help explain why the highest ozone concentrations occurred on 10 August.

Conditions were not as conducive to high ozone on 9 August because extensive showers and thunderstorms occurred that reduced insolation and increased mixing. On 11 August, stronger winds and deeper mixing resulted in only one exceedance, well downwind of Houston at the Northwest Harris site.

The three dominant mesoscale features were the land breeze, the bay breeze, and the gulf breeze. A significant feature that distinguished 10 August from 9 and 11 August was the delay in the pressure gradient reversal from offshore to onshore, which produced a land breeze of longer duration. On 10 August, the reversal occurred about 2 hours later than on 9 or 11 August. This delay allowed the land breeze to continue until midmorning. It is thus likely that emissions from the Houston region were transported southward in the morning to the south side of the city. Ozone began forming by midmorning and then moved northwestward as the bay breeze and gulf breeze moved through the area. On 9 and 11 August, the duration of the land breeze was too short to allow emissions to accumulate and produce significant levels of ozone before the gulf breeze ventilated the area. The persistence of the gulf breeze during the nighttime hours suggests that it was an efficient mechanism for removing ozone-polluted air from the region.

The location of the 500-mb ridge over eastern New Mexico and the 850-mb high over southeast Texas weakened the synoptic-scale pressure gradient and produced conditions favorable for the flow reversal and higher ozone concentrations observed on 10 August. These conditions included increased subsidence, which reduced cloud development and suppressed thunderstorms, and increased insolation, which enhanced diurnal forcing and augmented ozone chemistry.

Strong convection that preceded the bay and gulf breezes deepened the CBL and mixed ozone and NO_x throughout the CBL. When the gulf breeze passed surface monitoring sites, ozone concentrations generally decreased as stronger winds increased dilution and transported cleaner marine air into the region. The afternoon aircraft spiral on 10 August at Galveston showed relatively low pollutant concentrations because the gulf breeze had passed Galveston about 3 hours earlier. Pollutants that were mixed upward into the upper portions of the CBL, and perhaps subsequently vented into the lower troposphere by convective activity, were then subjected to steady transport conditions that carried the air westward. These conditions, along with ventilation by the gulf breeze, help explain the apparent lack of day-to-day carryover of pollutants, as was indicated by the aircraft data; this in turn helps explain why 11 August was not a day on which higher ozone concentrations were observed.

CASE STUDY OF THE 7-11 SEPTEMBER 1993 OZONE EPISODE IN SOUTHEAST TEXAS

During the period 7-11 September 1993, a total of 37 exceedances of the NAAQS for ozone occurred in the southeast Texas region, with 15 exceedances measured at sites located at or near the Gulf coast. This episode was substantially different from the 9-11 August and 17-21 August episodes because the highest ozone concentrations were measured at monitoring sites located within 10 to 20 km of the shoreline, whereas during the August episodes, they occurred within or north of the urban-industrial regions of Houston. Other meteorological and air quality differences between the September and August episodes are discussed in this case study. This section first describes the air quality and meteorological conditions observed on each day. After these descriptions, some of the phenomena that produced and transported ozone and ozone precursors during this episode are examined.

An overview of the ozone air quality for 7-11 September was discussed in an earlier section. As previously shown in Figure 3-13, this episode was unique because the highest ozone concentrations occurred near the coastline and at sites surrounding Galveston Bay. The episode consisted of a buildup day on 7 September with ozone concentrations generally less than 110 ppb, and four exceedance days when the maximum ozone concentrations ranged from 120 to 214 ppb. On 8, 9, and 10 September, the spatial pattern of ozone exceedances shown in Figures 3-13a, 3-13b, and 3-13c was similar, with highest concentrations measured at sites along the shoreline and near Galveston Bay. In fact, five of the eight sites that measured ozone concentrations greater than 170 ppb during this episode were located within 20 km of the coast. By 11 September, the region of exceedances shifted northward into the Houston region and the exceedance pattern was similar to that of the August episodes.

The time that each site measured its maximum ozone concentration during this episode was substantially different from the times in the August episodes, when peaks typically occurred during the period 1300–1500 CST. On 8, 9, and 11 September, most sites measured peak concentrations during the period 1200–1300 CST. However, on 10 September many sites extending from near the shoreline northward to Houston measured two ozone maxima. The first maximum occurred around midday; a second maximum occurred during the period 1600–1800 CST. Examples of these late ozone peaks are presented in Figure 3-56, which shows a time series of hourly ozone concentrations measured at four sites from Galveston to Houston on 10 September. At Galveston, ozone reached a maximum of 162 ppb at 1400 CST and remained above 100 ppb until 1900 CST. Notice that ozone at the Texas City and Seabrook sites peaked at 1200 CST, decreased during the period 1300–1500 CST, and then increased again after 1600 CST. In Houston, the two peaks at the Lang site were not very distinct. Many other sites in the Houston region measured two ozone maxima on this day. Another interesting feature was that ozone concentrations generally increased for 3 to 4 hours after the start of the onshore flow associated with the gulf breeze as shown by the arrows in Figure 3-56. This type of dual peak in the ozone data could have been caused by two distinct "clouds" of high ozone passing the monitoring sites or by ozone titration in the air parcels between the two peaks, or by shifts in wind direction. Additional analyses of transport on this day are presented later in this case study.

Figure 3-57 shows hourly ozone concentrations and surface winds at 0600 and 1400 CST for each day of this episode. Morning ozone conditions in this region were characterized by low concentrations ranging from 0–20 ppb in the urban regions to about 20–40 ppb at rural sites to the south and east of Houston. One exception to this observation occurred on 9 September, when ozone concentrations at 0600 CST were 10 to 40 ppb higher in the urban region of Houston, which may suggest that the background levels of ozone increased. Highest ozone concentrations in the afternoon showed considerable spatial variability from day to day as indicated in Figure 3-57. On the buildup day (7 September), ozone concentrations were low due to persistent offshore (northerly) flow observed throughout the day. Ozone concentrations on 8 and 9 September were highest between the ship channel and the shoreline, with the highest concentrations measured during offshore flow. In contrast, on 10 September the highest ozone concentrations were measured at shoreline sites, where the winds indicated onshore flow associated with the gulf breeze. On 11 September, ozone concentrations were highest at sites north of Houston.

Meteorological conditions observed during this episode were substantially different from those observed during the August episodes and were discussed in an earlier section. These differences included prevailing wind directions aloft, the location and origin of the high-pressure systems, and the 500-mb pattern. During the period 6–11 September, a series of three weak stationary fronts followed by continental high-pressure systems moved southeastward through the region and produced some clouds, but little or no precipitation. Northerly flow behind these continental high-pressure systems brought drier air into the region, which produced sunnier skies over the land and the Gulf on 7, 8, and 10 September. On 9 September, skies were clear over the Gulf, but the southeast Texas region was cloudy. Winds aloft during this episode were northerly and westerly and generally weaker than the synoptic easterly winds observed during the August episodes.

As was previously discussed, the gulf/land breeze circulation occurred during all ozone episodes in southeast Texas. Figure 3-58 shows time-series plots of wind and ozone concentrations measured at Gilchrist, Smith Point, and Seabrook during the period 7–11 September 1993. Typically, diurnal variations from onshore flow associated with the gulf breeze to offshore flow of the land breeze were observed at these sites. However, the onset times were earlier and the durations were longer than those observed during the August episodes. The offshore flow associated with the land breeze began during the period 0000–0200 CST, which was about 4 hours earlier than observed during other episodes. This offshore flow persisted until about 1200 CST at coastal sites and until 1500 CST at inland sites, which was about 2 hours longer than observed in August. The stronger land breezes were due to the synoptic-scale offshore pressure gradient reinforcing the mesoscale pressure gradient that was directed offshore during the night and early morning. When the land warmed during the daytime, the mesoscale pressure gradient switched to onshore and the synoptic pressure gradient (still offshore) inhibited the inland penetration of the gulf breeze. The strength and duration of the onshore flow generally matched that of the offshore flow. As discussed below, the gulf breeze did not push inland as far as during the August episodes.

Surface winds revealed many day-to-day differences during this episode, as shown in Figure 3-57. On 7 September, persistent offshore flow lasted most of the day; a weak gulf breeze flowed onshore at 1800 CST but did not penetrate far inland. Morning winds on the remaining days were somewhat similar, with offshore (northerly to northwesterly) flow measured at most sites. Although not shown in Figure 3-57g, the winds during the morning of 10 September were stronger than on most mornings. On 9 and 10 September, visible satellite images at 0730 CST showed a narrow line of clouds over the Gulf associated with the land breeze front, which indicated the farthest extent of the offshore flow. The land breeze front had generally passed the High Island Platform site by 0730 CST, as shown in Figures 3-57e and 3-57g. On the afternoons of 8 and 9 September, the gulf breeze pushed inland as indicated in Figure 3-57, but was opposed by northwesterly winds in the Houston region. The highest ozone concentrations occurred in the offshore flow ahead of the gulf breeze front, and lower ozone concentrations were measured behind it. By late evening the gulf breeze front had only reached about 100 km inland (just north of Houston). Early the next morning, when the flow reversal occurred, this air started flowing southward. On 10 September, the gulf breeze front penetrated further inland by 1400 CST. More important, highest ozone concentrations occurred in the marine air behind the gulf breeze, suggesting that ozone may have formed over the Gulf; these observations are addressed in greater detail later in this case study.

Winds aloft measured by the radar profilers also showed the features revealed in the surface data. Figure 3-59 shows winds from the Southeast Houston, Galveston, and High Island profiler sites for 9–10 September 1993. Note that missing winds at night were caused by interferences from migrating birds. On 9 September, the land breeze lasted from 0300 to 1100 CDT at the Galveston site. Offshore flow at the Southeast Houston site lasted from 0400 to 1800 CDT and hindered the inland propagation of the gulf breeze, which finally passed this site at 2100 CDT. On 10 September, the duration of the land breeze was much shorter and the gulf breeze penetrated inland faster. Also notice that aloft winds were weaker and varied more in direction than the persistent easterly winds measured aloft during the August episodes.

The rest of this case study examines the air quality and meteorological data in more detail to identify phenomena responsible for transporting ozone and ozone precursors during this episode.

A major distinguishing feature of this episode was that the large-scale synoptic weather patterns, which were different from those associated with other episodes, created conditions conducive to formation of high ozone concentrations. These conditions included:

- A synoptic pressure gradient directed offshore for much of the episode, which enhanced the land breeze and retarded the inland penetration of the gulf breeze
- Clearer skies over land and over the Gulf, which increased insolation
- Weaker and more variable winds aloft, which increased the chances of carryover of ozone or ozone precursors from one day to the next.

The synoptic-scale meteorological patterns during this episode produced longer periods of offshore flow that were stronger than those observed during the August episodes. Two types of offshore flow were observed: northerly synoptic flow on 7 September and northerly to northwesterly flow associated with the land breeze on 8–11 September. This offshore flow provided a mechanism for transporting shore-based ozone and ozone precursors over land as well as offshore into the Gulf of Mexico. Detailed analysis of these periods of offshore flow and the resultant onshore flow associated with the gulf breeze are presented below.

The episode began on 7 September with an 18-hour period of northerly to northeasterly winds associated with a high-pressure system moving into the area. These winds transported emissions from major source regions in the Beaumont/Port Arthur and the Houston regions southward over the Gulf. This southward transport was confirmed by a visible satellite image at 1630 CST on 7 September that showed a smoke plume from an agricultural burn near High Island, Texas extending southward over the Gulf. In a 2.5-hour period this plume was transported about 50 km over the Gulf. Trajectories computed with a diagnostic wind field model also indicated this type of offshore transport to the south and southwest; these trajectories are discussed in the next section. During this offshore flow, shore-based emissions were transported over the Gulf of Mexico and likely combined with OCSPD emissions.

On 8 and 9 September, the offshore flow associated with the land breeze was another important mechanism for transporting ozone and ozone precursors originating in the onshore source regions. As previously shown in Figure 3-57 for 8 and 9 September, highest ozone concentrations occurred ahead (i.e., to the north) of the gulf-breeze front when winds were offshore. Surface wind and air quality data during the period 0900–1100 CST suggest that the land breeze transported ozone and ozone precursors from the source regions in Houston southward to sites near the coast. For example, Figure 3-58b shows that the ozone concentrations at Smith Point on 8 September increased from 50 to 214 ppb during this period of offshore flow during the period 0700–1400 CST. Similar observations of this southward transport by the land breeze

were observed again on 9 September at Smith Point and other sites. The southward transport ceased when it encountered the northward-moving gulf-breeze front. This resulted in the highest ozone concentrations occurring ahead of the gulf-breeze front.

When the gulf breeze penetrated inland on 8 and 9 September, it generally took about 1 to 2 hours of steady onshore flow for the ozone concentrations to decrease significantly (i.e., below about 100 ppb). After about 2 hours of onshore transport, the marine air flowing onshore transported air with lower ozone and NO_x concentrations inland. This "clean-out" behind the gulf breeze was also observed during the August episodes. This observation suggests that the land breeze likely transported some shore-based emissions slightly offshore (e.g., less than 10 km), which underwent photochemistry over the Gulf. The resultant ozone was then recirculated back onshore in the marine air immediately ahead of the gulf breeze. After several hours of onshore transport, the ozone concentrations at coastal sites decreased substantially, indicating that the region of high ozone concentrations did not extend far out into the Gulf.

Air quality conditions on 10 September were an exception to the above discussion. On this day, the gulf breeze passed the Gilchrist site at 1200 CST, and ozone concentrations rose to 128 ppb at 1400 CST and remained above 100 ppb until 2000 CST during a period of persistent onshore flow of about 4 m/s. This 8-hour period of high ozone concentration implies that a region of high ozone extended significantly farther into the Gulf than on other days. Higher ozone concentrations in the marine air were also measured at Galveston (Figure 3-56) and Sabine Pass and at sites farther inland (see Figures 3-56 and 3-58).

The strong offshore flow (3 to 5 m/s) on the night of 10 September appeared to transport ozone and ozone precursors offshore. Once over the Gulf, these shore-based emissions likely commingled with OCSPD emissions and underwent photochemical change. Trajectories indicated that air parcels (and presumably shore-based emissions) originating over land during the morning (i.e., 0400–0900 CST) were transported between 10 to 50 km out into the Gulf before being recirculated back onshore by the gulf breeze.

Carryover of ozone and ozone precursors from one day to the next was an important aspect of this episode and one that was not generally observed during the August episodes. Two factors produced carryover of pollutants: an equal duration of the land and gulf breeze and weaker and more variable winds aloft. During the August episodes, the onshore flow associated with the gulf breeze lasted from 15 to 18 hours; consequently, it transported (i.e., ventilated) pollutants from the region. However, during this episode the duration of the gulf breeze was much shorter and did not penetrate far inland; thus, when the land breeze formed at night, the offshore flow recirculated ozone and ozone precursors back through the southeast Texas region. This "sloshing" of air back and forth likely allowed ozone and ozone precursor concentrations to build up. Winds aloft were light and variable, which likely produced little or no ventilation of pollutants out of the region as was observed during the August episodes.

Evaluating the contribution of OCSPD sources to ozone exceedances during this episode is difficult due to the extended periods of offshore flow that transported shore-based emissions over the Gulf. On 8, 9, and 11 September, the offshore extent of the land

breeze was not significantly far into the Gulf and lower ozone concentrations were observed in the marine air behind the gulf breeze than in front of the gulf breeze. However, on 10 September, emissions from onshore sources were transported offshore at least 50 km and likely commingled with OCSPD emissions over the Gulf. Photochemistry likely took place and the gulf breeze transported this marine air with higher ozone concentrations back onshore, and ozone concentrations behind the gulf breeze were higher than in front of it.

CASE STUDY OF THE 17–19 AUGUST 1993 OZONE EPISODE IN BATON ROUGE

The 17–19 August 1993 period was the only multiday episode during the summer of 1993 during which ozone concentrations exceeded the NAAQS in this region. Air quality data collected by surface monitors and aloft by aircraft were examined for evidence of transport of ozone and ozone precursors from OCSPD source regions in the Gulf of Mexico to the exceedance sites in the Baton Rouge area. Surface air quality and meteorological conditions are summarized first, followed by conditions aloft measured at the profiler sites. Next, detailed analyses examining the potential for transport of pollutants into the Baton Rouge area are discussed.

An overview of air quality and synoptic meteorological conditions was presented in Section 3.4, and plots of maximum ozone concentrations on each day of this episode are shown in Figure 3-14. Briefly, on the buildup day (17 August), the maximum ozone concentration reached 118 ppb at a site located southeast of Baton Rouge. By 18 August, exceedances occurred at a site in the East Baton Rouge Parish at 1400 CST and a second site in Dutchtown, 25 km southeast of Baton Rouge. The maximum ozone concentration measured on this day was 127 ppb. On 19 August, the site in Dutchtown exceeded at 1400 CST with an ozone concentration of 126 ppb. The synoptic meteorological conditions were conducive to high ozone concentrations when a high-pressure system moved westward into the area on 17 August and became stationary over southern Louisiana on 18 and 19 August. This high-pressure system produced clearer skies, lighter winds, and weaker pressure gradients.

Surface air quality and meteorological conditions during the period were analyzed for each hour of the episode. As examples, Figure 3-60 shows morning (0800 CST) and afternoon (1400 CST) ozone concentrations and surface winds for each day. During the buildup day (Figure 3-60a), strong northwesterly winds of 3 to 5 m/s were observed throughout the morning. By afternoon, the winds in Baton Rouge had weakened but still remained northwesterly until 1600 CST. Consequently, ozone concentrations of 90 to 118 ppb were measured at downwind sites southeast of Baton Rouge. The Cocodrie site on the Louisiana coast measured offshore winds (i.e., northerly) during the period 0000–1300 CST. By 1400 CST, the winds had switched to onshore, and ozone concentrations reached a peak of 98 ppb.

By morning of 18 August, winds were calm at most inland stations, and regional ozone concentrations were about 10 ppb higher than those measured on the previous morning.

Winds at Cocodrie were weak and directed offshore. In the Baton Rouge area, calm winds during the morning and early afternoon produced stagnation over the area. Highest ozone concentrations were measured at sites near Baton Rouge, with a peak concentration of 127 ppb measured at 1400 CST. Winds at coastline sites in Cocodrie and over the Gulf at Ship Shoal Platform changed from offshore to onshore at 1400 CST.

On the morning of 19 August, stronger northwesterly winds were observed, as shown in Figure 3-60e. Maximum ozone concentrations were again about 10 ppb higher than on the morning of 18 August, which suggests an increase in background concentrations. By the afternoon (Figure 3-60f), surface winds remained northwesterly at inland sites. These offshore winds persisted until 1800 CST before switching to onshore. Higher ozone concentrations were likely transported by these northwesterly winds from the Baton Rouge area to sites located 25 to 50 km to the southeast.

Wind data aloft, collected by profilers deployed at inland, shoreline, and offshore locations, were reviewed to identify periods of onshore flow capable of transporting OCSPD emissions from source regions over the Gulf of Mexico to the exceedance sites near Baton Rouge. Figure 3-61 shows the winds measured on 18 and 19 August by profilers at the Louisiana State University in Baton Rouge, at Cocodrie, and on the Ship Shoal Platform. Two periods of onshore flow were identified: the evening of 17 August and the evening of 18 August. The first period of onshore flow on 17 August was short-lived (i.e., 3 to 5 hours) and was only observed at Cocodrie and at Baton Rouge. At Cocodrie the winds were onshore with speeds of 5 to 7 m/s from the surface to 750 m agl during the period 1500-1700 CDT. Further inland at Baton Rouge, onshore flow occurred later during the period 1900-2300 CDT and was weaker (2 to 4 m/s). Over the Gulf at the Ship Shoal site, surface and winds aloft remained offshore all day on 17 August and until 1200 CDT on 18 August.

The second period of onshore flow on the evening of 18 August and overnight lasted longer and was observed aloft at all three profiler sites, as shown in Figure 3-61. By 1300 CDT, winds in Baton Rouge changed from light and variable to southerly at 2 to 4 m/s and remained southerly to southwesterly until 2300 CDT. At the Cocodrie and Ship Shoal sites, this onshore flow started about 2 hours later and persisted until about 0400 CDT on 19 August. Later in this section, these periods of onshore flow are examined as possible mechanisms for transporting OCSPD emissions onshore.

Another feature observed in the winds aloft on both nights preceding exceedance days was strong westerly to northwesterly winds associated with a low-level jet. Low-level jets form at night when the stable conditions in the nocturnal boundary layer decouple the winds aloft from surface frictional effects, causing the winds aloft to accelerate. As shown in Figure 3-61, this jet was noted only in the Baton Rouge area and was observed at around 300 m agl during the period 0000-0800 CDT on 18 August with speeds ranging from 5 to 8 m/s. Note that the surface winds at this time were calm. By midmorning on 18 August, the mixed layer began growing and convective mixing dissipated the low-level jet. The low-level jet observed on the morning of 19 August was stronger than the one noted on the previous night, with wind speeds of 5 to 10 m/s measured between 140 to 500 m agl. The ability of these low-level jets to transport ozone and ozone precursors is examined later in this case study.

The remainder of this section provides a conceptual model of the 17-19 August ozone episode and examines other data sources for evidence of transport of ozone and ozone precursors from OCSPD and other source regions into the Baton Rouge area.

On 17 August, meteorological conditions were not yet ideal for high ozone formation because the strong northwesterly winds during the morning diluted precursors and clouds reduced insolation. These northwesterly winds transported ozone concentrations ranging from 80 to 118 ppb to the southeast of Baton Rouge and appear to have transported higher ozone concentrations southward to Lafourch Parish and Cocodrie. Air quality conditions at Cocodrie for 17-19 August 1993 are shown in Figure 3-62. Notice in this figure that ozone concentrations increased during this period of offshore flow and then reached a peak of 98 ppb at 1400 CST, when the winds switched to southerly (onshore) associated with the gulf breeze. This high ozone concentration appears to have originated over land and to have been transported briefly over the Gulf and then recirculated back onshore. Also notice that the onshore flow period 1400-1600 CST was short-lived; winds returned to northerly and remained offshore until 1000 CST the next morning (18 August). Given the short duration of this onshore flow, it was unlikely that air parcels associated with OCSPD emissions were transported during this onshore flow more than 20 to 30 km inland and consequently did not contribute to the ozone episode on the following day (19 August).

During the period 0000-0800 CST on 18 August, the low-level jet observed in Baton Rouge could have transported ozone and ozone precursors into the region from regions to the west and southwest of Baton Rouge. This regional transport would increase the background ozone concentrations, and, when combined with locally produced ozone, would increase the chances for an ozone exceedance. By daybreak, the low-level jet dissipated as momentum, heat, and pollutants from the surface were mixed upward. In addition, any pollutants existing in layers aloft could have been mixed downward and combined with locally produced pollutants. Stagnant conditions developed over the areas as surface and winds aloft weakened, and insolation increased. This 3-hour period of stagnation was one major difference between conditions observed on 18 August and those of 17 and 19 August.

By the afternoon of 18 August, the onshore-offshore pressure gradient reversed and winds at all three profiler sites became southerly. This southerly flow was the longest period of onshore flow capable of transporting OCSPD emissions onshore. Surface air quality at Cocodrie was examined during this onshore flow for evidence of higher ozone or ozone precursor concentrations, as shown in Figure 3-62. During this onshore flow, ozone and NO_x concentrations ranged from 50 to 65 ppb and 3 to 5 ppb, respectively. One plume of aged NO_x (10 and 20 ppb) passed this monitor during the period 1900-2000 CST. Surface and upper-air trajectories from a diagnostic wind field model were used to determine how far north air parcels might have been transported during this period of onshore flow. These trajectories are discussed in greater detail in the next section. Forward trajectories started at Cocodrie and Ship Shoal every hour during onshore flow indicated that the farthest north that air parcels reached was New Orleans by 0600 CST on 19 August. These air parcels were then transported southeastward to Grand Isle, Louisiana by 1200 CST.

Conditions on 19 August were similar to those on the two previous days, but the low-level jet was stronger and winds remained offshore (northwesterly) at Baton Rouge throughout most of the day. Consequently, the highest ozone concentrations were measured 20 to 50 km southeast of Baton Rouge.

On 19 August, an aircraft flew morning and midday flights in this region to monitor air quality conditions aloft. The aircraft flew from Beaumont, Texas to the Ship Shoal Platform, and then northward to Baton Rouge during the morning and reversed this flight path during the afternoon (Anderson et al., 1993 contains details about the aircraft data). Aircraft data collected offshore and during spirals over Cocodrie and the Ship Shoal Platform showed low ozone concentrations of 40 to 60 ppb and low NO_x concentrations of about 2 ppb in the marine boundary layer (surface to about 600 m msl) during both the morning and midday flights. Ozone concentrations above the marine layer increased slightly to 60 to 70 ppb in the easterly, synoptic-scale flow aloft. As the aircraft flew northward toward Baton Rouge, higher ozone and NO_x concentrations were measured. During both flights, the highest ozone and NO_x concentrations were measured in the Baton Rouge area, while the lowest ozone and NO_x concentrations were typically measured during flights over the Gulf and the Louisiana coast.

Figure 3-63 shows ozone, NO, and NO_x concentrations and temperature measured during an aircraft spiral over Baton Rouge on the morning of 19 August. A layer aloft from 400 to 1000 m msl had high ozone concentrations ranging from 75 to 90 ppb. These high ozone concentrations were measured above the mixed layer, and winds at these altitudes were northwesterly at 2 to 3 m/s. Concentrations of NO were very low in this layer, suggesting that the air was aged. It was likely that the northwesterly winds associated with the low-level jet observed in the profiler data transported these high ozone concentrations from source areas to the west. These observations of low-level jets preceding ozone episodes are consistent with a 1992 ozone study in Baton Rouge (OGDEN, 1992) that observed similar winds.

Backward surface and upper-air trajectories from the Baton Rouge region were computed starting around the exceedance time on 19 August (see later discussion of trajectory procedures and Figure 3-71). These trajectories indicated that air parcels were transported into the Baton Rouge area from regions to the west and southwest. By 0000 CST on 19 August, the air parcels were generally located north of Lafayette and Lake Charles, Louisiana. At 1800 CST on the previous day, the air parcels were located at the coastline of Louisiana about 50 km southeast of Lake Charles. Given the error in these trajectories after 24 hours of transport, these air parcels could have originated in either the southeast Texas or southwestern Louisiana regions. Other analyses discussed in the next section support this type of regional transport from locations to the west of Baton Rouge. These trajectories indicated that second-day transport of air parcels could have occurred from regions over the western Gulf of Mexico (i.e., offshore of southwestern Louisiana and southeastern Texas).

3.6 ANALYSES OF TRANSPORT PROCESSES AND ONSHORE-OFFSHORE FLUX

ANALYSES OF VENTILATION AND RECIRCULATION

To investigate in more detail transport conditions aloft that occurred during the GMAQS, a procedure was developed to characterize ventilation conditions and the structure of the flow reversal. This procedure was based on integral quantities computed from the radar profiler data. The method used for this analysis was based on the work of Allwine and Whiteman (1994), who developed a technique to analyze mesoscale transport conditions in complex terrain (such as mountain-valley wind systems and upslope/downslope flows) using continuously measured upper-air data provided by radar profilers and Doppler sodars (Richards et al., 1991). Their approach was adapted to analyze transport conditions in the shoreline environment of the Gulf Coast. Following the work of Allwine and Whiteman (1994), the specific quantities that were computed for this study, and which were used to perform the "ventilation analyses" described in this section, included the following:

$$S = \int_{t}^{t+\tau} |\vec{V}(t)|\,dt \tag{3-1}$$

$$L = \sqrt{x^2 + y^2} \tag{3-2}$$

where:

$$x = \int_{t}^{t+\tau} u(t)\,dt \quad \text{and} \quad y = \int_{t}^{t+\tau} v(t)\,dt$$

$$\Theta = \tan^{-1}\left[\frac{x}{y}\right] \tag{3-3}$$

$$R = \frac{L}{S} \tag{3-4}$$

The quantities described by equations 3-1 through 3-4 represent, respectively, the scalar wind run S (km), the resultant (vector) transport distance L (km), the resultant (vector-averaged) wind direction Θ (degrees clockwise from true north adjusted to the proper quadrant), and the recirculation factor, R. The recirculation factor is the ratio of the resultant transport distance to the scalar transport distance (wind run). When R is equal to 1, straight-line, steady transport has occurred during the integration period. When R is equal to zero, no net transport has occurred during the integration period. Values of R close to 1, combined with transport distances of a few hundred kilometers, would typically characterize good ventilation conditions. Conversely, low values of R represent periods of stagnation or recirculation. Stagnation would be indicated by short scalar wind runs (i.e., low wind speeds); recirculation would be characterized by low values of the vector transport distance (e.g., L less than 50 km) compared to the scalar wind run. For example, if R were 0.25 and the vector-averaged wind run were 50 km, the scalar

wind run would be 200 km. Over a diurnal cycle, this would not be characteristic of stagnant conditions. For such conditions to have occurred, air must have circulated back and forth through the area of interest. A sea/land breeze or diurnal upvalley/downvalley wind system would be examples of such a recirculation.

For the analyses of the GMAQS data, the quantities described in equations 3-1 through 3-4 were computed for each radar profiler data set at each measurement height, using wind observations with 100 m vertical resolution. The integration time, T, was specified as 12 hours, and the transport statistics described by equations 3-1 through 3-4 were computed for each day during the period 18 July–15 September 1993 for consecutive 12-hour periods 0600–1700 CDT and 1800–0500 CDT. These integration periods were chosen to represent average daytime and nighttime conditions, respectively. At least six wind observations were needed at a sampling height to compute a valid set of transport statistics.

Figure 3-64 presents an example of the results of the ventilation analysis for a nonexceedance day when no flow reversal occurred. The figure uses a bar chart format to show the vertical distribution of the 12-hour integrated wind direction, resultant transport distance (L), and the recirculation factor (R) computed from the hourly averaged wind data collected at the Southeast Houston, Galveston, and High Island radar profiler sites. These analyses were performed using data collected during the period 0600–1700 CDT on 16 August 1993, a period judged to be representative of daytime conditions during nonexceedance conditions. The ventilation analysis shows that on this day steady transport occurred in the lowest 1000 m or so of the atmosphere (values of R close to 1), with onshore, southerly winds throughout the period, and transport distances of 150 to 250 km (integration periods over 24 hours showed that vector transport distances on nonexceedance days often exceeded 400 to 500 km). These results indicated relatively good ventilation conditions and short residence times for pollutants in the region, which probably contributed to keeping ozone concentrations low on days when the flow reversal did not occur.

By way of contrast, Figure 3-65 shows the results of the ventilation analysis for the period 0600–1700 CDT on 19 August 1993 in southeast Texas, the day on which the highest ozone concentration observed during the GMAQS occurred. On 19 August, the effect of the flow reversal was evident in the first 1000 to 1200 m of the atmosphere: resultant transport distances were reduced to 30 to 50 km, and values of the recirculation factor were less than about 0.25. The vector-averaged wind directions at all three Texas stations indicated onshore flow, but the occurrence of the offshore winds of the flow reversal was reflected in the low values of R. Above about 1200 m, the recirculation factor showed steady transport, and transport distances increased to about 200 km under steady southeasterly winds, up to approximately 1800 m msl. The depth of the gulf/land breeze circulation was marked by the rapid increase in R and L above about 1200 m msl. These results agree favorably with the analyses of the development of the mixed layer presented earlier. They indicate that if ozone and precursors were mixed upward during the day out of the gulf/land breeze layer, then they could have been "ventilated" northward out of the area under the steady transport conditions that existed aloft in the lower troposphere.

The results of the ventilation analysis for the 19 August 1993 episode in Louisiana are shown in Figure 3-66. As discussed previously, an onshore-offshore-onshore flow reversal was observed in the data collected by the Louisiana surface and upper-air stations, but the offshore (northerly) portion of the flow reversal persisted during most of the daylight hours on 19 August. The results presented in Figure 3-66 confirm that relatively steady transport from the northwest toward the southeast occurred aloft during the daytime hours. A similar analysis for the period preceding the maximum ozone concentrations observed in Baton Rouge (1200 CDT 18 August to 0600 CDT 19 August; see Appendix J) indicated that onshore transport (mean winds from the southeast to southwest) had occurred aloft in the boundary layer over Louisiana. Vector-integrated transport distances calculated at the shoreline and offshore at the Ship Shoal Platform indicated net transport distances of only 50 to 100 km in the mixed layer. At Louisiana State University, the ventilation analysis indicated transport from the southwest over distances of 200 to 250 km in the mixed layer, prior to the reversal of the winds and the development of northwesterly winds during the morning hours of 19 August.

Figure 3-67 shows results of the ventilation analysis in a time-height cross section format, based on the analyses of the Galveston upper-air data for the period 18 July–15 September. The three panels show contours of the recirculation factor, resultant (vector) transport distance, and the mean wind direction, respectively. The integration periods used for the analyses shown in Figure 3-67 were the same as those described previously. Time is plotted along the horizontal axis in Julian day format. The Julian days corresponding to the ozone episodes identified in Figure 3-19 are as follows:

Date	Julian Day
29 July–2 August	210–214
10–11 August	222–223
13 August	225
18–21 August	230–233
25 August	237
1–3 September	244–246
6 September	249
8–11 September	251–254

Similar analyses were performed for the upper-air data collected at all the radar profiler stations, and are included in Appendix J. The results for Galveston shown in Figure 3-67 are considered representative of the results obtained from the other profiler data sets.

Figure 3-67 shows that each of the exceedance days listed above was characterized by values of the recirculation factor between about 0.1 and 0.6. The vector transport distances on exceedance days were also characteristically low, typically less than about 50 to 75 km. Conversely, on nonexceedance days, the recirculation factor in the lower 1000 m or so of the atmosphere was typically greater than 0.9, and vector transport distances usually exceeded 200 km over any 12-hour period. The diurnal nature of the flow reversal is indicated by the increase in R and L during the night (during the steady onshore winds of Stage 6 of the conceptual model of the flow reversal), compared to daytime values. Interestingly, above the layer in which the gulf/land breeze circulation

was observed, the mean wind direction on exceedance days during the July–August period was usually northeasterly to southeasterly. This result is consistent with flow around the Bermuda high if the center of the high had shifted westward, as was discussed above. On nonexceedance days, winds aloft above the boundary layer were more southerly to southwesterly, which was characteristic of clockwise flows around the Bermuda high when the high was centered east of the study region. During the September episodes, winds aloft in the lower troposphere and above the boundary layer were northwesterly to northerly, which is consistent with flows around the continental high that moved into the region during this episode.

The results of the ventilation analyses support the conclusion that on exceedance days during the July–August period, the gulf breeze winds transported ozone through the Houston area and into the rural areas northwest, north, and northeast of the city. The general absence of carryover of pollutants aloft suggested by the aircraft data is most likely explained by the vertical venting of ozone and precursors to altitudes where relatively steady, synoptic-scale transport was occurring, and by the transport of pollutants out of the region by the gulf breeze. It appears as though the gulf breeze was an efficient ventilation mechanism for transporting pollutants out of the area overnight. The flow reversal on subsequent days of a multiday episode was not extensive enough to transport prior day's ozone and precursors back into exceedance areas.

Several important differences in the meteorological conditions accompanied the 8–11 September ozone episode, compared to the episodes in July and August. The ventilation analyses revealed several of these differences, as well as the similarities associated with the development of the flow reversal. One important difference was mentioned earlier in this section, namely, that mean wind directions aloft above the mixed layer were northwesterly to northeasterly during the September episode, reflecting airflow around a continental high (as opposed to the Bermuda high) that had moved into the region prior to the start of the episode. In addition, the ventilation analyses revealed that mean transport conditions preceding the start of the episode were characterized by relatively steady northerly to northeasterly (i.e., offshore) winds, as opposed to the steady onshore winds that preceded the flow reversal and the start of ozone episodes in July and August.

Values of the recirculation factor R during the September episode were comparable to values observed during the episodes earlier in the summer, and indicated the development of the onshore-offshore-onshore winds of the gulf/land breeze circulation. However, the ventilation analyses also showed that the nature of the flow reversal during the September episode was more of a true 180-degree reversal in the winds: 12-hour integrated mean wind directions computed for the ventilation analyses performed on the Southeast Houston and High Island profiler data showed the northerly to northeasterly winds of the land breeze during the early morning hours and through much of the day, and the southerly to southeasterly winds of the gulf breeze during the late afternoon and much of the nighttime hours. In addition, the vector-integrated transport distances were usually less than 80 to 100 km, and did not display as strong a diurnal trend as in the analyses of the July and August episodes.

The results summarized above suggest that it was likely that a period of good, persistent ventilation conditions (created by a prolonged gulf breeze), which could have transported

ozone and precursors out of the region overnight never developed during the September episode. Instead, it was likely that carryover of ozone and precursors from one day of the episode to the next occurred during the September episode, unlike the July–August episodes.

ANALYSES OF POLLUTANT TRANSPORT USING TRAJECTORIES

Mass-conservative wind fields for each hour of two ozone exceedance periods (18–21 August and 7–11 September) were calculated using surface (two-dimensional) and upper-air (three-dimensional) wind field models. The models were developed at the California Institute of Technology by Goodin et al. (1980), and later modified by the California Air Resources Board (ARB). The two-dimensional model calculated surface wind fields from hourly averaged surface data collected at the 48 sites shown in Appendix K. The upper-air model calculated aloft wind fields using the results computed by the surface model and aloft winds measured by seven doppler radar profilers, two doppler sodars, and four rawinsonde systems, as illustrated in Appendix K. Both models included parameterizations to account for the effects of atmospheric stability and mixing depth. The upper-air model calculated wind fields at user-specified altitudes and then adjusted those fields to minimize any anomalous divergence. After the wind fields were computed, air parcel trajectories (forward and backward) were created using a trajectory generation program developed by the ARB.

It is important to note that these models are not rigorous in their treatment of the physical processes that govern the flows within the modeling domain. They are simply data interpretation tools whose results are only as good as the quality and the resolution of the original observations collected during the field study. Only data that had been quality-controlled and validated were used in these analyses. Missing data were interpolated linearly in time by both the surface and upper-air models, and a cubic polynomial was used to interpolate missing data vertically in the upper-air model. Because the general topography within the selected modeling domain is relatively flat, no topography data were utilized by either model.

Figure 3-68 shows a map of the domain over which the wind fields were prepared. The domain dimensions were 900 km (east-west) by 450 km (north-south), with the center of the domain located near Lafayette, Louisiana. This domain was selected to include receptor sites in Texas and Louisiana, and to illustrate onshore-offshore as well as east-west flow regimes. A horizontal grid of 100 by 50 square cells, 9 km on a side, was defined over this area. Six vertical levels were specified in the upper-air model: 10, 100, 300, 500, 1000, and 2000 m msl. The data at 10 m were supplied by the output from the surface model. Figure 3-68 also illustrates the distribution of the surface and upper-air sites used by the models. The modeling domain was data-sparse to the north of Houston, over the Gulf of Mexico, and in the region between Texas and Baton Rouge, Louisiana. It is important to note that upper-air transport computed between Texas and Louisiana was primarily driven by data from the Lake Charles rawinsonde site, where soundings were performed two to three times daily depending on whether an intensive operation period was under way.

The wind field models and the trajectory generating program were tested using a data set where all wind speed and wind directions were set to 5 m/s and 180 degrees, respectively, and the resultant trajectories were plotted. Several randomly selected trajectories were validated by hand. In addition, backward trajectories were calculated from the end points of forward trajectories to test the continuity of the trajectory generating program. Good results were obtained from all of the tests.

Families of trajectories with a range of starting locations, times and altitudes were computed to describe potential transport paths and to illustrate the range of variability in air parcel locations. A total of 3264 forward and 3216 backward trajectories were computed. The backward trajectories were calculated for periods when high ozone concentrations were recorded at receptor sites. Trajectories were typically prepared at 10 m, 100 m, and 300 m, and the results compared. These trajectories were used to determine the general path that an air parcel arriving at the receptor site might have followed. Forward trajectories were calculated for periods with high emissions from potential source areas. These trajectories were used to determine the general path that air parcels might have followed on their way from a source region to a receptor area, and do not represent observed trajectories. Forward trajectories starting at shoreline sites were also computed during periods of offshore flow to estimate how far offshore an air parcel might have traveled during the flow reversal. In the following discussion, results are illustrated using trajectories at one altitude; however, results at other altitudes were typically similar.

The August Episode

The highest ozone concentration (231 ppb) measured during the summer of 1993 occurred at 1600 CST on 19 August, at Aldine, Texas. Figure 3-69 shows a backward trajectory starting from Aldine at the time of the peak measurement. This trajectory suggests that the air arriving at Aldine at the time of the maximum ozone concentration had previously been transported southeastward by the land breeze from slightly north of Aldine through the Houston region, during the morning daylight hours. At 1200 CST, the onset of the southerly winds of the gulf breeze produced a nearly 180-degree flow reversal, which recirculated air northwestward over the source areas east of Houston and back to Aldine.

Figure 3-70 shows an example of one of the forward trajectories computed from Baytown, Texas, an industrial area east of Houston. These trajectories indicated that during the morning daylight hours, air was transported southeastward toward (and possibly over) Galveston Bay by the land breeze. Again, an almost 180-degree flow reversal occurred at about 1200 CST, after which a northwestward flow carried air back over the Houston region and to Aldine, arriving near the time that the peak ozone concentration was measured.

Forward trajectories were also computed from coastal sites at Galveston and Gilchrist, Texas. These trajectories indicated that during the morning hours coastal air was transported no farther than approximately 40 km offshore before the start of the onshore flow reversal, and that air transported in the onshore flow did not reach Aldine until well

after the maximum ozone concentration was recorded. This suggests that emissions from offshore sources most likely did not contribute to this exceedance.

The 17–19 August episode was the only multiday episode observed in the Baton Rouge area during the summer of 1993. As shown in Figure 3-71, a backward trajectory was started at 1400 CST from Ascension Parish, Louisiana, the site where the maximum ozone concentration (126 ppb) was observed in the Baton Rouge area on 19 August. This trajectory indicates that air reaching the receptor at 1400 CST originated approximately 25 km off the coast of southeast Texas on the previous day, although this 1- to 2-day trajectory is speculative and may include significant errors. The airflow paralleled the coastline until noon, at which time it was directed shoreward by the gulf breeze. The air arrived at the shore around 1600 CST on the day before the exceedance, and was transported northeastward until the onset of the flow reversal at 0500 CST on the exceedance day. Beginning at 0500 CST, the air was redirected southeastward until it arrived at the exceedance site at 1400 CST. This trajectory suggests that carryover of ozone and ozone precursors from the previous day, and regional transport from offshore sources in southeast Texas, may have been components of the 19 August exceedance episode in Louisiana.

In addition, forward trajectories were computed for 18 and 19 August, starting at the profiler sites located at Cocodrie and at the Ship Shoal Platform. As shown in Appendix K, these trajectories indicate that significant onshore transport from either of these two sites was unlikely. Forward trajectories starting at Galveston for 18 and 19 August, as presented in Figure 3-72, show some evidence of regional transport of prior day's ozone from the Houston region toward northwest Louisiana. However, accumulated errors along trajectories dictate that inferences based on trajectories after 24 hours are speculative.

Conclusions and observations from the transport analysis for the August episode are as follows:

- Same-day emissions from offshore sources most likely did not contribute to the exceedances measured in Texas and Louisiana.

- There was evidence of regional transport in a northeastward direction.

The September Episode

For each day of the 7–11 September episode, forward trajectories were computed from source and coastal areas, and back trajectories were computed from exceedance areas for the times of maximum ozone concentration. These trajectories revealed that the characteristics of the flow regimes on 8 and 9 September were similar, and different from the flow characteristics on 10 September.

As shown in Figure 3-73, back trajectories computed from exceedance areas near the coast indicated that air arriving at these sites had originated from the urban-industrial

areas in the Houston region during the early morning hours on 8 and 9 September. In general, transport was slow and southeastward until approximately 1200 CST, at which time transport was redirected onshore by the flow reversal accompanying the arrival of the gulf breeze. Most of the maximum ozone concentrations were measured during or shortly after the transition to onshore flow. These results suggest that emissions from onshore sources were responsible for the high concentrations observed on 8 September, and that the participation of pollutants from offshore sources was unlikely.

For 8 and 9 September, forward trajectories starting from source areas in the Houston region were computed. These trajectories implied early morning transport in a southeastward direction along the western shore of Galveston Bay. As seen in Figure 3-74, air had reached the coastline by approximately 1100 CST, and was then recirculated back inland by onshore flow. When compared with measurements of high ozone concentrations at coastal sites (Gilchrist at 1300 CST and Smith Point at 1400 CST), the trajectories suggest that the primary cause of the exceedances on these 2 days was same-day transport of ozone and ozone precursors from source areas in the Houston region.

To determine the extent of onshore/offshore transport, forward trajectories were computed starting at the coastal sites of Galveston and Gilchrist. As shown in Figure 3-75, these trajectories (and others not illustrated) suggest that onshore air was carried no farther than approximately 50 km offshore in the morning, then returned back onshore with the flow reversal, and arrived onshore several hours after the ozone exceedance. This leads to the possibility of onshore air mixing with offshore sources and then coming back onshore.

Conclusions and observations from the transport analysis for 8 and 9 September are as follows:

- For both days there was evidence of same-day transport of ozone and ozone precursors from source areas in the Houston region to exceedance sites near Galveston Bay and along the coast.

- Due to timing, the possibility of onshore air mixing with offshore air and returning with the gulf breeze to participate in exceedances on the same day was unlikely.

- General transport was slow during the day.

As previously stated, the flow regimes associated with the 10 September exceedances were different from those observed on the preceding two days. As shown in Figure 3-76, backward trajectories from several exceedances illustrate a clockwise recirculating pattern over the 24-hour period preceding occurrence of the maximum ozone concentrations. This pattern suggests that carryover of ozone from the previous day's exceedances was likely an important factor. Along with evidence of carryover, there is also evidence of direct, same-day transport from source areas within the Houston region.

The back trajectory from Gilchrist, shown in Figure 3-77, is particularly interesting because it clearly illustrates how air from Galveston on the previous day was likely

transported overnight to Gilchrist and onward to Smith Point, and how the arrival of these air parcels coincided with the maximum observed ozone concentrations at these two sites, respectively. Another noteworthy feature of this trajectory is the northward transport of polluted air from Galveston over the main source areas in the Houston region. After the air passed through the Houston region, it was gradually redirected southward by the offshore flow reversal and reached the coast by late morning. While the magnitude of the offshore transport on 10 September was the largest observed, very little over-water transport was observed, due to the timing of the onshore flow reversal.

In addition, ozone concentrations measured at Galveston remained high for 5 hours after the initial onset of the gulf breeze on 10 September. Figure 3-78 shows two back trajectories started at 1400 CST and 1900 CST from Galveston. These trajectories illustrate how air parcels originating over land during the early morning hours were transported from 10 to 50 km offshore, where they were possibly mixed with offshore emissions before being recirculated back onshore by the gulf breeze.

To investigate the extent of the offshore transport on 10 September, forward trajectories were computed from Galveston and Gilchrist, which are shown in Figure 3-79. These trajectories illustrate how air that left the coastline during the early morning hours was transported offshore approximately 80 km before the onshore flow reversal recirculated the air back to the coast. These represent the farthest, same day, offshore transport observed in any of the trajectories computed. While the air transported back onshore likely contained pollutants from offshore sources, its arrival back at the coast was significantly later than any ozone exceedance.

Conclusions and observations from the transport analysis for 10 September are as follows:

- Transport distances during the land breeze and the gulf breeze were comparable.
- The offshore transport during the land breeze was farther than on the previous episode day.
- The general transport patterns recirculated air clockwise and suggested that carryover of pollutants from the previous day was important.

RESULTS OF ONSHORE–OFFSHORE POLLUTANT FLUX CALCULATIONS

The remainder of this section discusses two methods to estimate the flux of pollutants across two-dimensional (2-D) planes parallel to the Gulf of Mexico shoreline near Galveston Bay. One method uses upper-air meteorological and air quality data; these data are only available during intensive sampling. The second method uses hourly pollutant and wind data collected at surface monitoring sites; results obtained using this method represent the 3-D transport of pollutants only during well-mixed conditions, but the availability of continuous data provides pollutant-transport information at various times.

It is important to note that these flux estimation methods are simple models based on data, and spatial and temporal interpolations of data, with a number of simplifying assumptions, which are listed in detail in the following discussions. These methods are simple data interpretation tools whose results are only as good as the quality and resolution of the original observations collected during the field study. Only data that had been quality-controlled and validated were used in these estimates.

Method 1: Ozone and NO_x Flux Calculations Using Upper-Air Data

Figure 3-80 illustrates a method to estimate the flux of pollutants across two imaginary planes along the shoreline at Galveston and Gilchrist. The method uses upper-air meteorological and air quality data to estimate the flux of pollutants across two-dimensional planes; these data are only available during intensive sampling. Results obtained by this method allow assessment of the mass flow rate of a given pollutant.

A simple flux can be calculated by multiplying the pollutant concentration by the wind speed in the direction perpendicular to a specific plane. The flux of ozone across an imaginary plane along the shoreline at Galveston, for example, is the rate of flow per unit area that passes through the plane. This flux depends on the ozone concentration, and on the speed and direction of the wind transporting the ozone. The ozone mass flow rate across the plane is the average ozone flux multiplied by the area of the flux plane.

To estimate the flow rates of ozone and NO_x through imaginary planes along the shoreline at Galveston and Gilchrist, the following steps were performed:

- Defined flux planes along the shoreline at Galveston and Gilchrist.
- Calculated the wind speed in the direction perpendicular to the flux planes using upper-air meteorological measurements made by the Galveston radar profiler.
- Interpolated wind speeds vertically using a simple distance-weighting procedure.
- Calculated the pollutant flux across the flux planes by using the air quality data collected aloft at Galveston and Gilchrist and the estimated upper-air meteorological data.
- Prepared profile plots of pollutant concentrations, wind speeds, and pollutant flux estimates.
- Calculated the pollutant mass flow rate across the flux planes.

Flux Plane Definition

Air quality measurements aloft were made on nine intensive sampling days at Galveston and Gilchrist. Upper-air winds were continuously measured at Galveston during the summer.

To estimate the flux across imaginary planes at the shoreline, two flux planes are defined: one at Galveston and the other at Gilchrist. The extension of both imaginary planes is assumed to be about 50 km, the base is at the ground (about 2 m msl both at Galveston and Gilchrist), and the top is at 600 m msl, corresponding to the top of the mixing height at Galveston on 10 August in the afternoon. Note that late morning and afternoon mixing heights ranged from about 600 to 1000 m msl inland (see "Analyses of Mixing Depths and Boundary Layer Development" in Section 3.4 for further details).

The data collected on 10 August were chosen to illustrate the calculation of ozone and NO_x flux across the imaginary planes at Galveston and Gilchrist. This date was selected because the air quality data aloft were collected at approximately the same time periods the offshore and onshore fluxes estimated with surface data (see Method 2 below) reached their maxima.

Data Preparation

Aircraft air quality measurements were made at 0623-0634 CST and 1301-1312 CST at Galveston and 0732-0742 CST and 1407-1418 CST at Gilchrist on 10 August. The Galveston radar wind profiler measured winds hourly, but only the data collected at approximately the same time periods the aircraft flew spirals over Galveston and Gilchrist were used.

The radar profiler data were reported as altitude above ground level (agl) and were reported in the vertical as averages in uniform intervals of 100 m starting at the lowest altitude—about 150 m agl. These data were first converted to msl. Next, the wind speed component perpendicular to the flux plane was determined. Then, the gridded estimated values were linearly interpolated in the vertical to estimate the southeasterly component of the wind speed at each given pollutant data point aloft. Finally, these values were multiplied by the corresponding pollutant concentration values to obtain the flux across the planes. The flux was reported in mass/time/area, typically in units of $mg/min/m^2$ for plotting convenience. The offshore flux (northwesterly flow) is reported as negative and the onshore flux (southeasterly flow) is reported as positive.

Flux Estimation Results

The two measurement components that are needed to perform ozone and NO_x flux calculations are upper-air winds, and ozone and NO_x measurements aloft at Galveston and Gilchrist. As an example, the profile plots at Gilchrist are shown in Figure 3-81. The profile plots at Galveston are provided in Appendix L.

Figure 3-81 shows the ozone concentrations, the southeasterly component of the wind, and the flux calculations at Gilchrist. Note that there are upper-air data from close to the ground to about 1500 m msl. However, mass flow rates are calculated using the data for the first 600 m msl, which corresponds to the top of the mixed layer at Galveston on 10 August in the afternoon. The early morning ozone concentrations

(Figure 3-81a) were about 30 ppb for the first 600 m. The afternoon ozone concentrations ranged from 90 ppb close to the surface to about 50 ppb at 600 m msl. The early morning southeasterly wind speed components (Figure 3-81b) were about −1 m/s for the first 600 m and ranged from about 5 m/s near the surface to about 2 m/s at 600 m msl in the afternoon. Figure 3-81c shows the profiles of the ozone flux across the imaginary plane at Gilchrist. The early morning ozone fluxes were about −4 mg/min/m^2 for the first 600 m and ranged from about 55 mg/min/m^2 near the surface to about 4 mg/min/m^2 at 600 m msl in the afternoon.

To obtain the ozone mass flow rate across the flux plane (mass/time), the average flux was determined and this quantity was multiplied by the total area of the flux plane, as shown in the following equation:

$$\underset{\text{altitude}}{(600-2\text{ m})} \times \underset{\text{distance}}{(50{,}000\text{ m})} \times \underset{\text{average flux}}{(38.2\text{ mg/m}^2\text{/min})} \times \underset{\text{unit conversions}}{(10^{-6}\text{ kg/mg})} \times (\text{min}/60\text{ s}) = \underset{\text{ozone mass flow rate}}{19\text{ kg/s}} \quad (3\text{-}5)$$

This is equivalent to an average concentration of 69 ppb being transported at about 4.7 m/s across the Gilchrist flux plane.

Figure 3-82a shows a profile plot of the NO_x concentrations at Gilchrist on 10 August. NO_x concentrations were nonuniform early in the morning, with values between 23 ppb near the surface and 2 ppb at 600 m msl. In the afternoon, NO_x concentrations were fairly uniform, about 2 ppb for the first 600 m. Figure 3-82c shows the profiles of the morning and afternoon NO_x fluxes across the imaginary plane at Gilchrist. The morning NO_x flux ranged from −2.9 mg/min/m^2 near the surface to about 0.1 mg/min/m^2 at 600 m msl. The afternoon flux ranged from about 1.9 mg/min/m^2 near the surface to about 0.2 mg/min/m^2 at 600 m msl.

Table 3-9 lists the average ozone and NO_x concentrations and southeasterly component of the wind speed at Galveston and Gilchrist, and the average ozone and NO_x flux and mass flow rate across the Galveston and Gilchrist imaginary planes for 10 August. During morning offshore flow conditions (negative flux), the ozone mass flow rates at Galveston and Gilchrist were similar, about −2 kg/s. During afternoon onshore flow conditions (positive flux), the ozone mass flow rate at Galveston was about half the flow rate at Gilchrist (about 11 and 19 kg/s, respectively). Offshore and onshore NO_x flow rates were very similar at both sites. During offshore flow conditions, NO_x flow rates were −0.2 and −0.1 kg/s and during onshore flow conditions, NO_x flow rates were 0.6 and 0.5 kg/s at Gilchrist and Galveston, respectively.

Assumptions for Flux Calculations

A number of assumptions need to be considered while performing flux calculations. These are summarized below:

- Upper-air winds at one sampling location are representative of upper-air winds at a nearby location. It was assumed that the upper-air winds at Galveston also represent the upper-air winds at Gilchrist.

Table 3-9. Average ozone and NO_x concentration and southeasterly component of the wind speed at Gilchrist and Galveston, and the average ozone and NO_x flux and mass flow rate across the Gilchrist and Galveston imaginary planes during 10 August 1993. Southeastward flux and mass flow rate are reported as negative and northwestward flux and mass flow rate are reported as positive.

	Gilchrist		Galveston	
	Morning	Afternoon	Morning	Afternoon
Wind speed (m/s)	−0.9	4.7	−1.3	4.0
Ozone				
Concentration (ppb)	30	69	26	48
Flux (mg/min/m^2)	−3	38	−4	23
Mass flow rate (kg/s)	−2	19	−2	11
NO_x				
Concentration (ppb)	3	2	3	2
Flux (mg/min/m^2)	−0.4	1.2	−0.3	1.0
Mass flow rate (kg/s)	−0.2	0.6	−0.1	0.5

- The distance-weighting procedure used to vertically interpolate wind speed properly represents aloft winds.

- The distributions of the ozone and NO_x concentrations measured at a specific location properly represent the distributions of ozone and NO_x concentrations along the flux plane.

- Any small "clouds" of high or low ozone or NO_x concentrations that were missed by the aircraft are small contributors to the total flux.

Note that an important limitation of this flux calculation method is that it provides only "snapshots" of the flux through a plane. More frequent data are needed to investigate temporal and spatial variations in the pollutant concentrations, winds, and flux. The second method presented below uses hourly pollutant and wind data taken at surface monitoring sites to investigate temporal and spatial variations, but without upper-air data.

Method 2: Ozone and NO_x Flux Calculations Using Surface Data

In this analysis, fluxes are calculated by multiplying hourly surface pollutant concentrations by hourly wind speeds in the direction perpendicular to five northeast-southwest planes at five surface monitoring sites (Figure 3-80): Galveston, Gilchrist, Seabrook, Smith Point, and Houston Regional Monitoring (HRM) Site 7. Results obtained by this method can represent the two-dimensional transport of pollutants only during well-mixed conditions, but the availability of data provides pollutant-transport

information at many times. As with method 1, the flux is reported in mass/time/area, typically in units of mg/min/m^2, and offshore flux (southeastward flow) is reported as negative and the onshore flux (northwestward flow) is reported as positive.

The flux calculations at Galveston and Gilchrist represent the flux of pollutants along the shoreline. The flux calculations at Seabrook and Smith Point represent the flux across planes parallel to the Gulf of shoreline west and east of Galveston Bay, respectively. Finally, the flux calculations at Houston Regional Monitoring Site 7 represent the flux across a plane parallel to the shoreline in the industrial ship channel region. Below, hourly ozone and NO_x flux calculations for the 9-11 August episode are discussed. In addition, summary tables are presented that show maximum ozone and NO_x flux calculations during offshore and onshore flow conditions for three days (10 August, 19 August, and 9 September) representative of the three 1993 ozone episodes. Ozone and NO_x flux time-series plots for Galveston, Gilchrist, Seabrook, Smith Point, and Houston Regional Monitoring Site 7 for 17-21 August and 7-11 September are provided in Appendix M.

During the 9-11 August episode, ozone flux plots for Galveston, Gilchrist, Seabrook, Smith Point, and Houston Regional Monitoring Site 7 (depicted in Figure 3-83) show a very consistent diurnal pattern of morning negative ozone flux followed by afternoon positive flux. That is, flow associated with the land breeze transports ozone offshore in the morning, and flow associated with the gulf breeze transports ozone onshore in the afternoon. However, because the highest ozone concentrations are reached during the afternoon, more ozone is transported northward with the gulf breeze than is transported southward with the land breeze.

Similar flux plots were prepared for NO_x (see Figure 3-84). The diurnal pattern of NO_x concentration is quite different from the pattern for ozone. NO_x concentrations are often highest in the morning and are significantly more variable and less smooth than ozone concentrations. In addition, there are significant differences among the sites. NO_x concentrations measured at Galveston and Gilchrist did not exceed 20 ppb early in the morning and were usually below 10 ppb the rest of the day, and those at Seabrook and Smith Point were between 20 and 50 ppb early in the morning and less than 10 ppb the rest of the day, but NO_x concentrations measured at Houston Regional Monitoring Site 7 were between 40 and 120 ppb early in the morning (60 to 80 percent NO) and between 20 and 40 ppb the rest of the day (about 90 percent NO_2). In addition, the diurnal pattern at Houston Regional Monitoring Site 7 was more variable than the diurnal patterns at the other four sites. These differences result in much larger NO_x fluxes across the plane at Houston Regional Monitoring Site 7 (from -10 to 15 mg/min/m^2) than at Galveston, Gilchrist, Seabrook, and Smith Point (from -5 to 3 mg/min/m^2). That is, it appears that NO_x emitted in the urban/industrial area is a major contributor of the NO_x transported offshore early in the morning, and the NO_x transported onshore in the afternoon is a minor contributor of the NO_x flux in the urban/industrial area.

Tables 3-10 and 3-11 list the maximum ozone and NO_x fluxes at Galveston, Gilchrist, Seabrook, Smith Point, and Houston Regional Monitoring Site 7 for 10 August, 19 August, and 9 September. The tables show that the transport of pollutants on 9 September was very different from that on 10 and 19 August. Table 3-10 shows that the

Table 3-10. Maximum ozone fluxes at Galveston, Gilchrist, Seabrook, Smith Point, and Houston Regional Monitoring (HRM) Site 7 and the corresponding southeasterly component of wind speed and ozone concentration for 10 August, 19 August, and 9 September 1993. Southeastward flux is reported as negative and northwestward flux is reported as positive.

		Southeastward Ozone Flow				Northwestward Ozone Flow			
Day	Site	Max. Flux ($mg/min/m^2$)	Time (CST)	Wind Speed (m/s)	Ozone (ppb)	Max. Flux ($mg/min/m^2$)	Time (CST)	Wind Speed (m/s)	Ozone (ppb)
10 August	Galveston	−2.1	05	−1.0	18	31.1	14	3.7	72
	Gilchrist	−4.3	08	−1.3	27	38.7	16	4.6	71
	Seabrook	−0.3	04	−0.9	3	36.8	16	3.9	80
	Smith Point	−10.8	12	−2.0	46	25.7	15	2.9	75
	HRM Site 7	−7.0	09	−1.5	40	27.9	17	4.3	55
19 August	Galveston	−6.3	09	−3.0	18	35.9	16	5.0	61
	Gilchrist	−7.0	11	−1.1	55	34.6	18	5.1	58
	Seabrook	−6.5	09	−2.5	22	45.6	15	3.9	100
	Smith Point	−20.4	11	−2.8	62	26.4	17	3.6	63
	HRM Site 7	−8.8	11	−1.6	47	46.8	15	3.5	112
9 September	Galveston	−37.1	04	−5.8	54	43.5	12	2.9	126
	Gilchrist	−37.9	13	−2.1	152	53.8	16	2.5	182
	Seabrook	−37.8	14	−2.0	159	9.6	21	1.2	67
	Smith Point	−68.8	12	−3.0	195	19.4	21	1.8	92
	HRM Site 7[a]	−35.7	14	−2.9	106	NA	NA	NA	NA

[a] The hourly ozone flux calculated at Houston Regional Monitoring Site 7 for September 9 was offshore for all hours.

Table 3-11. Maximum NO_x fluxes at Galveston, Gilchrist, Seabrook, Smith Point, and Houston Regional Monitoring (HRM) Site 7 and corresponding southeasterly component of wind speed and NO_x concentration for 10 August, 19 August, and 9 September 1993. Southeastward flux is reported as negative and northwestward flux is reported as positive.

		Southeastward NO_x Flow				Northwestward NO_x Flow			
Day	Site	Max. Flux ($mg/min/m^2$)	Time (CST)	Wind Speed (m/s)	NO_x (ppb)	Max. Flux ($mg/min/m^2$)	Time (CST)	Wind Speed (m/s)	NO_x (ppb)
10 August	Galveston	−0.9	07	−0.5	16	3.0	15	3.9	7
	Gilchrist	−3.8	07	−1.1	31	1.6	16	4.6	3
	Seabrook	−4.9	06	−0.9	47	2.2	18	2.8	7
	Smith Point	−0.7	10	−2.0	3	1.1	18	2.5	4
	HRM Site 7	−5.4	09	−1.5	32	13.4	19	3.0	39
19 August	Galveston	−3.2	07	−2.8	10	0.8	14	3.7	2
	Gilchrist	−1.9	08	−2.7	6	1.5	15	4.1	3
	Seabrook	−4.5	07	−1.7	24	4.9	14	3.6	12
	Smith Point	−2.6	07	−1.7	13	1.2	16	2.7	4
	HRM Site 7	−10.1	08	−1.6	57	21.7	19	5.3	36
9 September	Galveston	−15.0	08	−1.7	77	3.6	12	2.9	11
	Gilchrist	−7.2	07	−2.2	28	3.5	16	2.5	12
	Seabrook	−19.3	08	−3.0	57	4.5	19	0.6	67
	Smith Point	−11.7	06	−3.0	35	1.0	20	1.3	7
	HRM Site 7[a]	−7.7	13	−2.7	25	NA	NA	NA	NA

[a] The hourly NO_x flux calculated at Houston Regional Modeling (HRM) Site 7 for September 9 was offshore for all hours.

maximum offshore ozone fluxes on 9 September were between −35.7 and −68.8 mg/min/m^2, whereas on 10 and 19 August they were between −2.1 and −20.4 mg/min/m^2. The ozone concentrations that correspond to these fluxes ranged from 54 to 195 ppb on 9 September, whereas they ranged from 3 to 62 ppb on 10 and 19 August.

In addition, the flux at Houston Regional Monitoring Site 7 was negative all day, indicating that pollutants emitted and produced in the urban and industrial areas were transported southward all day.

Table 3-11 shows that maximum NO_x fluxes during offshore flows were between −7.2 and −19.2 mg/min/m^2 on 9 September, whereas they were between −0.7 and −10.1 mg/min/m^2 on 10 and 19 August. The NO_x concentrations corresponding to these fluxes ranged from 25 to 77 ppb on 9 September and from 3 to 47 ppb on 10 and 19 August.

The tables also show that the maximum onshore ozone and NO_x fluxes at Galveston and Gilchrist (along the shoreline) usually occurred during the period 1400–1800 CST and 1400–1600 CST, respectively; this is generally too late to influence the maximum ozone concentrations inland.

3.7 DATA ANALYSIS CONCLUSIONS, CONCEPTUAL MODEL OF OZONE EXCEEDANCES, AND ASSESSMENT OF OCSPD CONTRIBUTIONS

This section presents the conclusions of the data analyses and the conceptual model of ozone exceedances in the southeast Texas and Baton Rouge areas. The conceptual model includes a description of general important meteorological and chemical phenomena that influence high ozone concentrations in the two areas. In addition, this section provides a summary of the data analysis assessments of OCSPD emission contributions to ozone exceedances in the southeast Texas and Baton Rouge areas. Note that the data analysis methods used are limited by the spatial and temporal availability of the data (see detailed discussions in Sections 3.1-3.6).

CONCLUSIONS AND CONCEPTUAL MODEL

Synoptic Meteorological Conditions

- Synoptic meteorological conditions during the 9–11 August and 17–21 August episodes were characterized by a broad ridge of high pressure located over the southern United States, easterly to northeasterly winds aloft, and a westward extension of the Bermuda high-pressure system located over the Gulf Coast region. This synoptic pattern produced weak surface pressure gradients and subsidence over the region and resulted in weaker surface winds and clearer skies. Synoptic meteorological conditions observed during these episodes were representative of historical episodes.

- Meteorological conditions during the 7–11 September episode were substantially different from those observed during the August episodes. These differences included prevailing westerly to northerly winds aloft, a continental high-pressure system off the Gulf Coast region, and a trough at 500 mb over the eastern United States. Synoptic weather conditions during this episode were observed in a historical database, but not as frequently as in the August episodes.

- The synoptic-scale meteorology during summer in the Gulf Coast region was characterized by onshore (southeasterly to southwesterly) winds, associated with clockwise (anticyclonic) flows around the Bermuda high-pressure cell, the center of which was usually located east of the study region. Days were generally sunny, warm, and humid, and convective showers occurred on some days.

Surface and Upper-Air Meteorological Conditions

- On almost every study day during the summer in southeast Texas, a gulf breeze was observed, which was also characterized by onshore (southerly) winds. Both the synoptic-scale weather features and local mesoscale conditions combined to produce relatively steady onshore winds during daylight hours on most days.

- At night, an offshore-directed pressure gradient developed as the land became cooler than the Gulf. Theoretically, this would have resulted in a land breeze (winds blowing offshore), but most of the time the synoptic-scale pressure gradient maintained southerly winds that were stronger than the land breeze, so the winds continued to blow onshore throughout the night. Flows aloft during these periods of steady onshore surface flows were consistent with surface conditions. Upper-air winds measured by the radar profilers showed generally steady southeasterly to southwesterly winds.

- On occasion, a land breeze was observed in the region. When the "flow reversal" occurred, it was characterized by offshore (northerly) winds that usually began late at night or early in the morning (e.g., 0400–0600 CST). These offshore winds continued until the onshore, southerly winds of the gulf breeze were again established, which typically occurred anytime from late morning through early afternoon. This pattern of onshore winds during the afternoon and nighttime hours, followed by offshore winds during the morning hours, followed by the return of onshore flows, typically occurred for several days at a time.

- Every ozone exceedance observed in the southeast Texas portion of the GMAQS study area was accompanied by this onshore-offshore-onshore flow reversal. Days with flow reversals occurred that were not exceedance days, but they were usually associated with a buildup to, or ramp-down from, a multiday episode. Also of significance was the timing of the flow reversal: it occurred during the morning hours, when morning rush-hour emissions were potentially highest and photochemistry was beginning to occur. Conversely, when the flow reversal did not occur, and instead onshore winds persisted through the full diurnal cycle, no ozone exceedances were observed in southeast Texas (see Figure 3-19).

- The flow reversal usually developed when the Bermuda high shifted westward. This produced a reversal of the synoptic-scale pressure gradient across the Gulf. When differences in sea-level pressure between the GMAQS sites offshore of Texas and Louisiana were used to calculate the geostrophic wind, onshore winds were persistent so long as the geostrophic wind was directed onshore. The flow reversal generally coincided with a reversal in the synoptic-scale pressure gradient and the development of northerly geostrophic flow.

- Analyses of onshore-offshore temperature and pressure gradients demonstrated that the offshore (northerly) component of the flow reversal was part of the land breeze circulation; the return to onshore flows in the afternoon was due to the development of the gulf breeze. That is, the flow reversal was a diurnal process, i.e., a sea/land breeze circulation; a weak or negative synoptic-scale pressure gradient was needed before it developed.

- Once the onshore-offshore mesoscale pressure gradient reversed direction in the early morning, the offshore winds of the flow reversal developed over the entire region (onshore and offshore) within a few (1 to 3) hours. A land breeze "front," which was observed in the surface and upper-air data sets and in satellite imagery, marked the movement of air across the Gulf that had originated onshore. The land breeze "front" typically traveled 75 to 100 km offshore before the winds reversed and began blowing onshore again. Similarly, within 1 to 3 hours of when the mesoscale pressure gradient was again directed onshore, the southerly winds of the gulf breeze were observed at stations located both onshore and offshore. A gulf breeze "front," which marked the inland penetration of marine air that had originated over the Gulf, was observed in the meteorological data sets and in satellite imagery.

- There was also evidence of a bay breeze that formed off of Galveston Bay; the bay breeze typically preceded the arrival of the gulf breeze at stations in the Houston area located near the bay.

- There were six stages in the development of this onshore-offshore-onshore flow reversal pattern:

  — **Stage 1** commenced with the development of the gulf breeze on the day preceding an exceedance day, and was characterized by **steady onshore flow** at virtually all the onshore and offshore observing stations in the region. Stage 1 flows typically persisted from the afternoon/early evening preceding an exceedance day to 0400–0500 CST on the exceedance day.

  — **Stage 2** occurred during the early morning hours (0400–0700 CST), and was characterized by the development of offshore winds at inland sites and at the shoreline; onshore-directed winds continued at the offshore stations, out to distances of at least 125 to 150 km, which produced **a convergence zone near the shoreline**.

- **Stage 3** occurred during the morning daylight hours (0700–1000 CST), and was characterized by **steady offshore winds** at all stations, including the offshore stations. Offshore-directed winds were observed out to distances of at least 125 to 150 km over the Gulf.

- **Stage 4** occurred during the late morning and early afternoon (1100–1300 CST), and marked the start of the gulf breeze. The gulf breeze was first observed at the shoreline sites. Northerly (offshore) winds continued at stations farther inland, producing a **convergence zone onshore** as the gulf breeze "front" propagated inland; northerly (offshore) winds also continued at stations located in the Gulf, producing a **divergence zone offshore near the coastline.**

- **Stage 5** occurred during the early afternoon (1300–1500 CST), and was characterized by **steady onshore flow** at the inland stations, but offshore winds persisted at the offshore stations, maintaining the **divergence zone offshore.**

- **Stage 6** was characterized by the development of **steady onshore flow** accompanying the gulf breeze at all stations. It was first observed in the middle of the afternoon, and persisted the rest of the night. Stage 6 represented the **start of the Stage 1 flow pattern** for the next day. During Stage 6, the southerly winds of the gulf breeze turned clockwise, in response to the Coriolis force, and became southwesterly to westerly during the course of the night.

- The flow reversal was not limited to the surface layer. It was also observed in all the upper-air data collected by the radar profilers, including the observations collected at the sites located offshore on the High Island and Ship Shoal platforms, and at the other Louisiana profiler installations. The flow reversal was confined to the planetary boundary layer (PBL) and was typically a few hundred meters deep (usually less than about 700 to 900 m).

- After about 12 hours of onshore flow during Stage 1, concentrations decreased to about 20 to 30 ppb ozone and 1 to 2 ppb NO_x at the shoreline. Inland, the NO_x concentrations were higher and ozone was titrated, with concentrations near zero. During Stage 2, the flow reversal began and shoreline NO_x concentrations increased to 5 to 10 ppb. Ozone concentrations decreased to near zero because of titration. Inland, ozone and NO_x concentrations were similar to those in Stage 1 levels. During Stage 3, early production of ozone was observed both inland and at the shoreline, while NO_x concentrations remained relatively high at the shoreline compared to Stage 1 levels.

- The "normal" buildup of ozone precursors during the morning hours occurred during Stage 4, as the northerly winds of the land breeze transported emissions from Houston to the south side of the city. The highest ozone concentrations observed during Stage 4 were usually located south of Houston, after the winds had reversed at the shoreline and were again blowing onshore. Emissions from

onshore sources that had been carried offshore by the land breeze began to be transported back onshore during Stage 4.

- Maximum ozone concentrations occurred during Stage 5 or Stage 6. Southerly winds accompanying the onshore component of the flow reversal were present over the region at the time that maximum ozone concentrations were observed. The ozone "cloud" (or "plume") was pushed northward (inland), with the highest ozone concentrations usually observed north of Houston. The arrival of the gulf breeze "front" at a station, and with it air that had originated offshore several hours earlier, usually marked the time when ozone concentrations dropped dramatically at that station. Maximum ozone concentrations were usually observed 1 to 2 hours prior to the passage of the gulf breeze "front." Once the gulf breeze "front" passed, ozone concentrations decreased steadily, and were usually below exceedance levels within 2 to 3 hours.

- Offshore, the northerly winds of the flow reversal continued during Stage 5. Ozone and precursors transported offshore earlier in the day by the land breeze were likely still coming onshore in the gulf breeze. During Stage 6, the gulf breeze continued to push the ozone "plume" into the rural areas north of Houston. Ozone levels behind the gulf breeze "front" decreased from the shoreline inland to Houston under the steady onshore flow.

- In Louisiana, the same general pattern of the onshore-offshore-onshore flow reversal was observed on a number of study days, including 18–19 August, when the NAAQS for ozone was exceeded in Baton Rouge. The flow reversal occurred most often when the synoptic-scale pressure gradient was weak. Given the distance between Baton Rouge and the coast of Louisiana, there was little or no evidence of a gulf breeze "front" reaching Baton Rouge and bringing moist air of offshore origin into the Baton Rouge area on an exceedance day. Instead, the flow reversal in Baton Rouge appeared to be a regionwide response to the diurnal change in orientation (offshore versus onshore) of the mesoscale pressure gradient produced by the differential heat and cooling of the land relative to the water.

Mixing Depths and Boundary Layer Development

- Analyses of mixing depth using the radar profiler data and supporting aircraft observations indicated the following:

  — The marine layer offshore showed only modest diurnal variations; the average depth of the mixed layer offshore was 500 to 700 m agl. The most pronounced "growth" of the mixed layer offshore coincided with the passage of the land breeze "front."

  — At the shoreline, a convective boundary layer (CBL) typical of inland locations formed during the offshore component of the flow reversal. However, once the gulf breeze started at the shoreline, the growing CBL

was capped off, and the mixed layer at the shoreline resembled the mixed layer offshore. During periods of onshore flow, upper-air data collected near the shoreline were a good surrogate for diagnosing offshore conditions.

— Inland, the diurnal evolution of the PBL was generally typical of urban/rural areas. A deep CBL developed (1500 to 2000 m agl) by midafternoon on episode days. Thus, there was a relatively strong north-south gradient in mixing depth over the region, with the deepest development over urban areas. Aircraft data suggested that inland mixing depths over rural areas were not as deep as those observed over urbanized areas, which is consistent with urban heat island effects and previous studies of mixed layer development in urban versus rural areas.

- As the gulf breeze "front" pushed inland, it produced lifting, instability, and convection (often accompanied by clouds and sometimes by showers). This process helped augment vertical mixing of pollutants, and transported surface-produced ozone vertically to altitudes as high as 2300 m agl during one episode (maximum altitudes of 1500 to 2000 m agl were more typical).

- Venting of pollutants out of the PBL and into the lower troposphere by this convective activity was indicated both by the profiler data and by the aircraft observations. This venting mechanism probably represented a sink for local pollutants, which, after being mixed upward, were then transported out of the region.

- General subsidence and clearing behind the gulf breeze "front" was indicated by surface observations, the profiler data, and satellite imagery. However, maximum ozone concentrations were not observed in these cloud-free conditions; instead, they were observed ahead of the "front," where some convective cloudiness was often still present.

Estimates of Pollutant Transport Using Trajectories

- During non-episode periods, when steady onshore transport occurred over the full diurnal cycle, cumulative transport distances, integrated over 12- to 24-hour periods over the region, exceeded 200 to 400 km from near the surface to the upper altitudes sampled by the profilers (about 3000 to 4000 m agl). During ozone episodes, transport analyses indicated minimum cumulative transport in the lower portions of the PBL where the flow reversal had occurred.

- When the flow reversal occurred, transport conditions in the upper portions of the boundary layer and in the lower troposphere indicated generally steady easterly to southeasterly winds, consistent with anticyclonic flow around a synoptic-scale high-pressure system. Vector-integrated transport distances above the PBL usually exceeded 200 to 300 km over integration periods of 12 hours.

- The data aloft support the conclusion that the gulf breeze transported ozone through Houston and into the rural areas north of the city. The general absence of carryover aloft of pollutants from day to day, which was indicated by the aircraft data, is most likely explained by the vertical venting of pollutants into regions aloft of steady synoptic-scale transport, and the transport out of the region by the gulf breeze. The gulf breeze was an efficient ventilation mechanism for transporting ozone out of the area during some episodes. The flow reversal on subsequent days of a multiday episode was not extensive enough to transport prior day's ozone back into the exceedance area.

- Calculated trajectories indicate that marine air coming onshore on the day of an ozone exceedance did not reach the areas where ozone exceedances were observed until several hours after the highest ozone concentrations had occurred. Air coming onshore with the gulf breeze in Texas and Louisiana the evening prior to an exceedance day (i.e., during Stage 1) may have reached the areas where exceedances occurred, and may have been transported back and forth through the area by the flow reversal.

Summary of the 17–19 August Ozone Episode in Baton Rouge

- Synoptic meteorological conditions were conducive to high ozone concentrations when a high-pressure system moved westward into the area on 17 August and became stationary over Louisiana on 18 and 19 August. This system produced clear skies, light winds during the day, and weak pressure gradients.

- Exceedances in the Baton Rouge area were due to stagnation and local transport of ozone by weak northwesterly winds observed during the morning. These winds transported ozone from the source regions in Baton Rouge to exceedance sites located about 25 km southeast of the city.

- Low-level jets with winds of 5 to 8 m/s at night (0000–0800 CDT) preceded both exceedance days. These low-level jets had westerly to northwesterly winds between 100 and 500 m agl; surface winds during this period were calm. Air quality data collected aloft (by an aircraft) suggested that this low-level jet might have transported pollutants into the Baton Rouge area from regions to the west.

Summary of the 7–11 September Ozone Episode in Southeast Texas

- Synoptic meteorological conditions were different from those observed during the August episodes.

- The synoptic-scale meteorological conditions produced an 18-hour period of southward flow on 7 September and south- to southeastward offshore flow during the morning associated with the land breeze on 8–11 September. This offshore flow provided a mechanism for transporting shore-based ozone and ozone precursors over land as well as offshore to the Gulf of Mexico.

- Stronger land breezes were caused by the synoptic-scale offshore pressure gradient reenforcing the mesoscale pressure gradient that was directed offshore during the night and early morning. When the land warmed during the daytime, the mesoscale pressure gradient switched to onshore, but the synoptic pressure gradient (still offshore) and the presence in the area of a stationary cold front inhibited the inland penetration of the gulf breeze. The strength and duration of the onshore flow generally matched that of the offshore flow.

- Southeastward flow associated with the land breeze was an important mechanism for transporting ozone and ozone precursors from shore-based source regions. The southward transport ceased when it encountered the northward-moving gulf breeze front. This resulted in the highest ozone concentrations occurring ahead of, or just behind, the gulf breeze front on 8 and 9 September.

- Air quality conditions on 10 September were different from those observed on 8 and 9 September because ozone concentrations remained high for up to 8 hours after the gulf breeze passed (i.e., in the marine air flowing onshore). This indicated that the region of high ozone extended significantly farther into the Gulf than on other days.

- This region of high ozone over the Gulf was caused by strong offshore flow (3 to 5 m/s) during the morning of 10 September, which transported significant amounts of ozone and ozone precursors offshore to about 50 km. OCSPD emissions may have contributed to the ozone formation offshore, but the arrival of this air back onshore occurred several hours later than any ozone exceedances. Pollutants were then recirculated back onshore by the gulf breeze.

Hydrocarbon and Carbonyl Compound Analyses

- Most of the NMOC/NO_x ratios collected aloft and at the surface along both Texas and Louisiana coasts were greater than 10; 50 to 90 percent of the ratios were over 20.

- NMHC species distributions were highly variable both at the surface (Clinton) and aloft (all spiral locations); these variabilities might be due to variations in meteorological parameters (including wind speed, wind direction, and mixing height) at the sources or along the transport route, or to variations in emissions, or to variations in chemical reaction rates.

- The aircraft hydrocarbon composition measured near offshore platforms was similar to the shoreline hydrocarbon composition under onshore conditions. Trajectory analyses showed that air parcels originating near the shoreline could be carried offshore in the morning as far as High Island Platform prior to the wind shift to onshore flow later in the day.

- Carbonyl compounds account for a large fraction of the carbon, often more than 50 weight percent in the samples aloft and an average of 35 percent at the

surface. C3+ carbonyl compounds account for about a quarter of the total carbon and more than half of the total carbonyl compounds on average at the surface. However, current PAMS (Photochemical Assessment Monitoring Stations) guidelines call for results for only formaldehyde, acetaldehyde, and acetone.

ASSESSMENT OF OCSPD EMISSION CONTRIBUTIONS TO OZONE EXCEEDANCES IN SOUTHEAST TEXAS AND BATON ROUGE

- Based on the data collected, it appears that direct, same-day transport of OCSPD emissions from source regions in the Gulf of Mexico (south and east of Louisiana) to exceedance sites near Baton Rouge probably did not occur. Backward trajectories indicated that OCSPD emissions could have contributed to Baton Rouge exceedances via second-day transport from source regions off the shores of southwestern Louisiana and southeast Texas.

- Evaluating the contribution of OCSPD sources to ozone exceedances in southeast Texas during the September episode was difficult due to the extended periods of offshore flow that transported shore-based emissions over the Gulf. On 8, 9, and 11 September, most exceedances occurred during offshore flow or in the onshore flow just behind the gulf breeze front, thus indicating little, if any, OCSPD emission contribution. Surface and upper-air trajectories combined with data analyses suggested that air parcels reaching exceedance sites originated in the Houston/Ship Channel area and were transported southeastward, no farther than about 10 km offshore, before being recirculated back onshore.

- However, on 10 September, trajectories and data analyses suggested that emissions from shore-based sources were transported offshore at least 50 km and likely commingled with OCSPD emissions over the Gulf. Photochemistry probably took place and the gulf breeze transported this marine air with higher ozone concentrations back onshore, as observed by the 8-hour period with ozone concentrations greater than 100 ppb measured after the gulf breeze passed Gilchrist and Galveston.

Transport Onshore During Persistent Onshore Flow Conditions

- When onshore flow persisted for several days at a time, the ozone concentration at the shoreline slowly and steadily dropped from typically about 60 to 80 ppb on the first day to 20 to 40 ppb after several days. NO_x concentrations also dropped from about 4 to 6 ppb to less than 2 ppb during steady onshore flow conditions. In addition, NO concentrations during persistent onshore flow were typically zero (less than 0.5 ppb). These data indicate that offshore emissions alone did not produce ozone exceedances in the southeast Texas and Baton Rouge nonattainment areas during persistent onshore flow conditions.

Transport Distances During 19 August Episode in Southeast Texas

- Surface and trajectories aloft indicated that nighttime and early morning emissions from the Houston/Ship Channel area were transported toward the southeast in the offshore flow and reached the general area of the shoreline by about midday, when the flow reversal returned these now-reacting emissions toward Houston. Emissions from the Texas City/Galveston and Beaumont/Port Arthur areas had reached about 30 to 40 km offshore before the flow reversal returned them toward the northwest; however, these emissions likely did not reach the exceedance areas north and northwest of Houston.

- Surface and upper-air trajectories indicated that air parcels that arrived at Aldine on 19 August had likely not reached the coast and thus had not been transported offshore. Offshore emissions beyond about 20 km likely did not reach the Houston ship channel area or the exceedance areas north and northwest of Houston.

- Surface and upper-air trajectories indicated that the morning offshore flow carried onshore emissions up to about 40 km offshore. In addition, offshore emissions from beyond about 75 km likely did not even reach the shoreline before about 2000 CDT, well after the ozone exceedances were recorded.

Transport Distances During 8 September Episode in Southeast Texas

- Surface and trajectories aloft indicated that nighttime and early morning emissions from the Houston/Ship Channel area were transported toward the southeast in the offshore flow and reached the general area of the shoreline and up to about 10 km offshore by about midday, when the flow reversal returned these now-reacting emissions toward the northeast. Emissions from the Texas City/Galveston and Beaumont/Port Arthur areas reached about 30 to 50 km offshore before the flow reversal returned them toward the northeast; however, these emissions likely did not reach the exceedance areas at the shoreline and inland up to about 20 km.

- Surface and upper-air trajectories indicated that air parcels arriving at Smith Point and Gilchrist on 8 and 9 September may have originated in the Houston ship channel area. Offshore emissions beyond about 75 km likely did not reach the onshore exceedance areas.

- Surface and upper-air trajectories indicated that the morning offshore flow carried onshore emissions up to about 50 km offshore. In addition, offshore emissions from beyond about 75 km likely did not even reach the shoreline before about 2000 CDT.

Transport Distances During Louisiana Episode

- Surface and upper-air trajectories indicated that air parcels arriving at Baton Rouge exceedance sites on 18 and 19 August had originated in the general area of southeast Texas on the previous day. Offshore emissions likely did not reach more than about 70 km onshore, and not as far as the exceedances areas.

- Surface and upper-air trajectories indicated that the morning offshore flow carried coastal emissions up to about 50 km offshore. In addition, offshore emissions from beyond about 60 km likely did not even reach the shoreline before about 2000 CDT.

Pollutant Flux Estimates

- Ozone and NO_x fluxes across the southeast Texas shoreline during early morning offshore flow conditions were different for different episodes. For the 17–21 August episode, the ozone flux was typically 4 mg/min/m^2, corresponding to an ozone concentration of about 20 ppb being transported at about 2 m/s; the NO_x flux was about 1 mg/min/m^2, corresponding to a NO_x concentration of about 5 ppb being transported at about 2 m/s. For the 9–11 August episode, the ozone and NO_x fluxes were typically about 1 mg/min/m^2, corresponding to ozone and NO_x concentrations of 15 and 12 ppb, respectively, being transported at about 1 m/s. Finally, for the 7–11 September episode, the ozone flux was typically 15 mg/min/m^2, corresponding to an ozone concentration of 62 ppb being transported at about 2 m/s; the NO_x flux was about 4 mg/min/m^2, corresponding to a NO_x concentration of about 19 ppb being transported at about 2 m/s.

- Ozone flux across the southeast Texas shoreline during midday onshore flow conditions was typically 23 mg/min/m^2, corresponding to an ozone concentration of about 58 ppb being transported at about 3 m/s for the August episodes and to an ozone concentration of about 110 ppb being transported at about 2 m/s for the September episode. NO_x flux was typically between 1 and 2 mg/min/m^2, corresponding to a NO_x concentration of about 4 ppb being transported at about 3 m/s for the August episodes and to a NO_x concentration of about 9 ppb being transported at about 2 m/s for the September episode.

- The typical NO_x mass flow rate passing through an imaginary plane about 600 m deep across 50 km of shoreline during midday onshore flow conditions was estimated to be about 2 mg/min, which corresponds to about 4.7×10^{-7} percent of typical surface emission rates in the Houston/Ship Channel area. Therefore, the amount of NO_x crossing the shoreline during onshore flow, even including onshore and offshore emissions, is significantly less than the onshore emissions likely to contribute to onshore ozone exceedances.

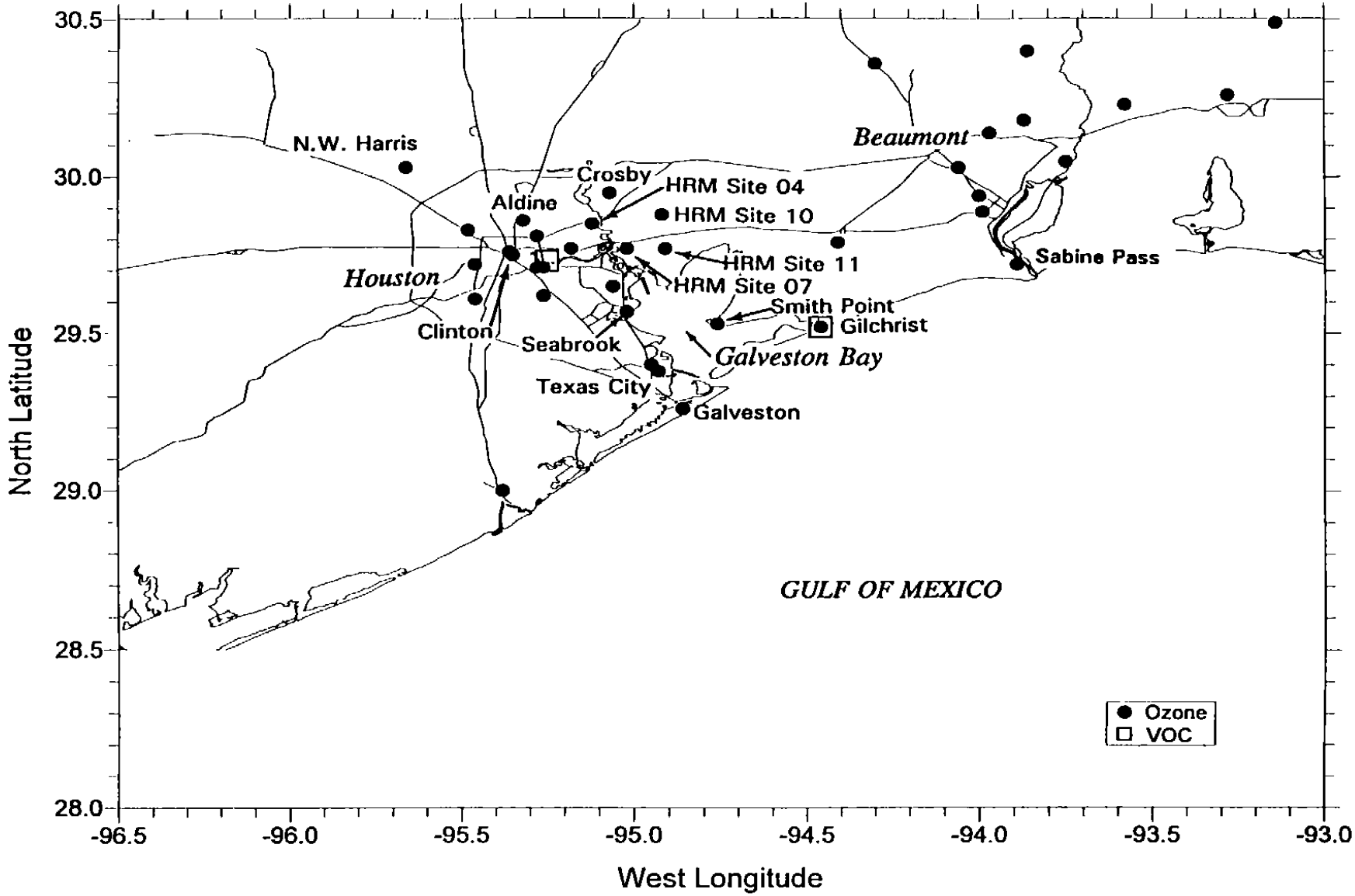

FIGURE 3-1a. Locations of surface air quality sites (ozone and NO/NO_y) and volatile organic compound samplers. Sites discussed in this report have been identified by name.

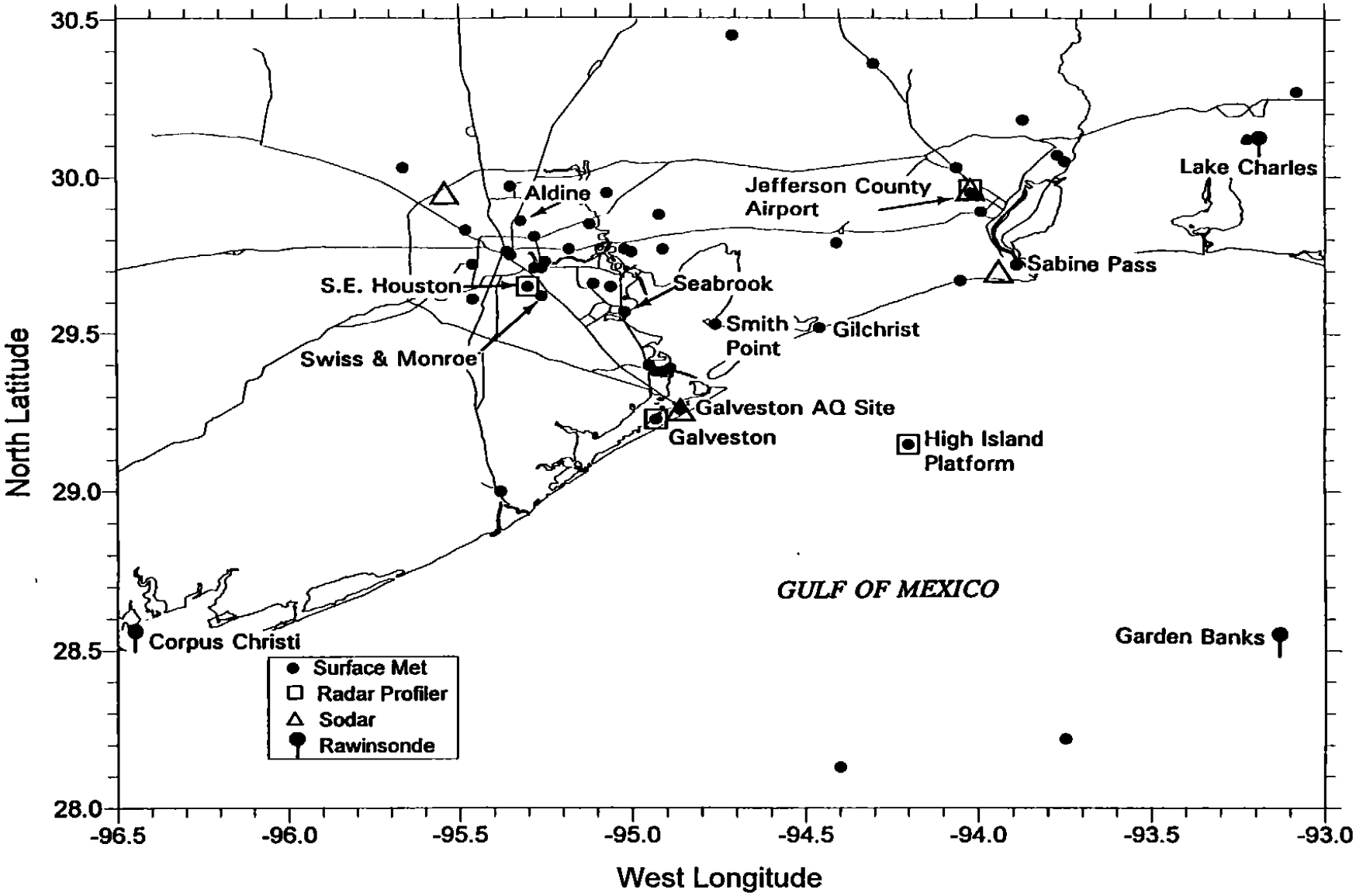

FIGURE 3-1b. Locations of surface and upper-air meteorological sensors. Sites discussed in this report have been identified by name.

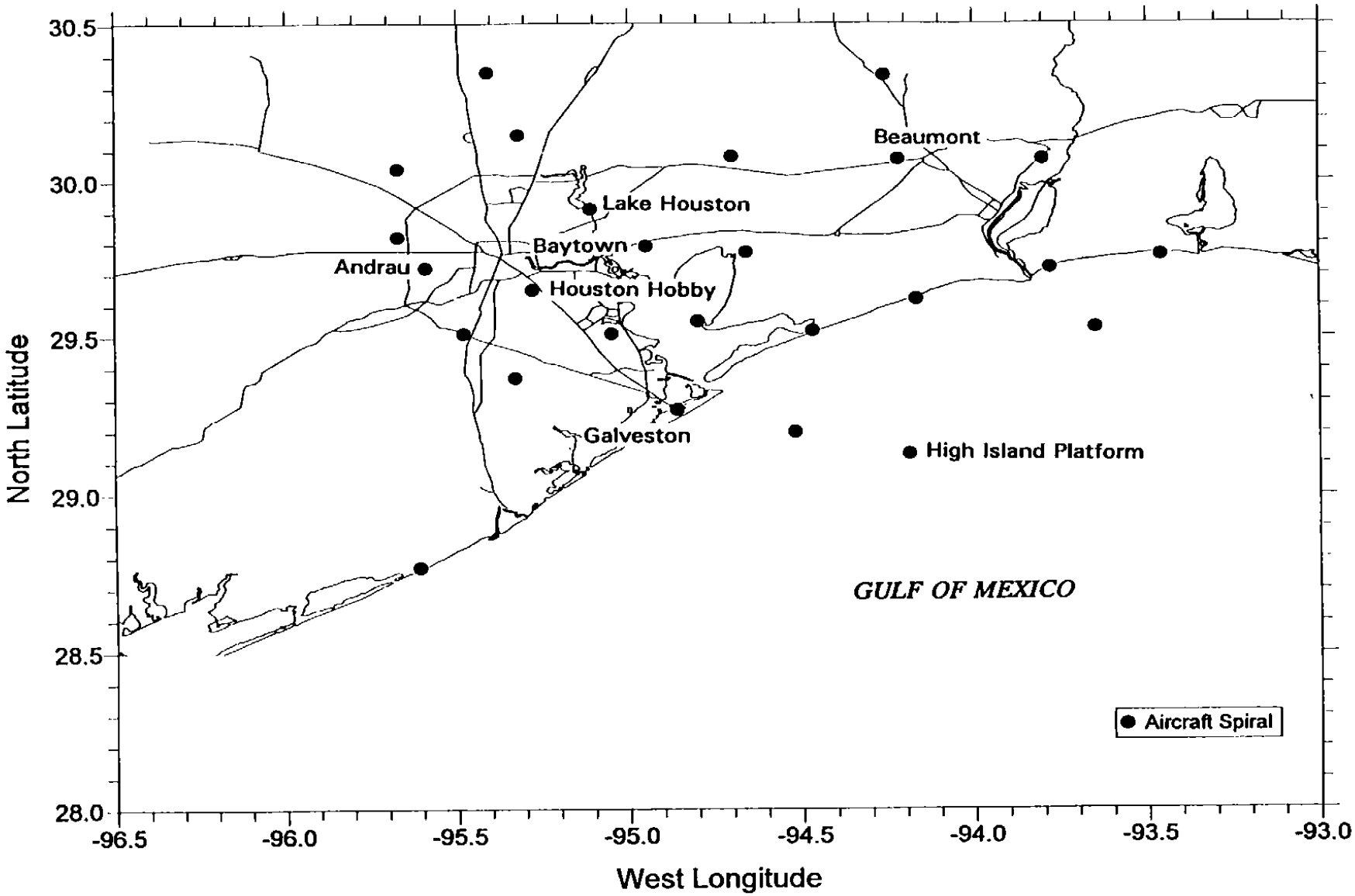

FIGURE 3-1c. Locations of aircraft spirals in the southeast Texas region. Sites discussed in this report have been identified by name.

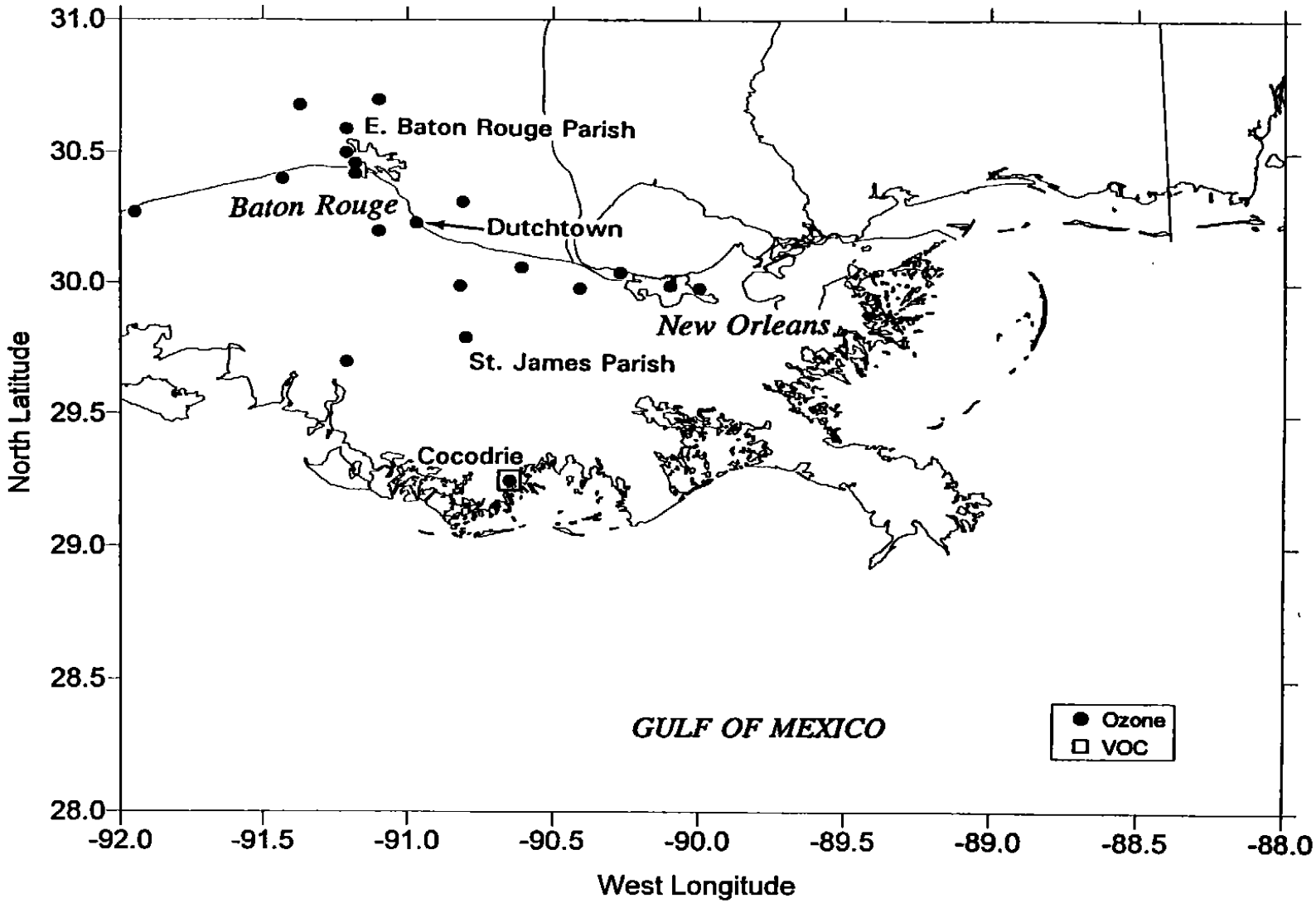

FIGURE 3-2a. Locations of surface air quality sites (ozone and NO/NO_x) and volatile organic compound samplers. Sites discussed in this report have been identified by name.

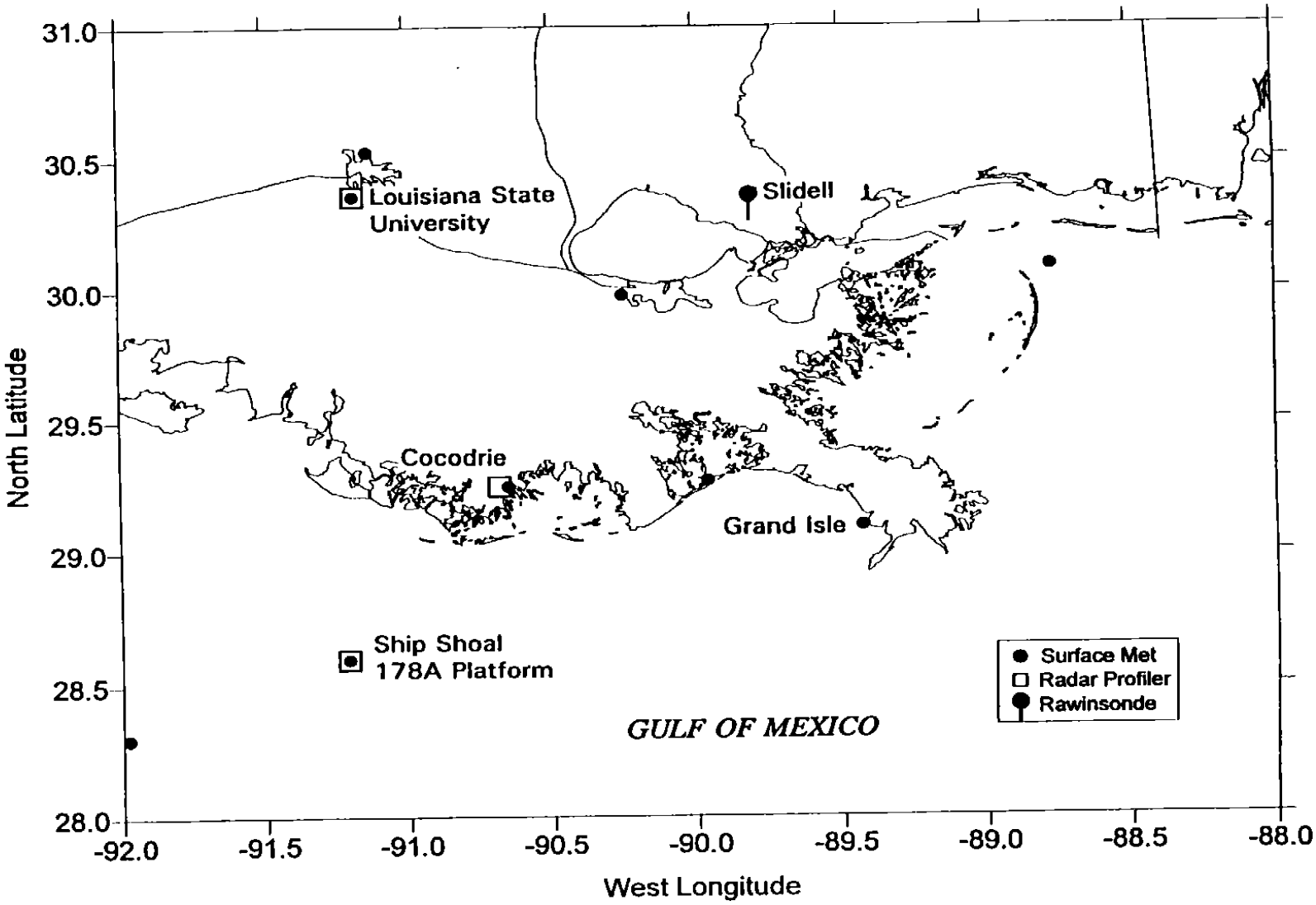

FIGURE 3-2b. Locations of surface and upper-air meteorological sensors. Sites discussed in this report have been identified by name.

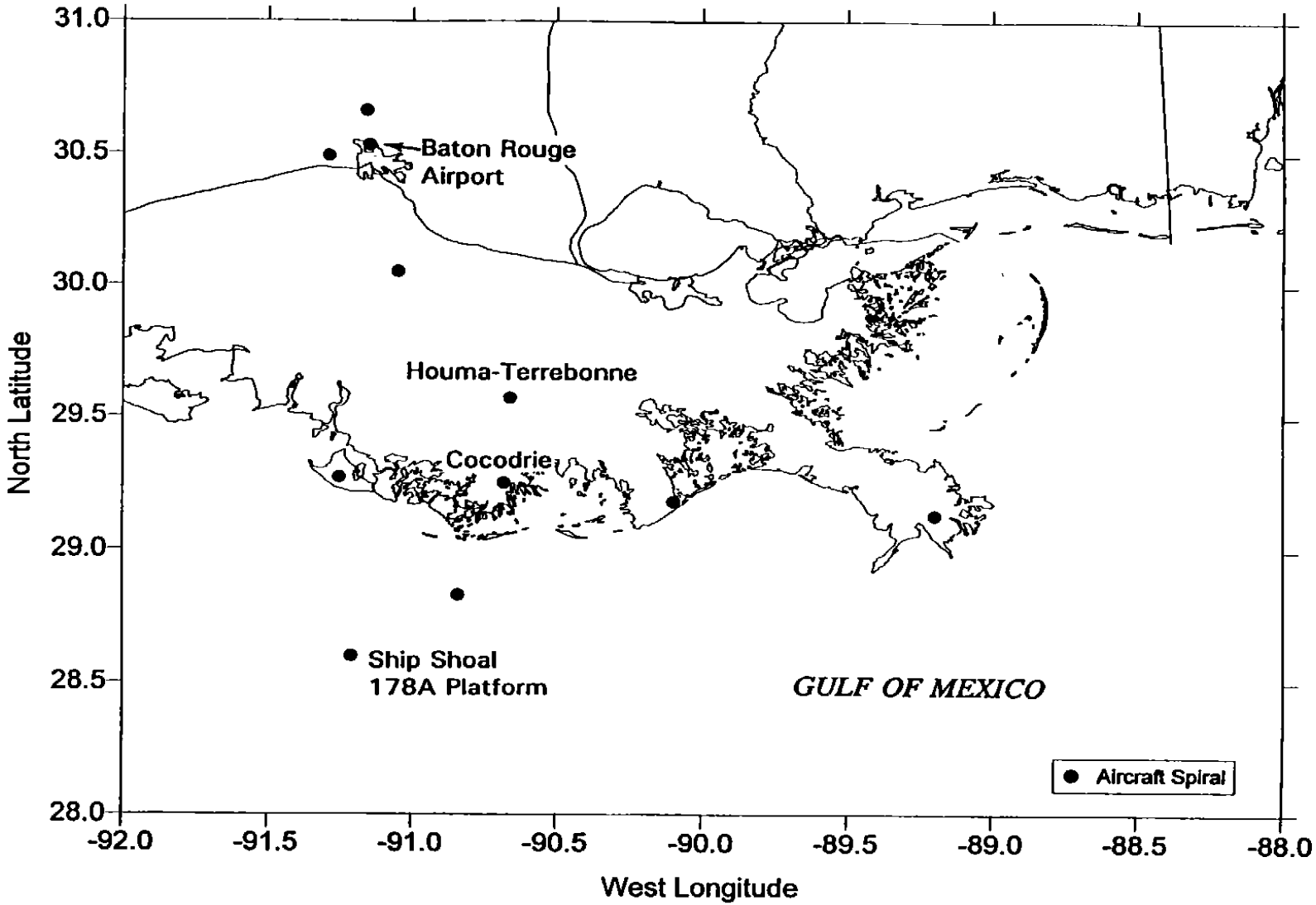

FIGURE 3-2c. Locations of aircraft spirals in the Louisiana region. Sites discussed in this report have been identified by name.

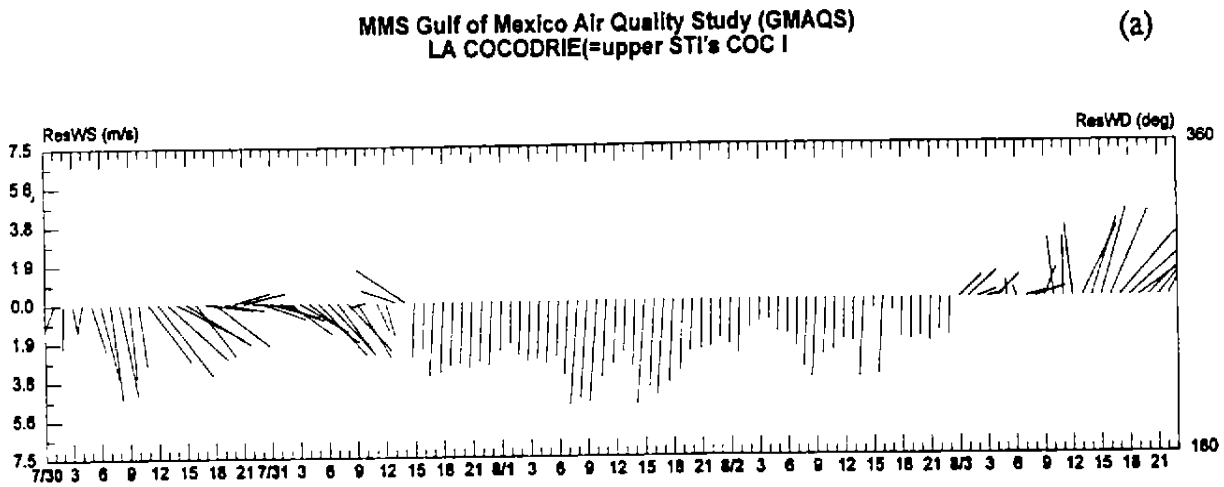

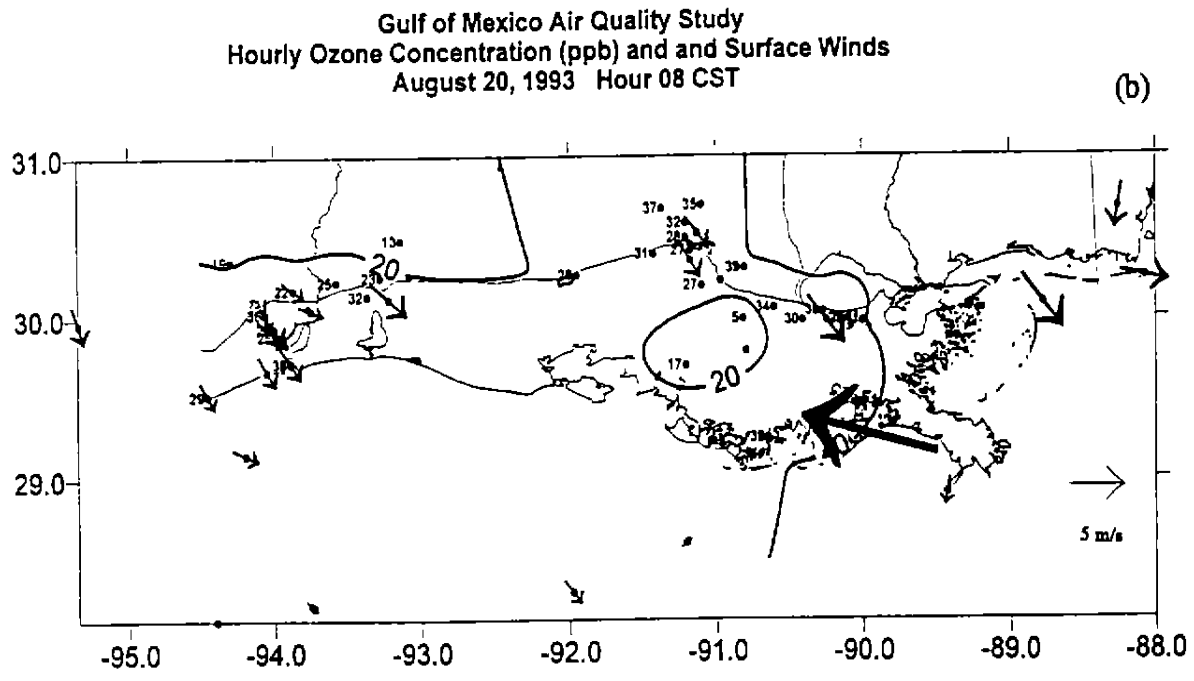

FIGURE 3-3. Examples of questionable data identified during the data validation: (a) constant wind directions measured at Cocodrie, Louisiana from July 31-2 August 1993 and (b) high surface winds at a surface station in Grand Isle, Louisiana on 29 August 1993 at 0800 CST.

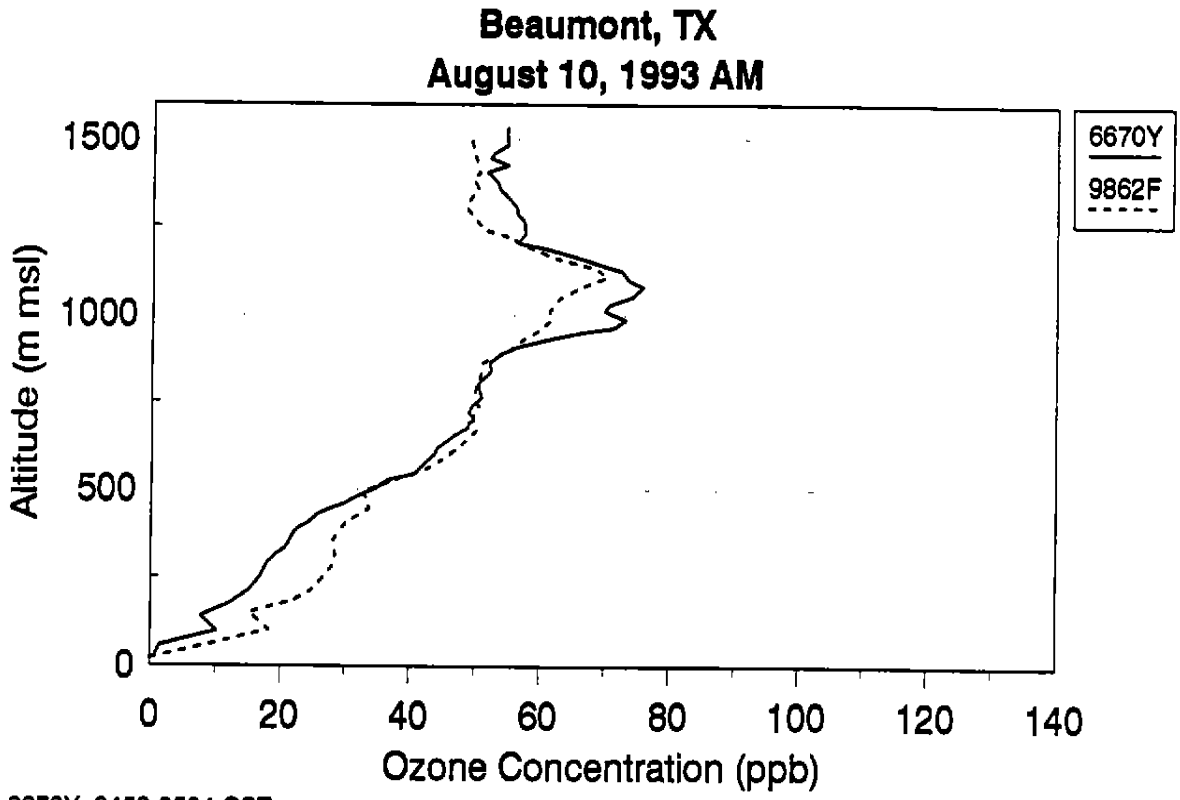

FIGURE 3-4. Comparison between 6670Y and 9862F aircraft ozone concentration profiles at Beaumont for the early morning flight on 10 August 1993. Altitude is in meters above mean sea level.

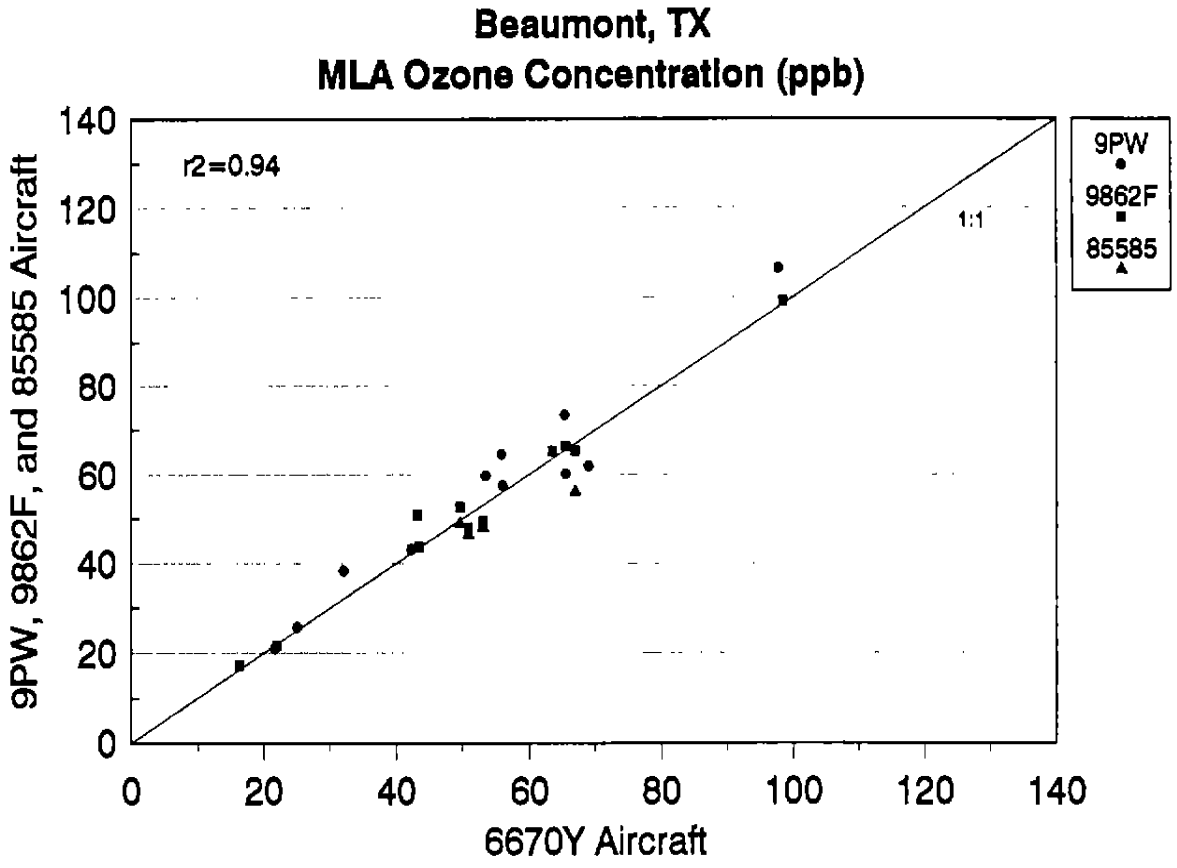

FIGURE 3-5. Scatter plot comparisons of 6670Y and 9PW, 9862F, and 85585 aircraft ozone mixed-layer averages (MLAs) for all the spirals over Beaumont during the summer of 1993.

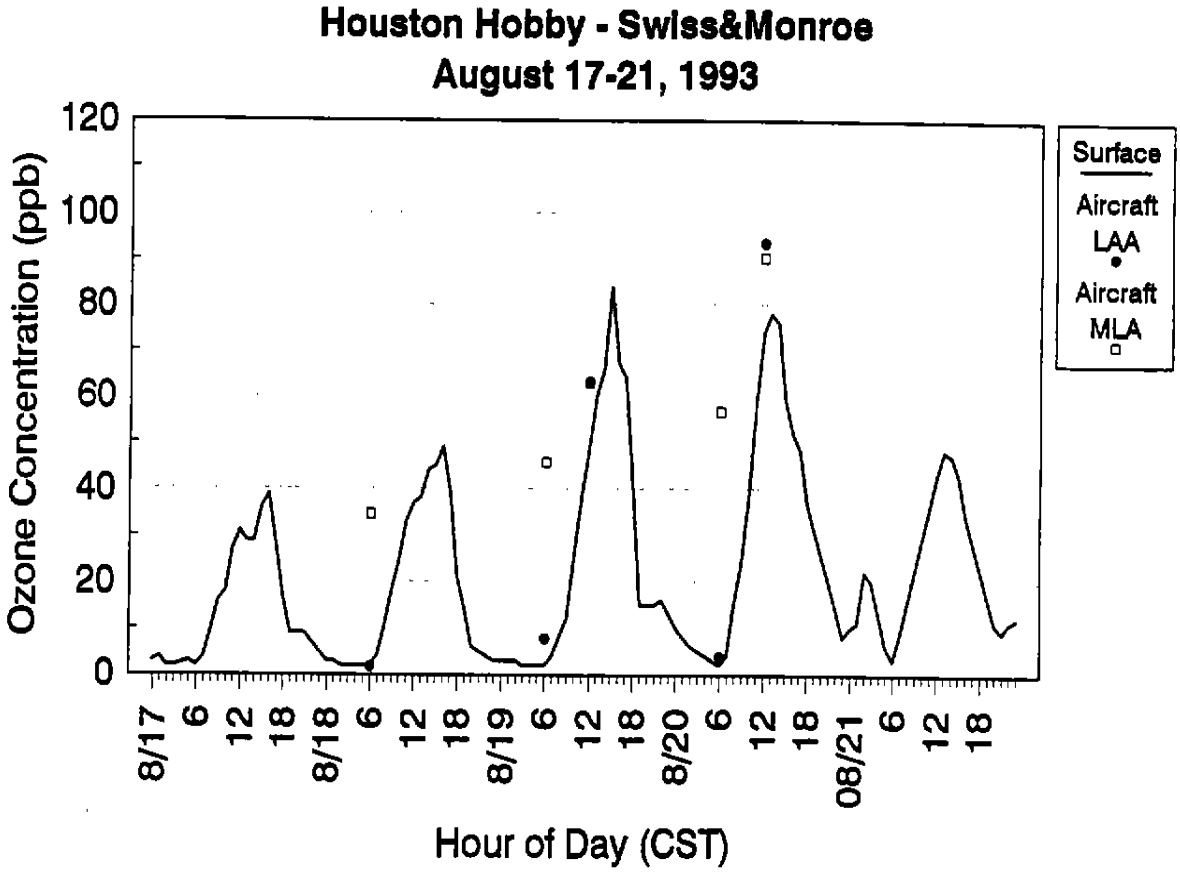

FIGURE 3-6. Comparison between surface ozone concentrations at the Swiss&Monroe surface site and mixed-layer averages (MLAs) and lowest-altitude averages (LAAs) at Houston Hobby Airport during the 17-20 August 1993 episode. (There were no flights on 17 August and 21 August.)

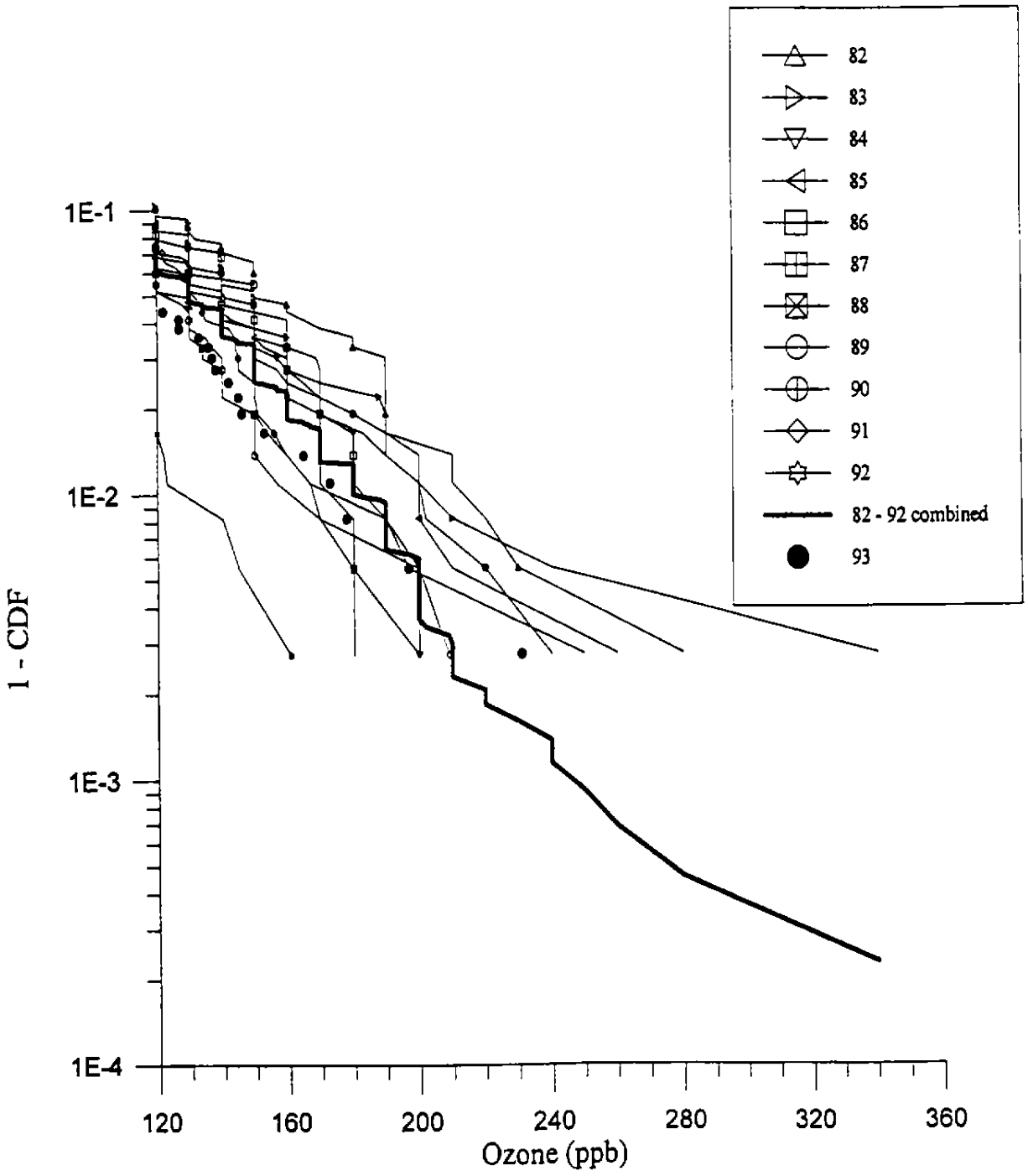

FIGURE 3-7. Cumulative distribution functions (CDF's) for ozone exceedances (C ≥ 120 ppb) in the GMAQS region. The daily maximum 1-hour ozone concentration anywhere in the GMAQS region is used. (Only one point is used in the figure to represent an ozone exceedance day even if multiple stations recorded ozone concentrations greater than or equal to 120 ppb.) The thin lines represent individual years (1982-1992), the filled circles represent 1993, and the thick line represents 1982-1992 combined.

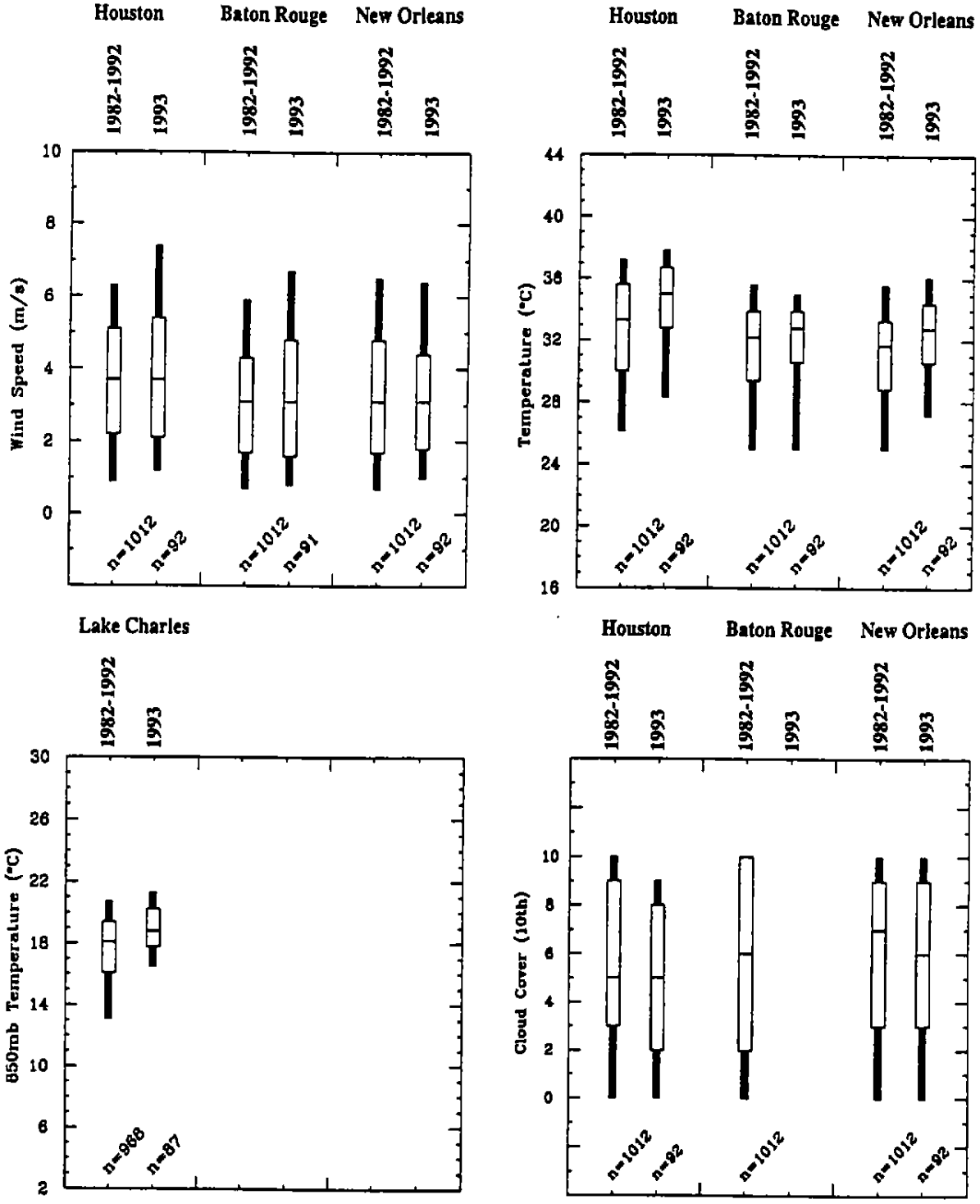

FIGURE 3-8. Probability distribution functions (pdf's) for meteorological variables in the GMAQS region for the historical period (1982-1992) and for 1993 for all days in the summer (July, August, September). The box plot format for the pdf's is used, with the median plus or minus one and two standard deviations indicated (i.e., the 2.5th, 16th, 50th, 84th, and 97.5th percentiles). The Houston, Baton Rouge, and New Orleans regions are included, except that the 850 mb temperatures were measured at Lake Charles for the ozone exceedance days in Houston.

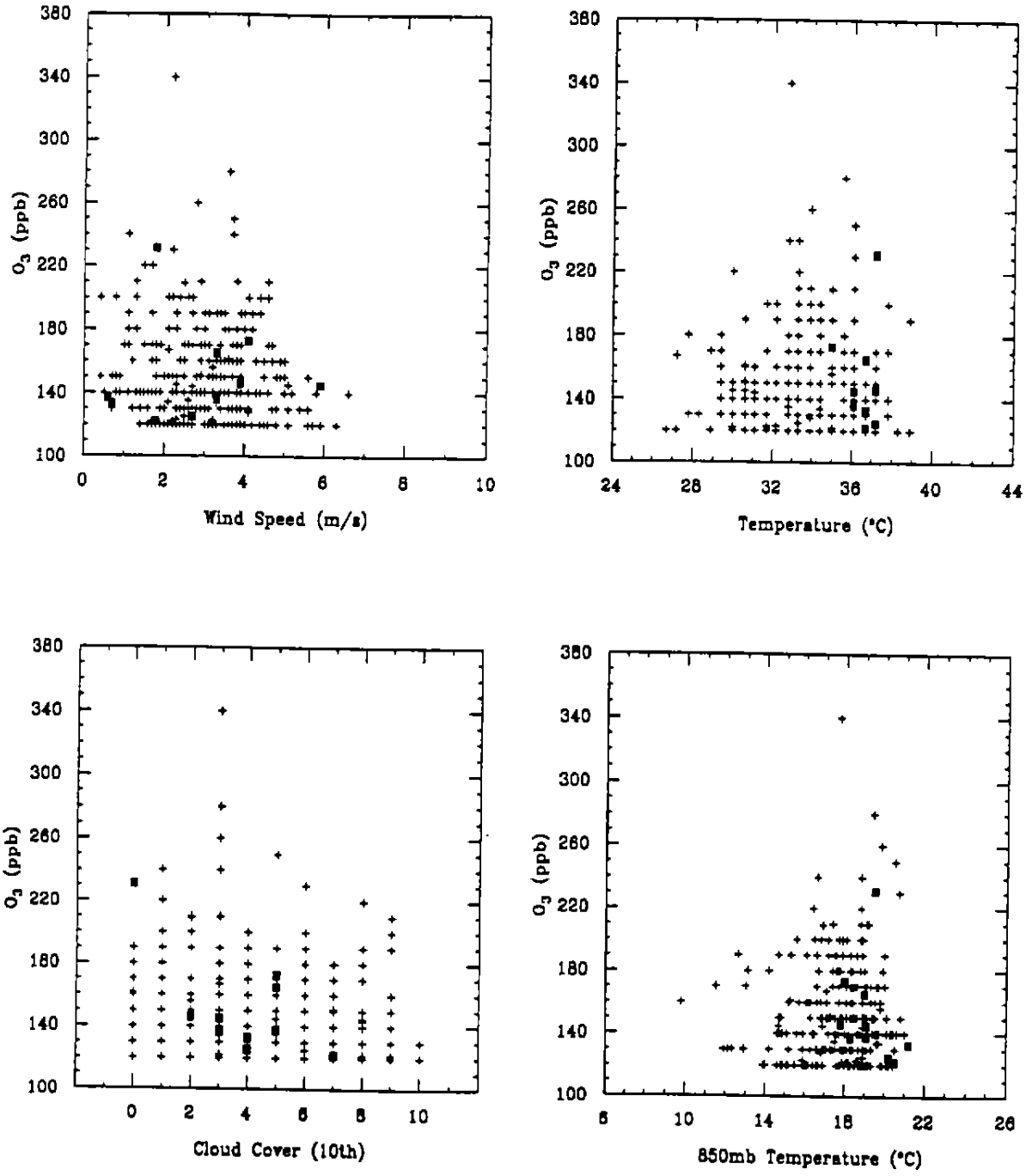

FIGURE 3-9. Maximum ozone concentrations in the Houston region for the 1982-1992 exceedance days (+) and for the 1993 episode days (■, those exceedance days included in the four GMAQS episode periods) plotted versus surface meteorological variables (wind speed, maximum surface temperature, and cloud cover) observed at Intercontinental Airport, and 850 mb temperature observed at Municipal Airport in Lake Charles.

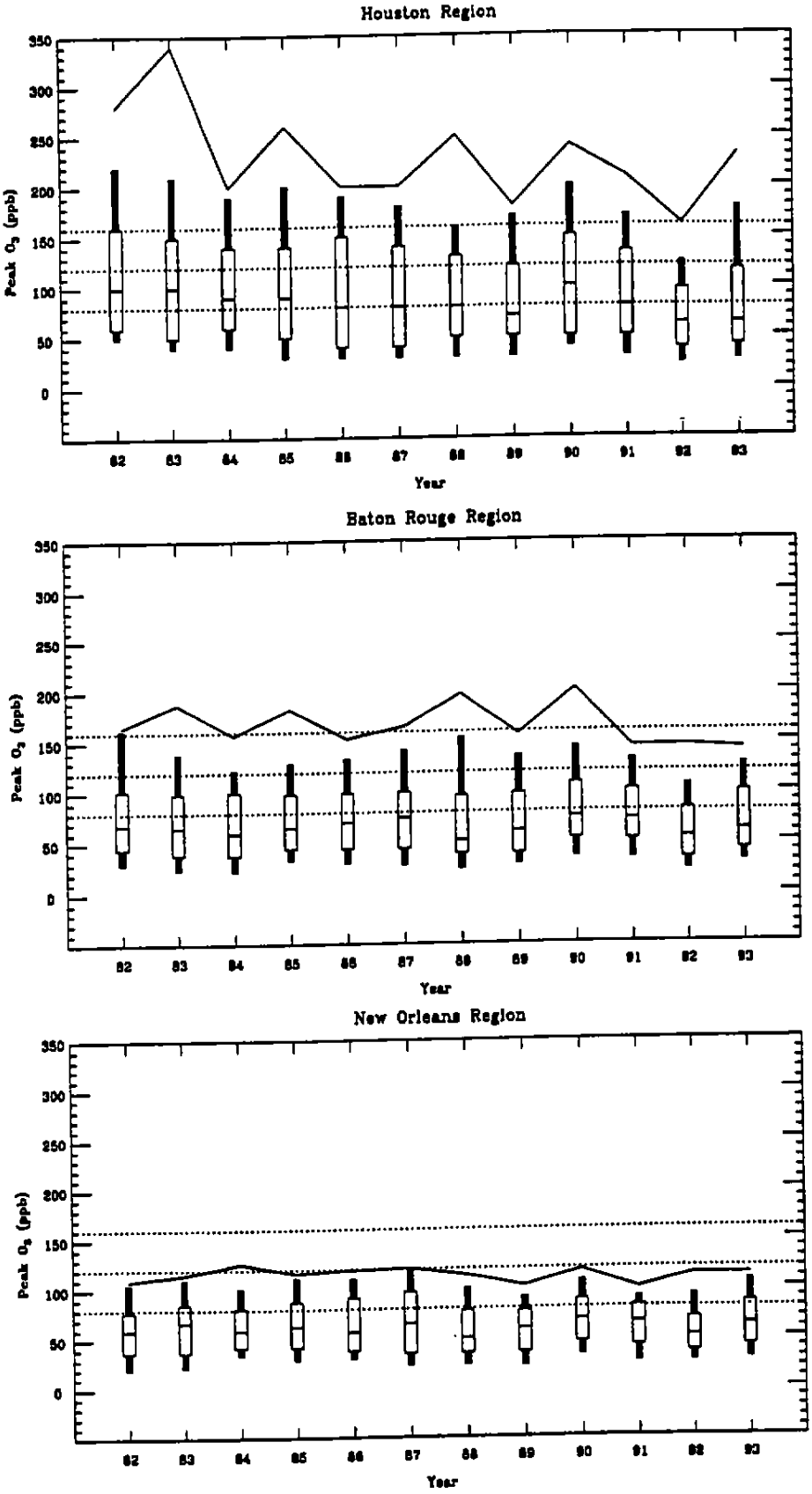

FIGURE 3-10. Box plot presentations of daily maximum ozone concentrations over the monitoring networks in the Houston, Baton Rouge, and New Orleans regions. The highest concentration and the 2.5th, 16th, 50th, 84th, and 97.5th percentiles are shown for each year from 1982-1993 for the summer (July, August, September) period. For each entry $n = 92$.

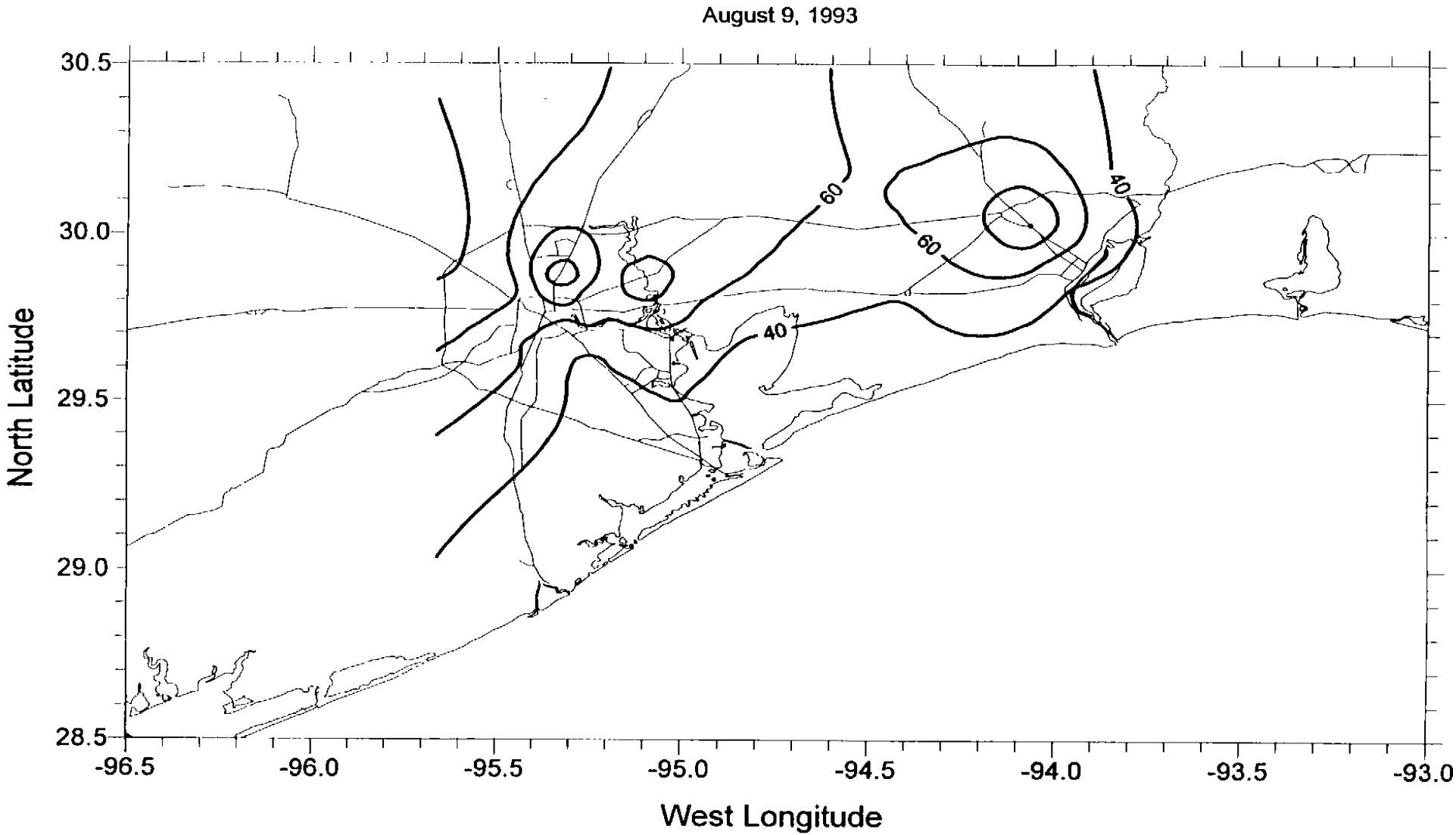

FIGURE 3-11a. Contour of maximum ozone concentrations (ppb) in the southeast Texas region on 9 August 1993. The location and concentrations of all exceedances are shown. No exceedances occurred on this initial day.

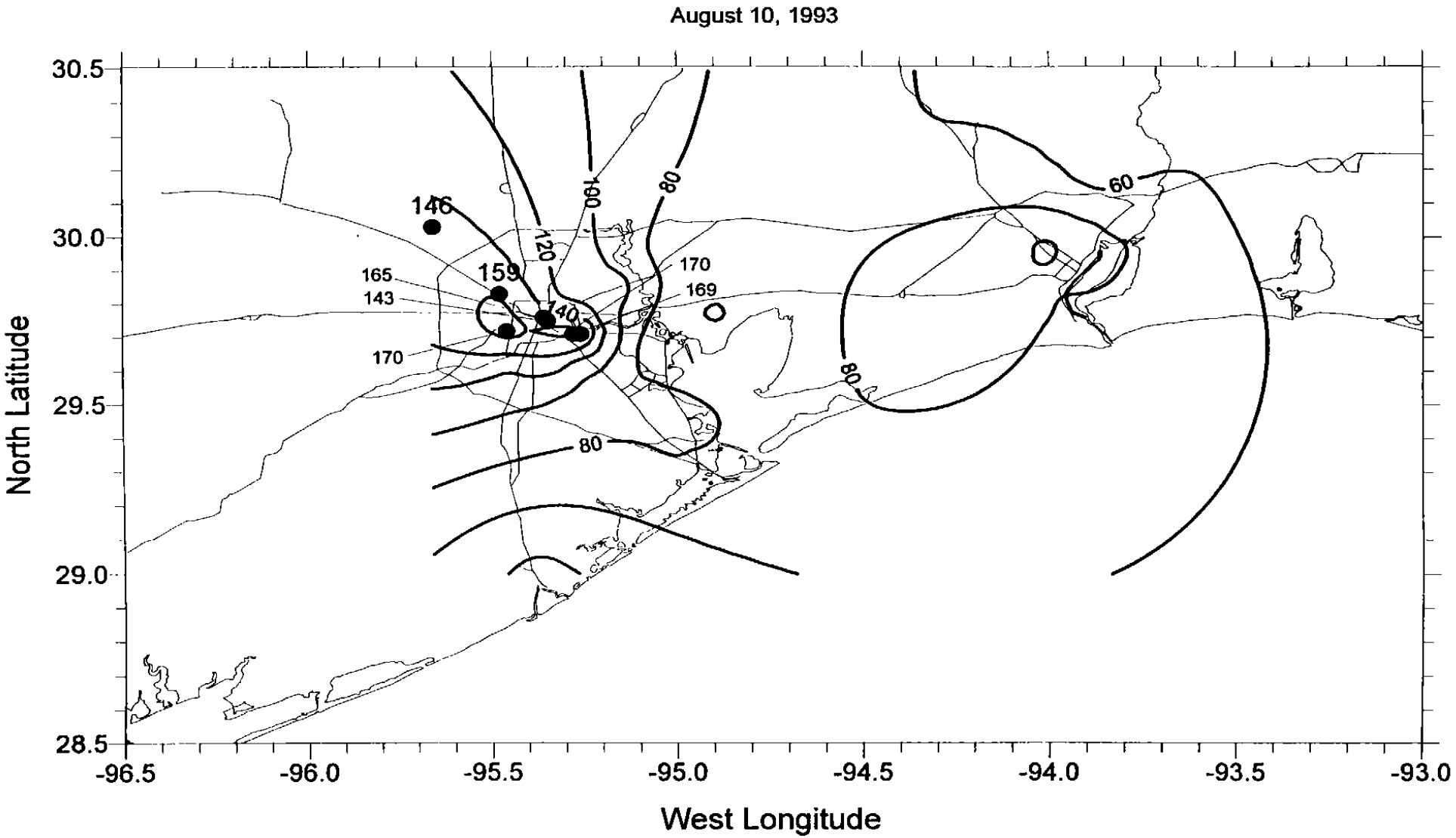

FIGURE 3-11b. Contour of maximum ozone concentrations (ppb) in the southeast Texas region on 10 August 1993.

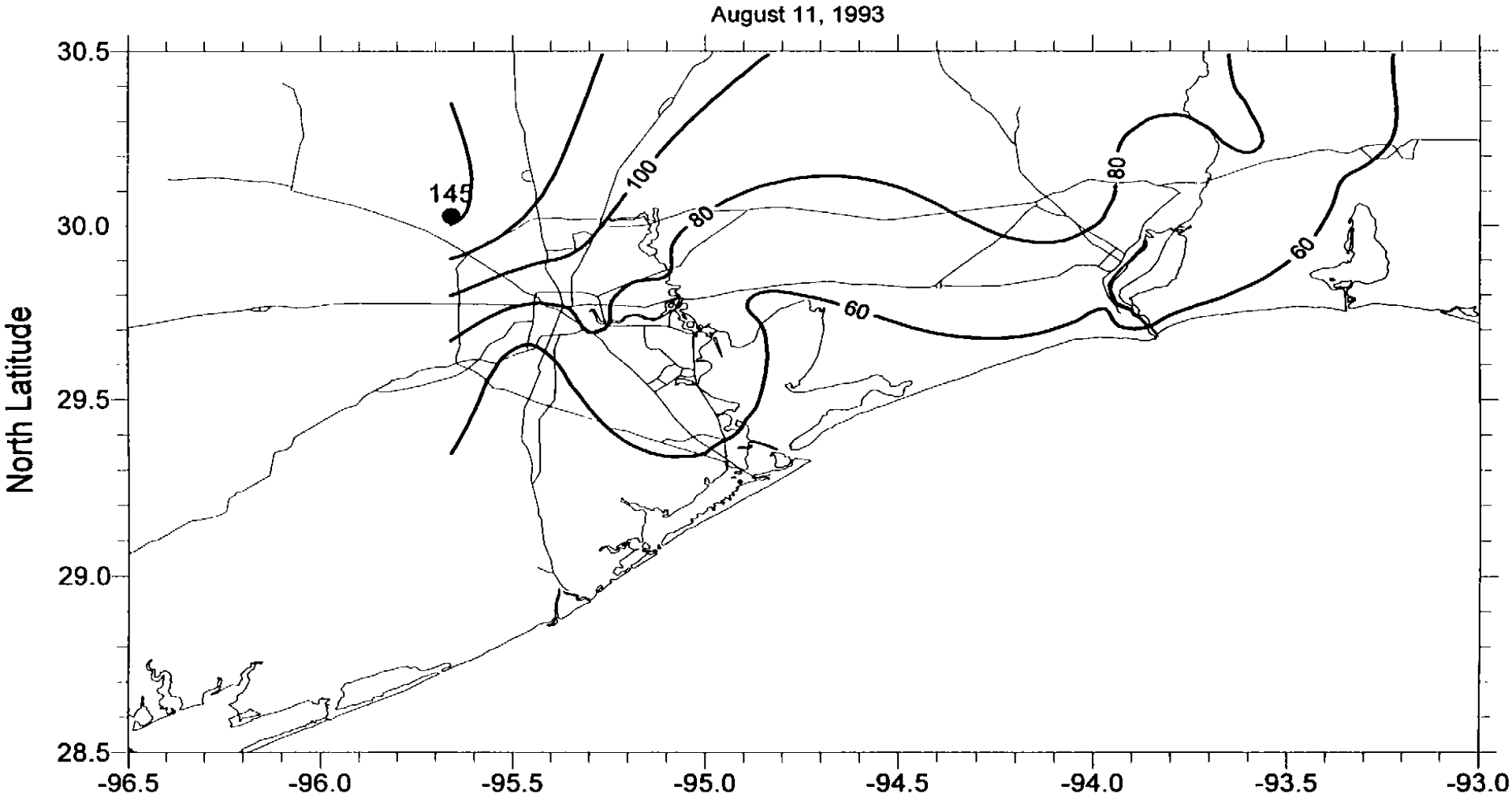

FIGURE 3-11c. Contour of maximum ozone concentrations (ppb) in the southeast Texas region on 11 August 1993.

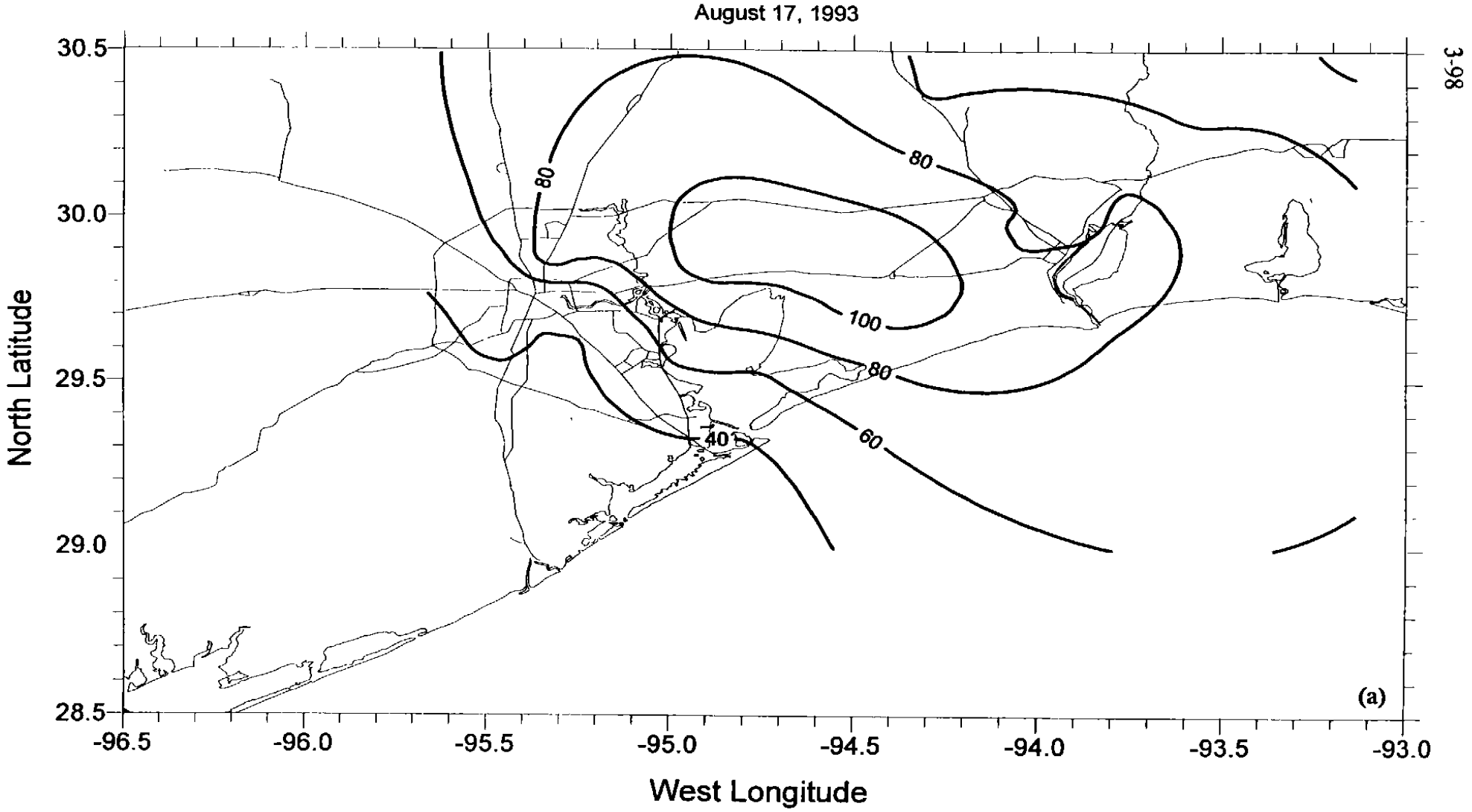

FIGURE 3-12a. Contour of maximum ozone concentrations (ppb) in the southeast Texas region on 17 August 1993. The locations and concentrations of all exceedances are shown. No exceedances occurred on this initial day.

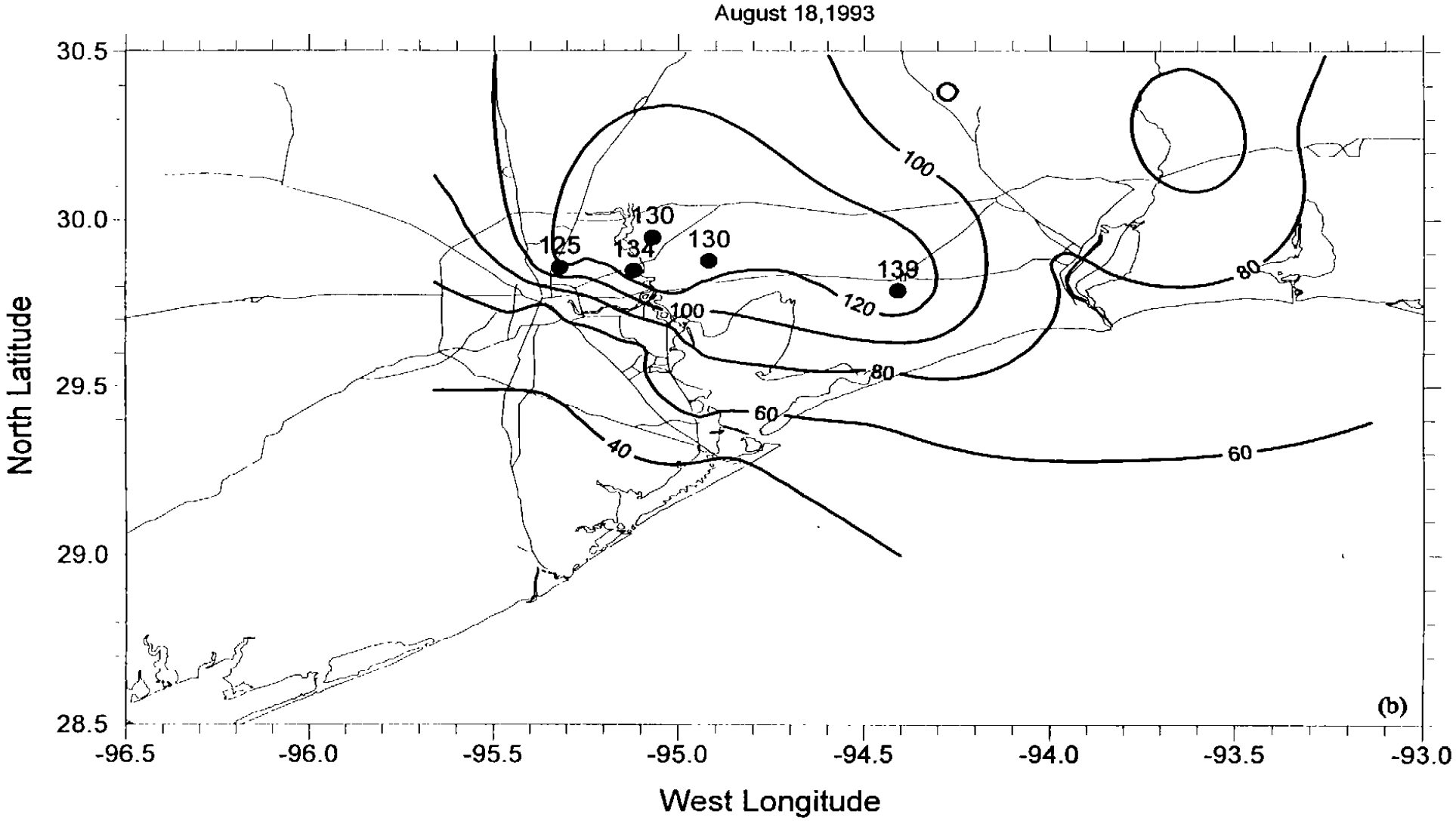

FIGURE 3-12b. Contour of maximum ozone concentrations (ppb) in the southeast Texas region on (b) 18 August 1993. The locations and concentrations of all exceedances are shown.

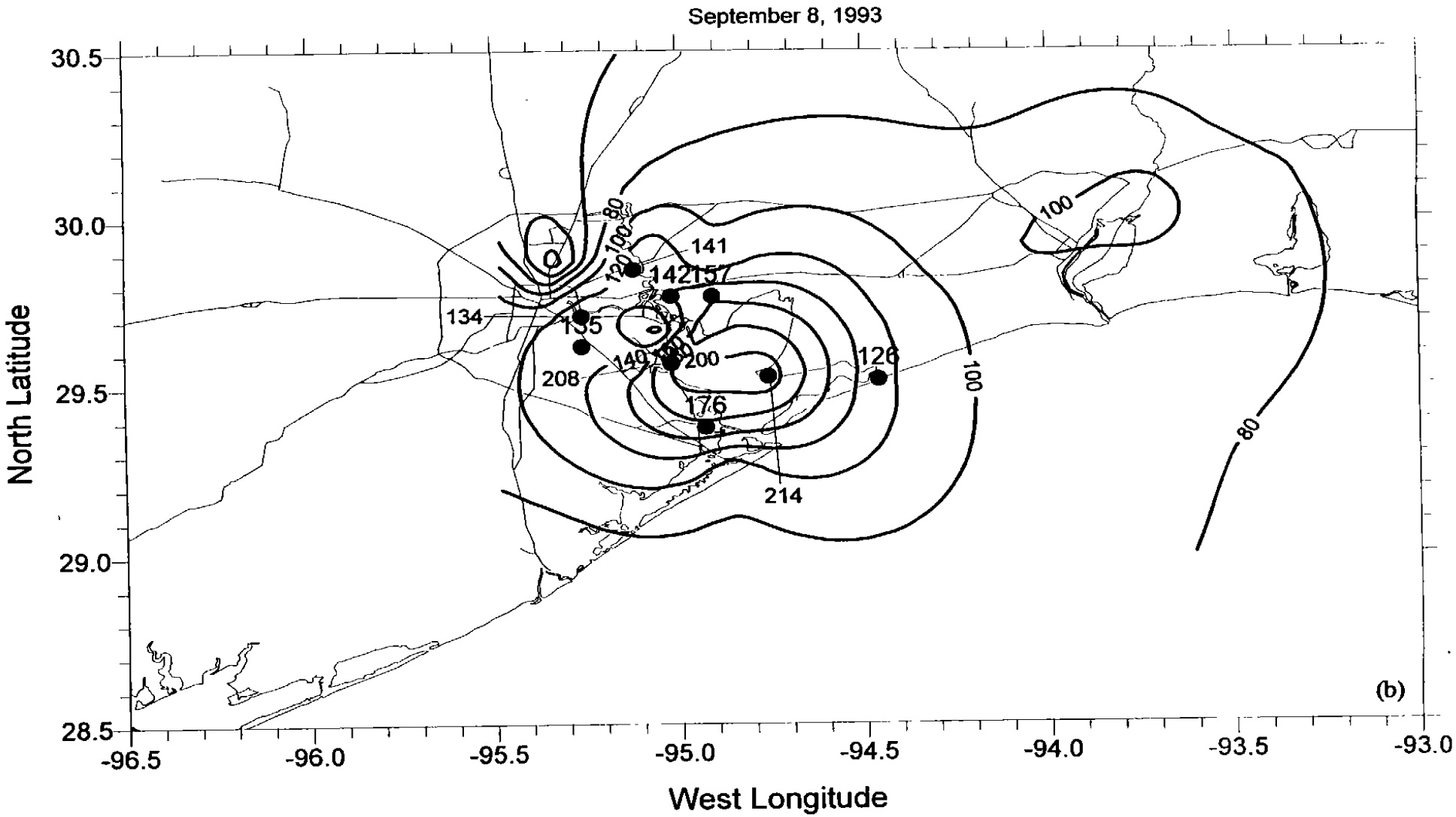

FIGURE 3-13b. Contour of maximum ozone concentrations (ppb) in the southeast Texas region on 8 September 1993. The locations and concentrations of all exceedances are shown. Note, the maximum concentration of 137 ppb at Tulosa (TN15) is not located within this map domain.

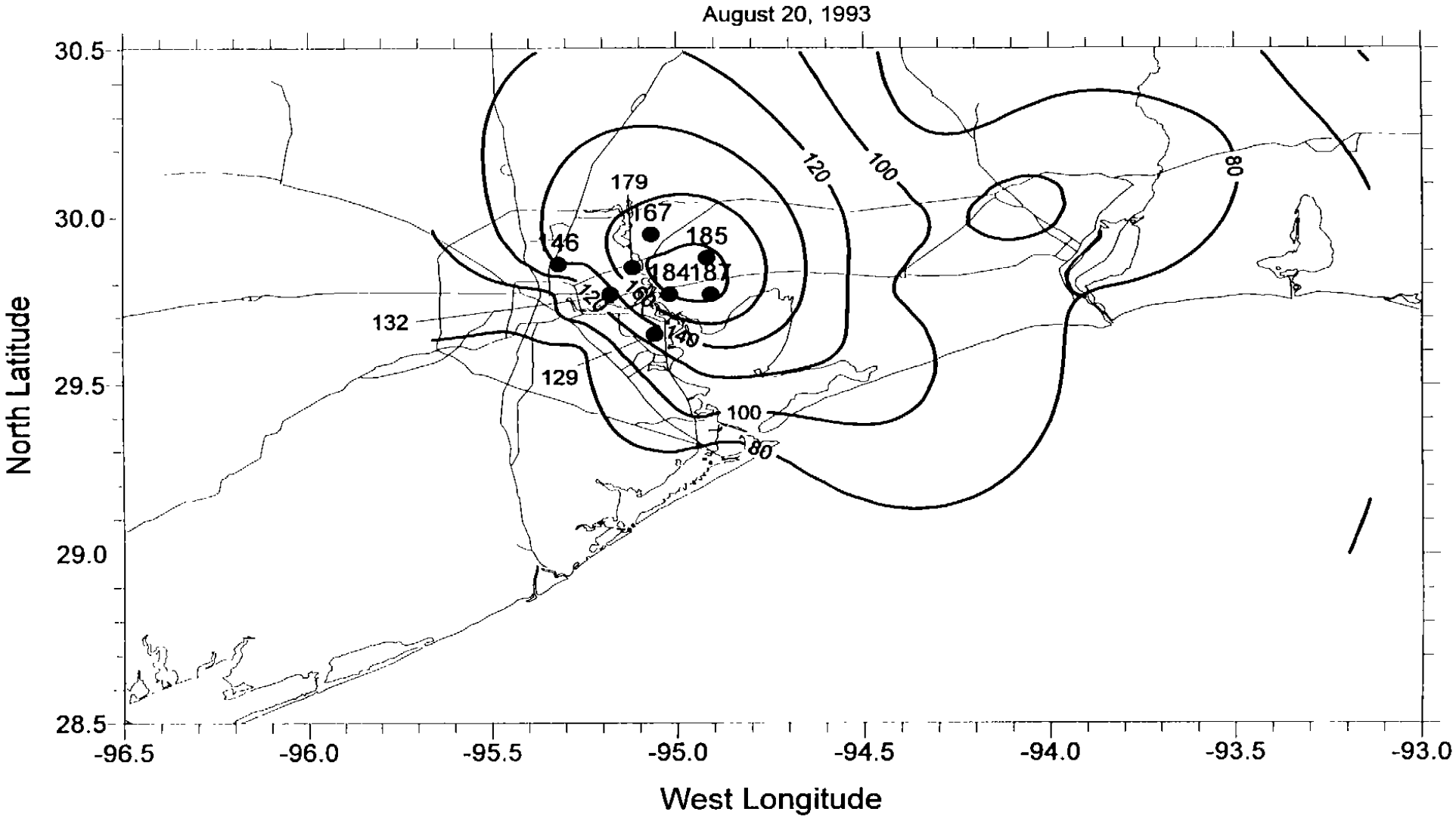

FIGURE 3-12d. Contour of maximum ozone concentrations (ppb) in the southeast Texas region on 20 August 1993. The locations and concentrations of all exceedances are shown.

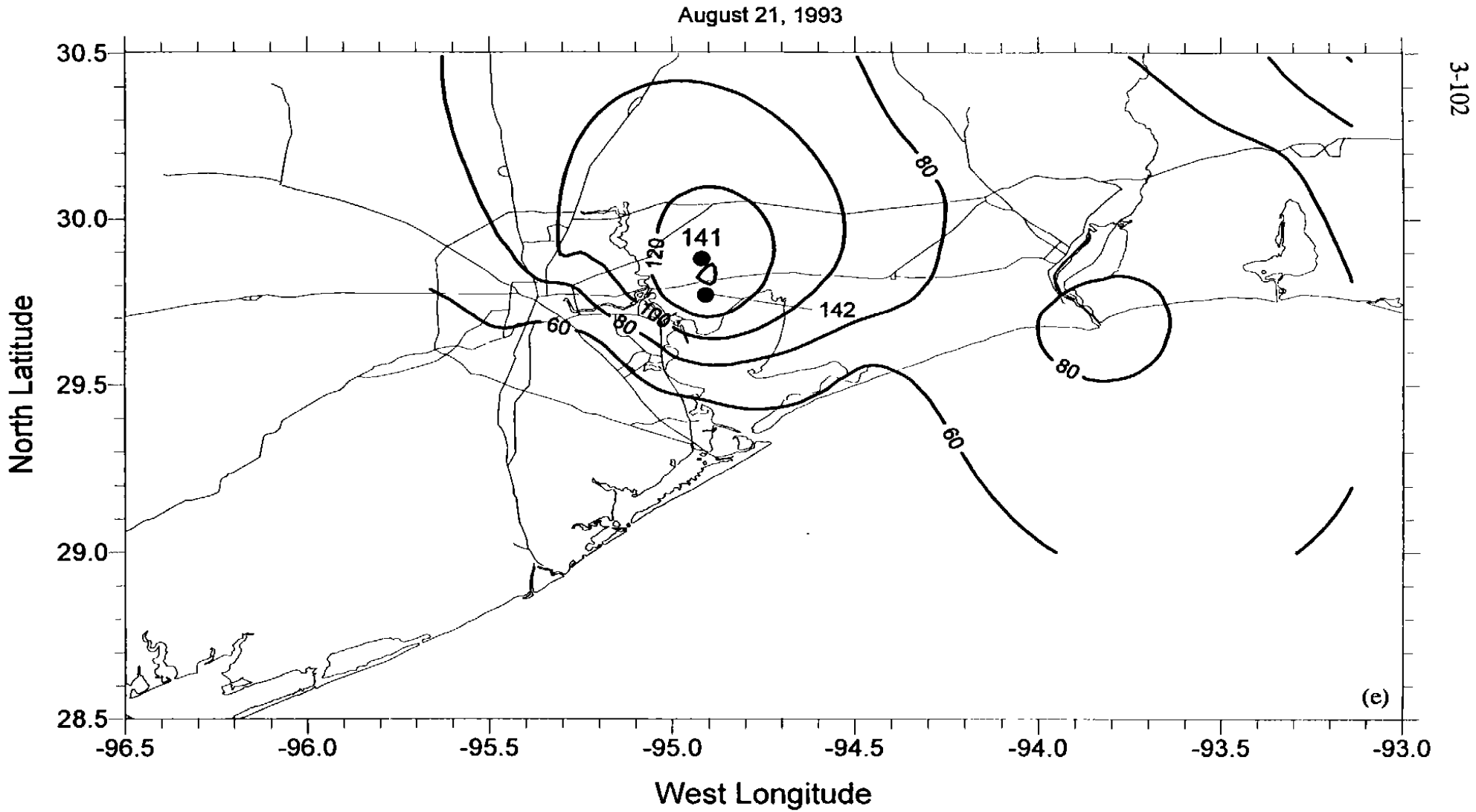

FIGURE 3-12e. Contour of maximum ozone concentrations (ppb) in the southeast Texas region on 21 August 1993. The locations and concentrations of all exceedances are shown.

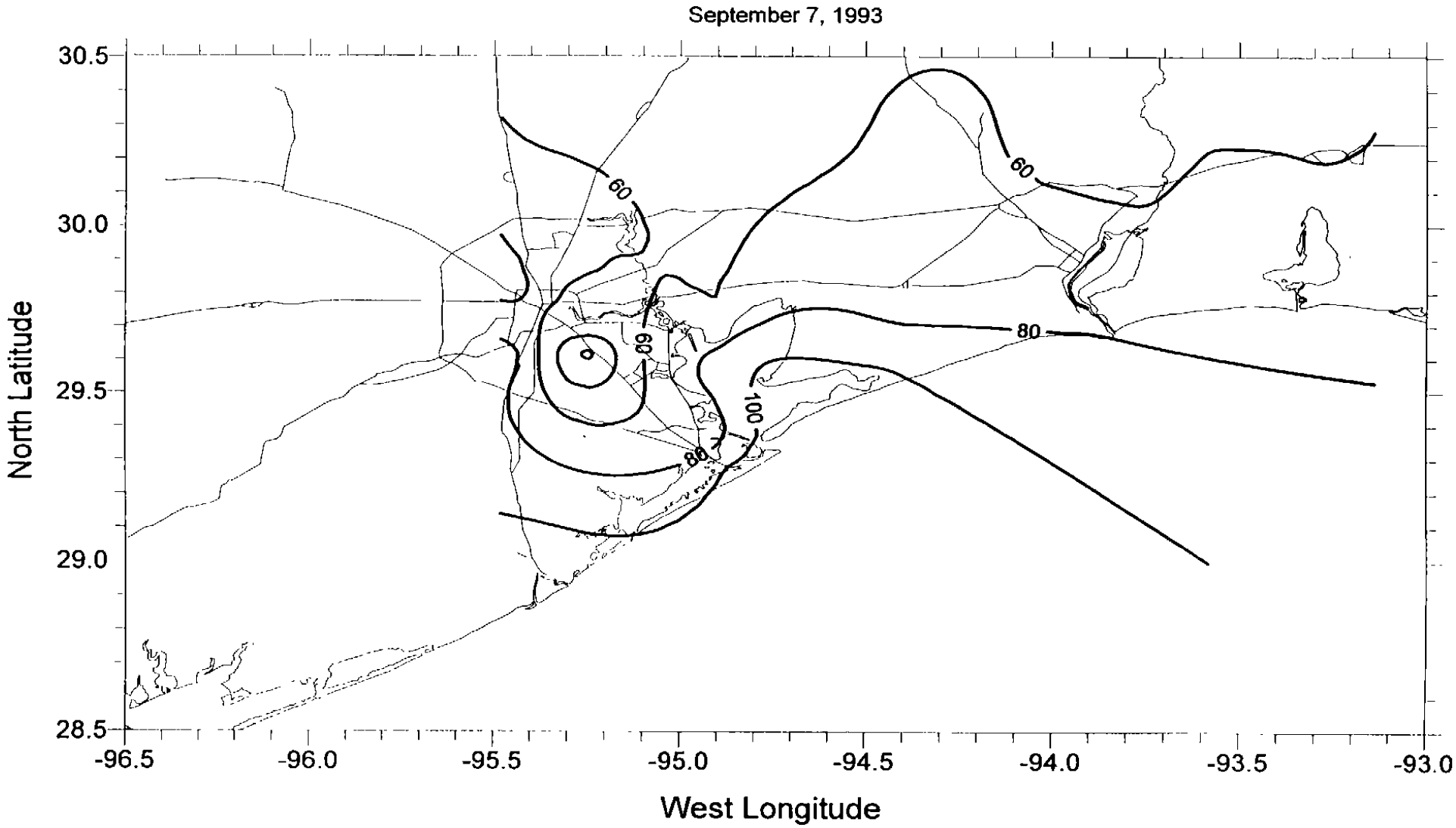

FIGURE 3-13a. Contour of maximum ozone concentrations (ppb) in the southeast Texas region on 7 September 1993. The locations and concentrations of all exceedances are shown. No exceedances occurred on this initial day.

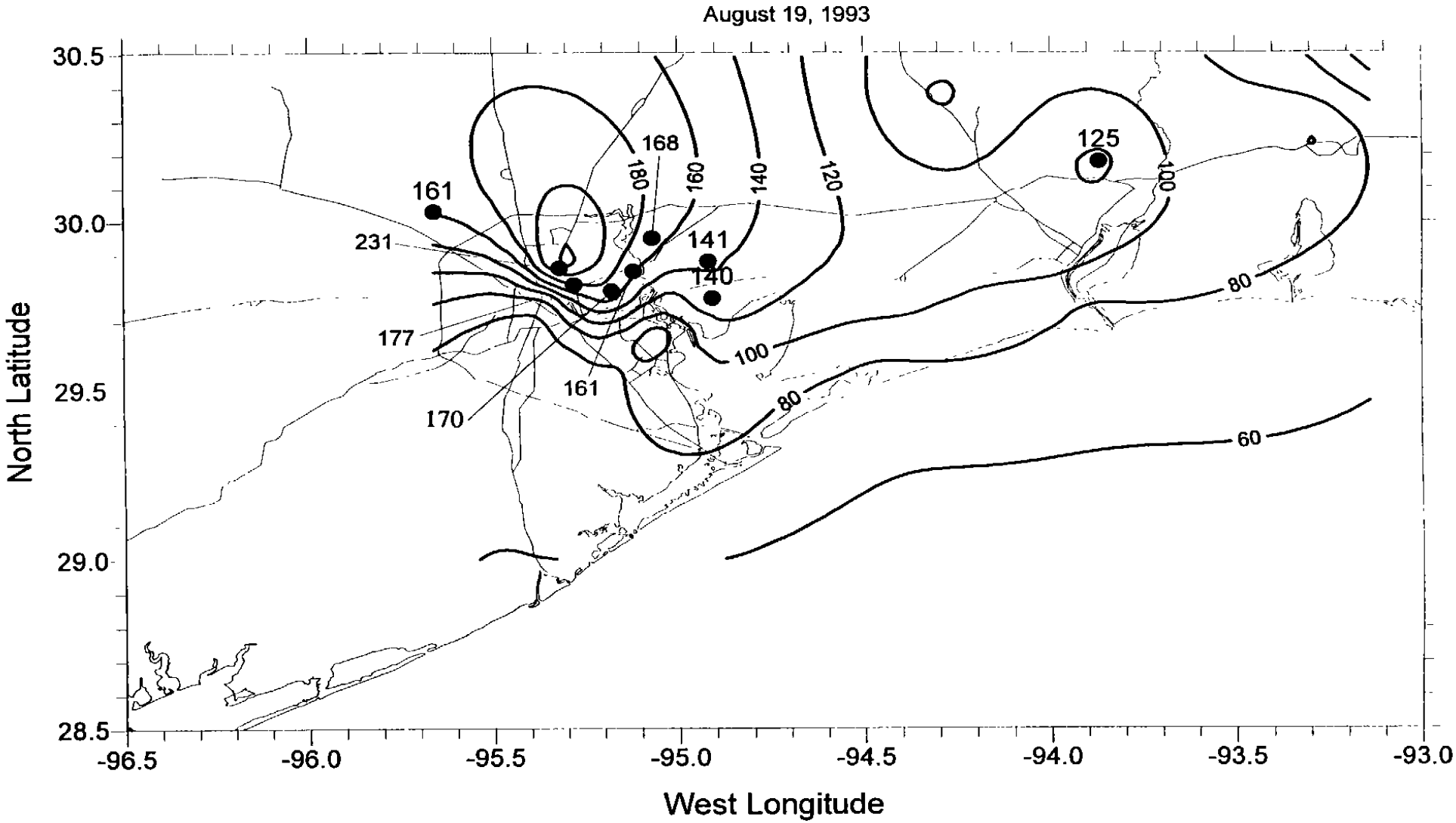

FIGURE 3-12c. Contour of maximum ozone concentrations (ppb) in the southeast Texas region on 19 August 1993. The locations and concentrations of all exceedances are shown.

September 15, 1995

To: Public Information Office, Gulf of Mexico OCS Region, (MS 5034)
From: Carla Langley, Leasing and Environment, Gulf of Mexico OCS Region, (MS 5430)
Subject: Environmental Studies Section Publications

The Environmental Studies Section is forwarding two copies each of the reports listed below. One copy of each report should be reserved as a reference copy and one copy as a loaner copy for use by MMS employees and the general public through the Public Information Office. For your information, the code in parentheses following the report names is the category under which each report is to be filed under Contract Deliverables. Note that a new category, J, is added for the Air Quality study series.

Publication charges for the public are available from Mike Dorner. Reprint authorizations for these or any other Studies' publications should be directed to Mike Dorner.

MMS Report No.	Title of the Report
OCS Study MMS 94-0044	Northeastern Gulf of Mexico Physical Oceanography Workshop: Proceedings of a Workshop Held in Tallahassee, Florida, April 5-7, 1994 (B.2)
OCS Study MMS 94-0046	A Description of the Gulf of Mexico Air Quality Study Data Archive Files (J)
OCS Study MMS 95-0019	Measurements of SO^2 Concentration and Atmospheric Structure in Delta and Breton Wildlife Refuges (J)
OCS Study MMS 95-0020	Bioavailability and Genotoxicity of Produced Water Discharges Associated with Offshore Production Operations (I.2)
OCS Study MMS 95-0027	Louisiana/Texas Shelf Physical Oceanography Program: Eddy Circulation Study; Annual Report: Year 2 (B.2)
OCS Study MMS 95-0028	Texas-Louisiana Shelf Circulation and Transport Processes Study: Year 2, Annual Report (B.2)
OCS Study MMS 95-0029	Synthesis of Available Biological, Geological, Chemical, Socioeconomic, and Cultural Resource Information for the South Florida Area (I.2)
OCS Study MMS 95-0031	Oil in the Gulf: Past Developments, Future Prospects (I.2)

OCS Study MMS 95-0038	Gulf of Mexico Air Quality Study, Final Report, Volume I: Summary of Data Analysis and Modeling (J)
OCS Study MMS 95-0039	Gulf of Mexico Air Quality Study, Final Report, Volume II: Data Analysis, Appendices A-M (J)
OCS Study MMS 95-0040	Gulf of Mexico Air Quality Study, Final Report, Volume III: Data Analysis, Appendices N-P (J)
OCS Study MMS 95-0045	Gulf of Mexico Offshore Operations Monitoring Experiment, Final Report; Phase I: Sublethal Responses to Contaminant Exposure (F.6)

If you have any questions, please give me a call at extension 2775.

Thanks,
Carla Langley

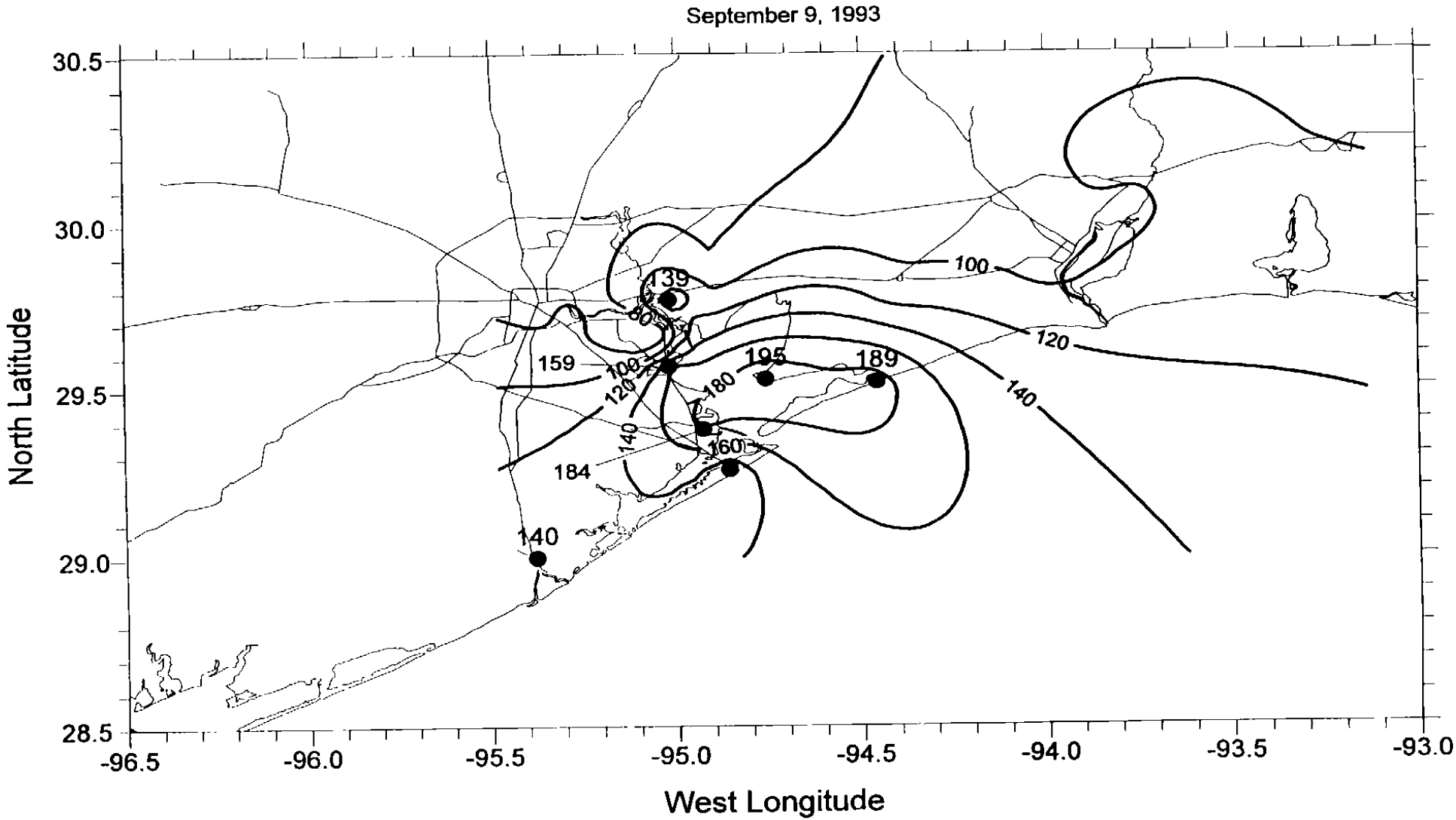

FIGURE 3-13c. Contour of maximum ozone concentrations (ppb) in the southeast Texas region on 9 September 1993. The locations and concentrations of all exceedances are shown.

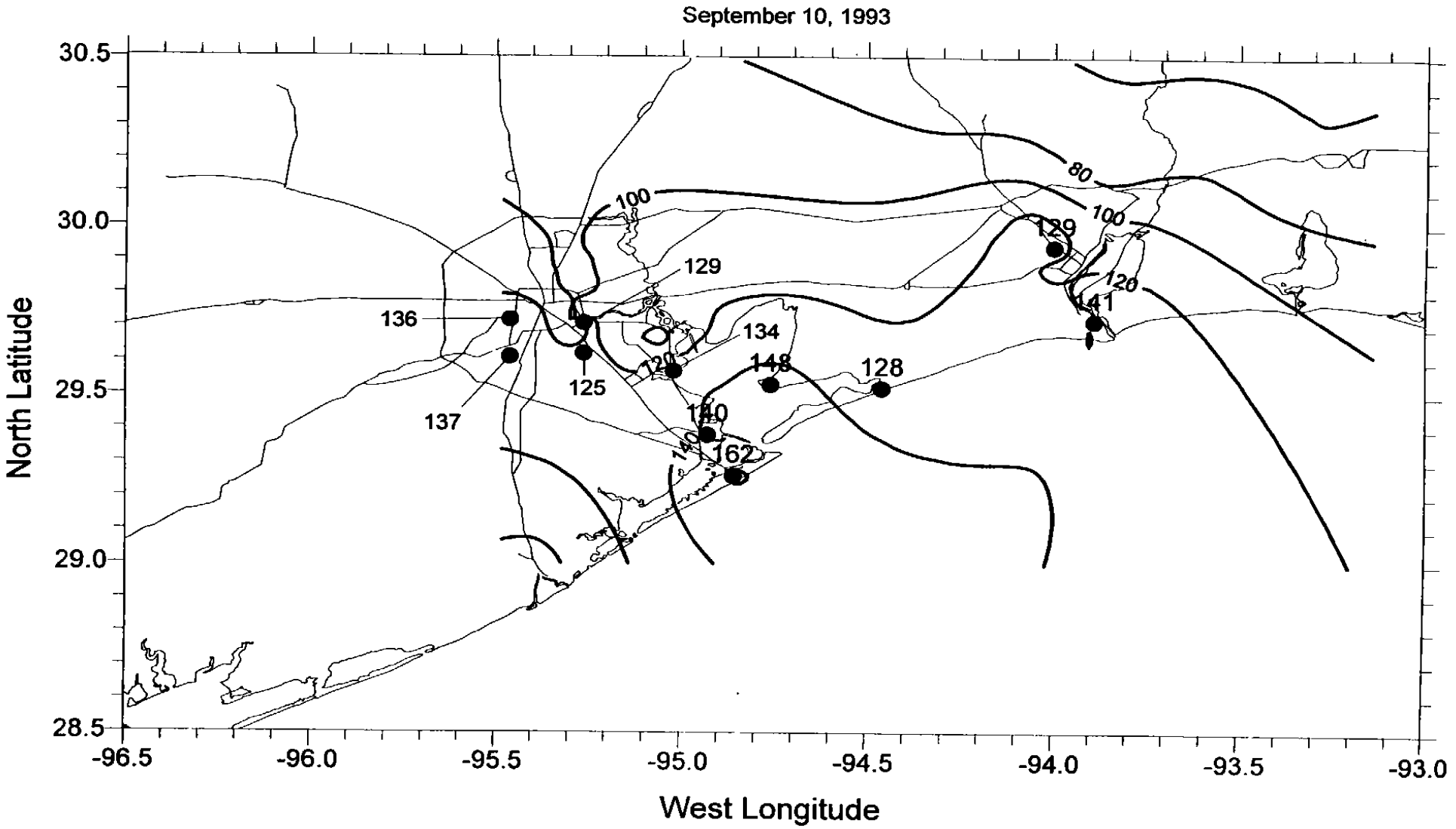

FIGURE 3-13d. Contour of maximum ozone concentrations (ppb) in the southeast Texas region on 10 September 1993. The locations and concentrations of all exceedances are shown.

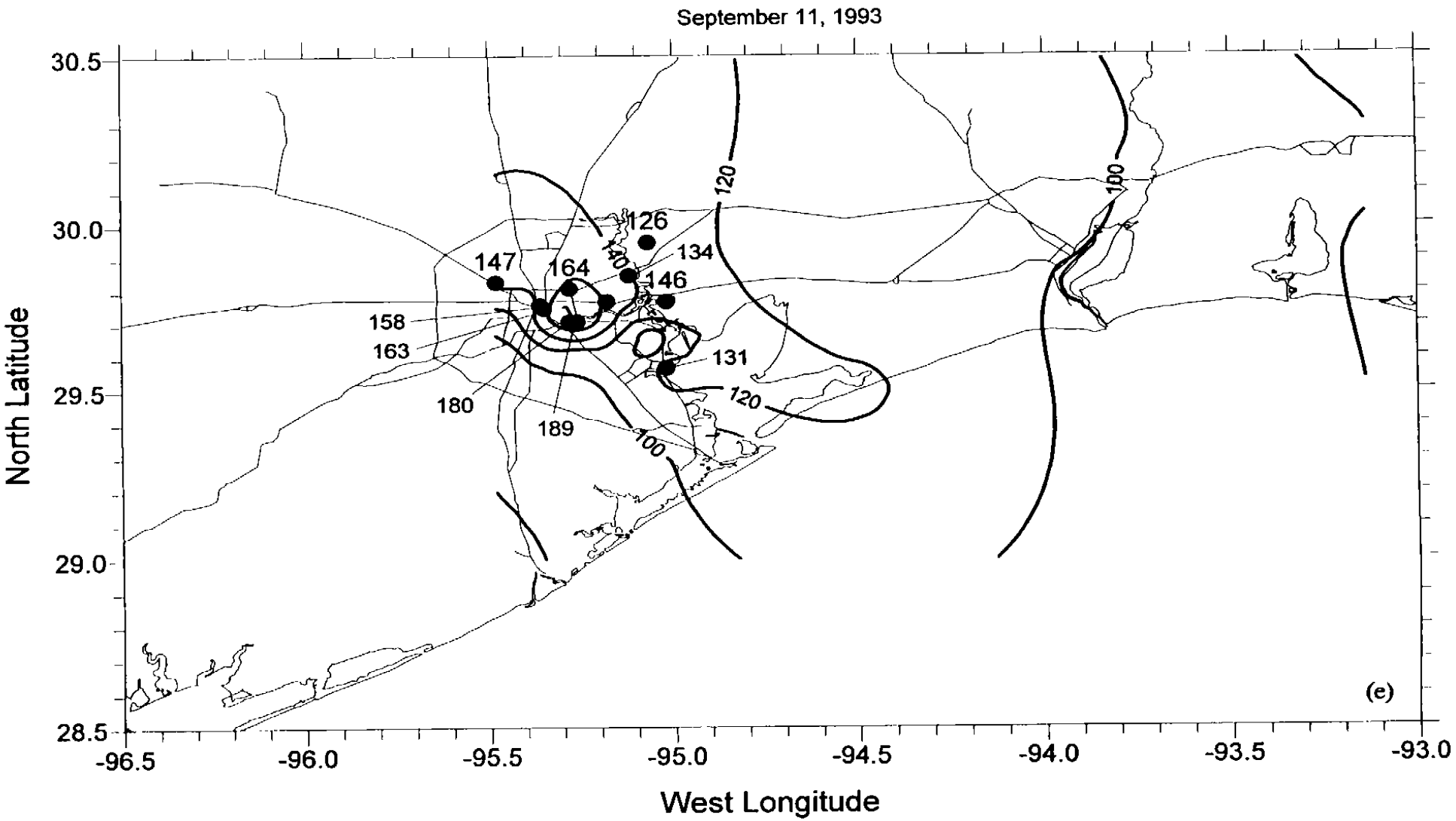

FIGURE 3-13e. Contour of maximum ozone concentrations (ppb) in the southeast Texas region on 11 September 1993. The locations and concentrations of all exceedances are shown.

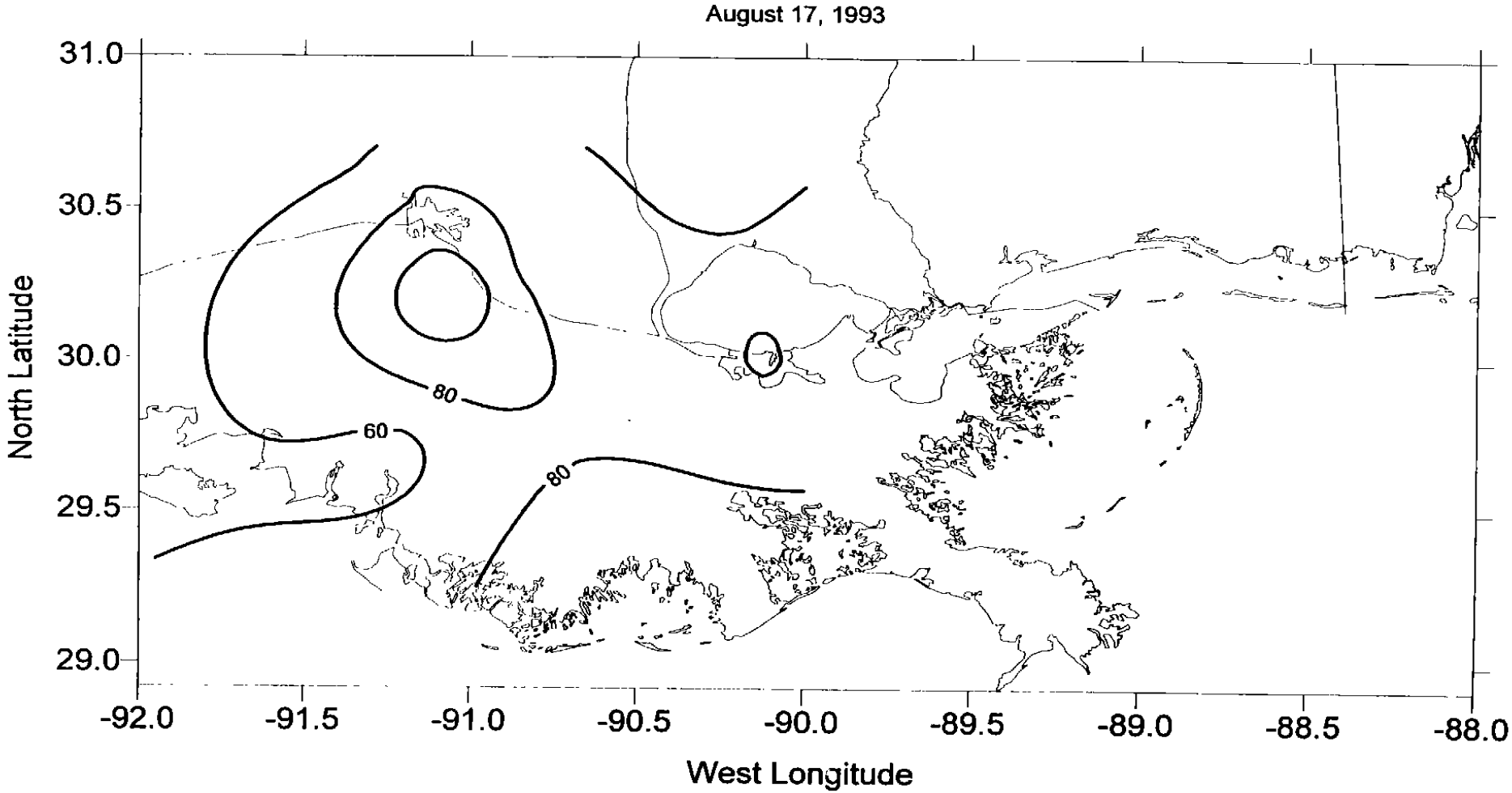

FIGURE 3-14a. Contour of maximum ozone concentrations (ppb) in the Baton Rouge, Louisiana, region on 17 August 1993. The locations and concentrations of all exceedances are shown. No exceedances occurred on this initial day.

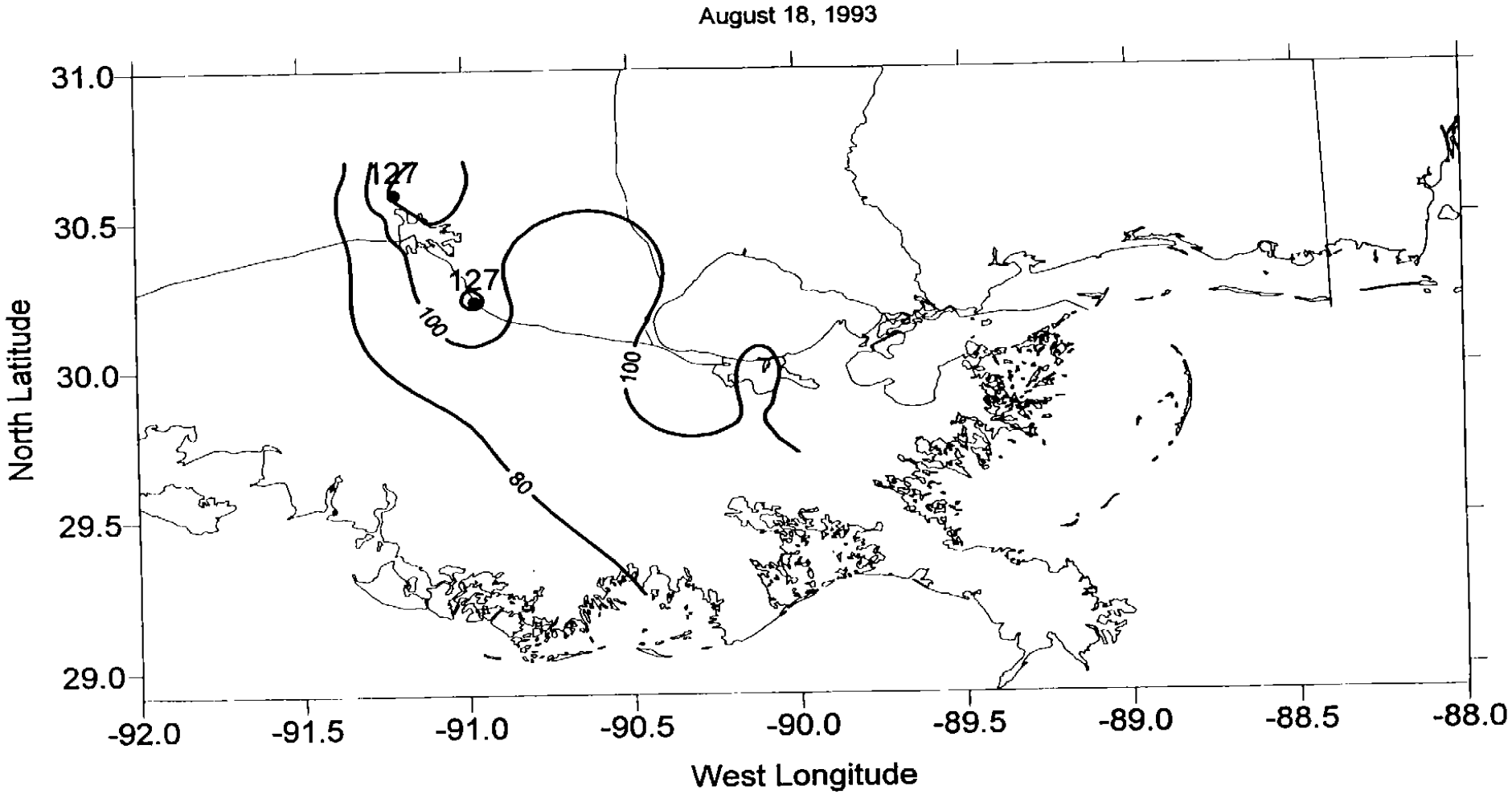

FIGURE 3-14b. Contour of maximum ozone concentrations (ppb) in the Baton Rouge, Louisiana, region on 18 August 1993. The locations and concentrations of all exceedances are shown.

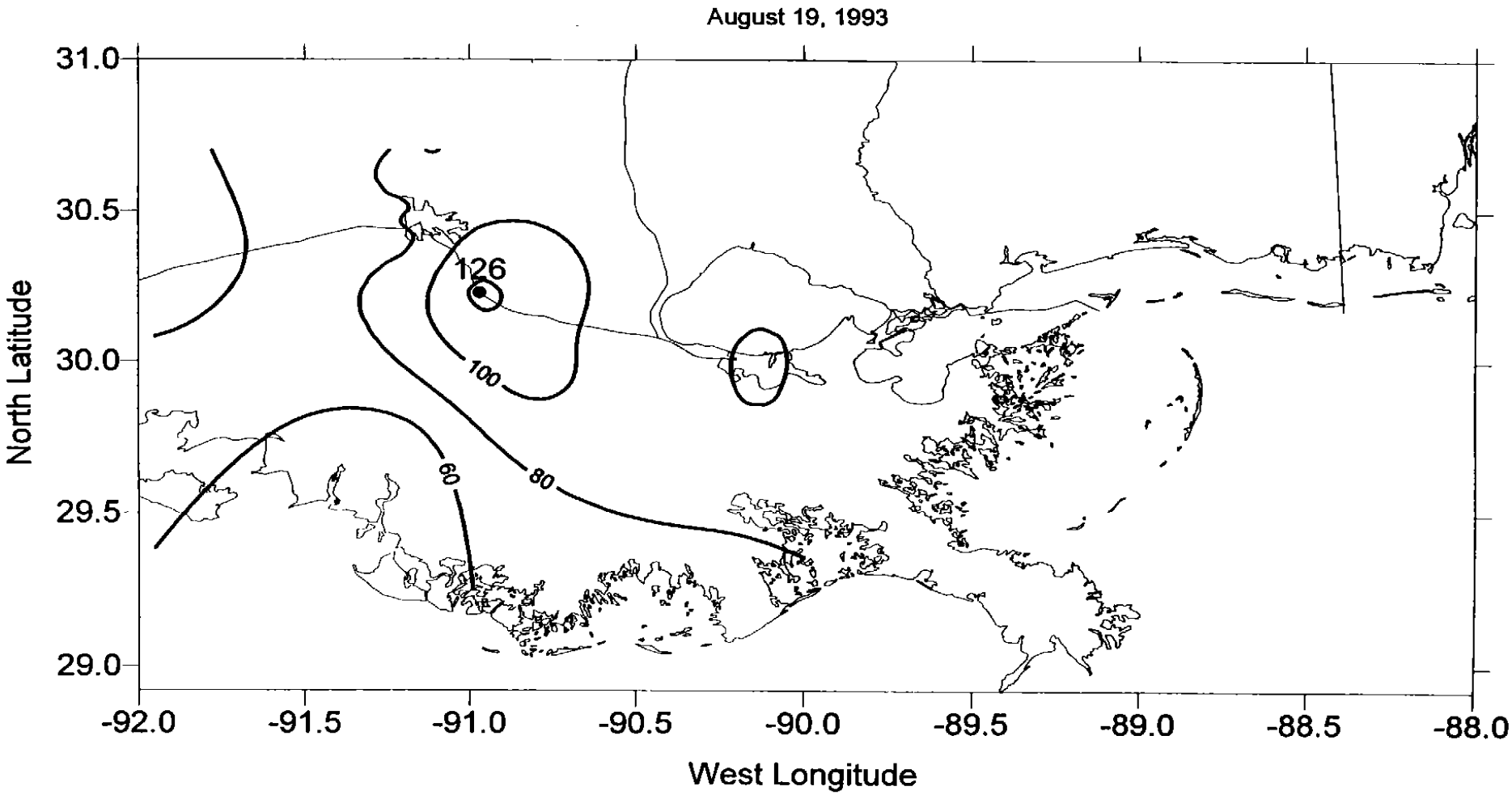

FIGURE 3-14c. Contour of maximum ozone concentrations (ppb) in the Baton Rouge, Louisiana, region on 19 August 1993. The locations and concentrations of all exceedances are shown.

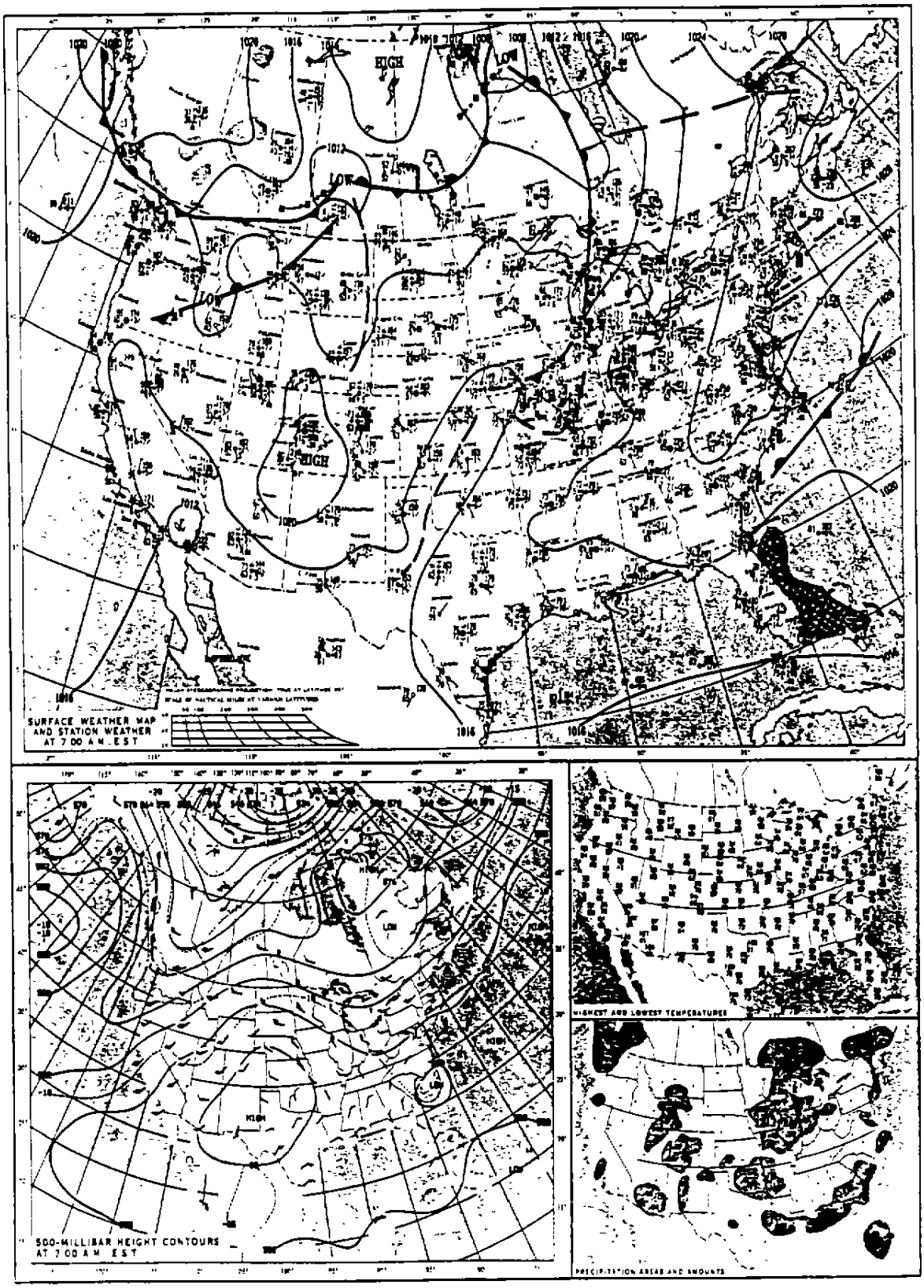

FIGURE 3-15. Daily weather map for 10 August 1993 at 0600 CST. The top panel shows the locations of the surface weather features (i.e., fronts, high- and low-pressure systems, etc.), surface winds, and isobars. The bottom-left panel shows the 500-mb heights and winds. The lower-right panels show the maximum and minimum temperatures and precipitation.

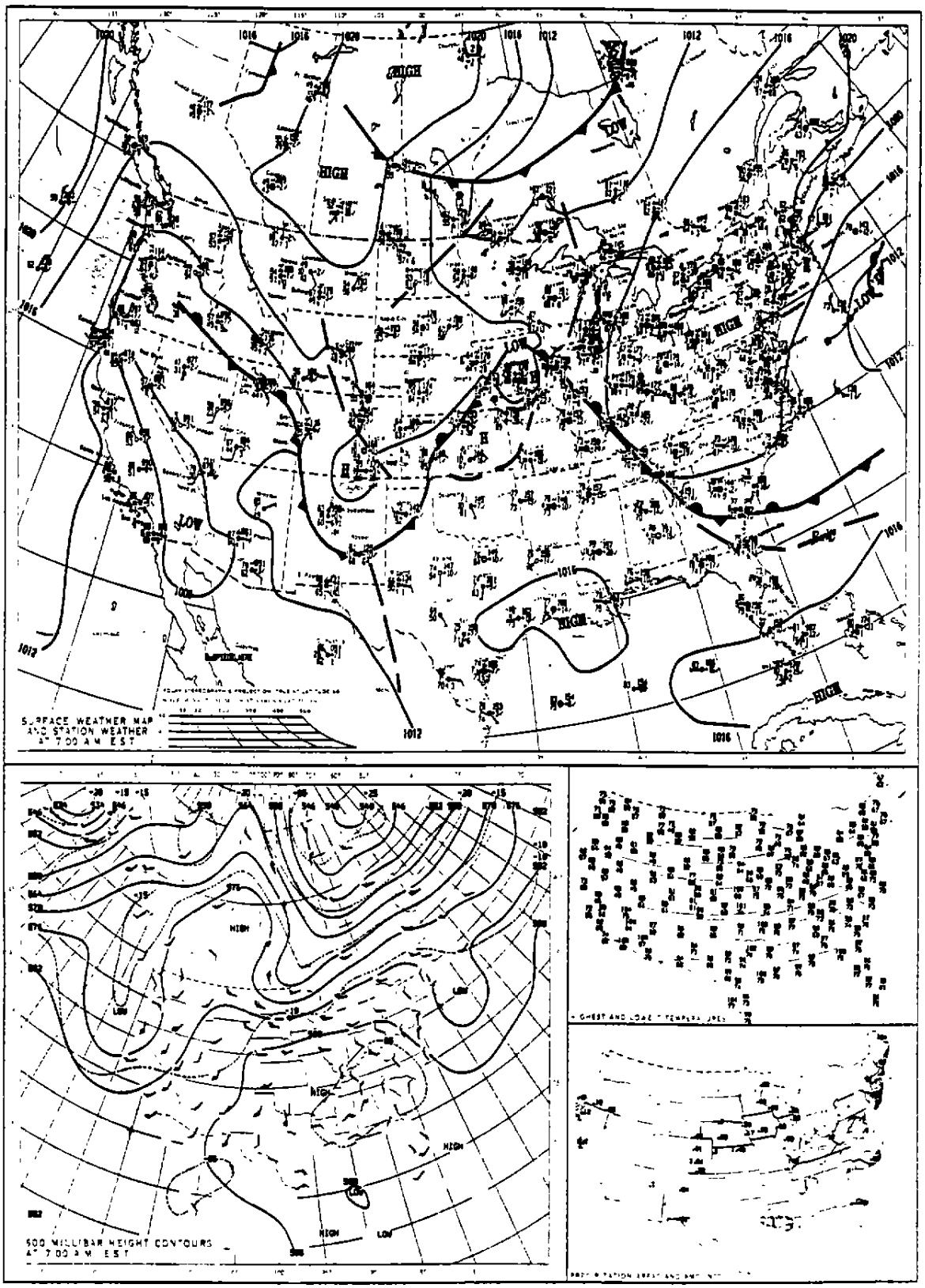

FIGURE 3-16. Daily weather map for 19 August 1993 at 0600 CST. The top panel shows the locations of the surface weather features (i.e., fronts, high- and low-pressure systems, etc.), surface winds, and isobars. The bottom-left panel shows the 500-mb heights and winds. The lower-right panels show the maximum and minimum temperatures and precipitation.

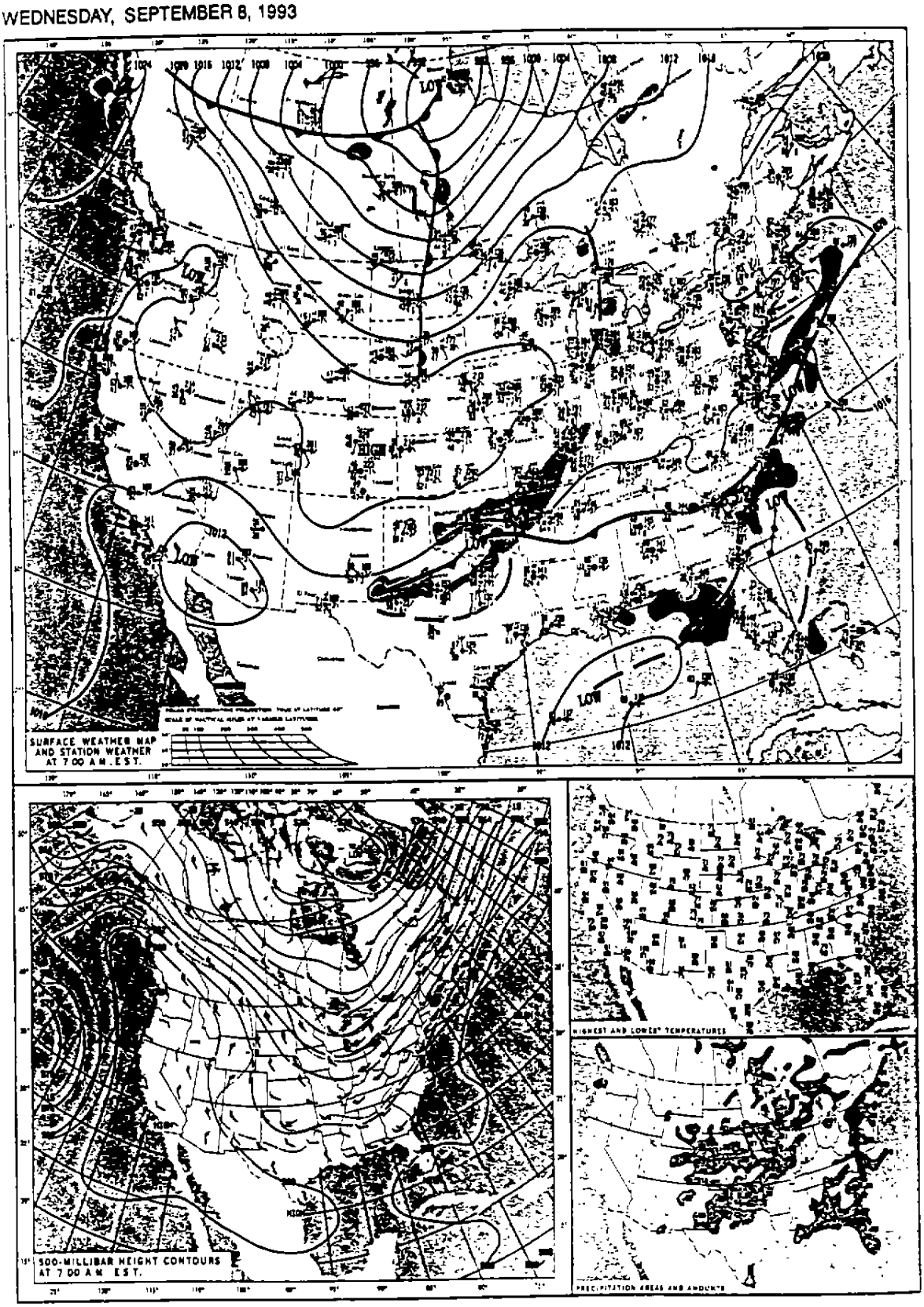

FIGURE 3-17. Daily weather map for 8 September 1993 at 0600 CST. The top panel shows the locations of the surface weather features (i.e., fronts, high- and low-pressure systems, etc.), surface winds, and isobars. The bottom-left panel shows the 500-mb heights and winds. The lower-right panels show the maximum and minimum temperatures and precipitation.

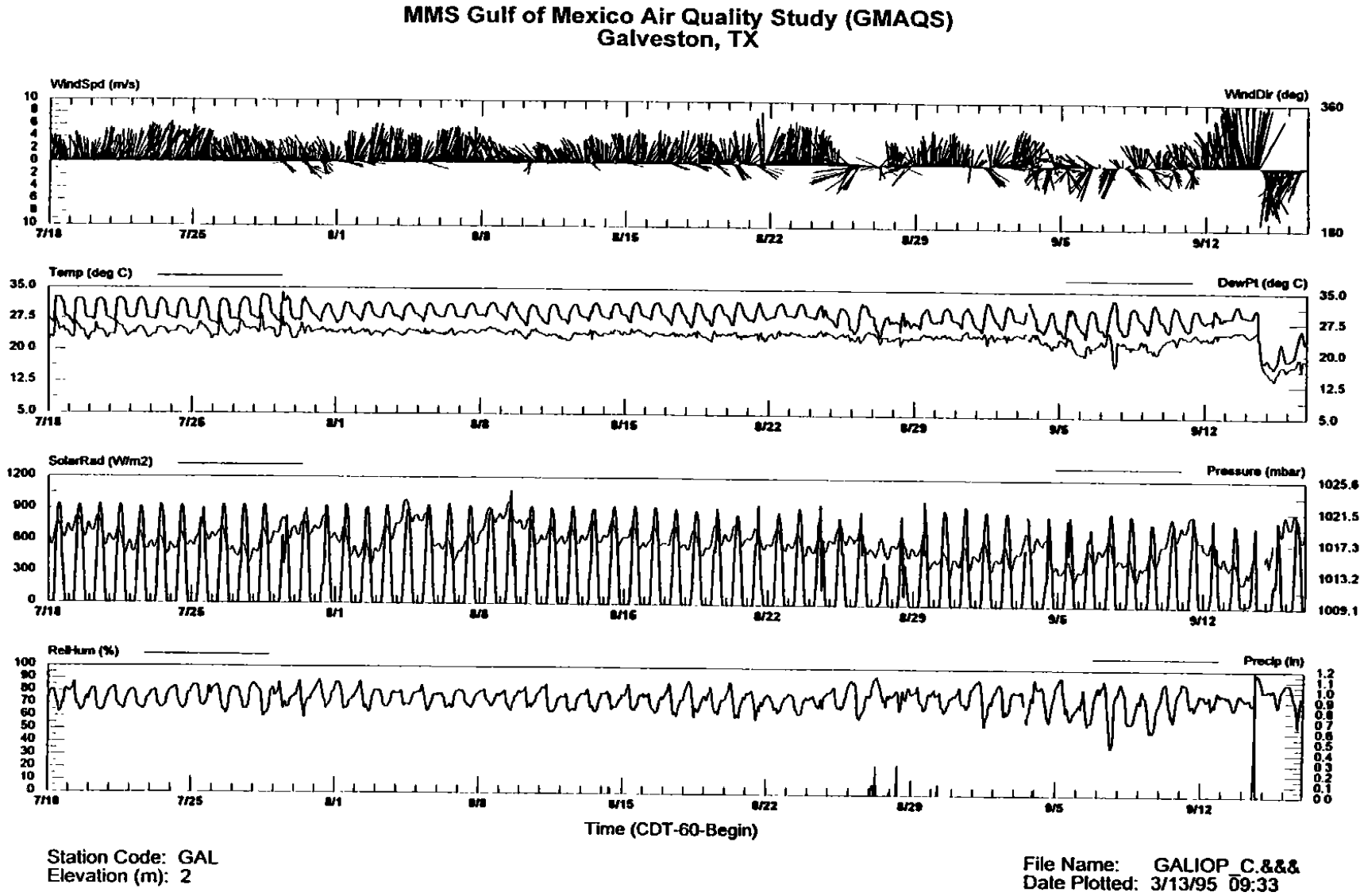

FIGURE 3-18a. Time series of surface winds, temperature and dew point, solar radiation and pressure, and relative humidity and precipitation measured at the Galveston (GAL) radar profiler site for the period 18 July – 15 September 1993.

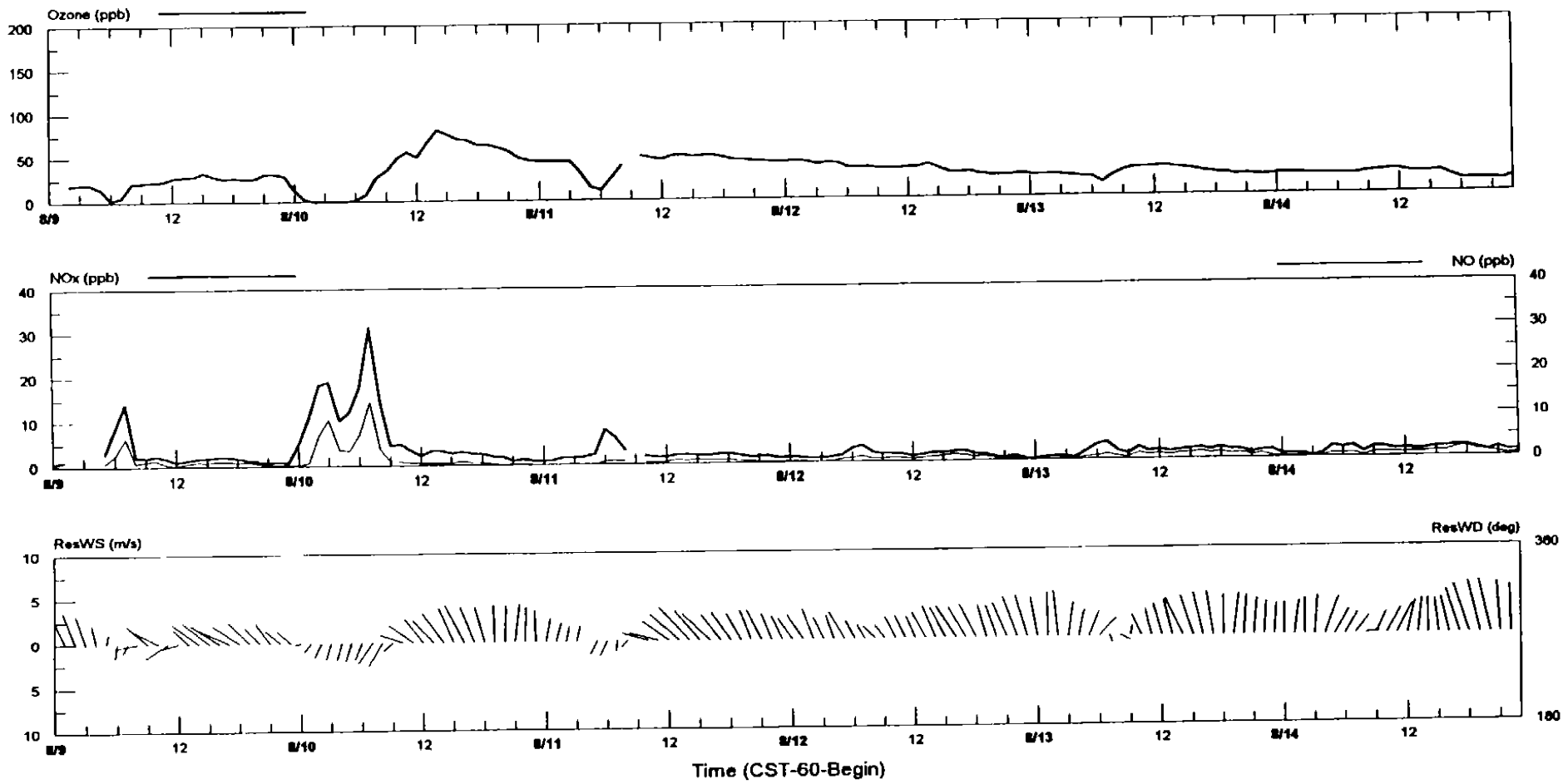

FIGURE 3-18b. Time series of ozone, NO, NO_x, wind speed, and wind direction measured at the Gilchrist, Texas surface monitoring site for the period 9–14 August 1993.

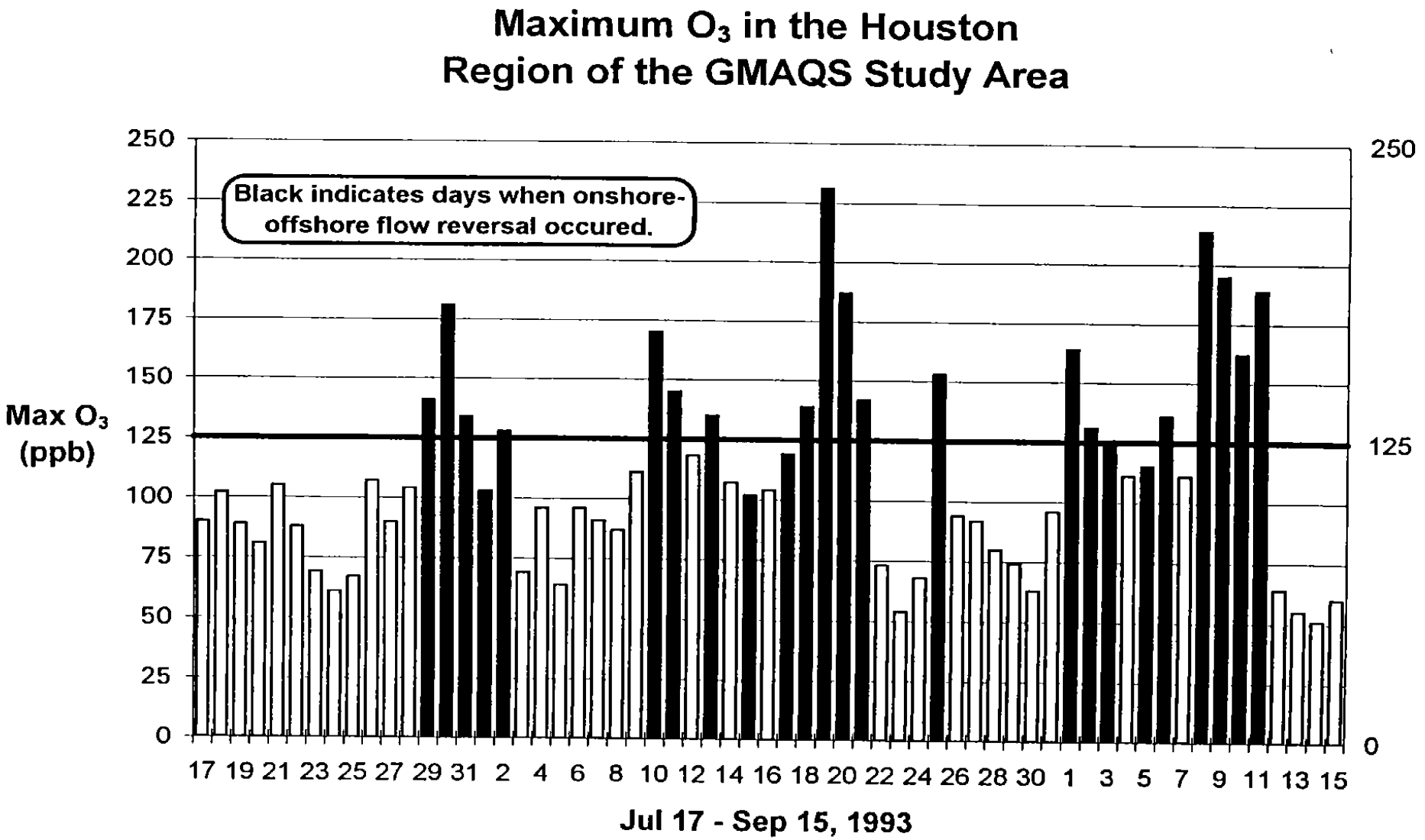

FIGURE 3-19. Maximum ozone concentrations observed in southeast Texas during the GMAQS project; the black bars indicate days on which a gulf/land breeze circulation formed that produced an onshore-offshore flow reversal in the region.

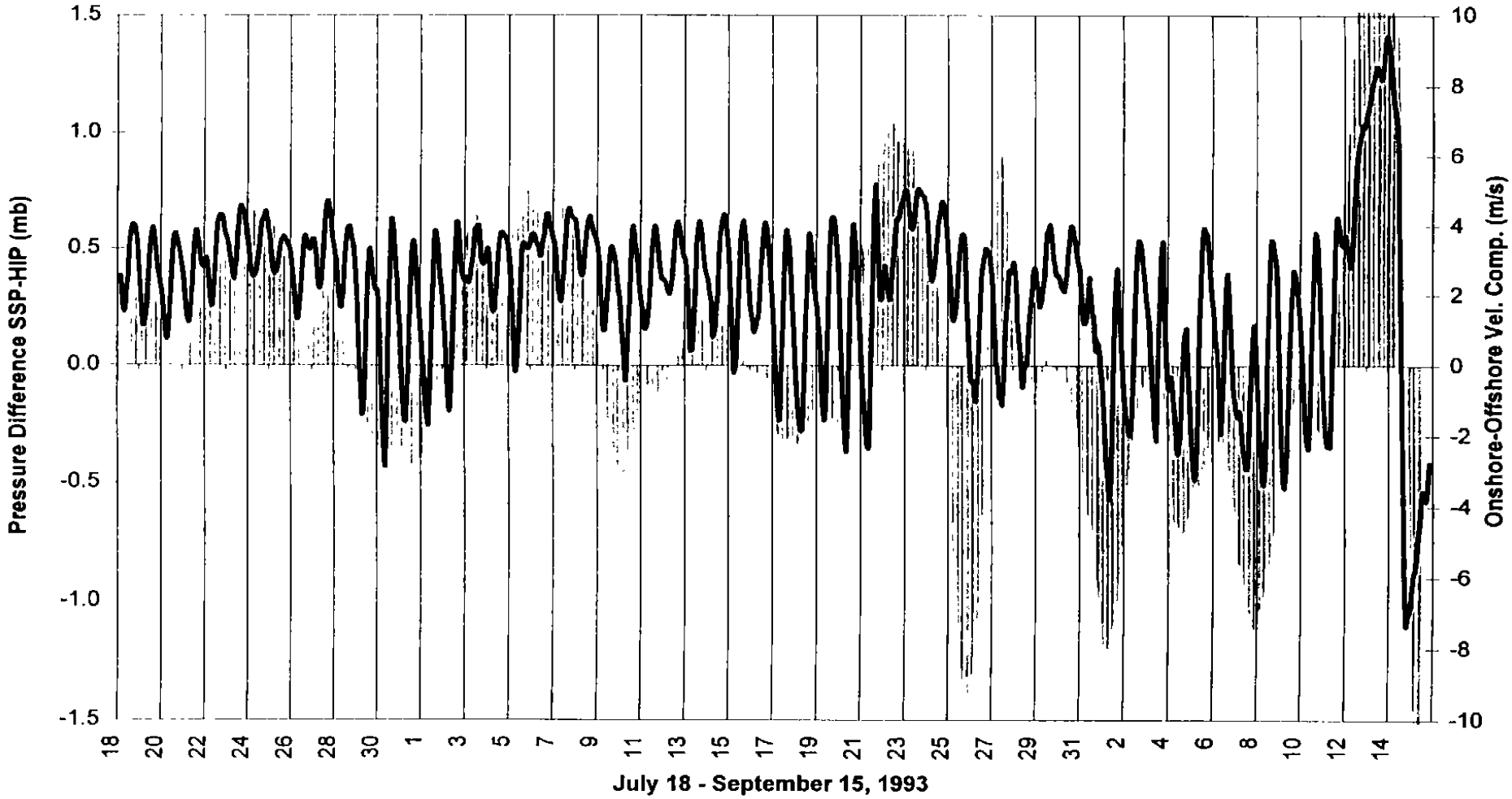

FIGURE 3-20. Sea-level pressure differences (mb) across the Gulf of Mexico between the High Island and Ship Shoal Platform radar profiler sites, and the component of the surface wind perpendicular to the coastline (V_n, m/s) at Galveston, Texas, for the period 18 July–15 September 1993.

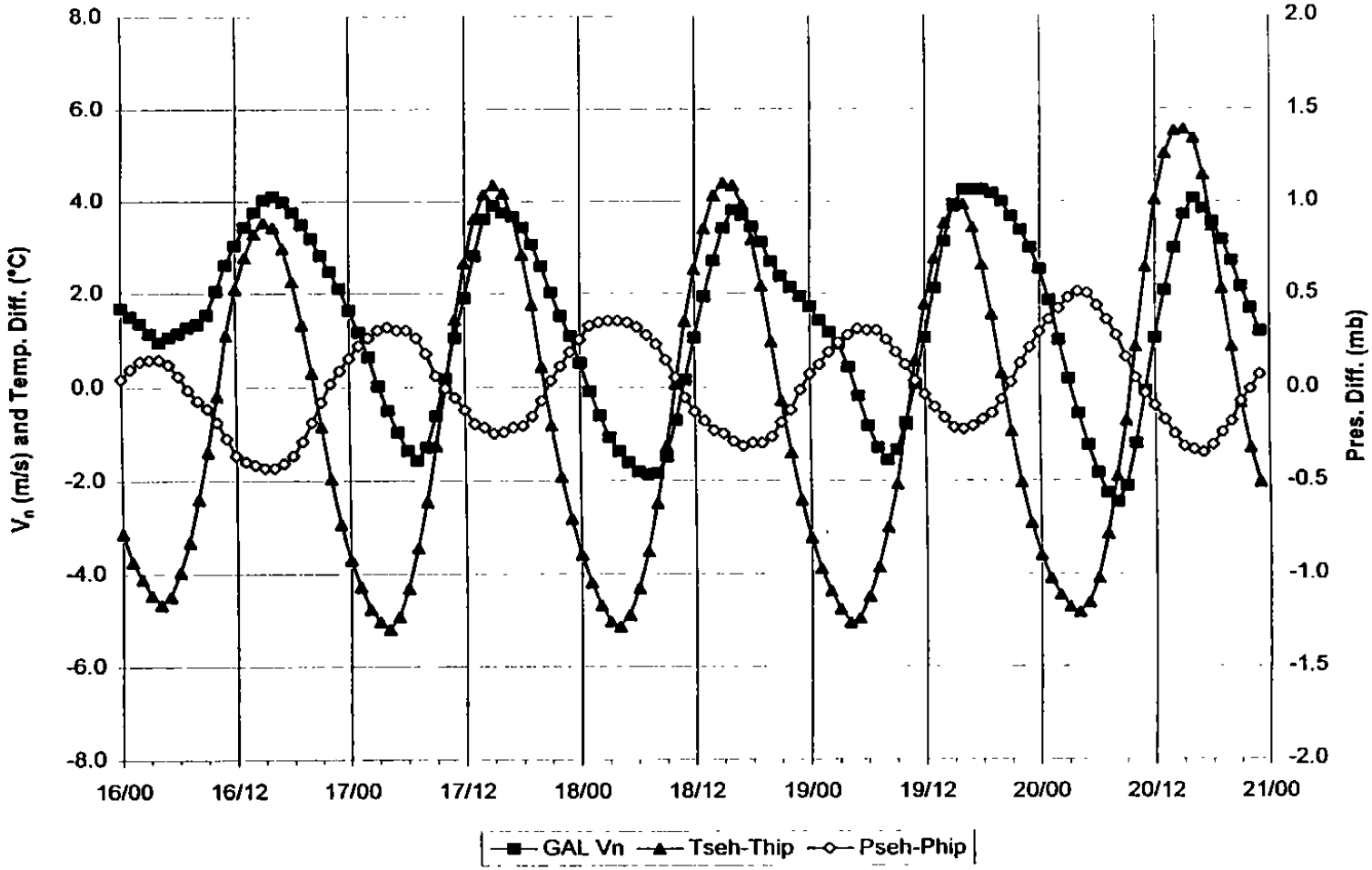

FIGURE 3-21. Onshore-offshore sea-level pressure differences (mb) and temperature differences (°C) between the Southeast Houston and High Island Platform radar profiler sites, and the component of the surface wind perpendicular to the coastline (V_n, m/s) at Galveston, Texas for the period 17–21 August 1993.

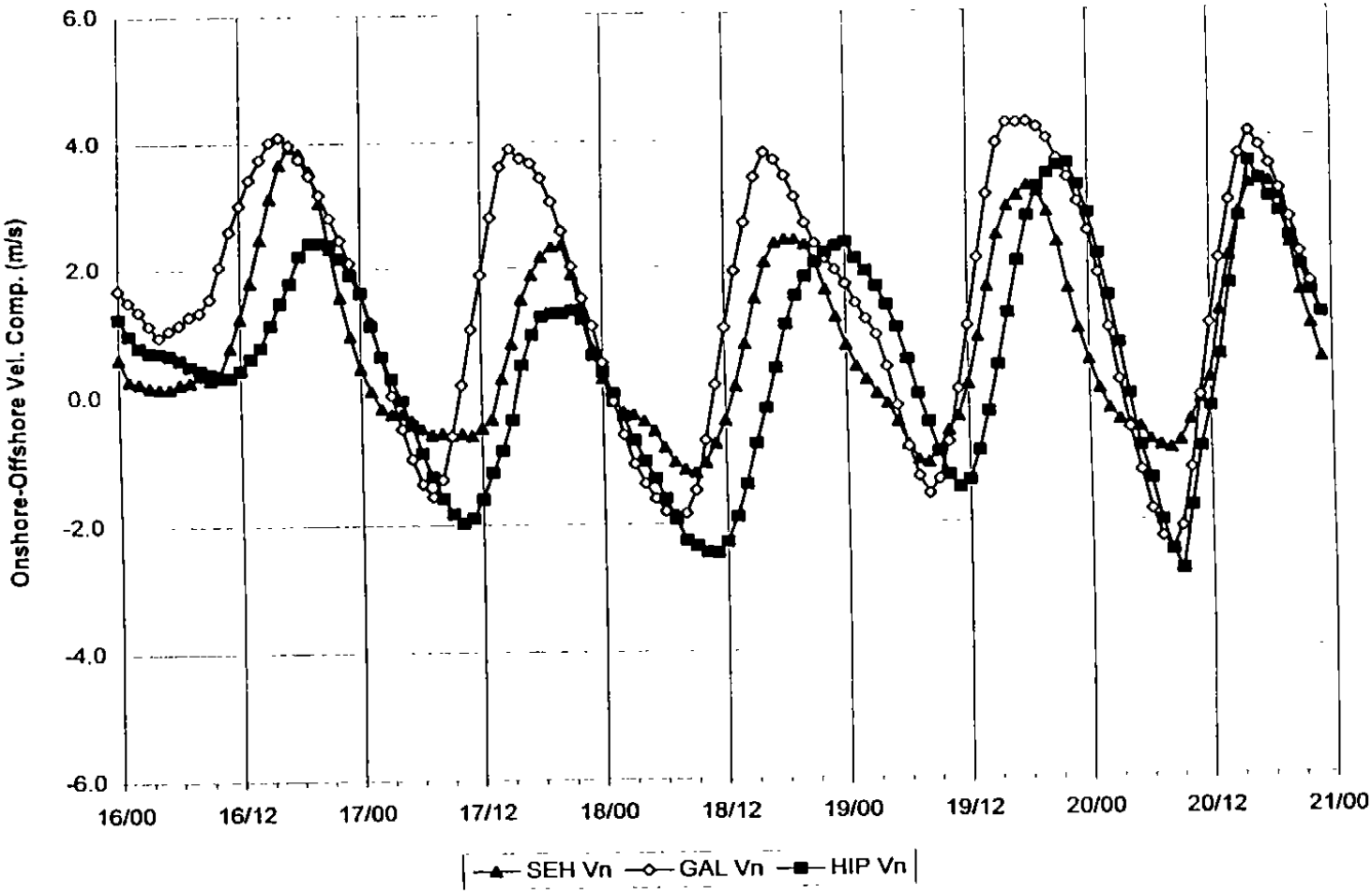

FIGURE 3-22. The component of the surface wind perpendicular to the coastline (V_n, m/s) at the Southeast Houston, Galveston, and High Island Platform radar profiler sites for the period 17–21 August 1993.

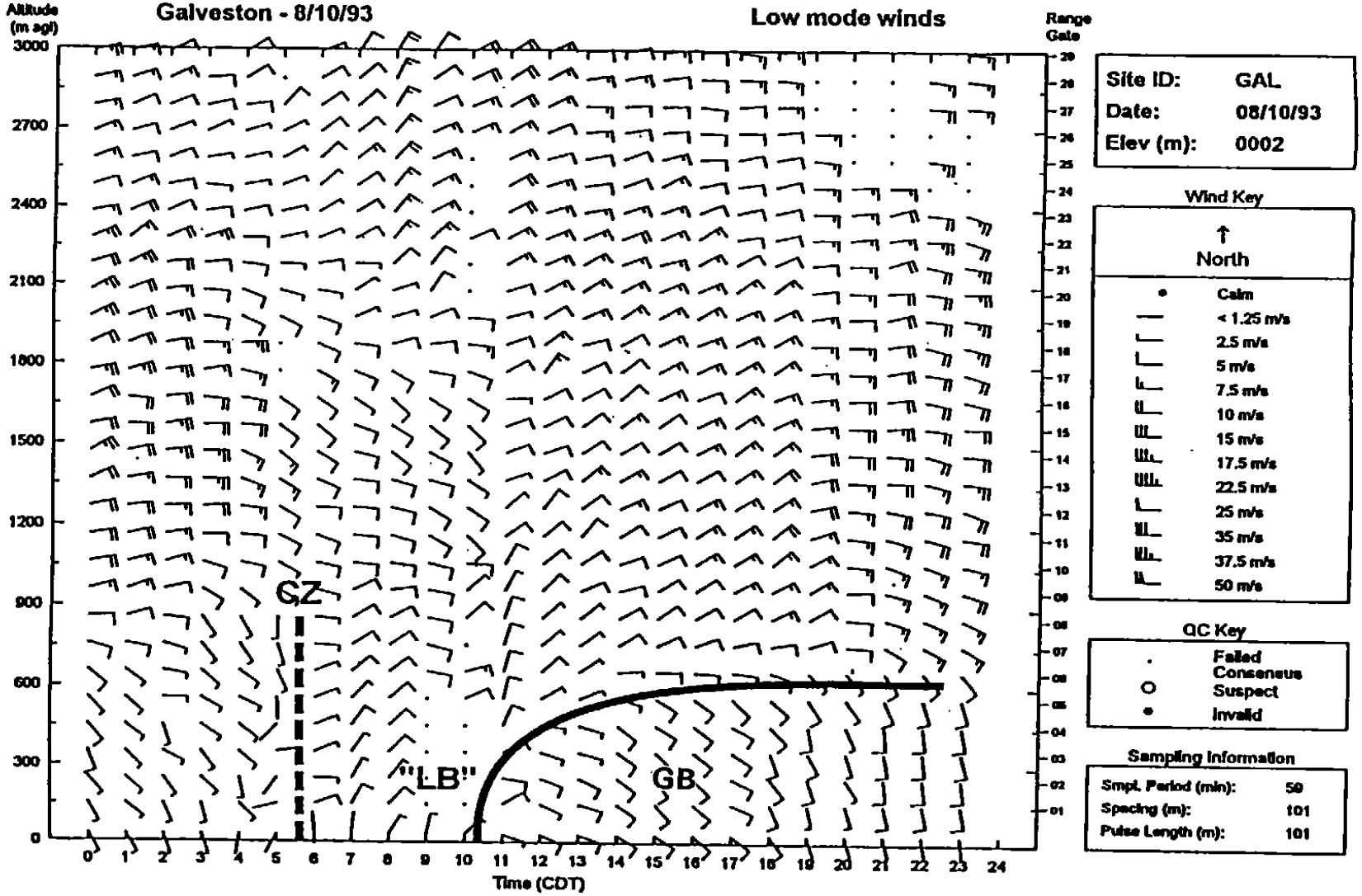

FIGURE 3-23. Wind profiles measured by the 915 MHz radar profiler at Galveston, Texas (GAL) 10 August 1993. Solid lines indicate gulf breeze (GB), land breeze (LB); dashed line indicates a convergence zone (CZ) that formed at the onset of the land breeze. The first level of winds was measured by the surface station that was collocated with the profiler.

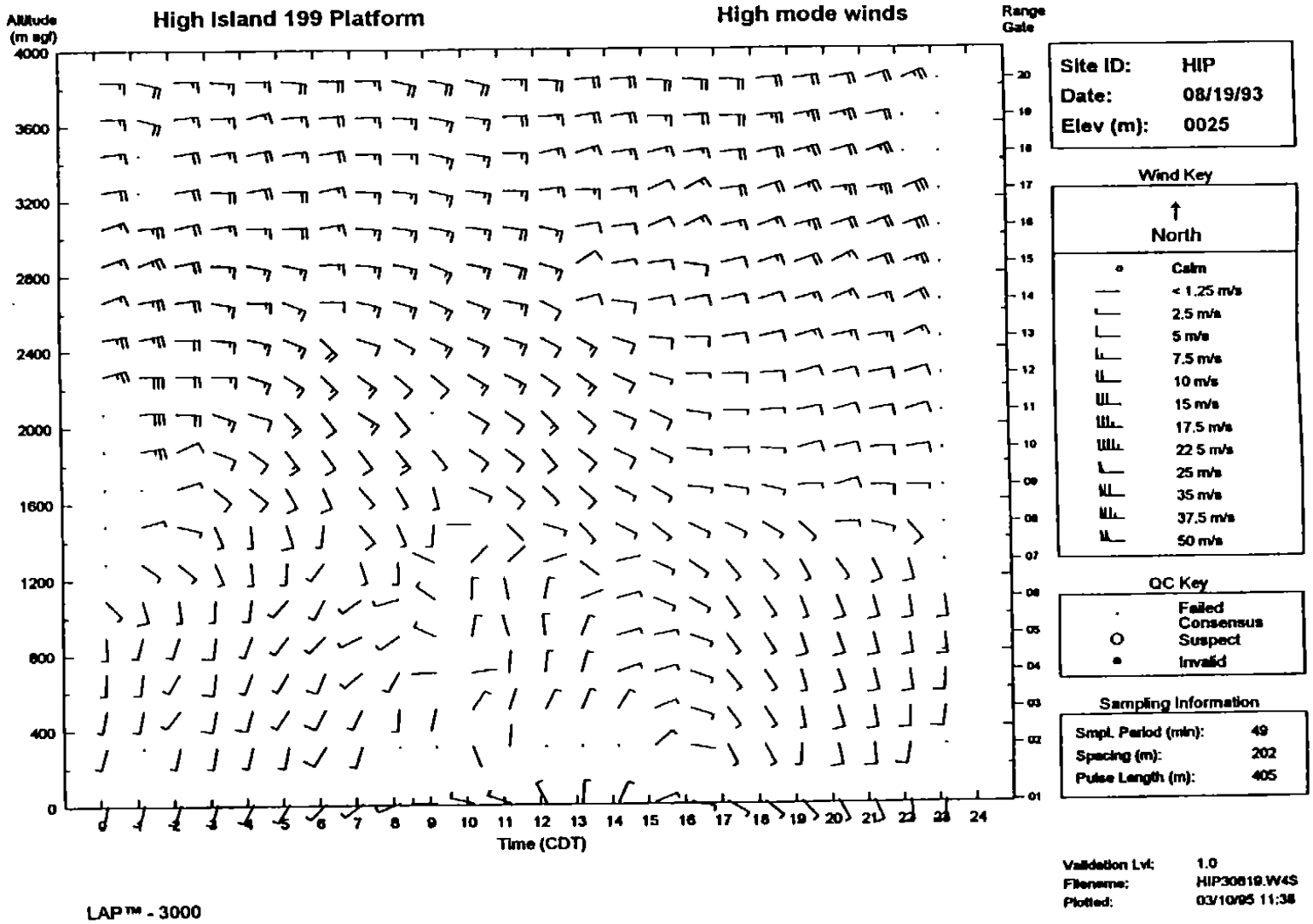

FIGURE 3-24. Wind profiles measured by the 915 MHz radar profiler at the High Island Platform (HIP) 19 August 1993. The first level of winds was measured by the surface station that was collocated with the profiler.

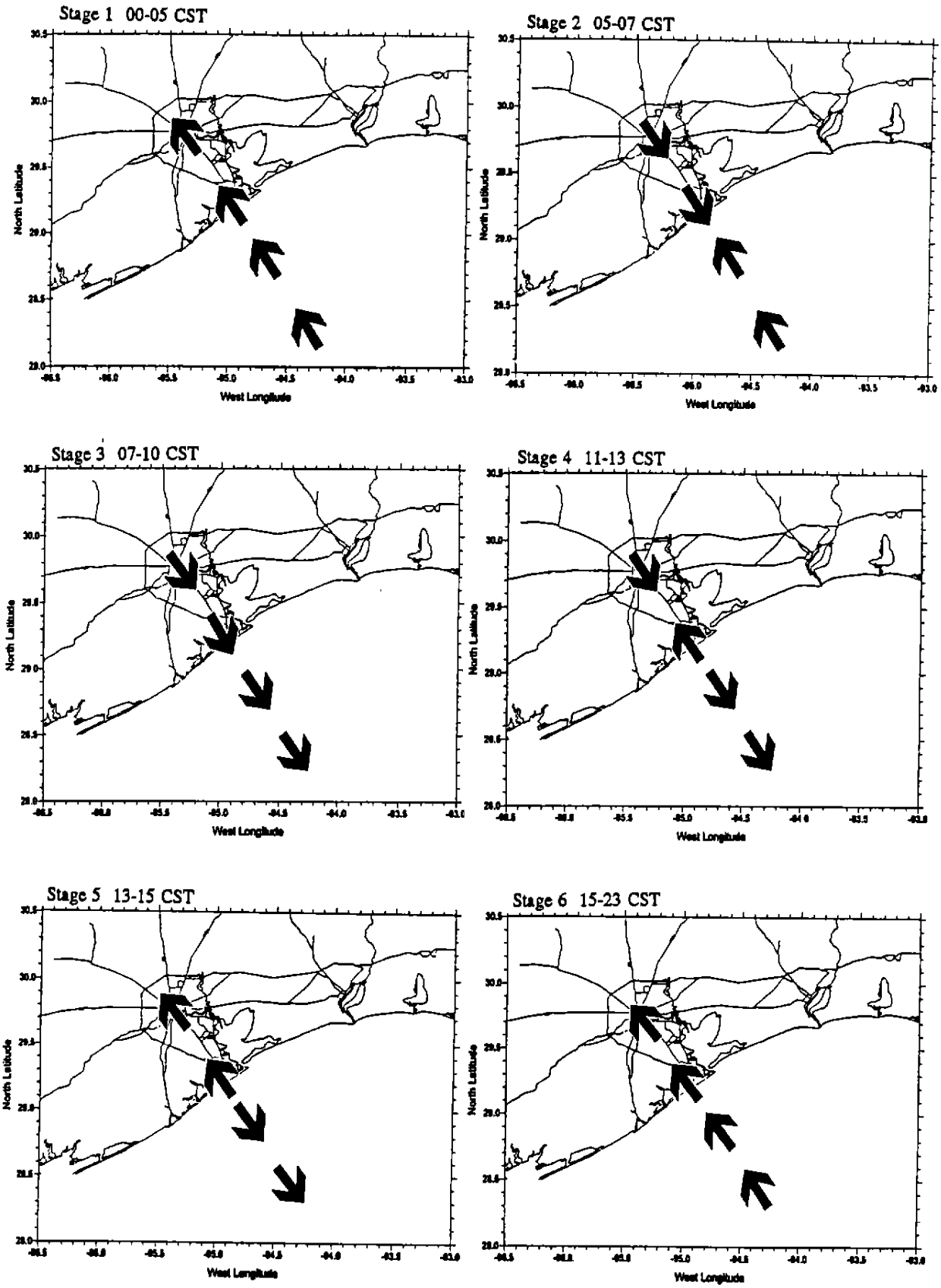

FIGURE 3-25. Conceptual model of the six stages of the onshore-offshore-onshore flow reversal in southeast Texas on episode days.

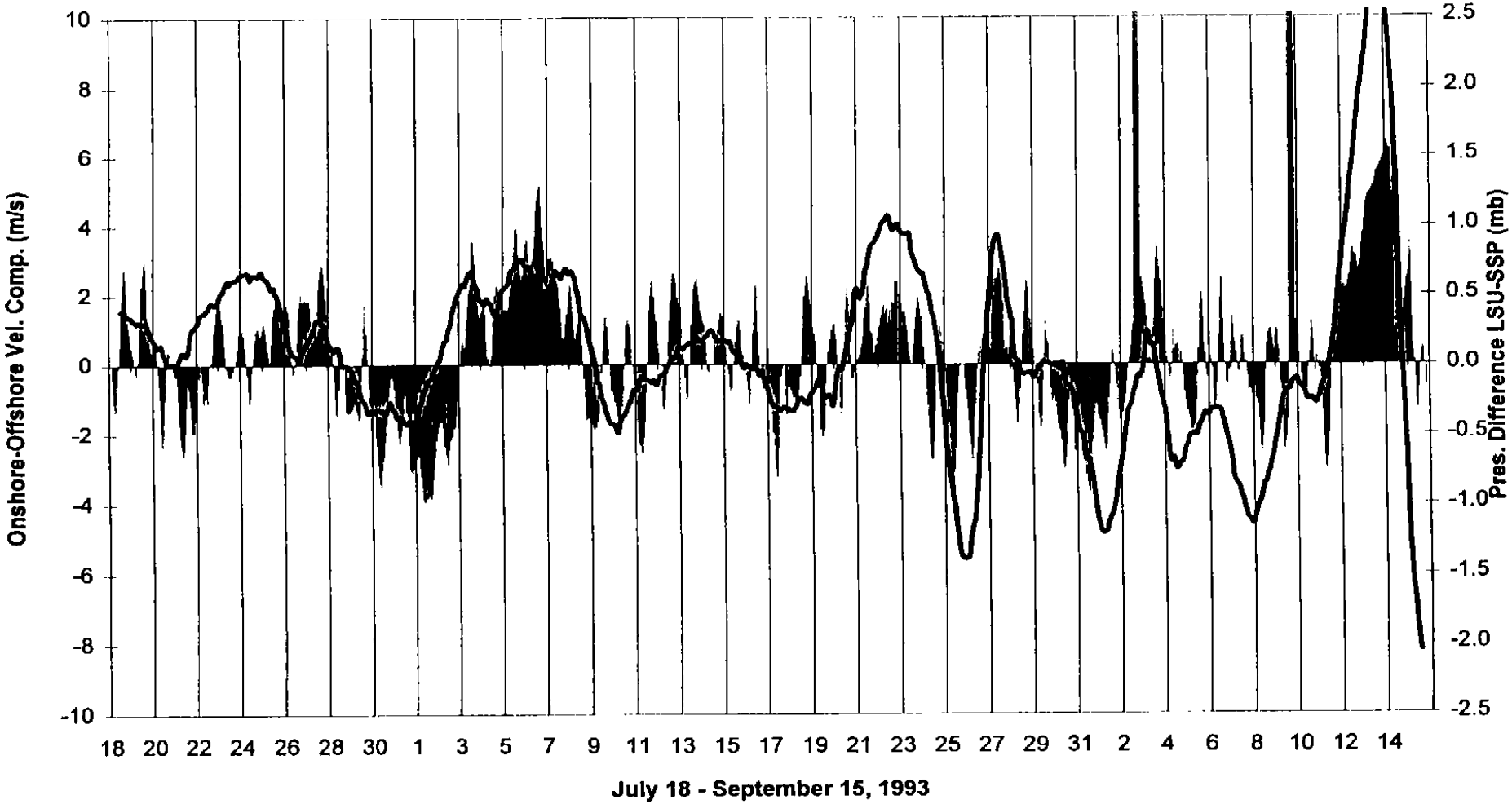

FIGURE 3-26. Sea-level pressure differences (mb) across the Gulf of Mexico between the High Island and Ship Shoal Platform radar profiler sites, and the component of the surface wind perpendicular to the coastline (V_n, m/s) at Cocodrie, LA, for the period 18 July–15 September 1993.

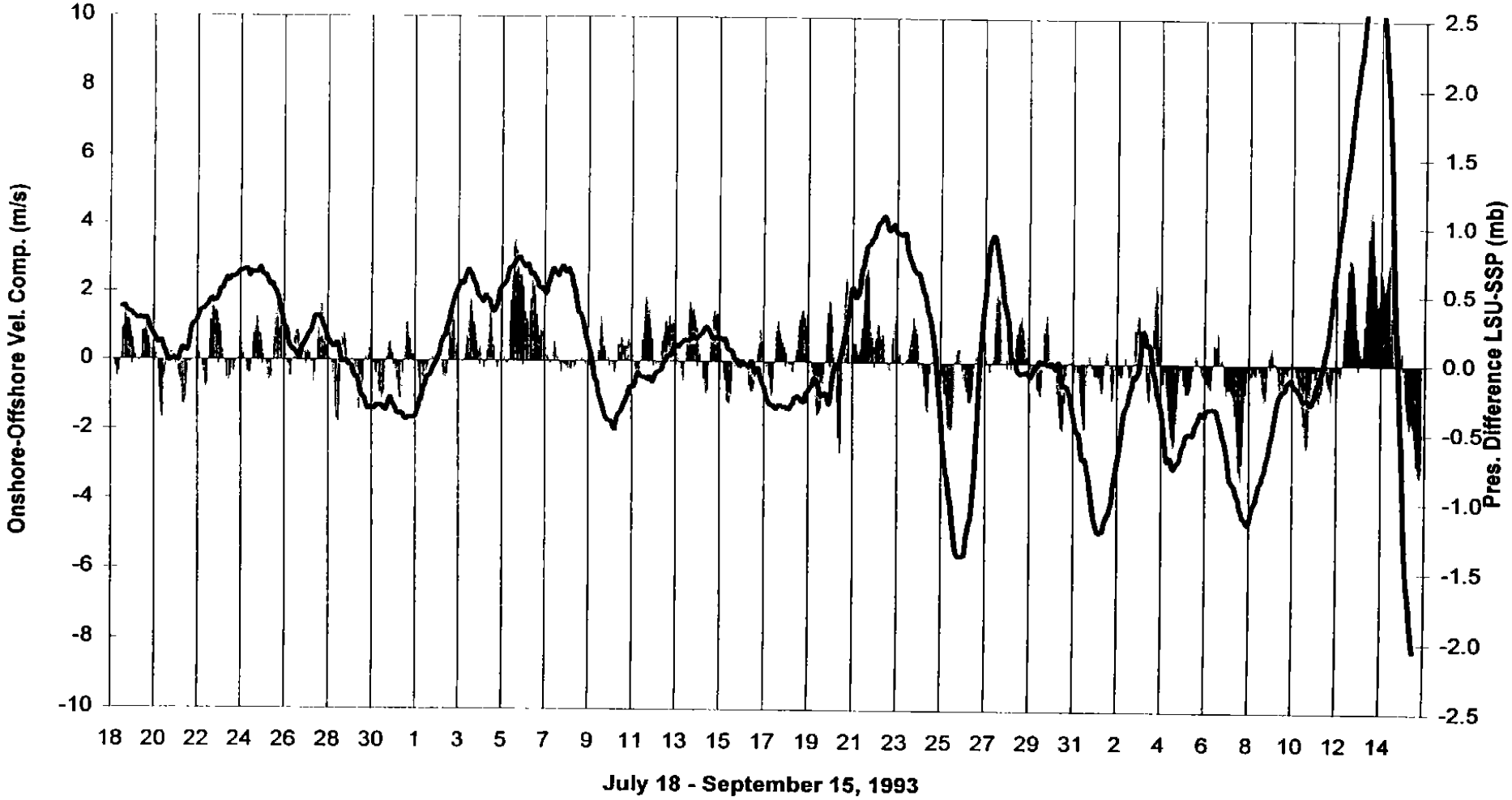

FIGURE 3-27. Onshore-offshore sea-level pressure differences (mb) between the Louisiana State University (LSU) and Ship Shoal Platform (SSP) radar profiler sites, and the component of the surface wind perpendicular to the coastline (V_n, m/s) at LSU, for the period 17–21 August 1993.

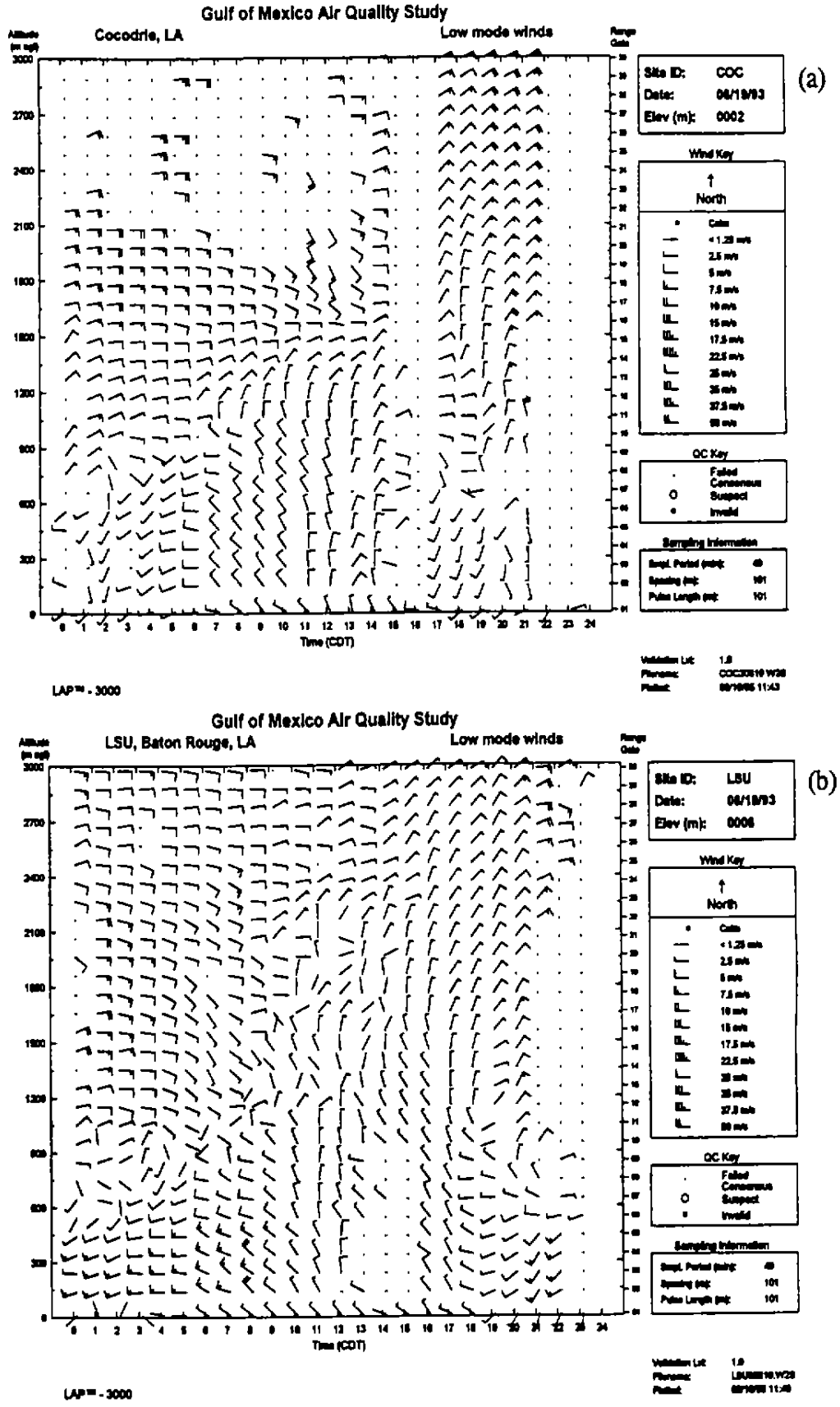

FIGURE 3-28. Wind profiles measured by the 915 MHz radar profilers at (a) Cocodrie, LA (COC) and (b) Louisiana State University (LSU) on 19 August 1993. The first level of winds was measured by the surface stations that were collocated with the profilers.

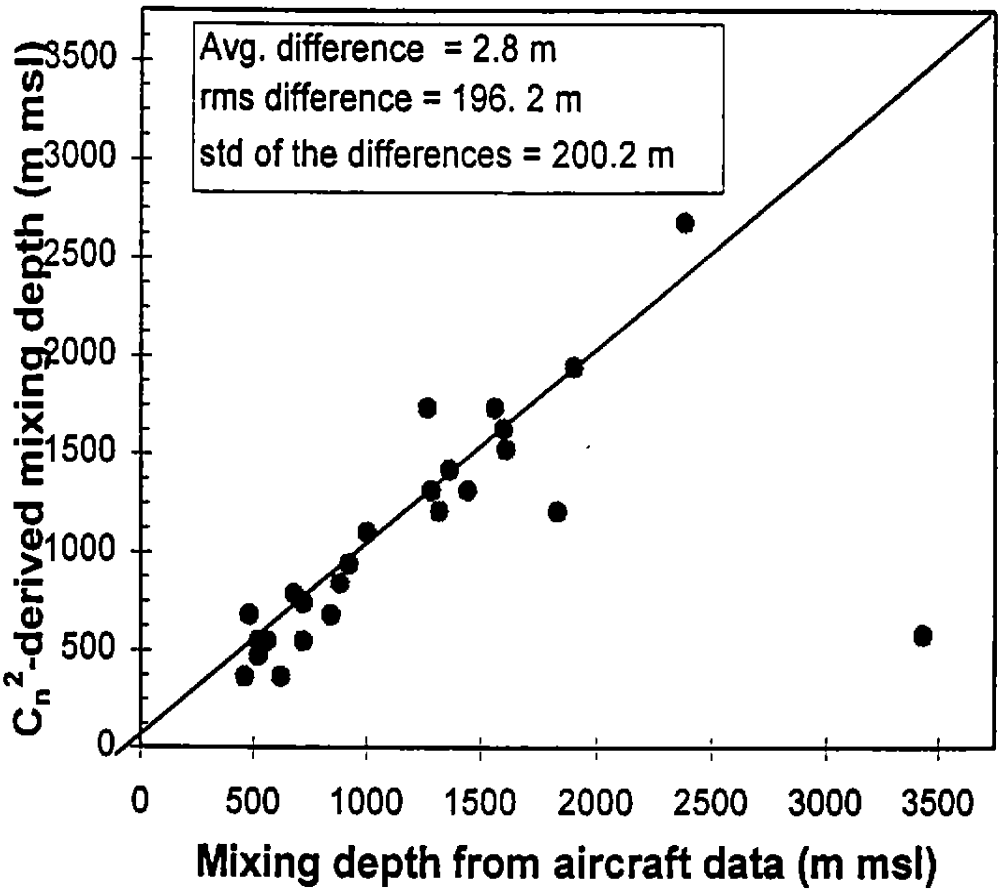

FIGURE 3-29. Scatter plot of C_n^2-derived mixing depths and mixing depths estimated from aircraft profiles of pollutant concentrations, turbulence, and temperature. Twenty-five comparisons were made using aircraft data collected in the afternoon near three profilers deployed in southeast Texas.

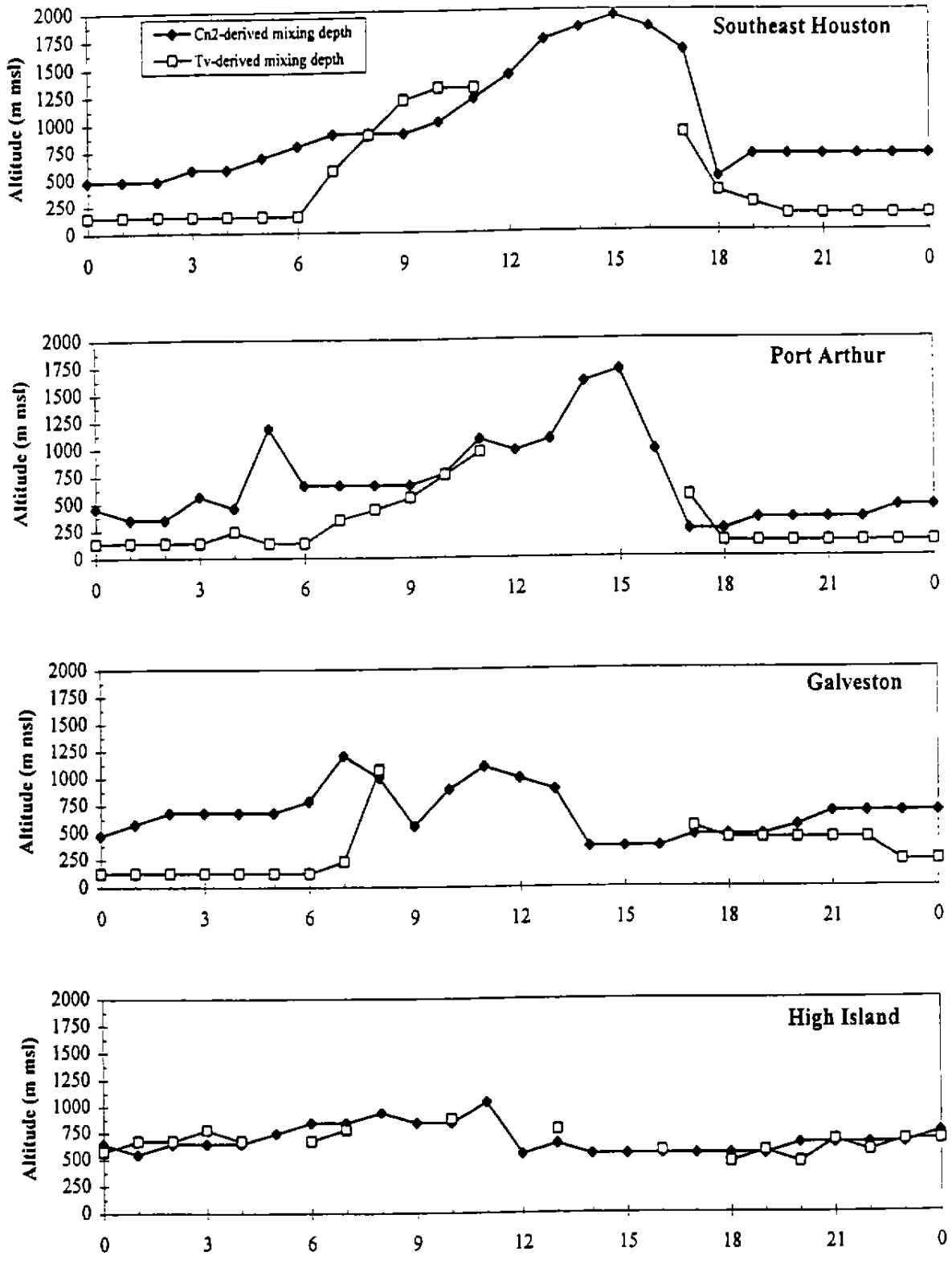

FIGURE 3-30. Time series plot of mixing depths estimated from C_n^2 and virtual temperature data for the profiler sites in southeast Texas located at Southeast Houston (SEH), Port Arthur (JCA), Galveston (GAL), and offshore at the High Island Platform (HIP) on 19 August 1993. Note that T_v-derived linking depths should be used from about 1800-0900 CST.

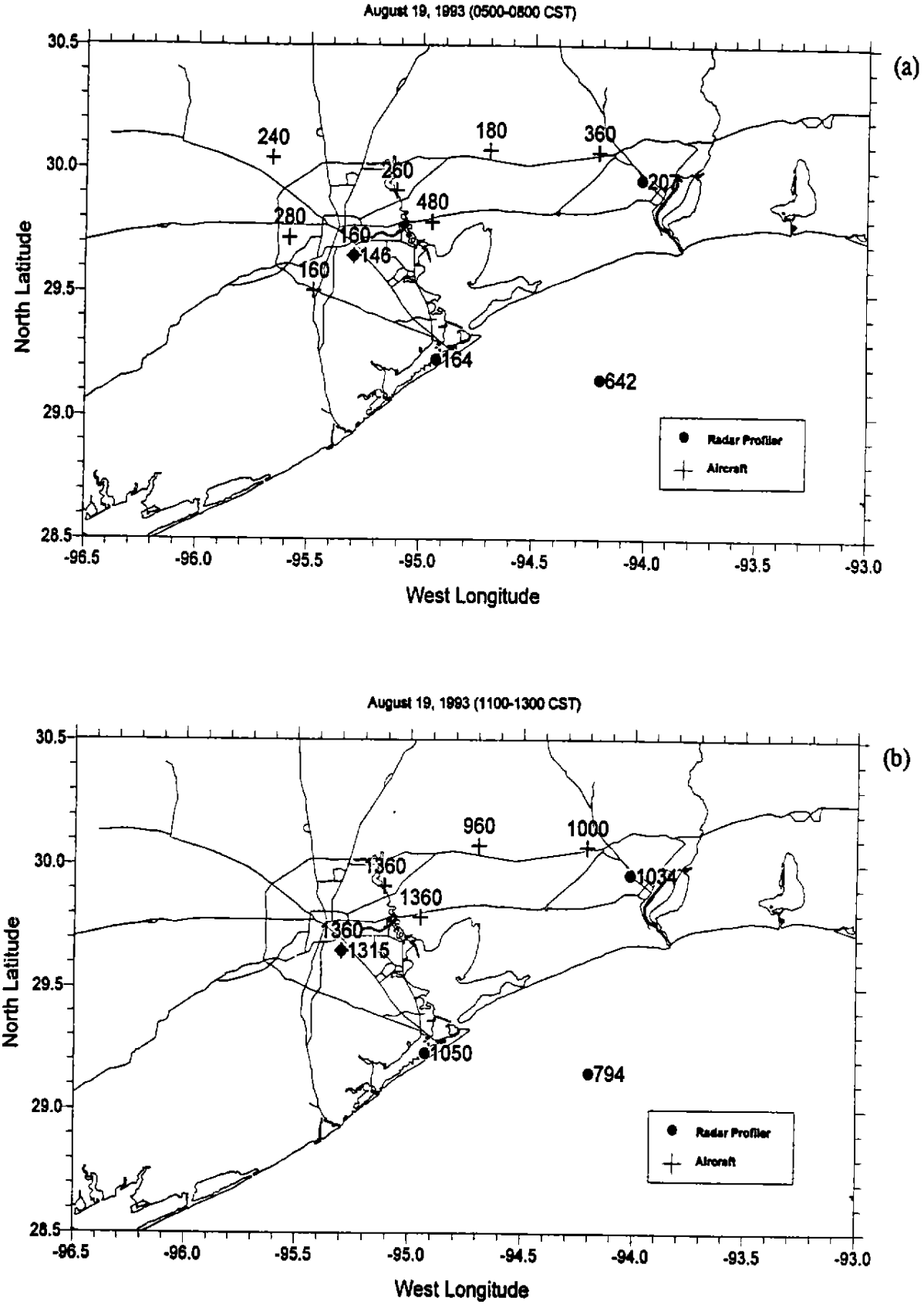

FIGURE 3-31. Mixing depth estimated on 19 August 1993 computed from (a) aircraft and RASS virtual temperature data for the period 0500-0800 CST and (b) aircraft and C_n^2 data for the period 1100-1300 CST.

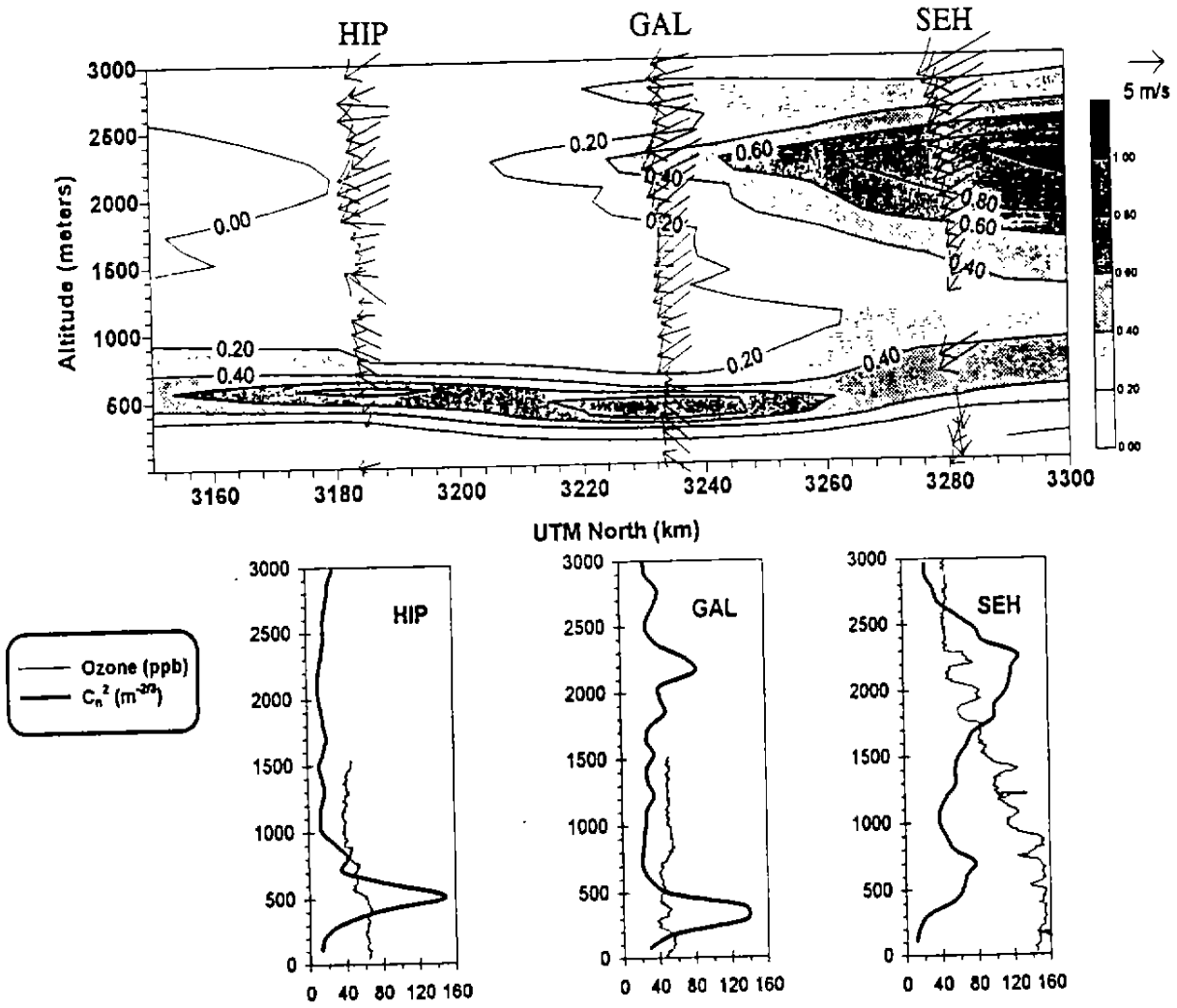

FIGURE 3-32. An example of mixing depth analysis during an ozone episode in southeast Texas using radar profiler data collected during the period 1300-1400 CDT on 10 August 1993. The top portion of the figure shows an offshore-to-onshore cross section of normalized C_n^2 ($C_n^2/C_{n\,max}^2$) and winds aloft measured at the Southeast Houston (SEH), Galveston (GAL), and High Island (HIP) radar profiler sites. Note that simple interpolation of the $C_n^2/C_{n\,max}^2$ data occurs between stations so some features shown may not be real. The top of the mixed layer corresponds to the maximum values of the parameter $C_n^2/C_{n\,max}^2$. The bottom three figures show the vertical profiles of C_n^2 measured at each profiler site, as well as aircraft profiles of ozone collected during the period 1226-1342 CST.

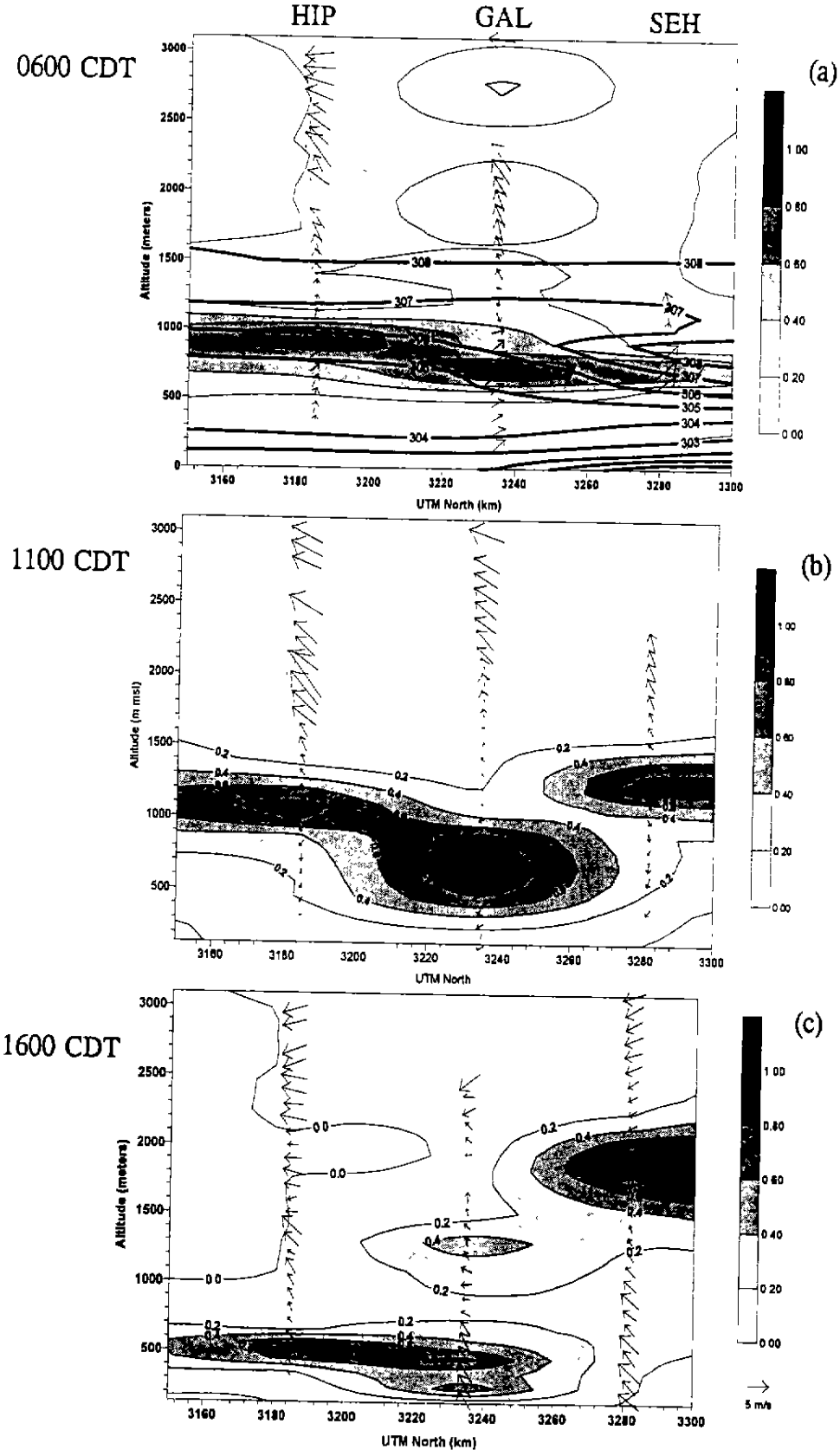

FIGURE 3-33. Offshore-to-onshore cross section of normalized C_n^2 ($C_n^2/C_{n\,max}^2$) and winds aloft measured at the Southeast Houston (SEH), Galveston (GAL), and High Island (HIP) radar profiler sites on 19 August 1993 at (a) 0600 CDT, (b) 1100 CDT, and (c) 1600 CDT. Contours of virtual potential temperature computed from RASS are also plotted at 0600 CDT.

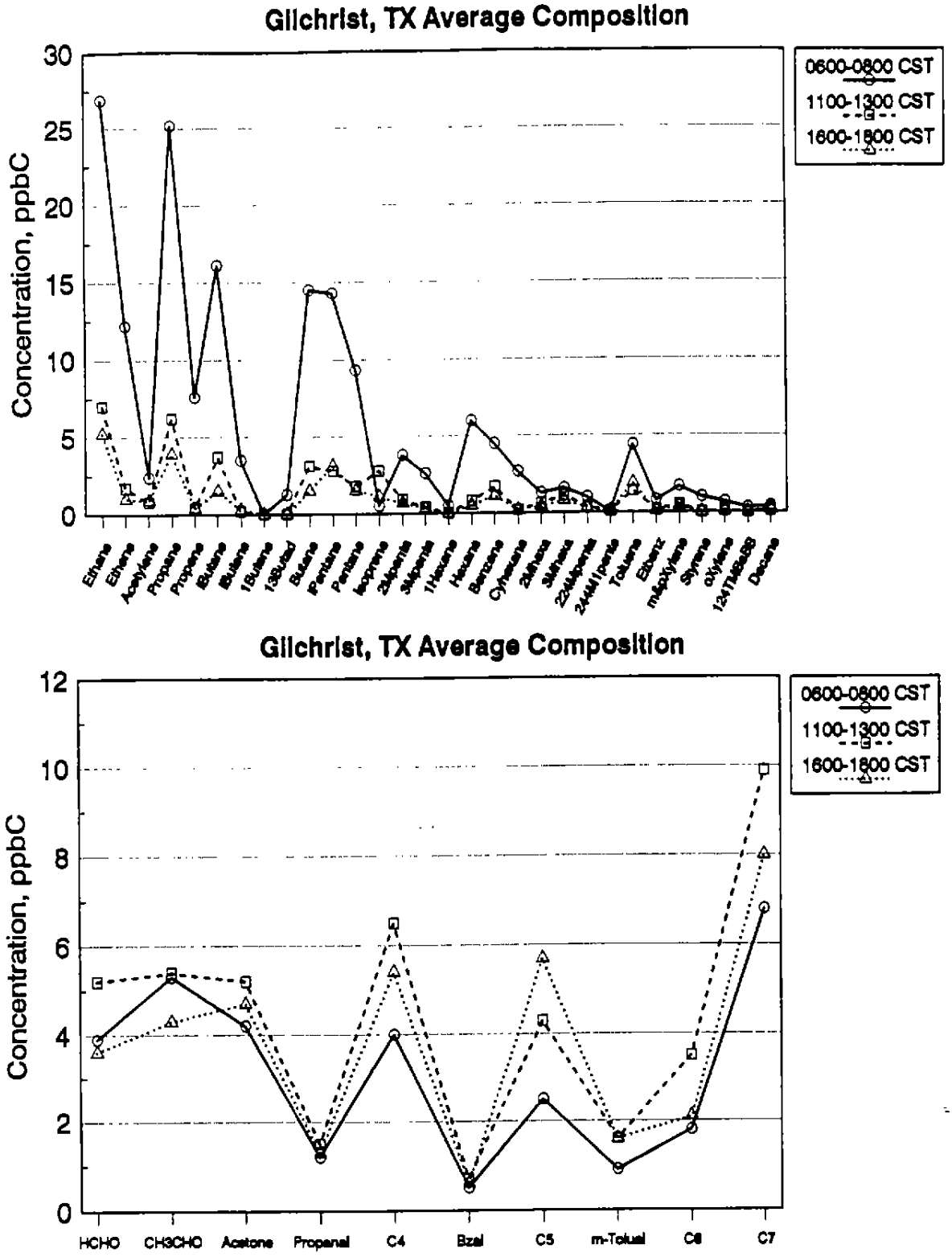

FIGURE 3-34. Average concentrations of abundant hydrocarbons (top) and carbonyl compounds (bottom) by time of day at Gilchrist, Texas. Average of all intensive sample-day data.

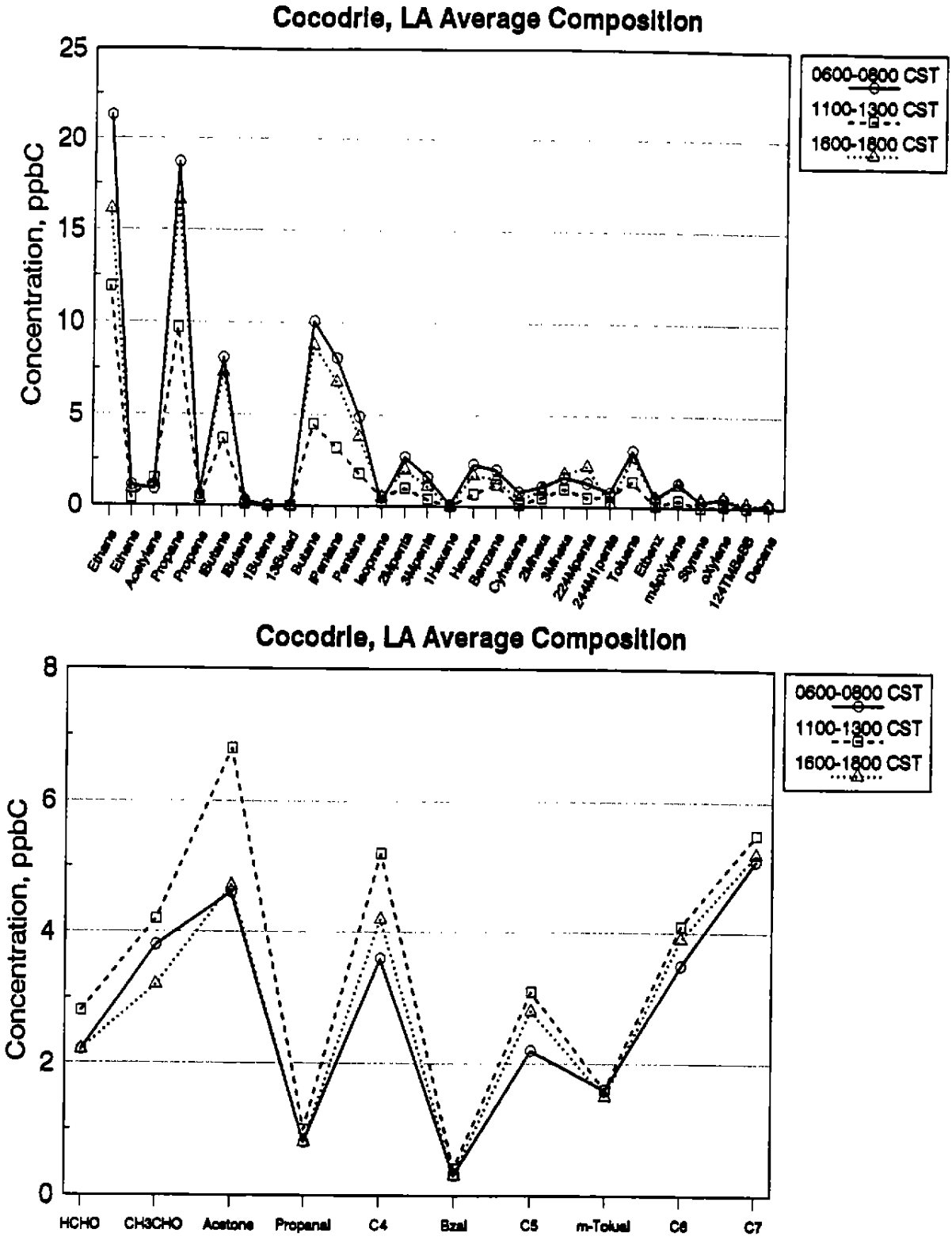

FIGURE 3-35. Average concentrations of abundant hydrocarbons (top) and carbonyl compounds (bottom) by time of day at Cocodrie, Louisiana (surface canisters). Average of all intensive sample-day data.

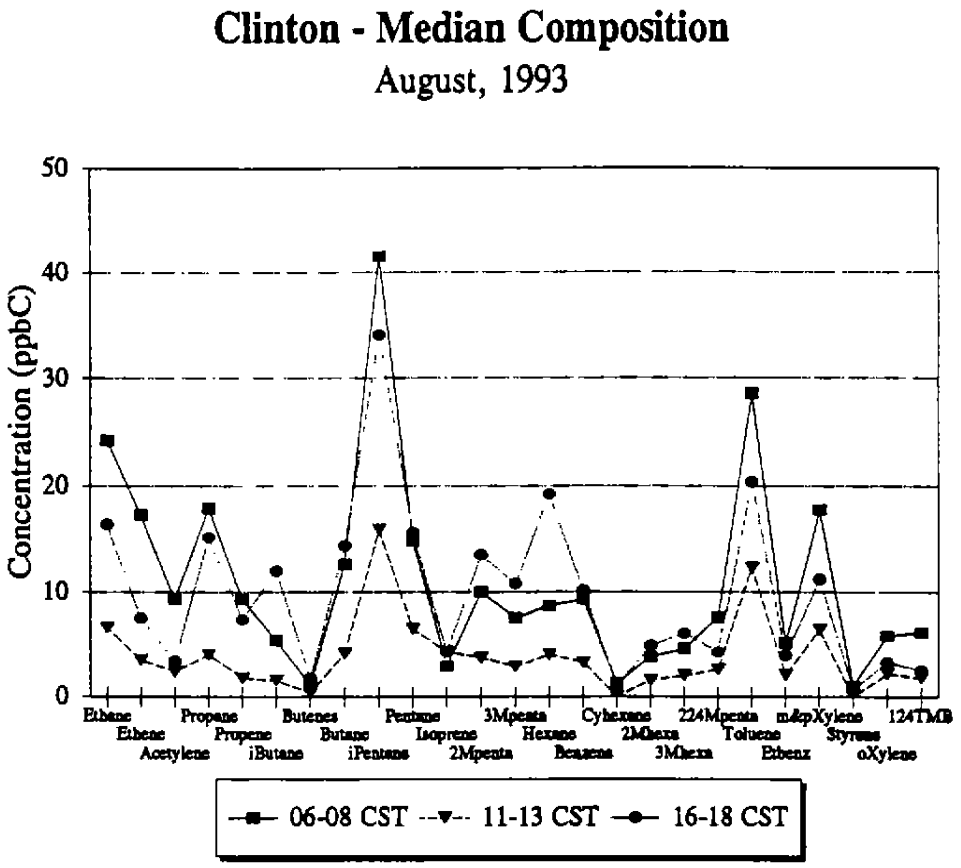

FIGURE 3-36. Median concentrations of abundant hydrocarbons by time of day at Clinton, Texas (surface continuous gas chromatograph results). Median of August 1993 data.

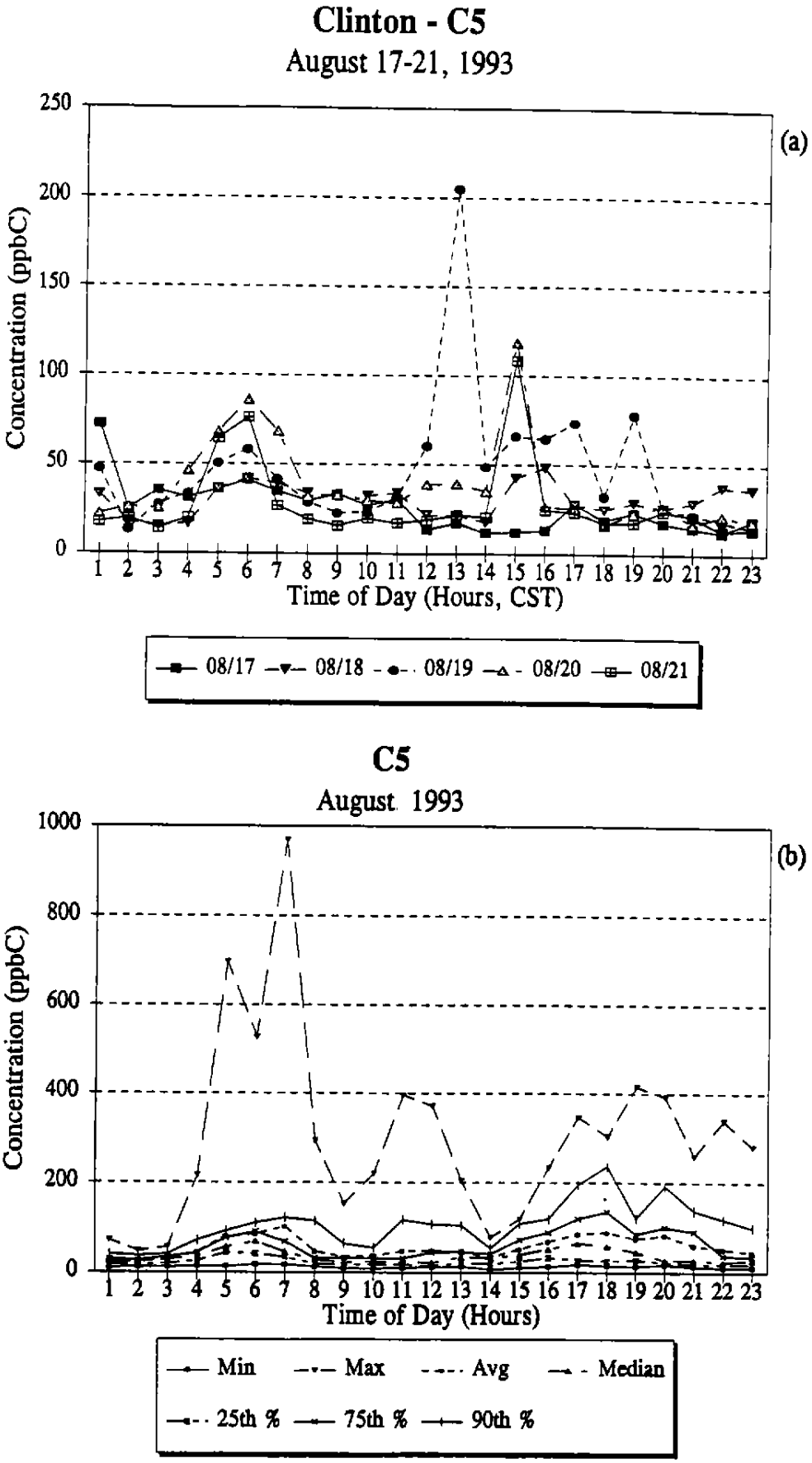

FIGURE 3-37. Diurnal plots of C5 paraffins at Clinton, Texas for (a) 17-21 August 1993 and (b) all of August 1993.

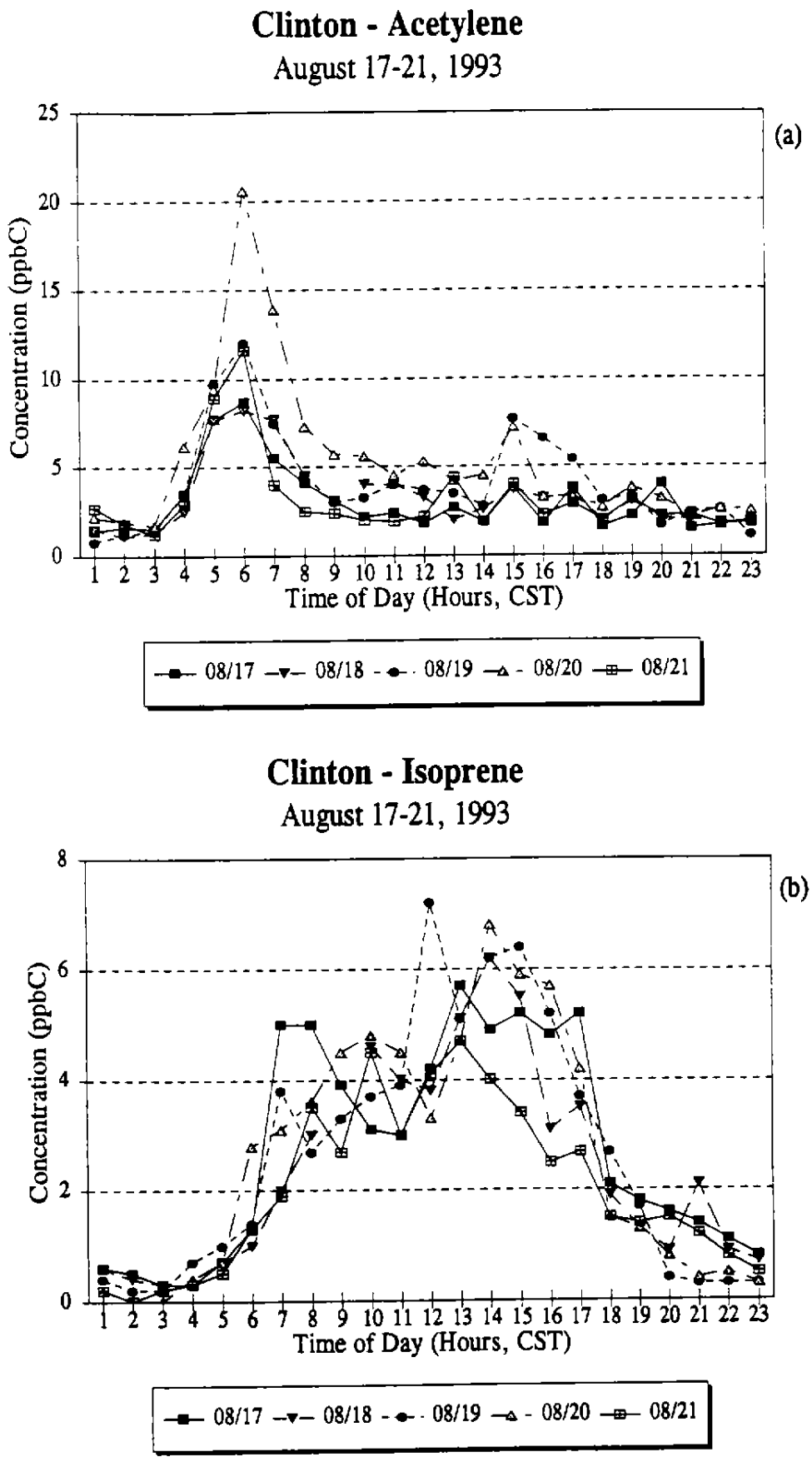

FIGURE 3-38. Diurnal plots of (a) acetylene and (b) isoprene at Clinton, Texas on 17-21 August 1993.

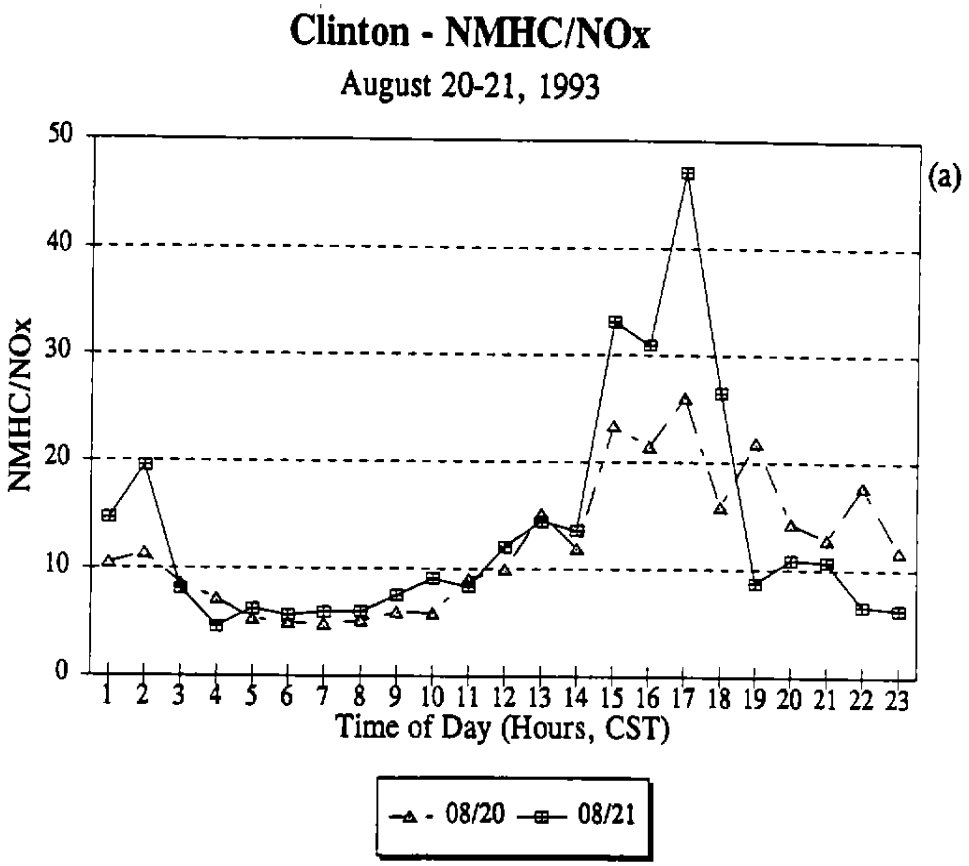

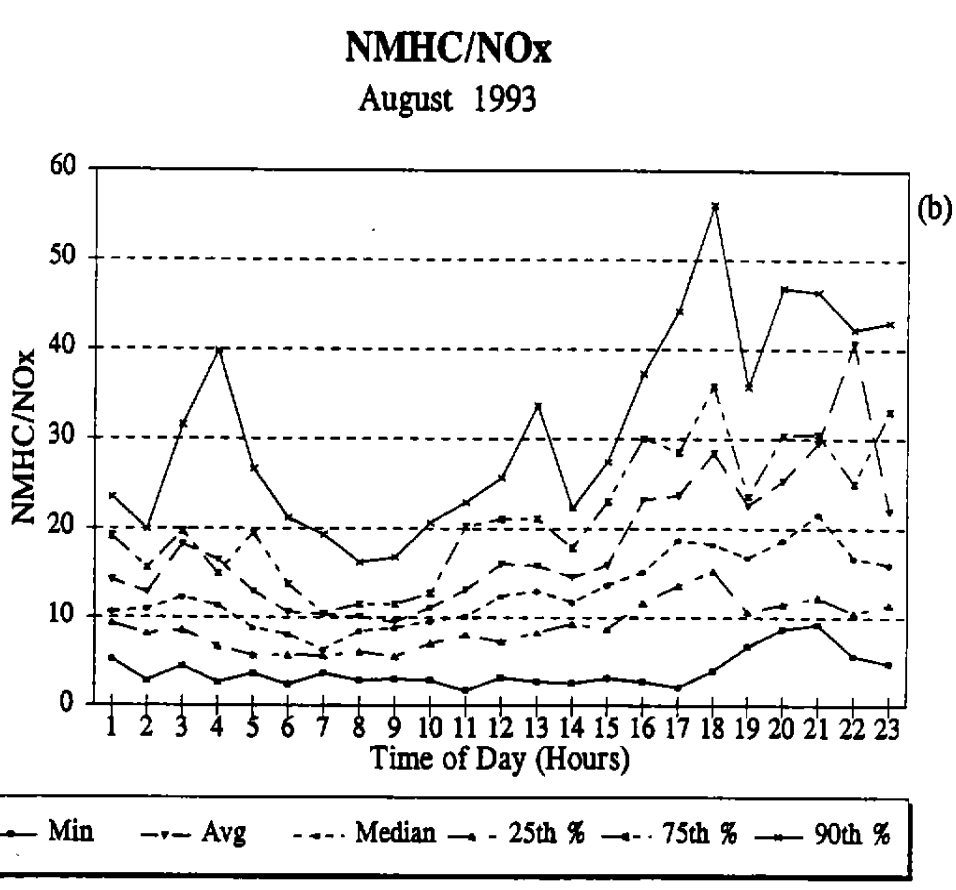

FIGURE 3-39. Diurnal plots of NMHC/NO_x ratios at Clinton, Texas during (a) 20-21 August 1993 and (b) all of August 1993.

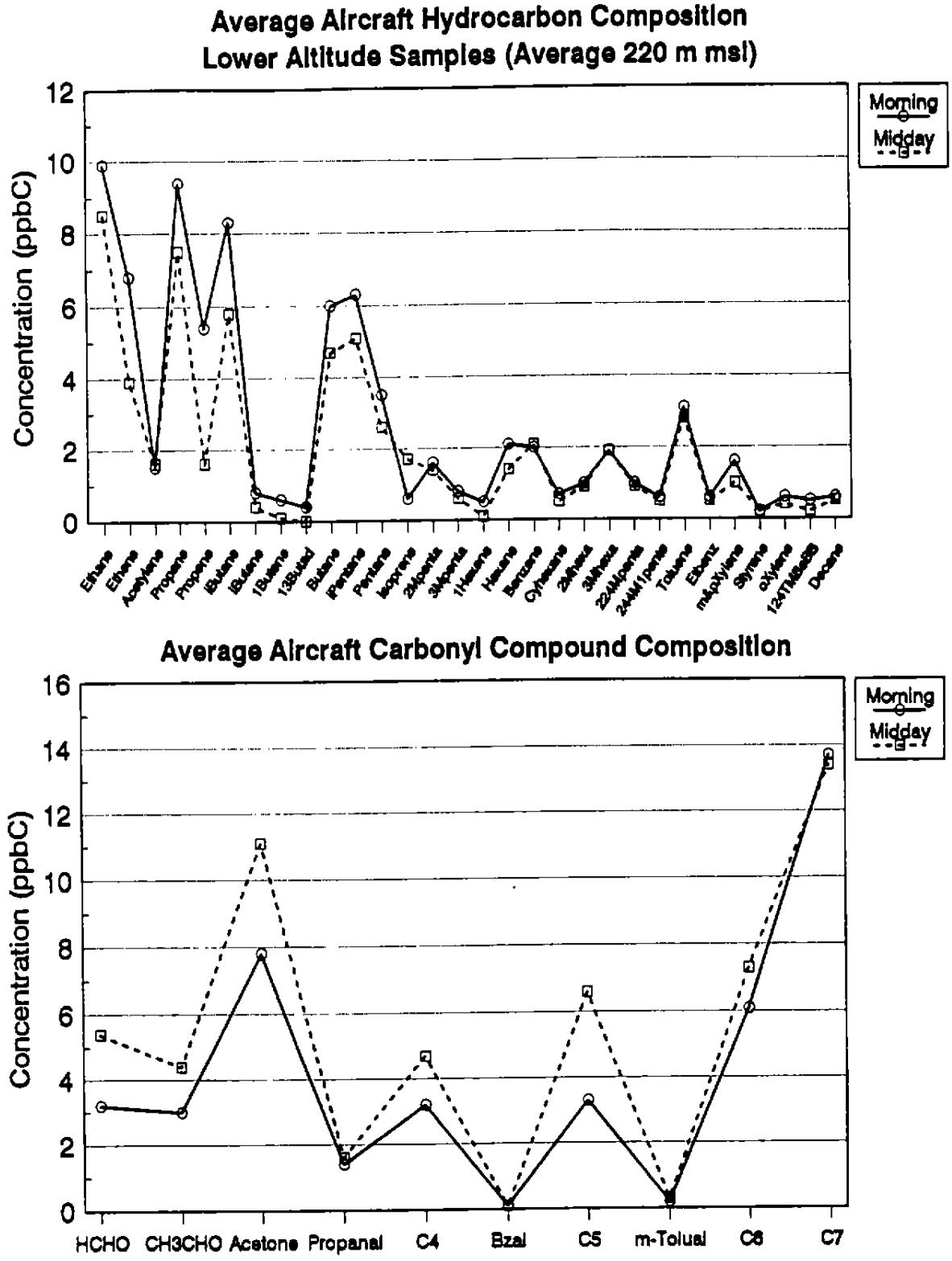

FIGURE 3-40. Average concentrations of abundant hydrocarbons (top) and carbonyl compounds (bottom) by sampling time collected by aircraft at lower altitudes (average of 220 m msl) during intensive sampling days.

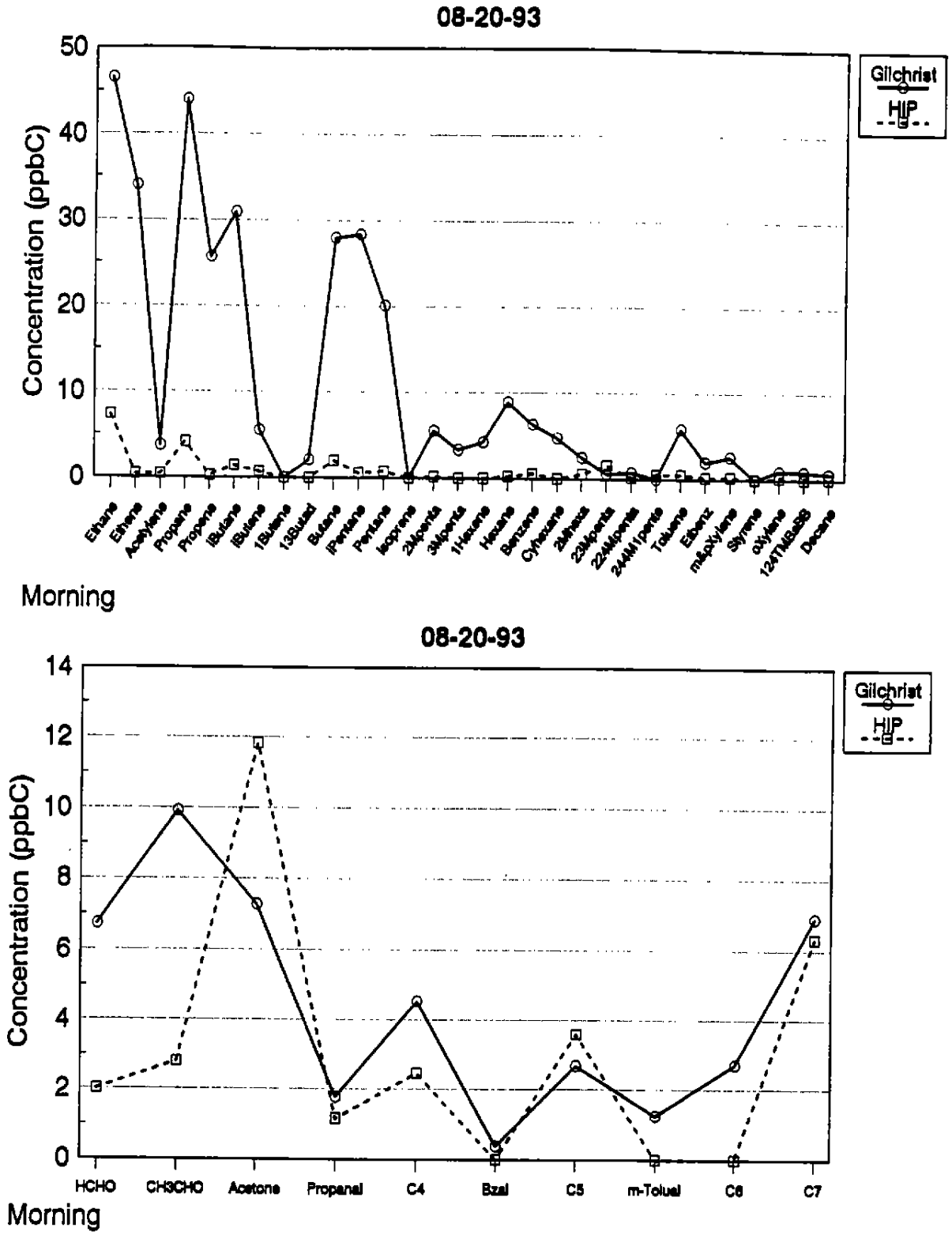

FIGURE 3-41. Concentrations of abundant hydrocarbons (top) and carbonyl compounds (bottom) aloft over High Island Platform and at the surface at Gilchrist on the morning of 20 August 1993. Winds at Gilchrist were offshore during sampling.

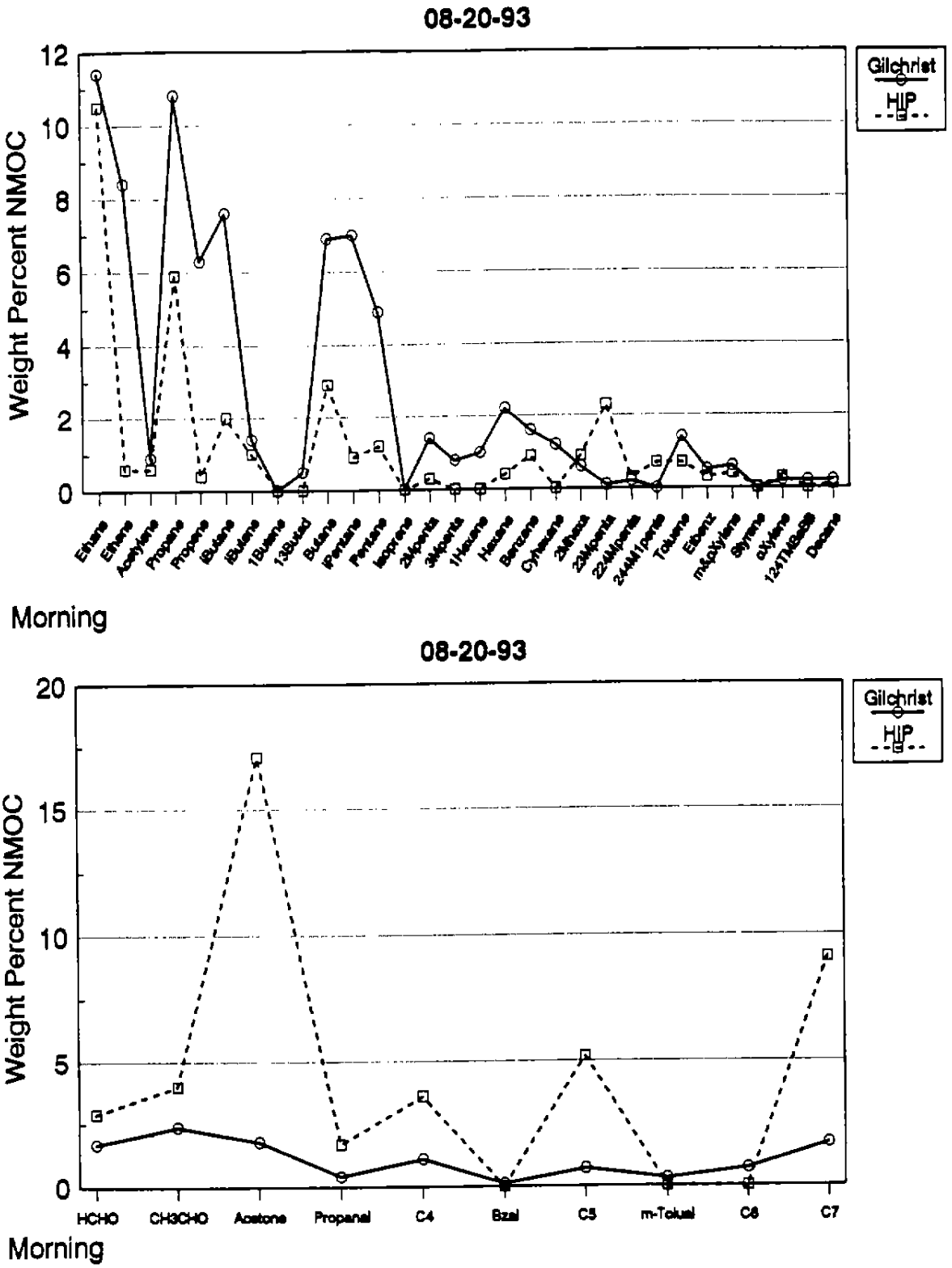

FIGURE 3-42. Weight percent of NMOC of abundant hydrocarbons (top) and carbonyl compounds (bottom) aloft over High Island Platform and at the surface at Gilchrist on the morning of 20 August 1993. Winds at Gilchrist were offshore during sampling.

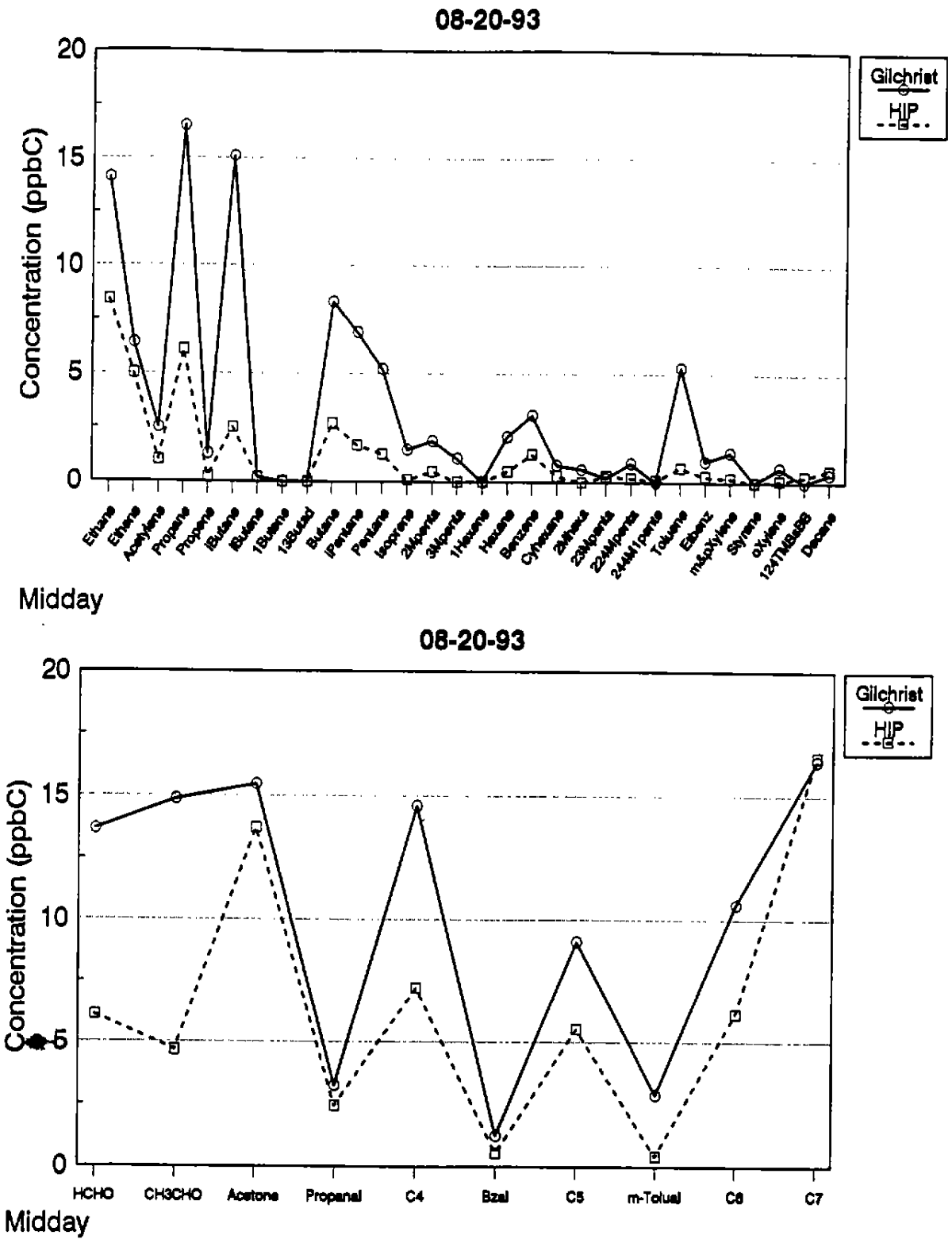

FIGURE 3-43. Concentrations of abundant hydrocarbons (top) and carbonyl compounds (bottom) aloft over High Island Platform and at the surface at Gilchrist midday on 20 August 1993. Winds at Gilchrist were mostly onshore during sampling.

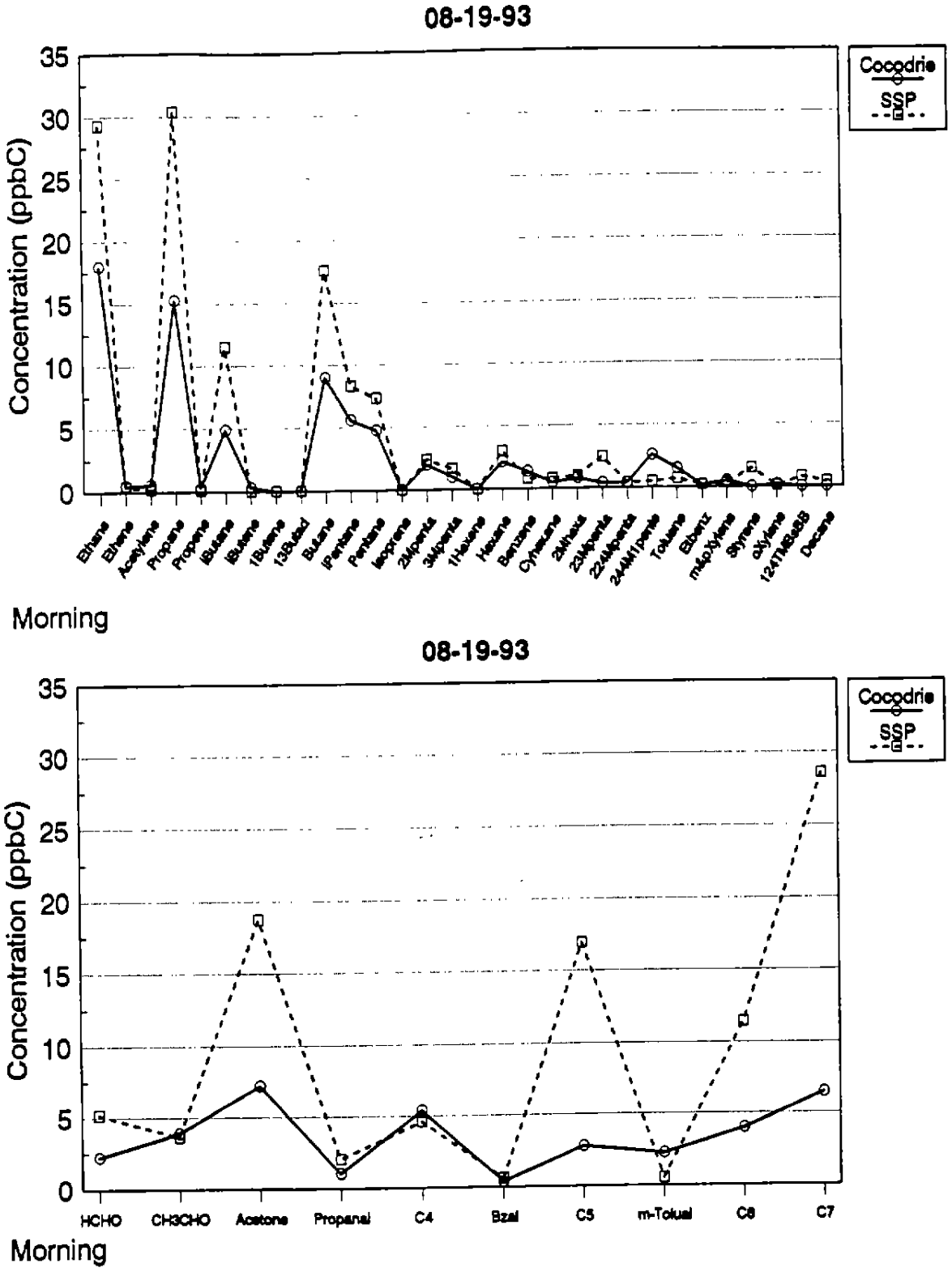

FIGURE 3-44. Concentrations of abundant hydrocarbons (top) and carbonyl compounds (bottom) aloft over Ship Shoal Platform and at the surface at Cocodrie on the morning of 19 August 1993. Winds at Gilchrist were mostly onshore during sampling.

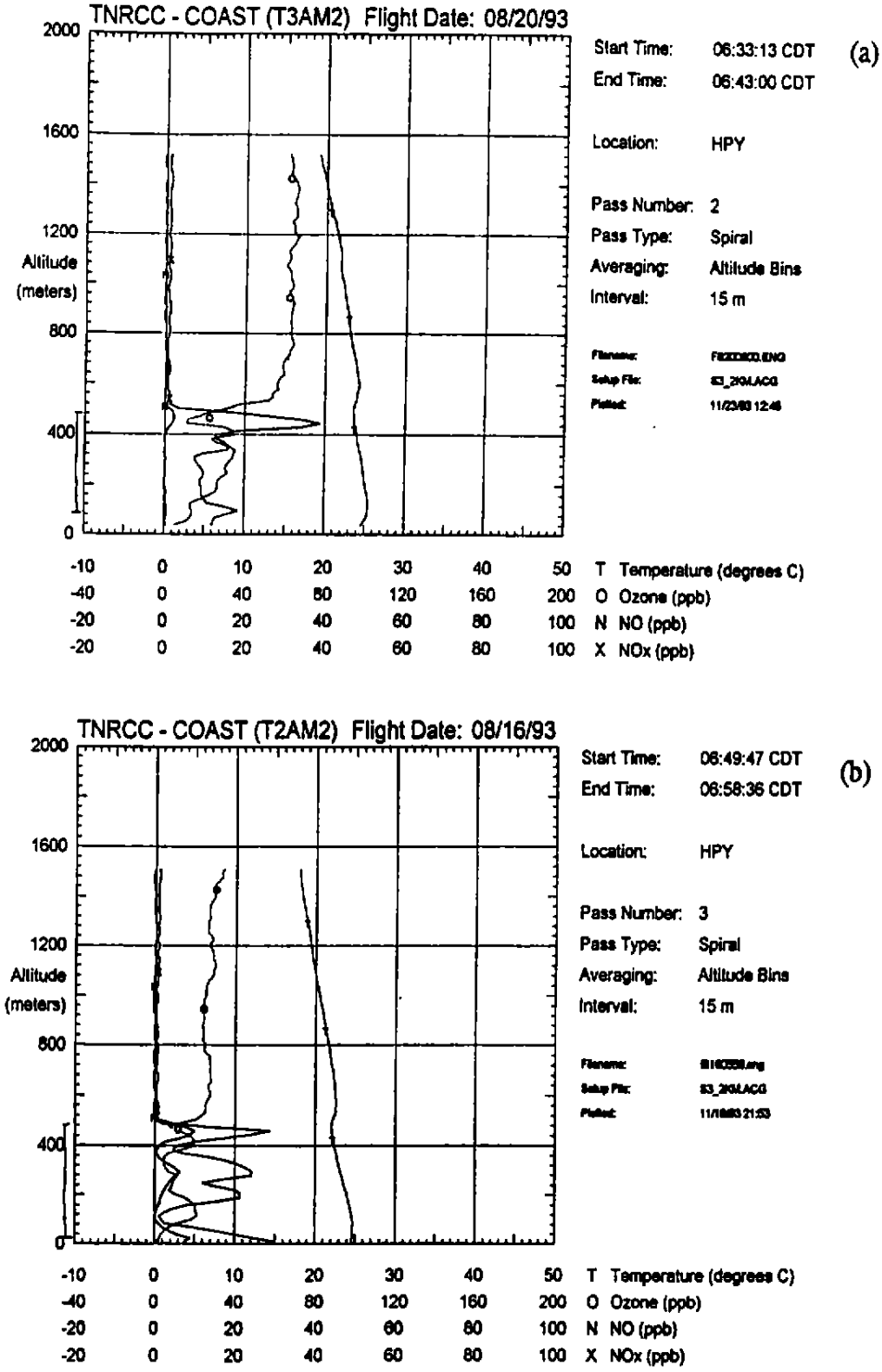

FIGURE 3-45. Temperature and NO, NO_x, and ozone concentrations measured by aircraft during a spiral over Baytown on the mornings of (a) August 20 and (b) 16 August 1993. Hydrocarbon and carbonyl compound samples were collected between 457 and 61 m msl on August 20 and between 457 and 30 m msl on August 16.

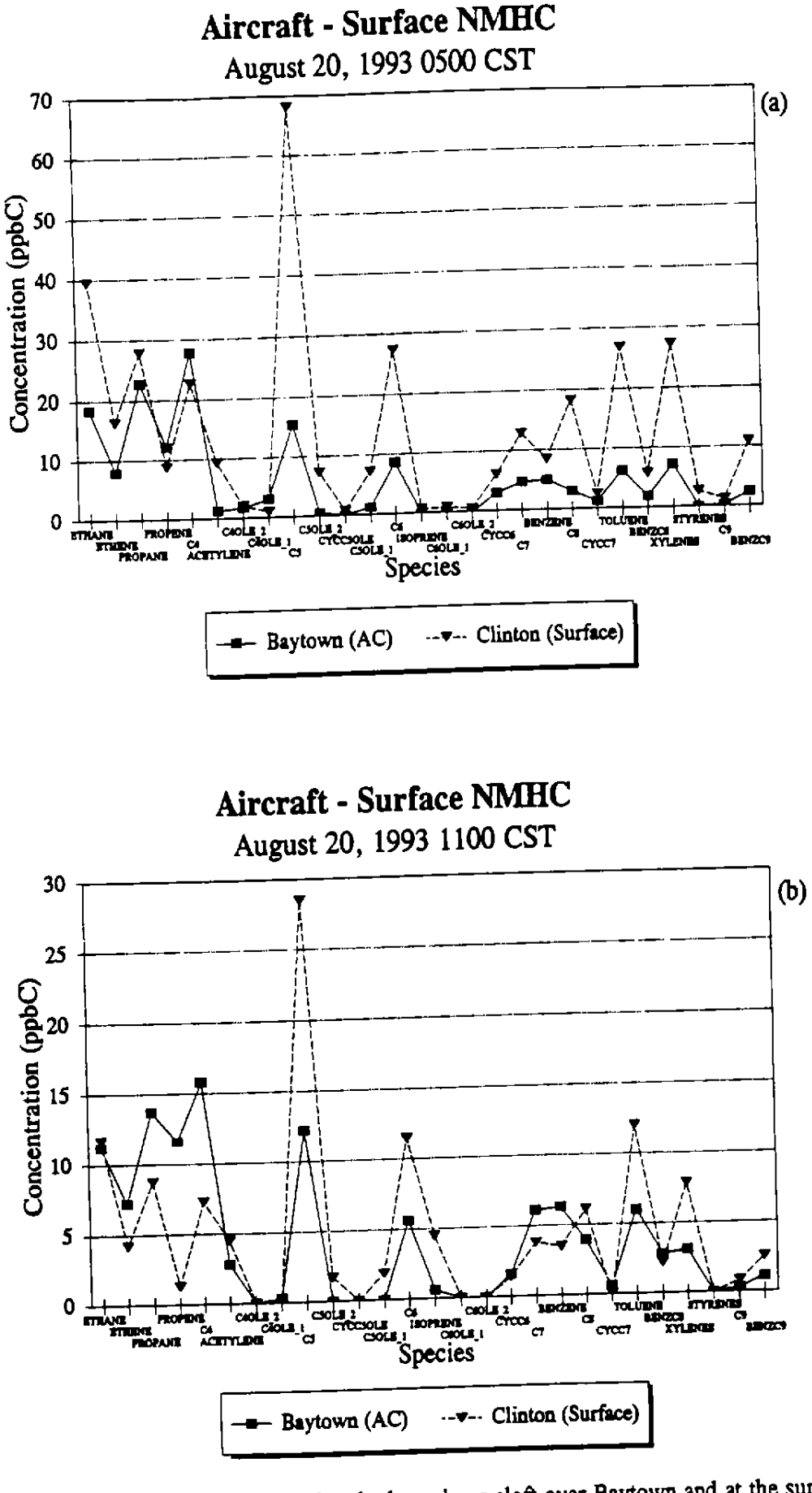

FIGURE 3-46. Concentrations of abundant hydrocarbons aloft over Baytown and at the surface at Clinton (a) in the morning and (b) midday on 20 August 1993.

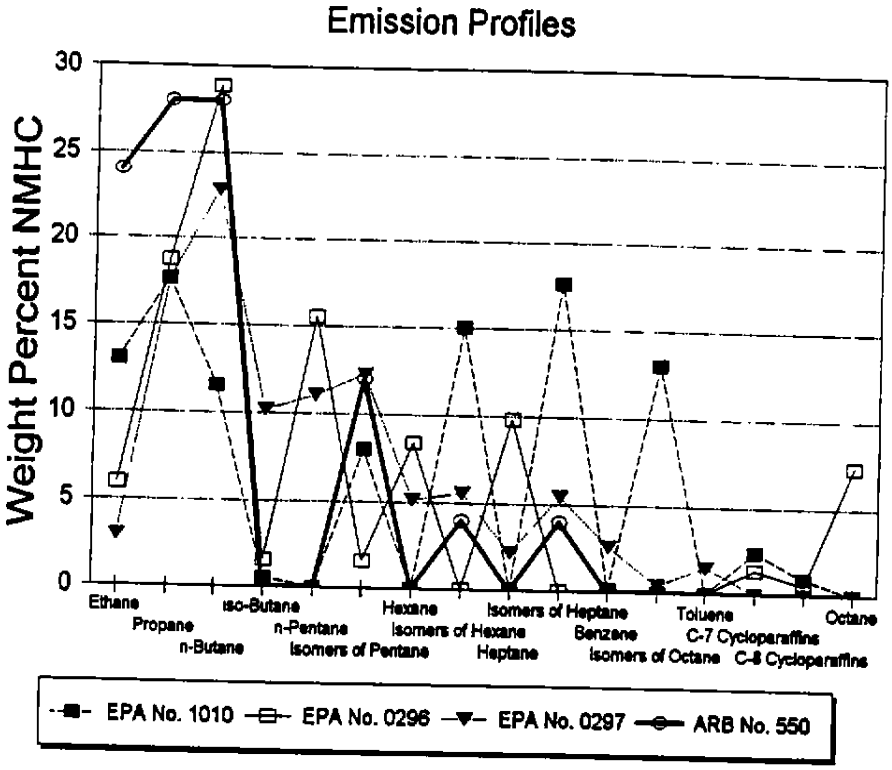

FIGURE 3-47. Normalized weight percent of NMHC of one California Air Resources Board and three EPA emission profiles: natural gas seeps (ARB no. 550), oil and gas production-fugitives-unclassified (EPA no. 1010), fixed roof tank-crude oil production (EPA no. 0296), and fixed roof tank-crude oil refinery (EPA no. 0297).

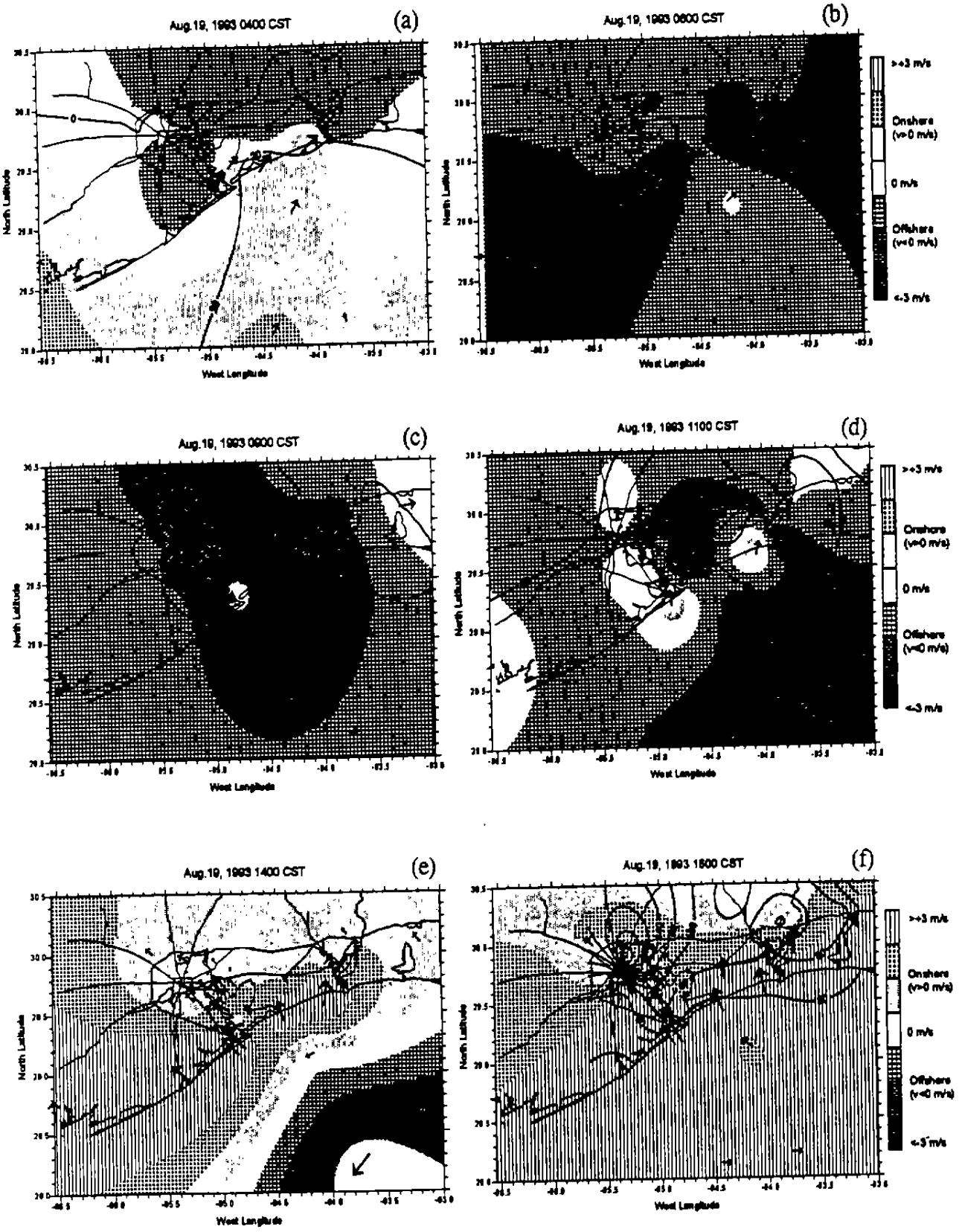

FIGURE 3-48. Isopleths of ozone concentrations (ppb), onshore-offshore component of the surface wind perpendicular to the shoreline (V_n, m/s), and surface winds on 19 August 1993 at (a) 0400 CST, (b) 0600 CST, (c) 0900 CST, (d) 1100 CST, (e) 1400 CST, and (f) 1600 CST.

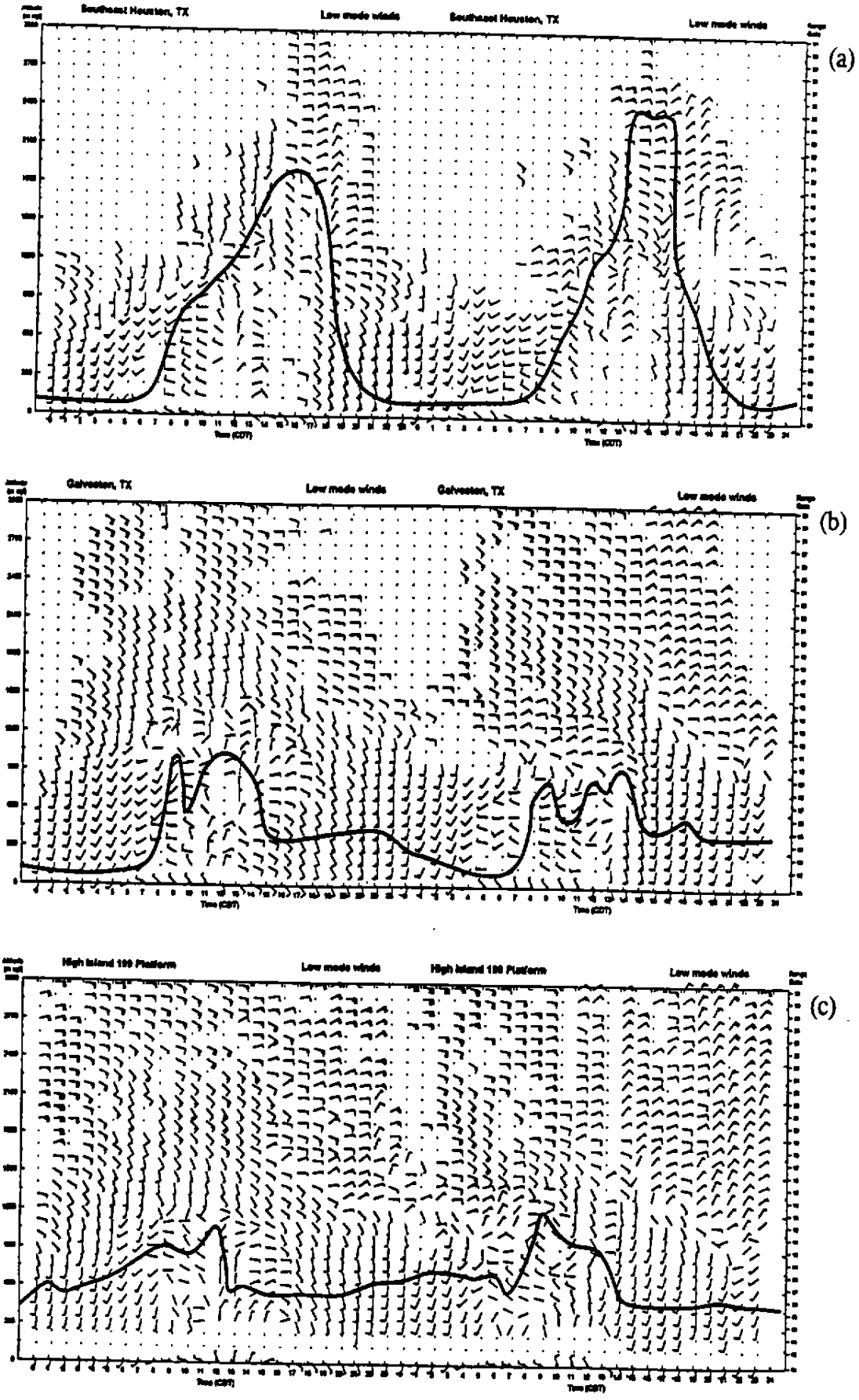

FIGURE 3-49. Time-height cross sections of winds from the (a) Southeast Houston, (b) Galveston, and (c) High Island Platform radar profilers on 19 and 20 August 1993. Hourly surface winds are also plotted at 10 m. Solid lines indicate the top of the mixed layer.

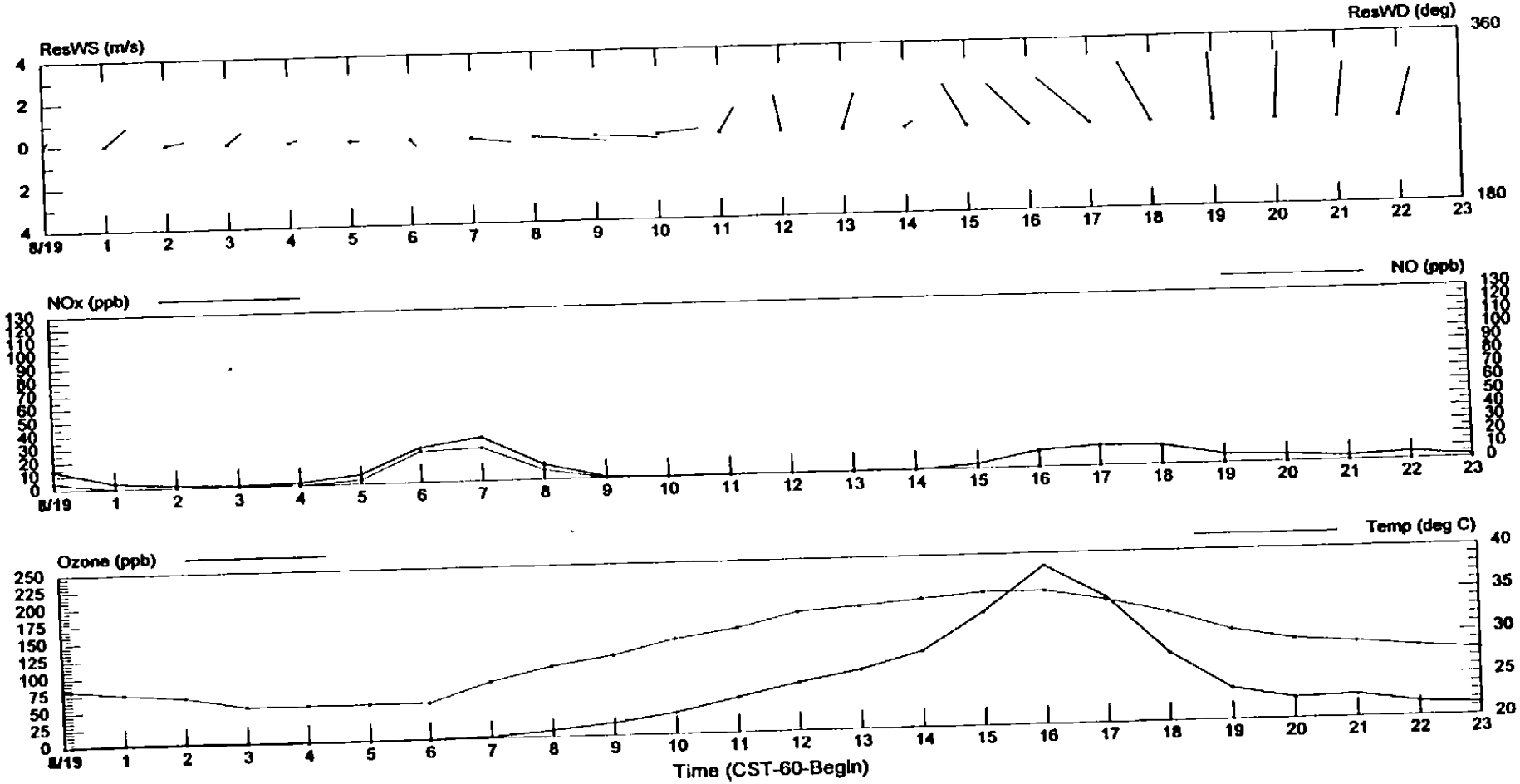

FIGURE 3-50. Time series of hourly averaged surface winds, temperature (°C), ozone (ppb), NO_x (ppb), and NO (ppb) measured at Aldine (TN10) on 19 August 1993.

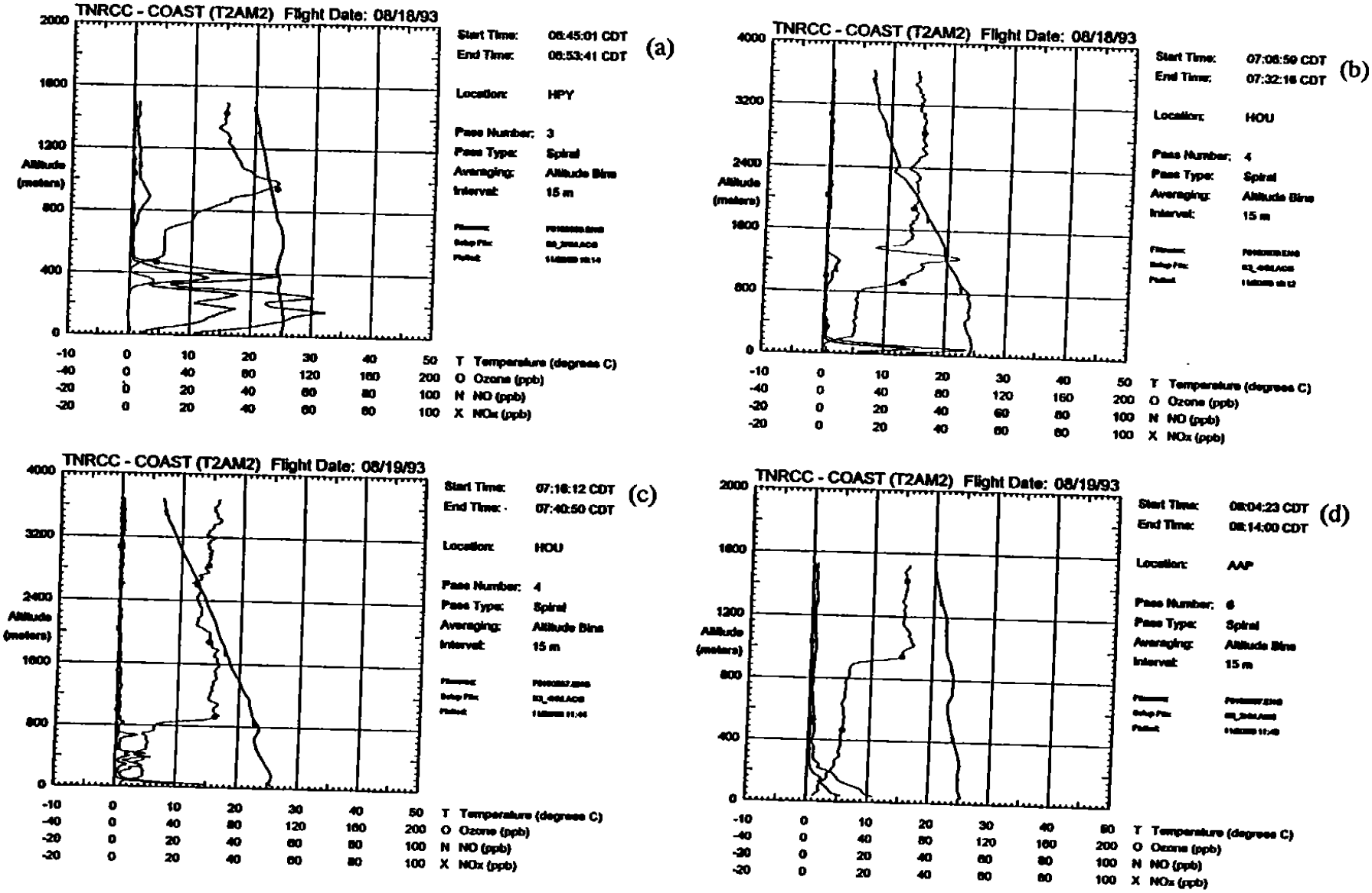

FIGURE 3-51. Early morning aircraft measurements of temperature, ozone, and oxides of nitrogen on 10 August 1993 over (a) Baytown (HPY) and (b) Houston Hobby Airport (HOU), and on 19 August 1993 over (c) Houston Hobby (HOU), and (d) Andrau (AAP).

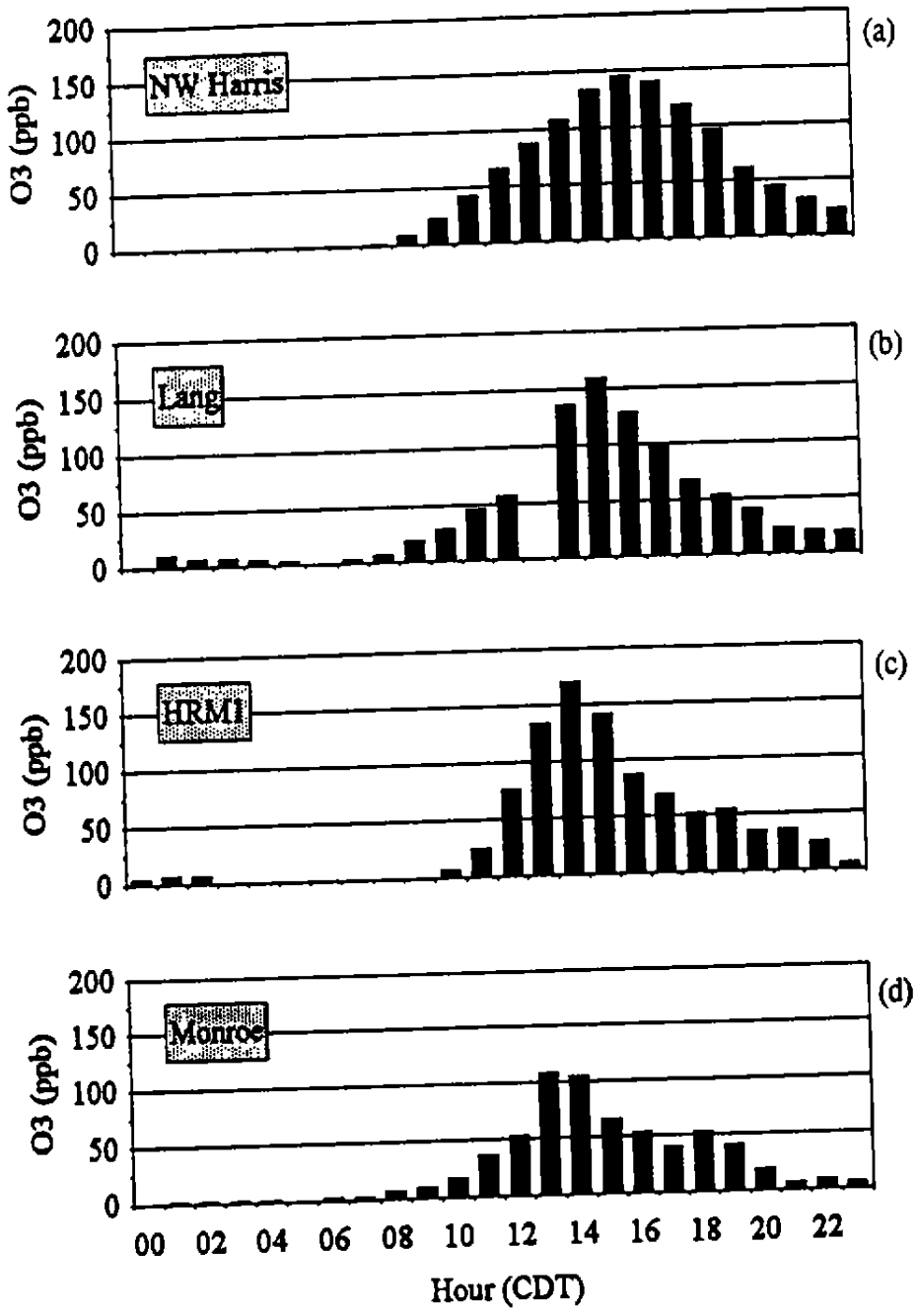

FIGURE 3-52. Hourly ozone concentrations at (a) Northwest Harris, (b) Lang, (c) Houston Regional Monitoring Site 1, and (d) Monroe on 10 August 1993.

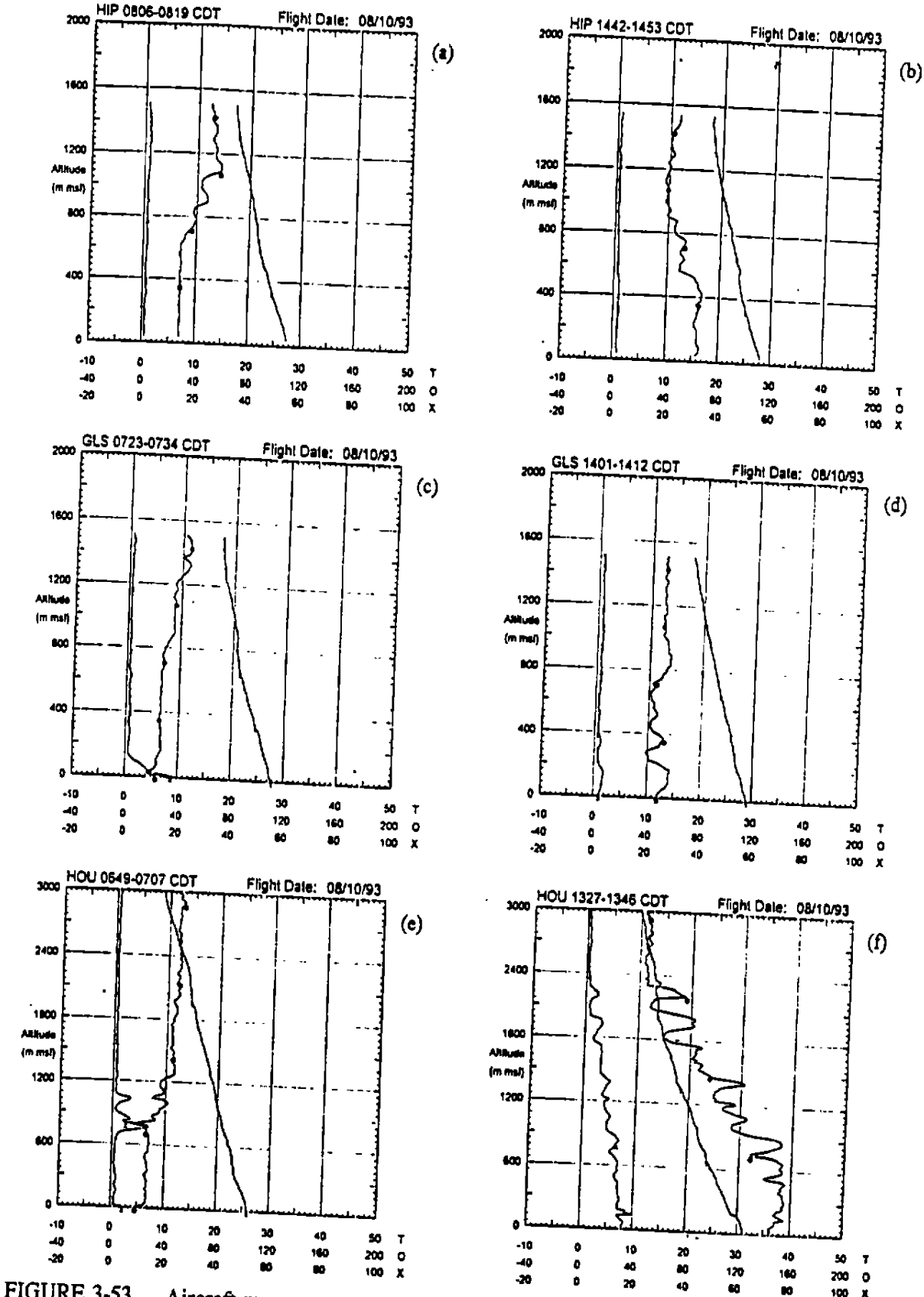

FIGURE 3-53. Aircraft measurements of temperature (T, °C), ozone (O, ppb) and oxides of nitrogen (NO_z, ppb) on 10 August 1993 over (a) High Island Platform (morning), (b) High Island Platform (afternoon), (c) Galveston Airport (morning), (d) Galveston Airport (afternoon), (e) Houston Hobby Airport (morning), and (f) Houston Hobby Airport (afternoon). The Galveston profiler was located 5 km southwest of Galveston Airport, and the Southeast Houston profiler was located 1 km west of Houston Hobby Airport.

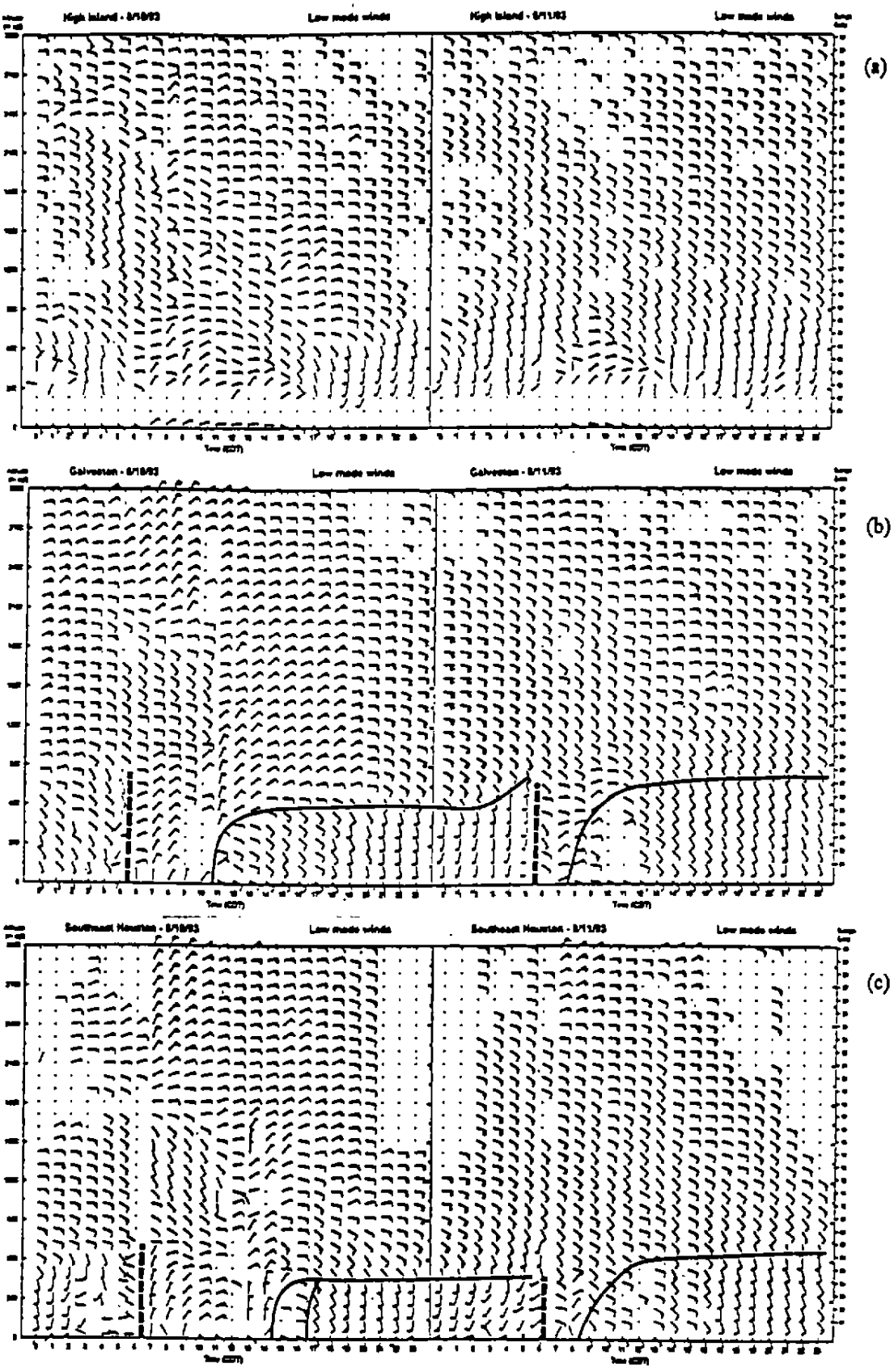

FIGURE 3-54. Time-height cross sections of winds from the (a) High Island Platform, (b) Galveston, and (c) Southeast Houston profilers on 10 and 11 August 1993. Hourly surface winds are also plotted at 10 m. Solid and dashed lines refer to the gulf/bay breezes and convergence zones, respectively.

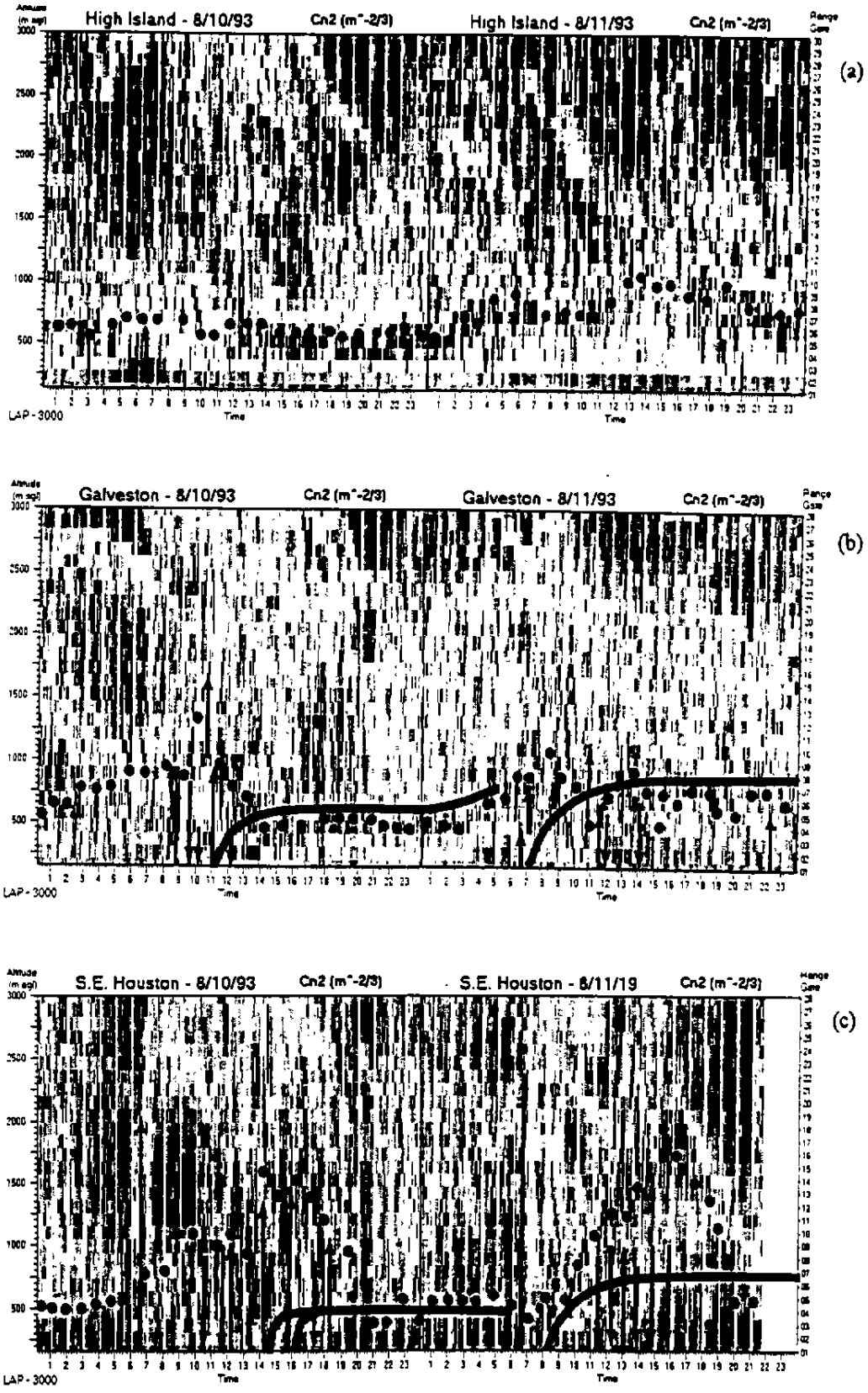

FIGURE 3-55. Time-height cross sections of C_n^2 from (a) High Island Platform, (b) Galveston, and (c) Southeast Houston profilers on 10-11 August 1993. Dotted line indicates top of the boundary layer. Vertical arrows denote regions with updrafts or downdrafts that exceeded 1 m/s. High values of Cn^2 are denoted by dark regions, with the highest values denoted by white regions within these dark regions.

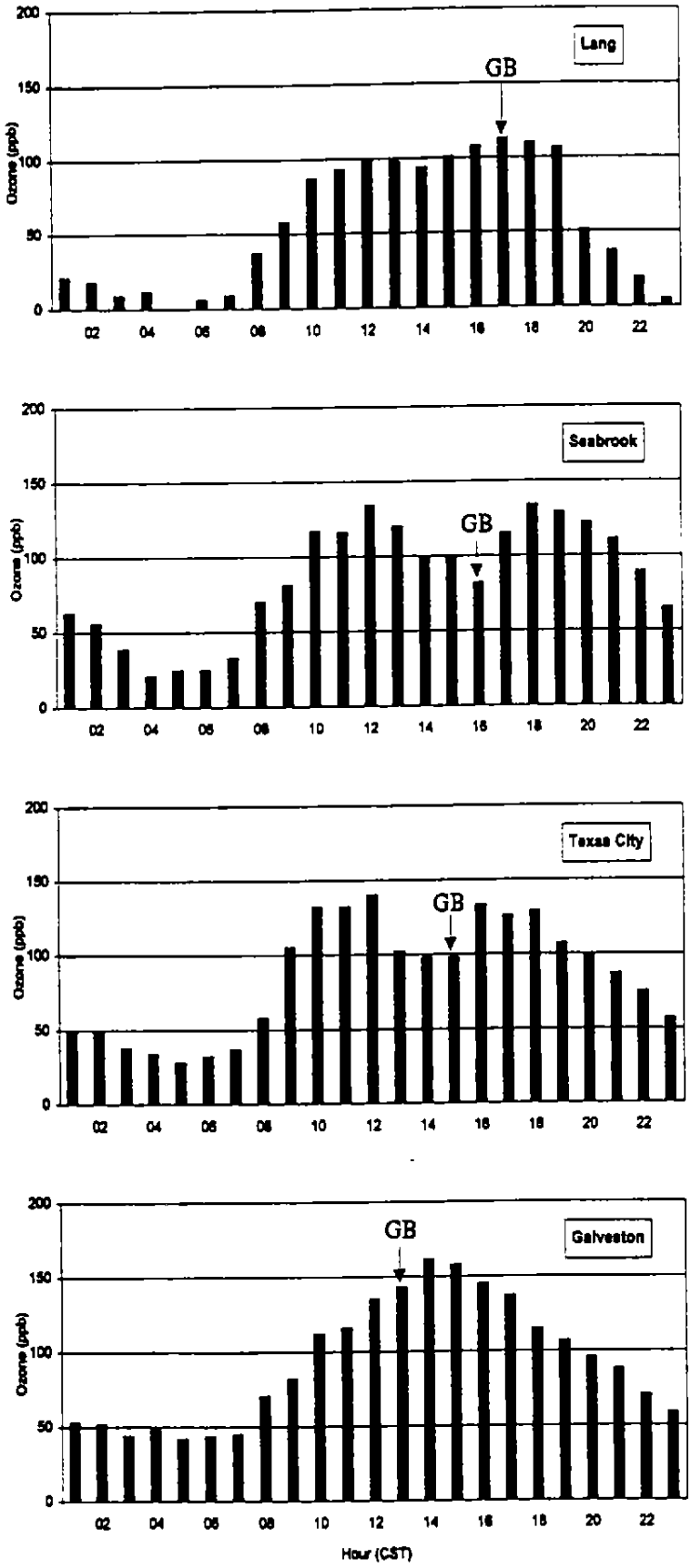

FIGURE 3-56. Hourly ozone concentrations on 10 September 1993 at Galveston, Texas City, Seabrook, and Houston (Lang). The arrows with "GB" indicate the time that the gulf breeze passed each site.

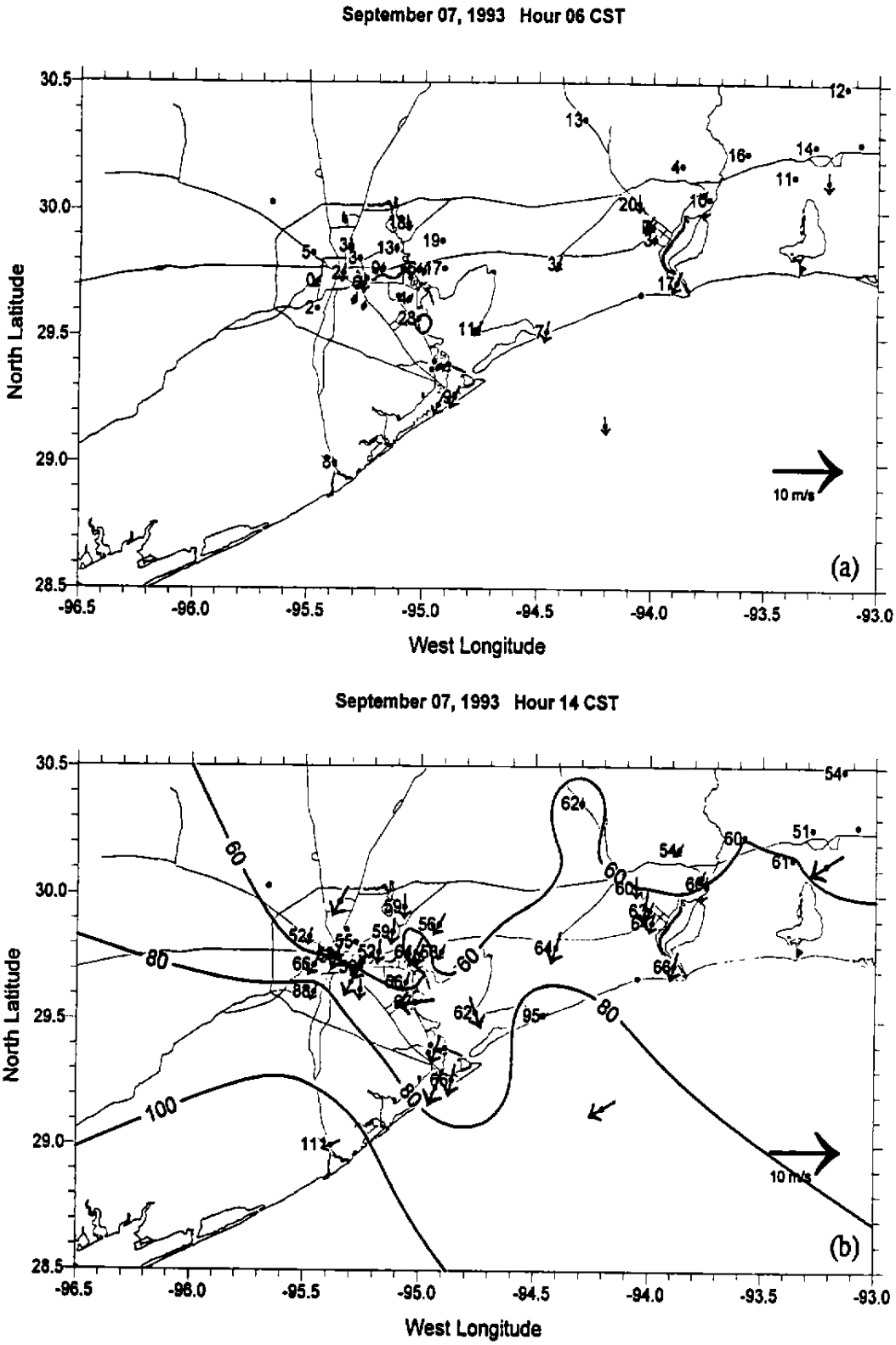

FIGURE 3-57. Plots of surface winds and ozone concentrations in the southeast Texas region at (a) 0600 CST and (b) 1400 CST on 7 September 1993, Dashed lines indicate the location of the gulf-breeze front.

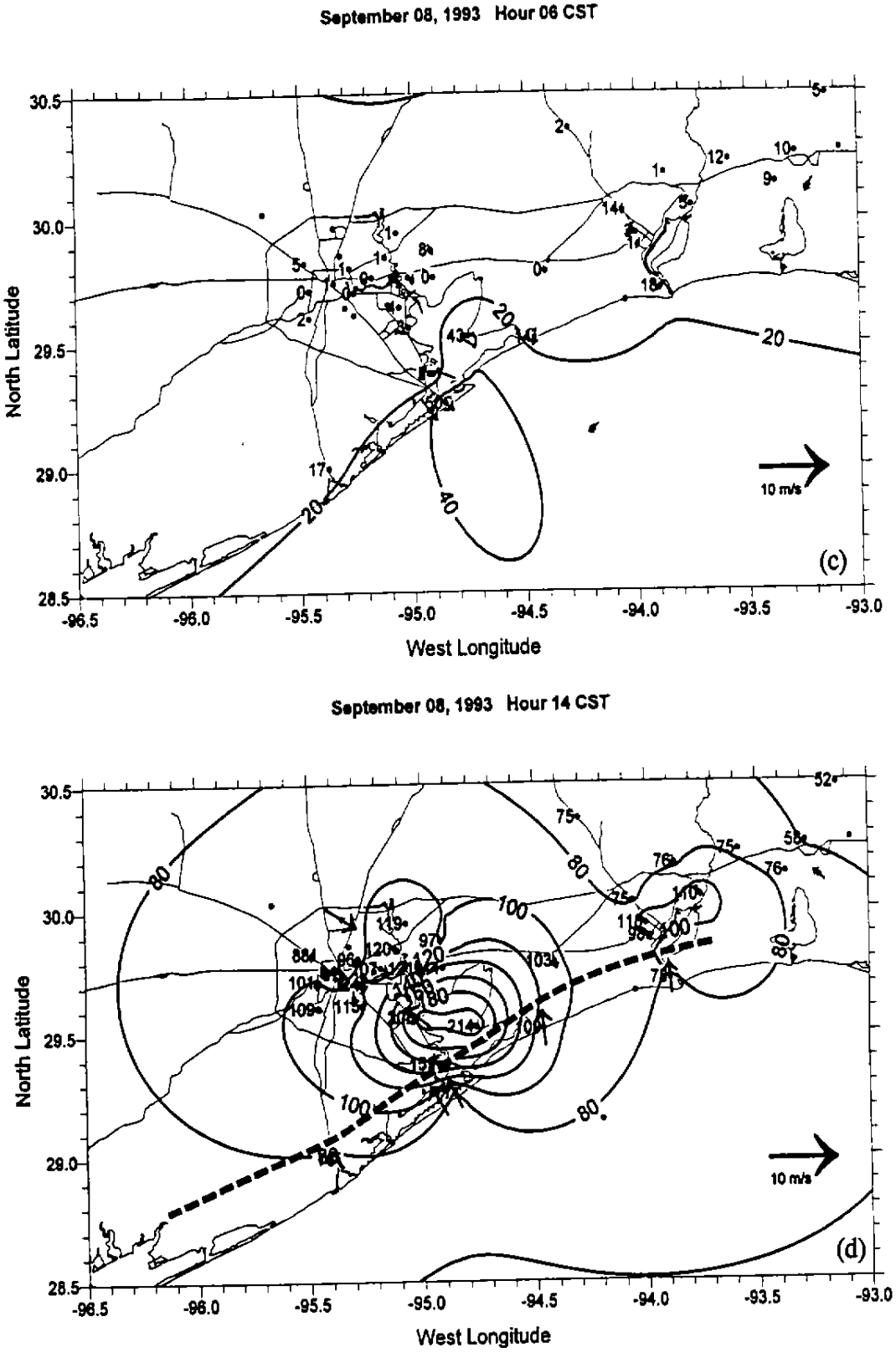

FIGURE 3-57. Plots of surface winds and ozone concentrations in the southeast Texas region at (c) 0600 CST and (d) 1400 CST on 8 September 1993. Dashed lines indicate the location of the gulf-breeze front.

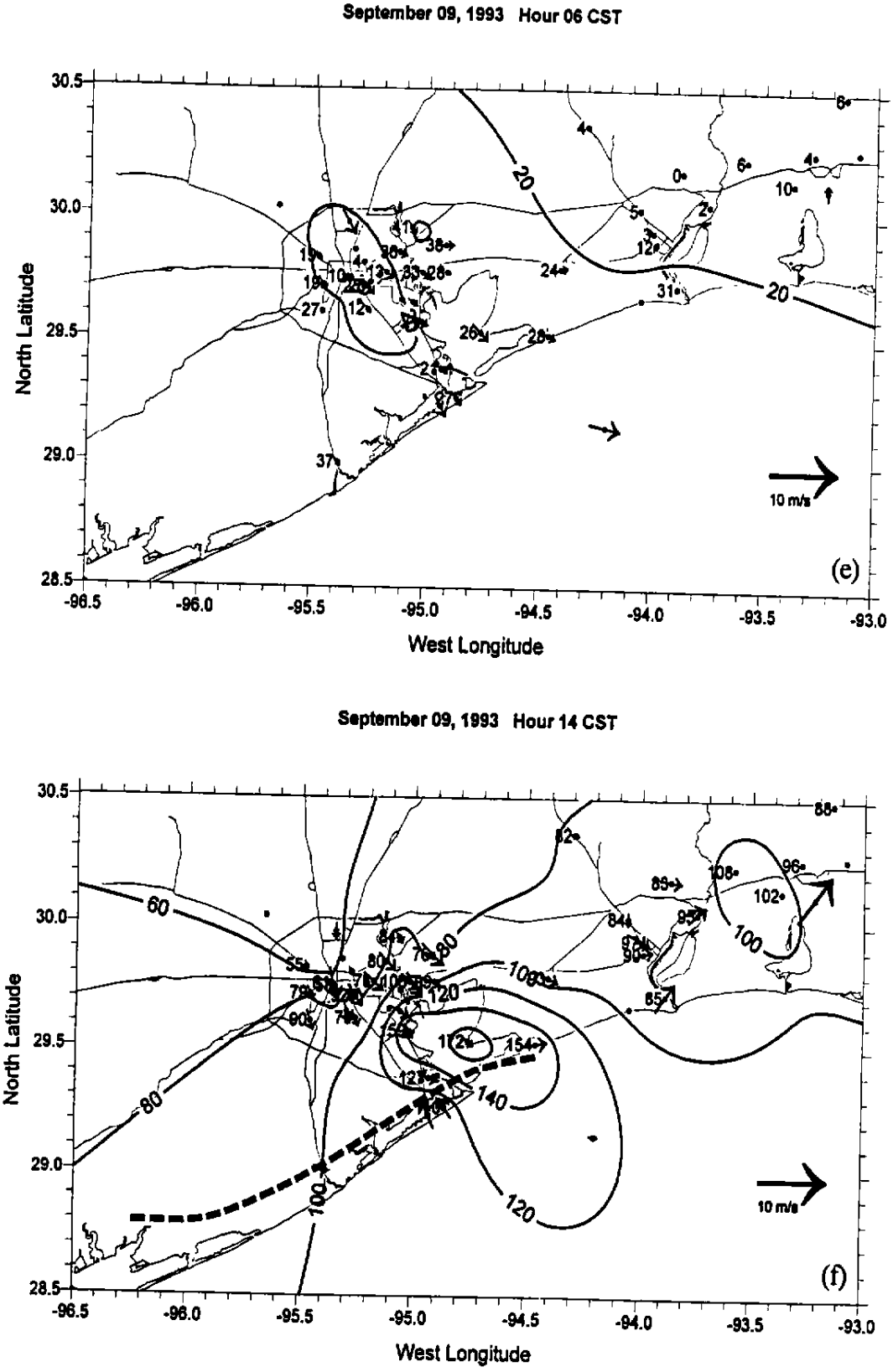

FIGURE 3-57. Plots of surface winds and ozone concentrations in the southeast Texas region at (e) 0600 CST and (f) 1400 CST on 9 September 1993. Dashed lines indicate the location of the gulf-breeze front.

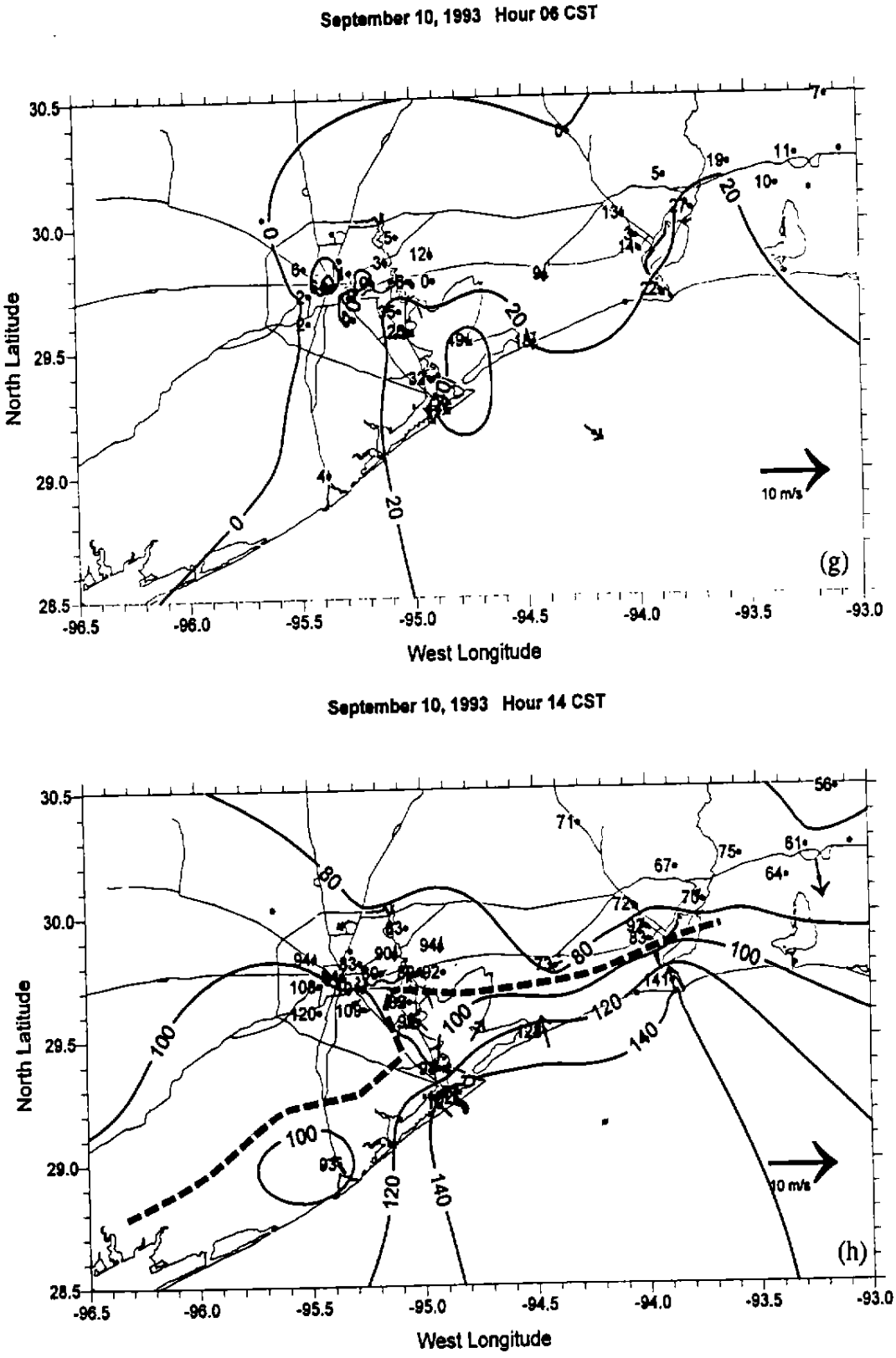

FIGURE 3-57. Plots of surface winds and ozone concentrations in the southeast Texas region at (g) 0600 CST and (h) 1400 CST on 10 September 1993. Dashed lines indicate the location of the gulf-breeze front.

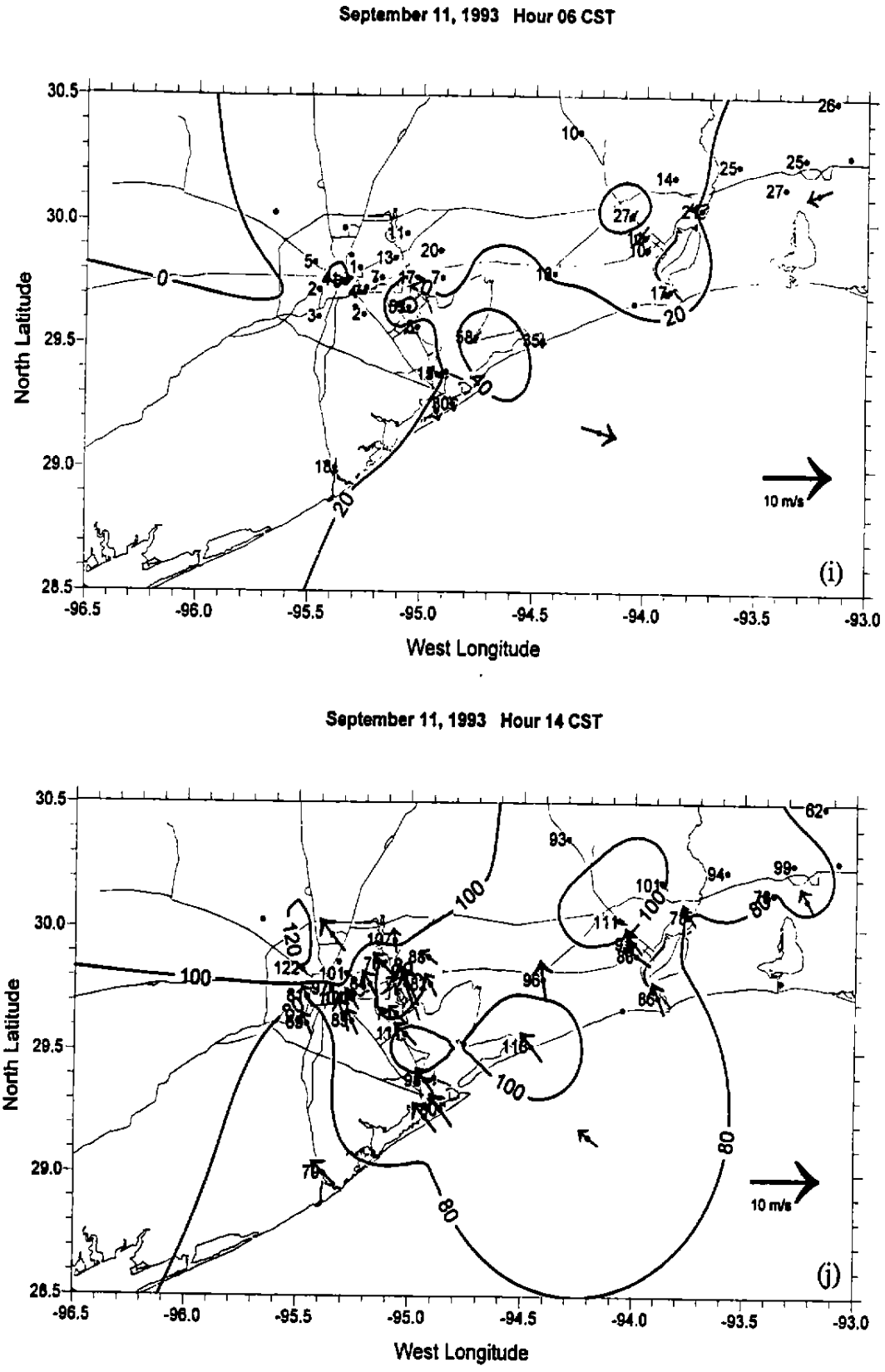

FIGURE 3-57. Plots of surface winds and ozone concentrations in the southeast Texas region at (i) 0600 CST and (j) 1400 CST on 11 September 1993. Dashed lines indicate the location of the gulf-breeze front.

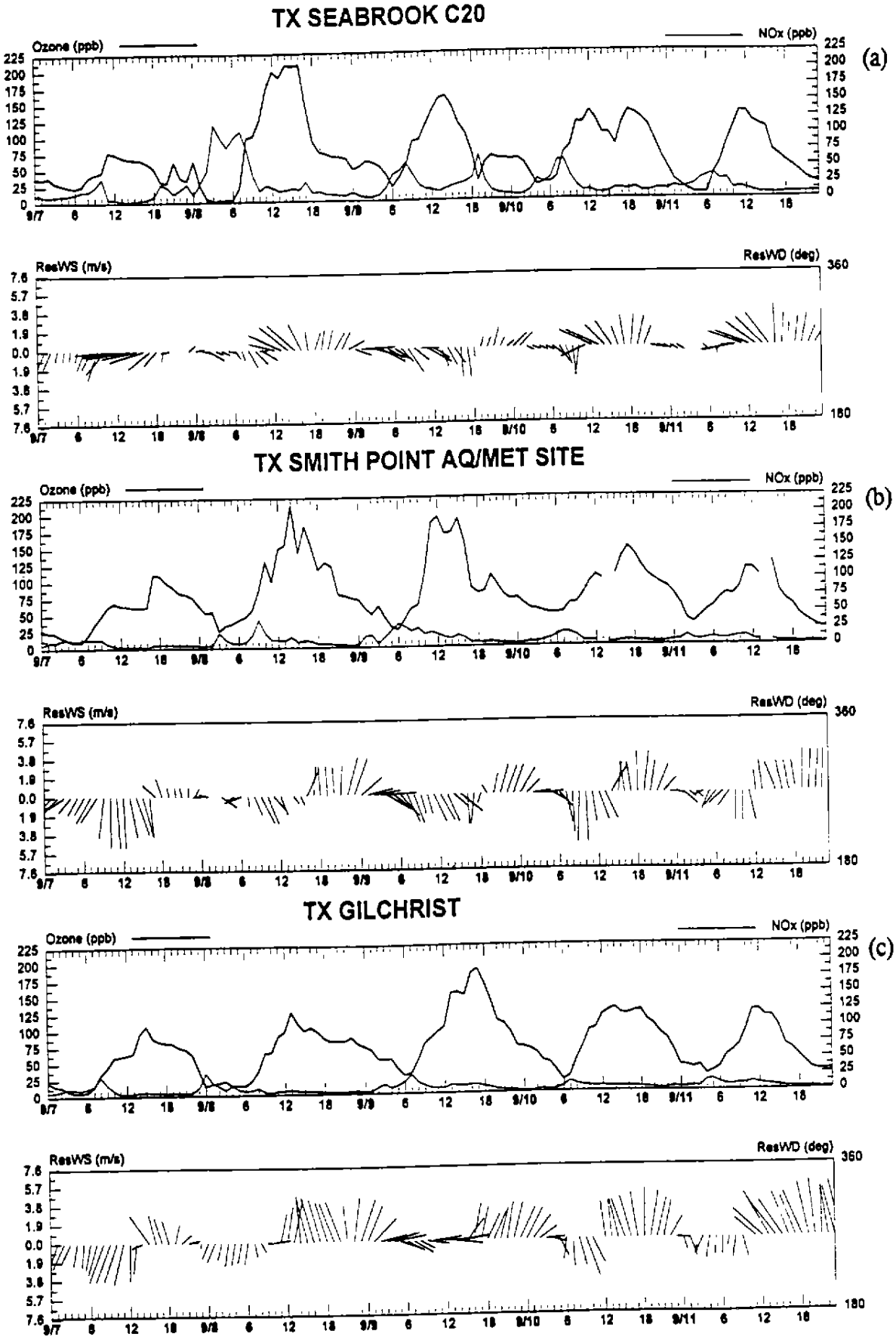

FIGURE 3-58. Time-series plots of ozone concentrations and surface winds at (a) Seabrook, (b) Smith Point, and (c) Gilchrist for the period 8-11 September 1993.

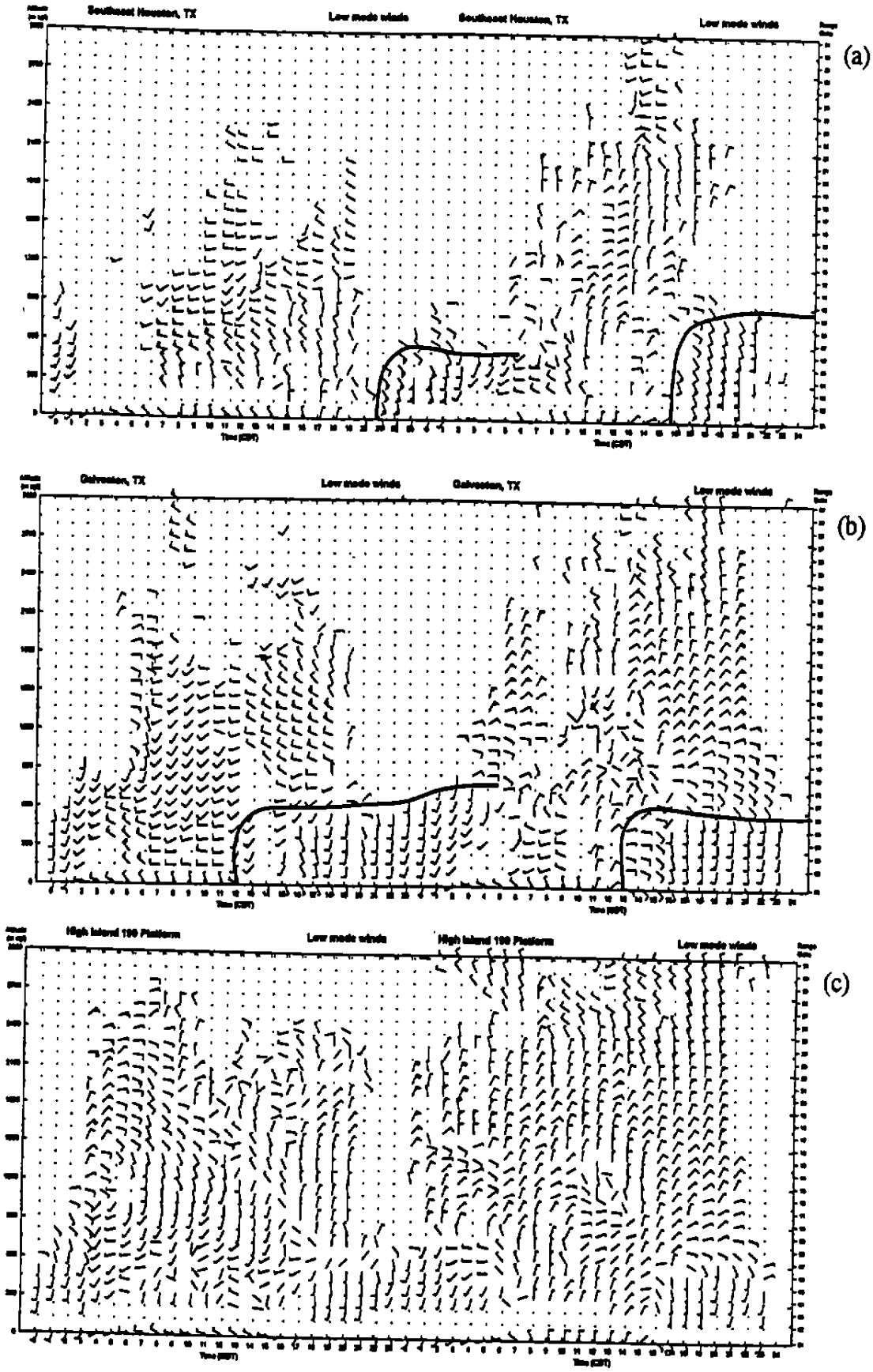

FIGURE 3-59. Time-height cross sections of winds from the (a) Southeast Houston, (b) Galveston, and (c) High Island Platform profilers on 9-10 September 1993. Hourly surface winds are also plotted at 10 m. Solid lines indicate the gulf breeze. Note that missing winds at night were caused by interferences from migrating birds.

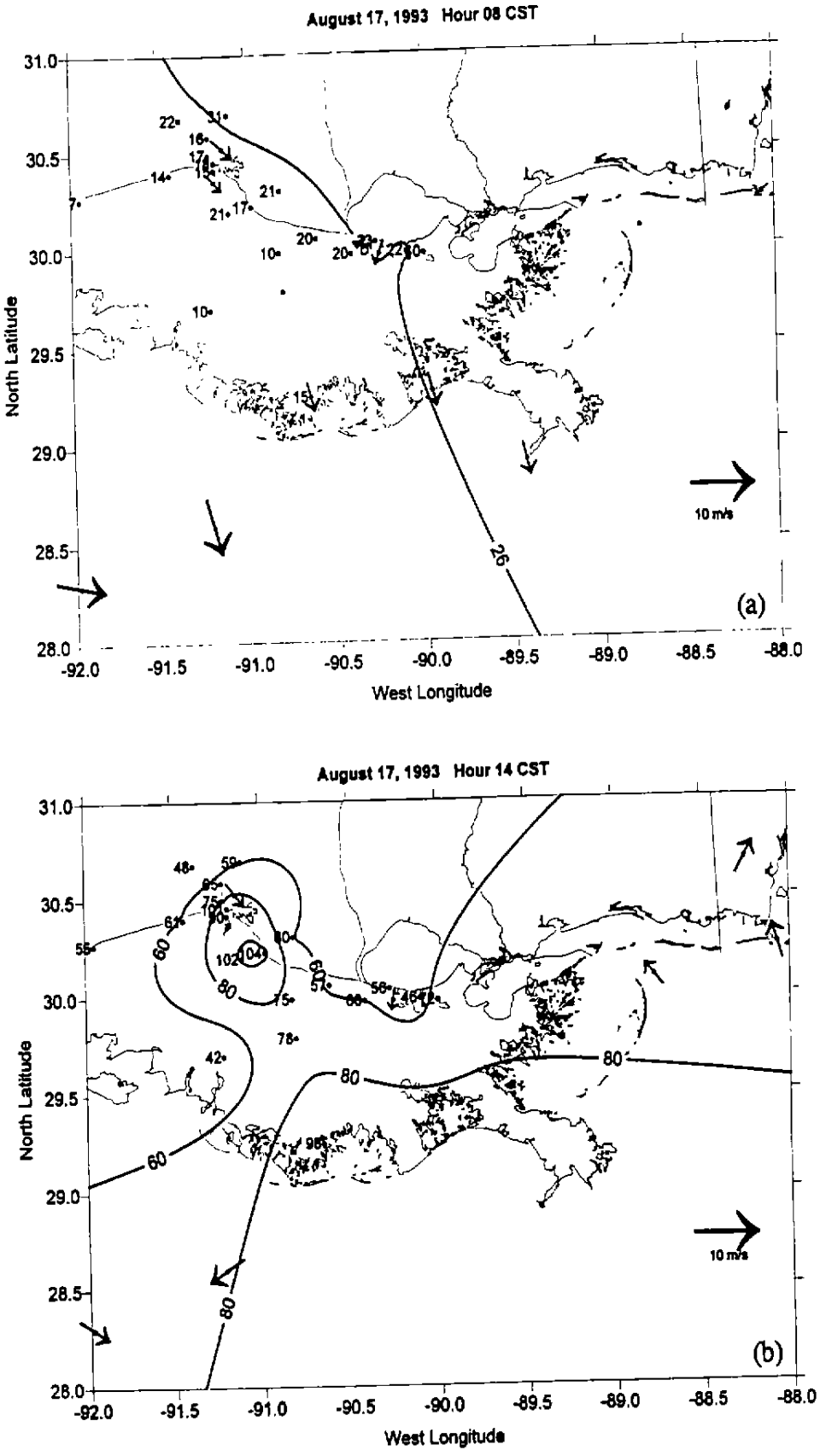

FIGURE 3-60. Surface winds and ozone concentrations at (a) 0800 CST and (b) 1400 CST on 17 August 1993.

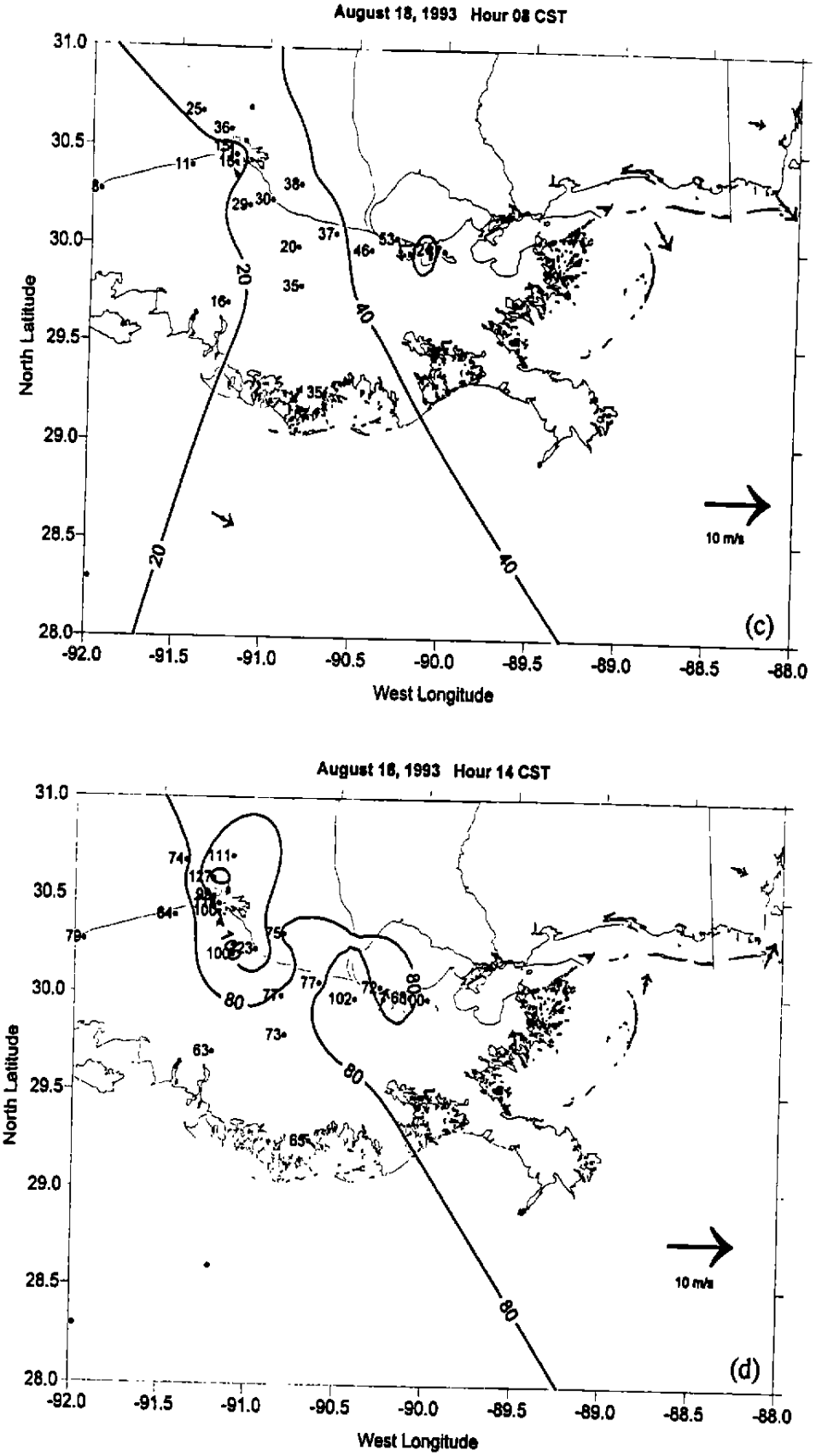

FIGURE 3-60. Surface winds and ozone concentrations at (c) 0800 CST and (d) 1400 CST on 18 August 1993.

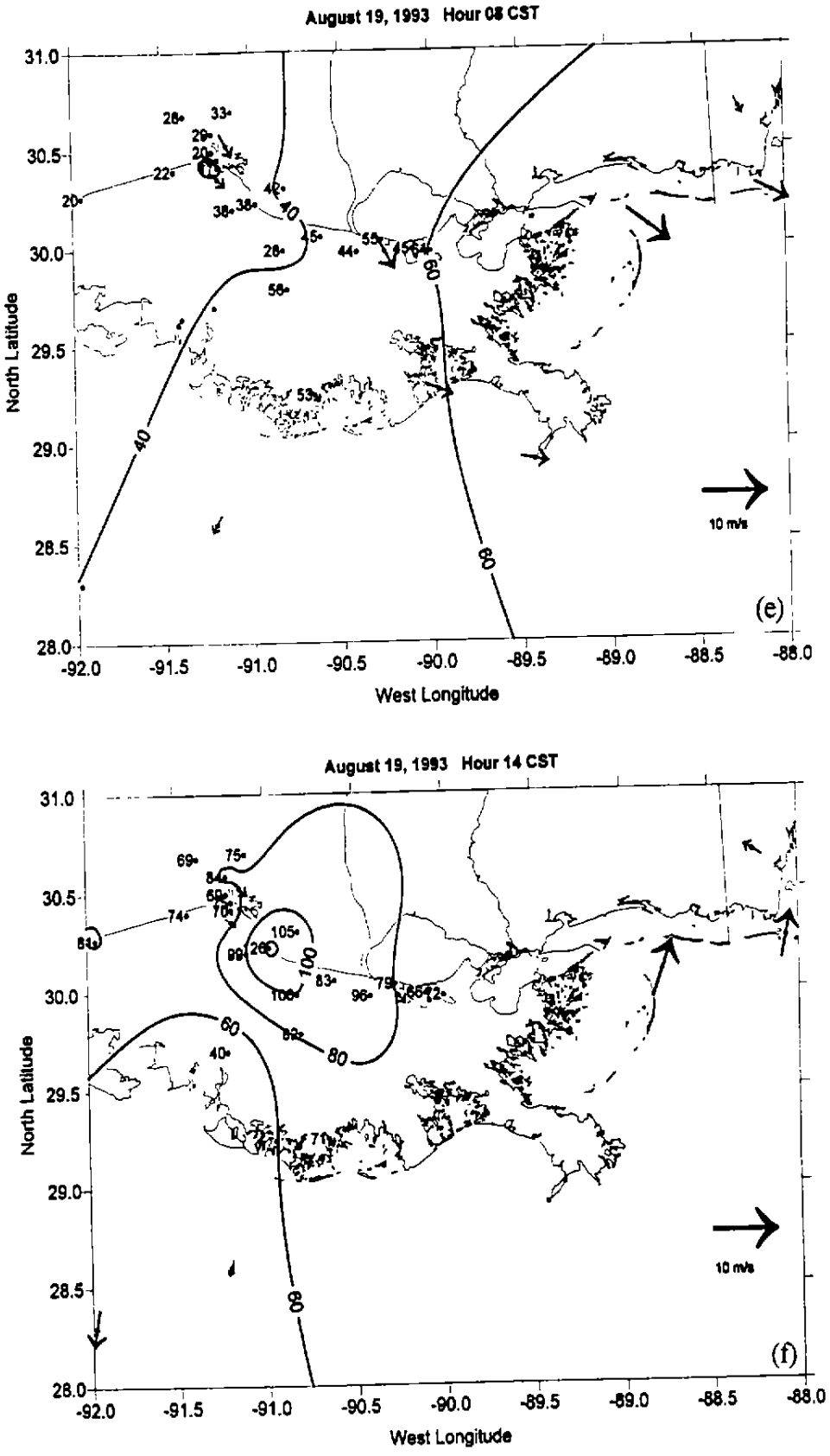

FIGURE 3-60. Surface winds and ozone concentrations at (e) 0800 CST and (f) 1400 CST on 19 August 1993.

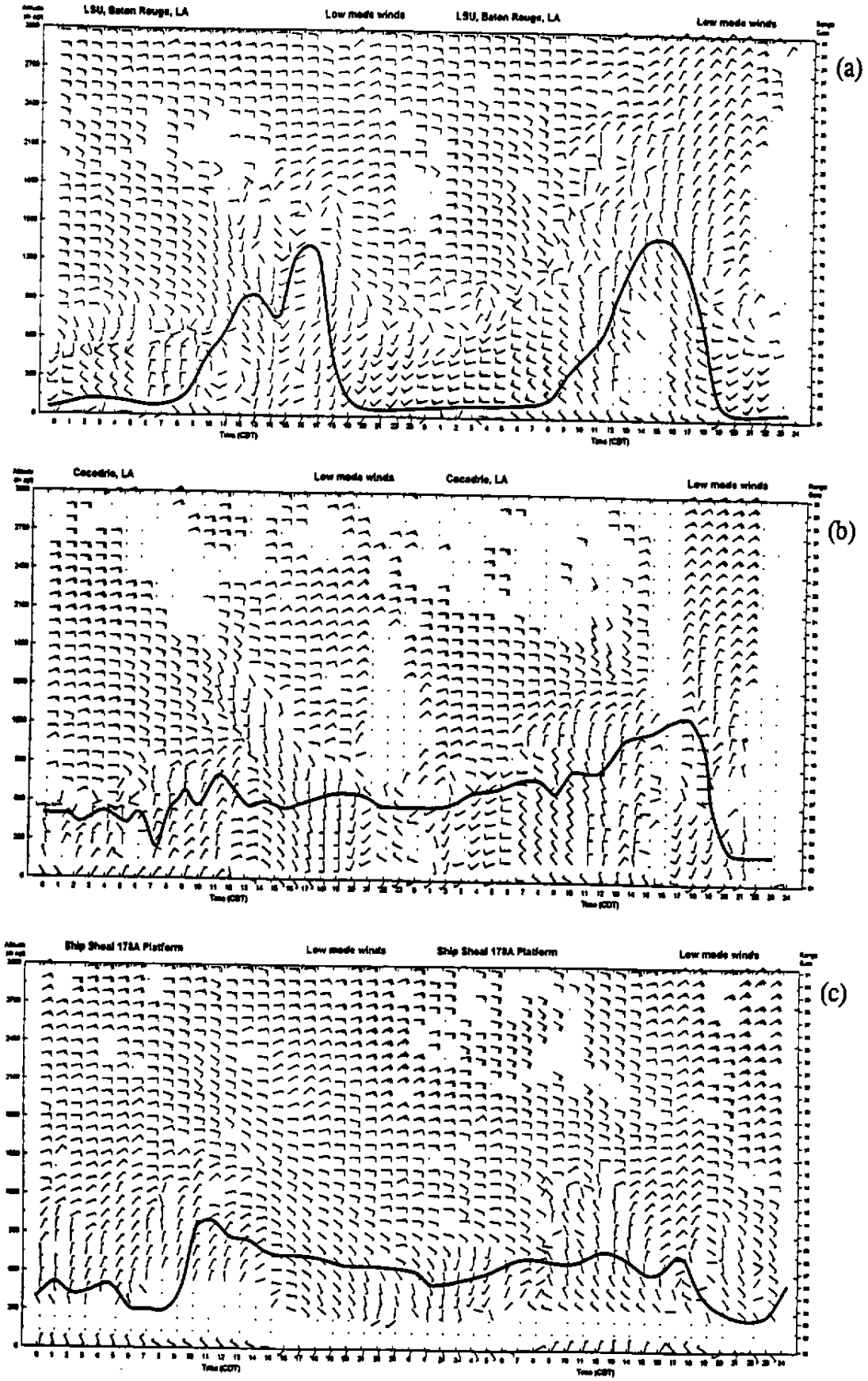

FIGURE 3-61. Aloft winds from the radar profiler sites in (a) Baton Rouge, Louisiana, (b) Cocodrie, Louisiana, and (c) Ship Shoal Platform in the Gulf of Mexico on 18-19 August 1993. Surface winds are plotted at 10 m agl. The solid line denotes the mixed layer depth estimated from radar profiler-based data.

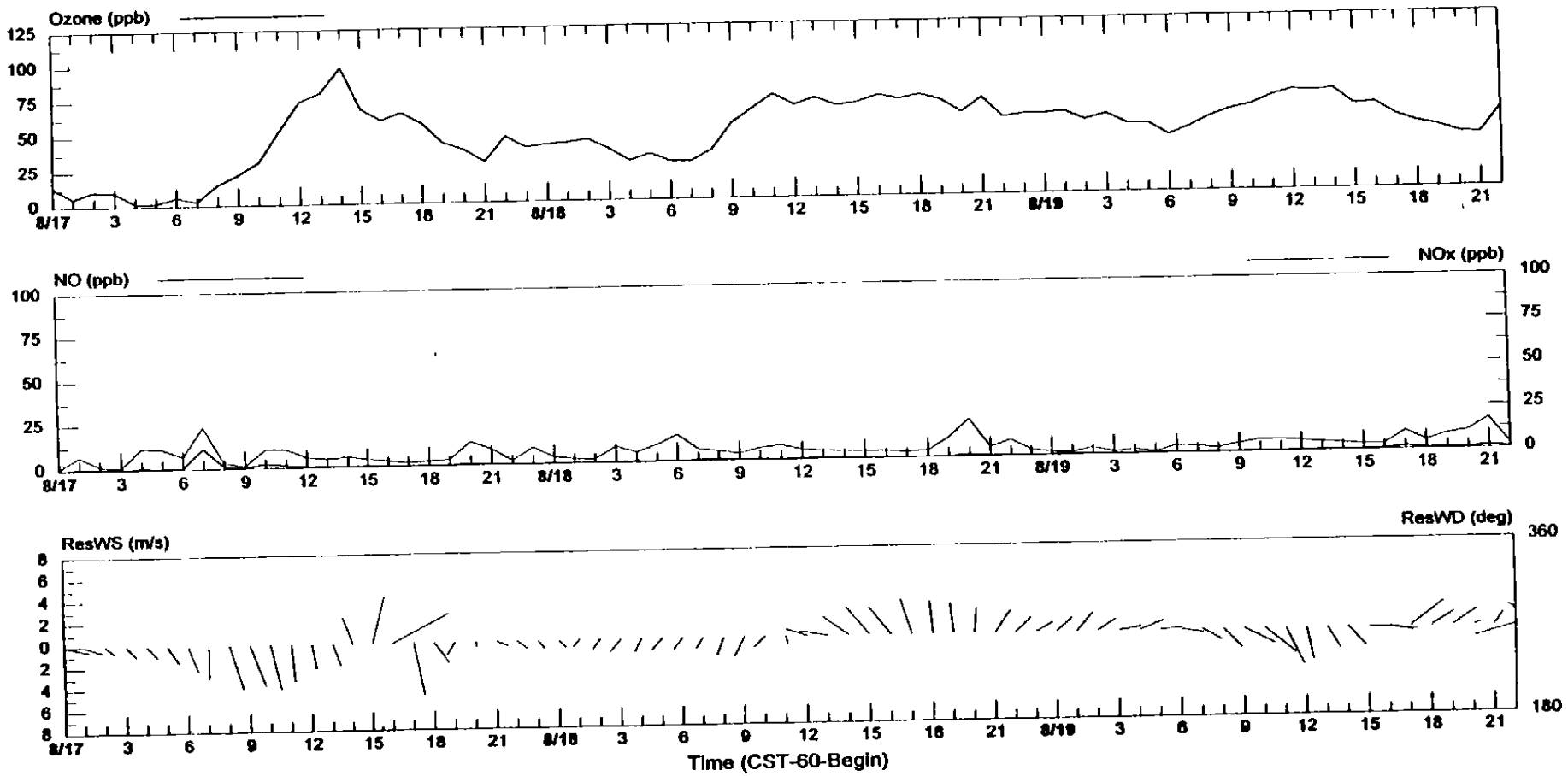

Station Code: COC
Elevation (m): 0

File Name: COCAUG.CDF
Date Plotted: 3/8/95 15:17

FIGURE 3-62. Surface ozone, NO, and NO_x concentrations and winds measured at the Cocodrie site for the period 17–19 August 1993.

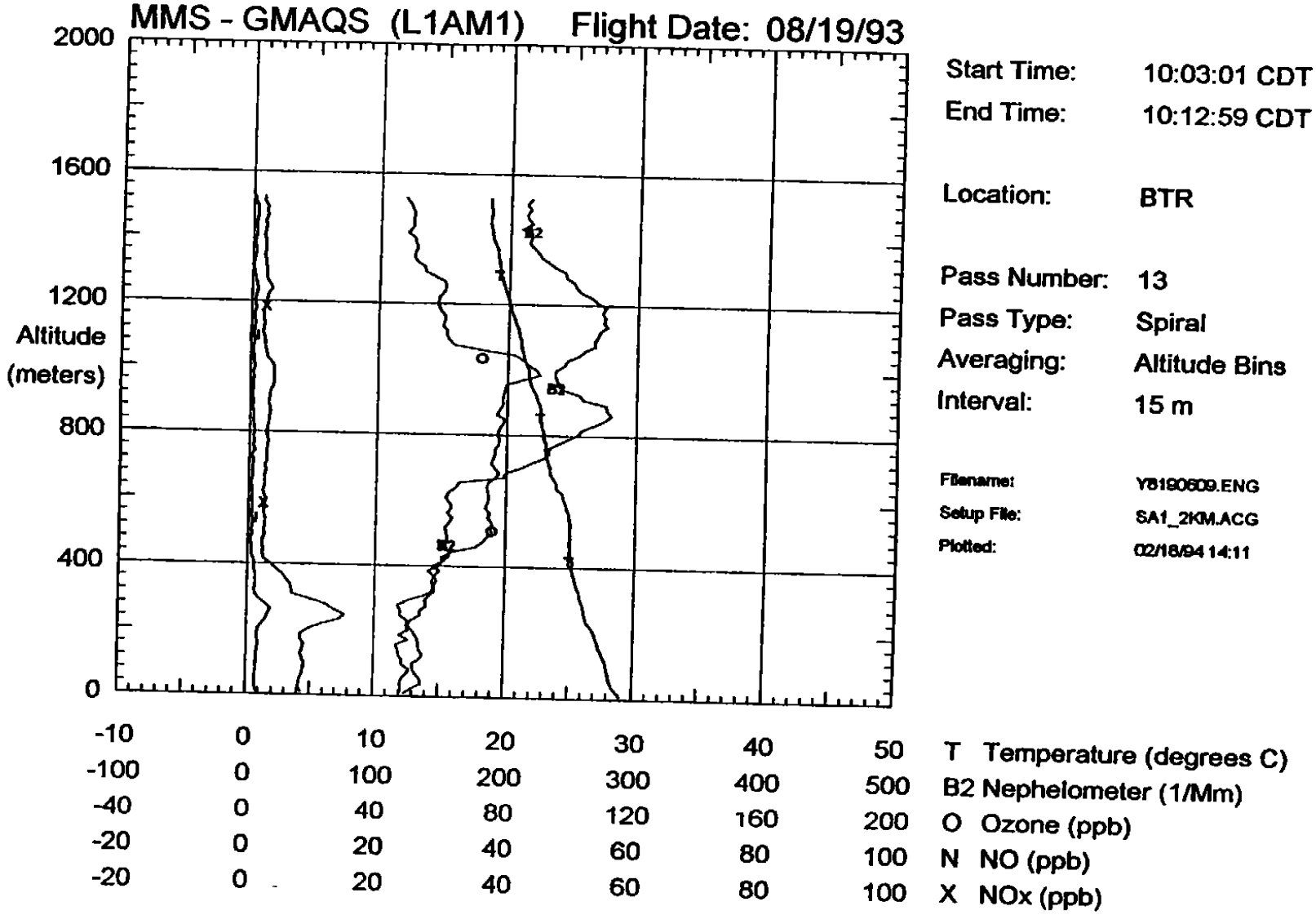

FIGURE 3-63. Ozone, NO, and NO_x concentrations and temperature measured during a descending aircraft spiral over Baton Rouge at 1010 CDT on 19 August 1993.

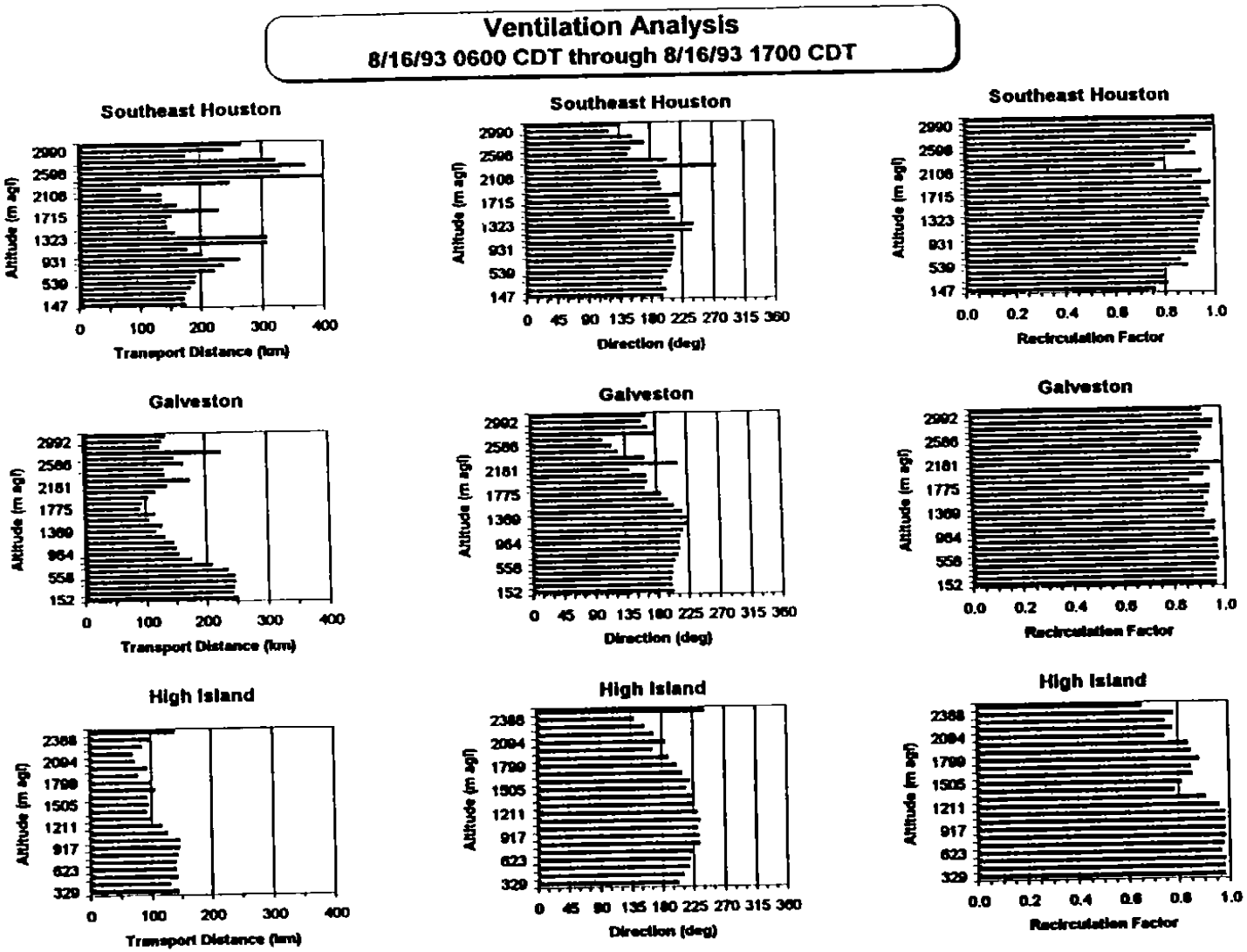

FIGURE 3-64. Vector-integrated transport distances, resultant wind directions, and recirculation factors, calculated from data collected by the Southeast Houston (SEH), Galveston (GAL), and High Island Platform (HIP) radar profilers for the period 0600–1700 CDT on 16 August 1993.

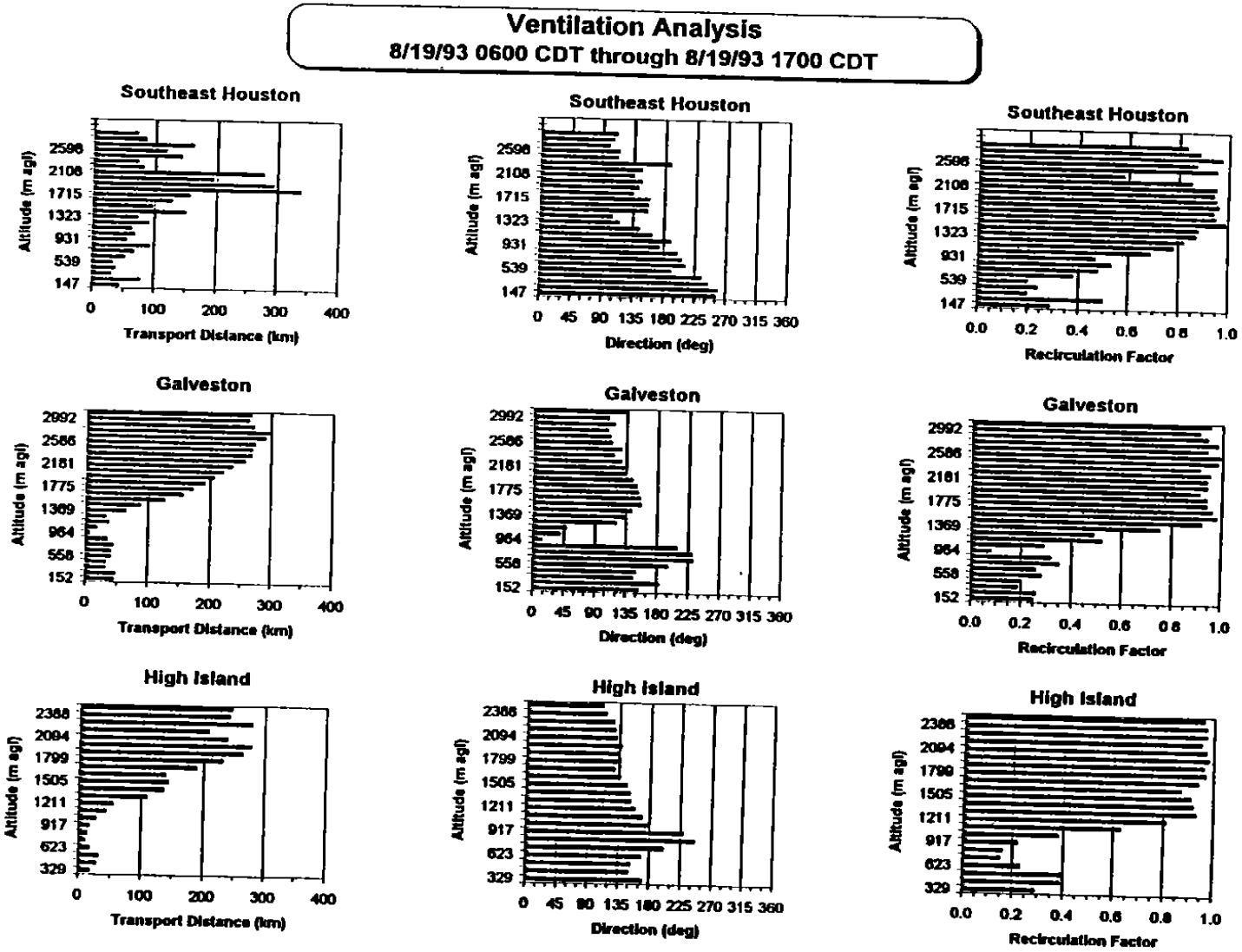

FIGURE 3-65. Vector-integrated transport distances, resultant wind directions, and recirculation factors, calculated from data collected by the Southeast Houston (SEH), Galveston (GAL), and High Island Platform (HIP) radar profilers for the period 0600-1700 CDT on 19 August 1993.

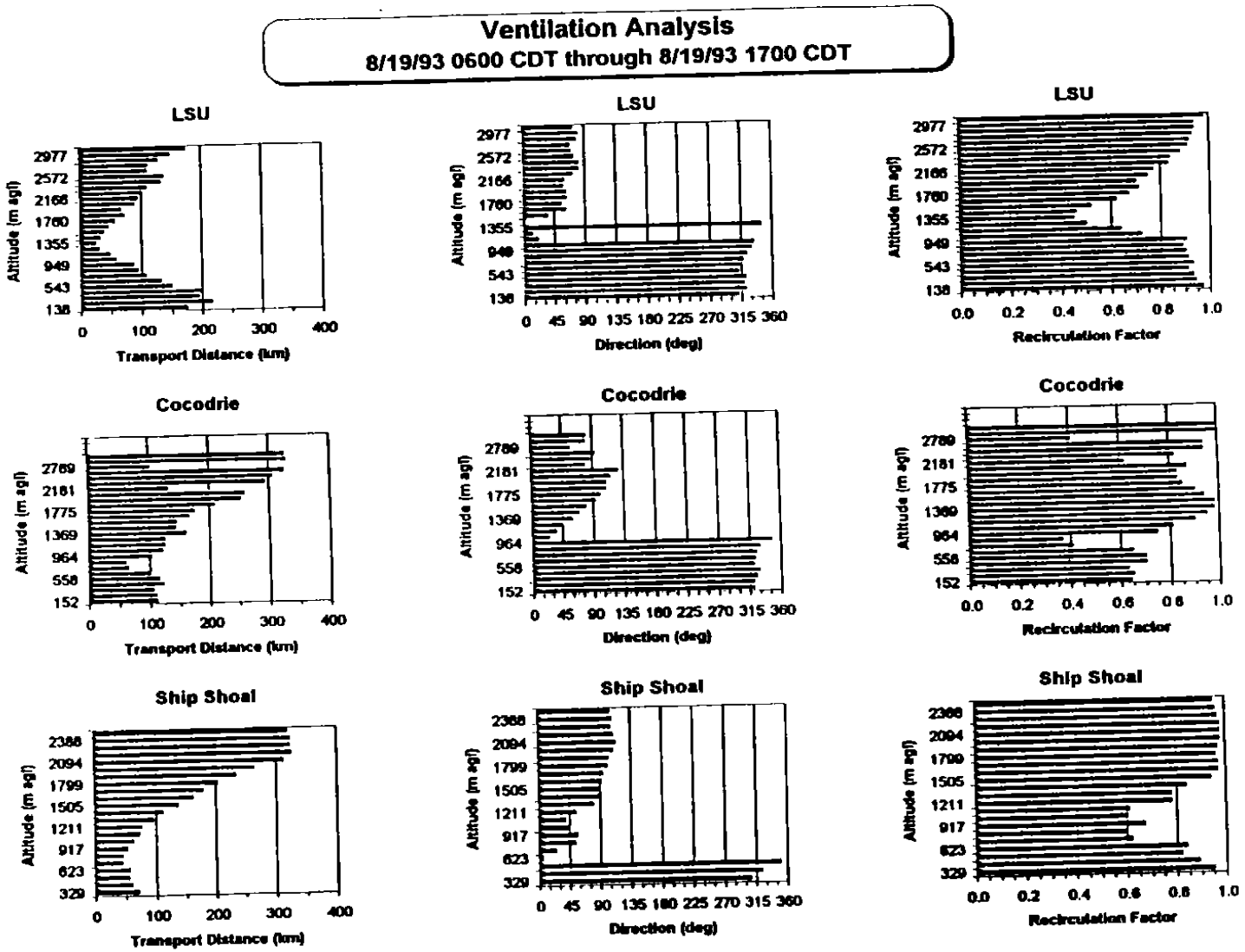

FIGURE 3-66. Vector-integrated transport distances, resultant wind directions, and recirculation factors, calculated from data collected by the LSU, Cocodrie (COC), and Ship Shoal Platform (SSP) radar profilers for the period 0600–1700 CDT on 19 August 1993.

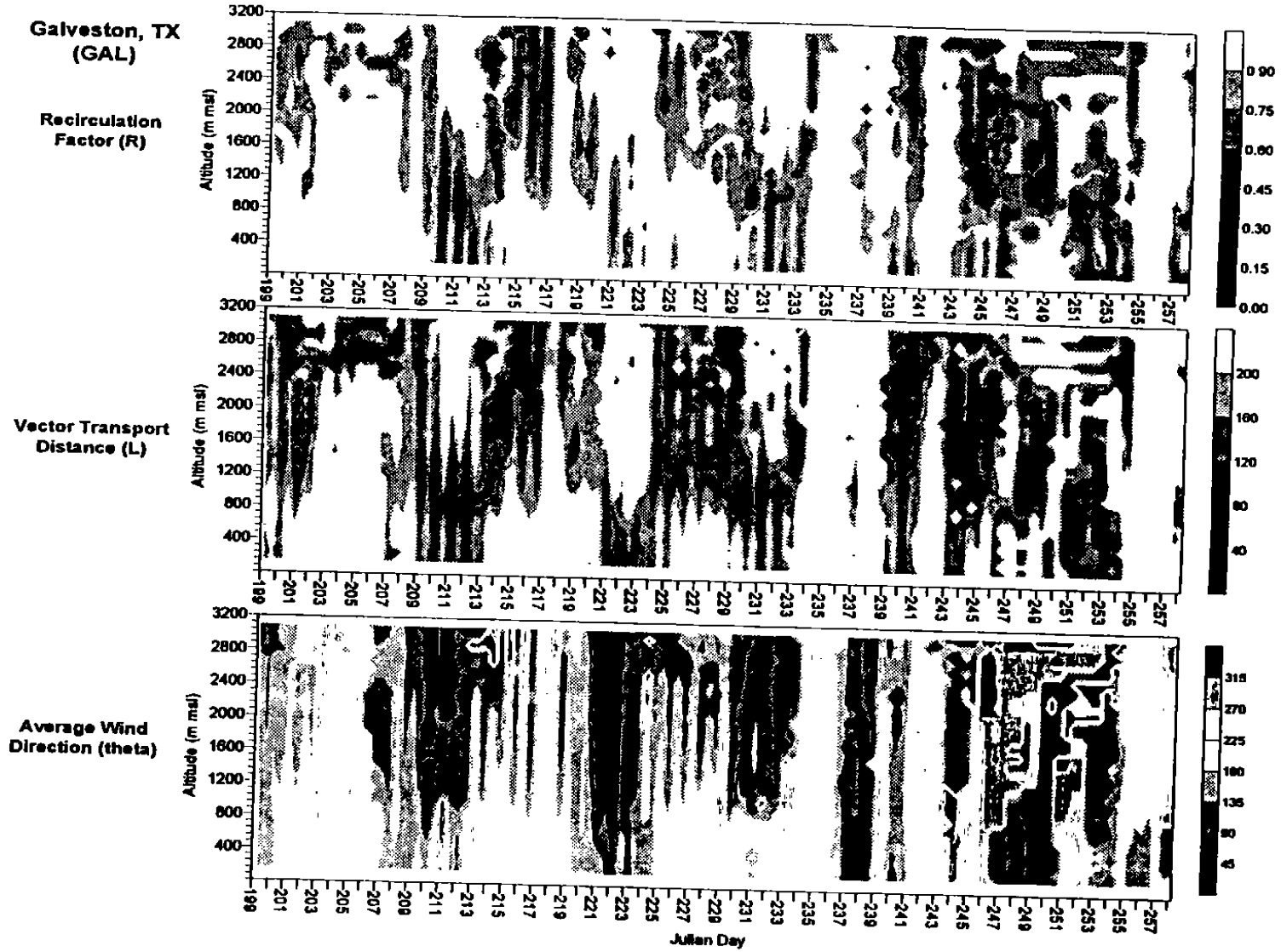

FIGURE 3-67. Time-height cross section of recirculation factor, vector-integrated transport distance, and resultant wind directions calculated from data collected at the Galveston (GAL) radar profiler for the period July 18–15 September 1993; the integration period was 12 hours in duration, 0600–1700 CDT and 1800–0500 CDT each day.

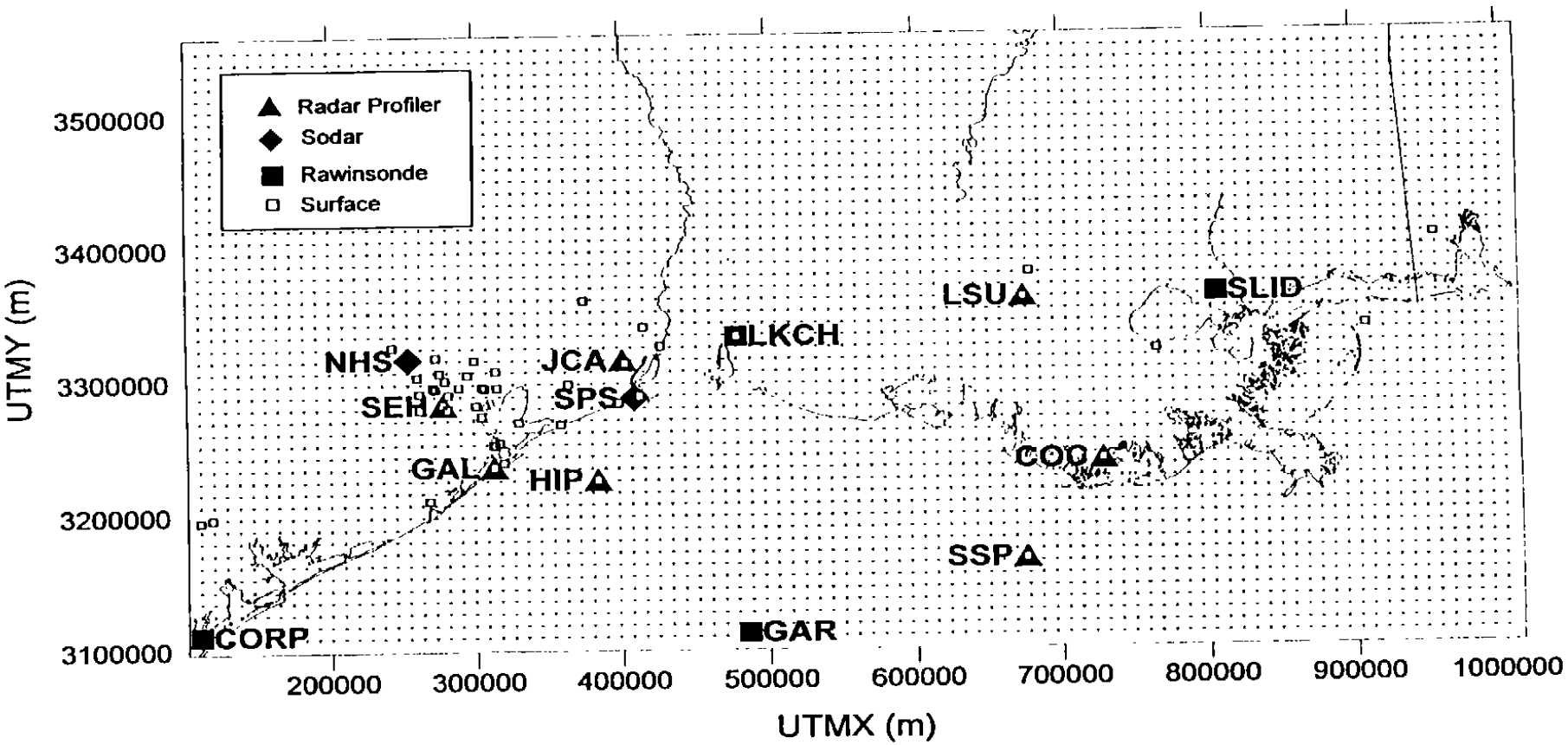

FIGURE 3-68. Map showing the modeling domain used by the surface and aloft wind fields, as well as the trajectory generation program (See Appendix K for site names and UTM coordinates). Dots are cell corners.

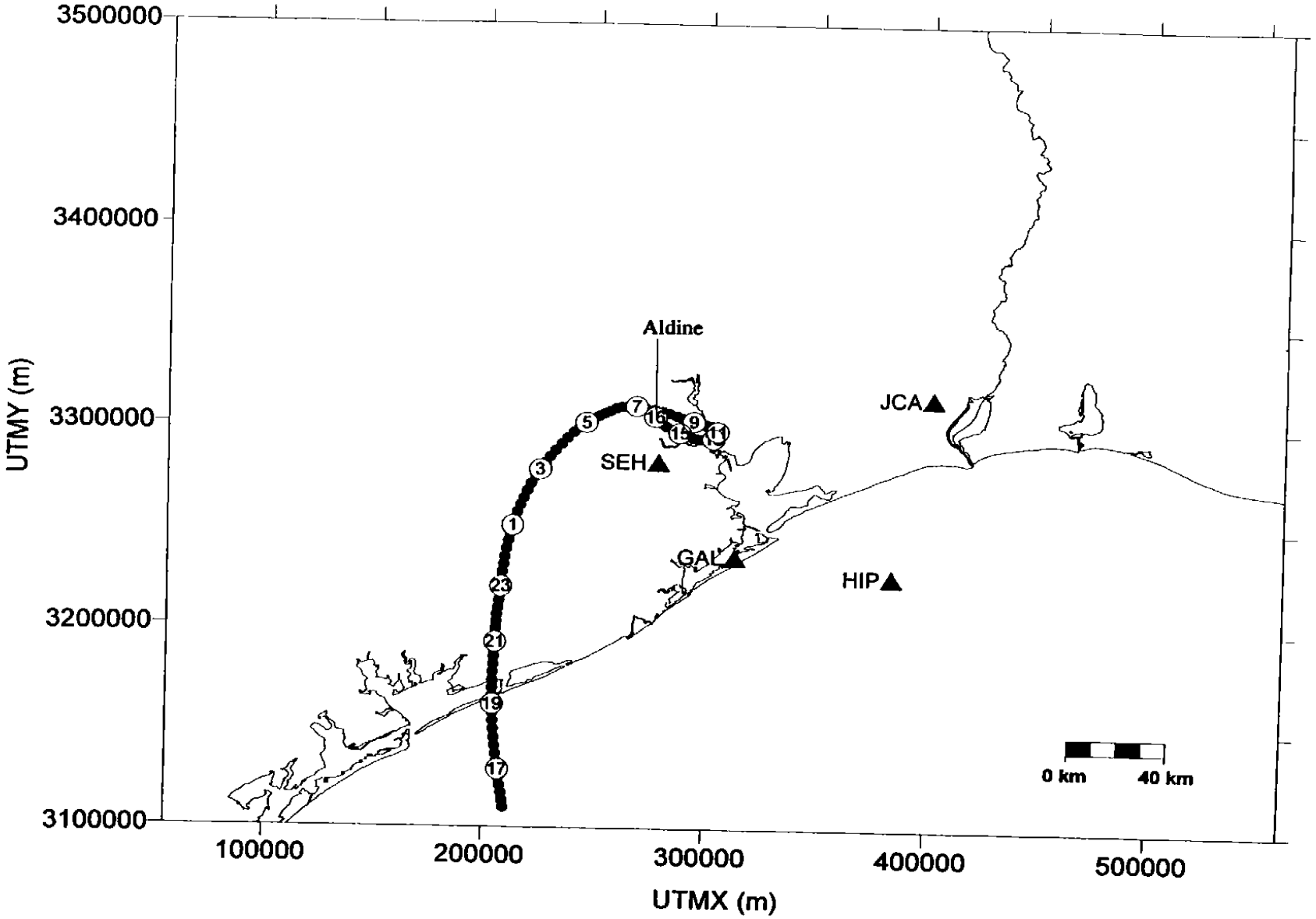

FIGURE 3-69. 300-m backward trajectory starting from Aldine, Texas, at 1600 CST on 19 August 1993.

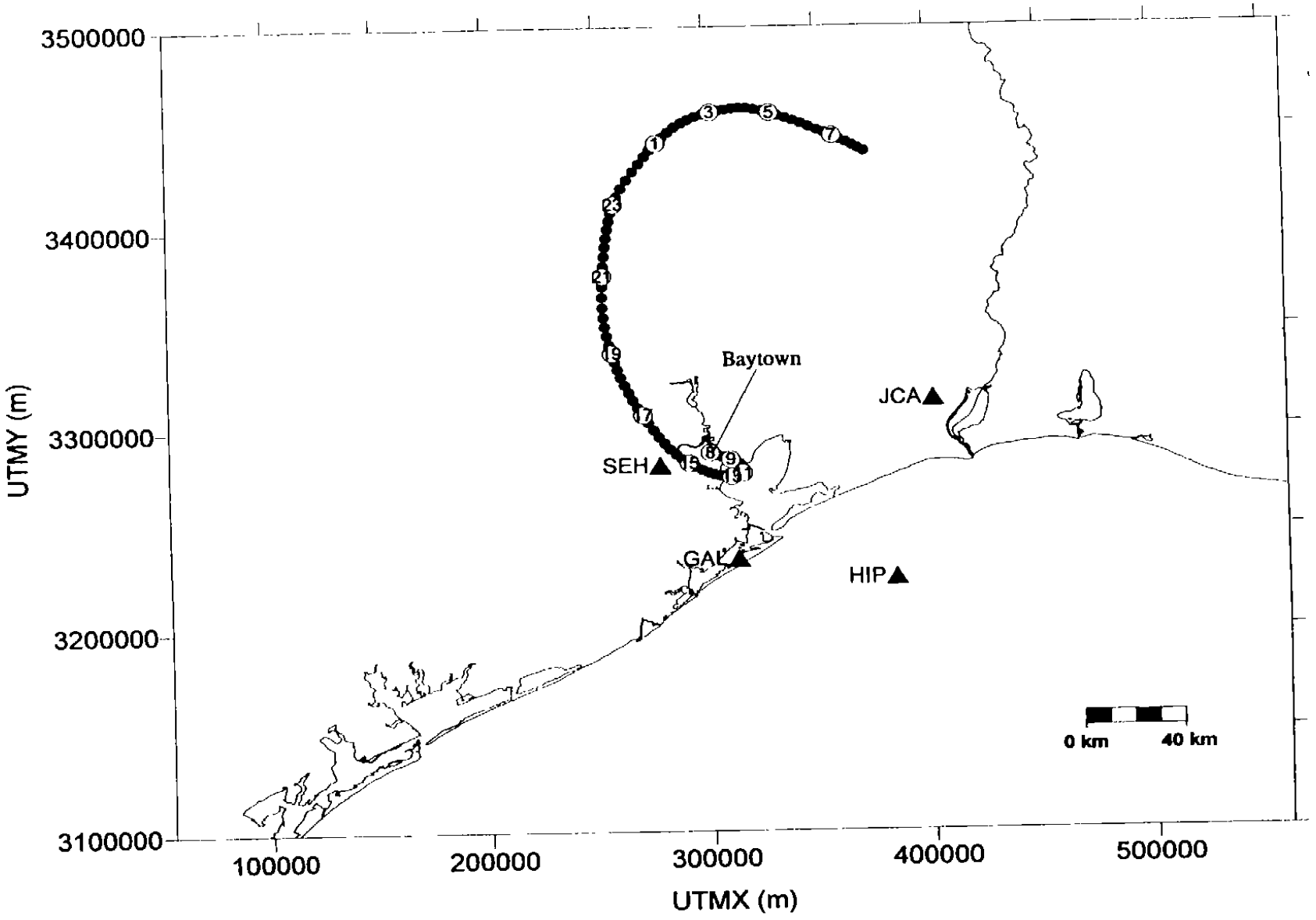

FIGURE 3-70. 300-m forward trajectory starting from Baytown, Texas, at 0800 CST on 19 August 1993.

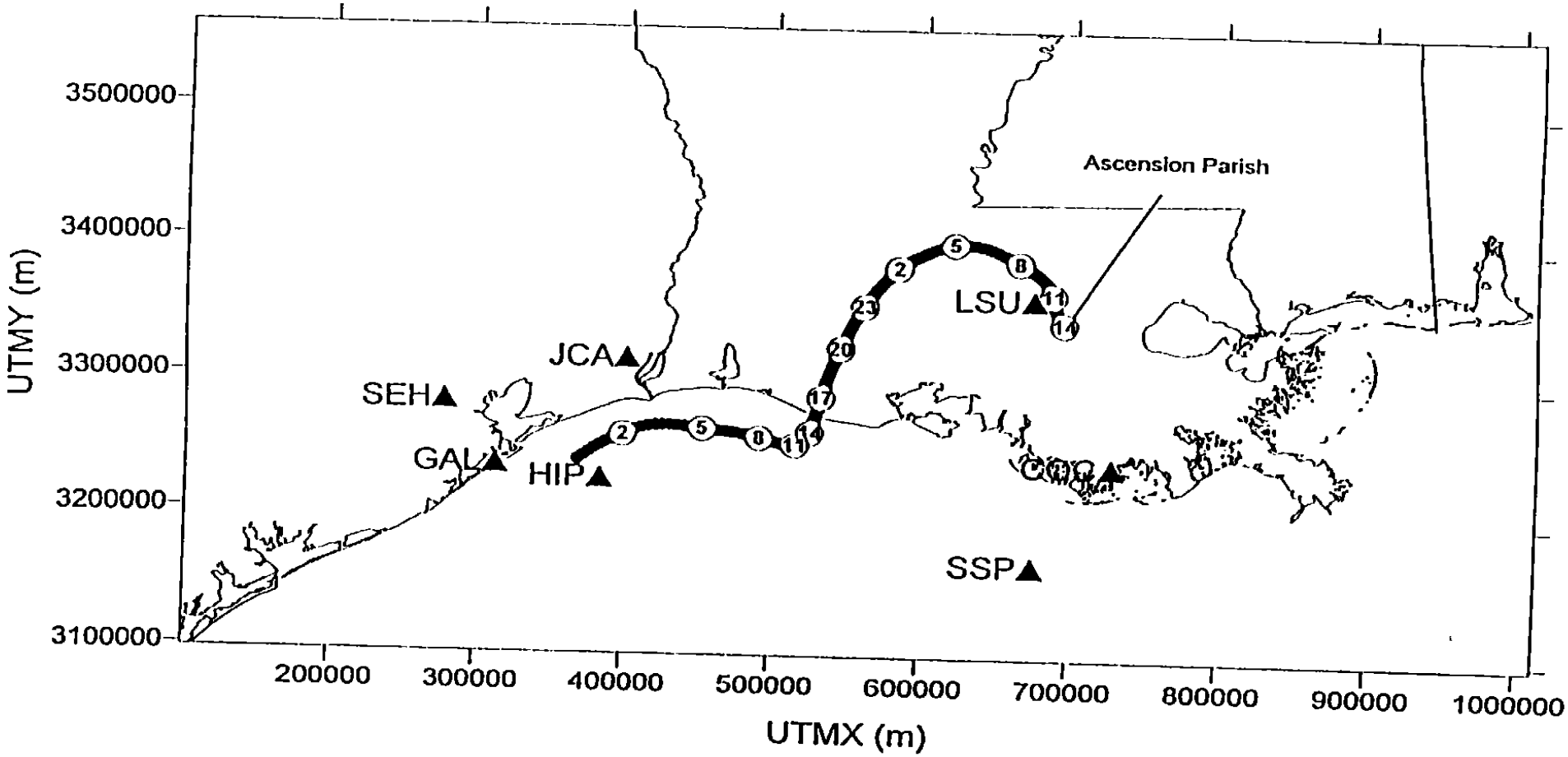

FIGURE 3-71. 300-m backward trajectory starting from Ascension Parish, Louisiana, at 1400 CST on 19 August 1993.

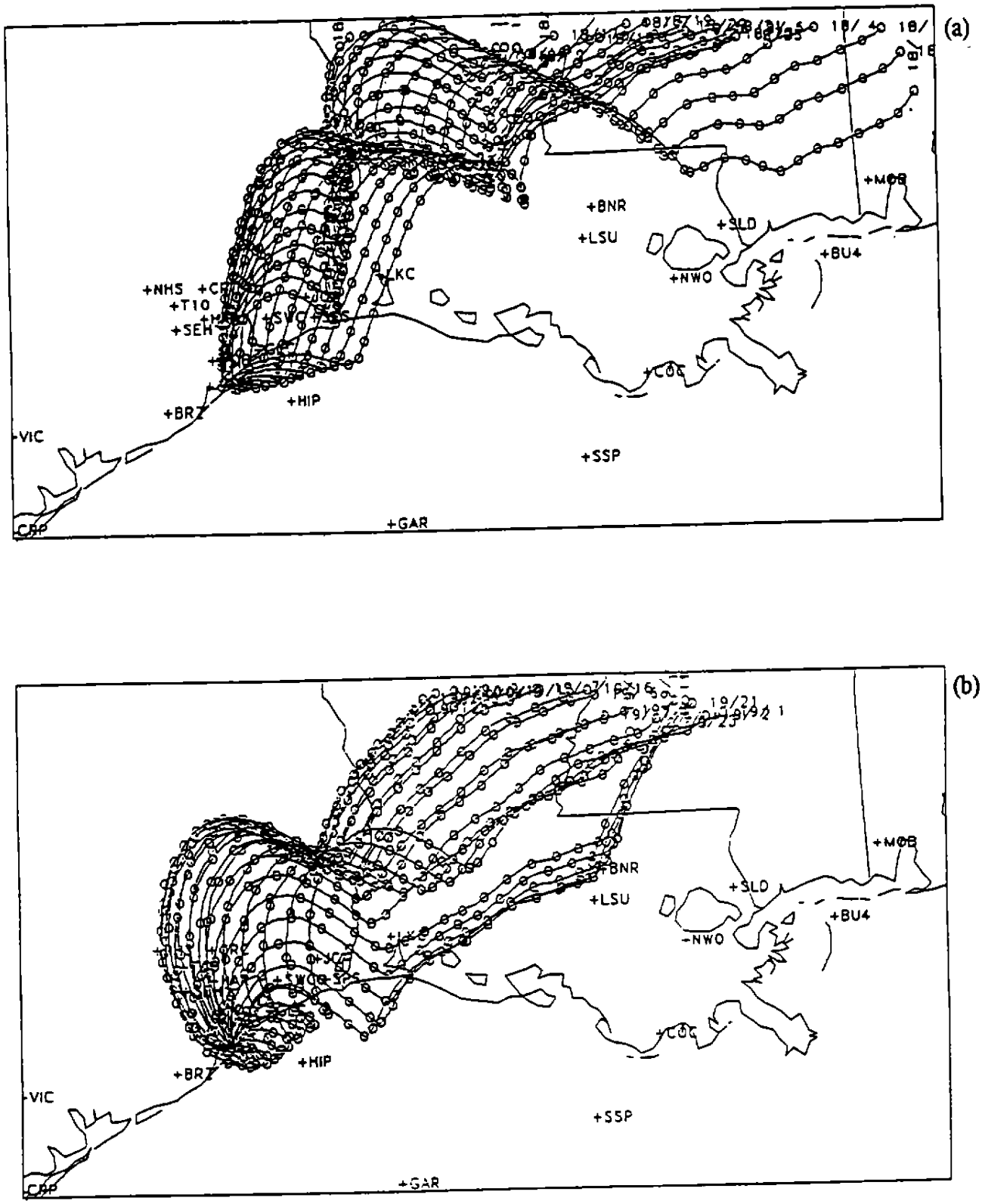

FIGURE 3-72. 300-m forward trajectories from Galveston, Texas at all hours on (a) 18 August and (b) 19 August 1993.

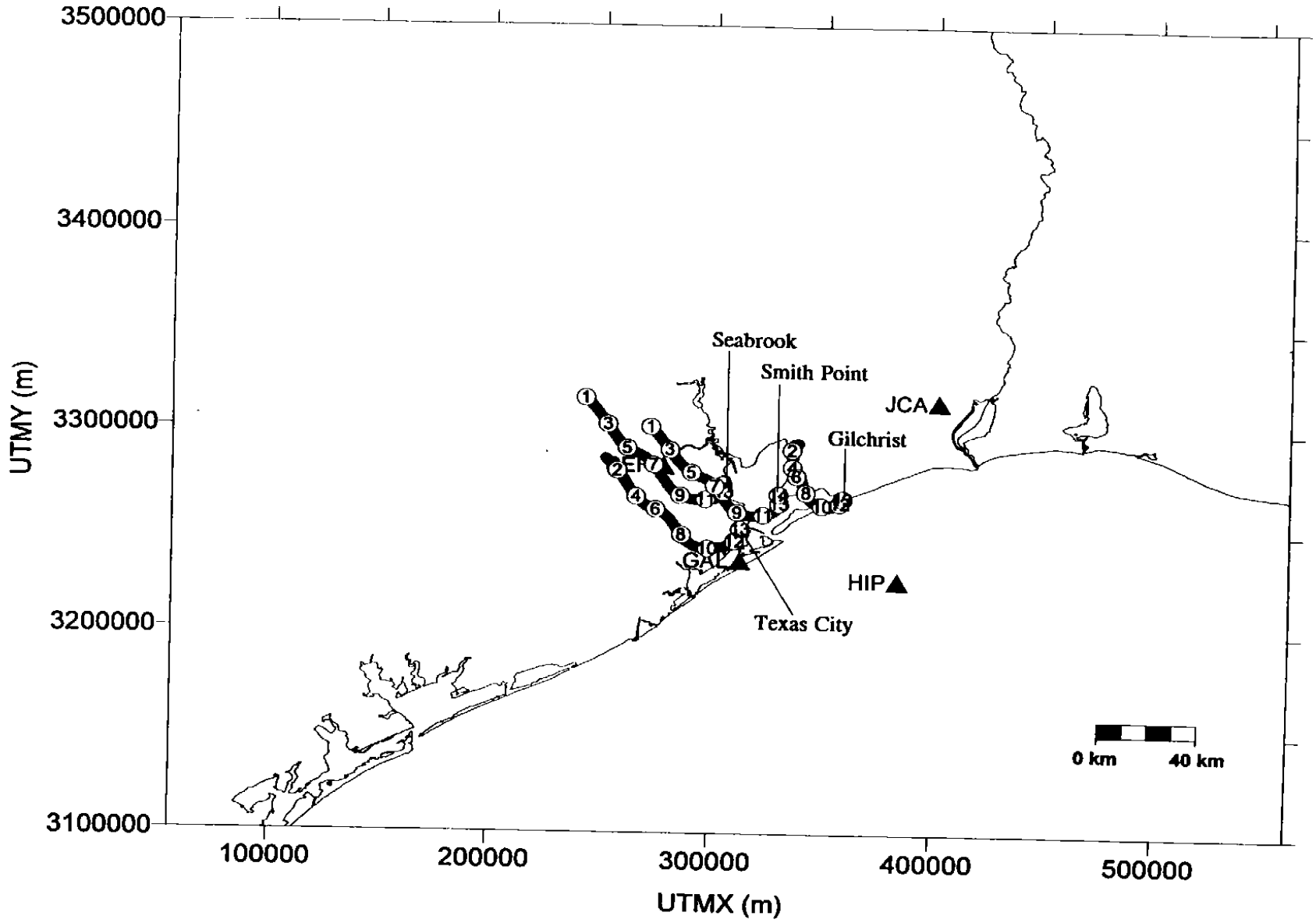

FIGURE 3-73. 100-m backward trajectories from Gilchrist at 1300 CST, Texas City at 1300 CST, Seabrook at 1400 CST, and Smith Point at 1400 CST, on 8 September 1993.

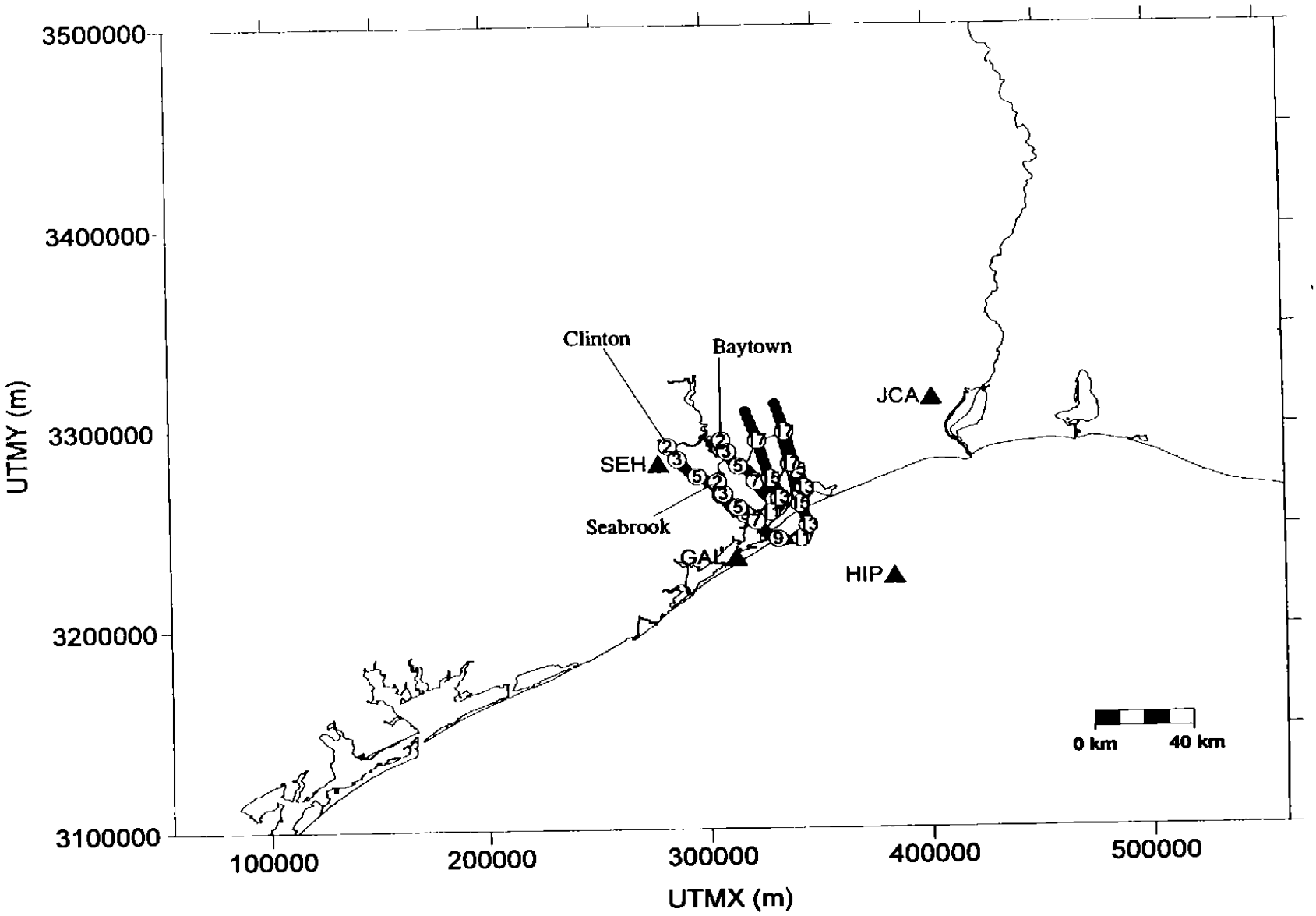

FIGURE 3-74. 100-m forward trajectories from Baytown, Seabrook, and Clinton at 0200 CST, on 8 September 1993.

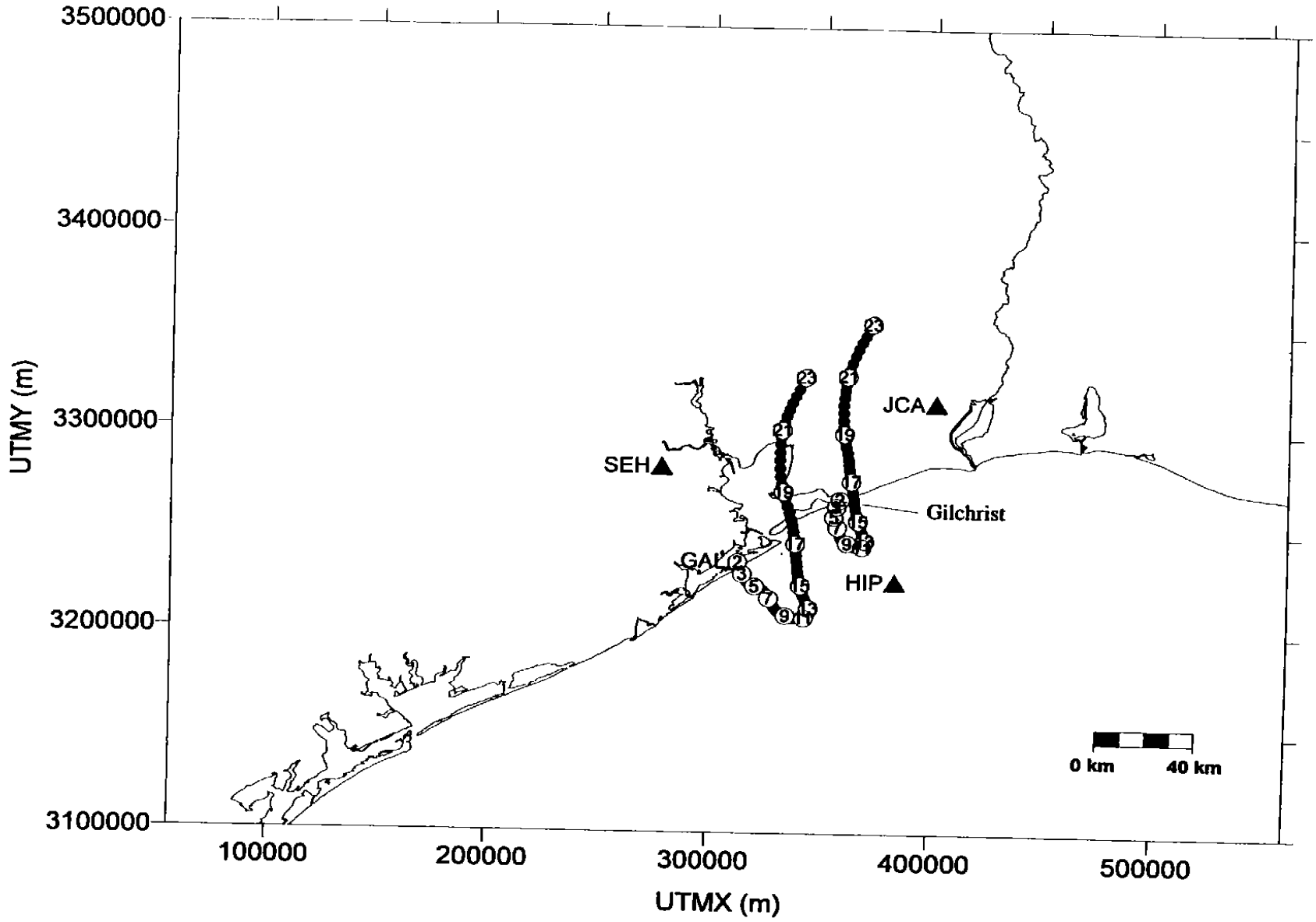

FIGURE 3-75. 100-m forward trajectories from Galveston and Gilchrist at 0200 CST, on 8 September 1993.

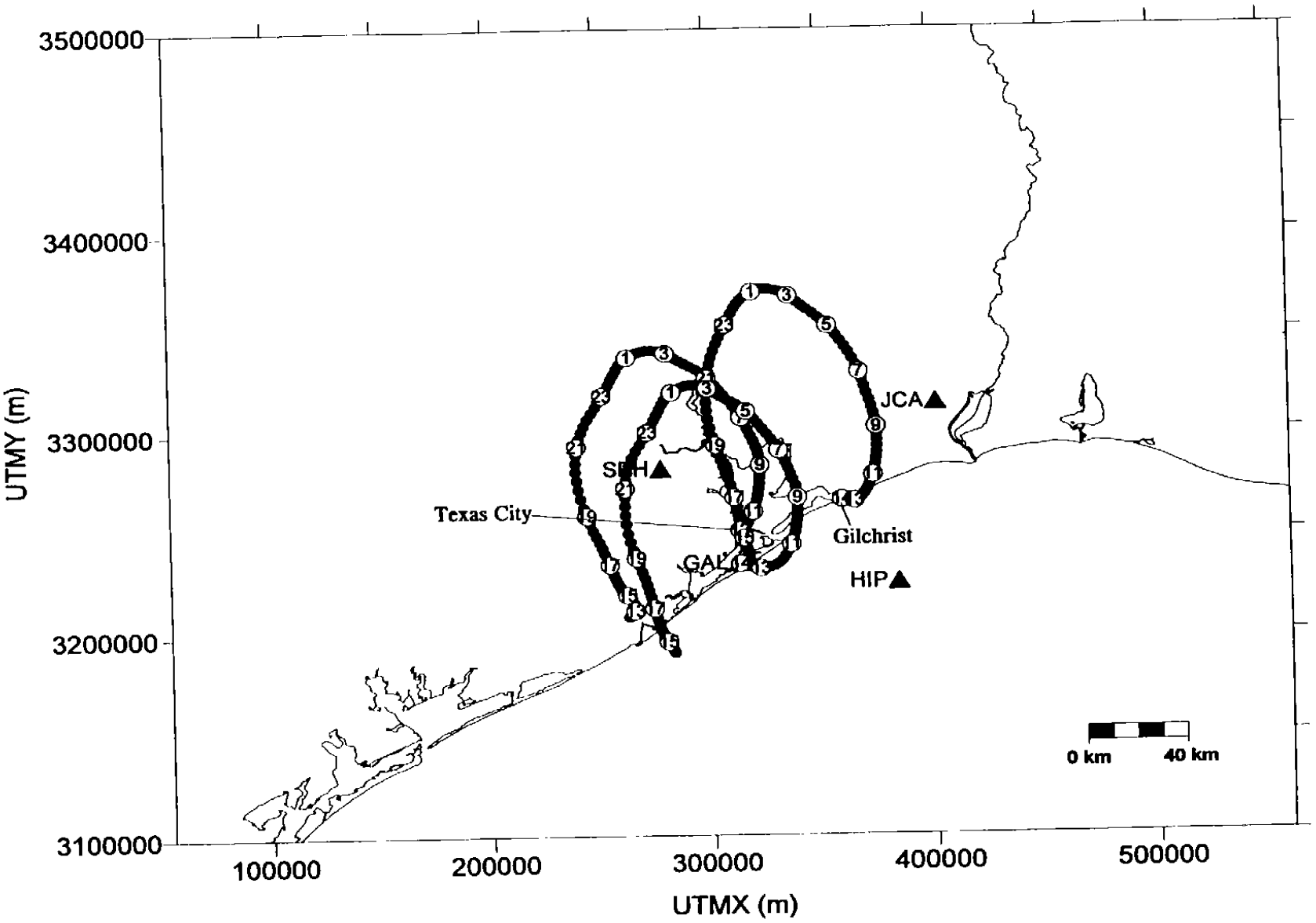

FIGURE 3-76. 100-m backward trajectory from Texas City at 1200 CST, Gilchrist at 1400 CST, and Galveston at 1400 CST, on 10 September 1993.

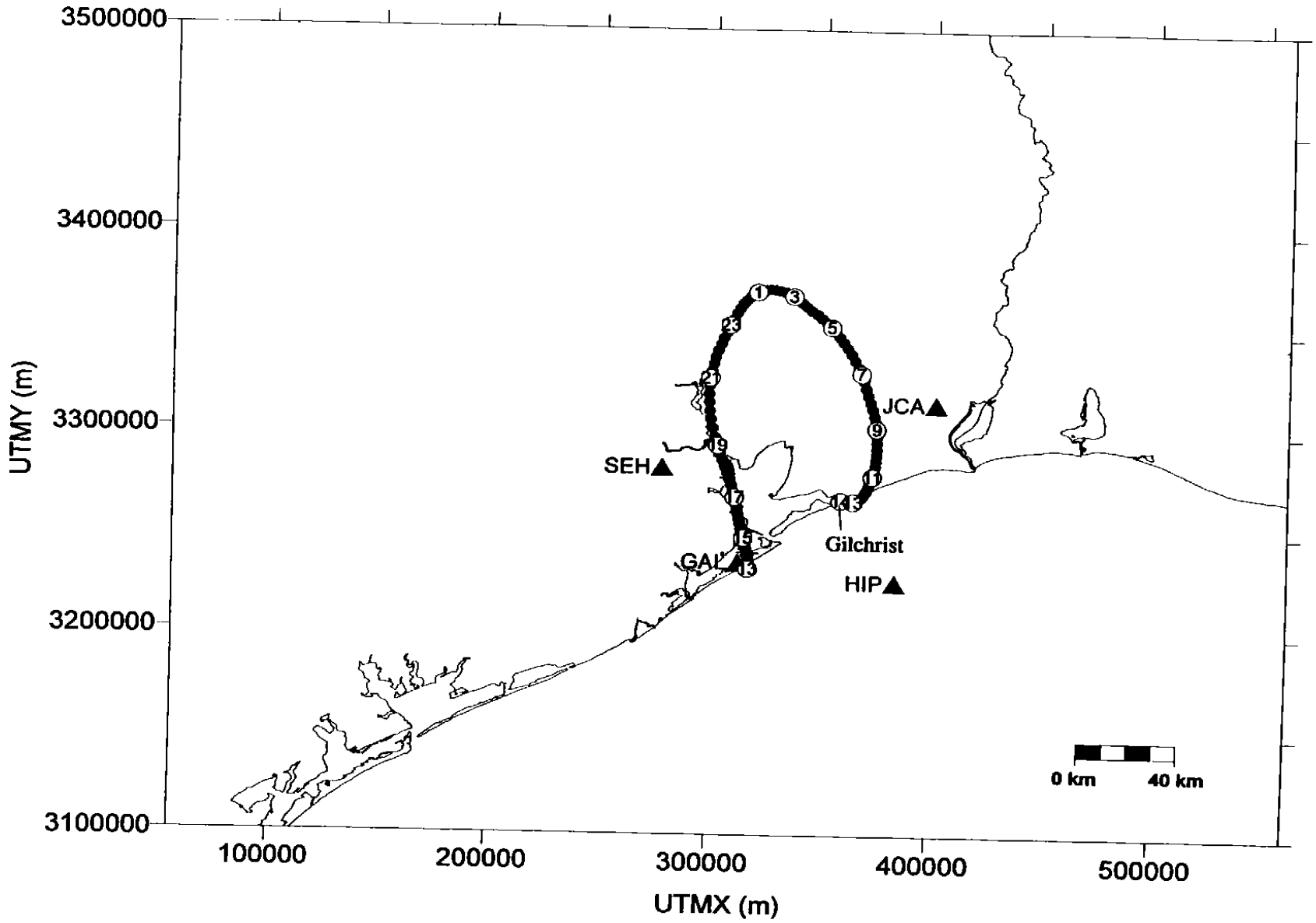

FIGURE 3-77. 100-m backward trajectory from Gilchrist at 1400 CST, on 10 September 1993.

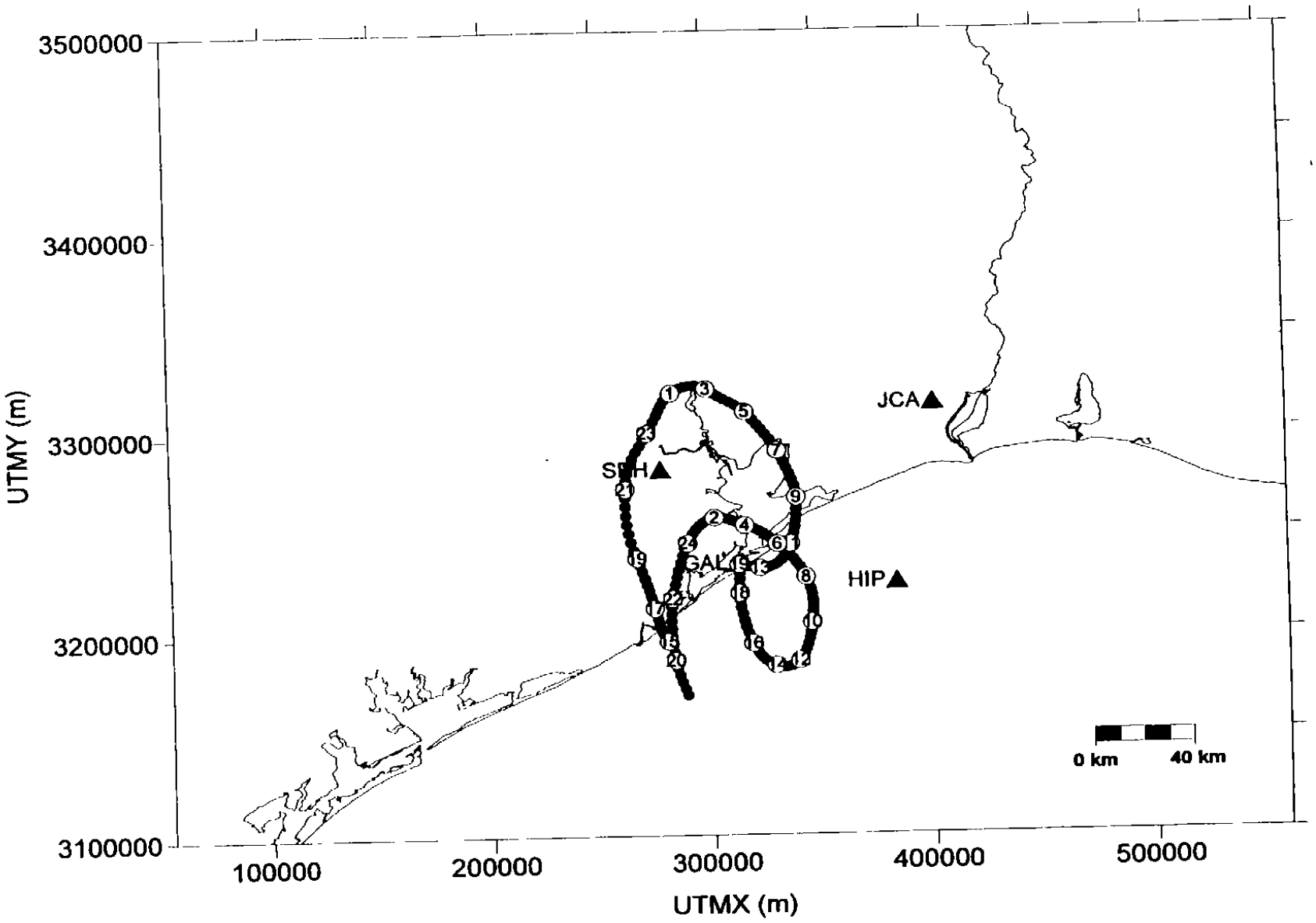

FIGURE 3-78. 100-m backward trajectory from Galveston at 1400 and 1900 CST, on 10 September 1993.

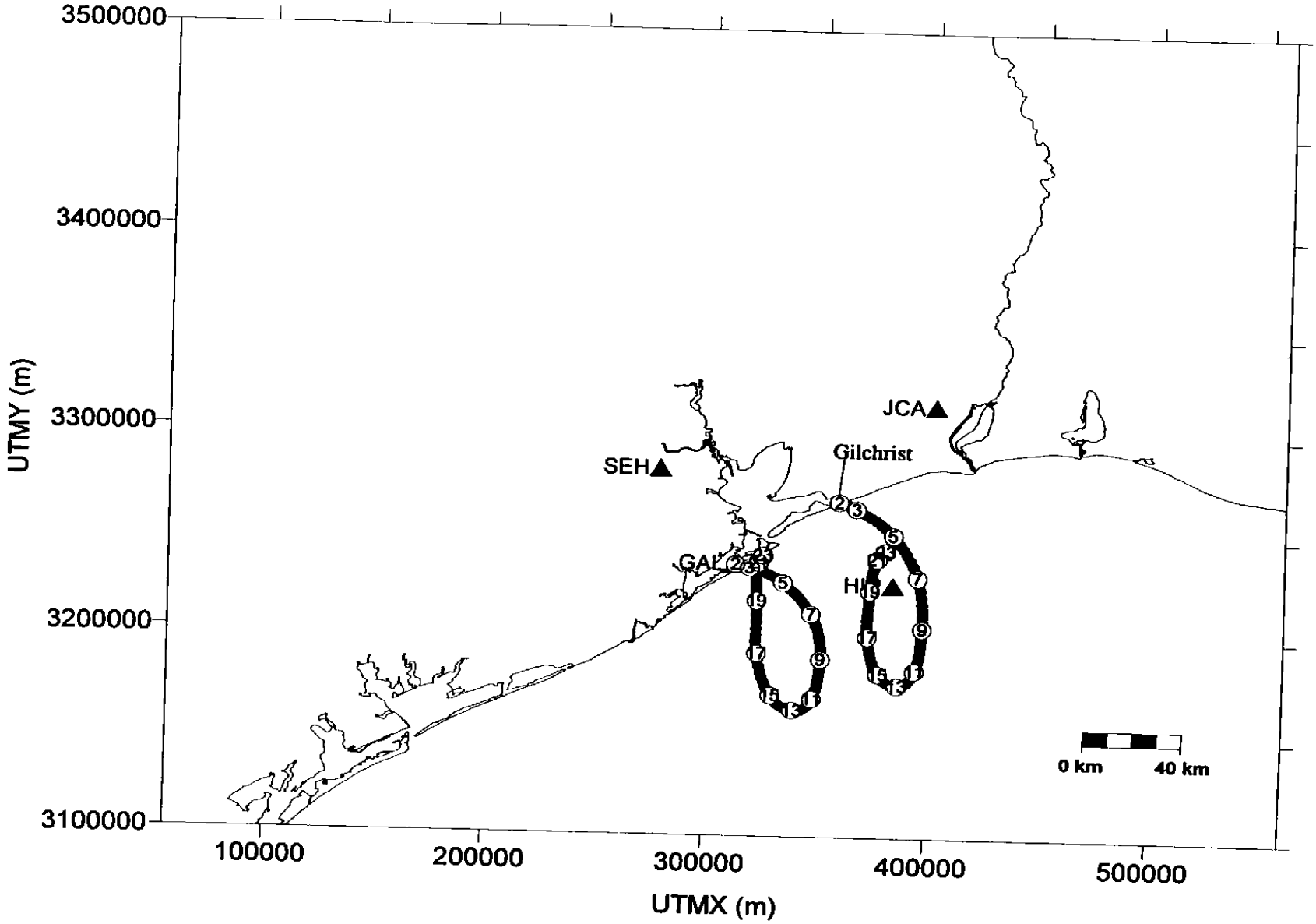

FIGURE 3-79. 100-m forward trajectory form Galveston and Gilchrist at 0200 CST, on 10 September 1993.

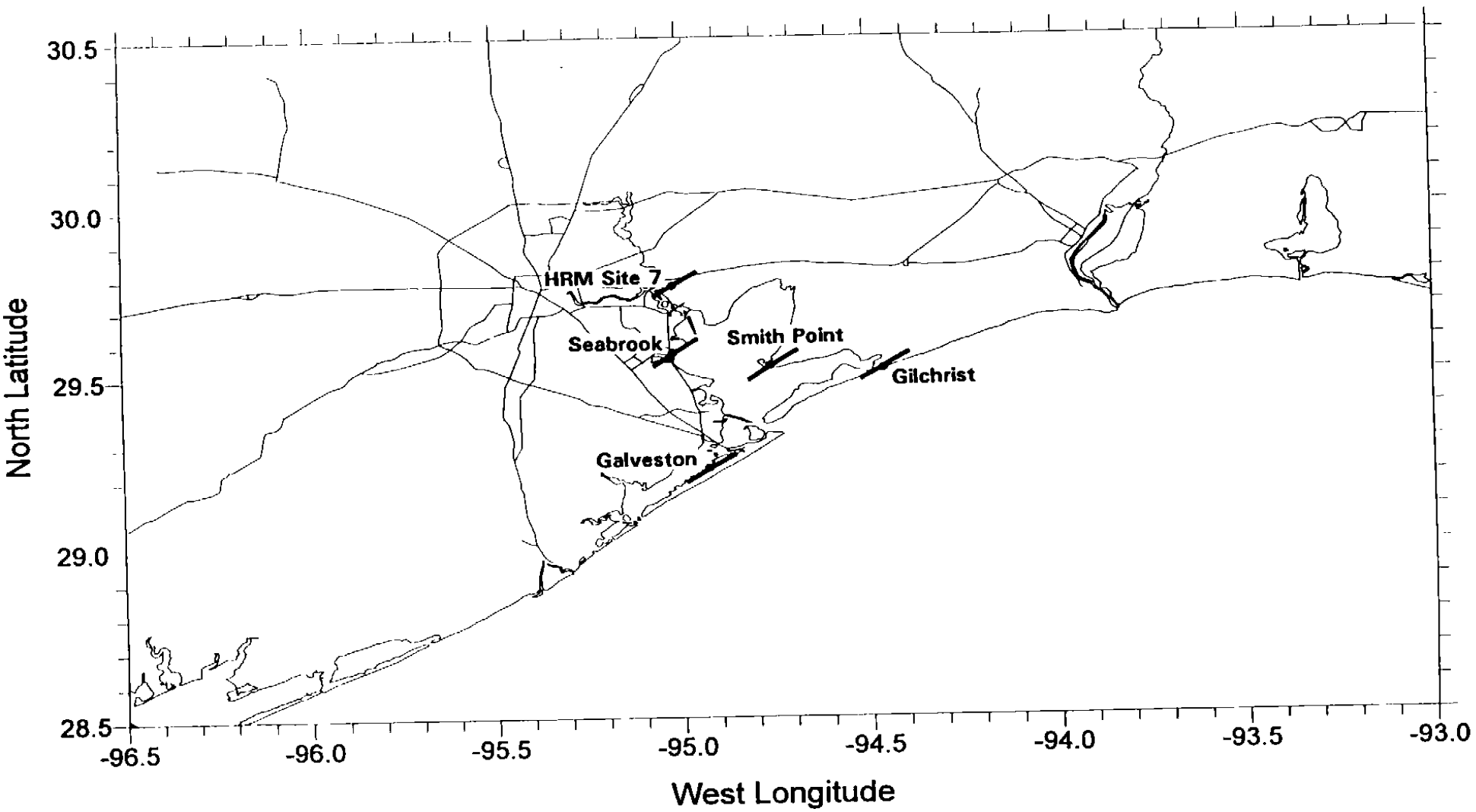

FIGURE 3-80. Five northeast-southwest flux planes specific to five surface monitoring sites: Galveston, Gilchrist, Seabrook, Smith Point, and Houston Regional Monitoring (HRM) Site 7.

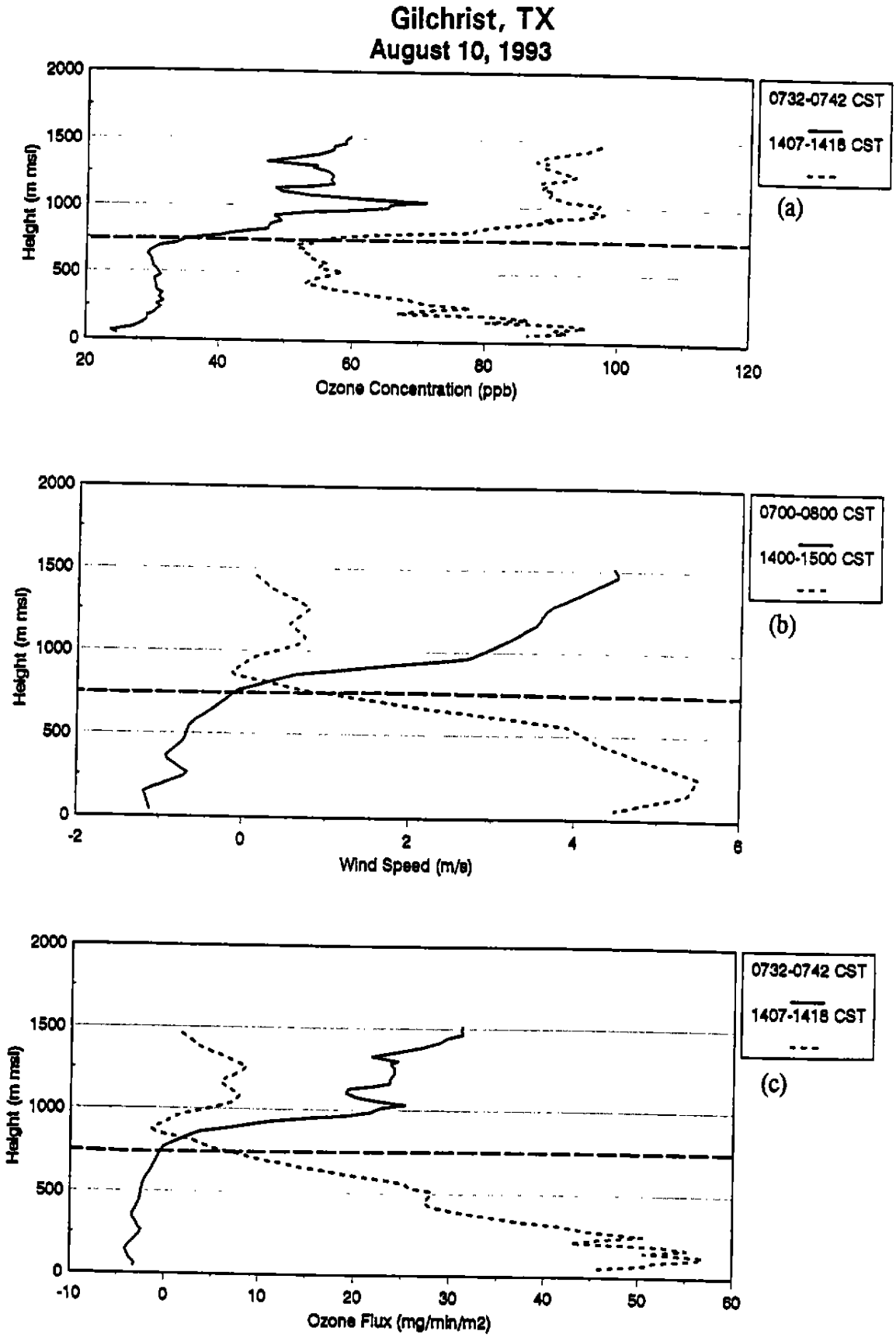

FIGURE 3-81. (a) Vertical profiles of ozone concentration, (b) southeasterly component of the wind speed, and (c) estimated ozone flux at Gilchrist on 10 August 1993. The longer dashed line indicates the top of the mixing layer at Galveston on 10 August in the afternoon.

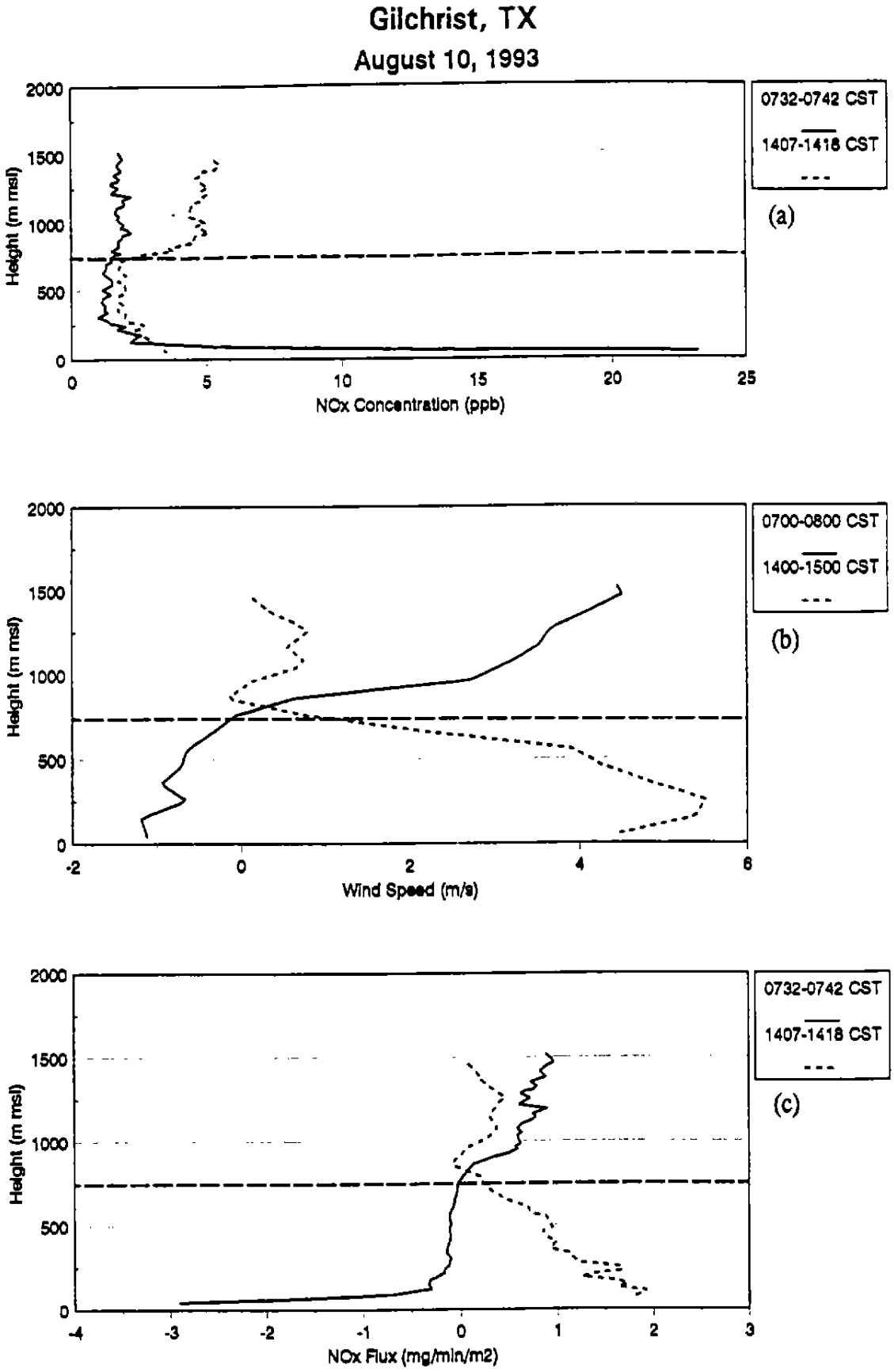

FIGURE 3-82. (a) Vertical profiles of NO_x concentration, (b) southeasterly component of the wind speed, and (c) estimated NO_x flux at Gilchrist on 10 August 1993. The longer dashed line indicates the top of the mixing layer at Galveston on 10 August in the afternoon.

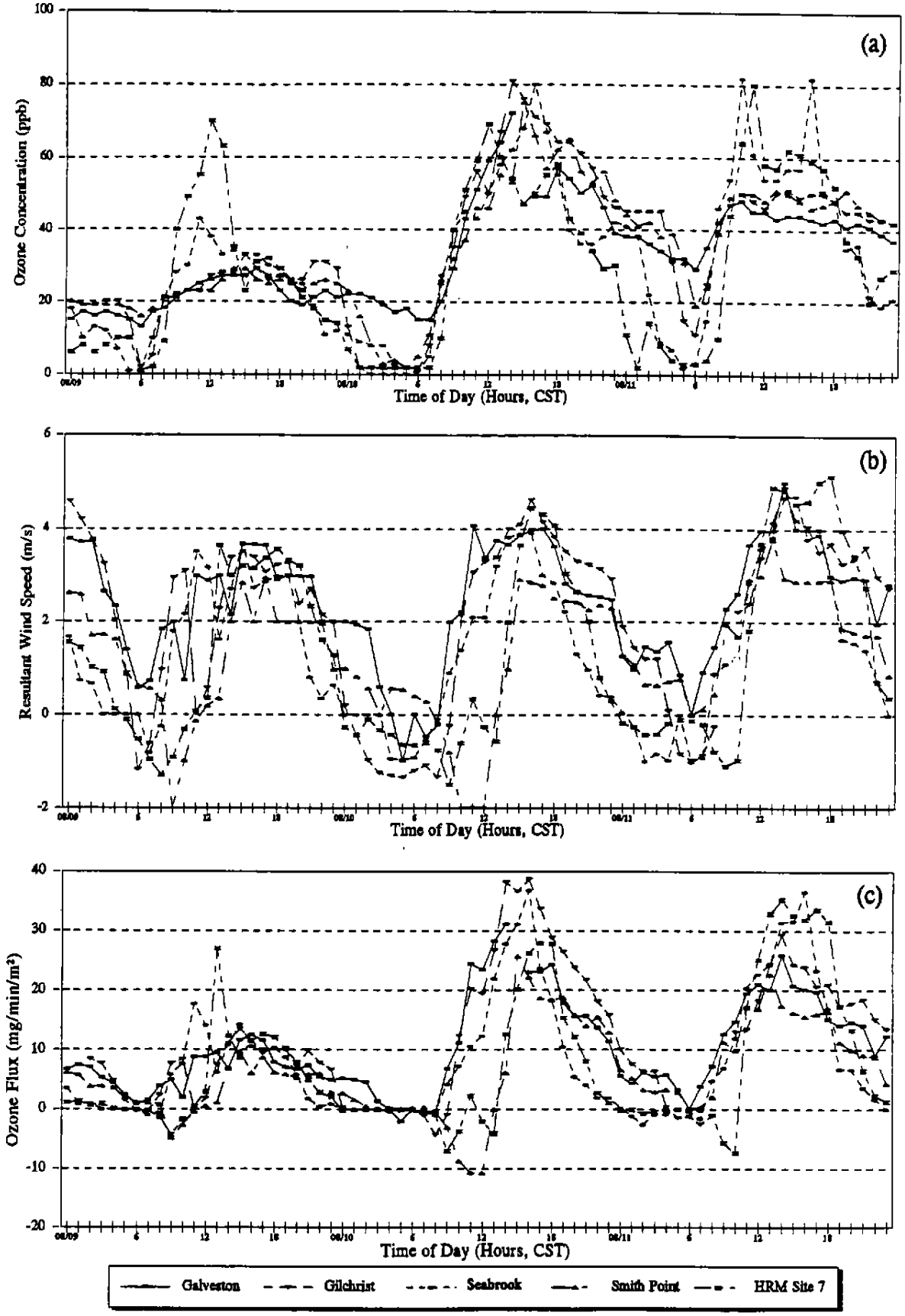

FIGURE 3-83. (a) Ozone concentration, (b) southeasterly component of the wind speed, and (c) estimated relative ozone flux at Galveston, Gilchrist, Seabrook, Smith Point, and Houston Regional Monitoring (HRM) Site 7 for 9-11 August 1993.

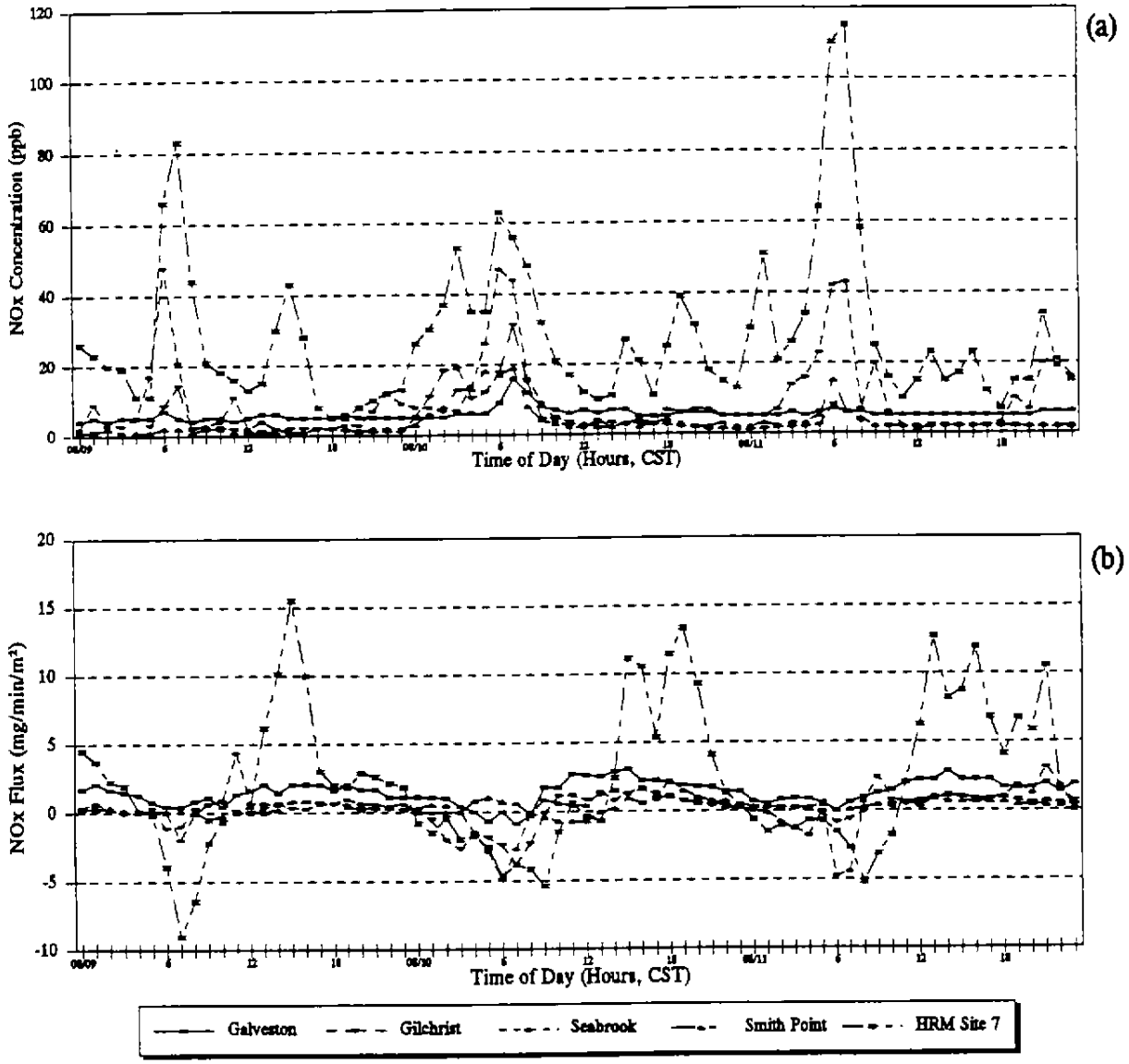

FIGURE 3-84. (a) NO_x concentration and (b) estimated relative NO_x flux at Galveston, Gilchrist, Seabrook, Smith Point, and Houston Regional Monitoring (HRM) Site 7 for 9–11 August 1993.

4 BASE YEAR MODELING ANALYSIS

4.1 INTRODUCTION

This section presents a summary of the meteorological and photochemical modeling analyses performed for the 1988 and 1993 ozone episodes. The modeling was performed to provide a database for use in estimating base-year and future-year impacts of OCS petroleum development (OCSPD) sources on ozone concentrations within onshore nonattainment areas in Texas and Louisiana. The modeling analysis was conducted using the SAI Mesoscale Model (SAIMM), a prognostic meteorological model, and an enhanced version of the Urban Airshed Model (UAM), known as UAM-V. The meteorological and photochemical modeling results are reviewed with regard to the data analysis results and conceptual models presented in Section 3.

4.2 OVERVIEW OF THE UAM-V

Version V of the Urban Airshed Model was applied to several ozone episodes to assess impacts of OCSPD emissions in the Texas-Louisiana Gulf Coast area. This model is an enhanced version of the current regulatory version of the UAM (EPA, 1991a). Like the UAM, the UAM-V is a three-dimensional grid model that numerically simulates the relevant emissions, transport, chemical reaction, and removal processes affecting tropospheric ozone production. Both models employ Version IV of the Carbon-Bond Chemical Mechanism (CB-IV); the UAM-V, however, includes several features that are not supported by the regulatory UAM. These enhancements correct identified deficiencies in the regulatory version (e.g., the fixed vertical grid structure) and allow an improved representation of atmospheric processes (e.g., use of three-dimensional fields for temperature and water vapor concentration). A summary of the new features follows.

1. Structured Modular Computer Code: The UAM computer code has been rewritten so that new modules can be easily included and the code can be vectorized to take advantage of modern computer architecture.

2. Vertical Grid Structure: The vertical layer structure in the UAM-V is defined by the user and is no longer based on the diffusion break (mixing height). This allows for higher resolution vertical layers near the surface and better matching with output from prognostic meteorological models, which typically use a terrain-following coordinate system with fixed levels above ground. The variable vertical structure of the UAM-V permits more realistic treatment of nighttime vertical structures and entrainment of elevated plumes into the grid calculations.

3. Three-Dimensional Inputs: Several meteorological variables that were spatially constant now may be varied temporally and spatially (e.g., temperature, water vapor, pressure, and photolysis rates). Furthermore, the vertical turbulent exchange coefficients are required as input and are usually obtained from a prognostic meteorological model. This feature allows the use of more realistic meteorological fields that may vary spatially over the region being simulated.

4. Two-Way Nested Grid Capability: A fine grid can be imbedded in a coarser grid for more detailed representation of advection/diffusion, chemistry, and emissions. Several levels of horizontal and vertical nesting can be accommodated. The UAM-V's nested grid structure permits high grid resolution where it is needed without the computational cost of carrying it over areas where it is not needed.

5. New Dry Deposition Algorithm: An updated dry deposition algorithm formulated by Wesely (1989) has been implemented in the UAM-V. This algorithm is similar to that used by the Regional Acid Deposition Model (RADM).

6. Plume-in-Grid (P-i-G) Capability: The updated model can treat the subgrid-scale chemistry and dynamics of point-source plumes. This P-i-G algorithm treats emissions as a series of multi-layered ellipsoidal puffs in which ambient air is entrained, chemical reactions take place, and concentrations are "shed" from the outer shells into the grid as the puff size grows to match the limiting cross-sectional area (X-Y or X-Z) of the grid cell. This feature avoids premature dilution and overdilution of emissions from large point sources, unlike other urban- and regional-scale photochemical grid models (such as the UAM and the EPA's Regional Oxidant Model, ROM).

The UAM-V was originally developed and tested for application to the South Coast Air Basin of California. Since its completion in 1992, the model has been distributed to a number of state agencies and research groups for evaluation. Recently, a comprehensive model comparison study of UAM and UAM-V was undertaken for the Atlanta area (Douglas et al., 1994) and based on this evaluation, the EPA permited the state of Georgia to use the UAM-V to evaluate SIP control strategies for the area. Other areas for which the model has been applied include the Lower Lake Michigan area (SIP modeling), the Northeast corridor, and the Lower Fraser Valley of British Columbia.

4.3 SPECIFICATION OF THE GMAQS MODELING DOMAIN

The GMAQS UAM-V modeling domain consists of a coarse-resolution outer domain and a fine-resolution inner domain that encompasses the Houston metropolitan area, Galveston Bay, and the Beaumont/Port Arthur area (see Figure 1-2). Both domains were specified in Zone 15 UTM coordinates. The following grid specifications (in kilometers) were used:

Outer Grid:

Grid origin (Easting, Northing) :	0, 2800
Cells in the west-east direction:	72
Cells in the south-north direction:	50
Horizontal grid spacing:	16

Inner Grid:

Grid origin:	204, 3180
Cells in the west-east direction:	62
Cells in the south-north direction:	54
Horizontal grid spacing:	4

Seven vertical layers were utilized:

Layer Interfaces (m)	Layer Midpoint (m)
0-50	25
50-150	100
150-450	300
450-900	675
900-1500	1200
1500-2200	1850
2200-3000	2600

These vertical layer heights were chosen such that the layer midpoints coincide with the heights of the SAIMM levels, minimizing the need for interpolation or averaging to convert the SAIMM output to UAM-ready format.

4.4 SELECTION OF HISTORICAL EPISODES (1987-1990)

This section summarizes the process followed in selecting historical (prior to 1993) and field program (1993) ozone episodes that were simulated in the meteorological and photochemical modeling analysis. One of the original objectives of the GMAQS program was to undertake an analysis of historical ozone air quality and meteorological data to (1) provide a basis for identifying the characteristics of ozone exceedance events to assist in forecasting such events in an intensive field program and (2) identify candidate episodes for modeling.

The analyses of historical data conducted by STI (Blumenthal et al., 1993) and Myers (1992) provided information for the historical episode selection performed by Douglas et al. (1992). The episode selection process consisted of statistical analysis of ozone data, examination of weather maps and local wind observations, and particle-path analysis for the period from 1987 to 1990. Candidate episodes were identified and classified according to their potential for onshore flow and thus potential for contribution of OCS emissions to onshore ozone concentrations. Only episode days with observed ozone concentrations greater than 12 pphm were considered. Utilizing several indicators of

onshore transport, including synoptic gradient, upper-air winds, and existence and onset of the gulf breeze, eight episodes for the Houston area and three episodes for the Baton Rouge area were selected for further consideration using particle-path analysis.

Gridded surface wind fields were generated using all available surface wind data for two subdomains, one encompassing the Houston nonattainment area and the other the Baton Rouge nonattainment area. Backward particle paths culminating at selected ozone monitoring sites at 1000 and 1600 CST were calculated and plotted. These times bracket the range of hours during which the highest ozone concentrations were measured at most sites. Based on the results of the particle-path analysis, the list of candidate episodes was reduced and the 28–29 July 1988 ozone episode was selected for modeling. The backward particle path culminating at 1600 CST for 29 July indicated persistent onshore flow (Figure 4-1; figures for this section begin on page 4-82). The maximum ozone concentration for this day was 13 pphm and occurred in the Houston area. The 29 July 1988 episode day represented one possible scenario for OCS emissions to cause a violation of the federal ozone standard on a day that otherwise was not characterized by meteorological conditions associated with high ozone concentrations. Although a detailed analysis of the meteorological conditions was not performed for this episode, a review of the climatological analysis (presented in Section 3) indicates that this episode is not representative of episodes that occurred during the 1982–1992 period.

4.5 SIMULATION OF THE 1988 MODELING EPISODE

The application of the UAM-V for the 28–29 July 1988 episode involved the use of the EPA's 1990 Interim emission inventory. This database includes emissions from major point sources and county-level emissions for area and mobile source categories. Biogenic emissions were prepared using the EPA's Biogenic Emissions Inventory System (BEIS) with episode-specific meteorological inputs, combined with special-study data for the Baton Rouge area. Emissions data were processed into UAM-V input files using the Emissions Preprocessor System (EPS 2.0), which handles spatial and temporal allocation and speciation of emissions. Files for the entire GMAQS domain were prepared at a resolution of 4 km and were aggregated or extracted as necessary.

Gridded fields of wind, temperature, water vapor concentration, pressure, and vertical exchange coefficients for the UAM-V were prepared using the Systems Applications International Mesoscale Model (SAIMM), a prognostic meteorological model. Procedures for applying SAIMM and processing into UAM-V input files were developed during preparation of data for the 1988 episode. Similar procedures were later used in preparing data for the 1993 episodes; these are described in Section 4.6. Considerably less meteorological data was available for the 1988 episode than for the 1993 episodes; in addition, for the 1988 episode the coarse-grid meteorological fields were used for both the coarse- and fine-grid UAM-V simulations.

Maximum ozone concentrations of 9 and 13 pphm, respectively, were observed within the Houston area on 28 and 29 July. On 28 July the observed peak in Baton Rouge was

20 pphm. However, based on the results of the episode selection analysis (outlined in the previous section), 28 July was not identified as a candidate episode for modeling of the Baton Rouge area as the potential for OCS impact was quite low. Thus, the focus of the modeling for this episode was on the Houston area.

A number of UAM-V simulations were performed to test the ability of the modeling system to replicate this episode. Maximum simulated ozone concentrations for the Houston area reached 14.6 pphm on 28 July and 13.8 pphm on 29 July. The results of the 1988 modeling effort indicated that the GMAQS modeling system was capable of simulating ozone formation and transport in the Gulf of Mexico area. However, given the relatively low observed ozone concentrations for this episode (compared to other Houston-area episodes) and the lack of a comprehensive database for input preparation and model performance evaluation, it was determined that the 1988 episode modeling might not provide a reliable framework for estimating OCS impacts. Besides identifying deficiencies in the existing data, the historical modeling effort also provided the opportunity to refine input methodologies followed in modeling the 1993 episodes.

4.6 SELECTION OF THE 1993 EPISODES

After the 1993 GMAQS and COAST field programs were completed, ozone air quality data were examined for the GMAQS domain. Based on an analysis of the candidate episode periods identified from the 1993 field program (described in Section 3), two candidate periods were selected for modeling: 17–20 August and 6–11 September 1993. Because the intensive GMAQS and COAST programs ended in late August, some supplemental data were not available for the September episode. Data availability for each of the episodes is described in Section 3.

The modeling episodes were selected based on the magnitude and extent of observed high ozone concentrations within the onshore ozone nonattainment areas and the estimated potential for OCS emissions to contribute to the onshore concentrations. The potential for contribution was estimated a priori based on analysis of the observed surface and upper-air wind data.

The air quality and meteorological characteristics of the 17–20 August and 6–11 September episodes are described in detail in Section 3. The August episode was characterized by high ozone concentrations and numerous exceedances of the NAAQS in the Houston area. The gulf-breeze circulation and associated flow reversal observed during this episode likely contributed to the ozone exceedances (by allowing the daily buildup of ozone precursors over the Houston area). At the monitoring sites, the highest ozone concentrations were observed prior to the passage of the gulf-breeze front; peak concentrations within the region were observed to the north of Houston. Aircraft data collected during this period do not indicate substantial day-to-day carryover of pollutants. Exceedances were also monitored in the Baton Rouge area during the August episode period.

The September episode was also characterized by high ozone concentrations within the Houston area, but for this episode the highest concentrations were measured near the coastline (between Houston and the coast and at sites along Galveston Bay). An offshore-directed pressure gradient during this episode period likely enhanced the offshore component of the gulf-breeze circulation (the land breeze) and suppressed the onshore component (limiting its inland penetration for example). Although no aircraft data are available for this episode, the data analysis results suggest that carryover of ozone and precursor pollutants contributed to the high observed ozone concentrations.

The representativeness analysis described in Section 3 concludes that the 1993 GMAQS episodes are representative of the period 1982–1992 and that the meteorological variables monitored during the 1993 episodes are within the ranges of distributions for ozone exceedance days during this historical period.

4.7 UAM-V BASE CASE INPUT PREPARATION FOR THE 1993 EPISODES

This section summarizes the input preparation methodologies and resulting input files prepared for the 1993 episodes for use in the UAM-V. Day-specific emission, meteorological, air quality, and land-use inputs were prepared for each episode day.

EMISSION INVENTORY DEVELOPMENT

Comprehensive gridded, hourly emission inventories were prepared for the entire study area, for both historical and future-year emission scenarios. These inventories cover an area of nearly 1 million square kilometers, encompassing portions of Texas, Louisiana, Mississippi, Alabama, Florida, and the western and central sections of the Gulf of Mexico OCS. Ozone nonattainment areas located within the modeling domain include the Houston/Galveston and Beaumont/Port Arthur nonattainment areas in Texas and the Lake Charles and Baton Rouge nonattainment areas in Louisiana. Figure 4-2 indicates the ozone attainment status for each county in the modeling domain.

The modeling inventories developed for this study include emissions of NO, NO_2, speciated VOC, and CO. These inventories were converted to formats suitable for input to the photochemical model using the UAM Emissions Preprocessing System, Version 2.0 (EPS 2.0) (EPA, 1992d). Quality assurance guidelines and procedures were developed, applied, and documented throughout the emission inventory process to ensure traceable emissions processing with minimal introduction of additional errors.

The emission inventories included both onshore and offshore emissions. All relevant emissions from anthropogenic and natural (biogenic) sources were considered, with special attention focused on offshore anthropogenic sources. The following sources have been addressed in this study:

Offshore anthropogenic sources:

- OCS and state waters oil and gas production facilities
- Crew and supply boats/helicopters serving OCS facilities
- Commercial shipping
- Recreational vessels
- Military vessels
- Pipeline vessels
- Exploratory vessels
- Intercoastal barges
- The Louisiana Offshore Oil Port (LOOP)

Onshore anthropogenic sources:

- Point sources
- Area sources
- Nonroad mobile sources
- Mobile sources

Natural sources:

- Biogenic sources

Data Sources

The MMS modeling domain consists of the western and central OCS sections and portions of Alabama, Florida, Louisiana, Mississippi, and Texas (see Figure 1-1). There are 328 counties/parishes within the domain, including 11 ozone nonattainment parishes in Louisiana and 11 nonattainment counties in Texas. Anthropogenic emissions data were obtained from the MMS and several state and local agencies, and were supplemented with the EPA 1990 Interim Inventory (EPA, 1993a). Figure 4-3 illustrates the origin of onshore emissions data by region for each of the three major source categories: point, area and nonroad mobile, and onroad motor vehicles.

Emissions data for onshore stationary point and area sources, nonroad mobile sources, and onroad motor vehicles were provided by the Texas Natural Resources Conservation Commission (TNRCC) and the Louisiana Department of Environment Quality (LDEQ) for the ozone nonattainment areas in the modeling domain. For the offshore region of the domain, emissions data were based on a survey conducted by MMS of OCS emission sources and existing data from the other emission sources (e.g., recreational boating). These sources are discussed in detail below.

Offshore Sources

To collect the information required to estimate emissions, the MMS and SAI developed a set of survey forms to solicit activity and operating data for OCS production platforms and crew/supply vessels and helicopters. The MMS distributed the platform surveys to platform operators located in OCS waters; the crew/supply vessel and helicopter surveys

were distributed to companies servicing the OCS facilities. The MMS entered all survey data into a database. The database files containing the platform-related activity data were inputted to the OCS Platform Inventory System (OPIS). OPIS was designed specifically for this study to access the survey database, assign quality assurance tracking codes, make data corrections, calculate emissions, and prepare the emission data file in the format required by EPS 2.0. The OPIS database contains 1,857 OCS platforms, corresponding to an 85 percent survey response rate. Since all of the major gas and oil production companies in the Gulf responded to the survey, these 1,857 platforms represent the great majority of operational production platforms in the Gulf. On the platforms, about 6,000 pieces of equipment, 1,800 storage tanks, 200 flares, and 500 vents are included as potential emission sources. These were treated explicitly as individual point sources in the modeling inventories. Platform fugitive emissions were estimated outside of OPIS, using a study of platforms off the coast of California (DOI, 1992). Information collected during the survey was also used to estimate emissions from other platform-related activities, including crew/supply boats and helicopters.

A.T. Kearney, Inc. (Kearney, 1993) provided information required to estimate emissions for other oil and gas related operations in the Gulf of Mexico including exploratory vessels and the Louisiana Offshore Oil Port (LOOP). A.T. Kearney also estimated emissions for sources not related to OCS oil and gas activities, including commercial shipping, recreational vessels, intercoastal barges, and commercial fishing. Activity data for these sources were collected and used with emission factors from the literature to estimate emissions. Activity data for military and pipeline vessels, including type and size of engine, fuel used, and area of operation, were obtained from the Navy and the MMS, respectively. A detailed discussion of the data sources and emission estimating methodologies for the Gulf of Mexico offshore region is provided in Appendix N, in Volume 3 of this report.

The OCS emission sources are classified as oil production or nonproduction activities. Table 4-1 provides the base-year inventory totals for each OCS source category, subtotaled by activity class.

Onshore Stationary and Nonroad Mobile Sources

Stationary area sources include those sources too numerous or too minor to be inventoried as individual point sources. Biogenic emissions, which may be classified as stationary, are discussed separately. Typical area sources include architectural coatings, solvent usage, and dry cleaning. Nonroad mobile sources include internal combustion sources other than onroad motor vehicles: lawn mowers, generator sets, marine vessels, construction equipment, and aircraft. For inventory processing the approach for these components is identical, and they are typically processed together.

The EPA 1990 Interim Inventory (EPA, 1993a) was used to provide baseline emissions estimates for the majority of the attainment counties/parishes in the UAM domain. For the four ozone nonattainment areas, preliminary 1990 SIP emissions data obtained from the state and local agencies were used to develop the modeling inventories.

Table 4-1. 1993 offshore emissions (tons/day): August episode, weekday.

Source Type	NO_x	VOC	CO
OCS Production Related Sources			
Area Sources			
Crew/Supply Vessels	26.60	2.11	6.47
Crew/Supply Helicopters	0.79	0.58	1.90
Exploration Vessels	71.99	2.87	8.19
Pipeline Vessels	49.43	8.41	7.79
Point Sources			
Platforms	325.84	75.39	76.12
OCS Subtotal	474.64	89.36	100.48
Non-OCS Production Related Sources			
Area Sources			
Barge Traffic	1.01	0.05	0.22
Recreational Boating	0.40	13.08	28.28
Military Vessels	0.10	0.00	0.01
LOOP	3.37	0.15	0.38
Commercial Fishing	34.20	6.28	16.34
Commercial Shipping	234.50	10.21	25.98
Point Sources			
LOOP	3.76	1.77	0.44
Non-OCS Subtotal	277.34	31.53	71.64
TOTAL	751.98	120.90	172.12

The EPA developed the 1990 Interim Inventory to provide a comprehensive national emissions database for use in regional modeling applications during the interim period in which the 1990 SIP inventories were being developed and incorporated into the national Aerometric Information Retrieval System (AIRS). For point sources, the Interim Inventory contains emissions and related data for individual sources at the process level. Table 4-2 lists the point source data fields from the 1990 Interim Inventory which were used to develop the modeling emission inventories. Emissions for area source categories (including nonroad mobile sources) in the 1990 Interim Inventory are reported as county-level totals by AIRS Area Source Category (ASC) code.

Table 4-2. Data variables from the EPA's 1990 Interim point source inventory.

Geographical Data
- FIPS state and county codes
- Source location (latitude and longitude)

Source Identification Data
- Plant identification code
- Point identification code
- Standard Industrial Classification Code
- Source Classification Code

Stack Characterization Data
- Height
- Diameter
- Exit gas temperature
- Exit gas flow rate
- Exit gas velocity

Operating Schedule Information
- Seasonal percentages of annual throughput
- Hours per day in operation
- Days per week in operation
- Weeks per year in operation

Control Technology Data for VOC, NO_x, CO, and SO_2
- Primary control equipment code
- Percent control efficiency
- Percent rule effectiveness

Emissions Data
- Tons per year of VOC, NO_x, CO, and SO_2

Houston/Galveston and Beaumont/Port Arthur. Preliminary stationary and nonroad mobile source annual emissions data were provided by TNRCC for 24 counties including and surrounding these two nonattainment areas. The 1990 emissions data included point source emissions in AIRS Facility Subsystem (AFS) format and county-level area and nonroad mobile source emissions in AIRS Area and Mobile Source (AMS) workfile format, the formats required for input to EPS 2.0. Projection factors were also provided by TNRCC to adjust these emissions to 1993 levels for the Houston/Galveston and Beaumont/Port Arthur nonattainment areas.

Baton Rouge and Lake Charles. LDEQ provided stationary and nonroad mobile source emissions data for 21 parishes in the Baton Rouge ozone SIP UAM modeling domain and for Calcasieu Parish (the Lake Charles nonattainment area). Point source emissions data were also provided for seven parishes surrounding Calcasieu. The data contained in these files included a combination of annual and typical weekday peak ozone season emission rates. These data were used to develop the 1993 emission inventory for the Baton Rouge and Lake Charles areas.

Onroad Motor Vehicles

For each county/parish in the modeling region, motor vehicle emission factors estimated with MOBILE5a (EPA, 1992a) were multiplied by vehicle miles traveled (VMT) estimates for 1990 to obtain the daily total mass of emissions by vehicle class, operating mode (e.g., exhaust, running losses), and roadway classification. The emission factors included the effects of local control requirements and Inspection and Maintenance (I/M) programs on a county-level basis. For this application, average daily speeds by vehicle type and roadway classification and average daily minimum and maximum temperatures

were used to calculate the emission factors (i.e., hourly temperature and speed adjustments were not made to the motor vehicle inventory).

For those counties/parishes for which locale-specific data were not available, motor vehicle emissions were estimated by multiplying the estimated 1990 VMT from the EPA 1990 Interim Inventory by emission factors generated by MOBILE5a. These VMT estimates are based on data collected as part of the U.S. Department of Transportation's Highway Performance and Monitoring Survey (HPMS), which is the preferred source of VMT estimates listed in EPA guidance (EPA, 1992c). Estimates of VMT by county/parish and roadway type (e.g., freeway, major arterial) were extracted from the 1990 Interim Inventory and projected to the 1993 base inventory year using national average annual projected VMT data published by Argonne National Laboratory (Saricks and Vyas, 1985). For each state, the resulting national-average VMT projection factor was adjusted using the ratio of projected population growth for the state to that of the nation.

Average speed data by roadway classification were also extracted from the 1990 Interim Inventory for input to the MOBILE5a model. Separate MOBILE5a scenarios were modeled using the average speed by roadway type obtained from the Interim Inventory as well as to simulate the various temperature ranges within the modeling regions. The I/M program characteristics for basic and enhanced I/M were obtained from descriptions of these programs in the *Federal Register* (1992). The refueling emissions are provided as part of the area component.

Houston/Galveston. Mobile inputs and daily VMT for 1990 were provided by HGAC for the Houston/Galveston nonattainment area (Jackson and Gram, 1994). The data provided by HGAC were compiled for the *Final 1990 Base Year Ozone State Implementation Plan, On-road Mobile Source Emission Inventory for the Houston-Galveston Ozone Nonattainment Area*, which was completed in May 1993. Refuel emissions were included with the area source emissions. The daily VMT were projected to 1993 values using the Argonne VMT projections. These data were then adjusted by a factor of 1.068 to account for the difference between the travel demand model VMT and HPMS VMT (HGAC, 1993). The 1990 MOBILE5a input files included daily average speeds for each county in the region. The total onroad mobile emissions prepared for the GMAQS application were underestimated in comparison to those estimated by HGAC because of differences in the emissions processing methodologies (e.g., the HGAC modeling incorporated period-specific link-based speeds and temperatures). Accordingly, adjustment factors were estimated for each county and pollutant and were applied to the modeling inventories to ensure that the emissions to be modeled reflected the values being used by the state for SIP modeling.

Further adjustments were made to the eight nonattainment counties. One adjustment was made to reflect a higher temperature in this area of the subdomain. Another was applied in order to reflect a similar magnitude as the preliminary SIP totals. Table 4-3 presents all of the adjustment factors applied to the Houston/Galveston area.

Table 4-3. Adjustment factors applied to the Houston/Galveston area onroad mobile emissions.

Adjustment	NO_x	VOC	CO
HGAC VMT adjustment	1.068	1.068	1.068
Temperature	0.9608–1.000	1.000–1.2433	1.0345–1.0871
TNRCC SIP	1.013–1.120	0.921–1.067	0.963–1.160

Beaumont/Port Arthur. For the Beaumont/Port Arthur nonattainment area, 1990 MOBILE5a inputs and daily VMT were received from TNRCC (Jackson and Kandalam, 1994). Refueling emissions were included with the area source emissions. The daily VMT were projected to 1993 using the Argonne VMT projections. The 1990 mobile input files were provided with daily average speeds on a county-by-county basis. The same daily minimum and maximum temperatures were used for both episodes for all counties in this region. As was the case for the Houston domain, adjustment factors were developed to adjust the emissions for TNRCC's use of period-specific link-based speeds and period-specific temperatures. The adjustment factors ranged from 0.993 to 1.24 for the nonattainment areas.

Baton Rouge and Lake Charles Nonattainment Areas. LDEQ (1993) provided 1990 VMT and MOBILE5a input files for the Baton Rouge subdomain and 1992 VMT and MOBILE5a input files for Calcasieu Parish (Lake Charles); these data were used to prepare the onroad mobile inventories. Estimates of VMT by parish and roadway type (e.g., freeway, arterial) were projected to the 1993 base inventory year using parish-specific projected VMT data, also provided by LDEQ. Episode-specific vehicle refueling emissions were calculated by multiplying the refueling emission factor in grams per gallon generated in MOBILE5a (based on the episodic minimum and maximum temperatures) by annual sales for each parish, provided by LDEQ.

Biogenic Emissions

Biogenic emissions estimates for the modeling domain were prepared using the EPA's Biogenic Emission Inventory System (UAM-BEIS), which is based on various biomass, emission, and environmental factors. The leaf biomass database used by UAM-BEIS was derived from land-use data in the Oak Ridge Laboratory's Geoecology Data Base (Olsen, 1980). The land-use database is resolved at the county level and includes acreage by forest types, agricultural crops, and other areas such as urban, grassland, and water. The emission factors used by BEIS are based largely on Zimmermann's (1979) study of biogenic emission rates in the Tampa/St. Petersburg Florida area. Emission factors are given for four hydrocarbon species: isoprene, α-pinene, monoterpene, and unidentified. The emission factors used by UAM-BEIS are standardized for full sunlight and 30° Celsius. Since biogenic emissions are strongly temperature dependent, and isoprene emissions also vary with solar intensity, UAM-BEIS adjusts the emission

factors to account for the effects of variations in ambient conditions using relationships derived by Tingey (Tingey, 1981; Tingey et al., 1980, 1981). UAM-BEIS also simulates the vertical variation of leaf temperature and sunlight within the forest canopy.

For this study, the UAM-BEIS was used to generate UAM-ready emission estimates for each episode day, using episodic meteorological data including hourly gridded surface wind speed, temperature, and relative humidity. Gridded temperature fields for BEIS were prepared by interpolation of surface temperature observations. Winds from the SAIMM and relative humidity observations were used. For each episode day, UAM-BEIS default county-level leaf biomass and land-use data were used to estimate biogenic emissions, except for the Baton Rouge area. The base biogenic emission rates for each grid cell were adjusted for temperature using the same hourly gridded surface temperature file used as input to the UAM for each episode day. Emissions for each county were spatially allocated to grid cells based on the fraction of county area located within each cell. For the Texas counties in the Houston/Galveston and Beaumont/Port Arthur subdomains, the resulting biogenic emissions were adjusted to correspond to the biogenic emission levels that were estimated using locale-specific land use for the COAST study.

The adjustments to the biogenic emissions within the Texas subdomain originated by comparing the biogenic emissions modeled using UAM-BEIS with those generated by TNRCC, also using the UAM-BEIS, for a 1990 July-August episode that exhibited similar meteorology. It was determined that the difference between the inventories was attributable to different biomass databases. Specifically, factors of 0.115 and 1.97 were applied across the board to NO and VOC, respectively. Since TNRCC had not modeled a September episode, these adjustments were not made to the day-specific biogenic emissions.

Table 4-4 presents biogenic emission totals for the 17 August and 6 September 1993 episode days. The distribution of the biogenic emissions is illustrated in Appendix P (in Volume 3 of this study): Figure P-6 presents the 17 August 1993 NO, isoprene, and other monoterpene densities, and Figure P-7 presents the 6 September 1993 biogenic emissions. In these displays, and in Table 4-4, NO is reported as NO_x and isoprene as methane (mol. wt. 80 g/mol). The distribution of the NO biogenic emissions is associated with agricultural land use and is the densest in the southwestern portion of the domain. The isoprene emissions, emitted from deciduous and broadleaf evergreen forested areas, is concentrated in the Houston area and northern Louisiana.

Table 4-4. Biogenic emission totals for the MMS domain (ton/day).

Episode	NO	Isoprene	Other Monoterpene
August 17, 1993 (adjusted)	443.3	8,233.3	8,863.4
September 6, 1993	1,138.1	4,347.0	5,333.0

For Baton Rouge, locale-specific gridded biogenic emissions were estimated by the Georgia Institute of Technology (GIT, 1993). The information provided by GIT included biogenic emission rates for one hour, calculated at 30°C and full solar intensity, at a 2-km grid cell resolution. To prepare the episode-specific biogenic modeling inventories, the emission rates provided by GIT were adjusted for hourly variations in temperature and solar intensity.

Modeling Inventory Preparation

Photochemical grid models such as the UAM-V require detailed emission inventories, containing hourly emissions for each grid cell in the modeling domain for each species being simulated. To facilitate development of these emission inventories for this analysis, the EPA's UAM Emissions Preprocessor System, Version 2.0 (EPS 2.0) was used. This system is a series of computer programs designed to perform the intensive data manipulations necessary to adapt a county-level annual or seasonal emission inventory for modeling use.

The core EPS 2.0 system consists of a series of FORTRAN modules that incorporate spatial, temporal, and chemical resolution into an emission inventory used for photochemical modeling. The resulting, gridded anthropogenic emissions files are then merged with the biogenic emissions file into a single low-level emissions file as the final step prior to input to the UAM. In addition to a low-level emission file, the UAM requires a separate file containing elevated source emission data.[1] Accordingly, EPS 2.0 also generates the ASCII input file for the UAM elevated point source emissions preprocessor, PTSRCE.

As part of the processing by EPS 2.0, an estimated plume rise is calculated by the Briggs effective plume height algorithm using the stack parameters provided on the emissions records and default meteorological conditions. If this estimated value is greater than a user-specified plume height (25 meters for MMS), the point source is flagged for possible elevated treatment. The final vertical allocation of the point source emissions is determined by the UAM.

Emissions data were processed separately through EPS 2.0 for four subregions: (1) Texas, (2) Louisiana, (3) Alabama, Florida, and Mississippi, and (4) the western and central regions of the Gulf of Mexico OCS (see Figure 4-4). These four subregions were defined to facilitate quality control tracking and the incorporation of local data. The nested grid employed by the UAM-V for this study required that gridded emissions be prepared for three different grid resolutions. To accomplish this, the emission inventory for the entire region was first gridded at the smallest resolution, 4 × 4

[1] "Low-level" emissions are emitted into the first layer of the grid. "Elevated" emissions are those point sources with an effective stack height of 25 meters or higher, and these emissions may be released in layers above the surface layer.

kilometers. For the portions of the modeling domain to be modeled at larger grid resolutions, the emissions data were prepared by aggregation of the 4 × 4 km cells to 8 × 8 or 16 × 16 km cells.

Chemical Speciation

Since every reaction of all of the organic species found in an urban atmosphere is not known and cannot be considered, photochemical models generally group pollutants to limit the number of reactions and species to a reasonable level while permitting reasonable accuracy in predicting ozone formation. The UAM employs version IV of the Carbon Bond Mechanism, which classifies each carbon atom in an organic molecule according to its bond type. Accordingly, VOC emissions must be assigned to their respective carbon bond classes prior to model application. The UAM also requires that NO_x emissions be distributed as NO and NO_2.

For this study, the default NO_x speciation (90 percent NO and 10 percent NO_2 by weight) included in the EPS 2.0 carbon-bond split factors file was assumed for all sources. For nearly all regions of the modeling domain, hydrocarbon emissions were assigned to the carbon bond species required by the UAM using speciation profiles developed by the EPA (1991b), carbon bond assignments for each chemical species, and the default speciation profile assignments by source category (Source Classification Code for point sources and AIRS AMS Area Source Category code for area and mobile sources) provided with EPS 2.0. For point sources within the Baton Rouge and Lake Charles domains, LDEQ developed point source-specific chemical speciation profiles that were incorporated into the modeling inventories for this study.

Temporal Allocation

The UAM requires hourly estimates of emissions for each grid cell in the modeling domain in order to accurately predict hourly ozone concentrations. Accordingly, annual average or peak ozone season daily emission rates must be adjusted to reflect the conditions of the ozone episode being modeled, including seasonal adjustments for temperature or activity levels (if baseline emissions are reported as annual averages) as well as adjustments for the day of the week. In addition, emissions must be allocated to each hour of the episode day.

For point sources, the operating schedule data provided in the AIRS AFS workfiles for each source were used to determine the appropriate episodic and diurnal adjustments for each source. The operating schedule information included hours per day, days per week, and hours per year in operation, as well as seasonal fractions of annual throughput. For area and mobile source categories, the default temporal variation profiles by source category provided with EPS 2.0 were used.

Spatial Allocation

To provide spatially resolved estimates of ozone and various other pollutants at the grid cell level, the UAM must be supplied with emission data that have the same degree of spatial resolution (i.e., by grid cell). The amount of effort required to implement this resolution varies depending on the type of source. For point sources, locations for each source (typically reported to within a fraction of a kilometer) can be used to assign emissions to the appropriate grid cells. For this study, this method was used to allocate emissions from both onshore point sources and OCS production platforms, based on the location data included in the AFS workfiles and OPIS database for each source.

By contrast, spatial resolution of emissions reported as county totals (as is usually the case for area sources and motor vehicles) requires substantially more effort. The most common approach for apportioning county-level emissions to grid cells is to use a surrogate indicator for spatial distribution of emission levels or activity (e.g., population, type of land use, or location of major links such as interstate roadways or shipping channels). A spatial allocation surrogate is a quantity whose areal distribution either is known or has been estimated and is assumed to be similar to the areal distribution of emissions from some source category whose spatial distribution is unknown.

For area and mobile sources, this allocation is based on a combination of gridded spatial surrogates and link data. As input, EPS 2.0 requires a gridded spatial allocation surrogate file which includes fractions by grid cell of total county area, population, and land use for each county. EPS 2.0 supports the spatial distribution of emissions by link for those categories for which such data are available and appropriate (e.g., onroad motor vehicles, railroad locomotives, aircraft landings and takeoffs, and shipping vessels). Emissions distributed by a specified link type are apportioned evenly along all the links of a given type within a county based solely on the length of the links.

To prepare the gridded spatial allocation surrogate file for the onshore portion of the domain, gridded land-use data were obtained from the U.S. Geological Survey (DOI, 1990). The land-use database, which has a spatial resolution of approximately 200 by 200 meters, includes data for over 30 land-use categories. The 200 $\times$ 200 m data for each land-use type were aggregated to the 4-km grid resolution of the UAM modeling domain, and the land-use categories in the USGS database were combined to form the 13 spatial surrogate categories. The final gridded spatial allocation surrogate file also contains county/parish area and population gridded surrogates. Population data for 1990 obtained from the Census Bureau (DOC, 1991) were gridded based on the location of the centroid of each census block.

Special spatial allocation factors were also developed to allocate the offshore emissions not directly assigned to a specific platform. These factors include offshore state water area, lease block area, and a lease block "platform density" surrogate based on the number of platforms located within each lease block. For the Baton Rouge SIP modeling domain, gridded VMT data provided by LDEQ were used to spatially allocate onroad mobile emissions.

The locations of OCS crew/supply helicopter airport and platform locations and shipping channels located in Galveston and Harris counties in Texas were electronically digitized for use in spatially allocating emissions from helicopter landings and take-offs and commercial vessels, respectively. Links were also used to allocate emissions from onroad motor vehicle on limited access roadways for the Lake Charles subdomain.

Table 4-5 shows the spatial surrogates used to allocate emissions from each source category. Plots of these surrogates are contained in Appendix O.

Emission Results

UAM modeling emission inventories were generated for the MMS modeling domain for 17-20 August 1993 and 6-11 September 1993, using the data sources and processing methodologies described previously. Table 4-6 summarizes the anthropogenic VOC, NO_x, and CO emissions by subregion and data source for a typical weekday during the August episode. Note that no temporal or spatial variation was assumed between the days for the August episode. Area sources contribute about 29 percent of the total anthropogenic NO_x and 45 percent of the total low-level VOC emissions. About 18 percent of the total anthropogenic NO_x and 19 percent of the total anthropogenic VOC result from onroad motor vehicles.

In the OCS region (subregion IV), the NO_x, VOC, and CO emissions are about 10 percent, 2 percent, and 1 percent of the total emissions in the modeling domain, respectively. The total low-level and elevated sources contribute about the same NO_x emissions to the inventory (approximately 3,700 tons per day for each), while the elevated VOC and CO emissions are much smaller compared to the low-level emissions. Tables 4-7 and 4-8 summarize overall emissions by major source category for each episode day during the August and September modeling inventories. On average, the area, motor vehicle, point, and biogenic sources contribute about 27, 16, 50, and 6 percent of the total NO_x emissions in August, respectively. Total VOC emissions consist of 11, 4, 8, and 77 percent area, motor vehicle, point, and biogenic sources, respectively. Biogenic and onroad mobile emission totals included in the tables have been adjusted to match the levels estimated by TNRCC. Emissions are relatively constant between the two episodes by major source category, except for biogenics.

Figure 4-5 shows the spatial distribution and magnitude of total low-level anthropogenic NO_x, VOC, and CO emissions for the modeling domain. As expected, emissions are concentrated in the urban areas. In the OCS region, higher emissions are seen in the grid cells with the larger platforms. Plots showing the spatial distribution and magnitude of the emissions for the area, mobile, low-level point, and biogenic sources for the domain are presented in Appendix P. Because the spatial distribution of these sources is constant from episode to episode, plots are presented for only one episode day.

Table 4-5. Special and EPS 2.0 default spatial allocation surrogate assignments.

Surrogate	Source Category Description
Onshore	
1 - County Area	Biogenic Sources
	Miscellaneous Sources - Lightning
2 - Population	Lawn & Garden Equipment
	Paved Road Dust
	Architectural Coatings
	Dry Cleaning
	Misc. Non-Industrial Solvent Utilization
	Asphalt Application
	Gasoline Service Stations
	Municipal Landfills
	Publicly Owned Wastewater Treatment Plants
	Misc. Combustion Processes
3 - Residential	Residential Fuel Combustion
	Residential On-Site Incineration & Open Burning
4 - Urban Land	Electric Utilities
	Industrial Fuel Combustion
	Commercial/Institutional Fuel Combustion
	Total Area Source Fuel Combustion
	Highway Vehicles - Gasoline & Diesel (Urban Roads)[a]
	Off-Highway Gasoline & Diesel Vehicles - Construction Equipment
	Paved Road Dust
	Chemical Manufacturing
	Food and Kindred Products
	Primary & Secondary Metal Production
	Mineral Processes
	Petroleum Refining
	Wood Products
	Rubber and Plastics
	Fabricated Metals
	Industrial Processes - Construction
	Machinery
	Mining and Quarrying
	In-Process Fuel Use
	Surface Coating - Solvent Utilization
	Degreasing Operations
	Graphic Arts
	Misc. Industrial Solvent Utilization
	Petroleum Product Storage and Transport

Continued

Table 4-5. Continued.

Surrogate	Source Category Description
Onshore (continued)	
4 - Urban Land (continued)	Organic & Inorganic Chemical Storage and Transport Bulk Materials Storage and Transport On-Site Incineration (Industrial and Commercial) Open Burning (Industrial and Commercial) Waste Disposal and Treatment Facilities Biogenic Sources - Urban Vegetation Misc. Combustion Cooling Towers Catastrophic/Accidental Releases Automotive Repair Shops Misc. Repair Shops Hospitals
5 - Agriculture	Off-Highway Gasoline & Diesel Vehicles - Farm Equipment Pesticide Application Biogenic - Vegetation/Agriculture Agricultural Production - Livestock
6 - Range Land	Oil & Gas Production Biogenic - Grassland/Alpine Meadows
7 - Deciduous Forest	Biogenic - Forests/Oak Forests
8 - Coniferous Forest	Biogenic - Coniferous Forests
9 - Mixed Forest	Biogenic - Non-Oak Forests/Scrubland
10 - Water	Recreational Marine Vessels Miscellaneous - Water
11 - Barren Land	Miscellaneous - Water/Barren
12 - Nonforested Wetlands	Biogenic - Soil/Wetlands
15 - Rural Land	Highway Vehicles - Gasoline & Diesel (Rural Roads)[a] Off-Highway Recreational Vehicles Off-Highway Logging Equipment Off-Highway Industrial Equipment Unpaved Road Dust Geogenic Sources Natural Sources Misc. Combustion Sources (Forest Fires, etc.)
101 - Limited Access Roads	Highway Vehicles - Gasoline & Diesel (Interstates)[a]

Continued

Table 4-5. Concluded.

Surrogate	Source Category Description
Offshore/OCS Region	
6 - Lease Blocks Areas weighted by Platform density	OCS Crew & Supply Aircraft (Cruise Mode) OCS Crew & Supply Boats
10 - Surface Area of Lease Blocks	OCS Barge OCS Commercial Fishing OCS Commercial Shipping OCS Recreational Boating OCS Exploratory Vessels OCS Pipeline Vessels LOOP
11 - State Water Area	State Exploratory Vessels State Commercial Fishing State Crew & Supply Boats State Pipeline Vessels State Military Vessels
103 - Helicopter Links	Helicopter Landing and Take-Offs
104 - River Links	State Commercial Fishing

[a] Link data were used for interstate mobile emissions for Lake Charles. Note that gridded VMT was used for the Baton Rouge mobile emissions. For all of the other mobile emissions in the region, assignment was to either urban or rural land use.

The location and relative magnitude of elevated source NO_x, VOC, and CO emissions are presented in Figure 4-6. As with the low-level anthropogenic sources, the elevated point source emissions are concentrated in urban areas onshore and platform locations offshore. Figure 4-7 shows the spatial distribution and magnitude of the biogenic VOC and NO emissions.

Emission Inventory Uncertainties

A rigorous quantification of emission inventory uncertainty is a substantial undertaking and was not within the scope of this study. The variability of inventory components (point, area, mobile, and biogenic) among geographic areas makes it difficult to form general statements about the uncertainty bounds of a particular inventory. Variability in the physical parameters inputted to the emissions equations and calculational errors are reflected in uncertainty of the inventory assessment of total emissions (Leadbetter and Huang, 1993). The uncertainty of each parameter contributes to the total uncertainty of the emission estimate and inventory. The majority of the available emission factor data (e.g., EPA AP-42 documentation) provide uncertainty calculations related to establishing the factors. However, activity data, unless emission source data are established directly, can contribute an unknown level of uncertainty.

Table 4-6. Baseline 1993 anthropogenic emissions (tons per day) by subregion and data source for the August 1993 episode.*

Source Category	Area			Onroad Mobile			Low-Level Point			Elevated Point		
	NO_x	VOC	CO	NO_x	VOC	CO	NO_x	VOC	CO	NO_x	VOC	CO
Subregion I												
Interim 90	598.5	617.7	1,248	358.6	268.6	2,449	43.1	196.4	10.5	1,116	290.2	313.4
TNRCC	245.2	539.5	1,594	364.5	245.4	2,474	67.4	545.7	22.6	1,115	126.5	476.3
Subtotal	843.7	1,157	2,842	723.1	514.0	4,924	110.5	742.0	33.1	2,231	416.7	789.7
Subregion II												
Interim 90	465.5	362.6	952.7	196.9	155.1	1,418	9.9	37.7	1.4	280.2	18.1	87.5
Baton Rouge	116.9	121.3	371.7	129.1	91.1	737.1	17.5	89.6	23.2	388.5	34.4	283.0
Lake Charles	18.3	21.7	83.7	20.6	13.5	105.0	20.0	57.8	4.5	158.6	17.0	107.8
Subtotal	600.7	505.6	1,408	346.5	259.7	2,260	47.5	185.2	29.0	794.7	69.4	478.4
Subregion III												
Interim 90	269.7	639.5	901.0	232.6	196.9	1,701	2.0	284.6	16.8	430.5	76.4	331.9
Subregion IV												
OCS	413.8	42.6	93.8	—	—	—	140.1	64.6	30.8	189.5	12.6	45.7
Total	2,128	2,345	5,245	1,302	970.6	8,885	300.1	1,276	109.8	3,646	575.1	1,646

* The totals for the OCS portion of the domain are slightly different in this table than those presented in Table 4-1. This is due to the fact that Table 4-1 represents the entire emission inventory and this table represents the gridded modeling inventory. Differences exist because some pieces of lease tracts included in the emission inventory are not included in the modeling inventory.

Table 4-7. 1993 baseline emission totals (tons per day) by major source category for the 17–20 August 1993 modeling episode.

Source Type	17 August			18 August		
	NO_x	VOC	CO	NO_x	VOC	CO
Anthropogenic - Low Level						
Area Sources	2,129	2,345	5,245	2,128	2,345	5,245
Mobile Sources[1]	1,302	970.6	8,885	1,302	970.6	8,885
Low Level Point Sources	300.1	1,276	109.8	300.1	1,276	109.8
Subtotal	3,730	4,592	14,240	3,730	4,592	14,240
Anthropogenic - Elevated						
Elevated Point Sources	3,646	575.1	1,646	3,646	575.1	1,646
Biogenic[1]	442.9	17,081	—	450.0	17,340	—
Total	7,819	22,248	15,885	7,826	22,507	15,885

Source Type	19 August			20 August		
	NO_x	VOC	CO	NO_x	VOC	CO
Anthropogenic - Low Level						
Area Sources	2,128	2,345	5,245	2,128	2,345	5,245
Mobile Sources[1]	1,302	970.6	8,885	1,302	970.6	8,885
Low Level Point Sources	300.1	1,276	109.8	300.1	1,276	109.8
Subtotal	3,730	4,592	14,240	3,730	4,592	14,240
Anthropogenic - Elevated						
Elevated Point Sources	3,646	575.1	1,646	3,646	575.1	1,646
Biogenic[1]	439.3	16,853	—	415.9	15,905	—
Total	7,815	22,020	15,885	7,792	21,072	15,885

[1] The biogenic and onroad mobile emissions in Texas are adjusted to match TNRCC levels.

Table 4-8. 1993 baseline emission totals (tons per day) by major source category for the 6–11 September 1993 modeling episode.

Source Type	6 September			7 September			8 September		
	NO_x	VOC	CO	NO_x	VOC	CO	NO_x	VOC	CO
Anthropogenic - Low Level									
Area Sources	2,086	2,361	5,694	2,086	2,361	5,694	2,086	2,361	5,694
Mobile Sources	1,303	959.1	8,791	1,303	959.1	8,791	1,303	959.1	8,791
Low Level Point Sources	241.4	1,283	96.7	241.4	1,283	96.7	241.4	1283	96.7
Subtotal	3,630	4,603	14,582	3,630	4,603	14,582	3,630	4,603	14,582
Anthropogenic - Elevated									
Elevated Point Sources	3523	576.4	1,662	3,523	576.4	1,662	3,523	576.4	1,662
Biogenic	1,137	9,671	—	1,177	9,442	—	1,183	9,846	—
Total	8,290	14,851	16,243	8,330	14,622	16,243	8,336	15,026	16,243

Source Type	9 September			10 September			11 September		
	NO_x	VOC	CO	NO_x	VOC	CO	NO_x	VOC	CO
Anthropogenic - Low Level									
Area Sources	2,086	2,361	5,694	2,086	2,361	5,694	2,141	2,522	9,094
Mobile Sources	1,303	959.1	8,791	1,303	959.1	8,791	1,303	960.0	8,793
Low Level Point Sources	241.4	1,283	96.7	241.4	1,283	96.7	240.4	1,253	100.4
Subtotal	3,630	4,603	14,582	3,630	4,603	14,582	3,708	4,734	17,988
Anthropogenic - Elevated									
Elevated Point Sources	3,523	576.4	1,662	3,523	576.4	1,662	3,516	567.2	1,657
Biogenic	1,175	10,005	—	1,200	9,894	—	1,145	9,718	—
Total	8,328	15,185	16,243	8,353	15,074	16,243	8,369	15,019	19,645

The emission inventory data incorporated into the final modeling inventory were obtained from five independent sources: (1) survey and emission estimation for OCS sources, (2) the EPA 1990 Interim Inventory for all attainment areas, (3) LDEQ for the Louisiana nonattainment regions, (4) TNRCC for the Houston/Galveston and Beaumont/Port Arthur areas, and (5) UAM-BEIS for biogenic sources (except that LDEQ provided biogenic emissions estimates for the Baton Rouge domain). The fact that the data were obtained from such a variety of sources contributes to the overall uncertainty. Throughout this project, analysis of the inventory and modeling results has provided insight into instances of identifiable uncertainty in the MMS modeling inventory.

OCS Sources. This study gave particular attention to offshore anthropogenic sources, including OCS oil and gas production facilities, crew and supply vessels and helicopters serving OCS facilities, commercial shipping and fishing, recreational boating, intercoastal barge traffic, and other sources located in the adjacent state waters. As a result of the quality assurance and quality control procedures employed in this study, the total OCS emissions decreased by more than two orders of magnitude from the originally estimated values (Steiner et al., 1993). Table 4-9 provides an overview of uncertainties associated with this component of the inventory.

Biogenics. At the time of the development of UAM-BEIS, it was recognized that areas of needed improvement for the biogenic modeling included development of additional emission factors, speciation of unidentified biogenic hydrocarbon compounds, a better understanding of the environmental influences, and an update of the land-use patterns. The uncertainty in biogenic emission estimates prepared with this version of the model has been estimated to be factor of ± 300 percent (Pierce et al., 1990).

Study of the differences between the Texas and MMS BEIS application revealed two elements contributing to the differences in the biogenic NO and VOC. The TNRCC version did not incorporate new soil NO emission fluxes attributed to agricultural practices. The NO estimates generated by BEIS are associated with grasslands and are relatively small, hence the large differences between the two NO_x totals. Differences in land-use data entered into BEIS accounted for the differences in the hydrocarbon emissions.

Fugitive Emissions. Two areas contribute to the uncertainty associated with the inventorying of fugitive emissions: (1) the number of fugitive emission sources within a facility and (2) differences in the methods used to quantify emissions. Experience has shown that facilities underestimate the actual number of fugitive sources by as much as 300–500 times. Additionally, differences in the five quantification methods commonly used to estimate fugitive emission result in varying levels of uncertainty. For instance, estimates using AP-42 "per component" emission factors may yield totals that are over 100 times those determined by monitoring the individual components.

For this study, it was ascertained that the monitoring practices at a certain Baytown refinery resulted in a significant underestimation of the facility's fugitive emissions. This underestimation is suspected to be as much as a factor of 5. In the absence of additional data, the fugitive VOC emissions for this facility were adjusted by that factor.

Table 4-9. Uncertainties associated with the OCS production-related emissions inventory.

Inventory Component	Basis of Uncertainty	Description
Survey	Survey respondent expertise	Different levels of expertise of survey recipients could lead to incorrect or incomplete survey responses because of incorrect interpretation.
	Unknown answers	Some platform equipment is very old and equipment ratings cannot be read, or equipment has been modified and manufacturer's ratings no longer are applicable.
	Incorrect responses	Many problems corrected in the database were a result of incorrect units. Some flow rates in the survey were metered; others were not metered and respondents had to estimate activity levels.
	Data entry	Although we used a double data entry system to minimize typographical and data omission errors, some may have occurred. Some respondents had their survey responses typed onto forms; this could also lead to data entry errors.
	Omitted sources	15 percent of the companies operating platforms in the Gulf that were contacted did not return surveys. Some of them may have multiple platforms. All major corporations operating in the Gulf returned surveys. Some emissions sources (e.g., equipment) on the platforms may have been inadvertently omitted. 6 percent of the helicopter companies (the smaller companies) contacted did not return the survey. 26 percent of the vessel companies contacted did not return the survey. The companies that did not return the surveys conduct the smaller operations.
Emissions Methodology	Emission factors	Emission factors represent an average population. Gulf population may not be representative of the emission factor mix.
	Fugitive emissions	Used empirical formula derived from Pacific OCS facilities. Gulf OCS platforms are not configured exactly the same as those in Pacific and the product mix may be different.
	Applicability/ usage	Even though methodologies were reviewed for applicability, it is possible that more applicable emissions methodologies exist or that the methodology was applied incorrectly because of an incorrect assumption.

Day-Specific Emissions. Ideally, day-specific emissions for all sources should be entered into the model to best represent the existing conditions. The effort to procure these emissions is costly and primarily limited to major point sources or modeled emissions such as onroad mobile and biogenic sources. While the uncertainty of the modeled emissions may be quantified, the final results are dependent upon the preciseness of the user-supplied inputs or the accuracy of the recorded data, as is the case with major point sources.

Emission Events. Events can be characterized by a number of activities which release unexpected emissions to the atmosphere. These may result from upset conditions, special events, or uninventoried sources. An in-depth investigation of the August 1993 episode indicated that a suspected hydrocarbon release near the turning basin of the shipping channel occurred at midday on 19 August. This event was simulated by assuming that about 15,000 gallons of gasoline was introduced into the channel between 10 a.m. and 1 p.m. A search of upset records by TNRCC indicated that an incident did occur at the location; however, the time of occurrence and magnitude were not available.

Uninventoried sources may also be classified as events. These are activities which regularly occur and which result in emissions but for one reason or another have not been included in the inventory. One emission source not included in the inventory for the MMS domain are the lightering activities that occur in the Gulf outside of the main harbors. Based on proposed regulations and estimated petroleum product transfer, these emissions may account for 8.3 to 21.6 tons VOC per day, not including emissions associated with the propulsion of the vessels.

Temporal Allocation. Processing of emissions for modeling requires temporal, spatial, and chemical allocation of the input pollutant data. Temporal allocation data, while often available for point source stack emissions, are typically based on national averages or engineering judgment. Activities which can occur at all times are typically assigned a flat temporal profile. That is, the activity is assumed to occur evenly for each month, each day of the week and 24 hours of the day. Generally, first-hand exposure to these activities indicates that they often occur sporadically and exhibit periods of no activity at all. The modeling process simulates an artificially even level of emissions from such a source rather than a peaking pattern which may be more realistic. Within the MMS domain, the commercial shipping emissions are suspected to incorporate this temporal uncertainty. The uncertainty associated with this source may be reduced in the future by obtaining shipping activity information from the port authorities.

METEOROLOGICAL INPUTS

Methodology

Introduction

The Systems Applications International Mesoscale Model (SAIMM) (Kessler and Douglas, 1992) was used in this study to generate meteorological input fields for the

application of the UAM-V for the GMAQS study area. The SAIMM is a prognostic meteorological model; that is, beginning with a set of initial conditions that represent the state of the atmosphere at the initial simulation time, the model simulates the response of the atmosphere to differential surface heating and terrain irregularities and thus provides information on the development and evolution of mesoscale meteorological features within the modeling domain. Observed meteorological data are incorporated into the SAIMM using a four-dimensional data assimilation (FDDA) procedure. The model produces hourly, three-dimensional fields of several meteorological variables including wind, temperature, specific humidity, pressure, planetary-boundary-layer height, and vertical turbulent exchange coefficients.

The SAIMM was used for this study to accommodate (1) the lack of sufficient data to properly characterize, using interpolative and diagnostic techniques, the meteorology within the modeling domain and (2) the input requirements of the UAM-V (three-dimensional fields of wind, temperature, water-vapor concentration, pressure, and vertical diffusivities). The SAIMM has the attributes necessary to simulate the gulf/land breeze circulations that characterize the Gulf Coast area, and the assimilation of observed data using the FDDA procedure allows the simulation of day-specific meteorological features.

The application of the SAIMM to the GMAQS study area is described in this section, which includes an overview of the SAIMM and a summary of the application procedures and modeling results for 17–20 August and 6–11 September 1993.

Overview of the SAIMM

The SAIMM is a hydrostatic, incompressible, primitive-equation, prognostic meteorological model designed to simulate the mesoscale airflows generated by differential heating of the earth's surface and terrain irregularities. The SAIMM is an enhanced version of the Colorado State University Mesoscale Model (CSUMM). The basic model formulation is given by Mahrer and Pielke (1977); the numerical advection scheme (upstream interpolation of cubic splines) is described by Mahrer and Pielke (1978).

The SAIMM is formulated in the terrain-following coordinate $z^* = s(z - z_G)/(s - z_G)$, where z is height above sea level, z_G is terrain height, and s is fixed height of the model top. This model includes a surface heat budget and relatively detailed treatments of the atmospheric surface and planetary boundary layers. Vertical exchange coefficients are based on predicted turbulent kinetic energy, as described by Ulrickson and Mass (1990).

The SAIMM is particularly well suited to the study of thermally forced mountain-valley airflow patterns, urban heat-island effects, and sea-breeze circulations with horizontal scales of 10 to 300 km. It has been used to generate meteorological inputs for air quality modeling of California's San Joaquin Valley (Morris et al., 1990), South Central Coast Air Basin (Kessler and Douglas, 1991), South Coast Air Basin (Douglas et al., 1992), and Sacramento Valley (Douglas, Shepard, and Haney, 1993), as well as the Texas–Louisiana Gulf Coast (Douglas, Lolk, and Mitsutomi, 1993).

The SAIMM requires external input of gridded terrain data (topographic heights, land and water coverage) and initial profiles of temperature and specific humidity. The SAIMM supports FDDA, a procedure by which observational data are incorporated into the prognostic model simulation using the Newtonian relaxation or "nudging" technique (Stauffer and Seaman, 1990; Stauffer et al., 1991). Using this methodology, one or more of the time-dependent variables are relaxed or "nudged" toward observed values during the course of the simulation. The nudging is effected by the addition of artificial tendency terms to the prognostic model equations. The general form of the prognostic equation for a variable a is

$$\frac{\partial a}{\partial t} = F(a, x, t) + G \times w_t \times w_{xyz} \times (a' - a)$$

The first term on the right-hand side of this equation, F, represents all of the model's physical processes. The second term is the nudging term. G determines the relative weight of the nudging term with respect to the model's physical processes. Typical values of G are 10^{-3} s^{-1} for strong nudging and 10^{-4} s^{-1} for moderate nudging. The variables w_t and w_{xyz} are temporal and spatial weighting functions, respectively, and the quantity a' represents the observed value.

Incorporation of observational data into the prognostic model simulation using FDDA should improve the agreement between the observations and the prognostic model results. The influence of the data may be propagated throughout the simulation and thus may also improve the simulated fields in areas removed from observations.

Application of the SAIMM to the Texas–Louisiana Gulf Coast Region

A nested-grid approach was used for the SAIMM application. The modeling domain (Figure 4-8) consists of a coarse-resolution outer domain and a fine-resolution inner domain that encompasses the Houston metropolitan area, Galveston Bay, and the Beaumont–Port Arthur area. (The modeling domain used for the application of the SAIMM was similar to that used for the UAM-V except that the origins of the SAIMM domains were shifted one-half grid cell such that the SAIMM grid points coincide with the UAM grid-cell centers.) The origin of the SAIMM coarse-grid domain is 8 Easting and 2808 Northing and the domain consists of 72 grid cells in the west-east direction and 50 grid cells in the south-north direction. The origin of the fine-grid domain is 206 Easting and 3182 Northing and consists of 62 grid cells in the west-east direction and 54 grid cells in the south-north direction. Both domains were specified in zone 15 UTM coordinates. The horizontal resolution is 16 km for the outer (coarse) grid and 4 km for the inner (fine) grid. Based on analysis of the observed wind profiles, 18 vertical levels were used. Table 4-10 summarizes the vertical resolution.

Several test applications of the SAIMM were performed for the coarse-grid domain to establish the most appropriate set of input parameters and modeling procedures. For the

Table 4-10. Vertical structure of the SAIMM modeling domain for application to the GMAQS study area.

Level	Height (m agl)	Level	Height (m agl)
1	25	10	1500
2	50	11	1850
3	100	12	2600
4	200	13	3400
5	300	14	4200
6	450	15	5000
7	675	16	6000
8	900	17	7000
9	1200	18	8000

test applications, the SAIMM was exercised for the 29 July 1988 ozone episode day using episode-specific temperature and humidity profiles. In the first application, the SAIMM was exercised without the FDDA option to test the model's response to initial conditions, boundary conditions, and input parameters. This simulation also served as a basis for evaluation of the consequent FDDA simulations (i.e., to test whether the observations were successfully assimilated). Subsequent simulations tested the sensitivity of the SAIMM to specification of (1) the various FDDA parameters, (2) sea-surface temperature (SST), and (3) variable surface characteristics (e.g., roughness length or soil moisture availability). Changing the SST from 25°C (77°F) to 28.8°C (84°F) resulted in only minor changes in the wind fields. However, use of the variable surface characteristics option significantly improved the simulation of the gulf breeze along the Louisiana Gulf Coast because specification of surface characteristics corresponding to coastal wetlands mitigated the onshore flow. The SAIMM also allows for the specification of time-varying boundary conditions and large-scale (geostrophic) forcing. Both of these simulation options facilitate the incorporation of large-scale information about synoptic-scale meteorological gradients that influence the mesoscale airflows inside the SAIMM domain. For larger, regional-scale domains such as the GMAQS domain, using the FDDA option to assimilate upper-air data is frequently sufficient to capture the large-scale gradients. Following analysis of the test simulation results, it was determined that simulation of the Texas-Louisiana Gulf Coast area should include zero geostrophic forcing, FDDA, variable surface characteristics, and zero-gradient boundary conditions.

Application of the SAIMM to the Texas-Louisiana Gulf Coast area for the 1993 ozone episodes included (1) specification of the SAIMM input parameters, (2) preprocessing of the surface and upper-air meteorological data, (3) preparation of the FDDA analyses, (4) exercise of the SAIMM, and (5) graphical analysis of the results. Input parameters include albedo, soil diffusivity, soil density, soil specific heat, soil moisture availability,

roughness length, SST, and time step. The albedo, soil parameters, and roughness length were specified according to the dominant land-use category for each grid cell and were based on surface characteristics described by Sailor, Douglas, and Kessler (1992); SST was based on buoy data, and the time step was determined based on maximum wind speeds and grid resolution. Table 4-11 summarizes the land-use categories and the corresponding surface parameters, and other input parameters are listed in Table 4-12. Note that the surface characteristics vary with land use and distinguish between land-use differences, for example, between the coastal areas of Louisiana and Texas. SST was estimated using episode-specific buoy data but, as noted earlier, the effects of small changes in this parameter are expected to be quite small.

Table 4-11. Land-use categories and surface characteristics used in the application of the SAIMM to the Texas–Louisiana Gulf Coast region.

Land-Use Category	Albedo	Roughness Length (cm)	Soil Moisture Availability Parameter	Soil Density ($g\ cm^{-3}$)	Soil Thermal Diffusivity ($cm^2\ s^{-1}$)	Soil Specific Heat ($g^{-1}\ K^{-1}$)
Urban	0.18	40	0.15	1.5	0.0028	0.24
Agricultural	0.20	10	0.50	2.4	0.0038	0.44
Range	0.20	5	0.30	2.0	0.0050	0.40
Deciduous forest	0.18	125	0.25	2.0	0.0057	0.35
Coniferous forest (including wetland)	0.18	125	0.25	2.0	0.0057	0.35
Mixed forest	0.18	125	0.25	2.0	0.0057	0.35
Water	0.20	5	0.50	1.8	0.0050	0.25
Barren land	0.30	5	0.03	2.0	0.0050	0.30
Nonforest wetland	0.20	10	0.50	2.4	0.0038	0.44
Mixed agricultural/ range	0.20	10	0.40	2.2	0.0044	0.44
Rocky/low shrub	0.20	50	0.10	2.0	0.0050	0.30

Meteorological data from several sources were used to prepare gridded fields for data assimilation and for evaluation of the meteorological fields. Wind, temperature, and humidity data collected by STI and ESE during the 1993 GMAQS field study were archived and quality-assured by SAI. This database was supplemented with data acquired from Desert Research Institute (DRI) and collected during the COAST and HRM field programs. In addition, data were acquired from several routine monitoring or special study networks including (1) the TNRCC, (2) the Southeast Texas Regional Planning Commission (SETRPC), (3) the LDEQ, (4) the Texas–Louisiana Shelf Circulation Program (LATEX), and (5) the National Climatic Data Center (NCDC).

Table 4-12. Input parameters for application of the SAIMM to the Texas–Louisiana Gulf Coast region.

Parameter	Coarse Grid (16 km)	Fine Grid (4 km)
Time step (s)	120	60
Horizontal filter coefficient	0.05	0.05
Vertical filter coefficient	0.0	0.0
Sea surface temperature (°C):		
17–20 August 1993	30.8	30.8
6–11 September 1993	29.8	29.8
Nudging coefficients (s^{-1}):		
Wind	5×10^{-4}	10^{-3}
Temperature/humidity	10^{-4}	10^{-4}

Locations of surface and upper-air meteorological monitoring sites within the SAIMM modeling domain are plotted in Figure 4-9a and listed in Table 4-13.

Preparation (preprocessing) of the meteorological data for FDDA includes temporal interpolation of the data to the assimilation time interval (hourly) and vertical interpolation of the upper-air wind, temperature, and humidity data to the SAIMM levels. A temporal influence range of 3 hours was used for the surface wind data and 12 hours was used for the upper-air data. The surface temperature and humidity data were not used in the FDDA procedure as these may result in erroneous unstable lapse rates near the surface when the observed surface temperatures are warmer than the simulated surface temperatures. The interpolated data were plotted and examined for spatial and temporal consistency. Questionable data were eliminated from the data files.

Although the raw meteorological data from the COAST and GMAQS field studies were processed and quality-assured as part of the data collection and archival programs, some additional quality assurance was performed before the data could be reliably used for data assimilation. The upper-air data were plotted and examined subjectively for spatial consistency following the vertical and temporal interpolation to the SAIMM vertical layer heights. For each hour, wind profiles for all the upper-air monitoring sites were plotted on a single page to facilitate the comparison of wind observations from different but sometimes collocated instruments. Wind observations that appeared to be incoherent in the vertical direction and inconsistent with nearby observations were omitted. Many of the rejected data points consisted of SODAR wind measurements near the upper range of the instrument, which after interpolation to the SAIMM layers occurred most frequently at 300 m or 450 m, corresponding to SAIMM levels 5 and 6.

Table 4-13. Meteorological surface and upper-air sites used in the application of the SAIMM to the Texas–Louisiana Gulf Coast region.

Site ID	UTM-easting (km)	UTM-northing (km)	Latitude	Longitude	Site Name	Source
Surface Sites:						
ACT	99.9	3505.5	31.62	97.22	Waco, TX	NCDC
ALI	3.5	3077.7	27.73	98.03	Alice, TX	NCDC
AUS	47.7	3359.4	30.29	97.70	Austin, TX	NCDC
BRO	55.7	2872.0	25.90	97.43	Brownsville, TX	NCDC
BSM	50.6	3351.8	30.22	97.67	Bergstrom, TX	NCDC
CEW	1121.0	3423.4	30.78	86.52	Crestview, FL	NCDC
CLL	177.1	3388.6	30.58	96.37	College Station, TX	NCDC
EFD	290.2	3278.1	29.62	95.17	Ellington, TX	NCDC
ESF	566.6	3472.1	31.38	92.30	Alexandria, LA	NCDC
GGG	344.7	3580.2	32.35	94.65	Longview, TX	NCDC
GLS	318.6	3238.8	29.27	94.87	Galveston (Scholes Field), TX	NCDC
GPT	878.0	3369.5	30.40	89.07	Gulfport, MS	NCDC
GRK	38.6	3446.9	31.07	97.83	Robert Gray AAF, TX	NCDC
HOU	279.0	3282.0	29.65	95.28	Houston/Hobby Airport, TX	NCDC
HRL	33.6	2909.8	26.23	97.67	Harlingen, TX	NCDC
HURL	1143.6	3395.0	30.52	86.30	Hurlbert Field, FL	NCDC
HUM	726.1	3272.9	29.57	90.67	Houma, LA	NCDC
JAN	774.6	3579.1	32.32	90.08	Jackson, MA	NCDC
LFK	333.3	3456.6	31.23	94.75	Lufkin, TX	NCDC
LFT	596.3	3341.2	30.20	92.00	Lafayette, LA	NCDC
MCB	741.4	3452.5	31.18	90.47	McComb, TX	NCDC
MEI	900.1	3585.1	32.33	88.75	Meridian, MS	NCDC
MGM	1122.0	3592.7	32.30	86.40	Montgomery, AL	NCDC
MXF	1124.5	3602.2	32.38	86.37	Maxwell AFB, AL	NCDC
NBG	788.3	3303.9	29.83	90.03	New Orleans NAS, LA	NCDC
NEW	786.1	3326.0	30.03	90.03	Lakefront Airport, LA	NCDC
NGP	77.5	3071.2	27.70	97.28	Corpus Christi, TX	NCDC
NPA	1046.7	3371.1	30.35	87.32	Pensacola, FL	NCDC
NQI	23.9	3050.9	27.50	97.82	Kingsville NAS, TX	NCDC
WHIT	1073.4	3413.4	30.72	87.02	Milton NAS, TX	NCDC
PNS	1057.2	3384.7	30.47	87.20	Pensacola FSS, FL	NCDC
POE	482.5	3435.0	31.05	93.18	Ft. Polk AFB, LA	NCDC
RND	0.0	3278.6	29.53	98.28	Randolph AFB, TX	NCDC

Continued

Table 4-13. Continued.

Site ID	UTM-easting (km)	UTM-northing (km)	Latitude	Longitude	Site Name	Source
SEP	11.3	3576.1	32.22	98.18	Stephenville, TX	NCDC
SHV	423.2	3592.3	32.47	93.82	Shreveport, LA	NCDC
TYR	274.2	3583.4	32.37	95.40	Tyler, TX	NCDC
VPS	1121.3	3390.0	30.48	86.52	Eglin AFB, FL	NCDC
5R0	426.4	3121.2	28.22	93.75	Hugh Island Platform A323	NCDC
7R3	683.8	3286.9	29.67	91.10	Amelia, LA	NCDC
7R5	471.0	3294.6	29.78	93.30	Cameron, LA	NCDC
9F2	772.5	3222.1	29.10	90.20	Fourchon, LA	NCDC
AXO	796.4	3241.2	29.27	89.95	Grand Isle, LA	NCDC
7R4	583.8	3294.9	29.78	92.13	Intracoastal City, LA	NCDC
7R1	853.0	3246.5	29.30	89.37	Venice, LA	NCDC
RKP	103.5	3112.8	28.08	97.03	Rockport, TX	NCDC
RPE	408.1	3285.7	29.60	93.95	Sabine Pass, TX	NCDC
LBX	264.9	3228.7	29.17	95.42	Brazoria City Airport, TX	NCDC
KEES	892.3	3371.9	30.42	88.92	Keesler AFB, MS	NCDC
ARA	607.7	3322.8	30.03	91.88	New Iberia, LA	NCDC
CILC	485.6	3341.9	30.21	93.15	Lake Charles (Chennault), LA	NCDC
A511	363.5	3112.3	28.13	94.40	High Island Platform A511	NCDC
7R8	599.7	3130.6	28.30	91.98	South Marsh Platform 130	NCDC
W556	500.2	3131.4	28.31	93.00	West Cameron, LA	NCDC
H18	918.6	3226.5	29.10	88.70	South Pass Platform 62A	NCDC
S58	724.9	3115.7	28.15	90.72	South Timbalier Platform 300A	NCDC
7W2	548.9	3153.6	28.51	92.50	Vermilion Platform 265	NCDC
H01Z	281.8	3289.1	29.71	95.26	HRM Site 1, TX	TNRCC
H03Z	289.1	3294.6	29.77	95.18	HRM Site 3, TX	TNRCC
H04Z	295.1	3303.8	29.85	95.12	HRM Site 4, TX	TNRCC
H07Z	305.0	3294.7	29.77	95.02	HRM Site 7, TX	TNRCC
H08Z	300.9	3281.1	29.65	95.06	HRM Site 8, TX	TNRCC
H10Z	314.4	3306.7	29.88	94.92	HRM Site 10, TX	TNRCC
H11Z	315.3	3294.2	29.77	94.91	HRM Site 11, TX	TNRCC
AVAT	309.4	3250.9	29.37	94.96	Avenue A, TX	TNRCC
34ST	311.2	3253.9	29.40	94.95	34th Street, TX	TNRCC
SWLT	316.8	3252.8	29.39	94.89	Seawall, TX	TNRCC
ME5T	314.0	3251.2	29.38	94.91	MET 5, TX	TNRCC
MOBT	316.8	3252.8	29.39	94.89	Mobile, TX	TNRCC
S40S	413.2	3287.7	29.72	93.89	SETRPC Site 40, TX	TNRCC

Continued

Table 4-13. Continued.

Site ID	UTM-easting (km)	UTM-northing (km)	Latitude	Longitude	Site Name	Source
S41S	425.9	3327.2	30.07	93.77	SETRPC Site 41, TX	TNRCC
S42S	416.0	3338.9	30.18	93.87	SETRPC Site 42, TX	TNRCC
S43S	403.1	3312.0	29.94	94.00	SETRPC Site 43, TX	TNRCC
BLOG	119.2	3174.3	28.64	96.89	Bloomington, TX	TNRCC
PCOG	152.8	3181.1	28.71	96.55	Point Comfort, TX	TNRCC
SDRG	135.3	3148.8	28.42	96.72	Sea Drift, TX	TNRCC
VICG	118.9	3185.8	28.74	96.90	Victoria, TX	TNRCC
LAX1	706.7	3087.7	27.90	90.90	Shell Bullwinkle Platform	LATEX
LAX2	303.1	3087.6	27.90	95.00	Buoy 42019	LATEX
LAX3	600.6	3230.0	29.19	91.96	Buoy 42026	LATEX
LAX4	594.3	3148.9	28.46	92.03	Buoy 42027	LATEX
LAX5	396.6	3237.1	29.26	94.06	Buoy 42028	LATEX
LAX6	394.7	3190.3	28.83	94.08	Buoy 42029	LATEX
LAX7	406.3	3136.9	28.35	93.96	Buoy 42030	LATEX
LAX8	301.4	3196.3	28.88	95.04	Buoy 42031	LATEX
LAX9	699.1	3187.4	28.80	90.96	Buoy 42033	LATEX
LX10	152.6	2991.1	27.00	96.50	Buoy 42020	NCDC
LX11	363.9	3230.8	29.20	94.40	Buoy 42035	NCDC
BUO1	835.3	2871.8	25.93	89.65	Buoy 42001	NCDC
BUO2	443.3	2863.4	25.89	93.57	Buoy 42002	NCDC
BUO3	1210.6	2887.7	25.94	85.91	Buoy 42003	NCDC
BUO4	907.8	3336.1	30.09	88.77	Buoy 42007	NCDC
BURL	848.3	3202.5	28.91	89.43	Southwest Pass C-MAN, LA	NCDC
CSBF	1240.7	3306.7	29.67	85.36	Cape San Blas C-MAN, FL	NCDC
DPIA	974.3	3356.4	30.25	88.07	Uphine Island C-MAN, AL	NCDC
GDIL	796.4	3240.5	29.27	89.96	Grand Isle C-MAN, LA	NCDC
PTAT	100.9	3084.5	27.83	97.05	Port Aransas C-MAN, TX	NCDC
SMKF	1709.1	2776.1	24.63	81.11	Sombrero C-MAN, FL	NCDC
SRST	398.4	3282.5	29.67	94.05	Sabine C-MAN, TX	NCDC
VENF	1549.6	3038.3	27.07	82.45	Venice C-MAN, FL	NCDC
LKCH	479.2	3331.5	30.12	93.22	Lake Charles, LA	NCDC
VCT	117.9	3197.5	28.85	96.92	Victoria, TX	NCDC
MSY	765.3	3319.9	29.98	90.25	New Orleans, LA	NCDC
BPT	401.9	3313.5	29.95	94.02	Port Arthur, TX	NCDC
CORP	56.3	3079.2	27.77	97.50	Corpus Christi (International), TX	NCDC

Continued

Table 4-13. Continued.

Site ID	UTM-easting (km)	UTM-northing (km)	Latitude	Longitude	Site Name	Source
IAH	273.2	3317.2	29.97	95.35	Houston, TX	NCDC
MOB	955.2	3403.9	30.68	88.25	Mobile, AL	NCDC
BTR	679.1	3378.8	30.53	91.13	Baton Rouge, LA	NCDC
GAL	312.7	3235.0	29.23	94.93	Galveston (RWP), TX	GMAQS
HIP	383.7	3225.4	29.15	94.20	Texaco's High Island 199 Platform (RWP)	GMAQS
LSU	675.1	3359.9	30.36	91.18	Louisiana State University (RWP), LA	GMAQS
SEH	277.9	3281.8	29.65	95.30	Southeast Houston (RWP), TX	GMAQS
SSP	675.4	3164.7	28.60	91.21	Arco's Ship Shoal 178A Platform (RWP)	GMAQS
GILC	358.5	3266.6	29.52	94.46	Gilchrist, TX	GMAQS
COC	728.0	3238.1	29.25	90.65	Cocodrie (RWP), LA	GMAQS
TN1	282.3	3290.8	29.73	95.25	Clinton, TX	TNRCC
TN2	272.7	3293.2	29.75	95.35	Crawford, TX	TNRCC
TN3	279.6	3299.7	29.81	95.28	N. Wayside, TX	TNRCC
TN4	260.4	3302.3	29.83	95.48	Lang, TX	TNRCC
TN5	261.8	3277.9	29.61	95.46	Croquet, TX	TNRCC
TN6	281.2	3278.6	29.62	95.26	Swiss & Monroe, TX	TNRCC
TN7	286.3	3294.1	29.76	95.21	East C01, TX	TNRCC
TN8	397.8	3322.4	30.03	94.06	Beaumont C02, TX	TNRCC
TN9	63.2	3077.2	27.75	97.43	West C04, TX	TNRCC
TN10	275.9	3305.3	29.86	95.32	Aldine C08, TX	TNRCC
TN11	427.7	3324.4	30.05	93.75	West Orange C09, TX	TNRCC
TN12	312.7	3251.5	29.38	94.93	Texas City C10, TX	TNRCC
TN13	268.1	3210.1	29.00	95.38	Clute C11, TX	TNRCC
TN14	295.8	3282.8	29.66	95.11	Deer Park C18, TX	TNRCC
TN15	51.6	3086.5	27.83	97.55	Tulosa C21, TX	TNRCC
TN16	306.6	3293.7	29.76	95.00	Baytown C24, TX	TNRCC
TN17	243.5	3324.9	30.03	95.66	NW Harris C26, TX	TNRCC
TN18	375.1	3359.2	30.36	94.30	Kountze C85, TX	TNRCC
TN19	109.6	3195.6	28.83	97.00	Victoria, TX	TNRCC
TN20	279.3	3288.2	29.71	95.28	Manchester C22, TX	TNRCC
TN21	338.9	3583.9	32.38	94.71	Longview C19, TX	TNRCC
TN22	404.6	3307.2	29.89	93.99	Port Arthur C28, TX	TNRCC
CRSC	299.9	3315.0	29.95	95.07	Crosby, TX	COAST
GALC	319.6	3238.4	29.26	94.86	Galveston (SODAR), TX	COAST

Continued

Table 4-13. Concluded.

Site ID	UTM-easting (km)	UTM-northing (km)	Latitude	Longitude	Site Name	Source
GLRC	261.8	3290.3	29.72	95.46	Galleria, TX	COAST
SBRC	304.6	3272.9	29.57	95.02	Seabrook C20, TX	COAST
STWC	364.0	3296.5	29.39	94.92	Stowell (Winnie), TX	COAST
SPTC	329.7	3268.3	29.53	94.76	Smith Point, TX	COAST
Upper-Air Sites:						
GAL	312.7	3235.0	29.23	94.93	Galveston (RWP), TX	GMAQS
HIP	383.7	3225.4	29.15	94.20	Texaco's High Island 120 A Platform (RWP)	GMAQS
LSU	675.1	3359.9	30.36	91.18	Louisiana State University (RWP), LA	GMAQS
SEH	277.9	3281.8	29.65	95.30	Southeast Houston (RWP), TX	GMAQS
SSP	675.4	3164.7	28.60	91.21	Arco's Ship Shoal Platform 178A (RWP)	GMAQS
JCA	401.6	3314.4	29.96	94.02	Jefferson County Airport (RWP), TX	GMAQS
COC	728.0	3238.2	29.25	90.65	Cocodrie (RWP), LA	GMAQS
GALC	319.6	3238.4	29.26	94.86	Galveston (SODAR), TX	COAST
JCS	401.7	3314.5	29.93	93.01	Jefferson County Airport (SODAR), TX	COAST
NHS	254.5	3315.6	29.94	95.53	Northwest Houston (SODAR), TX	COAST
SPS	409.4	3286.0	29.71	93.93	Sabine Pass (SODAR), TX	COAST
LKCH	478.8	3331.9	30.12	93.22	Lake Charles (Radiosonde), LA	NCDC
CORP	56.3	3078.6	27.77	97.5	Corpus Christi (Radiosonde), TX	NCDC
SLID	806.6	3361.7	30.35	89.82	Slidell (Radiosonde), LA	NCDC
GAR	486.1	3070.4	27.76	93.14	Chevron's Garden Banks 236A Platform (Radiosonde)	GMAQS

Upper-air virtual temperature data measured by Radio Acoustic Sounding Systems (RASS) located at the six MMS upper-air monitoring sites (see Table 4-13) were converted to air temperature using surface humidity and temperature data. For each of the RASS monitoring sites, the surface virtual temperature was calculated. The difference between the virtual temperature and the observed air temperature, estimated using the surface data, was then assumed to apply throughout the mixed layer. The vertical extent of the virtual temperature data was limited (up to 800–2300 m) and, thus, the conversion was applied at all levels for all hours. As indicated by Tables 4-14 through 4-16, comparison of the derived upper-air temperatures with those observed by NWS radiosondes indicate reasonable agreement.

Table 4-14a. Comparison of observed and estimated air temperature using observed virtual temperature profiles and surface temperature and humidity data for 19 August 1993: Slidell, LA NWS (observed) and Louisiana State University, LA RASS site (estimated).

SAIMM Levels (m)	Slidell		Louisiana State University	
	0600 CST	1800 CST	0600 CST	1800 CST
37.5	26.6	30.5	—	—
75.0	27.2	30.3	—	—
150.0	27.9	30.1	26.0	31.3
250.0	27.6	30.0	25.7	30.9
375.0	27.2	29.0	25.5	29.8
562.5	26.6	27.6	26.0	27.9
787.5	25.0	25.9	25.6	26.0
1050.0	23.1	24.2	—	23.4
1350.0	21.0	21.7	—	21.2
1675.0	19.1	19.4	—	18.3
2225.0	15.9	16.2	—	15.3

Table 4-14b. Comparison of observed and estimated air temperature using observed virtual temperature profiles and surface temperature and humidity data for 19 August 1993: Lake Charles, LA NWS (observed) and Jefferson County Airport, TX RASS site (estimated).

SAIMM Levels (m)	Lake Charles		Jefferson County Airport	
	0600 CST	1800 CST	0600 CST	1800 CST
37.5	26.2	33.1	—	—
75.0	26.3	32.6	—	—
150.0	26.4	31.6	26.3	29.7
250.0	26.6	30.7	26.2	29.1
375.0	26.3	29.6	26.1	28.6
562.5	24.8	28.0	24.8	27.4
787.5	24.5	26.1	23.0	25.5
1050.0	22.6	23.9	21.3	23.5
1350.0	20.9	21.5	—	21.1
1675.0	18.7	19.2	—	18.2
2225.0	15.5	16.4	—	—

Table 4-14c. Comparison of observed and estimated air temperature using observed virtual temperature profiles and surface temperature and humidity data for 19 August 1993: Garden Banks radiosonde (observed) and High Island Platform RASS site (estimated).

SAIMM Levels (m)	Garden Banks		High Island Platform	
	0600 CST	1800 CST	0600 CST	1800 CST
37.5	28.3	29.4	—	—
75.0	28.0	29.0	26.4	—
150.0	27.3	28.3	26.4	—
250.0	26.3	27.3	26.3	27.1
375.0	25.2	26.2	25.4	26.4
562.5	23.4	24.4	23.8	25.3
787.5	23.4	22.3	22.1	24.0
1050.0	21.5	20.5	20.9	22.3
1350.0	19.8	18.7	19.1	20.6
1675.0	17.9	16.8	18.2	—
2225.0	12.6	13.0	—	—

Table 4-15a. Comparison of observed and estimated air temperature using observed virtual temperature profiles and surface temperature and humidity data for 8 September 1993: Slidell, LA NWS (observed) and Louisiana State University, LA RASS site (estimated).

SAIMM Levels (m)	Slidell		Louisiana State University	
	0600 CST	1800 CST	0600 CST	1800 CST
37.5	21.5	27.8	—	—
75.0	21.2	27.6	—	—
150.0	22.2	26.9	23.9	28.4
250.0	22.6	26.0	24.3	27.8
375.0	21.9	24.8	23.3	26.8
562.5	20.8	23.4	21.9	24.9
787.5	19.5	22.1	20.3	22.9
1050.0	19.0	20.7	19.2	20.5
1350.0	17.7	19.4	18.1	18.3
1675.0	17.7	17.4	14.6	16.1
2225.0	13.1	13.8	12.6	13.2

Table 4-15b. Comparison of observed and estimated air temperature using observed virtual temperature profiles and surface temperature and humidity data for 8 September 1993: Lake Charles, LA NWS (observed) and Jefferson County Airport, TX RASS site (estimated).

SAIMM Levels (m)	Lake Charles		Jefferson County Airport	
	0600 CST	1800 CST	0600 CST	1800 CST
37.5	23.3	31.7	—	—
75.0	24.5	31.2	—	—
150.0	25.8	30.5	26.0	27.2
250.0	25.8	29.7	25.7	26.8
375.0	25.1	28.5	24.9	26.5
562.5	23.7	26.8	23.4	25.4
787.5	22.3	24.6	21.8	23.5
1050.0	20.5	22.3	19.4	21.6
1350.0	18.0	19.5	16.8	18.9
1675.0	15.8	16.7	14.5	16.0
2225.0	15.8	13.1	13.7	13.2

Table 4-16a. Comparison of observed and estimated air temperature using observed virtual temperature profiles and surface temperature and humidity data for 9 September 1993: Slidell, LA NWS (observed) and Louisiana State University, LA RASS site (estimated).

SAIMM Levels (m)	Slidell		Louisiana State University	
	0600 CST	1800 CST	0600 CST	1800 CST
37.5	23.9	29.6	—	—
75.0	25.4	29.4	—	—
150.0	25.6	28.9	24.8	28.9
250.0	24.8	28.3	26.0	28.3
375.0	23.8	27.5	25.1	27.3
562.5	22.6	25.9	23.8	25.6
787.5	21.7	23.6	22.7	23.5
1050.0	20.0	21.8	—	21.2
1350.0	18.2	19.7	—	18.6
1675.0	16.6	17.3	—	15.8
2225.0	13.3	13.3	—	—

Table 4-16b. Comparison of observed and estimated air temperature using observed virtual temperature profiles and surface temperature and humidity data for 9 September 1993: (b) Lake Charles, LA NWS (observed) and Jefferson County Airport, TX RASS site (estimated).

SAIMM Levels (m)	Lake Charles		Jefferson County Airport	
	0600 CST	1800 CST	0600 CST	1800 CST
37.5	25.2	30.4	—	—
75.0	25.8	29.9	—	—
150.0	26.3	29.2	25.4	29.2
250.0	26.0	28.5	25.8	28.7
375.0	25.1	27.7	25.8	28.1
562.5	23.8	26.4	24.5	26.6
787.5	22.0	24.9	22.3	24.4
1050.0	20.7	22.6	20.0	21.9
1350.0	18.9	20.0	—	19.1
1675.0	16.4	17.3	—	16.8
2225.0	13.9	14.3	—	—

Gridded fields of wind, temperature, and specific humidity for FDDA were calculated using an objective analysis procedure. The scheme employs an inverse-distance-squared interpolation procedure to grid the variables at each model level for each assimilation time. The interpolation is governed by a number of user-specified parameters including the maximum radius of influence, number of stations to be used in the interpolation, and number of smoothing passes. The maximum radius of influence should be based on data representativeness (which may vary under different meteorological conditions) and should reflect the limiting influence of terrain features on the interpolation of data. The same values of interpolation parameters are used for the entire grid. A 160-km maximum radius of influence was used for the surface wind data and 800 km was used for the upper-air data. Note that it is not necessary that every grid point be influenced by an observation. The interpolation of data to a grid point was further limited to the four nearest observation points at the surface and the three nearest observation points aloft.

Following interpolation of the data, a spatial weighting factor was assigned to each grid cell depending on data availability. This factor ranged from 1.0 at the data point to 0.0 within a user-specified radius of influence. The weighting factor determines the strength of the nudging (or data assimilation) at each grid point in the domain. The gridded fields of wind, temperature, and humidity data and the spatial weighting factors were plotted and examined (a sample plot is provided in Figure 4-10). Note that the

weighting coefficients are larger near the observation sites (the nudging is stronger in these cases). The blank spaces in Figure 4-10 indicate data-sparse areas where the weighting factors are zero and where the prognostic variables are not nudged.

The SAIMM was then exercised for the coarse-grid domain using the FDDA procedure and the results evaluated using graphical analysis. As described above, several sensitivity simulations were performed to determine the optimum set of nudging coefficients for this application. As a result of these tests, moderate nudging ($G = 5 \times 10^{-4}$) of the winds and weak nudging ($G = 10^{-4}$) of the temperature and moisture variables was applied. The resulting simulated fields were evaluated using graphical displays of horizontal cross sections for selected levels (not shown); wind observations were overplotted on the simulated wind fields.

A procedure was developed for extracting information from the coarse-grid SAIMM simulated fields to provide time- and space-varying (along the lateral boundaries and in the vertical) boundary conditions for the fine-grid simulation. Using this procedure, the SAIMM was exercised for the fine-grid domain using domain-scale initial temperature and humidity profiles, zero-geostrophic wind, FDDA, variable surface characteristics, and zero-gradient boundary conditions. Wind, temperature, and specific humidity fields from the coarse-grid simulation were used as the first-guess field for the preparation of FDDA analyses for the fine-grid simulation. Data were incorporated into the first-guess field using an objective analysis procedure. This provided the FDDA analysis for the fine-grid simulation. Several fine-grid simulations were run to determine how to best achieve the one-way nesting (i.e., which of the prognostic variables to nudge and the optimum strength of the nudging coefficients) in the fine-grid simulations.

The one-way nesting procedure is designed to preserve the features of the coarse-grid simulation near the grid interface. This is important to ensure mass-flux consistency across the interface in the photochemical simulation (i.e., the coarse- and fine-grid wind fields must be consistent across this boundary). The nesting procedure allowed for improved simulation of small-scale features in the interior of the inner domain as a result of the model's response to the higher resolution as well as to the high-resolution FDDA analyses.

As a final step, the simulated fields of wind, temperature, humidity, pressure, and vertical exchange coefficients were converted to the format and vertical resolution used in the UAM-V simulations. The general procedure for converting the output from the SAIMM to input for the UAM-V is described by Schulhof and Douglas (1992). The SAIMM vertical layer heights were transformed from the SAIMM vertical coordinate system to the terrain-parallel, fixed-height vertical coordinate system employed in the UAM-V. The SAIMM output was then either averaged (wind) or linearly interpolated (temperature, specific humidity, pressure, and vertical exchange coefficients) to the UAM-V layers. To minimize the potential for loss of emissions and entrainment of air of unknown composition through the model top, the O'Brien vertical velocity adjustment procedure (O'Brien, 1970), which minimizes vertical velocity at the top of the modeling domain, was invoked in preparing the UAM-V input wind fields. Note that no horizontal interpolation was necessary for this application as similar grid definitions were used for the SAIMM and the UAM-V simulations.

Simulation Results for 17–20 August 1993

The presentation of results in this section focuses on 19 August, the day on which the maximum ozone concentration of 231 ppb was observed.

The observed meteorological conditions for this episode, summarized here, are described in detail in Section 3. The regional airflow patterns were characterized by anticyclonic circulation associated with a high-pressure system located over the Gulf of Mexico. In the Galveston Bay–Houston area, observed near-surface winds were mostly southwesterly on 17 and 18 August and southerly on 19 and 20 August. A gulf breeze developed on all days with a relatively early onset between 1000 and 1200 CST and a duration of 10 to 12 hours. The maximum vertical extent of the observed gulf breeze was between 700 and 1000 m, and it extended inland to north of the Houston area. Observed upper-air wind profiles indicate that the wind was predominantly easterly above approximately 1000 m; significant diurnal variations below 1000 m resulted from the thermally forced bay/gulf breeze circulations.

Wind Fields

Because the wind fields are the most important of the meteorological inputs (they determine the transport and dispersion of pollutants within the modeling domain), the evaluation of the meteorological modeling results focused on the wind fields. Figures 4-11 and 4-12 show the simulated coarse-grid wind fields for 1000 and 1600 CST respectively for three levels (25, 675, and 1200 m agl). To facilitate comparison with observations, the observed wind vectors are overplotted in bold.

Over the Gulf of Mexico, the surface winds at 1000 CST on 19 August (Figure 4-11a) are generally northwesterly over the Gulf. The observed synoptic-scale anticyclonic circulation is well represented in the simulated upper-layer wind fields (Figures 4-11a and b). In particular, the weak wind speeds over Louisiana (1200 m agl) are replicated. The observed wind speeds and wind directions over the Houston area are also represented (although less well). Note that the coarse-resolution simulation is not expected to replicate the airflow features influenced by a relatively small-scale feature like Galveston Bay. At 675 m (Figure 4-11b), observed winds over the Houston area are northwesterly while the simulated winds are more westerly, and at 1200 m (Figure 4-4-11c), the observed winds are east-southeasterly while the simulated winds are from the south-southeast.

At 1600 CST (Figure 4-12a), the winds over the Gulf are onshore along most of the Texas–Louisiana coast to approximately 100 km from the shoreline. Northerly and easterly winds persist south of the location of the Garden Banks monitor. While the observed winds are well represented in the simulated fields over the Houston area, observed winds over eastern Louisiana are more variable than the simulated winds. Winds at 675 m (Figure 4-12b) are from the southeast over the Houston area and the western Gulf and very light and variable over Louisiana and the eastern portion of the

Gulf. At 1200 m (Figure 4-12c), the wind field is dominated by an anticyclonic circulation over southern Louisiana. Observed wind directions and wind speeds aloft are generally well simulated.

In summary, the coarse-grid wind fields for 19 August illustrate that the regional flow patterns were dominated by an anticyclonic circulation, characterized in Section 3 as an extension of the Bermuda high-pressure system westward into the Gulf of Mexico. The model is able to simulate associated regional-scale airflow patterns.

Figures 4-13 and 4-14 show the fine-grid wind fields for 1000 and 1600 CST for the same three levels (25, 675, and 1200 m agl). Note that some distortion of the geographical features, including smoothing of the coastline, occurs when the plots are generated. Some sites may appear to be displaced with respect to the geographical features. At 1000 CST, near-surface winds (Figure 4-13) have westerly components across the domain. Offshore flow at approximately 1–2 ms^{-1} is evident along the Texas Gulf Coast and over Galveston Island. Simulated and observed wind speeds in Galveston Bay and over the Gulf of Mexico are generally comparable. In the Houston area, the simulated surface winds exhibit less variation than the observations. At 675 m agl (Figure 4-13b), the airflow is eastward throughout the domain. Wind speeds are weak (1 ms^{-1}) over the Gulf and somewhat stronger (2–3 ms^{-1}) north of Houston and over the Beaumont–Port Arthur area. At 1200 m agl (Figure 4-13c), winds are variable with mostly southerly components. The observed winds are very well replicated at this level.

The near-surface winds at 1600 CST (Figure 4-14a) are characterized by a relatively strong (3–5 ms^{-1}) onshore flow. Observed wind speeds are well simulated south and east of Galveston Bay, but in some portions of the Houston area the simulated onshore airflow is stronger than observed. Aloft, the onshore flow is also evident at 675 (Figure 4-14b) and 1200 m agl (Figure 4-14c) over the western half of the domain. Over Beaumont and Port Arthur, wind directions are southerly at 675 m agl and easterly at 1200 m agl.

While the good agreement between the simulated and observed winds as presented in these figures is indicative of good model performance, there is no reliable way to evaluate the wind fields in those areas for which observed data are not available. A comparison with the data analysis results, however, indicates that the fine-grid SAIMM simulated airflow patterns throughout the domain conform to the conceptual model of offshore-onshore flow reversal presented in Section 3. The steady offshore flow at 1000 CST corresponds to Stage 3 of the flow reversal pattern; the onshore flow at 1600 CST corresponds to Stage 6.

Particle-path analysis was used in this study to illustrate the airflow characteristics of the SAIMM-generated wind fields and to support the development of a conceptual model for ozone formation during this episode. The particle paths are intended to complement the graphical displays and to further illustrate the airflow characteristics of the simulated surface wind fields by suggesting possible transport pathways. Particle paths are two-dimensional and represent advection by the horizontal wind components only. Labels along the particle path indicate the number of hours since release (forward) or prior to

reception (backward) in 3-hour intervals. Backward particle paths culminating at the locations and the hour of the peak observed ozone concentrations were computed and plotted. Twenty-four-hour backward particle paths ending at 1600 CST on 19 August at the locations of four ozone monitors in the Houston area are shown in Figure 4-15. These paths illustrate the flow reversal that marks the arrival of the gulf breeze in the Houston area around 1200 to 1300 CST. The southernmost trajectory is influenced by the simulated gulf breeze at 1200 CST while the other trajectories show this influence at 1300 CST. This is consistent with the description of gulf breeze development presented for this episode day in Section 3.

The vertical and temporal evolution of the simulated gulf breeze is illustrated in Figure 4-16. In this plot the y-axis represents the vertical dimension and the x-axis represents the south-north direction. Wind vectors represent horizontal wind components and may be interpreted similarly to the wind vectors plotted on the x-y cross section plots; the vertical variation of potential temperature is indicated by the contours. This cross section illustrates the vertical variation of wind and potential temperature along the south-north segment corresponding to the west-east grid cell number 20; it starts near the southern end of Galveston Island (south-north grid cell number 2) and ends north of Houston (south-north grid cell number 40). At 1000 CST on 19 August (Figure 4-16a), winds are northwesterly (offshore) at approximately 1 ms^{-1} over the coastal waters south of Galveston Island while winds over land are more westerly (alongshore). At 1200 CST (Figure 4-16b), the gulf breeze is evident south of Houston in Brazoria County and is characterized by southeasterly winds below about 500 m. At 1400 and 1600 CST (Figures 4-16c and d), the gulf breeze is apparent along the entire cross section and extends up to approximately 1000 m agl at 1400 CST and 1300 m agl at 1600 CST. The vertical and temporal evolution of the gulf breeze as illustrated by the vertical cross sections emphasize the ability of the model to realistically represent the complex, three-dimensional circulation patterns associated with the development of the gulf breeze including the transition from weak offshore flow to steady onshore flow, the inland propagation of the gulf breeze front, and the vertical development of the gulf-breeze layer. This simulation of the gulf breeze is consistent with the conceptual gulf-breeze model developed for this episode in Section 3 as well as the radar profiler data (this comparison is presented later in this section).

Temperature and Moisture Fields

Simulated temperatures for the coarse-grid domain at 0400 and 1600 CST on 19 August are shown in Figure 4-17. Temperatures over the Gulf remain fairly uniform between 29°C and 30°C day and night. At 0400 CST, the level 1 (37.5 m agl) temperature field is characterized by warmer temperatures offshore and a gradient along the shoreline. Inland, temperatures range from 24°C over western Texas to 29°C over portions of Mississippi and Alabama. At 1600 CST, temperatures are fairly uniform near 30°C over the inland portions of the domain. The daytime temperature field is relatively featureless due to the flat terrain across the modeling domain.

Although these fields are not used in the UAM-V simulations (only the coarse-grid fields are used by UAM-V), the fine-grid temperature and humidity fields are presented and discussed here because the quality of these fields reflects the quality of the fine-grid wind fields as well. Compared with the coarse-grid temperature field for 0400 CST, the 4-km temperatures are characterized by a more pronounced coastal temperature gradient along Galveston Bay and the Gulf of Mexico (Figure 4-18a). The near-surface temperatures for 0400 CST on 19 August are 25°C inland northwest of Houston, 27°C along the coast, and 29°C over Galveston Bay and the Gulf. During the afternoon, temperatures increase to over 31°C over land in the 4-km domain compared with about 30° for the 16-km domain (Figure 4-18b).

While the simulated temperature gradients along the coast and diurnal temperature profiles generally agree with the observed surface temperature data, the inland spatial temperature patterns and maximum temperature values are generally not well simulated by the relatively spatially invariant level 1 (37 m agl) temperature fields. Temperatures aloft (and vertical temperature profiles) are better represented since the upper-air temperature data were assimilated into the simulation.

The level 1 simulated specific humidity fields for the coarse- and fine-grid domains are presented in Figures 4-19 and 4-20 for 0400 and 1600 CST on 19 August, respectively. The water vapor content of the air is relatively high during this episode; at 0400 CST on 19 August the specific humidity is mostly between 19 and 20 g kg^{-1}. The predominant feature of the moisture fields for both domains is a west-east gradient from low humidity over west Texas to higher humidity over Louisiana, Mississippi, and Alabama. At 1600 CST, the specific humidity ranges from 16 g kg^{-1} over western Texas to 20 g kg^{-1} over Louisiana, Mississippi, and Alabama. As for the surface temperature fields, the simulated specific humidity fields do not capture the magnitudes or spatial patterns associated with the observed surface moisture. The coastal gradients and vertical profiles are, however, represented.

Vertical Exchange Coefficients

The vertical turbulent exchange coefficients (or diffusivities) control the diffusion of pollutants between the UAM-V layers. In the SAIMM, the diffusivities are estimated using a turbulent kinetic energy (TKE) scheme. These calculations are described briefly in the SAIMM user's guide (Kessler and Douglas, 1992) and in more detail by Ulrickson and Mass (1990). The vertical exchange coefficients exhibit a diurnal variation similar to mixing heights with maxima during the afternoon hours.

For this application, the SAIMM-generated diffusivities were interpolated from the SAIMM vertical structure to the UAM-V layer interfaces and smoothed using four passes of a five-point smoothing routine. In addition, a land-use dependent minimum value was imposed at the interface between layers 1 and 2 in order to maintain a physically realistic well-mixed nocturnal boundary layer. The minimum values applied were 5 m^2 s^{-1} over urban areas, 2 m^2 s^{-1} over forested areas, and 1 m^2 s^{-1} elsewhere. Figure 4-21 illustrates the postprocessed diffusivities for each UAM-V layer interface for 1600 CST on 19 August. The magnitude of the exchange coefficients indicates the

strength rather than the depth of the mixing. Differences between the inland and offshore simulated vertical turbulent exchange coefficients and the associated profiles are consistent with the mixing-depth analysis results presented in Section 3. Maximum diffusivities occur over northern portions of Texas and Louisiana at the interface between layers 3 and 4; diffusivities over land drop off gradually and become very small above layer 5 (900–1500 m agl). Over the Gulf, diffusivities decrease above layer 3 (150–450 m), which suggests a mixed-layer height of approximately 450 m over the water.

Comparison with Observed Data

An important consideration in the evaluation of the SAIMM-generated meteorological fields is the ability of the model to represent the gulf- and bay-breeze circulations. Wind profiler data collected at the Galveston Island (GAL) and Southeast Houston (SEH) monitoring sites provide a basis for the examination of the timing, depth, and inland extent of these features of the simulation. Plots comparing vertical profiles of the observed and simulated winds for these sites between the hours of 1000 and 1600 CST on 18 and 19 August are provided in Figures 4-22 through 4-25. For this comparison, the observed data were interpolated to the SAIMM levels; the lowest 12 levels are plotted. Although the observed data have been incorporated into the simulation using the FDDA procedure, the nudging term represents only one term in the model equations and it is not expected that the data will be identically replicated. Good agreement between the simulated and observed winds indicates successful assimilation; differences indicate that one or more of the other terms in the equations oppose the nudging term and that the assimilation, and thus the simulation, is less successful.

For 18 August, the midday profiler observations for GAL (Figure 4-22) are well represented by the simulated fields. Both the observed and simulated values indicate significant vertical shear. The timing and depth of the gulf breeze, as indicated by the southerly flow components, is well replicated. The comparison for SEH (Figure 4-23) also indicates good agreement between the simulated and observed values. The development of southerly flow components during the afternoon hours and the associated increase in wind speed is simulated. The observed data, however, indicate more of an easterly component below 1000 m agl than the simulated values.

The observed variability in the 19 August morning profiler data for GAL poses a challenge for the model (Figure 4-24). The transition from southward to northwestward flow below 500 m is not well simulated, especially at 1100 CST. The observations and the vertical shear, however, are well simulated throughout the remainder of the midday period. Similarly, some directional disagreement is indicated in the light winds below 500 m at the SEH monitoring site (1300 and 1400 CST) (Figure 4-25). The southwestward flow indicated by the profiler data is, however, not supported by surface observations. Good agreement is achieved for 1500 and 1600 CST.

UAM-V Tracer Simulations

To further examine the airflow characteristics of the simulated wind fields, especially the extent of offshore transport of onshore emissions, an inert UAM-V simulation was performed in which emissions of several tracer species from the Houston/Galveston Bay area were tagged. Continuous emission sources (surface and elevated) were placed in four areas: Houston, Baytown, Texas City, and the Ship Channel area east of Houston. The tracer simulations were performed for 18–19 August and 8–9 September. The following discussion focuses on the transport of mass emitted during the nighttime and morning hours when the mixed layer is still relatively shallow and when the possibility exists that the emissions might be transported offshore by the north to westerly winds of the land breeze. Figures 4-26 to 4-29 show the simulated concentrations of selected tracer species for 18 and 19 August.

Figure 4-26 shows the surface-level concentrations of the Houston surface (HOU) and elevated (HOUPT) tracer species for 1000 CST on 18 August. (Note that the simulated concentrations of the tracer species are not proportional to the actual mass of emissions from these areas, but are approximately equivalent to 1 ppm per grid cell per hour.) The spatial patterns of the HOU tracer suggest eastward transport to the Louisiana state border. Similarly, the HOUPT tracer is advected eastward into the Beaumont/Port Arthur and Calcasieu Parish nonattainment areas (Figure 4-26b). The Texas City surface tracer (TEX) (Figure 4-27a) does not appear to be transported out of the local area whereas the elevated tracer (TEXPT) is advected to the southeast over the northern portion of Galveston Island to a distance of approximately 50 km offshore (Figure 4-27b) (no other tracer species were transported offshore on 18 August). Simulated concentrations of all the tracer species decrease rapidly during the late morning hours as the depth of the mixed layer increases.

As illustrated in Figure 4-28, the HOU and HOUPT tracers are again advected eastward on 19 August; first to the east-southeast over the Galveston Bay and then to the northeast into the Beaumont/Port Arthur area. Simulated concentrations of the Ship Channel tracer (SHP and SHPPT), though of smaller magnitude than the Houston tracer, indicate similar eastward transport patterns (Figure 4-29). In the afternoon (not shown), the extent of the HOU and SHP tracer concentrations is limited to the Houston area. Simulated concentrations of the Baytown and Texas City tracers are comparatively small on this day.

Unlike the two-dimensional trajectories presented earlier in this report, the tracer simulations incorporate vertical advection and horizontal and vertical dispersion and, thus, allow a much more realistic examination of potential transport pathways. Note that the reliability of both methodologies is dependent upon the quality of the objectively analyzed (Section 3) or simulated (Section 4) wind fields. The tracer simulation results, however, support the general conclusions from the data analysis that southeastward transport of pollutants occurred during this episode and that carryover of ozone and precursor pollutants was unlikely.

Simulation Results for 6–11 September 1993

The observed air quality data for the 6–11 September episode indicate a buildup of ozone concentrations over the Houston and Galveston Bay areas with maximum ozone concentration occurring on 8 and 9 September. Thus, the following discussion focuses on those two primary ozone episode days.

Peak ozone concentrations during this episode were measured south of Houston (at Smith Point on 8 and 9 September and at Galveston on 10 September). The observed upper-air wind data are characterized by northerly components associated with a high-pressure system located north of Houston. In general, the synoptic-scale northerly airflow delayed the onset and inhibited the inland extent of the gulf breeze on 7–10 September. The gulf breeze did not reach the Houston area on several of the episode days; the maximum inland extent of the gulf breeze was approximately to Texas City and Smith Point on 7, 8, and 9 September. The observed meteorological conditions for this episode are described in detail in Section 3.

Wind Fields

Figures 4-30 and 4-31 show the coarse-grid wind fields for three levels (25, 675, 1200 m agl) for 1000 and 1600 CST on 8 September. Note that wind directions above approximately 1500 m are persistently from the north during this episode. It is proposed in Section 3 that the northerly wind components aloft enhanced the offshore and suppressed the onshore component of the gulf breeze. The 1000 CST surface winds are weak and variable over Texas and Louisiana and from the north at approximately 5 ms^{-1} over the Gulf. Wind directions over the Houston and Baton Rouge areas are well simulated while surface wind speeds over Texas and northern Louisiana generally are underestimated at this hour. Winds aloft over Louisiana are northeasterly at 675 m agl and northerly at 1200 m agl. Winds aloft are weak and variable over the Galveston Bay–Houston area.

At 1600 CST, the surface wind fields indicate that a gulf breeze has developed along the Texas coast while further inland wind directions maintain an easterly or northeasterly component. Surface winds offshore (about 100 km from the Texas coast) are northeasterly as a result of cyclonic circulation over the Gulf. The surface winds for this hour illustrate Stage 5 of the flow reversal pattern as presented in Section 3 (onshore flow along the coast, southward flow offshore, and a divergence zone between the onshore- and offshore-directed flows). Southeasterly winds at 2–3 ms^{-1} are present over the Mississippi River Delta; the southeasterly winds converge with northwesterly winds near Baton Rouge. Aloft, south to southeasterly winds continue over Louisiana though with stronger wind speeds near 2–4 ms^{-1}. Over Houston and Galveston, the observed and simulated winds have a southerly component at 675 m agl and a northerly component at 1200 m agl.

As indicated in Section 3, the regional-scale meteorological conditions associated with this episode period were significantly different than for the August episode. These differences are apparent in the coarse-grid airflow patterns and confirm that the model is able to simulate the day-to-day variations in the regional-scale meteorological conditions.

Twenty-four-hour surface-level forward particle paths initiated at 0000 and 1200 CST on 8 September from possible OCSPD source locations along the Texas–Louisiana Gulf Coast are shown in Figure 4-32. The initiation points of these particle paths represent the locations of several platforms in the OCS region (not necessarily the maximum extent of the gulf breeze) with high (relative to other OCS sources) emissions of oxides of nitrogen and hydrocarbons. The particle paths released at midnight illustrate that some of the platforms located within approximately 100 km from the coast are influenced by the diurnal changes in wind patterns associated with land/gulf breeze circulations. The 1200 CST particle paths illustrate the southerly gulf breeze and suggest that emissions from the selected source locations may have been advected onshore during this episode. The particle paths initiated at midnight, especially those originating near the Texas coast, indicate a nearly 180 degree change in wind direction. This is consistent with the findings of the ventilation analysis presented in Section 3.

The simulated fields for the fine-grid domain for 1000 and 1600 CST on 8 September are shown in Figures 4-33 and 4-34. The surface winds for 1000 CST are weak and from the west over most of the domain. The northwesterly (offshore) winds with speeds of approximately 2–3 ms^{-1} that were present over Galveston Bay and Galveston Island are well simulated. However, simulated winds in the Houston area are somewhat less variable than those observed. Note that the simulated surface winds replicate the observed winds indicating southeastward flow around Galveston Bay (e.g., at Smith Point). Westerly components dominate the wind fields aloft. Winds are weak and from the southwest at 675 m agl. Westerly winds dominate at 1200 m agl with some southwestward flow over the Gulf east of Galveston Island. The simulated winds agree very well with the observations.

By 1600 CST, the gulf breeze has fully developed along the Texas–Louisiana Gulf Coast. The inland extent of the northward flow is near the southeastern portion of Houston and appears to be well simulated. However, north of the gulf-breeze front observed winds indicate southwestward flow while the simulated winds are more easterly. This is especially true just northeast of Galveston Bay and suggests that the simulated gulf/bay breeze penetrates too far inland in this area. The gulf breeze is also evident in the 675 m agl wind fields but not in the 1200 m fields. Winds at 675 m are from the south over the Gulf and along the coastline and mostly easterly inland. Winds at 1200 m are northeasterly throughout the domain.

Vertical cross-sections of the 4-km wind fields show the evolution of the simulated gulf breeze for 8 September. The cross-section shown in Figure 4-35 illustrates the vertical variation of wind and potential temperature along the south-north segment corresponding to west-east grid cell number 20 (eastern Houston). The cross-section extends from near the southern boundary of the domain to approximately 50 km north of Houston. At 1000 CST, winds are northwesterly over the Gulf and westerly inland up to about 1200

m agl. At 1200 CST, wind speeds are very weak and variable everywhere. In the afternoon, the gulf breeze develops first over the Gulf and extends inland to Texas City by 1400 CST and to Southeast Houston by 1600 CST. The maximum vertical extent of the simulated gulf breeze on this day is approximately 900 m agl. Comparison with the vertical cross-section plots for 19 August shows that the gulf breeze develops later on 8 September and the extent of inland penetration is significantly less. This is consistent with the findings of the data analysis.

Backward particle paths culminating at the location and hour of the peak observed ozone concentration for several monitoring sites were also used to examine the potential for transported ozone and precursor emissions to influence the peak ozone concentrations in the Houston/Galveston areas. Figure 4-36 shows the twenty-four-hour backward particle path ending at 1400 CST (the time of the observed peak ozone concentrations of 214 ppb) at the Smith Point and Seabrook monitoring site locations on 8 September. The backward particle paths for this day appear to pass over areas of possible high emissions in and around Houston. They also illustrate that the simulated wind fields support the hypothesis that the build-up of ozone concentrations observed at Smith Point and Seabrook was associated with offshore flow (refer to Figure 3-58).

On 9 September at 1000 CST, surface winds are northerly again over most of the Gulf of Mexico (Figure 4-37a). Over Louisiana, surface winds are southwesterly over Calcasieu Parish and northwesterly in the Baton Rouge–New Orleans area at about 3–4 ms^{-1}. Winds over Galveston are very weak and variable while winds over Houston and most of Texas are weak and from the east-northeast. Simulated surface-level wind speeds are generally lower than observed. The airflow aloft is characterized by anticyclonic circulation over the Gulf of Mexico (Figures 4-37b and c). As a result, winds are generally southerly along the Texas coast and northerly along the Louisiana coast. Inland, winds are from the west at 3–5 ms^{-1}.

At 1600 CST, winds over the Gulf are variable with onshore flow along the coastline (Figure 4-38a). In the Houston area and over most of Texas, winds are weak (near 1 ms^{-1}) and variable. Wind speeds in Houston are not simulated well in the coarse-grid fields as observed winds in the Houston area indicate offshore flow at 2–3 ms^{-1}. While observed wind directions in general appear to be replicated in the simulated fields, simulated surface wind speeds at this hour appear to be overestimated over the Gulf of Mexico and underestimated over land. The upper-level wind observations are very well replicated by the simulation. Anticyclonic circulation continues to dominate the 675 m agl wind fields over the Gulf of Mexico (Figure 4-38b). The simulated winds over Texas for this level are still weak and variable and thus do not replicate very well the observations over Houston and Port Arthur, which at this time indicate northwesterly winds at 4–5 ms^{-1}. At 1200 m, winds are northerly or northwesterly throughout the domain and wind speeds are better simulated at this level (Figure 4-38c).

Surface-level forward particle paths initiated from the locations of several OCS platforms at midnight on 9 September mostly illustrate the anticyclonic circulation noted above (Figure 4-39). Some recirculation associated with the land/gulf breeze is suggested in the particle path initiated from the platform located about 50 km south of Galveston

Island. It is possible that Calcasieu Parish and other portions of Louisiana may have been influenced by OCS emissions on this day. Possible onshore transport all along the Texas-Louisiana Gulf coast is also suggested by the particle paths initiated at 1200 CST from the platforms located within 50–100 km of the coast.

The 4-km wind fields for 9 September are presented in Figure 4-40 and 4-41. At 1000 CST, the surface winds are northwesterly to the west of Galveston Bay and southwesterly to the east of Galveston Bay. Around Galveston Bay from Texas City to Smith Point, the simulated surface winds are mostly westerly while observed winds indicate a northerly component. This may have resulted in the underestimate of simulated onshore-to-offshore pollutant transport during the morning of 9 September. To the south of Texas City and over Galveston Island, simulated and observed winds are northwesterly. Winds along the coast and over the Gulf of Mexico appear to be well simulated. Aloft, winds are generally northwesterly to westerly at 675 m agl and southwesterly to southerly at 1200 m.

During the afternoon, the gulf breeze develops along the coast and by 1600 CST extends inland to Texas City. Although simulated wind speeds are lower than observed throughout the Houston area, northerly wind over Houston and Smith Point are simulated. The gulf-breeze front is also located near Texas City in the 675 m agl winds. Away from the coast, winds are weak and from the northwest over land and from the southwest over the Gulf. Westerly to northwesterly winds prevail at 1200 m.

As indicated by the surface-level backward particle path for 9 September (Figure 4-42), surface winds over Galveston Bay maintained northerly components for most of the day. These particle paths (ending at the locations of the Smith Point and Gilchrist monitoring sites) thus suggest possible transport of ozone and precursors from source areas in and around Houston and the Houston Ship Channel. This is consistent with the findings of the data analysis which suggests that the offshore-directed flow was an important mechanism for transporting ozone and precursor pollutants from onshore source regions to the coastal monitoring sites at which high ozone concentrations were monitored.

As a result of the strong southwestward flow on 9 September, the vertical and horizontal extent of the gulf breeze is inhibited. The vertical cross sections of the wind fields through southeast Houston at 1000 CST indicate weak winds from the north-northwest along the entire south-north extent of the section (Figure 4-43). At 1200 CST, southerly components appear near the coast and by 1400 CST the gulf breeze has developed over the Gulf of Mexico and the gulf-breeze front is located between Galveston Island and Texas City. The southeasterly gulf breeze on this day extends up to approximately 500 m. At 1600 CST, the gulf breeze front has reached its maximum inland extent at about 25 km northwest of Texas City. The vertical and inland extent of the simulated gulf breeze is even less than for 8 September. The more limited inland extent is consistent with the higher observed ozone concentrations nearer to the coast than on the previous day. Surface observations indicate, however, that even though it is quite limited, the inland extent may have been overestimated.

Temperature and Humidity Fields

The diurnal variation in the 37.5 m agl temperature fields on 8 September is illustrated in Figures 4-44 and 4-45. Early morning temperatures over West Texas on 8 September range from 28°C near the coast to 26°C inland. Near-surface temperatures over Louisiana are somewhat cooler and range from 23–25°C inland to 26–27°C along the coast. Over the Gulf of Mexico, the warmest temperatures are higher than 29°C and occur offshore. Eastern portions of the Gulf of Mexico experience cooler near-surface temperatures between 26°C and 28°C. In the afternoon, temperatures over the Gulf of Mexico warm up by 1 to 2°C while temperatures over land warm up to a uniform 30°C throughout the domain. Near-surface temperatures for the fine-grid domain are near 27°C during the early morning hours (Figure 4-45a). In the afternoon, temperatures vary from 29°C over the Gulf of Mexico to greater than 31°C over land (Figure 4-45b).

On 9 September at 0400 CST, near-surface temperatures over Texas are between 27°C and 28°C whereas temperatures over Louisiana and Mississippi are cooler and range from 25°C to 27°C (Figure 4-46a). Over the Gulf of Mexico, near-surface temperatures are near 28°C. In the afternoon, air temperatures over the water warm up to more than 29°C near the coast (Figure 4-46b). Over land, near-surface temperatures are near 30°C and are uniform across the domain. The fine-grid 37.5 m temperatures again suggest somewhat stronger surface heating as afternoon temperatures reach 31°C over land (Figure 4-47b). Simulated temperatures over land exhibit a more pronounced diurnal profile than those over water.

As for 19 August, the relatively uniform level 1 simulated temperatures over the land do not capture the observed spatial variations in surface temperature. The temperature gradients along the coast are less pronounced than for the August episode, possibly due to the increased strength and duration of the offshore-directed flow during the September episode days.

The early morning near-surface specific humidity for 8 September is around 17 g kg^{-1} over most of the domain (Figure 4-48a). Diurnal variation in the moisture fields is most evident over Texas and the western Gulf where the specific humidity decreases by 1 to 2 g kg^{-1} in the afternoon (Figure 4-48b). The fine-grid humidity fields show somewhat more variation over land; an area of increased specific humidity is indicated near the simulated gulf-breeze front (Figure 4-49b).

On 9 September at 0400 CST, the near-surface specific humidity ranges from 18 g kg^{-1} over portions of Louisiana, Mississippi, and Alabama to 16 g kg^{-1} over Texas (Figure 4-50a). The moisture content over the Gulf of Mexico is uniformly around 17 g kg^{-1}. At 1600 CST, specific humidity increases to 18 g kg^{-1} over the Gulf and to 19 g kg^{-1} south of Galveston Island (Figure 4-50b). Inland, the moisture content is spatially uniform near 17 g kg^{-1}. Again, more detail is evident in the fine-grid fields (Figure 4-51). At 1600 CST, a gradient has developed along the coastline and around the outline of Galveston Bay. In addition, the specific humidity is around 16 g kg^{-1} north of the gulf breeze front whereas the specific humidity behind it is higher at 18–19 g kg^{-1}. This drier air ahead of the gulf-breeze front is consistent with the conceptual model of the

gulf breeze presented in Section 3. Simulated specific humidity is slightly lower for this episode (17–19 g kg^{-1}) than for the September episode (19–20 g kg^{-1}); this is consistent with the findings of the data analysis which suggest that the southward flow aloft brought dry continental air into the region during the September episode.

Vertical Exchange Coefficients

The vertical variation in diffusivities at 1600 CST for 8 and 9 September are presented in Figures 4-52 and 4-53. The afternoon fields are generally characterized by diffusivities that increase then decrease with height. The UAM-V layer interface at which the maximum values occur and the rate at which they decrease above the maximum may be used to infer the height of the mixed layer. On 8 September, the maximum values over the Gulf of Mexico appear to occur at the interface between layers 2 (50–150 m agl) and 3 (150–450 m agl), above which the diffusivities drop off sharply. This suggests a mixed layer height near 450 m. Over coastal Louisiana, the maximum value is also found at the interface between UAM-V layers 2 and 3, but here the diffusivities are higher, near 50–60 m^2 s^{-1}, and drop off more gradually. Over Houston and northern portions of Texas, the maximum is found between UAM-V layers 4 (450–900 m) and 5 (900–1500 m).

On 9 September, the spatial patterns are similar with relatively low diffusivities over the Gulf of Mexico and higher values over land. On this day, maximum diffusivities are found over Louisiana and it appears that very little vertical diffusion occurred above UAM-V layer 5 (1500 m).

Comparison with Observed Data

The simulated winds corresponding to the Galveston (GAL) and Southeast Houston (SEH) monitoring sites were compared with observed profiler data to examine the timing, depth, and inland extent of the simulated gulf- and bay-breeze features. Vertical profiles of the observed and simulated winds for these sites between the hours of 1000 and 1600 CST on 8 and 9 September are compared in Figures 4-54 through 4-57.

For 8 September, the observed vertical wind shear at GAL (Figure 4-54) is well simulated as is the transition to northward flow (between 1100 and 1300 CST). During the afternoon hours, the simulated winds maintain a southeasterly component while the observed winds are more southerly. The depth of the gulf breeze, as indicated by the vertical extent of the northward flow, is well characterized but slightly overextended at 1600 CST. The observed winds for the SEH site (Figure 4-55) are generally well simulated although the transition to westward flow below approximately 800 m (1300 CST) is delayed in the simulation.

The onset of the gulf breeze on 9 September is well timed at the GAL site (Figure 4-56). The transition from northwestward to northeastward flow, however, occurs earlier in the simulated fields than is indicated by the observations. Further inland, at SEH (Figure 4-57), wind speeds and directions are well represented at all levels until 1300 CST. The

strength of the northerly components below 800 m agl is underestimated throughout the remainder of the midday period.

UAM-V Tracer Simulation

UAM-V tracer simulations were performed to examine the potential for offshore transport of onshore emissions. Simulated concentrations of four tracer species emitted in Houston, Baytown, Texas City, and the Ship Channel area east of Houston for 8 and 9 September were examined. Figures 4-58 through 4-65 show the simulated surface concentrations of selected tracer species for 1000 and 1600 CST on 8 and 9 September.

For 8 September, the 1000 CST spatial patterns of the HOU and HOUPT surface concentrations indicate offshore transport to a distance of approximately 32 km south of Galveston Island (Figure 4-58). The SHP and SHPPT tracers are also advected out over the Gulf during the morning (Figure 4-59). The afternoon HOU and HOUPT concentrations (Figure 4-60) are highest over Houston and the Galveston Bay/Smith Point area, suggesting that the northerly winds continue for some time after 1000 CST but then reverse before 1600 CST. Simulated concentrations of the Ship Channel tracers for 1600 CST show similar patterns of transport (Figure 4-61). Concentrations of the elevated tracer SHPPT south and east of Houston are higher than the surface tracer SHP, indicating that transport above the surface layer may be important.

The pattern of offshore-onshore transport is repeated on 9 September. During the morning hours, the HOU and HOUPT tracers are advected to the southeast over the Gulf to a distance of approximately 32 km from Gilchrist (Figure 4-62). The southeastward advection is also evident in the SHP and SHPPT tracer concentrations for 1000 CST (Figure 4-63). Both the HOUPT and SHPPT tracer clearly have been advected back onshore between Gilchrist and Sabine Pass; the flow reversal had already occurs over the Gulf and near the coastline before 1000 CST (Figure 4-64). In the afternoon, the SHPPT and HOUPT tracers are still present over the Bay and in the Smith Point and Gilchrist areas (Figure 4-65).

The repeated sequence of offshore-onshore transport on 8 and 9 September revealed by the UAM-V tracer simulation results illustrates the multi-day aspects of the September episode and supports the suggestion that day-to-day OCS impacts may be greater during this episode compared to the August episode. Again, the tracer simulations allow a much more realistic examination of potential transport pathways, as represented by the simulated wind fields, than the two-dimensional particle path analyses. The tracer simulation results clearly show that the simulated wind fields represent the carryover/recirculation of pollutants from onshore sources that was determined, through data analysis, to have occurred during this episode. On both 8 and 9 September, the tracers are advected approximately 32 km offshore; the data analysis results (Section 3) suggest that this distance is somewhere between 10 and 50 km.

AIR QUALITY INPUTS

The UAM-V requires gridded initial concentrations for all species for the entire coarse-grid domain, boundary concentrations for all species along each lateral boundary, and concentrations at the top boundary of the domain. Considering the length of the lateral boundaries, sufficient monitoring data do not exist to determine, based on observations, appropriate concentrations along the boundaries. A few surface monitors measuring ozone and NO_x are located near the west and north boundaries, but there are no available hydrocarbon measurements near the boundaries. Furthermore, no measurements are available to define a vertical profile for pollutant concentrations near any of the boundaries. The boundary concentrations used were therefore based primarily on past model applications and estimates of continental background concentrations of ozone and ozone precursors. Because of the large modeling domain used in this application, the effects of the boundary conditions on the interior of the modeling domain, especially the Houston subdomain, should be minimal.

Most of the south and east boundaries are located well out over the Gulf of Mexico. Concentrations along these boundaries were therefore set to values representative of clean marine air. Hydrocarbon samples collected off the coast of southern California have been analyzed to give estimates of concentrations in marine air (Moore et al., 1991) indicating a marine hydrocarbon concentration of around 10 ppb. Based on this information, we estimated the split of marine hydrocarbon into CB-IV species to be 76 percent PAR, 10 percent OLE, 3 percent ETH, and 11 percent aromatics which were split equally between TOL and XYL. Trace amounts of FORM, ALD2, and other CB-IV species were assumed. To be consistent with this small amount of hydrocarbons, NO_x concentrations must also be small. A rough estimate based on maintaining a HC/NO_x ratio less than or equal to the HC/NO_x ratio in the emissions inventory limits the total NO_x to 0.74 ppb. Conservatively, therefore, NO2 was set to 0.5 ppb and NO to 0.01 ppb. The resulting marine air concentrations are summarized in Table 4-17. These concentrations were used for the south and east boundaries in all simulations.

Table 4-17. Marine air concentrations of CB-IV species (ppb).

NO	0.0100	OLE	0.5000	OPEN	0.0010
NO2	0.5000	PAR	7.6000	PAN	0.0010
O3	40.0000	TOL	0.0786	PNA	0.0010
CO	200.0000	XYL	0.0688	H2O2	0.0010
ALD2	0.0500	ISOP	0.0010	HONO	0.0010
ETH	0.1500	CRES	0.0010	HNO3	0.0010
FORM	0.0500	MGLY	0.0010	NXOY	0.0001

Because numerical tracer simulations made prior to photochemical modeling of the August episode indicated that pollutant mass from the north and top boundaries would not reach the Houston area during the episode, concentrations at these boundaries were also set to the marine air concentrations for the August episode. After an examination of aircraft measurements of ozone and other pollutants collected during the GMAQS and COAST programs, the ozone concentration was increased to 60 ppb for the top boundary

prior to the final base-case simulation. Along the west boundary for the August episode, EPA default boundary concentrations (2 ppb NO_x, 22 ppbC RHC) (EPA, 1991a) are used for 0 to 700 m altitude and the marine concentrations are used above 700 m. The few measurements available on this boundary are not inconsistent with this choice. The west boundary concentrations are listed in Table 4-18.

Table 4-18. EPA default boundary concentrations of CB-IV species (ppb).

NO	0.0100	OLE	0.3000	OPEN	0.0010
NO2	2.0000	PAR	14.9400	PAN	0.0010
O3	40.0000	TOL	0.1800	PNA	0.0010
CO	350.0000	XYL	0.0975	H2O2	0.0010
ALD2	0.5550	ISOP	0.1000	HONO	0.0010
ETH	0.5100	CRES	0.0010	HNO3	0.0010
FORM	2.1000	MGLY	0.0010	NXOY	0.0001

Boundary concentrations for the September episodes were prepared in a similar manner. However, since the north and east boundaries were inflow boundaries for some hours, these were not simply set to clean background conditions. Surface observations near the north boundary were averaged to obtain a separate boundary concentration for CO, NO, NO_2, and ozone. For these species, the average concentrations were used for the lowest 700 meters on the north boundary and the assumed marine concentrations were used above this level. For the other species on the north boundary, EPA default concentrations were used for the lowest 700 meters and assumed marine concentrations were used above this level. Since measurements of NO, NO_2, and CO are nonexistent near the west and east boundaries, the observed values near these boundaries were used only to specify the boundary values for ozone. Concentrations of all other species were set to EPA background values near the surface. The range of the average boundary concentrations and inflow time periods is shown in Table 4-19. Along the south boundary, marine concentrations were used for all layers at all times.

Table 4-19. Average surface concentrations for north, east and west boundaries.

Boundary	Time Period	CB-IV Species	Concentration Range (ppb)
North	6–11 Sept	CO	0–1000
		NO	1–15
		NO2	0–19
		O3	40–75
West	0000–0600, 9 Sept	O3	40
East	11 Sept	O3	40–60

Initial concentrations for both the August and September episodes were interpolated from surface observations for NO, NO2, O3, and CO. The interpolation included many pseudo-sites for which concentrations were set either to EPA background concentrations over land or to marine concentrations over the Gulf. Figure 4-66 illustrates the regions over which the different pseudo-site concentrations were used: the gray region used marine concentrations while the unshaded region used EPA default concentrations. The interpolated values (displayed in Figure 4-67 for ozone and NO_2) were used for the lowest 300 meters of the modeling region with the marine concentrations above. Hydrocarbon values were set to the marine concentrations for all grid cells and layers.

LAND-USE INPUTS

Land-use data are used by the UAM-V in calculating deposition rates for the chemical species and by the albedo/haze/ozone column preprocessor in calculating the albedo and hence in setting up the photolysis rates file. The UAM-V SURFACE file contains fractional coverage for 11 categories of land use. The SURFACE file for this application was prepared using USGS land-use data (the format of which is described in DOI, 1990) which is available at 200-m horizontal resolution for approximately 30 land-use categories. The USGS categories were mapped into the UAM-V categories and then the data were regridded to the appropriate resolution for each of the modeling grids. The resulting gridded distributions of the urban, water, and forest categories are shown in Figure 4-68.

OTHER INPUTS

The albedo/haze/ozone column file contains codes which correspond to specific values of these parameters. Photolysis rates are calculated for the full range of albedo, haze, and ozone column present in a given simulation by the *calcj* light model program. The model then uses the appropriate set of rates for each grid cell during the model run. Because detailed data on turbidity were unavailable, the value for haze was set to 0.094 uniformly, which is typically representative of rural conditions. Albedo is derived automatically by the *alhzoz* preprocessor program from the UAM-V SURFACE file; values range from 0.04 to 0.08. Ozone column data were obtained through the National Space Science Data Center, which archives data from satellite-based Total Ozone Mapping Spectrometers.

4.8 DIAGNOSTIC AND SENSITIVITY ANALYSIS

This section summarizes the UAM-V diagnostic and sensitivity analysis that was performed for the August and September 1993 episodes. The simulations were performed to diagnose possible problems in the input assumptions, to test the sensitivity to various input parameters, and to assess the performance of the model to changes in the inputs. Although it is acknowledged that the potential for OCSPD emission impacts

may be greater for the September episode, because of the availability of supplemental data collected for the August episode during the 1993 GMAQS field study (e.g., aircraft and profiler) a more comprehensive diagnostic and sensitivity analysis was performed for the August episode. Information obtained through analysis of the August episode benefited the September modeling exercises. Per the direction of the GMAQS Technical Review Group (TRG), the modeling analysis focused on the Houston urban area. Thus, the diagnostic and sensitivity analysis was directed toward understanding, assessing, and improving model performance within the Houston subdomain.

During the course of the analysis, two base emissions inventories were prepared for each of the 1993 episodes simulated. The "baseline" inventory represents the modeling inventory prepared and processed using standard procedures and data received from the MMS, the states of Texas and Louisiana, and local agencies. The inventory for the Houston subdomain was modified during the course of the diagnostic analysis—various components were adjusted within their range of uncertainty. The meteorological and air quality inputs as well as several of the UAM-V input parameters were also examined as part of the diagnostic and sensitivity analysis. In total, 64 simulations were performed for the August episode and 14 simulations were performed for the September episode. Many of these simulations were partial simulations (i.e., the model was exercised for only a subset of the episode days).

The results of the diagnostic and sensitivity simulations for these episodes, presented in the following sections, emphasize those simulation results that provide useful information regarding model performance or the effects of input uncertainty.

Throughout the analysis, the simulation results were used to investigate the following possible explanations for the high observed ozone concentrations, especially in the Greater Houston area: (1) the high observed peaks resulted from day-specific emissions that are not incorporated into the current emissions inventories, (2) the high observed peaks were due to especially adverse meteorological conditions combined with high emissions, or (3) the high peaks were due to synergistic interactions of the local, diverse emissions. This third possibility exists due to the high concentrations of industrial emissions at some locations around Galveston Bay: with certain combinations of near-stagnant wind conditions it is possible for local combinations of VOC and NO_x emissions to form air parcels with mixtures that have optimal ratios for ozone formation.

ANALYSIS OF THE 17-20 AUGUST 1993 EPISODE

Initial Simulation Results

The initial UAM-V simulation for the August episode, using the baseline emissions inventory, produced a maximum simulated ozone concentration in the Houston area of 106 ppb (on 18 August). The maximum observed ozone concentration during this episode was 231 ppb, measured at the Aldine site on 19 August. This underestimation of the observed ozone concentrations indicated significant deficiencies in the emissions

and/or meteorological inputs. The majority of the diagnostic and sensitivity simulations performed for this episode were designed to address the model performance deficiencies.

Emission-Related Diagnostic and Sensitivity Simulations

A number of diagnostic simulations were performed for this episode to investigate possible problems with the emission inventory. Based on analysis of the initial simulation results, it was hypothesized that the inability of the UAM-V to replicate the high ozone concentrations observed in the Houston area was due to a non-ozone-conducive emission-based VOC-to-NO_x ratio. The anthropogenic-emission-based estimated molar VOC-to-NO_x ratio is approximately 2.5 for the Houston-area baseline inventory (see Tables 4-6 and 4-7). This indicates that ozone production is limited by the amount of VOC emissions (e.g. VOC-limited conditions) and is contrary to the findings of the data analysis. Following several corrections to the baseline inventory (incorporating, for example, updated emission factors and improved emission estimates), several sensitivity simulations were performed to investigate the sensitivity to NO_x emissions. The majority of these simulations found that reducing NO_x emissions increased simulated peak ozone concentrations. This response, although somewhat counterintuitive, is partially explained by the fact that high NO_x concentrations enhance the removal of radical species to form nitrates. Moreover, the removal of radicals by NO_x can significantly retard or slow the ozone-forming process so that the reduction of NO_x emissions leads to ozone formation earlier in the day and not as far downwind from high-emissions areas.

A sensitivity simulation in which NO_x emissions within the Houston subdomain were reduced by half was performed using an updated version of the baseline emission inventory and simulated ozone concentrations within the Houston area (especially near major emissions sources) increased significantly. Consistent with hypothesis number 3 (synergistic interactions of local emissions), the across-the-board NO_x reduction test produced significantly different results for 17, 18, and 19 August. For 17 August the half NO_x scenario produced a 14 ppb increase in the peak simulated ozone concentration; for the 18th the maximum increase was 37 ppb; but on the 19th the increase in simulated peak ozone was as high as 75 ppb. Moreover, when the updated baseline NO_x emissions were used, the simulated maximum ozone concentration at Aldine (where the maximum observed concentration of 231 ppb was measured) was only 110 ppb (a peak of 148 ppb was simulated downwind). When the NO_x emissions were halved, the simulated peak essentially matched both the observed concentration and its location because the ozone formation rate was so much faster with the reduced NO_x emissions. That is, for the site where the highest ozone concentration was observed, the simulated ozone concentration increased by a factor of two (essentially matching the observed concentration) when NO_x emissions were assumed to decrease by a factor of two.

This sensitivity simulation was repeated several times throughout the course of the diagnostic and sensitivity analysis (with either updated emissions or updated meteorological data) but in most other cases the results were less dramatic. Following some additional minor revisions to the meteorological and emission inputs, the increases in peak simulated ozone concentration due to reduction of the NO_x emissions by half

were 21, 34, and 44 ppb for 17, 18, and 19 August, respectively. This different response, using slightly different meteorological fields provides even more support for hypothesis number 3 (synergistic interactions of local precursors).

This apparent sensitivity to NO_x emissions led to further examination of the emission inventory. Tracer simulations were used to determine the relative importance of the various sources of NO_x emissions including area, mobile, low-level point, and elevated point sources. The results indicated that NO_x emissions from mobile sources were most predominant within the region where the highest ozone concentrations were observed on 19 August. The tracer simulation results were confirmed by an analysis of the emissions inventory in the grid cells along the ship channel (located upwind of the maximum concentration area during this episode), which showed that mobile NO_x clearly dominated (by as much as 80 percent) the NO_x emissions in this region. The tracer simulations also indicated that NO_x from elevated sources principally affected the area north of Baytown (where the simulated ozone concentrations were also lower than observed). Figures 4-69 and 4-70 illustrate the relative contributions of the elevated and surface NO_x emission tracers. The contours represent the percentage contribution for each of the tracers and thus provide an estimate of the potential "contribution" of the NO_x emissions. This potential for NO_x emissions from elevated point sources to influence the simulated surface ozone concentrations might be the result of using default stack parameters to replace missing values. This would result in more of the emissions from the elevated sources being emitted into the lowest layer of the model.

The potential for sensitivity to radicals from HONO was also studied by assigning a small fraction (1 percent) of all nitric oxide emissions to HONO. This approach is consistent with recent measurement data. The sensitivity to HONO emissions at this level produced only small increases in simulated peak ozone of 2 to 4 ppb. Because of the small effect and an adverse impact on computing time, the HONO assignment was not retained through the remainder of the modeling analysis.

Uncertainties in the VOC emission estimates were also examined as part of the diagnostic and sensitivity analysis for the August episode. Using information derived from other measurement and modeling studies, such as Harley et al. (1992) and Wagner and Wheeler (1991), a sensitivity simulation was performed in which the mobile-source VOC emissions were adjusted by a factor of 2. Simulated ozone concentrations throughout the Houston subdomain generally increased as a result of this modification; the peak simulated ozone concentration for 19 August increased by 16 ppb. However, this increase in VOC emissions alone did not result in significantly improved simulated concentration patterns.

The effects of increased VOC emissions were also examined by increasing, in another sensitivity simulation, the stationary (area and point) source VOC emissions by 50 percent. This increased the domain-wide maximum ozone concentrations by approximately 10 to 20 ppb but, as for the mobile-source VOC sensitivity simulation, this alone did not dramatically improve the simulation results.

Meteorology-Related Diagnostic and Sensitivity Simulations

Additional diagnostic and sensitivity simulations were performed to examine the effects of uncertainties in the meteorological fields on the UAM-V simulation results. To examine the degree to which differences between the simulated and observed winds affected the simulation results, alternate wind fields for the Houston fine-grid modeling domain were prepared using the Diagnostic Wind Model (DWM) (Douglas et al., 1990). Observed wind data are incorporated into the DWM using an objective analysis procedure, so good agreement between the modeled and observed winds is ensured. Unlike the SAIMM, however, the DWM is unable to provide a physically realistic representation of complex mesoscale airflow features (e.g., the gulf breeze) that are not directly supported by observed data. Use of the DWM wind fields did not improve the simulation results. Although both simulations were performed with an intermediate version of the emissions inventory, model performance for the corresponding simulation with the SAIMM fine-grid wind fields was better.

The magnitude and spatial distribution of the vertical exchange coefficients K_v was also examined. Varying the K_v values by either a factor of 5 higher or lower changed simulated peak ozone concentrations by as much as 30 ppb: increased K_vs gave lower ozone by generally about 15 ppb, reduced K_vs gave higher ozone with a range from about 10 ppb to 31 ppb. Changing the K_vs only between the lowest two layers had little impact (generally less than 4 ppb) on midday ozone peaks but affected the simulated surface nighttime ozone and precursor concentrations. Based on the K_v sensitivity simulations, a land-use-dependent minimum K_v value was prescribed. This improved the nighttime simulated concentrations but had little effect on the daytime peaks.

Alternate horizontal dispersion parameters and numerical advection schemes were also tested but produced very small differences in simulated ozone peak concentrations when 4 km or larger grid resolution was used. At 4 km grid cell resolution, a finite-element advection scheme produced simulated ozone peaks only 3 or 4 ppb higher than the standard (Smolarkiewicz) scheme for the days 18 and 19 August, but 8 ppb higher ozone for the peak well downwind of an assumed "spill" (see discussion below) on 19 August.

In the initial simulations of this episode, cloud cover was estimated using available data. Gridded cloud-cover fields were prepared by interpolating the observed values. Given the paucity of the available measurements, however, the gridded fields were quite uncertain. To avoid introducing errors associated with this uncertainty into the simulations, clear-sky conditions were assumed for the base-case modeling. This increased the simulated ozone concentrations by about 20 ppb. Comparison of the interpolated cloud fields with satellite images later revealed that the interpolated fields spread the cloud cover over much too broad an area, lending support to the decision to use clear sky conditions.

To test the sensitivity of the model to the specification of photolysis rates, spatially invariant photolysis rates corresponding to those used in the regulatory version of the UAM were substituted for the UAM-V photolysis rate estimates. In general, these are higher than those used with the UAM-V. A moderate sensitivity was indicated: using

the higher photolysis rates, simulated ozone peak concentrations increased by 15, 38, and 25 ppb for 17, 18, and 19 August, respectively.

Initial- and Boundary-Condition-Related Diagnostic and Sensitivity Simulations

For the August episode the UAM-V was started two days prior to the day with highest ozone peaks in order to minimize any dependency on initial conditions. To assure that the effects of initial conditions were, in fact, minimized, the UAM-V was run in an inert mode and the advection of "initial-condition" tracers was examined. Based on these simulations, the initial conditions were not expected to influence the simulated concentrations beyond 17 August.

Measurements taken from aircraft during the August episode showed that ozone concentrations aloft (up to a height well above the top of the modeling domain) were 60 ppb or higher. Ozone concentrations along the top boundary of the modeling domain were therefore increased from 40 to 60 ppb to examine the influence of the upper boundary conditions on the simulated ozone concentrations. The simulated ozone concentrations were increased only slightly and model performance was not improved; nevertheless, the higher top boundary concentration was retained because it was consistent with the observed upper-air data.

Sensitivity to Other Input Parameters

Use of the plume-in-grid (P-i-G) treatment for elevated point sources was investigated for this episode. However, the effects of P-i-G were small compared to the other emissions-related sensitivity simulations.

Sensitivity to grid cell size was examined with a coarse-grid only simulation and the addition of a 1-km nested grid over the Houston ship channel area. The coarse-grid only simulation was primarily used as an initial test of the model inputs. With 1-km resolution, simulated ozone concentrations were affected only slightly.

Evidence for a Hydrocarbon Spill Affecting the 19 August 1993 Episode

The peak observed ozone concentration in the Houston area on 19 August (231 ppb) was the highest ozone concentration observed within the modeling domain during 1993. As reported in Section 3, high VOC concentrations were observed at the Clinton monitoring site (also located within the Houston area) between the hours of 1300 and 1400 CST on this day and a petroleum product spill was reported to have occurred in the ship channel area. This information, coupled with the localized nature of the observed ozone peak, suggested that such an incident may have contributed to the observed high ozone concentrations. Several diagnostic simulations were performed to examine this possibility.

Figure 4-71 illustrates, through interpolation of the observed data, the daily maximum ozone concentrations for 19 August 1993. The peak ozone value of 231 ppb (at the Aldine site) is quite localized, even though the ozone values in this figure do not represent simultaneous observations. Site-specific peaks were also measured one hour earlier at the site just upwind (southeast) of the Aldine site and one hour later at the site just downwind (northwest) of Aldine. The afternoon winds were very light and generally from the southeast, indicating possible transport of ozone and precursors from the nearby Houston Ship Channel region. At the upwind site, which is 6.6 km away, the observed ozone concentration was 177 ppb for the hour before the 231 ppb was measured at Aldine but 163 ppb at the time of the measured peak at Aldine. At the downwind site, an ozone concentration of 130 ppb was observed at the time of the maximum ozone concentration at Aldine; one hour later this value increased to 161 ppb. Observed concentrations at another nearby monitor site (10 km away) reached only 90 ppb ozone on this day. Backward particle paths calculated using the SAIMM wind field for the sites at which the four highest ozone concentrations were observed (Figure 4-72) indicate that shortly before arriving at the observation sites, the particles slowly passed through the industrial region near the ship channel. Additionally, a high level of hydrocarbons was detected at the Clinton monitoring site (located near the ship channel) during the midday period (Figure 4-73).

Figure 4-74 shows the flight path and sampling locations for aircraft measurements taken on the afternoon of 19 August around the region of the high ozone peak in Houston. The aircraft data, taken within two hours of the observed ground-level peaks, showed no indications of high ozone except for the traverse into and near Baytown on the eastern part of the ozone "cloud" depicted in Figure 4-71. The data thus tend to confirm a boundary for the localized peak ozone values of this event.

A petroleum product spill of about 15,000 gallons in the ship channel area between 1000 and 1300 CST was simulated by locally adjusting the emissions inventory. Daily maximum simulated ozone concentrations for the simulation of 19 August without the spill but with the previously described adjustments to the emissions inventory are shown in Figure 4-75. The maximum simulated ozone concentration is 190 ppb, located between the sites which registered peak concentrations of 231 and 161 ppb. At observation sites away from the area impacted by the ship channel emissions the simulated values are considered to be in satisfactory agreement with observations.

In simulation results with the spill, shown in Figure 4-76, the ozone peak is closer to the ship channel source region and the maximum is 241 ppb. The increase in VOC-to-NO_x ratio has accelerated the photochemistry so that the peak occurs earlier in the day. Due to highly concentrated emissions in the ship channel area, a delay in peak ozone formation translates into a lower peak concentration due to dispersion of these highly concentrated precursors as they move downwind. The highly localized ozone produced by this combination of ship channel emissions and an assumed petroleum product spill is depicted by the three-dimensional plot shown in Figure 4-77, which is the same information as shown in Figure 4-76, except for the method of plotting.

Summary

The results of the diagnostic and sensitivity simulations suggested that adjustment of the emissions inventory was required to simulate ozone concentrations that approached the observed concentrations. An adjusted inventory that includes (1) double the mobile VOC, (2) increased stationary VOC emissions (50 percent), and (3) reduced elevated NO_x emissions (50 percent) was prepared and was used for the base-case and future-year simulations. Emissions corresponding to the petroleum product spill were also included in the base-case modeling for the August episode.

ANALYSIS OF THE 6-11 SEPTEMBER 1993 EPISODE

The diagnostic and sensitivity analysis for the September episode benefited from the information obtained during the analysis of the August episode. Emission-related sensitivity simulations were performed to determine whether the adjustments that were made for the August episode were also appropriate for the September episode (that is, whether the adjustments improved model performance). Sensitivity simulations involving the meteorological inputs were also performed.

Initial Simulation Results

The initial UAM-V simulation for the September episode, using the baseline emissions inventory and the coarse- and fine-grid wind fields, produced a maximum simulated ozone concentration in the Houston area of 135 ppb (on 9 September). Observed concentrations at most sites were significantly underestimated (concentrations greater than 200 ppb were observed at two sites on 8 September). As with the August episode, the initial simulation results indicated deficiencies in the emissions or meteorological inputs. Several diagnostic and sensitivity simulations were performed to examine whether the changes made to the inventory for the August episode (with the exception of the spill) also improved model performance for the September episode. The changes produced a similar positive response for this episode, providing additional support for the adjustments. Given the magnitude of the adjustments that were needed for September and based on the diagnostic and sensitivity simulation results for August, it was also apparent that the errors and uncertainties associated with the emission inventory outweighed any that might be present in the other inputs. Only two meteorological input sensitivity simulations were performed for this episode.

Emissions-Related Diagnostic and Sensitivity Simulations

A number of sensitivity simulations were performed to examine the response of the model to changes in emissions, in particular those adjustments that were made for the August episode. Reducing all elevated NO_x emissions by a factor of 2 resulted in increased maximum ozone concentrations on all but one day of the episode. These increases ranged from 7 to 49 ppb for 6-10 September; the peak was reduced by 1 ppb

for 11 September. Increasing the mobile-source VOC emissions (by a factor of 2) and the stationary (area and point) source VOC emissions (by a factor of 1.5) further increased concentrations throughout the Houston area and resulted in peak simulated concentrations of 190, 234, 164, and 186 ppb for 8, 9, 10, and 11 September, respectively.

Maximum observed ozone concentrations on 8 and 9 September occurred nearer to the coastline than for the August episode. Even with the above-mentioned emission inventory adjustments, simulated ozone concentrations at several of the sites where the highest concentrations were observed were low relative to the observations (e.g., at the Gilchrist, Texas City, Seabrook, and Smith Point monitoring sites). Several additional simulations were performed to investigate the possible causes of these underestimates.

In one such simulation, all NO_x emissions for the lower Galveston Bay ship channel were assumed to be zero (Figure 4-78 shows the location of these emissions). These NO_x emissions amounted to about 50 tons per day. In another simulation, all point source NO_x emissions in the two grid cells containing Texas City were set to zero; this also amounted to a local NO_x reduction of approximately 50 tons per day.

Both of these sensitivity simulations showed ozone increases of 30 to 50 ppb for the lower Galveston Bay region for 8 and 9 September. While such ozone increases significantly improve model performance and confirm that high NO_x emissions in the inventory suppressed simulated ozone locally in this region, we cannot conclude which of the two changes that were made might be more indicative of any specific errors in the emissions inventory. Figures 4-79 through 4-82 show the ozone changes produced for the two sensitivity simulations for the two days of 8 and 9 September. Presumably, some combination of too much NO_x in the inventory for the Texas City point sources and the ship channel plus a substantial underrepresentation of VOC in this region would be consistent with these results as well.

Meteorology-Related Diagnostic and Sensitivity Simulations

Two simulations designed to investigate the effect on the UAM-V simulation results of certain assumptions related to meteorological modeling were also performed as part of the diagnostic and sensitivity analysis for the September episode.

As for the August episode, a land-use-dependent minimum K_v value was prescribed and the K_v fields were smoothed to reduce the sharp gradients along the coastline. This improved the nighttime simulated concentrations but had little effect on the daytime peaks.

To investigate the effects of differences between the simulated and observed surface winds on the UAM-V simulation results, alternate meteorological fields for 8 and 9 September were prepared by including a large-scale forcing term in the SAIMM simulation. The simulated gulf breeze penetrated too far inland during the afternoon of 8 September, and the simulated northerly wind components to the north of the gulf breeze front were weaker than observed for the afternoon of 9 September. These

differences may have contributed to the apparent displacement of the simulated high ozone concentrations to the north of where the peaks were observed. Incorporation of a large-scale forcing term enhanced the SAIMM-simulated southward flow component but degraded the wind fields such that the agreement between the simulated and observed winds was lessened. Use of the alternate wind fields resulted in some improvement in the UAM-V simulation for 8 September, but results for 9 September were slightly degraded. The alternate wind fields were not used for the base-case simulation.

Summary

The results of the diagnostic and sensitivity simulations for this episode indicated that emission inventory adjustments were required to simulate ozone concentrations that compared favorably with those observed. The adjustments that were made for the August episode were similarly beneficial for this episode and were used for the base-case and future-year simulations, but these were not sufficient to provide good model performance at key monitoring sites located between Houston and the coast.

SUMMARY OF DIAGNOSTIC AND SENSITIVITY ANALYSIS RESULTS

The diagnostic and sensitivity simulations that were performed for the August and September episodes support the following conclusions:

1. The steep ozone gradients observed for all high ozone days in the Houston-Galveston region could not be properly simulated with coarse (16 km) grid cells. To simulate such steep ozone gradients, a fine resolution (1 to 4 km) is required for the model and for the meteorological fields and emissions inventory. For this analysis, only the ship channel and point source emissions could be resolved to 1 km; although the 1-km resolution of these emissions was tested, it appears not to be necessary. A full 1-km test (with 1-km resolution for all emissions and for the meteorological fields) was not performed, however, and any potential benefits of such an enhancement remain unknown.

2. Either lower localized NO_x or higher VOC emissions in the Houston/Galveston Bay area or some combination of these two appears to provide a better simulation of ozone for all the high ozone days. Use of day-specific emissions data, such as the petroleum product spill on 19 August, might improve model performance even further.

3. The especially steep gradients and high ozone concentrations observed on 19 August appear to be caused by an extreme localized fluctuation in the day-to-day emissions in the highly industrialized ship-channel region combined with the local meteorological conditions. We have reproduced the observed 19 August ozone "spike" using only a local VOC increase at a location where a spill was known to have occurred on that day. However, the actual size of the spill remains unknown, and the results of the one-half NO_x emissions sensitivity simulations suggest that

lowering the NO_x emissions can give similar results. Some combination scenario (higher VOC, lower NO_x) cannot be ruled out as having possibly existed during this episode.

4. Simulation results for the September episode indicate that underestimation of the high ozone concentrations at some sites in the Galveston Bay area may be due to local suppression of ozone by high local NO_x emissions. However, low VOC emission estimates or inaccurate representation of the gulf breeze could also be contributing factors.

5. Some overestimation of observed ozone concentrations for some of the days with the lowest values using the adjusted inventory may actually be due to the prescribed solar radiation associated with the assumption of clear skies; cloud cover seen in satellite photos was not incorporated into the simulation.

6. Significant uncertainty exists in the emission inventory estimates. Although the uncertainty in the emission inputs precluded a comprehensive examination of the meteorological or other inputs as part of the diagnostic and sensitivity analysis, the information derived from such an analysis proved useful in identifying the key inputs that influenced the simulation results.

4.9 BASE-CASE SIMULATIONS: 1993 EPISODES

Base-case UAM-V model performance for the August and September episodes is summarized in this section. The simulations described were performed using the adjusted emissions inventory summarized in the previous section.

AUGUST EPISODE

On three of the four days modeled for the August episode (18, 19, and 20 August 1993) ozone exceedances were observed in the Houston area. Observed concentrations on 17 August also approached the ozone standard. Although this discussion touches on model results and model performance for 17 and 18 August, these days were simulated primarily as initialization days for 19 and 20 August. The following discussion focuses primarily on the two latter days. For easy reference, the locations of selected ozone monitoring sites are plotted in Figure 4-83.

During all days of this episode, both the observed and simulated ozone peaks are located to the north or northwest of Galveston Bay. On 17 August, the simulated and observed peaks in the Houston area are in close proximity, but the simulated concentrations are higher than observed (see Figure 4-84). To the south toward the ship channel, both the observed and simulated values decrease considerably. South of the ship channel, simulated concentrations are fairly uniform at around 60 ppb, but the observed concentrations vary from about 25 ppb to 75 ppb in this area. In the rest of the domain (Figure 4-85), observed ozone concentrations are for the most part between 60 ppb and

90 ppb, although some concentrations above 100 ppb are observed near Baton Rouge. Simulated values are also in this range, but are higher than observed in the Beaumont/Port Arthur/Lake Charles area and lower than observed in the Baton Rouge area.

On 18 August, the observed and simulated ozone peaks in the Houston area are considerably higher than on the previous day. The location of the simulated maximum is near that of the observed maximum, but, as on 17 August, the value is overestimated (Figure 4-86). The characteristics of the simulated and observed ozone concentration patterns are rather similar between the two days. Concentrations once again decrease near the ship channel, and concentrations south of the ship channel are relatively low (lower in the observations than the simulation). In eastern Louisiana (see Figure 4-87), ozone concentrations greater than 120 ppb were observed, and the simulated concentrations are nearly as high. The hourly simulated concentration patterns indicate transport of ozone from southeast Texas to Baton Rouge during the nighttime hours. As described in Section 3, this may have been associated with the presence of a low-level jet between the hours 0000 and 0800 CST. Around Beaumont/Port Arthur/Lake Charles (BPA/LC), simulated concentrations are somewhat higher than the observed maximum of 116 ppb.

Numerous ozone exceedances were observed on 19 August. The maximum simulated ozone concentration is 242 ppb while the observed maximum is 231 ppb. The distribution of ozone (see Figure 4-88) is somewhat different on this day than on the other days of this episode. Both the observed and simulated peaks are located farther west than on the other days with a pronounced ozone plume extending northwestward from the ship channel area. This plume is more evident in the simulation, but is also somewhat supported by the observations. The simulation results indicate that this plume extends more than 70 km north of Houston, but there are no observations in this area to confirm the extent of the plume. An observation of 161 ppb located about 40 km northwest of the observed ozone peak lends some support to this simulated feature. Addition of VOC emissions in the ship channel clearly contributes to formation of this ozone plume, but sensitivity simulations have shown that this pattern occurs even without the additional emissions. Ozone concentrations south of the ship channel are higher on 19 August than on other days of this episode, with observed and simulated values consistently 60 ppb or higher. Agreement between the observed and simulated ozone distributions is better on this day than on 17 and 18 August. In the rest of the domain (see Figure 4-89), the observed and simulated ozone patterns are in fairly good agreement. Simulated values in the BPA/LC area are somewhat higher than the observations, but an exceedance was observed in this area. Values slightly above the standard are present in both the observations and simulation in eastern Louisiana, with the simulated maximum value occurring about 40 km north of the observed maximum.

The simulated ozone concentration pattern for 20 August (Figure 4-90) resembles those for the 17th and 18th. High observed ozone concentrations along the northern edge of Galveston Bay are not well simulated. The simulated and observed peaks on this day are 168 ppb and 187 ppb, respectively. Although the steep gradient in observed ozone concentrations is again present along the ship channel, ozone concentrations south of the

ship channel are highest for this episode on 20 August. Local ozone maxima (observed and simulated) again occur near BPA/LC and Baton Rouge (see Figure 4-91). The simulated peak is located northeast of the observed peak in the BPA/LC area but is of about the right magnitude. The peak is overestimated somewhat in the Baton Rouge area.

Table 4-20 presents some selected model performance statistics for ozone for all four days of the episode for a subdomain around Houston. The statistics include the unpaired accuracy of the peak concentration (in which the domain-wide simulated peak is compared to the observed peak), the average accuracy of the peak (averaged over all monitoring sites), the normalized bias, the normalized gross error, and the root-mean-square error (RMSE). The normalized bias and gross error statistics are calculated using a cutoff concentration of 40 ppb (i.e., observation/simulation pairs are not included in the calculation of these statistics if the observed values is less than 40 ppb). For reference, the EPA-recommended ranges for the unpaired accuracy of the peak, the normalized bias, and the normalized gross error are also provided. These represent the range of values associated with acceptable model performance for urban-scale photochemical modeling, and although they are not directly relevant for this modeling study, they provide some perspective regarding statistical model performance. As noted in Section 3, good agreement between the surface and low-altitude ozone concentrations was observed during this episode, so comparison of the UAM-V layer 1 concentrations with surface observations is a reasonable approach to evaluating model performance.

Table 4-20. Selected model performance statistics for the August 1993 episode (Houston subdomain).

	Recommended range	17 Aug	18 Aug	19 Aug	20 Aug
Observed maximum (ppb)		119	139	231	187
Simulated maximum (ppb)		163	185	223	166
Unpaired accuracy of the peak (%)	< 15–20	37	33	−3	−11
Average accuracy of the peak (%)	—	50	24	−8	−13
Normalized bias (%)	< 5–15	32	17	−12	−21
Normalized gross error (%)	< 30–35	41	27	25	26
RMSE (ppb)	—	27	20	25	24

The statistics on 17 and 18 August are not within the EPA-recommended ranges because of considerable overestimation, but the performance on 19 August is quite good with all statistics falling within the recommended range. Since predictions on 20 August tend toward underestimation, performance is not as good as on the 19th.

Further insight into model performance for this episode can be gained by examining time-series displays of observed and simulated ozone concentrations for monitoring sites

within the Houston subdomain. Figure 4-92 shows time-series plots for selected sites within this subdomain. In these plots, the box symbols represent the observed concentrations, the solid line represents the four-cell weighted average simulated concentrations, and the dashed lines indicate the maximum and minimum simulated values within one grid cell of the monitoring site location. Thus, the shaded area represents the range of simulated concentrations within one grid cell of the monitoring site. Simulated and observed concentrations for the sites TN12, SBRC, TN10, and TN17 (Texas City, Seabrook, Aldine, and Northwest Harris County) are shown in Figure 4-92a. Overall, observed concentrations are well represented at these sites. The peak simulated concentrations are lower than observed at all four sites on 19 August and at the TN12, SBRC, and TN17 sites on 20 August. The timing of the peaks, however, is very well represented with the simulated peaks occurring ahead of the gulf breeze front and simulated concentrations decreasing following its passage. This is consistent with the findings of the data analysis and suggests that the timing and inland penetration of the gulf breeze is well represented by the simulated wind fields.

Time-series plots for sites TN5, TN2, TN3, and CRSC, which are located southwest of (TN5), within (TN2 and TN3), and northeast of (CRSC) Houston, are shown in Figure 4-92b. The relatively low concentrations at TN5 are well simulated on all four days. At the other sites, the simulated peaks are higher than observed on 17 and 18 August and very close to what was observed on the 19th and the 20th. The observed diurnal concentration profiles are well simulated, especially for the latter two days of the simulation period.

Statistics for sites in the Beaumont/Port Arthur/Lake Charles area, presented in Table 4-21, indicate a considerable bias toward overestimation on 17 and 18 August with a smaller bias toward underestimation on the 19th and 20th. Peaks on the 17th through the 19th are not reproduced well, but performance on 20 August is quite good. Time-series plots for sites located in the Beaumont/Port Arthur/Lake Charles area are presented in Figure 4-93. Observed ozone concentrations are underestimated at the TN8 site (Beaumont) on 19 and 20 August and overestimated at the LO24 site (Lake Charles) on all days of the simulation period. It is not likely that this is due to differences between the emissions estimates for Texas and Louisiana since simulated concentrations at the TN18 and LO5 sites, also located in Texas and Louisiana, respectively, are generally quite consistent with the observed values.

Statistics for the Baton Rouge area are presented in Table 4-22. Performance on 17–19 August is fairly good except for the overestimation on the 19th. Performance degrades on 20 August with a consistent bias toward overestimation and gross error that is rather large. Time-series plots for sites within the Baton Rouge area are presented in Figure 4-94. Simulated concentrations are generally higher than observed during the nighttime hours probably due to the coarse resolution of the grid in this portion of the domain. Agreement between the simulated and observed concentrations during the daytime hours varies from site to site and from day to day.

Maximum values for the full modeling domain are found within the Houston subdomain, and therefore the statistics on the peaks for the full domain do not differ from those for

Table 4-21. Selected model performance statistics for the August 1993 episode (Beaumont/Port Arthur/Lake Charles subdomain).

	Recommended range	17 Aug	18 Aug	19 Aug	20 Aug
Observed maximum (ppb)		95	116	125	110
Simulated maximum (ppb)		117	139	160	116
Unpaired accuracy of the peak (%)	< 15–20	23	20	28	6
Average accuracy of the peak (%)	—	19	18	−12	8
Normalized bias (%)	< 5–15	21	26	−12	−7
Normalized gross error (%)	< 30–35	28	30	19	22
RMSE (ppb)	—	18	21	15	17

Table 4-22. Selected model performance statistics for the August 1993 episode (Baton Rouge subdomain).

	Recommended range	17 Aug	18 Aug	19 Aug	20 Aug
Observed maximum (ppb)		118	127	126	112
Simulated maximum (ppb)		97	119	127	140
Unpaired accuracy of the peak (%)	< 15–20	21	−6	−6	13
Average accuracy of the peak (%)	—	−5	−7	8	25
Normalized bias (%)	< 5–15	3	10	17	37
Normalized gross error (%)	< 30–35	21	20	25	39
RMSE	—	15	16	19	24

the Houston subdomain (see Table 4-23). On a domain-wide basis, the bias is very small (indicating both under- and overestimation of the observed concentrations), but the gross error is slightly larger than for the Houston subdomain.

COMPARISON OF UAM-V SIMULATED CONCENTRATIONS WITH AIRCRAFT MEASUREMENTS

Measurements of ozone and precursor concentrations from aircraft flights were made on 18–20 August 1993 in several parts of the modeling domain, including the Houston and Beaumont areas. Figures illustrating the comparison of these measurements with UAM-V simulated concentrations from the base case have been prepared. A discussion of that comparison is presented in this section along with a selected subset of the plots.

Table 4-23. Selected model performance statistics for the August 1993 episode (full modeling domain).

	Recommended range	17 Aug	18 Aug	19 Aug	20 Aug
Observed maximum (ppb)		119	139	231	187
Simulated maximum (ppb)		163	185	223	166
Unpaired accuracy of the peak (%)	< 15–20	37	33	−3	−11
Average accuracy of the peak (%)	—	14	6	−3	0
Normalized bias (%)	< 5–15	0	6	0	−5
Normalized gross error (%)	< 30–35	35	32	29	33
RMSE (ppb)	—	27	25	25	26

On 18 August, agreement between the aircraft observations of ozone and NO_x is fairly good. The examples shown in Figure 4-95, displaying ozone and NO_x concentrations as a function of height above ground, are representative of the agreement between observations and predictions for that morning. In these displays, the solid line represents the instantaneous aircraft measurement of ozone or NO_x. Dashed lines running across the plot depict the height of the UAM-V model layer interfaces. The simulated concentrations are displayed as the numerical value of the concentration with a bar underneath that shows the range of predicted concentrations within one grid cell of the location of the aircraft spiral. If a surface observation is available near the spiral location, a triangle which points to the value of the observed concentration is plotted along the x axis. Figure 4-95 presents data collected during an aircraft spiral flown in a location a few kilometers north of Galveston Bay. Up to about 300 m agl, observed concentrations of ozone are virtually zero, while the simulated concentrations are a few ppb. Simulated and observed ozone concentrations increase at nearly the same rate from 300 to 1000 m, both reaching a value aloft of about 60 ppb. Simulated and observed NO_x concentrations near the ground range from 20 to 90 ppb and drop to near zero above 500 m. The agreement in the simulated and observed vertical profiles for NO_x and ozone indicates that the mixing depth (represented in the model by the vertical exchange coefficients, K_v) is accurately prescribed in the model. The morning simulated and observed vertical profiles of NO_x and ozone agree in most of the aircraft data plots. The absence of carryover in the simulation, as indicated by the simulated vertical profiles of ozone concentrations, is consistent with the conceptual model of this episode presented in Section 3.

Later in the simulation, the simulated ozone concentrations tend to be low compared to the aircraft measurements, especially above 1000 m. Figure 4-96 displays the NO_x and ozone concentrations above Houston on the morning of 19 August 1993. Agreement between observed and simulated ozone is good below 1000 m, but aloft the simulated concentrations are lower than observed. This may be due to improper specification of

boundary conditions aloft, underrepresentation of vertical mixing on the previous day, or the fact that the aircraft is providing an instantaneous sample of the atmosphere while the modeled concentrations are hourly averages. Agreement between observed and simulated NO_x, however, is good throughout the entire vertical profile.

On the afternoon of 19 August (Figure 4-97), agreement between observed and simulated ozone concentrations in the spiral taken above the Crosby site (CRY), located about 20 km northwest of Baytown, is good in the mixed layer, but above 1000 m simulated ozone concentrations are again lower than observed. Other aircraft spirals confirm that the simulated ozone aloft is low compared to aircraft observations on both 19 and 20 August. Simulated ozone concentrations typically are around 40 ppb aloft on these two days while observed concentrations are 60–70 ppb. Again, this may be due to boundary conditions, vertical mixing, or the discrepancy between the instantaneous measurements and the hourly averaged simulated values. NO_x concentrations are quite low in both the observed and simulated data in Figure 4-97b. The simulated hydrocarbon concentrations agree well with the single measurement of hydrocarbon available during this flight.

In summary, for the majority of the spirals flown in the Houston area for the August episode, the UAM-V simulated concentrations compare favorably to the aircraft measurements for both ozone and NO_x. This agreement indicates that the models are properly replicating the physical and chemical processes that influence the vertical structure of observed ozone and NO_x concentration patterns at various locations and at various times throughout the day and lends support to the emission inventory adjustments.

SEPTEMBER EPISODES

The September simulation period includes two episodes and six days, 6–11 September 1993; ozone exceedances occurred in the Houston area on all days except 7 September. During this period, the maximum ozone concentrations were observed in very different locations on different days of the episodes. This is characteristically different from the August episode during which the ozone peak consistently occurred north or northwest of Galveston Bay. The first two days, 6 and 7 September, were simulated primarily as initialization days, but they will be discussed to some extent along with the primary episode days.

On 6 September, the observed and simulated ozone maxima are located just southwest of Houston, but the simulated peak is somewhat lower than the observed peak (see Figure 4-98). Observed and simulated ozone concentrations throughout the rest of the Houston subdomain range from about 60 to 70 ppb. Outside of the Houston subdomain (see Figure 4-99), concentrations are for the most part 60 ppb or less. Southeast of the Beaumont/Port Arthur/Lake Charles (BPA/LC) area, observed ozone concentrations exceed 100 ppb while the maximum simulated ozone concentrations are about 90 ppb.

Although observed ozone concentrations on 7 September do not exceed 120 ppb, ozone concentrations of more than 140 ppb are simulated over the Gulf of Mexico (likely due to the offshore advection of pollutants). In the southern part of the Houston subdomain

(see Figure 4-100), a maximum ozone concentration greater than 100 ppb was observed at several monitoring sites, and the simulated values agree fairly well with these observations. No data are available to confirm the high simulated ozone concentrations over the Gulf. In and north of Houston, both observed and simulated ozone concentrations are around 60 ppb. In the remainder of the modeling domain (Figure 4-101), both observed and simulated ozone concentrations are fairly low (60 ppb or lower).

September 8 is the first day of the episode that has very high ozone concentrations. In the Houston subdomain, the observed data indicate an ozone cloud that resides over Galveston Bay and extends a few kilometers onshore (see Figure 4-102). The simulated ozone peak, however, is onshore, approximately over Baytown with a finger of high ozone extending about 40 km to the west. Simulated ozone concentrations approach the observations at some of the shoreline sites, but at Texas City, on the west side of the mouth of the bay, simulated values are well below the observed peak. There is a rather sharp gradient in the simulated ozone concentrations to the north of Texas City. The full modeling domain is shown in Figure 4-103. The high simulated ozone concentrations extend outward into the Gulf of Mexico from Galveston Bay. High ozone is also simulated for the BPA/LC area, but the observed ozone reaches only about 110 ppb. Near Baton Rouge, ozone concentrations over 100 ppb are observed, but the simulated values are only about 80 ppb.

The simulated distribution of ozone on 9 September in the Houston subdomain (Figure 4-104) is similar to that for 8 September with the simulated peak located over the bay, but the ozone cloud is located a little farther southeast than on the 8th and the simulated concentrations are higher. Nevertheless, the simulated ozone cloud is again located too far north, but the high concentrations do not extend nearly as far west as on the 8th. The high ozone concentrations observed at Gilchrist (189 ppb) and Texas City (184 ppb) are underestimated, but the simulated concentration pattern shows that higher concentrations extend toward these areas. The modeling results indicate a rather large area of high ozone concentrations north of Galveston Bay, but there are insufficient observations to determine if this is appropriate. In the BPA/LC area (see Figure 4-105), observed and simulated values are both a little over 100 ppb. Similarly, in the Baton Rouge area, observed and simulated ozone concentrations are also a bit over 100 ppb.

As shown in Figure 4-106, moderately high ozone concentrations are observed in several portions of the Houston subdomain on 10 September: the peak of 162 ppb on Galveston Island, 130–150 ppb along the shore of Galveston Bay, and over 130 ppb at the western side of Houston. The simulated peak of 167 ppb is located on the western side of Houston with values that approach, but do not quite reach, the observed values in other parts of the domain. There is also an area of relatively high simulated ozone concentrations (>130 ppb) about 40 km north of Galveston Bay, but there are no monitors in this area. Simulated ozone concentrations in the BPA/LC area (see Figure 4-107) are quite high with the domain-wide peak of 206 ppb sitting just offshore, south of Port Arthur. Observed concentrations in this area are also fairly high, with a value of 141 ppb observed at a nearby coastal site. In eastern Louisiana, observed and simulated ozone concentrations are in the neighborhood of 100 ppb.

On 11 September, the display of the simulated ozone concentrations in the Houston subdomain (see Figure 4-108) exhibits a pattern similar to that seen for the August episode. The maximum simulated ozone concentration of 186 ppb is located about 70 km northwest of Galveston Bay. However, the highest observed concentrations, with a peak of 189 ppb, are located in Houston while the simulated ozone concentrations in this part of the domain are only about 110 ppb. A gradual gradient exists across the southern portion of the subdomain, with both observed and simulated ozone concentrations dropping from about 120 ppb on the eastern side to 80 ppb on the west side. In the BPA/LC area (see Figure 4-109), simulated and observed ozone concentrations agree fairly well, both showing ozone higher than 110 ppb. There is a local simulated maximum between Houston and Beaumont that exceeds the value observed in that part of the domain. In eastern Louisiana, observed and simulated concentrations both reach about 100 ppb.

Selected statistical performance measures for the Houston subdomain are presented in Table 4-24 for all days of the September episodes. Performance on 6 September is poor but improves on the 7th and remains improved for the rest of the episode days. There is a bias toward underestimation during most of the episode days, and the peak is underestimated on three of the six days. Time-series plots comparing the simulated and observed concentrations at selected monitoring sites are provided in Figure 4-110. For sites located south and east of Houston (GALC, GILC, SPTC, and SBRC) (Figure 4-110a), model performance with regard to the timing and magnitude of the peak ozone concentrations is variable. The timing of the observed peak concentrations at the Galveston (GALC) and Gilchrist (GILC) sites is well simulated; simulated concentrations are lower than observed at GALC on 10 September and at GILC on 9 September. Simulated ozone concentrations for Smith Point (SPTC) and Seabrook (SBRC) are lower than observed on 8–11 September (except at Seabrook on 9 September) but the day-to-day variation in magnitude is simulated (e.g. the highest concentrations occur on the 8th and 9th). The simulated peaks lag the observed peaks by about one hour on 9 September. In general, the time-series plots for 8 September indicate that although the simulated winds are from the north (see Figure 4-111), insufficient quantities of ozone and precursor pollutants from the Houston area are advected toward SPTC and SBRC during the mid- to late-morning hours. This also seems to be true for SPTC on 9 September and might also explain the lower than observed concentrations at the Gilchrist site on 9 September (i.e., concentrations do not continue to increase following flow reversal because not enough material was carried offshore during the morning hours).

These discrepancies between the observed and simulated concentrations indicate that inaccuracies in either the emissions or the wind fields or some combination of both may have adversely influenced the simulation results. As noted earlier, the simulated gulf breeze penetrated too far inland during the afternoon of 8 September, and the simulated northerly wind components to the north of the gulf breeze front were weaker than observed for the afternoon of 9 September. These differences may have contributed to the apparent displacement of the simulated high ozone concentrations to the north of where the peaks were observed. Alternatively, additional emission inventory adjustments or day-specific-emission estimates may have improved the simulation for the September episode.

Table 4-24. Selected model performance statistics for the September 1993 episode (Houston subdomain).

	Recommended range	6 Sep	7 Sep	8 Sep	9 Sep	10 Sep	11 Sep
Observed maximum (ppb)		136	111	214	195	162	189
Simulated maximum (ppb)		112	133	188	234	164	169
Unpaired accuracy of the peak (%)	< 15–20	−18	20	−12	20	1	−11
Average accuracy of the peak (%)	—	−25	8	−8	28	1	−16
Normalized bias (%)	< 5–15	−39	−10	−14	6	−10	−6
Normalized gross error (%)	< 30–35	40	22	25	34	28	31
RMSE (ppb)	—	30	16	28	31	31	29

Time-series plots for sites within the Houston area are presented in Figure 4-110b. Much better agreement between the simulated and observed concentrations is exhibited for these sites, although the simulated peaks at TN2 and TN3 (in Houston) are higher than observed for 8 and 9 September.

Selected statistical performance measures for the BPA/LC subdomain are presented in Table 4-25 for all days of the September episodes. Although most performance measures are within the EPA-recommended ranges, on 6 and 10 September the bias and gross error are quite high. The bias toward overestimation on the 10th might be mitigated if the simulated ozone cloud were located just a short distance farther offshore, and there is an indication in the observations that ozone increases toward the coastline. Accuracy for the peak is in general not very good for this subdomain. Time-series plots for sites within this area are presented in Figure 4-111. High nighttime simulated concentrations at the TN18 sites are likely related to the rural location of this site and the northerly flow components (i.e., no NO emissions are available to titrate the simulated ozone).

In the Baton Rouge area, the statistics (presented in Table 4-26) indicate good performance for 6 through 9 September but show a bias toward overestimation on the 10th and 11th. Accuracy of the peak is fairly good except on 7 September. The time-series display for simulated and observed ozone shown in Figure 4-112 is consistent with the implications of the statistics.

The statistics for the full domain, presented in Table 4-27, do not indicate a strong bias in the simulation other than on 6 September, the first day of the simulation. While the peak is fairly well simulated on most days, the gross error is quite large in some cases.

Table 4-25. Selected model performance statistics for the September 1993 episode (Beaumont/Port Arthur/Lake Charles subdomain).

	Recommended range	6 Sep	7 Sep	8 Sep	9 Sep	10 Sep	11 Sep
Observed maximum (ppb)		94	78	113	110	141	116
Simulated maximum (ppb)		85	121	148	120	207	151
Unpaired accuracy of the peak (%)	< 15–20	−10	55	31	9	47	30
Average accuracy of the peak (%)	—	−17	20	9	−5	31	8
Normalized bias (%)	< 5–15	−27	12	−1	9	29	11
Normalized gross error (%)	< 30–35	31	21	22	17	34	20
RMSE (ppb)		24	14	17	14	25	16

Table 4-26. Selected model performance statistics for the September 1993 episode (Baton Rouge subdomain).

	Recommended range	6 Sep	7 Sep	8 Sep	9 Sep	10 Sep	11 Sep
Observed maximum (ppb)		73	63	108	124	105	107
Simulated maximum (ppb)		74	84	97	109	124	107
Unpaired accuracy of the peak (%)	< 15–20	2	33	−11	−12	18	−0.2
Average accuracy of the peak (%)	—	3	25	−2	8	32	34
Normalized bias (%)	< 5-15	−6	15	1	10	41	34
Normalized gross error (%)	< 30–35	21	22	13	18	43	35
RMSE (ppb)	—	13	12	10	15	29	22

Table 4-27. Selected model performance statistics for the September 1993 episode (full modeling domain).

	Recommended range	6 Sep	7 Sep	8 Sep	9 Sep	10 Sep	11 Sep
Observed maximum (ppb)		136	111	214	195	162	189
Simulated maximum (ppb)		112	146	188	234	207	184
Unpaired accuracy of the peak (%)	< 15–20	−18	31	−12	20	28	−3
Average accuracy of the peak (%)	—	−15	12	−6	4	11	−2
Normalized bias (%)	< 5–15	−29	−4	−10	3	9	6
Normalized gross error (%)	< 30–35	34	24	23	28	35	31
RMSE (ppb)	—	25	18	24	25	29	26

4.10 SUMMARY OF AND INTERPRETATION OF THE RESULTS OF THE UAM-V PERFORMANCE EVALUATION FOR THE AUGUST AND SEPTEMBER EPISODES

A number of diagnostic and sensitivity simulations were performed during the evaluation of the UAM-V to develop a final set of meteorological, air quality, and emission inputs that provide adequate base-case model performance for each of the episodes. The performance of the model was assessed using graphical techniques and statistical measures that illustrate and quantify the uncertainty (error) in the simulated concentration estimates. In applying models such as the SAIMM and UAM-V, it is widely accepted that a number of contributing factors add to the uncertainty of the meteorological and photochemical modeling analyses. These include (1) errors inherent in model formulation (assumptions, parameterizations, condensed chemical mechanisms, numerical approximations), (2) errors associated with the inputs to the models (errors in the measurement data, errors in estimating temporal, spatial, and speciation features of emissions, and errors associated with model input preparation techniques, including those introduced by interpolation or extrapolation of the data to create the gridded fields), and (3) errors associated with the differences in the spatial and temporal attributes of the processes occurring in the atmosphere versus the spatial and temporal resolution/representativeness of the data and the model's grid structure. Some of these errors can be minimized and some cannot.

Efforts were made in the GMAQS study to minimize the input errors by using the latest state-of-the-science monitoring equipment and techniques (RWP, aircraft, etc.) to collect high-quality supplemental data at additional locations throughout the study domain, and by employing an advanced prognostic meteorological model with data-assimilating

capabilities in an effort to prepare physically realistic meteorological fields using the supplemental data. Efforts were also made to reduce the resolution errors by using the variable nested-grid capability of the prognostic and photochemical models to better resolve the complex physical mechanisms that affect ozone concentrations on multiple scales.

However, even with the high quality, supplemental data, and the advanced modeling tools available for this study, some errors are expected in simulating the complex features of ozone production, deposition, and transport that were observed for each of the episodes in the GMAQS study domain. In particular, uncertainties in the emission estimates were sufficiently large such that reasonable model performance could not be achieved using the baseline emissions inventory. The modeling emission inventories were adjusted (similarly for both episodes) and the base-case modeling was performed using the adjusted inventories.

SUMMARY OF UAM-V PERFORMANCE FOR THE AUGUST EPISODE

Overall, the spatial and temporal ozone concentration patterns observed during this multi-day episode are represented in the UAM-V simulation results. During this episode, the highest ozone concentration observed during the 1993 GMAQS field program (231 ppb) occurred on 19 August, and the model nearly replicated this peak concentration by simulating a maximum concentration of 223 ppb in the vicinity of the observed peak. Except for the initial day of the episode (17 August), during which the model is affected most by initial conditions and good performance is not expected, the normalized gross error statistics for the Houston subdomain are well within EPA-recommended performance criteria for a UAM SIP application. Because of the resolution of the coarse grid (16 km) used in the Baton Rouge area, the model is not expected to perform as well as an application with a higher resolution grid for the area. However, even with the coarse resolution, the UAM-V does a good job in replicating the observed spatial and temporal patterns, and the magnitude of the observed concentrations in Baton Rouge as indicated by the time-series plots (Figure 4-94) and the statistical measures (Table 4-22). Comparison of the UAM-V simulated concentrations with aircraft measurements also indicates that the model does a good job in replicating the vertical structure of observed ozone and precursor profiles at various locations and at various times throughout the day after adjustments were made to the inventory.

Despite uncertainties in the emission inventory inputs, good model performance was achieved for this episode. The simulated characteristics of the episode are consistent with the conceptual model presented in Section 3 (e.g. pollutants were advected offshore during the morning hours, the highest simulated ozone concentrations occurred ahead of the simulated gulf-breeze front, and day-to-day carryover of pollutants did not contribute significantly to the simulated concentrations).

SUMMARY OF UAM-V PERFORMANCE FOR THE SEPTEMBER EPISODE

Overall, the spatial and temporal ozone concentration patterns observed during this period were represented in the UAM-V simulation results, with some exceptions. Within the Houston subdomain, the high ozone concentrations that were observed at sites located between Houston and the coastline on 8, 9, and 10 September were underestimated in the simulation. Nevertheless, except for the initial day of the simulation period (6 September), the calculated performance measures for the Houston subdomain are within EPA-recommended performance criteria for a UAM SIP application. In the Baton Rouge area, the model (with 16 km horizontal resolution) replicates the observed ozone concentrations (although peak observed concentrations were fairly low) (Table 4-26).

The lack of aircraft data for this episode precluded a comprehensive model performance evaluation, especially with regard to the simulation of day-to-day carryover. Despite the model performance problems noted for certain of the more coastal sites, the simulated characteristics of the episode are consistent with the conceptual model developed through analysis of the meteorological and air quality data (Section 3). For example, the simulated concentrations over the Gulf are significantly higher than for the August episode (greater than 100 ppb offshore from Houston and Beaumont/Port Arthur on 7, 8, 9 and 10 September). This is consistent with the buildup of ozone offshore resulting from the extended duration of the offshore-directed flow. Although concentrations at some of the more coastal sites were not replicated, the simulated concentrations for this episode occur further south than for the August episode. Because the observed ozone peaks were monitored at sites located in the more industrialized portions of the domain, uncertainty in the emission estimates may have affected model performance for this episode more significantly than for the August episode.

Although the ozone isopleth figures for 8 September indicate that the simulated ozone plume may be located too far north of the Seabrook and Smith Point monitoring sites where high concentrations were observed (Figure 4-102), sensitivity simulations involving a reduction of localized NO_x emissions from industrial and shipping channel sources indicate that the local NO_x emissions have a large (localized) effect on simulated ozone concentrations and that simulated concentrations around Galveston Bay may actually be suppressed because of localized overestimation of NO_x (or underestimation of VOC) in the emission inventory. The sensitivity simulation indicates that an increase in the hydrocarbon to NO_x ratio would be necessary to dramatically change the simulated ozone concentrations in this area. While it is possible that the VOC/NO_x ratio might be changed by significantly changing the spatial distribution of emissions, it is more likely that the emission inventory either overestimates NO_x or underestimates hydrocarbon in this area.

Although the UAM-V is underestimating observed ozone concentrations at Texas City on 8 and 9 September, and to some extent, at Seabrook and Smith Point, it should be noted that the performance of the model at the Stowell-Winnie site (STWC) (Figure 4-113), located north of Gilchrist (more inland and away from the industrial sources around Galveston Bay) is very good for all episode days. Also, indicators of how well the

model is simulating ozone along the coast (the area of primary focus for potential OCSPD impacts) are provided in examining UAM-V performance at the coastal monitors as presented in Figure 4-113 for TN13, Galveston Island (GALC), and Sabine Pass (S40S), which are located in areas not likely influenced by local high NO_x emissions from industrial sources. With the exception of the underestimation of ozone at the Gilchrist monitor for one day of this episode (9 September) (Figure 4-111), these results indicate that the model is properly replicating the production and transport (both offshore and onshore) of ozone along the coast in those areas not affected by local sources.

In summary, the model is adequately replicating observed concentrations in the Houston subdomain and throughout the domain as indicated by the performance statistics, and although the model is underestimating peak ozone concentrations at a few of the monitors around Galveston Bay on some of the episode days, sensitivity simulations and additional analyses have indicated that localized emission uncertainties or wind field inaccuracies may be the cause. However, the performance of model in simulating the temporal and spatial features and magnitude of ozone concentrations at the coastal monitors (TN13, Galveston, Gilchrist, Sabine Pass) is quite good (although simulated concentrations are lower than observed at Galveston on 10 September and at Gilcrist on 9 September). This indicates that the model is properly replicating ozone concentrations in the area along the coast and supports the use of this modeling database for OCS impact assessment.

RECOMMENDATIONS REGARDING USE OF THE MODELING SYSTEM FOR ESTIMATING THE IMPACTS OF OCSPD EMISSIONS

This qualitative and quantitative assessment of model performance for the August and September episodes gives strong indication that the meteorological and photochemical modeling system has provided a reasonable simulation of each of the episodes. The simulation results are generally consistent with the conceptual models of the episodes developed through analysis of the air quality and meteorological data. Uncertainty in the model inputs, especially the emissions, appears to have affected performance. Use of the modeling system to assess the impacts of OCSPD sources on ambient concentration levels offshore and onshore must consider these inherent uncertainties.

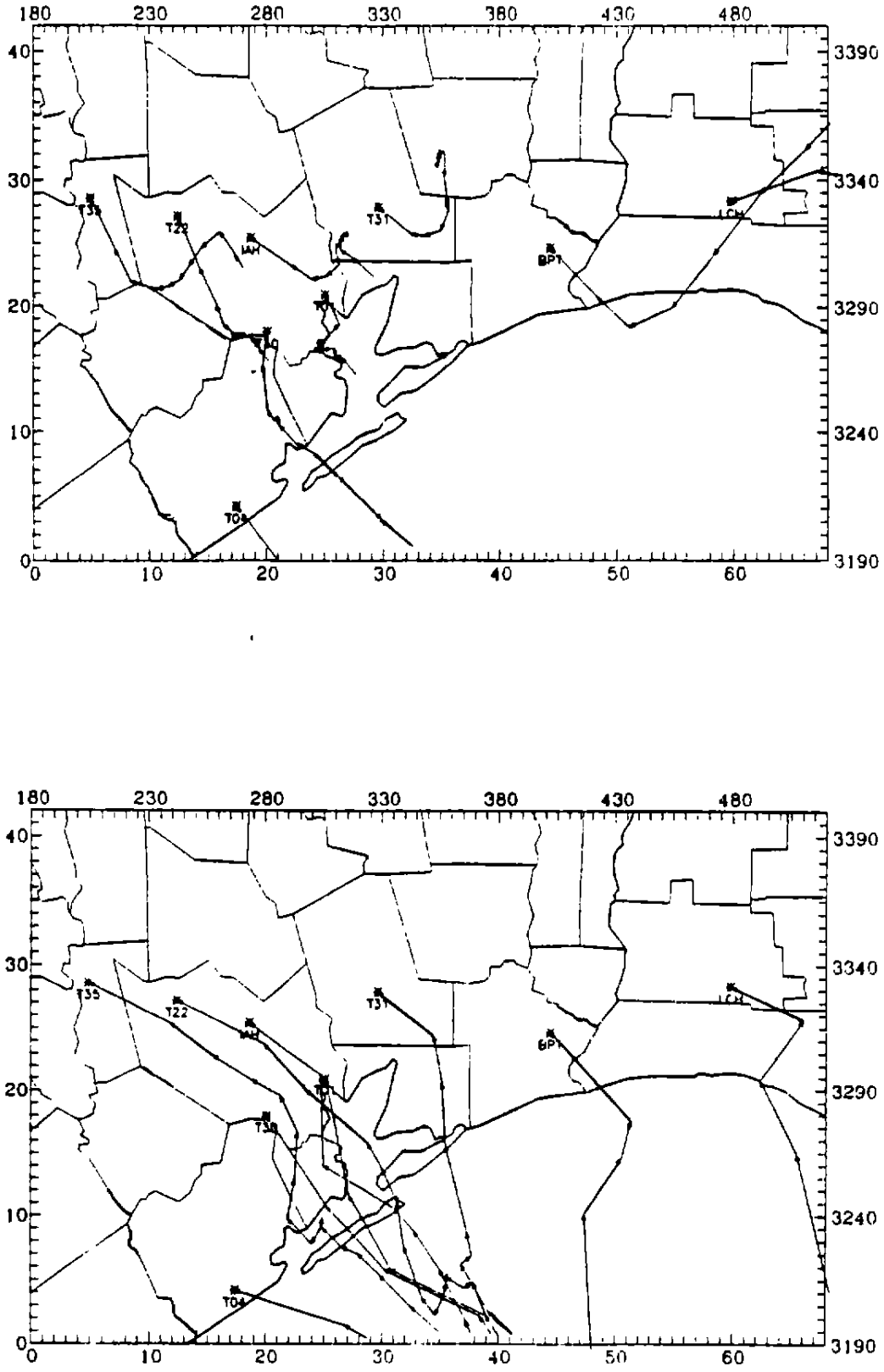

Figure 4-1. Backward particle paths for the Houston region on 29 July 1988 culminating at 1000 and 1600 CST.

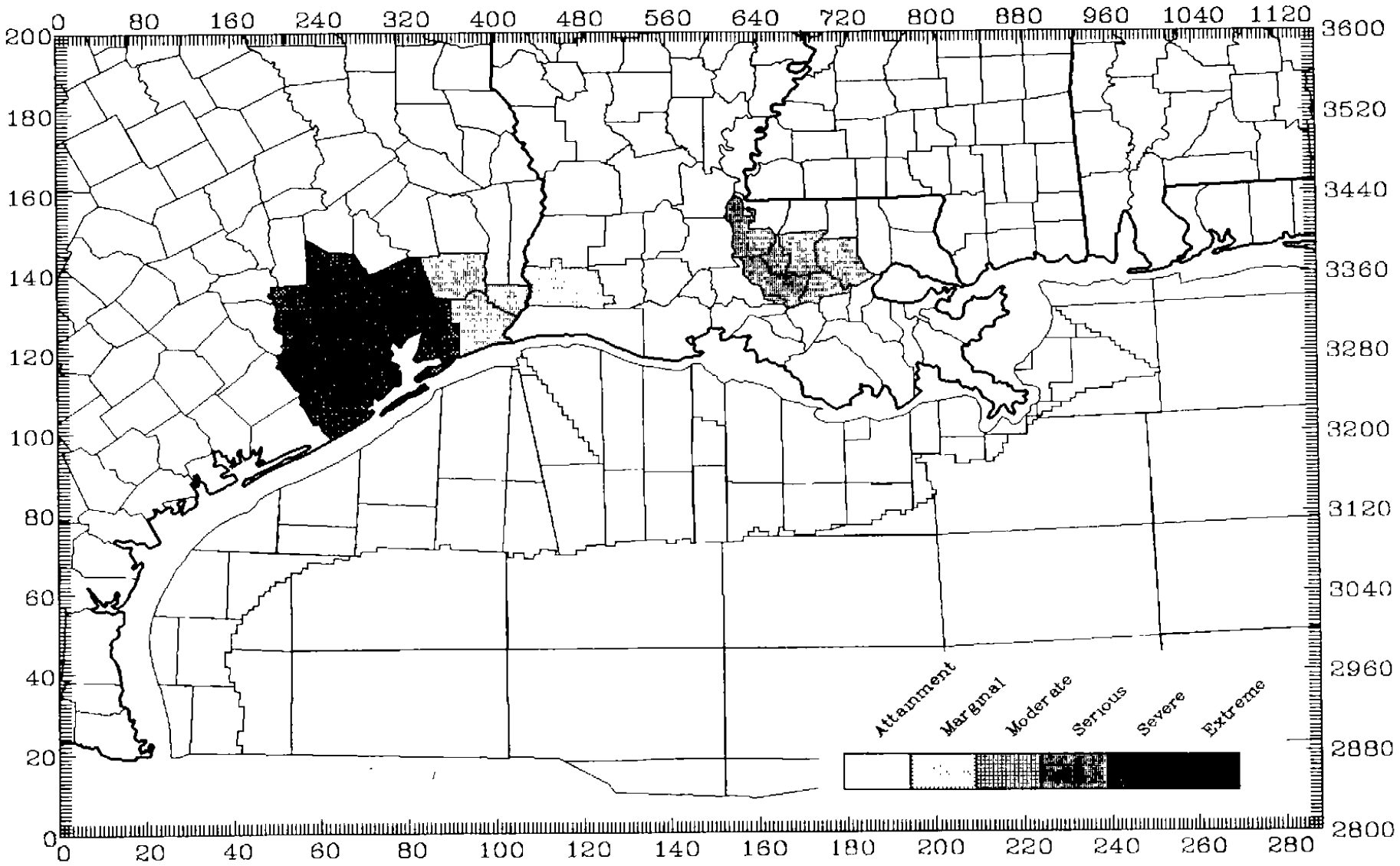

Figure 4-2. Ozone nonattainment status by county for the MMS GMAQS modeling domain.

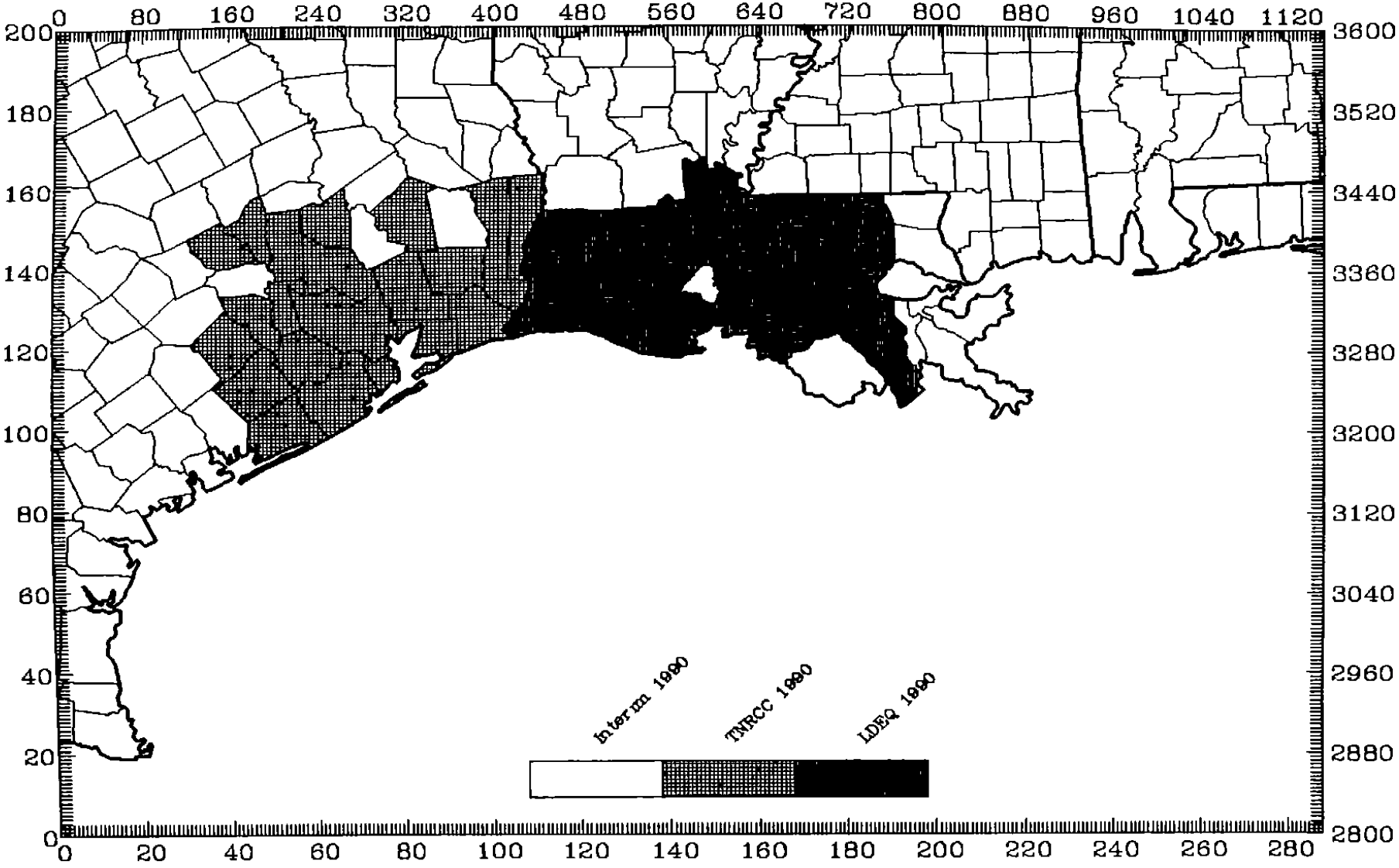

Figure 4-3a. Data sources for onshore point source emissions.

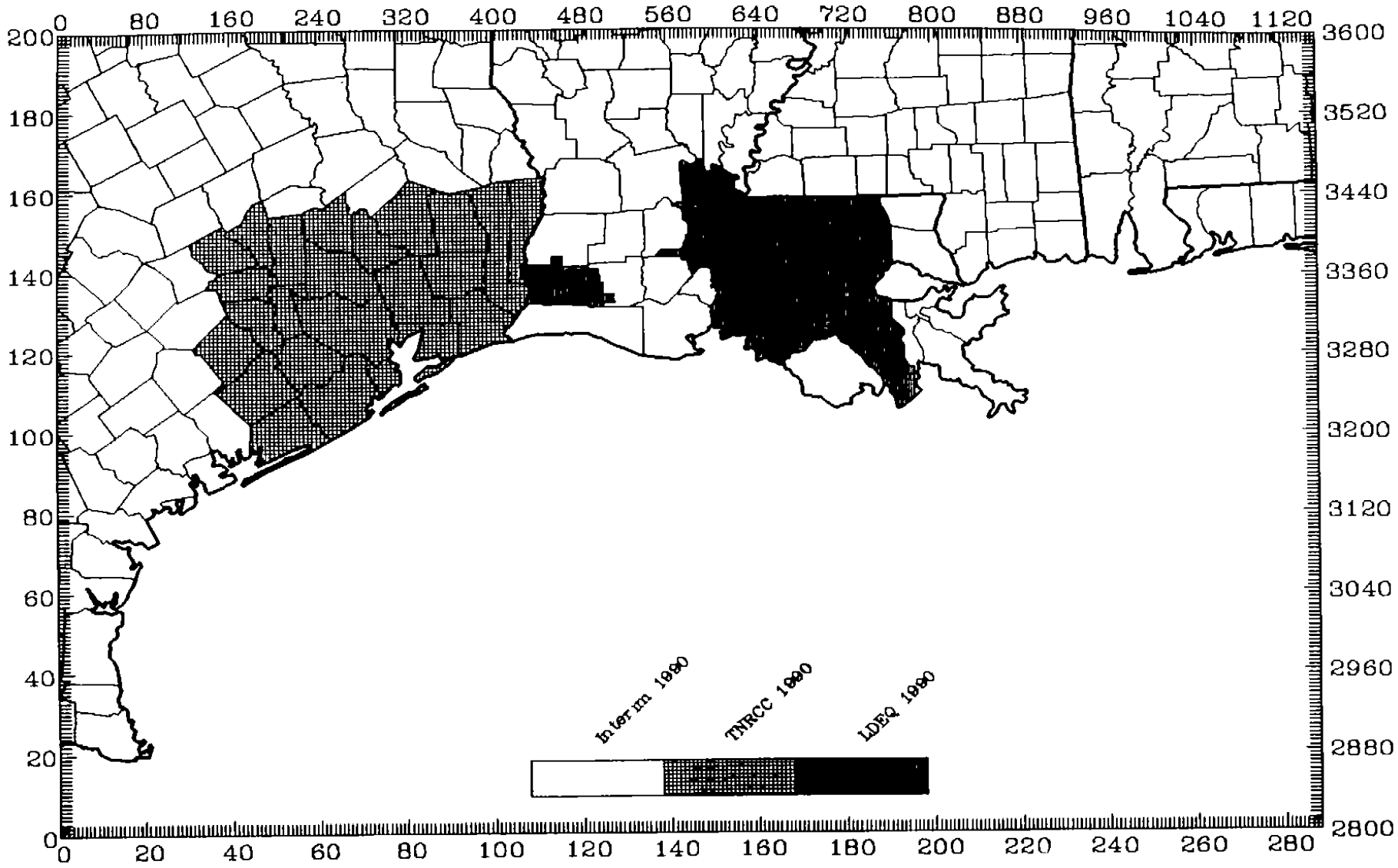

Figure 4-3b. Data sources for onshore area source and nonroad mobile source emissions.

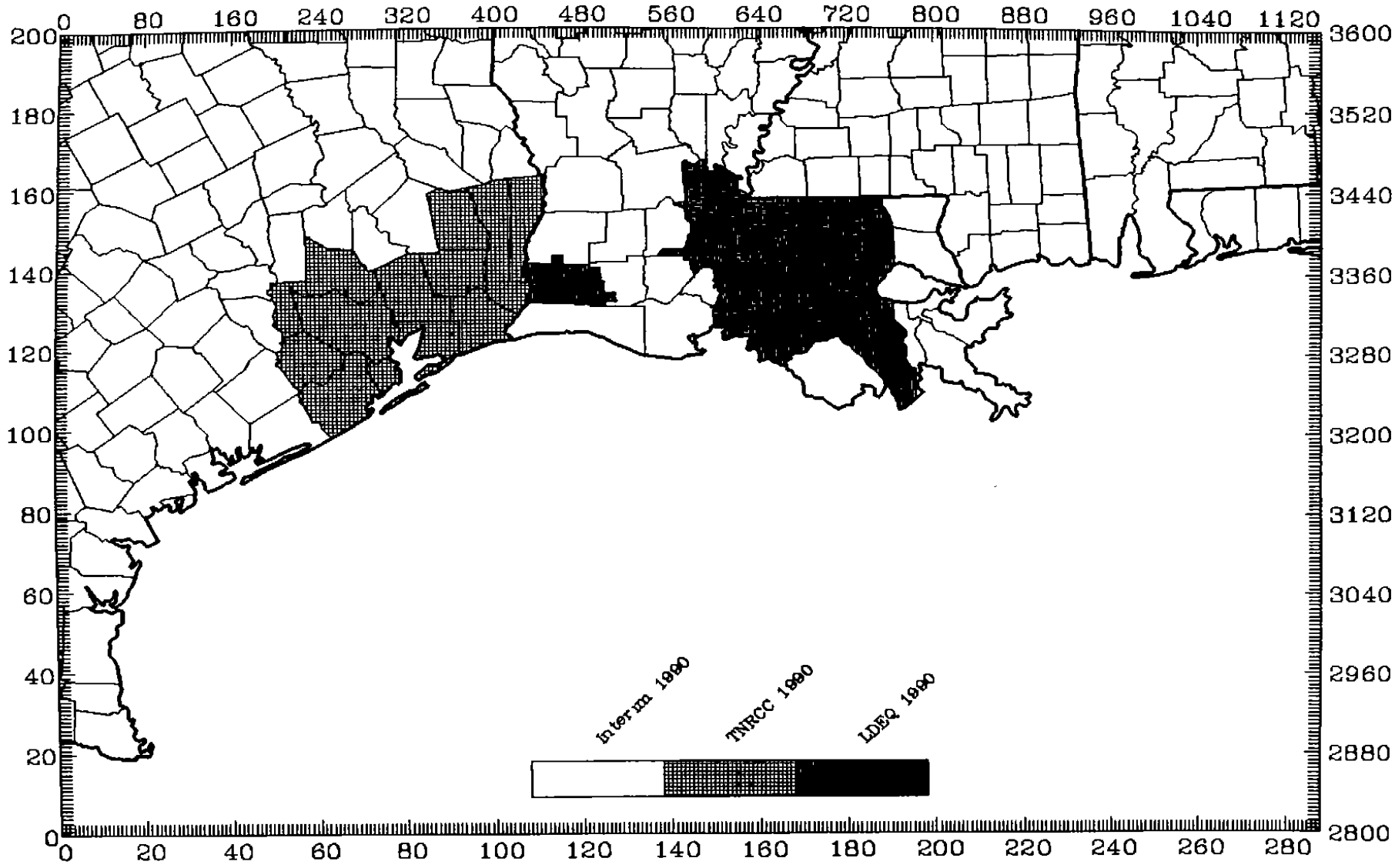

Figure 4-3c. Data sources for onroad motor vehicle emissions.

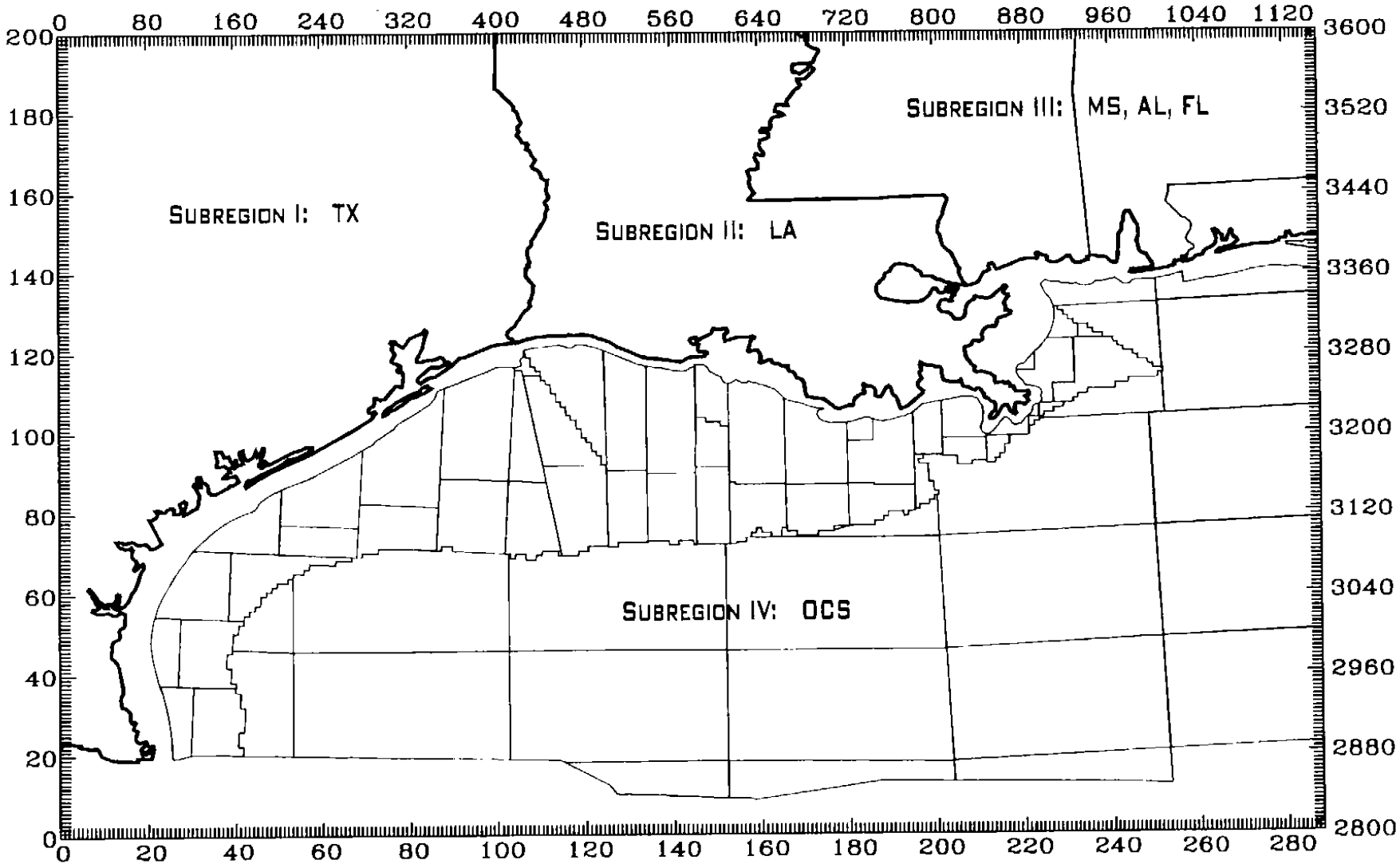

Figure 4-4. Subregions used for EPS 2.0 emissions processing.

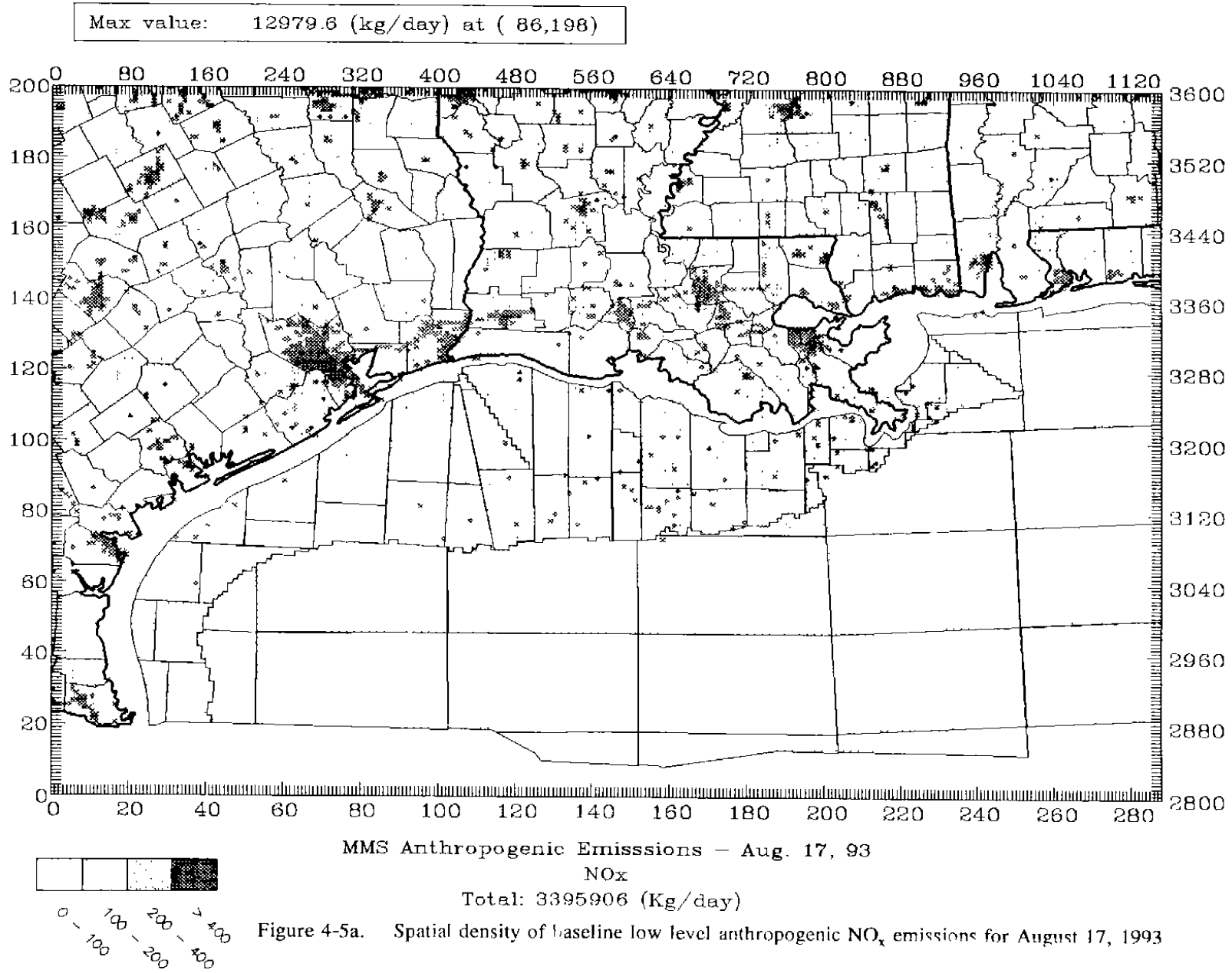

Figure 4-5a. Spatial density of baseline low level anthropogenic NO_x emissions for August 17, 1993

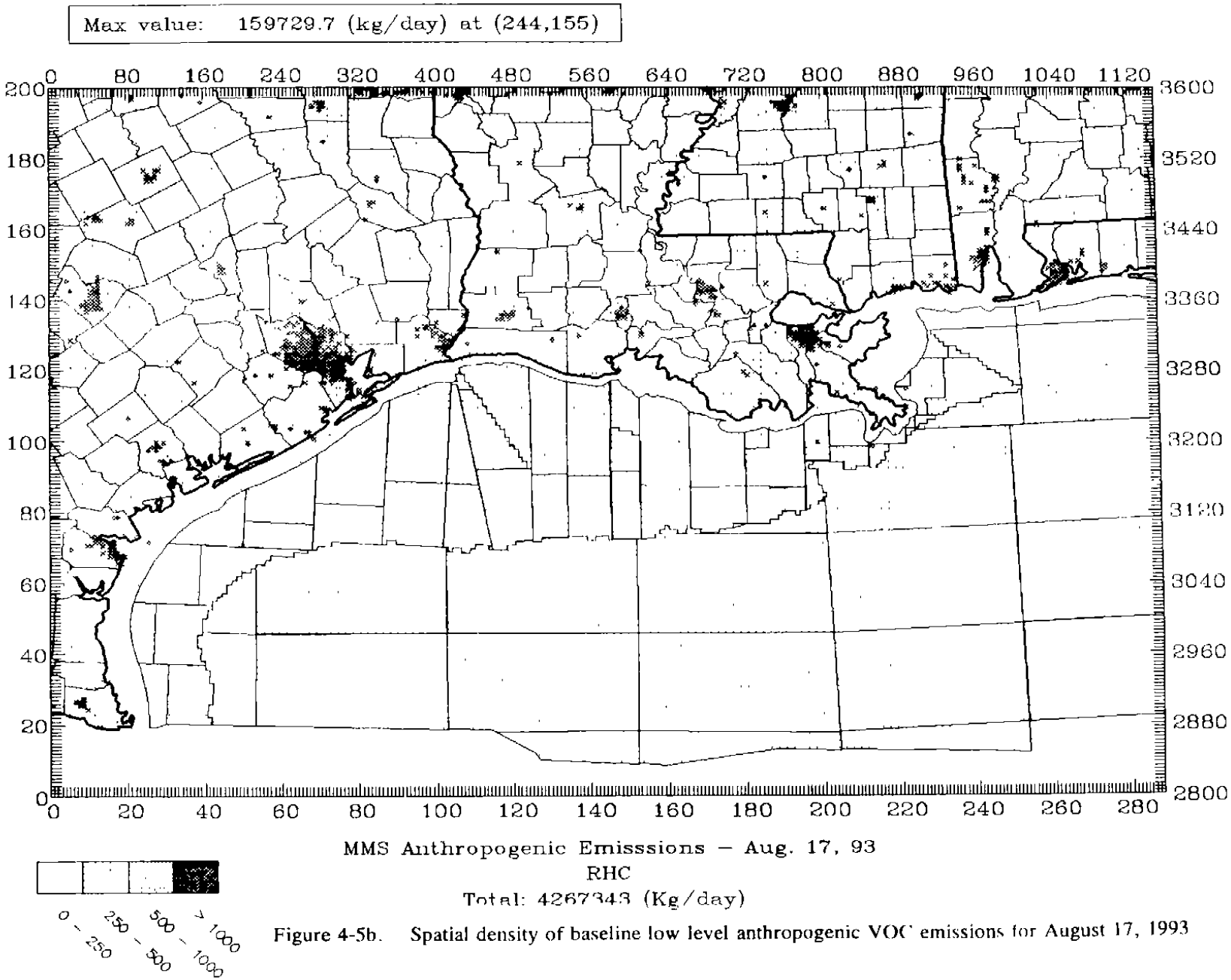

Figure 4-5b. Spatial density of baseline low level anthropogenic VOC emissions for August 17, 1993

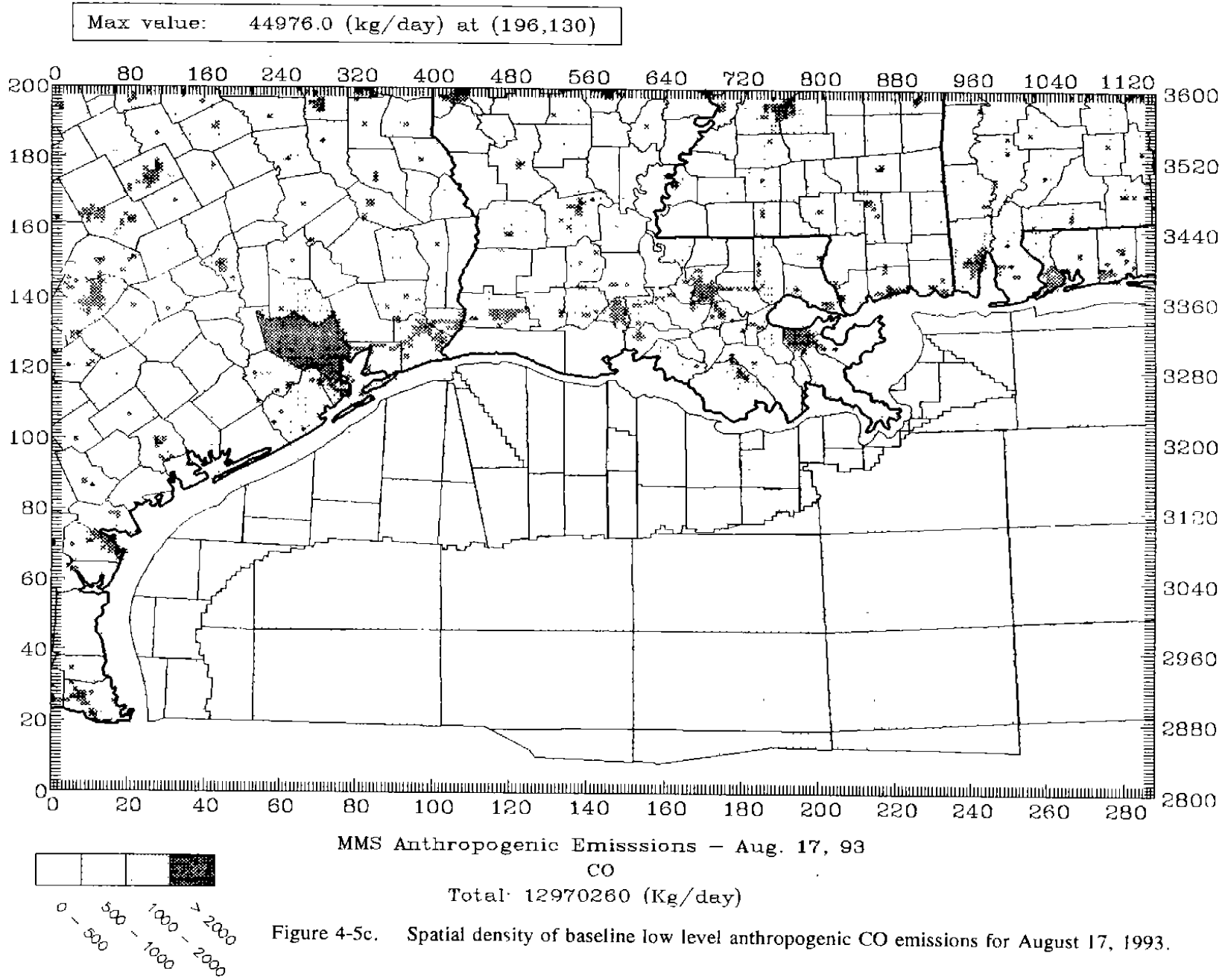

Figure 4-5c. Spatial density of baseline low level anthropogenic CO emissions for August 17, 1993.

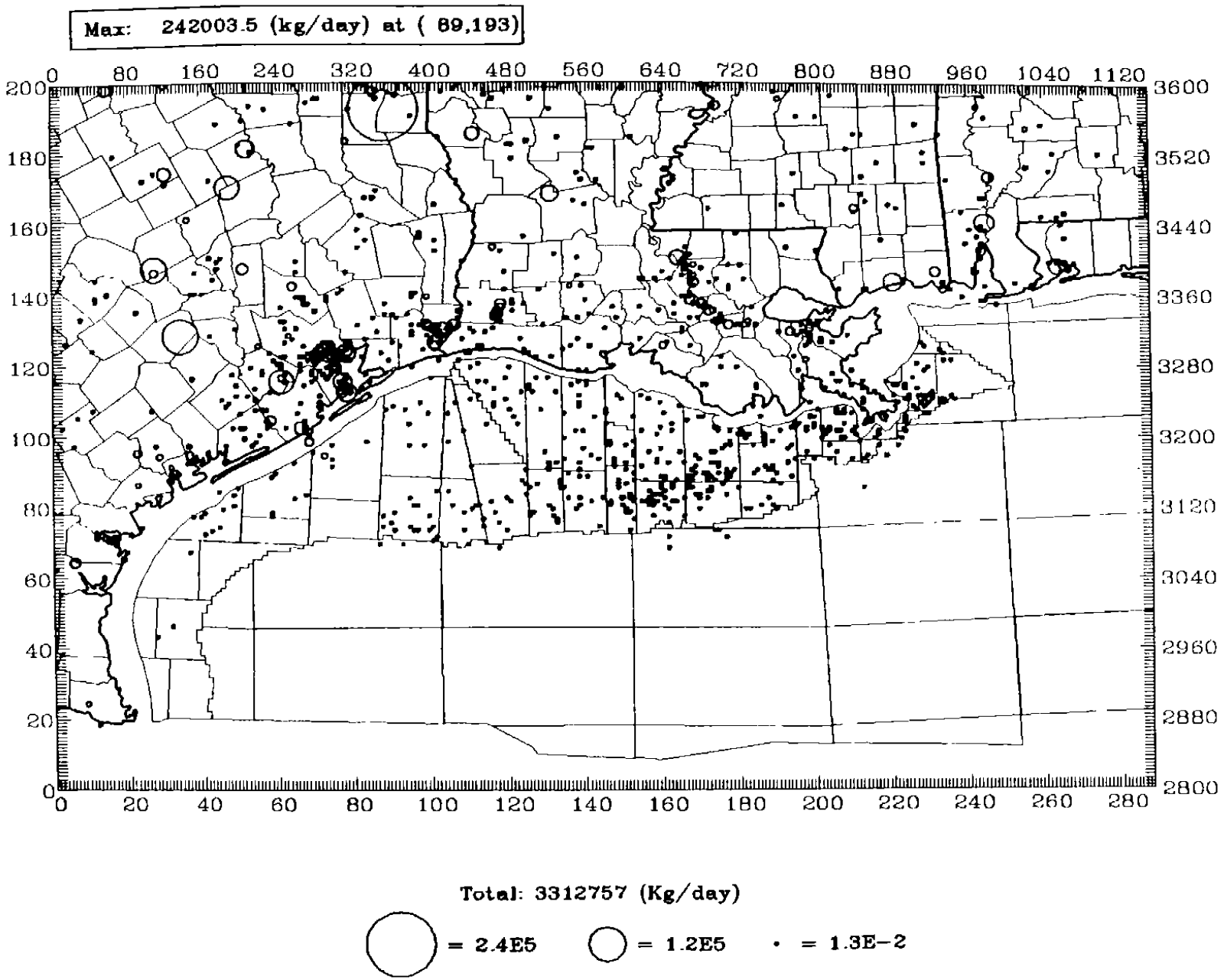

Figure 4-6a. Spatial distribution of baseline elevated NO_x emissions for August 17, 1993.

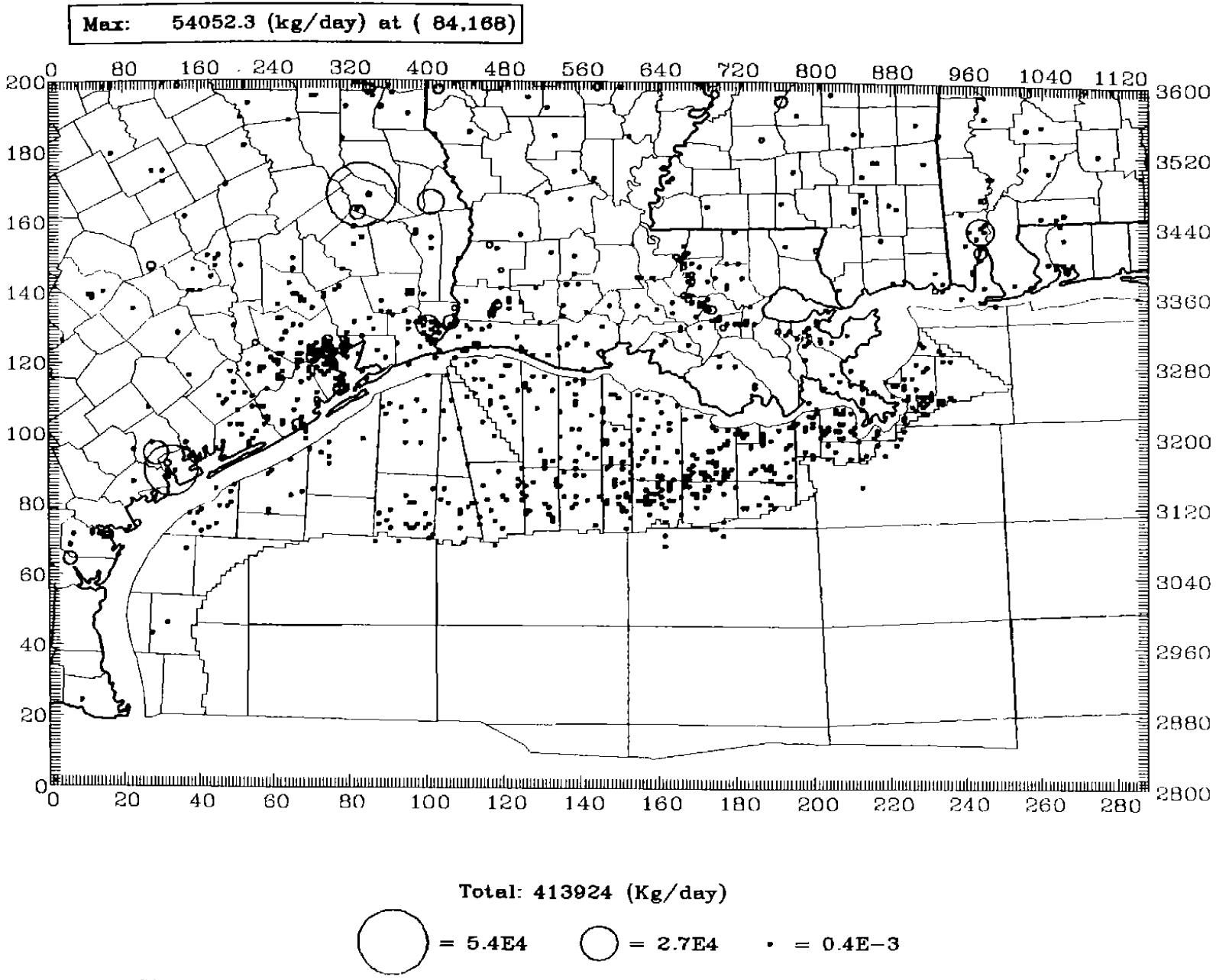

Figure 4-6b. Spatial distribution of baseline elevated VOC emissions for August 17, 1993

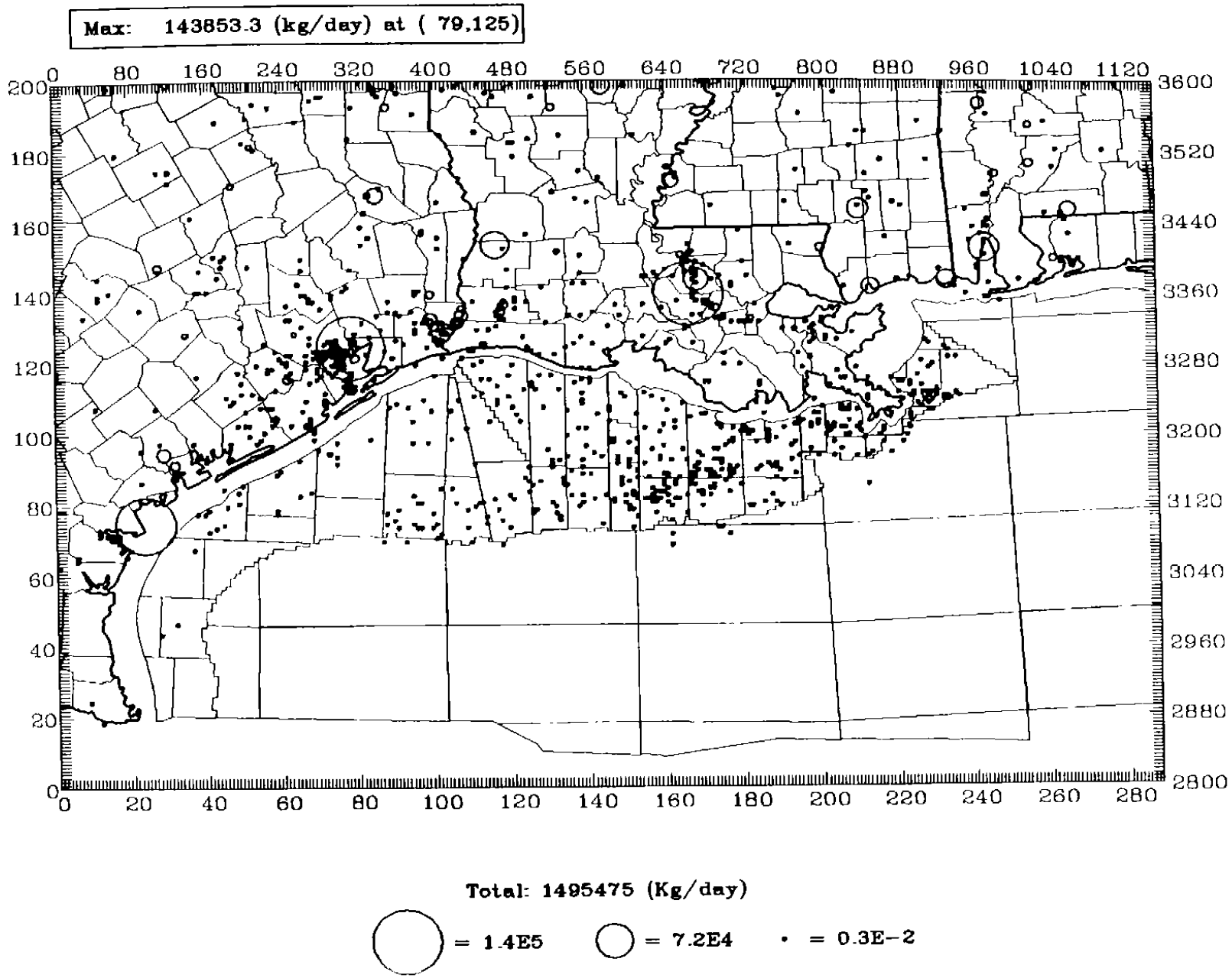

Figure 4-6c. Spatial distribution of baseline elevated CO emissions for August 17, 1993

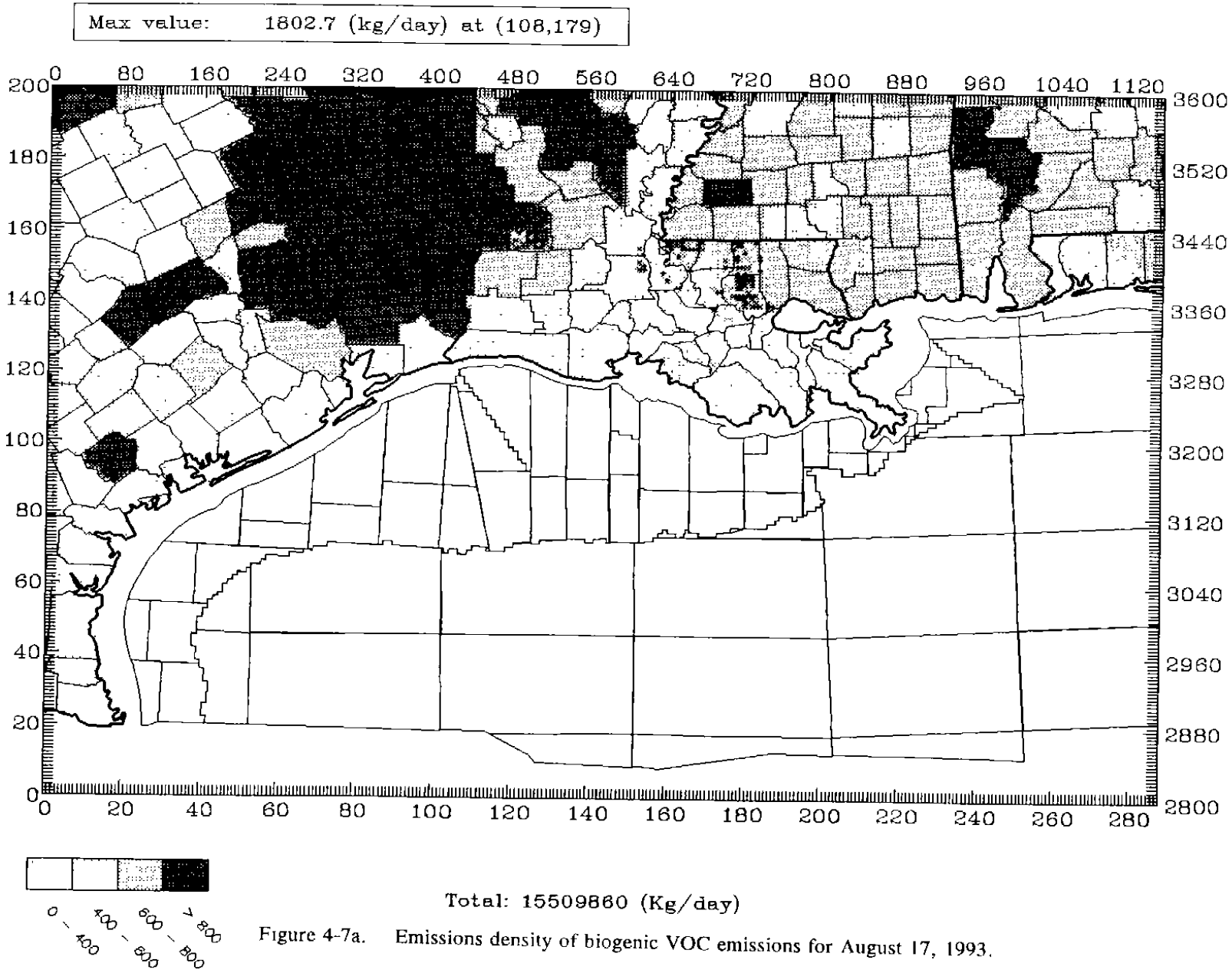

Figure 4-7a. Emissions density of biogenic VOC emissions for August 17, 1993.

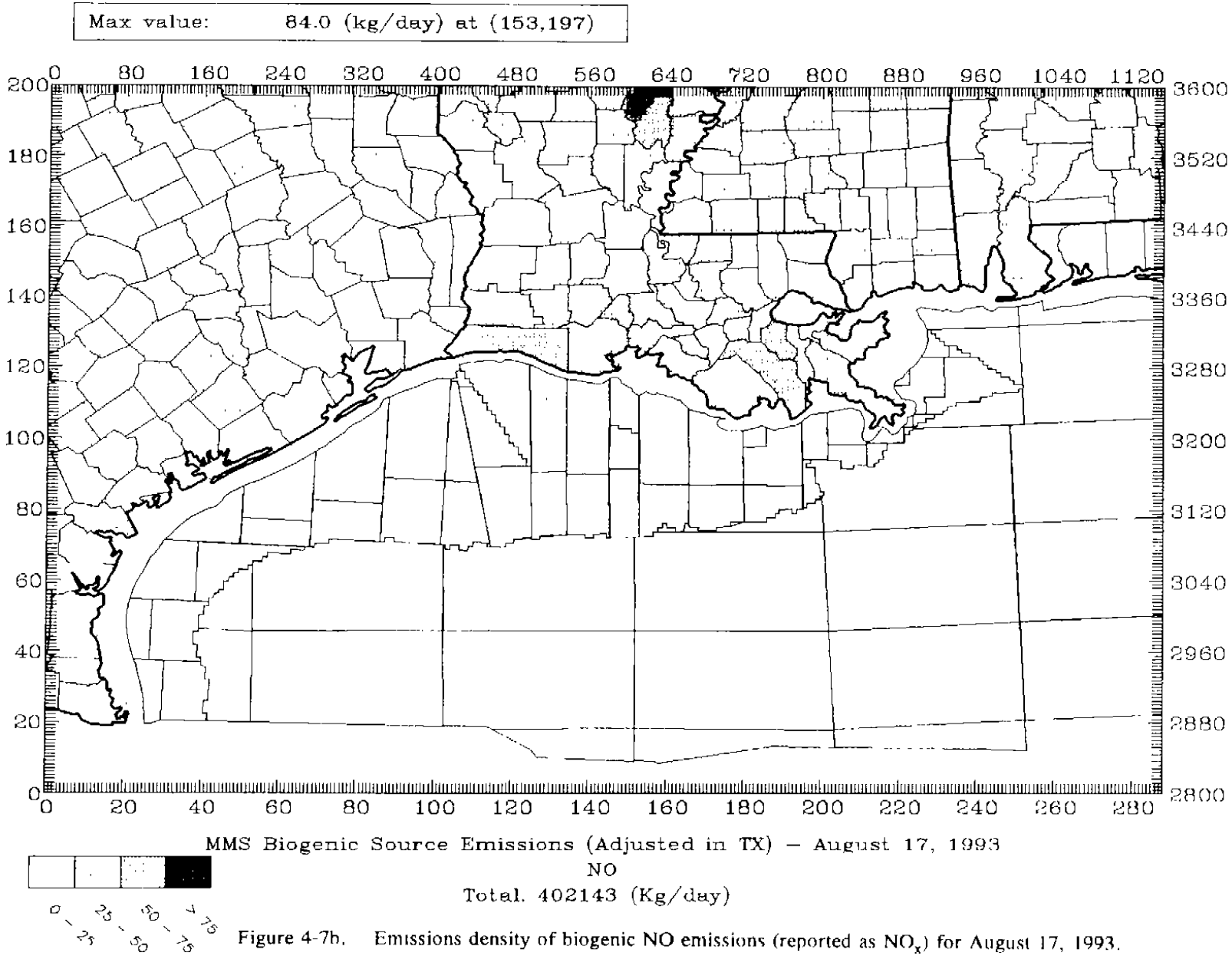

Figure 4-7h. Emissions density of biogenic NO emissions (reported as NO_x) for August 17, 1993.

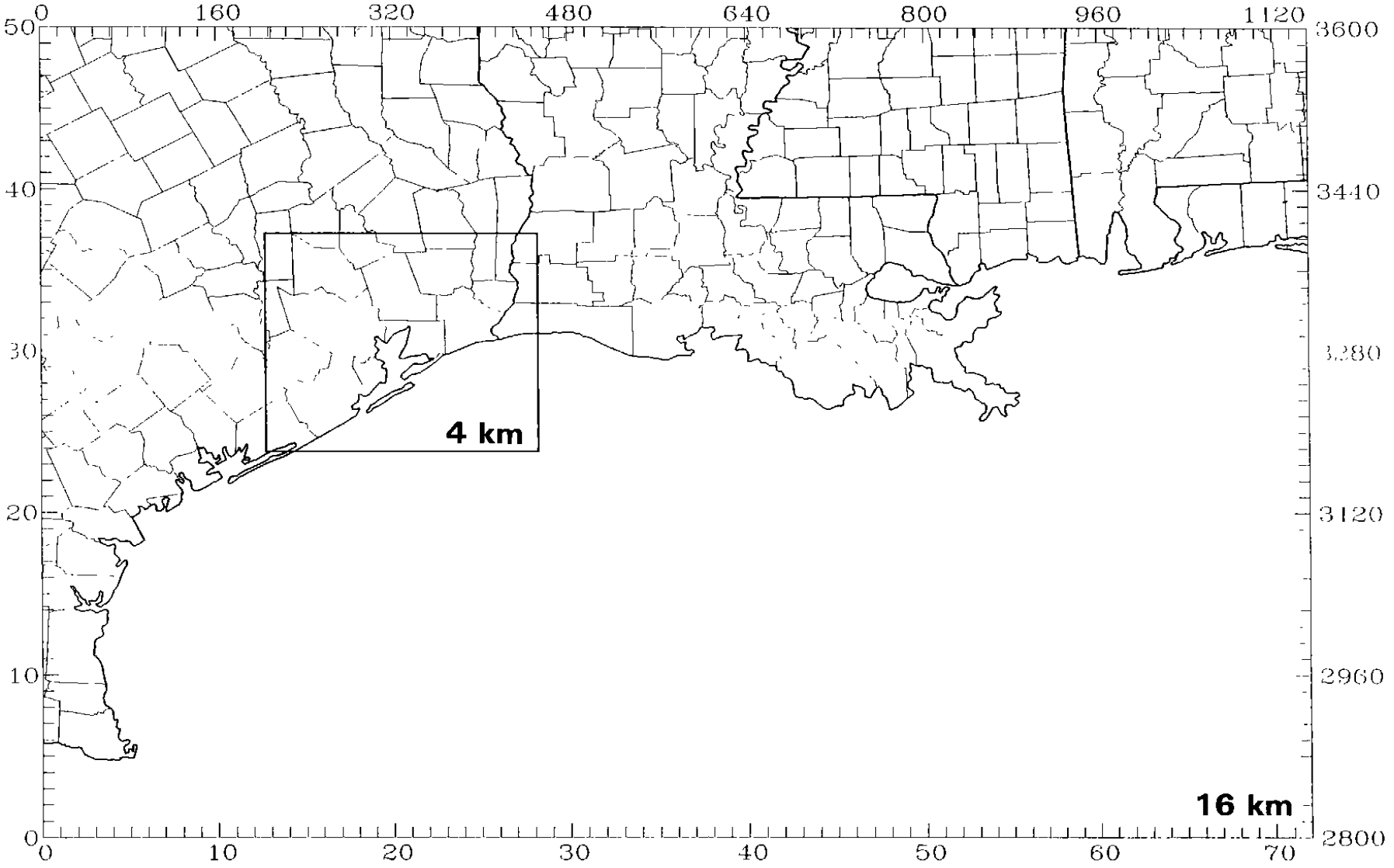

Figure 4-8. The MMS GMAQS meteorological modeling domains.

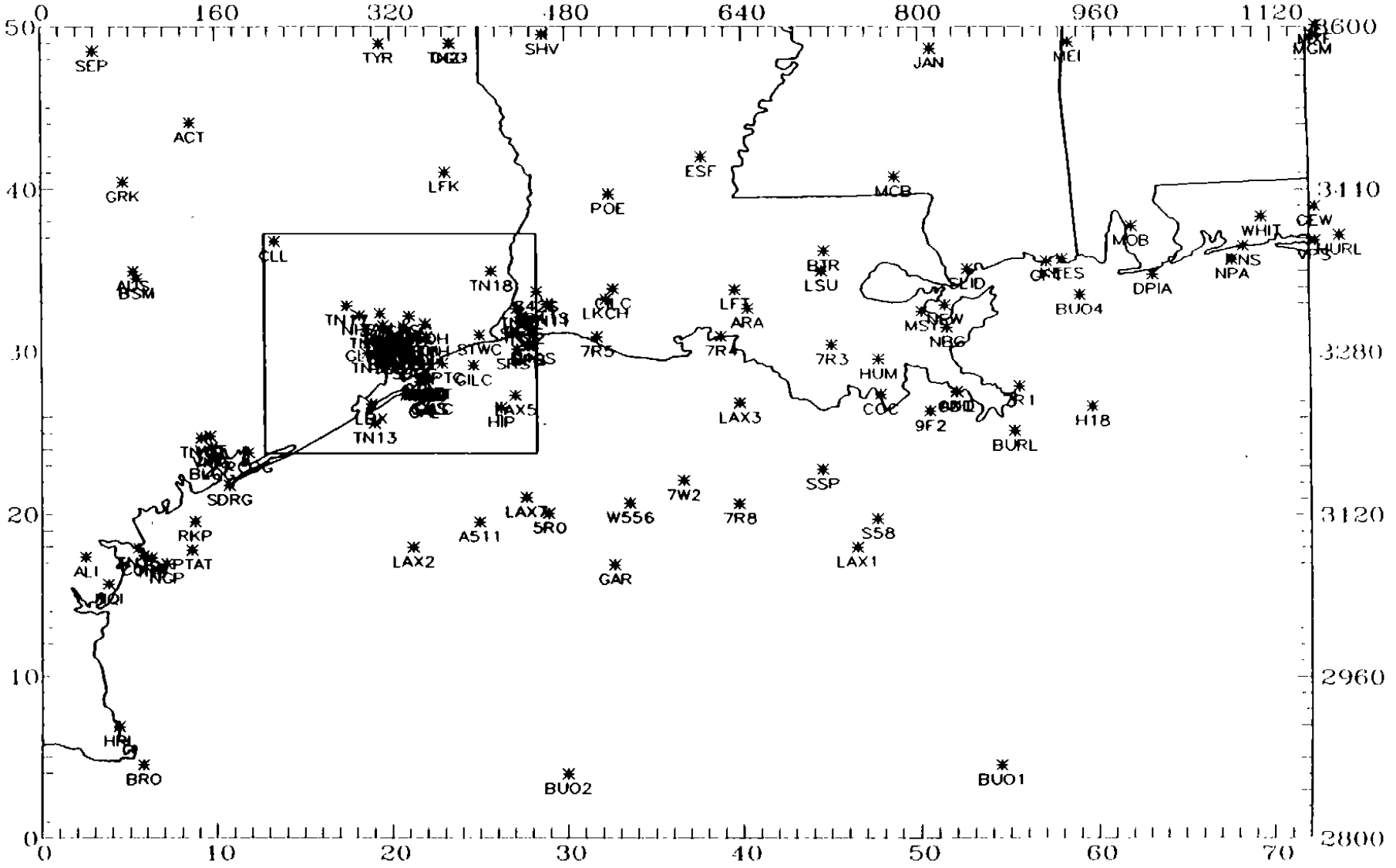

Figure 4-9a. Locations of meteorological monitoring sites in the outer, coarse-grid domain.

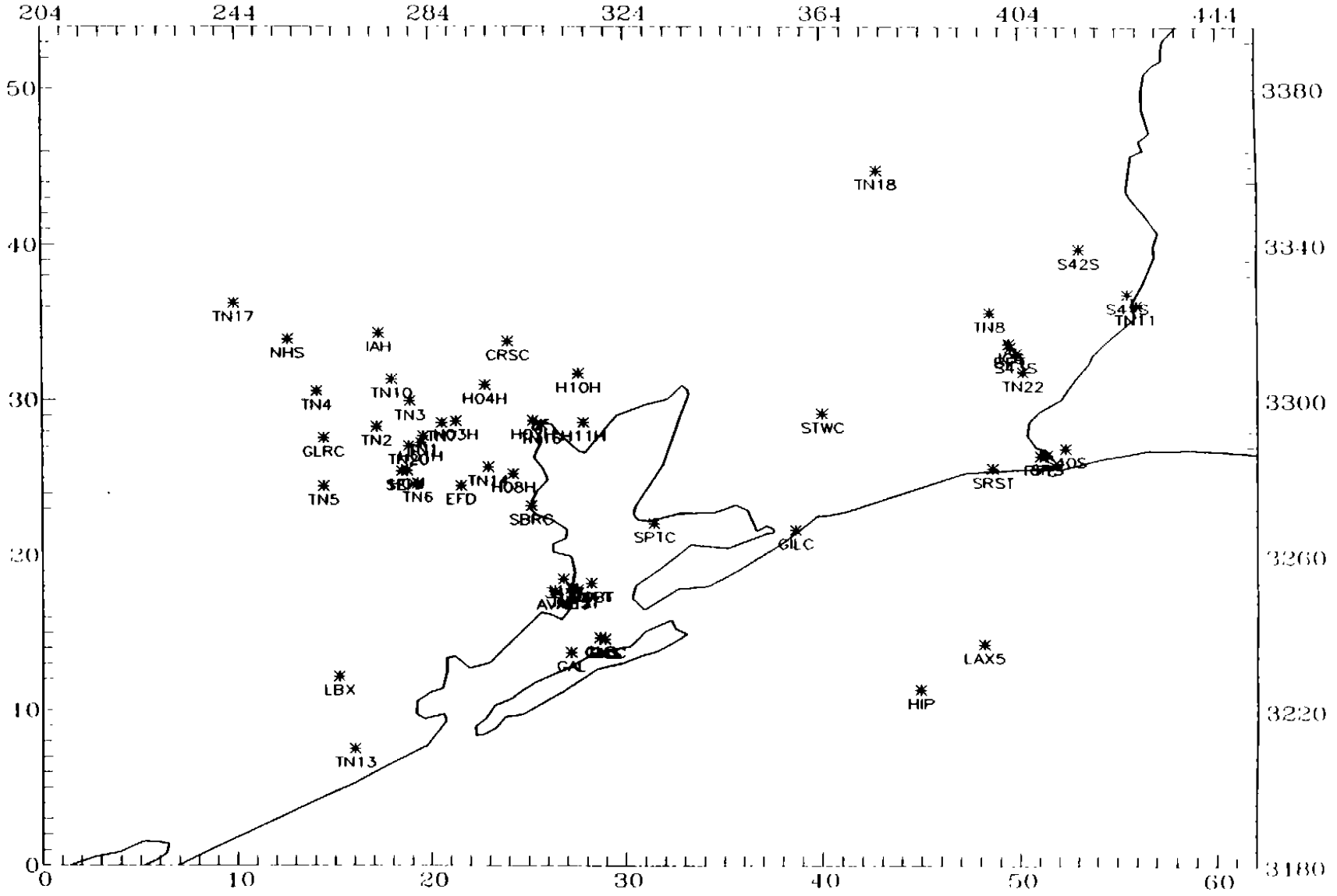

Figure 4-9b. Locations of meteorological monitoring sites in the inner, fine-grid domain.

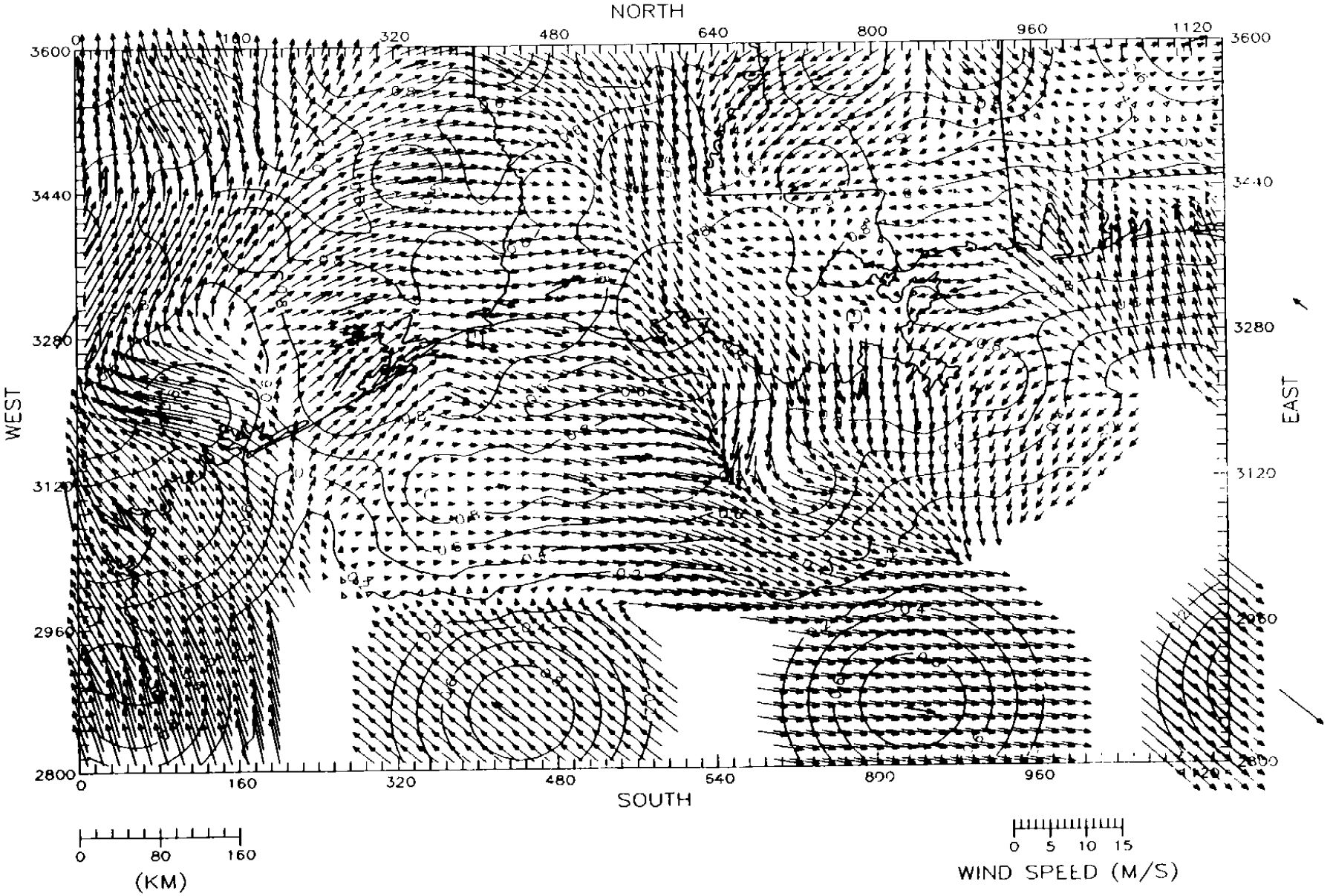

Figure 4-10. Objective analysis of surface wind observations (vectors) and spatial weighting coefficients (contours). Observed wind vectors are overplotted in bold.

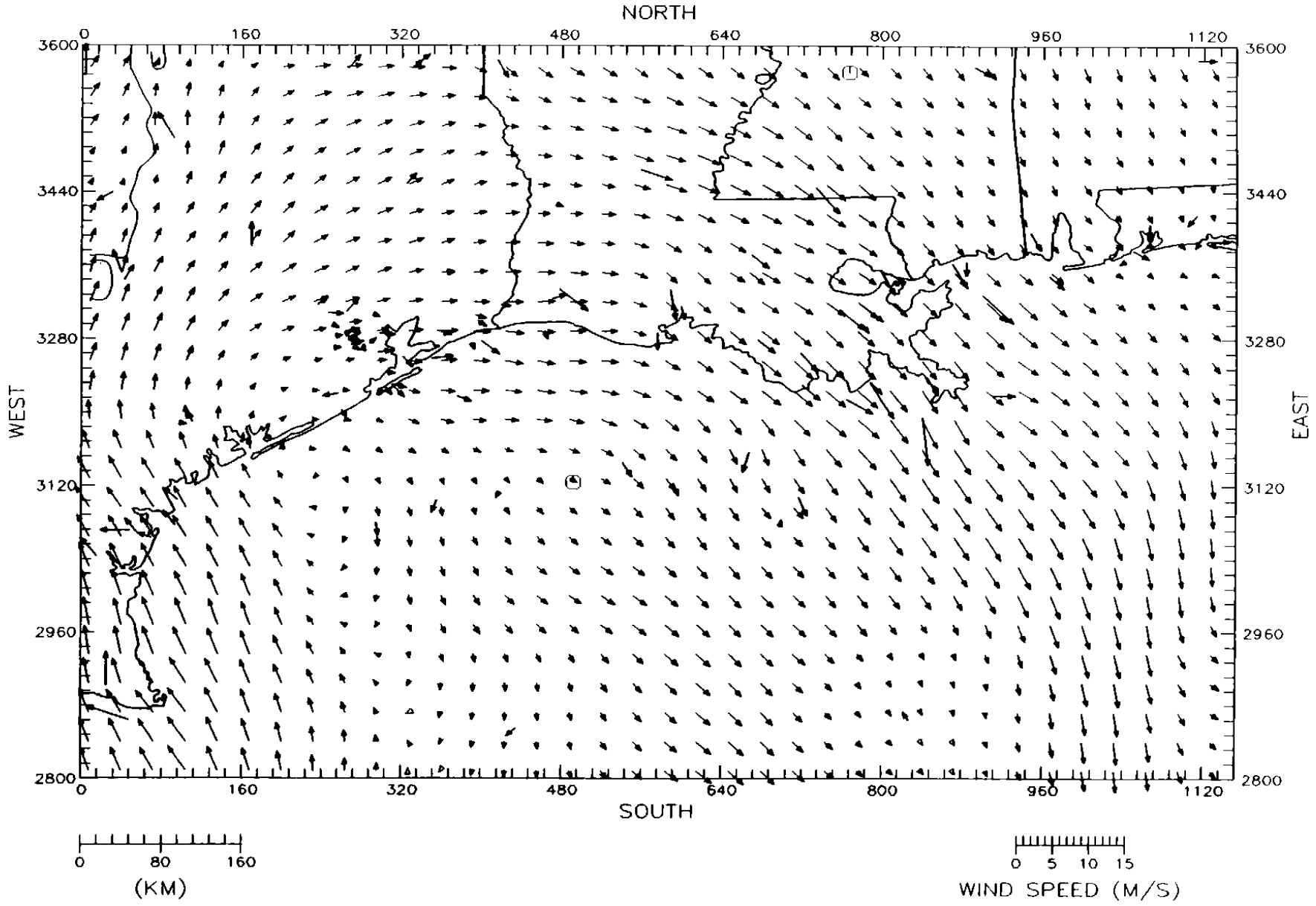

Figure 4-11a. SAIMM wind fields for the coarse-grid domain on 19 August 1993 at 1000 CST. Level 1 (25 m).

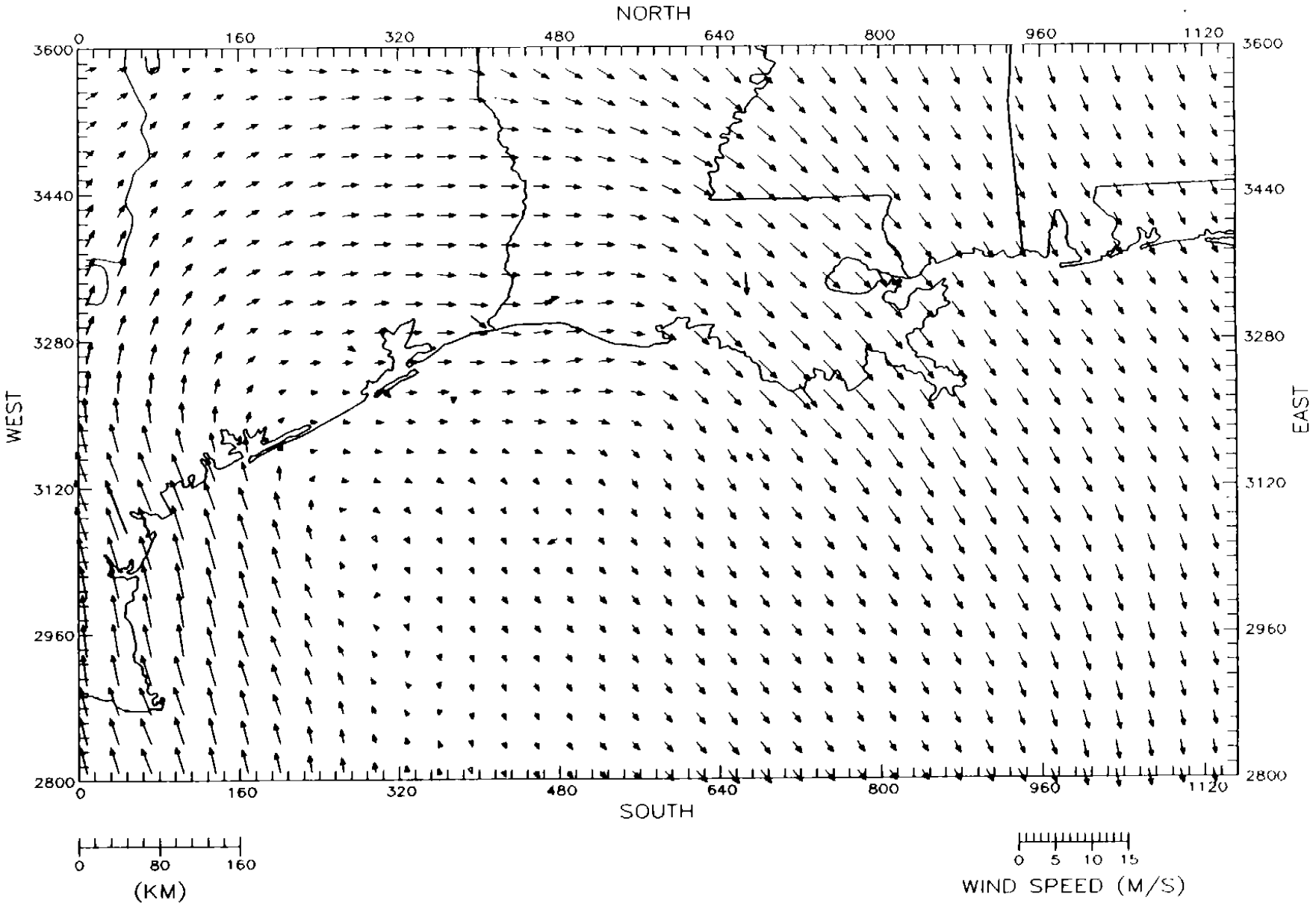

Figure 4-11b. SAIMM wind fields for the coarse-grid domain on 19 August 1993 at 1000 CST. Level 7 (675 m).

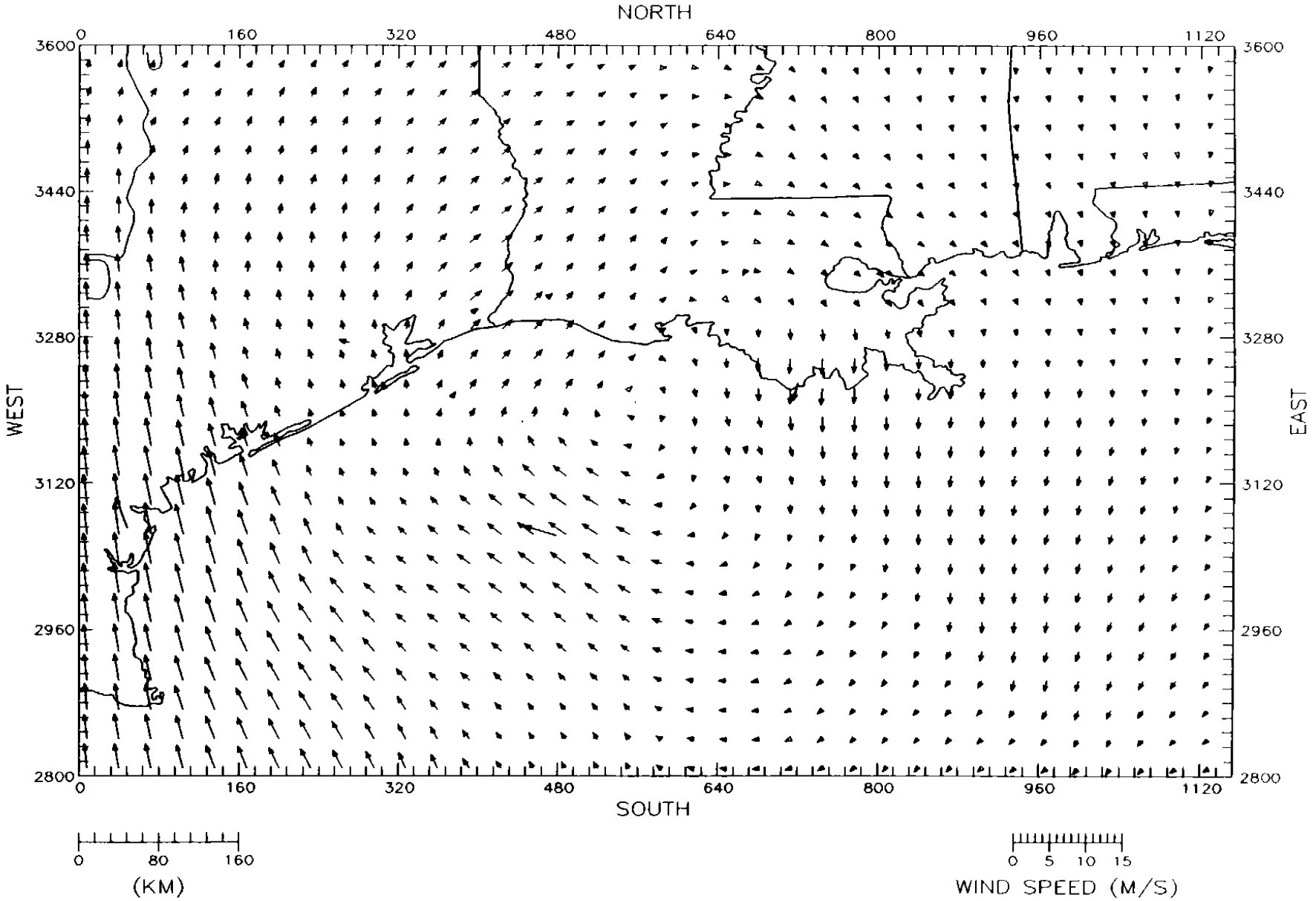

Figure 4-11c. SAIMM wind fields for the coarse-grid domain on 19 August 1993 at 1000 CST. Level 9 (1200 m).

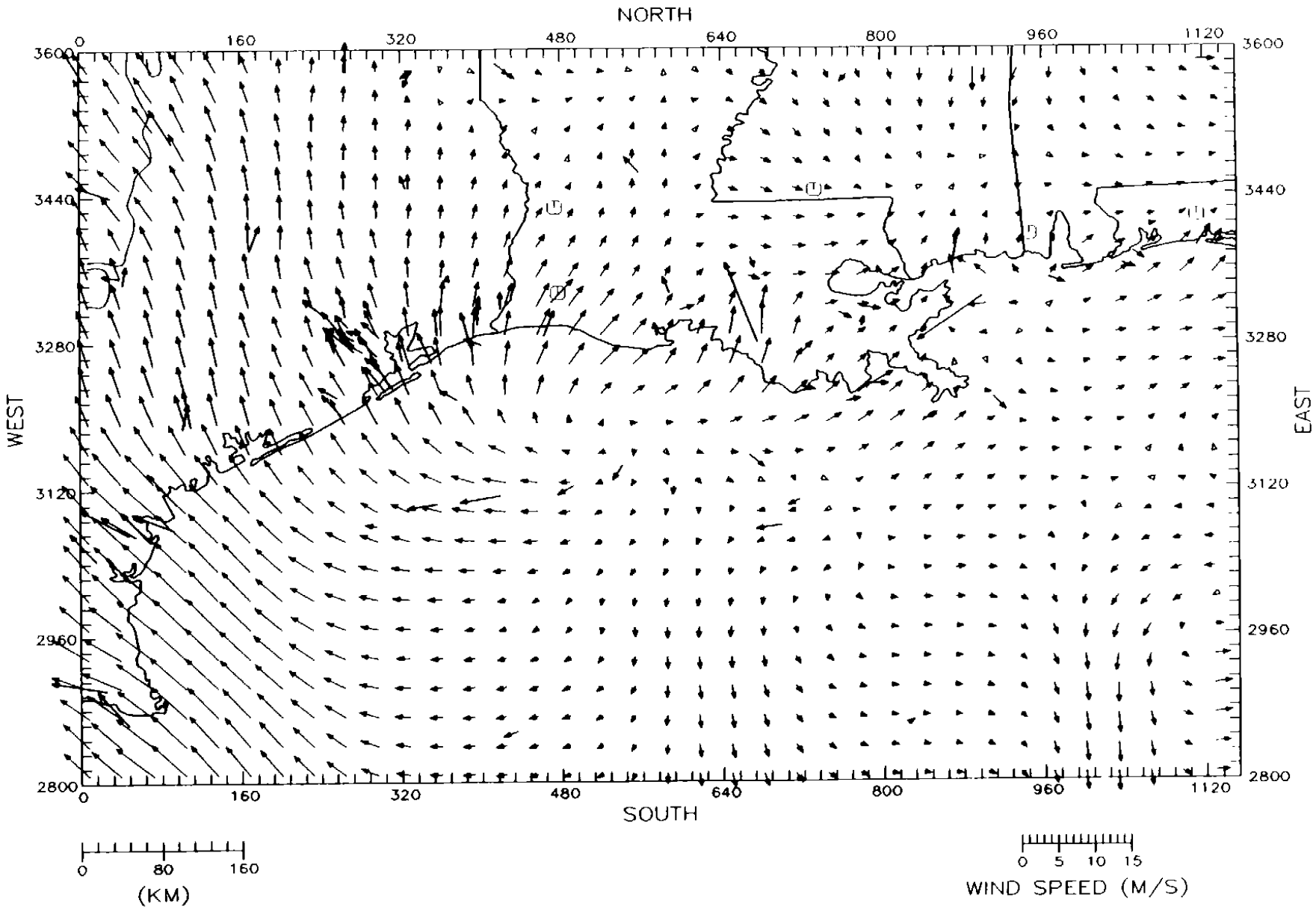

Figure 4-12a. SAIMM wind fields for the coarse-grid domain on 19 August 1993 at 1600 CST. Level 1 (25 m).

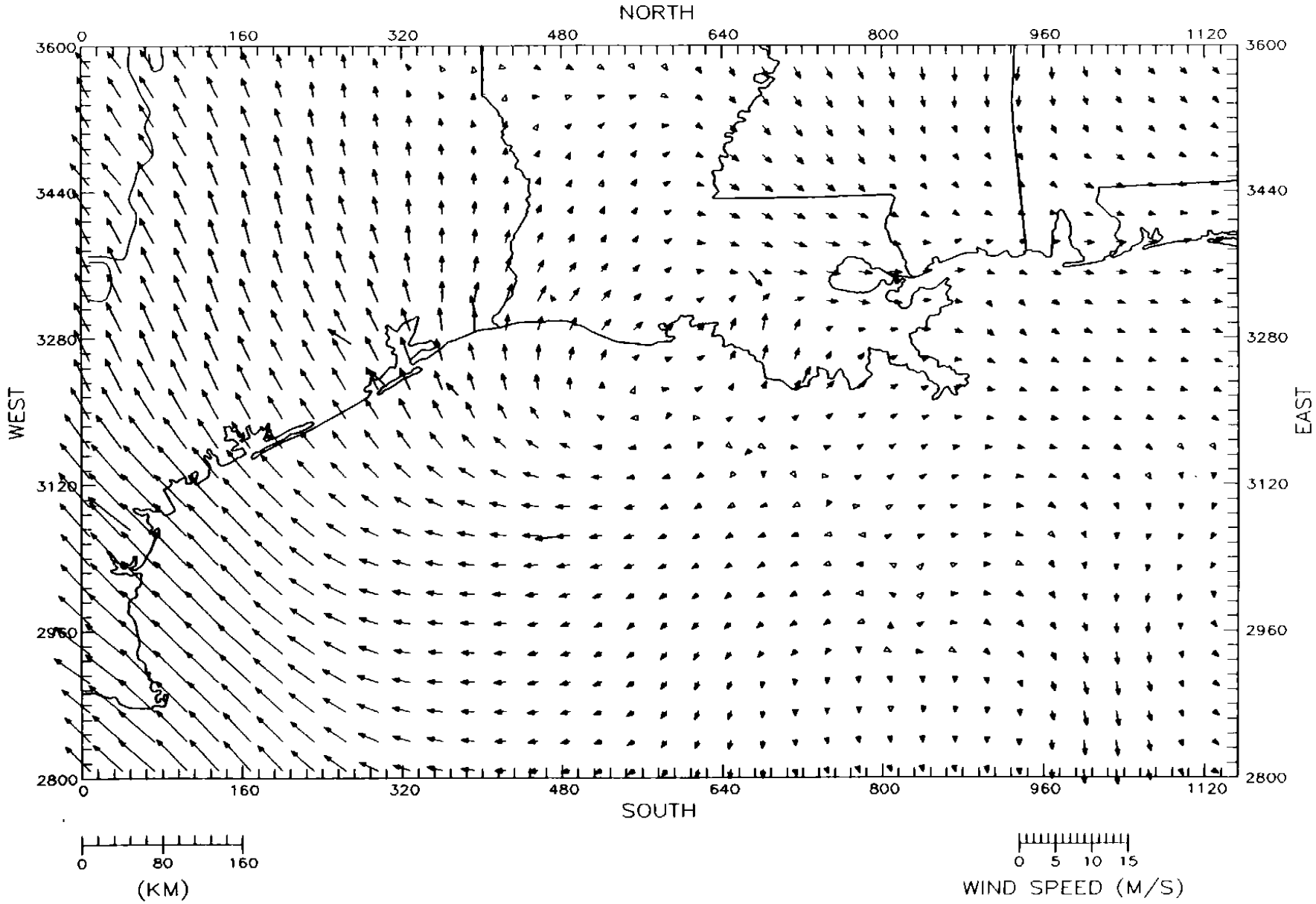

Figure 4-12b. SAIMM wind fields for the coarse-grid domain on 19 August 1993 at 1600 CST. Level 7 (675 m).

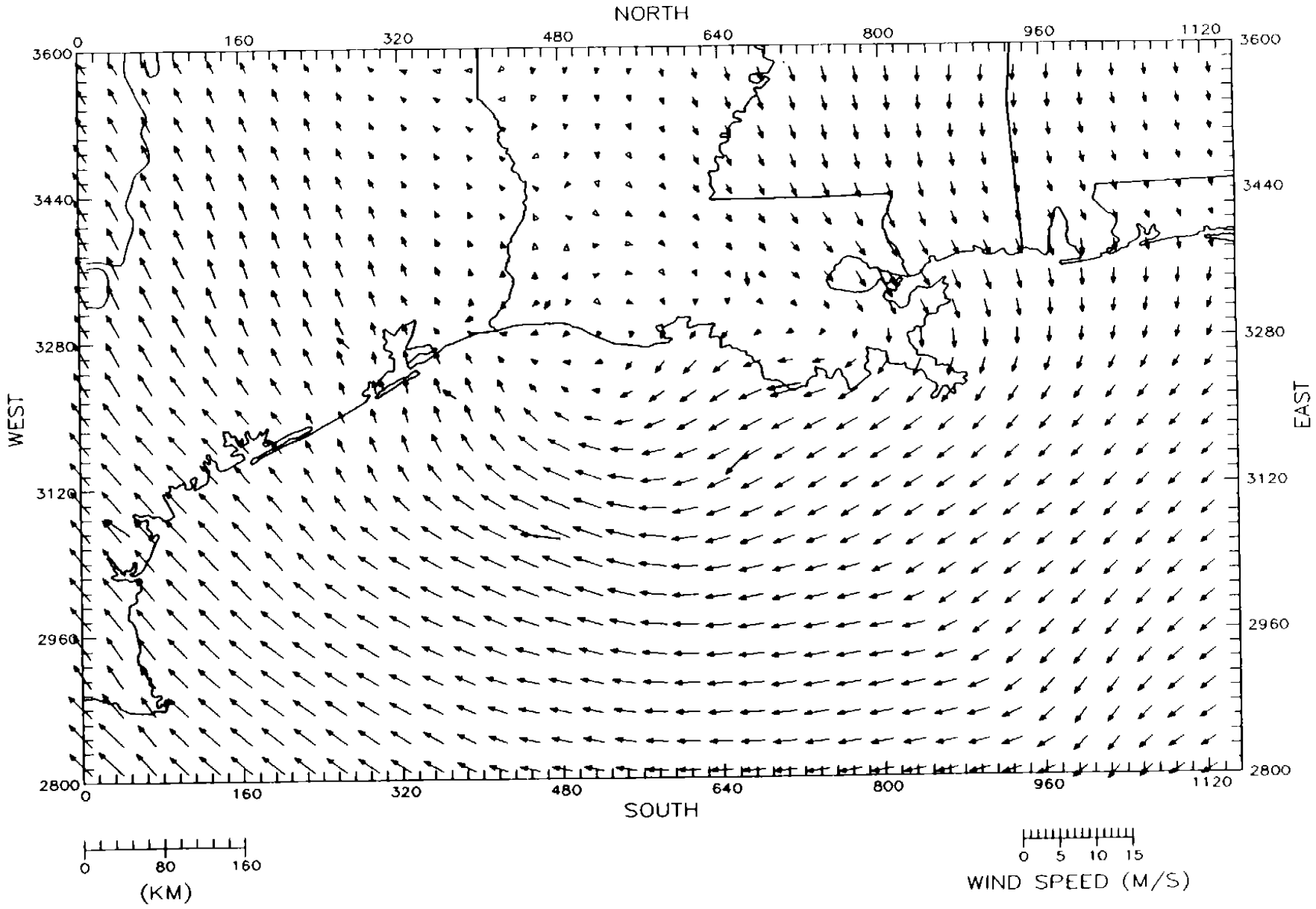

Figure 4-12c. SAIMM wind fields for the coarse-grid domain on 19 August 1993 at 1600 CST Level 9 (1200 m).

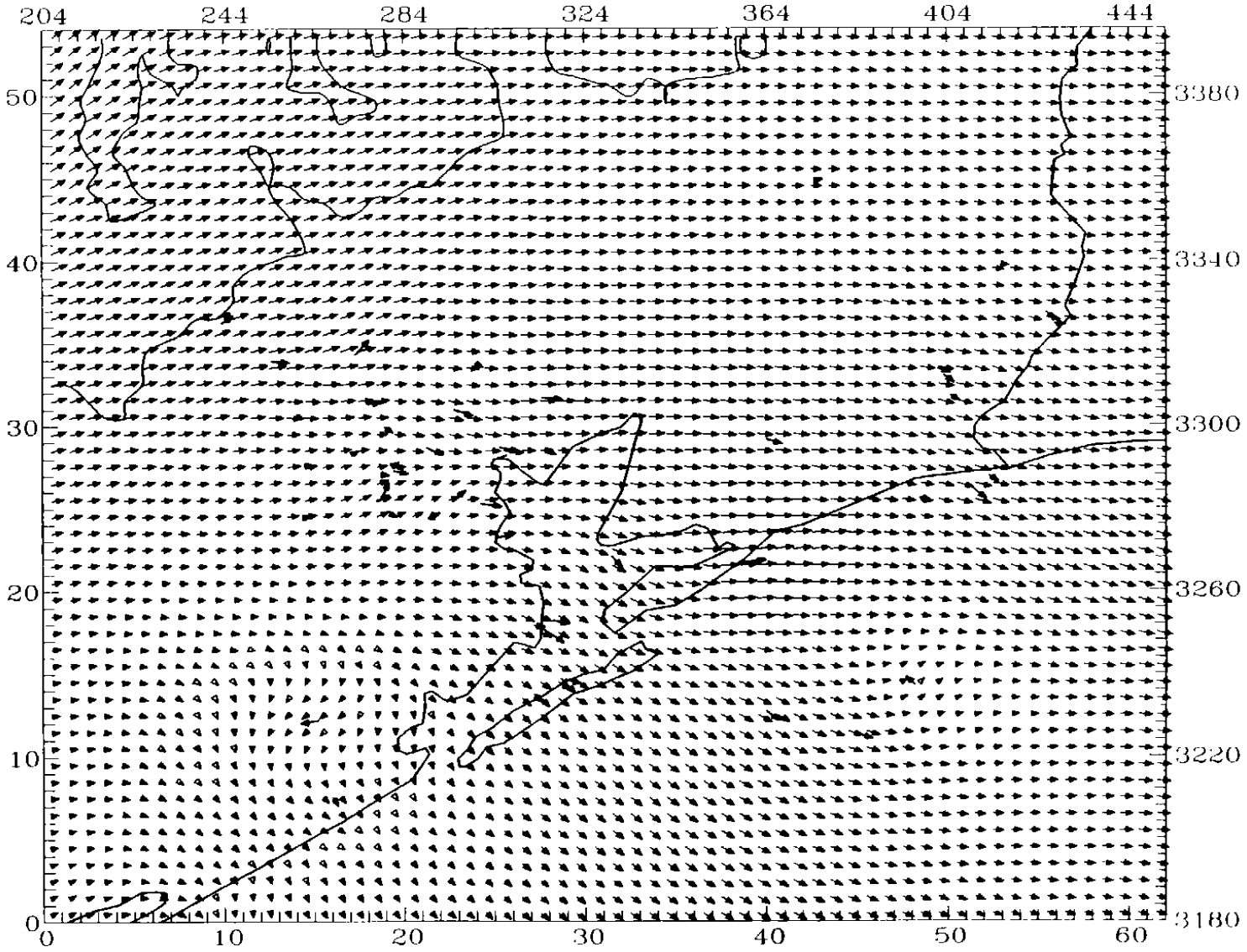

Figure 4-13a. SAIMM wind fields for the fine-grid domain on 19 August 1993 at 1000 CST. Level 1 (25 m).

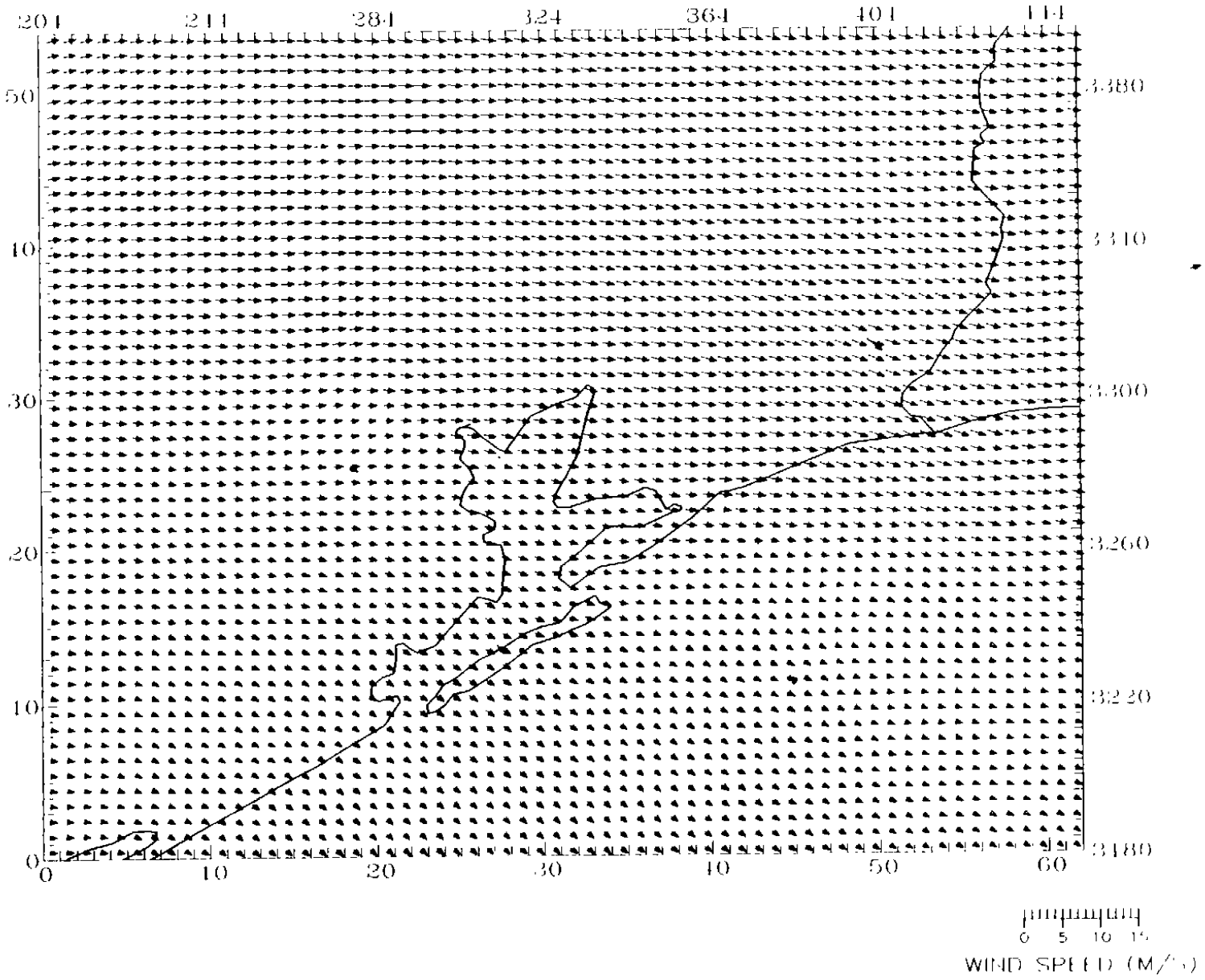

Figure 4-13b. SAIMM wind fields for the fine-grid domain on 19 August 1993 at 1000 CST Level 7 (675 m)

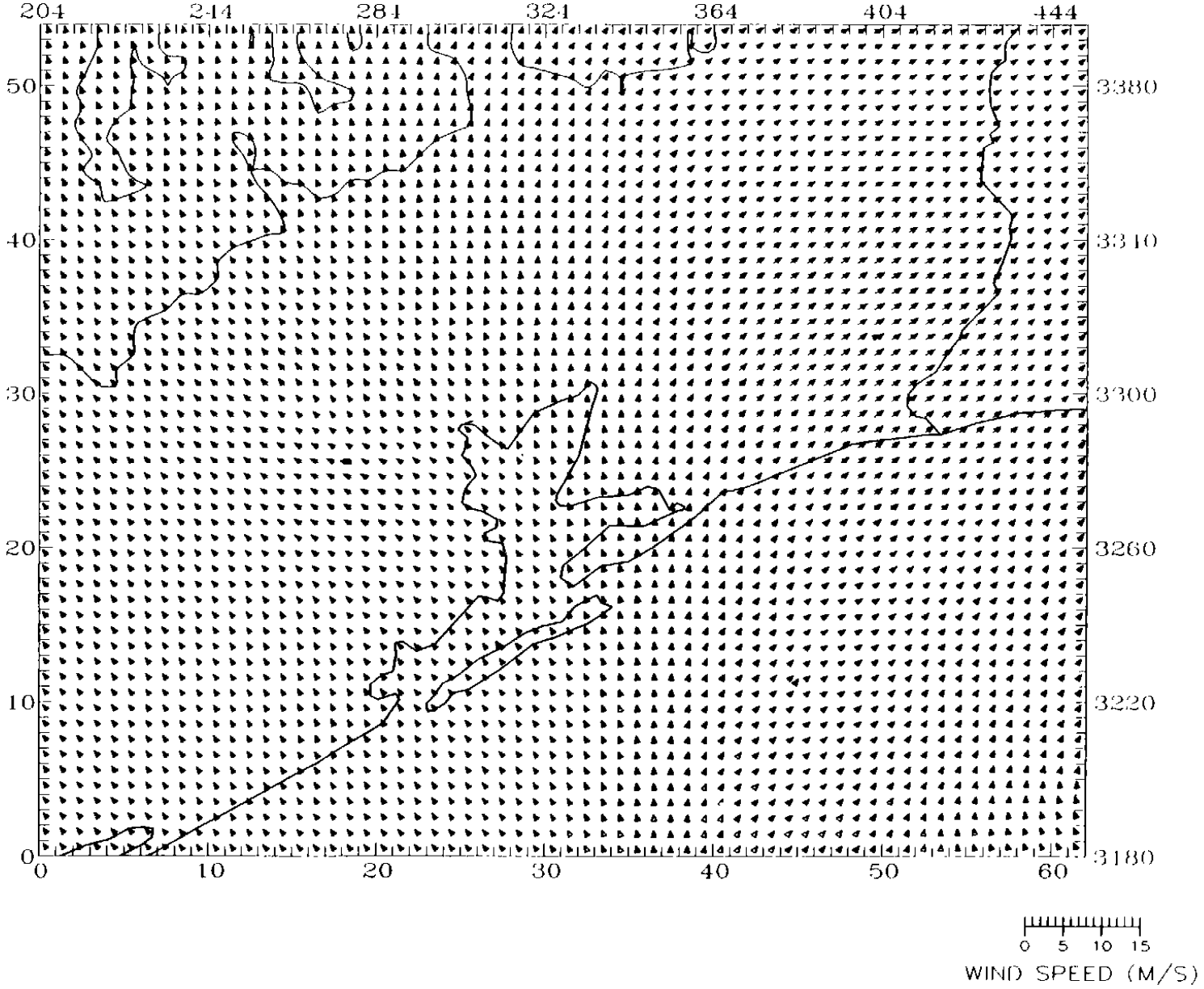

Figure 4-13c. SAIMM wind fields for the fine-grid domain on 19 August 1993 at 1000 CST. Level 9 (1200 m).

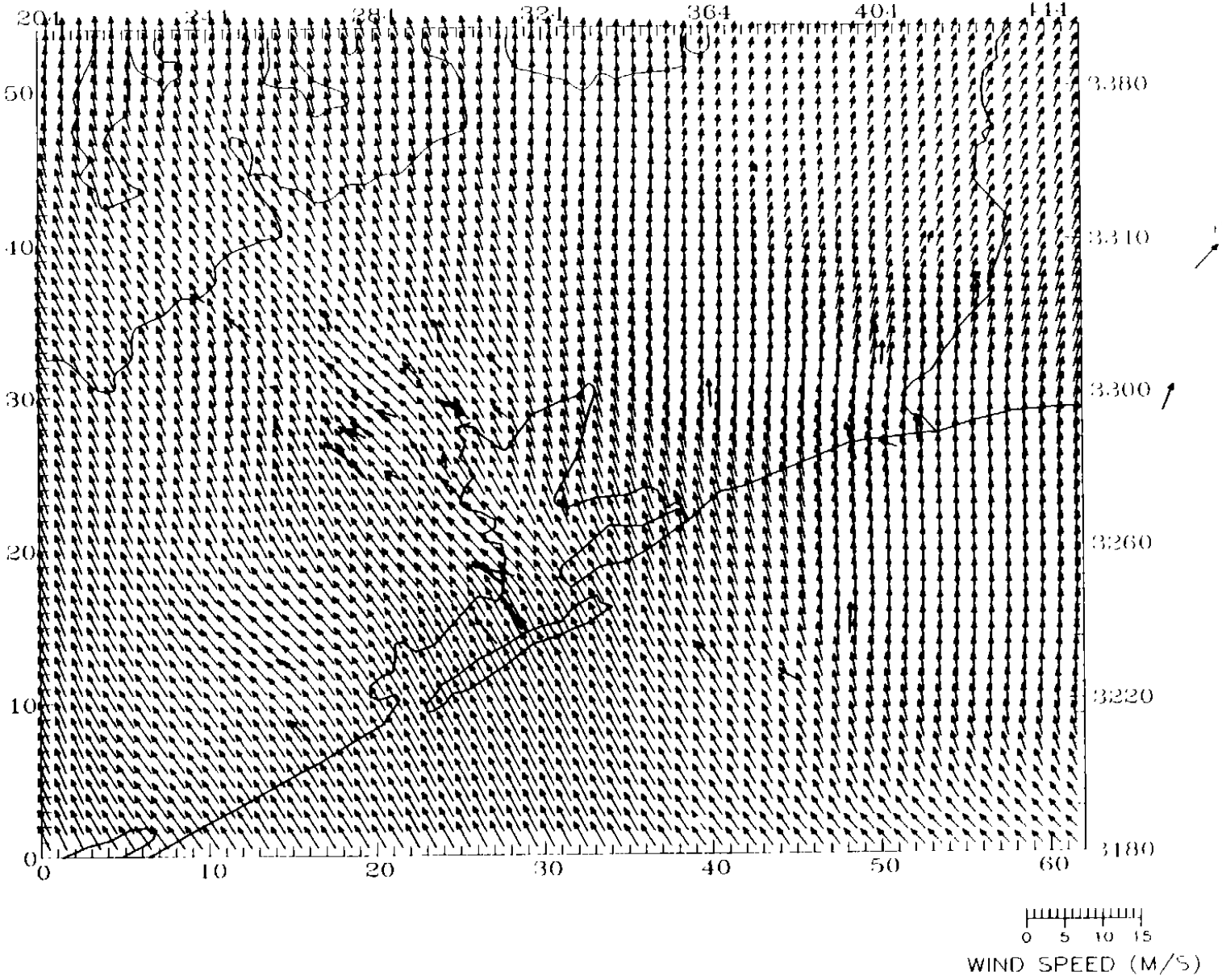

Figure 4-14a. SAIMM wind fields for the fine-grid domain on 19 August 1993 at 1600 CST Level 1 (25 m).

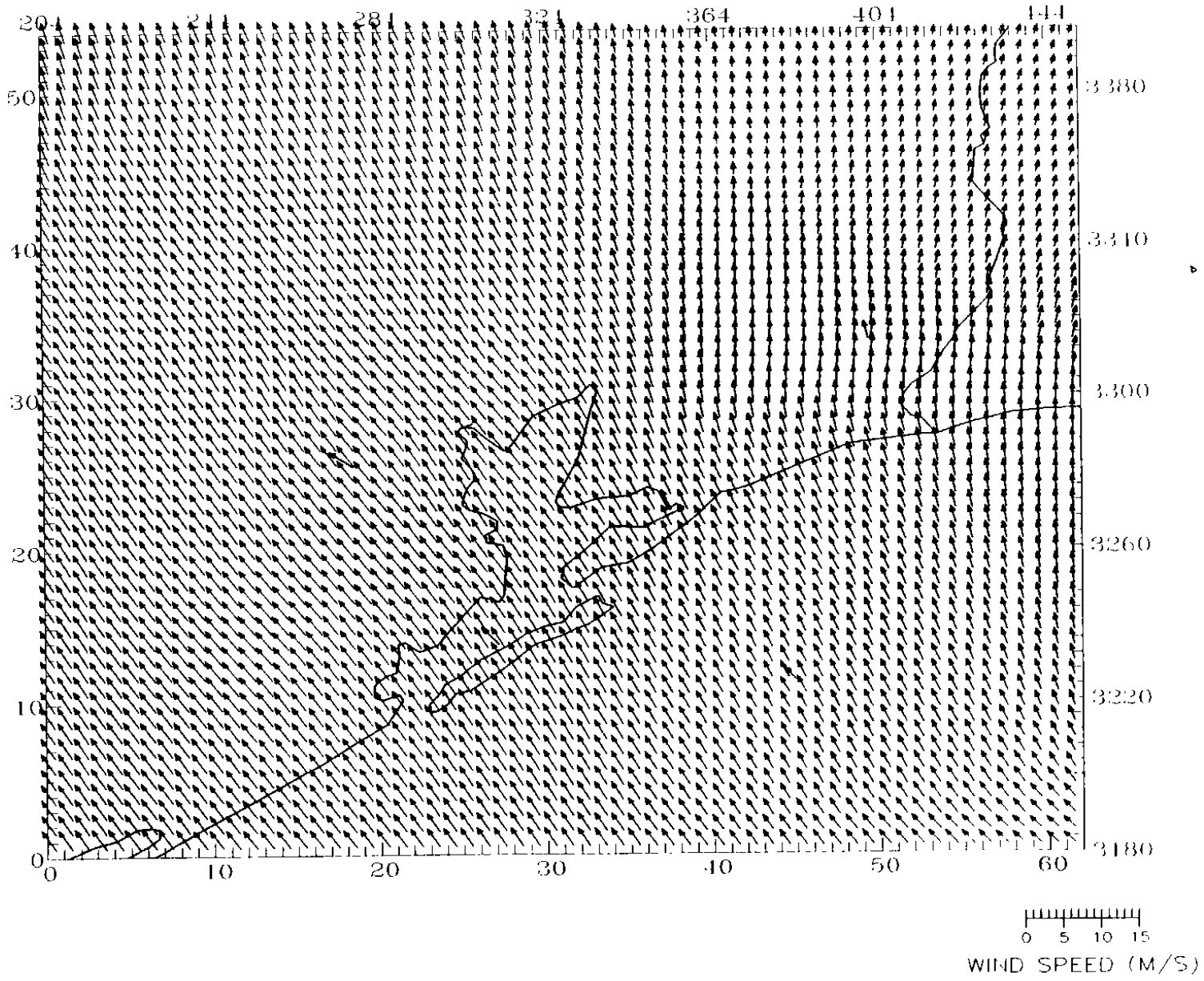

Figure 4-14b. SAIMM wind fields for the fine-grid domain on 19 August 1993 at 1600 CST. Level 7 (675 m).

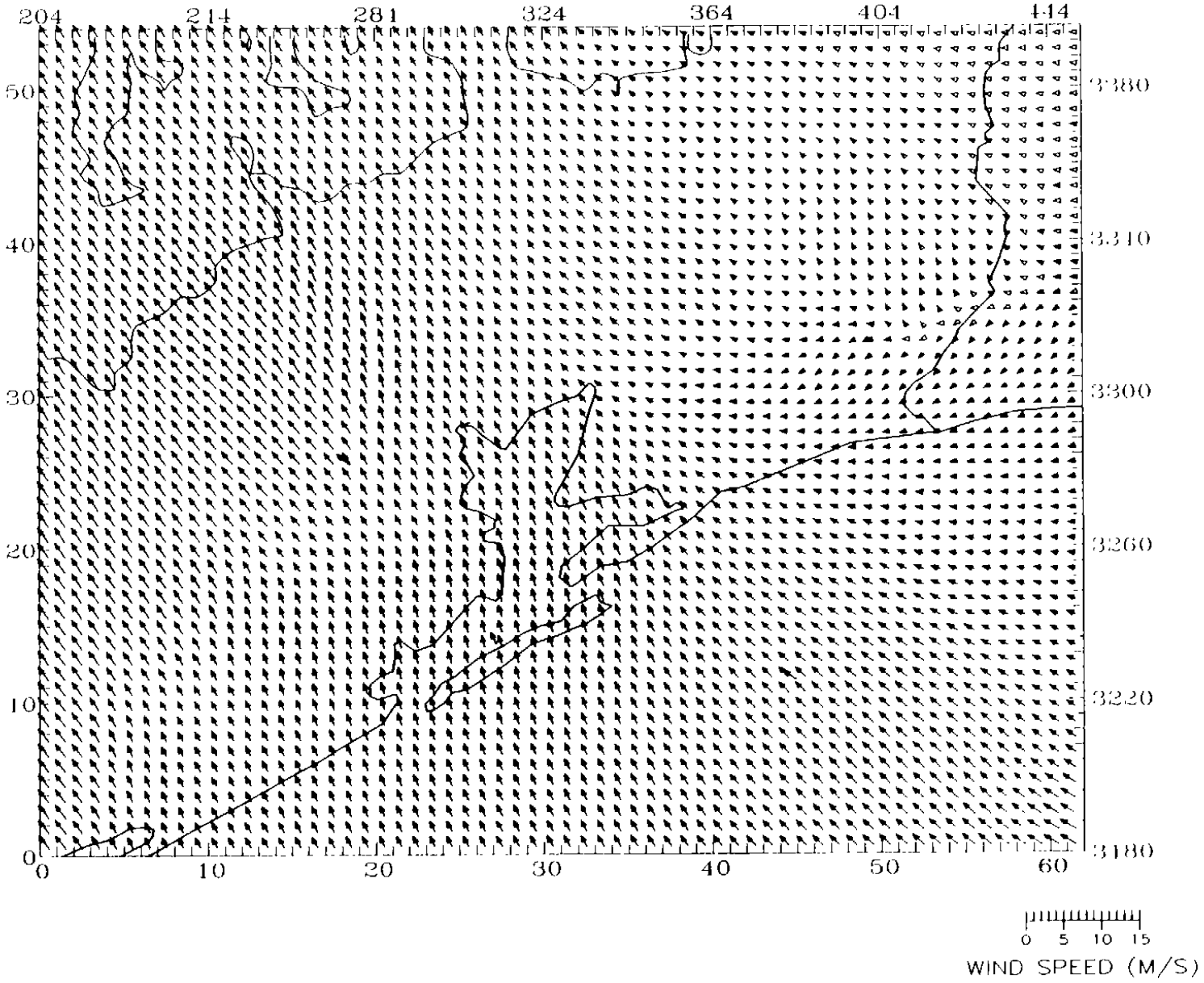

Figure 4-14c. SAIMM wind fields for the fine-grid domain on 19 August 1993 at 1600 CST. Level 9 (1200 m).

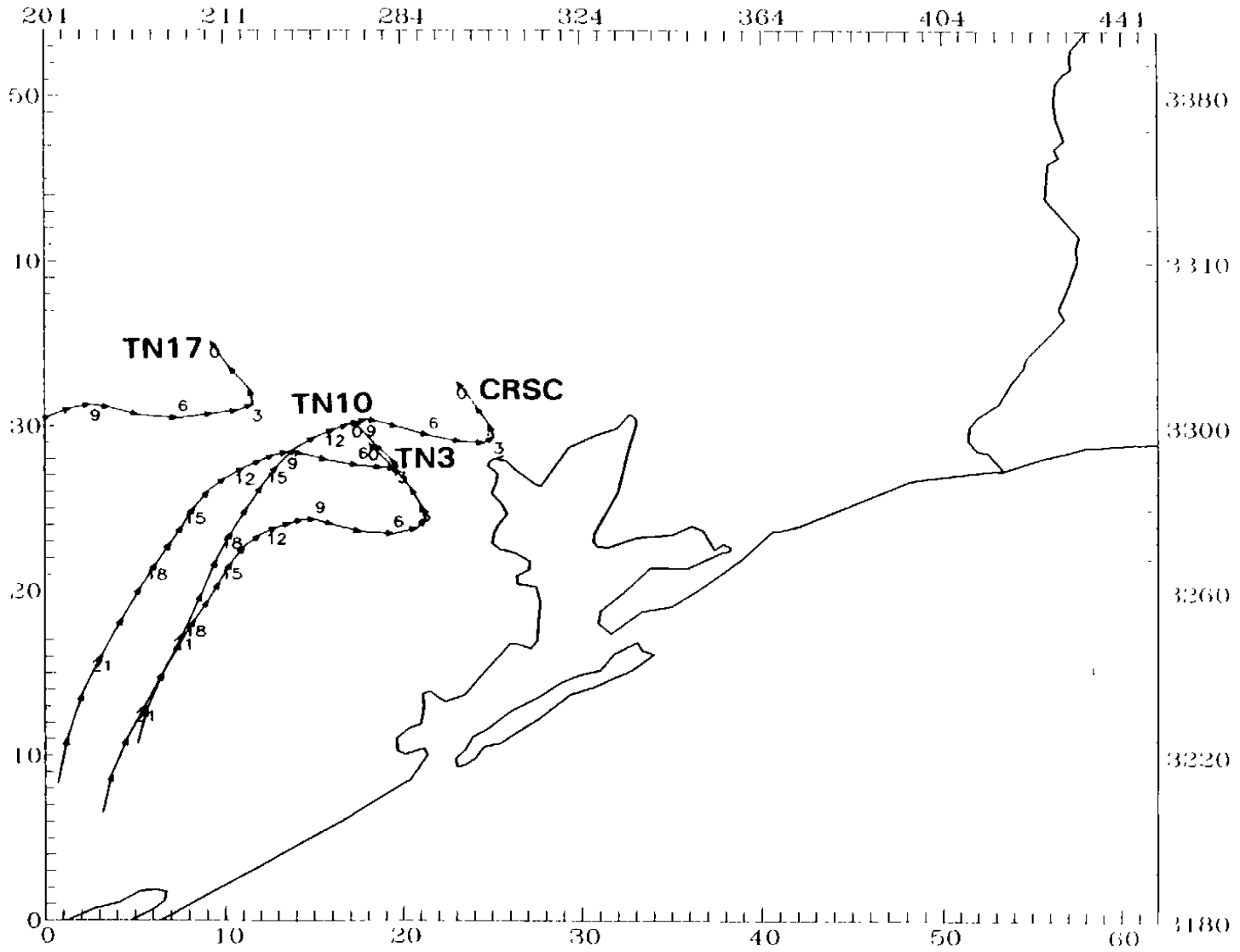

Figure 4-15. Twenty-four-hour backward particle paths ending at 1600 CST on 19 August 1993.

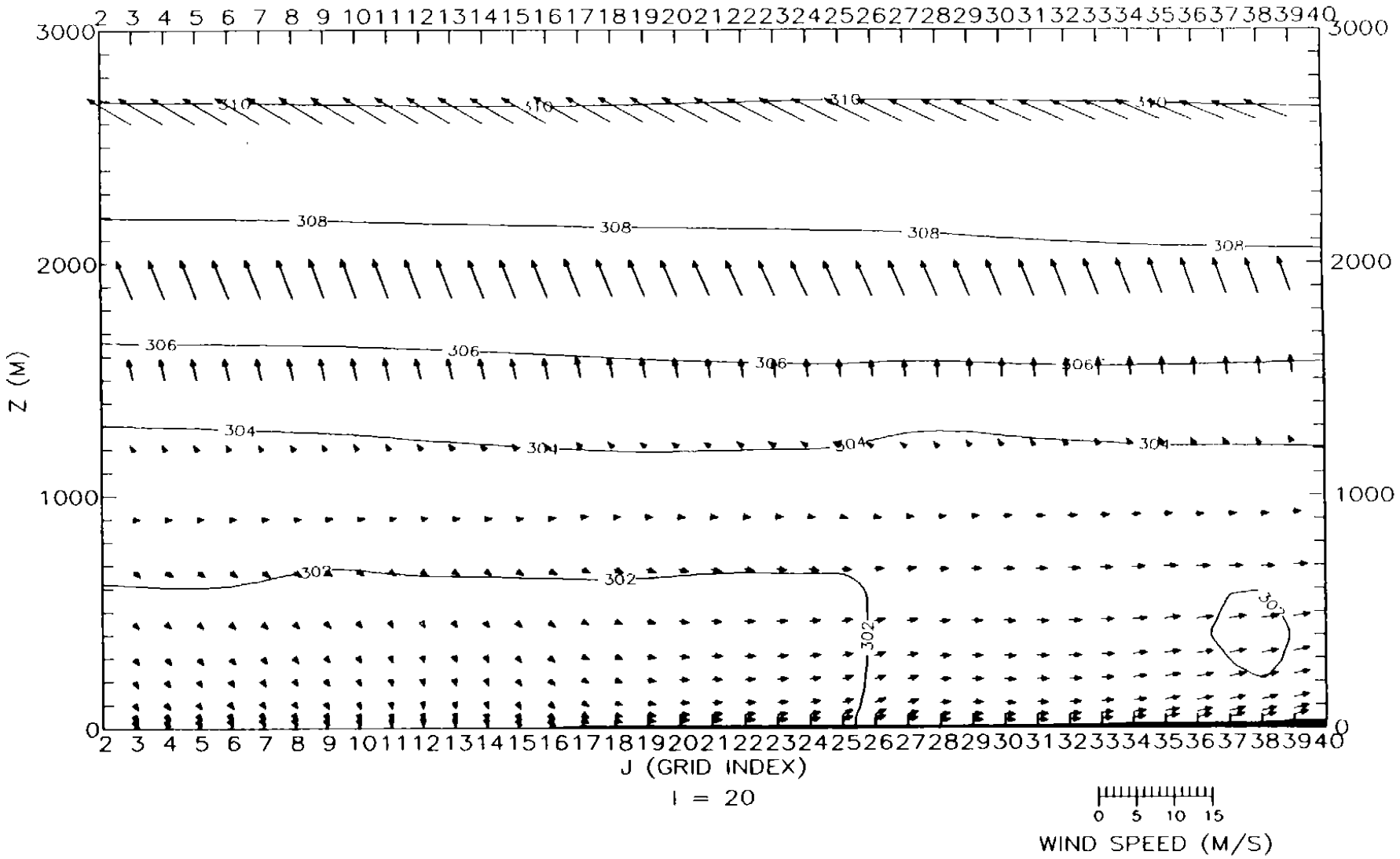

Figure 4-16a. Vertical cross section of wind and potential temperature for the fine-grid domain along west-east grid cell number 20 from south-north grid cells 2 to 40 on 19 August, 1000 CST.

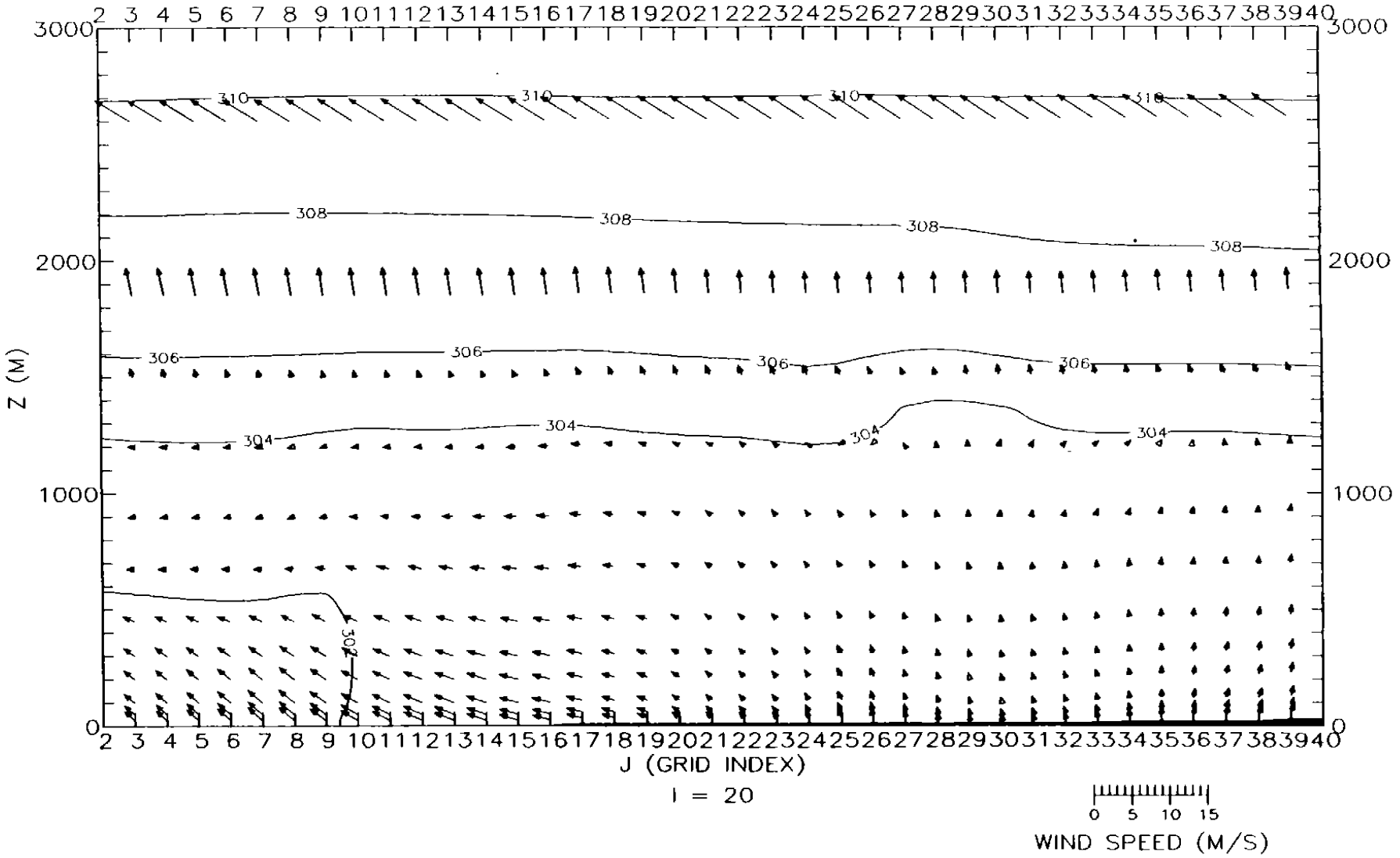

Figure 4-16b. Vertical cross section of wind and potential temperature for the fine-grid domain along west-east grid cell number 20 from south-north grid cells 2 to 40 on 19 August, 1200 CST.

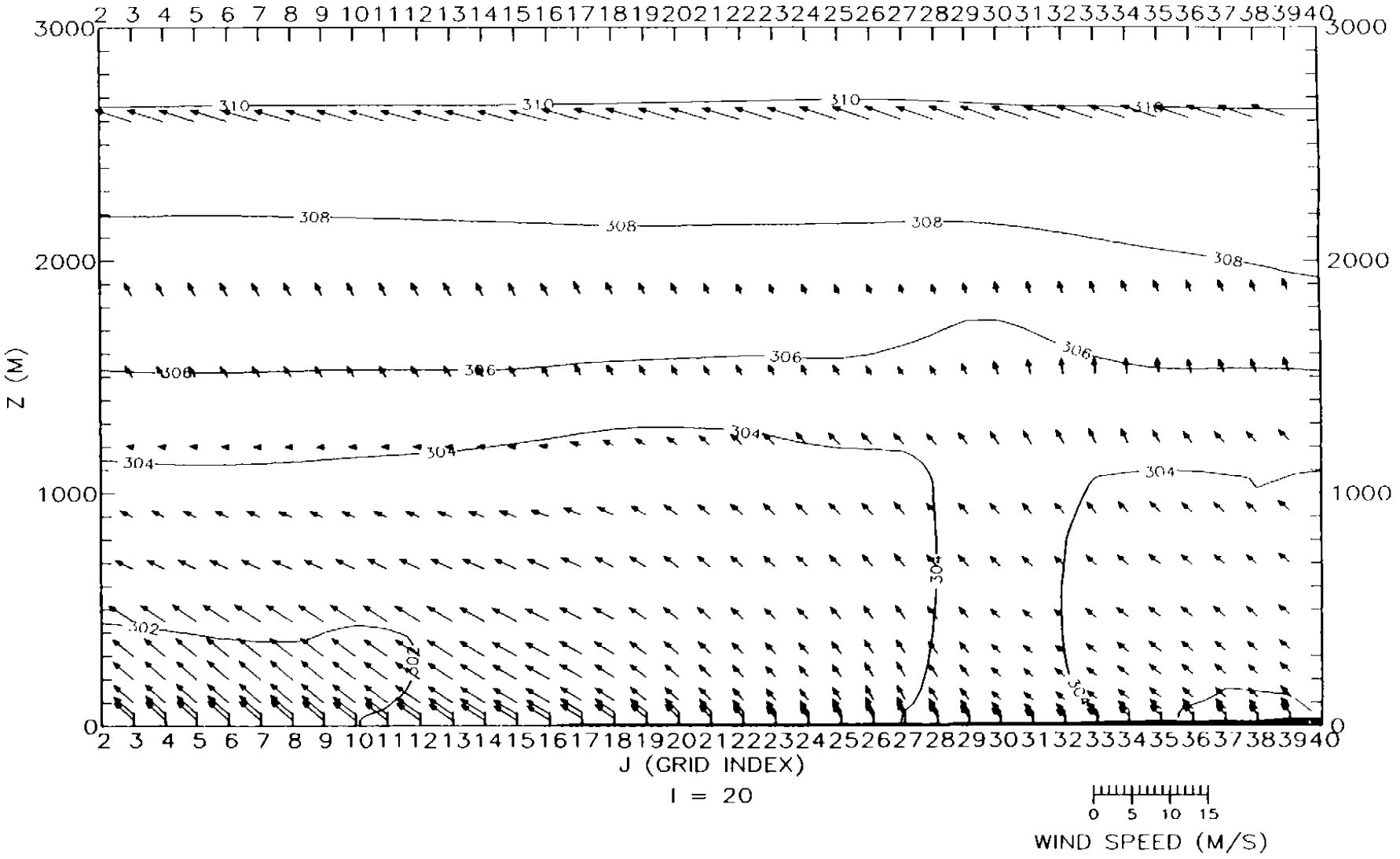

Figure 4-16c. Vertical cross section of wind and potential temperature for the fine-grid domain along west-east grid cell number 20 from south-north grid cells 2 to 40 on 19 August, 1400 CST.

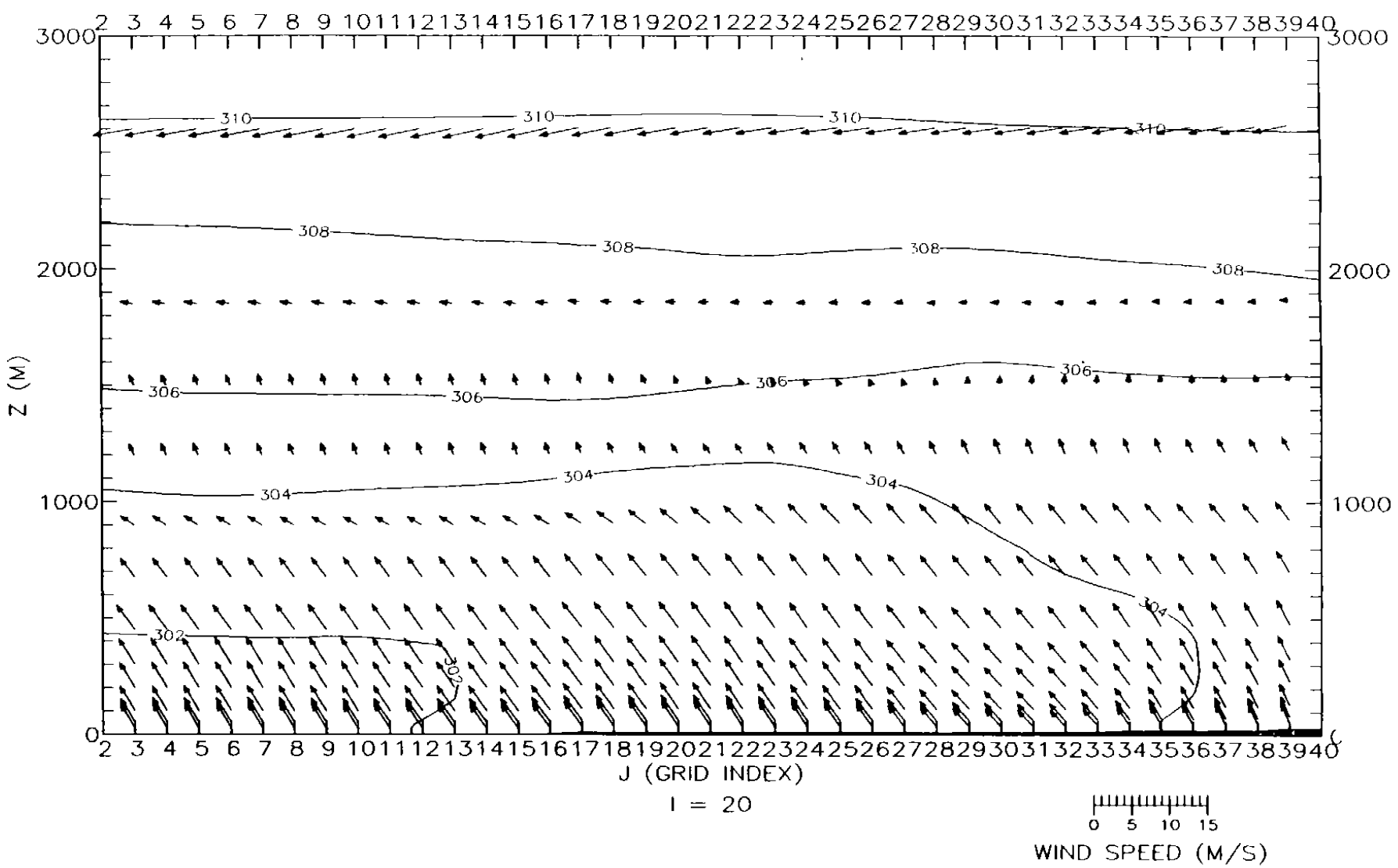

Figure 4-16d. Vertical cross section of wind and potential temperature for the fine-grid domain along west-east grid cell number 20 from south-north grid cells 2 to 40 on 19 August, 1600 CST.

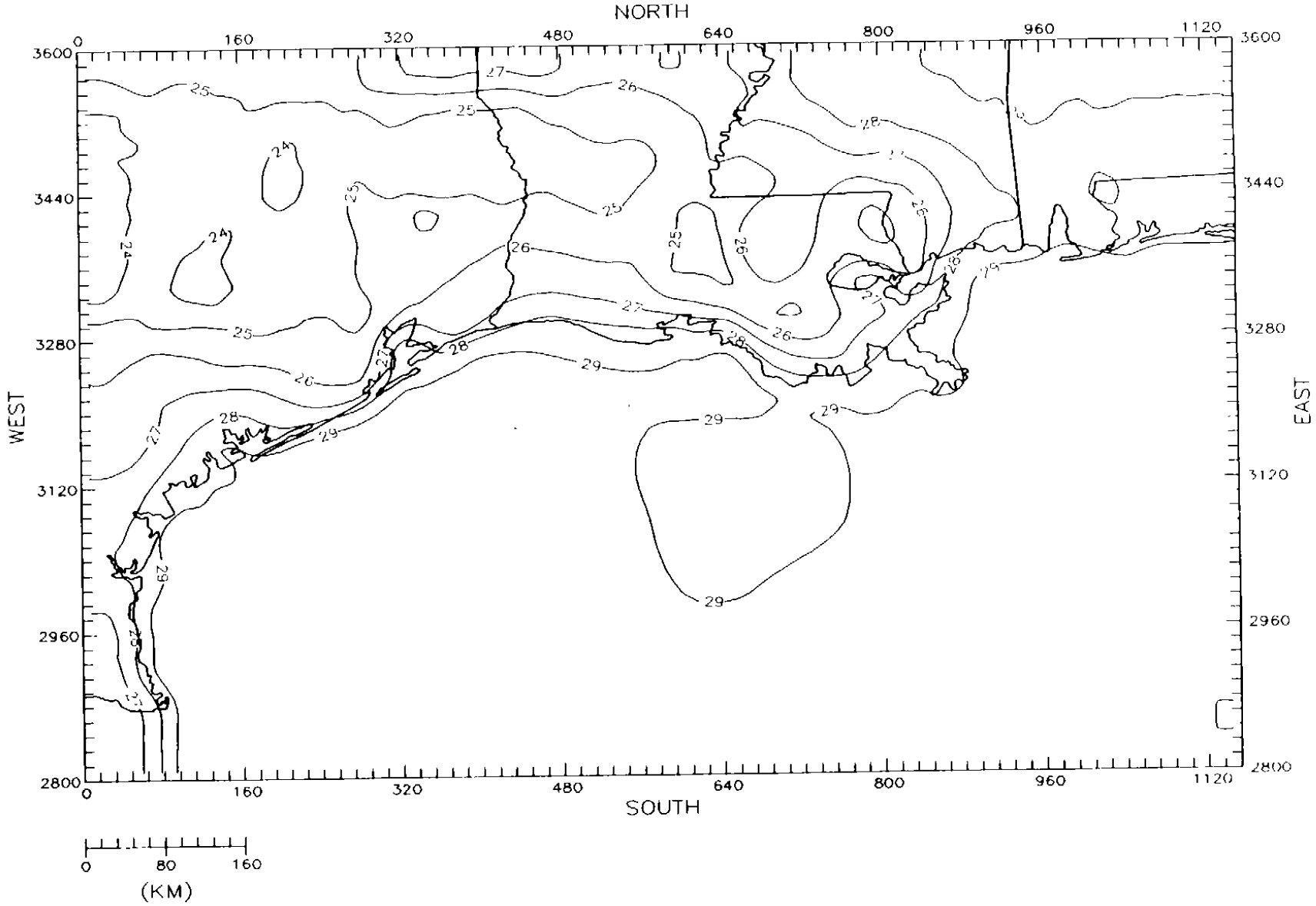

Figure 4-17a. SAIMM surface-level temperature fields (°C) for the coarse-grid domain on 19 August 1993 at 0400 CST

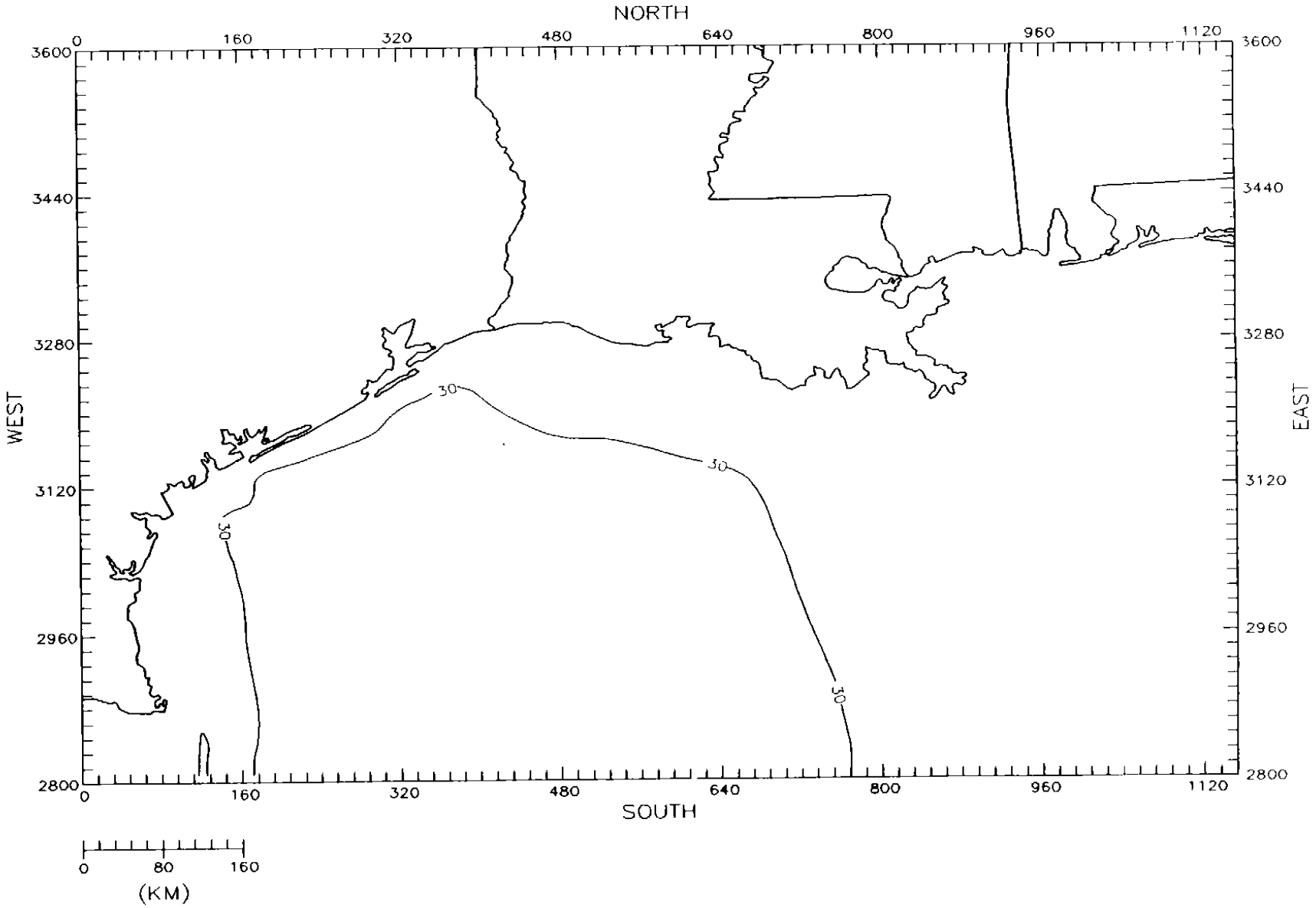

Figure 4-17b. SAIMM surface-level temperature fields (°C) for the coarse-grid domain on 19 August 1993 at 1600 CST.

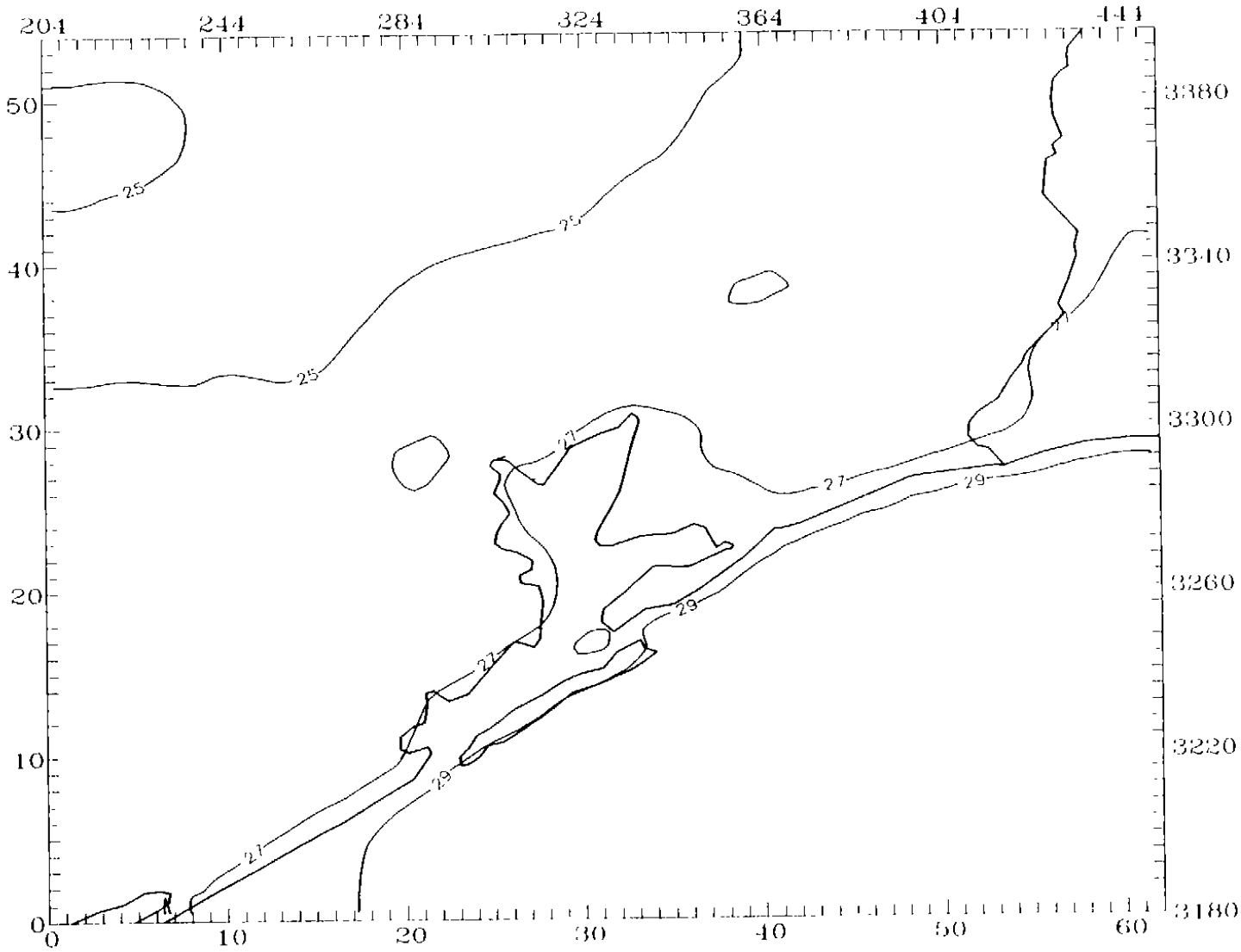

Figure 4-18a. SAIMM surface-level temperature fields (°C) for the fine-grid domain on 19 August 1993 at 0400 CST.

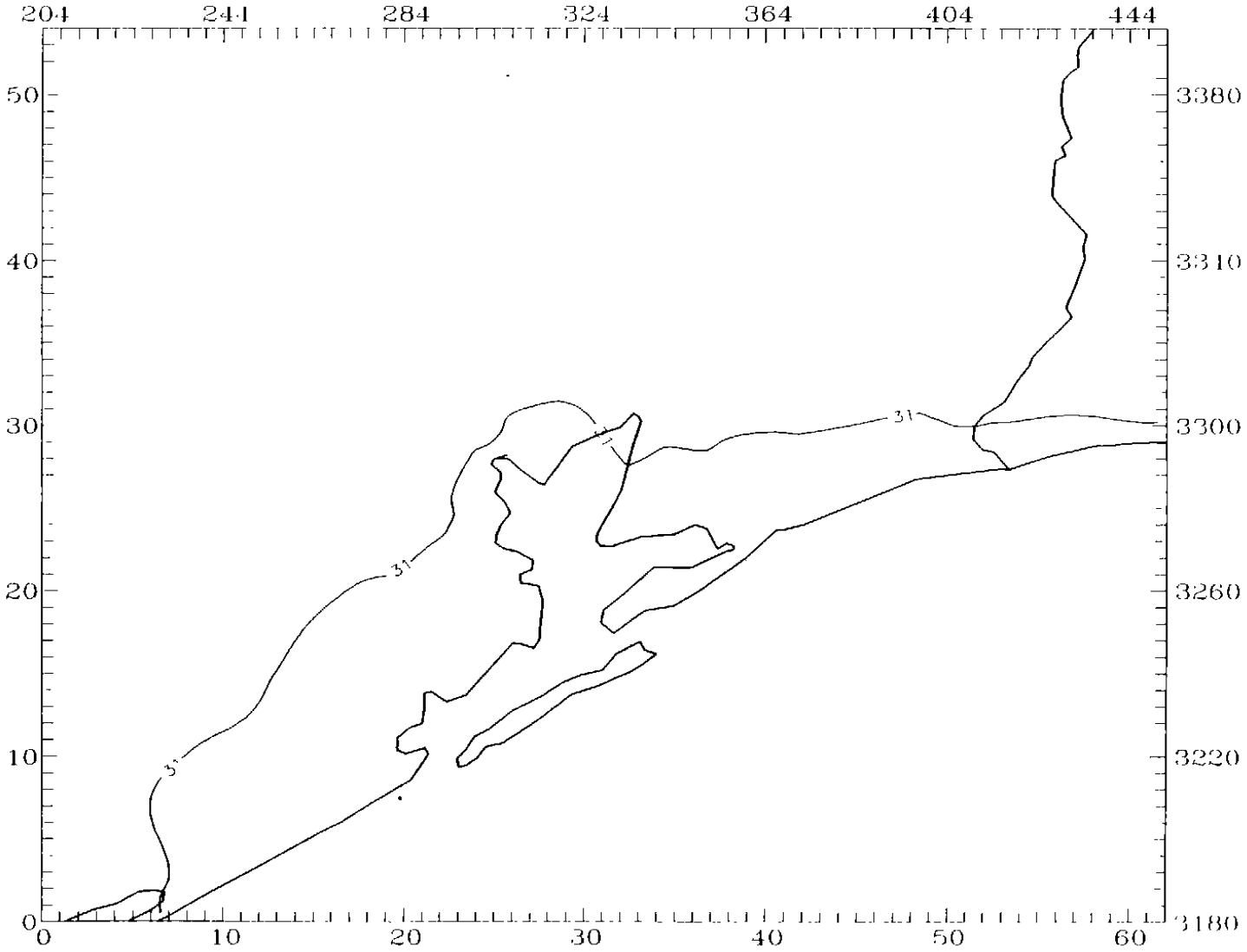

Figure 4-18b. SAIMM surface-level temperature fields (°C) for the fine-grid domain on 19 August 1993 at 1600 CST.

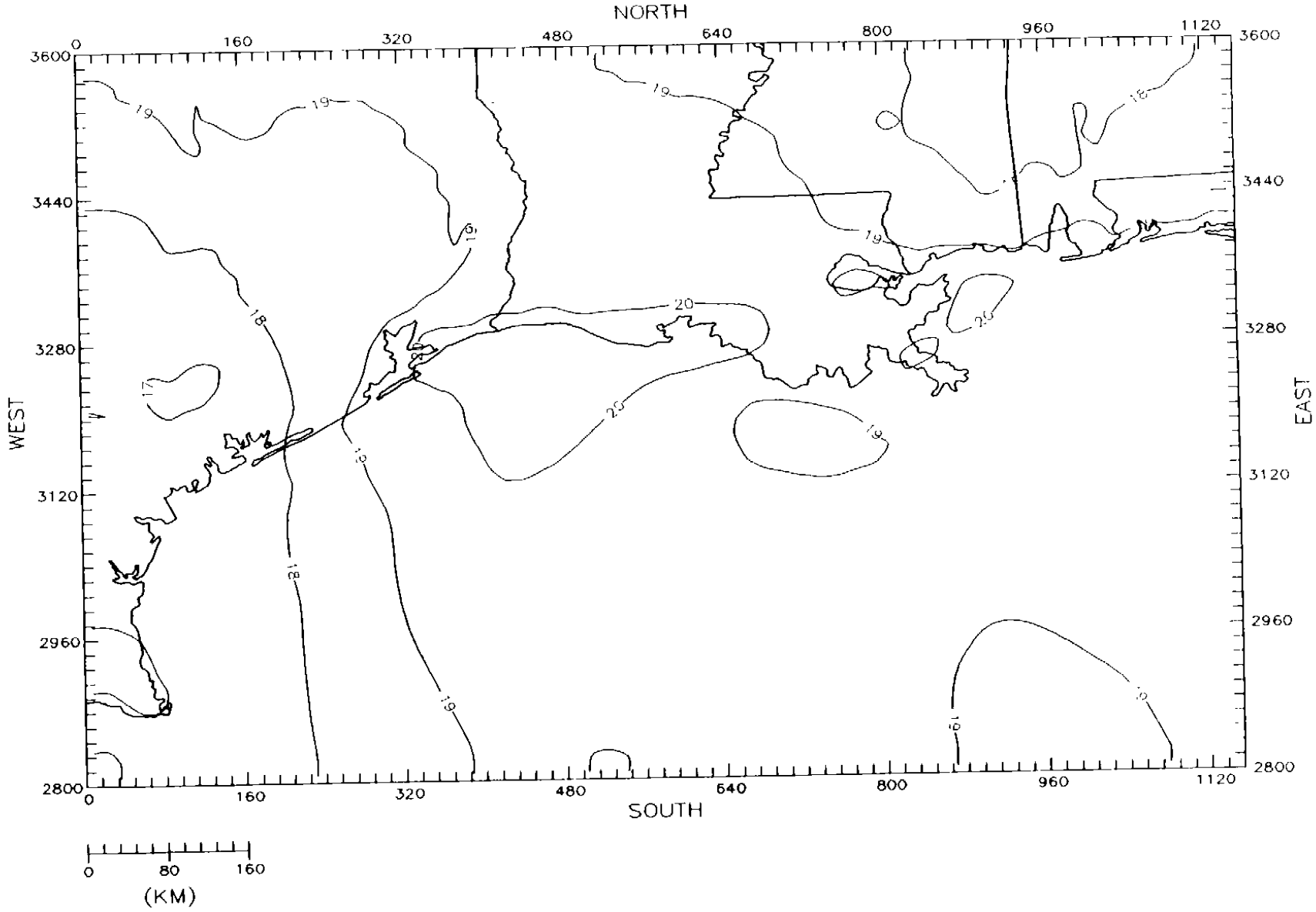

Figure 4-19a. SAIMM surface-level specific humidity fields (gkg^{-1}) for the coarse-grid domain on 19 August 1993 at 0400 CST.

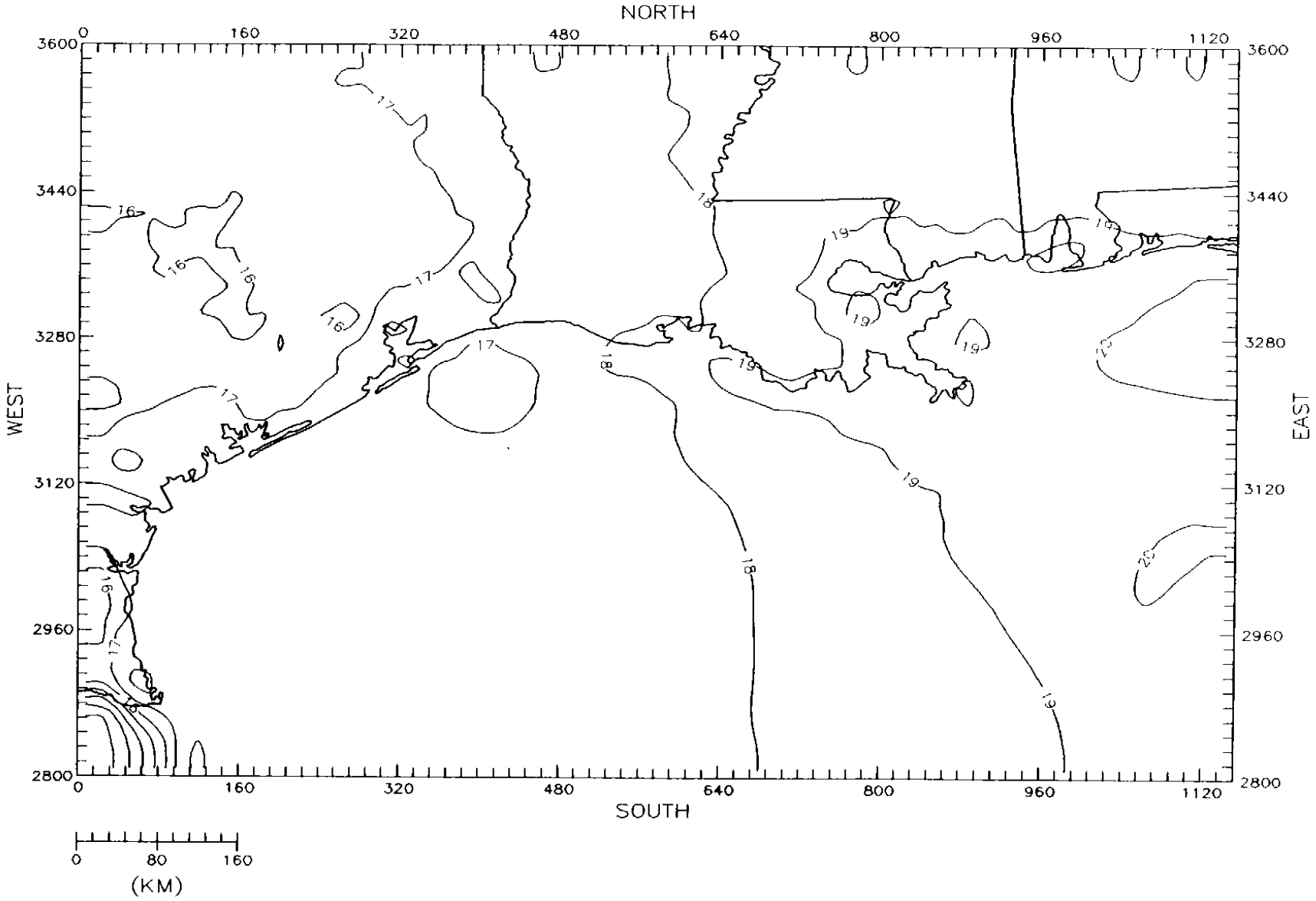

Figure 4-19b. SAIMM surface-level specific humidity fields (gkg^{-1}) for the coarse-grid domain on 19 August 1993 at 1600 CST

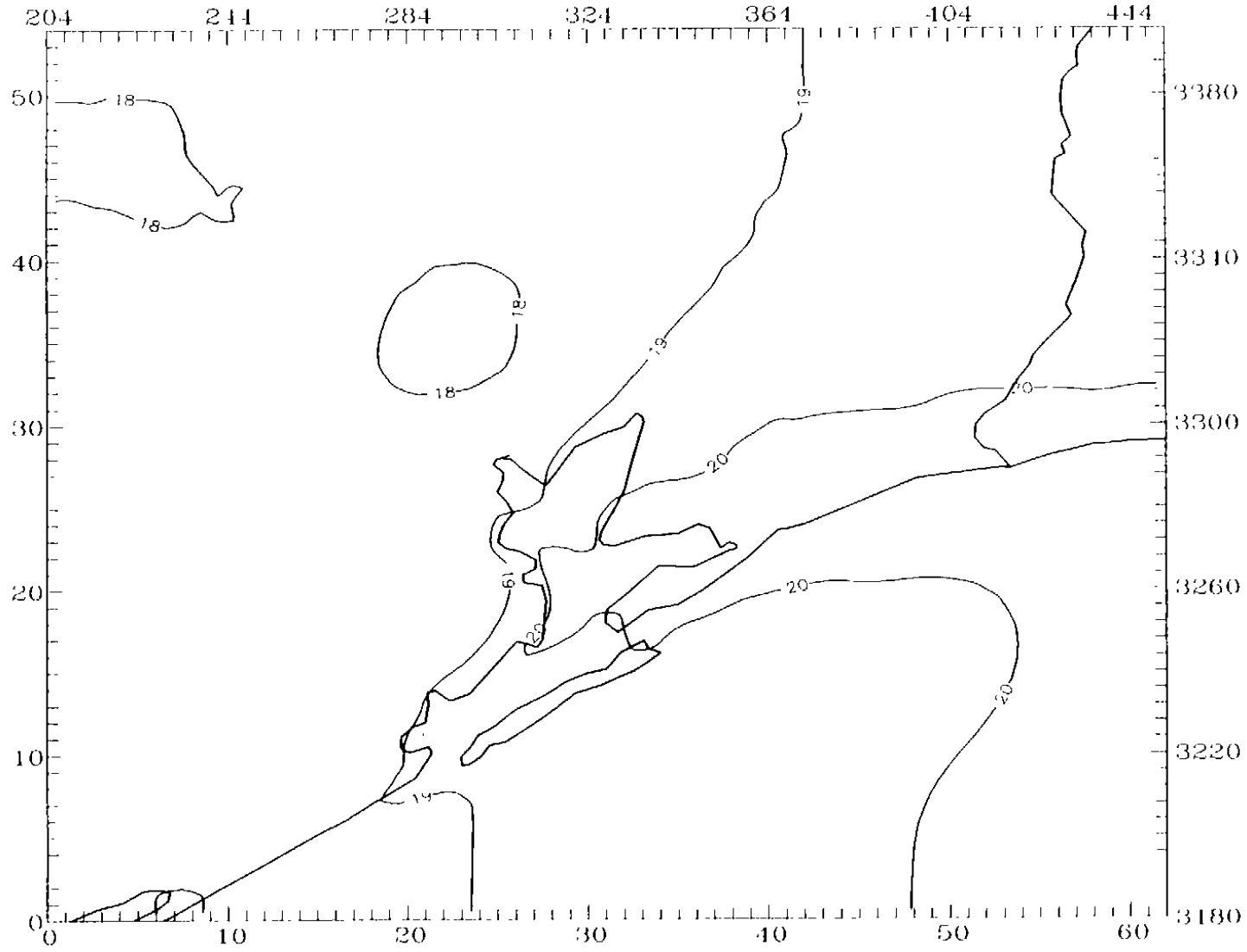

Figure 4-20a. SAIMM surface-level specific humidity fields (gkg^{-1}) for the fine-grid domain on 19 August 1993 at 0400 CST.

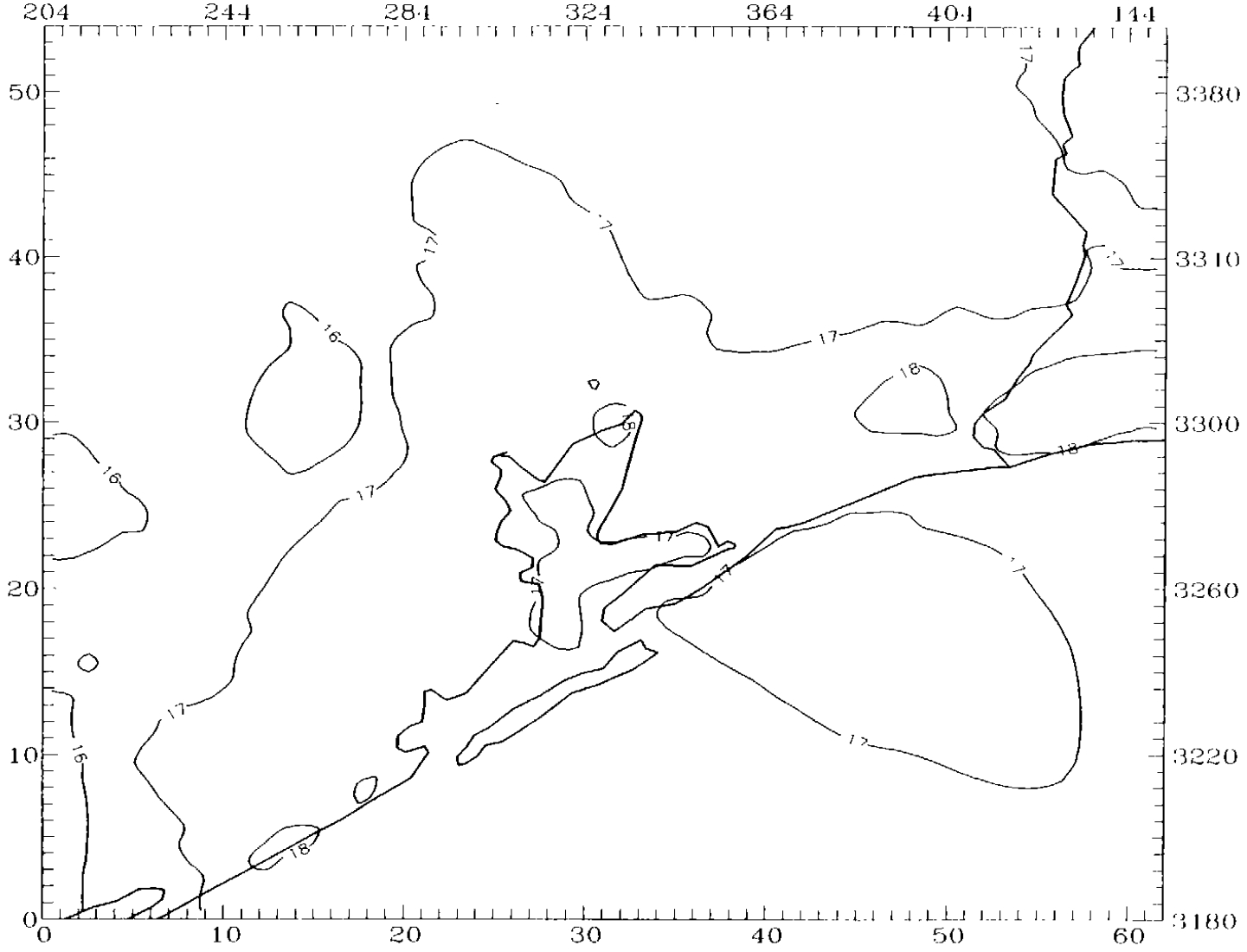

Figure 4-20b. SAIMM surface-level specific humidity fields (gkg^{-1})for the fine-grid domain on 19 August 1993 at 1600 CST.

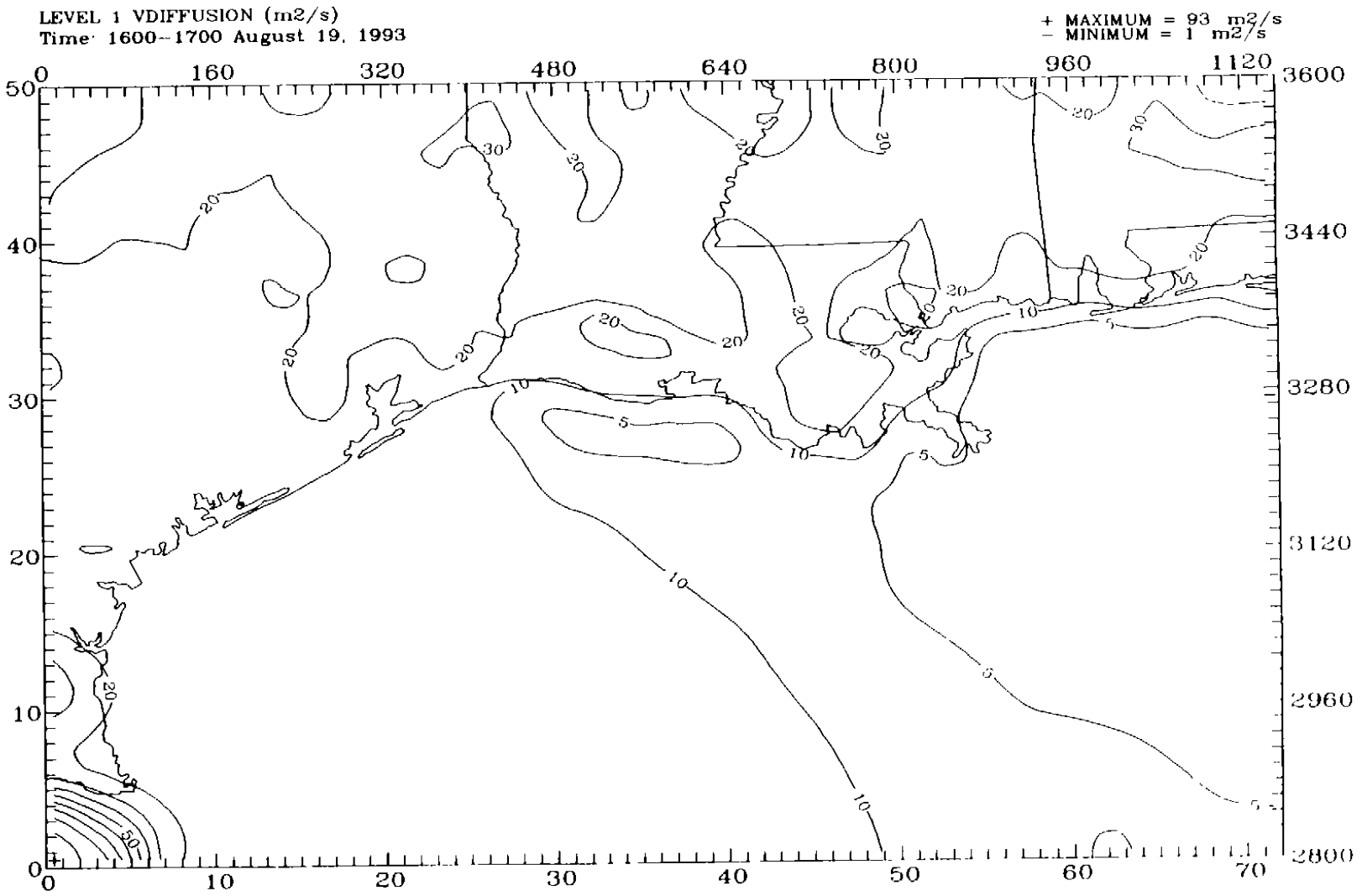

Figure 4-21a. UAM-V-ready vertical turbulent exchange coefficients (m^2s^{-1}) for the coarse-grid domain on 19 August 1993 at 1600 CST Interface between UAM-V layers 1 and 2.

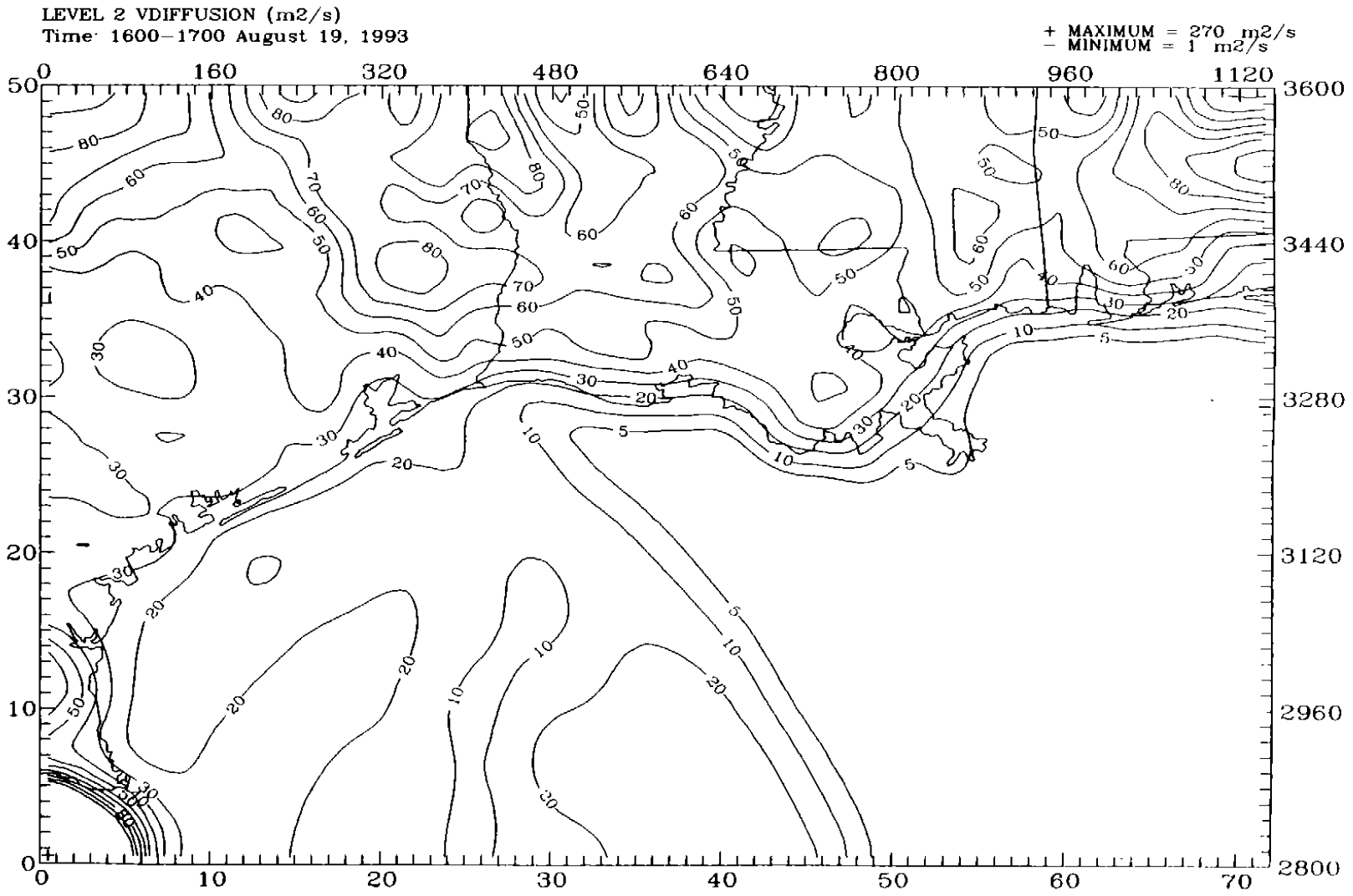

Figure 4-21b. UAM-V-ready vertical turbulent exchange coefficients (m^2s^{-1}) for the coarse-grid domain on 19 August 1993 at 1600 CST Interface between UAM-V layers 2 and 3.

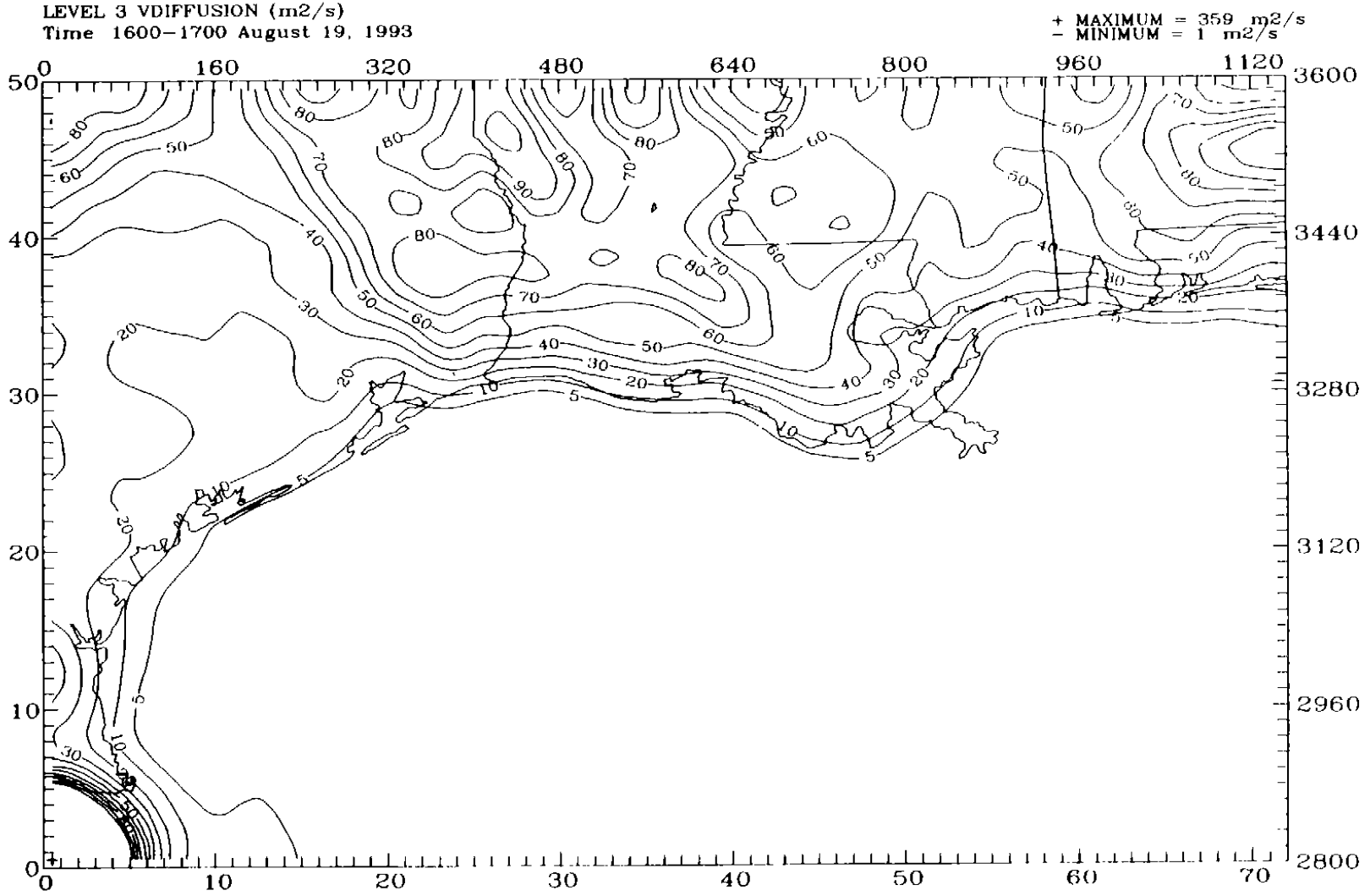

Figure 4-21c. UAM-V-ready vertical turbulent exchange coefficients (m^2s^{-1}) for the coarse-grid domain on 19 August 1993 at 1600 CST Interface between UAM-V layers 3 and 4.

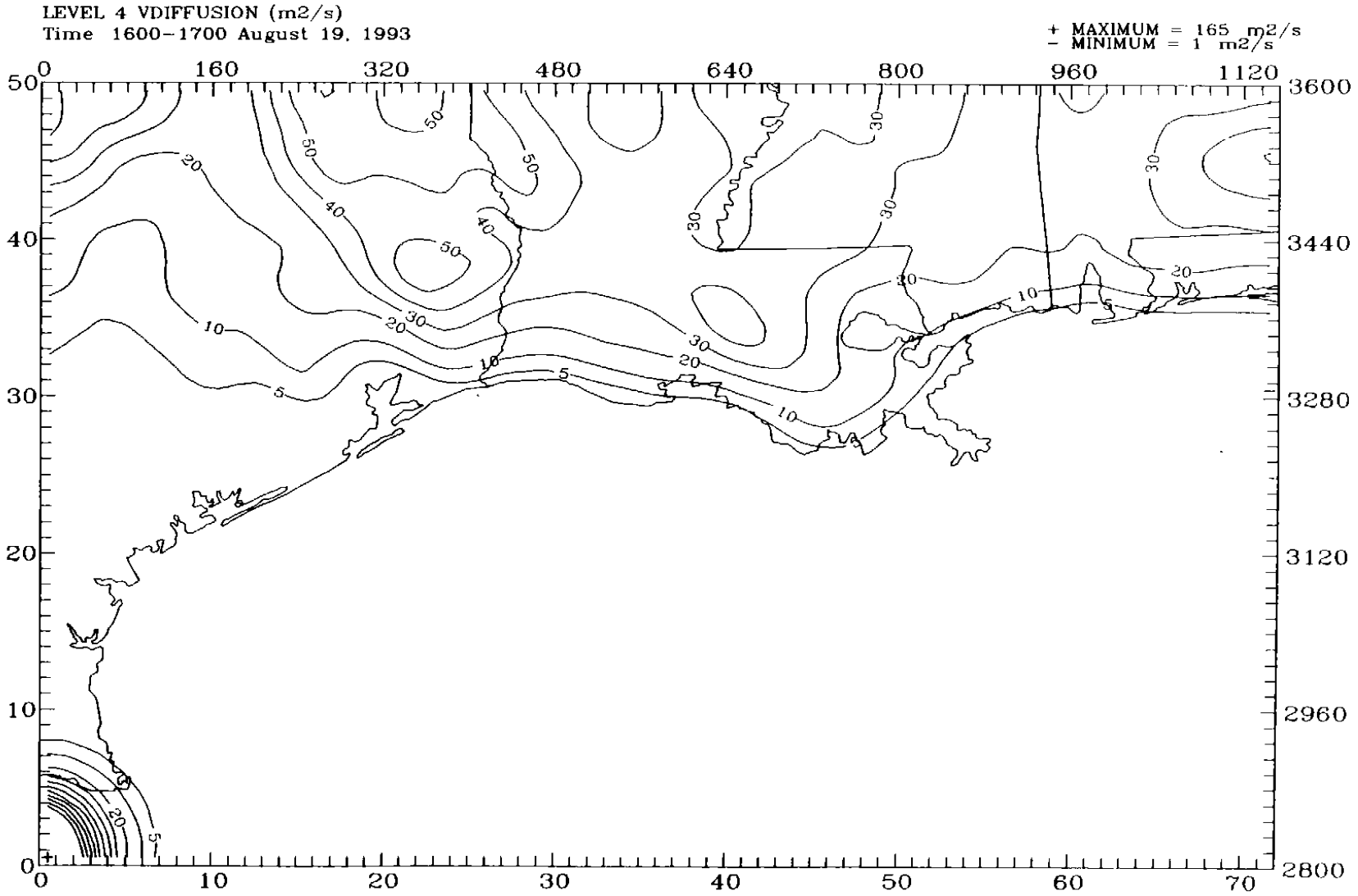

Figure 4-21d. UAM-V-ready vertical turbulent exchange coefficients (m^2s^{-1}) for the coarse-grid domain on 19 August 1993 at 1600 CST Interface between UAM-V layers 4 and 5.

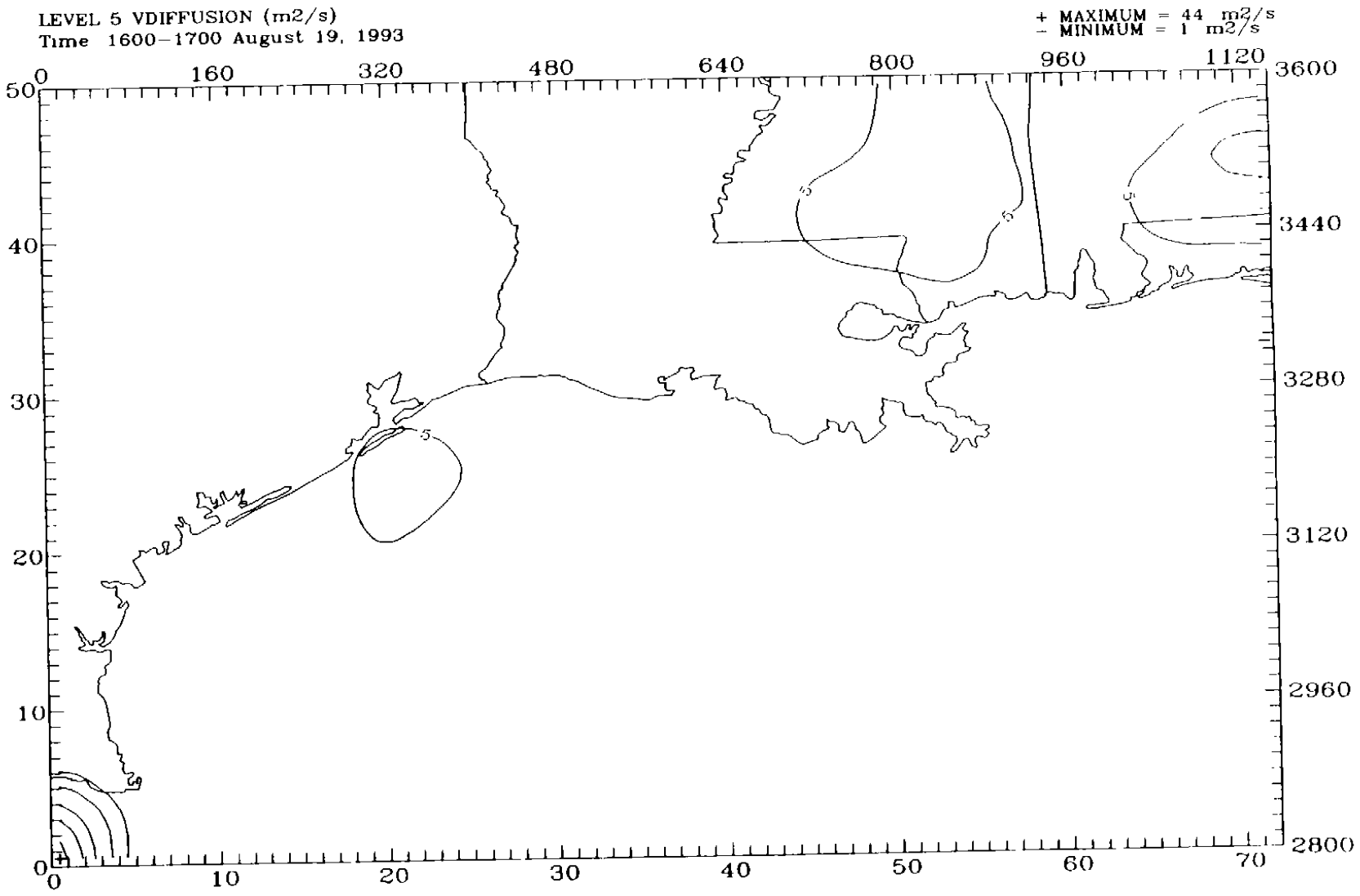

Figure 4-21e. UAM-V-ready vertical turbulent exchange coefficients (m^2s^{-1}) for the coarse-grid domain on 19 August 1993 at 1600 CST. Interface between UAM-V layers 5 and 6.

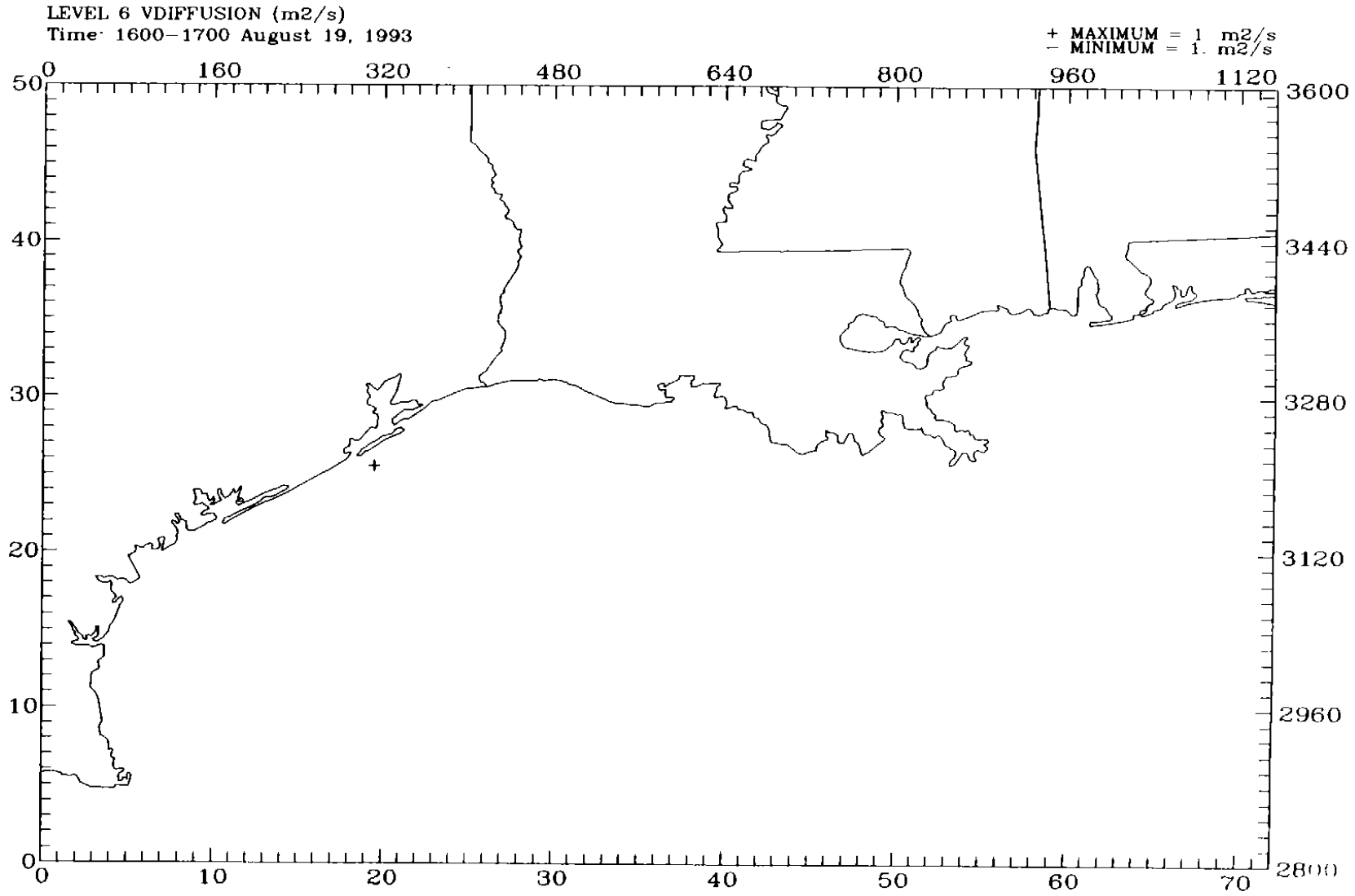

Figure 4-21f. UAM-V-ready vertical turbulent exchange coefficients (m^2s^{-1}) for the coarse-grid domain on 19 August 1993 at 1600 CST Interface between UAM-V layers 6 and 7.

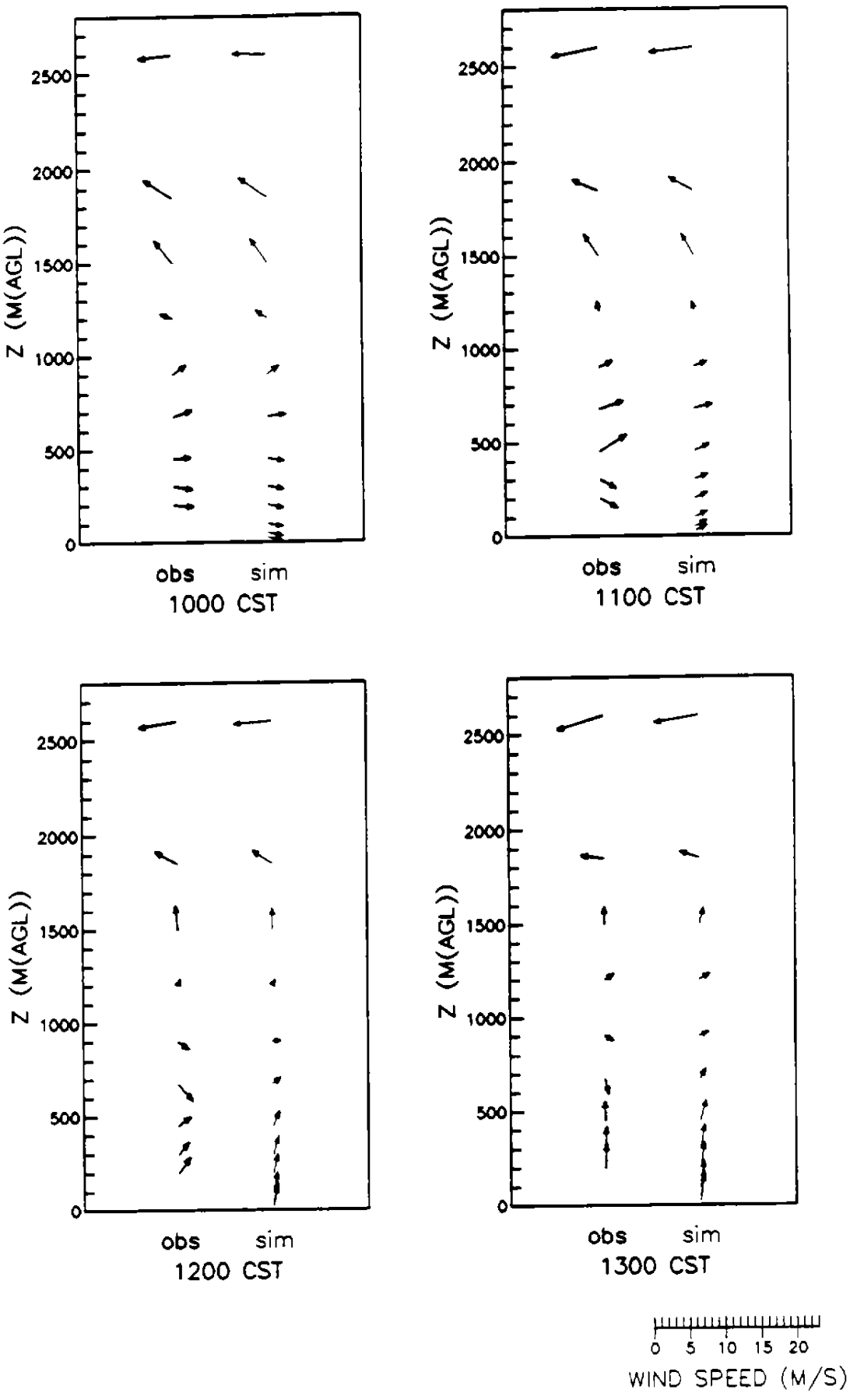

Figure 4-22a. Comparison of midday observed and simulated wind profiles for Galveston (GAL) on 18 August 1993.

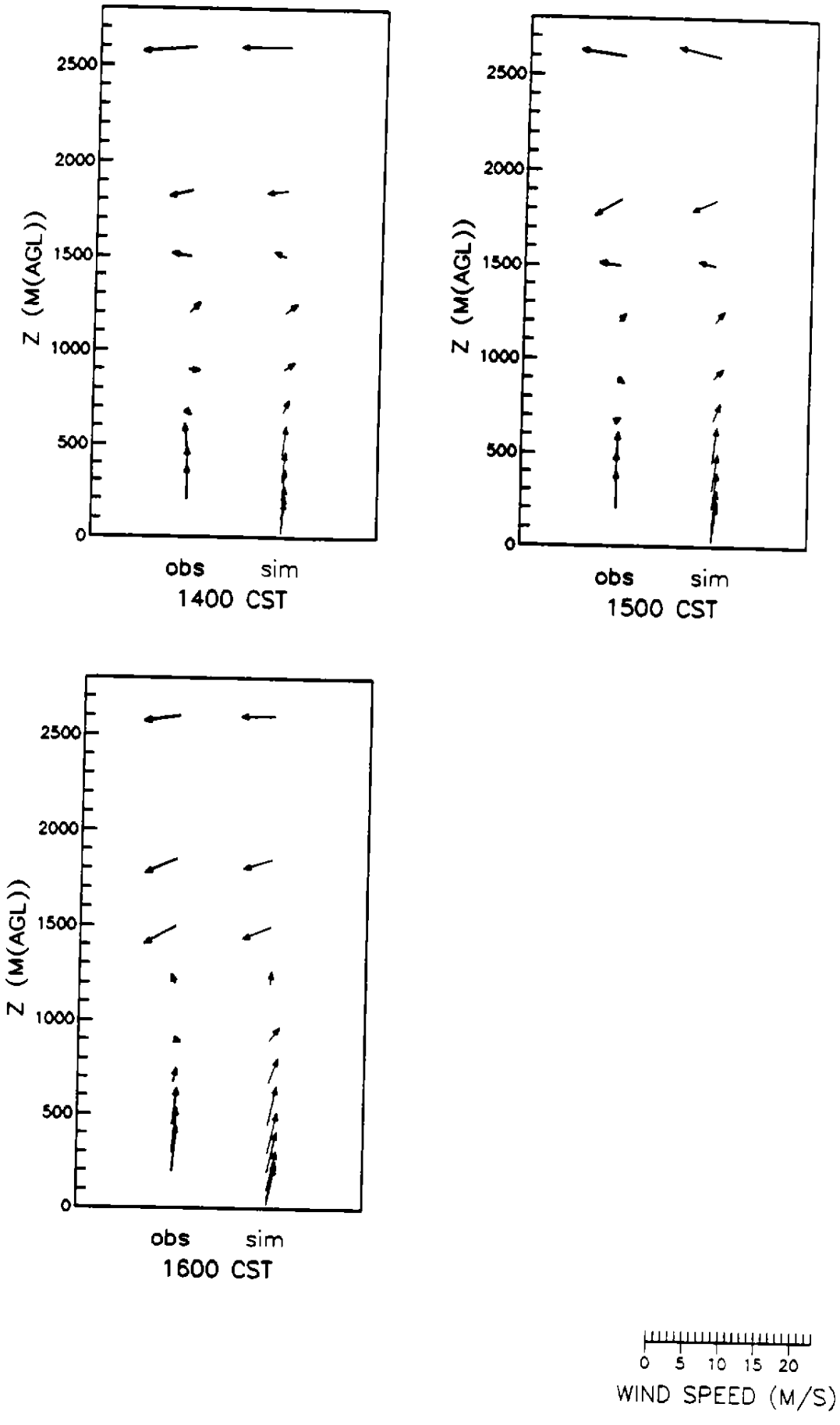

Figure 4-22b. Comparison of midday observed and simulated wind profiles for Galveston (GAL) on 18 August 1993.

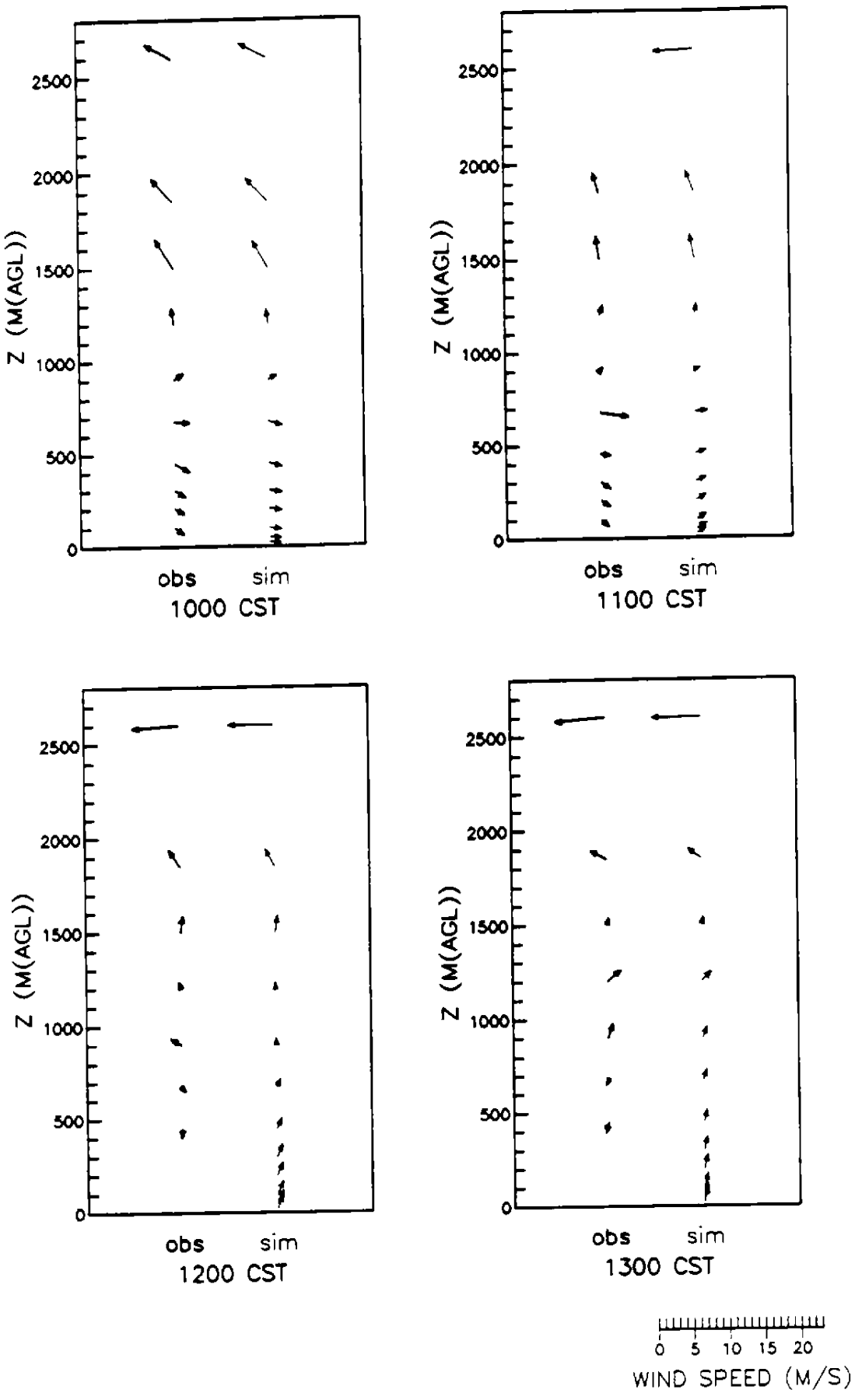

Figure 4-23a. Comparison of midday observed and simulated wind profiles for Houston (SEH) on 18 August 1993.

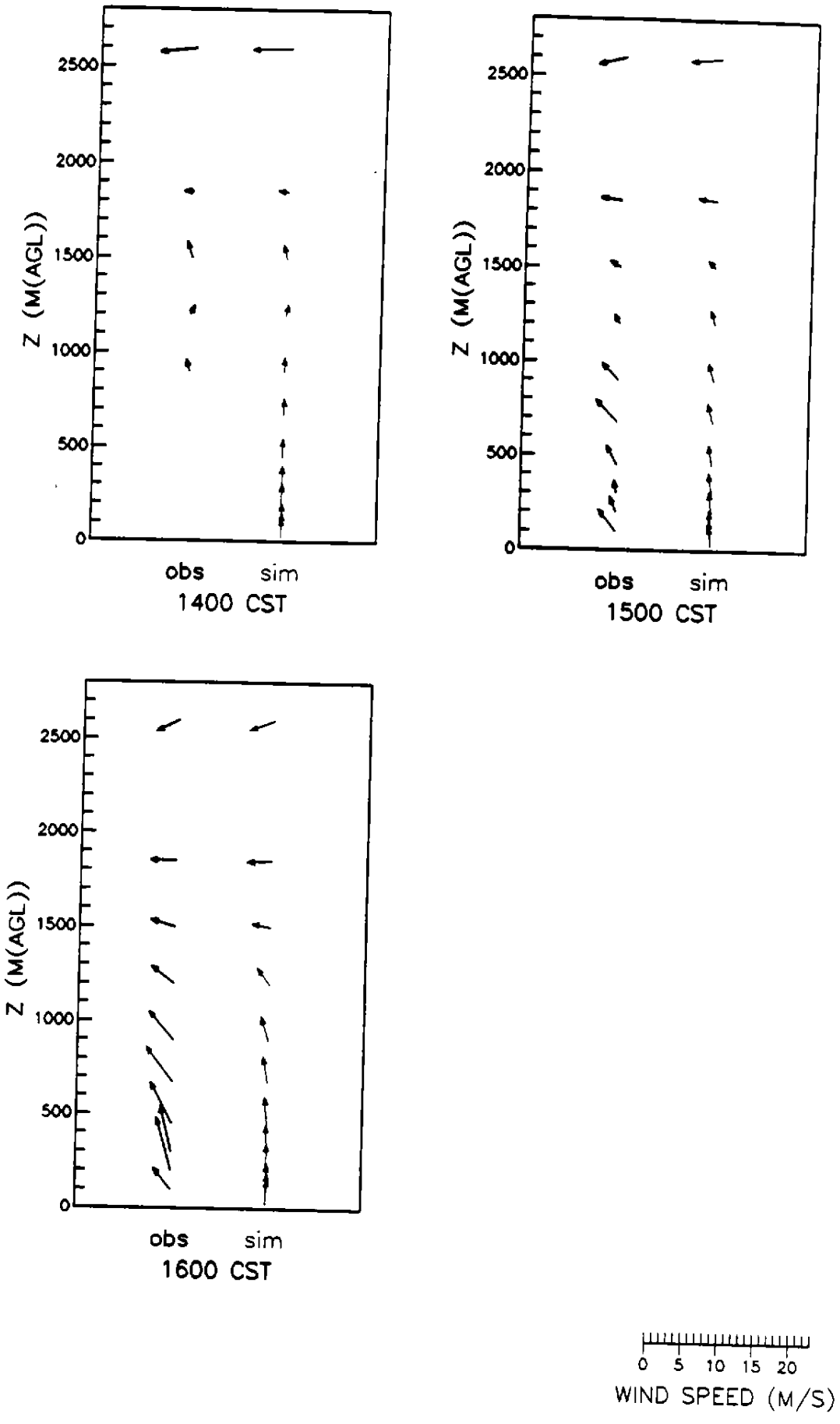

Figure 4-23b. Comparison of midday observed and simulated wind profiles for Houston (SEH) on 18 August 1993.

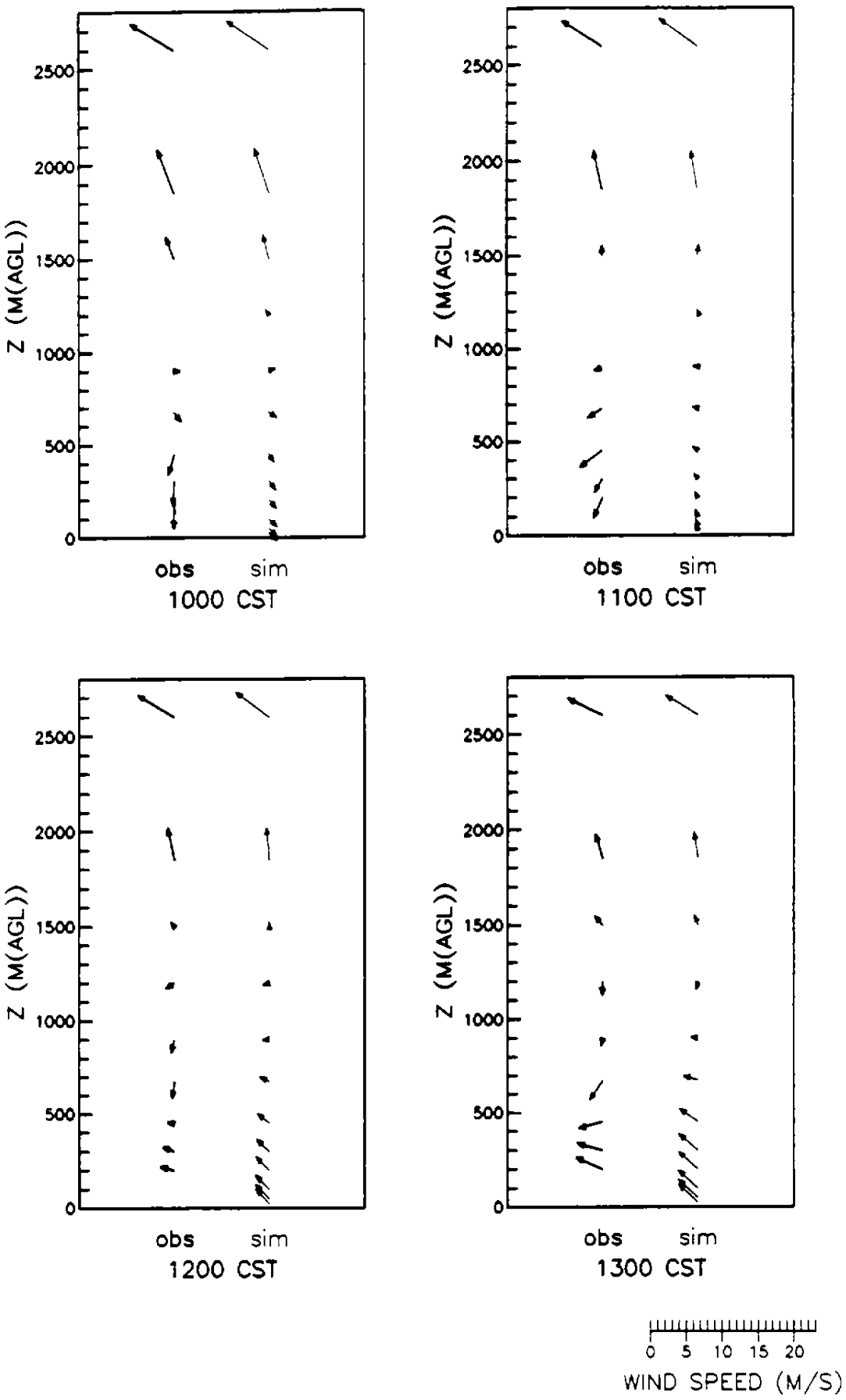

Figure 4-24a. Comparison of midday observed and simulated wind profiles for Galveston (GAL) on 19 August 1993.

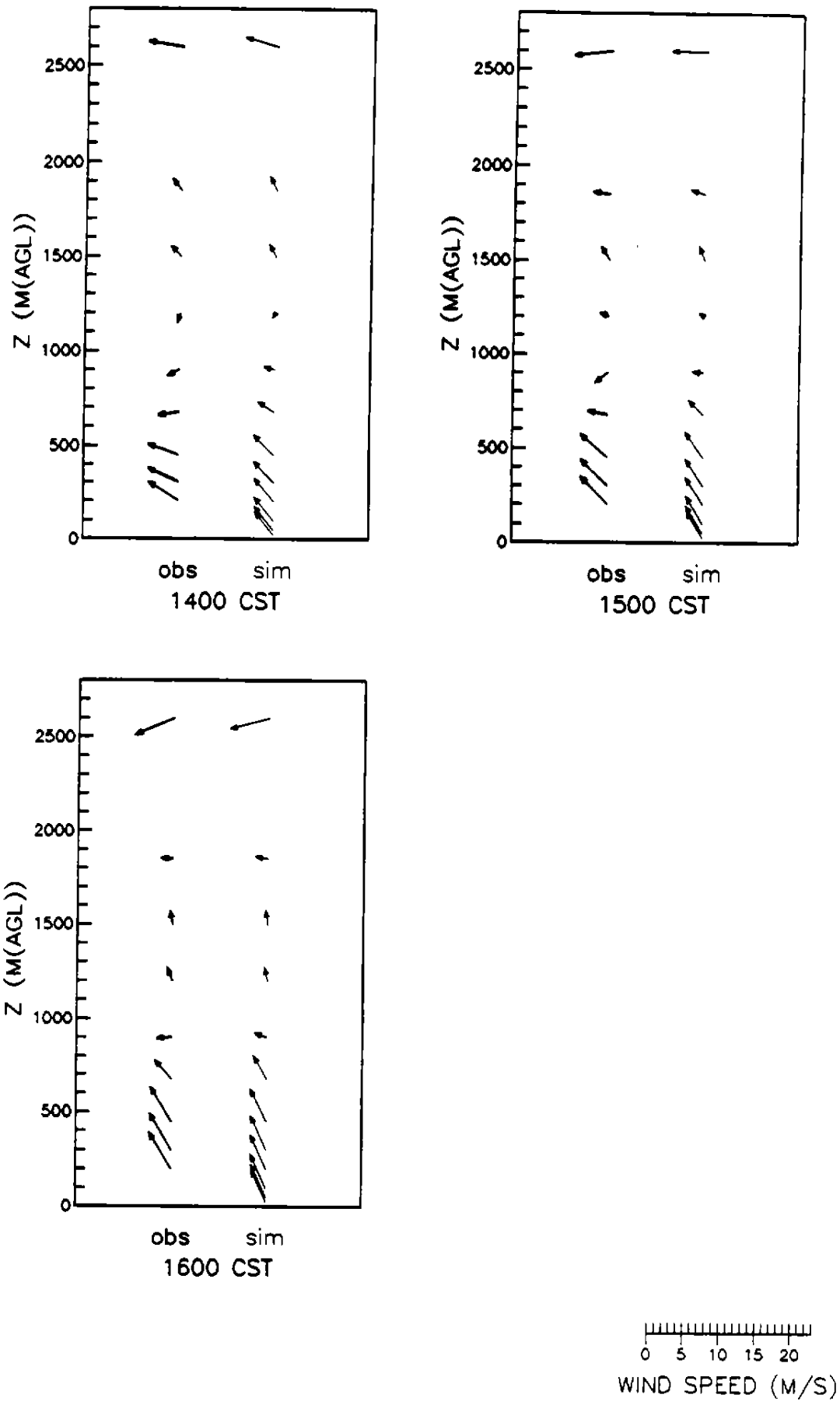

Figure 4-24b. Comparison of midday observed and simulated wind profiles for Galveston (GAL) on 19 August 1993.

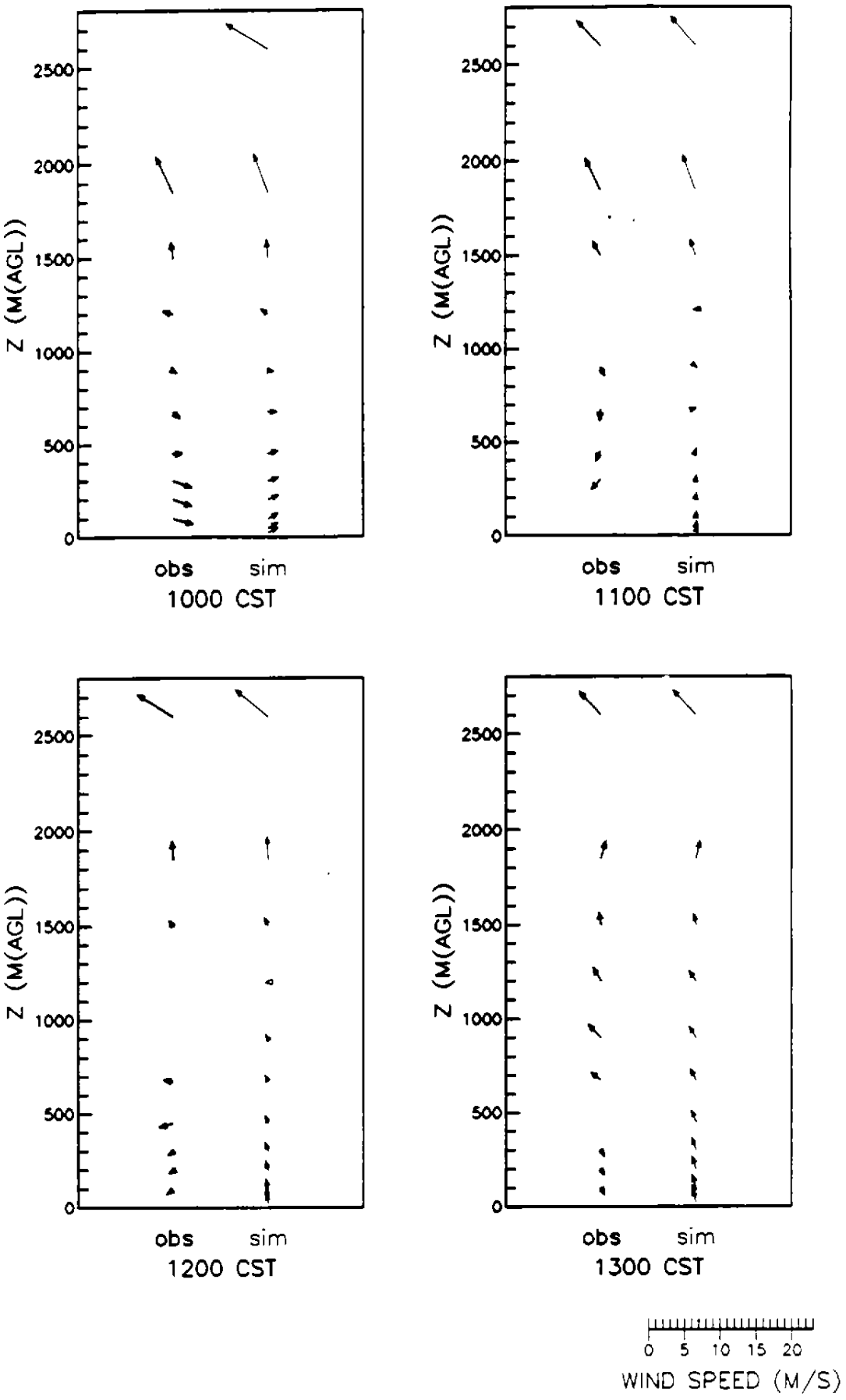

Figure 4-25a. Comparison of midday observed and simulated wind profiles for Houston (SEH) on 19 August 1993.

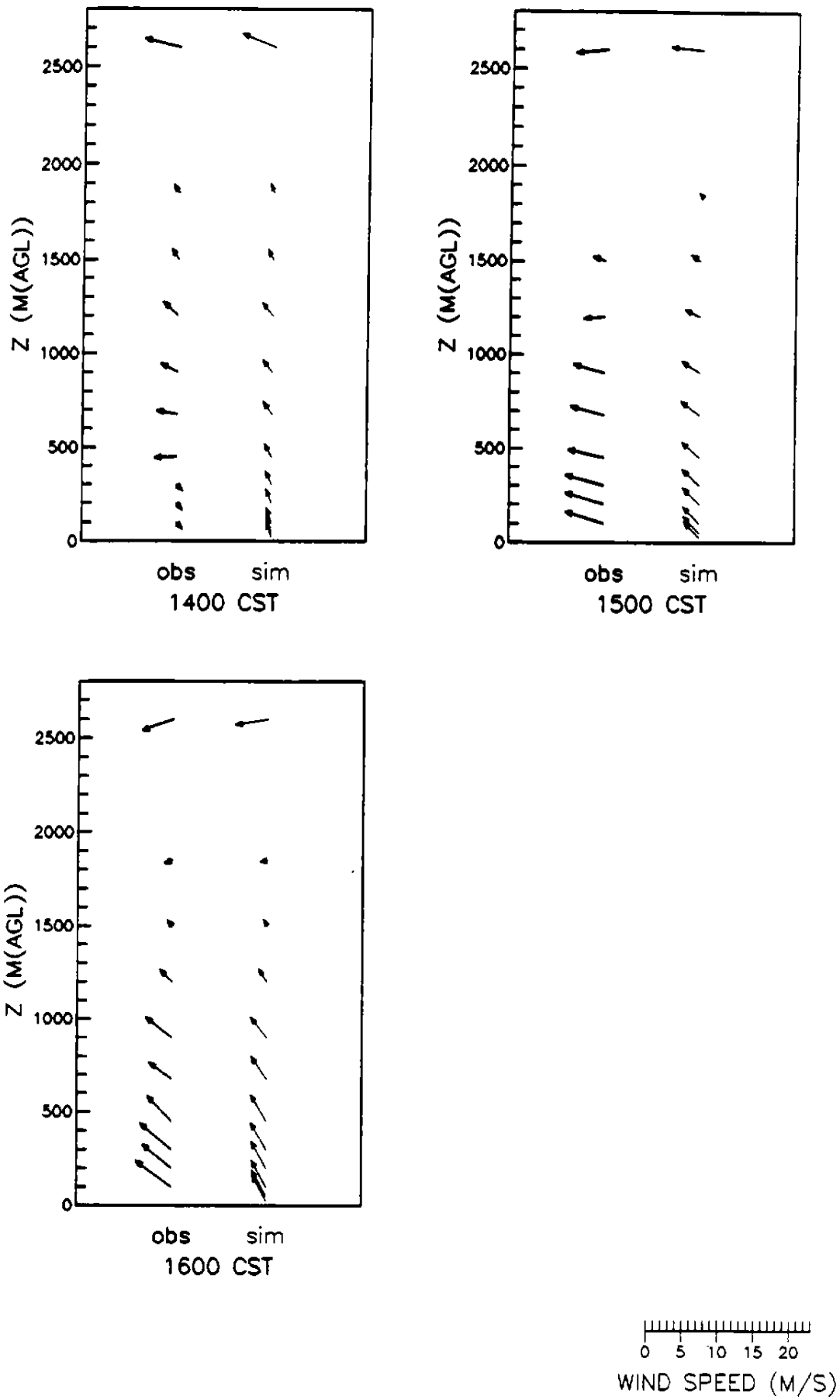

Figure 4-25b. Comparison of midday observed and simulated wind profiles for Houston (SEH) on 19 August 1993.

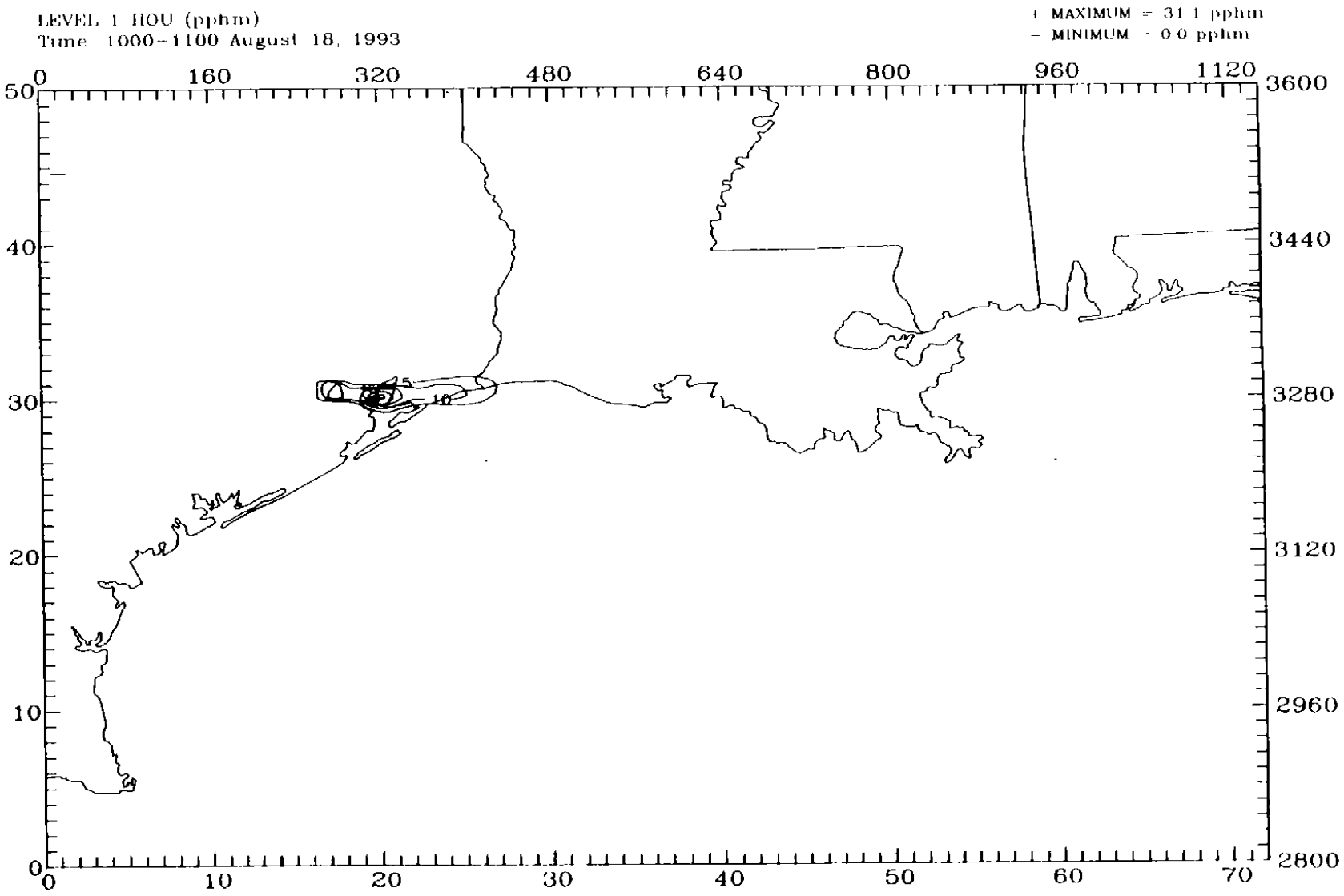

Figure 4-26a. Layer 1 concentrations of the low-level emission tracer HOU on 18 August 1993 at 1000 CST.

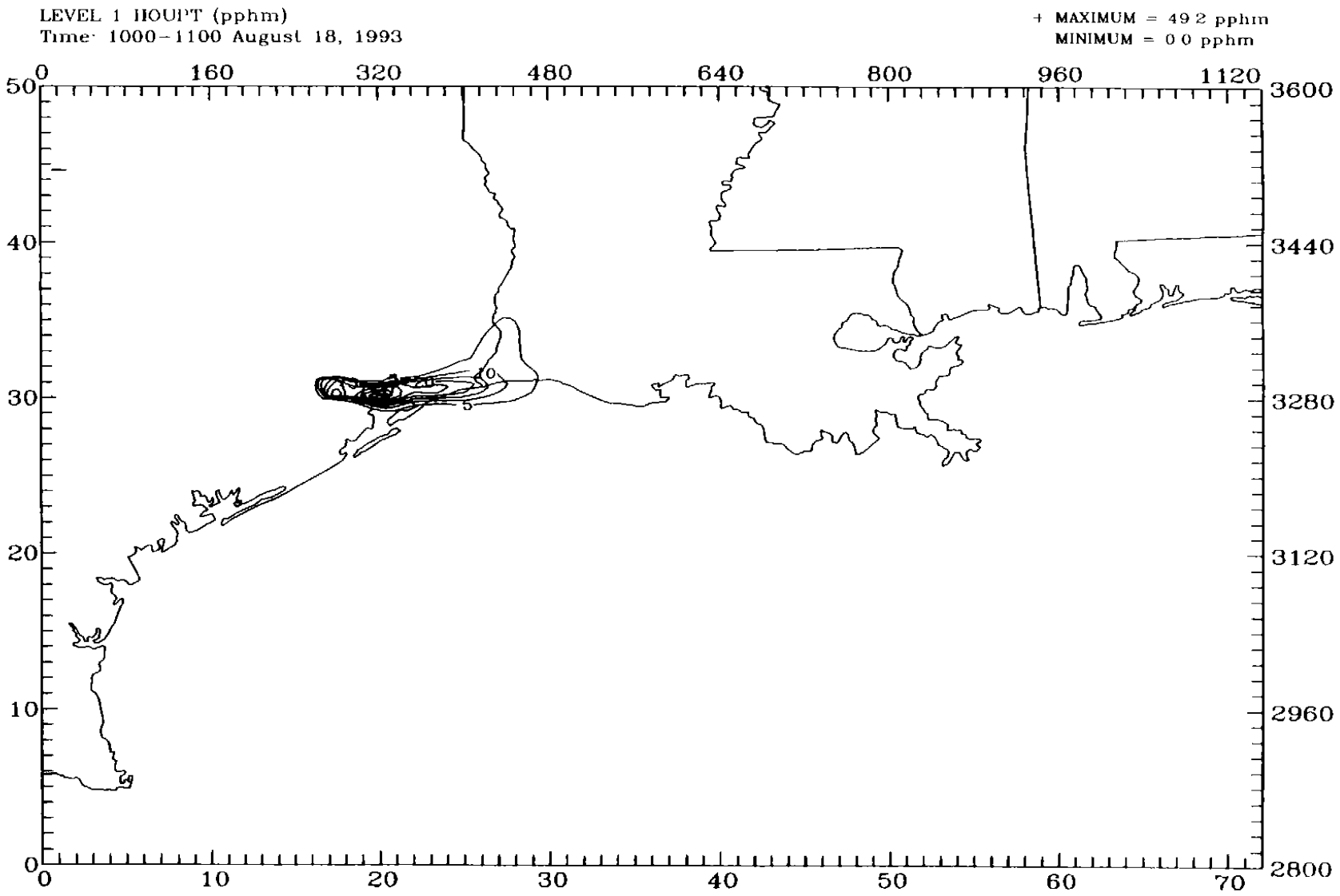

Figure 4-26b. Layer 1 concentrations of the elevated emission tracer HOUPT on 18 August 1993 at 1000 CST.

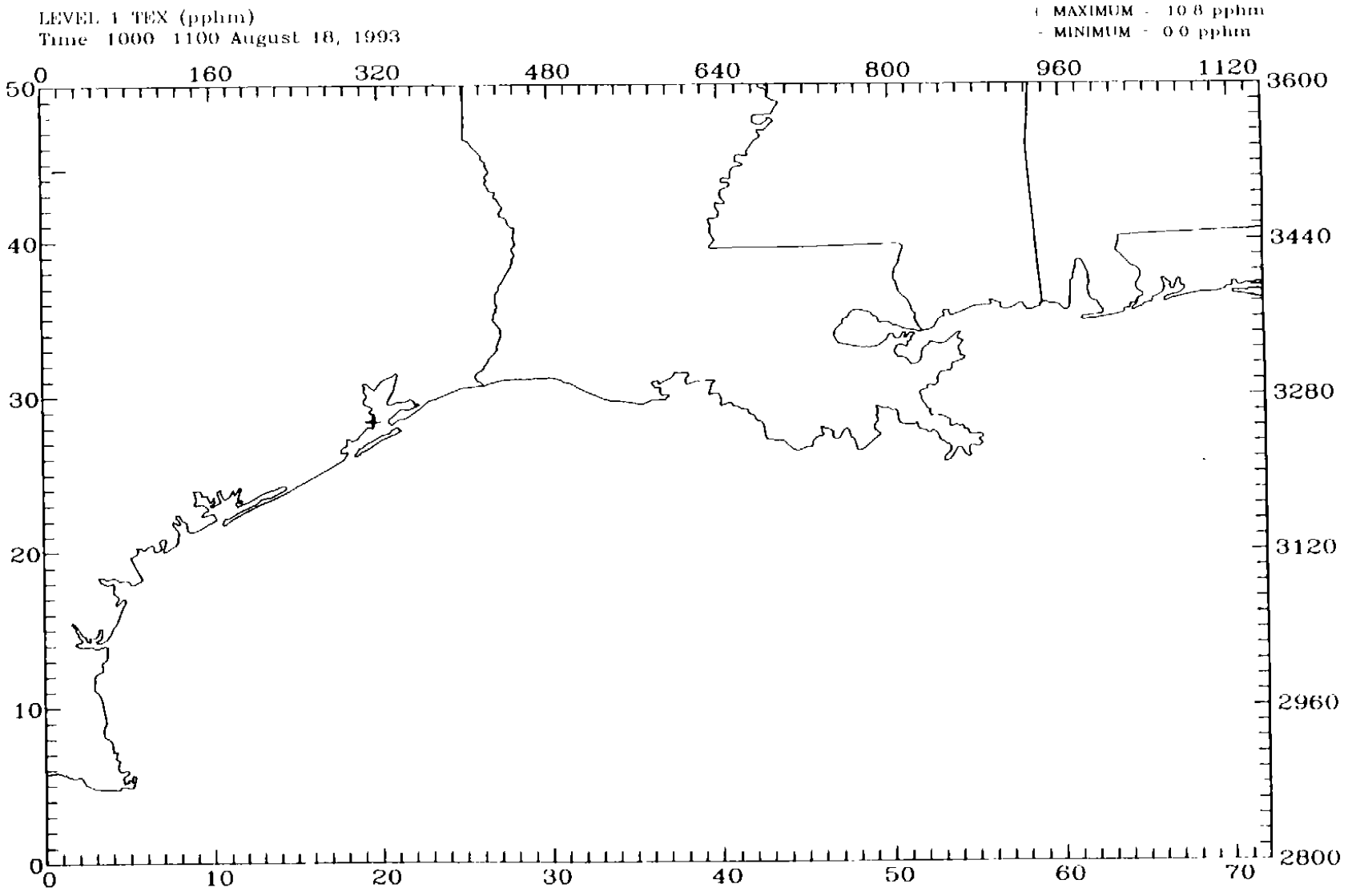

Figure 4-27a. Layer 1 concentrations of the low-level emission tracer TEX on 18 August 1993 at 1000 CST.

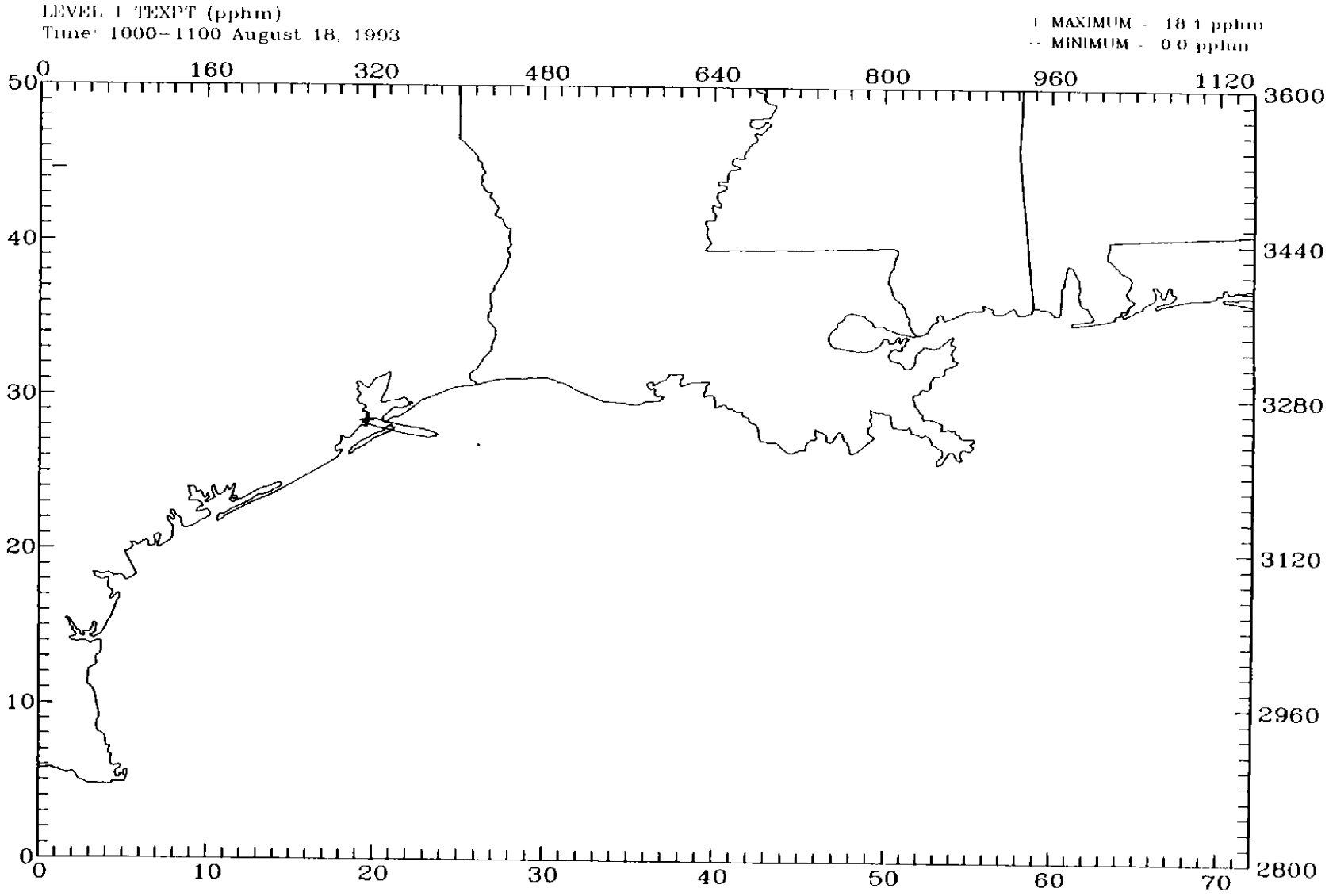

Figure 4-27b. Layer 1 concentrations of the elevated emission tracer TEXPT on 18 August 1993 at 1000 CST.

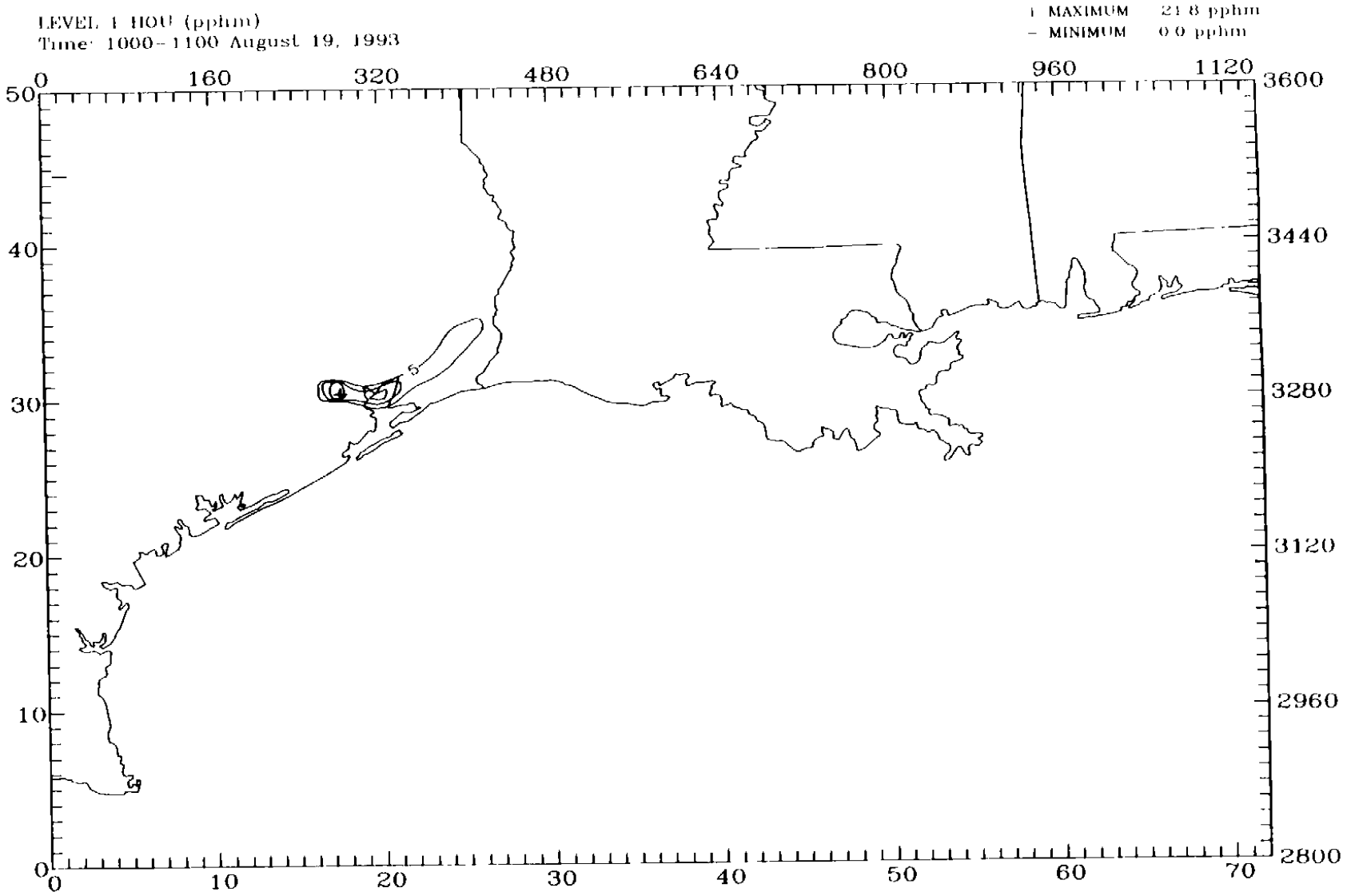

Figure 4-28a. Layer 1 concentrations of the low-level emission tracer HOU on 19 August 1993 at 1000 CST

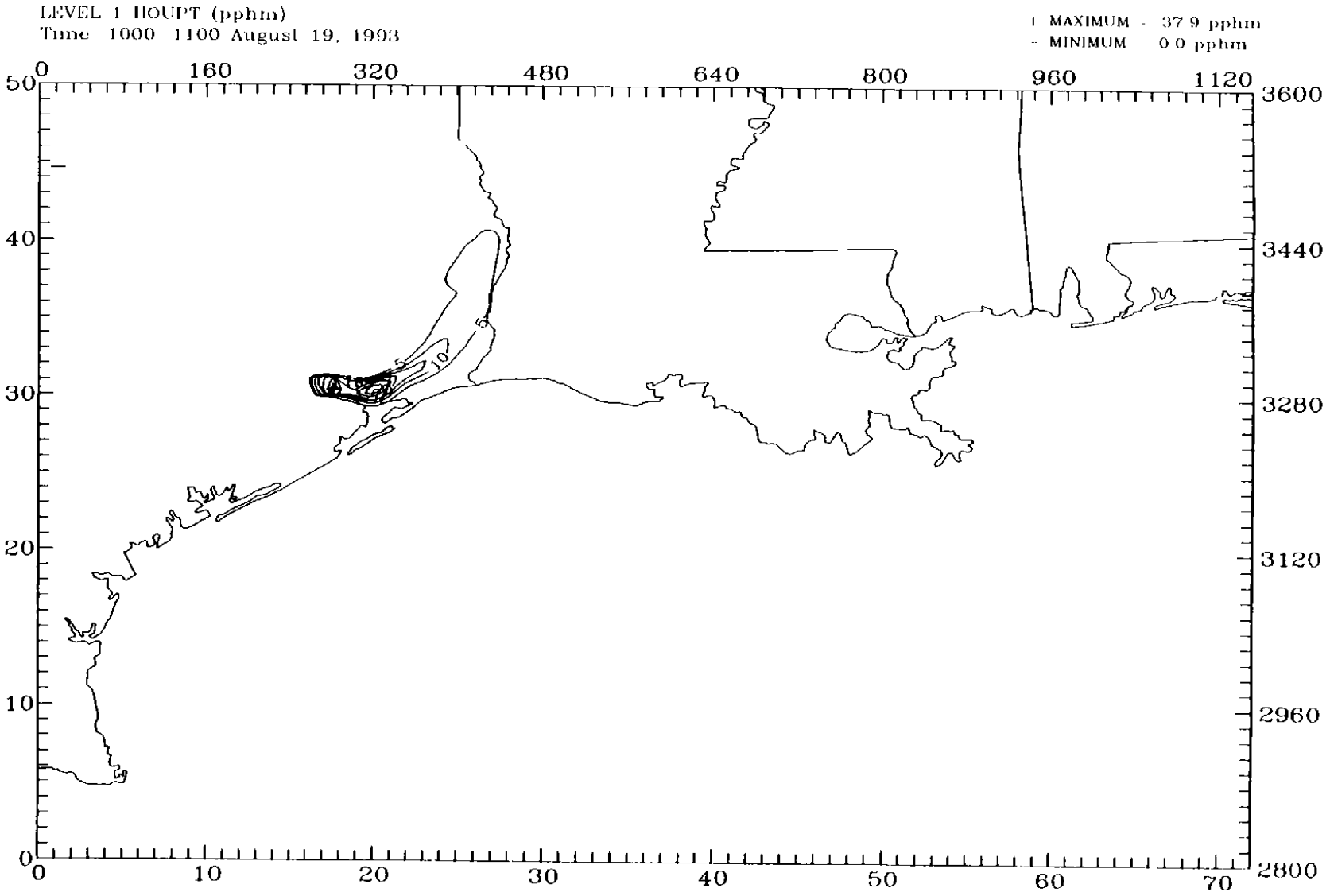

Figure 4-28b. Layer 1 concentrations of the elevated emission tracer HOUPT on 19 August 1993 at 1000 CST

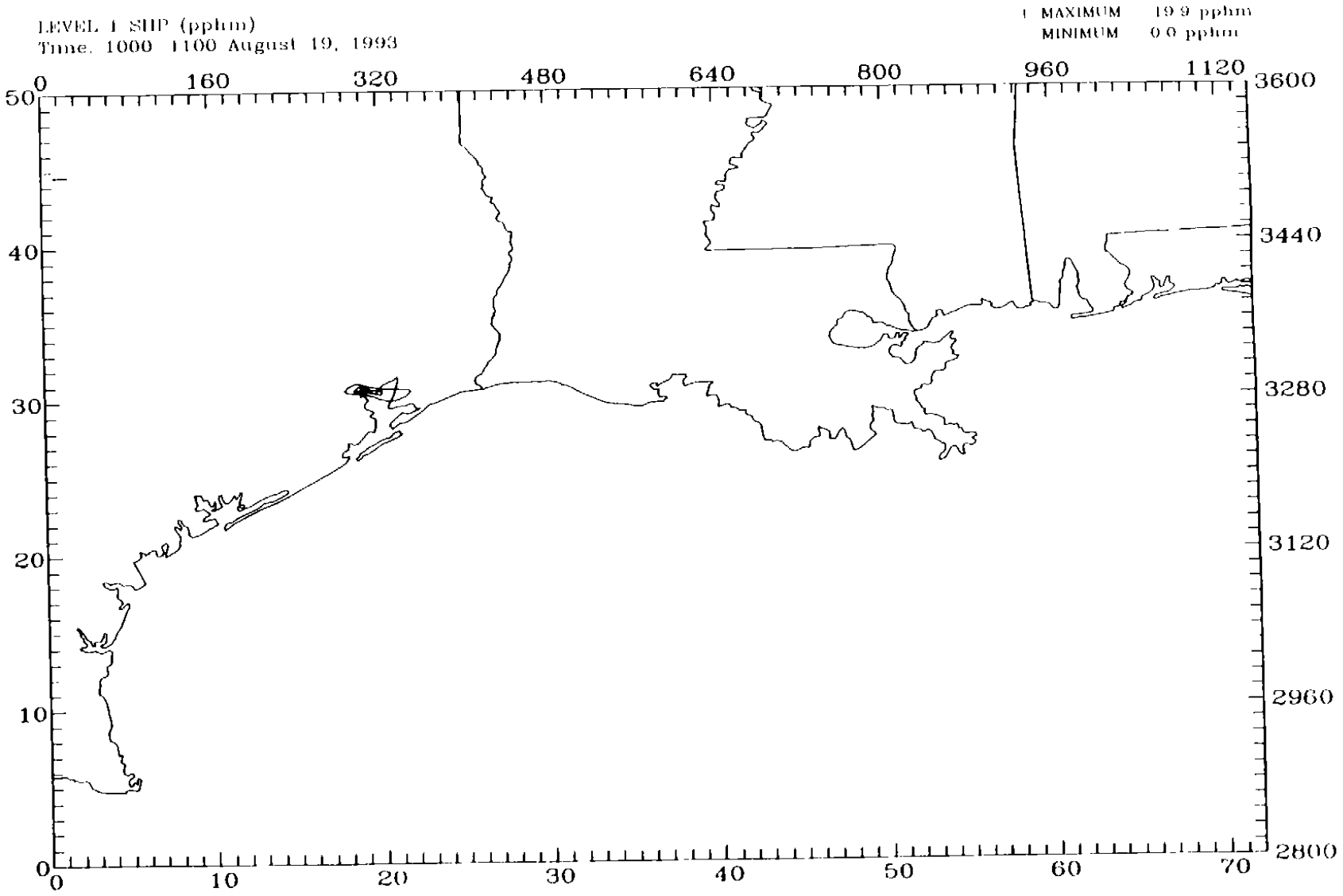

Figure 4-29a. Layer 1 concentrations of the low-level emission tracer SHP on 19 August 1993 at 1000 CST

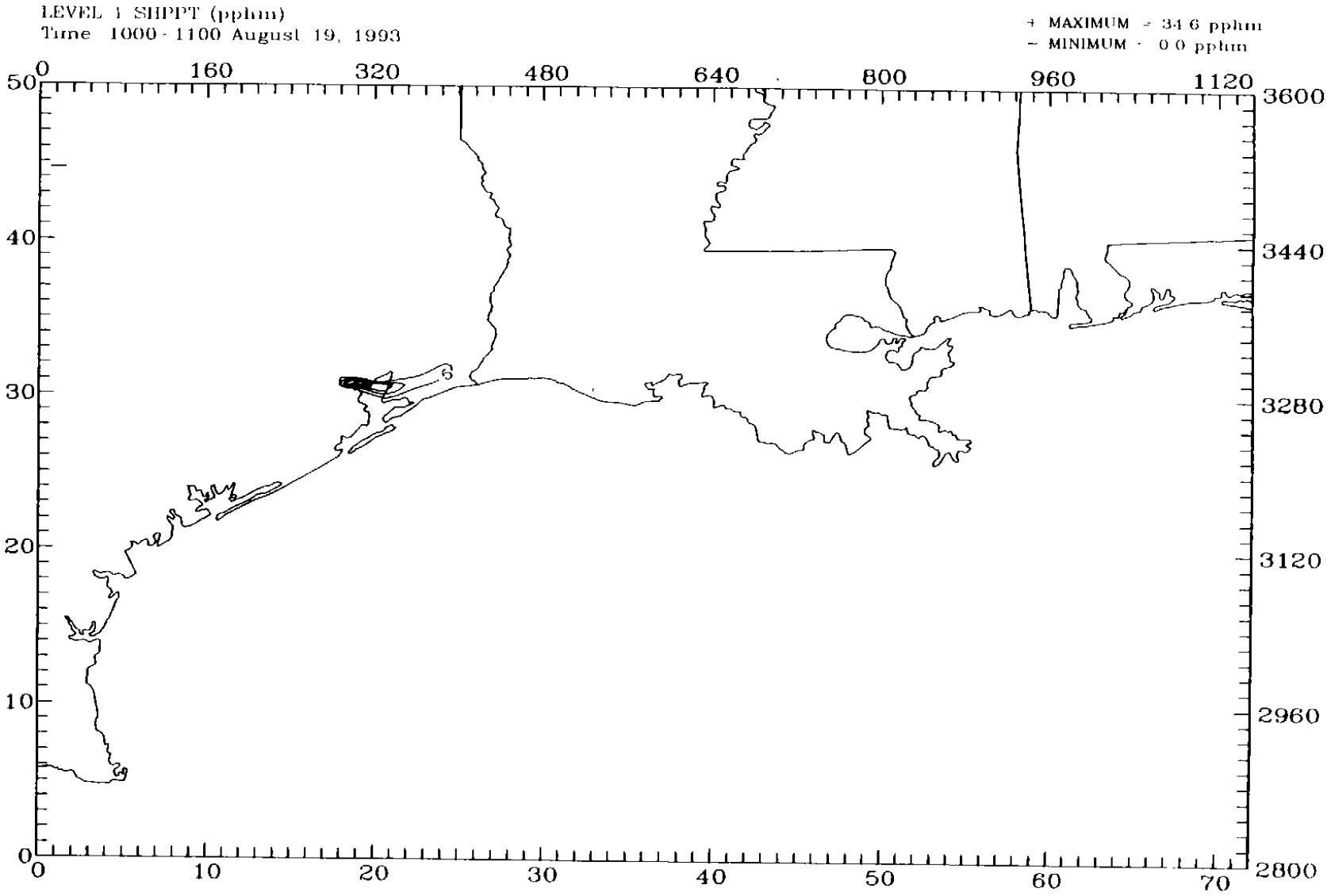

Figure 4-29b. Layer 1 concentrations of the elevated emission tracer SHPPT on 19 August 1993 at 1000 CST.

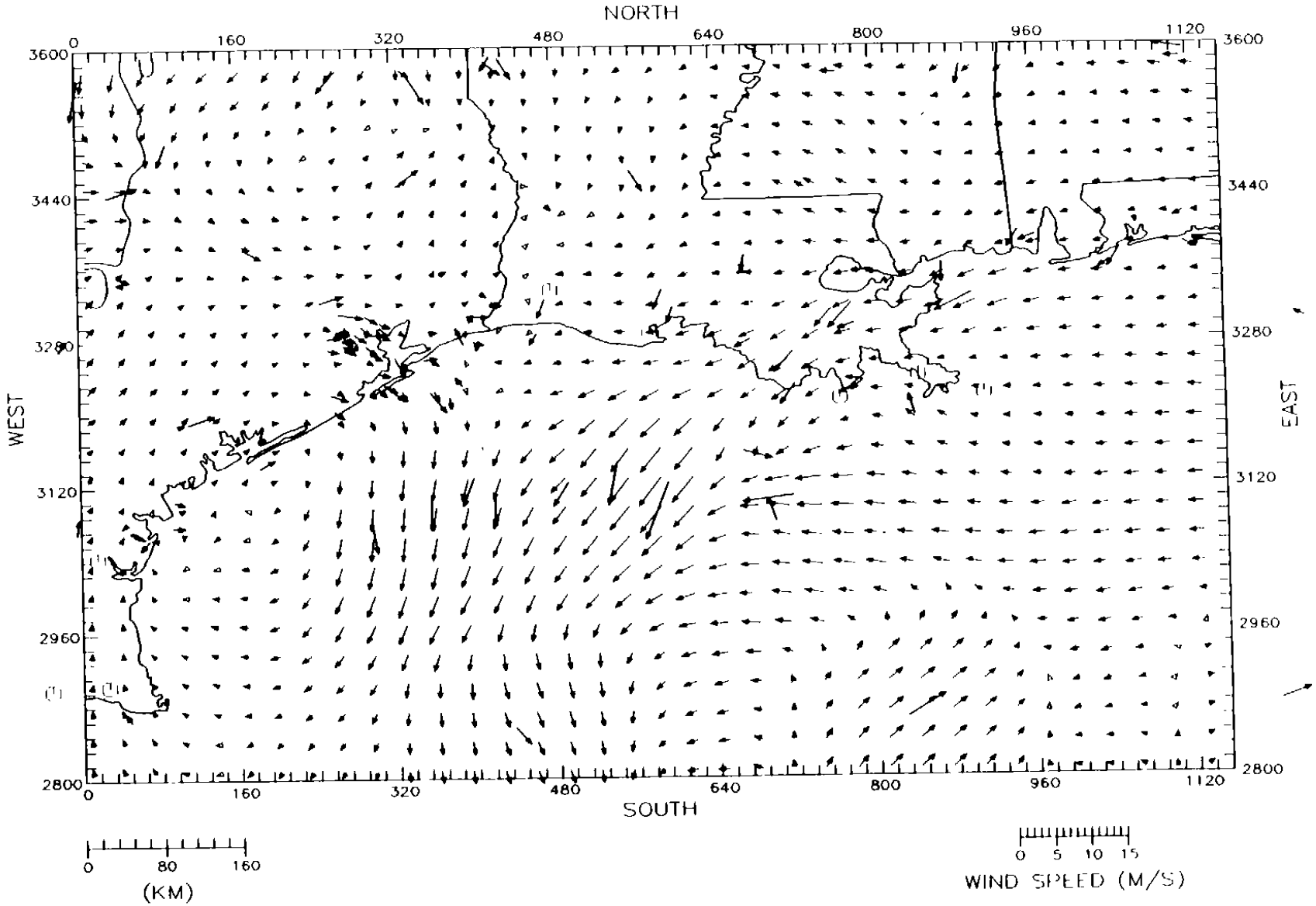

Figure 4-30a. SAIMM wind fields for the coarse-grid domain on 8 September 1993 at 1000 CST. Level 1 (25 m).

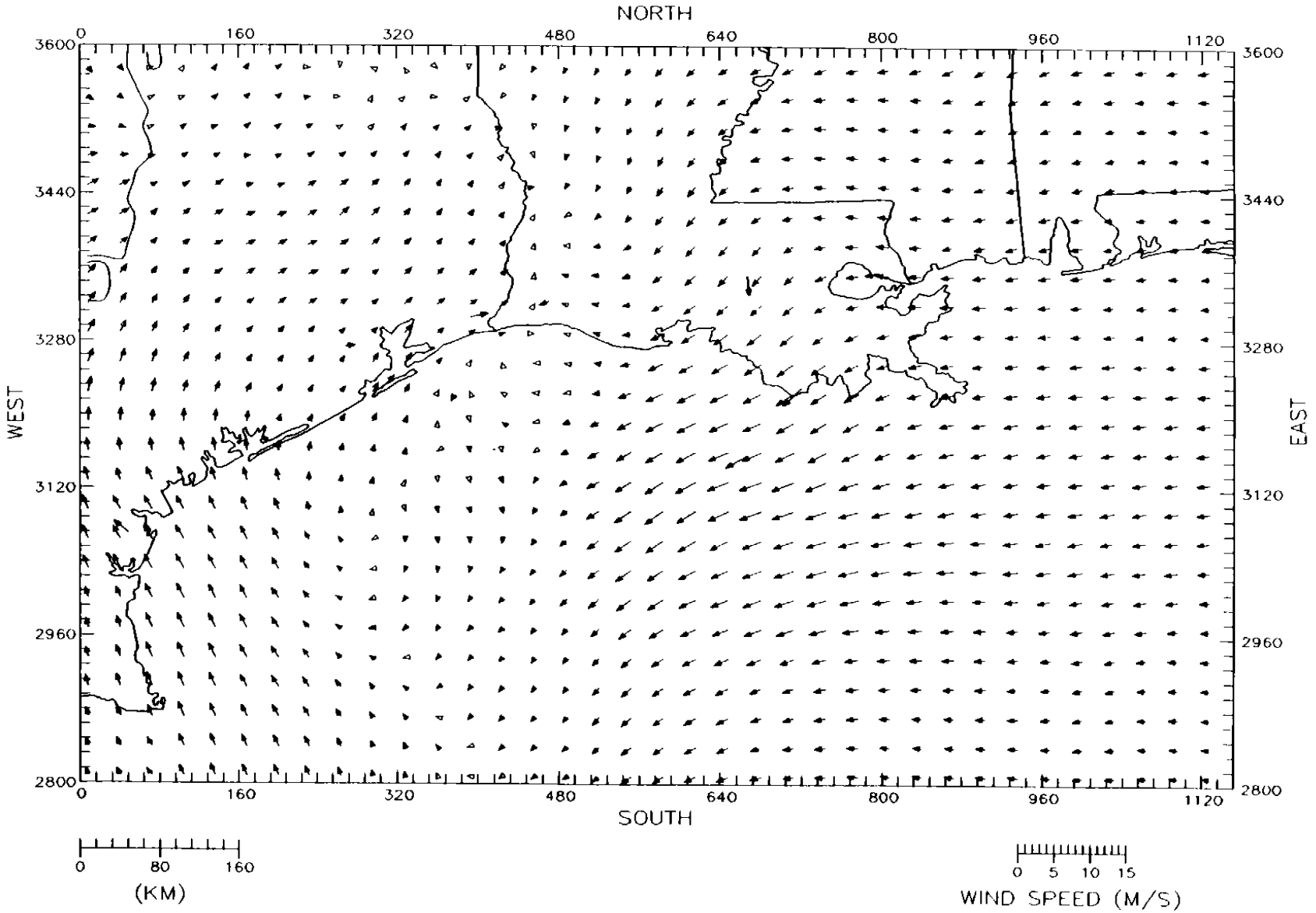

Figure 4-30b. SAIMM wind fields for the coarse-grid domain on 8 September 1993 at 1000 CST. Level 7 (675 m).

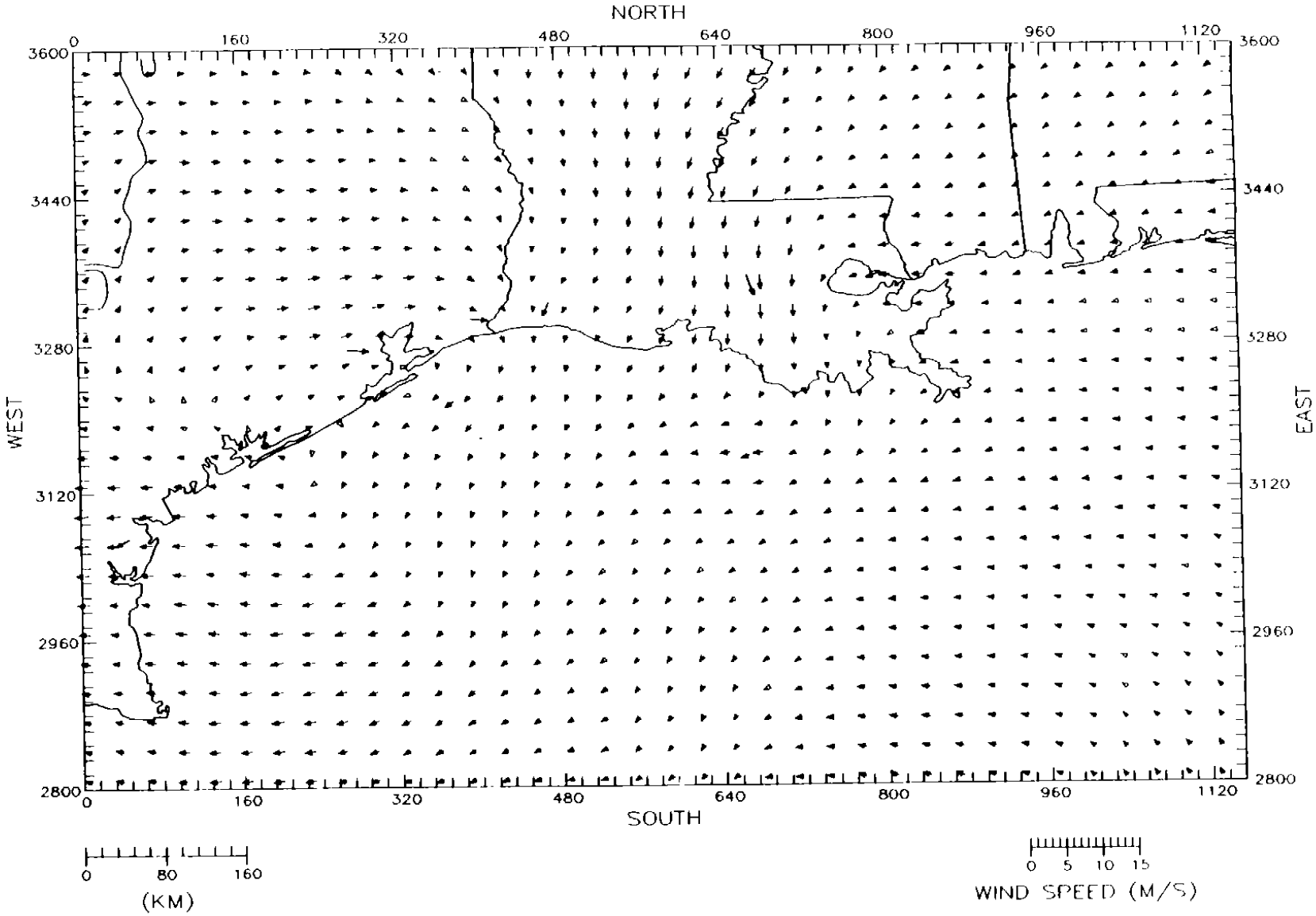

Figure 4-30c. SAIMM wind fields for the coarse-grid domain on 8 September 1993 at 1000 CST Level 9 (1200 m).

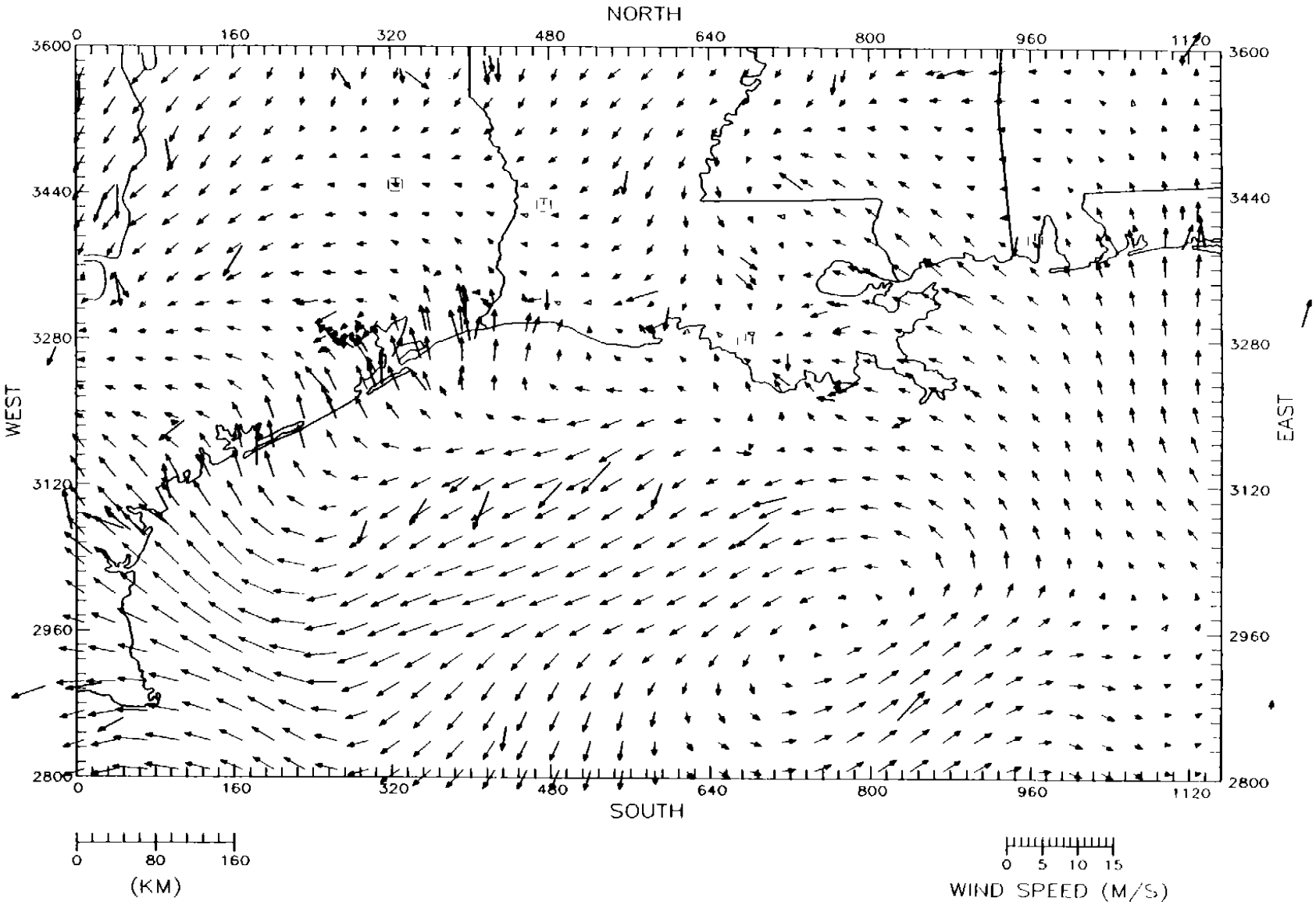

Figure 4-31a. SAIMM wind fields for the coarse-grid domain on 8 September 1993 at 1600 CST. Level 1 (25 m).

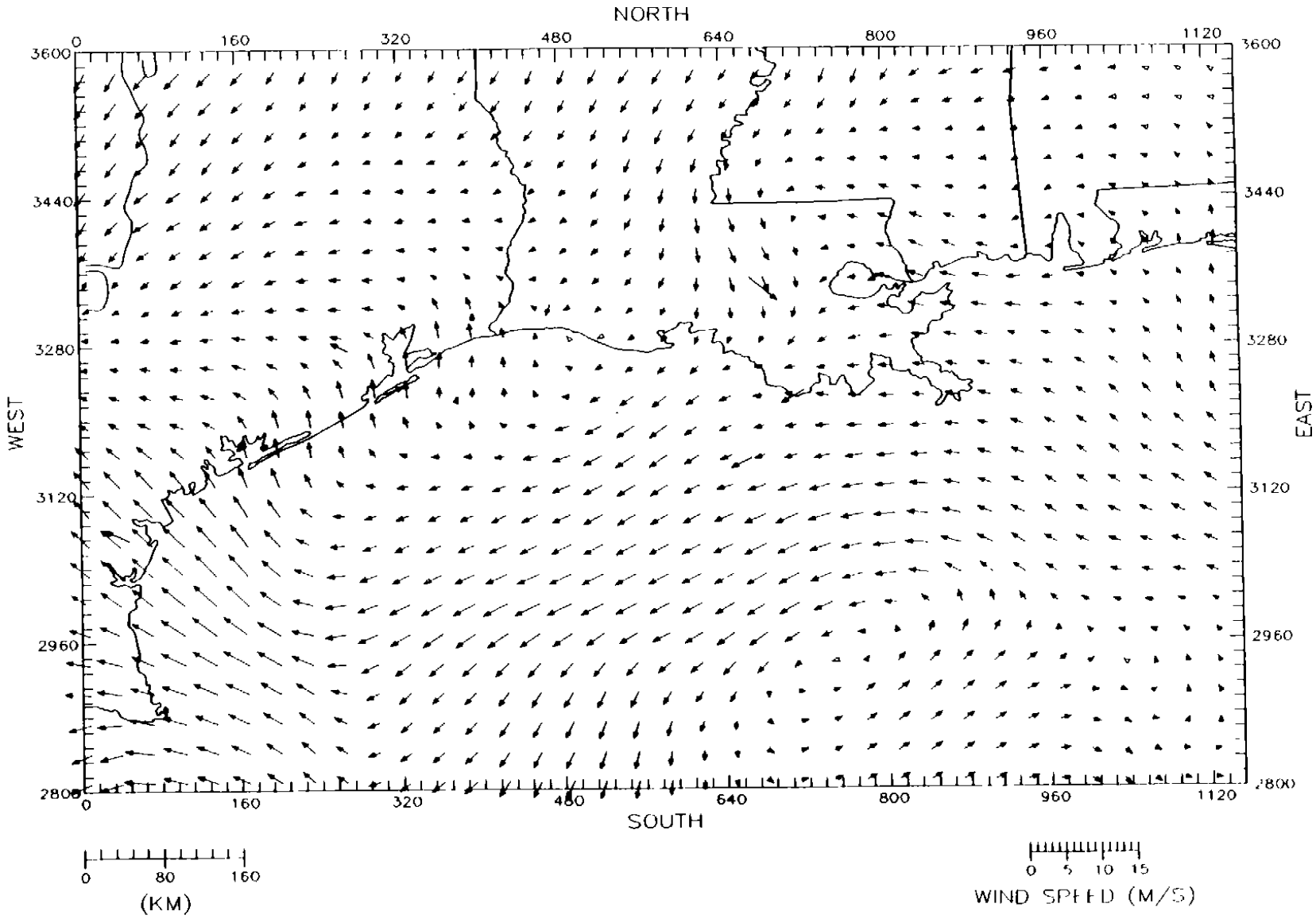

Figure 4-31b. SAIMM wind fields for the coarse-grid domain on 8 September 1993 at 1600 CST Level 7 (675 m)

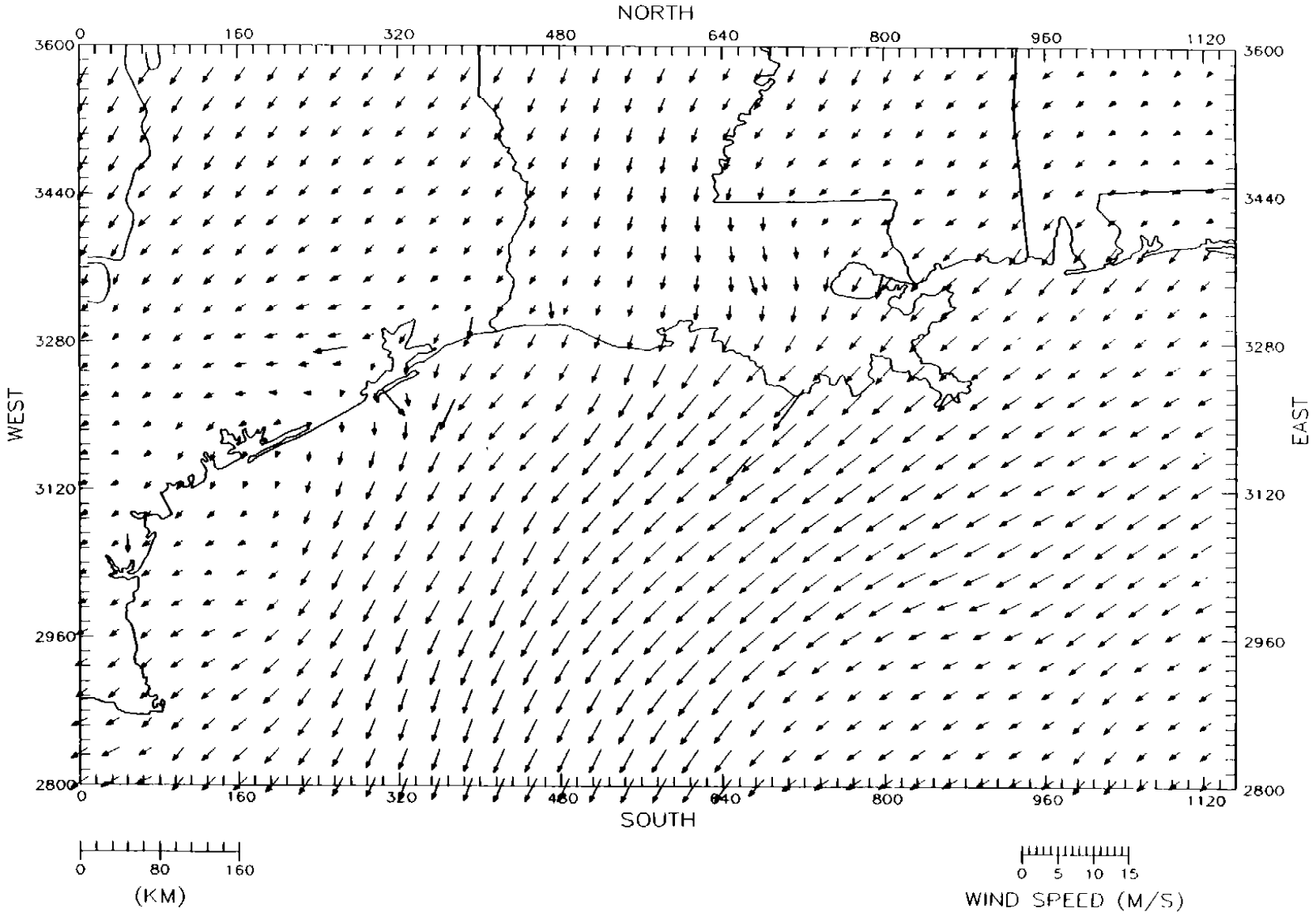

Figure 4-31c. SAIMM wind fields for the coarse-grid domain on 8 September 1993 at 1600 CST Level 9 (1200 m)

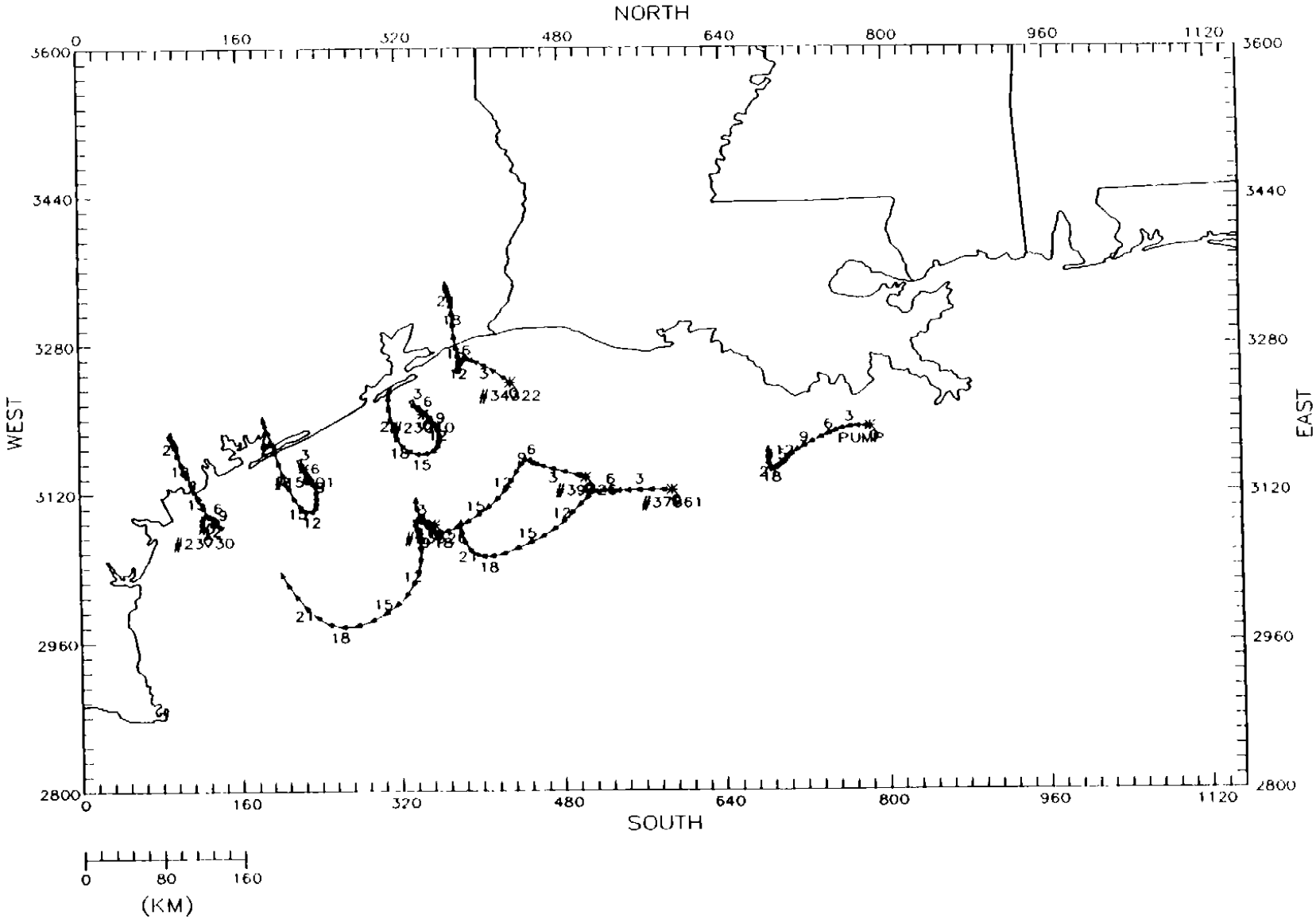

Figure 4-32a. Twenty-four-hour forward particle paths for the surface layer initiated at 0000 CST on 8 September 1993.

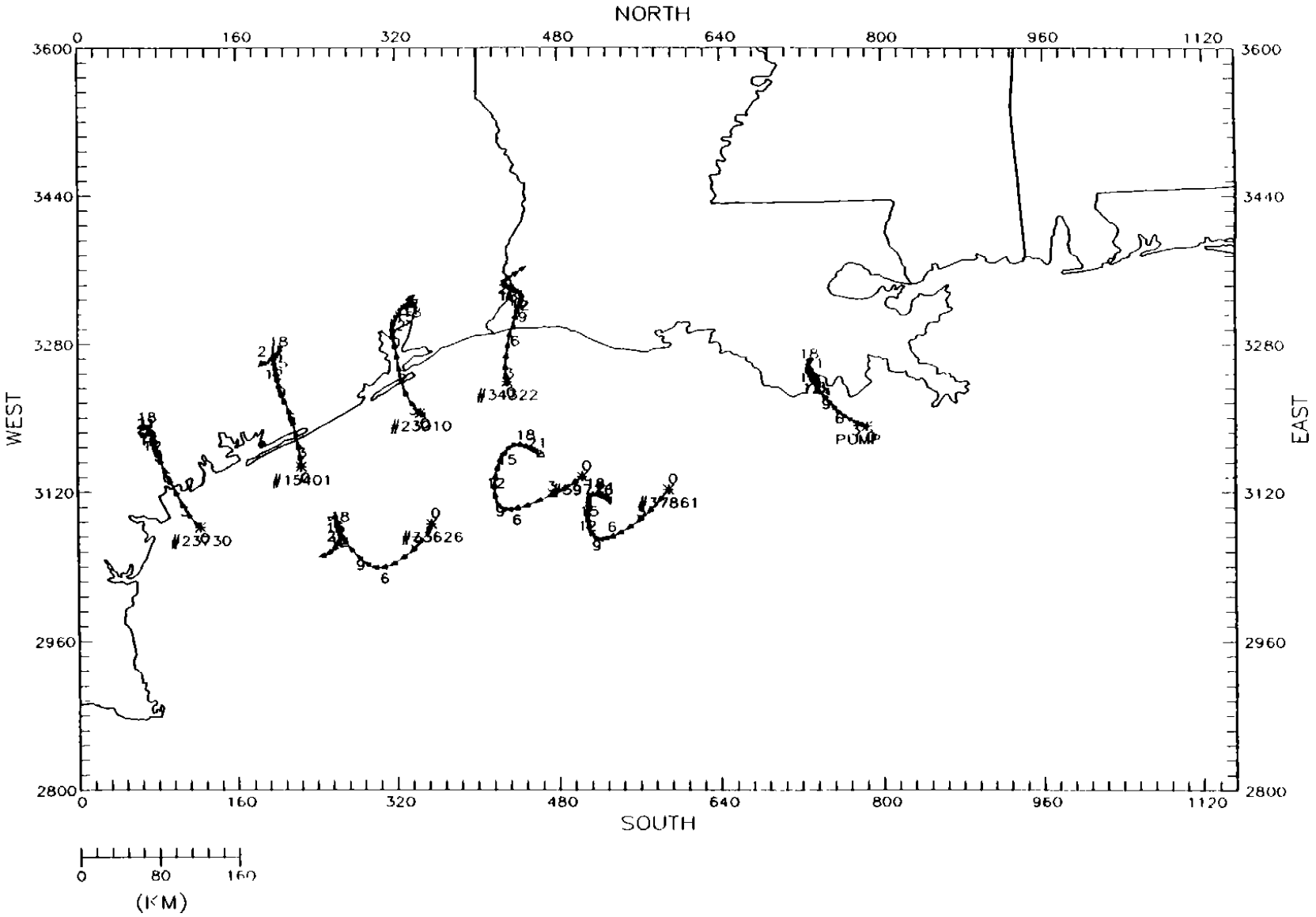

Figure 4-32b. Twenty-four-hour forward particle paths for the surface layer initiated at 1200 CST on 8 September 1993.

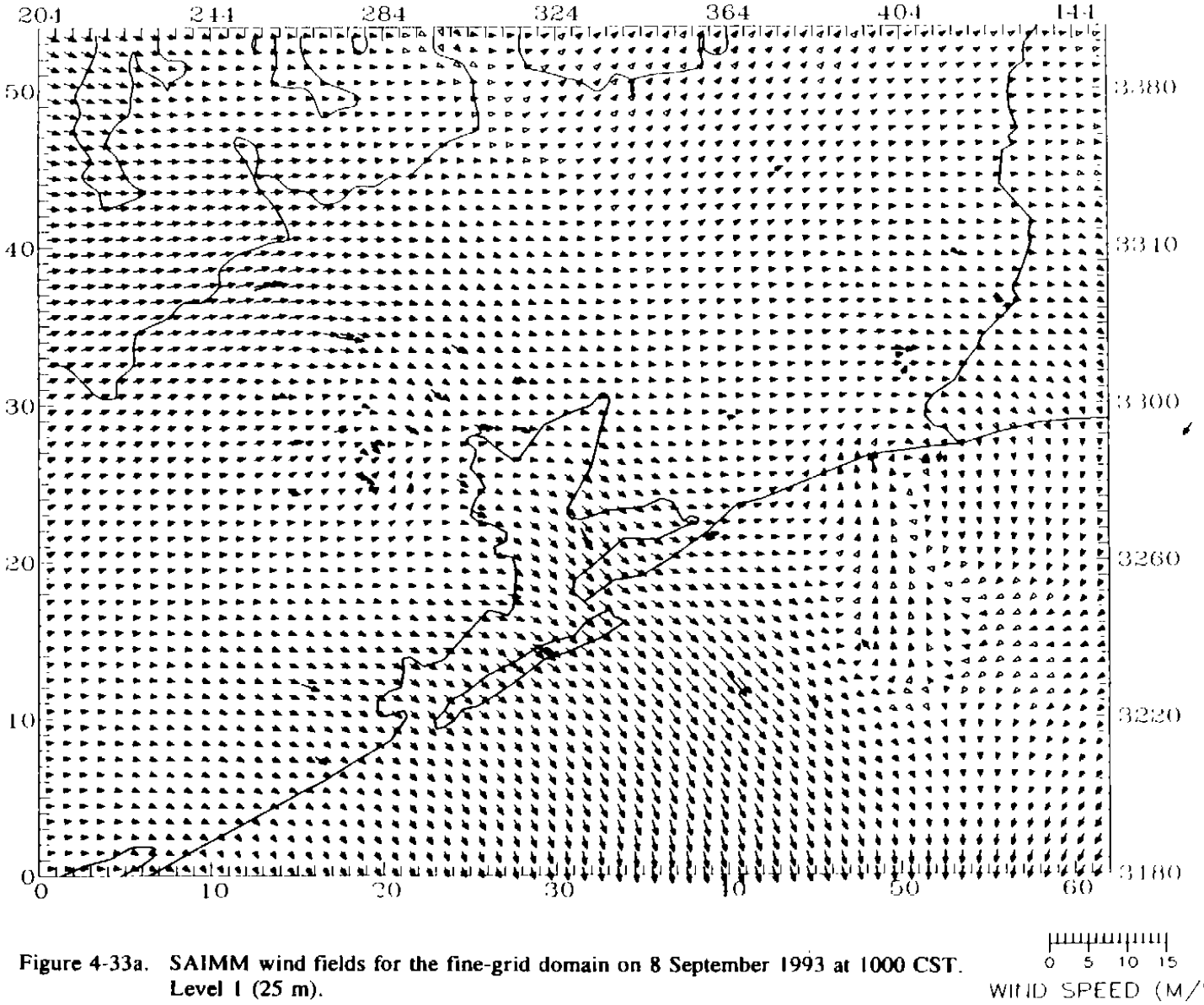

Figure 4-33a. SAIMM wind fields for the fine-grid domain on 8 September 1993 at 1000 CST. Level 1 (25 m).

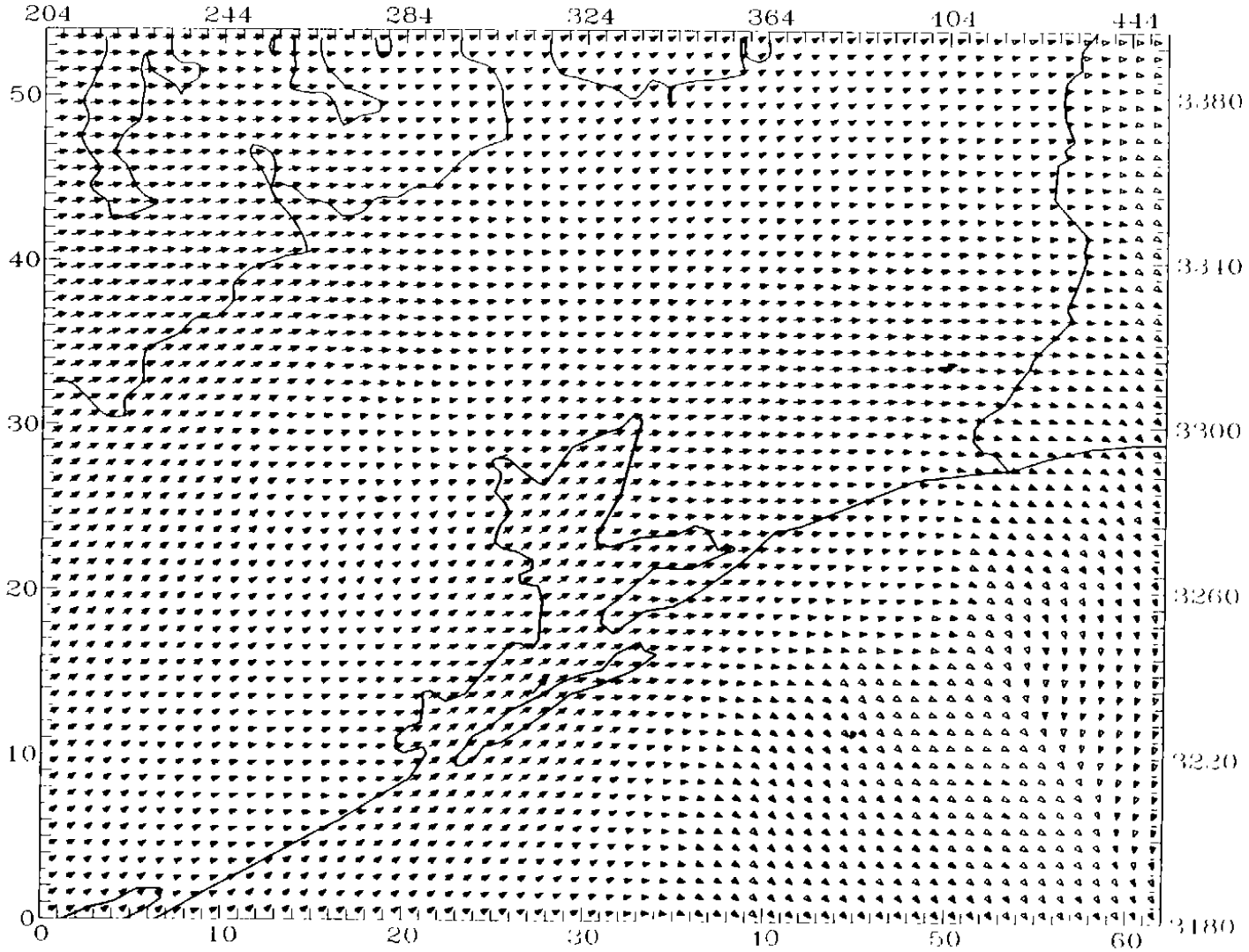

Figure 4-33b. SAIMM wind fields for the fine-grid domain on 8 September 1993 at 1000 CST. Level 7 (675 m).

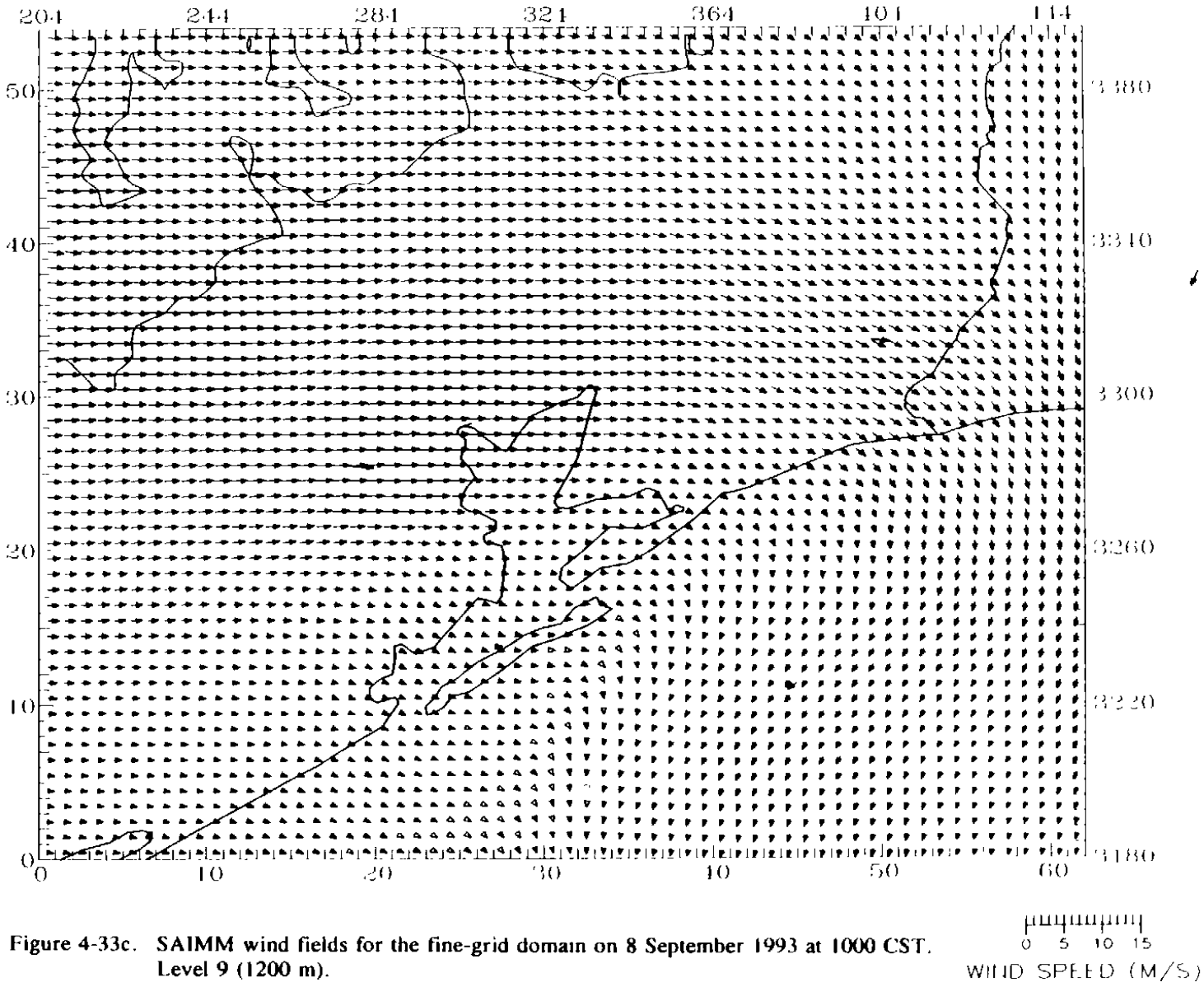

Figure 4-33c. SAIMM wind fields for the fine-grid domain on 8 September 1993 at 1000 CST. Level 9 (1200 m).

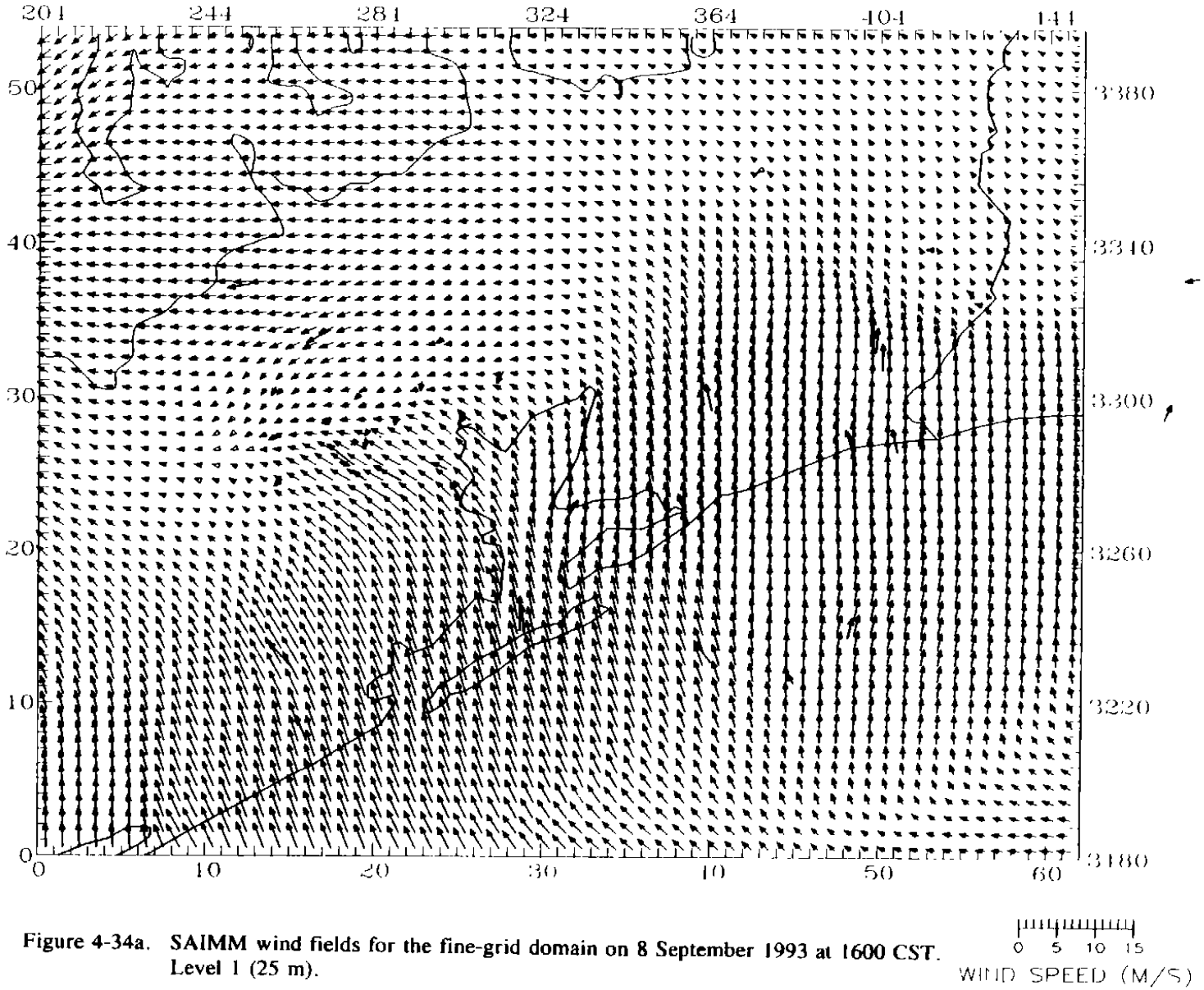

Figure 4-34a. SAIMM wind fields for the fine-grid domain on 8 September 1993 at 1600 CST. Level 1 (25 m).

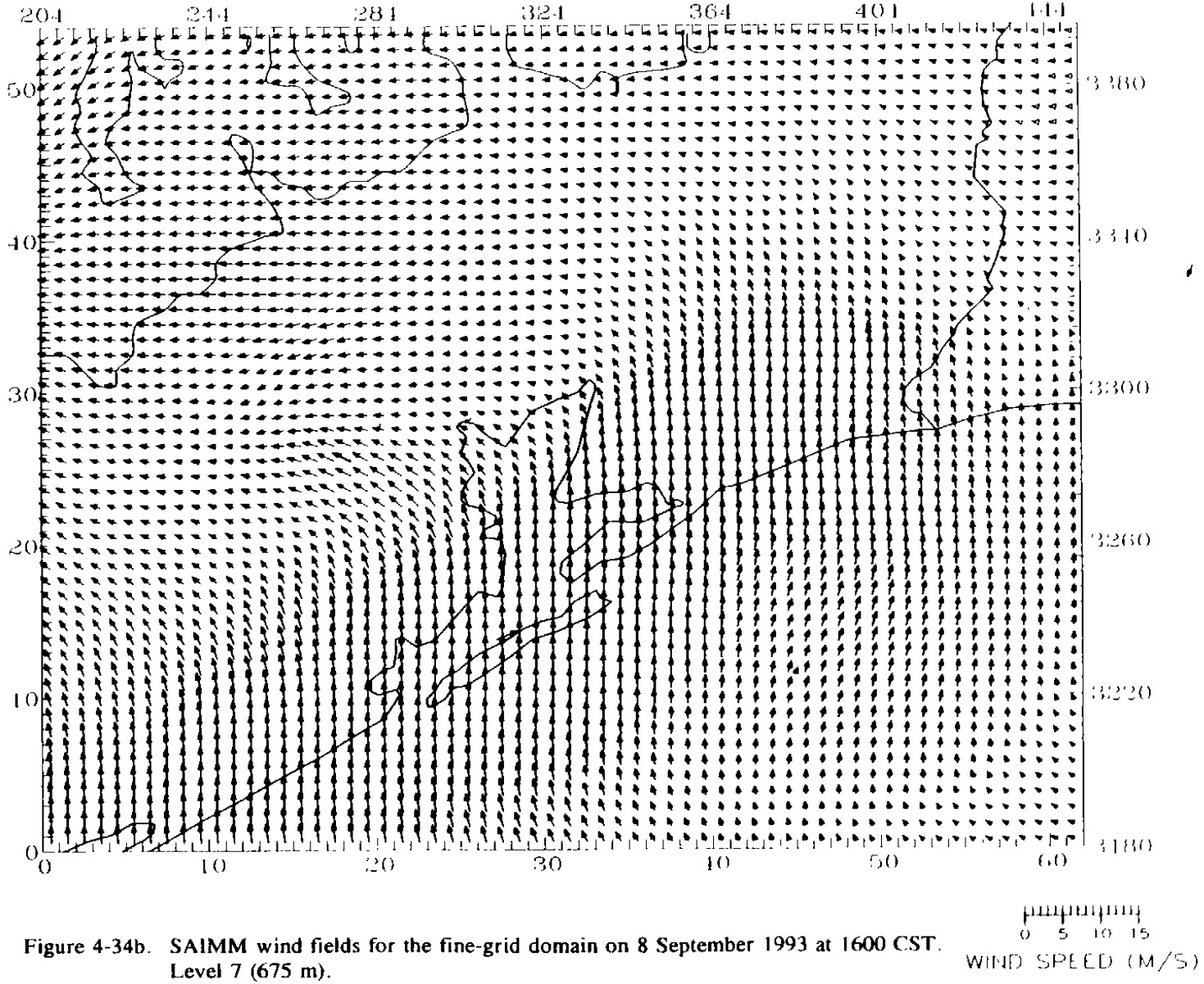

Figure 4-34b. SAIMM wind fields for the fine-grid domain on 8 September 1993 at 1600 CST. Level 7 (675 m).

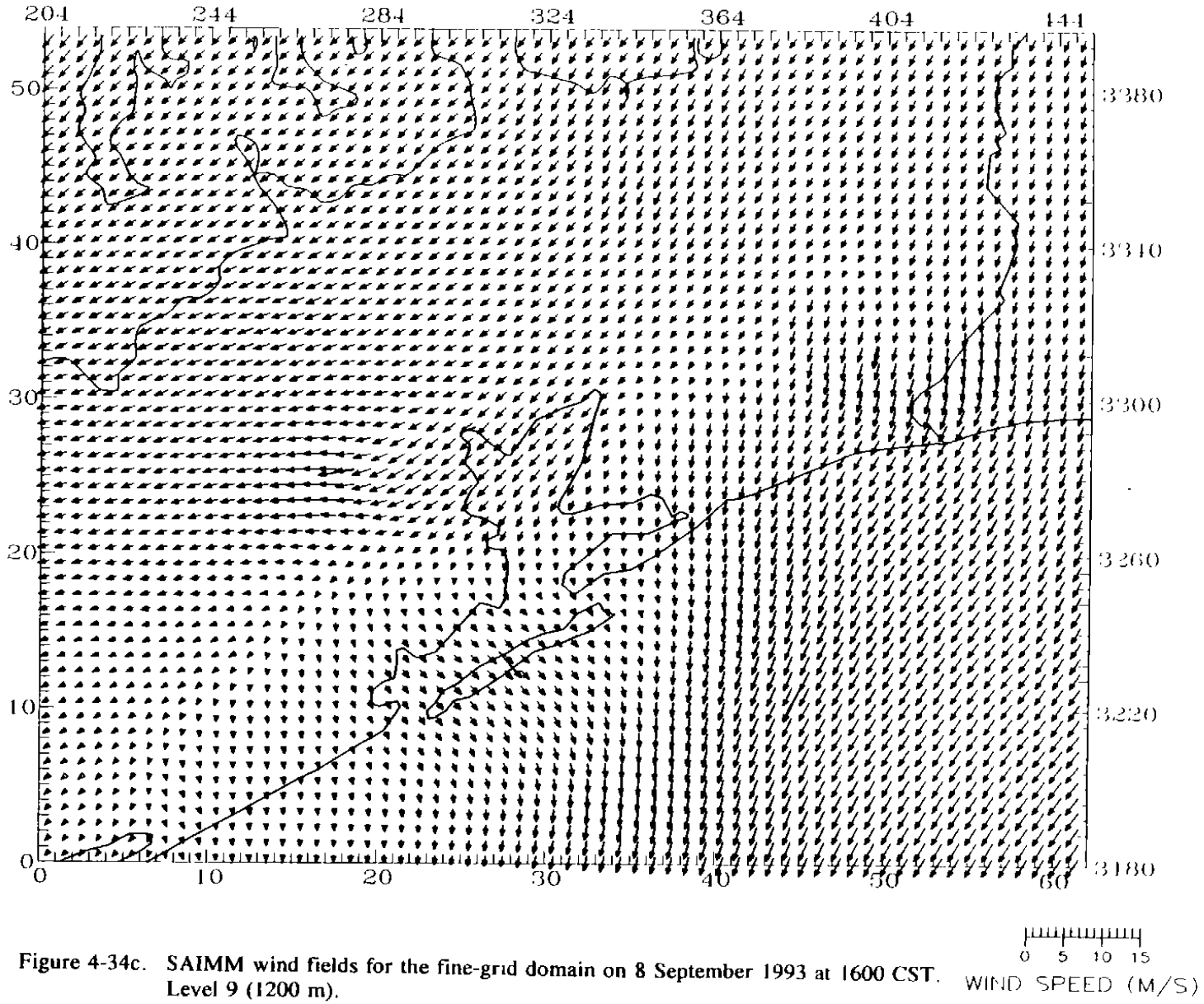

Figure 4-34c. SAIMM wind fields for the fine-grid domain on 8 September 1993 at 1600 CST. Level 9 (1200 m).

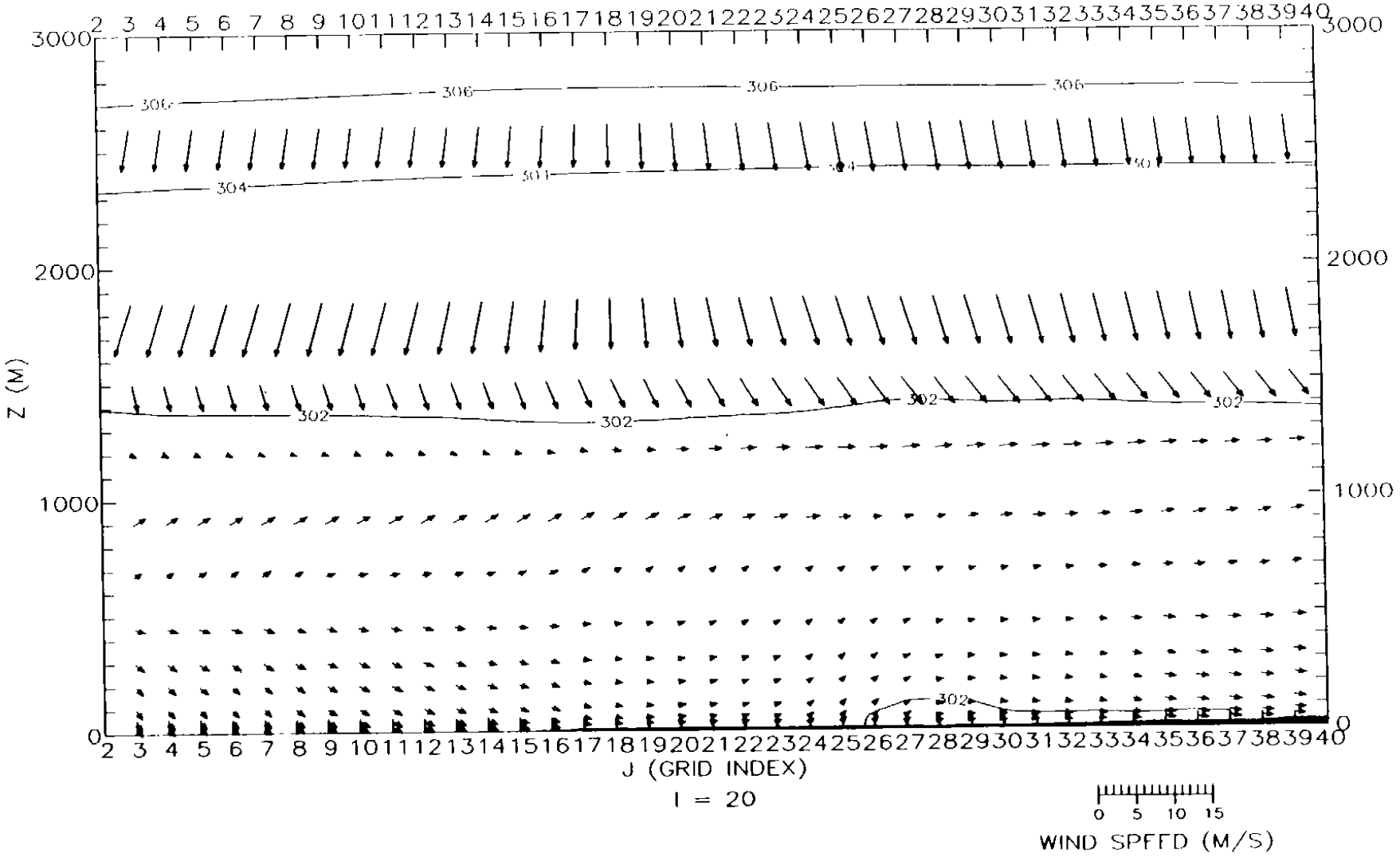

Figure 4-35a. Vertical cross section of wind and potential temperature for the fine-grid domain along west-east grid cell number 20 from south-north grid cells 2 to 40 on 8 September 1993 at 1000 CST.

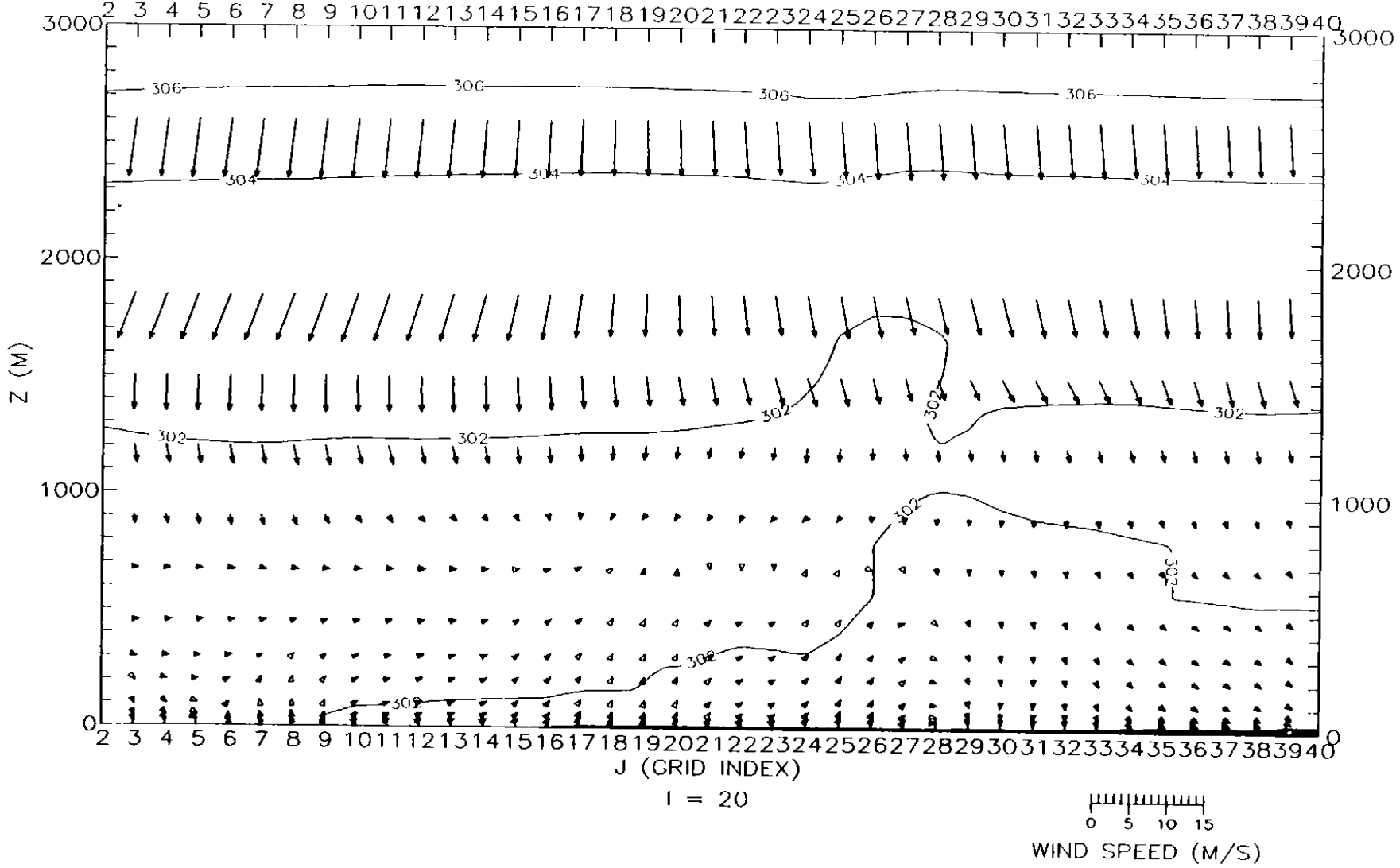

Figure 4-35b. Vertical cross section of wind and potential temperature for the fine-grid domain along west-east grid cell number 20 from south-north grid cells 2 to 40 on 8 September 1993 at 1200 CST.

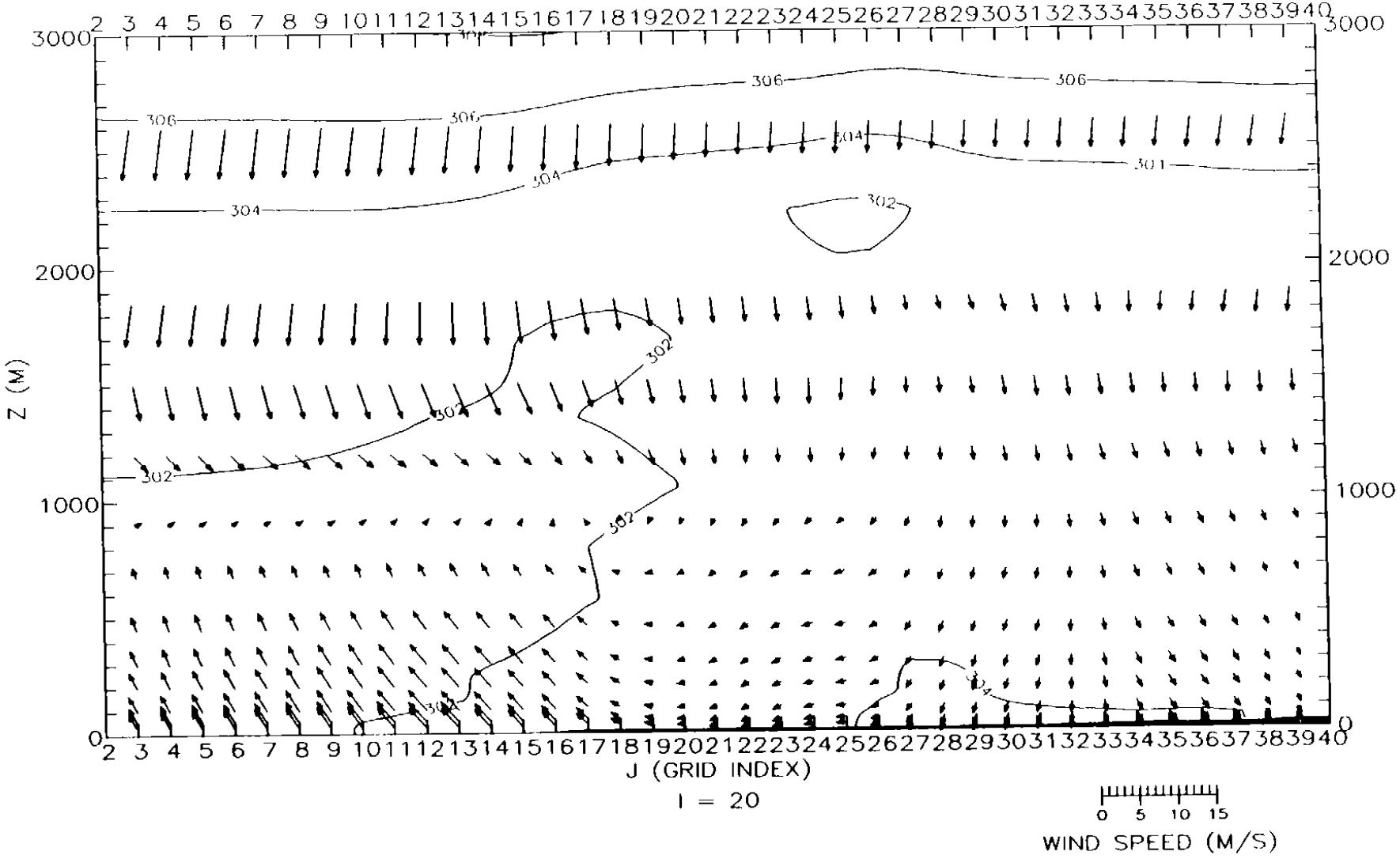

Figure 4-35c. Vertical cross section of wind and potential temperature for the fine-grid domain along west-east grid cell number 20 from south-north grid cells 2 to 40 on 8 September 1993 at 1400 CST.

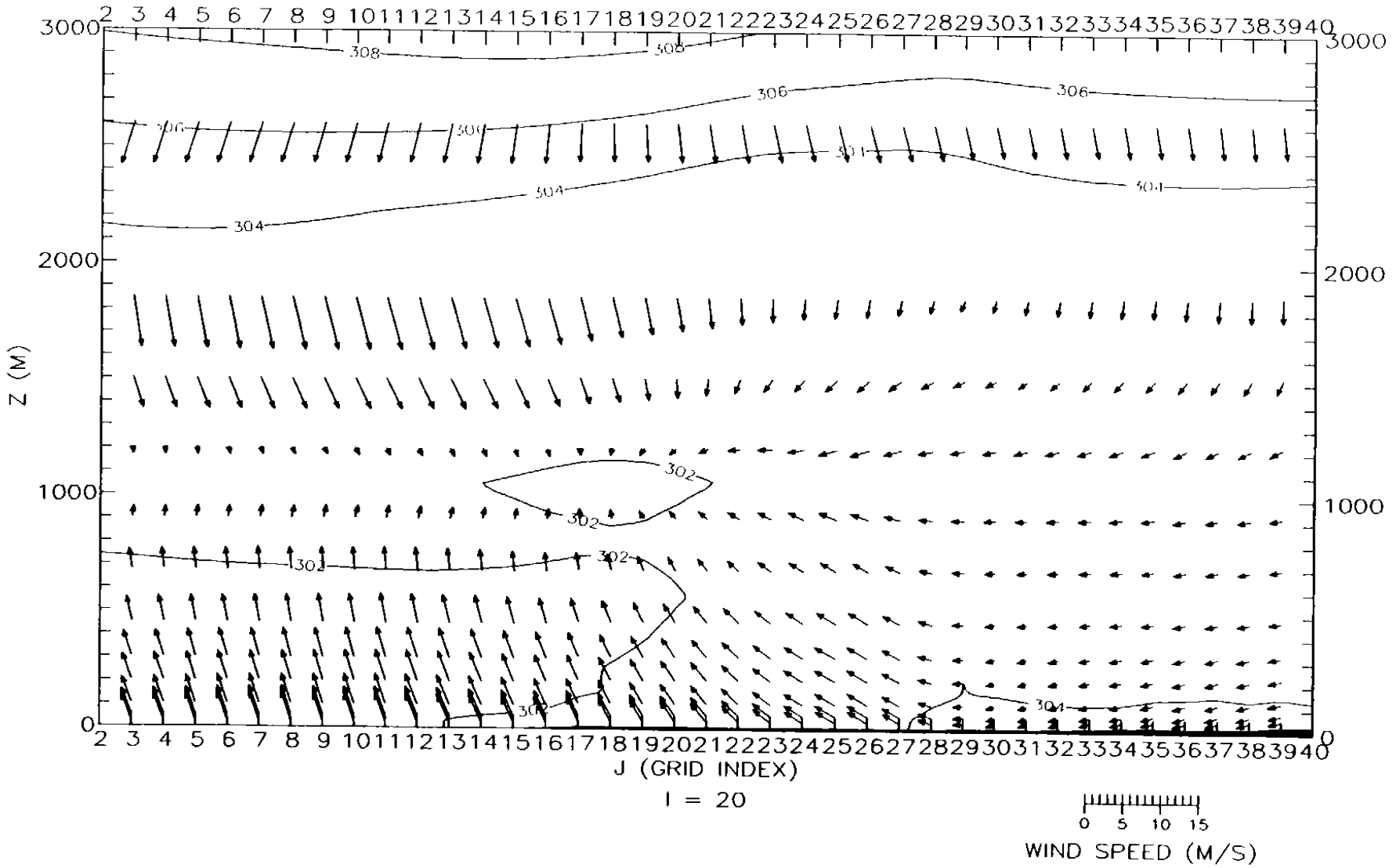

Figure 4-35d. Vertical cross section of wind and potential temperature for the fine-grid domain along west-east grid cell number 20 from south-north grid cells 2 to 40 on 8 September 1993 at 1600 CST.

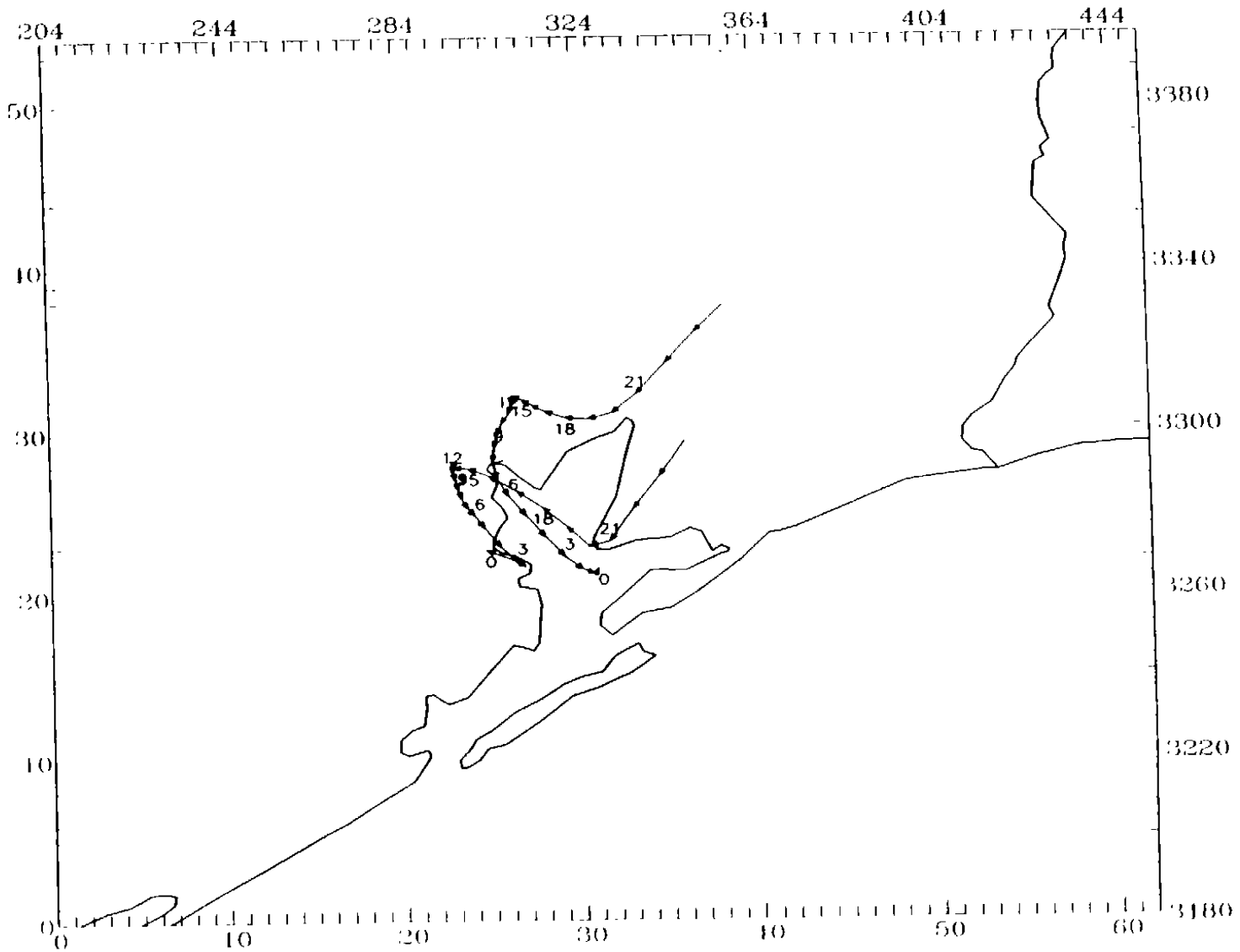

Figure 4-36. Twenty-four-hour backward particle paths for the surface layer ending at 1400 CST on 8 September 1993

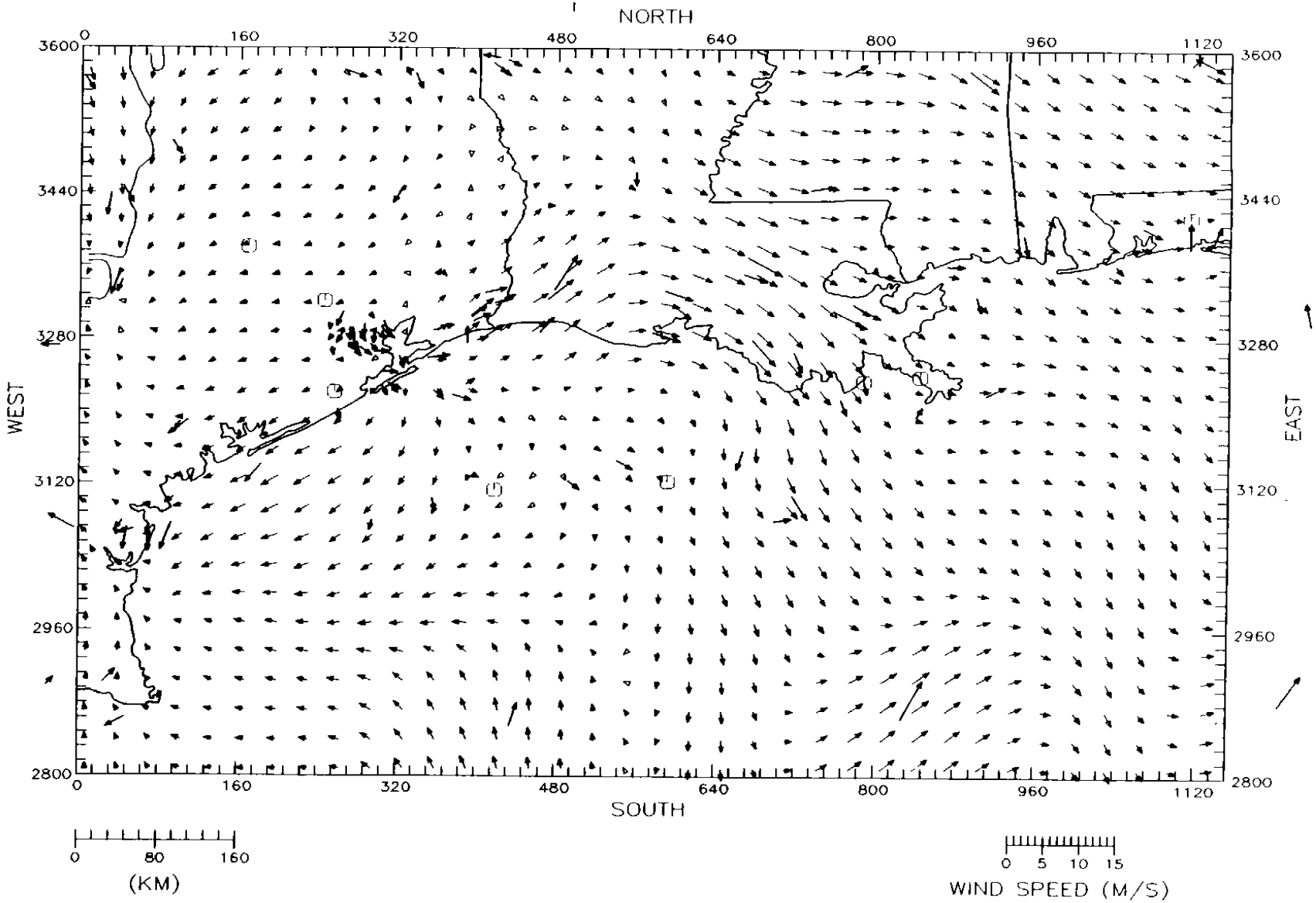

Figure 4-37a. SAIMM wind fields for the coarse-grid domain on 9 September 1993 at 1000 CST. Level 1 (25 m)

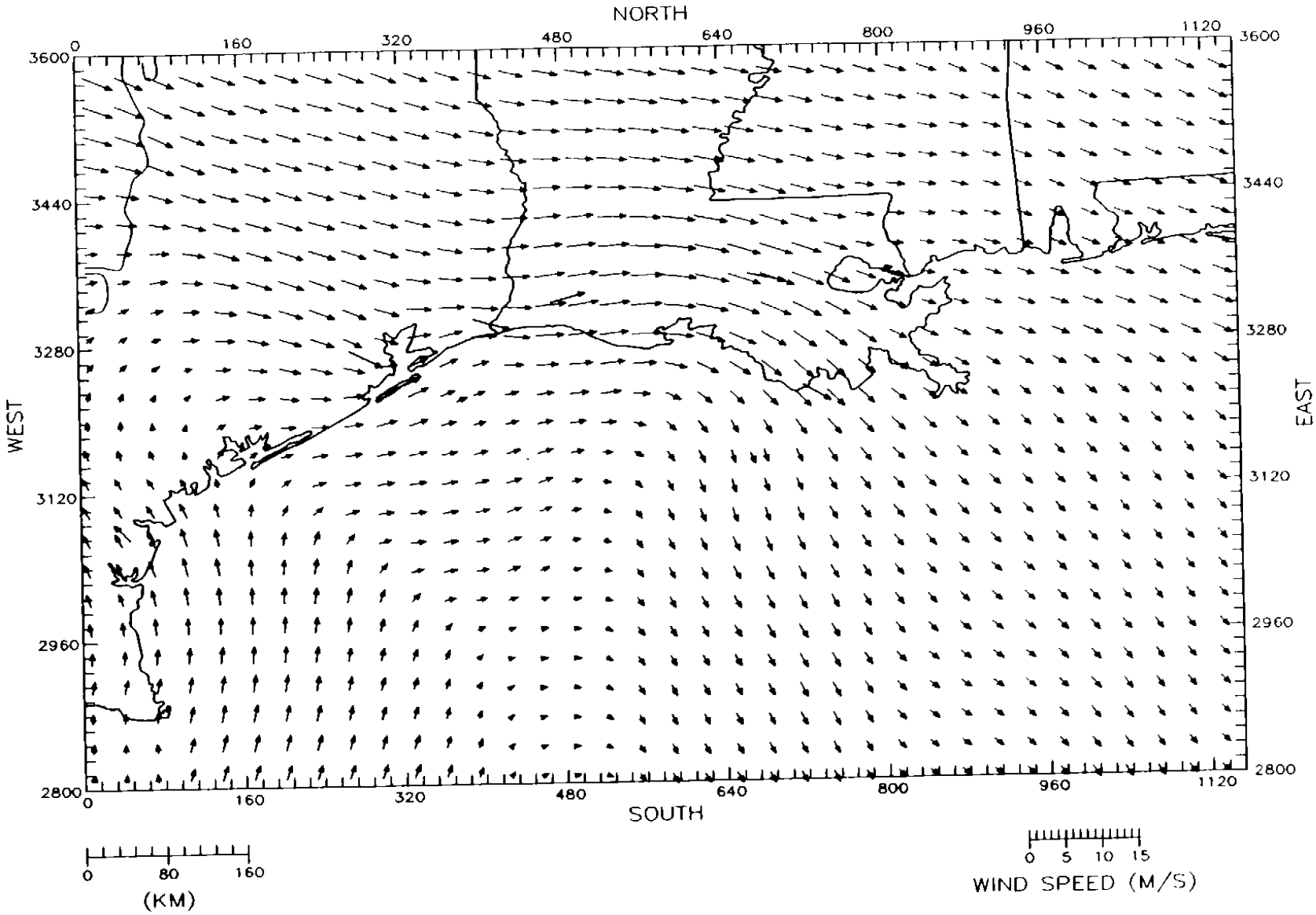

Figure 4-37b. SAIMM wind fields for the coarse-grid domain on 9 September 1993 at 1000 CST. Level 7 (675 m).

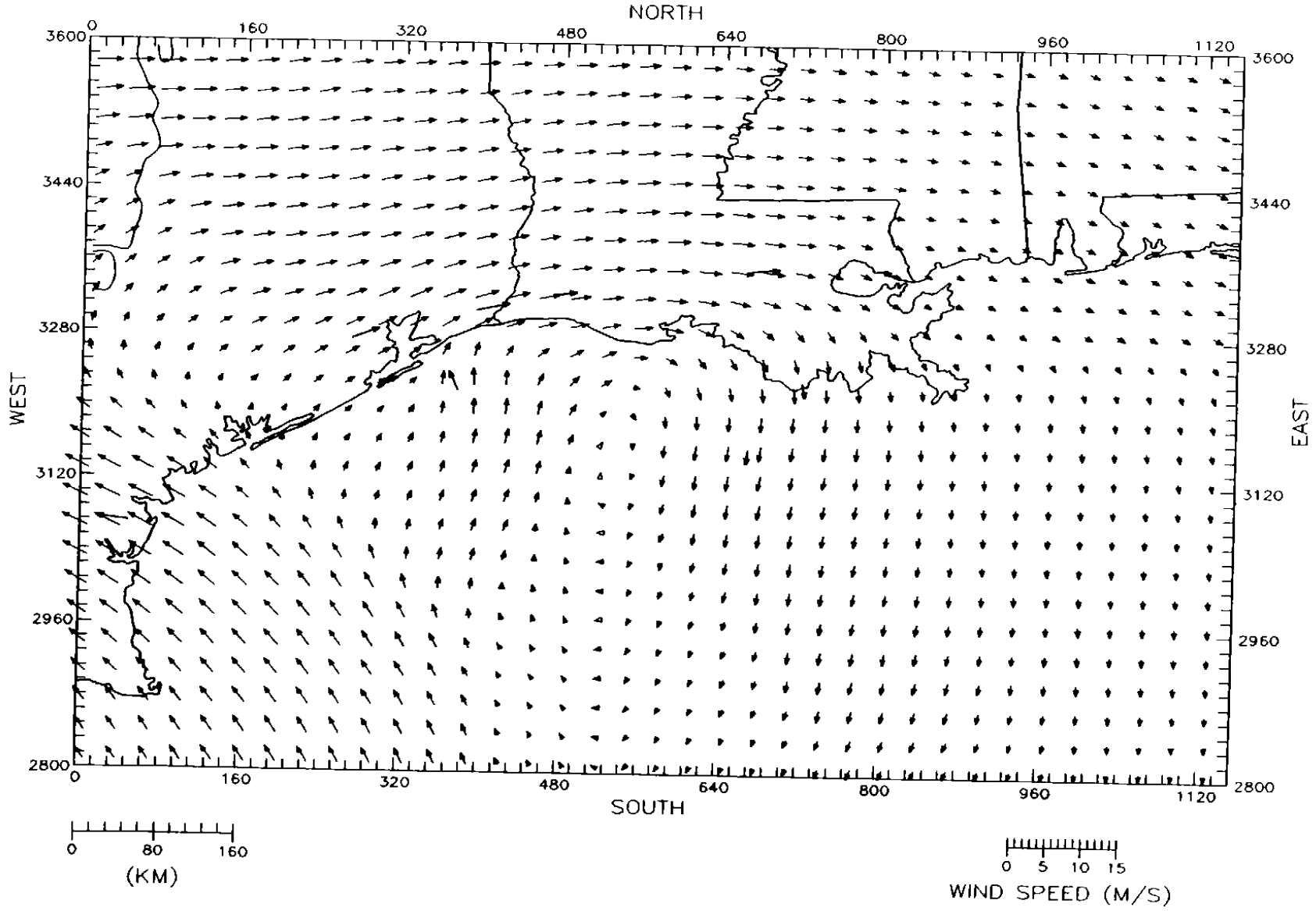

Figure 4-37c. SAIMM wind fields for the coarse-grid domain on 9 September 1993 at 1000 CST. Level 9 (1200 m).

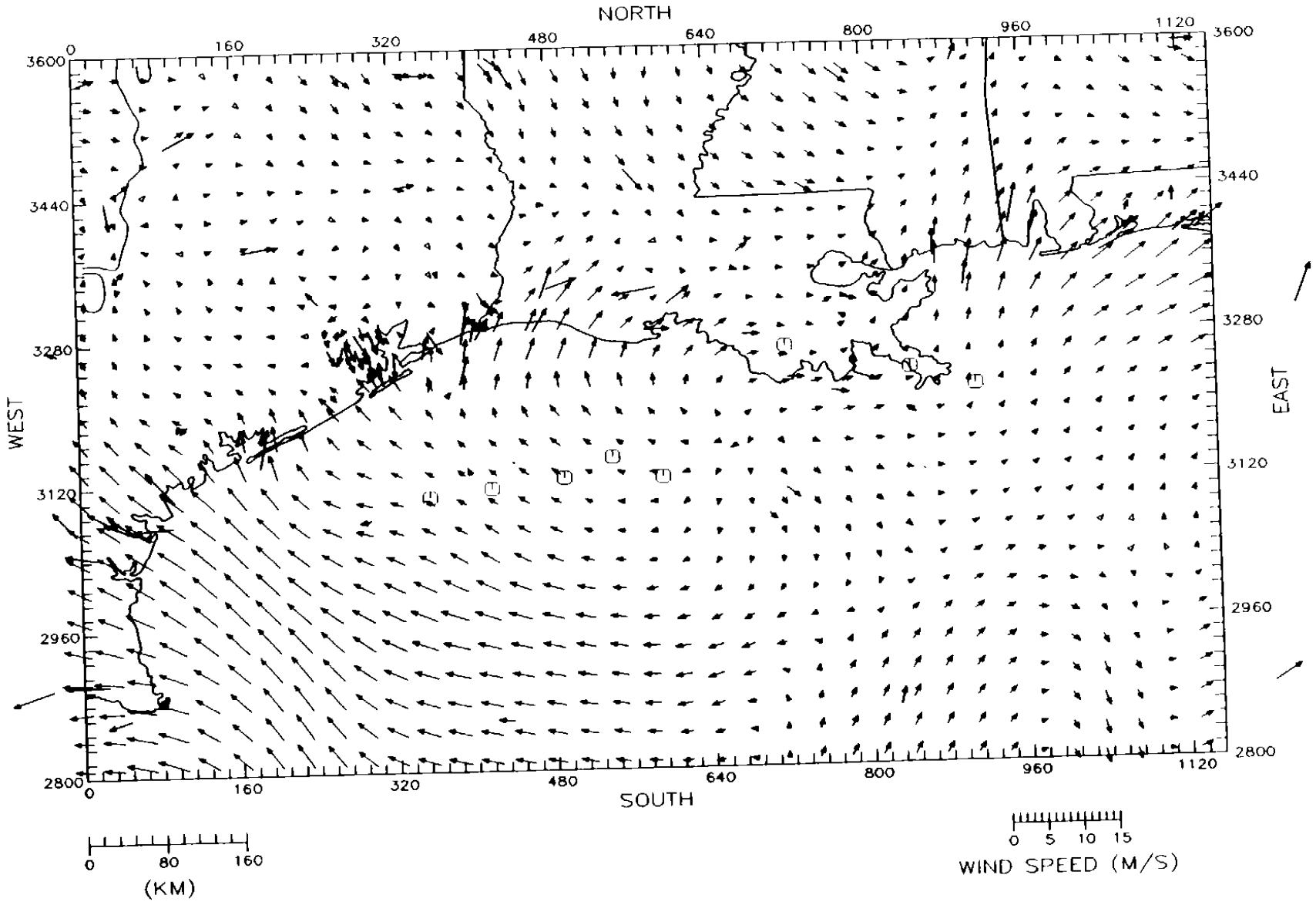

Figure 4-38a. SAIMM wind fields for the coarse-grid domain on 9 September 1993 at 1600 CST. Level 1 (25 m).

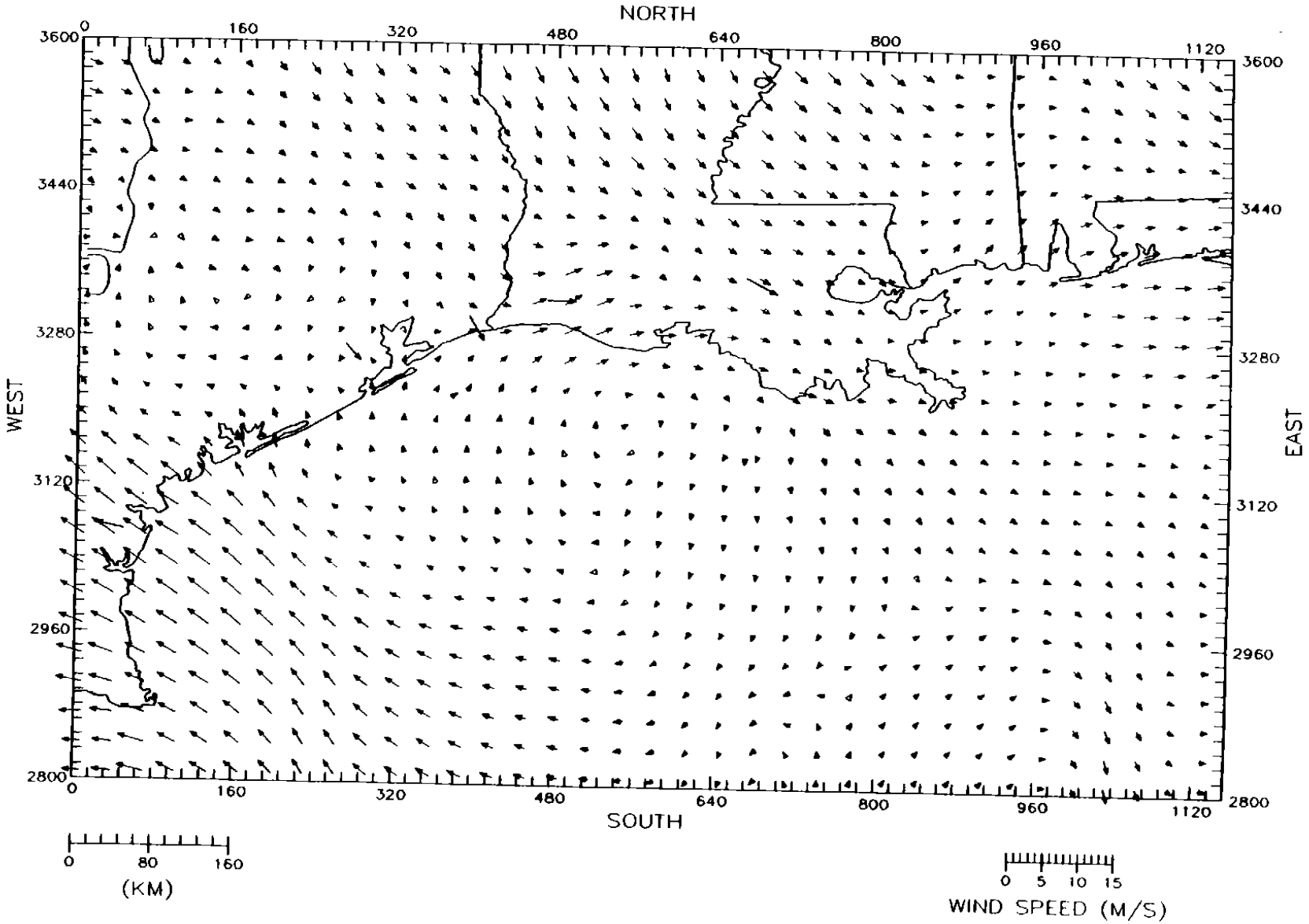

Figure 4-38b. SAIMM wind fields for the coarse-grid domain on 9 September 1993 at 1600 CST. Level 7 (675 m).

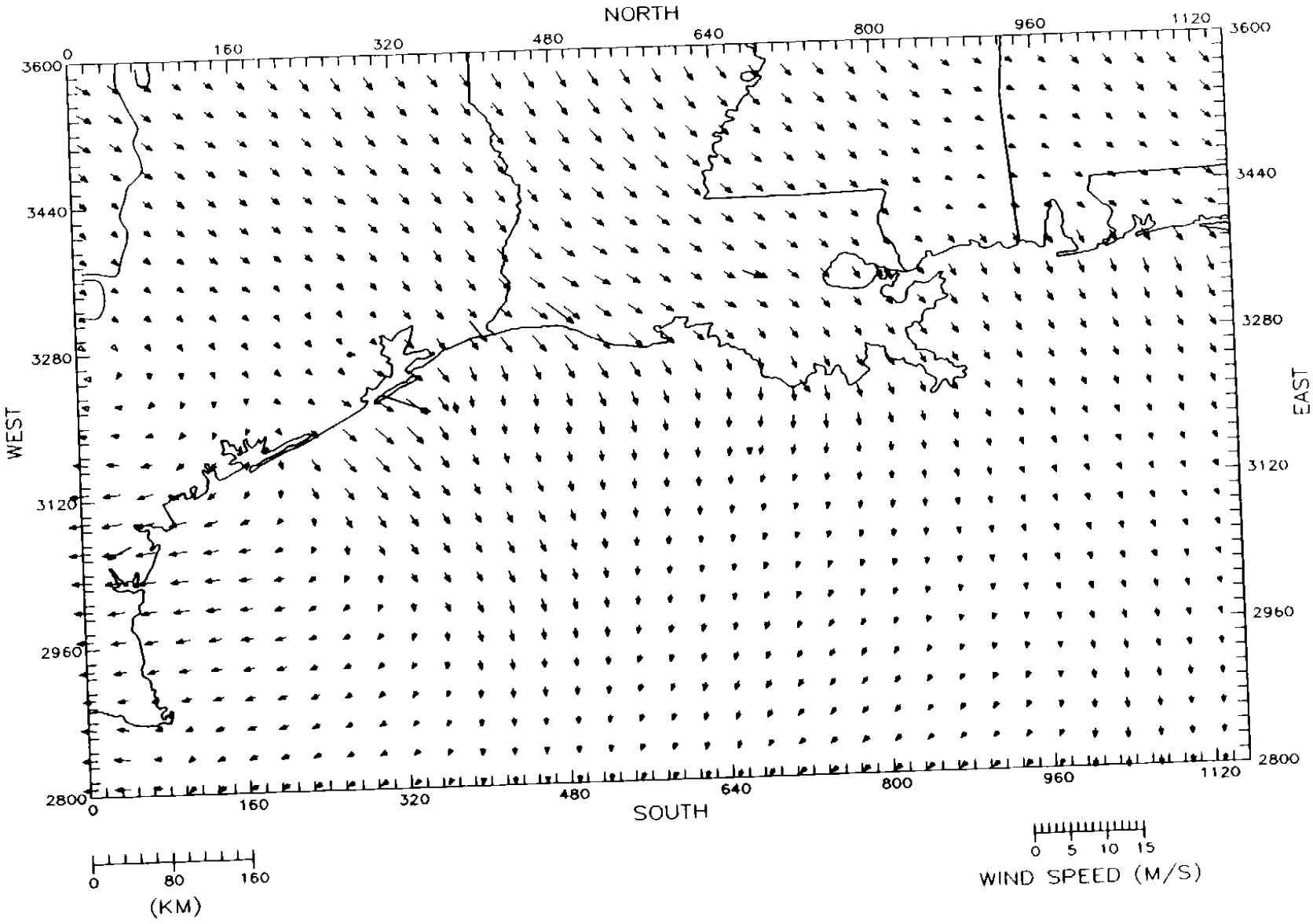

Figure 4-38c. SAIMM wind fields for the coarse-grid domain on 9 September 1993 at 1600 CST Level 9 (1200 m).

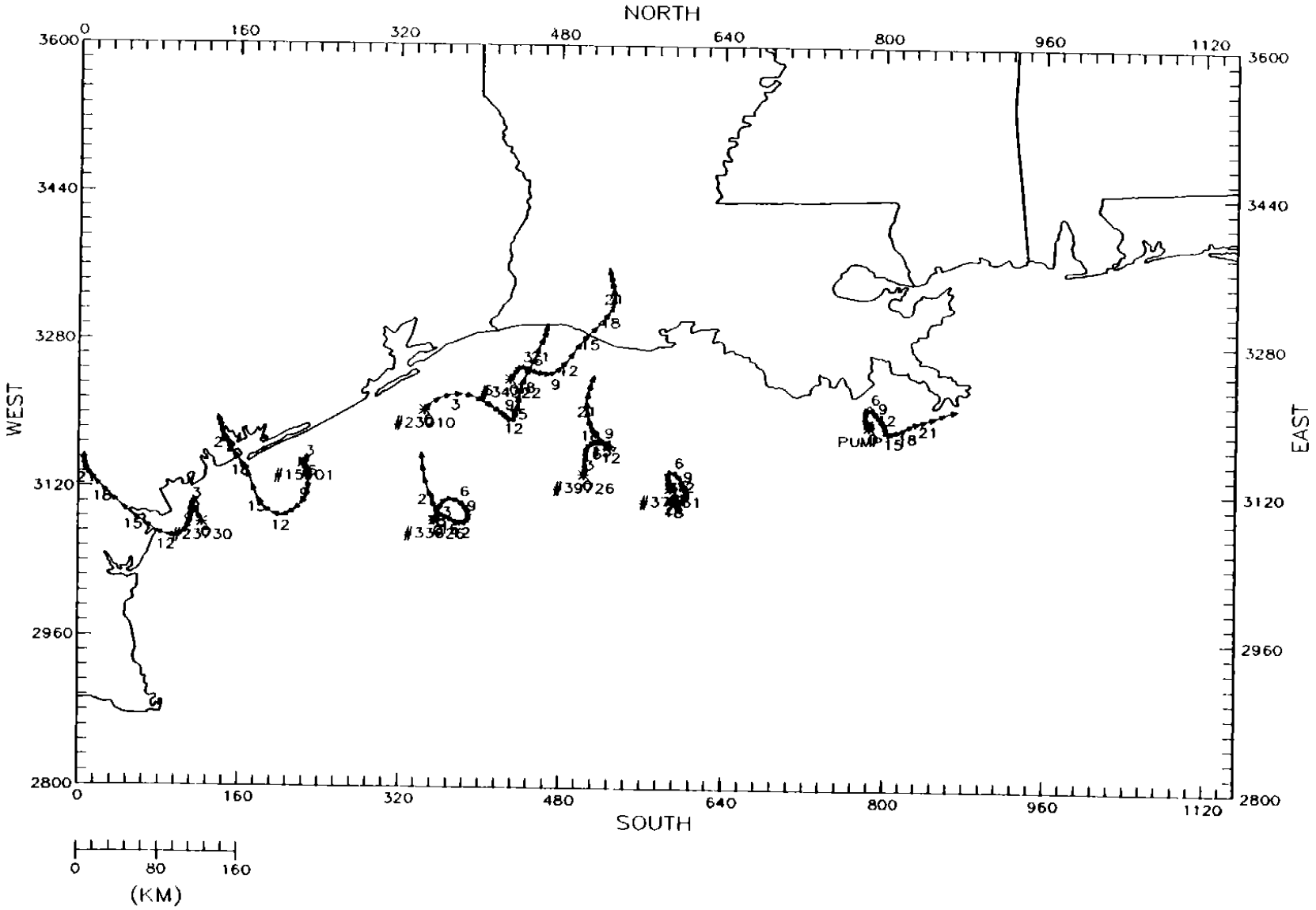

Figure 4-39a. Twenty-four-hour forward particle paths for the surface layer initiated at 0000 CST on 9 September 1993

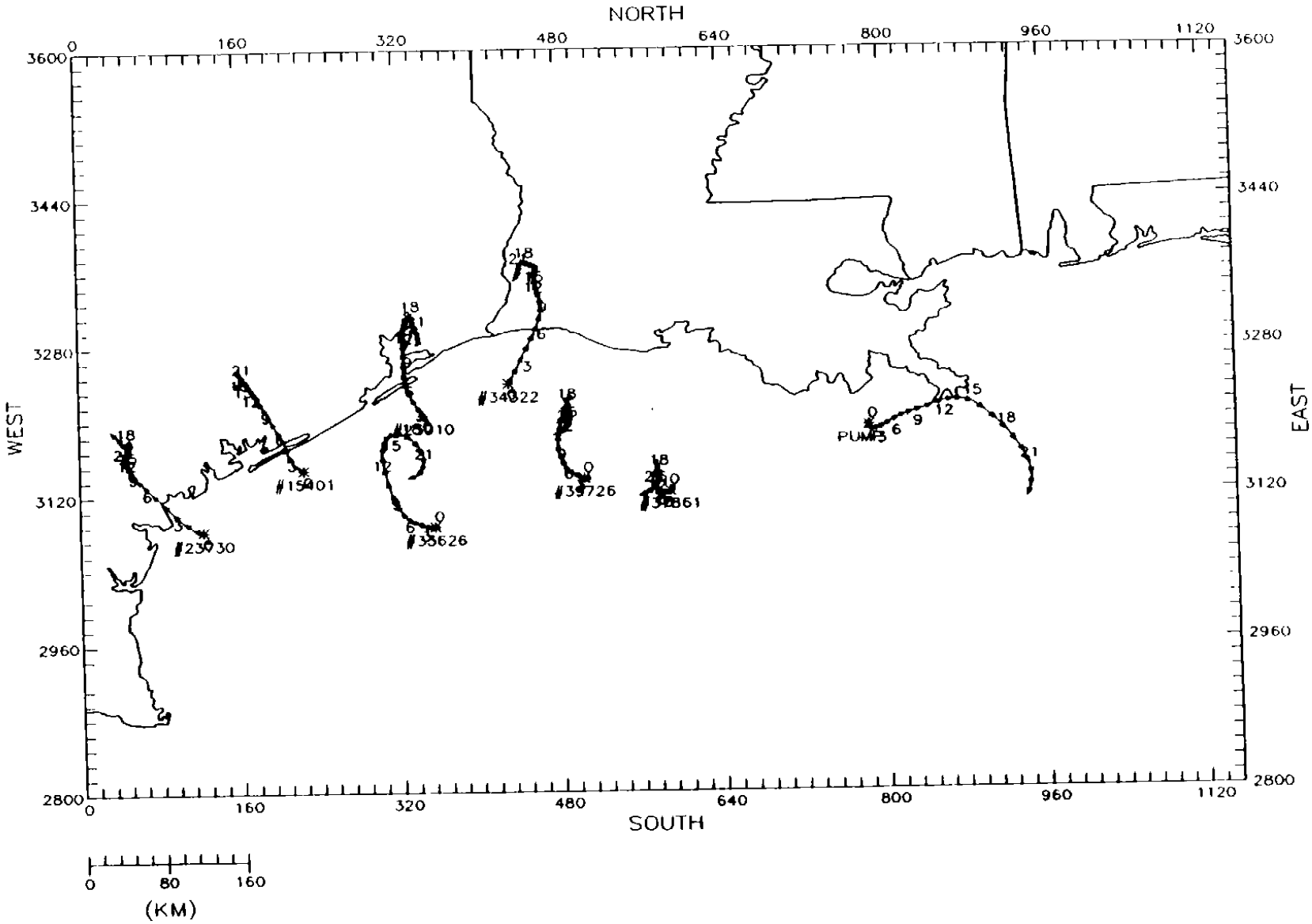

Figure 4-39b. Twenty-four-hour forward particle paths for the surface layer initiated at 1200 CST on 9 September 1993.

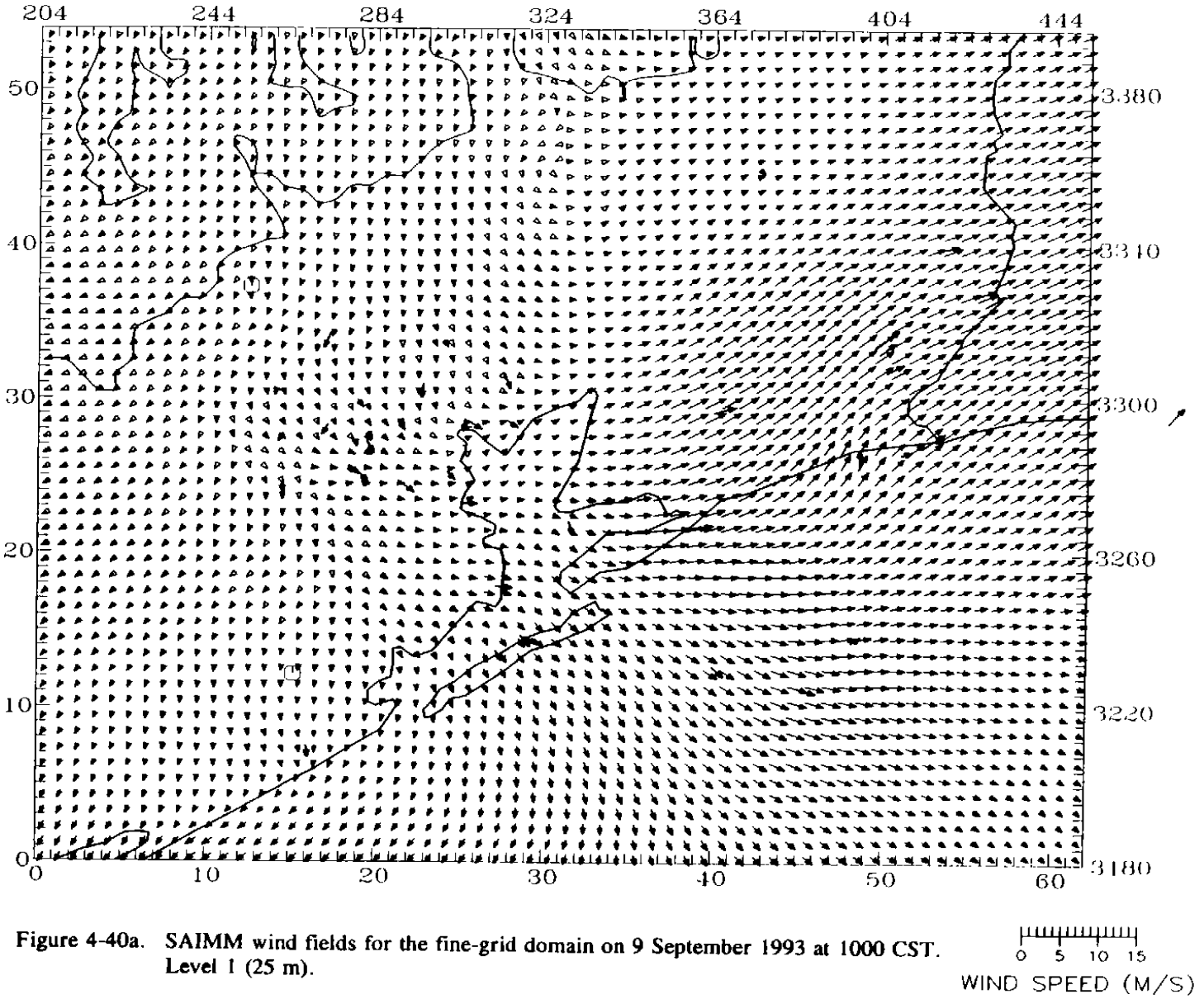

Figure 4-40a. SAIMM wind fields for the fine-grid domain on 9 September 1993 at 1000 CST. Level 1 (25 m).

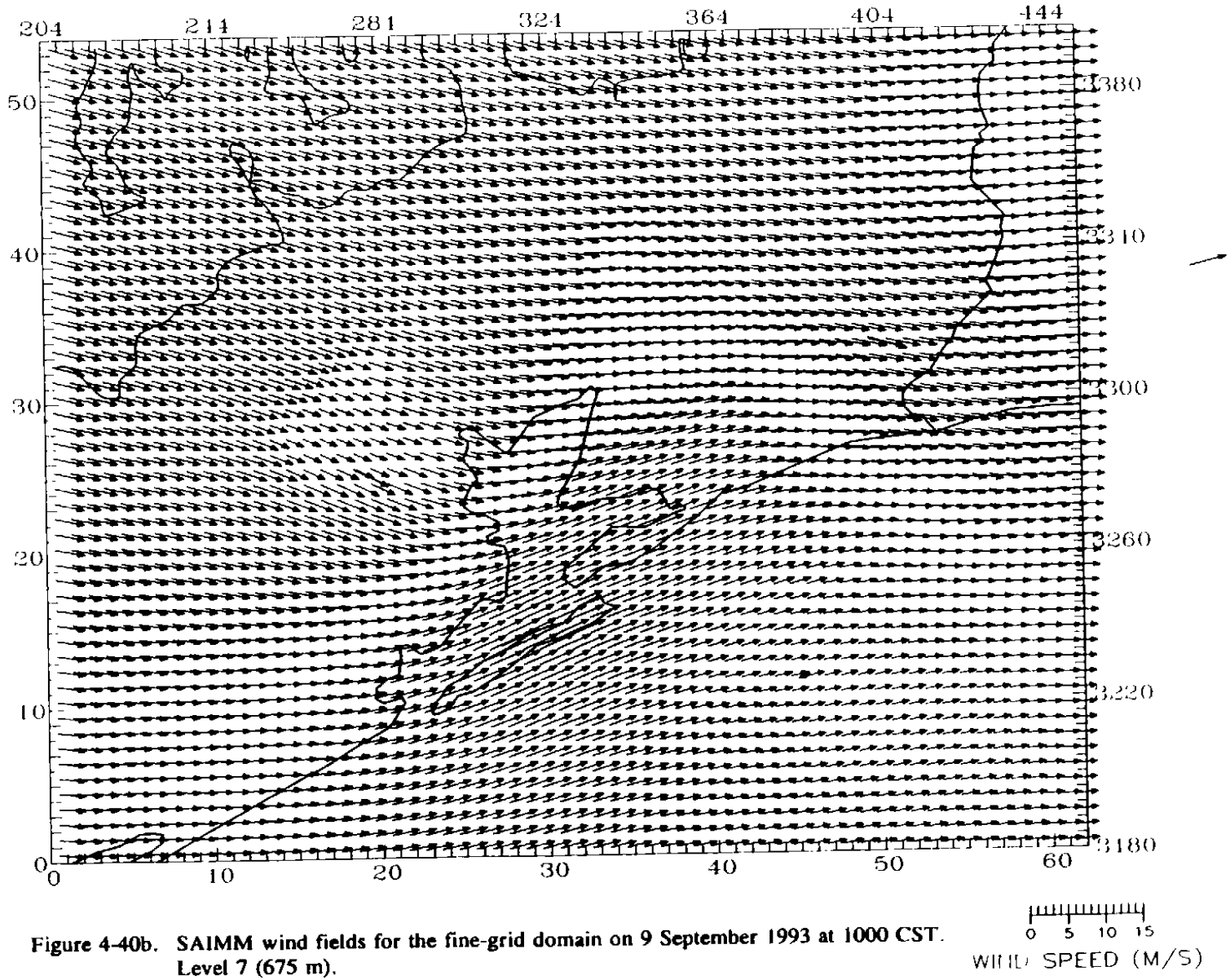

Figure 4-40b. SAIMM wind fields for the fine-grid domain on 9 September 1993 at 1000 CST. Level 7 (675 m).

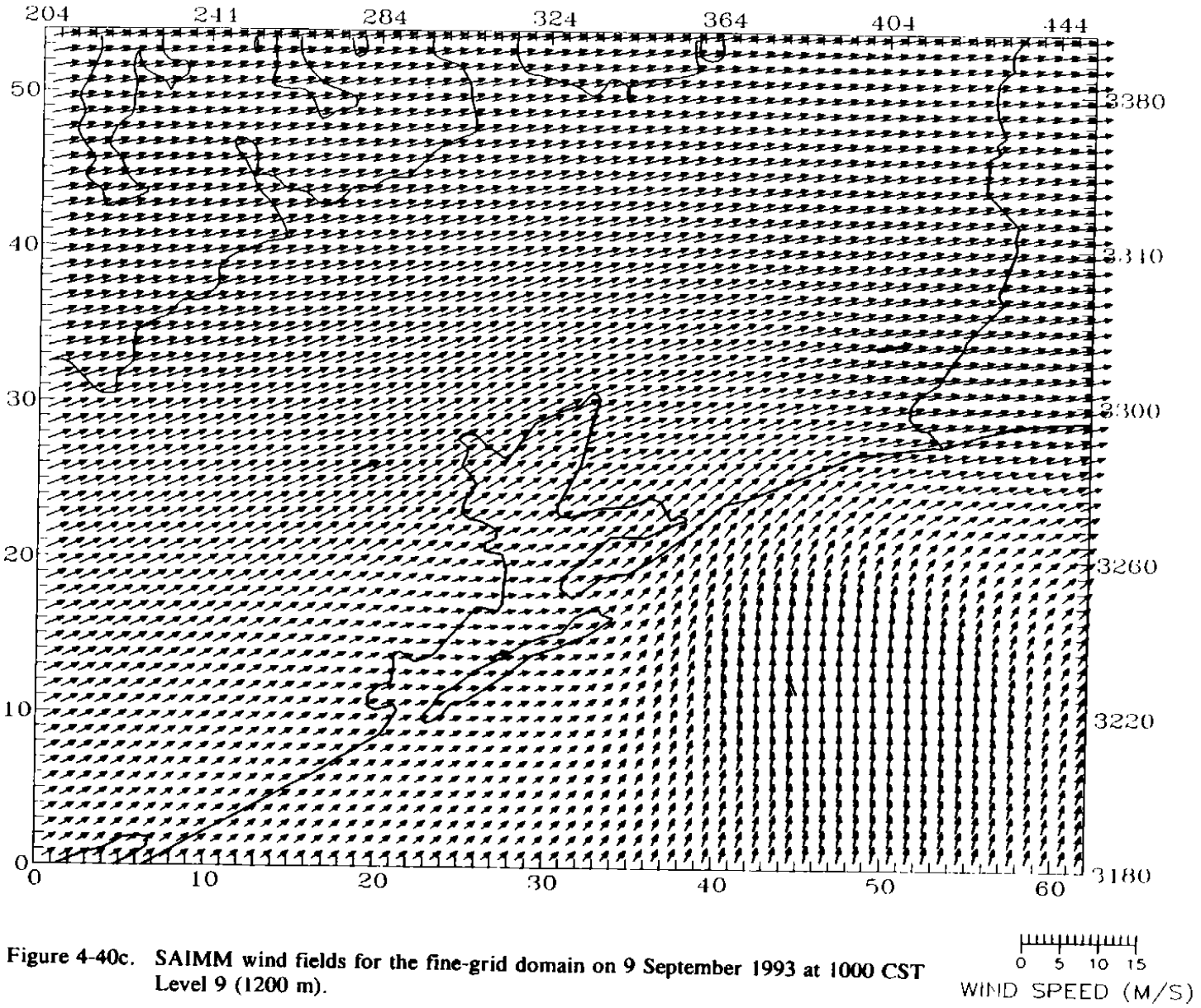

Figure 4-40c. SAIMM wind fields for the fine-grid domain on 9 September 1993 at 1000 CST Level 9 (1200 m).

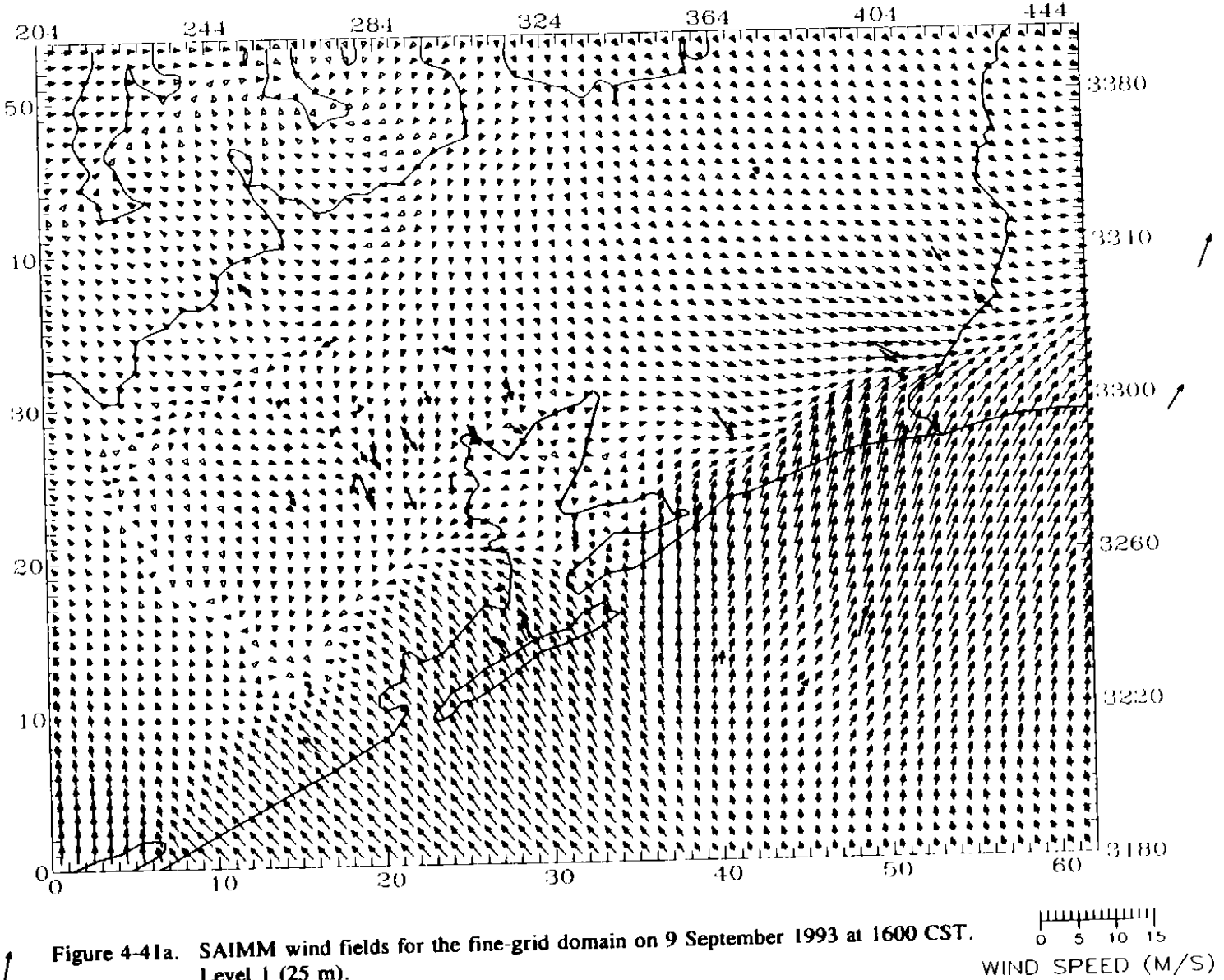

Figure 4-41a. SAIMM wind fields for the fine-grid domain on 9 September 1993 at 1600 CST. Level 1 (25 m).

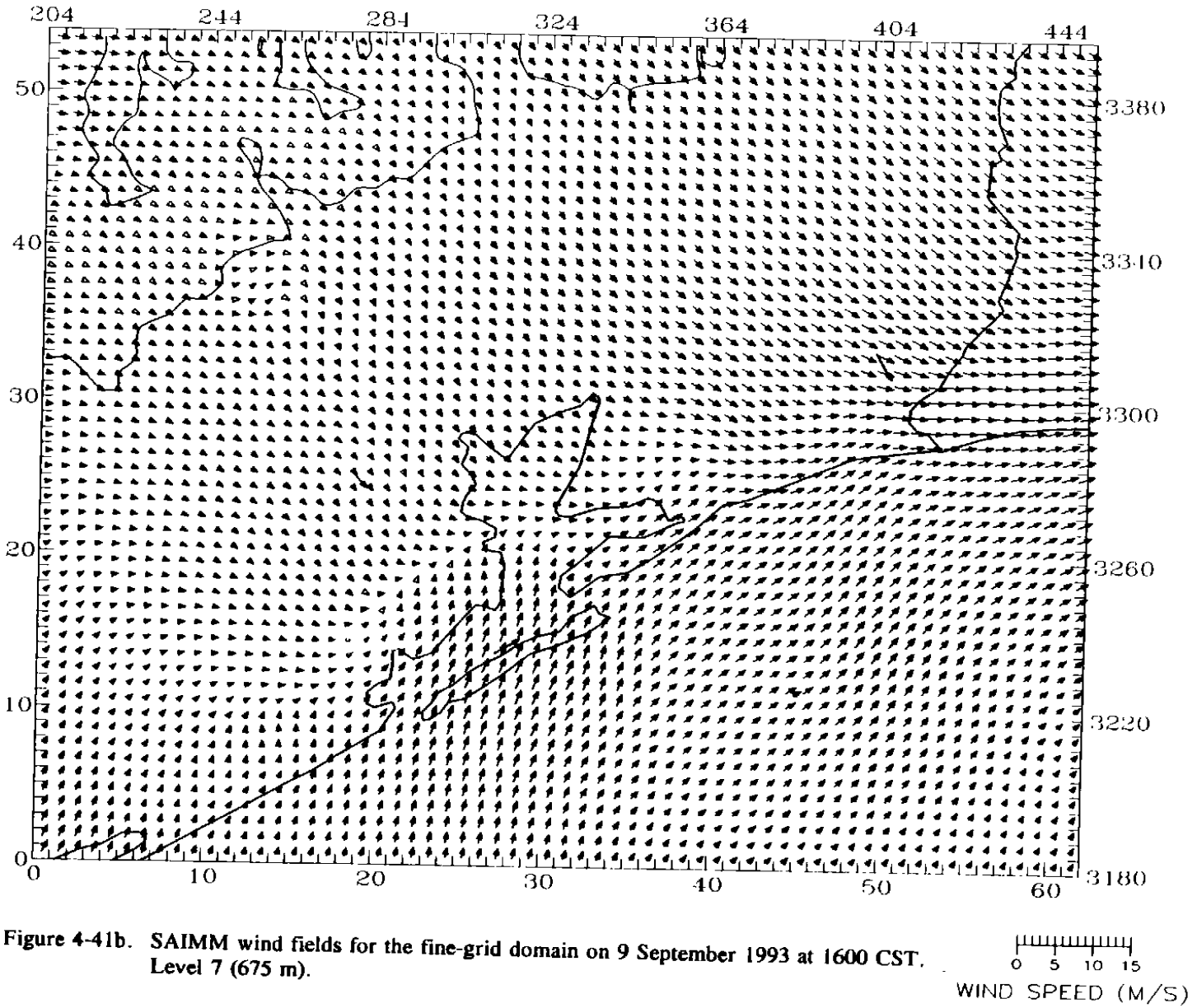

Figure 4-41b. SAIMM wind fields for the fine-grid domain on 9 September 1993 at 1600 CST. Level 7 (675 m).

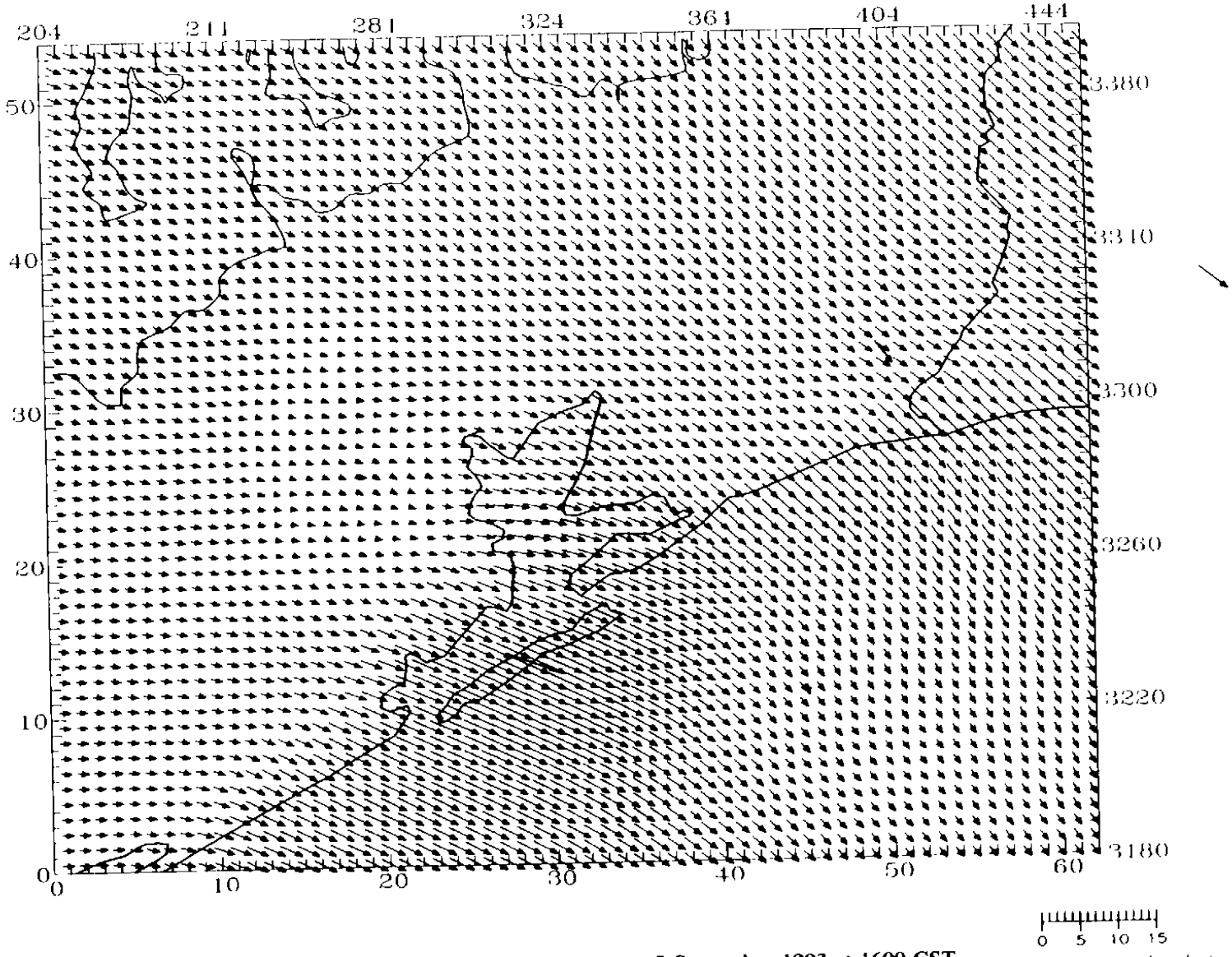

Figure 4-41c. SAIMM wind fields for the fine-grid domain on 9 September 1993 at 1600 CST. Level 9 (1200 m).

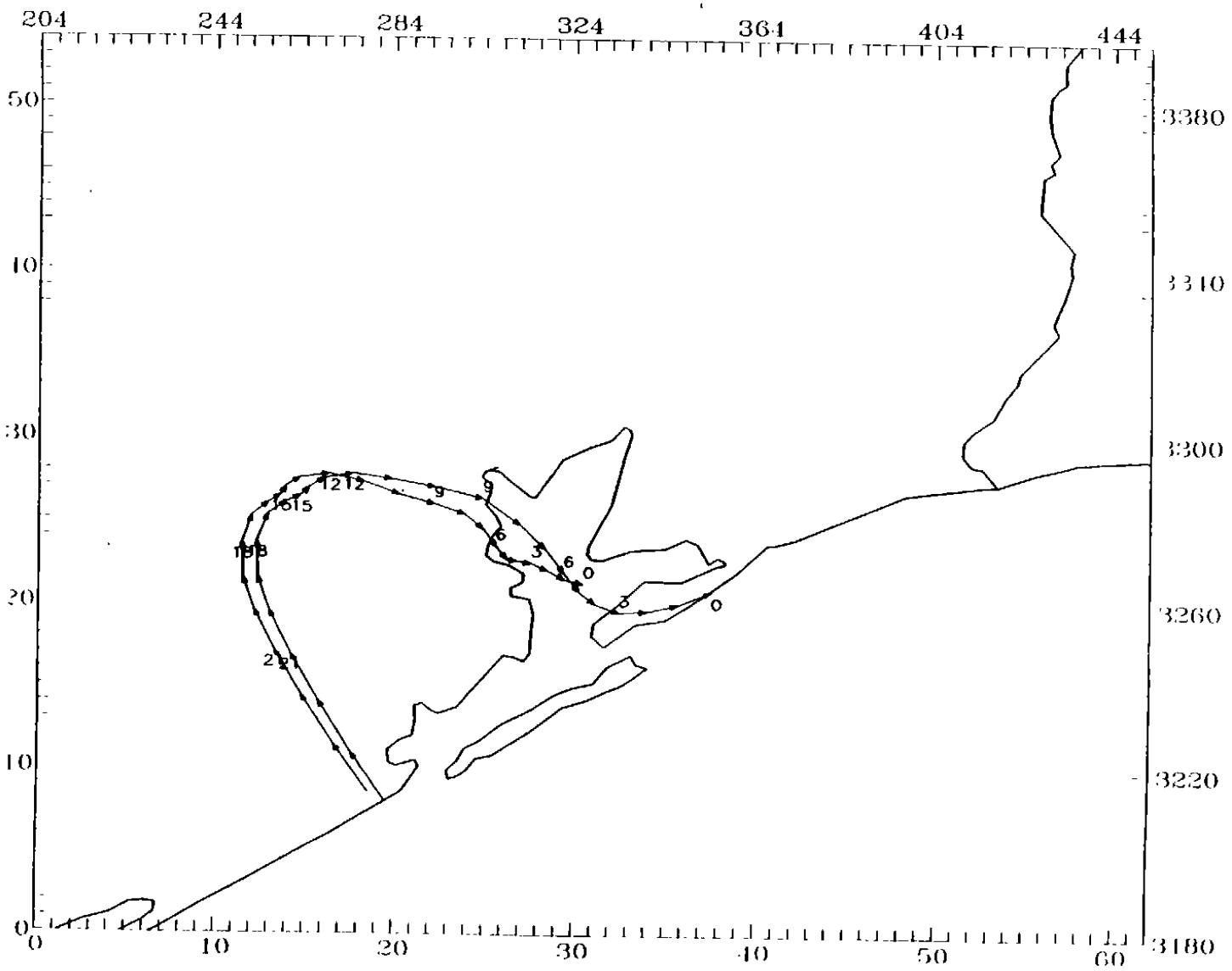

Figure 4-42. Twenty-four-hour backward particle path for the surface layer ending at 1500 CST on 9 September 1993.

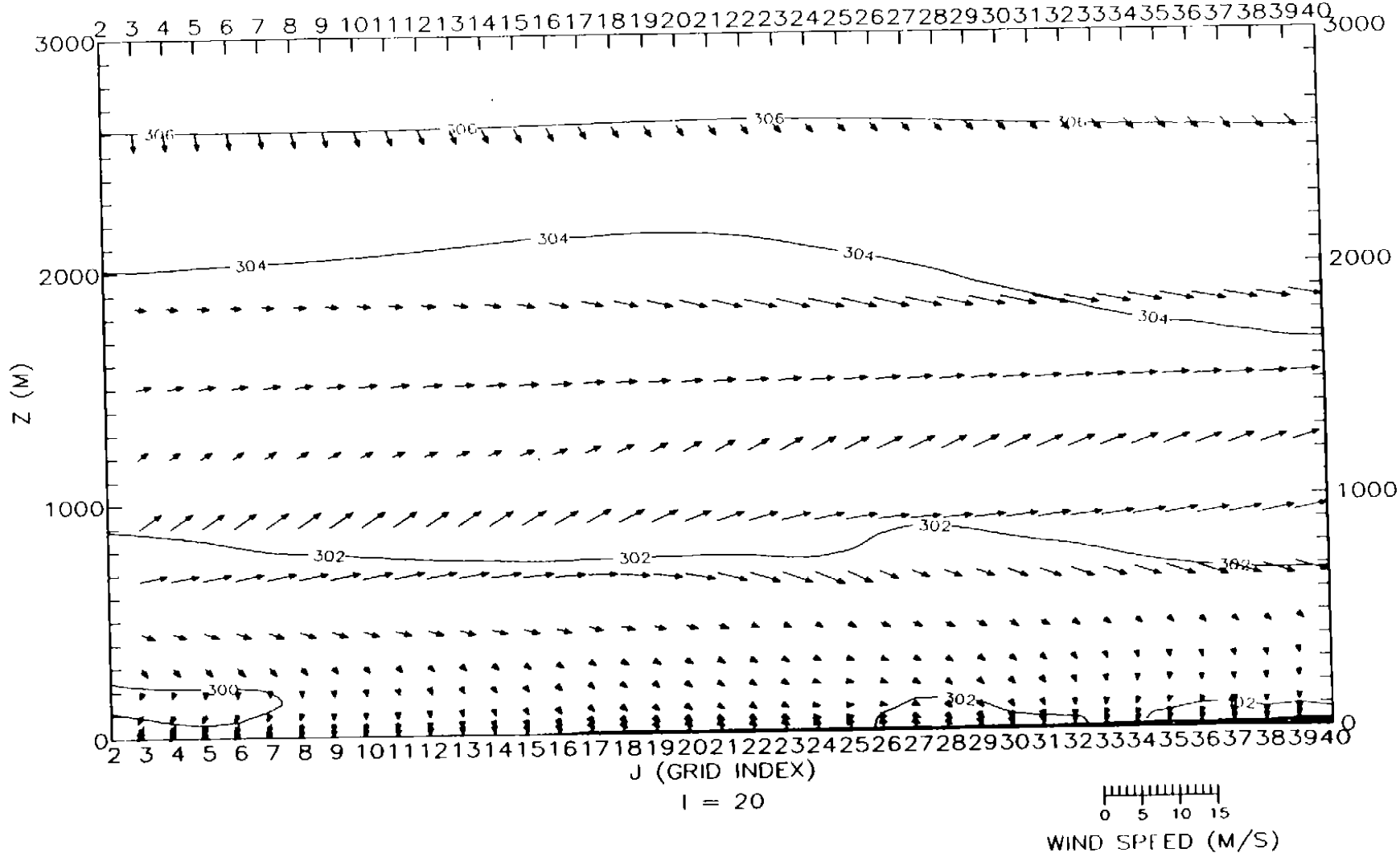

Figure 4-43a. Vertical cross section of wind and potential temperature for the fine-grid domain along west-east grid cell number 20 from south-north grid cells 2 to 40 on 9 September 1993 at 1000 CST.

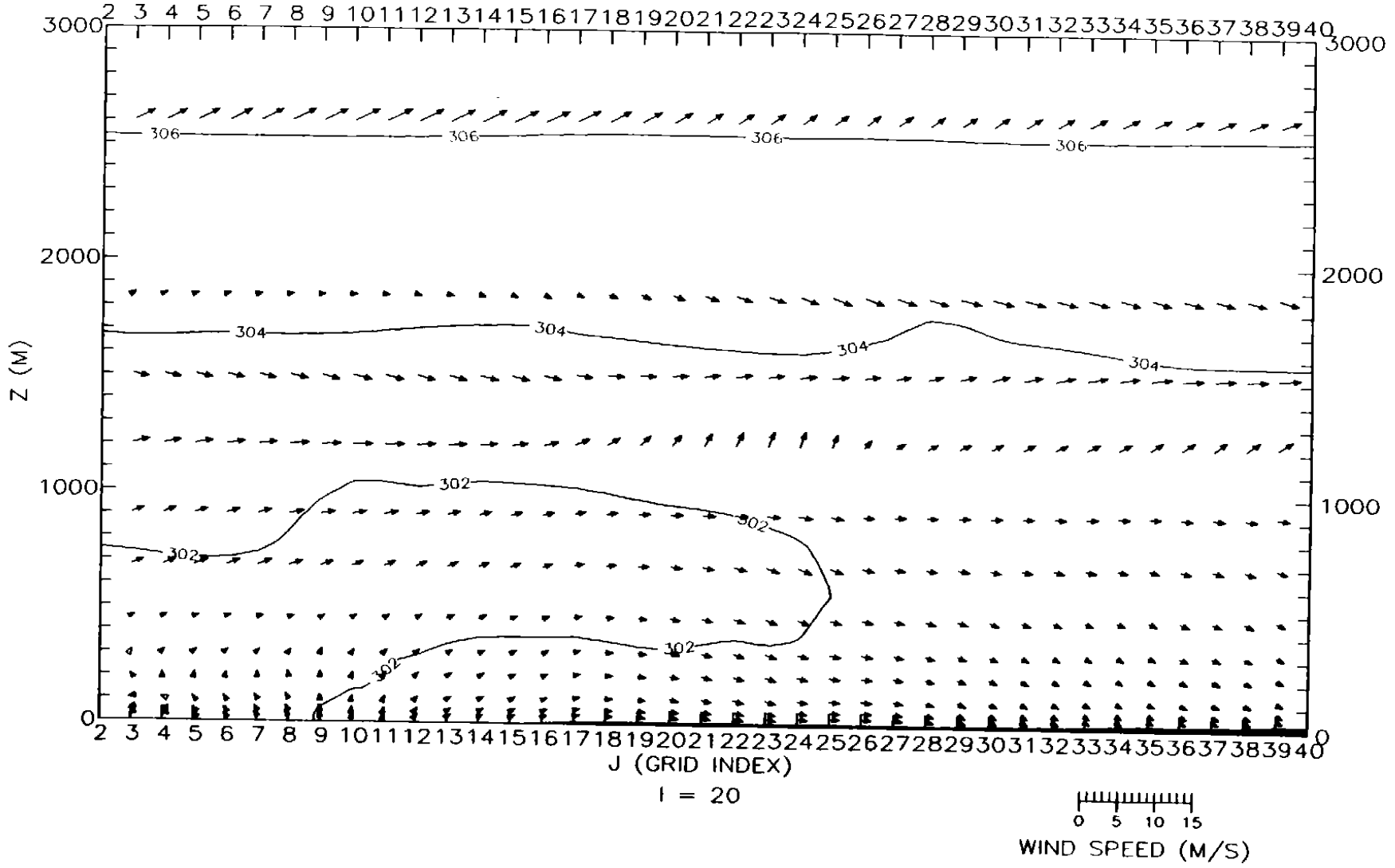

Figure 4-43b. Vertical cross section of wind and potential temperature for the fine-grid domain along west-east grid cell number 20 from south-north grid cells 2 to 40 on 9 September 1993 at 1200 CST.

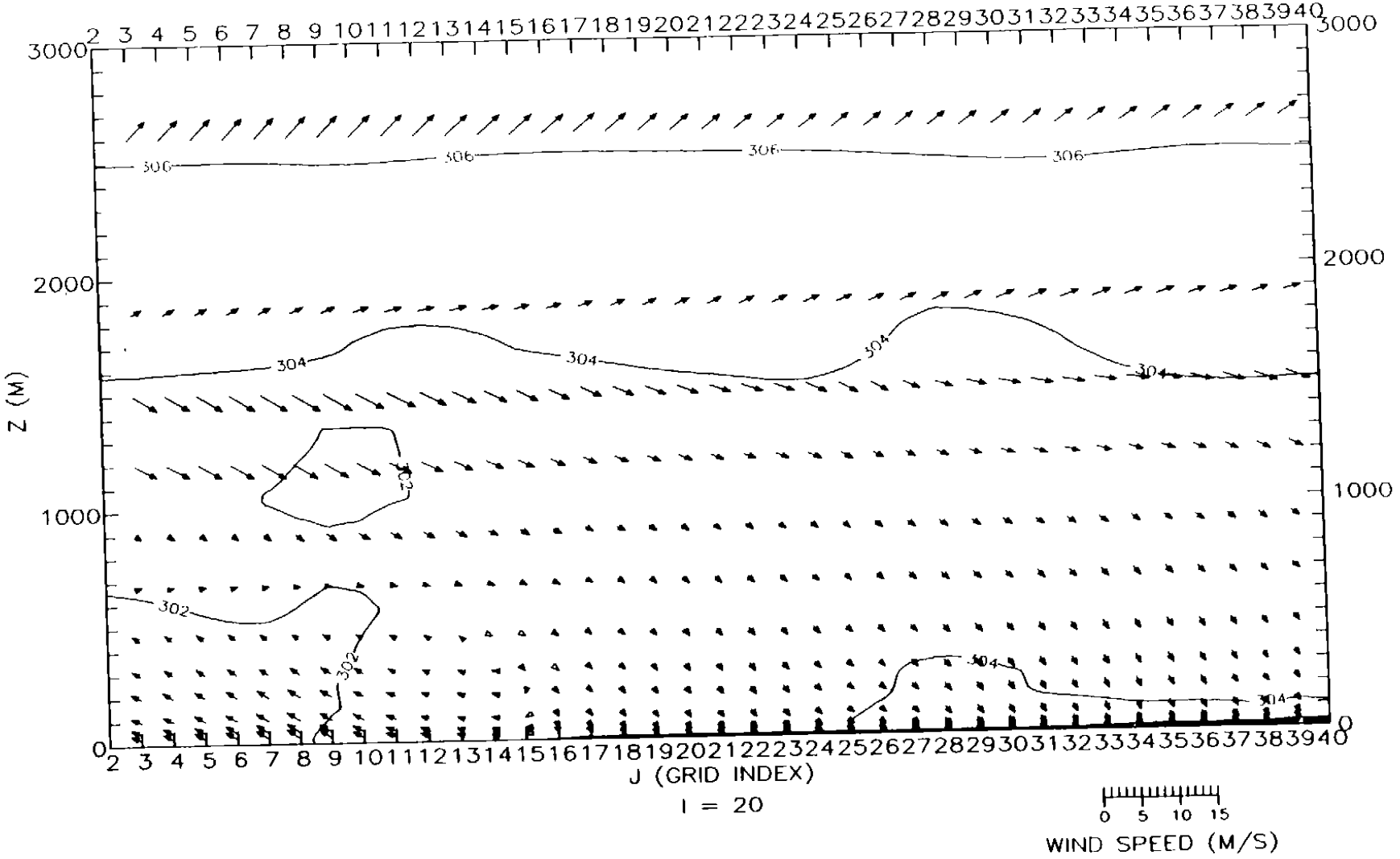

Figure 4-43c. Vertical cross section of wind and potential temperature for the fine-grid domain along west-east grid cell number 20 from south-north grid cells 2 to 40 on 9 September 1993 at 1400 CST.

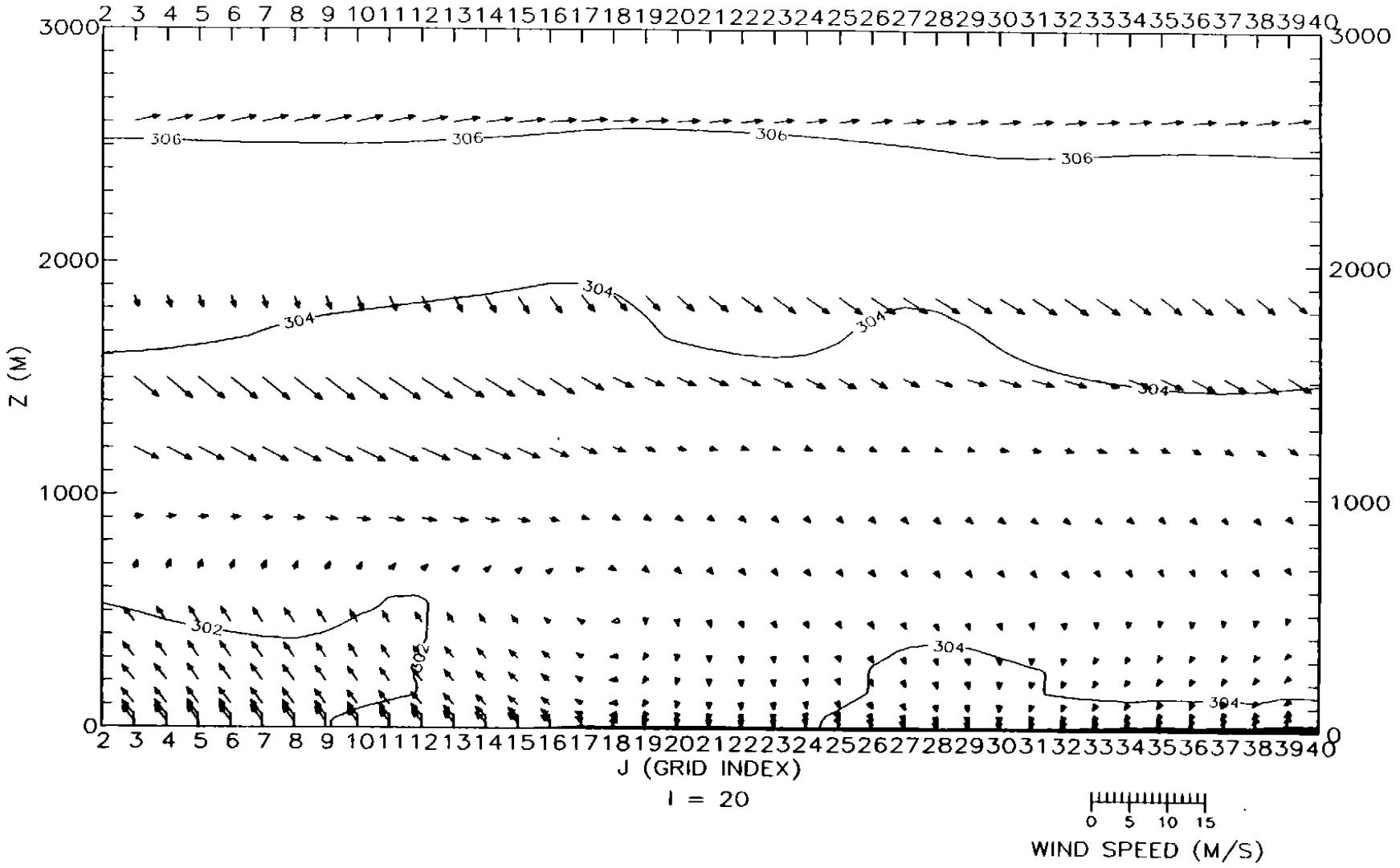

Figure 4-43d. Vertical cross section of wind and potential temperature for the fine-grid domain along west-east grid cell number 20 from south-north grid cells 2 to 40 on 9 September 1993 at 1600 CST.

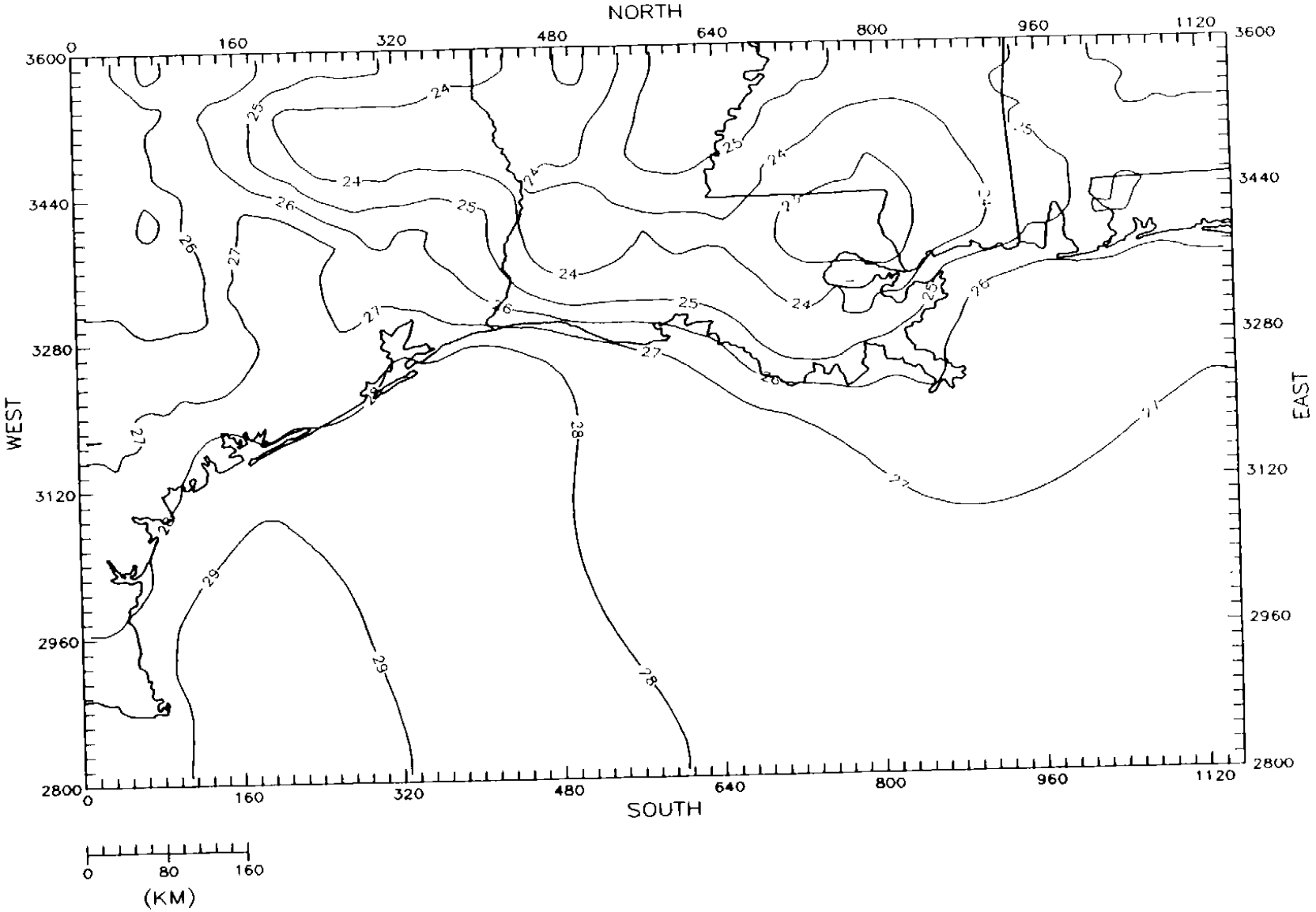

Figure 4-44a. SAIMM surface-level temperature fields (°C) for the coarse-grid domain on 8 September 1993 at 0400 CST.

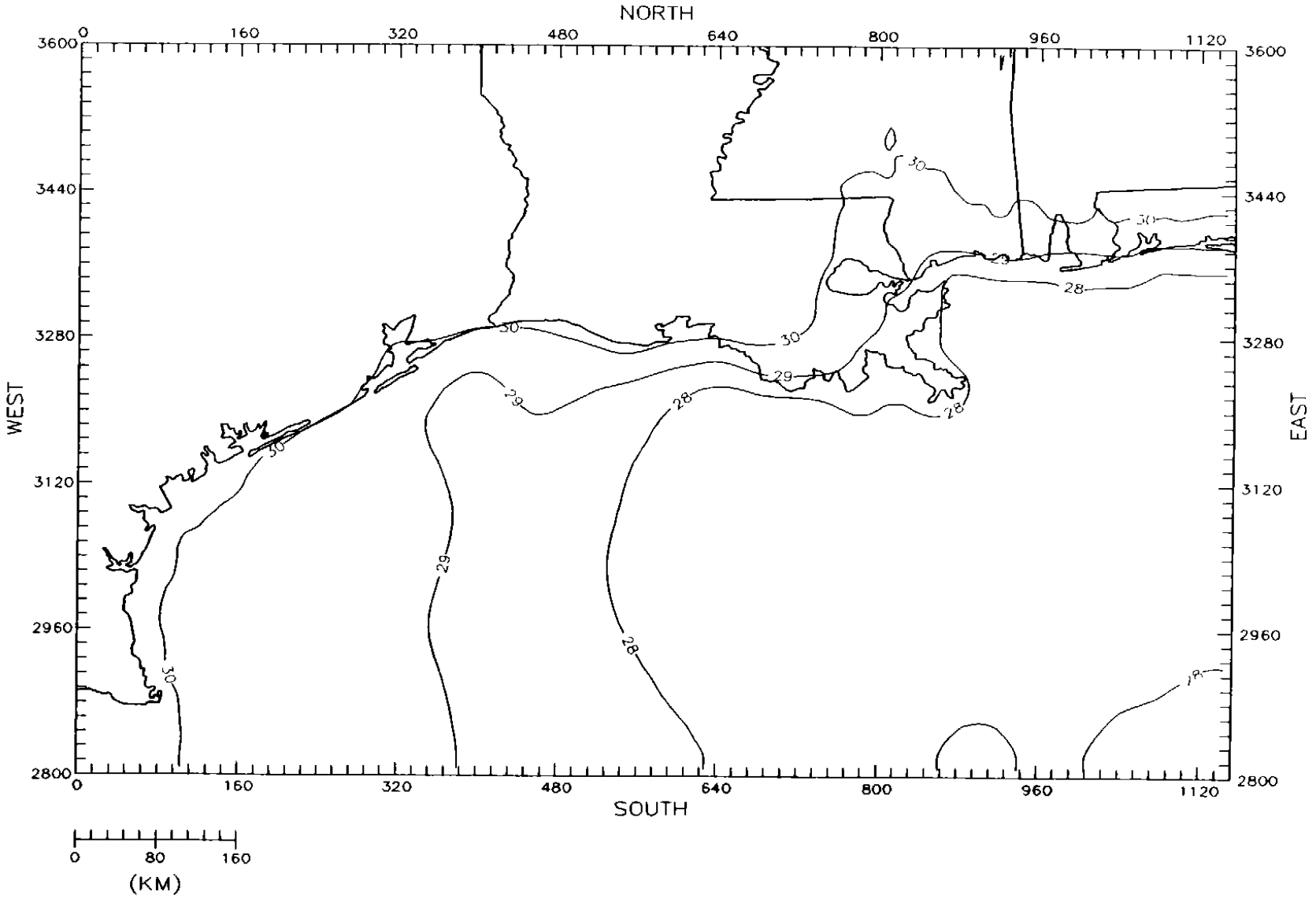

Figure 4-44b. SAIMM surface-level temperature fields (°C) for the coarse-grid domain on 8 September 1993 at 1600 CST.

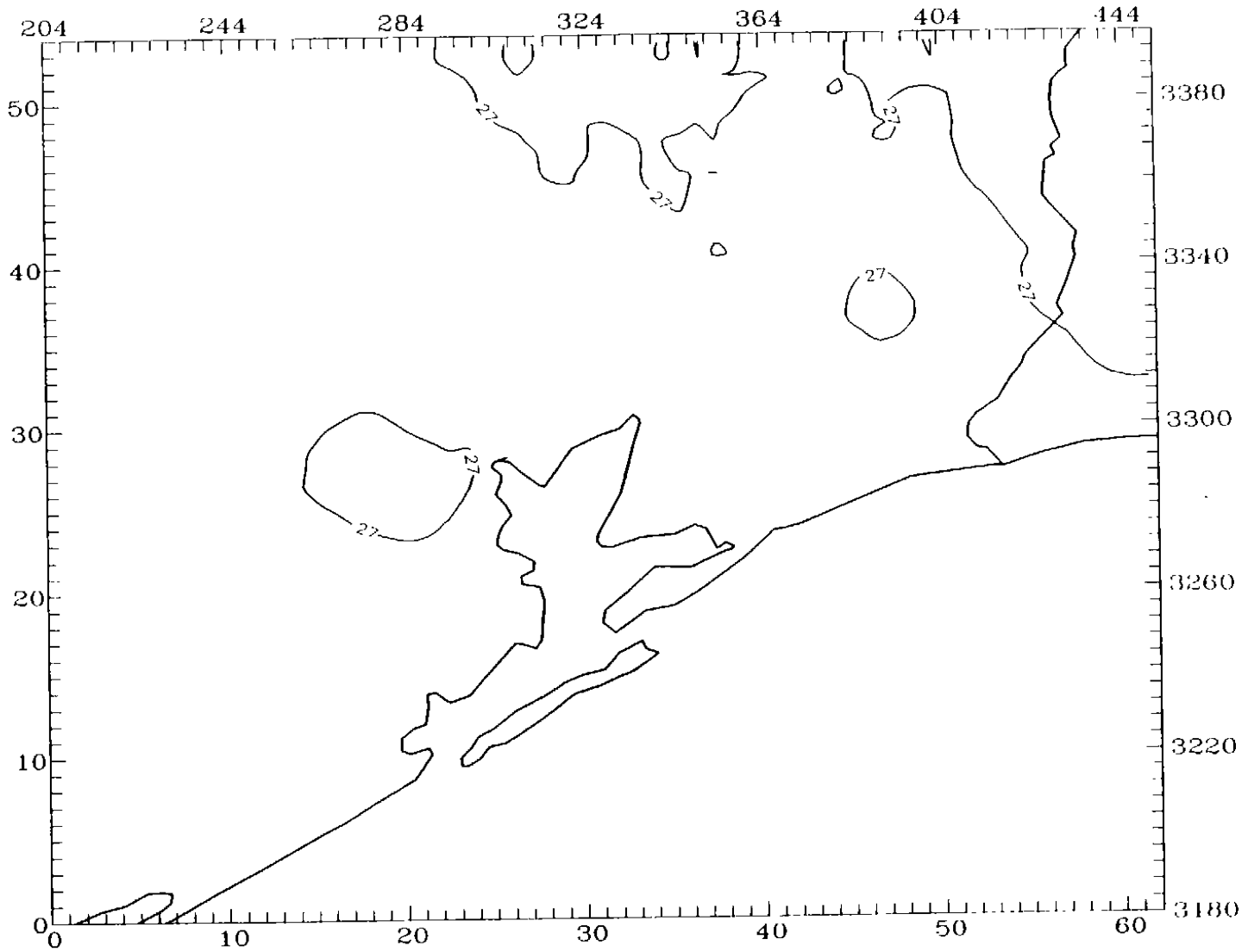

Figure 4-45a. SAIMM surface-level temperature fields (°C) for the fine-grid domain on 8 September 1993 at 0400 CST.

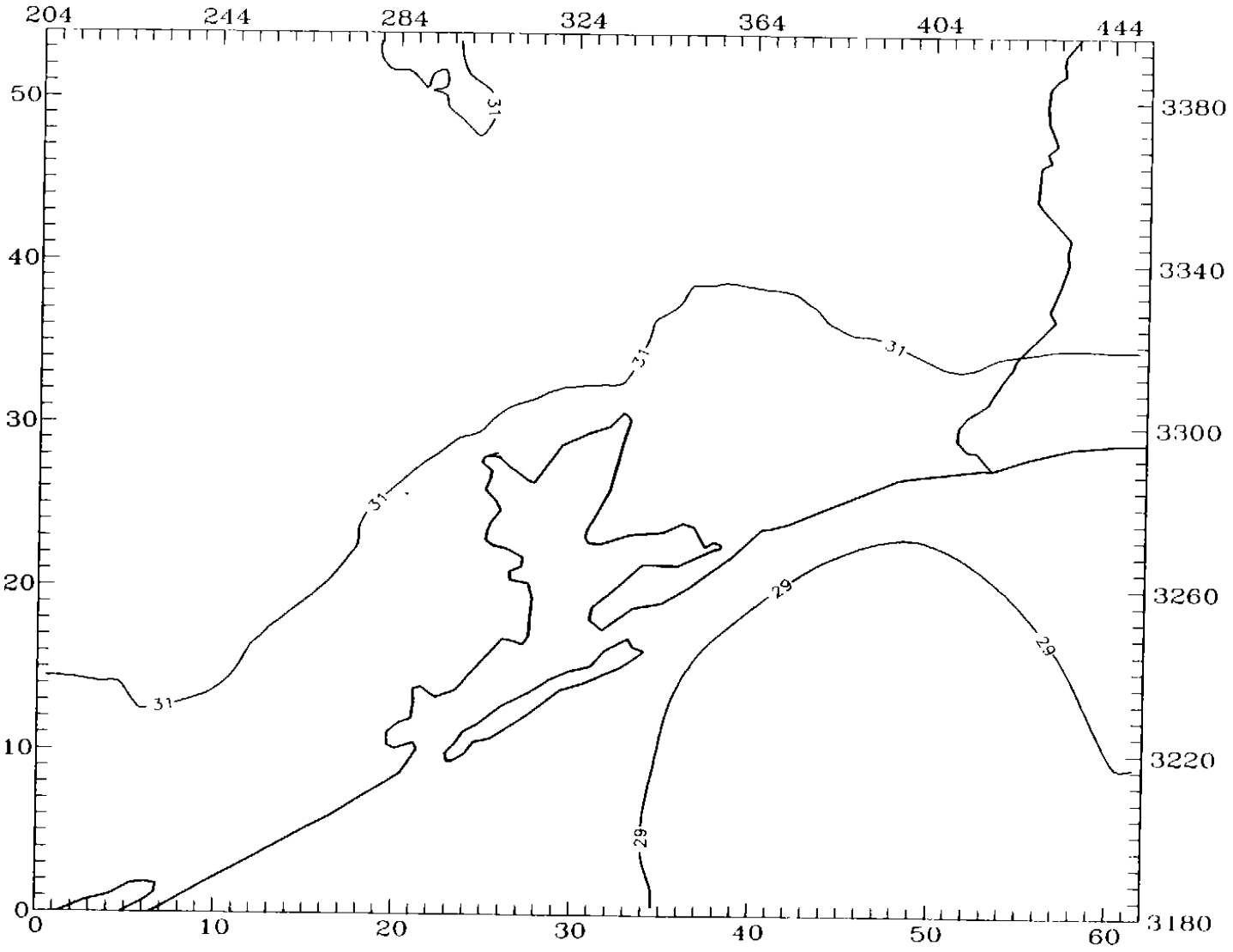

Figure 4-45b. SAIMM surface-level temperature fields (°C) for the fine-grid domain on 8 September 1993 at 1600 CST.

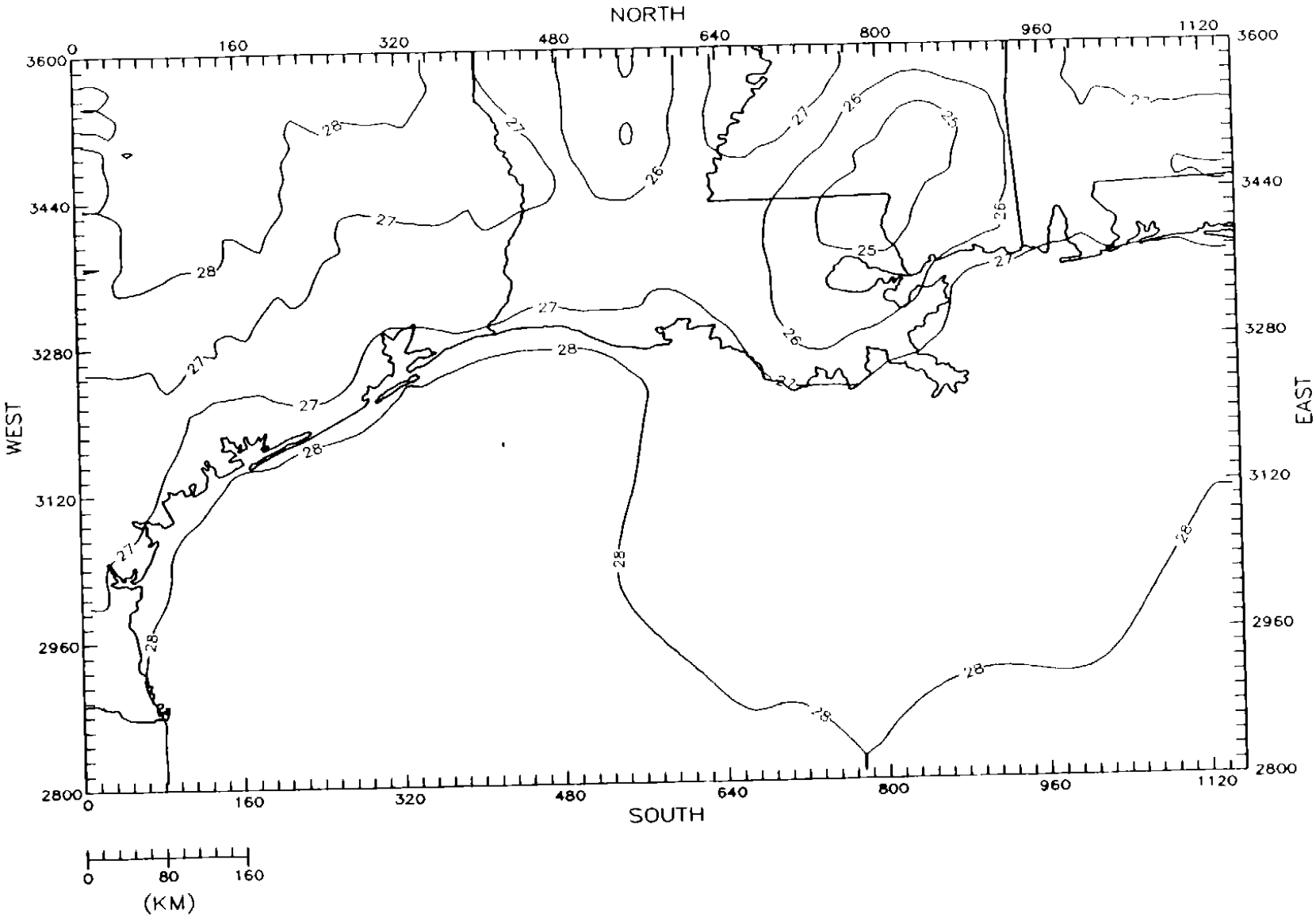

Figure 4-46a. SAIMM surface-level temperature fields (°C) for the coarse-grid domain on 9 September 1993 at 0400 CST.

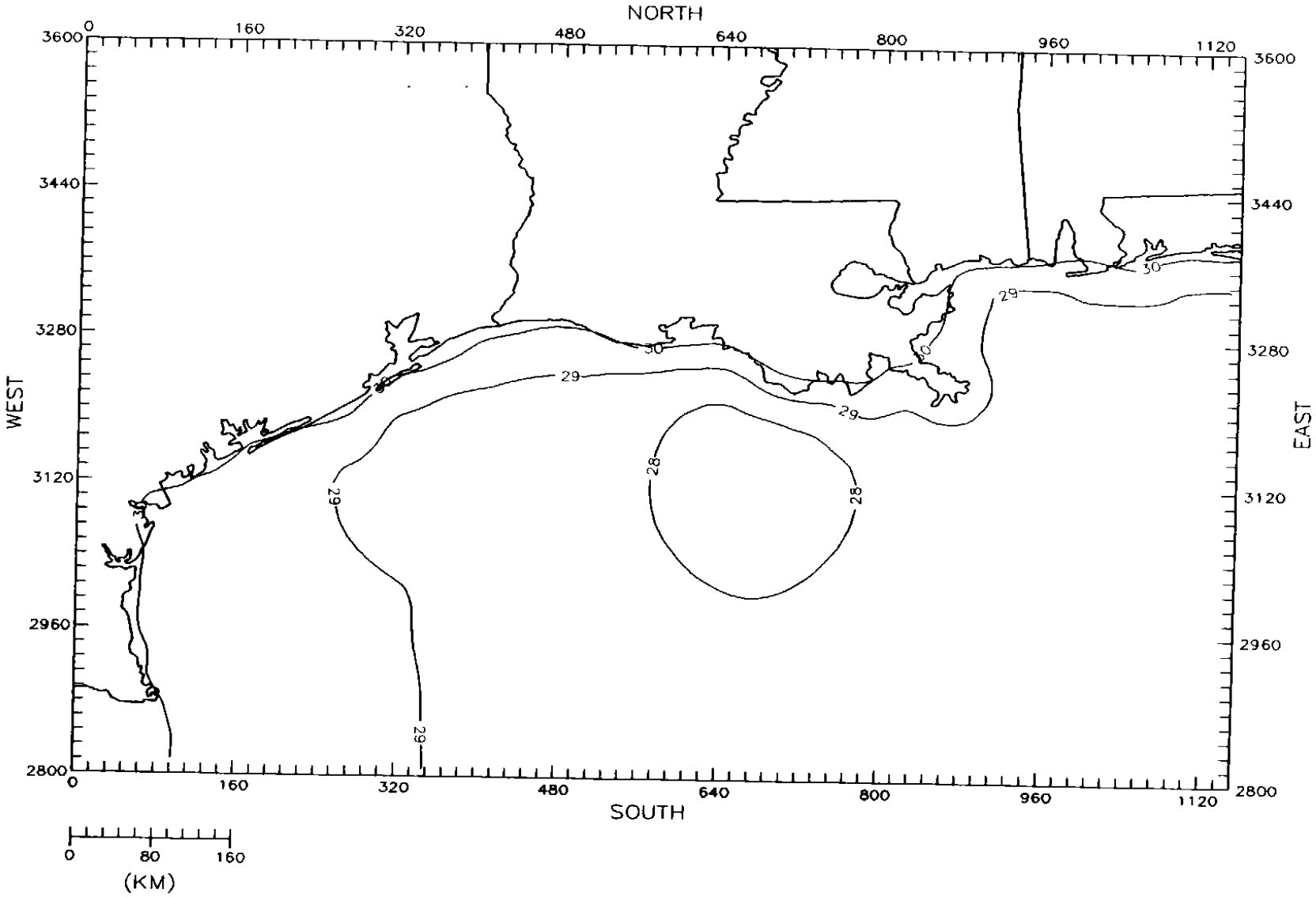

Figure 4-46b. SAIMM surface-level temperature fields (°C) for the coarse-grid domain on 9 September 1993 at 1600 CST

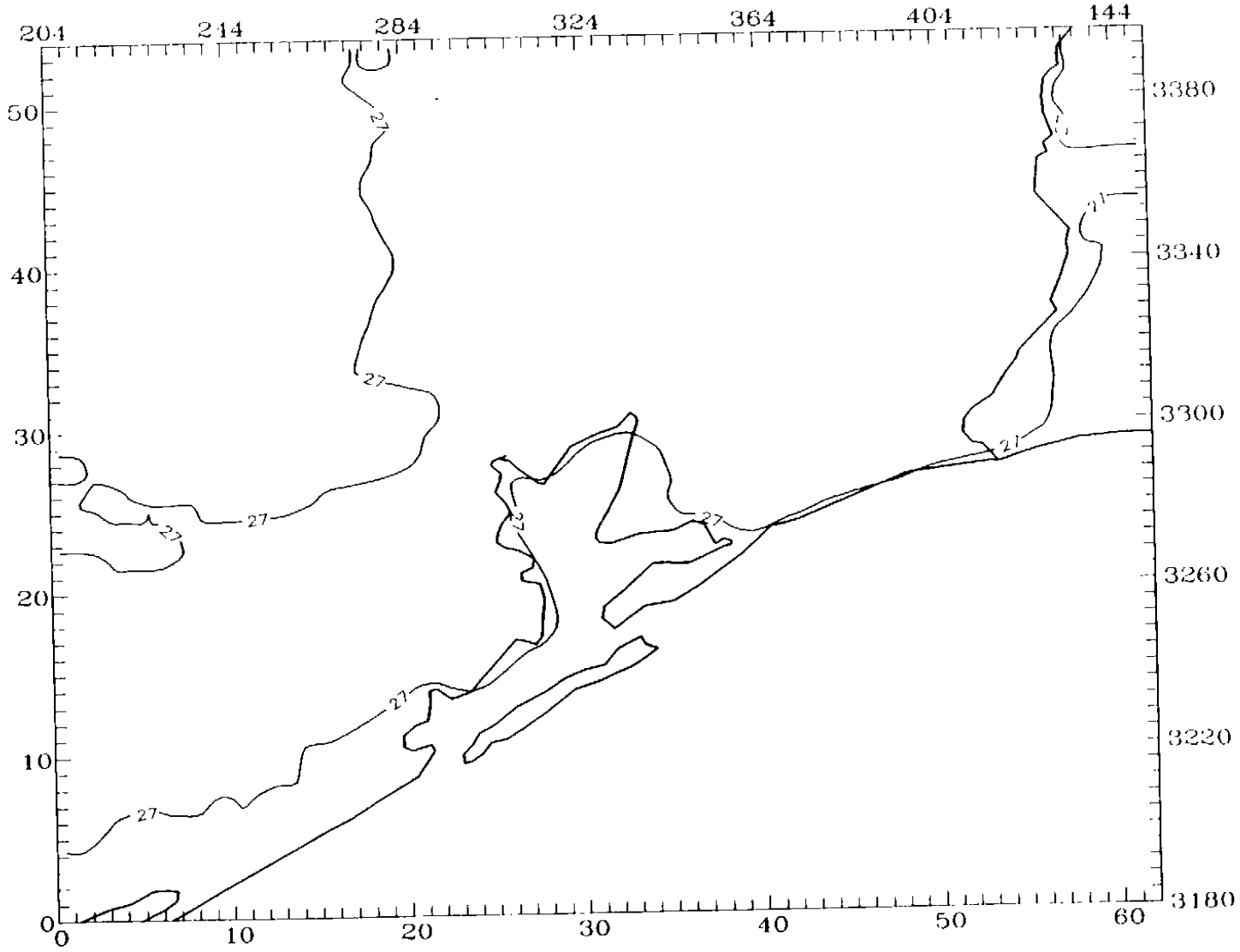

Figure 4-47a. SAIMM surface-level temperature fields (°C) for the fine-grid domain on 9 September 1993 at 0400 CST.

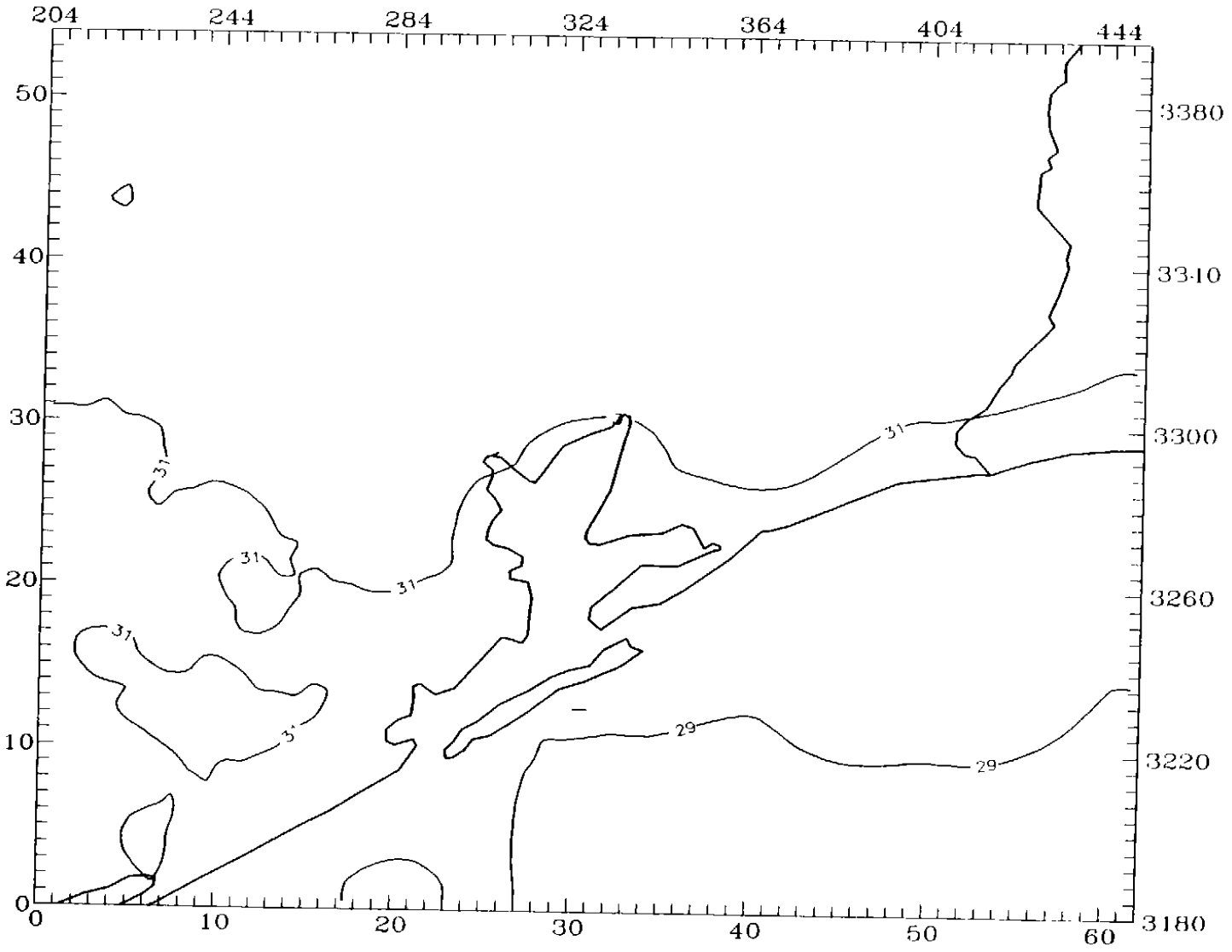

Figure 4-47b. SAIMM surface-level temperature fields (°C) for the fine-grid domain on 9 September 1993 at 1600 CST.

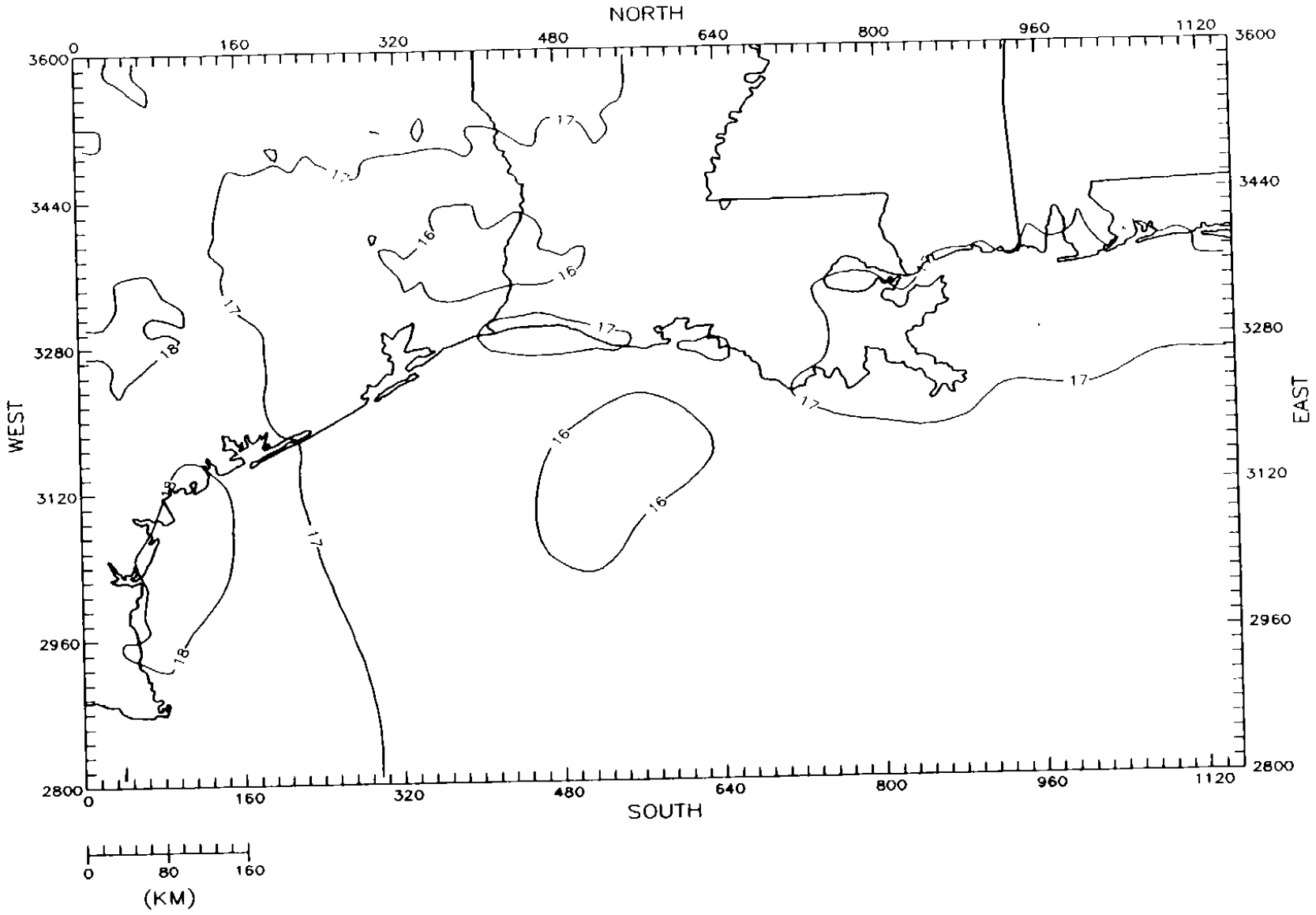

Figure 4-48a. SAIMM surface-level specific humidity fields (gkg^{-1}) for the coarse-grid domain on 8 September 1993 at 0400 CST.

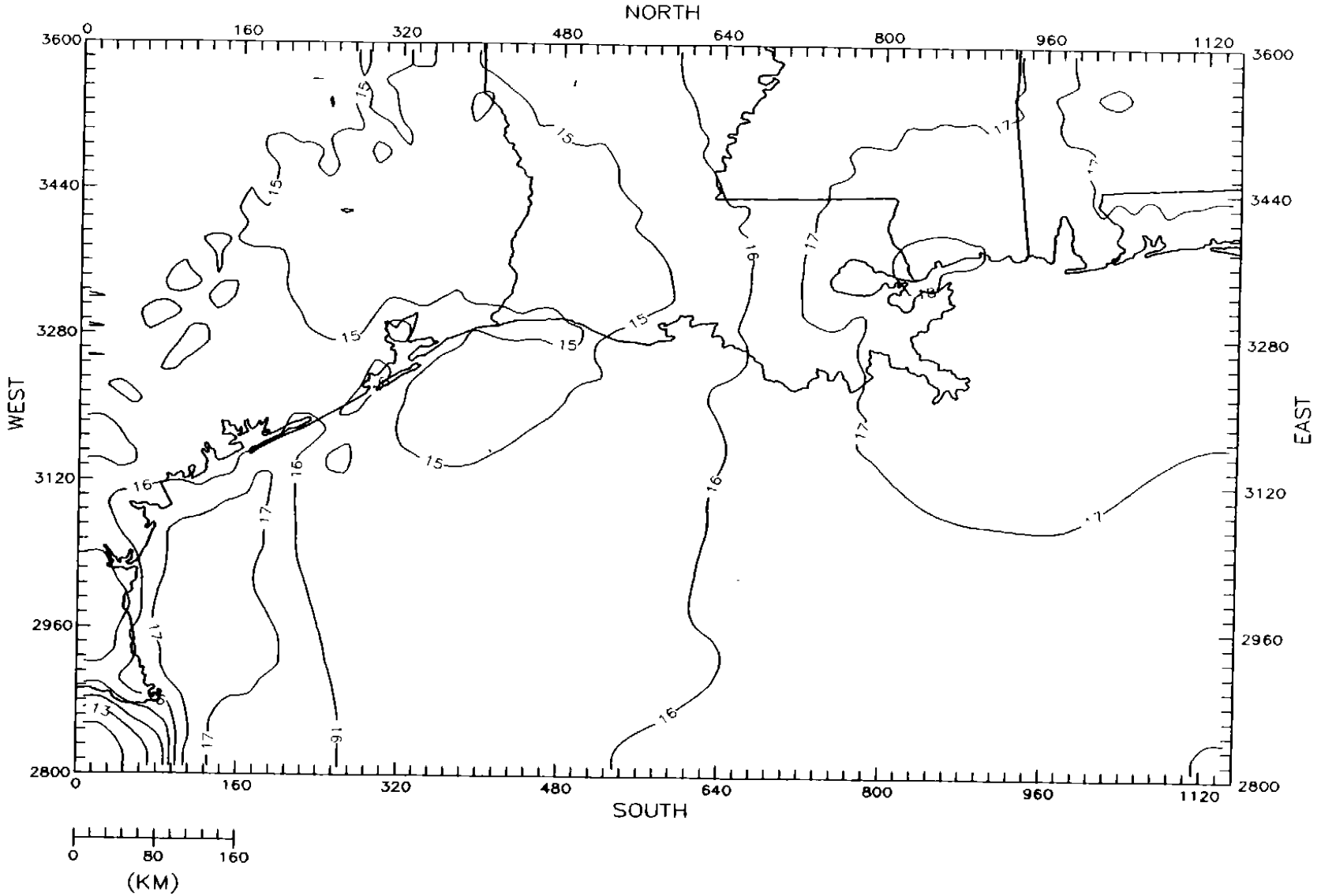

Figure 4-48b. SAIMM surface-level specific humidity fields (gkg^{-1}) for the coarse-grid domain on 8 September 1993 at 1600 CST.

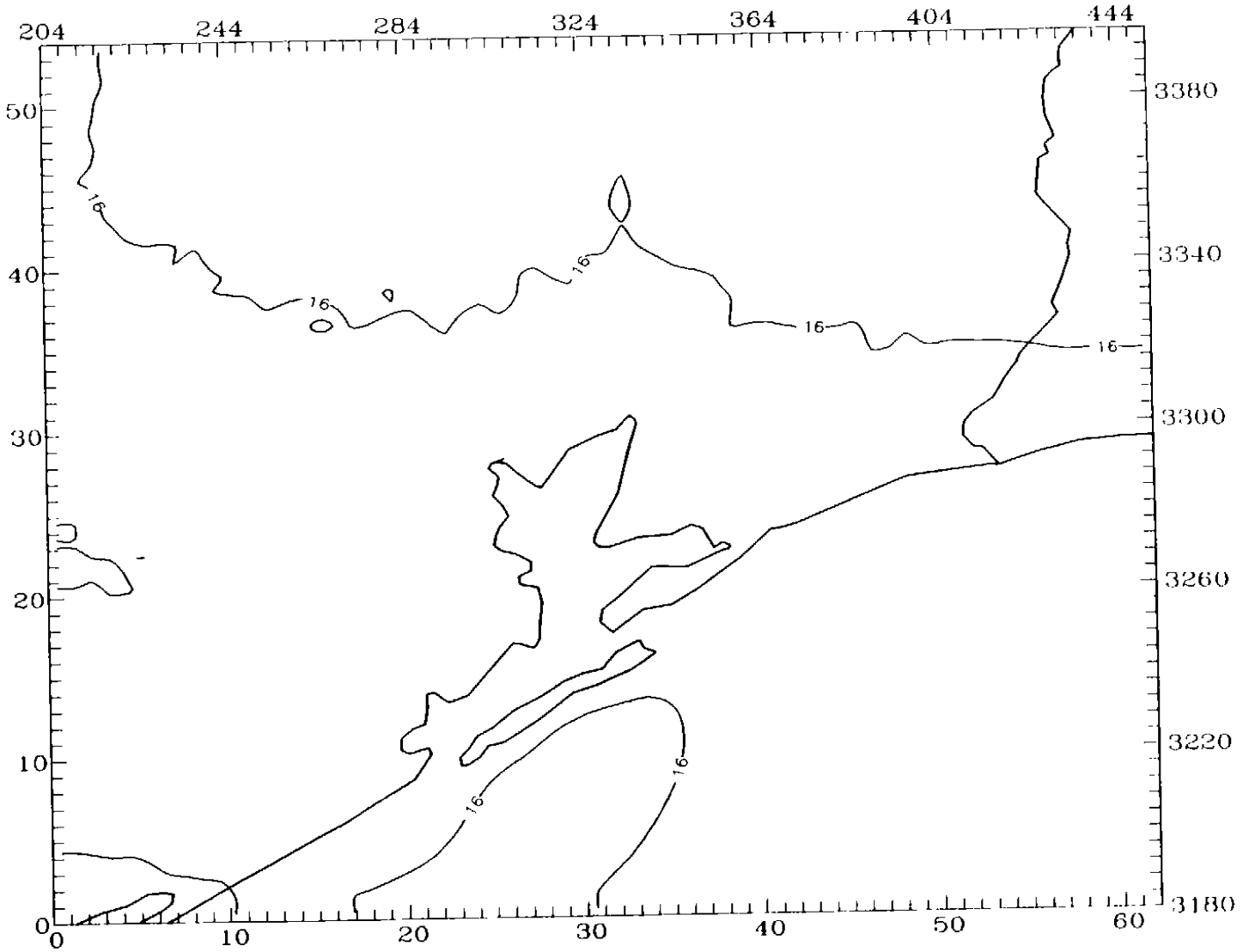

Figure 4-49a. SAIMM surface-level specific humidity fields (gkg^{-1}) for the fine-grid domain on 8 September 1993 at 0400 CST.

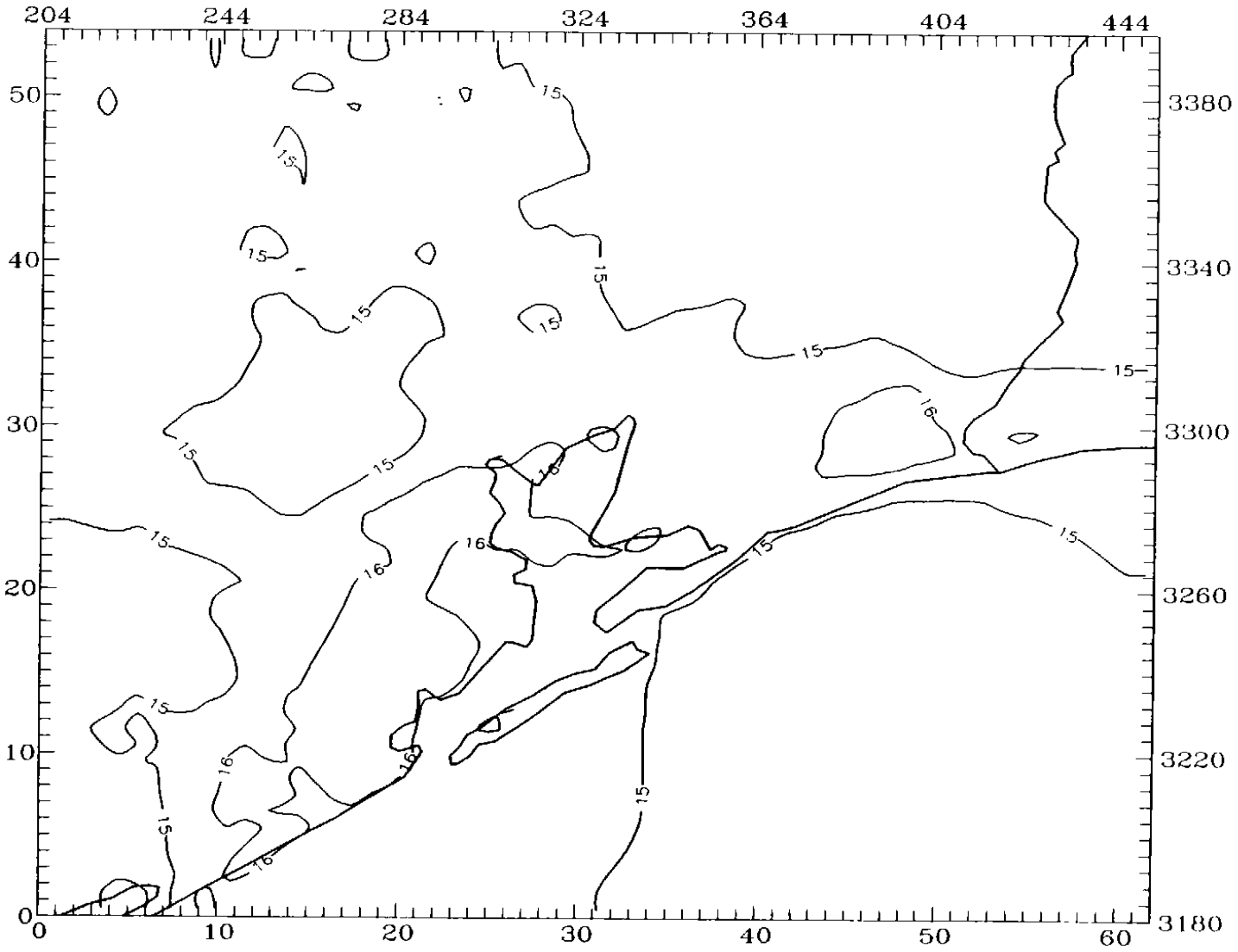

Figure 4-49b. SAIMM surface-level specific humidity fields (gkg^{-1})for the fine-grid domain on 8 September 1993 at 1600 CST.

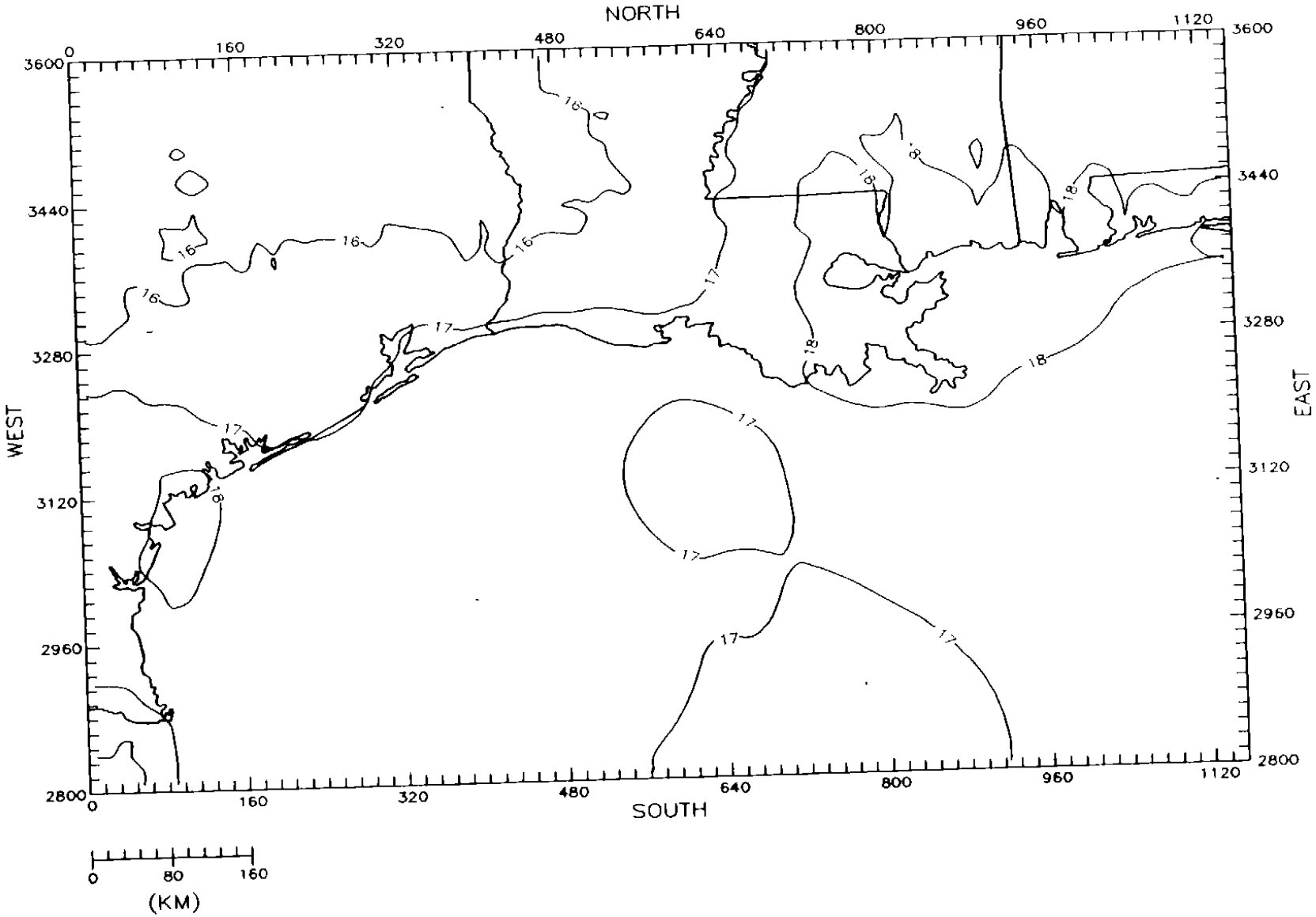

Figure 4-50a. SAIMM surface-level specific humidity fields (gkg^{-1}) for the coarse-grid domain on 9 September 1993 at 0400 CST.

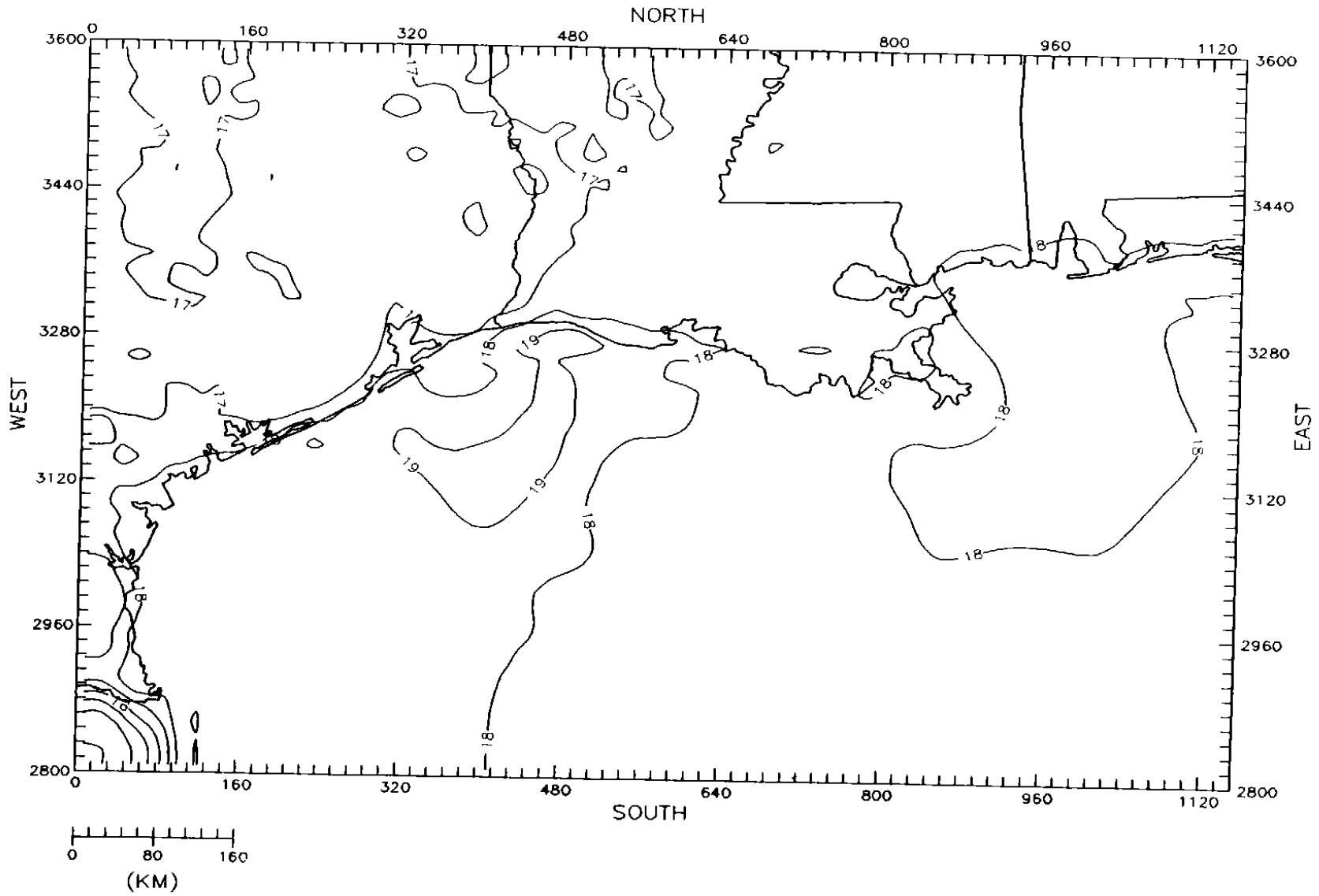

Figure 4-50b. SAIMM surface-level specific humidity fields (gkg^{-1}) for the coarse-grid domain on 9 September 1993 at 1600 CST.

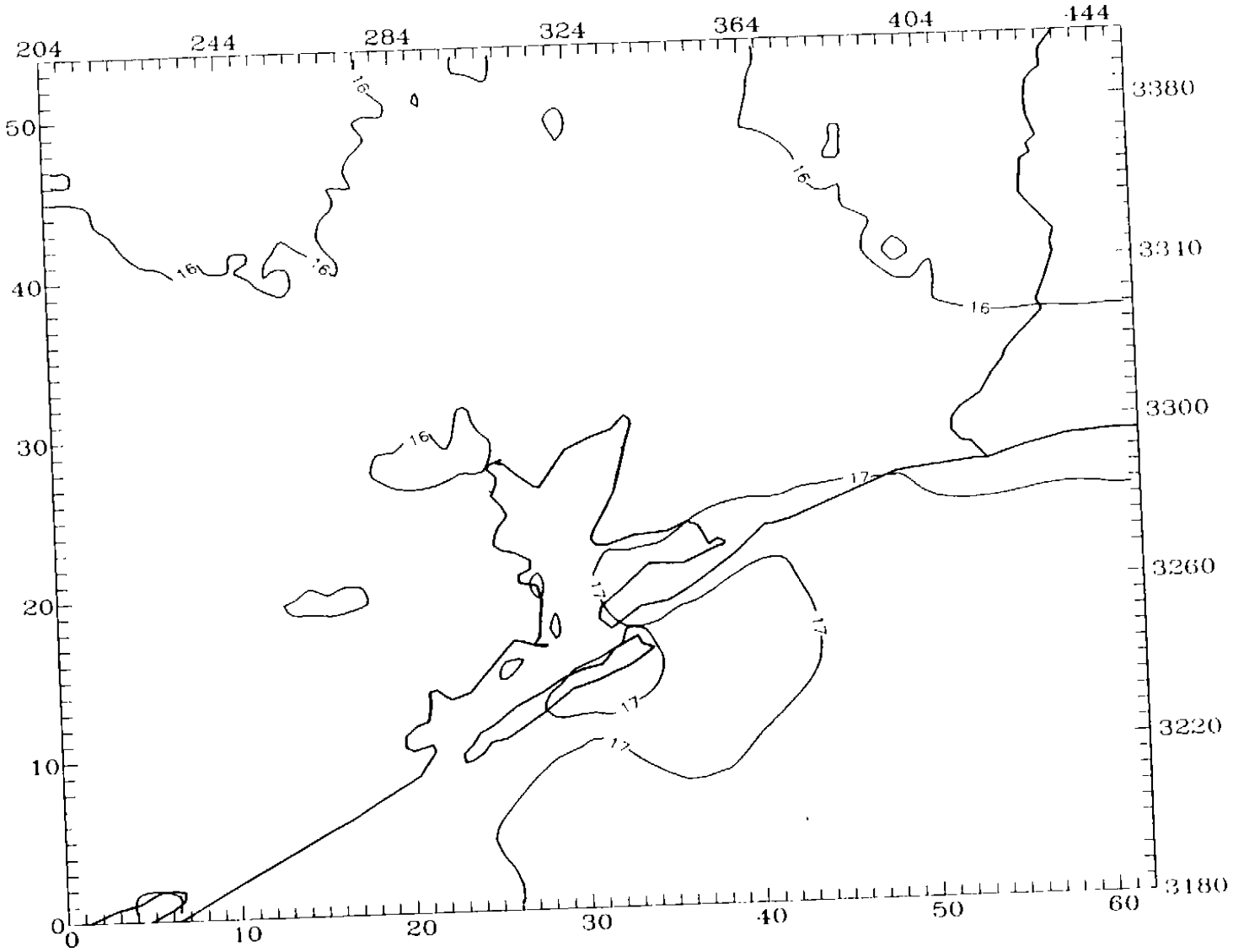

Figure 4-51a. SAIMM surface-level specific humidity fields (gkg^{-1}) for the fine-grid domain on 9 September 1993 at 0400 CST.

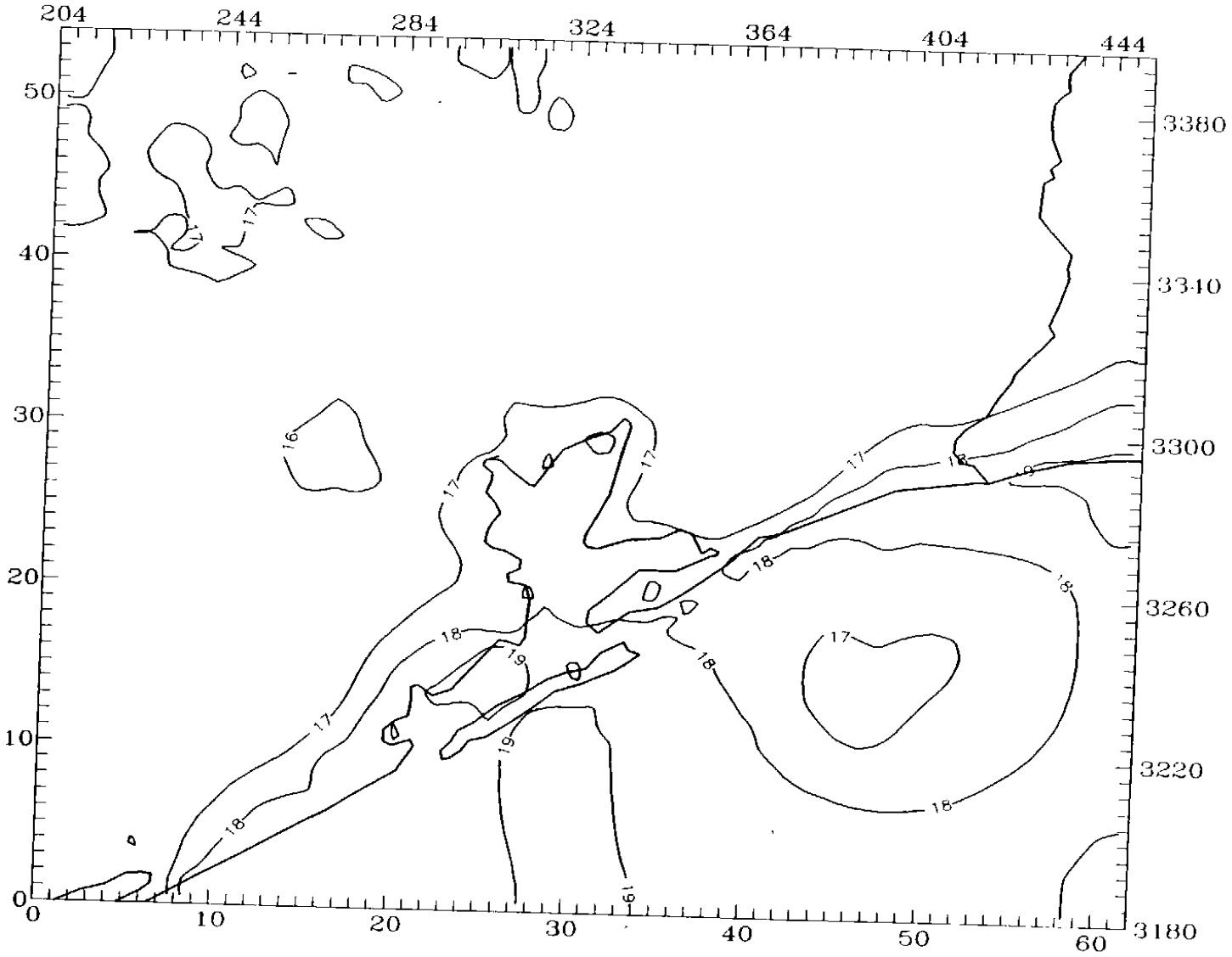

Figure 4-51b. SAIMM surface-level specific humidity fields (gkg^{-1})for the fine-grid domain on 9 September 1993 at 1600 CST.

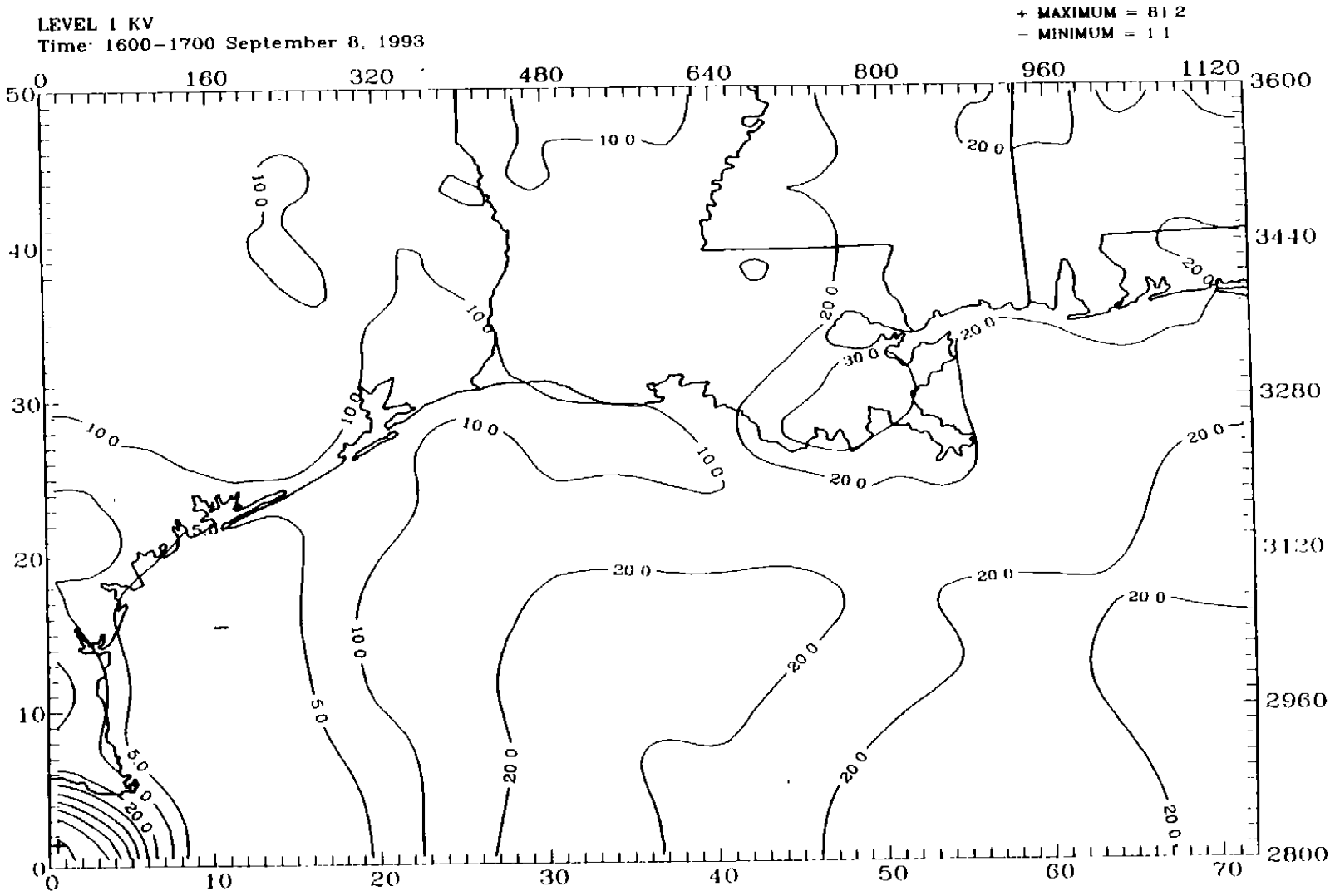

Figure 4-52a. UAM-V-ready vertical turbulent exchange coefficients (m^2s^{-1}) for the coarse-grid domain on 8 September 1993 at 1600 CST. Interface between UAM-V layers 1 and 2.

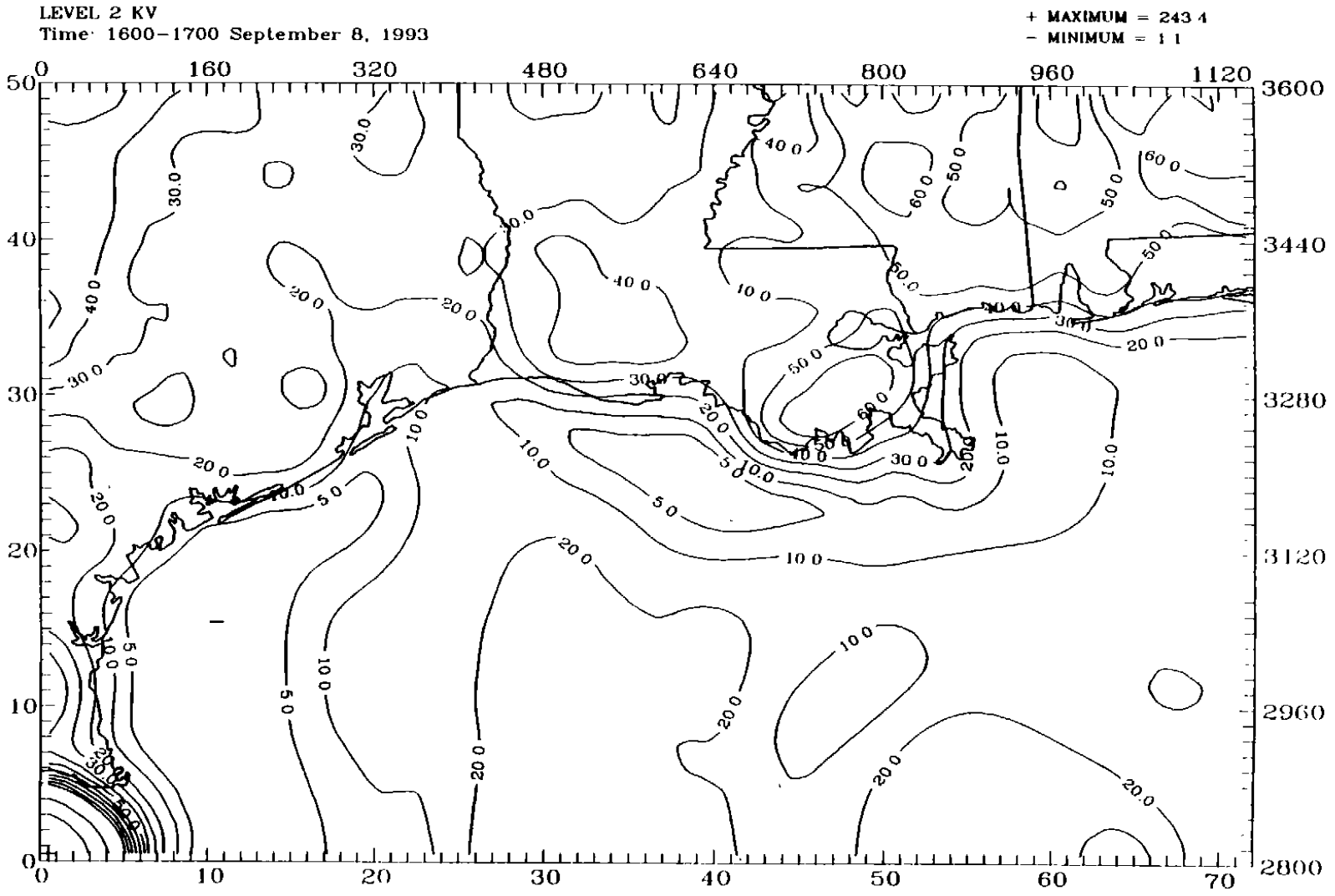

Figure 4-52b. UAM-V-ready vertical turbulent exchange coefficients (m^2s^{-1}) for the coarse-grid domain on 8 September 1993 at 1600 CST. Interface between UAM-V layers 2 and 3.

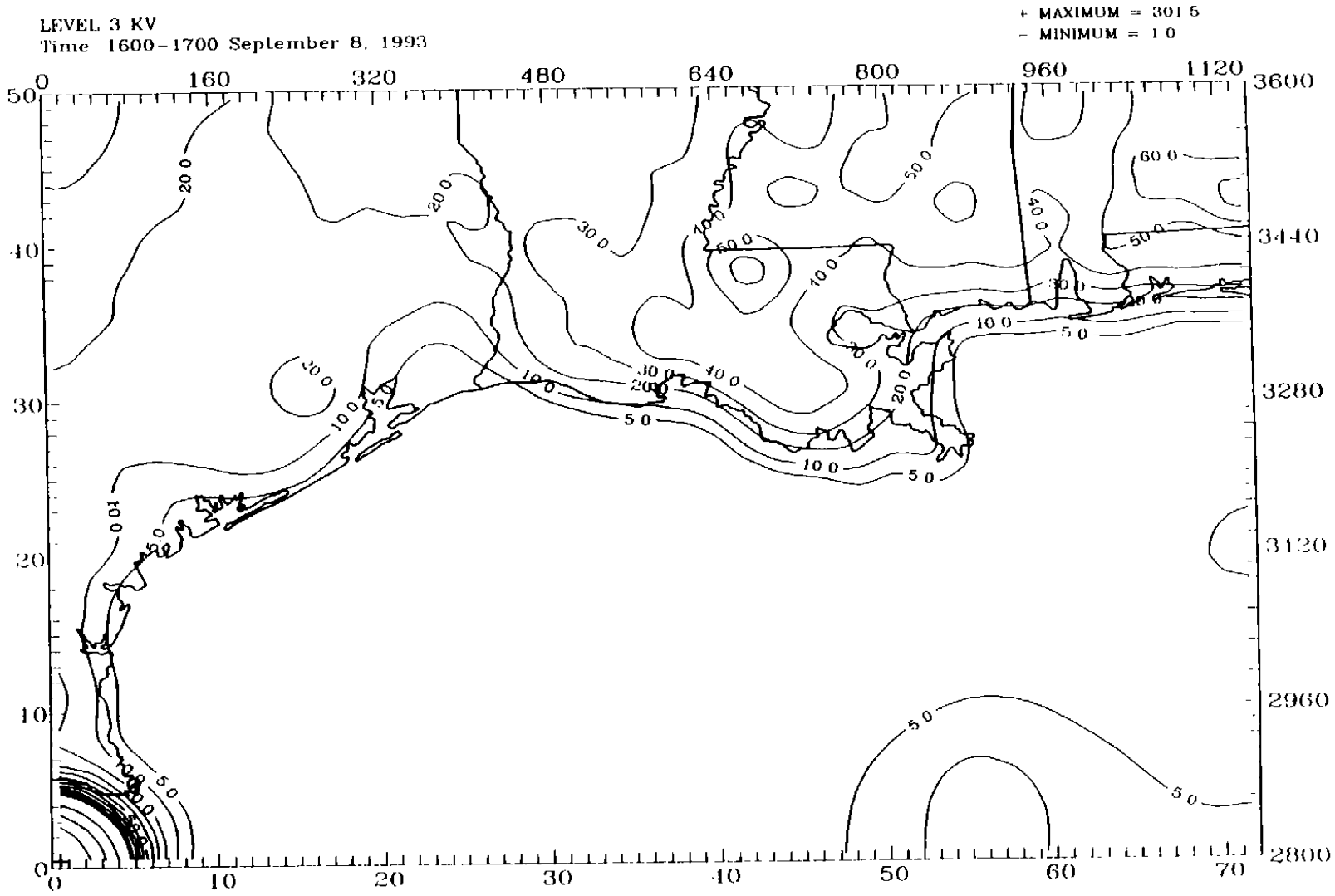

Figure 4-52c. UAM-V-ready vertical turbulent exchange coefficients (m^2s^{-1}) for the coarse-grid domain on 8 September 1993 at 1600 CST. Interface between UAM-V layers 3 and 4.

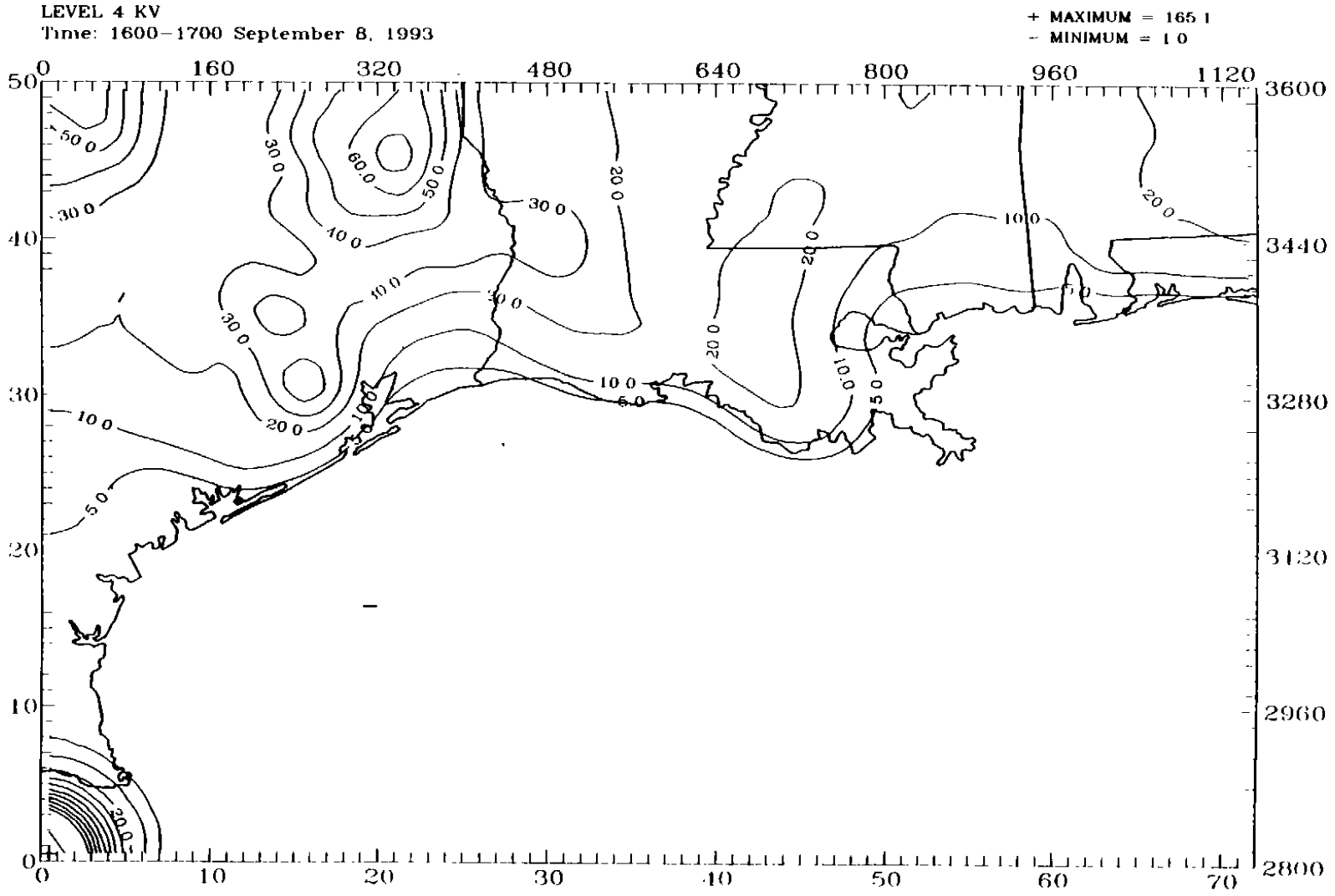

Figure 4-52d. UAM-V-ready vertical turbulent exchange coefficients (m^2s^{-1}) for the coarse-grid domain on 8 September 1993 at 1600 CST. Interface between UAM-V layers 4 and 5.

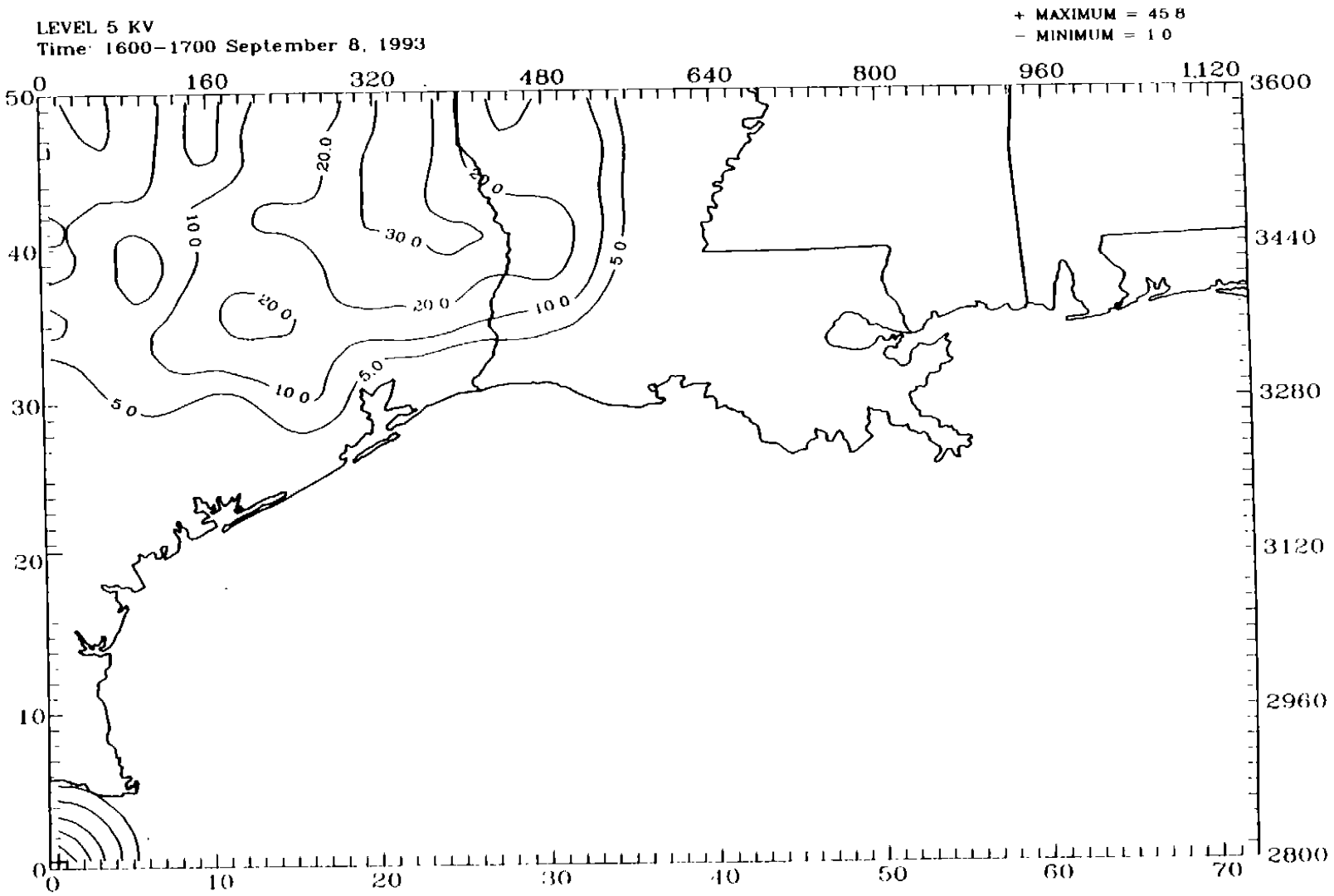

Figure 4-52e. UAM-V-ready vertical turbulent exchange coefficients (m^2s^{-1}) for the coarse-grid domain on 8 September 1993 at 1600 CST. Interface between UAM-V layers 5 and 6.

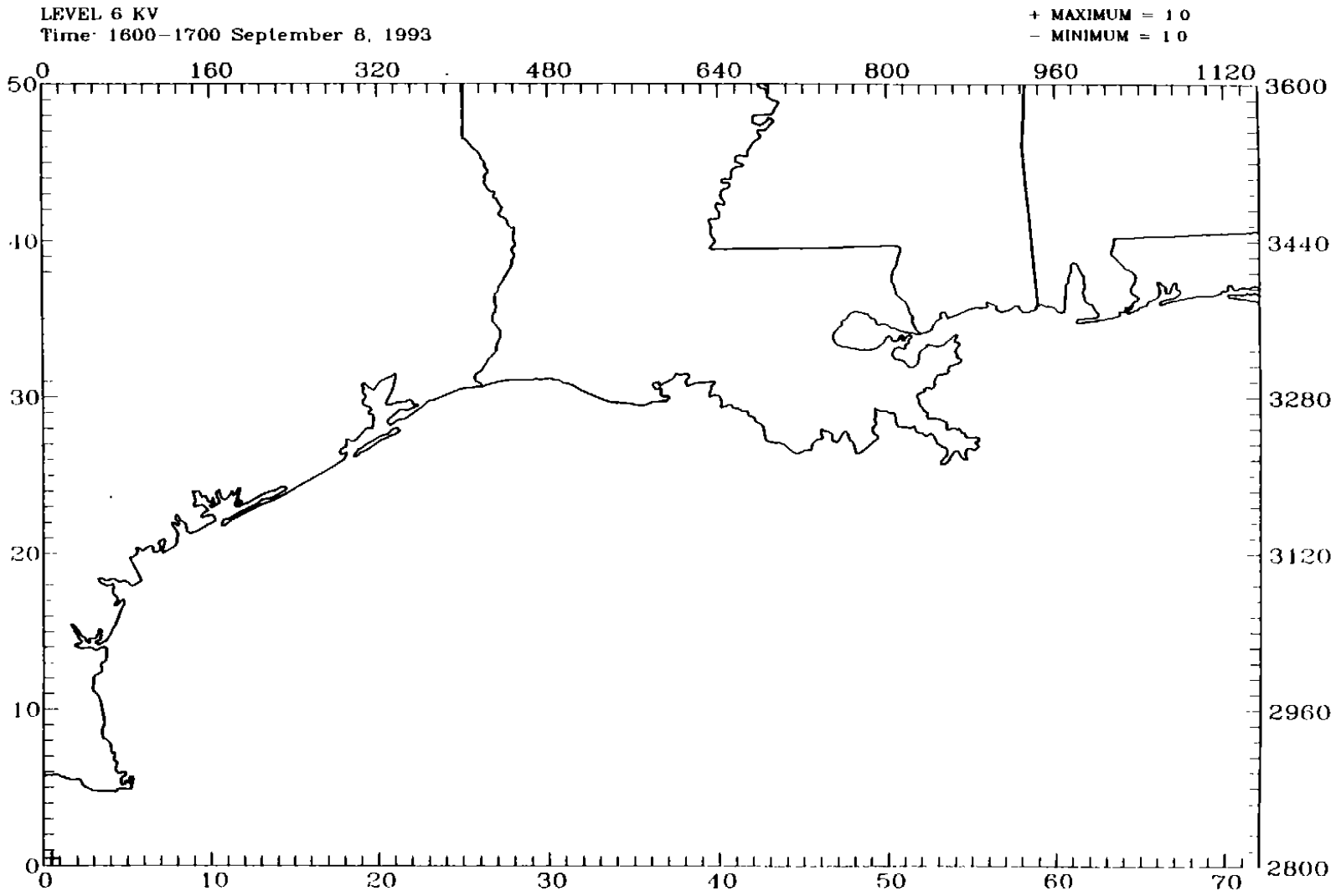

Figure 4-52f. UAM-V-ready vertical turbulent exchange coefficients (m^2s^{-1}) for the coarse-grid domain on 8 September 1993 at 1600 CST. Interface between UAM-V layers 6 and 7.

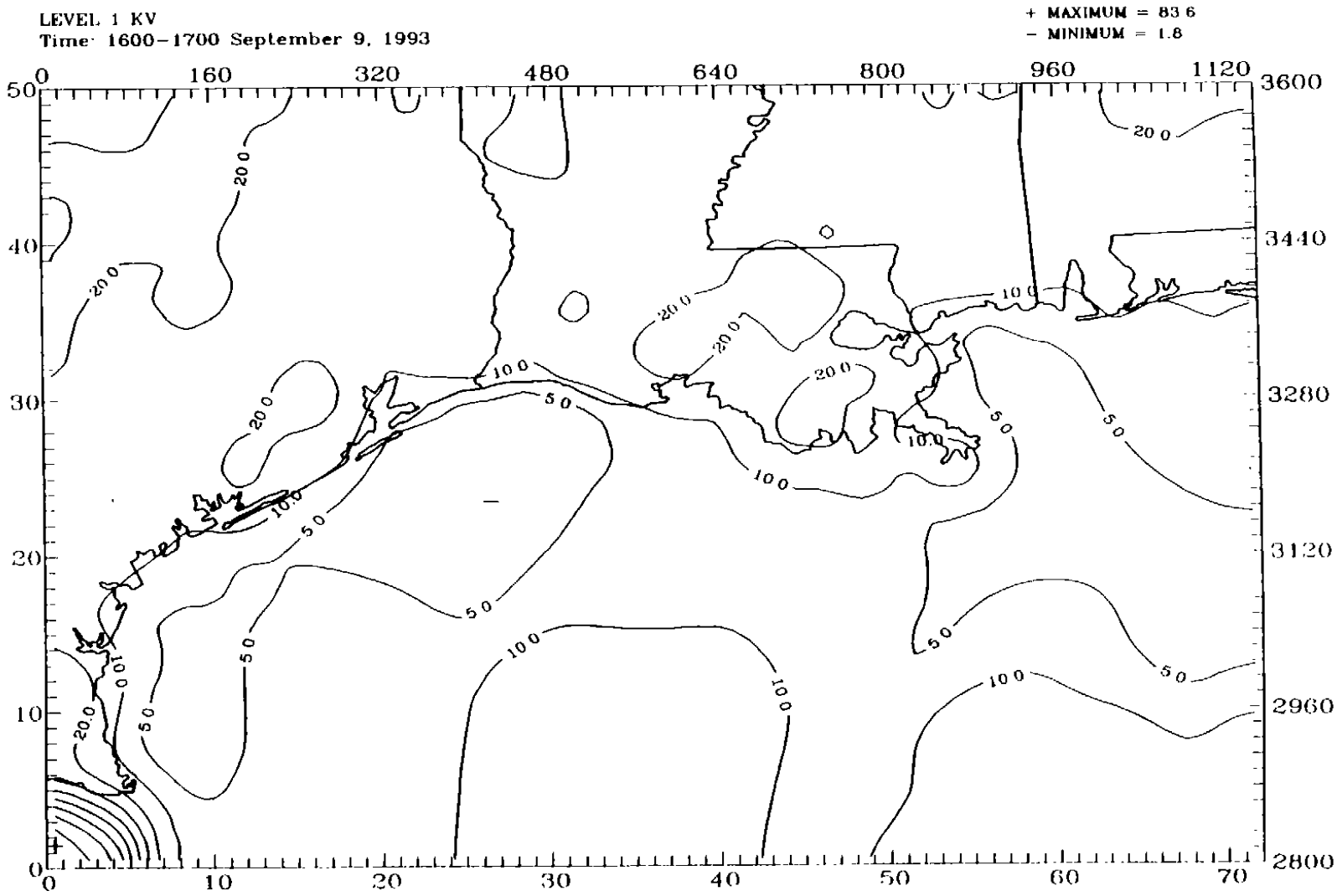

Figure 4-53a. UAM-V-ready vertical turbulent exchange coefficients (m^2s^{-1}) for the coarse-grid domain on 9 September 1993 at 1600 CST. Interface between UAM-V layers 1 and 2.

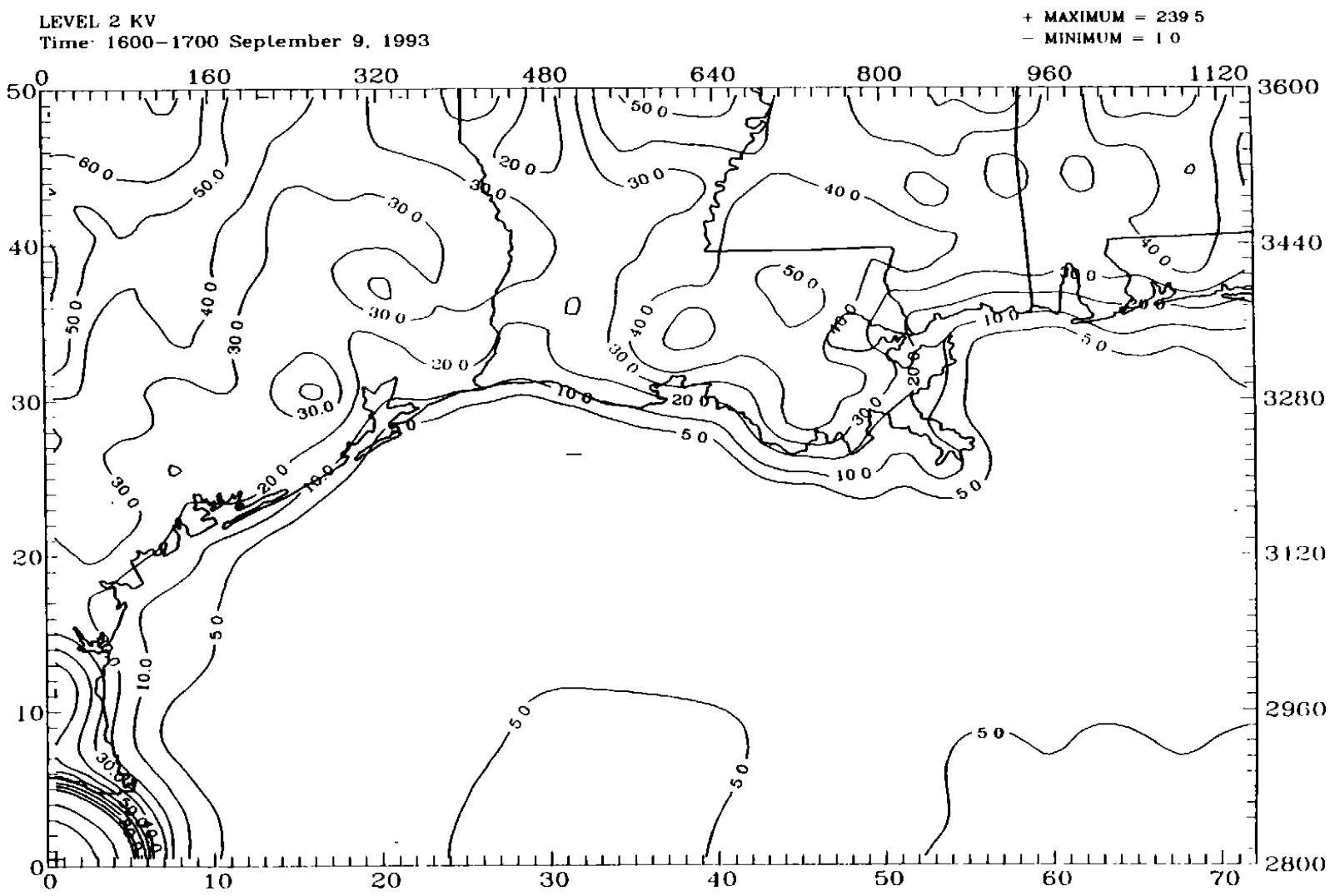

Figure 4-53b. UAM-V-ready vertical turbulent exchange coefficients (m^2s^{-1}) for the coarse-grid domain on 9 September 1993 at 1600 CST. Interface between UAM-V layers 2 and 3.

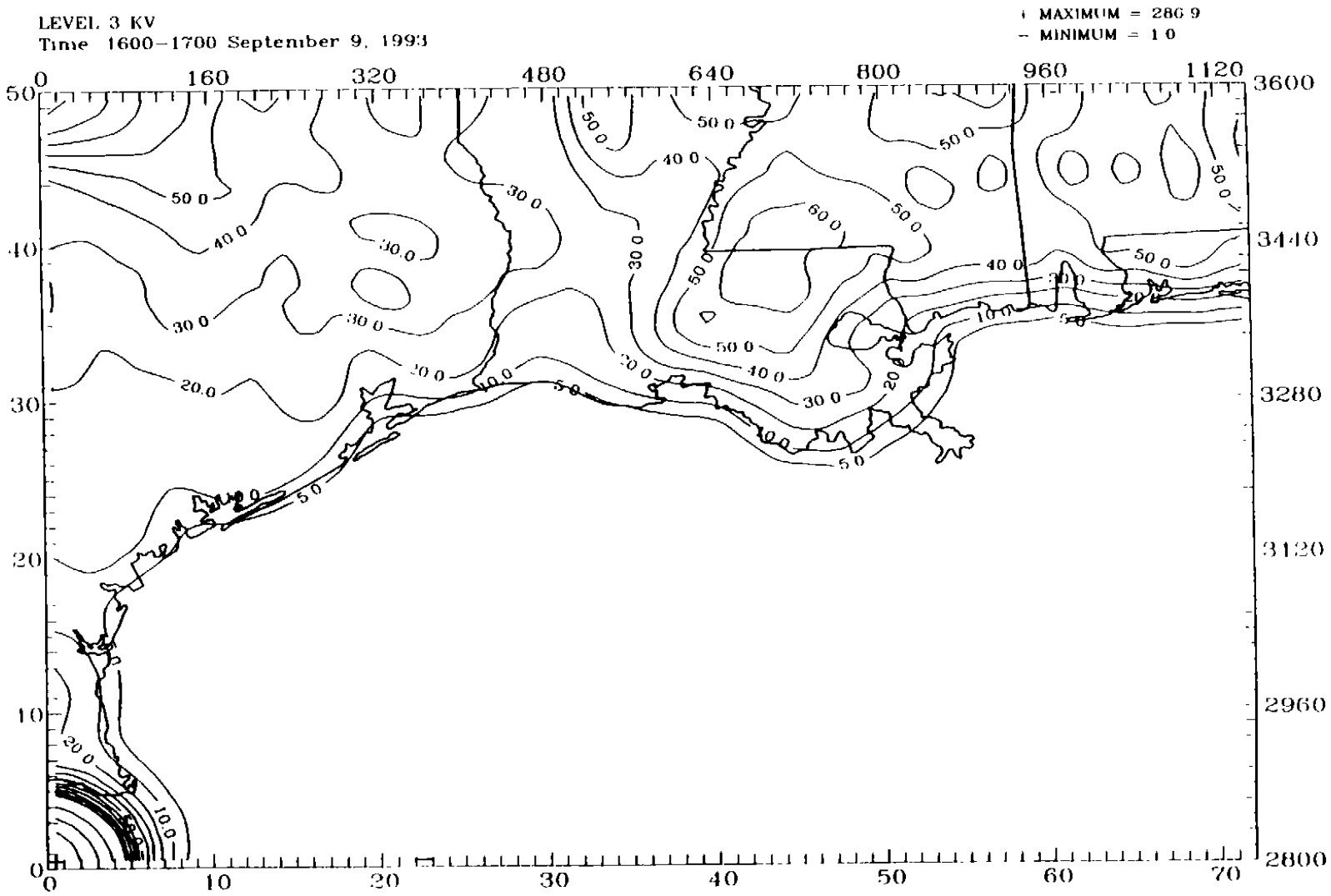

Figure 4-53c. UAM-V-ready vertical turbulent exchange coefficients (m^2s^{-1}) for the coarse-grid domain on 9 September 1993 at 1600 CST. Interface between UAM-V layers 3 and 4.

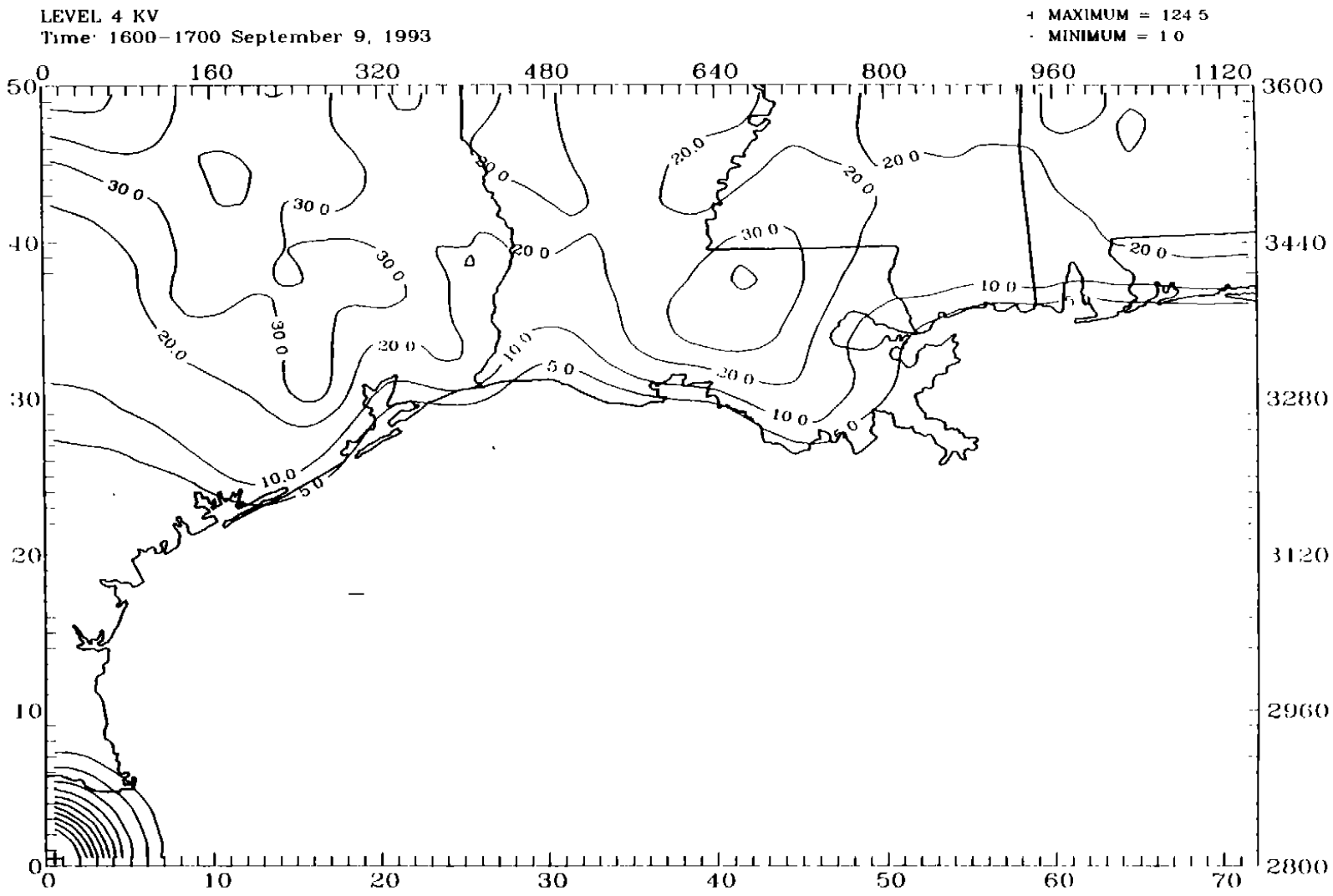

Figure 4-53d. UAM-V-ready vertical turbulent exchange coefficients (m^2s^{-1}) for the coarse-grid domain on 9 September 1993 at 1600 CST. Interface between UAM-V layers 4 and 5.

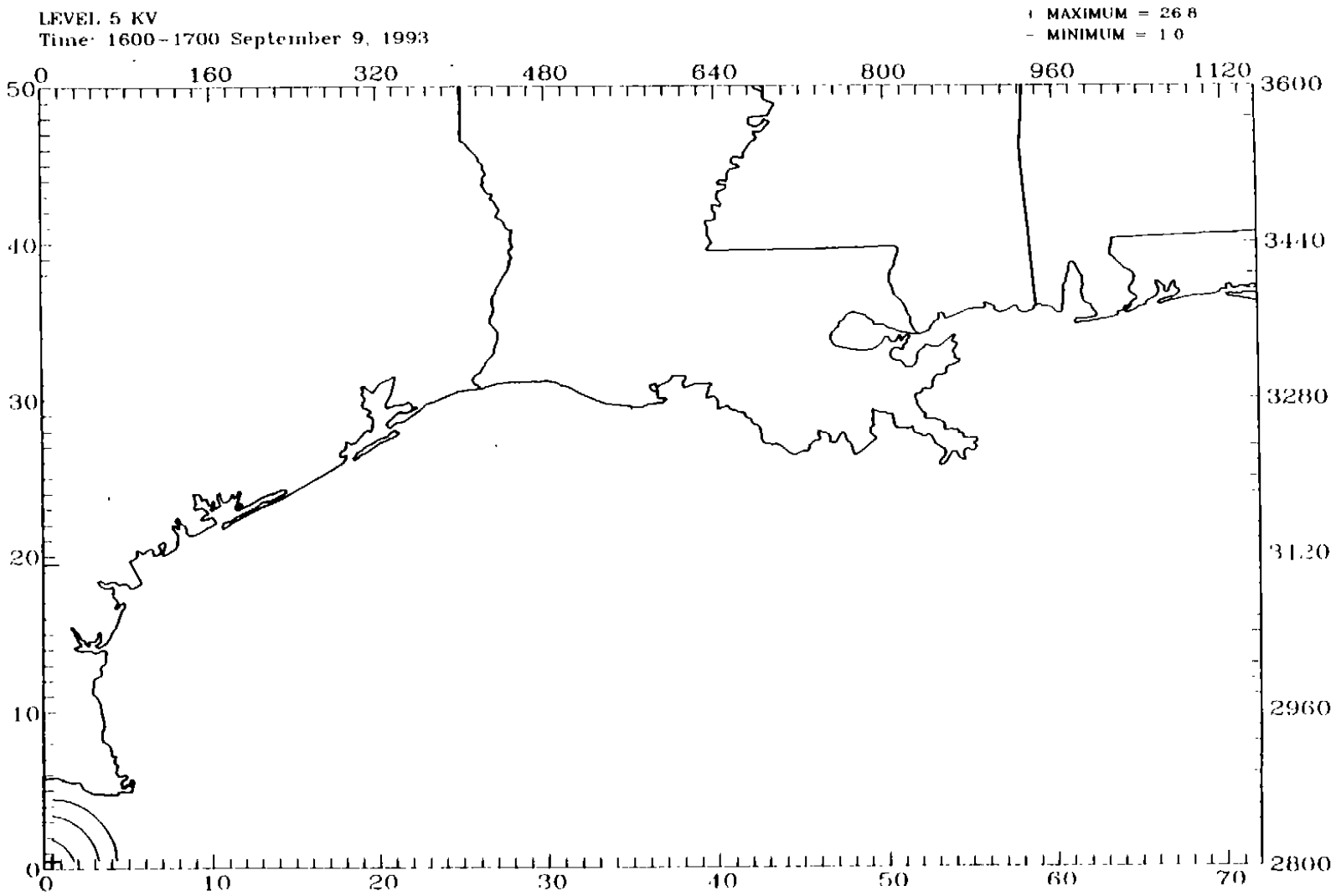

Figure 4-53e. UAM-V-ready vertical turbulent exchange coefficients (m^2s^{-1}) for the coarse-grid domain on 9 September 1993 at 1600 CST. Interface between UAM-V layers 5 and 6.

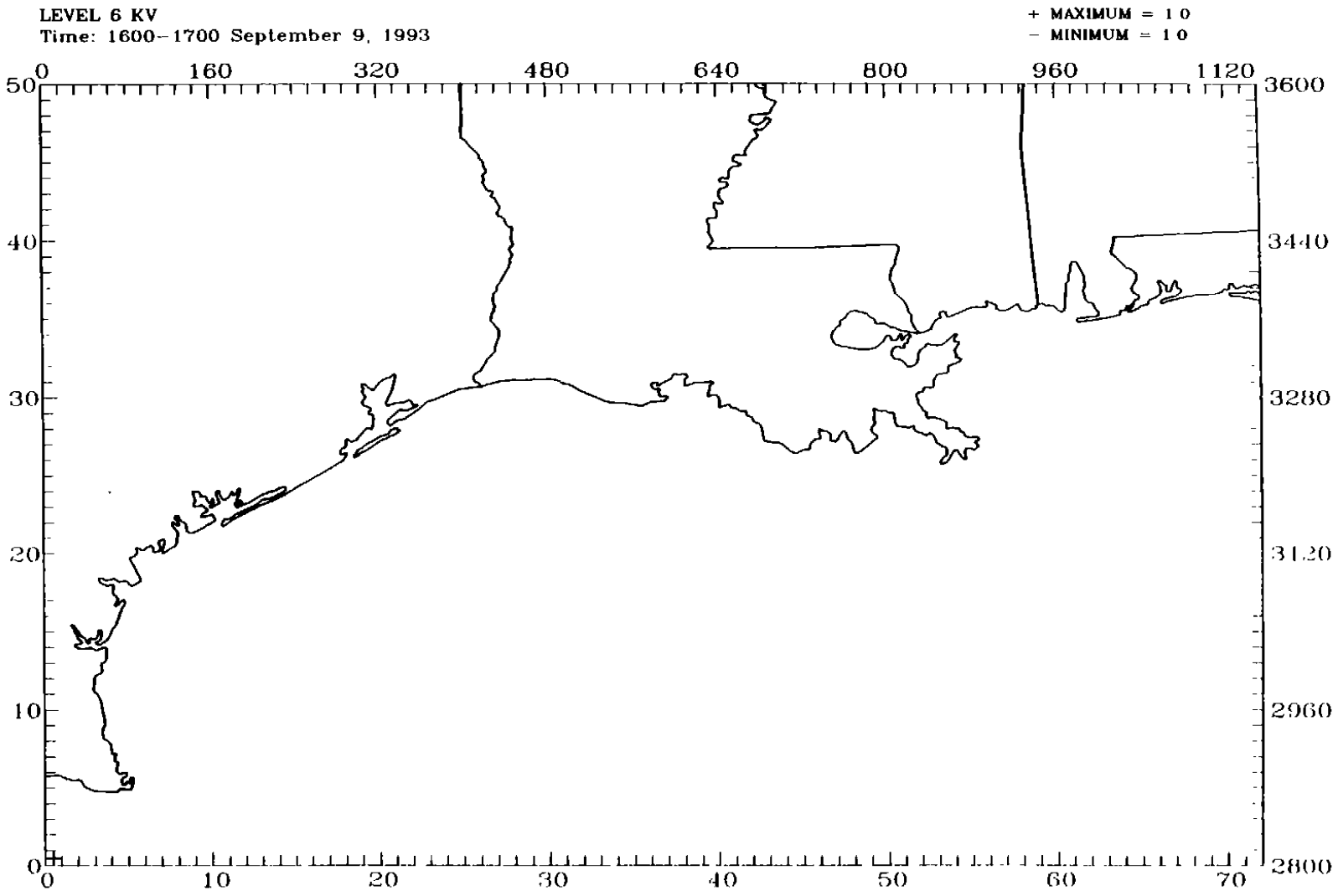

Figure 4-53f. UAM-V-ready vertical turbulent exchange coefficients (m^2s^{-1}) for the coarse-grid domain on 9 September 1993 at 1600 CST. Interface between UAM-V layers 6 and 7.

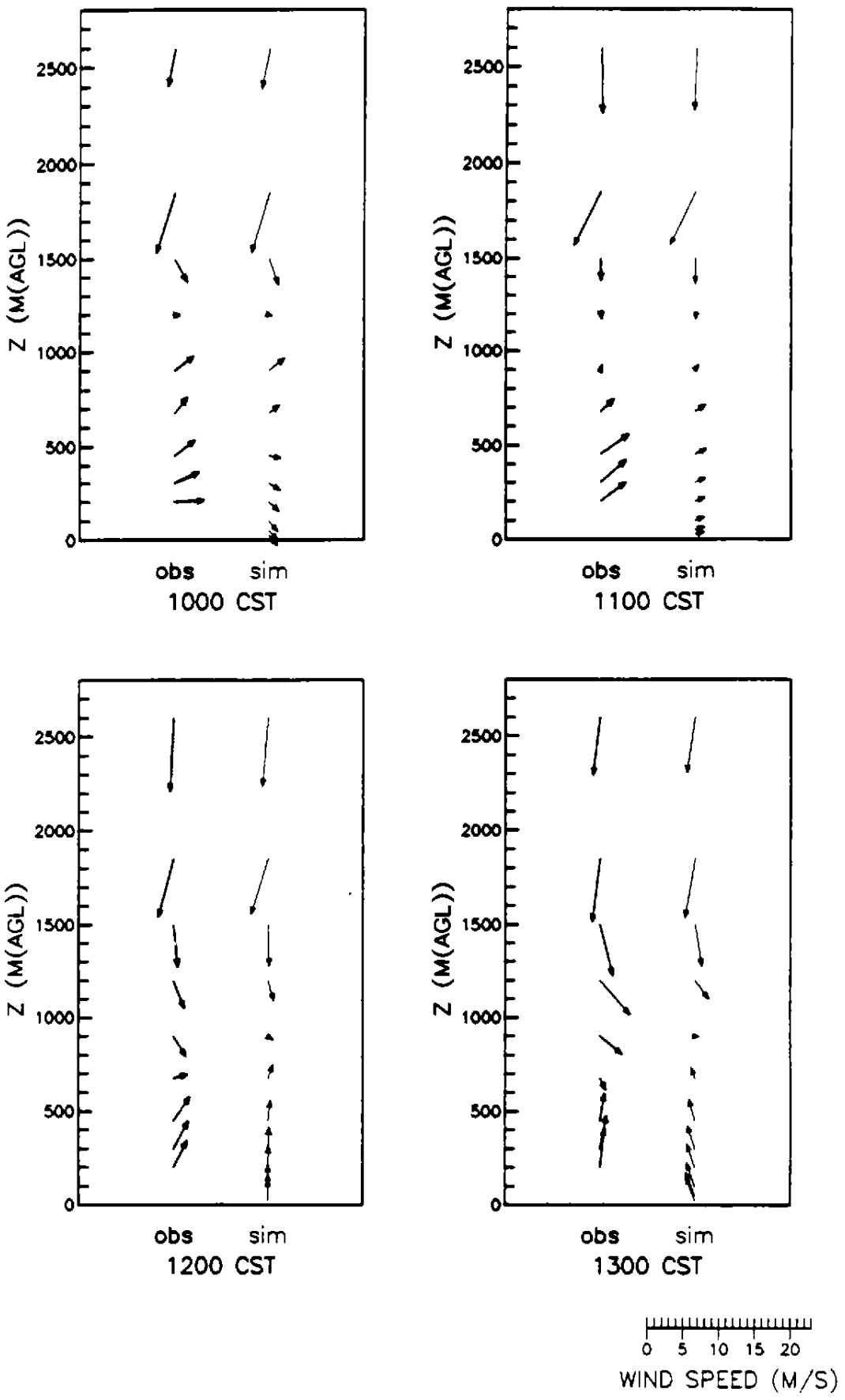

Figure 4-54a. Comparison of midday observed and simulated wind profiles for Galveston (GAL) on 8 September 1993.

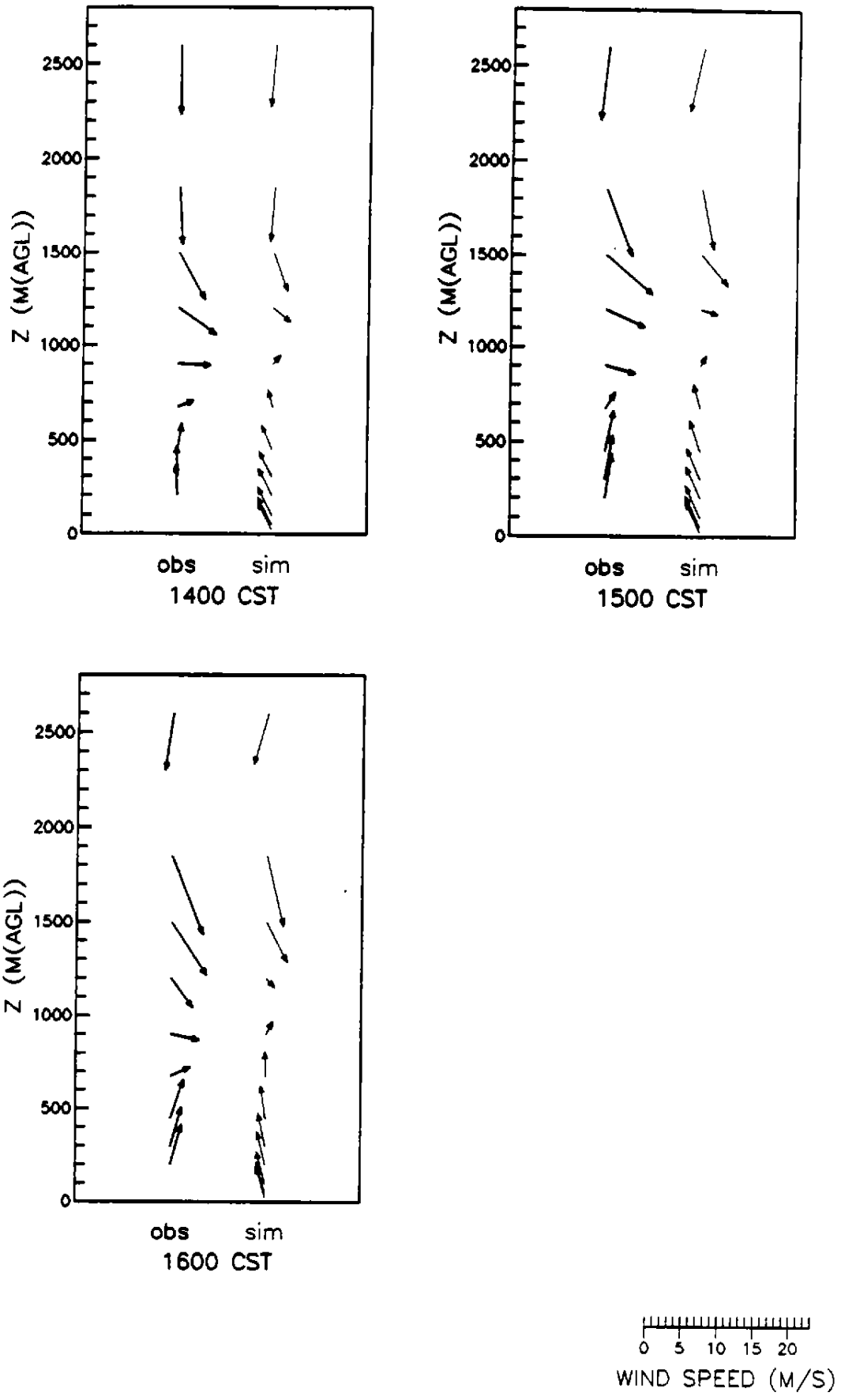

Figure 4-54b. Comparison of midday observed and simulated wind profiles for Galveston (GAL) on 8 September 1993.

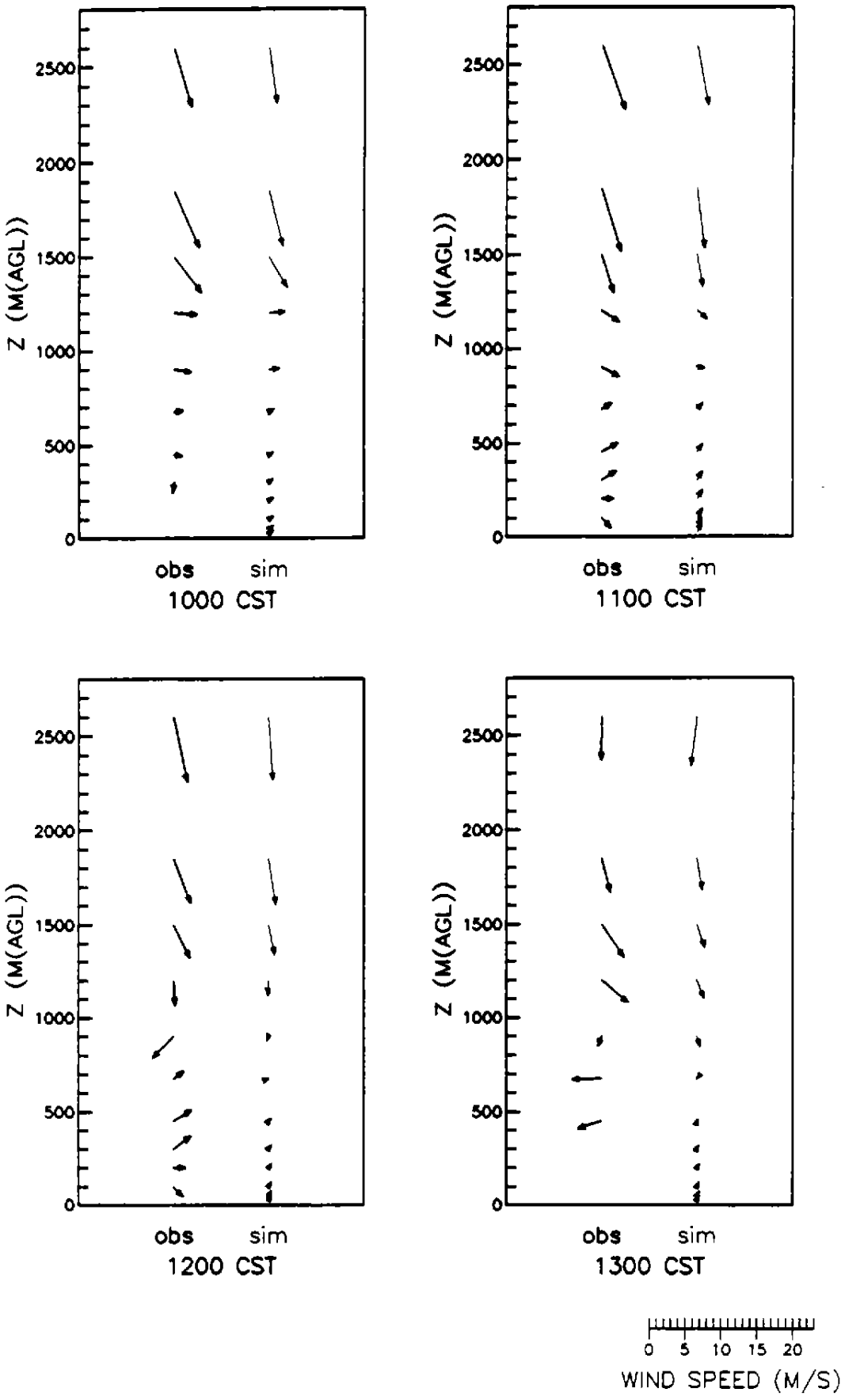

Figure 4-55a. Comparison of midday observed and simulated wind profiles for Houston (SEH) on 8 September 1993.

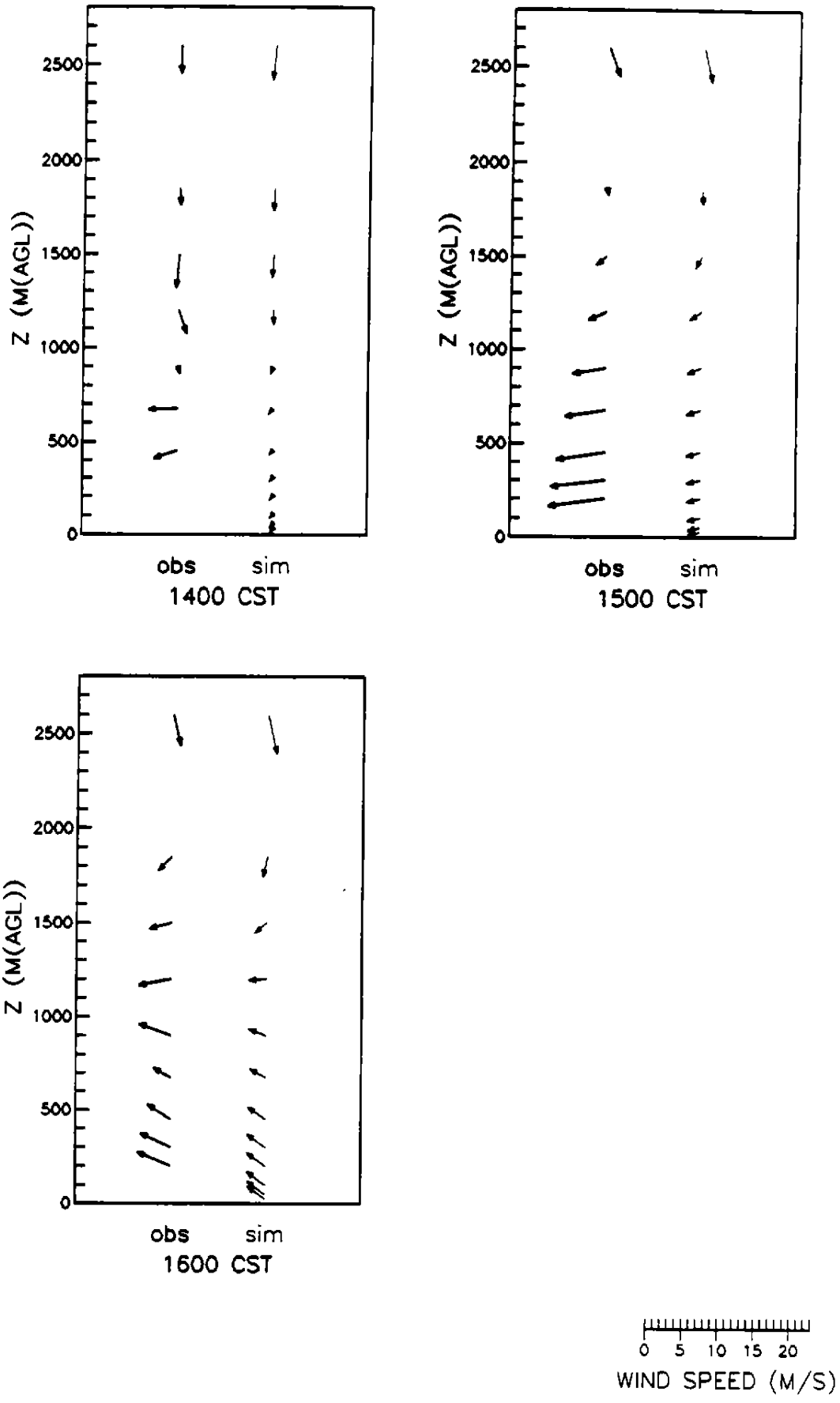

Figure 4-55b. Comparison of midday observed and simulated wind profiles for Houston (SEH) on 8 September 1993.

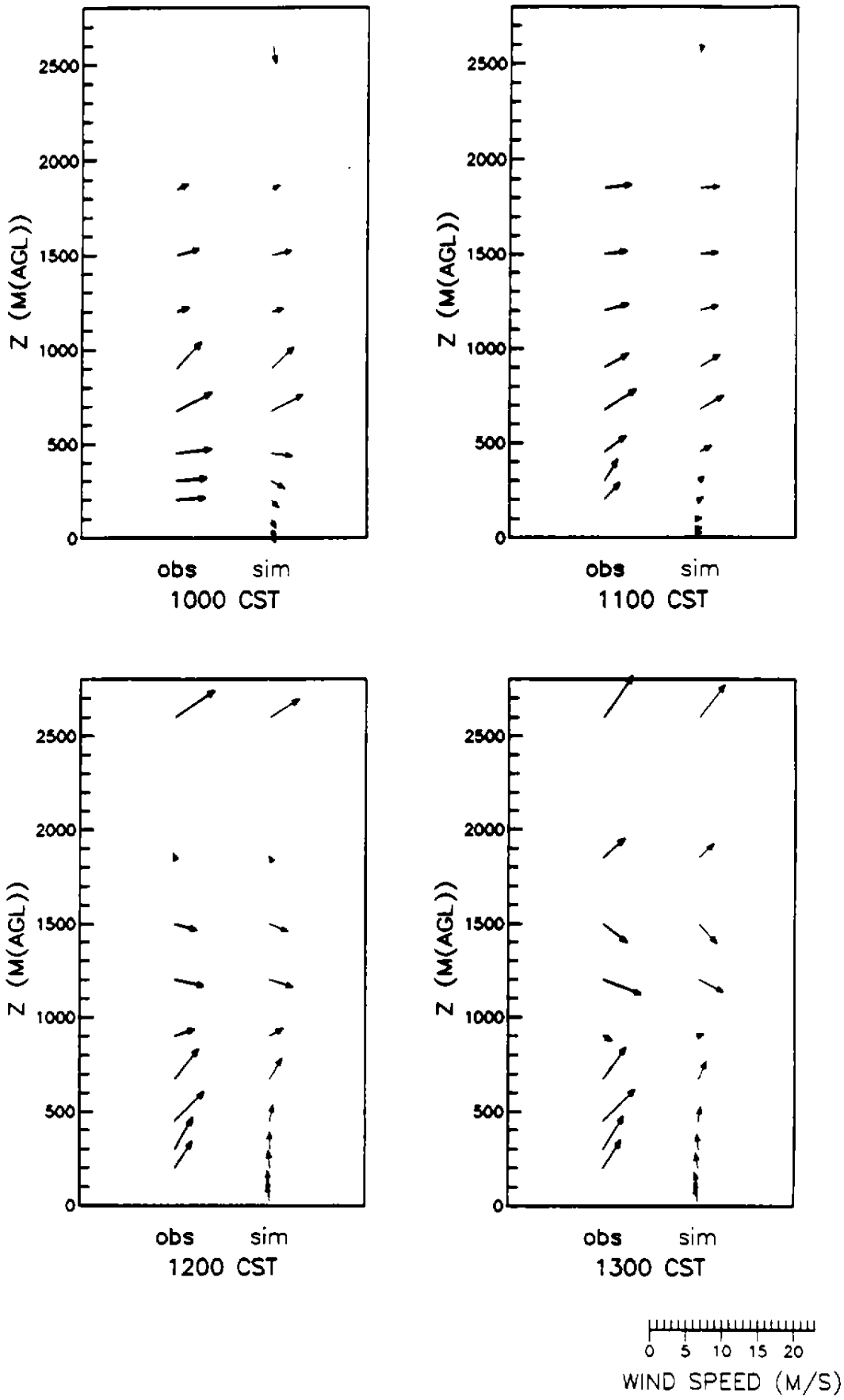

Figure 4-56a. Comparison of midday observed and simulated wind profiles for Galveston (GAL) on 9 September 1993.

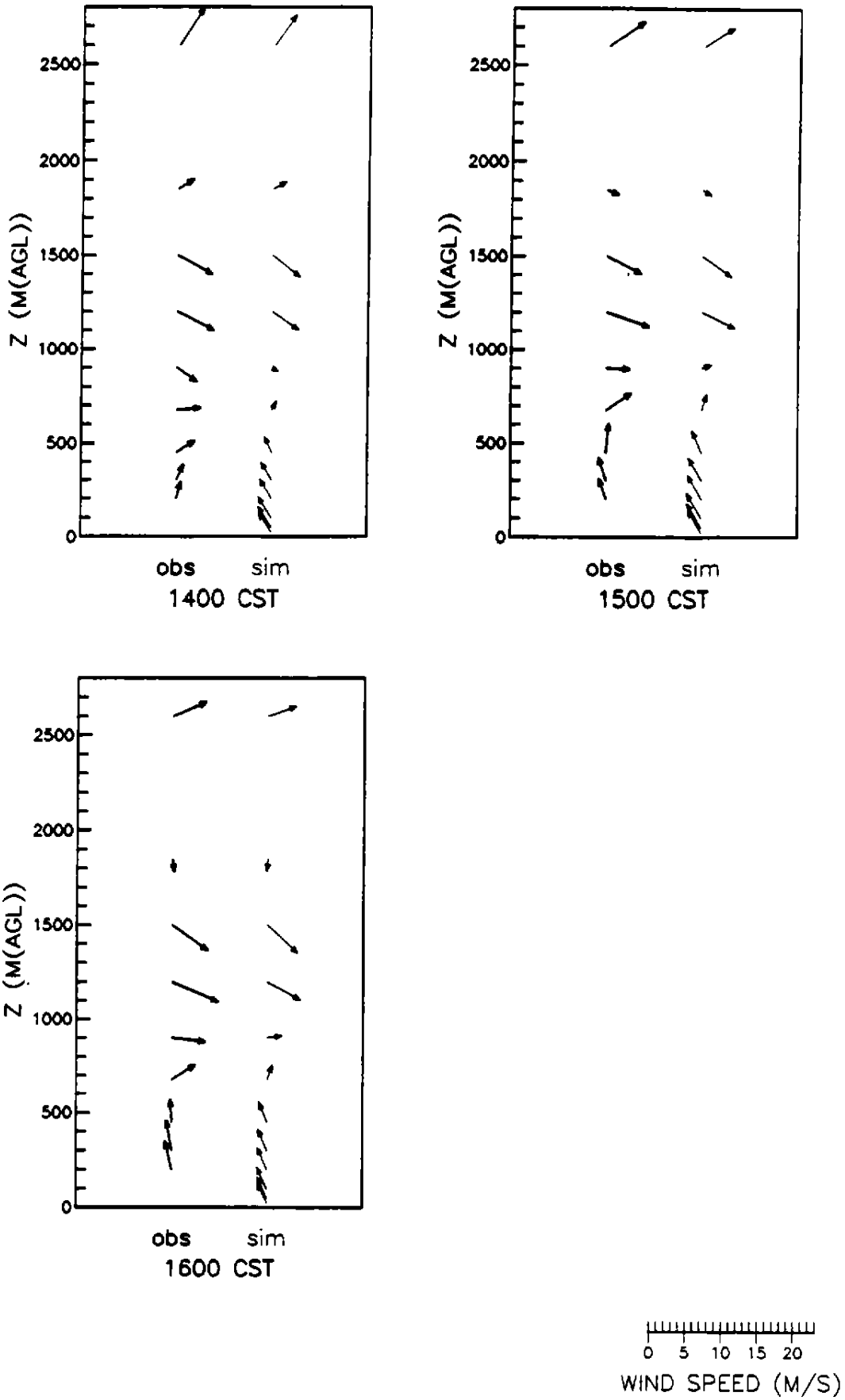

Figure 4-56b. Comparison of midday observed and simulated wind profiles for Galveston (GAL) on 9 September 1993.

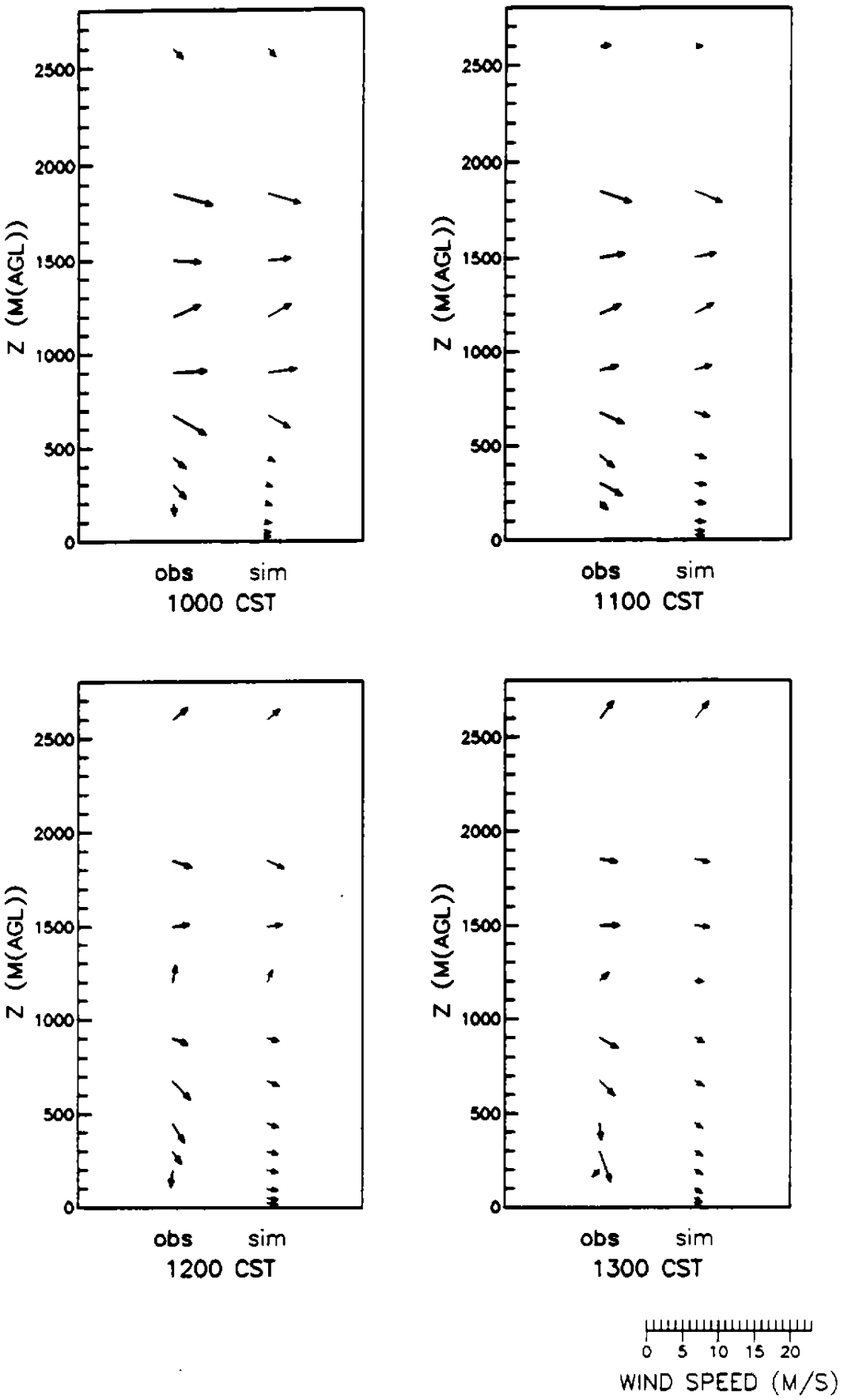

Figure 4-57a. Comparison of midday observed and simulated wind profiles for Houston (SEH) on 9 September 1993.

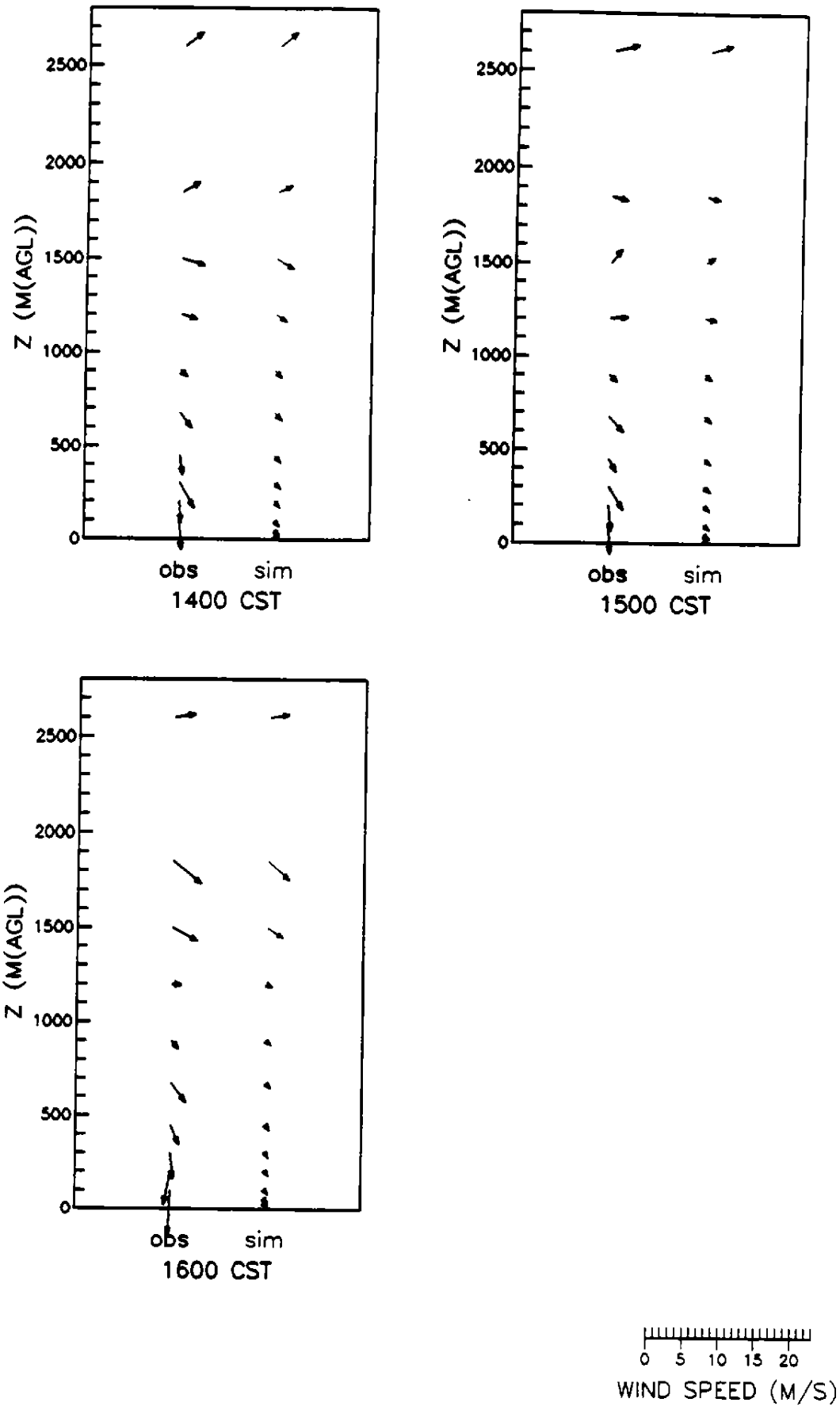

Figure 4-57b. Comparison of midday observed and simulated wind profiles for Houston (SEH) on 9 September 1993.

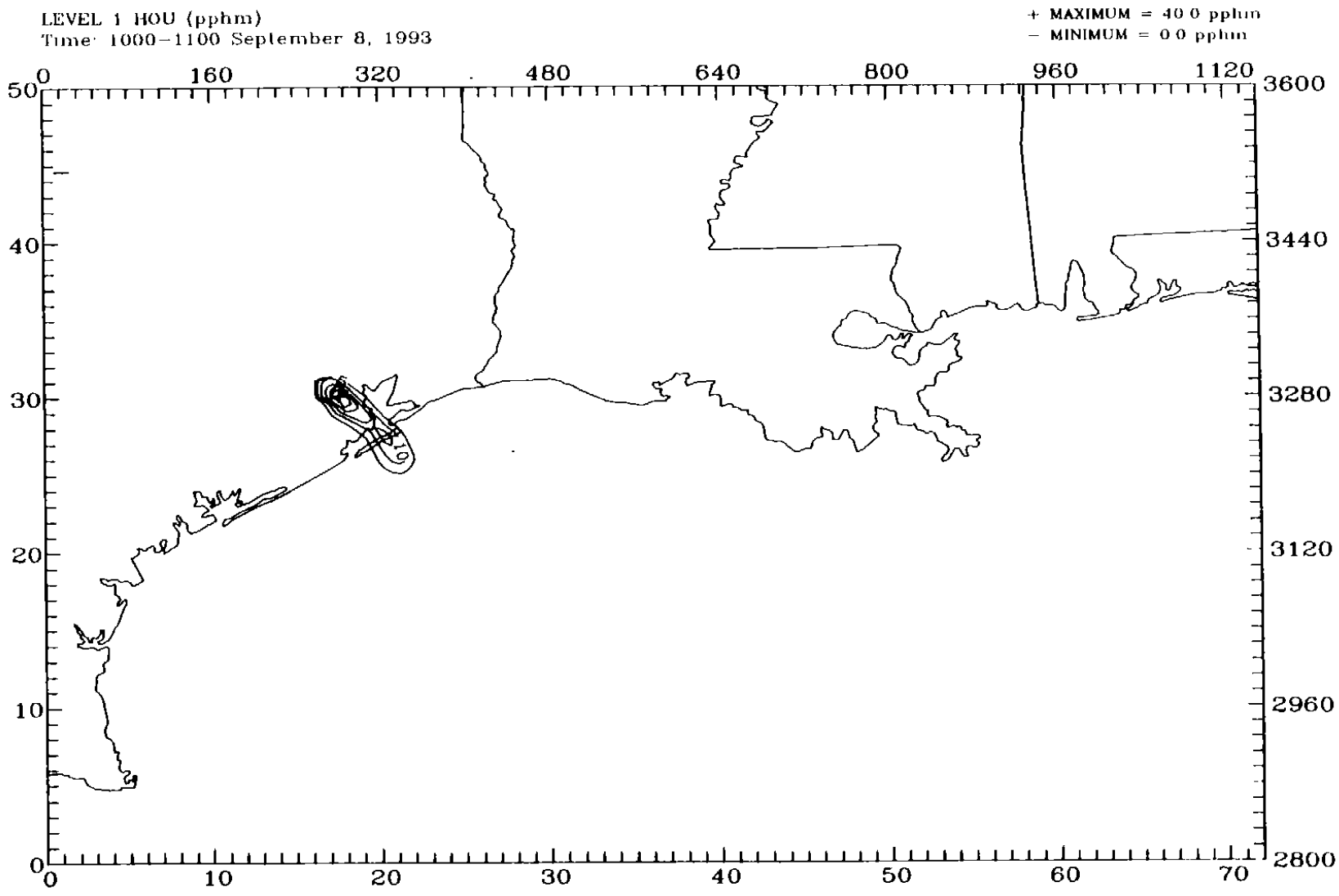

Figure 4-58a. Layer 1 concentrations of the low-level emission tracer HOU on 8 September 1993 at 1000 CST

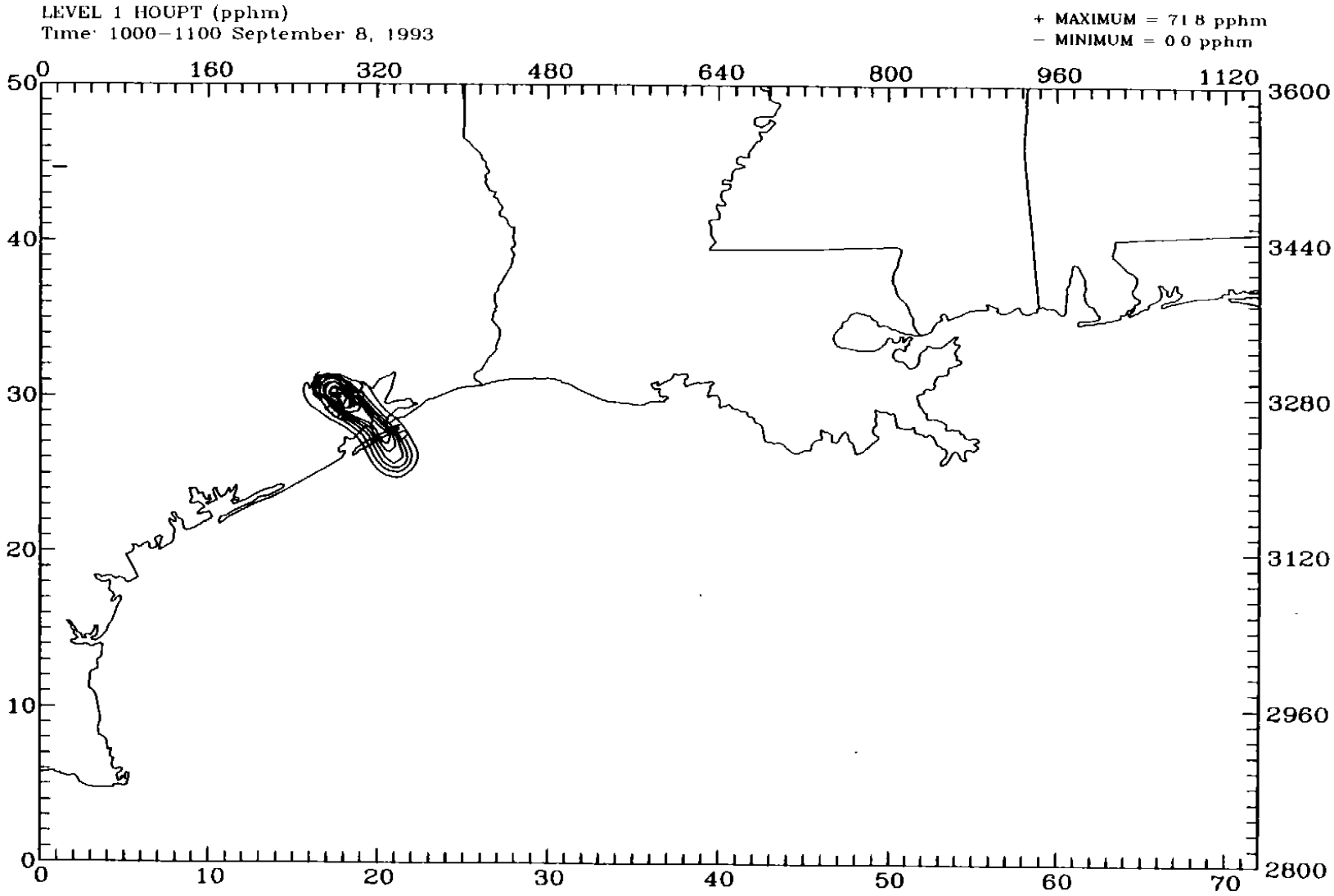

Figure 4-58b. Layer 1 concentrations of the elevated emission tracer HOUPT on 8 September 1993 at 1000 CST.

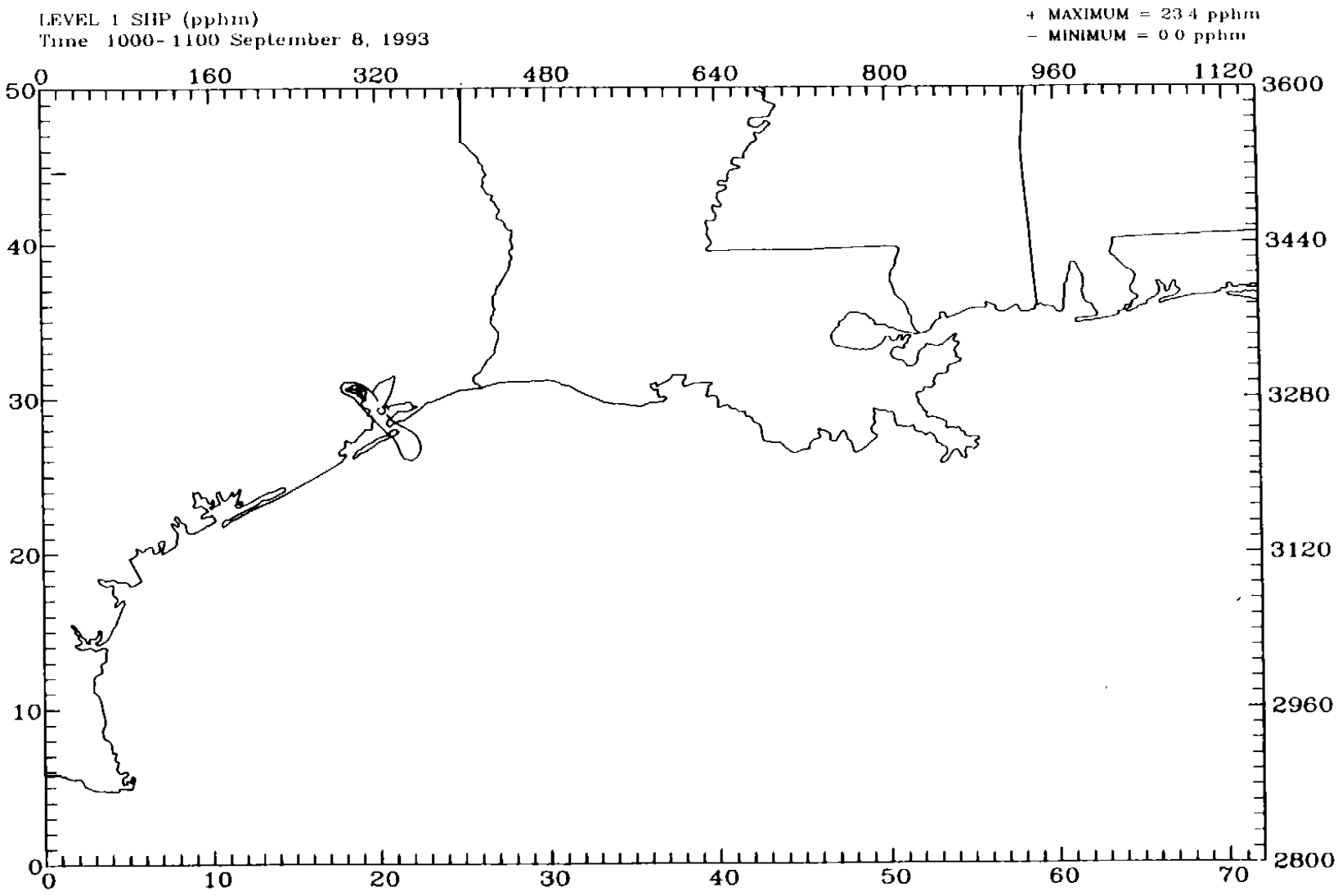

Figure 4-59a. Layer 1 concentrations of the low-level emission tracer SHP on 8 September 1993 at 1000 CST.

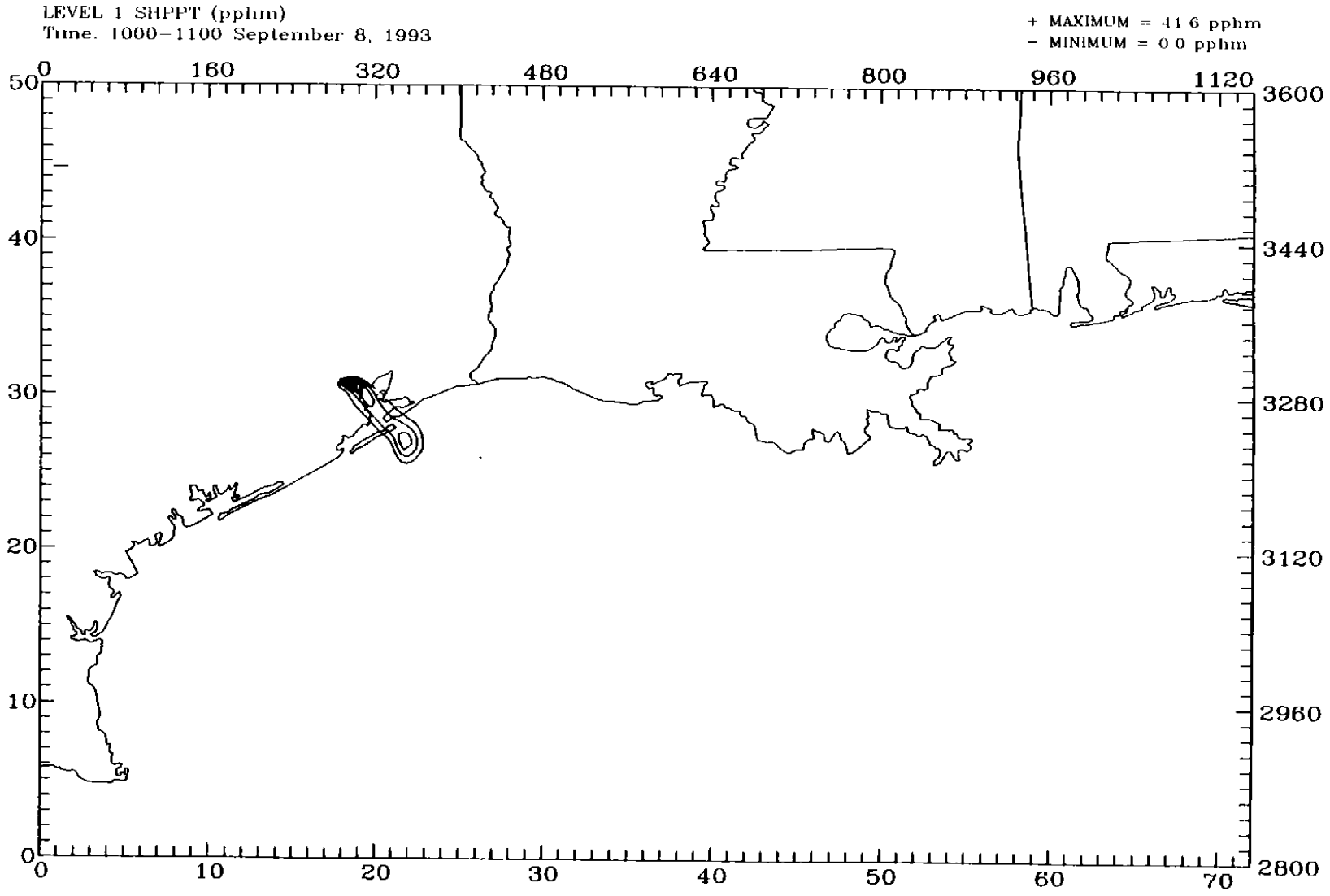

Figure 4-59b. Layer 1 concentrations of the elevated emission tracer SHPPT on 8 September 1993 at 1000 CST.

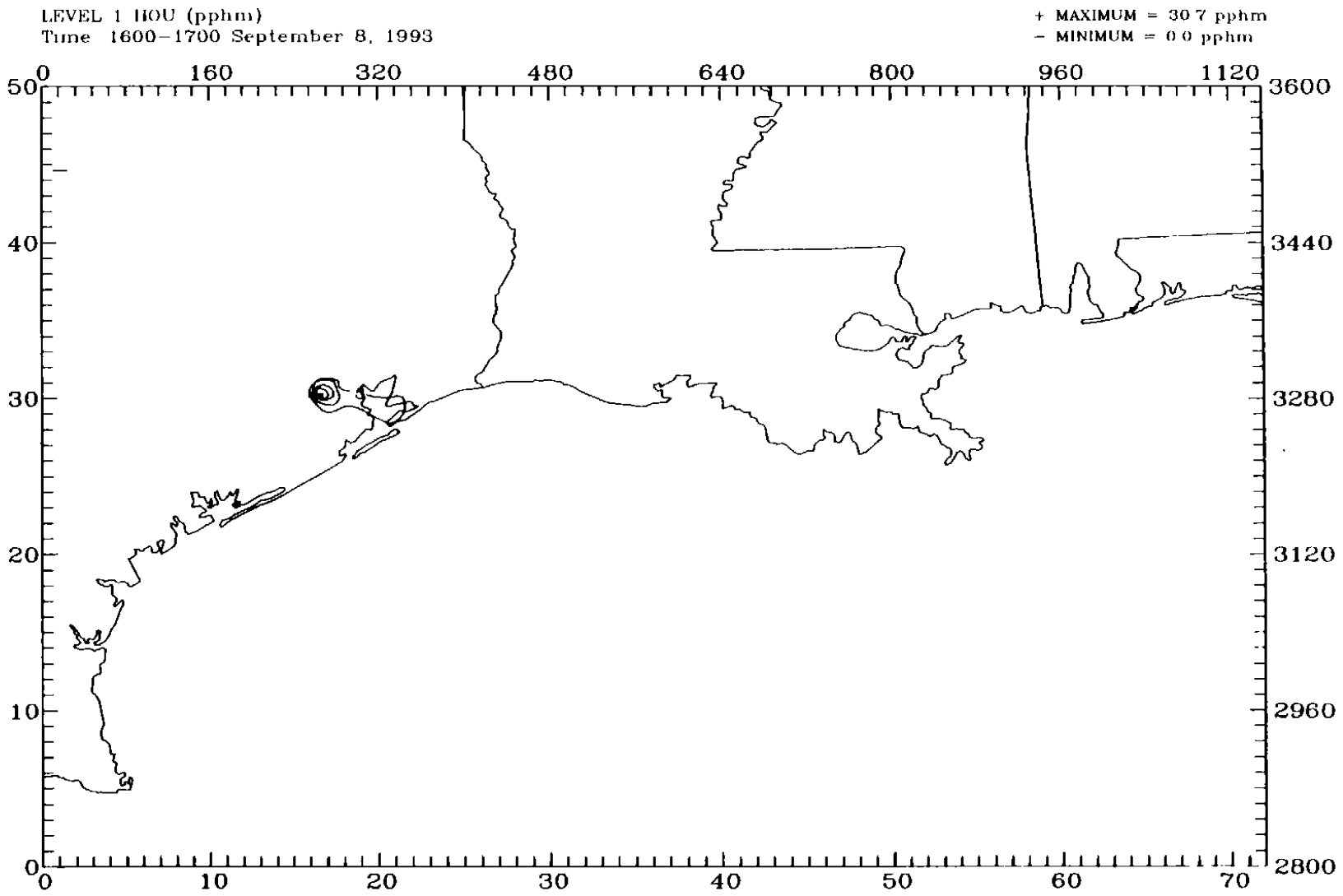

Figure 4-60a. Layer 1 concentrations of the low-level emission tracer HOU on 8 September 1993 at 1600 CST.

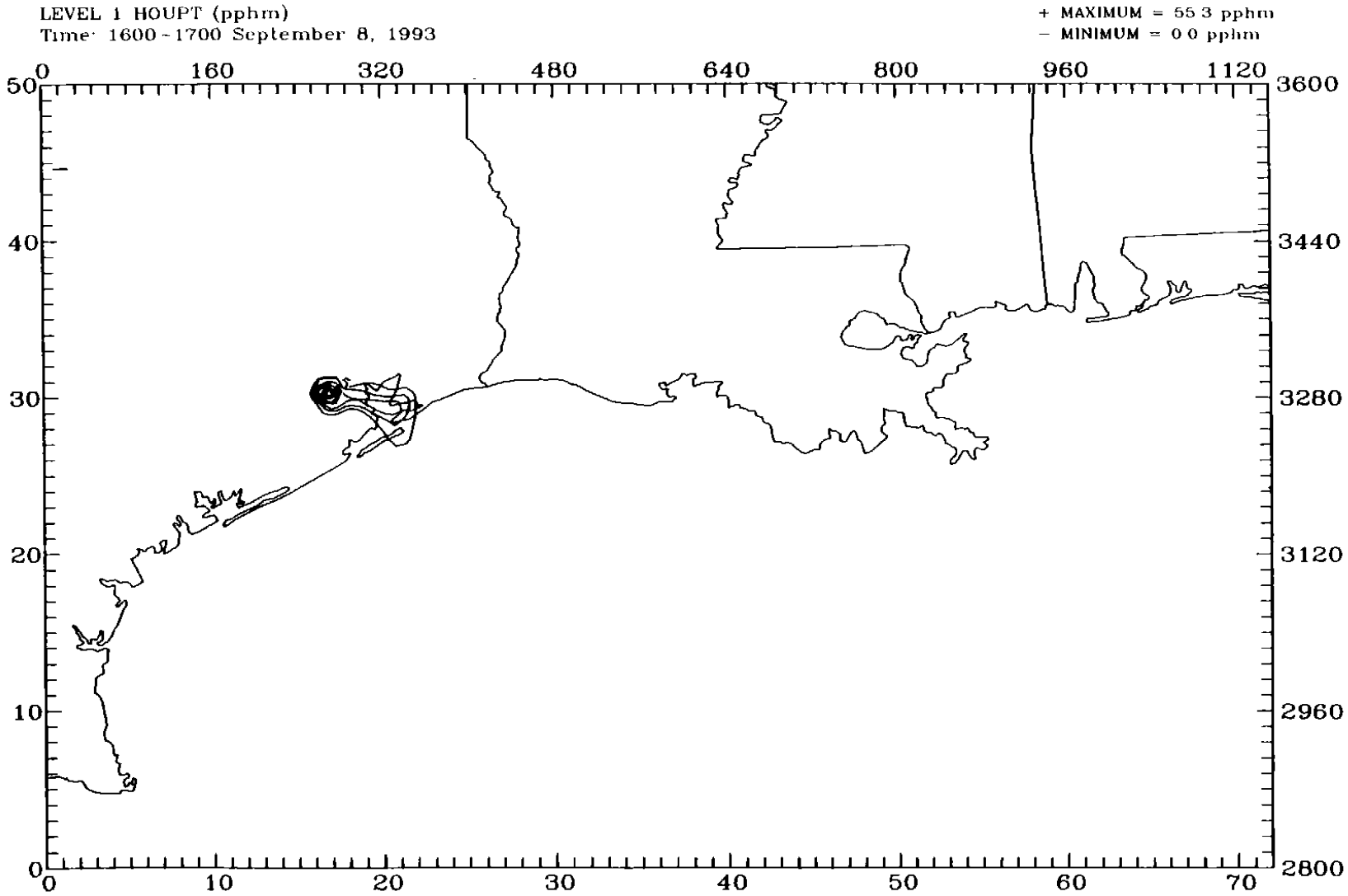

Figure 4-60b. Layer 1 concentrations of the elevated emission tracer HOUPT on 8 September 1993 at 1600 CST.

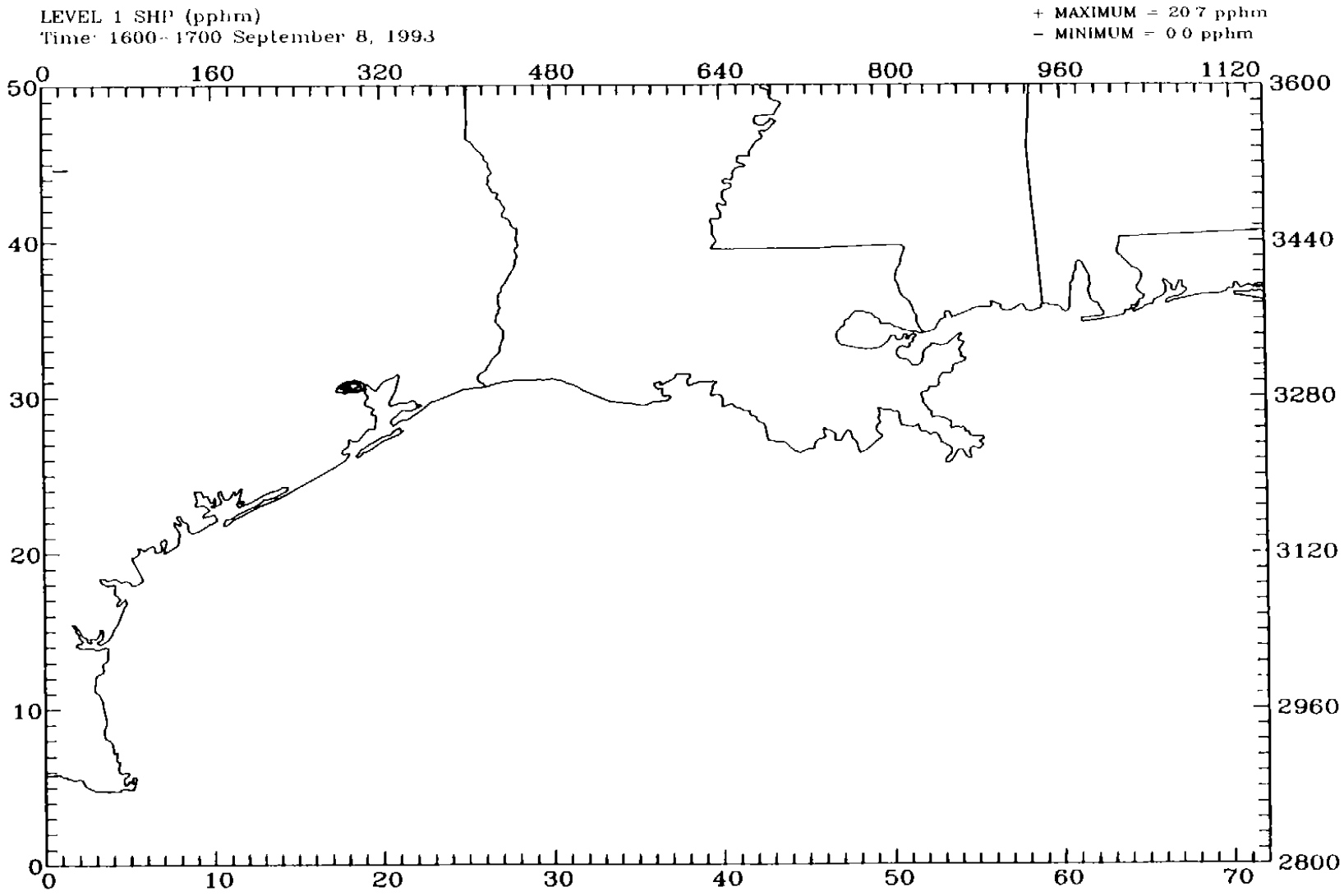

Figure 4-61a. Layer 1 concentrations of the low-level emission tracer SHP on 8 September 1993 at 1600 CST.

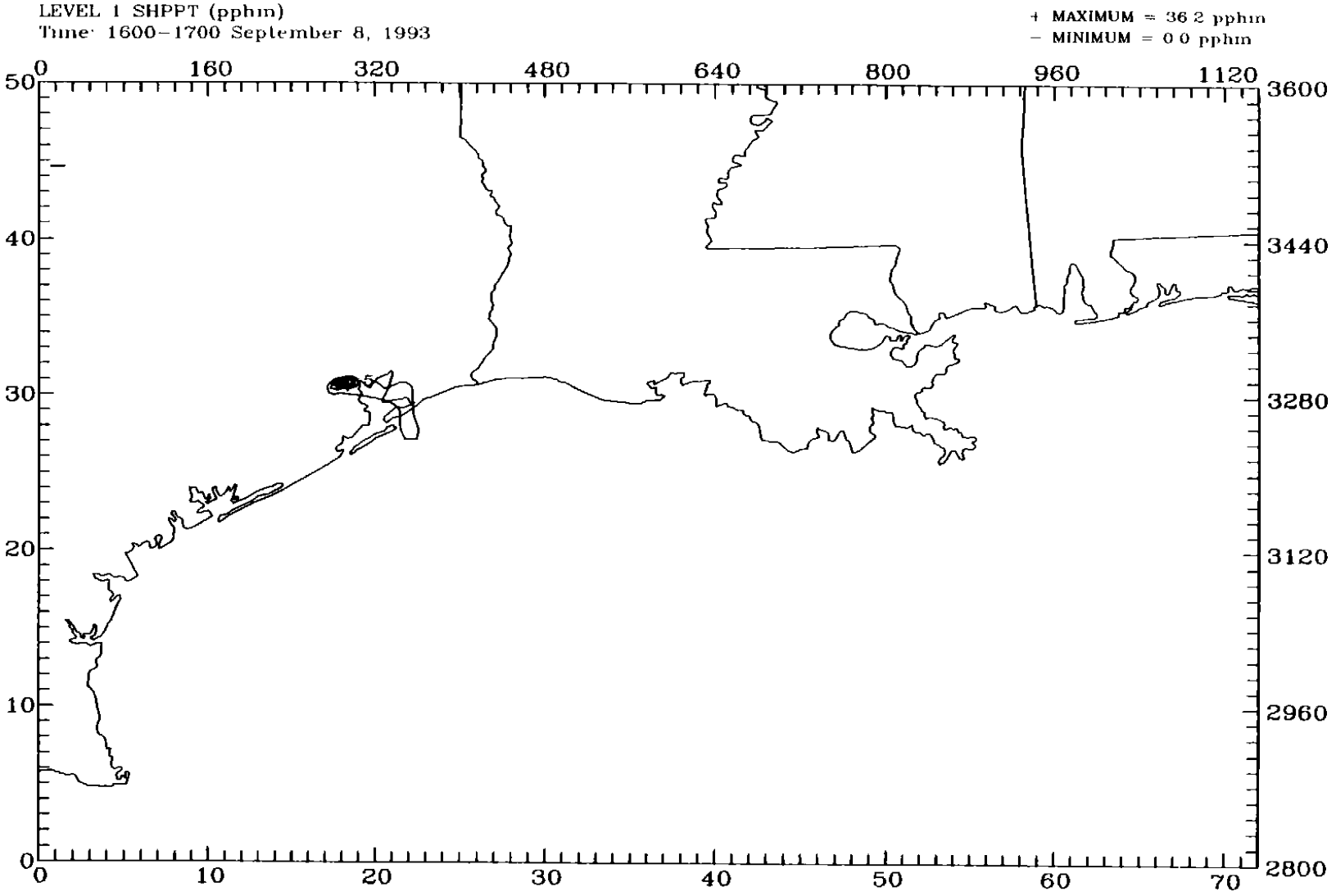

Figure 4-61b. Layer 1 concentrations of the elevated emission tracer SHPPT on 8 September 1993 at 1600 CST.

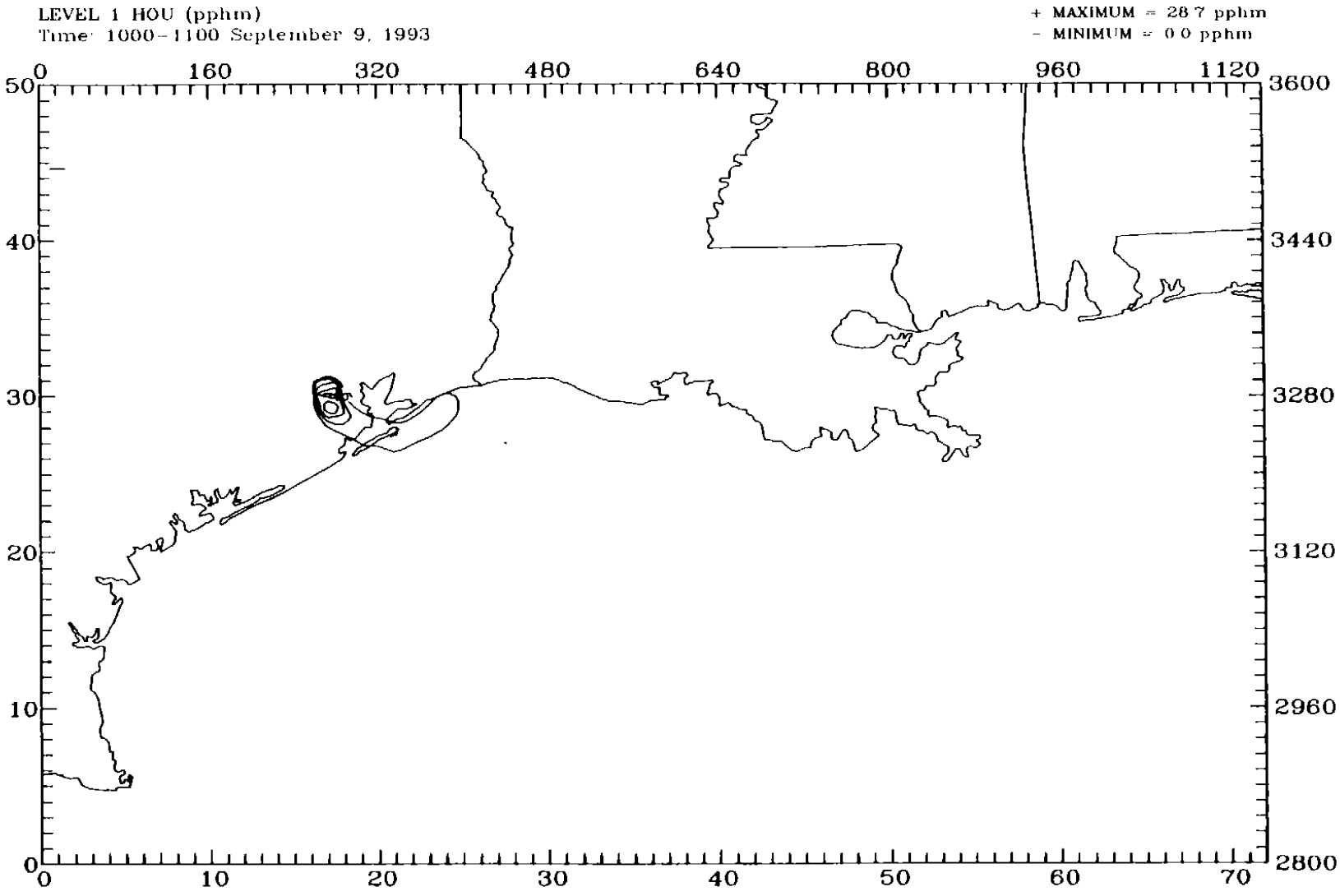

Figure 4-62a. Layer 1 concentrations of the low-level emission tracer HOU on 9 September 1993 at 1000 CST.

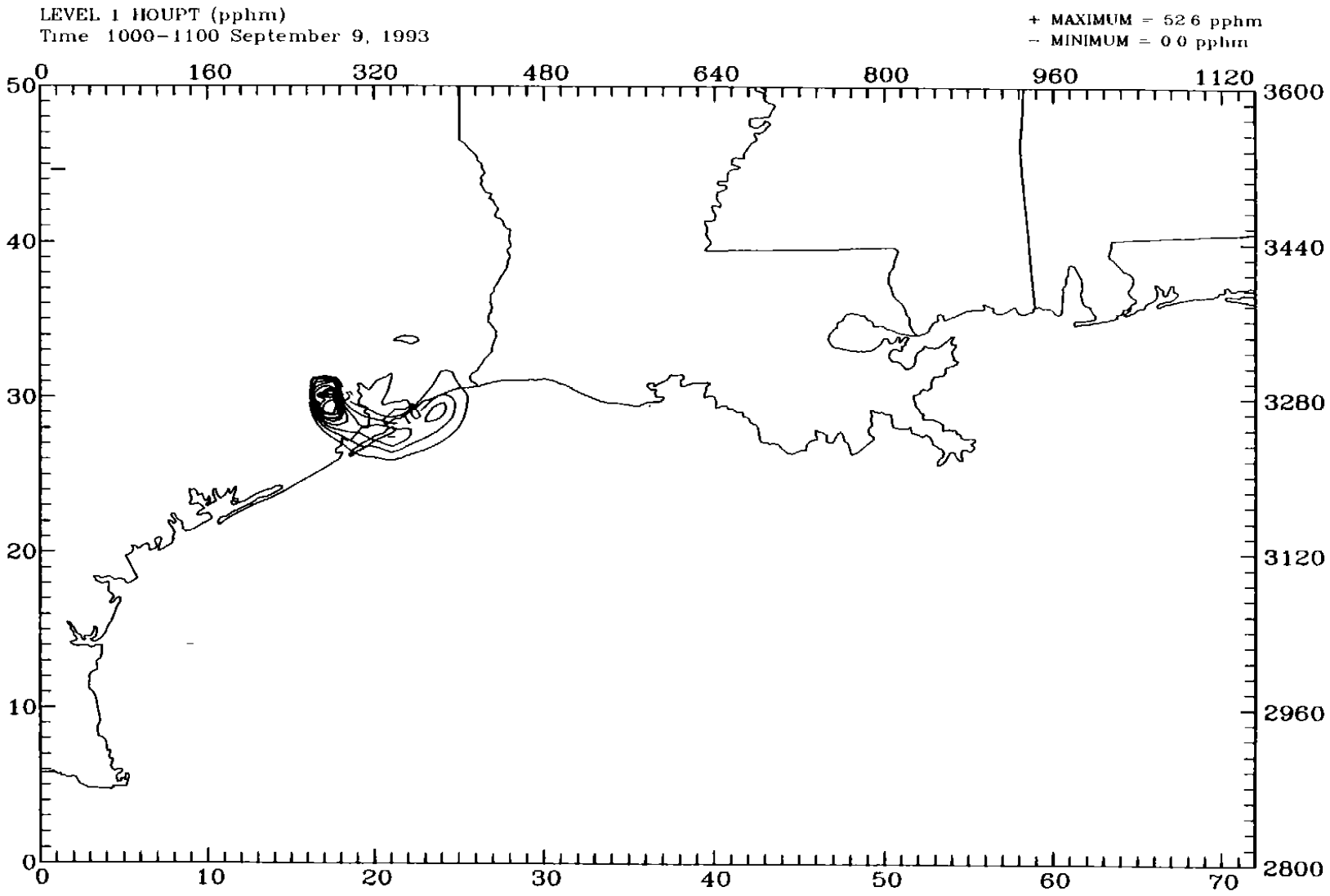

Figure 4-62b. Layer 1 concentrations of the elevated emission tracer HOUPT on 9 September 1993 at 1000 CST.

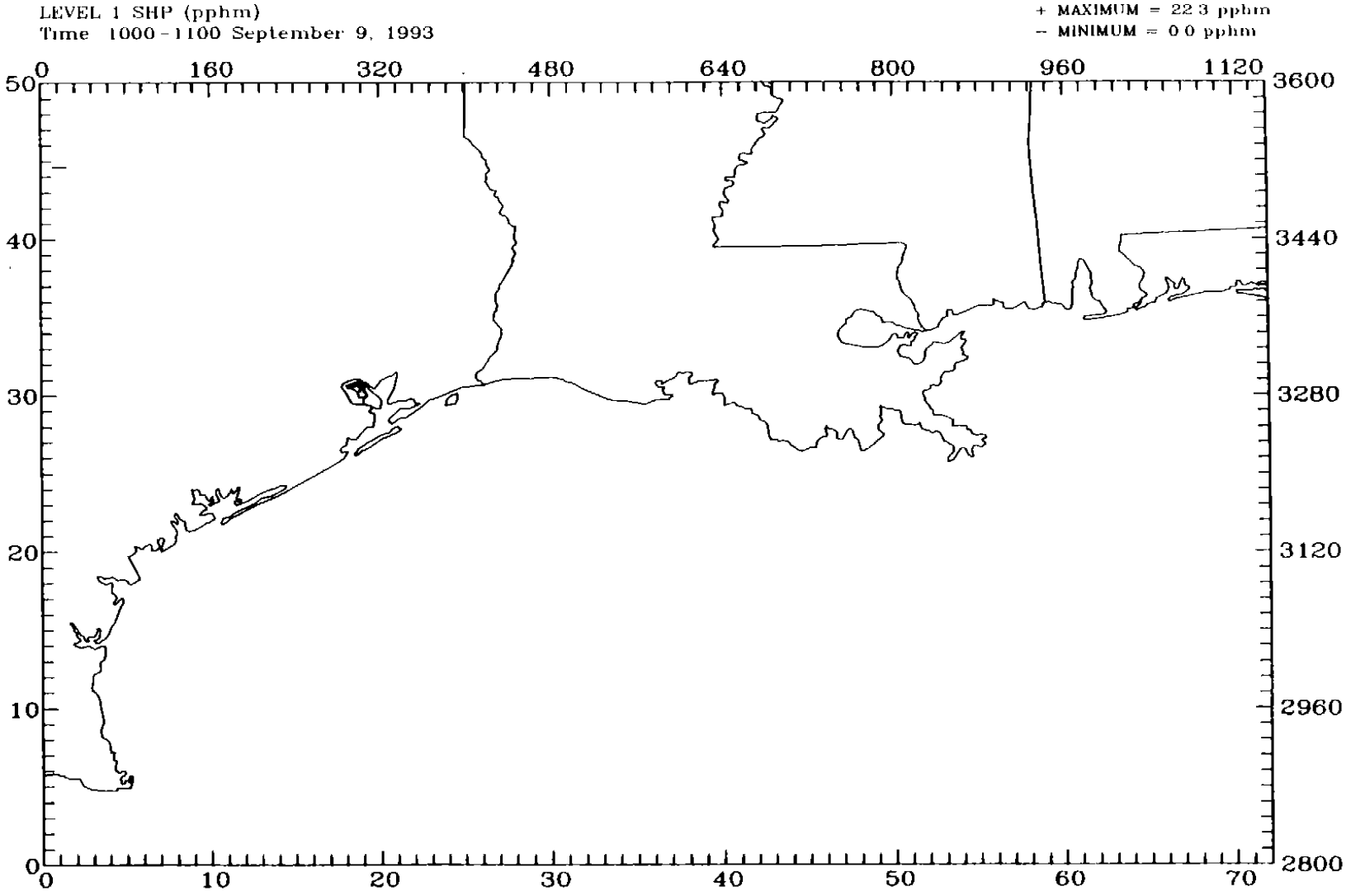

Figure 4-63a. Layer 1 concentrations of the low-level emission tracer SHP on 9 September 1993 at 1000 CST.

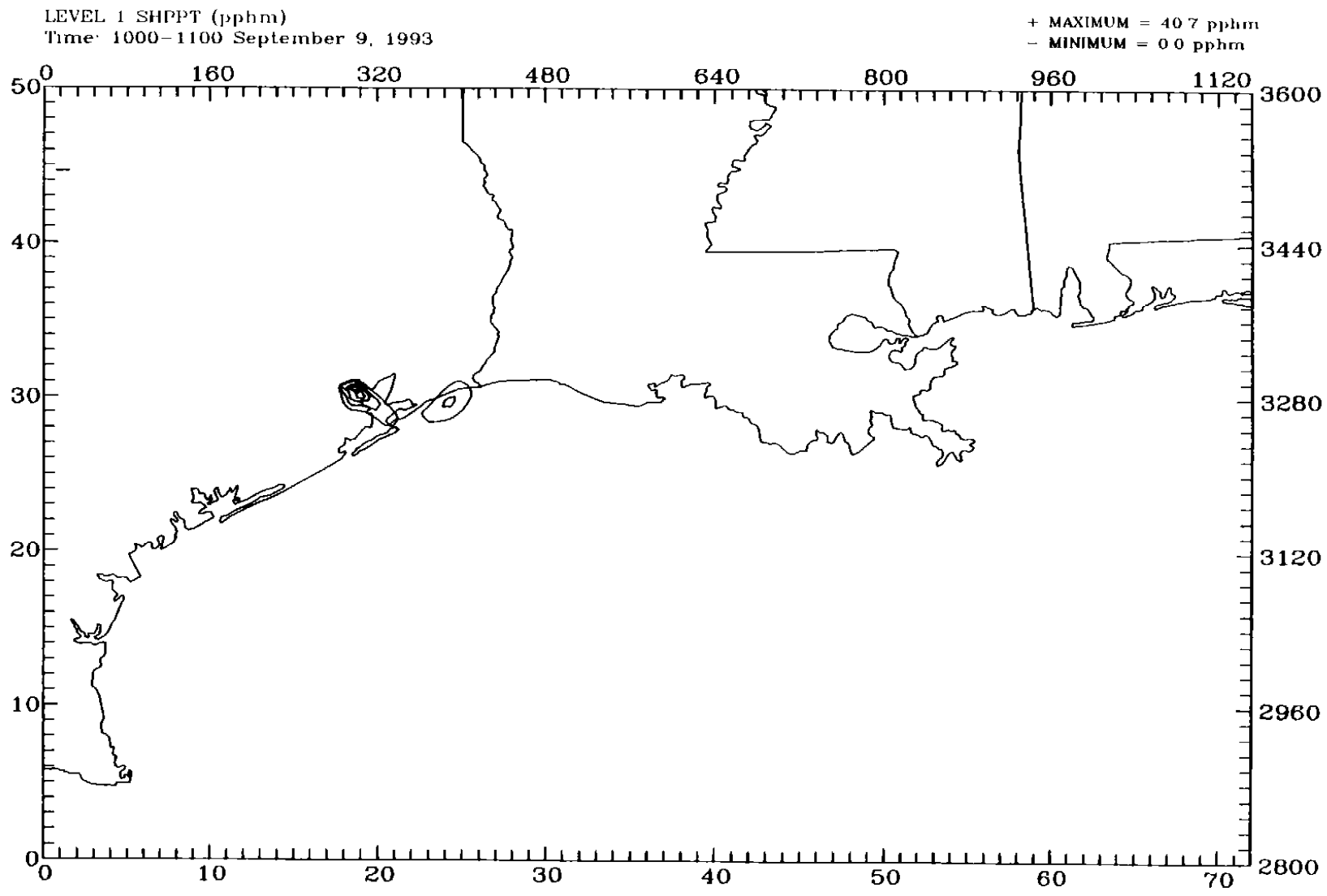

Figure 4-63b. Layer 1 concentrations of the elevated emission tracer SHPPT on 9 September 1993 at 1000 CST.

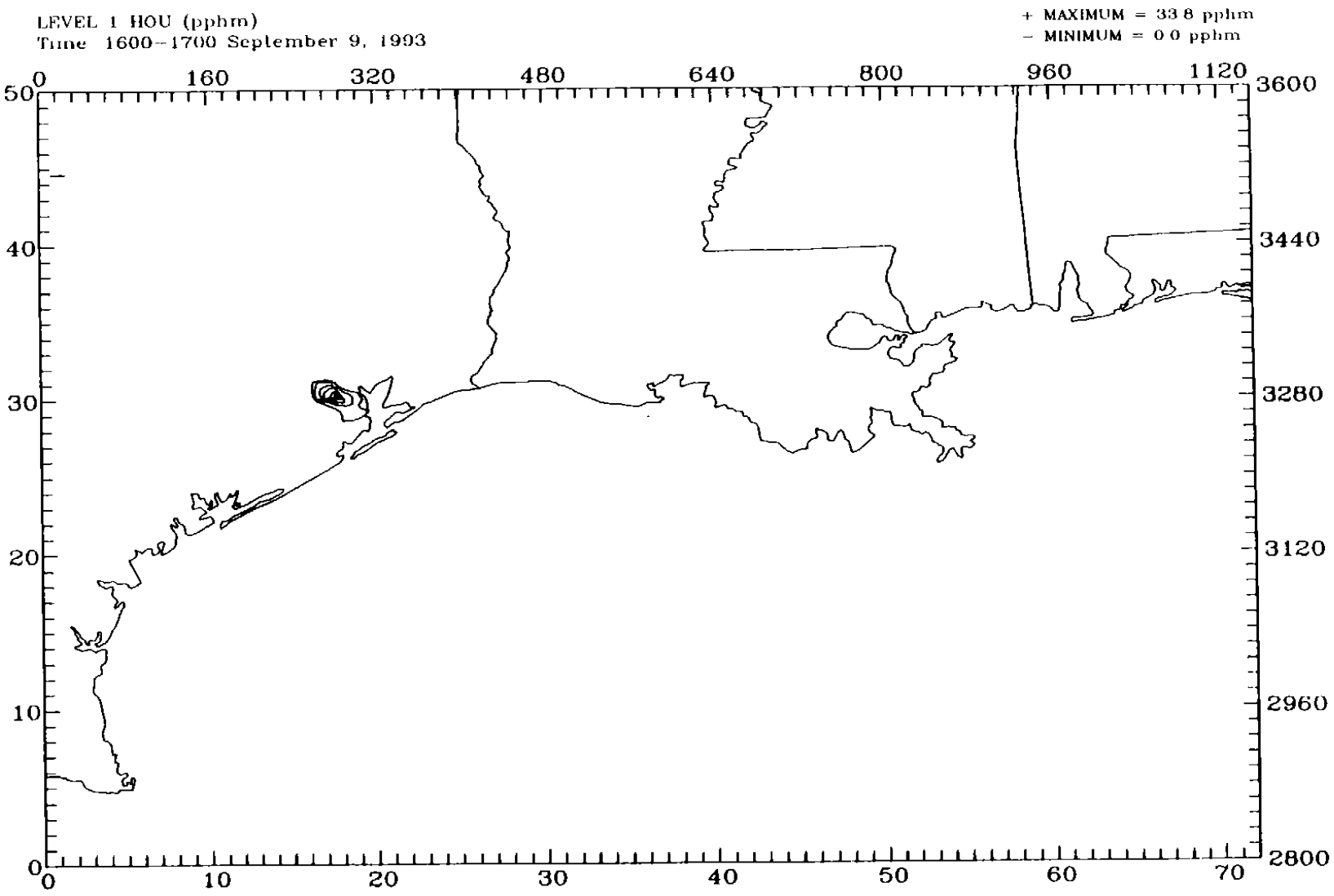

Figure 4-64a. Layer 1 concentrations of the low-level emission tracer HOU on 9 September 1993 at 1600 CST.

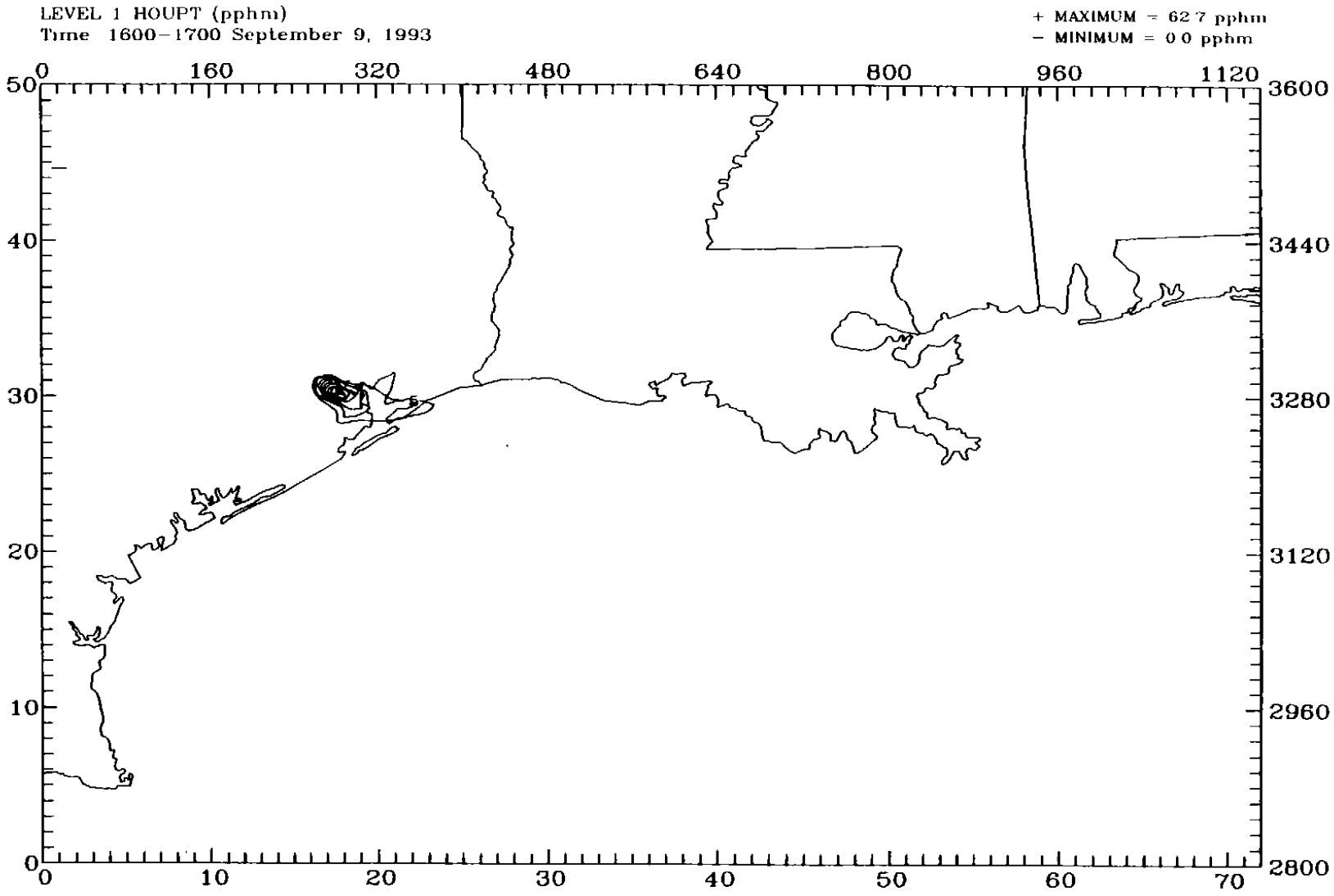

Figure 4-64b. Layer 1 concentrations of the elevated emission tracer HOUPT on 9 September 1993 at 1600 CST.

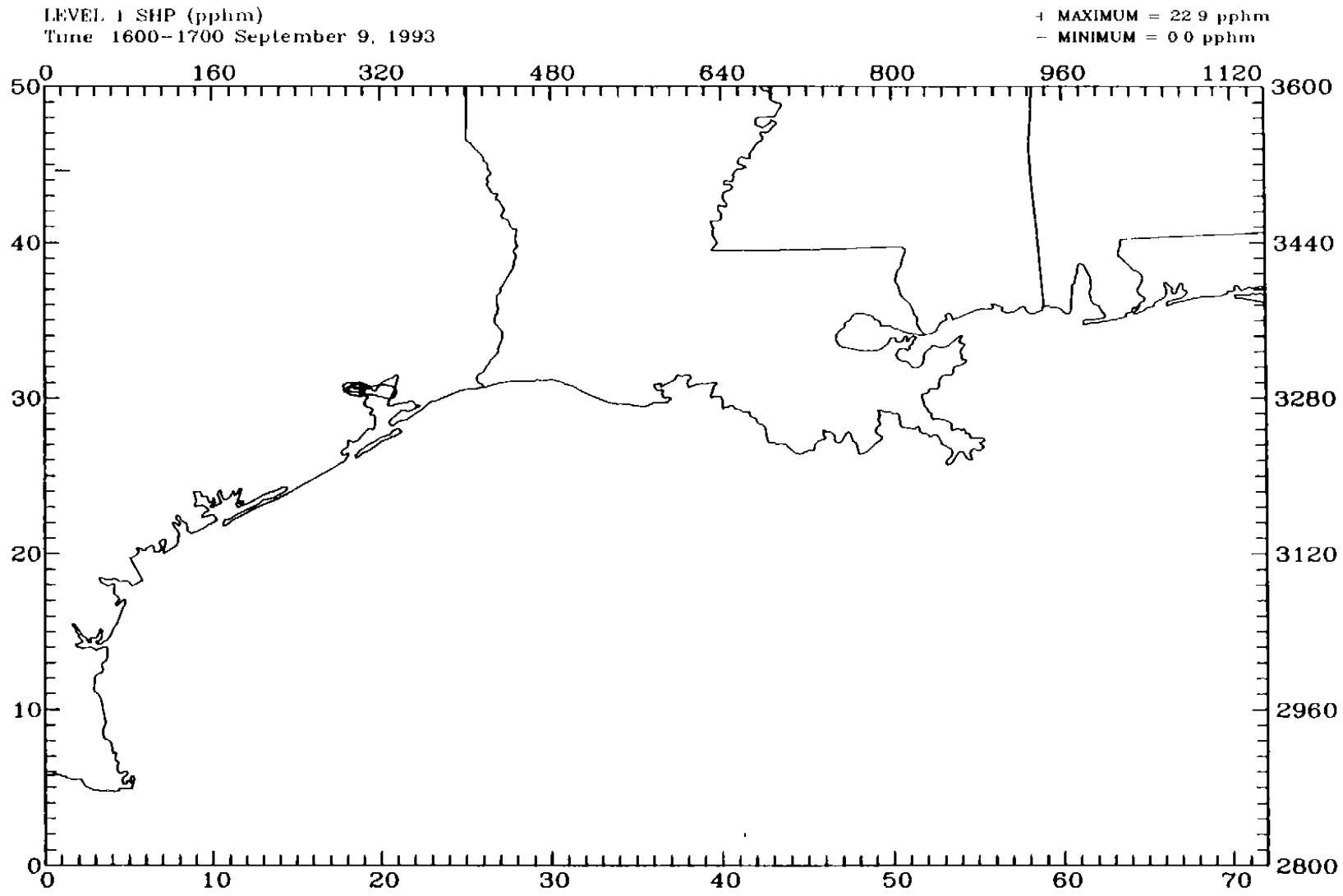

Figure 4-65a. Layer 1 concentrations of the low-level emission tracer SHP on 9 September 1993 at 1600 CST.

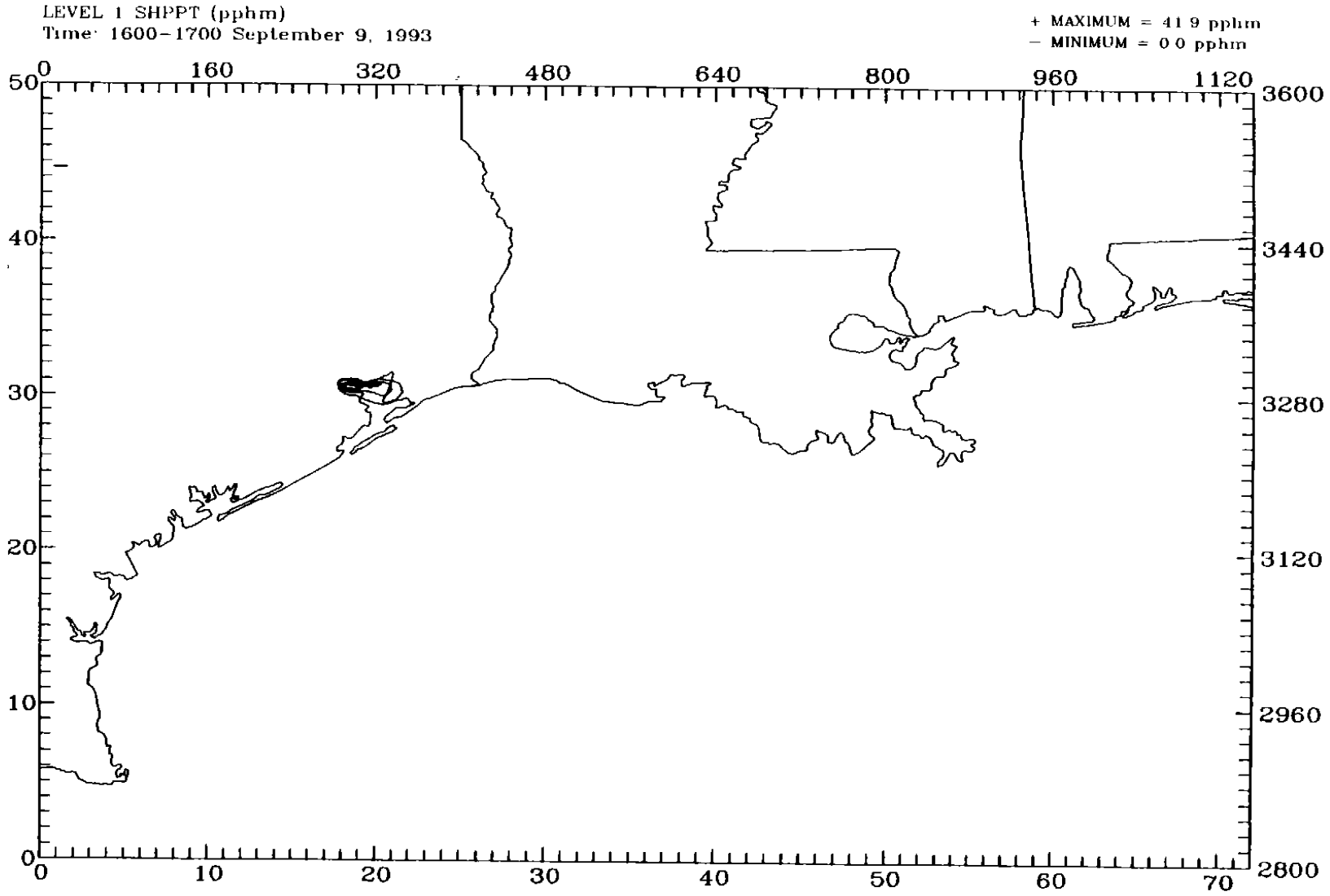

Figure 4-65b. Layer 1 concentrations of the elevated emission tracer SHPPT on 9 September 1993 at 1600 CST.

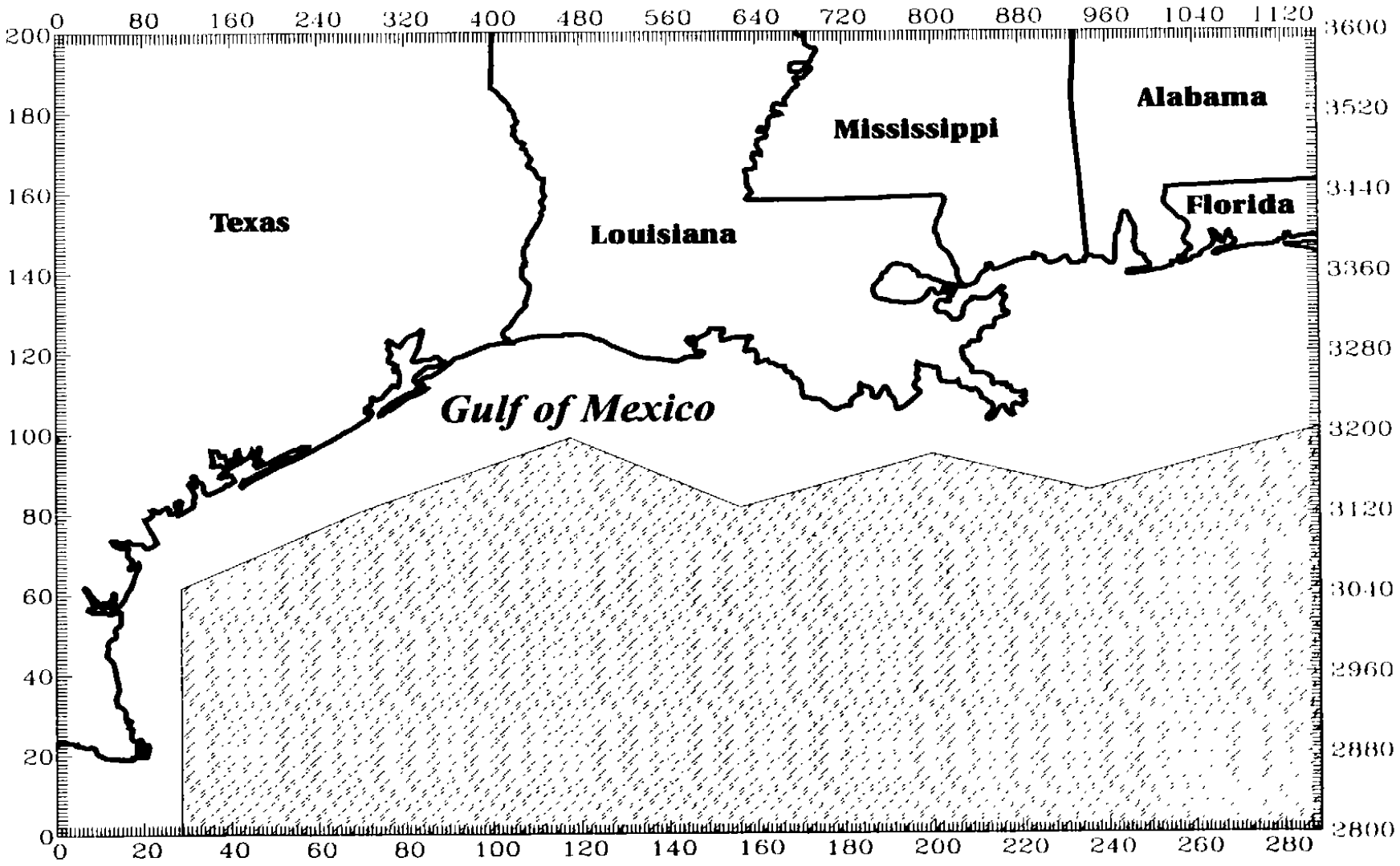

Figure 4-66. Subdomains used to develop background concentration for the modeling domain. Patterned area is marine area.

cdr5\mmsa002

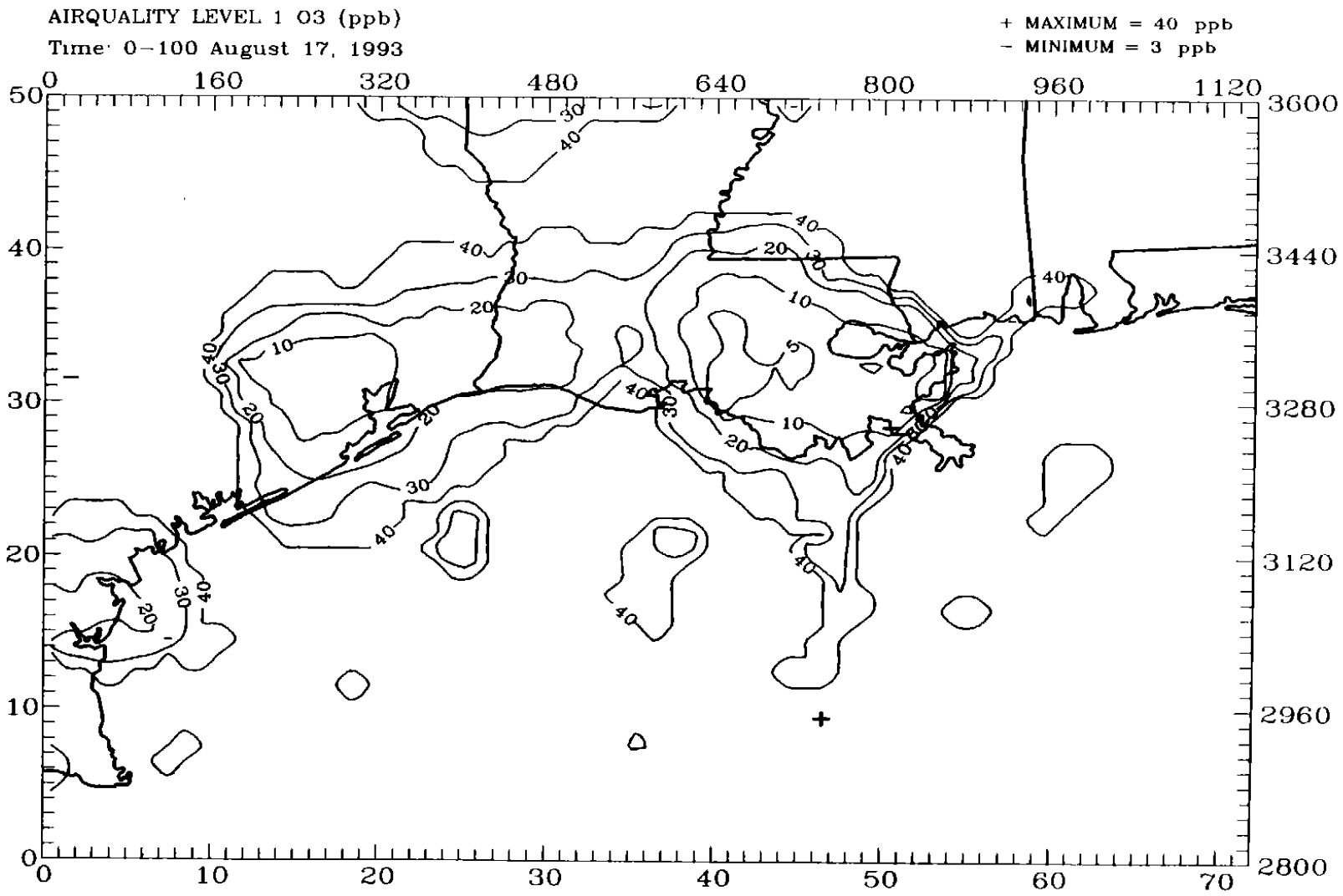

Figure 4-67a. Initial UAM concentrations of ozone (ppb) in the modeling domain on 17 August 1993.

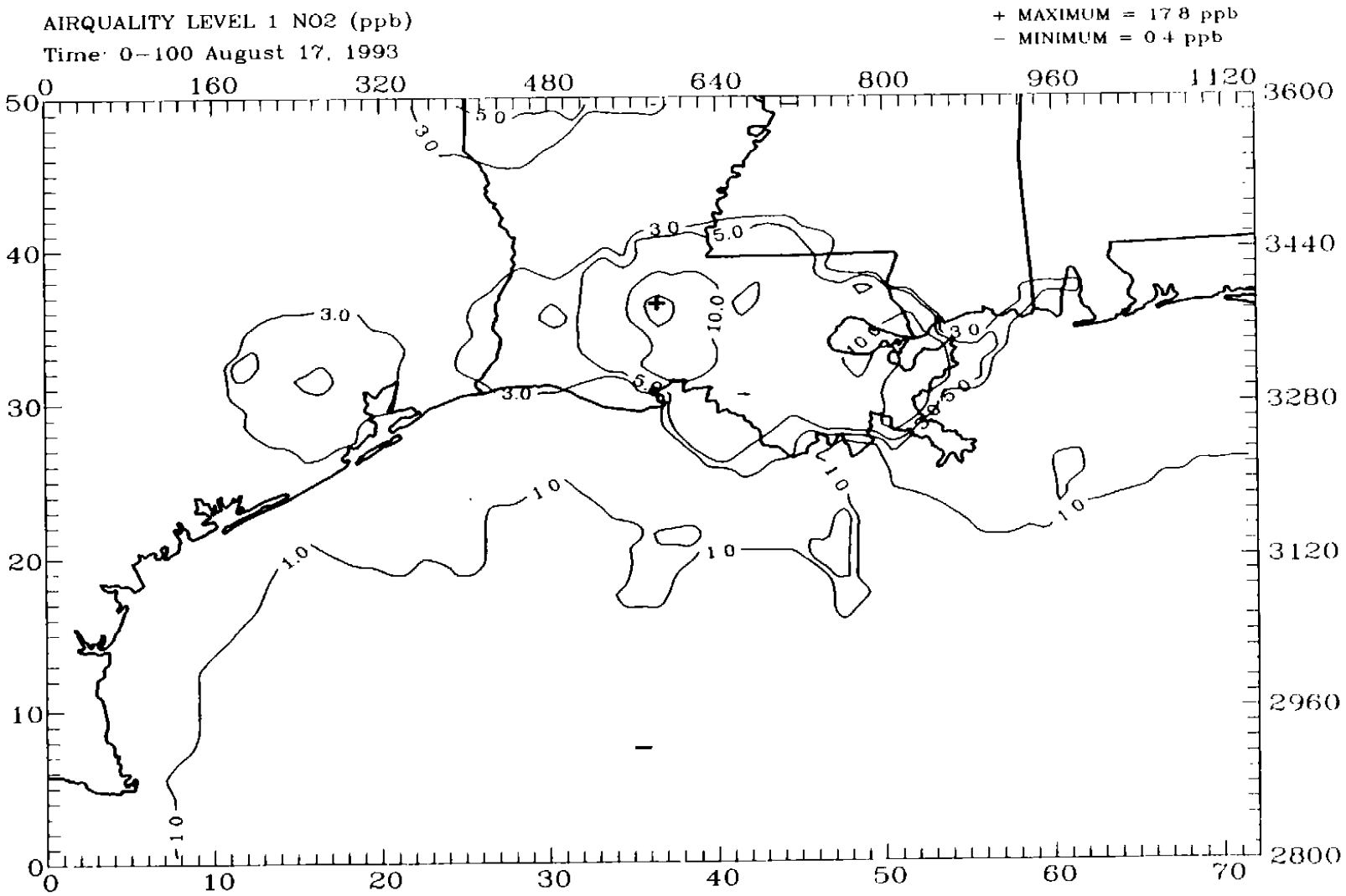

Figure 4-67b. Initial UAM concentrations of NO_2 (ppb) in the modeling domain on 17 August 1993.

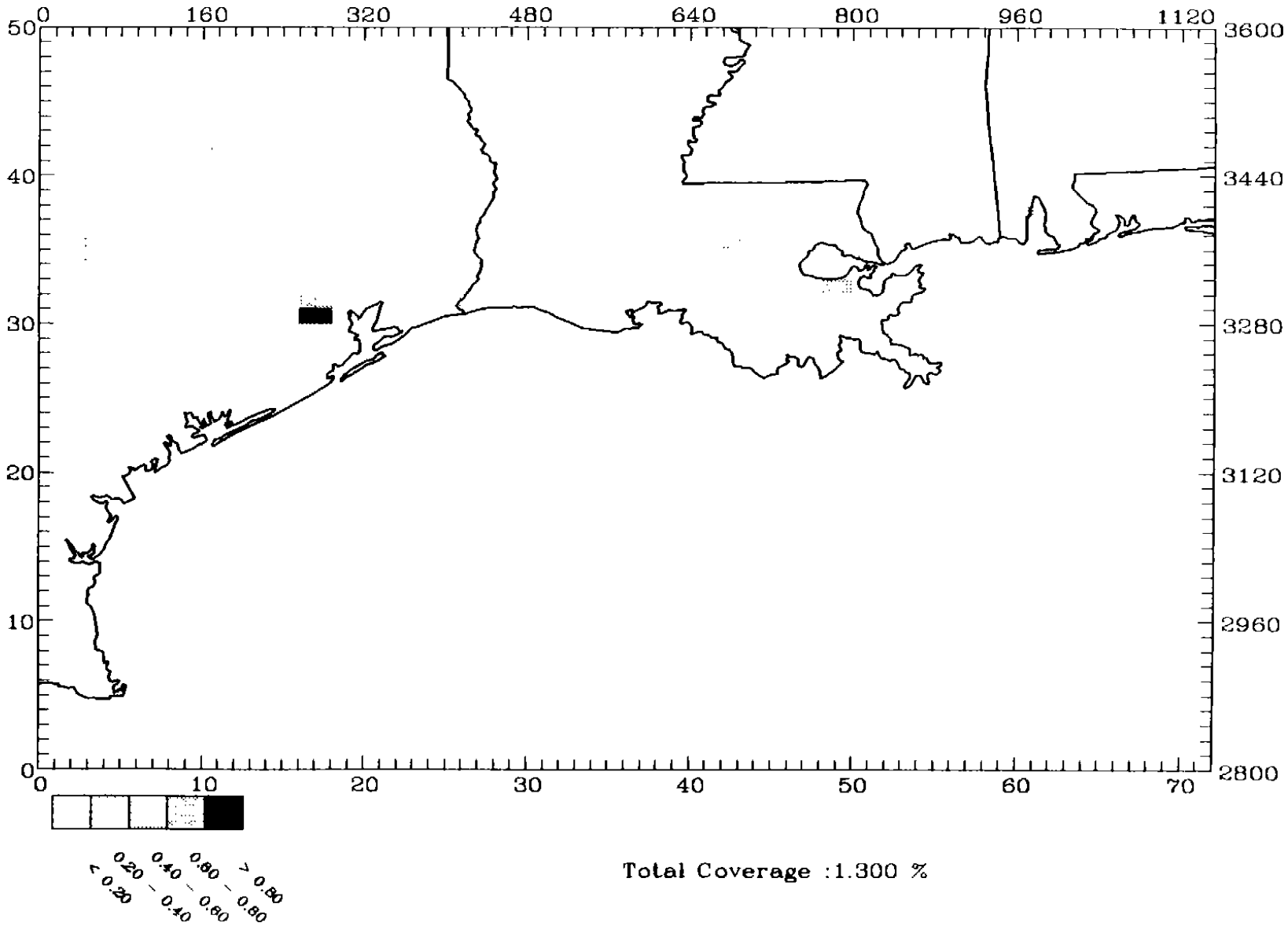

Figure 4-68a. Fractional coverage of the urban land-use category in the GMAQS domain.

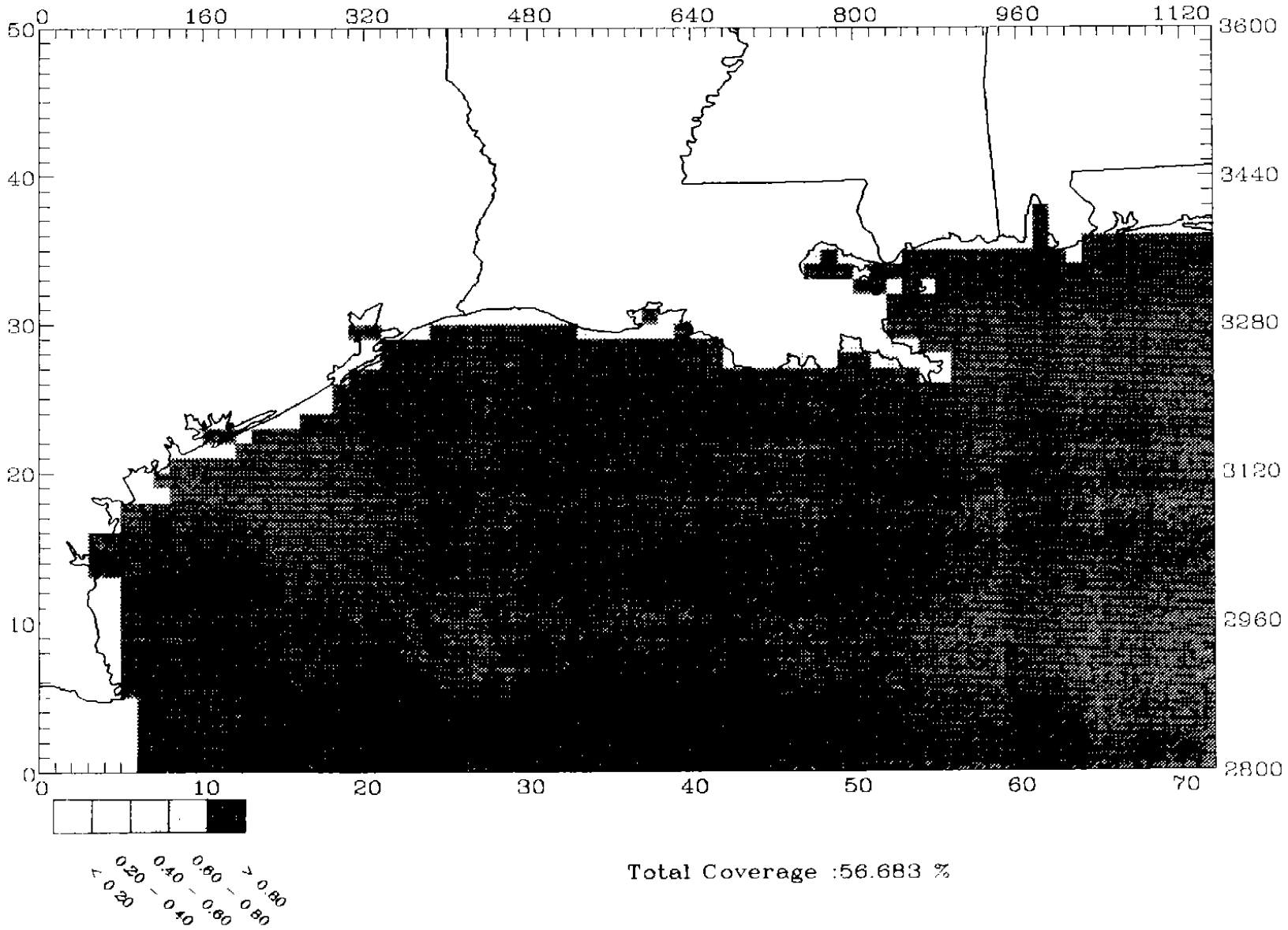

Figure 4-68b. Fractional coverage of the water land-use category in the GMAQS domain.

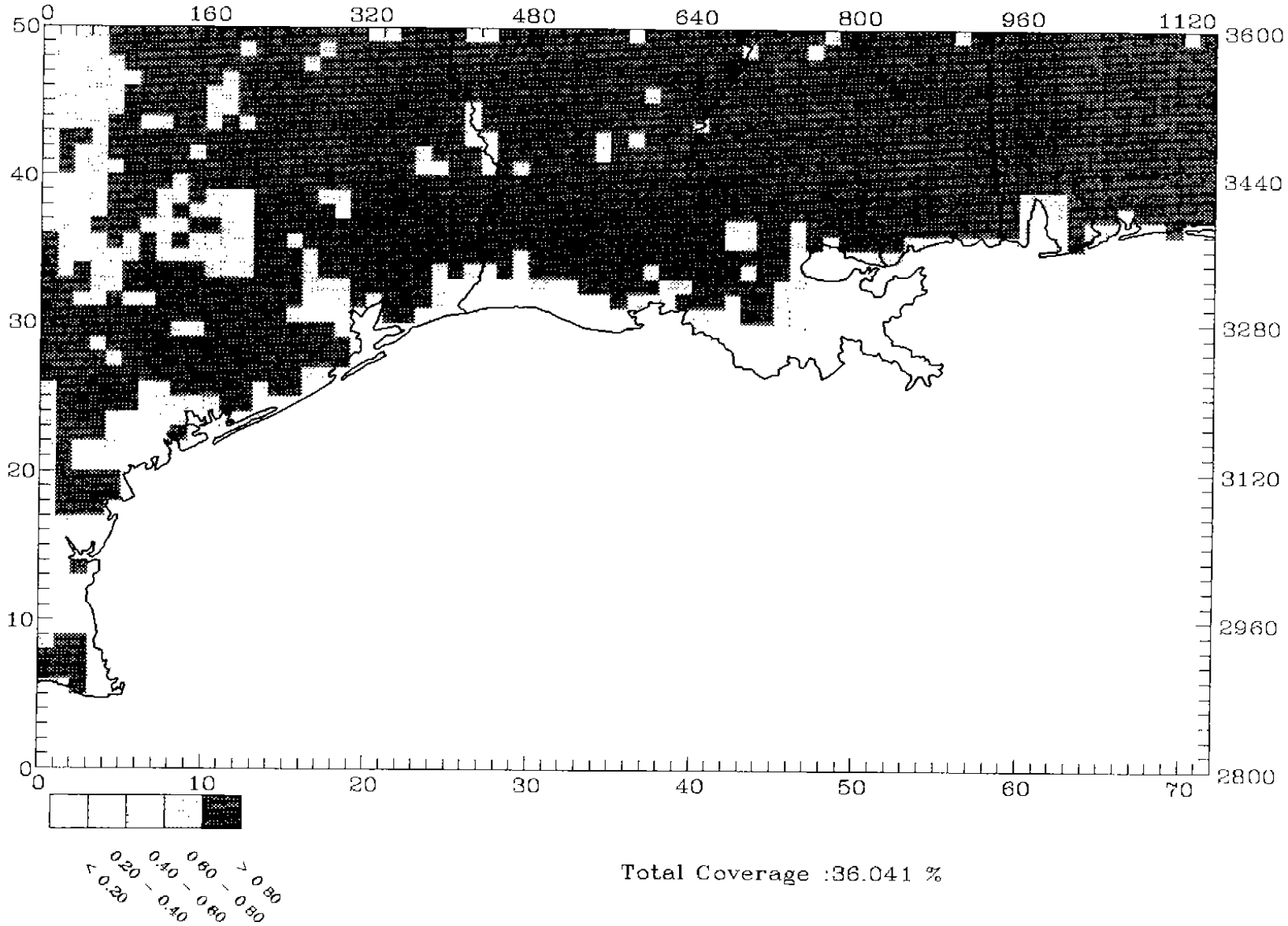

Figure 4-68c. Fractional coverage of the forest land-use category in the GMAQS domain.

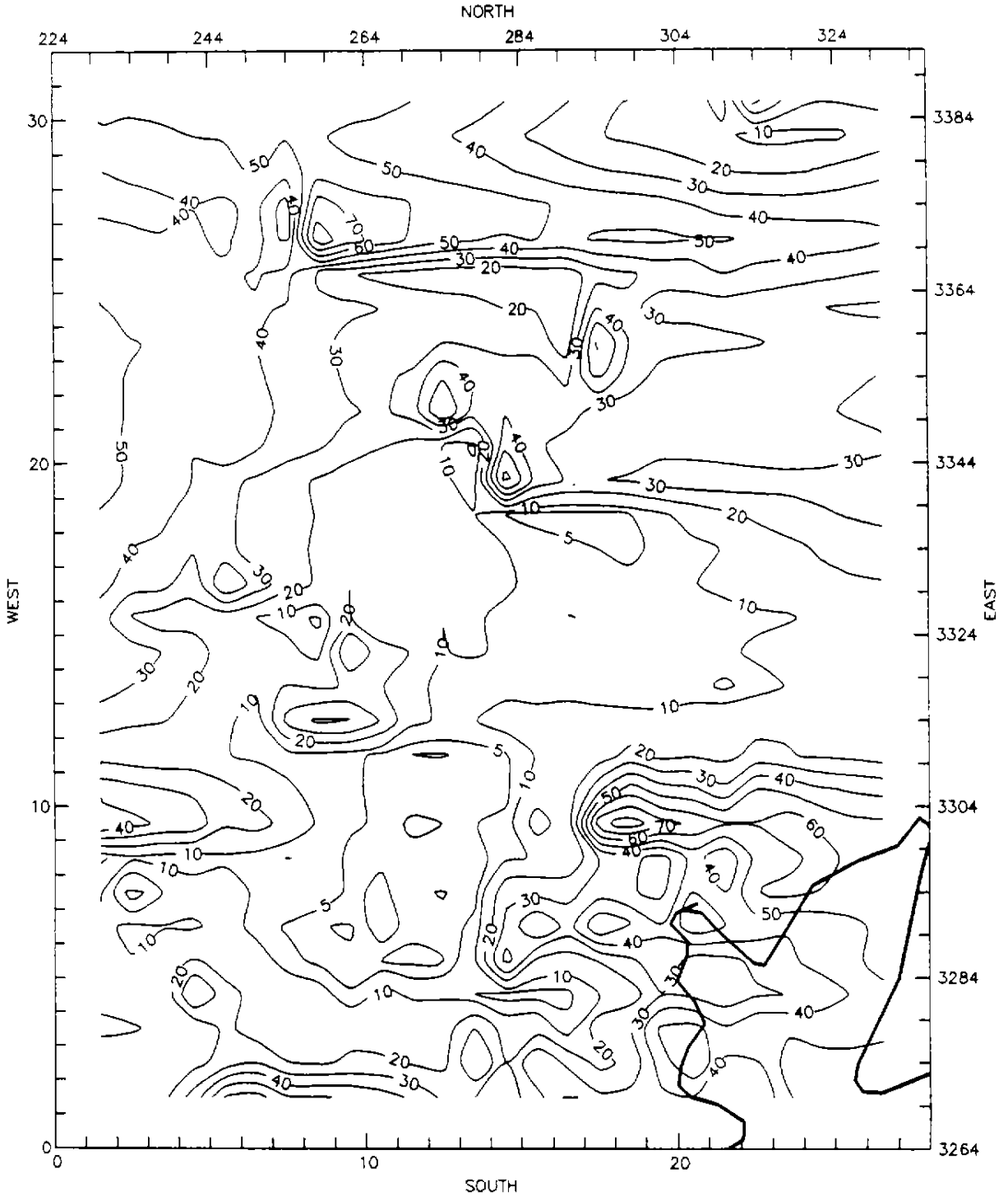

Figure 4-69. Percent contribution of 19th elevated NO_x tracer at 1200 EST, 19 August 1993.

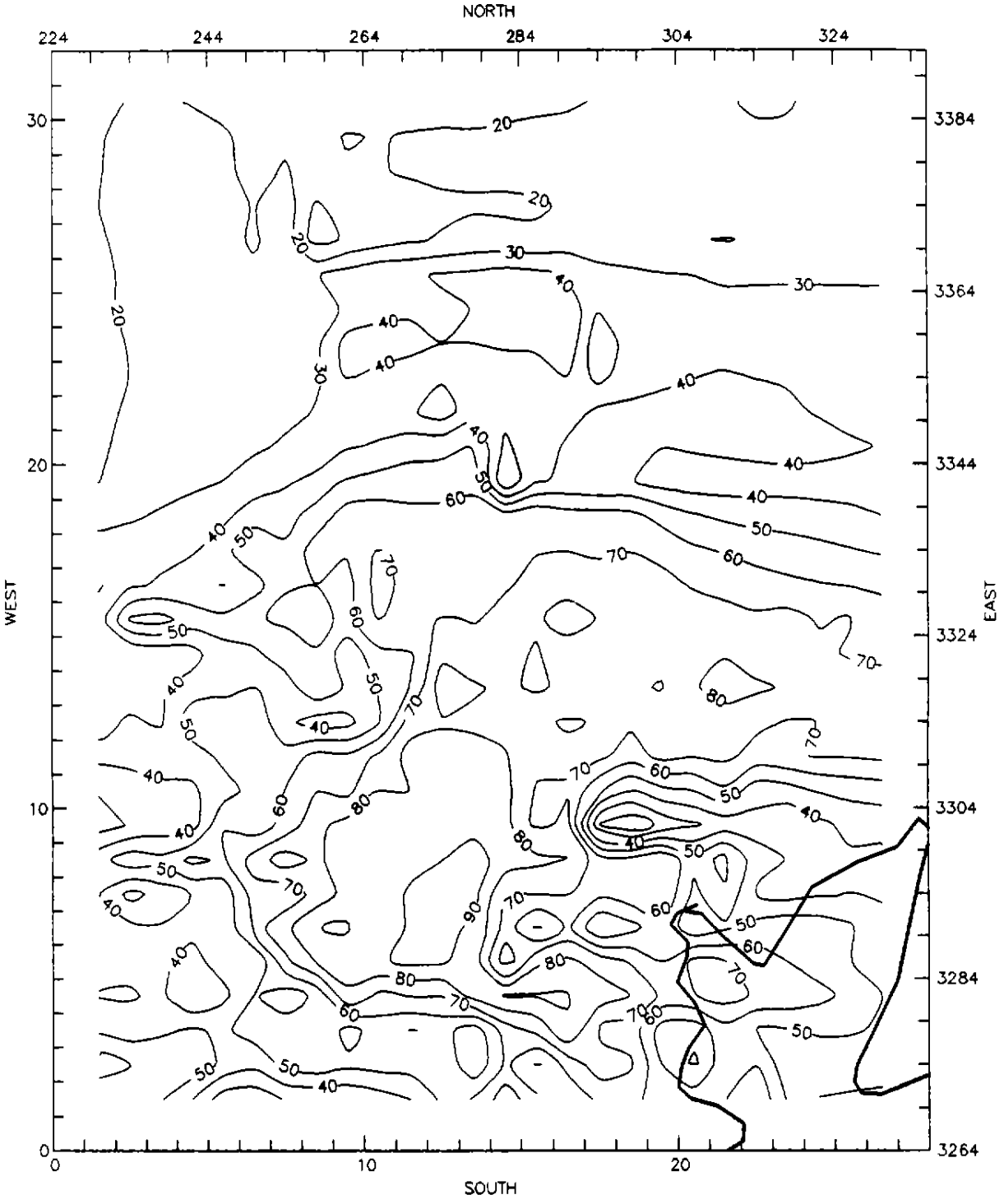

Figure 4-70. Percent contribution of 19th low-level NO_x tracer at 1200 EST, 19 August 1993.

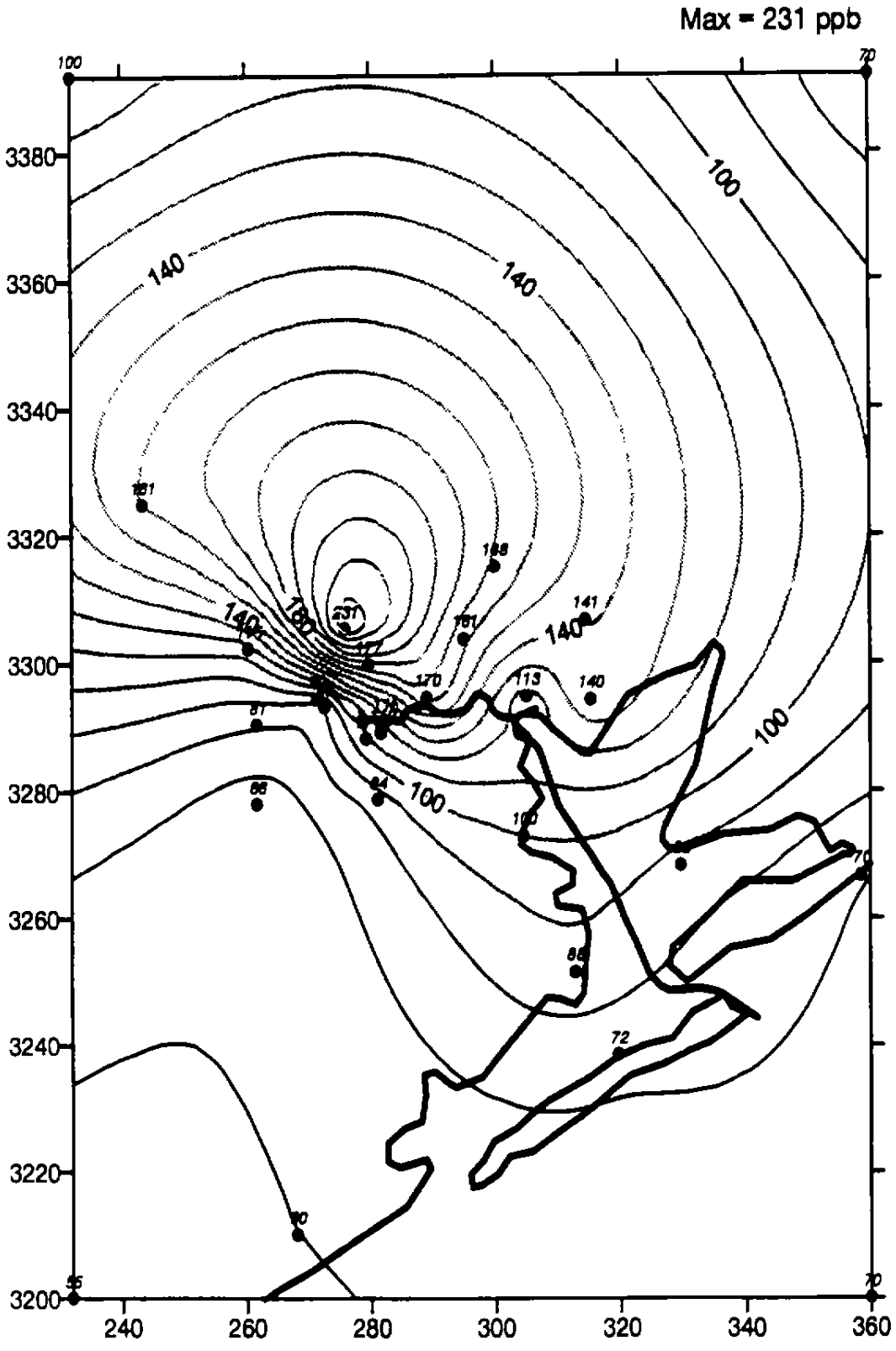

Figure 4-71. Interpolated observations of daily maximum ozone on 19 August. Note steep gradient leading to maximum of 231 ppb and sparsity of data to north of the maximum.

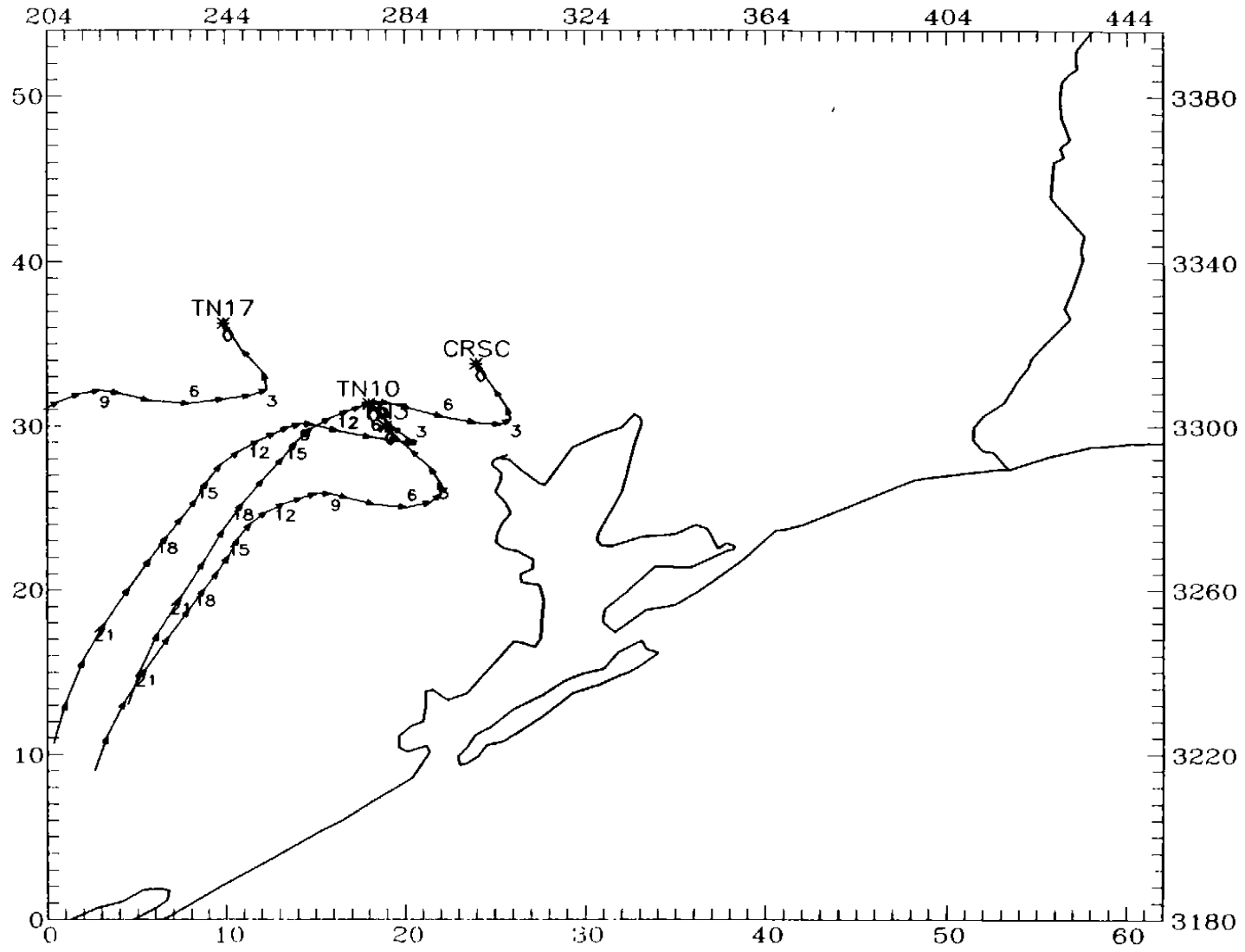

Figure 4-72. Back trajectories using UAM-V windfield from four of the highest ozone observation sites starting at the time (1600) that the 231 ppb observation occurred (at site TN10) on 19 August. Arrows indicate hourly locations.

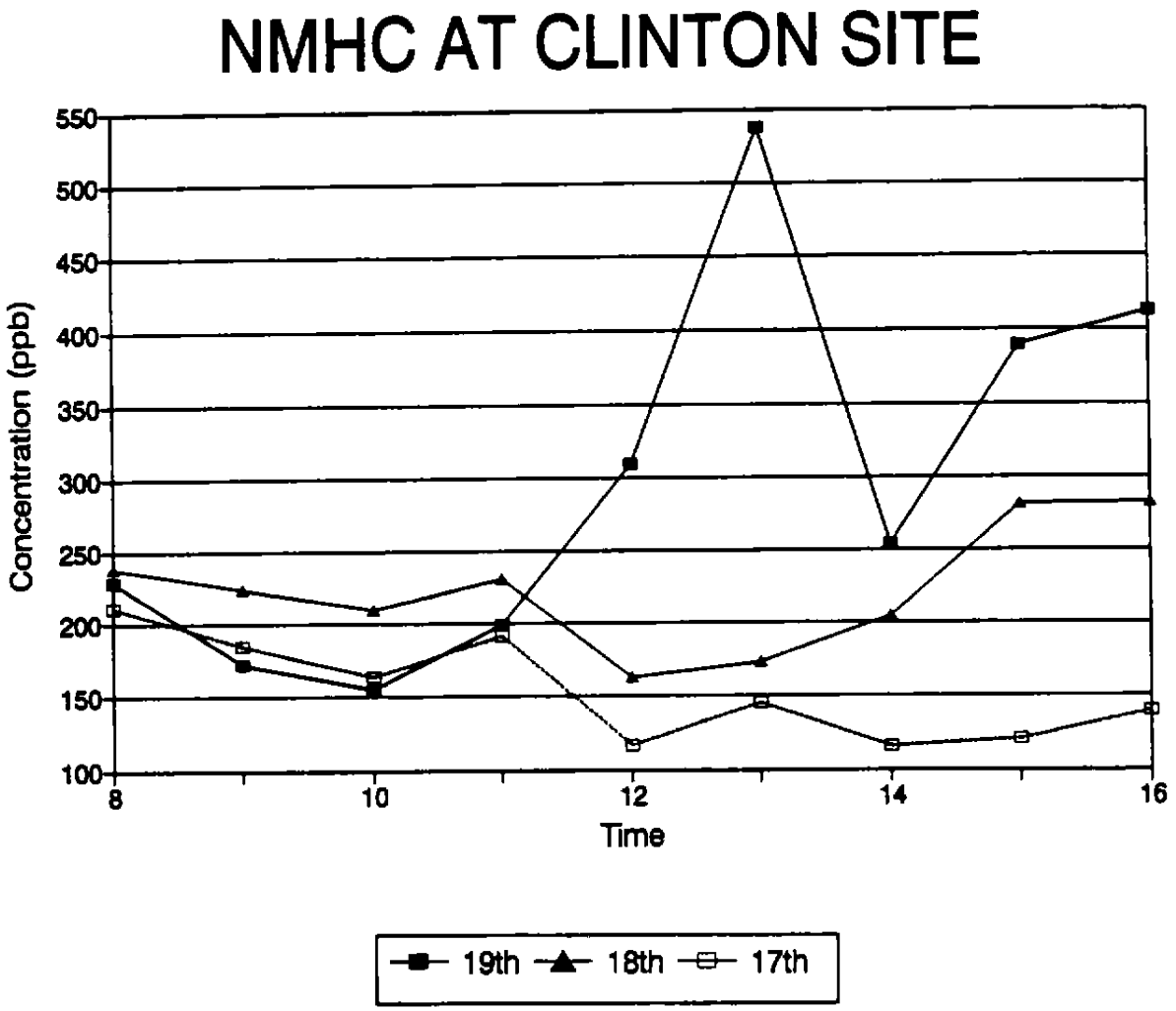

Figure 4-73. Mid-day NMHC concentration (in ppbC) observed near the ship channel (at Clinton) for the 17th through 19th of August.

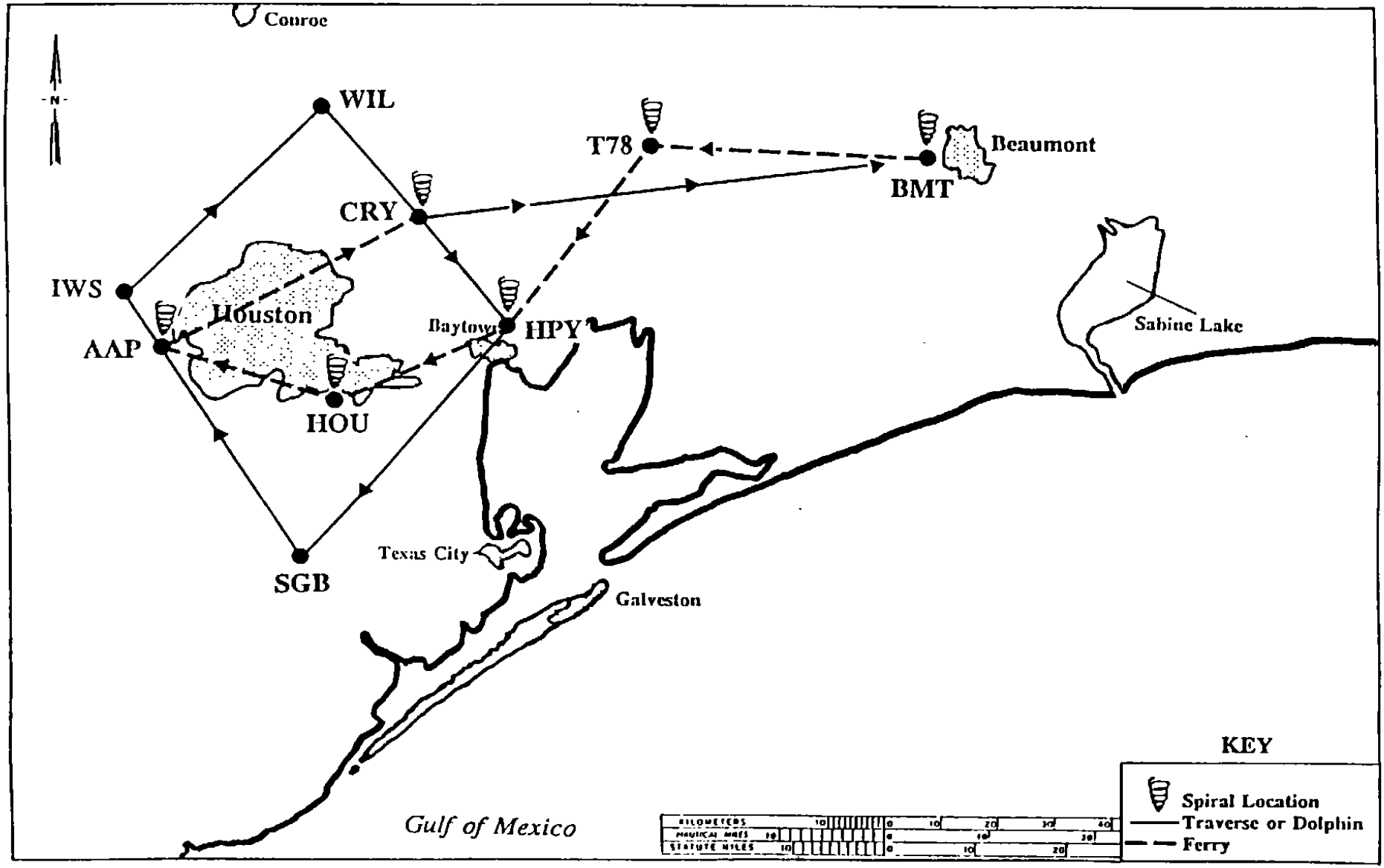

Figure 4-74. Flight route used on the early afternoon of 19 August.

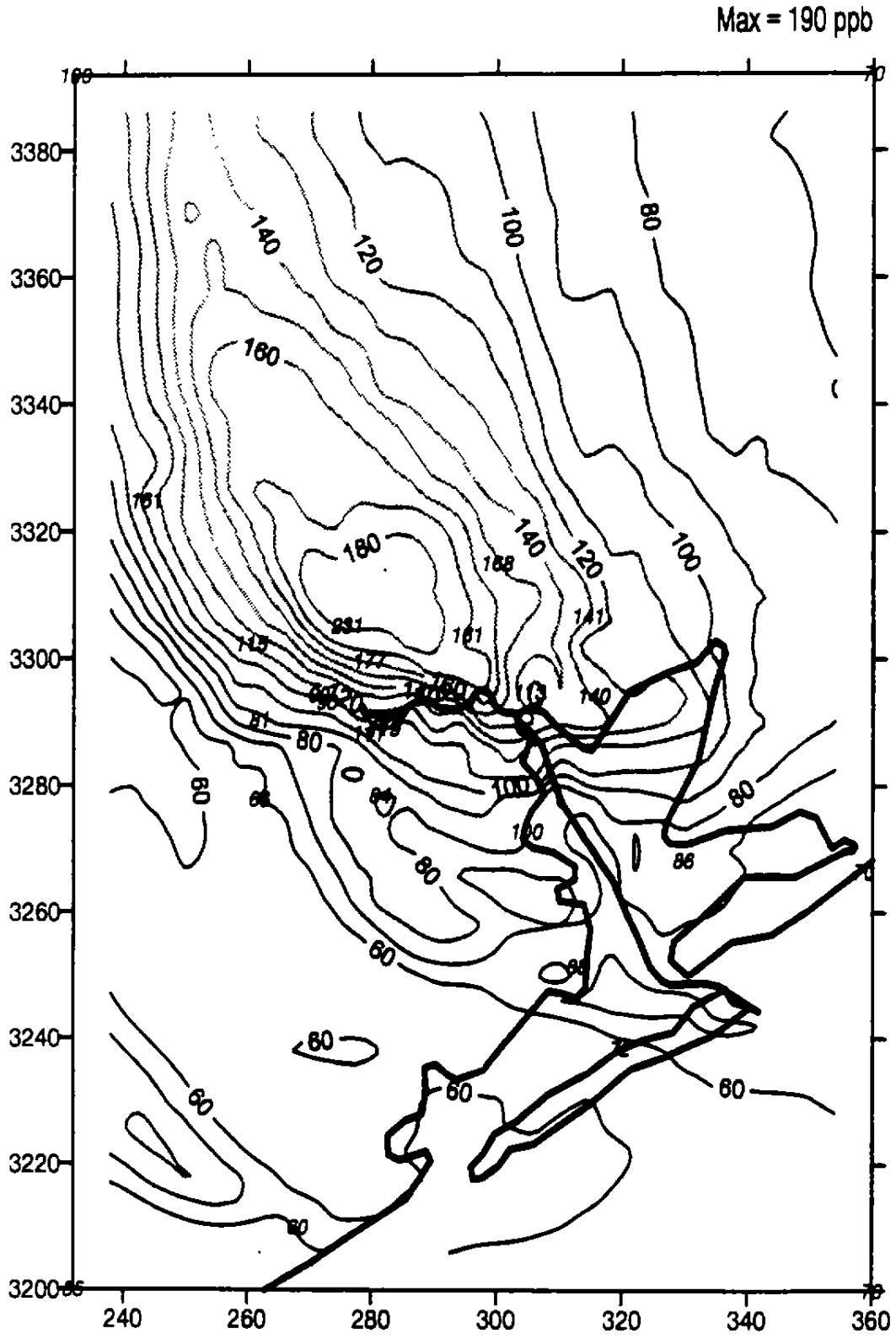

Figure 4-75. Contour plot of UAM-V simulated ozone for 19 August without HC spill on ship channel.

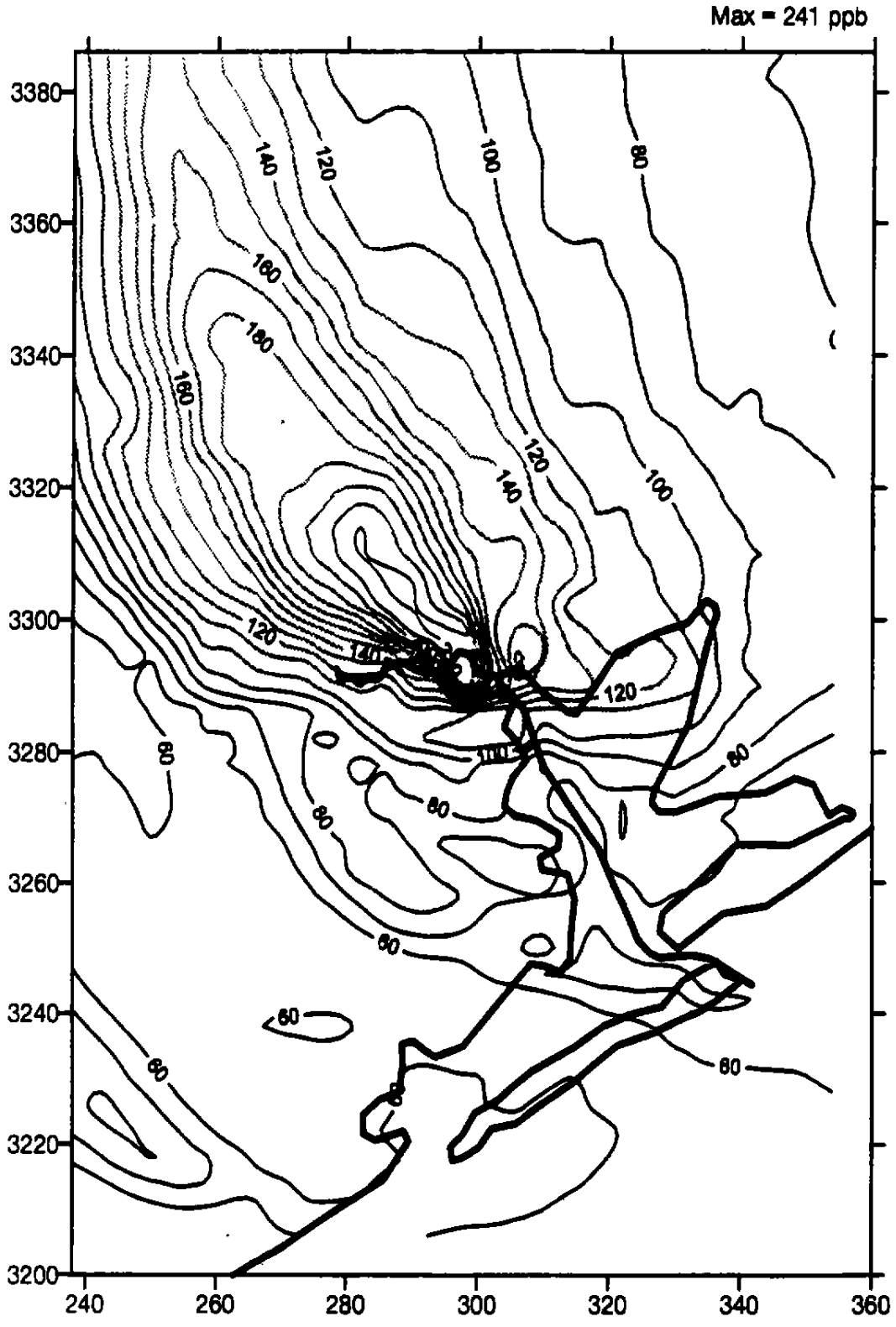

Figure 4-76. Contour plot of UAM-V simulated ozone for 19 August with HC spill on ship channel.

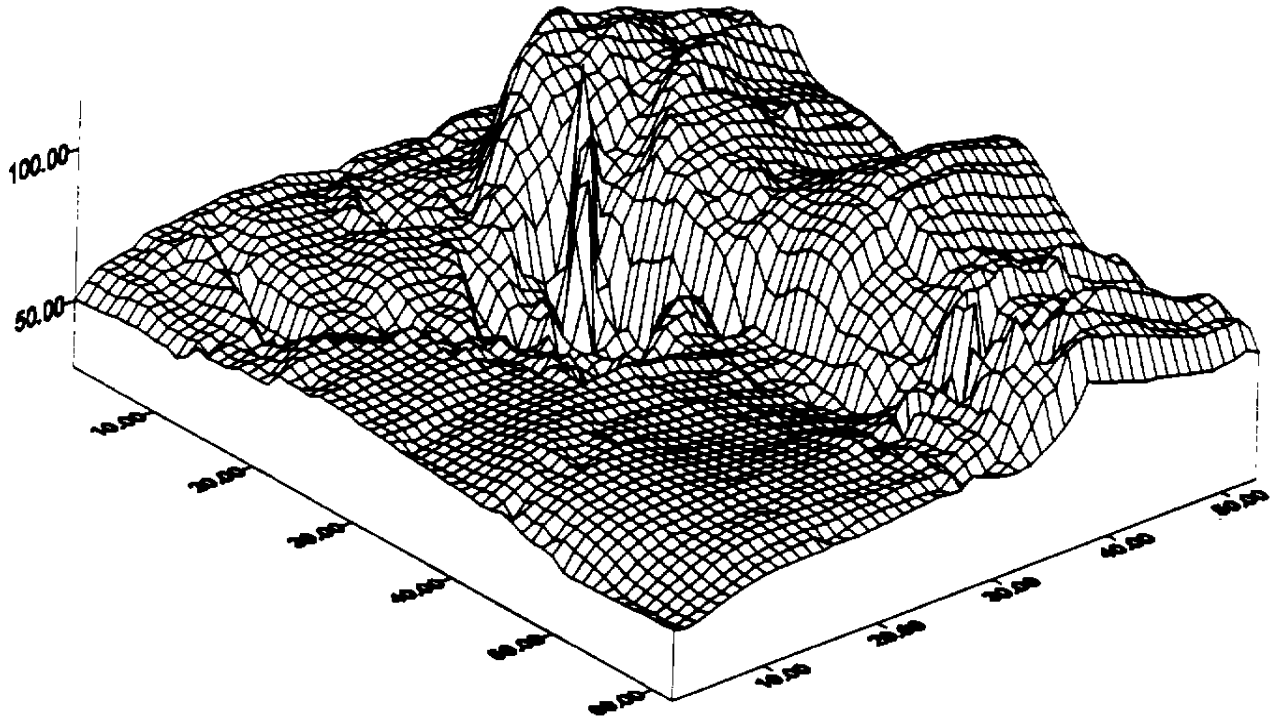

Figure 4-77. 3-D plot of Figure 4-76 looking to the northwest. Note the ozone "spike" in the center of the figure.

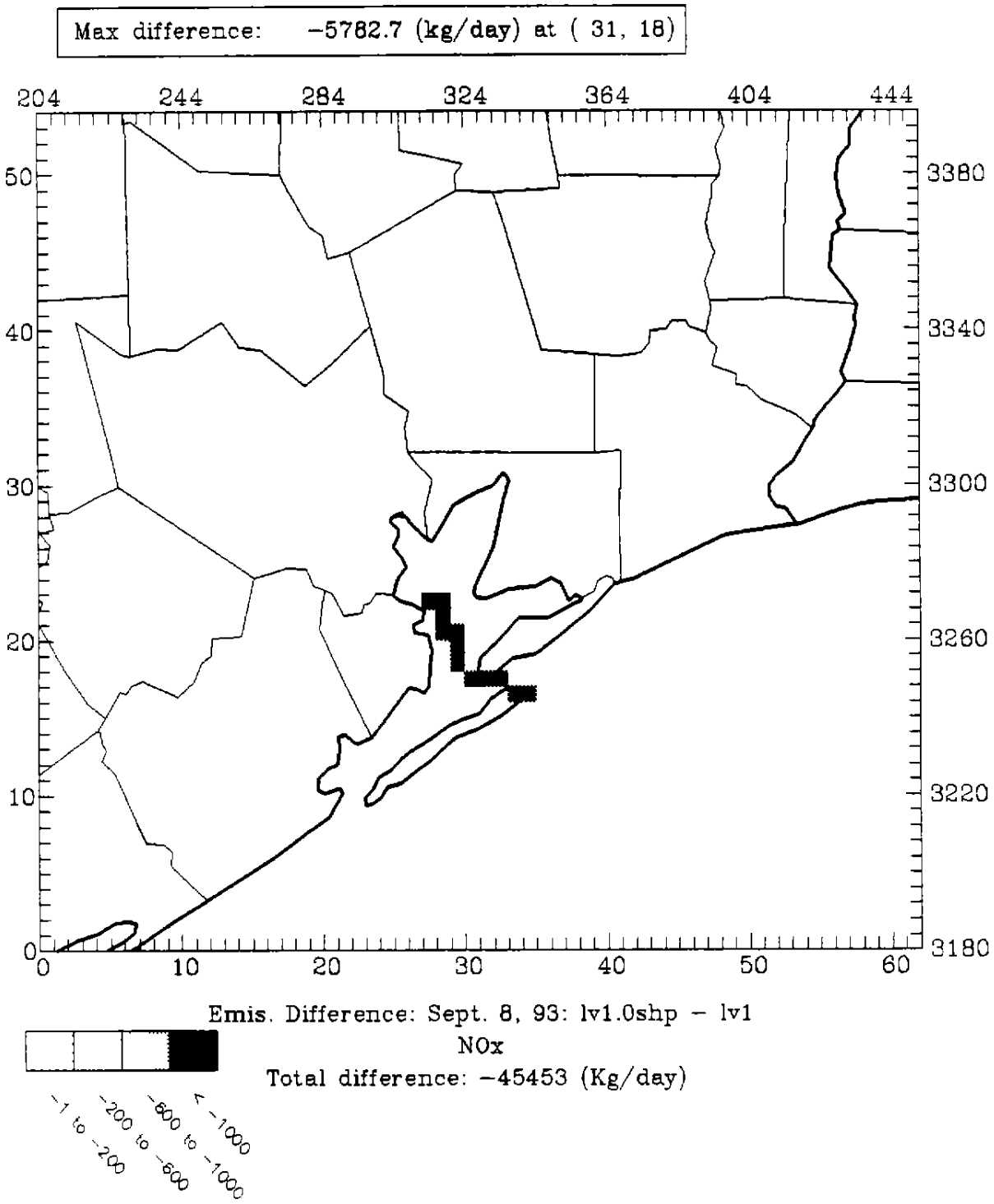

Figure 4-78. Grid cells of the Houston ship channel that were set to zero for one of the September sensitivity tests.

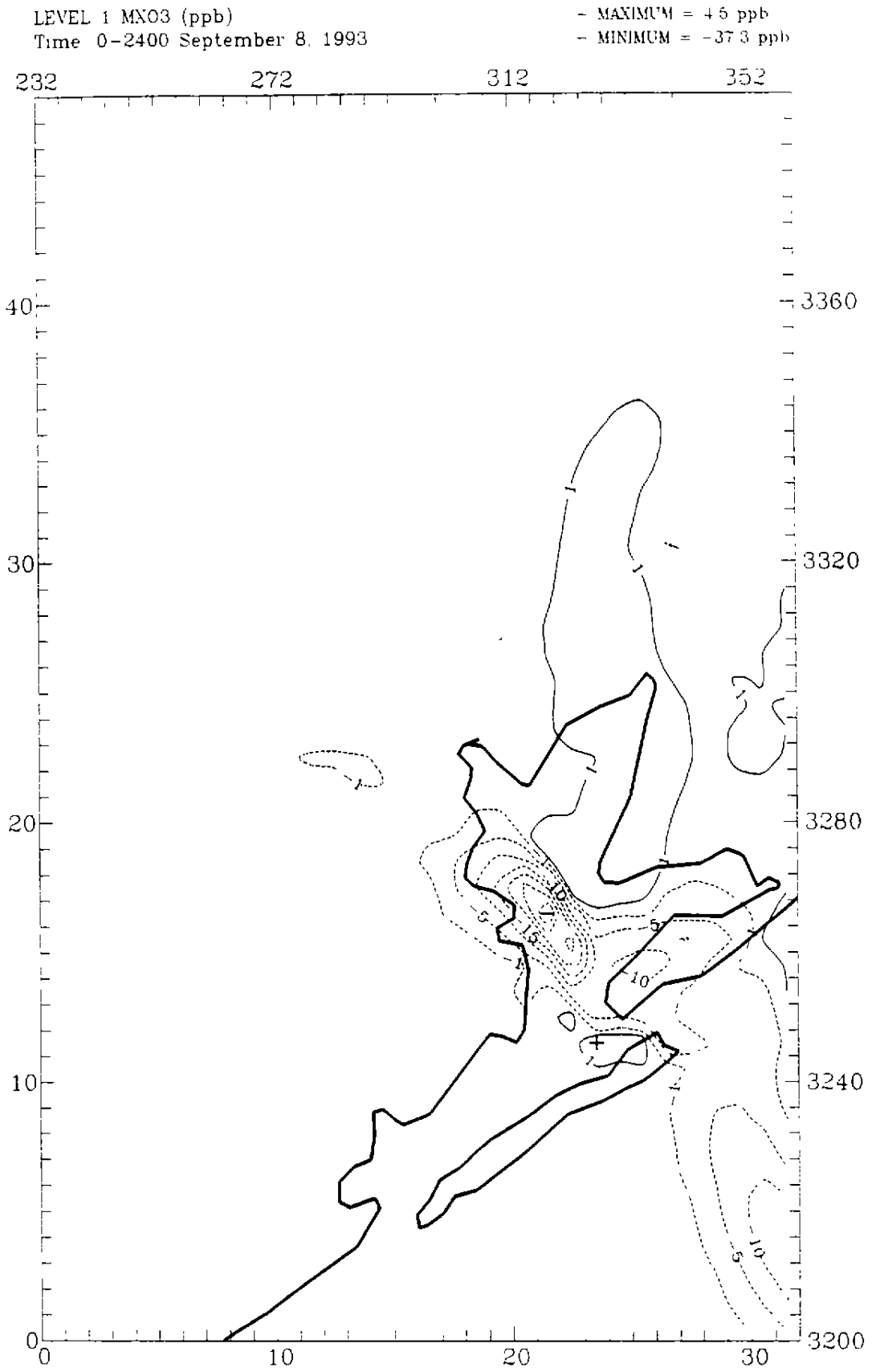

Figure 4-79. Changes in maximum simulated ozone (base minus sensitivity) for 8 September when 50 tons of ship channel NO_x emissions located as shown in Figure 4-78 are set to zero.

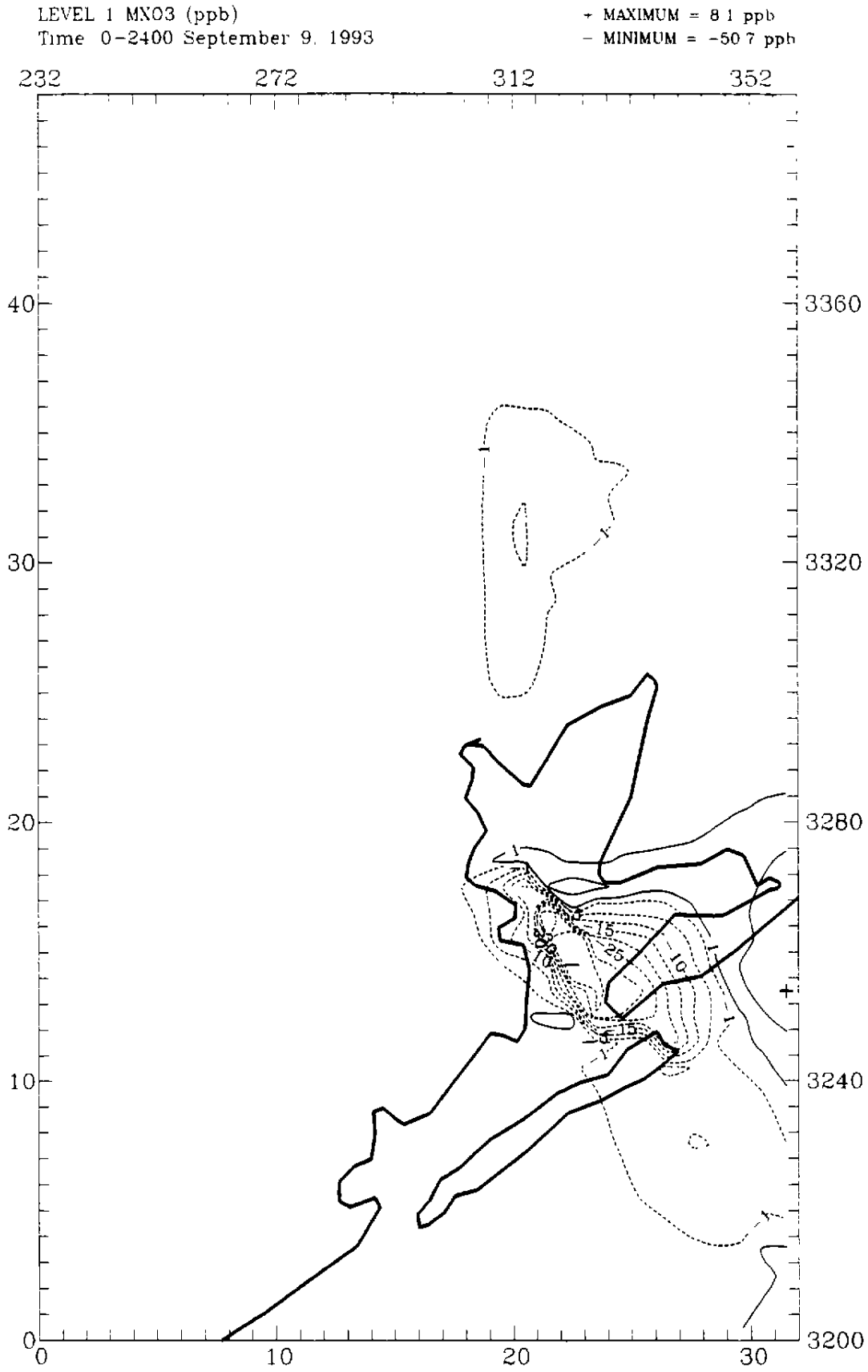

Figure 4-80. Changes in maximum simulated ozone (base minus sensitivity) for 9 September when 50 tons of ship channel NO_x emissions located as shown in Figure 4-78 are set to zero.

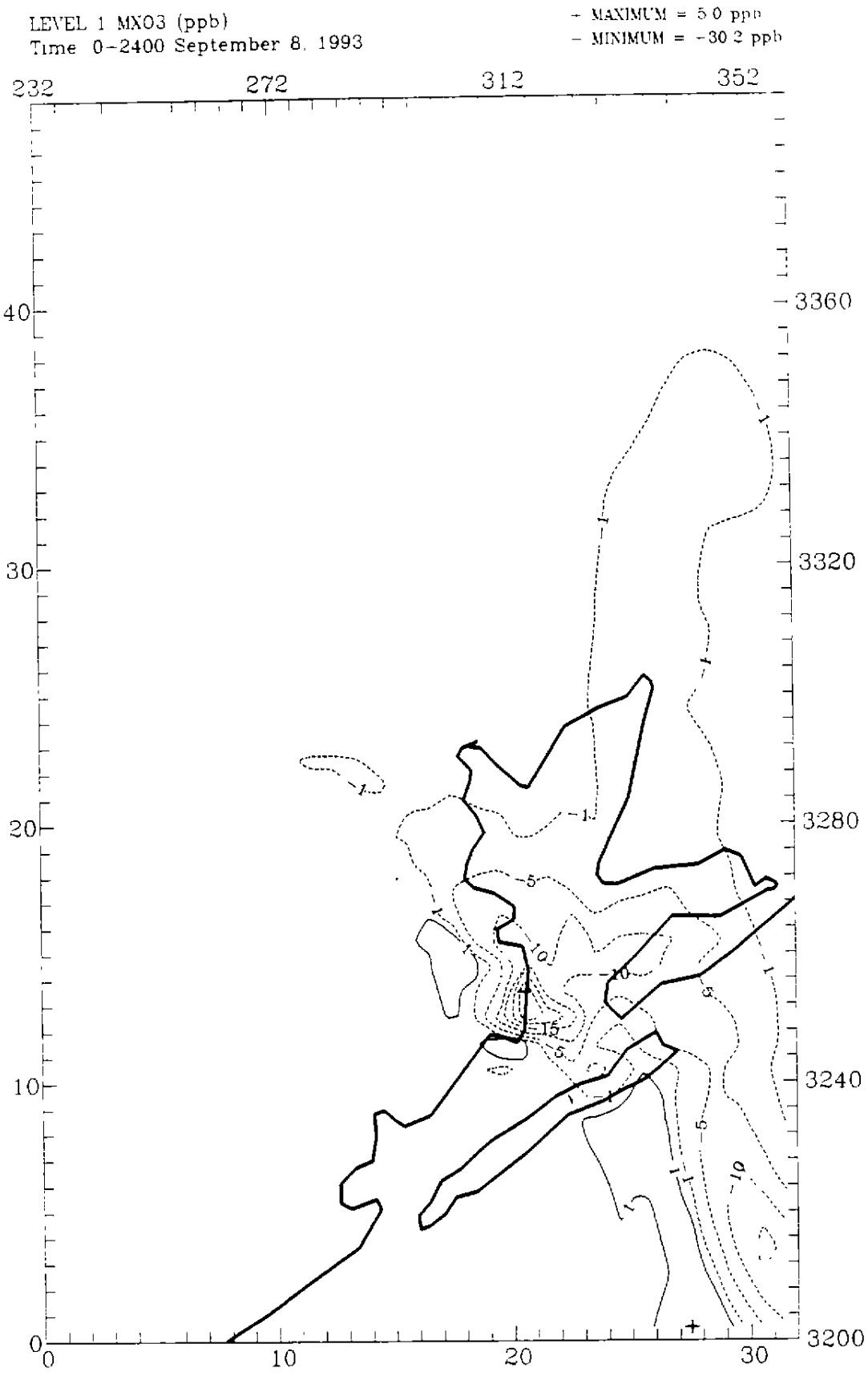

Figure 4-81. Changes in maximum simulated ozone (base minus sensitivity) for 8 September when 50 tons of point NO_x emissions located near Texas City are set to zero.

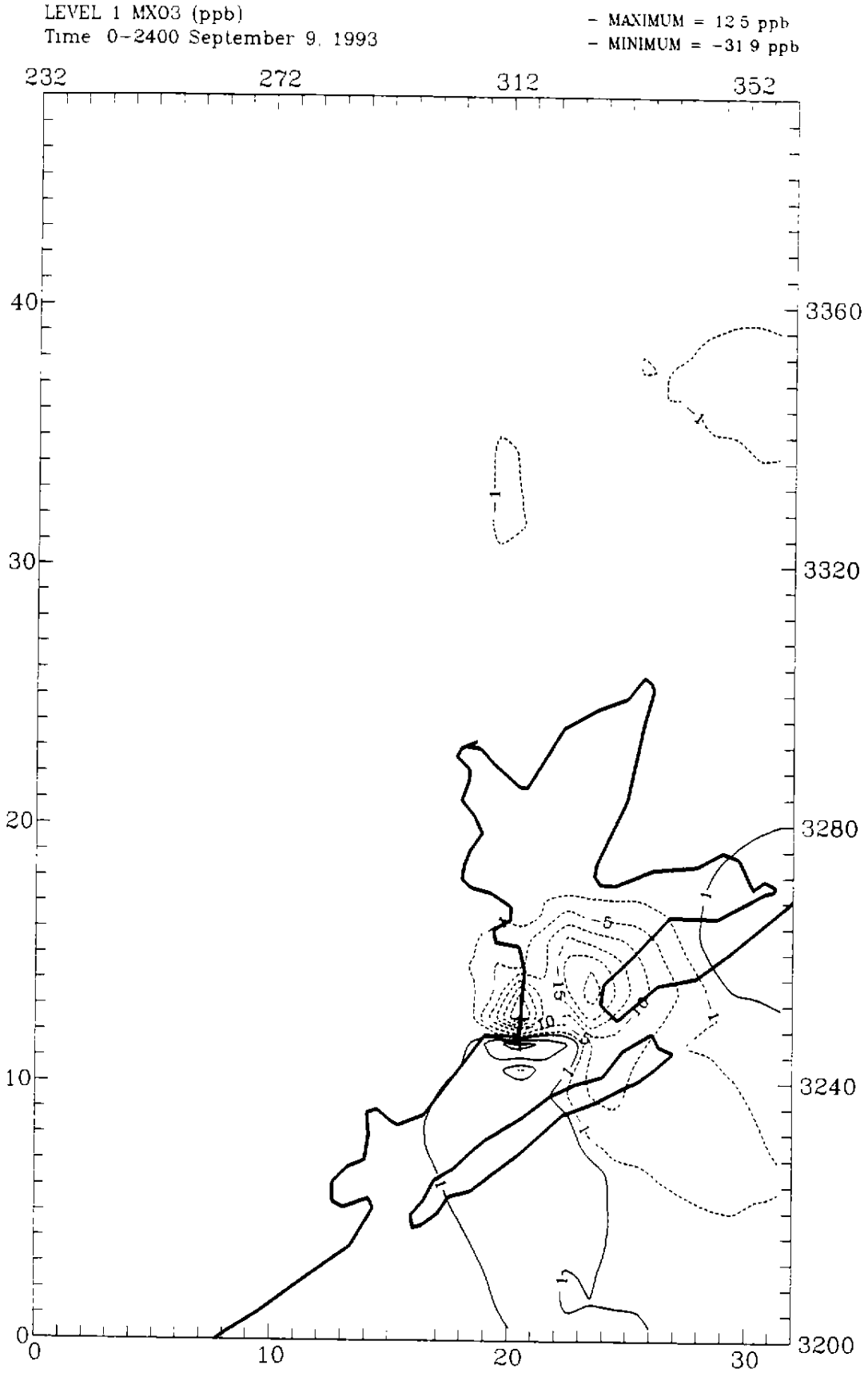

Figure 4-82. Changes in maximum simulated ozone (base minus sensitivity) for 9 September when 50 tons of point NO_x emissions located near Texas City are set to zero.

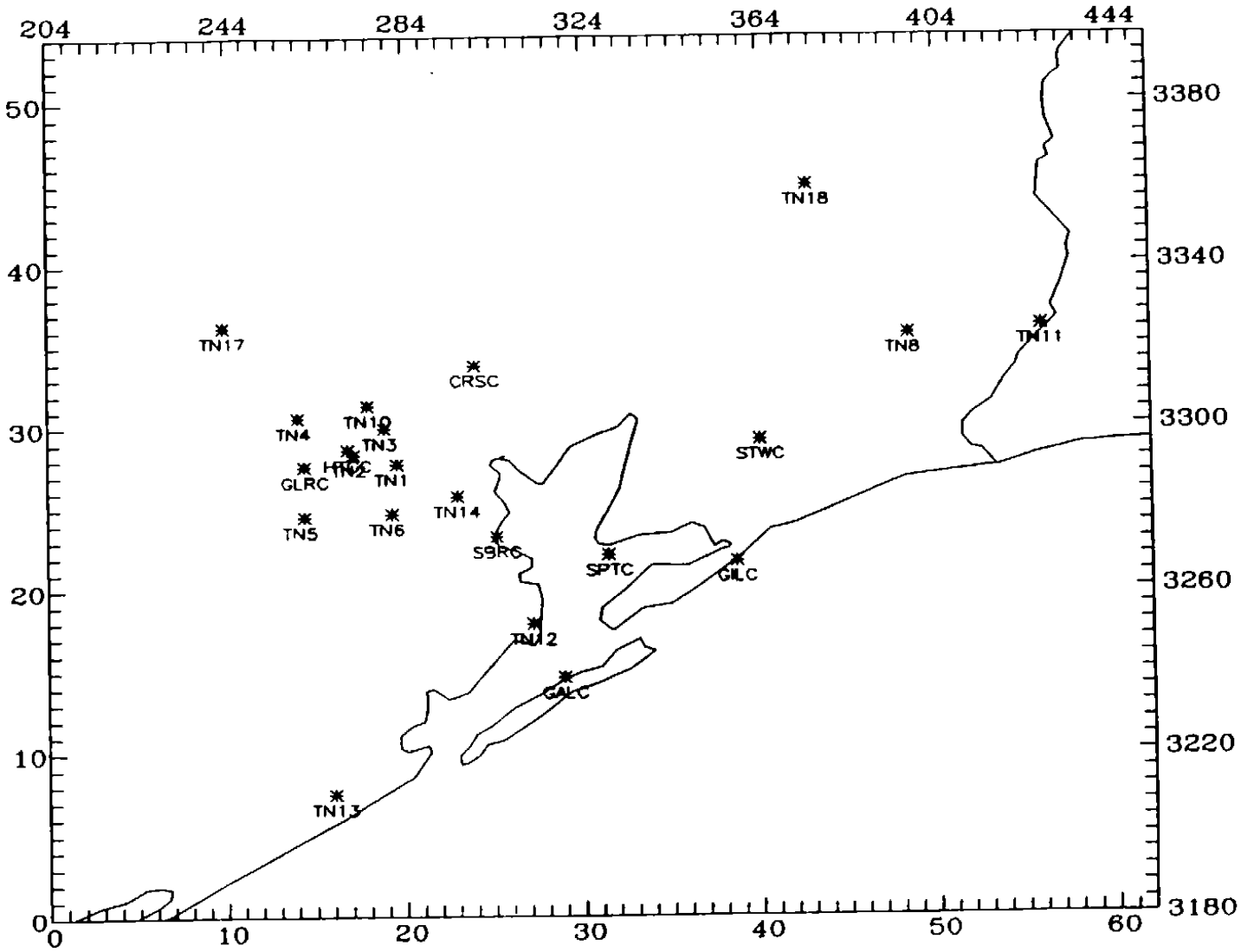

Figure 4-83. Locations of selected ozone monitoring sites within the Houston subdomain.

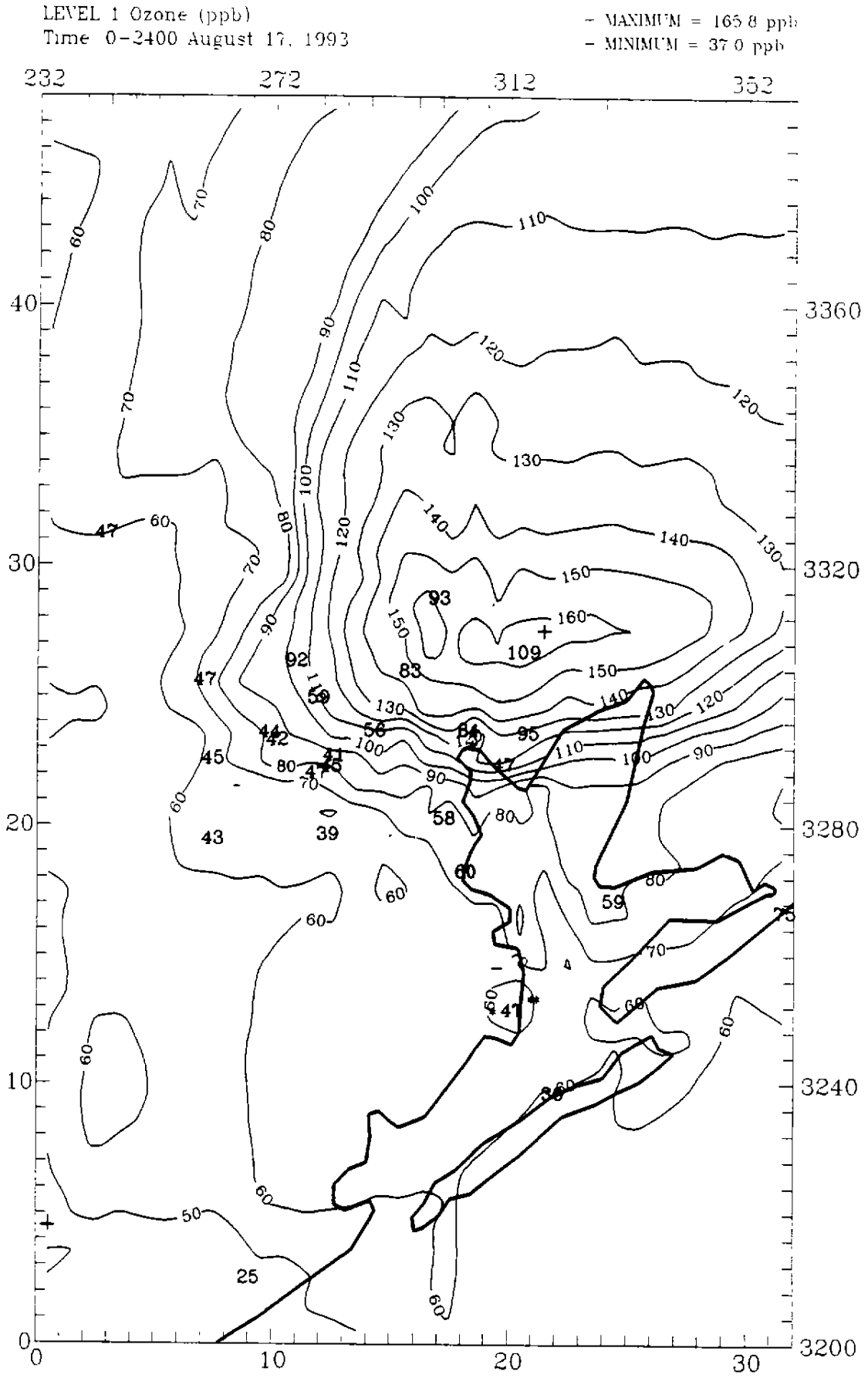

Figure 4-84. Maximum simulated (hourly averaged) ozone concentrations (ppb) in the Houston area on 17 August 1993 for the base-case simulation. Observed maxima are also shown.

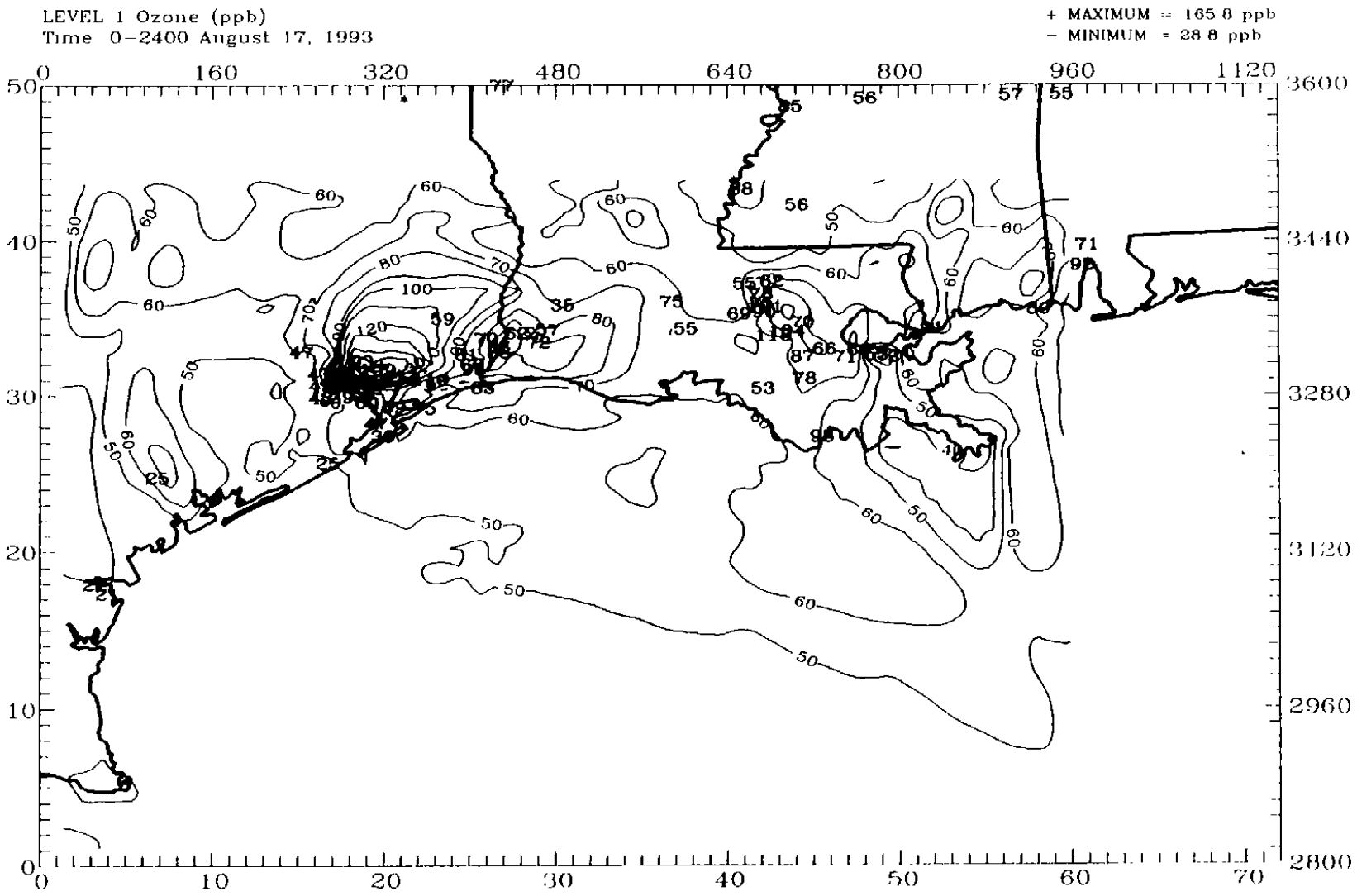

Figure 4-85. Maximum simulated (hourly averaged) ozone concentrations (ppb) in the GMAQS domain on 17 August 1993 for the base-case simulation. Observed maxima are also shown.

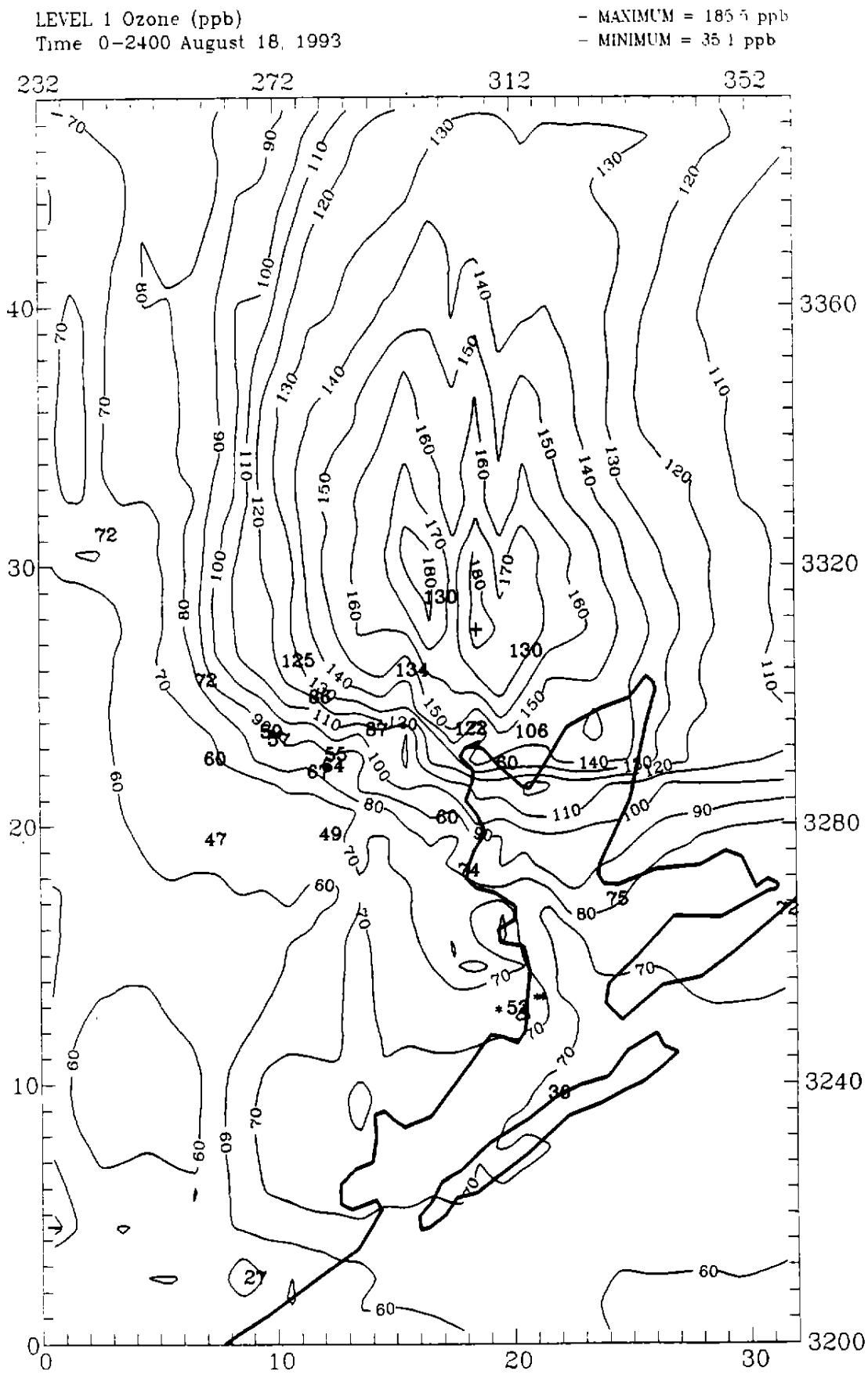

Figure 4-86. Maximum simulated (hourly averaged) ozone concentrations (ppb) in the Houston area on 18 August 1993 for the base-case simulation. Observed maxima are also shown.

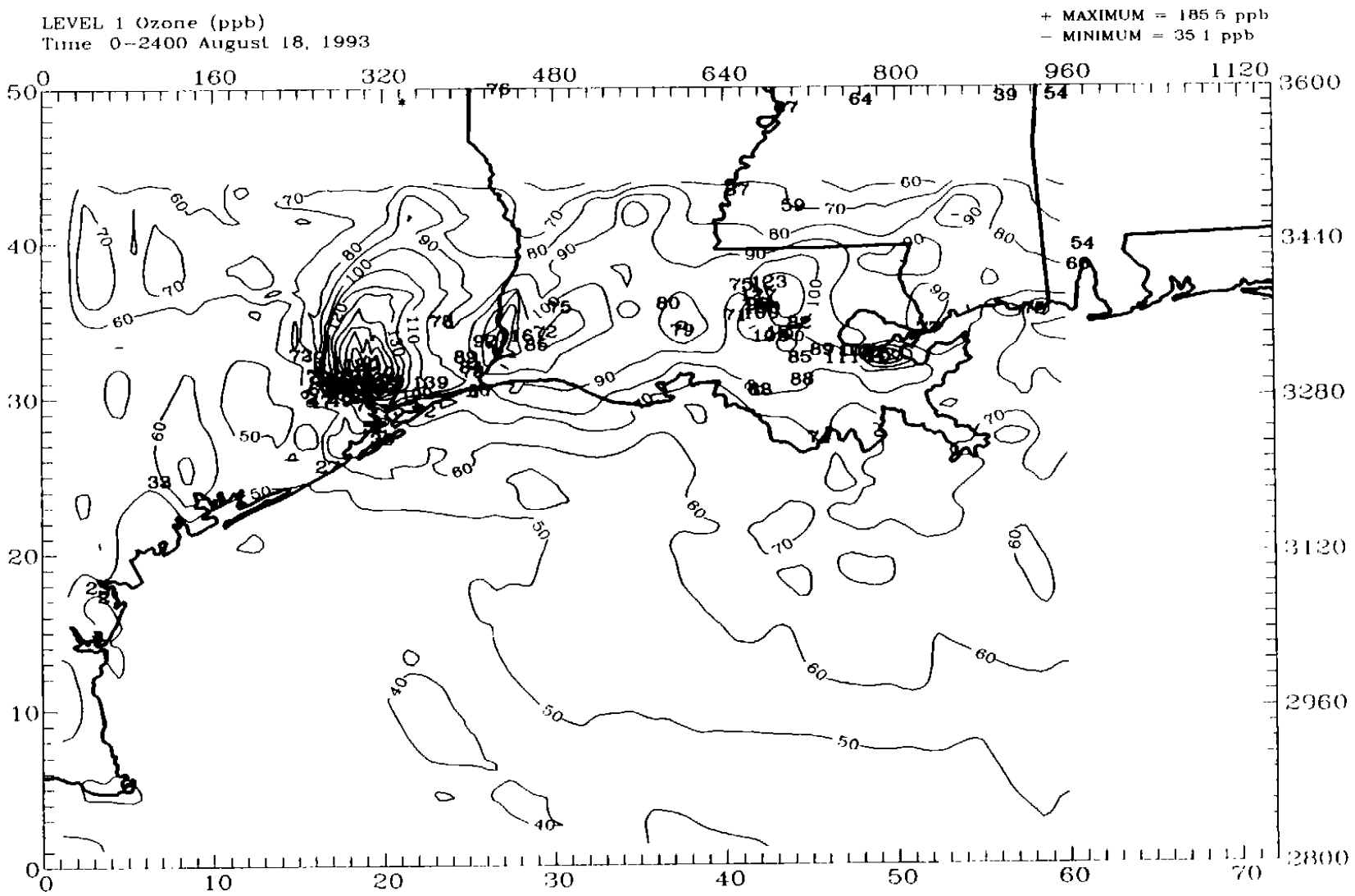

Figure 4-87. Maximum simulated (hourly averaged) ozone concentrations (ppb) in the GMAQS domain on 18 August 1993 for the base-case simulation. Observed maxima are also shown.

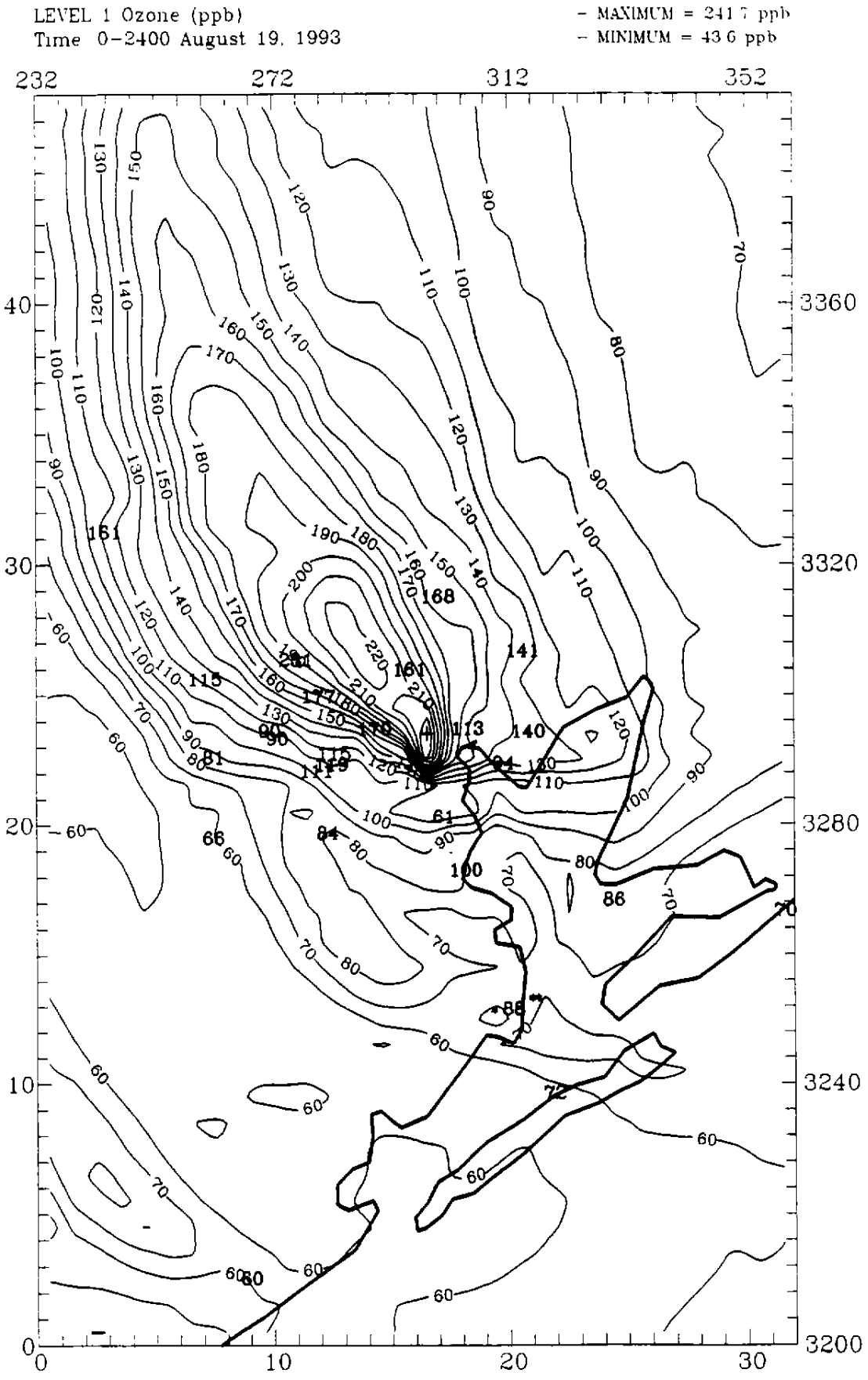

Figure 4-88. Maximum simulated (hourly averaged) ozone concentrations (ppb) in the Houston area on 19 August 1993 for the base-case simulation. Observed maxima are also shown.

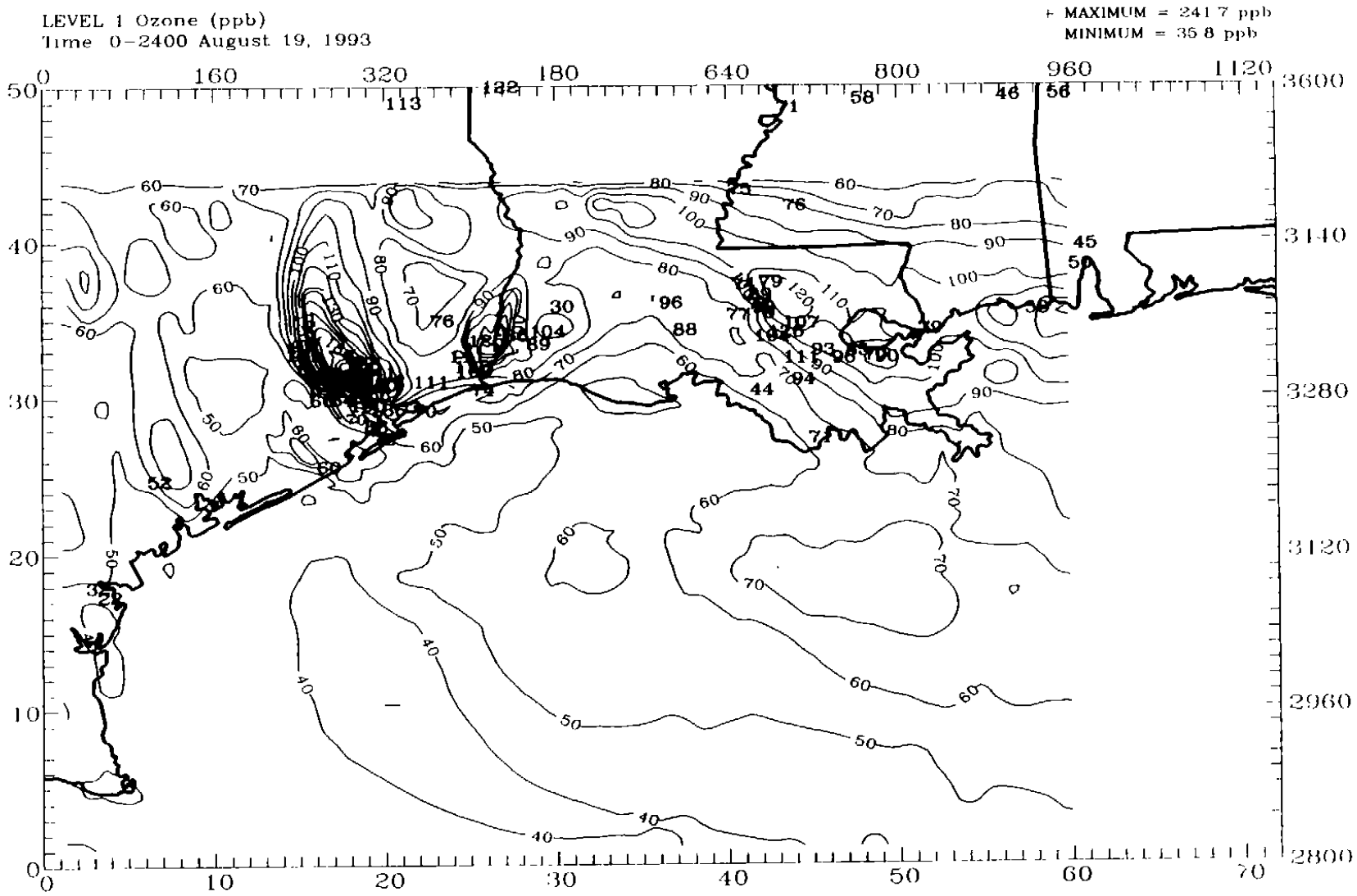

Figure 4-89. Maximum simulated (hourly averaged) ozone concentrations (ppb) in the GMAQS domain on 19 August 1993 for the base-case simulation. Observed maxima are also shown.

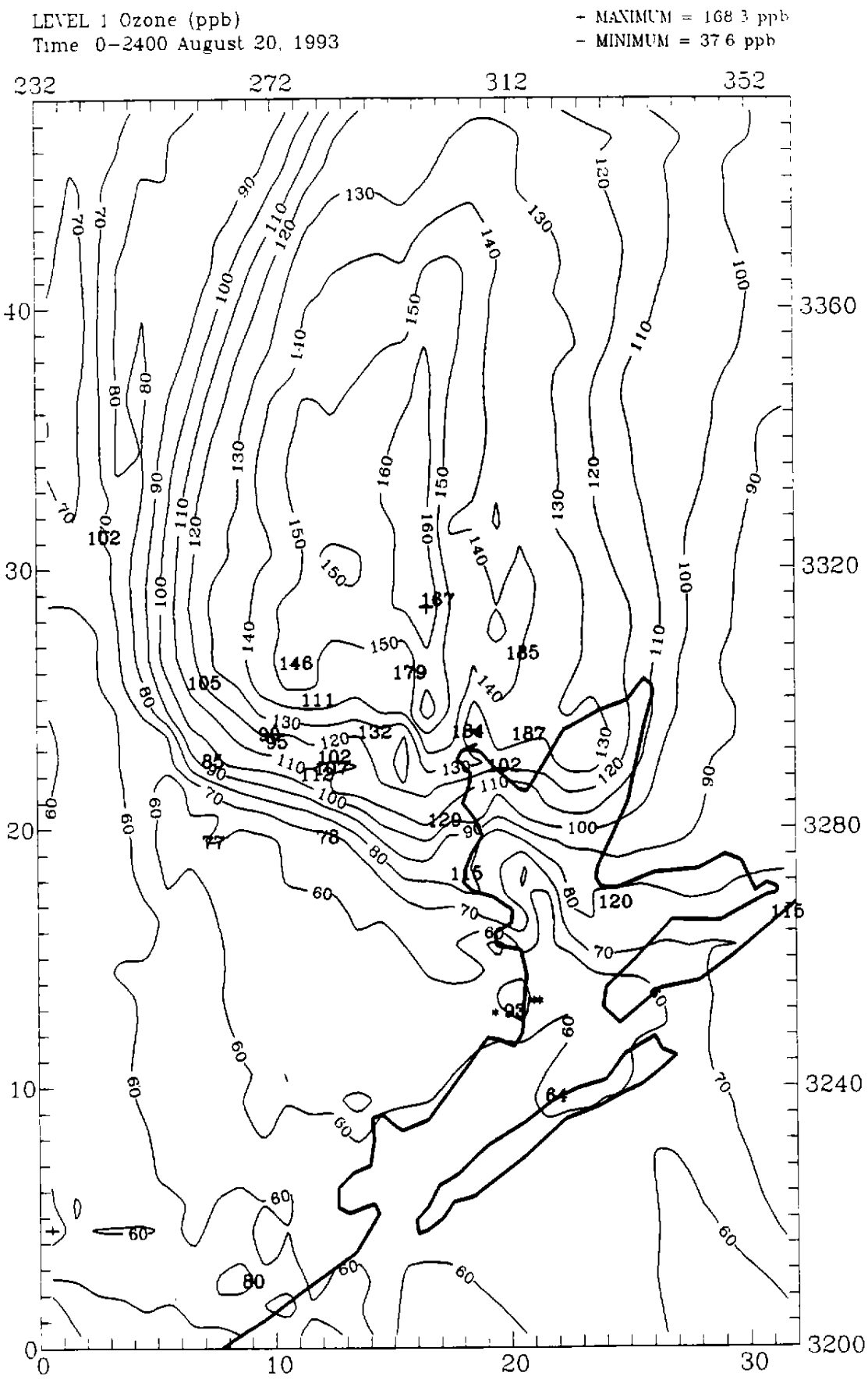

Figure 4-90. Maximum simulated (hourly averaged) ozone concentrations (ppb) in the Houston area on 20 August 1993 for the base-case simulation. Observed maxima are also shown.

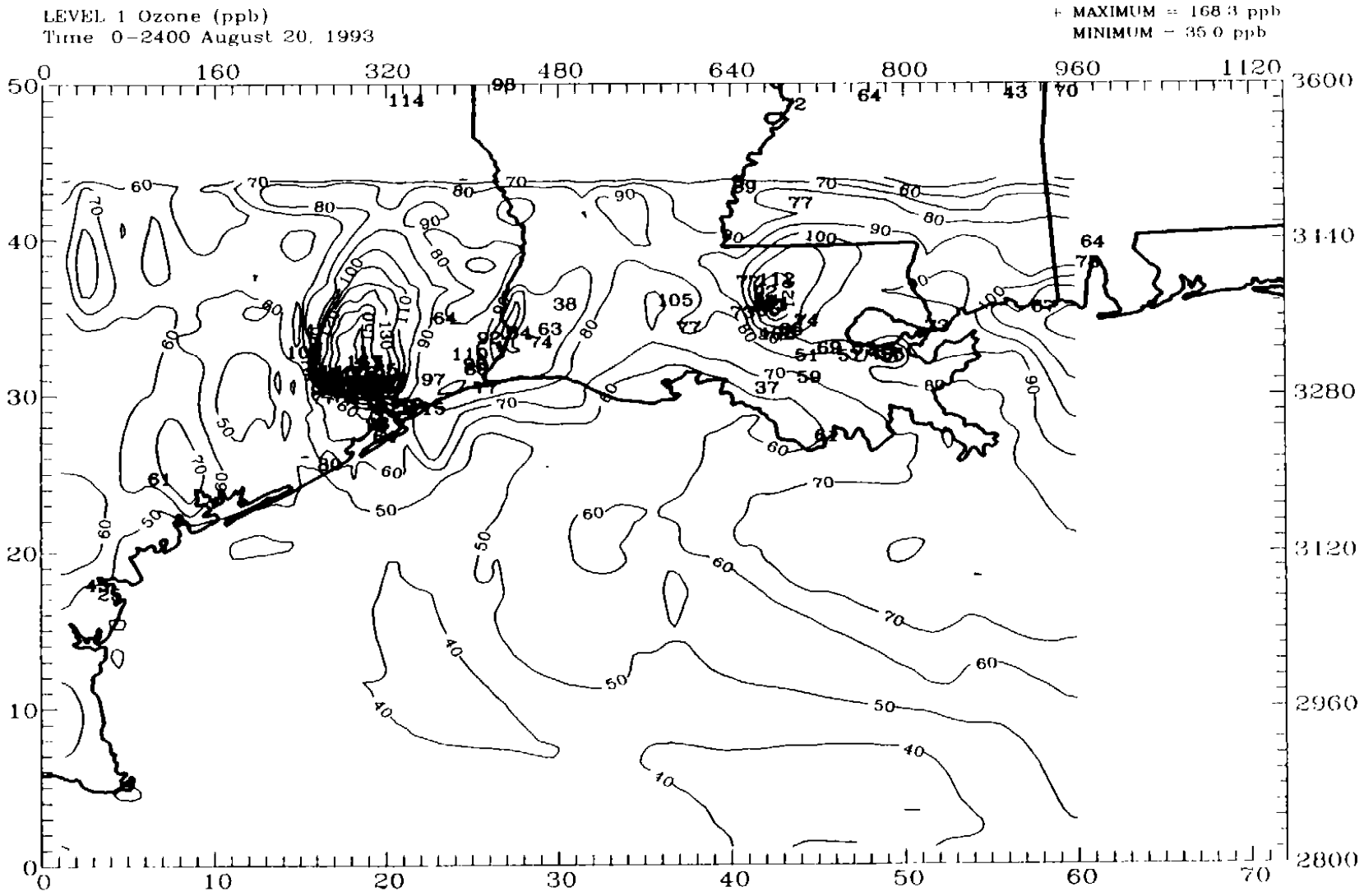

Figure 4-91. Maximum simulated (hourly averaged) ozone concentrations (ppb) in the GMAQS domain on 20 August 1993 for the base-case simulation. Observed maxima are also shown.

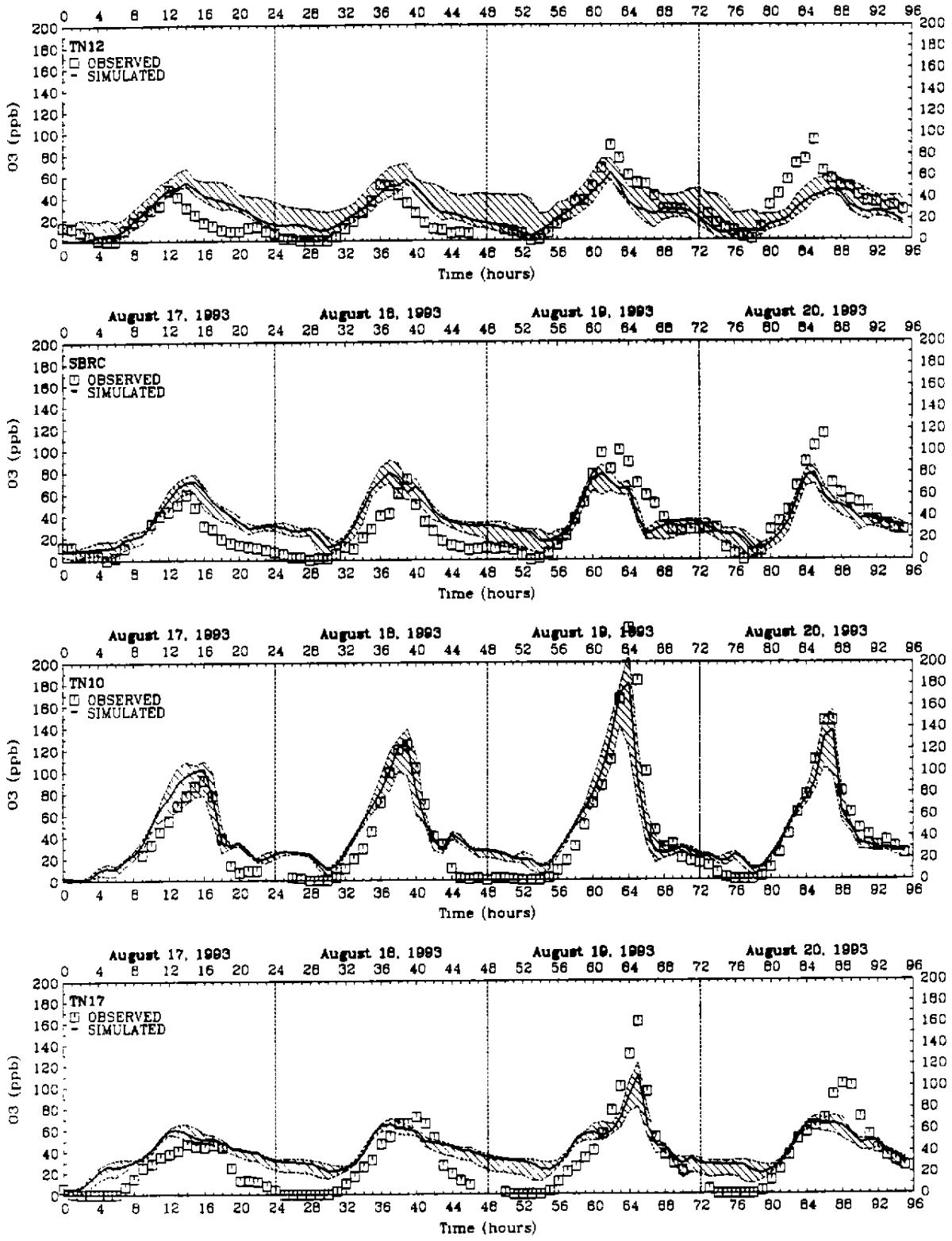

Simulated Ozone Concentrations on August 17–20 1993. (Base Case)

Figure 4-92a. Time-series plots comparing simulated and observed ozone concentrations (ppb) for selected monitoring sites within the Houston subdomain for the 17-20 August 1993 period. Base-case simulation.

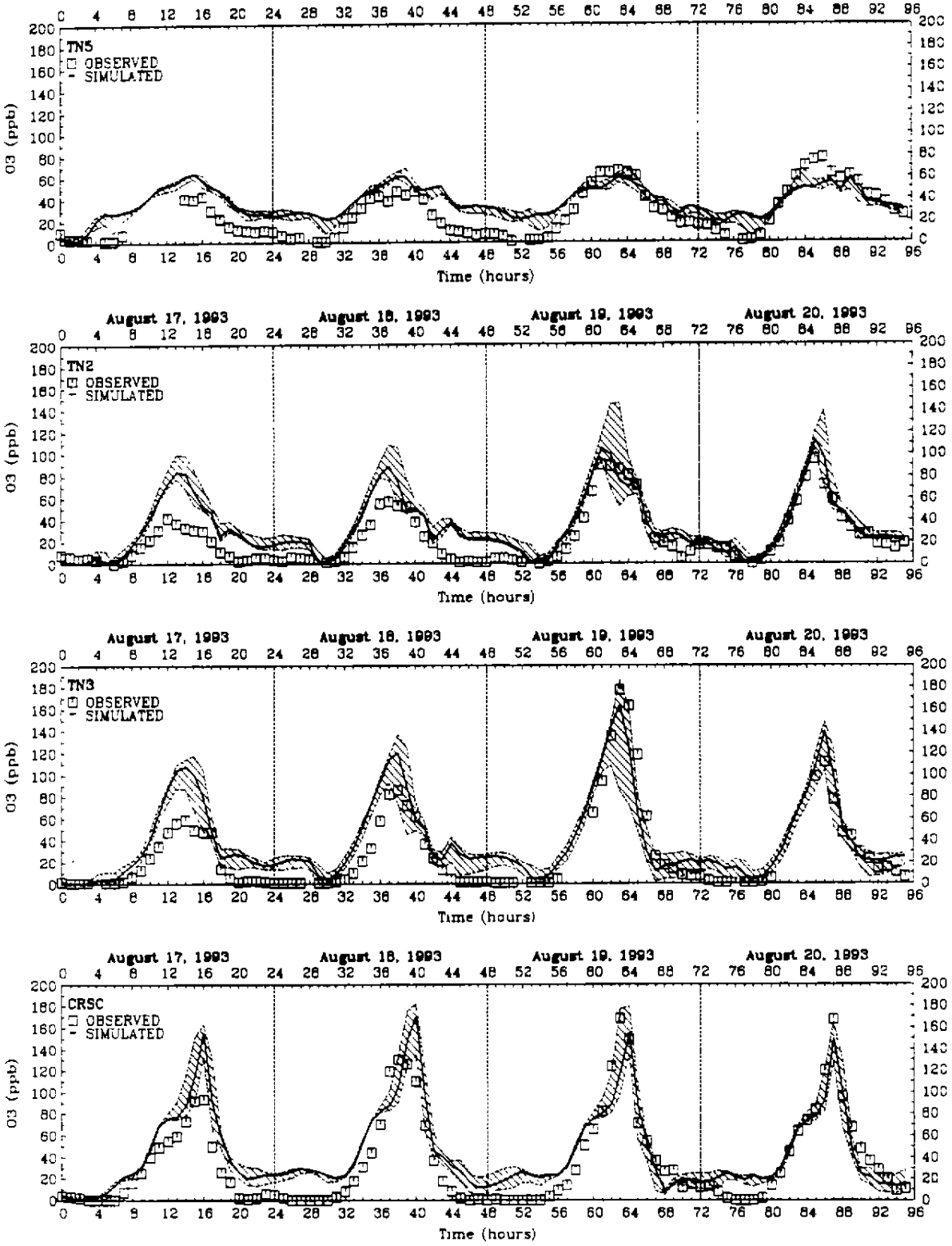

Simulated Ozone Concentrations on August 17-20 1993 (Base Case)

Figure 4.92b. Concluded

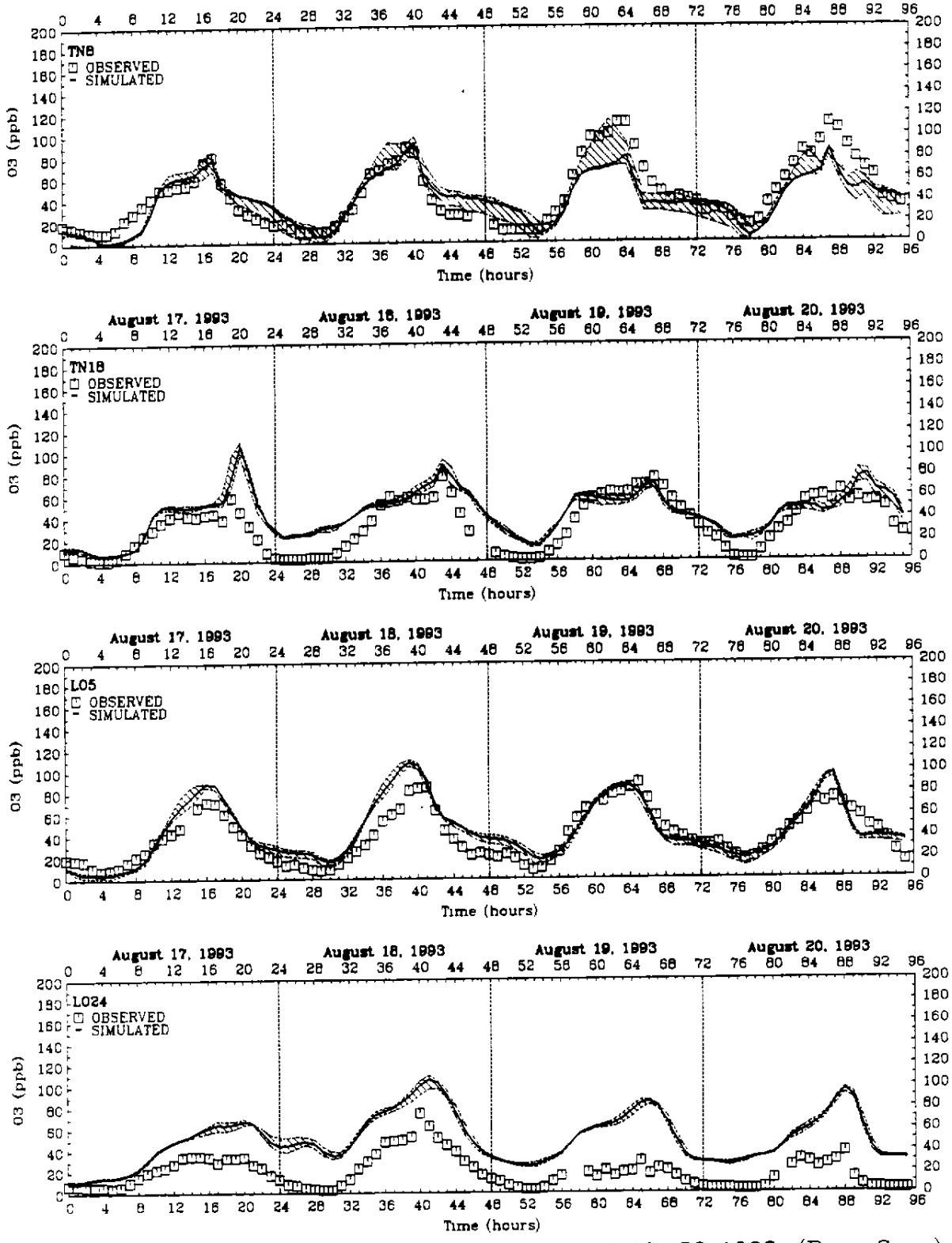

Simulated Ozone Concentrations on August 17–20 1993. (Base Case)

Figure 4-93. Time-series plots comparing simulated and observed ozone concentrations (ppb) for selected monitoring sites in the Beaumont/Port Arthur/Lake Charles area for the 17-20 August 1993 period. Base-case simulation.

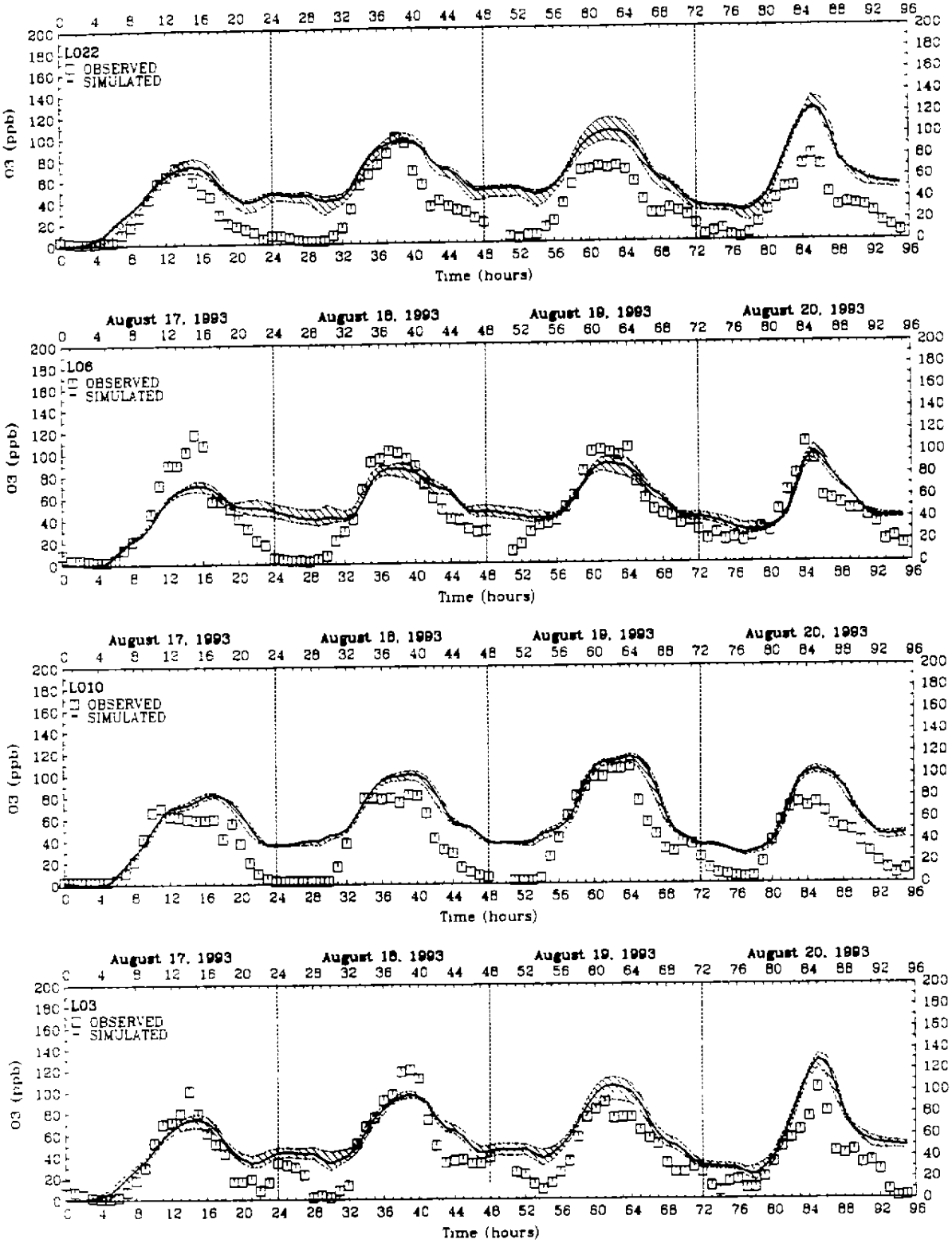

Simulated Ozone Concentrations on August 17–20 1993. (Base Case)

Figure 4-94. Time-series plots comparing simulated and observed ozone concentrations (ppb) for selected monitoring sites within the Baton Rouge area for the 17-20 August 1993 period. Base-case simulation.

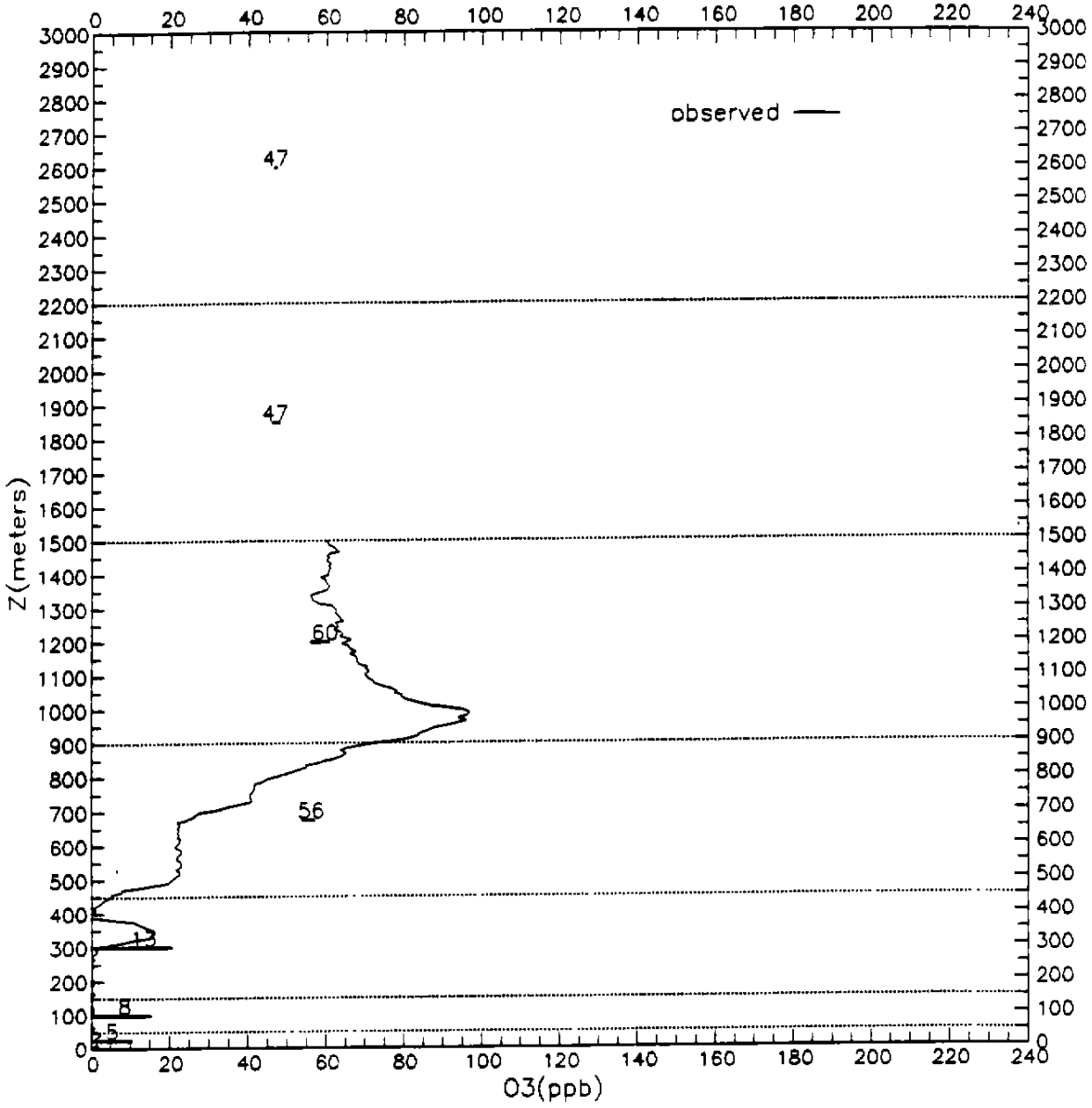

Figure 4-95a. Comparison of upper-air simulated and observed ozone concentrations for the HPY aircraft spiral location on 18 August 1993 at 0545 -0553 CST for the base-case simulation. The solid line represents the instantaneous aircraft measurements and the numerical values represent the simulated values within each UAM-V layer (indicated by horizontal dashed lines). The nearest surface observation is 0 ppb at H11H (5 km from HPY) at 0600 CST.

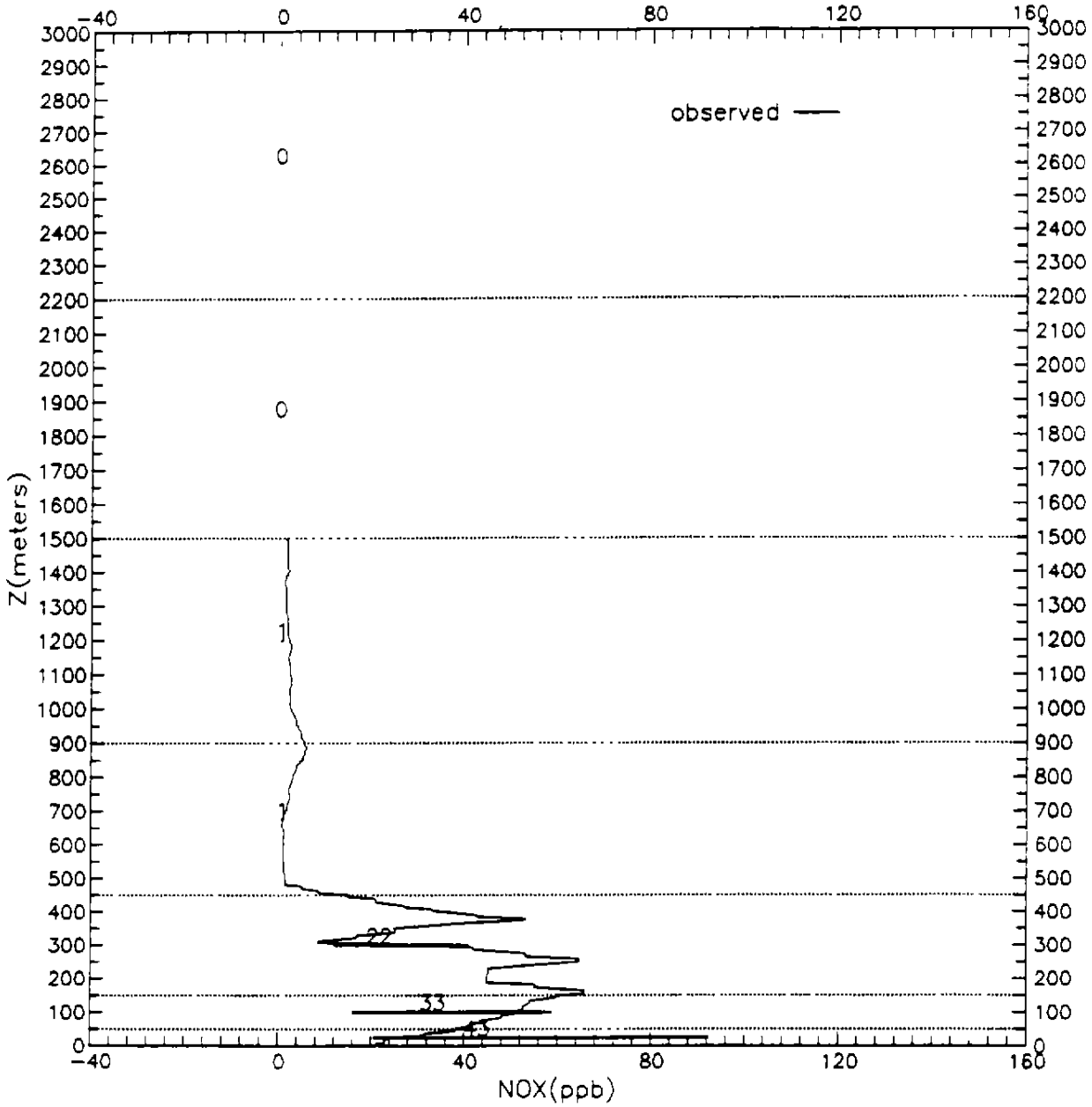

Figure 4-95b. Comparison of upper-air simulated and observed NO_X concentrations for the HPY aircraft spiral location on 18 August 1993 at 0545-0553 CST for the base-case simulation. The solid line represents the instantaneous aircraft measurements and the numerical values represent the simulated values within each UAM-V layer (indicated by horizontal dashed lines). The nearest surface observation at H11H was missing for this hour.

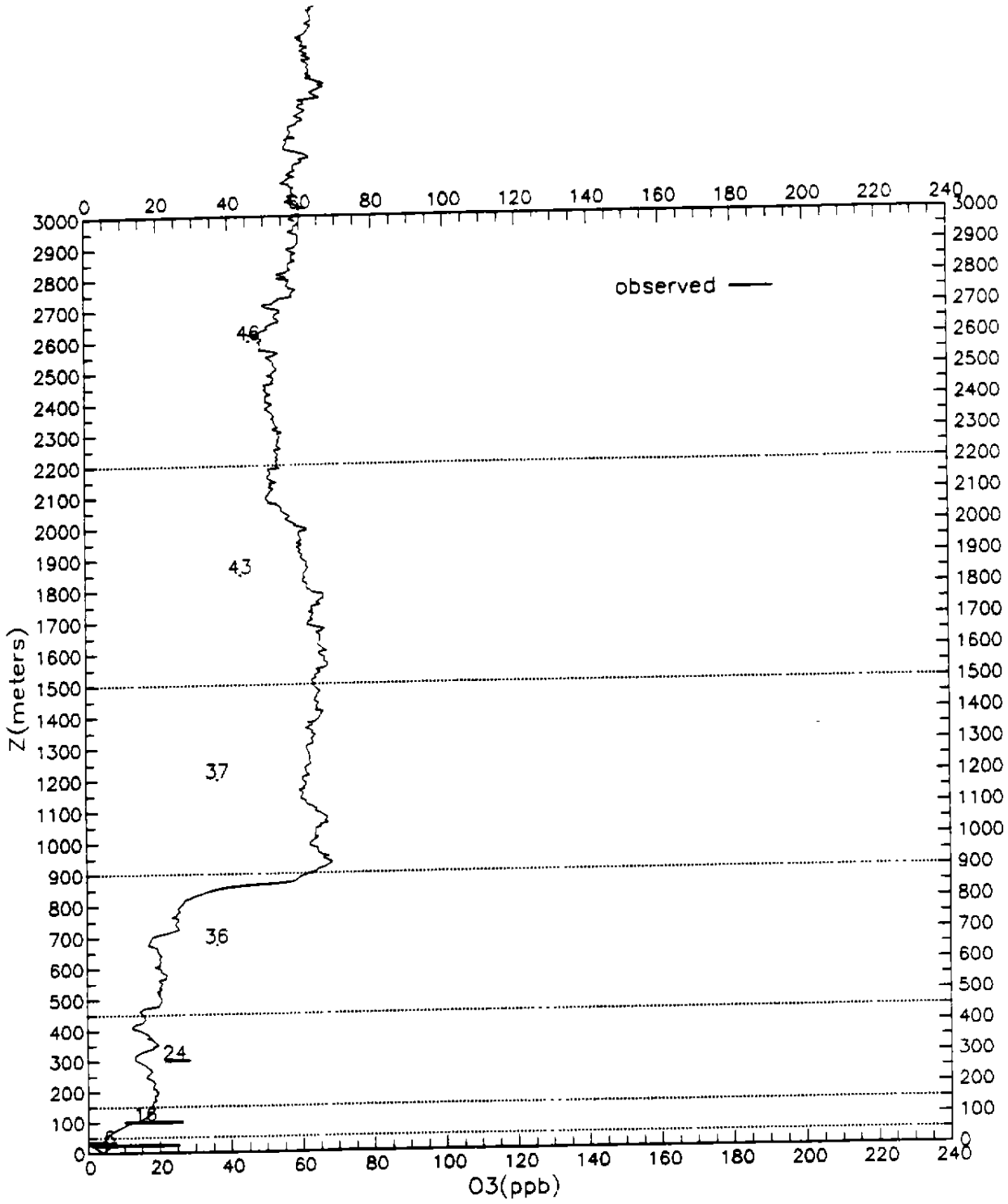

Figure 4-96a. Comparison of upper-air simulated and observed ozone concentrations for the HOU aircraft spiral location on 19 August 1993 at 0616-0640 CST for the base-case simulation. The solid line represents the instantaneous aircraft measurements and the numerical values represent the simulated values within each UAM-V layer (indicated by horizontal dashed lines). The nearest surface observation is 4 ppb at TN6 (3 km from HOU) at 0700 CST.

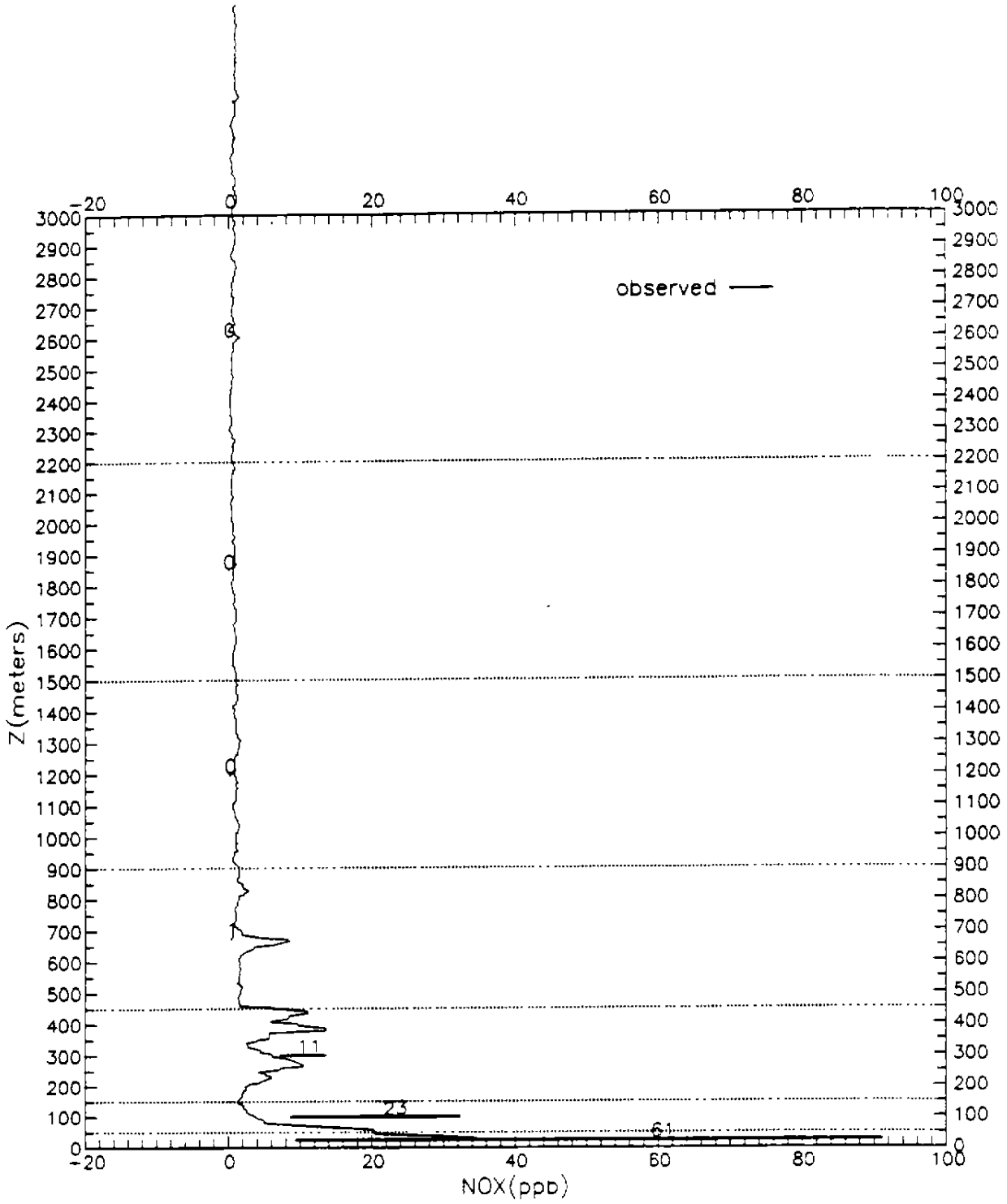

Figure 4-96b. Comparison of upper-air simulated and observed NO_X concentrations for the HOU aircraft spiral location on 19 August 1993 at 0616-0640 CST for the base-case simulation. The solid line represents the instantaneous aircraft measurements and the numerical values represent the simulated values within each UAM-V layer (indicated by horizontal dashed lines). The nearest surface observation is 139 ppb at H01H (8 km from HOU) at 0700 CST.

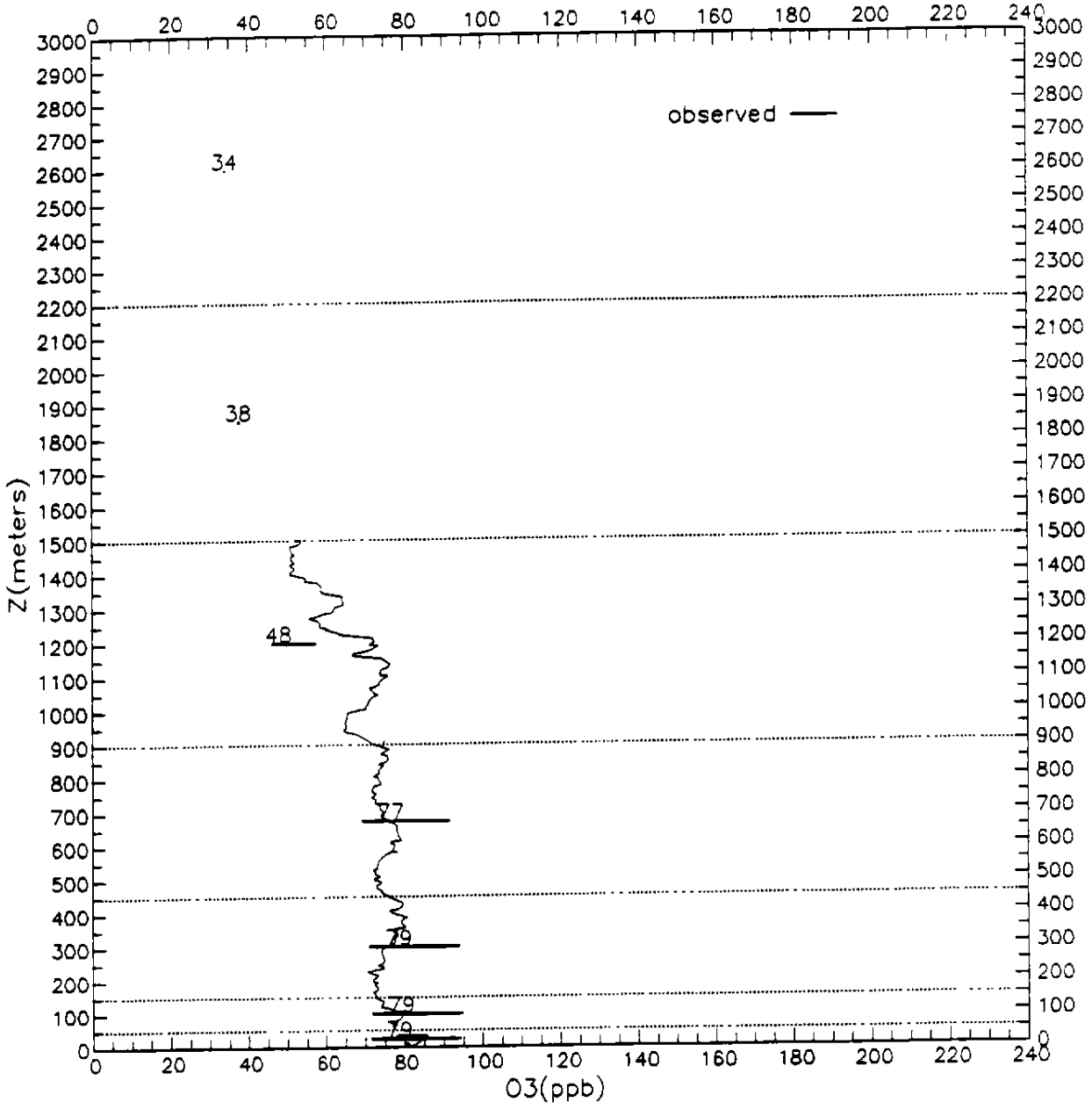

Figure 4-97a. Comparison of upper-air simulated and observed ozone concentrations for the CRY aircraft spiral location on 19 August 1993 at 1248-1257 CST for the base-case simulation. The solid line represents the instantaneous aircraft measurements and the numerical values represent the simulated values within each UAM-V layer (indicated by horizontal dashed lines). The nearest surface observation is 82 ppb at CRSC (6 km from CRY) at 1300 CST.

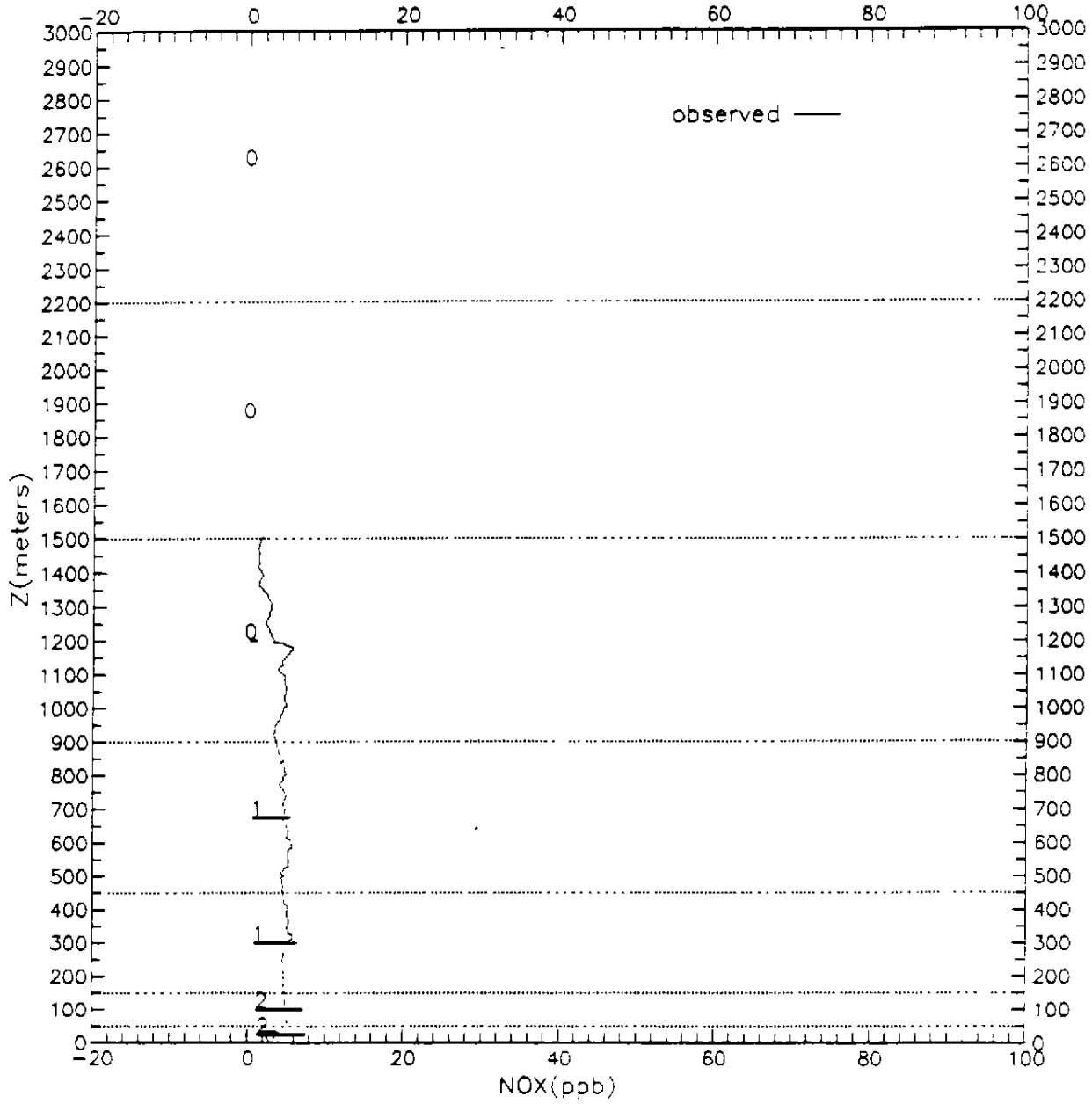

Figure 4-97b. Comparison of upper-air simulated and observed NO_X concentrations for the CRY aircraft spiral location on 19 August 1993 at 1248-1257 CST for the base-case simulation. The solid line represents the instantaneous aircraft measurements and the numerical values represent the simulated values within each UAM-V layer (indicated by horizontal dashed lines). The nearest surface observation is 3 ppb at CRSC (6 km from CRY) at 1300 CST.

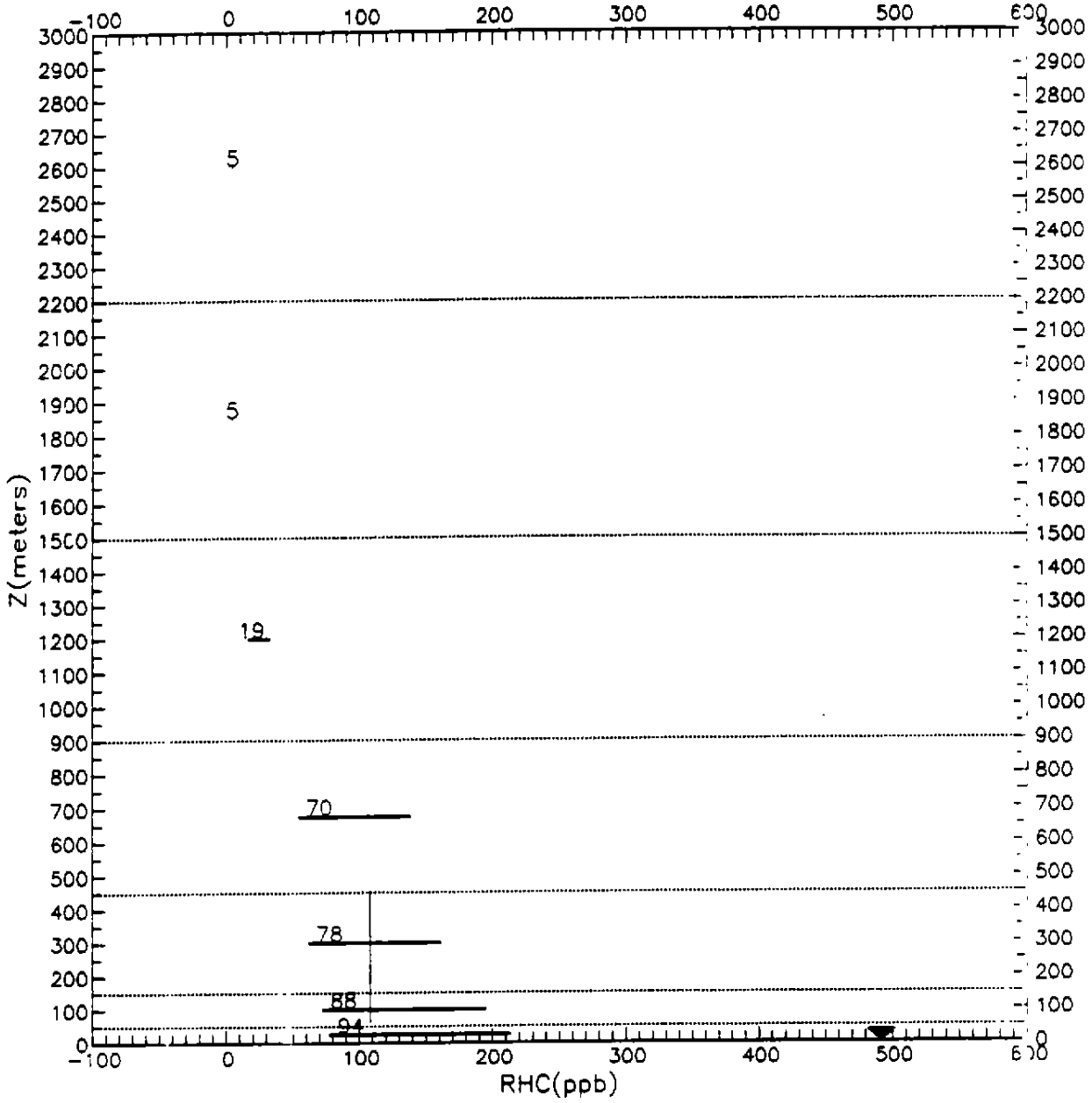

Figure 4-97c. Comparison of upper-air simulated and observed RHC concentrations for the CRY aircraft spiral location on 19 August 1993 at 1248-1257 CST for the base-case simulation. The solid line represents the instantaneous aircraft measurements and the numerical values represent the simulated values within each UAM-V layer (indicated by horizontal dashed lines). The nearest surface observation is 492 ppb at C35C (24 km from CRY) at 1300 CST.

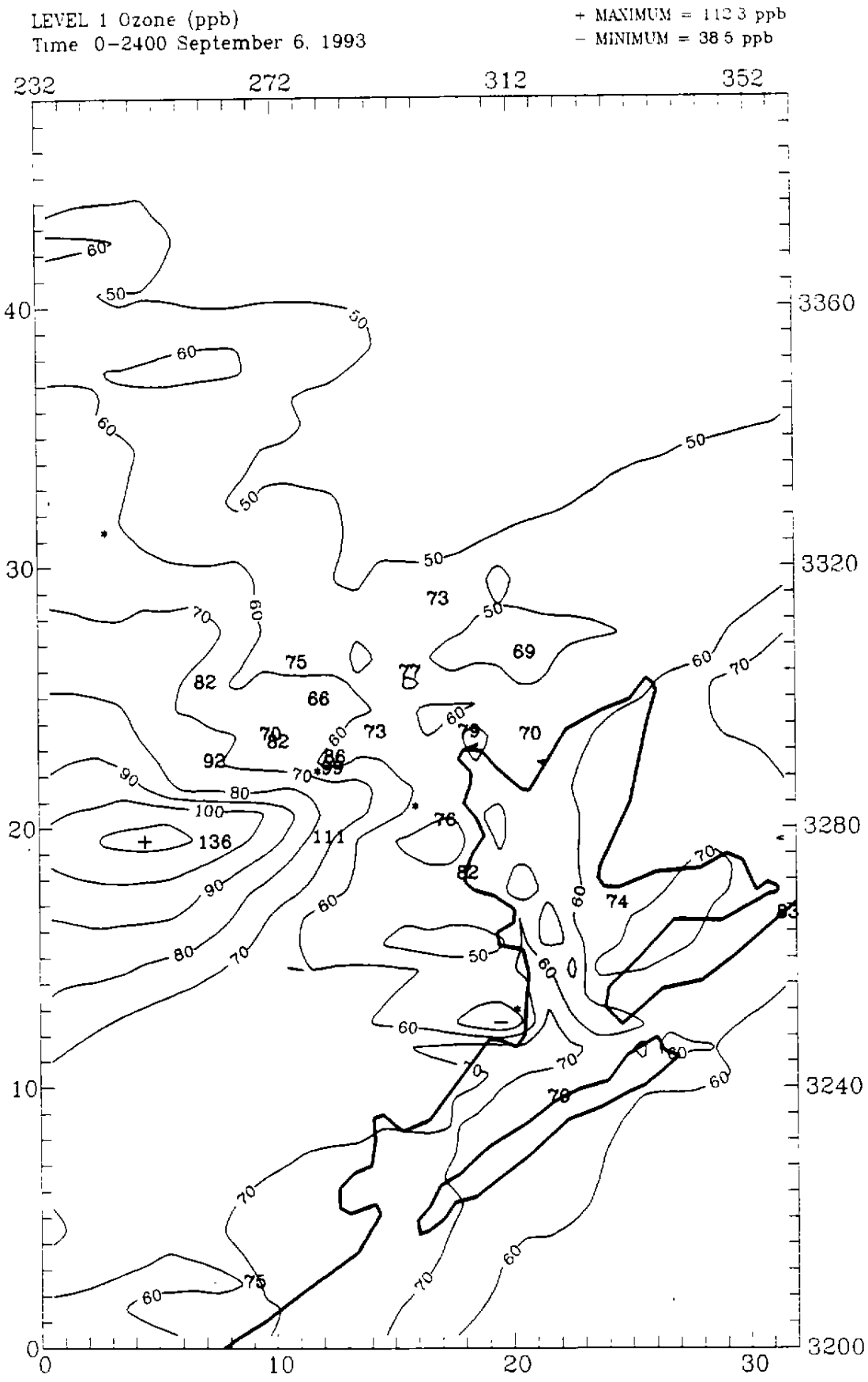

Figure 4-98. Maximum simulated (hourly averaged) ozone concentrations (ppb) in the Houston area on 6 September 1993 for the base-case simulation. Observed maxima are also shown.

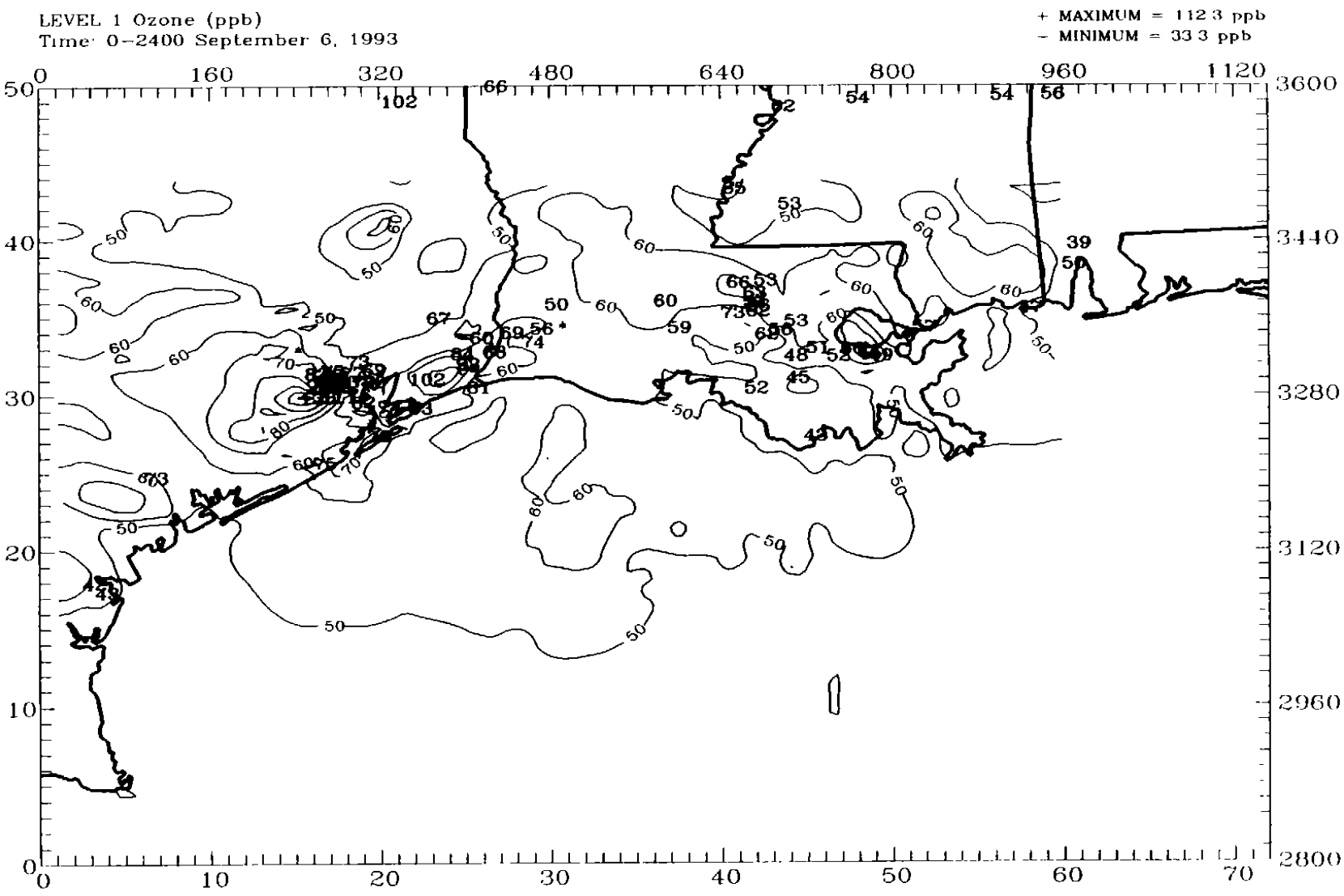

Figure 4-99. Maximum simulated (hourly averaged) ozone concentrations (ppb) in the GMAQS domain on 6 September 1993 for the base-case simulation. Observed maxima are also shown.

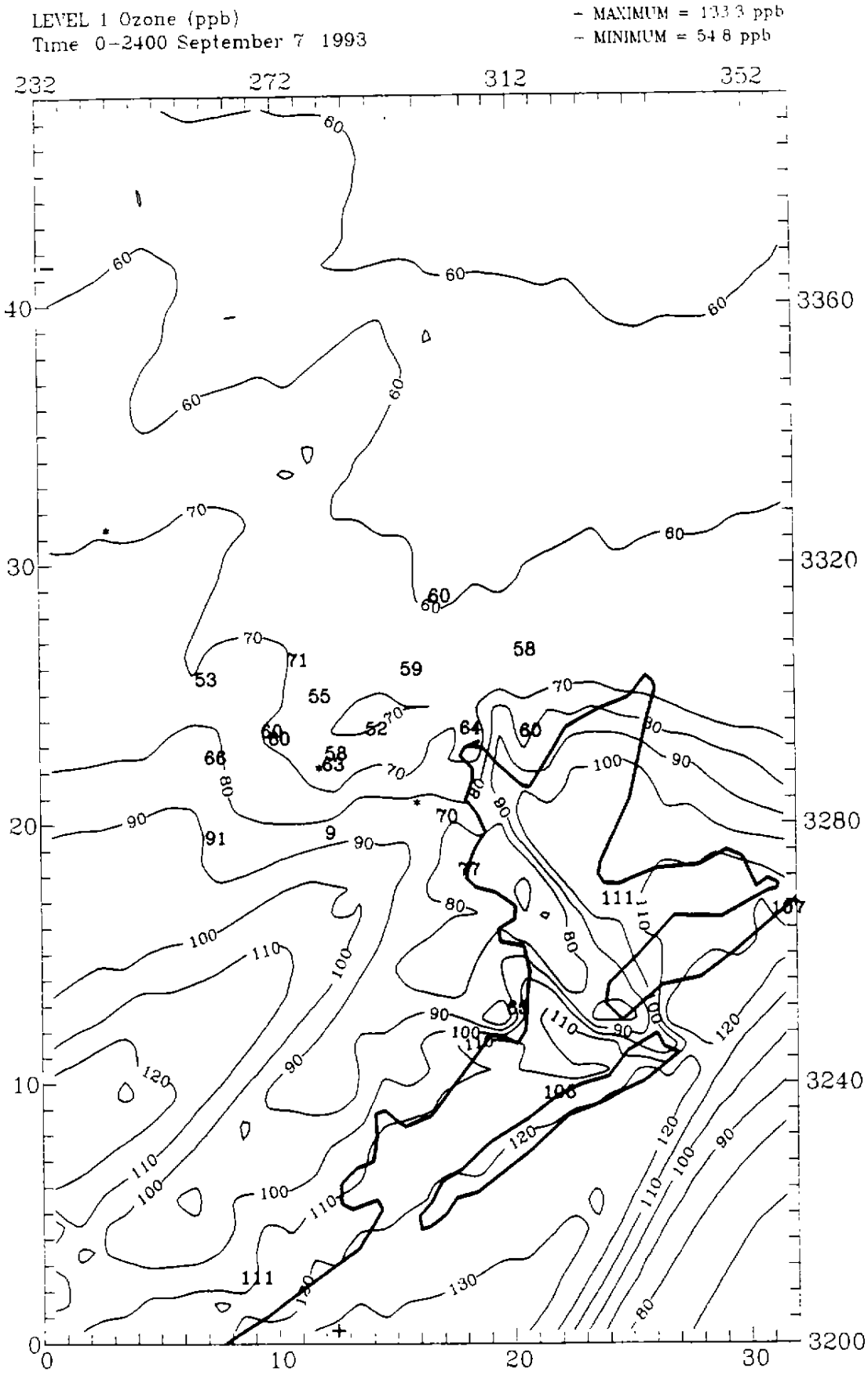

Figure 4-100. Maximum simulated (hourly averaged) ozone concentrations (ppb) in the Houston area on 7 September 1993 for the base-case simulation. Observed maxima are also shown.

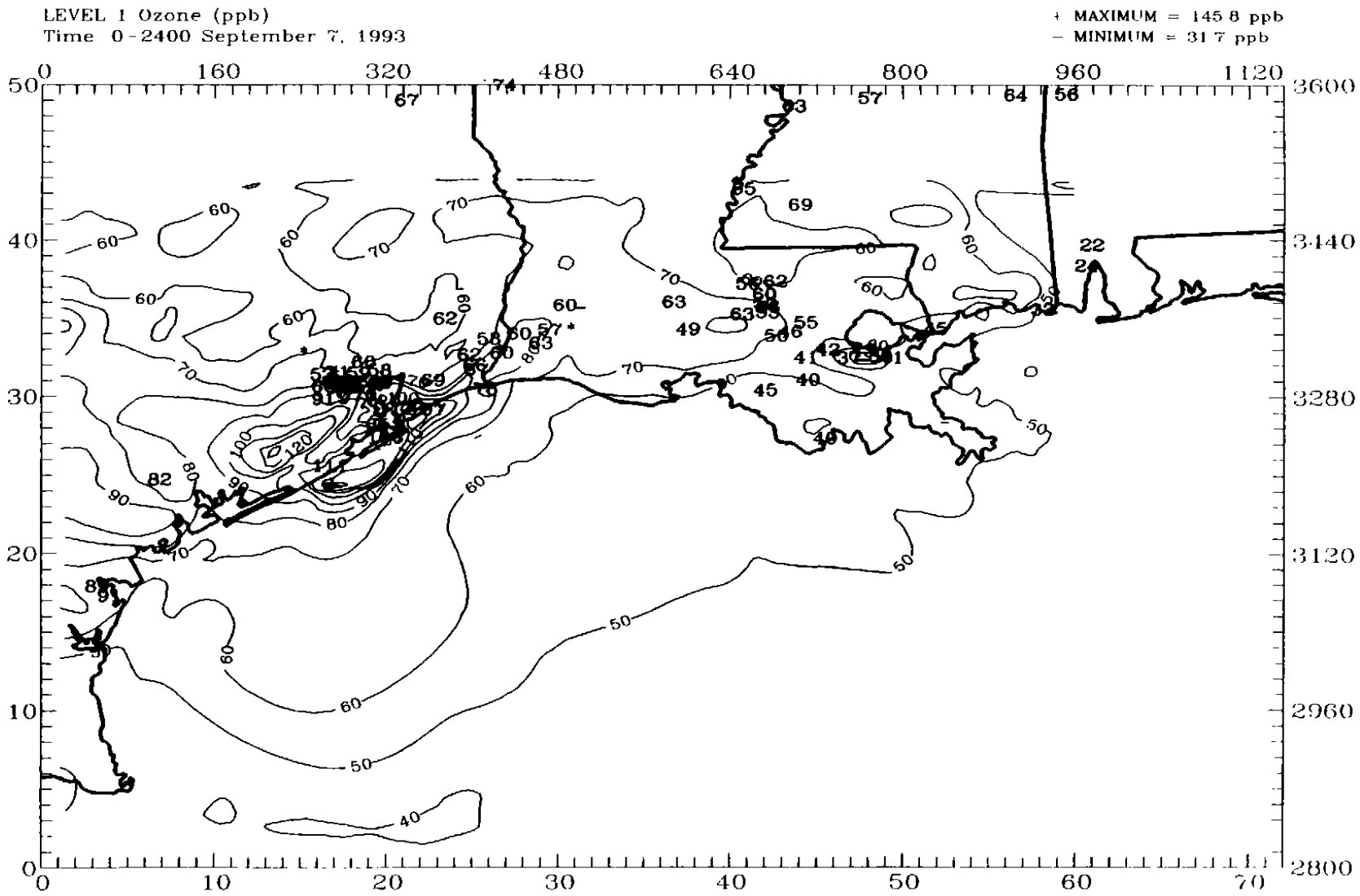

Figure 4-101. Maximum simulated (hourly averaged) ozone concentrations (ppb) in the GMAQS domain on 7 September 1993 for the base-case simulation. Observed maxima are also shown.

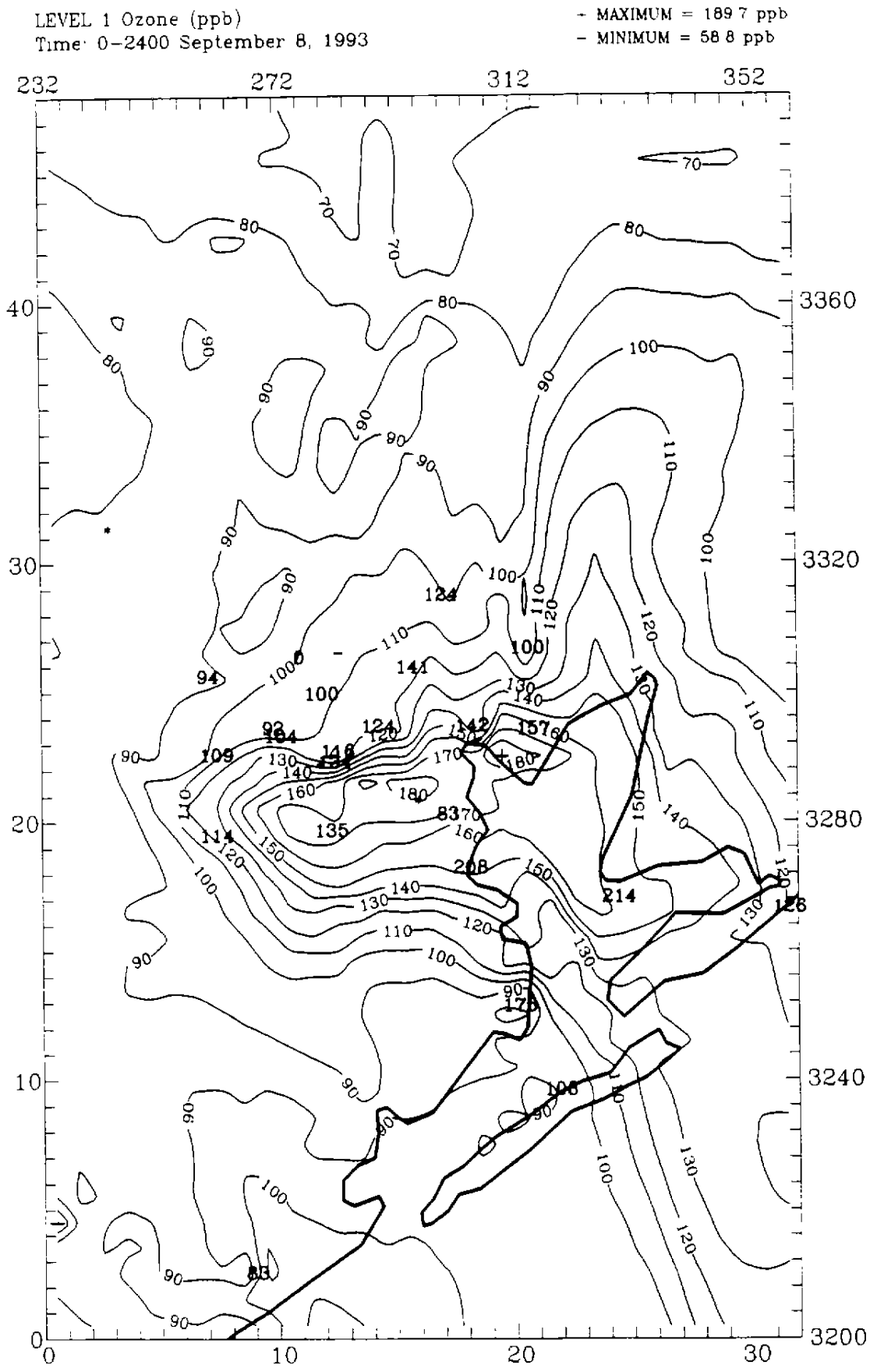

Figure 4-102. Maximum simulated (hourly averaged) ozone concentrations (ppb) in the Houston area on 8 September 1993 for the base-case simulation. Observed maxima are also shown.

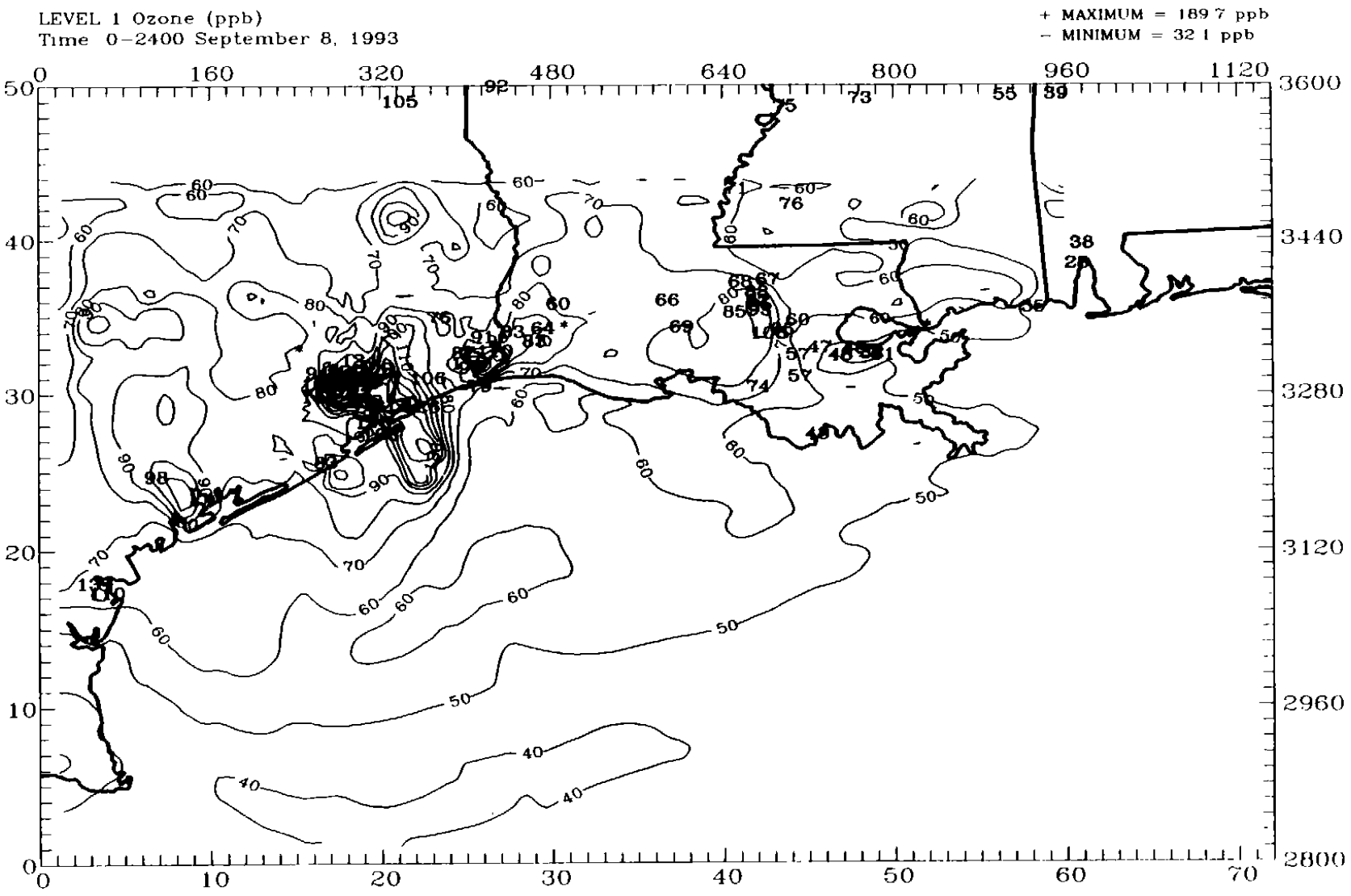

Figure 4-103. Maximum simulated (hourly averaged) ozone concentrations (ppb) in the GMAQS domain on 8 September 1993 for the base-case simulation. Observed maxima are also shown.

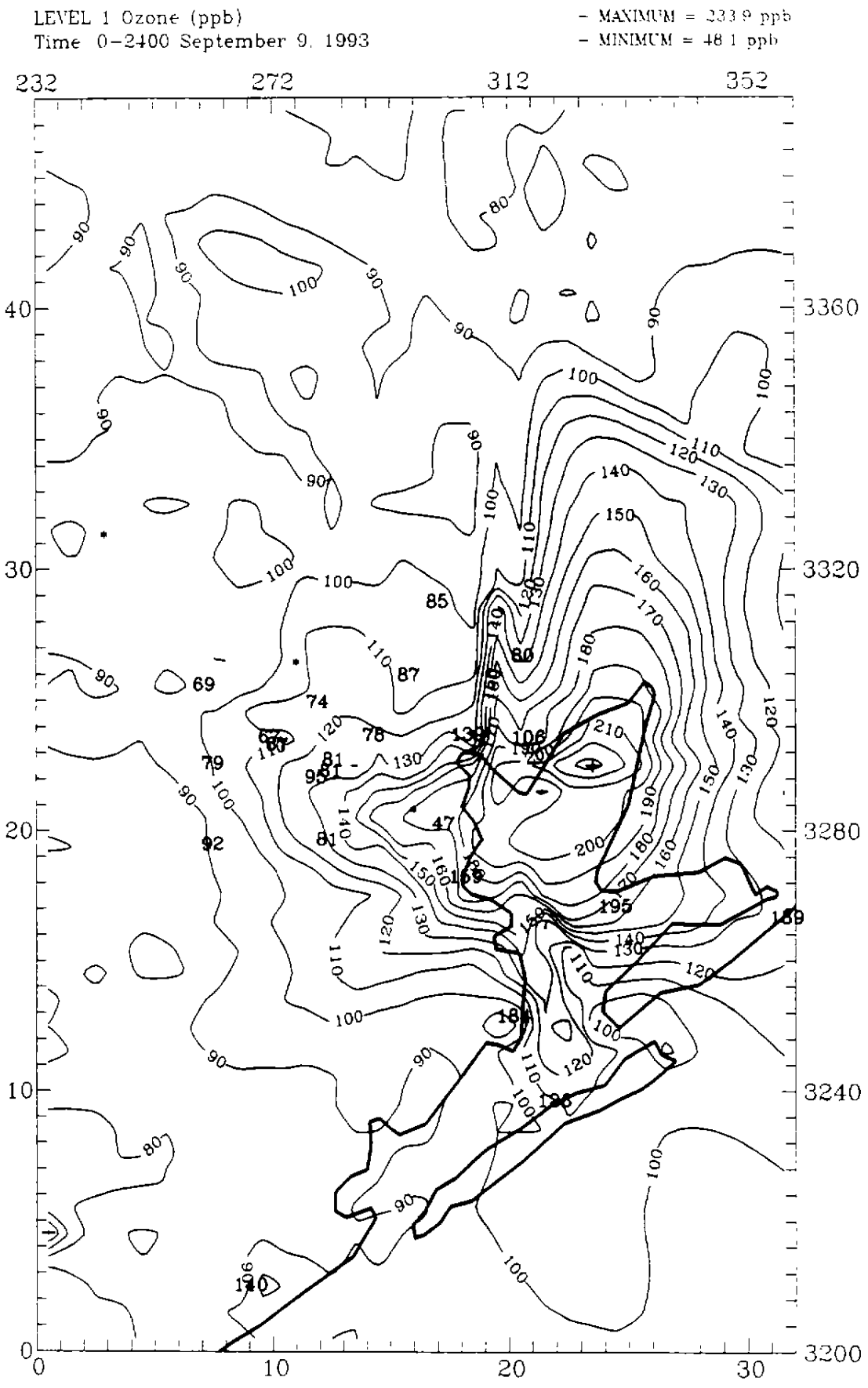

Figure 4-104. Maximum simulated (hourly averaged) ozone concentrations (ppb) in the Houston area on 9 September 1993 for the base-case simulation. Observed maxima are also shown.

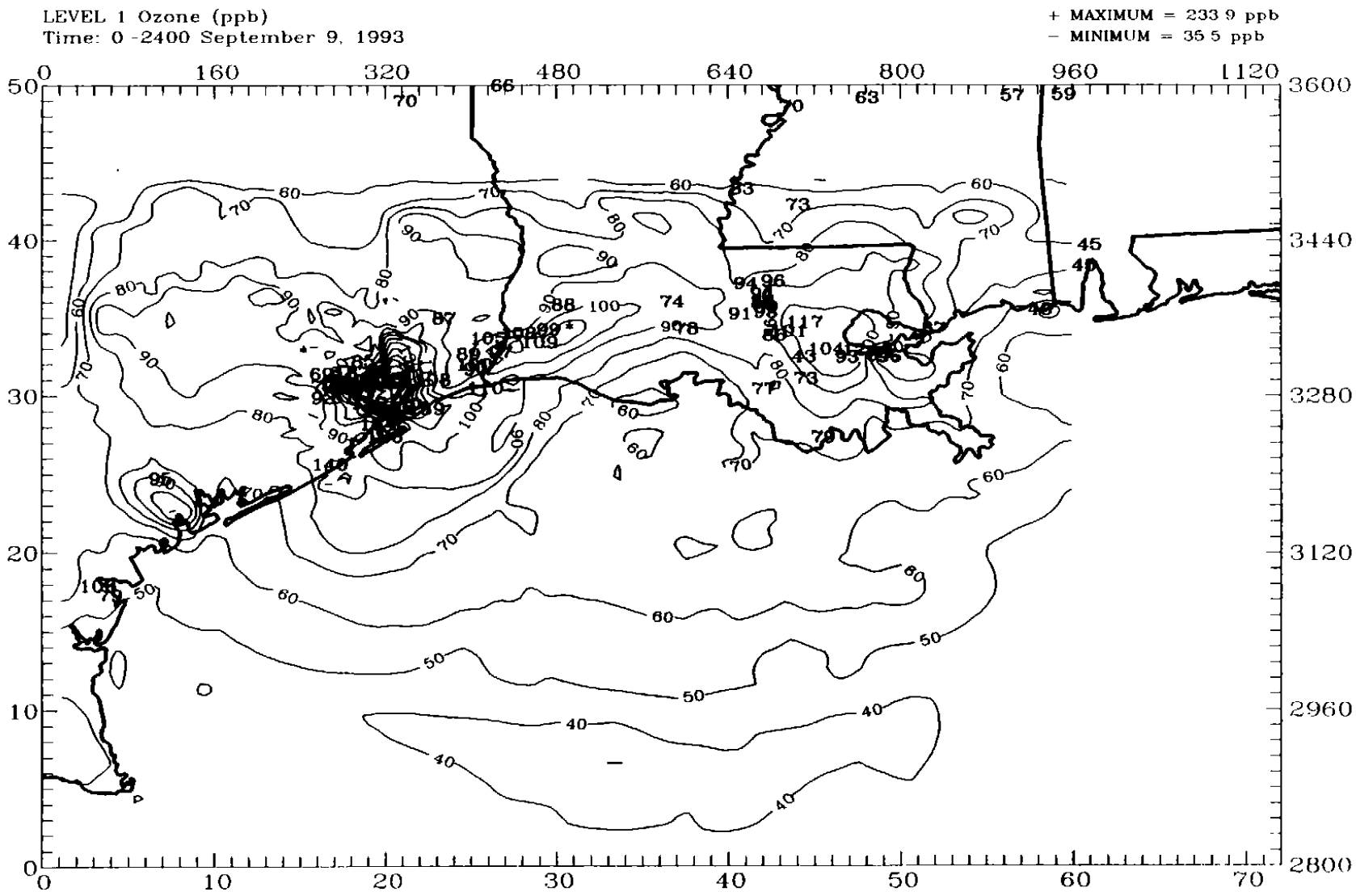

Figure 4-105. Maximum simulated (hourly averaged) ozone concentrations (ppb) in the GMAQS domain on 9 September 1993 for the base-case simulation. Observed maxima are also shown.

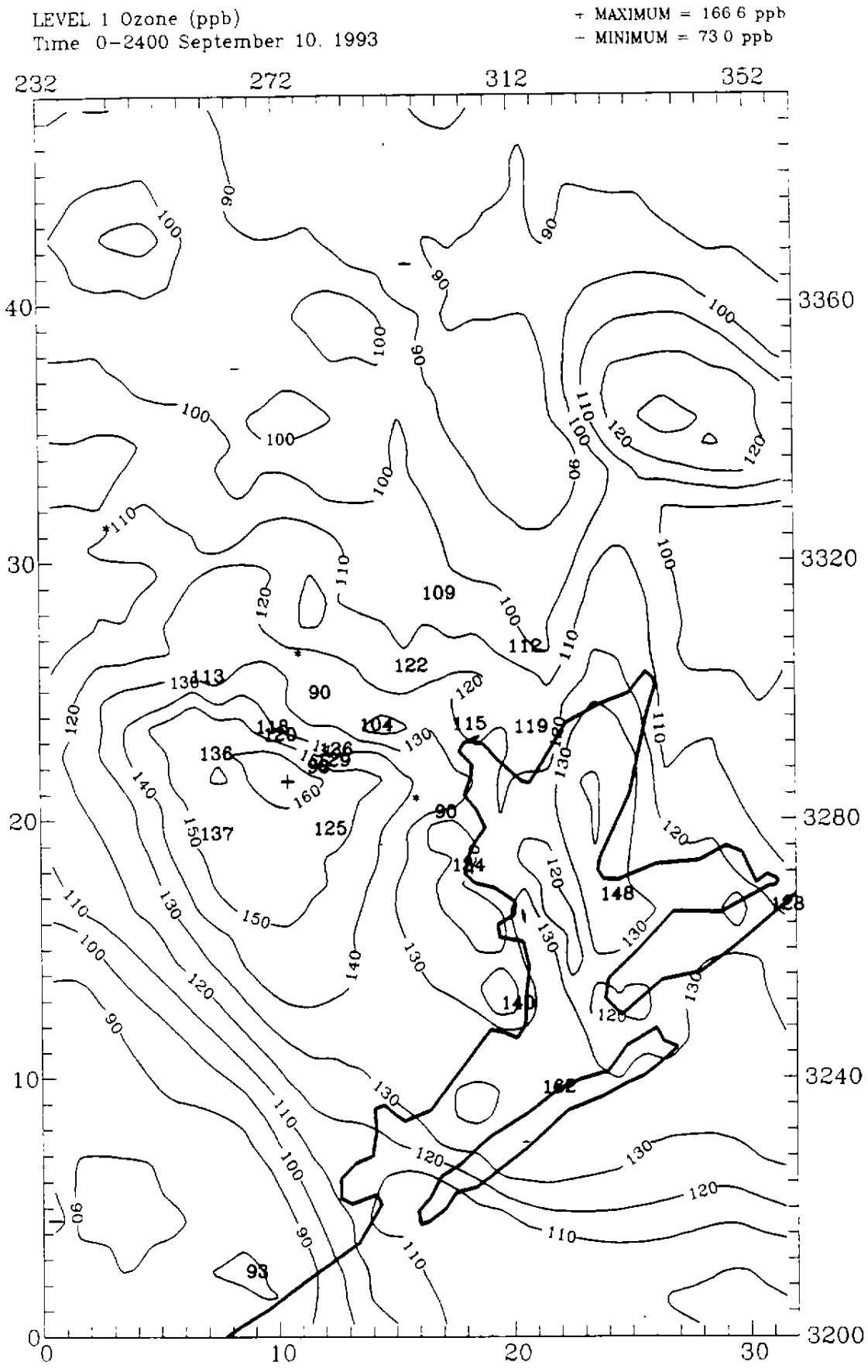

Figure 4-106. Maximum simulated (hourly averaged) ozone concentrations (ppb) in the Houston area on 10 September 1993 for the base-case simulation. Observed maxima are also shown.

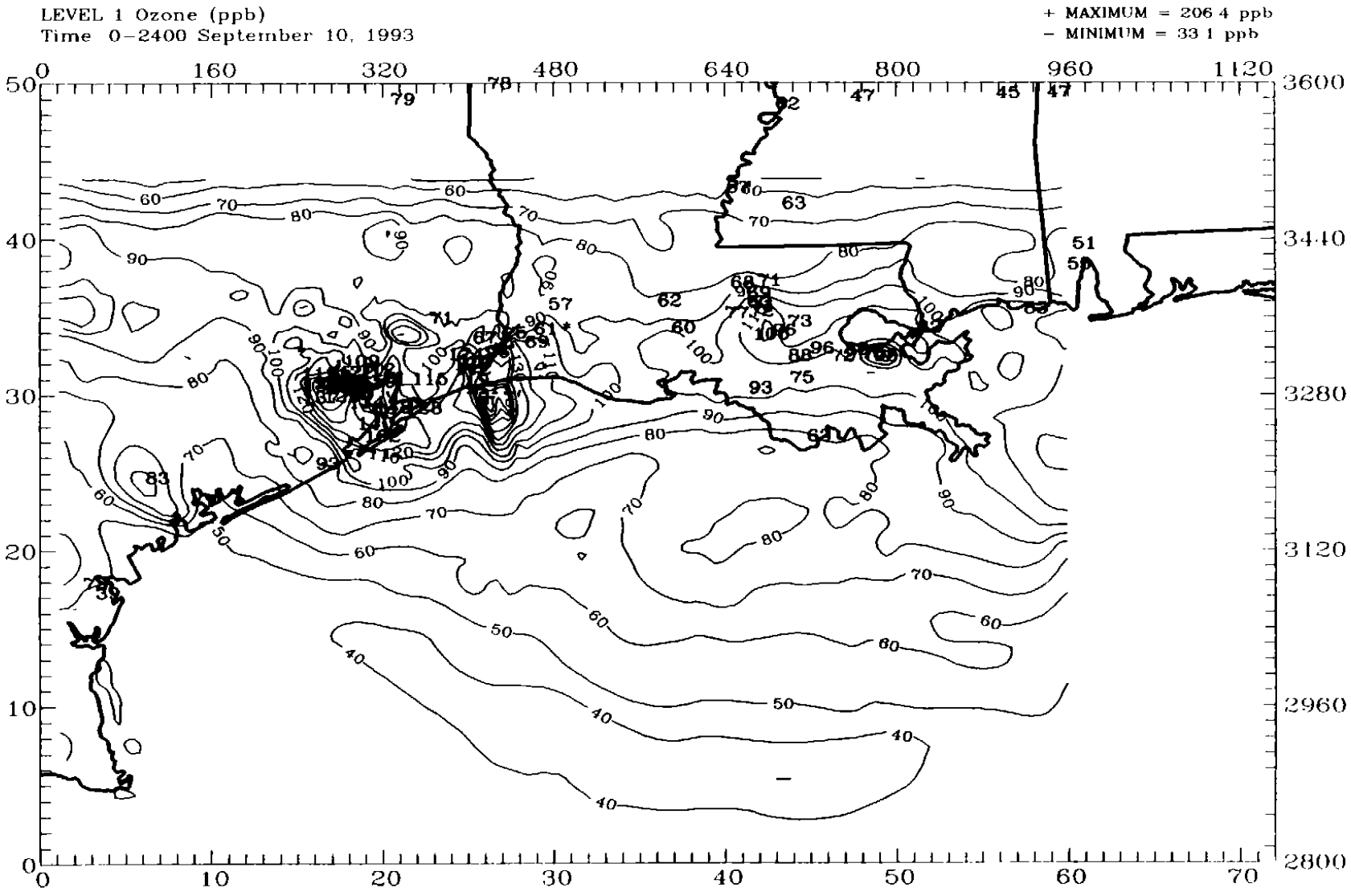

Figure 4-107. Maximum simulated (hourly averaged) ozone concentrations (ppb) in the GMAQS domain on 10 September 1993 for the base-case simulation. Observed maxima are also shown.

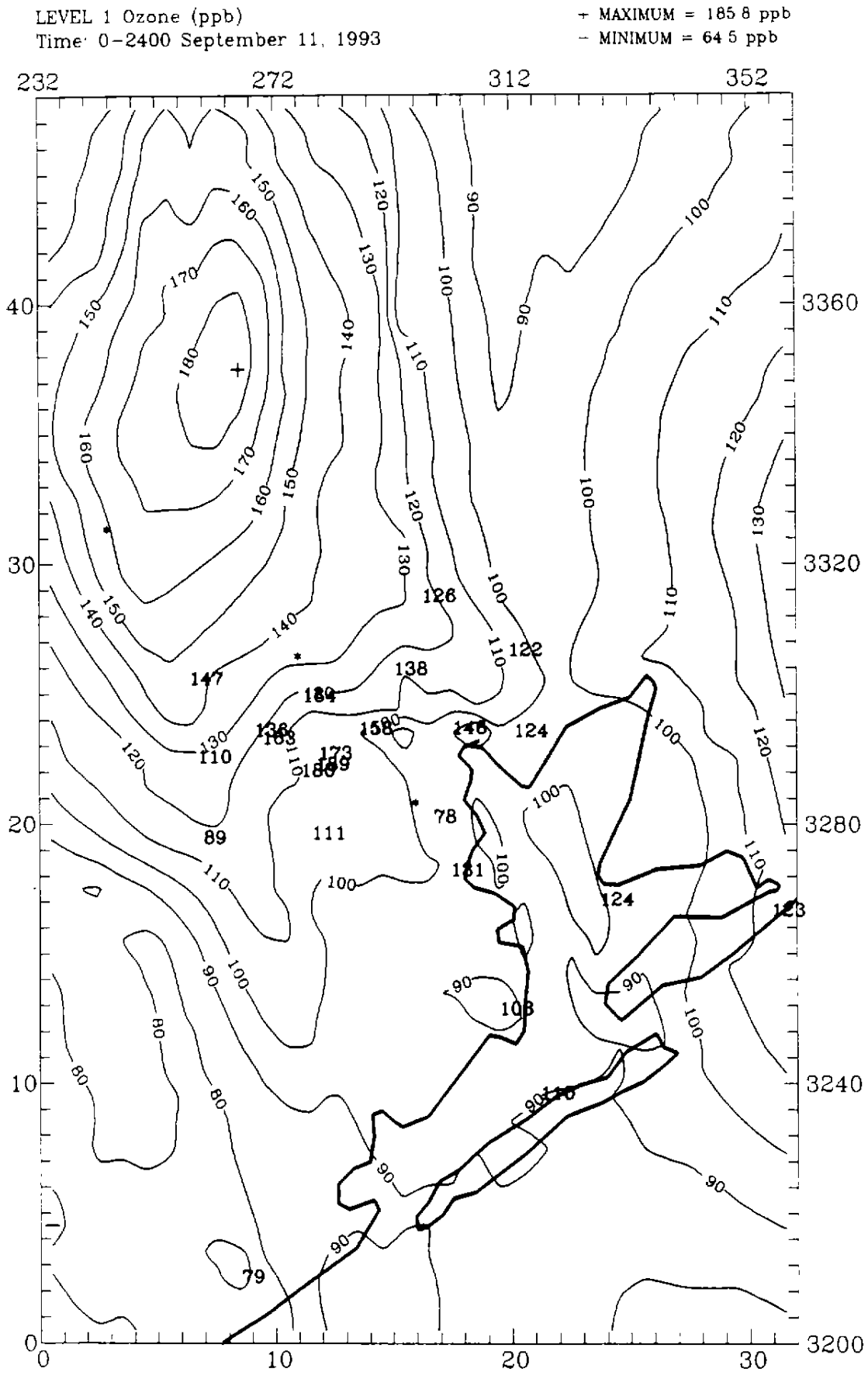

Figure 4-108. Maximum simulated (hourly averaged) ozone concentrations (ppb) in the Houston area on 11 September 1993 for the base-case simulation. Observed maxima are also shown.

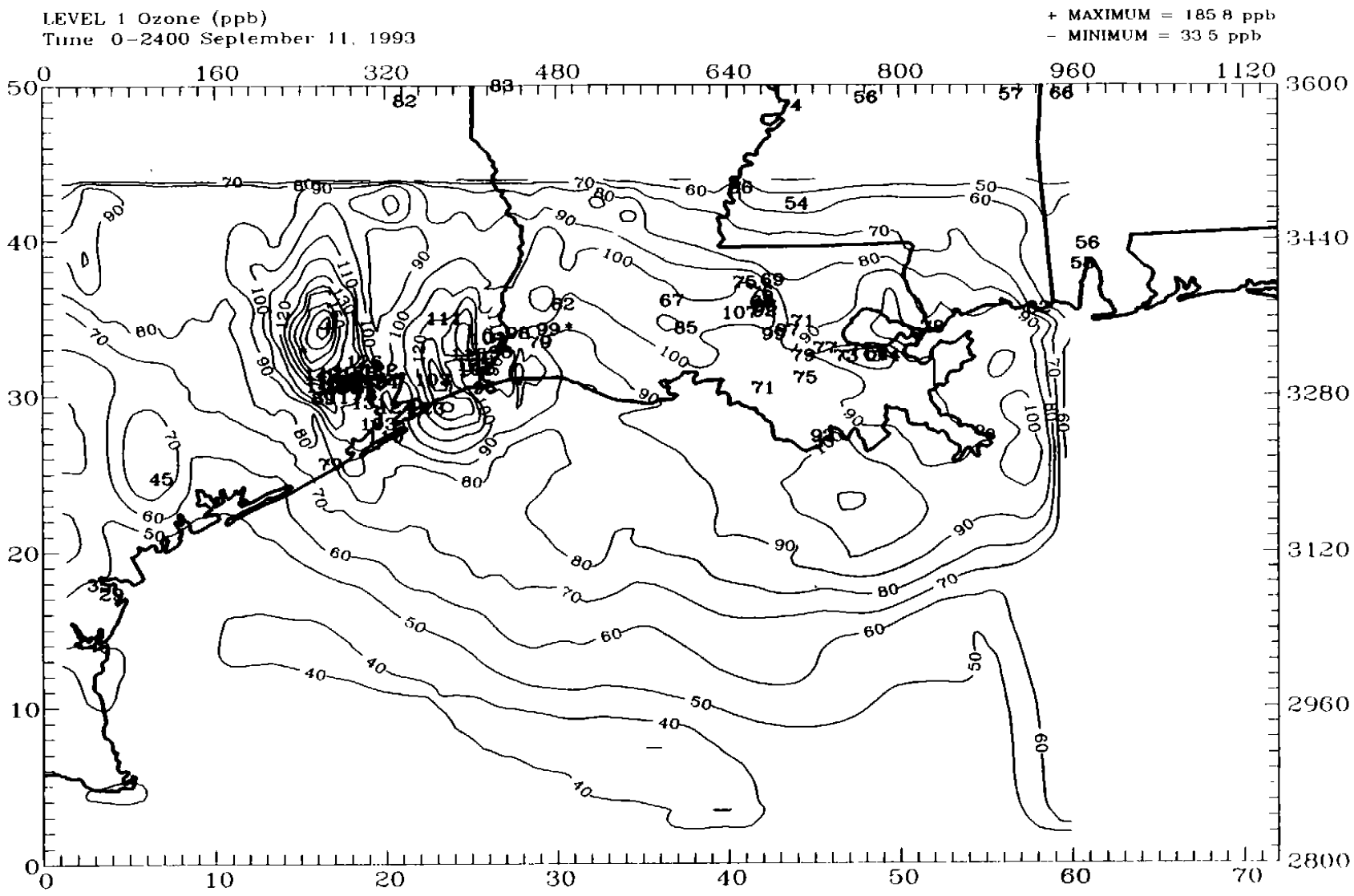

Figure 4-109. Maximum simulated (hourly averaged) ozone concentrations (ppb) in the GMAQS domain on 11 September 1993 for the base-case simulation. Observed maxima are also shown.

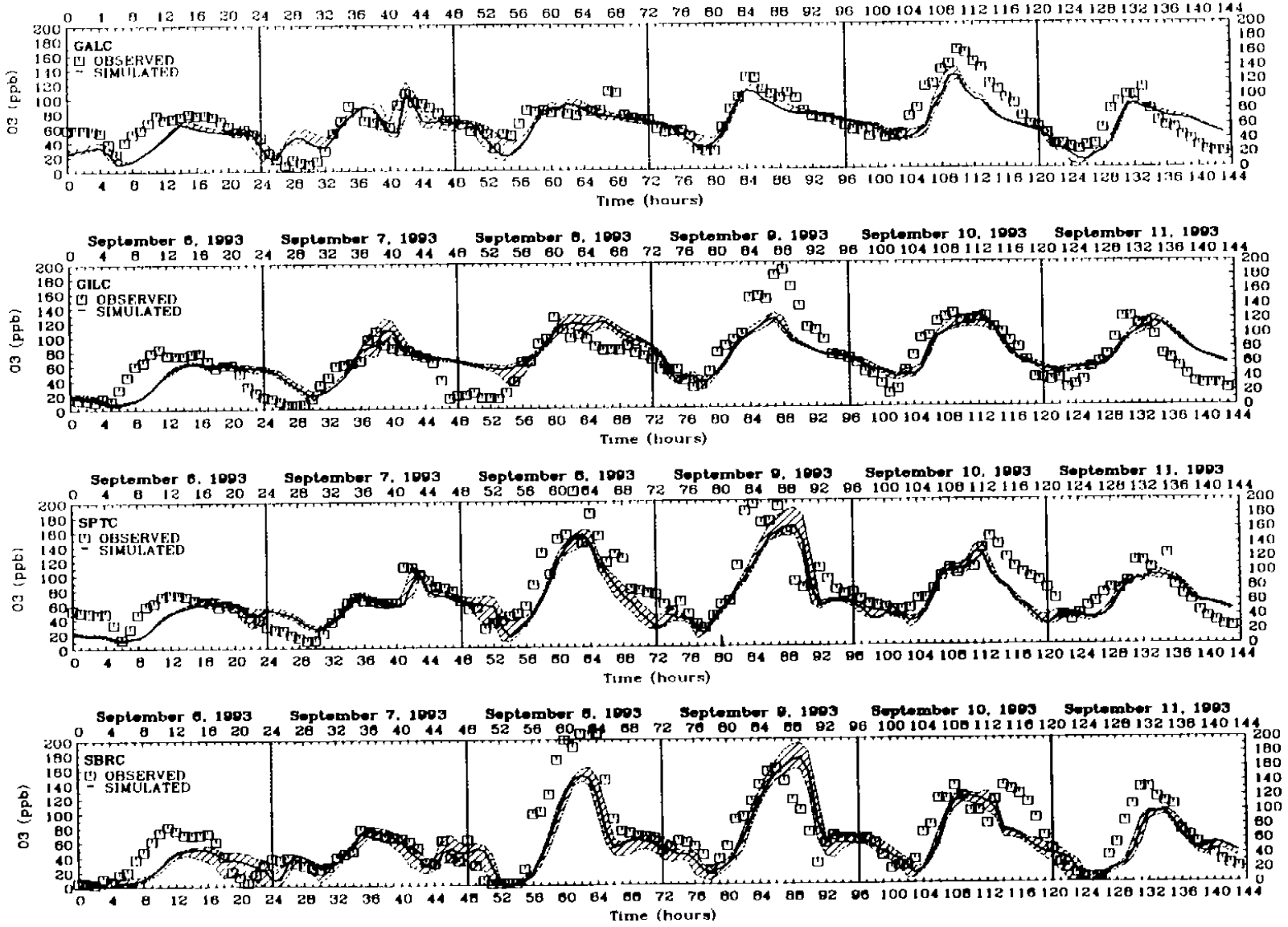

Figure 4-110a. Time-series plots comparing simulated and observed ozone concentrations (ppb) for selected monitoring sites located to the south and east of the Houston area for the 6-11 September 1993 period. Base-case simulation

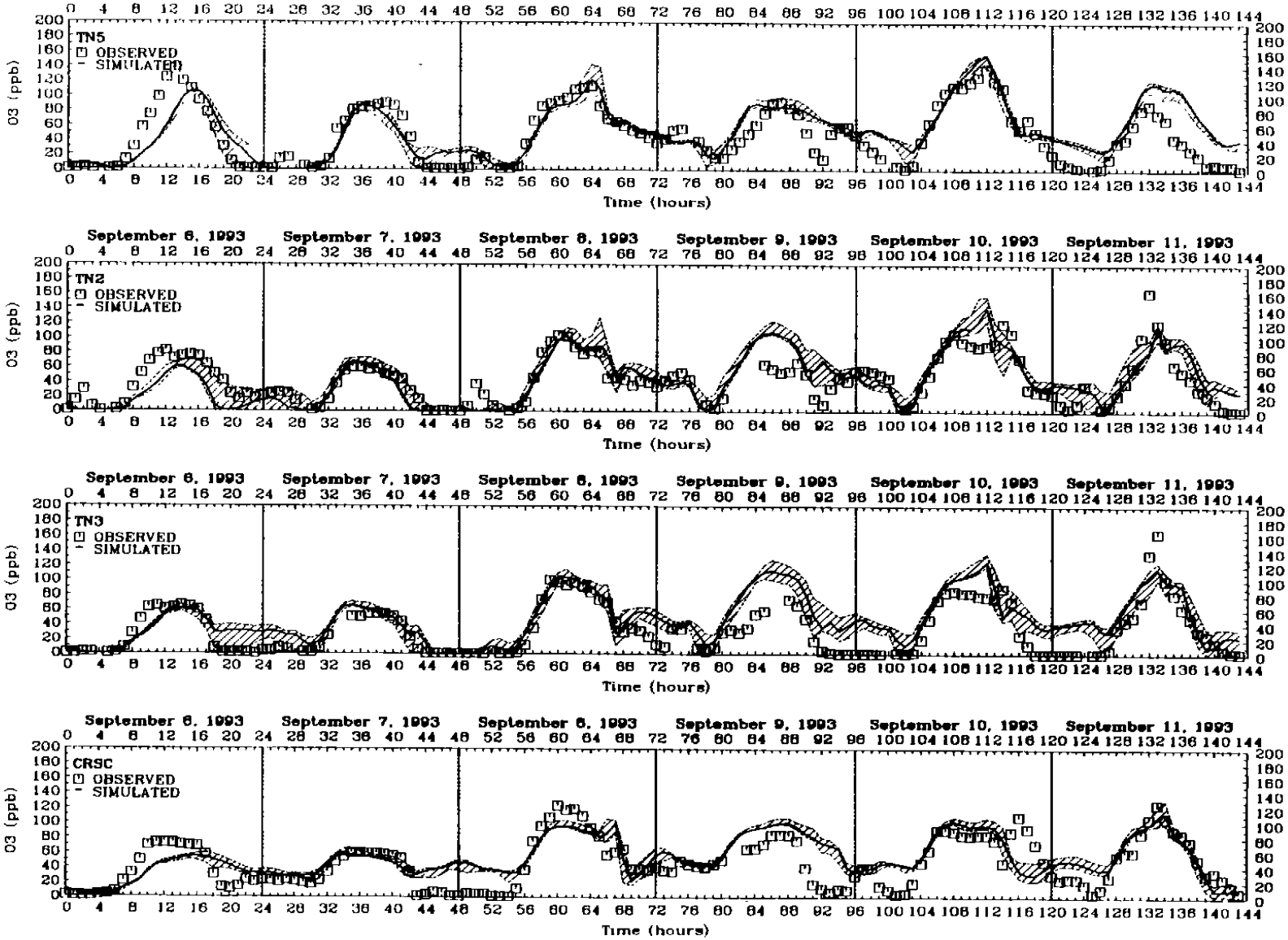

Figure 4-110b. Time-series plots comparing simulated and observed ozone concentrations (ppb) for selected monitoring sites located within the Houston area for the 6-11 September 1993 period. Base-case simulation.

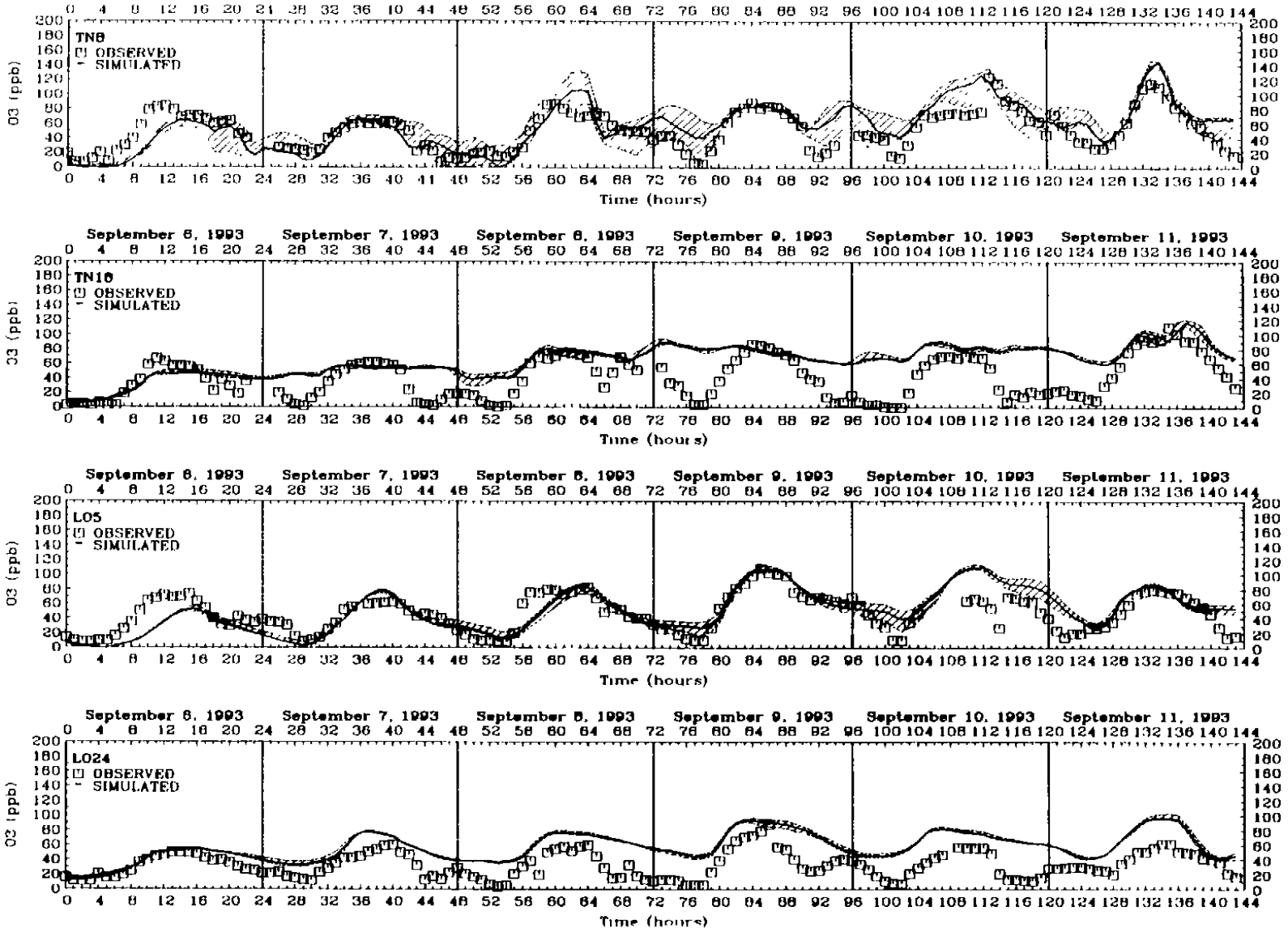

Figure 4-111. Time-series plots comparing simulated and observed ozone concentrations (ppb) for selected monitoring sites located within the Beaumont/Port Arthur/Lake Charles area for the 6-11 September 1993 period. Base-case simulation.

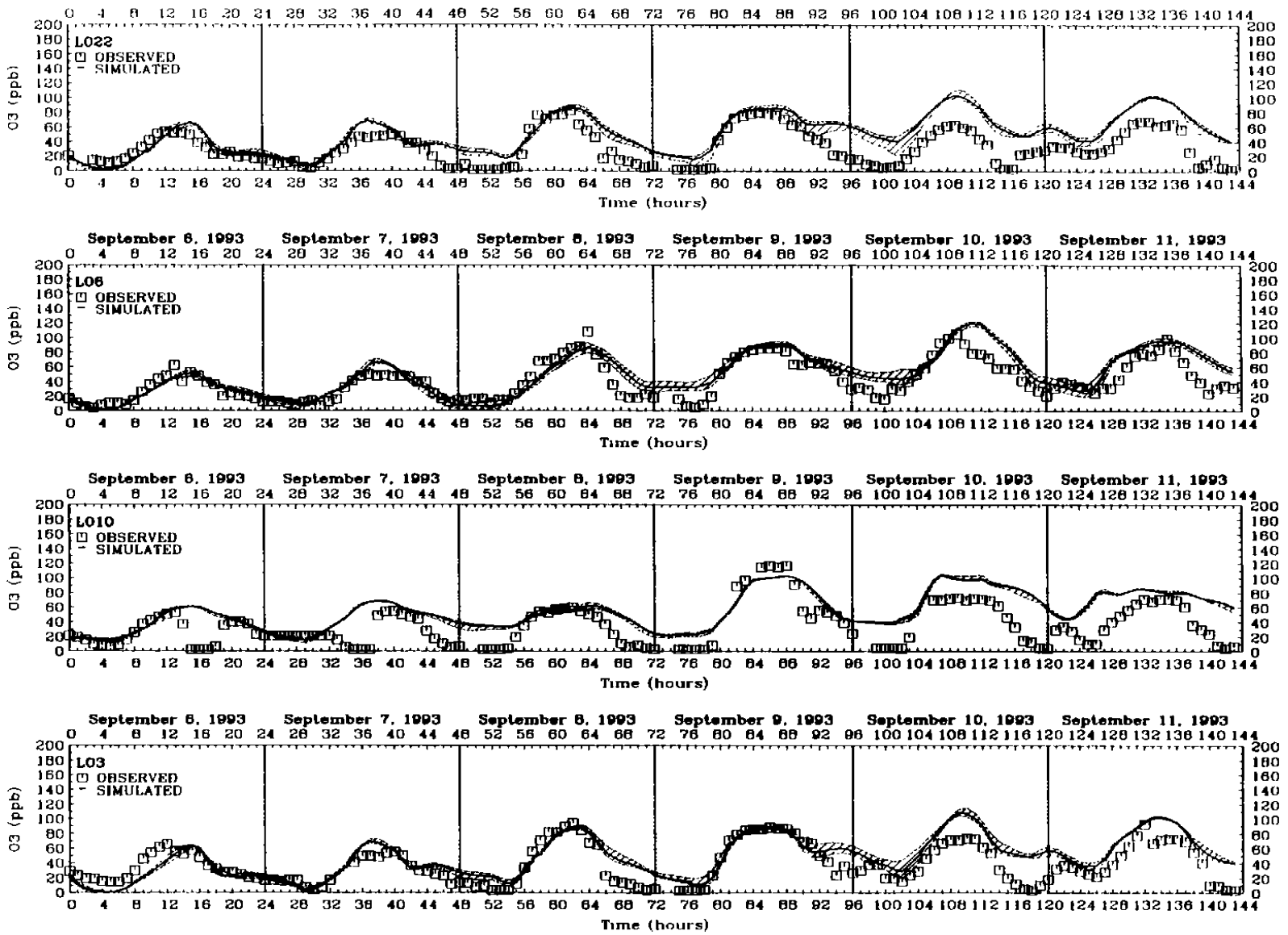

Figure 4-112. Time-series plots comparing simulated and observed ozone concentrations (ppb) for selected monitoring sites located within the Baton Rouge area for the 6-11 September 1993 period. Base-case simulation.

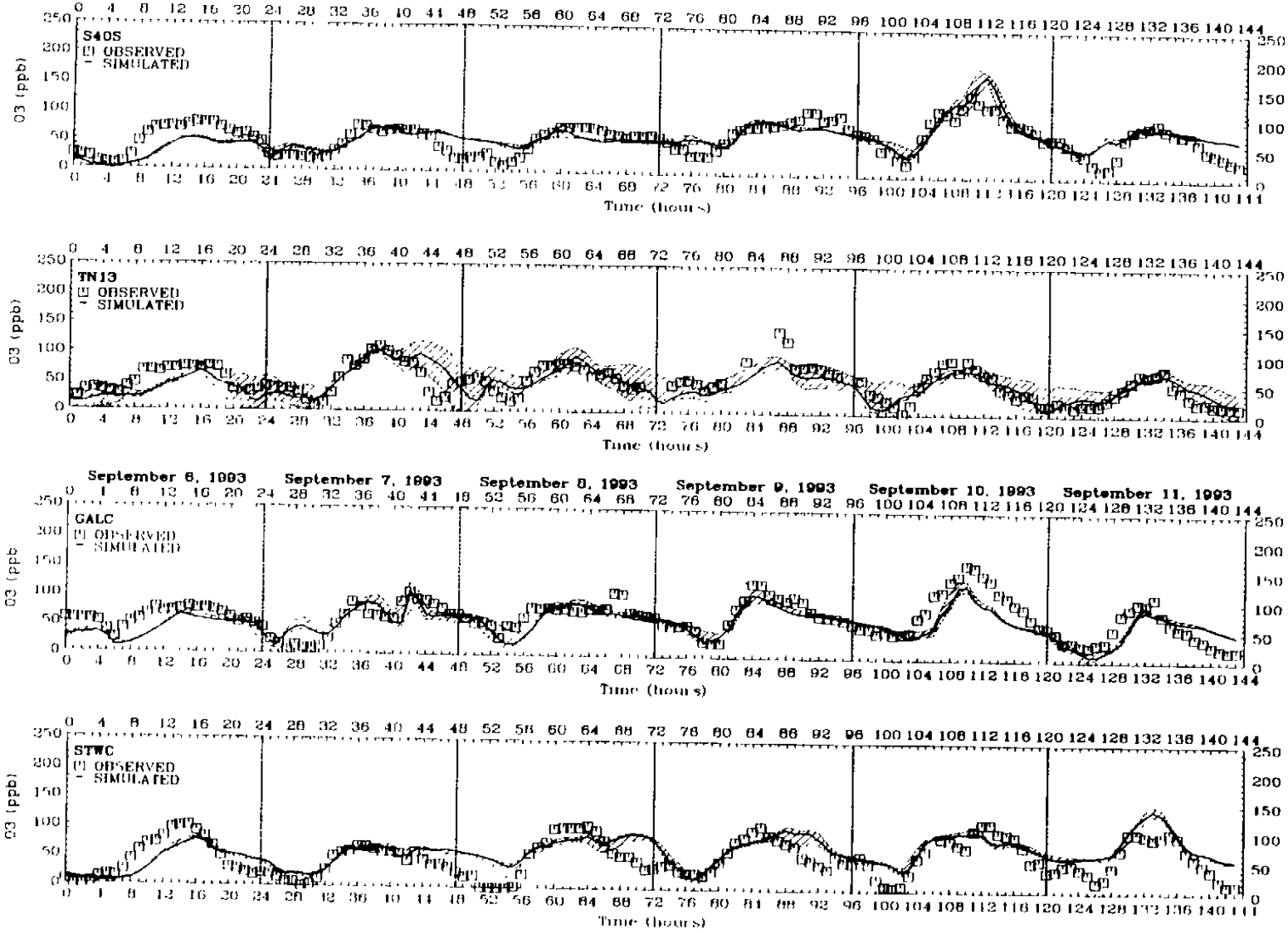

Figure 4-113. Time-series plots comparing simulated and observed ozone concentrations (ppb) for selected monitoring sites located along the Texas gulf coast for the 6-11 September 1993 period. Base-case simulation.

5 OCSPD IMPACT ANALYSIS FOR 1993 AND 1999

This section summarizes the photochemical modeling analysis performed to assess ozone impacts of OCS petroleum development (OCSPD) emissions under the "current" (1993) and anticipated future-year (1999) emission scenarios. The 1993 analysis used the base-case files developed for the August and September episodes, as detailed in Section 4. Emission estimates for 1999 for the onshore and offshore portions of the domain were made by projecting the 1993 estimates to 1999 using growth and control factor information obtained from various agency sources having jurisdiction within the study domain. Issues regarding the uncertainty in various components of the onshore emission inventory for the Houston area were identified during the UAM-V model performance evaluation and were presented in Section 4. Because these uncertainties could potentially influence the OCSPD impact assessment, the impact analysis simulations were performed using various combinations of onshore (for the Houston area) and offshore emissions that bracketed the uncertainties. The ensemble of simulations completed for each of the episodes provides a range of estimated OCSPD impacts under a variety of possible onshore and offshore emission scenarios. The modeling analysis of OCSPD emission impacts presented in this section is similar to that performed for the Gulf of Mexico area by the EPA for the MMS using the Regional Oxidant Model (MMS/EPA, 1993).

5.1 METHODOLOGY FOR ASSESSING OZONE IMPACTS FROM OCSPD EMISSION SOURCES USING THE UAM-V

The 1993 GMAQS field program provided meteorological and air quality measurement data for examination of the physical and chemical characteristics of ozone formation in the Gulf of Mexico area and estimation of the potential influence of OCSPD emissions on onshore areas. For example, hourly measurements of wind and ozone concentrations for monitors at coastal locations provided estimates of the daily surface flux of precursors and ozone along the coastal areas of Texas and Louisiana, and aircraft measurements taken during episodic conditions provided information regarding the three-dimensional distribution of precursor and ozone concentrations in these areas. However, interpolation and extrapolation (in time and space) of these data from a relatively small number of monitoring sites over such a large area limits the ability of the analyst to provide quantitative estimates of the impacts of OCSPD emissions.

While the analysis of meteorological and air quality data for selected 1993 episode periods (summarized in Section 3) has provided some qualitative indication of the potential for OCSPD emission impacts on onshore nonattainment areas, the main purpose of the photochemical modeling effort and one of the primary objectives of the MMS

GMAQS is to quantify these impacts on concentrations of ozone in the four nonattainment areas of interest: Houston/Galveston and Beaumont/Port Arthur in Texas, and Lake Charles/Calcasieu Parish and Baton Rouge in Louisiana (see Figure 1-1). Although uncertainties are inherent in model formulation, and errors exist in measurement data and are introduced by the methodologies used to create model inputs, the photochemical grid model is a tool that provides a perspective regarding the ozone formation and transport mechanisms that cannot be obtained from limited point measurements (i.e., a quantitative estimate of the impacts of OCSPD emissions can be made for all locations within the modeling domain).

In this study, ozone impacts from OCSPD emission sources were estimated by performing a series of UAM-V simulations for the "current" year (1993) and a future year (1999).

1993 OCSPD Impact Analysis—Using the meteorological inputs developed for the August and September 1993 episodes, pairs of simulations were performed. Both used a fixed set of onshore emissions, but one included and the other excluded OCSPD emission sources, which are made up of crew/supply vessels, crew/supply helicopters, exploration vessels, pipeline vessels, and point sources associated with platform operation. The impacts were assessed for the base-case simulations of the August and September 1993 episodes.

1999 OCSPD Impacts Analysis—Estimates of future-year emissions for 1999 were prepared based on the anticipated growth in population and industrial sources between 1993 and 1999. The UAM-V was exercised using the projected 1999 inventory and, as for 1993, simulations were performed with and without OCSPD emissions. The year 1999 corresponds to the attainment date for the Beaumont/Port Arthur and Baton Rouge areas, which are designated serious ozone nonattainment areas by the EPA. The Houston/Galveston area is designated by the EPA as a severe-17 ozone nonattainment area with an attainment date of 2007, and the Lake Charles area is designated a marginal area with an attainment date of 1993.

After the onshore and offshore emissions were processed and day-specific ambient temperature adjustments made, a number of future-year UAM-V simulations were performed using the meteorological and air quality conditions for the August and September 1993 episodes. Emissions from all sources expected to be operating in 1999 (including increases due to growth or new sources, and decreases due to source shutdowns, mobile-source fleet turnover, and other mandated controls) were included in the first scenario. This established the forecasted future baseline ambient concentrations. The second scenario ("no OCSPD") eliminated all OCSPD-related emission sources from the baseline inventory. The difference in these scenarios provides a bounding calculation of the total "impact" due to OCSPD emission sources in the western and central Gulf on ozone concentrations within the nonattainment areas. To address and evaluate the effects of uncertainty in estimating future-year emissions, combinations of onshore and offshore emission scenarios were simulated to provide a range of estimated OCSPD impacts.

Quantification and Assessment of Impacts—Ozone impacts resulting from the inclusion of the OCSPD emissions were "quantified" by subtracting the simulated ozone value for each grid cell in the "No OCSPD" simulation from the value in the corresponding grid cell in the simulation that included OCSPD emissions. For this study, the 1993 and 1999 UAM-V simulated impacts of OCSPD emissions were assessed as follows: The change in hourly ozone was calculated for each grid cell by subtracting the ozone concentration in the "No OCSPD" simulation from that in the baseline simulation. The incremental impacts due to the inclusion of OCSPD precursor emissions are illustrated graphically in an ozone "difference" plot. This type of plot depicts isopleths of absolute ozone concentrations for the "No OCSPD" simulation and various levels of shading depicting incremental ozone impacts from the "With OCSPD" scenario. (An example of this type of plot is presented in Figure 5-6, on page 5-12.) The total hourly ozone concentration estimated for the simulation is obtained by adding the increment (shading) to the value given by the ozone isopleth. For example, in Figure 5-6a, in the Gulf south of Galveston Island, the incremental impact is 2–4 ppb for this hour and the total ozone concentration is 42–44 ppb. Presenting the information this way provides the reader an estimate of the concentration derived from the simulation without OCSPD emissions along with the incremental impacts due to OCSPD emissions.

To provide a more focused analysis of the impacts, plots of this parameter are presented separately for the Houston/Galveston-Beaumont/Port Arthur subdomain and a subdomain for Louisiana that includes the Lake Charles/Calcasieu Parish and Baton Rouge nonattainment areas. Tabular summaries of incremental impacts due to OCSPD emissions are even more focused and are presented for only those portions of the domain covered by the four nonattainment areas, as illustrated in Figure 5-1.

To illustrate the OCSPD impacts, representative plots are provided for each of the scenarios for selected episode days. For the August episode, impacts are assessed for the 18th and 19th, and for the September episode, impacts are assessed for the 8th, 9th and 10th. The meteorological conditions of the episodes, as revealed by the data analysis and base-case UAM-V modeling results, indicate that the greatest potential for OCSPD impacts occurred on these particular days.

5.2 SUMMARY OF THE BASE-YEAR (1993) OCSPD IMPACT SIMULATIONS

This section summarizes the UAM-V simulations performed to estimate the impacts of OCSPD sources on ozone concentrations observed during the August and September 1993 episodes.

SUMMARY OF OCSPD EMISSIONS FOR 1993

Emission density plots depicting the location and magnitude of OCSPD emissions for 17 August 1993 are presented in Figure 5-2 and 5-3, respectively, for NO_x and VOC for the southeast Texas offshore area. Similarly, Figures 5-4 and 5-5 present NO_x and VOC

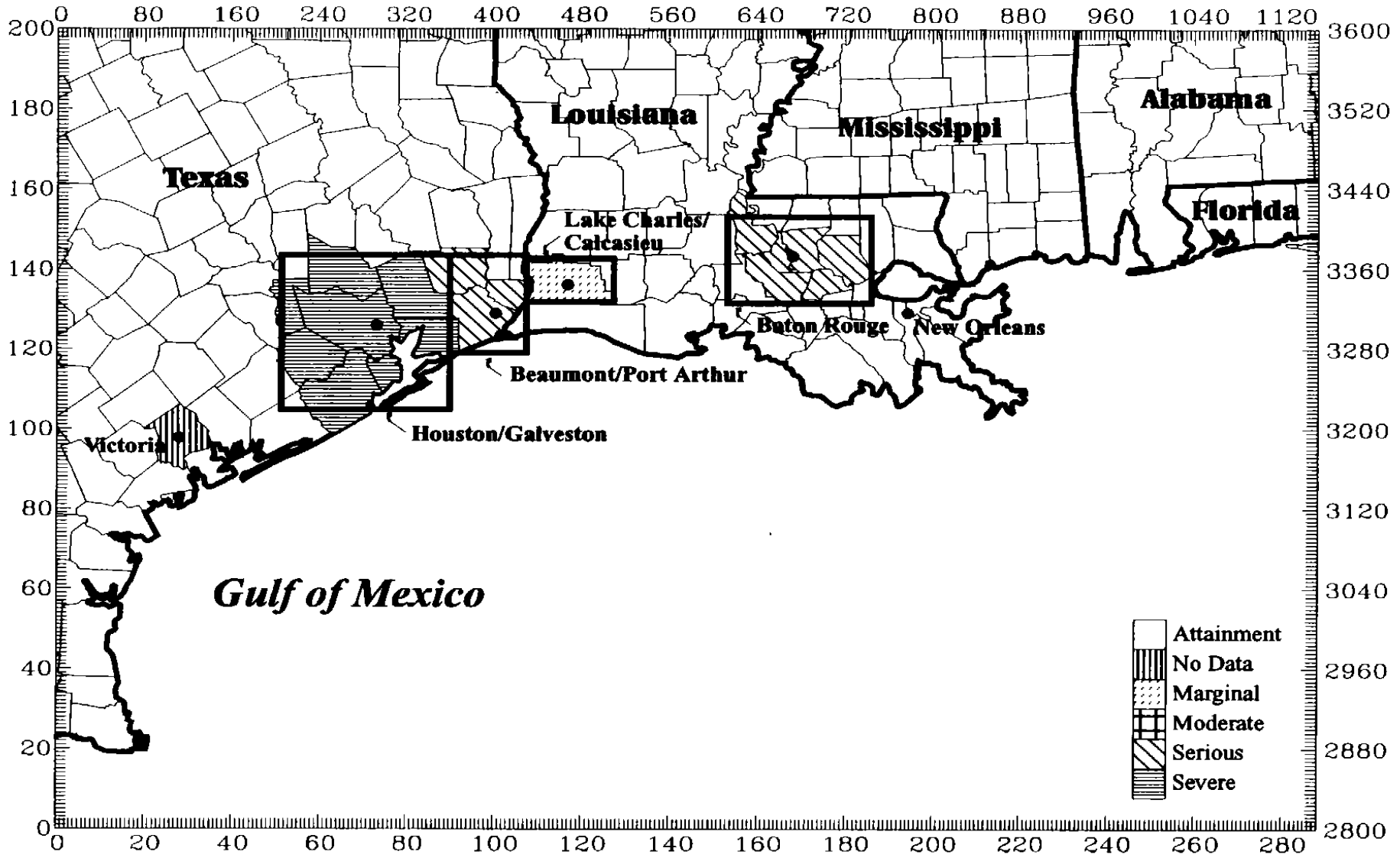

Figure 5-1. Depiction of nonattainment areas in the GMAQS domain for which daily ozone impacts from OCSPD emissions have been tabulated.

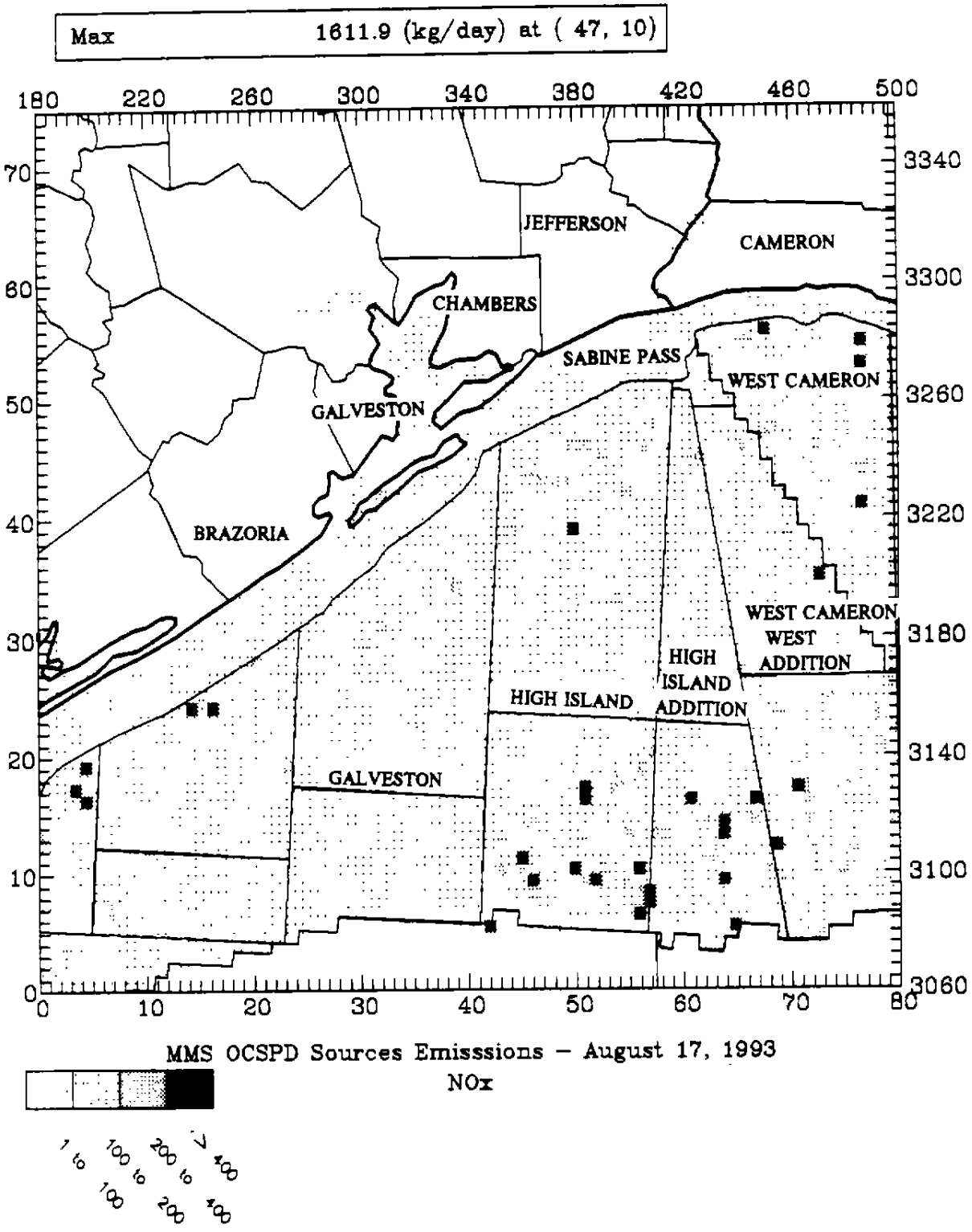

Figure 5-2. OCSPD NO_x emission totals (kg/day) for 17 August 1993 for the Texas portion of the GMAQS domain.

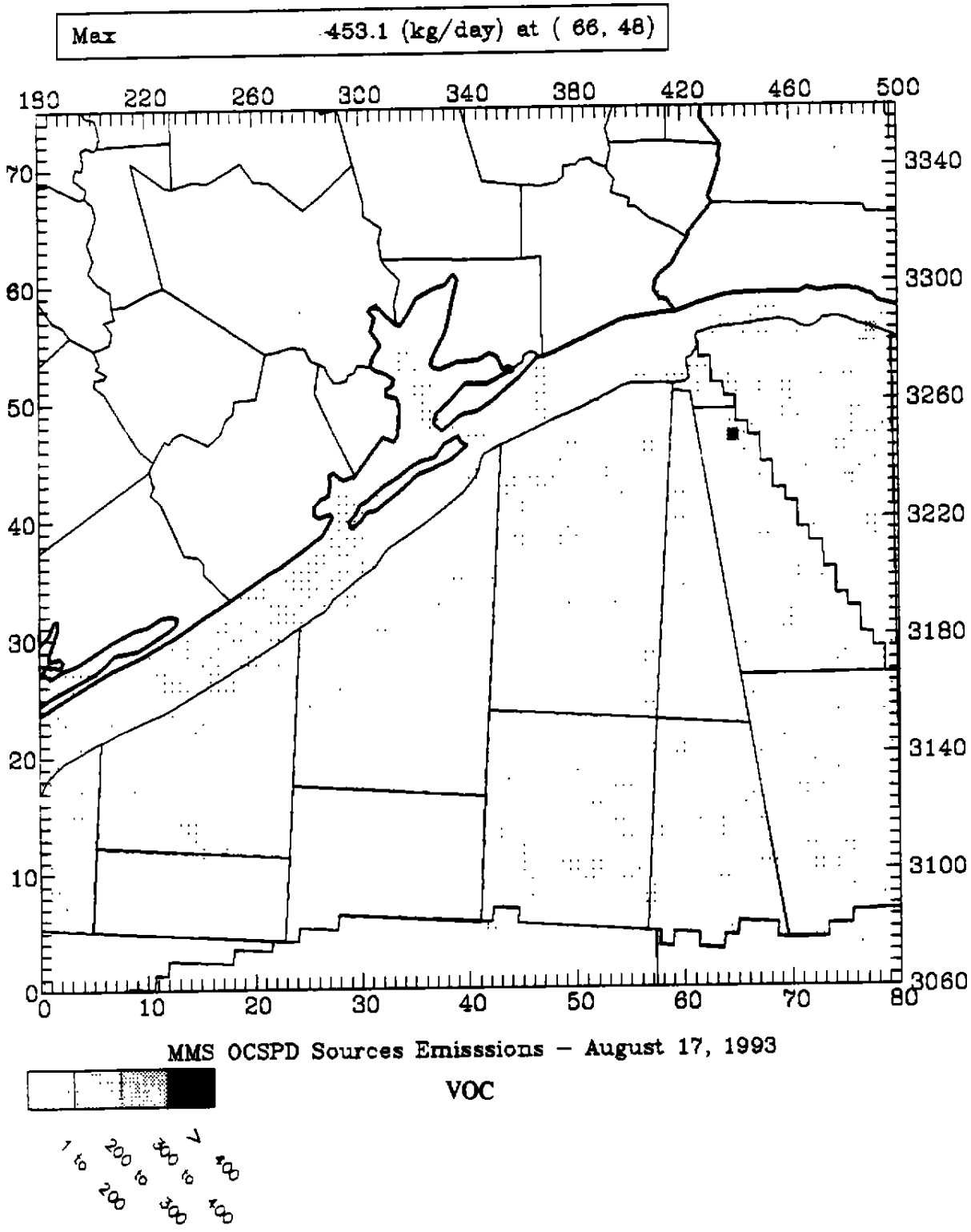

Figure 5-3. OCSPD VOC emission totals (kg/day) for 17 August 1993 for the Texas portion of the GMAQS domain.

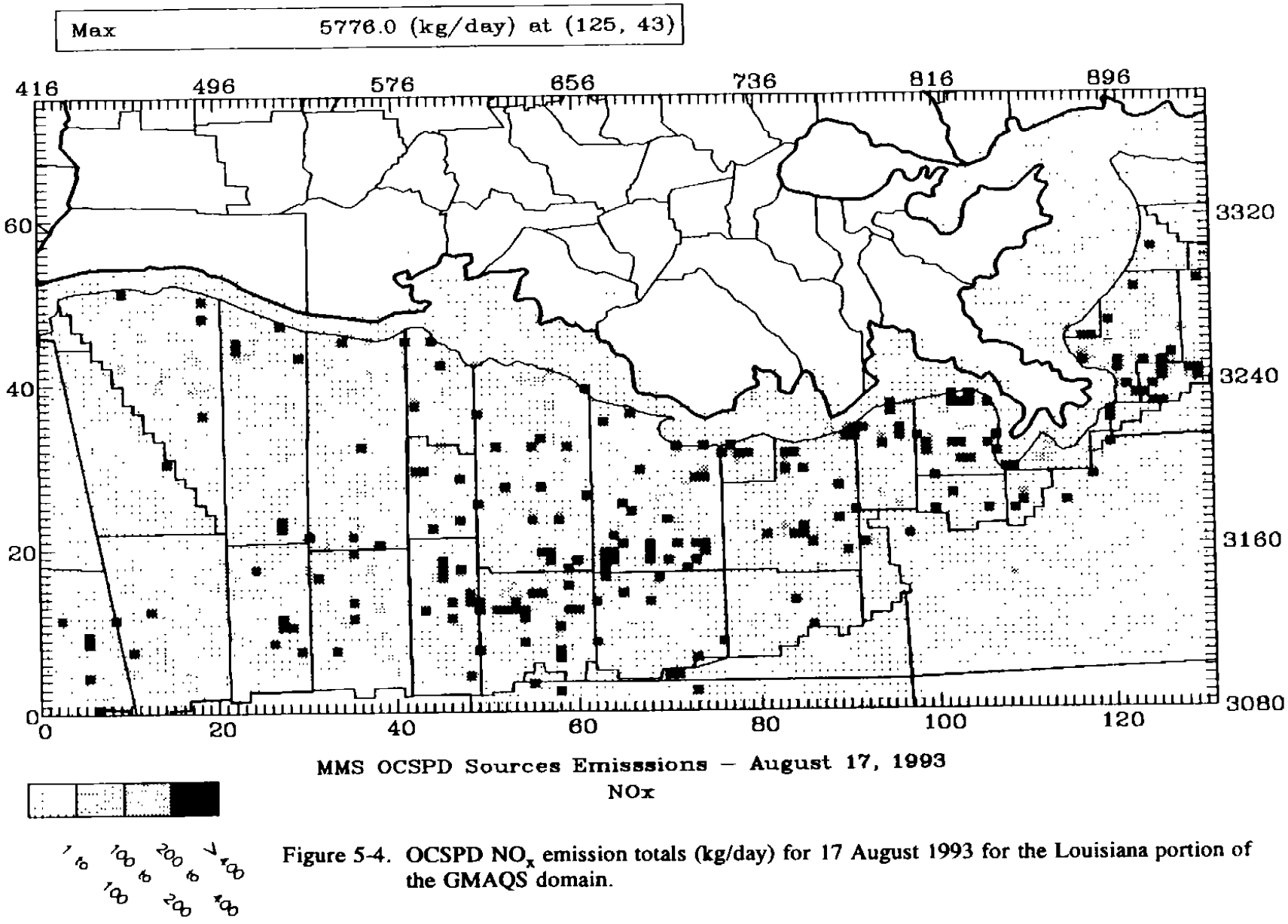

Figure 5-4. OCSPD NO_x emission totals (kg/day) for 17 August 1993 for the Louisiana portion of the GMAQS domain.

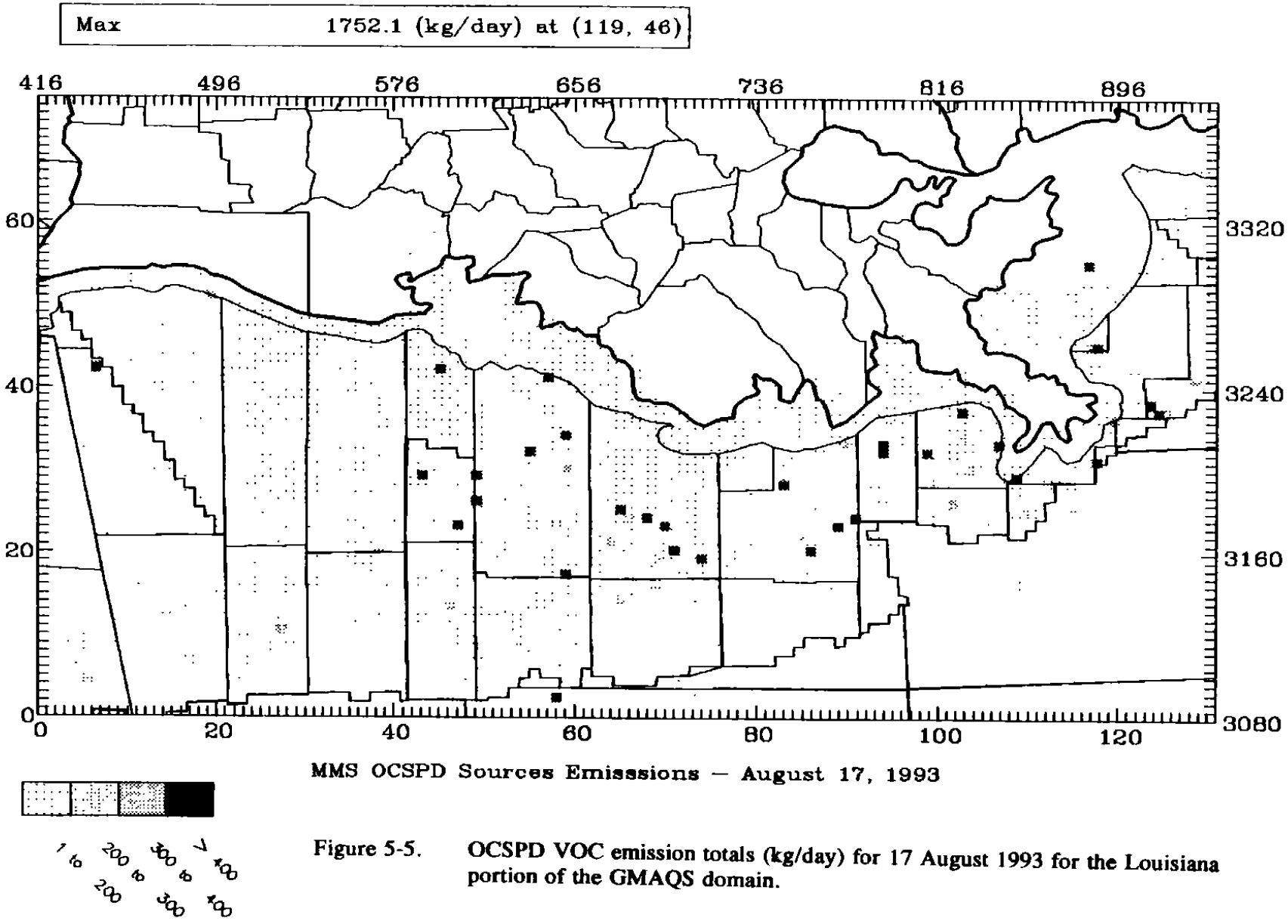

Figure 5-5. OCSPD VOC emission totals (kg/day) for 17 August 1993 for the Louisiana portion of the GMAQS domain.

OCSPD emissions for the offshore area south of Louisiana. The figures show that the majority of the OCSPD emissions are associated with platform operations, located in the central Gulf area south of Louisiana. (Future growth in OCS exploration and development activity is also expected to be greatest in this general area, but further from shore.) Because crew/supply vessels, pipeline vessels, and crew/supply helicopters are associated with OCS petroleum development and included as OCSPD emissions, some of these emissions are located along inland waterways (e.g., the Sabine River); at service ports, terminals, and airports in the Galveston Bay/Houston Ship Channel area; and at other locations along the Texas and Louisiana coast. These totals can be compared to those provided for all subdomains of the GMAQS domain in Table 4-6 for the August episode. As presented in Table 4-1, emissions from these nonplatform sources make up approximately 30 percent of the OCSPD NO_x inventory and approximately 15 percent of the OCSPD VOC inventory; the majority of the OCSPD emissions are associated with point sources located on platforms. In addition, the nonplatform OCSPD sources make up nearly 20 percent of the total offshore NO_x inventory and approximately 10 percent of the total offshore VOC inventory. To provide a comparison of the OCSPD emissions located just adjacent to the Houston and Beaumont/Port Arthur onshore nonattainment areas, the emissions associated with OCSPD activity in the offshore lease tracts are presented in Table 5-1. The lease blocks included in these totals are depicted in Figure 5-2. A comparison of these emissions with those from sources located in the adjacent Houston and Beaumont/Port Arthur areas (Table 4-6, Subregion I) indicates that the OCSPD emissions adjacent to the Houston and Beaumont/Port Arthur areas represent less than 2 percent of the total NO_x emissions and less than 1 percent of the total VOC emissions in the Houston/Beaumont/Port Arthur onshore area.

OCSPD IMPACT SIMULATION RESULTS FOR 1993

To estimate the ozone impacts of OCSPD emissions, the base-case UAM-V simulations (presented in Section 4) for the August and September episodes were rerun without OCSPD emissions. For the analysis of impacts, difference plots are provided for those hours during which the simulated peak concentrations occurred. In addition, to compare the impacts from OCSPD emissions with those from other sources, a simulation was performed for the September episode in which onroad mobile emissions were omitted.

17-20 August

As noted above, the analysis of OCSPD impacts for this episode focuses on 18 and 19 August. Figure 5-6 presents ozone impacts of OCSPD emissions for 18 August (hour 1700–1800, a representative hour near the time of the observed peak) for the Houston and Louisiana subdomains. It shows the incremental impacts as shades of gray and the absolute concentrations derived from the "No OCSPD" simulation as isopleths. The maximum onshore impact in the Houston area during this hour is 6 ppb, or less in the southwest corner of the figure, where ozone concentrations resulting from all other emission sources are approximately 50 ppb. The maximum impact in the Baton Rouge area for this hour is less than 2 ppb. Figure 5-7 presents the calculated impacts for 19

Table 5-1a. Emissions summary for OCSPD sources in Houston subregion, 17 August 1993.

Source Type	County/Lease Block	FIPS[1]	NO_x (tpd)	VOC (tpd)	CO (tpd)
Exploration Vessels					
	Galveston	99037	0.2056	0.0081	0.0215
	High Island	99049	0.1621	0.0064	0.0170
	Brazoria	48039	0.3207	0.0127	0.0336
	Chambers	48071	1.3314	0.0527	0.1396
	Galveston	48167	0.3693	0.0146	0.0387
	Jefferson	48245	0.5053	0.0200	0.0530
Subtotal			2.8944	0.1145	0.3034
Crew/Supply Vessels					
	Galveston	99037	0.6874	0.0545	0.1673
	High Island	99049	0.1640	0.0130	0.0399
	Brazoria	48039	0.5701	0.0452	0.1388
	Chambers	48071	0.0017	0.0001	0.0004
	Galveston	48167	0.1648	0.0131	0.0401
	Jefferson	48245	0.0536	0.0042	0.0131
Subtotal			1.6416	0.1301	0.3996
Crew/Supply Helicopters					
	Galveston	99037	0.0138	0.0071	0.0222
	High Island	99049	0.0188	0.0099	0.0331
	Brazoria	48039	0.0011	0.0012	0.0074
	Chambers	48071	0.0000	0.0000	0.0000
	Galveston	48167	0.0009	0.0009	0.0066
	Jefferson	48245	0.0023	0.0034	0.0122
Subtotal			0.0369	0.0225	0.0815
Pipeline Vessels					
	Galveston	99037	1.4301	0.2434	0.2255
	High Island	99049	1.5453	0.2631	0.2437
	Brazoria	48039	0.2752	0.0468	0.0434
	Chambers	48071	0.4260	0.0725	0.0672
	Galveston	48167	0.0641	0.0109	0.0101
	Jefferson	48245	0.2639	0.0449	0.0416
Subtotal			4.0046	0.6816	0.6315
Platforms					
	Galveston	99037	1.4250	0.2744	0.3102
	High Island	99049	5.1381	0.7154	1.1700
Subtotal			6.5631	0.9898	1.4802
TOTAL			15.1406	1.9385	2.8962

[1] FIPS 99xxx indicate OCS lease blocks.

Table 5-1b. Emissions summary for OCSPD sources in the Beaumont/Port Arthur subregion, 17 August 1993.

Source Type	County/Lease Block	FIPS[1]	NO_x (tpd)	VOC (tpd)	CO (tpd)
Exploration Vessels					
	High Island	99049	0.1621	0.0064	0.0170
	High Island East Addition	99051	0.4103	0.0162	0.0429
	Sabine Pass	99097	0.0000	0.0000	0.0000
	West Cameron West Addition	99141	0.1485	0.0059	0.0155
	Cameron	22023	0.3611	0.0143	0.0379
	Jefferson	48245	0.5053	0.0200	0.0530
Subtotal			1.5873	0.0628	0.1663
Crew/Supply Vessels					
	High Island	99049	0.1640	0.0130	0.0399
	High Island East Addition	99051	0.0568	0.0045	0.0138
	Sabine Pass	99097	0.0041	0.0003	0.0010
	West Cameron West Addition	99141	0.4496	0.0356	0.1094
	Cameron	22023	0.3482	0.0276	0.0848
	Jefferson	48245	0.0536	0.0042	0.0131
Subtotal			1.0763	0.0852	0.2620
Crew/Supply Helicopters					
	High Island	99049	0.0188	0.0099	0.0331
	High Island East Addition	99051	0.0079	0.0040	0.0141
	Sabine Pass	99097	0.0050	0.0032	0.0110
	West Cameron West Addition	99141	0.0123	0.0075	0.0260
	Cameron	22023	0.0013	0.0013	0.0097
	Jefferson	48245	0.0023	0.0034	0.0122
Subtotal			0.0476	0.0293	0.1061
Pipeline Vessels					
	High Island	99049	1.5453	0.2631	0.2437
	High Island East Addition	99051	0.5362	0.0913	0.0846
	Sabine Pass	99097	0.0544	0.0093	0.0086
	West Cameron West Addition	99141	0.7581	0.1291	0.1195
	Cameron	22023	0.2375	0.0404	0.0374
	Jefferson	48245	0.2639	0.0449	0.0416
Subtotal			3.3954	0.5781	0.5354
Platforms					
	High Island	99049	5.1381	0.7154	1.1700
	High Island East Addition	99051	1.2821	0.1918	0.3100
	Sabine Pass	99097	0.1322	0.0244	0.0288
	West Cameron West Addition	99141	2.1401	1.0061	0.4655
Subtotal			8.6925	1.9377	1.9743
TOTAL			14.7991	2.6931	3.0441

[1] FIPS 99xxx indicate OCS lease blocks.

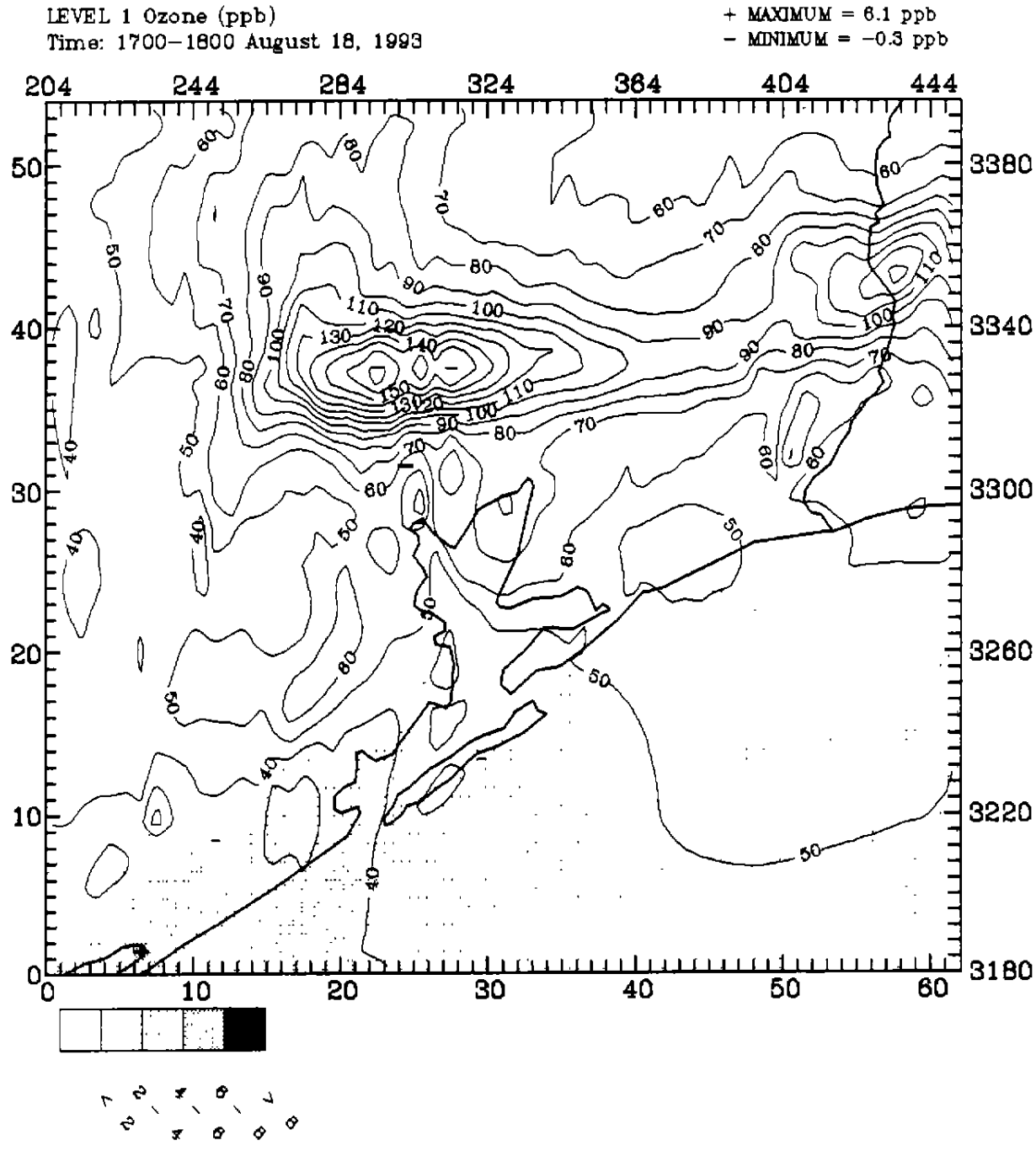

Figure 5-6a. UAM-V simulated ozone impacts (ppb) (shaded area) from OCSPD emissions for the Houston subdomain for 1700 CST 18 August 1993 (with OCSPD emissions minus without OCSPD emissions). Isopleths depict ozone from simulation without OCSPD emissions.

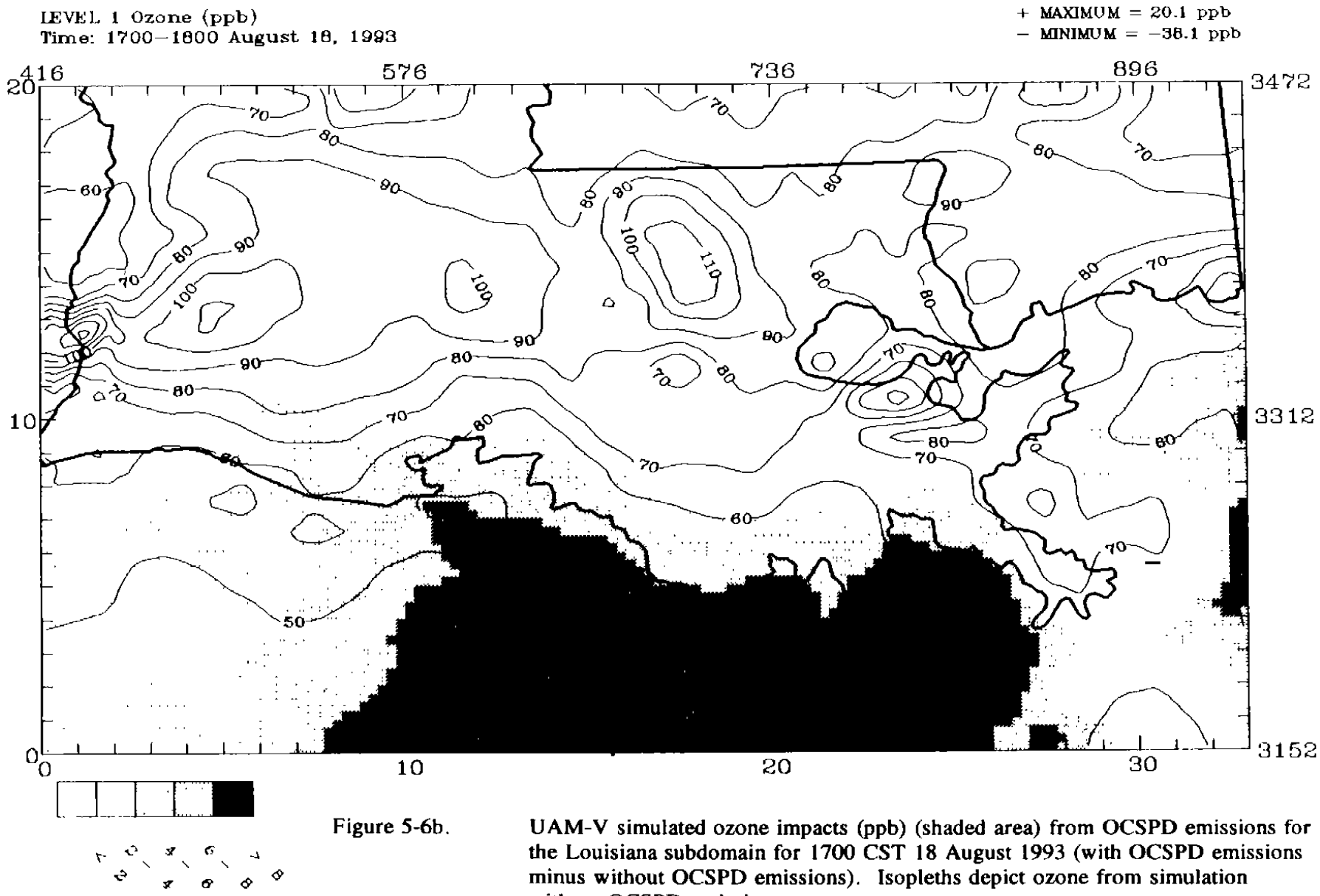

Figure 5-6b. UAM-V simulated ozone impacts (ppb) (shaded area) from OCSPD emissions for the Louisiana subdomain for 1700 CST 18 August 1993 (with OCSPD emissions minus without OCSPD emissions). Isopleths depict ozone from simulation without OCSPD emissions.

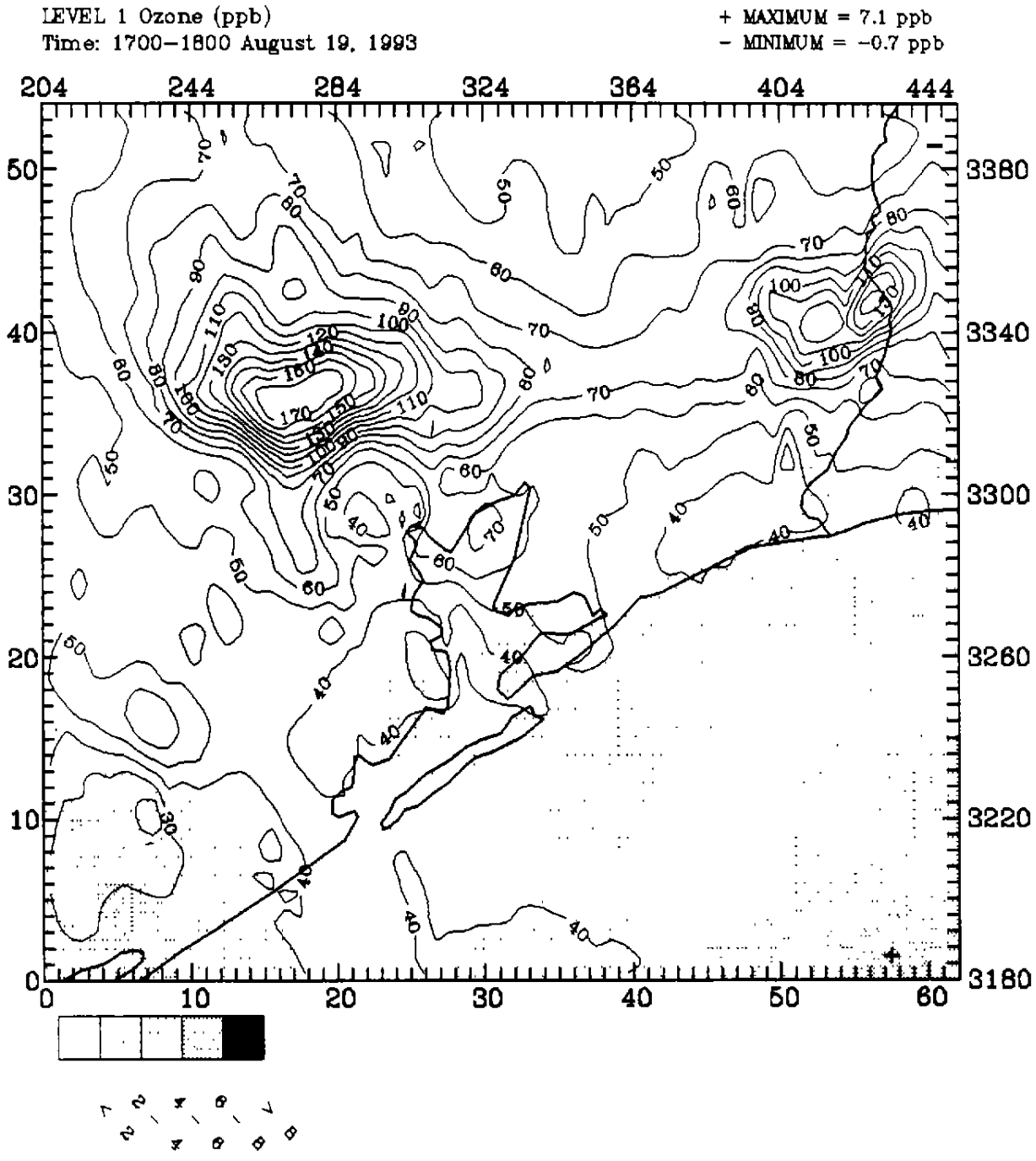

Figure 5-7a. UAM-V calculated ozone impacts (ppb) (shaded area) from OCSPD emissions for the Houston subdomain for 1700 CST 19 August 1993 (with OCSPD emissions minus without OCSPD emissions, Houston ship channel petroleum product spill not simulated). Isopleths depict ozone from simulation without OCSPD emissions.

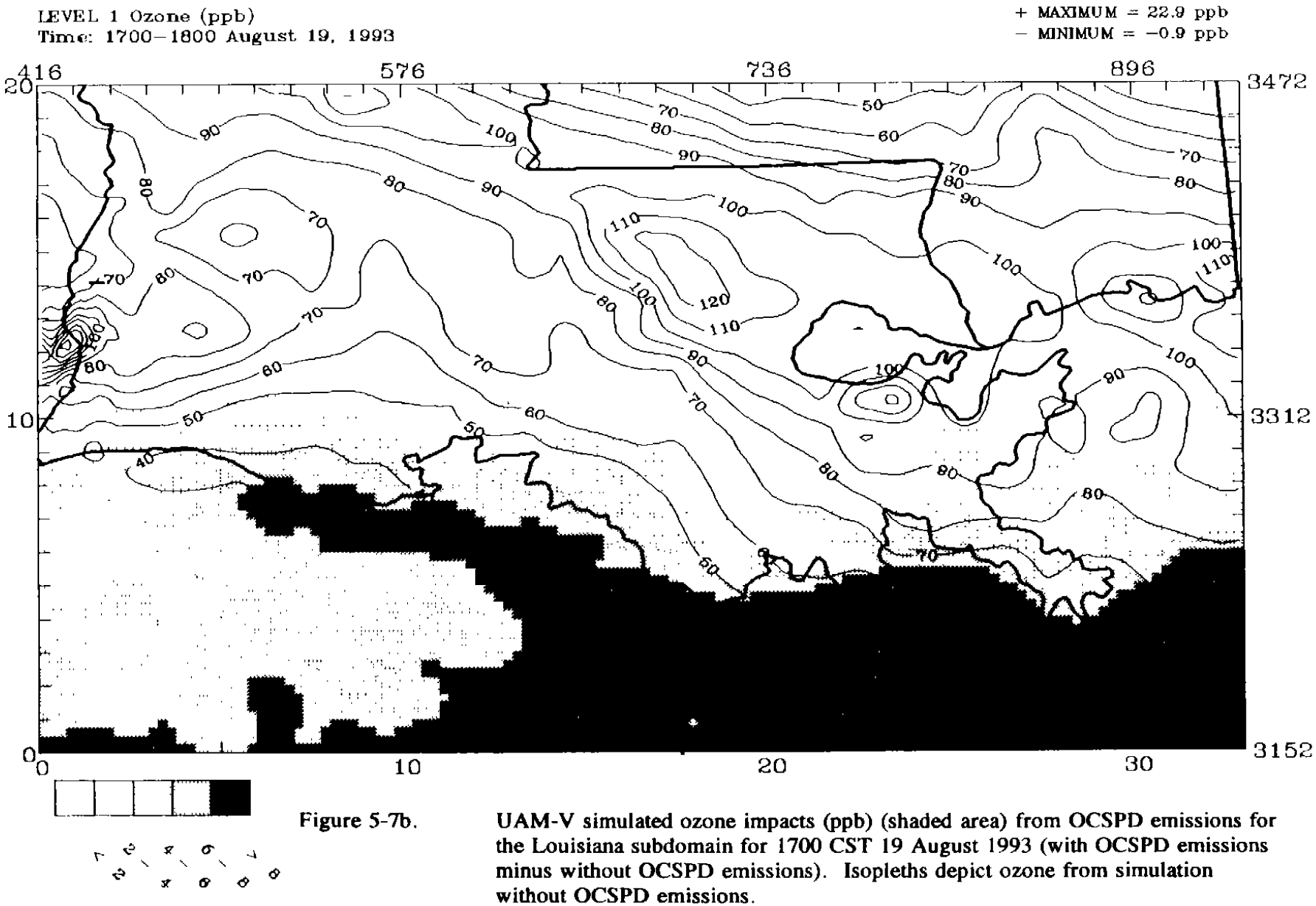

Figure 5-7b. UAM-V simulated ozone impacts (ppb) (shaded area) from OCSPD emissions for the Louisiana subdomain for 1700 CST 19 August 1993 (with OCSPD emissions minus without OCSPD emissions). Isopleths depict ozone from simulation without OCSPD emissions.

August (hour 1700-1800). The maximum impact due to OCSPD emissions in the Houston/Beaumont/Port Arthur area is less than 2 ppb in the area near the simulated peak concentration. In assessing OCSPD emissions for this episode day, emissions from the suspected petroleum product spill in the Houston Ship Channel area were not included in this simulation due to the accidental/episodic nature of this event. In the Baton Rouge area during this time, the peak impact is less than 2 ppb. Impacts along the Louisiana coast are near 8 ppb while the maximum difference in this subdomain is 23 ppb, located some 90 km offshore.

- For this episode, the maximum ozone impacts due to OCSPD operations in the Houston/Beaumont/Port Arthur area are estimated to be 6–8 ppb at a time when the hourly average ozone concentrations calculated from all other emission sources are approximately 50 ppb. During periods and at locations where ozone concentrations are simulated to equal or exceed 124 ppb, the incremental ozone impacts due to OCSPD emissions are simulated to be less than 2 ppb.

- For the Baton Rouge area, the maximum simulated incremental impacts from OCSPD emissions for this episode during the time of observed (and simulated) maximum concentrations is 0–2 ppb. Larger impacts from OCSPD emissions are simulated during other hours, and along the Louisiana coastline and over the Gulf, well south of the Baton Rouge nonattainment area.

6–11 September

As noted earlier, the analysis of OCSPD impacts for this episode focuses on 8, 9 and 10 September. Figure 5-8 presents the calculated impacts from OCSPD emissions on ozone concentrations within the Houston and Louisiana subdomains for 8 September (hour 1600–1700). For this hour, the maximum onshore impacts in the Houston area are 2–4 ppb, in the Beaumont/Port Arthur area 8–10 ppb, and in the Baton Rouge area less than 2 ppb. Figure 5-9 presents the calculated impacts from OCSPD emissions on ozone concentrations in the Houston and Louisiana subdomains for 9 September (hour 1600–1700). The maximum onshore impacts in the Houston area for this hour range from 2 to 4 ppb, and the maximum impact in the Baton Rouge area for this hour is less than 2 ppb. Figure 5-10 presents impacts for 10 September for hour 1500–1600. The maximum impacts for the Houston area range from 2 to 4 ppb and occur along the coast. In the Baton Rouge area the peak impact is less than 2 ppb. Impacts along the Louisiana coast are near 2–4 ppb while the maximum difference in this subdomain is 25 ppb, located some 100 km offshore, south of Vermilion Parish.

- The maximum simulated onshore impacts for the Houston area range between 2 and 4 ppb and in the Beaumont/Port Arthur area between 8 and 10 ppb. At locations and during periods when the onshore ozone concentration is simulated to equal or exceed 124 ppb, the simulated increment due to OCSPD operations in these areas is less than 2 ppb. In the Baton Rouge area, where the maximum simulated ozone concentrations are greater than 124 ppb, the maximum incremental impact is 0–2 ppb.

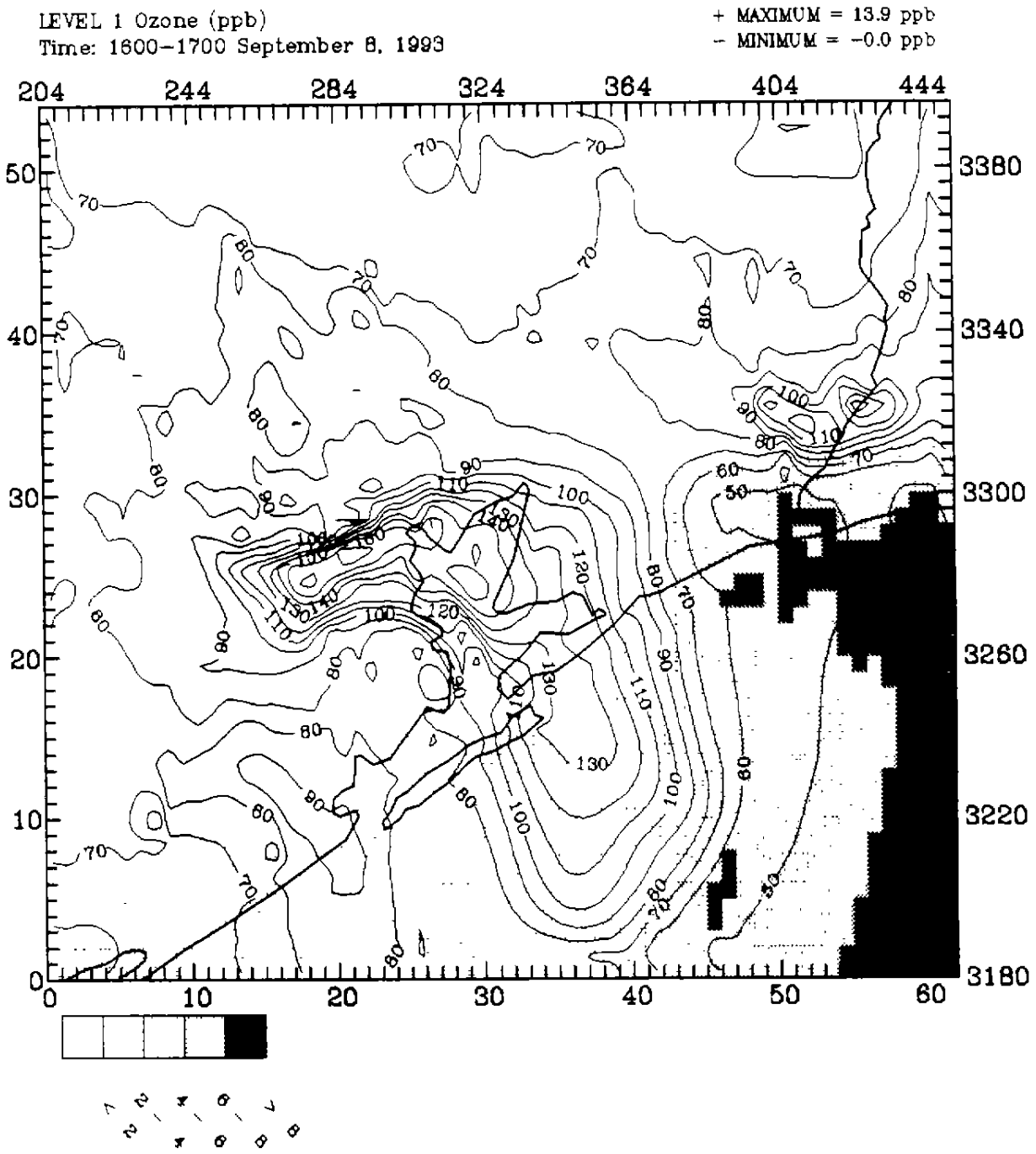

Figure 5-8a. UAM-V calculated ozone impacts (ppb) (shaded area) from OCSPD emissions for the Houston subdomain for 1600 CST 8 September 1993 (with OCSPD emissions minus without OCSPD emissions). Isopleths depict ozone from simulation without OCSPD emissions.

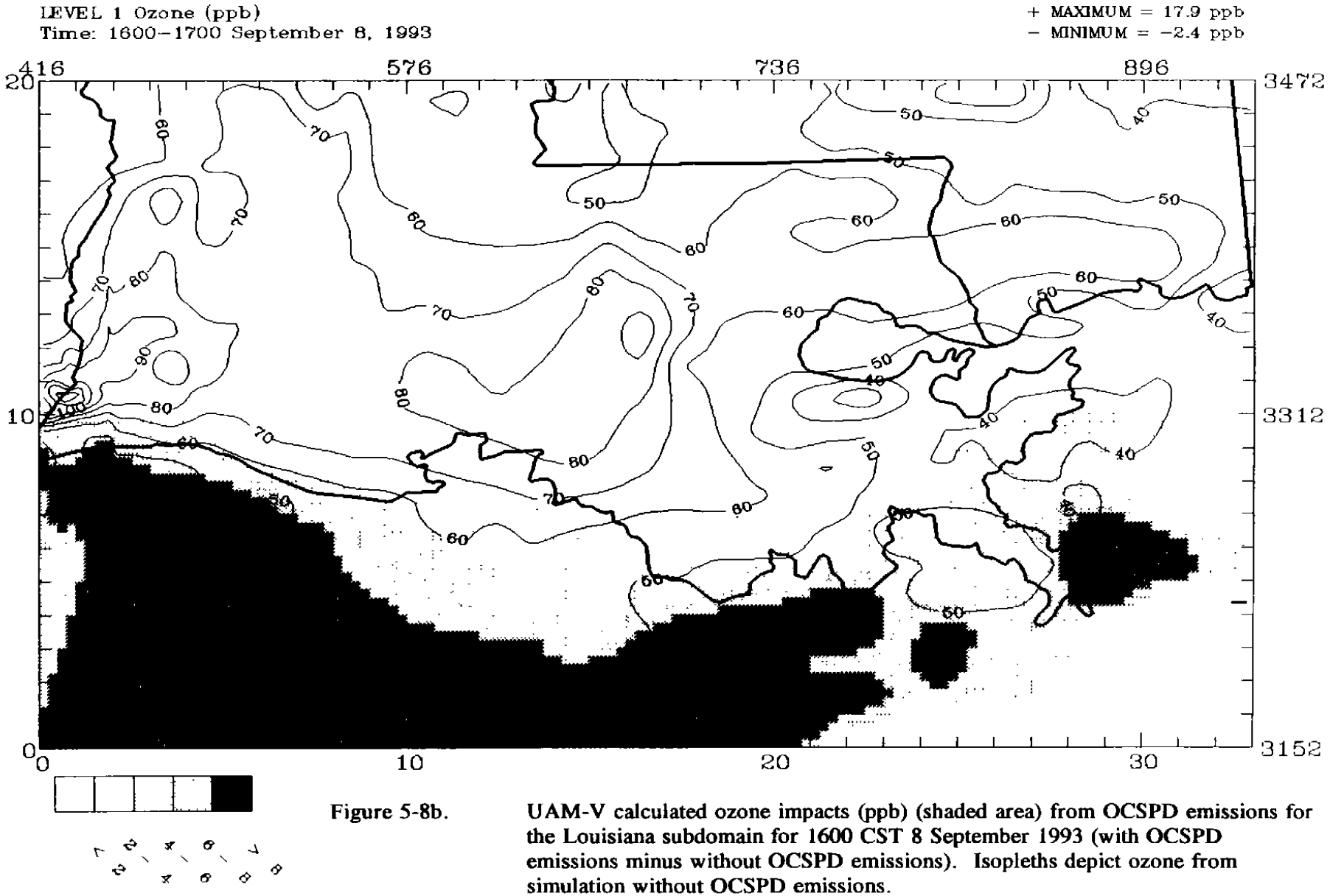

Figure 5-8b. UAM-V calculated ozone impacts (ppb) (shaded area) from OCSPD emissions for the Louisiana subdomain for 1600 CST 8 September 1993 (with OCSPD emissions minus without OCSPD emissions). Isopleths depict ozone from simulation without OCSPD emissions.

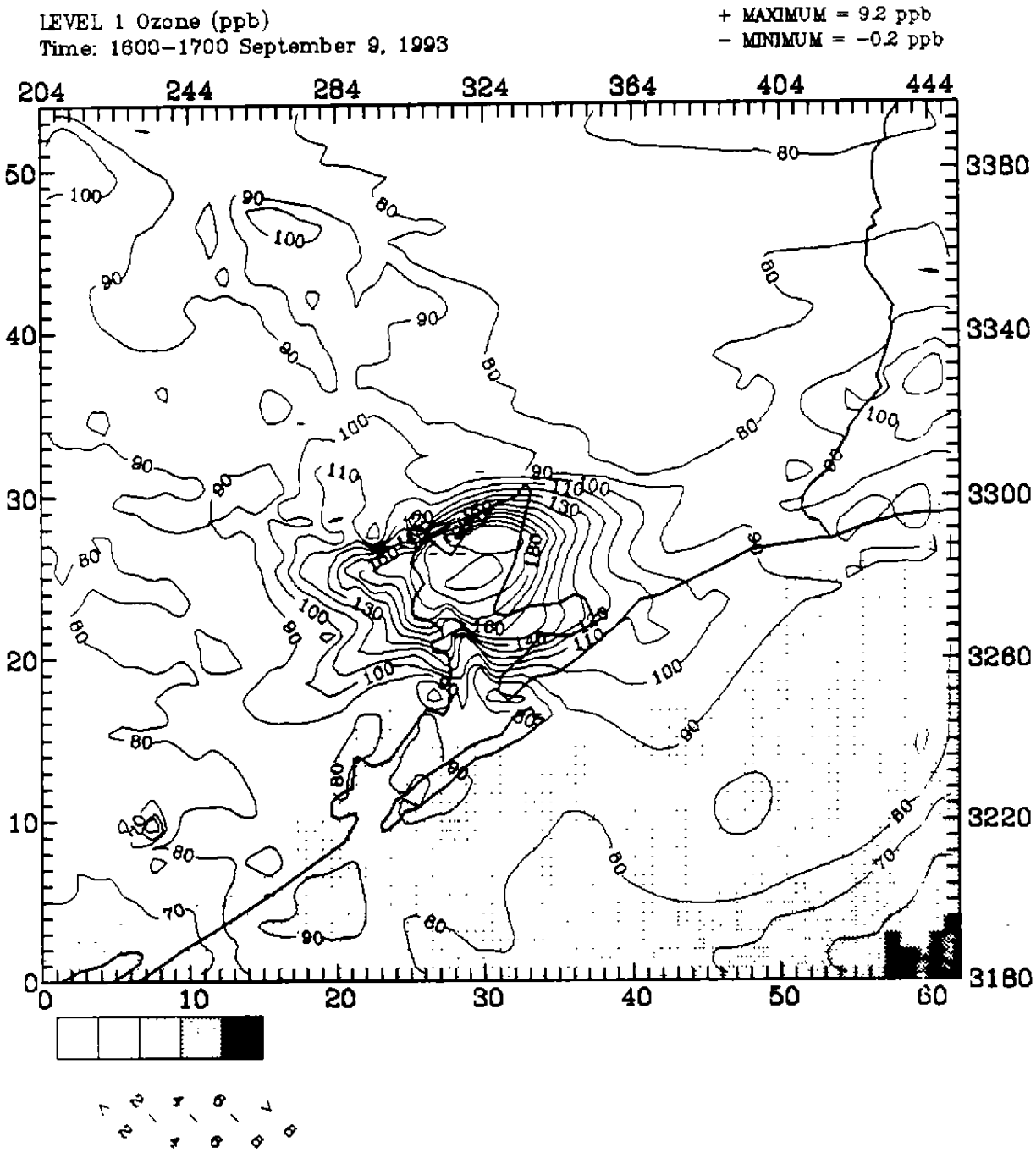

Figure 5-9a. UAM-V simulated ozone impacts (ppb) (shaded area) from OCSPD emissions for the Houston subdomain for 1600 CST 9 September 1993 (with OCSPD emissions minus without OCSPD emissions). Isopleths depict ozone from simulation without OCSPD emissions.

95013

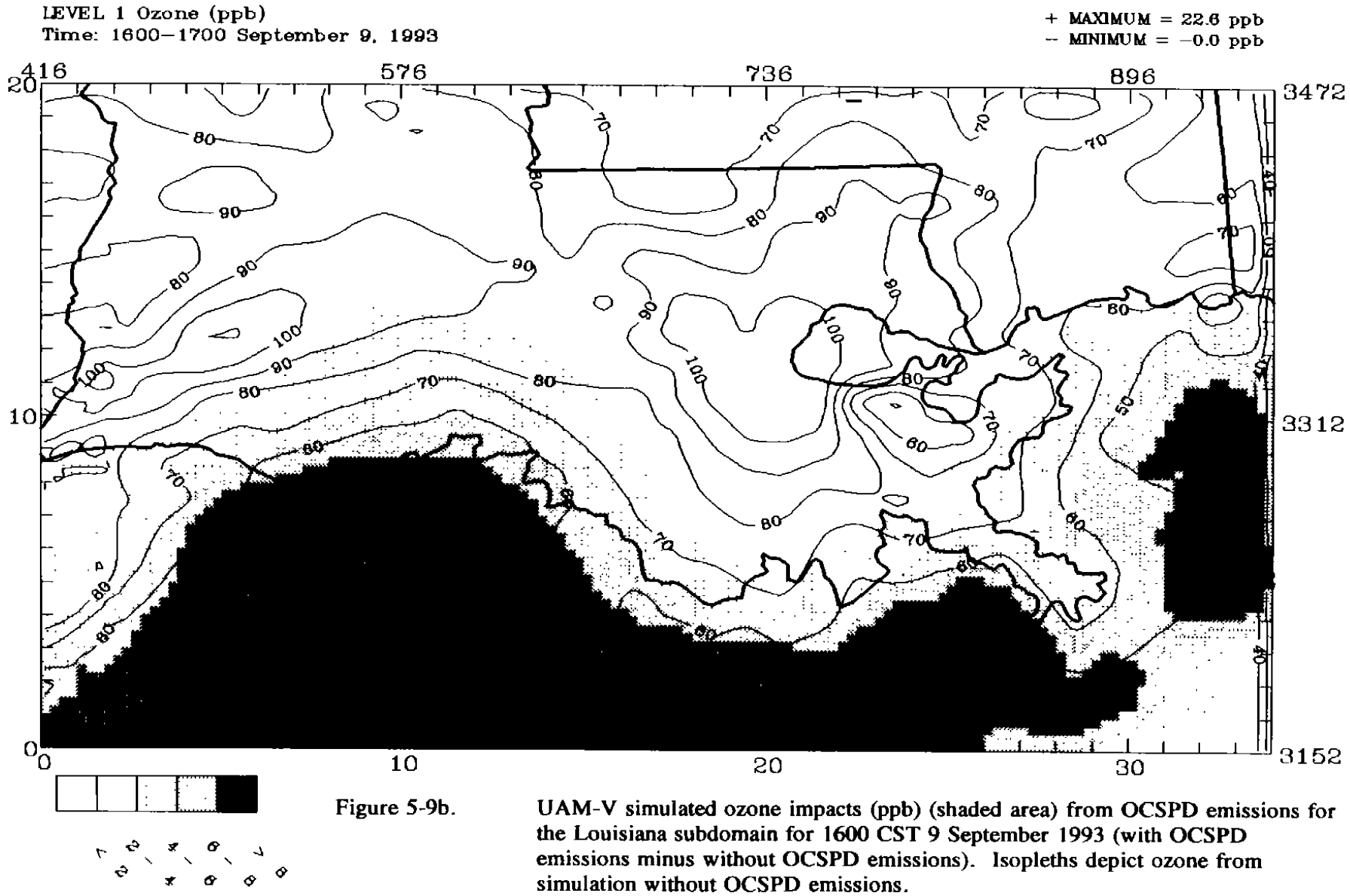

Figure 5-9b. UAM-V simulated ozone impacts (ppb) (shaded area) from OCSPD emissions for the Louisiana subdomain for 1600 CST 9 September 1993 (with OCSPD emissions minus without OCSPD emissions). Isopleths depict ozone from simulation without OCSPD emissions.

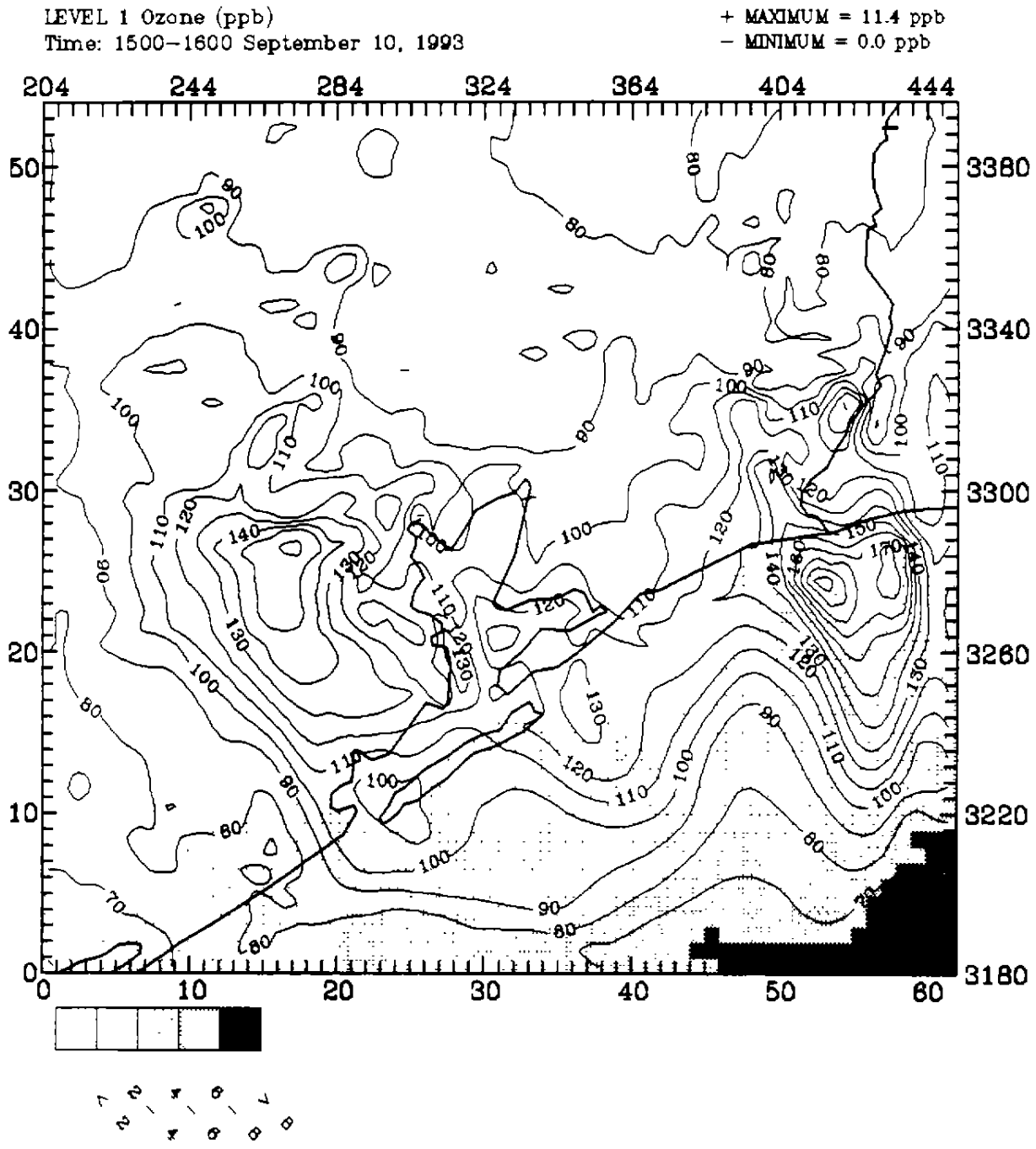

Figure 5-10a. UAM-V simulated ozone impacts (ppb) (shaded area) from OCSPD emissions for the Houston subdomain for 1500 CST 10 September 1993 (with OCSPD emissions minus without OCSPD emissions). Isopleths depict ozone from simulation without OCSPD emissions.

95013

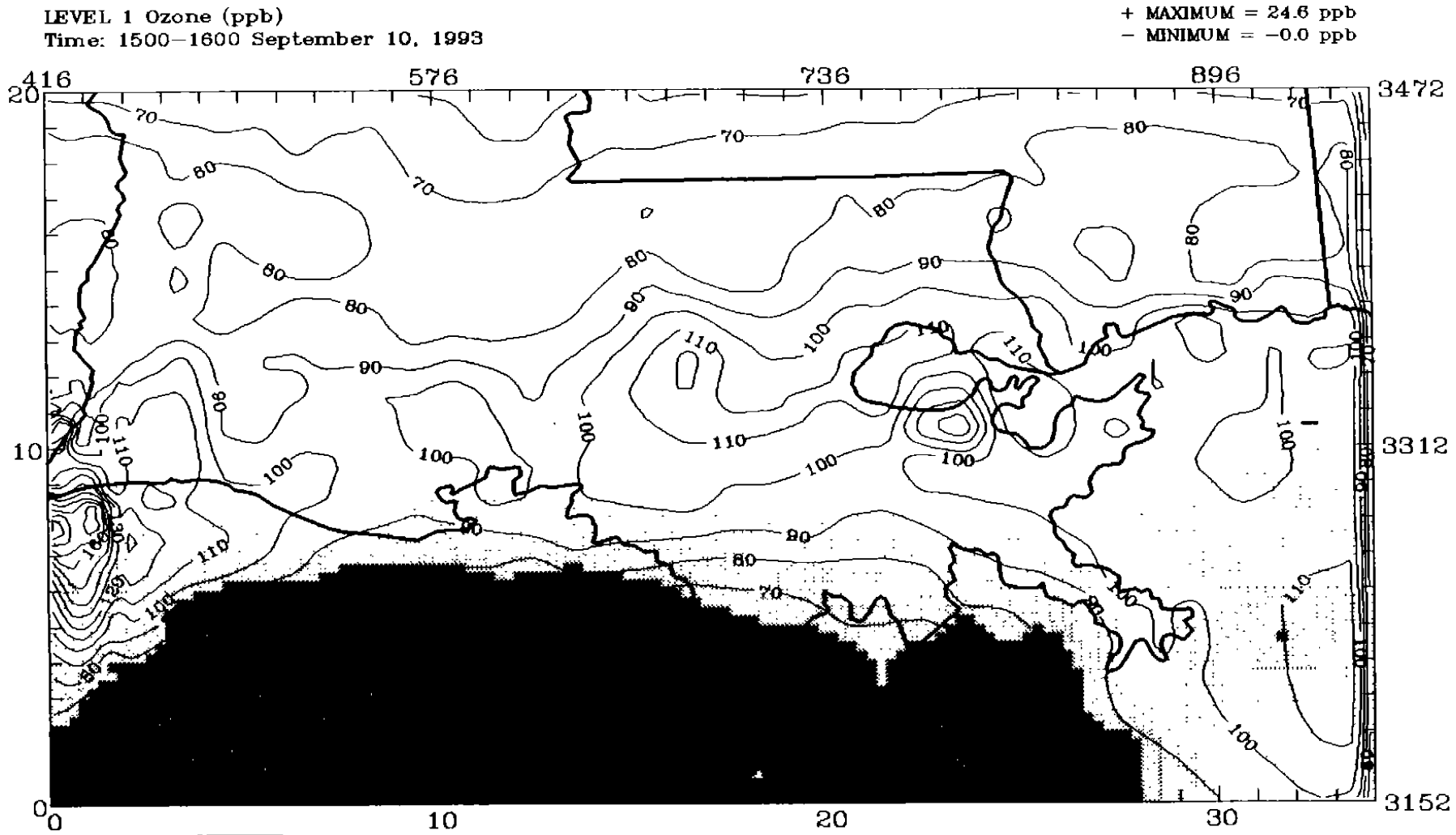

Figure 5-10b. UAM-V simulated ozone impacts (ppb) (shaded area) from OCSPD emissions for the Louisiana subdomain for 1500 CST 10 September 1993 (with OCSPD emissions minus without OCSPD emissions). Isopleths depict ozone from simulation without onroad mobile emissions.

Mobile-Source Emission Sensitivity

To compare the impacts of OCSPD emissions with those of another anthropogenic source category, an emission sensitivity simulation for the 6–11 September episode was performed. In this simulation, onroad mobile emissions were eliminated from the base-case simulation (OCSPD emissions were included). For comparison with impacts presented in Figure 5-8 through 5-10 from OCSPD sources, Figure 5-11 presents ozone impacts from mobile sources for 8 September (hour 1600–1700); Figure 5-12 provides ozone impacts from mobile sources for 9 September (hour 1600–1700), and Figure 5-13 presents impacts from mobile sources for 10 September. For 8 September the maximum impact from mobile emissions is 46.6 ppb, located in southern Houston, and the maximum impact in the Baton Rouge area is 11.7 ppb. For 9 September the maximum impact from mobile emissions is 50 ppb, located just southeast of Houston, while the maximum impact in the Baton Rouge area is 10–15 ppb. For 10 September the maximum impact in the Houston area is 51 ppb, located just west of Houston, and the maximum impact in the Baton Rouge area is 10–15 ppb. These impacts are large compared to the 2–4 ppb impact resulting from OCSPD emissions.

These results illustrate that the contribution of mobile-source emissions to total simulated ozone concentrations is considerably larger than that derived from OCSPD emissions for the September 1993 episode.

5.3 EMISSION PROJECTIONS—1990 TO 1999

The 1999 baseline emission inventory was estimated from the 1990 emission inventory. The BEAFAC program in EPS 2.0 uses the EPA's preferred data source for calculating changes in activity levels for most stationary source categories, the Bureau of Economic Analysis' *Regional Projections to 2040* (DOC, 1990). The BEA database contains state data related to population, personal income, and employment for 57 industrial groupings. For each of these categories, the BEA database contains historical data for 1973, 1979, 1983, and 1988, and projected data for 1995, 2000, 2005, 2010, 2020, and 2040. For each state specified by the user, BEAFAC calculates state-level projection factors for population and earnings by industry by dividing the data for the projection year by the data for the base year. If the year requested is not in the database, data values for that year are determined by linearly interpolating between the two closest years in the file.

Future-year projections were estimated from the 1990 base-year inventories using a variety of projection factors (population, economic, transportation, industry specific) supplied by LDEQ, TNRCC, MMS, and the EPA. The following describes the development of future-year inventories from base-year inventories for sources in the onshore and offshore regions of the domain.

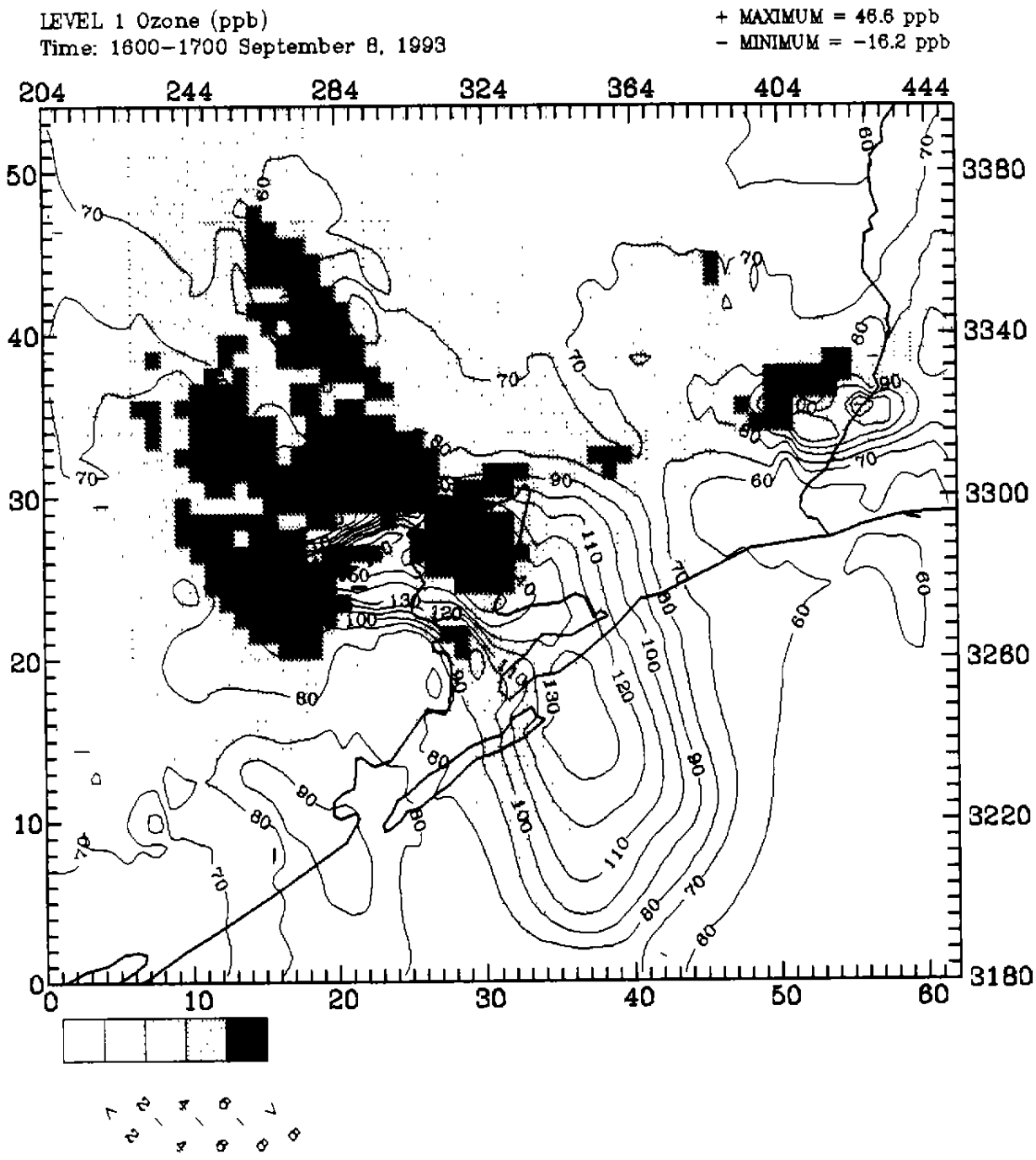

Figure 5-11a. UAM-V calculated ozone impacts (ppb) (shaded area) from onroad mobile emissions for the Houston subdomain for 1600 CST 8 September 1993 (with onroad mobile emissions minus without onroad mobile emissions). Isopleths depict ozone from simulation without onroad mobile emissions.

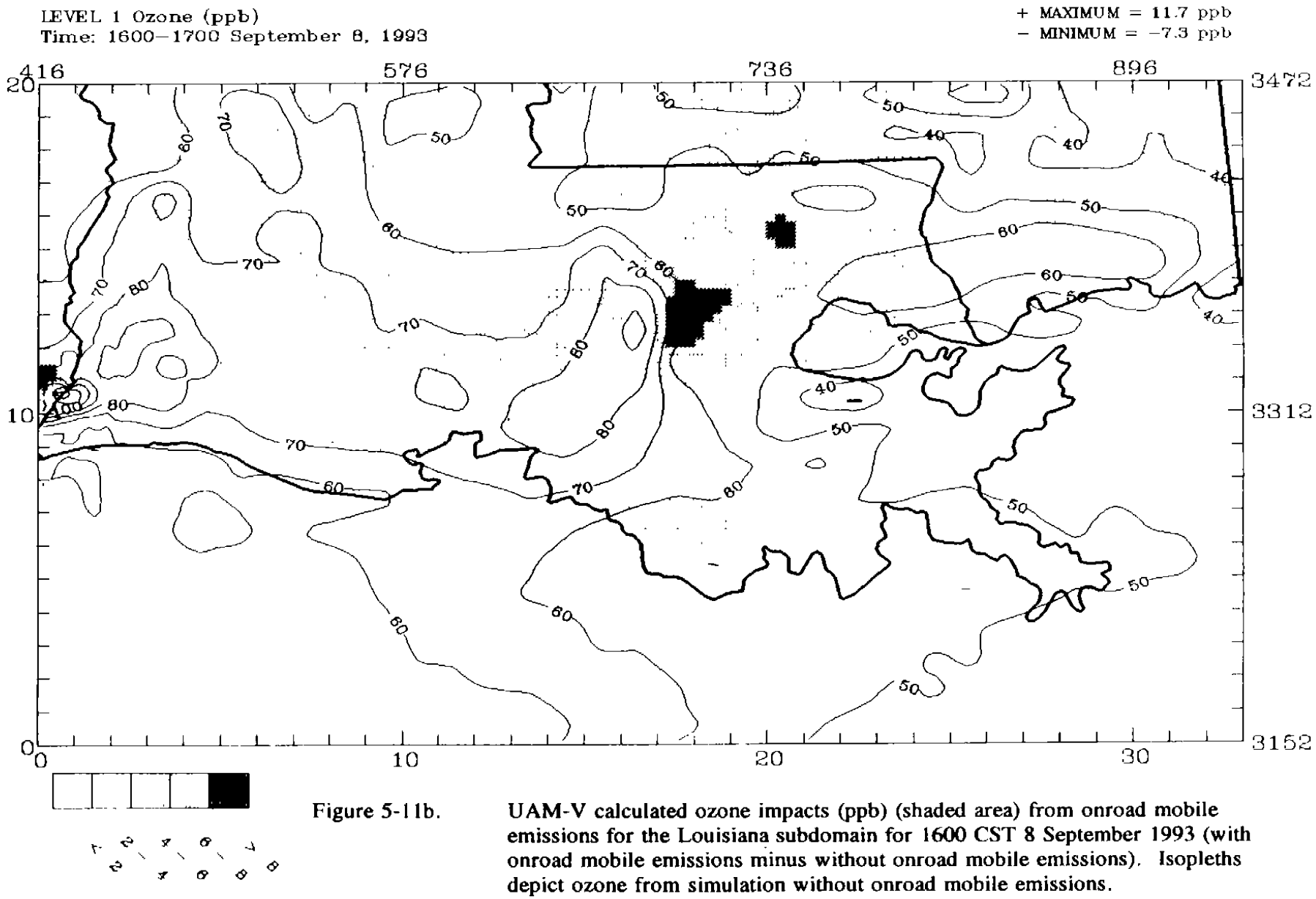

Figure 5-11b. UAM-V calculated ozone impacts (ppb) (shaded area) from onroad mobile emissions for the Louisiana subdomain for 1600 CST 8 September 1993 (with onroad mobile emissions minus without onroad mobile emissions). Isopleths depict ozone from simulation without onroad mobile emissions.

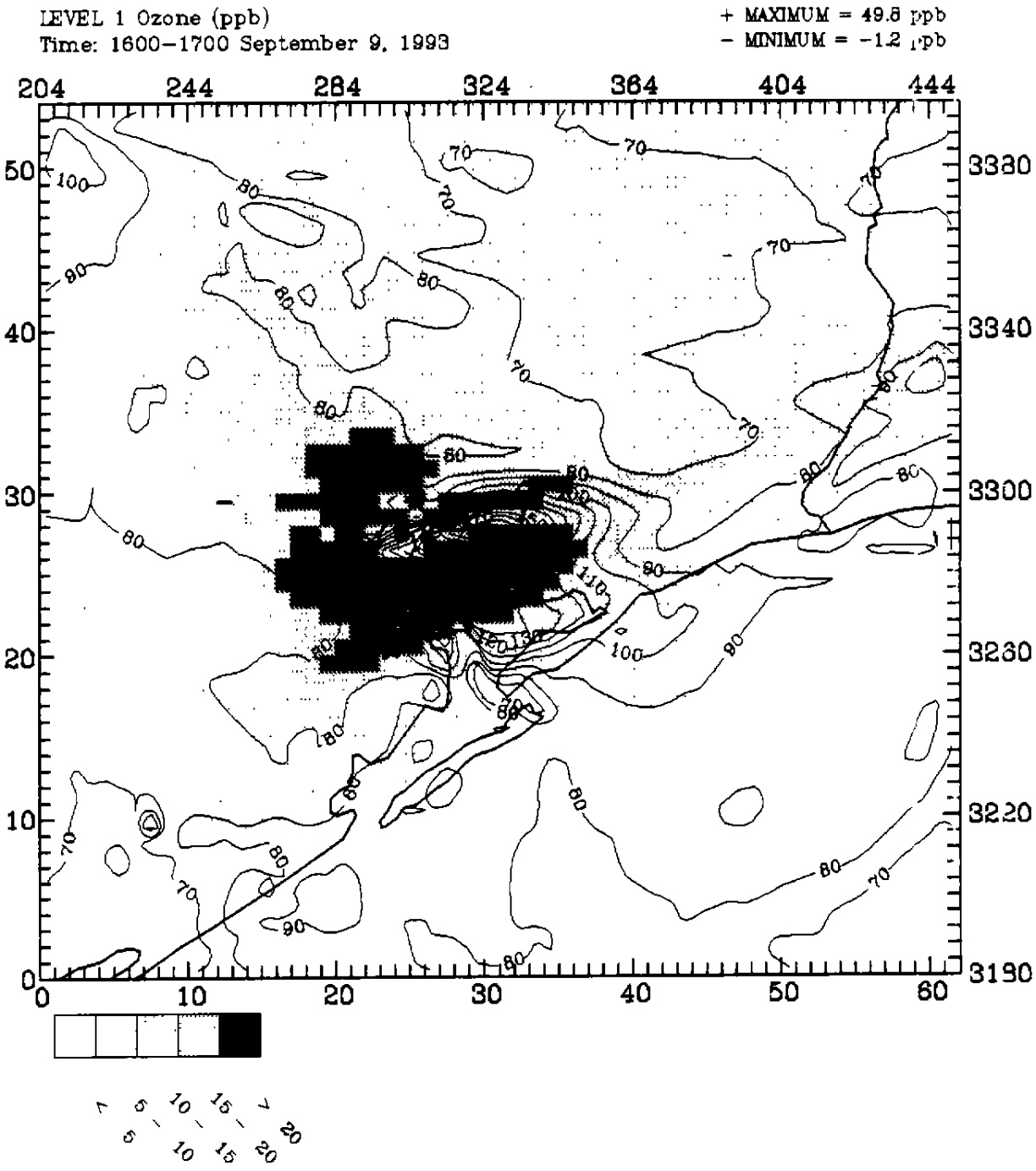

Figure 5-12a. UAM-V simulated ozone impacts (ppb) (shaded area) from onroad mobile emissions for the Houston subdomain for 1600 CST 9 September 1993 (with onroad mobile emissions minus without onroad mobile emissions). Isopleths depict ozone from simulation without onroad mobile emissions.

Stationary and Nonroad Mobile Sources

Texas. Growth and control factors provided by TNRCC were used to estimate 1999 stationary and nonroad mobile source emissions for the Houston/Galveston and Beaumont/Port Arthur subdomains. Separate projection factors were designated for three subregions: eight nonattainment counties in the Houston/Galveston area, three nonattainment counties in the Beaumont/Port Arthur area, and the remaining Texas counties in the subdomain. The point source growth factors were generated by Economic Growth Analysis System (E-GAS) (Randolph, 1993), and area and nonroad mobile source growth factors were generated using BEAFAC. The control factors included 15 percent VOC reductions and NO_x RACT emissions reductions. The rest of the attainment counties in Texas were projected to 1999 using the same methodology that was used for Alabama, Mississippi, and Florida (described further below).

Louisiana. For the Louisiana ozone attainment parishes (and the three marginal parishes), LDEQ provided a set of growth factors that were applicable for all Louisiana stationary source projections from the 1990 to the 1999 level. LDEQ also indicated that no controls would be applied for these sources. The LDEQ factors were applied to the 1990 EPA Interim Inventory area, nonroad mobile, and point source emissions to provide 1999 emission inventory estimates for the state. For the Baton Rouge area, growth and control factors provided by LDEQ were used to project point, area, and nonroad mobile sources. The emissions for the Baton Rouge subdomain were grown from 1990 to 1999 levels for all source categories using BEA employment factors, with the exception of those associated with electrical utilities, which were held constant at 1990 levels. VOC emissions from area and non-electric utility point sources were reduced 15 percent overall to accommodate the 1996 RFP requirements, and NO_x RACT reductions were applied to both utility and nonutility point sources.

Alabama, Florida, Mississippi, and Portions of Texas. For these areas, growth factors for non-utility point sources, area sources, and nonroad mobile sources were generated using BEAFAC. Growth factors for the electric utilities were calculated using state-specific utility generation information obtained from documentation of the ROMNET study (EPA, 1993b).

The control measures modeled for these areas included anticipated emissions reductions due to control regulations mandated under the Clean Air Act. The effects of nonutility, area, and nonroad mobile control measures required by the Clean Air Act on emissions levels for 1999 were estimated using methodologies and control parameter data obtained from documentation describing the ROMNET study (EPA, 1992b, 1993b). The level of required control for each area varies according to the ozone nonattainment status. The various types of mandated controls for the attainment counties are described briefly below.

- *National Measures*: National measures affect all sources nationwide, regardless of the nonattainment status of the area in which the source is located. For this analysis, the control requirements for the following sources and source categories were modeled as national measures: commercial and consumer solvent use; architectural surface coatings; traffic markings; hazardous waste Treatment,

Storage, and Disposal Facilities (TSDFs); marine vessel loading and unloading of crude oil and gasoline; landfills; and nonroad diesel engines.

- *Title III MACT Requirements*: Title III of the Clean Air Act requires that any facility emitting 10 tons per year or more of any hazardous air pollutant (as listed in Title III) or 25 tons per year or more of any combination of hazardous air pollutants must implement Maximum Available Control Technology (MACT). These requirements apply nationwide, regardless of nonattainment status. MACT controls were applied for both point and area source categories; since the MACT control efficiencies developed for the ROMNET study already included rule penetration factors for both area and point sources, these controls were applied to all appropriate sources without verifying individual source size.

- *Title IV NO_x Requirements:* Title IV NO_x emission control requirements for coal-fired electric utility boilers are specified in terms of an emission factor limit (lb NO_x/MMBtu). There were only two Title IV utilities included in the EPA Interim Inventory used for the study (one in Florida and one in Mississippi). To estimate the emissions reductions for the utility boilers for 1999, a 1990 baseline emission rate was calculated for each individual unit, based on the unit operating rate, fuel heat content, and reported annual emissions. The ratio of the applicable NO_x emission factor limit specified above to the 1990 baseline emission rate was then applied to the NO_x emissions of each unit to estimate future-year NO_x emission rates.

For the sources and source categories subject to more than one type of regulatory control, the most stringent control was applied.

Onroad Motor Vehicles

The 1999 modeling inventories for onroad mobile sources were prepared in a similar manner to the base-year inventories, but using 1999 vehicle miles traveled (VMT) projections and MOBILE5a input parameters. The same episodic daily minimum and maximum temperatures were assumed for the 1999 modeling inventories as were used for the 1993 base-year inventories. In the future-year inventories, the Inspection/Maintenance (I/M) program modeled for each county was determined based upon the county's ozone nonattainment status. Required future-year control measures (e.g., new vehicle emission standards, stage II and onboard vapor recovery controls, and reformulated gasoline usage) were incorporated directly into the onroad motor vehicle emission estimates using the MOBILE5a model.

For the attainment portions of the modeling domain, estimates of VMT by county and roadway type (e.g., freeway or arterial) were extracted from the 1990 Interim Inventory and projected to 1999 using national average annual projected VMT data, published by Argonne National Laboratory (Saricks and Vyas, 1985). For each state, the resulting VMT projection factors were adjusted using the ratio of projected population growth for the state to project population growth for the nation. Average speed data by roadway

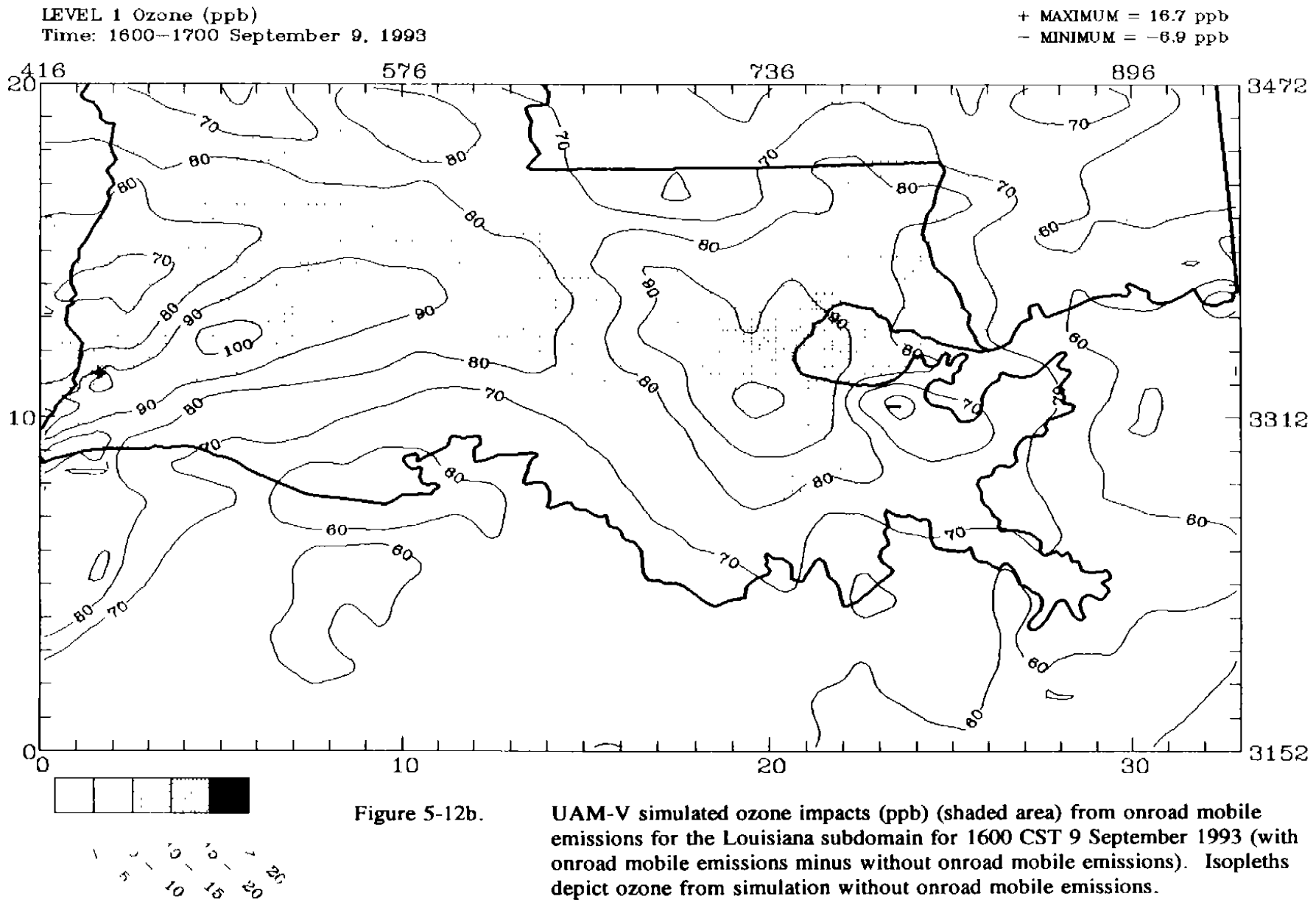

Figure 5-12b. UAM-V simulated ozone impacts (ppb) (shaded area) from onroad mobile emissions for the Louisiana subdomain for 1600 CST 9 September 1993 (with onroad mobile emissions minus without onroad mobile emissions). Isopleths depict ozone from simulation without onroad mobile emissions.

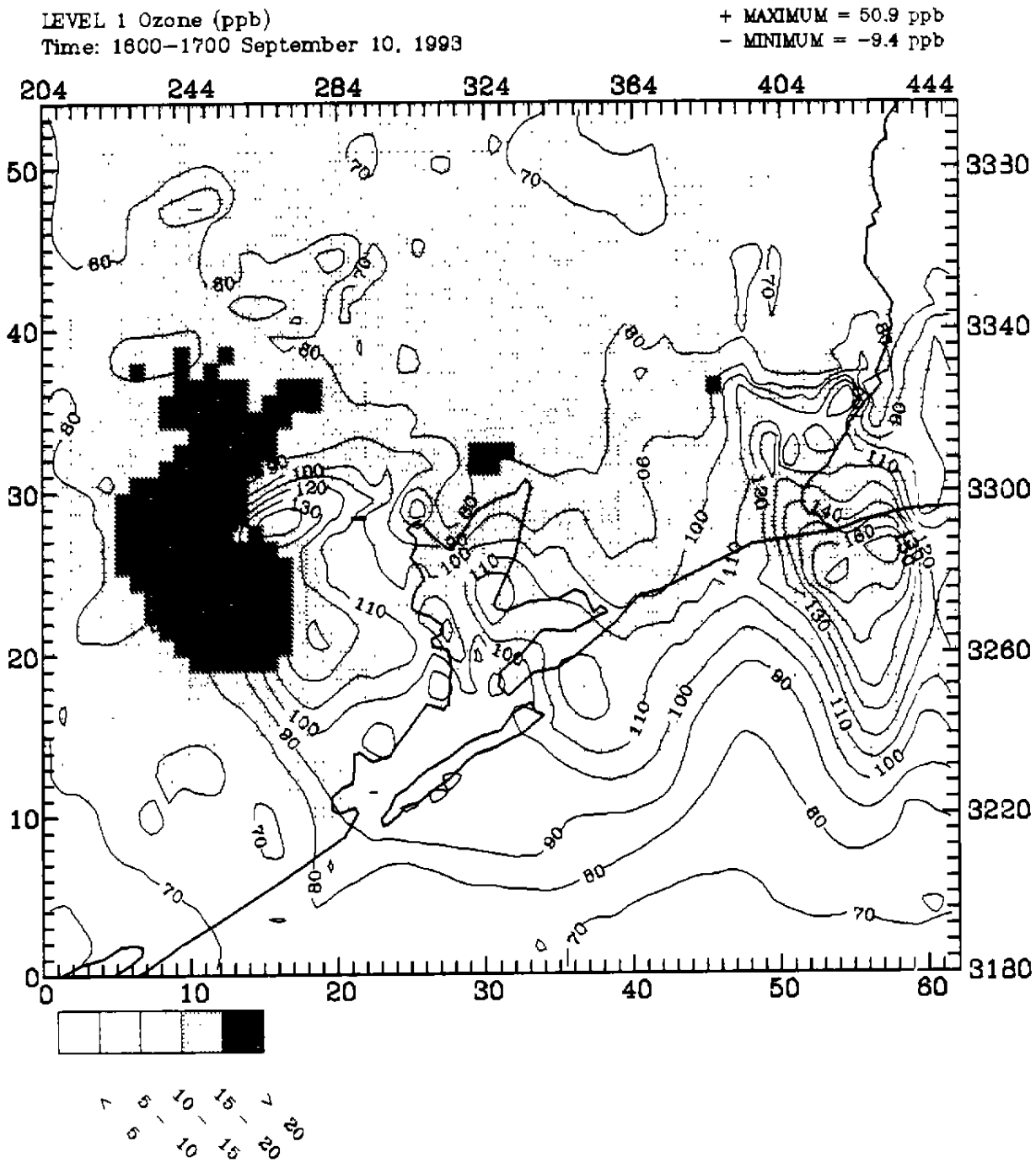

Figure 5-13a. UAM-V simulated ozone impacts (ppb) (shaded area) from onroad mobile emissions for the Houston subdomain for 1600 CST 10 September 1993 (with onroad mobile emissions minus without onroad mobile emissions). Isopleths depict ozone from simulation without onroad mobile emissions.

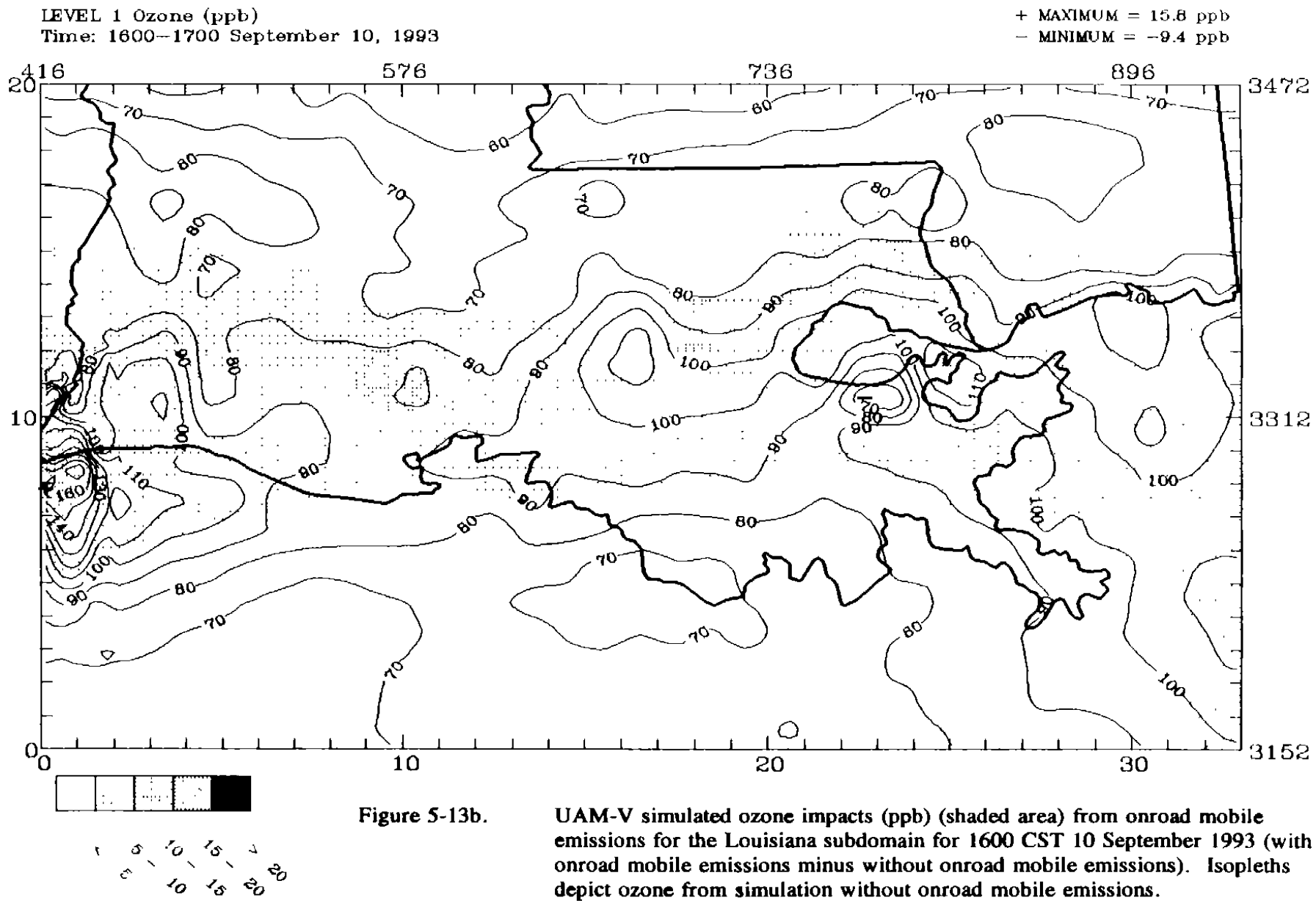

Figure 5-13b. UAM-V simulated ozone impacts (ppb) (shaded area) from onroad mobile emissions for the Louisiana subdomain for 1600 CST 10 September 1993 (with onroad mobile emissions minus without onroad mobile emissions). Isopleths depict ozone from simulation without onroad mobile emissions.

OFFSHORE REGION

Emissions were projected from the base to the future year using projection factors for each of the regional planning areas as identified by the MMS. These factors were estimated based on data from MMS, the Coast Guard, the Army Corps of Engineers, the Louisiana Offshore Oil Port, and the National Oceanic and Atmospheric Administration (National Marine Fisheries Service). The factors for production wells and exploration vessels were based on the number of production platforms and developmental wells projected for 1999 compared to those existing in 1992. For the platform support vessels and helicopters, crew/supply activity associated with the production platforms was assumed to increase proportionally with the increase in the number of production platforms. Table 5-2 presents the factors used to project the OCSPD emissions to 1999. These factors reflect the fact that Gulf of Mexico oil and gas production has been relatively steady during the decade prior to 1993 and is expected to decline slightly in the latter half of the 1990s. Most of the near-shore tracts have been in production for many years and are declining (especially offshore of the Houston and Beaumont/Port Arthur area), while larger new developments, the majority of which are located in the Central Gulf of Mexico area, are located further offshore in deepwater tracts. The 1999 inventory totals for all OCS sources (platforms, production, and nonproduction) are presented in Table 5-3. An additional column provides the percent change from the 1993 base-year inventory.

Table 5-2. Future-year projection factors for OCSPD emission sources.

Source Category	Modeling Base Year	MMS Planning Area		
		Western	Central	Eastern
Production Wells	1992	1.0	1.0	1.0
Crew/Supply Vessels	1992	1.0	1.0	1.0
Crew/Supply Helicopters	1992	1.0	1.0	1.0
Exploration Vessels	1988	0.87	0.57	7.0
Pipeline Vessels	1990	1.0	1.0	1.0
Military Vessels	1992	1.0	1.0	1.0
Commercial Fishing	1990	1.0	1.0	1.0
Commercial Shipping	1990	1.0	1.0	1.0
Barge Traffic	1990	1.0	1.0	1.0
LOOP	1990	1.039	1.039	1.039
Recreational Boating	1990	1.028	1.028	1.028

Table 5-3. Offshore emissions comparisons: 1999 vs. 1993 for the August episode, weekday (ton/day).

Source Type	NO_x			VOC			CO		
	1993	1999	Change	1993	1999	Change	1993	1999	Change
OCS Petroleum Development Sources									
Area Sources									
Crew/Supply Vessels	26.60	29.26	10%	2.11	2.32	10%	6.47	7.12	10%
Crew/Supply Helicopters	0.79	0.79	0%	0.58	0.58	0%	1.90	1.90	0%
Exploration Vessels	71.99	43.34	−40%	2.87	1.73	−40%	8.19	4.91	−40%
Pipeline Vessels	49.43	49.43	0%	8.41	8.41	0%	7.79	7.79	0%
Point Sources									
Platforms	325.84	370.28	14%	75.39	86.62	15%	76.12	86.25	13%
OCSPD Subtotal	474.64	493.09	4%	89.36	99.66	12%	100.48	107.96	7%
Non-OCS Petroleum									
Area Sources									
Barge Traffic	1.01	1.01	0%	0.05	0.05	0%	0.22	0.22	0%
Recreational Boating	0.40	0.42	3%	13.08	13.42	3%	28.28	29.02	3%
Military Vessels	0.10	0.10	0%	0.00	0.00	0%	0.01	0.01	0%
LOOP	3.37	3.37	0%	0.15	0.15	0%	0.38	0.38	0%
Commercial Fishing	34.20	34.21	0%	6.28	6.28	0%	16.34	16.34	0%
Commercial Shipping	234.50	234.50	0%	10.21	10.21	0%	25.98	25.98	0%
Point Sources									
LOOP	3.76	3.76	0%	1.77	1.77	0%	0.44	0.44	0%
Non-OCSPD Subtotal	277.34	277.35	0%	31.53	31.87	1%	71.64	72.38	1%
TOTAL	751.98	770.45	2%	120.90	131.53	9%	172.12	180.34	5%

The activity associated with commercial shipping and fishing vessels and barges was assumed to be constant from 1990 to 1999, based on the following:

- *Commercial Shipping*: The average annual increase in commercial shipping traffic between 1985 and 1989 was approximately 4.2 percent. Although foreign trade is expected to grow in the future, this industry has continued to make improvements in efficiency as a result of new, larger, more efficient vessels; improved port operations; and containerization. These latter two dramatically reduce port time. For these reasons, the 1999 emissions are equal to the baseline emissions.

- *Commercial Fishing*: The major fisheries in the Gulf of Mexico are essentially stable in terms of growth, since they are fully developed and further growth is precluded due to limitations imposed by biological and economic factors.

- *Barges*: This industry is mature and no future growth in barge traffic is anticipated (Kearney, 1993).

For pipeline vessels, MMS has assumed no growth from 1990 to 1999 (Steiner and Steorts, 1994). Accordingly, the emission totals for this category listed in Table 5-2 reflect no change from the 1993 base-year inventory. For military vessels, it was assumed that the activity levels would remain constant, since emissions are negligible compared to the total OCS inventory (less than 1 percent) and current political trends are toward reductions in military operations.

Projected activity levels for the Louisiana Offshore Oil Port (LOOP) were based on the average annual vessel traffic between 1987 and 1991. The average number of vessels from previous years was used for future traffic levels at the LOOP for the following reasons: (1) no expansion of the LOOP facilities is expected before the year 2000; (2) the number of tankers per year using the LOOP fluctuated an average of 9 percent per year from 1987 to 1991; (3) no direct correlation exists between the amount of throughput each year and the number of vessels using the port; and (4) the facility is operating near the effective annual operation capacity, thus precluding substantial growth (Kearney, 1993).

For recreational boating, the projected growth is based on the number of vessels registered from 1987 to 1991. The trend indicates that the number of vessels will increase by about 3 percent between 1990 and 1999. Growth in emissions was assumed to be proportional to the increase in vessels.

ONSHORE REGION

Projections of the emissions from 1990 level to future-year 1999 level include emissions growth, CAA-mandated controls, and state-specific controls. The emission projection procedures applied to 1990 EPA Interim Inventory data and state-specific data are described below.

classification were also extracted from the 1990 interim inventory to be used as input to the MOBILE5a model[1].

Houston/Galveston. For the Houston/Galveston nonattainment area, 1999 MOBILE5a inputs and VMT were received from the Houston/Galveston Area Council (HGAC, 1993). This information was compiled for the *Houston Metropolitan Transportation Conformity Plan*, completed in November 1994. The I/M program characteristics for basic and enhanced I/M used to estimate onroad motor vehicle emissions for Houston/ Galveston were also obtained from HGAC.

Some of the MOBILE5a input parameters received from HGAC varied by time of day, while other data represented a 24-hour average. The VMT data that varied by time of day were used to develop weighted averages for several of the MOBILE5a input parameters, including trip distributions, VMT mixes by vehicle type, and operating modes. For all counties in this region, the future-year inventory includes loaded/idle and transient I/M programs, as well as an antitampering program (ATP) with pressure and purge checks. The start years of these programs vary by county from 1984 to 1997. The HGAC designated entire counties as either rural or urban, so that only rural or urban ASC codes are used for emissions reporting. The 1999 emissions were calculated using these inputs and projected VMT.

Beaumont/Port Arthur. For the Beaumont/Port Arthur nonattainment area, 1999 MOBILE5a inputs were provided by the Texas Department of Transportation (TxDOT) for Hardin, Jefferson, and Orange counties (Jackson and Gram, 1994). These input files included I/M and an ATP. The 1999 MOBILE5a inputs were not available for Jasper, Newton, and Tyler counties. For these counties, the 1999 MOBILE5a inputs provided for Hardin County were used, with the exception that I/M and ATP programs were not modeled for these three counties. The 1999 average speeds and VMT by road type were not available from TxDOT for the Beaumont/Port Arthur nonattainment area. Accordingly, the same average speeds were used for the future-year inventory as were used for 1993. The 1990 VMT was projected to 1999 using the Argonne VMT projections. The I/M program characteristics for basic and enhanced I/M were obtained from TxDOT. The 1999 emissions which were calculated were then adjusted to account for TxDOT's use of hourly speeds and temperatures versus the average daily speeds and temperatures used for this application. The same daily minimum and maximum average temperatures used for the Houston/Galveston nonattainment area for the August and September 1993 episodes were used to develop the 1999 onroad motor vehicle inventories for the Beaumont/Port Arthur area.

---

[1] The onroad mobile emissions factors were estimated using average speed by roadway type. Diurnal influences on the onroad mobile emissions are incorporated into the emission factors generated by MOBILE5a and through the temporal allocation during the processing of the inventory. The effects of hourly ambient temperature on mobile emissions are accounted for by the MOBILE5a model using observed minimum and maximum temperatures and an internal diurnal profile to estimate the daily emission factors. Hourly activity patterns are based on a national average profile and accounted for during the temporal allocation step of the inventory processing.

Baton Rouge and Lake Charles. LDEQ provided EPS 2.0 onroad motor vehicle input emissions files for the Baton Rouge domain for 1999. However, the episodic temperatures used to estimate the emissions in the input files supplied by LDEQ were for an 1989 episode; accordingly, the emissions were adjusted to the 1993 episode temperatures before incorporation into the modeling inventories. For the Lake Charles subdomain, the 1992 VMT were projected to 1999 using the Argonne VMT projections. New emission factors were developed with MOBILE5a to reflect the newer vehicle fleet, onboard vapor recovery, and reduced Reid vapor pressure. Refueling emissions for 1999 were estimated from the MOBILE5a emission factors for Calcasieu Parish as described previously. For the Baton Rouge subdomain, refueling was already included in the EPS 2.0 input files provided by LDEQ.

Biogenic Emissions

Since detailed information regarding future land use, biomass, and crop acreage was not available for this study, the same biogenic emissions inputs were used for both the 1993 and 1999 modeling inventories. This assumes that the meteorological conditions and land-use patterns are the same for 1999 as those for 1993 in the UAM-V simulations.

RESULTS OF EMISSIONS PROCESSING FOR THE 1999 INVENTORIES

The UAM-V emission inventories for 1999 were prepared for the 17–20 August and 6–11 September episodes, using the projection methodologies presented previously. Tables 5-4 and 5-5 summarize the overall emissions by major source category for each episode day during the August and September modeling inventories. On average, the distribution of area, motor vehicle, point, and biogenic sources is about the same in 1993 and 1999.

Compared to the 1993 inventories, overall anthropogenic NO_X, VOC and CO emissions are about 1, 7, and 13.5 percent lower, respectively, for 1999 (for 9 September). Using the projection factors supplied by the MMS, the NO_X, VOC, and CO emissions for the offshore region are 2, 9, and 5 percent higher than the 1993 estimates. The offshore emissions for 1999 (OCSPD and non-OCSPD) comprise 11, 3, and 1 percent of the total anthropogenic NO_X, VOC, and CO emissions, respectively within the modeling domain. These values are slightly higher than the 1993 percentages, due to the slight increase in offshore emissions and the decrease in onshore emissions (i.e., emissions growth is offset by future-year emission controls).

The spatial distribution of both the low-level and elevated emissions are consistent between the base-year and future-year modeling inventories. Accordingly, spatial distribution plots are presented only for the base-year modeling inventory (see Appendix N).

In addition to the 1999 baseline emission inventories summarized in Tables 5-4 and 5-5, "adjusted" future baseline inventories were prepared by increasing stationary source

Table 5-4. Baseline emissions for 1999 including OCS, 17-20 August (ton/day).[1]

Source Type	17 August			18 August		
	NO_x	VOC	CO	NO_x	VOC	CO
Anthropogenic - Low Level						
Area Sources	2247.3	2288.2	5734.5	2247.3	2288.2	5734.5
Mobile Sources	1141.8	716.6	6343.0	1141.8	716.6	6343.0
Low Level Point Sources	325.5	1192.5	111.7	325.5	1192.5	111.7
	3714.6	4197.2	12189.2	3714.6	4197.2	12189.2
Elevated Point Sources	3641.4	620.3	1733.1	3641.4	620.3	1733.1
	442.9	17081.3		450.0	17340.3	
Total	7799.0	21898.9	13922.3	7806.0	22157.9	13922.3
	19 August			20 August		
	NO_x	VOC	CO	NO_x	VOC	CO
Anthropogenic - Low Level						
Area Sources	2247.3	2288.2	5734.5	2247.3	2288.2	5734.5
Mobile Sources	1141.8	716.6	6343.0	1141.8	716.6	6343.0
Low Level Point Sources	325.5	1192.5	111.7	325.5	1192.5	111.7
	3714.6	4197.2	12189.2	3714.6	4197.2	12189.2
Elevated Point Sources	3641.4	620.3	1733.1	3641.4	620.3	1733.1
	439.3	16852.7		415.9	15904.9	
Total	7795.4	21670.3	13922.3	7772.0	20722.5	13922.3

[1] New set of projections applied to offshore sources June 8, 1995.
[2] Biogenic emissions in Texas adjusted to TNRCC level.

VOC emissions by 50 percent, increasing motor vehicle VOC emissions by 100 percent, and decreasing elevated point sources NO_x emissions by 50 percent for the Houston/Galveston and Beaumont/Port Arthur subdomain. These adjustments were similar to those made for the 1993 base-case inventories for both modeling episodes (see Section 4).

5.4 SUMMARY OF FUTURE-YEAR UAM-V SIMULATION RESULTS FOR 1999

This section summarizes the UAM-V simulations performed for the future year (1999) to establish baseline concentration estimates and to estimate incremental impacts resulting from the emissions associated with expected future OCSPD activity.

Table 5-5. Baseline emissions for 1999 including OCS, 6–10 September (ton/day).[1]

Source Type	6 September			7 September			8 September		
	NO_x	VOC	CO	NO_x	VOC	CO	NO_x	VOC	CO
Anthropogenic - Low Level									
Area Sources	2204.0	2292.3	5881.7	2204.0	2292.3	5881.7	2204.0	2292.3	5881.7
Mobile Sources	1141.0	708.1	6324.9	1141.0	708.1	6324.9	1141.0	708.1	6324.9
Low Level Point Sources	258.7	1191.1	96.4	258.7	1191.1	96.4	258.7	1191.1	96.4
Subtotal	3603.8	4191.5	12303.0	3603.8	4191.5	12303.0	3603.8	4191.5	12303.0
Anthropogenic - Elevated									
Elevated Point Sources	3529.5	621.0	1747.3	3529.5	621.0	1747.3	3529.5	621.0	1747.3
Biogenic	1137.0	9671.3		1176.7	9441.8		1182.8	9845.8	
Total	8270.3	14483.8	14050.3	8310.0	14254.3	14050.3	8316.0	14658.3	14050.3

Source Type	9 September			10 September		
	NO_x	VOC	CO	NO_x	VOC	CO
Anthropogenic - Low Level						
Area Sources	2204.0	2292.3	5881.7	2204.0	2292.3	5881.7
Mobile Sources	1141.0	708.1	6324.9	1141.0	708.1	6324.9
Low Level Point Sources	258.7	1191.1	96.4	258.7	1191.1	96.4
Subtotal	3603.8	4191.5	12303.0	3603.8	4191.5	12303.0
Anthropogenic - Elevated						
Elevated Point Sources	3529.5	621.0	1747.3	3529.5	621.0	1747.3
Biogenic	1175.2	10004.8		1199.9	9893.8	
Total	8308.4	14817.3	14050.3	8333.2	14706.3	14050.3

[1] New set of projections applied to offshore sources June 8, 1995.

1999 OCSPD EMISSION SCENARIO SIMULATION RESULTS

The UAM-V base-case meteorological and air quality inputs for the September and August episodes were used along with future-year baseline (1999) projected emissions[2] to evaluate the impacts of OCSPD emissions. Because of the uncertainties in the onshore inventory for the Houston subdomain that were revealed during the model performance evaluation (Section 4), the future-year simulations used both a 1999 baseline and a 1999 "adjusted baseline" emission inventory for the Houston subdomain for each episode. The adjustments for the future year were identical to those used for the final base-case simulations. Because the 1999 OCSPD emissions were overestimated, the impacts estimated for 1999 are conservative.

As outlined above, to assess the incremental impacts of OCSPD emissions on ozone concentration, a number of OCSPD emission scenarios were run for the entire GMAQS domain with both the baseline and the adjusted baseline emissions for the Houston subdomain for each episode. Table 5-6 lists the simulations corresponding to these scenarios for the August and September episodes. For August, these include simulations

Table 5-6a. MMS GMAQS 1999 UAM-V simulations for the August episode.

AUG99-1:	Aug 1999 adjusted* with OCSPD emissions
AUG99-2:	Aug 1999 adjusted* without OCSPD emissions
AUG99-5:	Aug 1999 baseline with OCSPD emissions
AUG99-6:	Aug 1999 baseline without OCSPD emissions
AUG99-7:	AUG99-1 with double OCSPD emissions
AUG99-9:	AUG99-5 with double OCSPD emissions

* Adjustments made to 1999 Houston baseline inventory (100% VOC increase for mobile sources, 50% increase in point/area VOC, 50% decrease in point source NO_x).

Table 5-6b. MMS GMAQS 1999 UAM-V simulations for the September episode.

SEP99-1:	Sep 1999 adjusted* with OCSPD emissions
SEP99-2:	Sep 1999 adjusted* without OCSPD emissions
SEP99-3:	Sep 1999 baseline with OCSPD emissions
SEP99-4:	Sep 1999 baseline without OCSPD emissions
SEP99-5:	Sep 1999 adjusted* with double OCSPD emissions
SEP99-7:	Sep 1999 adjusted* with 50% decrease in OCSPD emissions
SEP99-8:	Sep 1999 baseline with 50% decrease in OCSPD emissions

* Adjustments made to 1999 Houston baseline inventory (100% VOC increase for mobile sources, 50% increase in point/area VOC, 50% decrease in point source NO_x).

[2] "All of the UAM-V simulations performed for each of the episodes reported in this document used a future-year OCSPD emissions inventory prepared using projection factors calculated from development figures provided by the MMS. It has since been discovered that the projection factors used were based on an incorrect interpretation of the MMS figures. The projection factors have since been revised and these are reflected in Tables 5-2 through 5-5. The original set of projection factors resulted in future-year OCSPD emissions that are about double that of the revised emissions.

(with and without OCSPD emissions) using the onshore adjusted inventory, the baseline inventory, and combinations of these onshore inventories with the 1999 estimated OCSPD emissions, including a doubling of the OCSPD emission estimates. For September, simulations include those using the onshore adjusted and baseline inventories (with and without OCSPD emissions) and those that included a doubling and a 50 percent decrease in OCSPD emissions. The doubling and 50 percent decrease simulations were performed to examine the sensitivity to OCSPD emissions and to account for potential uncertainties in the inventories.

August Episode Results for 1999

Table 5-7 presents the maximum simulated ozone concentrations for the August episode (18 and 19 August) for the Houston, Beaumont/Port Arthur, Lake Charles, and Baton Rouge nonattainment areas and compares the 1993 base-case results (with and without OCSPD emissions) with those obtained for the 1999 scenarios. The peak ozone concentrations in the Houston area derived from the baseline inventories are unrealistically low and close to the federal standard (0.12 ppm), while the peak concentrations derived from the adjusted inventory result in concentrations that are less than the 1993 base case, but more in line with the expected future-year (1999) concentrations, given the small decreases in estimated precursor emissions from 1993 to 1999. As indicated in the table, the calculated peak concentrations for the Houston area are lower with the baseline emissions than with the adjusted emissions. The peaks, however, remained relatively unchanged due to OCSPD emissions. This is also true for the other nonattainment areas. It should be noted that the uncertainties in the Houston area emission inventory did not significantly affect the conclusions reached in this study regarding the impacts of OCSPD emissions on ozone concentrations in the Houston area.

The impacts on hourly ozone concentrations in the Houston/Beaumont/Port Arthur and Louisiana domains resulting from OCSPD emissions are presented for hour 1700–1800 for 19 August in Figures 5-14 and 5-15, respectively for the "adjusted with OCSPD" simulation (AUG99-1) and the "adjusted with double OCSPD emissions" simulation (AUG99-7). In the Houston area (Figure 5-14), maximum incremental impacts are approximately 8 ppb in the southwest portion of the subdomain where maximum concentrations due to all other emission sources are 30–50 ppb. In the Baton Rouge area, during this hour, when peak simulated concentrations are nearly 120 ppb, the maximum impacts due to OCSPD emissions are less than 2 pbb. When OCSPD emissions are doubled, the impacts increase in magnitude (>8 ppb) and spatial extent in the Houston area, and increase to 2–4 ppb in the Lake Charles and Baton Rouge areas. The maximum hourly impacts in the offshore areas of the Houston subdomain for this day range from 6 to 16 ppb in an area approximately 80 km south of Gilchrist; these offshore hourly impacts increase to 8–20 ppb for this day in the same area when the OCSPD emissions are doubled. Offshore of Louisiana, maximum impacts range from 15 to 38 ppb in an area more than 60 km south of Terrebonne Parish; when the OCSPD emissions are doubled, the maximum impacts in this area increase by a few ppb. For the Houston area, the OCSPD impacts derived using the onshore baseline inventory are comparable to those obtained with the adjusted inventory.

Table 5-7a. Maximum simulated ozone concentrations (ppb) for the Houston/Galveston and Beaumont/Port Arthur subdomains for 1993 and 1999 for the August episode.

Simulation	18 Aug	19 Aug
Houston/Galveston		
1993 Base Case, without OCSPD	185	192
1993 Base Case, with OCSPD	185	192
1999 Baseline, without OCSPD emissions	114	116
1999 Baseline, with OCSPD emissions	114	116
1999 Baseline, with double OCSPD emissions	114	116
1999 Adjusted Baseline, without OCSPD emissions	143	133
1999 Adjusted Baseline, with OCSPD emissions	143	133
1999 Adjusted Baseline, with double OCSPD emissions	143	133
Beaumont/Port Arthur		
1993 Base Case, without OCSPD	128	160
1993 Base Case, with OCSPD	128	160
1999 Baseline, without OCSPD emissions	111	117
1999 Baseline, with OCSPD emissions	112	118
1999 Baseline, with double OCSPD emissions	112	119
1999 Adjusted Baseline, without OCSPD emissions	122	151
1999 Adjusted Baseline, with OCSPD emissions	122	152
1999 Adjusted Baseline, with double OCSPD emissions	123	152

Table 5-7b. Maximum simulated ozone concentrations (ppb) for the Lake Charles and Baton Rouge subdomains for 1993 and 1999 for the August episode.

Simulation	18 Aug	19 Aug
Lake Charles		
1993 Base Case, without OCSPD	138	160
1993 Base Case, with OCSPD	139	160
1999 Baseline, without OCSPD emissions	116	123
1999 Baseline, with OCSPD emissions	117	124
1999 Baseline, with double OCSPD emissions	117	124
1999 Adjusted Baseline, without OCSPD emissions	133	151
1999 Adjusted Baseline, with OCSPD emissions	133	152
1999 Adjusted Baseline, with double OCSPD emissions	134	152
Baton Rouge		
1993 Base Case, without OCSPD	118	127
1993 Base Case, with OCSPD	118	127
1999 Baseline, without OCSPD emissions	116	121
1999 Baseline, with OCSPD emissions	116	121
1999 Baseline, with double OCSPD emissions	116	122
1999 Adjusted Baseline, without OCSPD emissions	117	123
1999 Adjusted Baseline, with OCSPD emissions	117	124
1999 Adjusted Baseline, with double OCSPD emissions	117	125

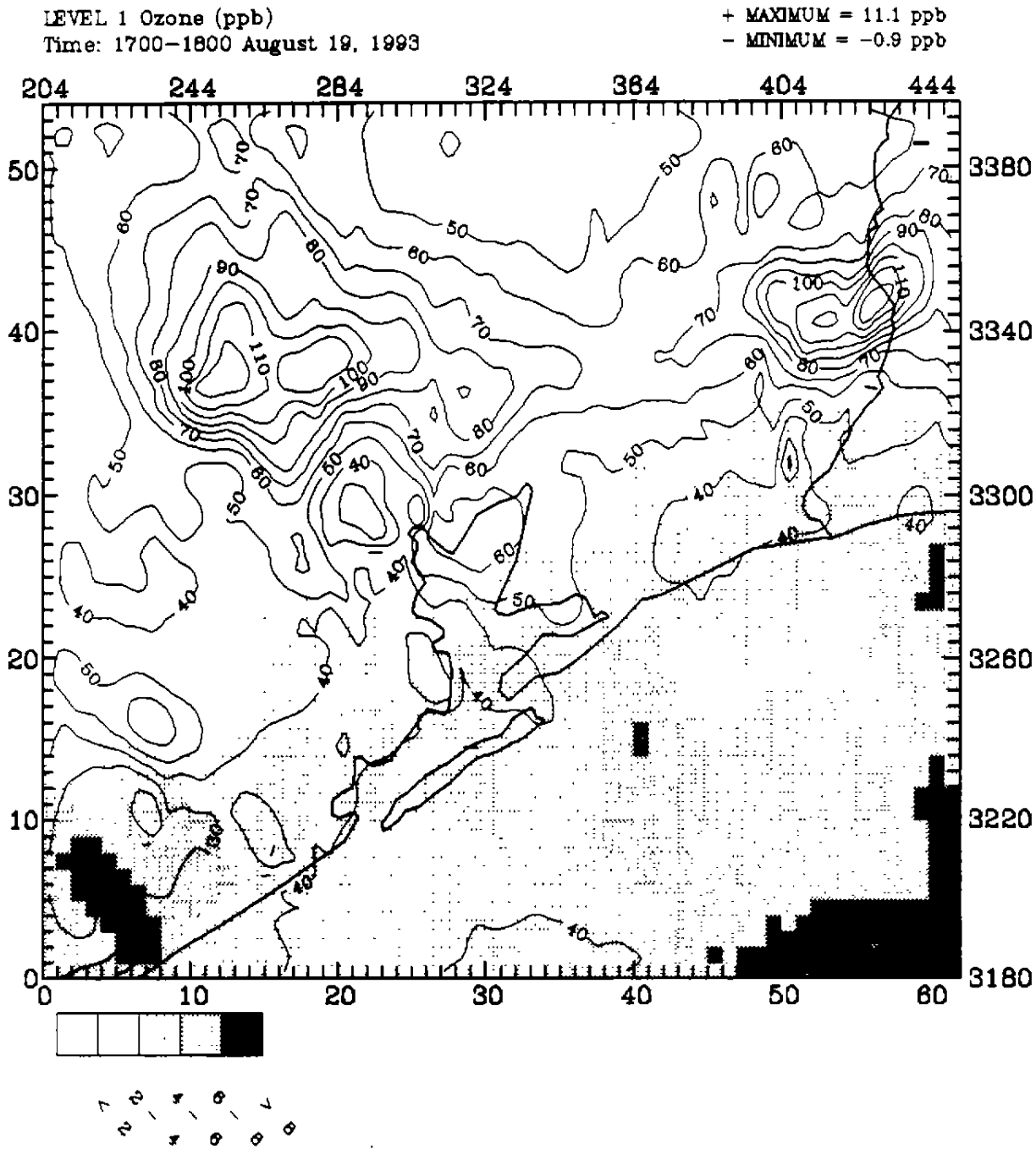

Figure 5-14a. UAM-V calculated ozone impacts (ppb) (shaded area) for 1999 from OCSPD emissions for the Houston subdomain for 1700 CST 19 August (with OCSPD emissions minus without OCSPD emissions). Isopleths depict ozone from simulation without OCSPD emissions.

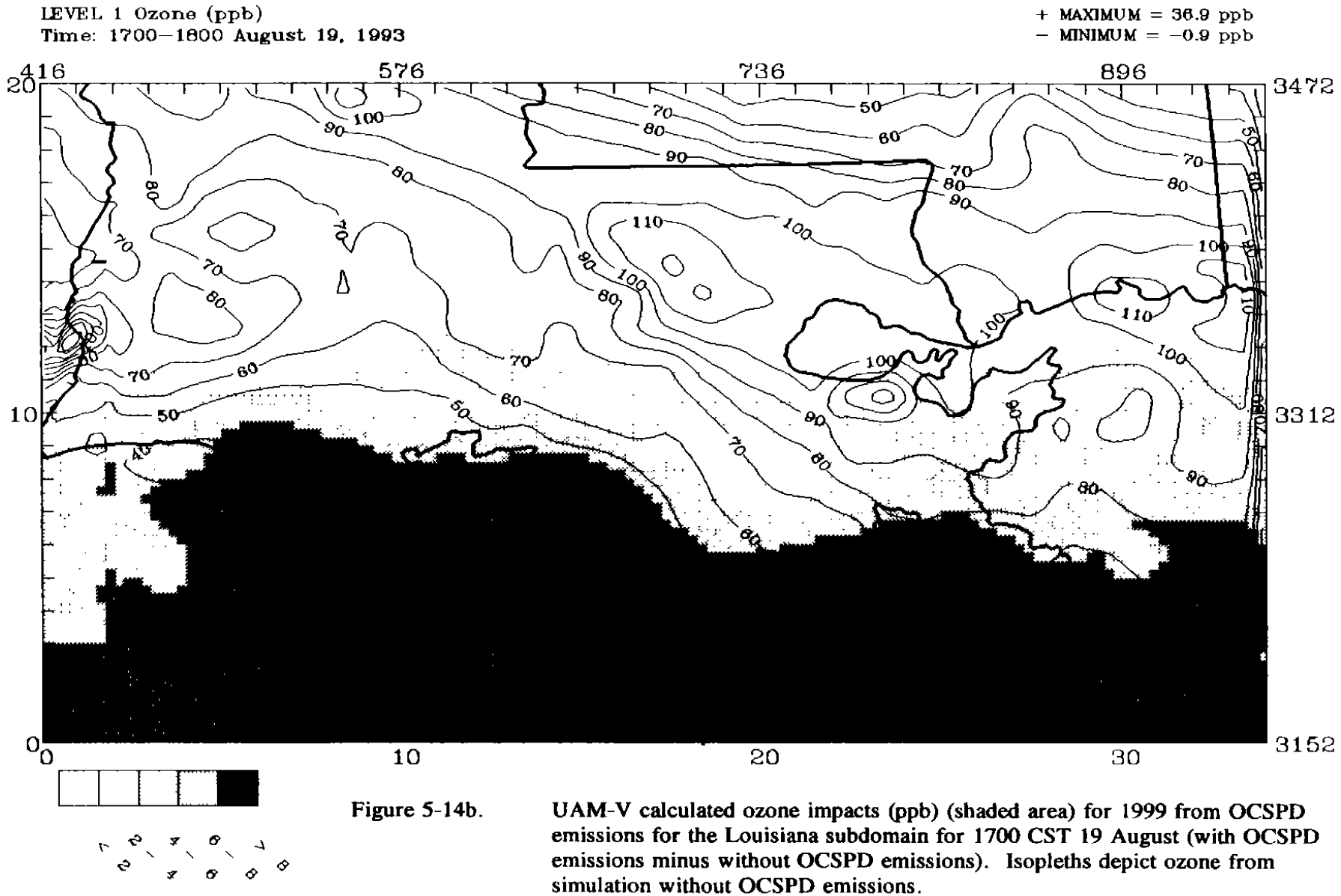

Figure 5-14b. UAM-V calculated ozone impacts (ppb) (shaded area) for 1999 from OCSPD emissions for the Louisiana subdomain for 1700 CST 19 August (with OCSPD emissions minus without OCSPD emissions). Isopleths depict ozone from simulation without OCSPD emissions.

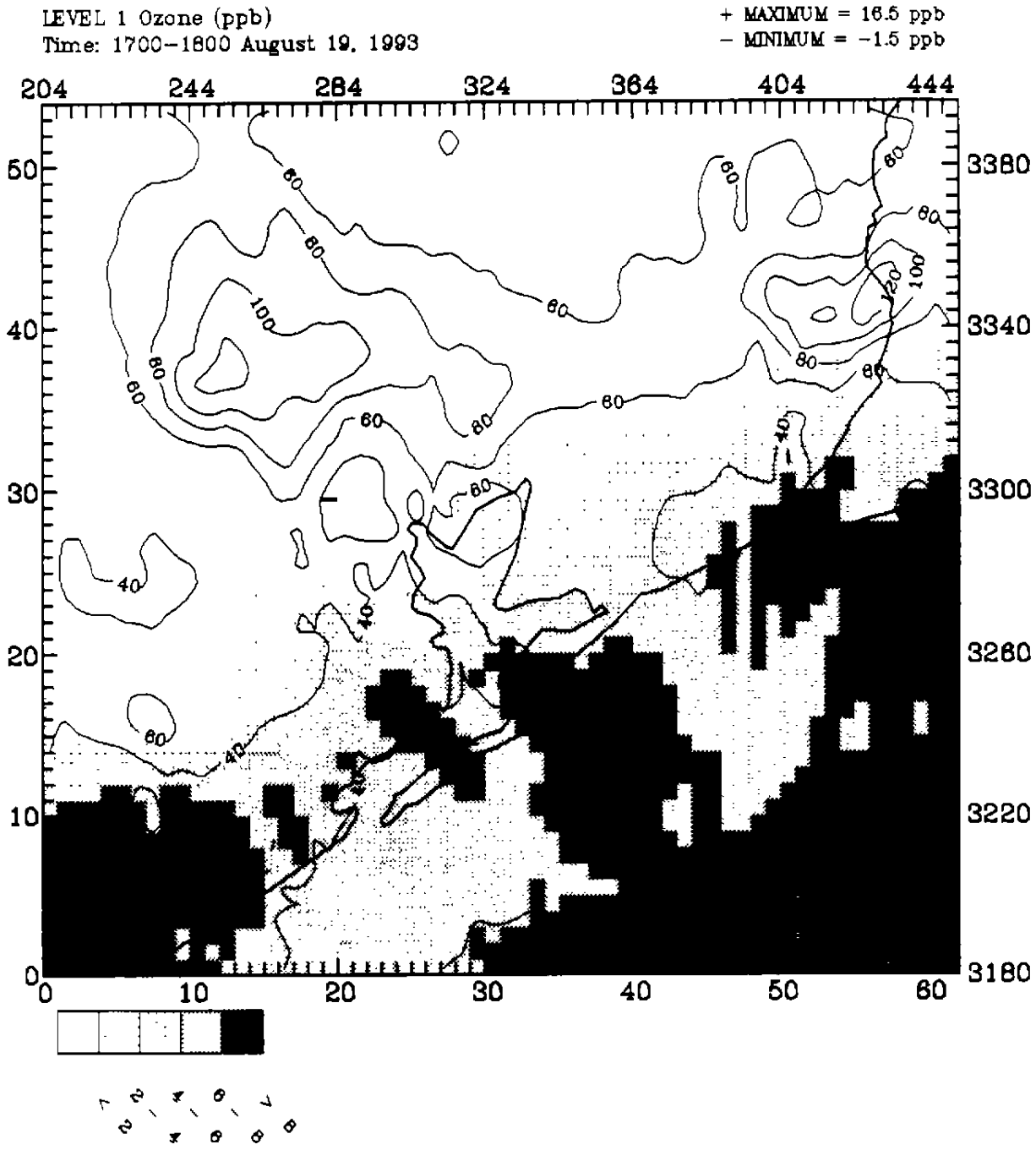

Figure 5-15a. UAM-V calculated ozone impacts (ppb) (shaded area) for 1999 from double OCSPD emissions for the Houston subdomain for 1700 CST 19 August (with double OCSPD emissions minus without OCSPD emissions). Isopleths depict ozone from simulation without OCSPD emissions.

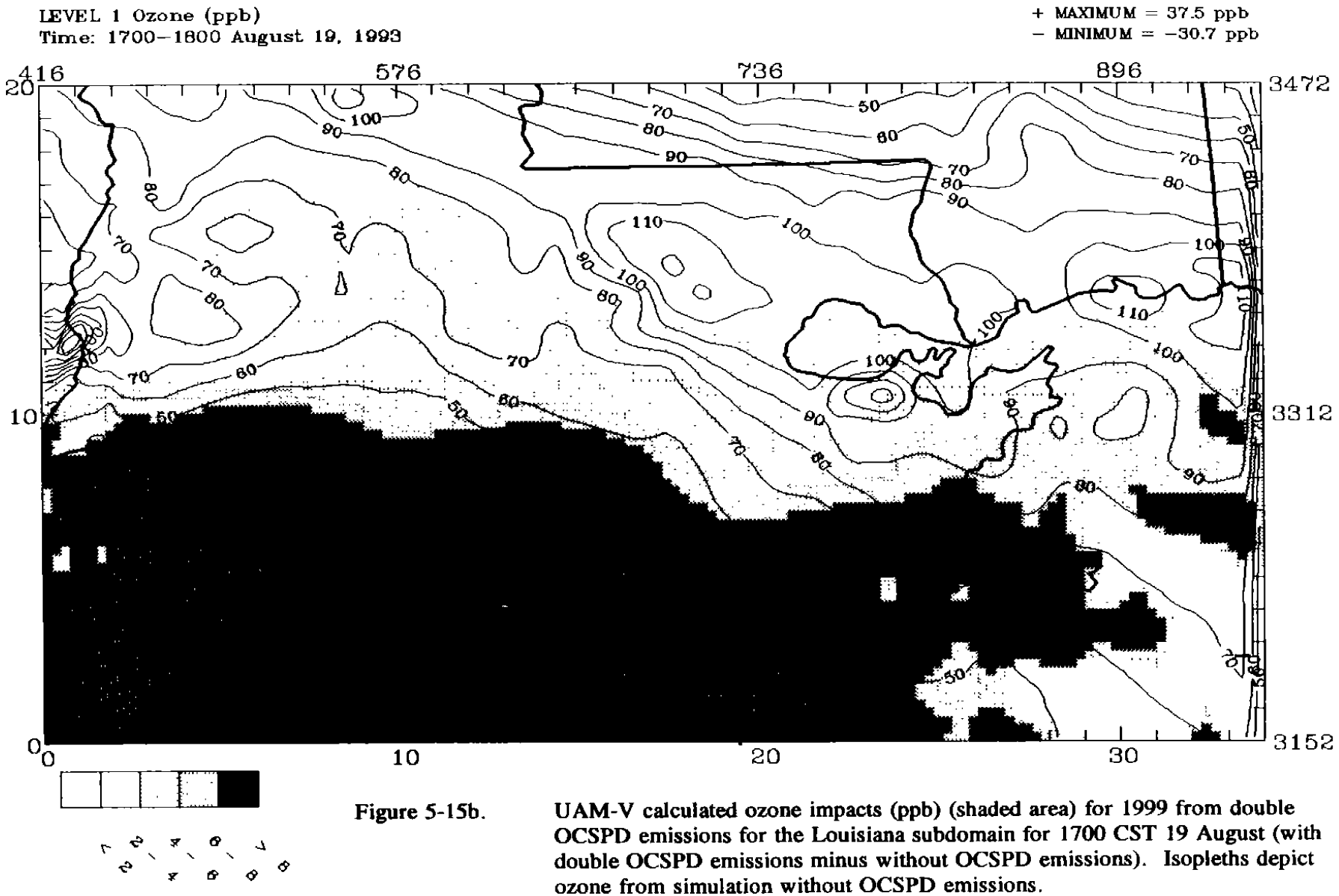

Figure 5-15b. UAM-V calculated ozone impacts (ppb) (shaded area) for 1999 from double OCSPD emissions for the Louisiana subdomain for 1700 CST 19 August (with double OCSPD emissions minus without OCSPD emissions). Isopleths depict ozone from simulation without OCSPD emissions.

The maximum impacts due to OCSPD emissions for 18 and 19 August for each of the nonattainment areas are provided in Table 5-8. The table provides the maximum impacts in grid cells where the simulated ozone concentration (with OCSPD emissions) exceeds 124 ppb along with the maximum impacts in grid cells where the simulated ozone concentration is less than 124 ppb. For this episode, the largest simulated OCSPD impacts in cells less than 124 ppb are approximately 20 ppb, while in cells with maximum simulated ozone concentrations greater than 124 ppb, the maximum impacts are less than 2 ppb in all nonattainment areas, even when OCSPD emissions are doubled.

- The maximum simulated ozone impacts due to estimated 1999 OCSPD operations in the Houston/Beaumont/Port Arthur area are 6–8 ppb at a time when the hourly average ozone concentrations calculated from all other emission sources are approximately 30–50 ppb. During periods and at locations where ozone concentrations are simulated to equal or exceed 124 ppb, the incremental ozone impact due to OCSPD emissions is simulated to be less than 2 ppb.

- For the Baton Rouge area, the maximum simulated incremental impacts from 1999 OCSPD emissions for this episode during the time of observed (and simulated) maximum concentrations is 0–2 ppb. Larger impacts from OCSPD emissions are simulated during other hours, and along the Louisiana coastline and over the Gulf, well south of the Baton Rouge nonattainment area.

September Episode Results for 1999

Table 5-9 presents the maximum simulated ozone concentrations for the September episode (9 and 10 September) for the Houston, Beaumont/Port Arthur, Lake Charles, and Baton Rouge nonattainment areas, comparing the 1993 base-case results with those obtained for the 1999 scenarios. The peak ozone concentrations in the Houston area derived from the baseline inventories are also unrealistically low and close to the standard (0.12 ppm), while the peak concentrations derived from the adjusted inventory result in concentrations that are less than the 1993 base case but more in line with the expected future-year concentrations, given the small decreases in overall precursor emissions from 1993 to 1999. As indicated in the table, the calculated peak concentrations are increased by only a few ppb in all nonattainment areas due to OCSPD emissions.

The impacts on hourly ozone concentrations in the Houston/Beaumont/Port Arthur and Louisiana domains resulting from OCSPD emissions are presented for hour 1500–1600 for 10 September in Figures 5-16 and 5-17, for the "adjusted with OCSPD" simulation (SEP99-1) and the "adjusted with double OCSPD emissions" simulation (SEP99-5), respectively. Incremental impacts are generally less than 2 ppb in the Houston and Baton Rouge areas during the afternoon hours (Figure 5-16); in the Beaumont/Port Arthur area, larger impacts (4–6 ppb) are present along the coast; when OCSPD emissions are doubled, greater impacts are simulated along the Texas coastal area, but impacts in the Baton Rouge area remain the same. The maximum hourly impacts in the offshore areas of the Houston subdomain for this day range from 12 to 18 ppb in an area

Table 5-8. UAM-V simulated maximum ozone impacts (ppb) for 1999 for the August episode due to OCSPD emissions.

Simulation	18 August		19 August	
	For Cells > 124 ppb	For Cells < 124 ppb	For Cells > 124 ppb	For Cells < 124 ppb
Houston Nonattainment Area				
Baseline	N/A*	8.6	N/A	14.3
Adjusted	0.5	8.8	0.4	14.3
Baseline, with double OCSPD	N/A	13.0	N/A	20.6
Adjusted, with double OCSPD	0.8	13.3	0.5	20.6
Beaumont/Port Arthur Nonattainment Area				
Baseline	N/A	4.6	N/A	9.8
Adjusted	N/A	4.8	1.1	9.8
Baseline, with double OCSPD	N/A	7.2	N/A	14.8
Adjusted, with double OCSPD	N/A	7.5	1.7	14.8
Lake Charles Nonattainment Area				
Baseline	N/A	4.2	N/A	7.7
Adjusted	0.9	4.1	1.1	7.8
Baseline, with double OCSPD	N/A	6.4	1.5	11.7
Adjusted, with double OCSPD	1.4	6.4	1.7	12.0
Baton Rouge Nonattainment Area				
Baseline	N/A	11.4	N/A	12.3
Adjusted	N/A	11.6	N/A	12.3
Baseline, with double OCSPD	N/A	14.7	N/A	16.7
Adjusted, with double OCSPD	N/A	15.0	1.6	16.7

* Not applicable—no simulated concentrations greater than 124 ppb.

Table 5-9a. Maximum simulated ozone concentrations (ppb) for the Houston/Galveston and Beaumont/Port Arthur subdomains for 1993 and 1999 for the September episode.

Simulation	9 Sept	10 Sept
Houston/Galveston		
1993 Base Case, without OCSPD	233	164
1993 Base Case, with OCSPD	234	164
1999 Baseline, without OCSPD emissions	114	111
1999 Baseline, with 50% OCSPD emissions	115	111
1999 Baseline, with OCSPD emissions	115	112
1999 Baseline, with double OCSPD emissions	116	112
1999 Adjusted Baseline, without OCSPD emissions	175	135
1999 Adjusted Baseline, with 50% OCSPD emissions	175	136
1999 Adjusted Baseline, with OCSPD emissions	175	136
1999 Adjusted Baseline, with double OCSPD emissions	175	137
Beaumont/Port Arthur		
1992 Base Case, without OCSPD	126	205
1993 Base Case, with OCSPD	127	207
1999 Baseline, without OCSPD emissions	100	125
1999 Baseline, with 50% OCSPD emissions	100	125
1999 Baseline, with OCSPD emissions	101	125
1999 Baseline, with double OCSPD emissions	101	125
1999 Adjusted Baseline, without OCSPD emissions	111	183
1999 Adjusted Baseline, with 50% OCSPD emissions	112	185
1999 Adjusted Baseline, with OCSPD emissions	112	187
1999 Adjusted Baseline, with double OCSPD emissions	113	189

Table 5-9b. Maximum simulated ozone concentrations (ppb) for the Lake Charles and Baton Rouge subdomains for 1993 and 1999 for the September episode.

Simulation	9 Sept	10 Sept
Lake Charles		
1993 Base Case, without OCSPD	120	144
1993 Base Case, with OCSPD	120	145
1999 Baseline, without OCSPD emissions	106	107
1999 Baseline, with 50% OCSPD emissions	106	107
1999 Baseline, with OCSPD emissions	107	107
1999 Baseline, with double OCSPD emissions	107	107
1999 Adjusted Baseline, without OCSPD emissions	111	131
1999 Adjusted Baseline, with 50% OCSPD emissions	111	132
1999 Adjusted Baseline, with OCSPD emissions	112	133
1999 Adjusted Baseline, with double OCSPD emissions	112	135
Baton Rouge		
1993 Base Case, without OCSPD emissions	109	122
1993 Base Case, with OCSPD	109	122
1999 Baseline, without OCSPD emissions	104	114
1999 Baseline, with 50% OCSPD emissions	104	114
1999 Baseline, with OCSPD emissions	104	114
1999 Baseline, with double OCSPD emissions	104	115
1999 Adjusted Baseline, without OCSPD emissions	104	115
1999 Adjusted Baseline, with 50% OCSPD emissions	104	115
1999 Adjusted Baseline, with OCSPD emissions	104	115
1999 Adjusted Baseline, with double OCSPD emissions	104	115

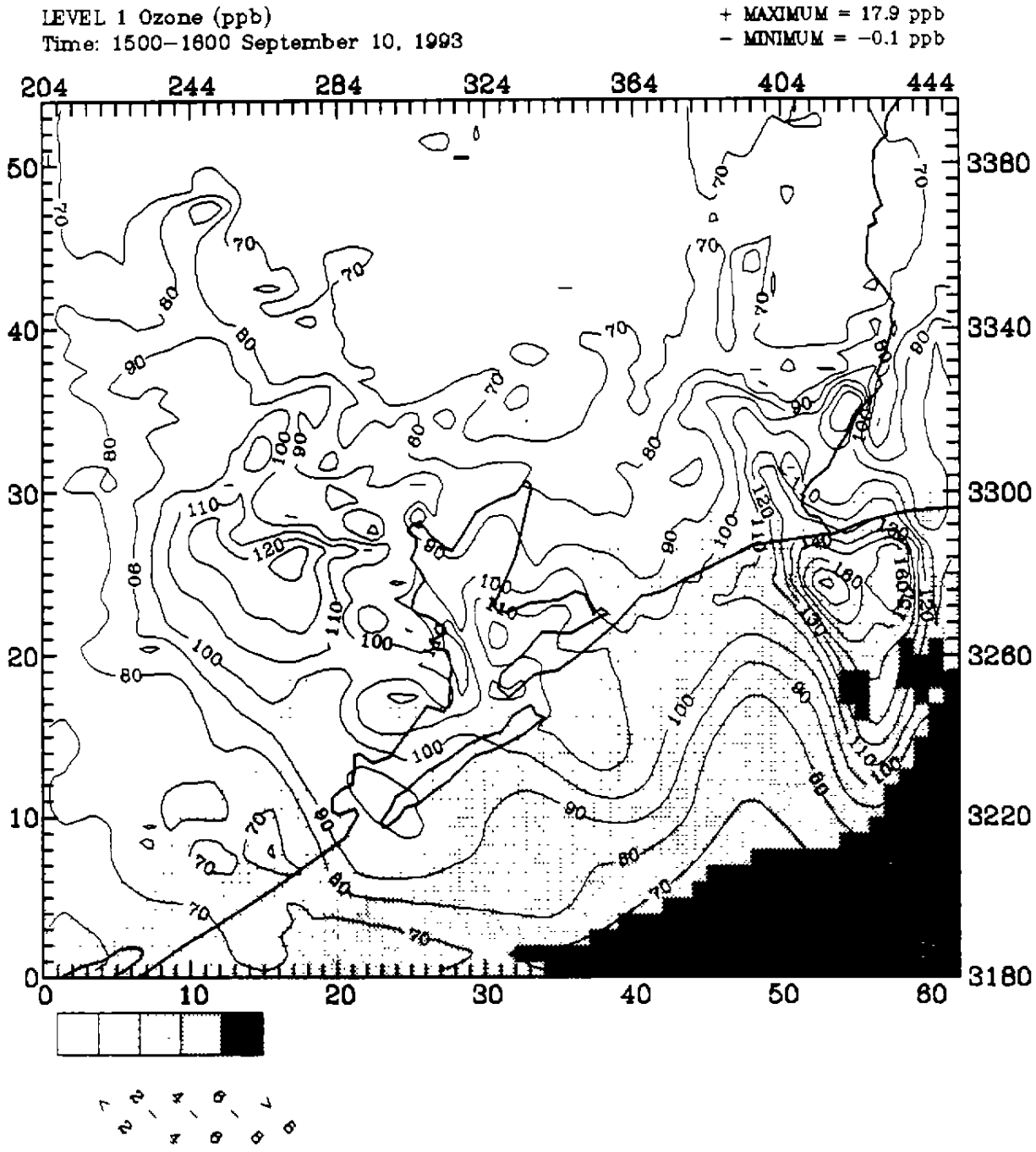

Figure 5-16a. UAM-V calculated ozone impacts (ppb) (shaded area) for 1999 from OCSPD emissions for the Houston subdomain for 1500 CST 10 September (with OCSPD emissions minus without OCSPD emissions). Isopleths depict ozone from simulation without OCSPD emissions.

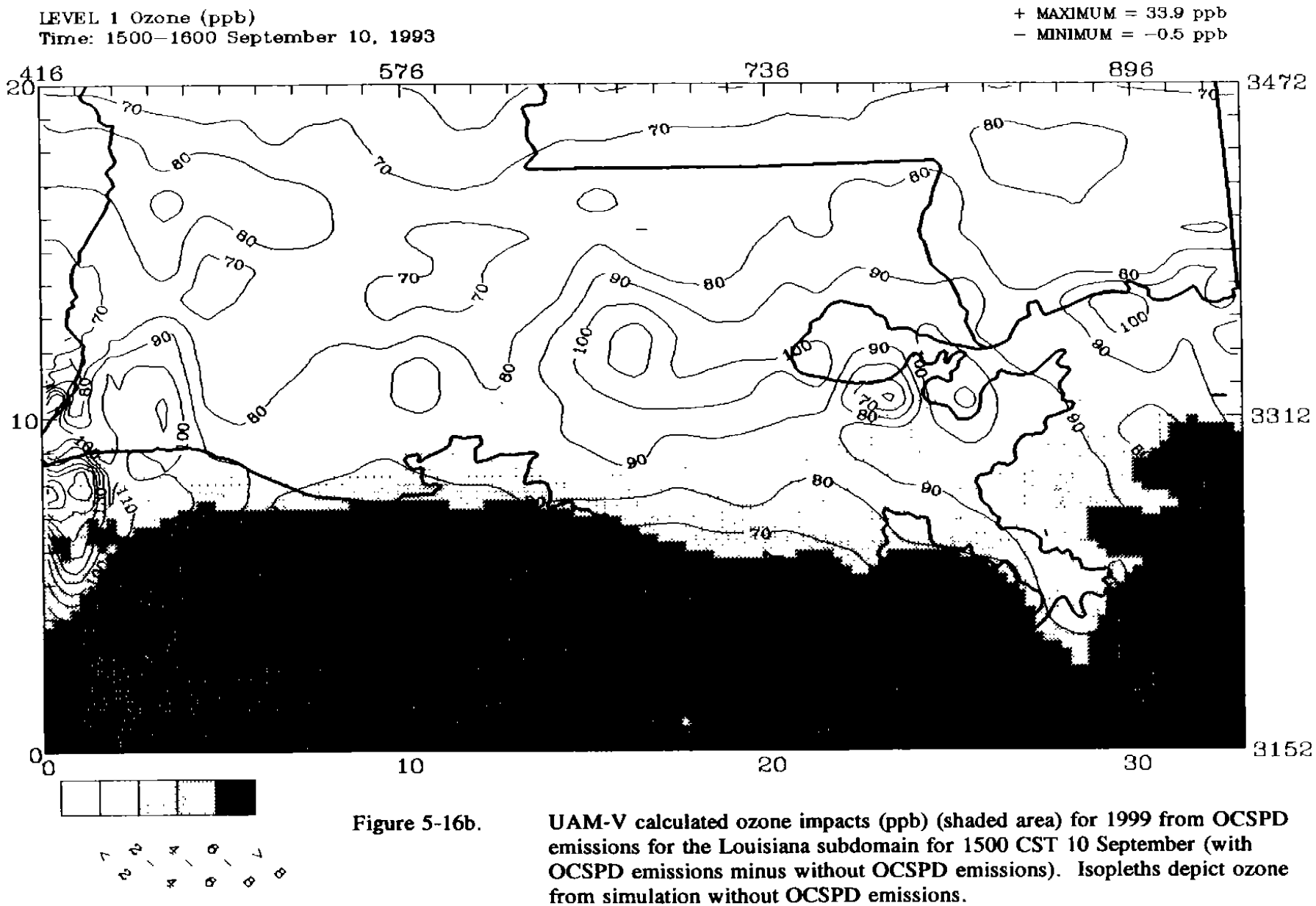

Figure 5-16b. UAM-V calculated ozone impacts (ppb) (shaded area) for 1999 from OCSPD emissions for the Louisiana subdomain for 1500 CST 10 September (with OCSPD emissions minus without OCSPD emissions). Isopleths depict ozone from simulation without OCSPD emissions.

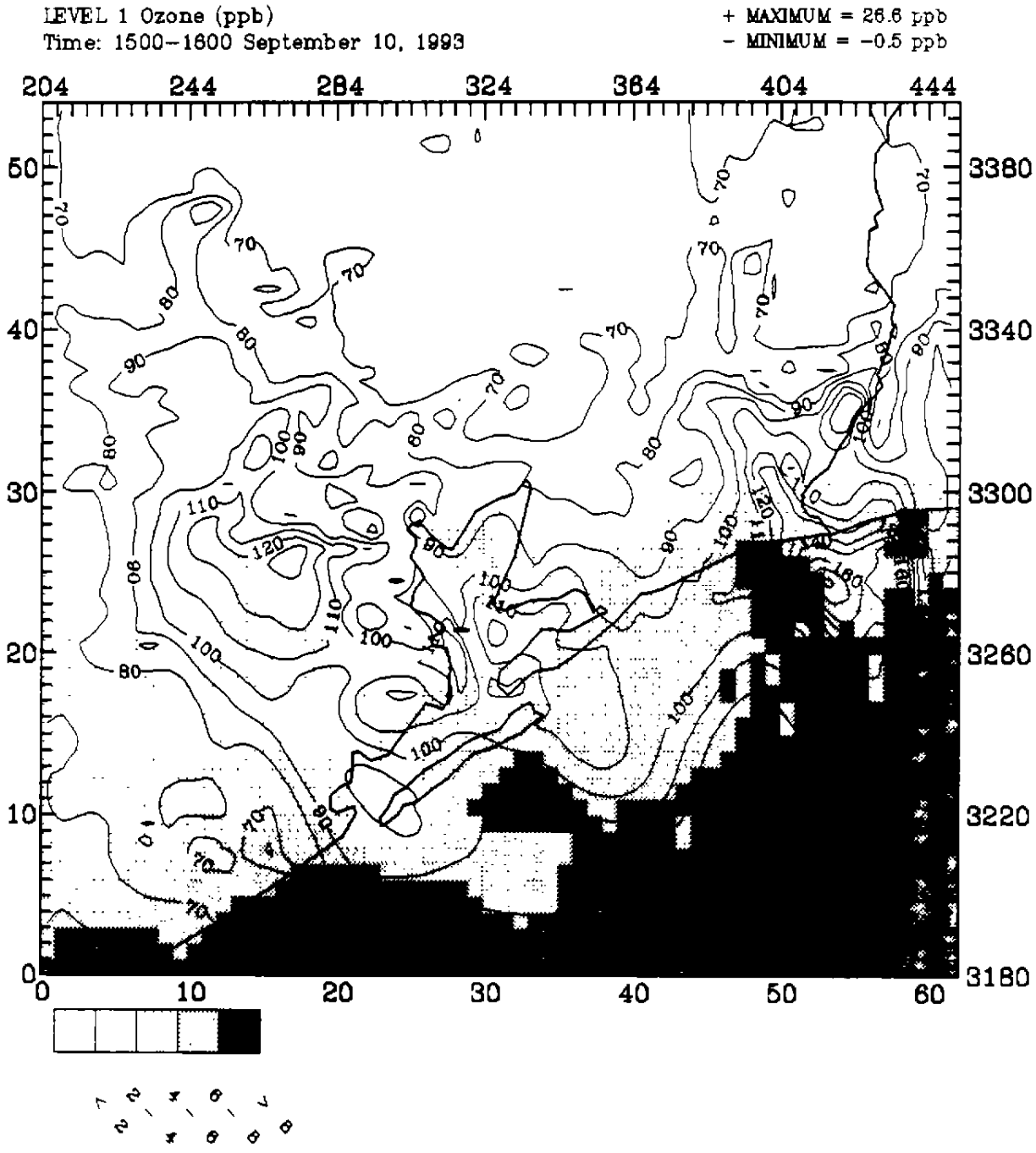

Figure 5-17a. UAM-V calculated ozone impacts (ppb) (shaded area) for 1999 from double OCSPD emissions for the Houston subdomain for 1500 CST 10 September (with double OCSPD emissions minus without OCSPD emissions). Isopleths depict ozone from simulation without OCSPD emissions.

95013

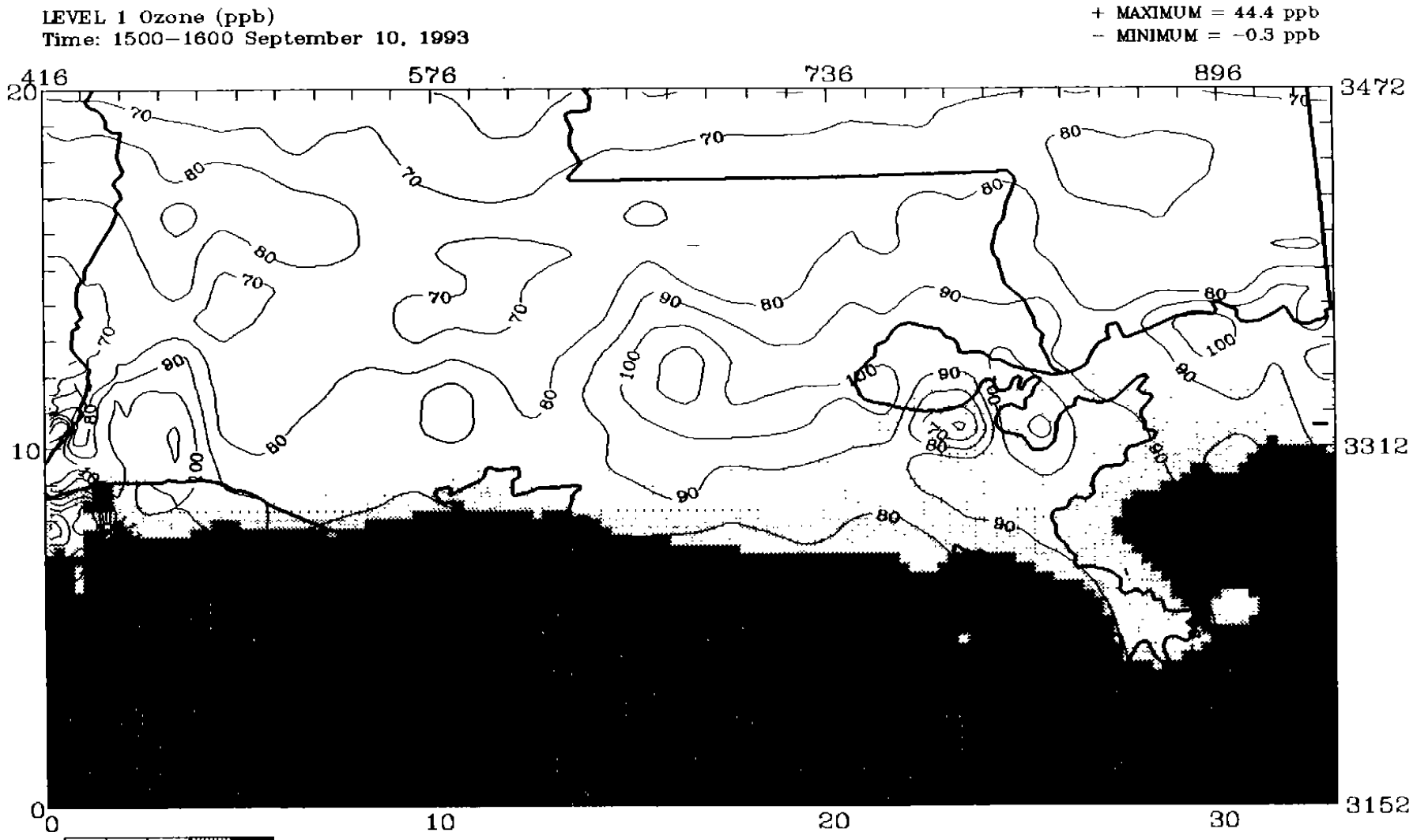

Figure 5-17b. UAM-V calculated ozone impacts (ppb) (shaded area) for 1999 from double OCSPD emissions for the Louisiana subdomain for 1500 CST 10 September (with double OCSPD emissions minus without OCSPD emissions). Isopleths depict ozone from simulation without OCSPD emissions.

approximately 80 km south of Gilchrist; these offshore impacts increase to 15-26 ppb in the same area when emissions are doubled (Figure 5-17). In the areas offshore of Louisiana, maximum differences range from 18 to 35 ppb in an area more than 100 km south of Vermilion Parish; when the OCSPD emissions are doubled, the maximum hourly impacts increase and range from 18 to 44 ppb. For the Houston area, the OCSPD impacts derived using the onshore baseline inventory are comparable to those obtained with the adjusted inventory.

The maximum impacts due to OCSPD emissions for 8, 9 and 10 September for each of the nonattainment areas are provided in Table 5-10. The table provides the maximum impacts in grid cells where the simulated ozone concentration (with OCSPD emissions) exceeds 124 ppb along with the maximum impacts in grid cells where the simulated ozone concentration is less than 124 ppb. For this episode, the largest simulated OCSPD impact in a cell with a concentration less than 124 ppb is 11.6 ppb in the Baton Rouge nonattainment area (there are no cells in the Baton Rouge area with maximum simulated ozone concentrations greater than 124 ppb). This impact increases to 17.3 ppb when emissions are doubled. For the Beaumont/Port Arthur area, the impact for grid cells greater than 124 ppb using the adjusted Houston emissions is 6.6 ppb for 10 September. This impact increases to 11.6 ppb when OCSPD emissions are doubled.

- The maximum simulated onshore impacts for the Houston area range between 4 and 6 ppb at locations in the southern portion of the subdomain where simulated concentrations due to all other emissions range between 60 and 80 ppb. At locations and during periods when the onshore ozone concentration in the Houston area is simulated to exceed 124 ppb, the simulated increment due to OCSPD operations for 1999 is less than 2 ppb. For the Beaumont area, the maximum incremental impact of OCSPD emissions is 6.6 ppb for 10 September. When OCSPD emissions are doubled, the maximum impact in the Beaumont area during the period when the onshore ozone concentration is simulated to exceed 124 ppb is 11.6 ppb. In the Baton Rouge area, the maximum simulated ozone impact is approximately 12 ppb; there are no cells in the Baton Rouge area with maximum simulated concentrations greater than 124 ppb.

Table 5-10. UAM-V simulated maximum ozone impacts (ppb) for 1999 for the September episode due to OCSPD emissions.

Simulation	8 September		9 September		10 September	
	For Cells > 124 ppb	For Cells < 124 ppb	For Cells > 124 ppb	For Cells < 124 ppb	For Cells > 124 ppb	For Cells < 124 ppb
Houston Nonattainment Area						
Baseline	N/A*	14.8	N/A	9.5	N/A	12.2
Adjusted	3.0	14.6	1.7	12.0	2.4	12.3
Baseline, with double OCSPD	N/A	18.4	N/A	14.3	N/A	17.5
Adjusted, with double OCSPD	2.0	18.1	2.7	18.7	4.8	17.6
Baseline, with 50% OCSPD	N/A	9.9	N/A	5.7	N/A	7.6
Adjusted, with 50% OCSPD	1.2	9.8	1.1	7.2	1.2	7.6
Beaumont/Port Arthur Area						
Baseline	N/A	15.9	N/A	10.0	N/A	6.8
Adjusted	1.3	16.0	N/A	10.0	6.6	6.7
Baseline, with double OCSPD	N/A	24.7	N/A	15.6	N/A	10.8
Adjusted, with double OCSPD	2.0	25.3	N/A	15.7	11.6	10.9
Baseline, with 50% OCSPD	N/A	9.6	N/A	6.0	N/A	4.0
Adjusted, with 50% OCSPD	0.8	9.6	N/A	6.0	3.4	3.9
Lake Charles Nonattainment Area						
Baseline	N/A	14.7	N/A	14.7	N/A	7.5
Adjusted	N/A	14.9	N/A	14.8	2.2	7.8
Baseline, with double OCSPD	N/A	22.1	N/A	21.4	N/A	10.4
Adjusted, with double OCSPD	N/A	22.8	N/A	22.0	4.4	11.1
Baseline, with 50% OCSPD	N/A	9.1	N/A	9.3	N/A	4.7
Adjusted, with 50% OCSPD	N/A	9.2	N/A	9.3	1.2	4.9
Baton Rouge Nonattainment Area						
Baseline	N/A	5.6	N/A	9.8	N/A	11.4
Adjusted	N/A	5.6	N/A	10.0	N/A	11.6
Baseline, with double OCSPD	N/A	8.8	N/A	14.9	N/A	16.9
Adjusted, with double OCSPD	N/A	8.8	N/A	15.3	N/A	17.3
Baseline, with 50% OCSPD	N/A	3.3	N/A	6.1	N/A	7.1
Adjusted, with 50% OCSPD	N/A	3.3	N/A	6.2	N/A	7.2

* Not applicable—no simulated concentrations greater than 124 ppb.

6 SUMMARY AND CONCLUSIONS

This report provides a summary of the activities conducted during the MMS Gulf of Mexico Air Quality Study (GMAQS), a study specifically mandated by Congress in the 1990 Clean Air Act Amendments (Title VIII, Sec. 801(b)). The major objective of the GMAQS was to collect supplemental data and apply state-of-the-science analysis methods and modeling tools to assess the potential impacts of OCS petroleum development (OCSPD) related sources located in the western and central regions of the Gulf of Mexico on ozone nonattainment areas located in Texas and Louisiana.

6.1 SUMMARY OF THE OCSPD IMPACT ANALYSIS

The impacts of OCSPD emissions on ozone concentrations within onshore nonattainment areas has been qualitatively assessed by analyzing supplemental meteorological and air quality data collected during the 1993 field program. Base-year and future-year OCSPD emission impacts have also been quantified with the application of a meteorological/photochemical modeling system, which was used to simulate a 1988 episode and two episodes that occurred during the summer of 1993. The results of the data analysis indicate that the OCSPD contribution to ozone concentrations in onshore nonattainment areas is very small. This is based on an analysis, including flux estimates, of ozone and ozone precursor data collected at surface sites and aloft along the Texas-Louisiana coastline during ozone-conducive conditions. The base-year and future-year UAM-V modeling results indicate that during the episodic conditions simulated, the maximum incremental increases to peak hourly ozone concentrations due to OCSPD emissions for both episodes were approximately 25-35 ppb, in locations over the central Gulf of Mexico region (near the area of highest OCSPD emission density), more than 120 km south of the Louisiana coastline. Peak simulated ozone concentrations in this area (with OCSPD emissions) ranged from 70 to 80 ppb. The maximum simulated onshore hourly incremental impacts due to OCSPD emissions were greatest during the nighttime hours for all episode days at coastal and inland locations throughout the GMAQS domain when observed and simulated ozone concentrations were relatively low. *During periods and at locations where ozone concentrations were simulated to equal or exceed 125 ppb, the incremental ozone impacts due to OCSPD emissions were simulated to be less than 2 ppb.*

6.2 GOALS AND OBJECTIVES OF THE GMAQS

The MMS GMAQS as originally planned entailed one major goal and six objectives. These are summarized in the following discussion.

> *The overall goal of this study was to quantitatively determine through modeling (meteorological and photochemical) the effects of current and future OCS development in the Gulf of Mexico on ozone nonattainment areas in Texas and Louisiana.*
>
> The overall goal of the GMAQS was achieved through the successful acquisition of supplemental air quality and meteorological data and through the combined application of meteorological and air quality analysis methods and advanced modeling tools to provide a quantification of the impacts, within nonattainment areas of Texas and Louisiana, of current and future OCSPD sources located in the western and central Gulf of Mexico.

The objectives of the GMAQS included the following:

(1) *Analyses of historical data, supplemented by recent meteorological measurements, that describe the conditions and likelihood of OCS emissions reaching coastal areas under conditions conducive to ozone formation.*

An analysis of historical ozone exceedance events for 1982–1990 was completed before the beginning of the 1993 field program. This analysis provided useful information for the design, implementation, and episode forecasting for the 1993 field program.

(2) *Preliminary meteorological and photochemical modeling of historical episodes of high onshore ozone concentrations to estimate OCS contributions to onshore ozone for historical high ozone episodes.*

Preliminary modeling using the SAIMM and UAM-V was undertaken in late 1992 and early 1993 involving the simulation of the 27–28 July 1988 episode. This preliminary modeling provided a preview for modeling the 1993 episodes. Information was obtained for setting model input parameters and for revealing the key features of the models that would be important in simulating the complex three-dimensional structure of the gulf breeze circulation and resulting ozone formation and transport characteristics of the area. For this episode, the preliminary modeling indicated that emissions from OCSPD sources had a small impact on ozone concentrations within onshore nonattainment areas.

(3) *Collection of extensive meteorological and air quality data during the summer ozone season.*

A wealth of supplemental air quality and meteorological measurements were obtained during the 1993 GMAQS field program. A number of exceedance days

were forecast, and intensive measurements were obtained. Two periods, 17–20 August and 6–11 September, which indicated the potential for onshore OCSPD impacts, were selected for modeling. High data recovery rates were achieved with all measurement systems. The data quality objectives were met with quality assurance audits. Intensive measurements were obtained for the 17–20 August episode. However, because the intensive field program ended on 28 August, intensive measurements (e.g., aircraft and supplemental radiosonde measurements) were not obtained for the 6–11 September exceedance episode; however, supplemental air quality and meteorological data were collected during this episode.

(4) *Extension, refinement, evaluation, and application of meteorological and photochemical modeling techniques using the data collected during the field study.*

The meteorological/photochemical modeling system was applied for the August and September episodes. The supplemental meteorological data collected, especially for the August episode, were assimilated into the prognostic meteorological model to improve the representation of the three-dimensional meteorological fields. Supplemental air quality measurements taken on the ground and aloft were used to set initial and boundary conditions and to assess the performance of the photochemical model in replicating the three-dimensional structure of observed ozone concentration patterns and in providing a reliable database for assessing and forecasting impacts from current and future OCSPD emission scenarios.

(5) *Evaluation of the sources of uncertainty in estimates of impacts.*

Although additional air quality and meteorological measurements were made during the 1993 GMAQS field program, compared to those taken routinely, uncertainties are still present in the modeling analysis. Additional measurements or modifications to the meteorological modeling approach may aid in refining the simulation of the complex gulf-breeze circulation. The photochemical modeling analysis revealed that the largest degree of uncertainty was associated with the emission estimates. Certain changes in the photochemical modeling approach (e.g., use of day-specific emission estimates and a higher resolution nested grid) may improve model performance further and lower the uncertainty associated with the quantification of the impacts of OCSPD emissions.

(6) *Recommendation of future monitoring and modeling efforts that can address these uncertainties.*

The data analysis and modeling efforts conducted in this study have revealed some areas of uncertainty that could be addressed in the future with additional monitoring, analysis, and modeling efforts. A set of recommendations have been formulated and are based on the experience and knowledge gained in the course of the GMAQS program, through analysis and modeling, regarding the physical mechanisms responsible for ozone production in the area, and, in particular, the

unique features that cause ozone exceedance events. These recommendations are provided in Section 7 of this report.

6.3 SUMMARY OF RESULTS OF GMAQS ACTIVITIES

The major activities of the GMAQS included:

(1) ***Field Study Design and Implementation*** — An intensive air quality and meteorological data collection effort was planned in late 1992 and early 1993. The program commenced in April 1993 with the deployment of supplemental surface air quality and meteorological monitoring systems. In addition, intensive measurements using aircraft and other systems were also conducted, on a number of forecasted ozone-conducive days, during a six-week period in July and August 1993.

(2) ***Data Analysis*** — The data collected during the field program were analyzed to provide a more thorough understanding of the physical processes affecting ozone production and transport in the GMAQS area. These analyses included the examination of episodic meteorological conditions; the calculation of particle trajectories, pollutant fluxes, ventilation parameters, and boundary layer parameters; and an episode representativeness and climatological analysis.

(3) ***Emission Inventory Preparation*** — As a major input required for simulating ozone exceedance events in the GMAQS domain, an inventory consisting of biogenic emissions and anthropogenic emissions from area, mobile, and industrial point sources was prepared. This included a comprehensive inventory of OCSPD-related sources.

(4) ***Application of a Meteorological/Photochemical Modeling System*** — Using historical data for 1988 and the supplemental data collected during two 1993 episodes, a data-assimilating prognostic meteorological model (SAIMM) and an advanced, variable nested-grid photochemical model (UAM-V) were applied to numerically simulate the physical and chemical features of the episodes to assess the potential current and future impacts of OCSPD sources throughout the GMAQS domain. After the models were evaluated with observed data and it was determined that they provide an acceptable representation of ozone production and transport for each of the episodes, the impacts of OCSPD emissions were assessed for 1993 and 1999.

RESULTS OF THE FIELD STUDY DESIGN AND IMPLEMENTATION

The GMAQS field program was designed to collect supplemental data for use in analyzing and simulating ozone exceedance events. Additional monitors were placed onshore to supplement the routine measurement network. Monitors were also placed at selected offshore locations to provide measurements in the Gulf. Aircraft measurements

were taken to provide information regarding the three-dimensional meteorological and air quality characteristics of the atmosphere during ozone exceedance events. Three offshore platforms and five onshore sites were selected for the installation of supplemental air quality and/or meteorological measurement systems for the study. The equipment was installed and began operating by mid-April 1993.

The intensive measurement portion of the field study extended from 18 July to 28 August 1993. During this time, two highly instrumented twin-engine aircraft were located in Beaumont and on alert to fly when conditions were favorable for ozone exceedances. In addition, the National Weather Service provided one additional upper-air meteorological measurement per day as needed, for Slidell and Lake Charles, Louisiana.

The 1993 GMAQS field study was successful. Several high ozone episodes were forecast and captured, including those with peak ozone concentrations at approximately the same levels as EPA-determined design values for the study area. High data recovery rates were achieved for all measurement systems. Reports for quality assurance auditors demonstrate that data quality objectives were achieved.

RESULTS OF THE DATA ANALYSES

Available data for monitoring sites within the GMAQS modeling domain were analyzed to provide information for selection of historical episodes for modeling and for the development of an episode forecasting methodology for the 1993 field program.

Descriptions and displays of air quality and meteorological data (objective data analysis) collected during the 1993 field program were prepared and apparent relationships between parameters were identified. Summary statistics and visual displays were prepared to characterize the important features of the air quality and meteorological conditions in the Gulf Coast region. The key findings of the data analysis include:

- Ozone exceedance days in the southeast Texas portion of the GMAQS study are associated with a distinct flow reversal; the strength and duration of the land breeze, and corresponding stagnation during transition to onshore flow is an important mechanism that causes a recirculation of precursor emissions and contributes to observed hourly ozone concentrations exceeding 0.12 ppm. Detailed analysis of the observed wind data for 10 exceedance days in 1993, suggests that the land breeze "front" typically traveled 75 to 100 km offshore before the winds reversed and began blowing onshore again. No exceedance events occurred in this area during 1993 without the observed flow reversal.

- Maximum ozone concentrations occurred during the period when southerly winds accompanying the onshore component of the flow reversal were present. The ozone "cloud" (or "plume") was pushed northward (inland), with the highest ozone concentrations usually observed north of Houston. Ozone concentrations dropped dramatically after the passage of the gulf-breeze front.

- In Louisiana, the same general pattern of the onshore-offshore-onshore flow reversal was observed on a number of study days, including 18–19 August, when the NAAQS for ozone was exceeded in Baton Rouge.

- The depth of the marine layer offshore showed only modest diurnal variations; the average depth of the mixed layer offshore was 500 to 700 m agl. The most pronounced "growth" of the mixed layer offshore coincided with the passage of the land breeze "front."

- Aircraft data suggested that mixing depths over inland rural areas were not as deep as those observed over urbanized areas, which is consistent with urban heat island effects and previous studies of mixed layer development in urban versus rural areas.

- As the gulf breeze "front" pushed inland, it produced lifting, instability, and convection (often accompanied by clouds and sometimes by showers). This process helped augment vertical mixing and venting of pollutants.

- The upper-air data for the August episode indicated that the gulf breeze transported ozone through Houston and into the rural areas north of the city. The general absence of carryover aloft of pollutants from day to day during this episode, which was indicated by the aircraft data, is most likely explained by the vertical venting of pollutants into regions aloft of steady synoptic-scale flow, and transport out of the region.

- Calculated trajectories for each of the episodes examined indicated that marine air coming onshore (from potential OCSPD source areas) on the day of an ozone exceedance did not reach the areas where maximum ozone concentrations were observed until several hours after the highest ozone concentrations had occurred.

- Trajectory analysis indicated that direct, same-day transport of offshore OCSPD emissions from source regions in the Gulf of Mexico (south and east of Louisiana) to exceedance sites near Baton Rouge did not occur during the August and September episodes.

- Surface and upper-air trajectories combined with data analyses for the September episode suggested that air parcels reaching Houston-area exceedance sites originated in the Houston ship channel area and were transported southeastward, no farther than 10 km offshore, before being recirculated back onshore.

- However, on 10 September, trajectories and data analyses suggested that emissions from shore-based sources in the Houston/Galveston area were transported offshore at least 50 km and commingled with OCSPD emissions over the Gulf.

- When steady onshore flow persisted for several days at a time, ozone concentrations at shoreline monitoring sites slowly and steadily dropped from typically about 60–80 ppb on the first day to 20–40 ppb after several days. NO_x

concentrations also dropped from about 4–6 ppb to less than 2 ppb during steady onshore flow conditions.

A range of data analysis methods were used to examine the potential for OCSPD emissions to contribute to ozone exceedances in the southeast Texas and Baton Rouge nonattainment areas. Flux estimates, calculated for both the August and September episodes, indicate that the amount of NO_x emissions transported into the Houston area from OCSPD sources is small compared to that from onshore sources. Similarly, for ozone, the flux calculations indicate that the amount of ozone transported onshore is small compared to that produced in the Houston area.

EMISSION INVENTORY PREPARATION

Gridded, hourly emissions inventories were prepared for the entire study area, for both historical and 1993 ozone episodes, and for future-year emissions scenarios. These inventories cover an area of nearly one million square kilometers, encompassing the western and central portions of the Gulf of Mexico and onshore ozone nonattainment areas (Houston/Galveston, Beaumont/Port Arthur, Calcasieu Parish/Lake Charles, and Baton Rouge).

Air pollutants inventoried include NO, NO_2, speciated VOC, and CO. The modeling emission inventories include emissions from both onshore and offshore sources and those specifically associated with OCS petroleum development (OCSPD) related emissions. Relevant emissions from anthropogenic and biogenic sources were inventoried, with special attention focused on offshore anthropogenic sources.

- OCSPD emissions in offshore lease tracts adjacent to the Houston and Beaumont/Port Arthur areas represent less than 2 percent of the total anthropogenic NO_x emissions and less than 1 percent of the total VOC emissions in the Houston/Beaumont/Port Arthur onshore nonattainment areas.

- OCSPD emissions in the western and central Gulf of Mexico comprise approximately 5 percent of the total anthropogenic NO_x emissions and less than 2 percent of the total anthropogenic VOC emissions within the entire GMAQS modeling domain.

Initial simulation results using the baseline modeling emission inventory suggested that VOC emissions were understated relative to NO_x emissions. The data analysis results support this inference.

- An anthropogenic emission-based VOC-to-NO_x ratio of approximately 2.5 is not consistent with measurement-derived estimates of 10 or greater.

The use of the inventory in the modeling analysis also indicated that uncertainties in the day-specific emission estimates, especially for mobile and industrial sources, may have affected model performance for both episodes.

- Based on the results of numerous diagnostic and sensitivity simulations performed using the UAM-V, modeling emission inventories for the Houston area were adjusted such that the NO_x emissions from elevated point sources were reduced by 50 percent, VOC emissions from stationary sources (including area, nonroad, and point sources) were increased by 50 percent, and VOC emissions for mobile sources were increased by a factor of 2 for both episodes.

- Based on an analysis of hydrocarbon data for the Clinton site and information obtained from county records, VOC emissions for 19 August were modified to incorporate the effects of a petroleum product spill in the Houston Ship Channel area. Emissions from this assumed accidental occurrence were included in the base-case performance evaluation simulations only; additional simulations for this day performed to assess OCSPD emission impacts, however, did not include these emissions.

It is anticipated that more refined emission inventory information collected as part of the 1993 COAST program (not available in time for use in the GMAQS) for anthropogenic and biogenic sources could be used to improve the GMAQS inventory and the modeling results.

RESULTS OF THE METEOROLOGICAL MODELING

Meteorological fields for application of the UAM-V to the GMAQS modeling domain were prepared using the SAI Mesoscale Model (SAIMM). For this application, the model was exercised using a one-way nested-grid approach with 16-km horizontal resolution for the coarse grid or outer domain and 4-km resolution for the inner domain. Routine and supplementary meteorological data collected during the GMAQS and COAST field programs were incorporated into the SAIMM simulations using four-dimensional data assimilation (FDDA).

The model evaluation using data collected during each of the episodes showed that the model provided a reasonable representation of the observed regional-scale flow patterns and the temporal and spatial features of the gulf breeze and associated airflow patterns.

- Good agreement between the simulated and observed winds aloft for both episodes indicates that the SAIMM was able to simulate the day-to-day variations in the regional-scale meteorological conditions (and, thus, the regional-scale transport patterns) associated with anticyclonic flow aloft during the August episode and northerly winds aloft during the September episode.

- The simulated vertical and temporal evolution of the gulf breeze (as illustrated by vertical cross-section plots) demonstrates the ability of the model to realistically represent the complex, three-dimensional circulation patterns associated with the development of the gulf breeze including the transition from weak offshore-directed flow to steady onshore flow, the inland propagation of the gulf breeze front, and the vertical development of the gulf-breeze layer.

- A comparison with the data analysis results for both episodes indicates that the fine-grid SAIMM-simulated airflow patterns conform to the conceptual models of offshore-onshore flow reversal suggested by the data. The various stages of flow reversal were identified in the simulated wind fields.

- The timing and inland extent of the simulated gulf breeze varies among the episode days in a manner that is consistent with the findings of the data analysis (i.e. the gulf breeze develops later and extends less far inland on the September episode days, likely due to the northerly flow aloft).

- Particle paths calculated using the simulated winds for 8 September indicate a nearly 180-degree change in wind direction. This is consistent with the ventilation analysis results for this day. Comparison with observed surface wind data, however, suggests that the simulated gulf/bay breeze penetrates too far inland on 8 September.

- Although particle paths illustrate that the simulated wind fields for 9 September support the hypothesis that the buildup of ozone concentrations observed near the coast was associated with offshore flow, weaker than observed northerly wind components may have resulted in an underestimate of simulated onshore-to-offshore pollutant transport during the morning of 9 September.

UAM-V tracer simulations were used to evaluate the three-dimensional meteorological fields with respect to the data analysis results.

- Tracer simulation results for the August episode support the general conclusions from the data analysis that northeastward transport of pollutants occurred during this episode and that carryover of ozone and precursor pollutants was unlikely.

- Results for the September episode show that the simulated wind fields represent carryover/recirculation of pollutants from onshore sources that was determined, through data analysis, to have occurred during this episode. On 8 and 9 September, the simulated tracers are advected approximately 32 km offshore; the data analysis results suggest that this distance is somewhere between 10 and 50 km.

The results of the modeling indicated that additional improvements in replicating the observed features of the Gulf and Galveston Bay breeze flow patterns could be achieved with a higher resolution grid, or possibly more advanced modeling techniques.

RESULTS OF THE PHOTOCHEMICAL MODELING ANALYSES

An advanced photochemical air quality model, the variable-grid version of the Urban Airshed Model (UAM-V), was applied for the GMAQS domain to provide computer simulations of the chemical and physical mechanisms affecting observed ozone concentrations within the study domain and to provide quantitative estimates of the impacts of OCSPD emissions on ozone concentrations within the Houston/Galveston, Beaumont/Port Arthur, Calcasieu Parish/Lake Charles, and Baton Rouge nonattainment

areas. The primary focus of the modeling analysis was the Houston area. Three multiday ozone episodes were simulated including 27–28 July 1988 and 17–20 August and 6–11 September 1993; supplemental air quality meteorological data were available for the 1993 episodes.

- The objective of the modeling effort for the 1988 episode was to test whether the GMAQS modeling system (consisting of EPS 2.0, SAIMM, and UAM-V) was capable of simulating ozone formation and transport in the Gulf of Mexico area. It provided an opportunity to test and refine input preparation methodologies and to identify deficiencies in the available meteorological and air quality databases for consideration in designing the 1993 field study.

- The 1993 modeling episodes were selected based on the magnitude and extent of observed high ozone concentrations within the onshore ozone nonattainment areas and the estimated potential for OCS emissions to contribute to the onshore concentrations.

- Analysis of historical ozone episodes indicated that the 1993 GMAQS episodes were representative of the period 1982–1992 and that the meteorological variables monitored during the 1993 episodes were within the ranges of distributions for ozone exceedance days during this historical period.

Numerous diagnostic and sensitivity tests were carried out to examine the response of the UAM-V to uncertainties in inputs to assess whether the model was able to perform reasonably well in replicating the temporal and spatial characteristics of the observed ozone concentration patterns.

- The diagnostic and sensitivity simulations showed that either lower localized NO_x or higher VOC emissions in the Houston/Galveston Bay area or some combination of the two provided a better simulation of ozone for all the high ozone days.

- The simulation results also indicated that the high observed ozone concentrations in the Houston area may have been the result of localized fluctuations in emissions combined with adverse meteorological conditions or synergistic interactions of the local, diverse emissions.

- The modeling emission inventories were adjusted within considered ranges of uncertainty to enable the UAM-V to reasonably depict the air quality characteristics of the ozone episodes. The adjustments included a 50 percent decrease in elevated point-source NO_x emissions, a 50 percent increase in stationary source VOC emissions, and 100 percent increase in mobile-source VOC emissions. VOC emissions corresponding to a petroleum product spill were also included for the simulation of 19 August for the base-case model evaluation only.

Evaluation of UAM-V model performance was completed using available air quality measurements and a variety of graphical and statistical analysis techniques.

- The qualitative and quantitative assessment of model performance for the August and September episodes indicated that the meteorological and photochemical modeling system provided a reasonable simulation of each of the episodes. The simulation results were generally consistent with the conceptual models of the episodes developed through analysis of the air quality and meteorological data and the statistical measures were generally within the ranges provided by EPA for acceptable photochemical model performance.

- Uncertainty in the model inputs, however, affected model performance, and the results of the model performance evaluation indicated that use of the modeling system to assess the impacts of OCSPD emissions on ozone concentrations within the GMAQS region should consider these uncertainties.

The impacts of OCSPD emissions have been assessed for each of the episodes for 1993 and 1999 by performing a series of UAM-V simulations. The impacts have been quantified by graphically illustrating and tabulating changes to the simulated hourly average ozone concentrations. To quantify impacts, the ozone concentrations obtained from the simulation without OCSPD emissions were subtracted from the corresponding simulation that included OCSPD emissions.

OCSPD Impact Analysis for 1993

Modeling of OCSPD impacts for 1993 for the August and September episodes revealed:

- The maximum incremental increases to peak hourly ozone concentrations due to OCSPD emissions for both episodes were approximately 25-35 ppb, in locations over the central Gulf of Mexico region, more than 120 km south of the Louisiana coastline (near the area of highest OCSPD emission density). Peak simulated ozone concentrations in this area (with OCSPD emissions) ranged from 70 to 80 ppb. The maximum simulated onshore incremental impacts due to OCSPD emissions were greatest during the nighttime hours for all episode days at coastal and inland locations throughout the GMAQS domain when observed and simulated ozone concentrations were relatively low.

- Maximum ozone impacts due to OCSPD operations for the August episode in the Houston area were estimated to be 6-8 ppb at a time when the hourly average ozone concentrations calculated from all other emission sources were approximately 50 ppb. During periods and at locations where ozone concentrations were simulated to equal or exceed 125 ppb, the incremental ozone impacts due to OCSPD emissions were simulated to be less than 2 ppb.

- For the Baton Rouge nonattainment area, the maximum simulated incremental impacts from OCSPD emissions for the August episode, during the time of observed (and simulated) maximum concentrations, was 0-2 ppb. Larger impacts from OCSPD emissions are simulated during other hours, and at locations along the Louisiana coastline and over the Gulf, well south of the Baton Rouge nonattainment area.

- For the September episode, the maximum simulated onshore impacts for the Houston area range between 6 and 8 ppb. At locations and during periods when the onshore ozone concentration is simulated to equal or exceed 125 ppb, the simulated increment due to OCSPD operations is less than 2 ppb. For Baton Rouge, in areas where the maximum simulated ozone concentrations are greater than 125 ppb, the maximum incremental impact is 0–2 ppb.

Simulations involving the elimination of OCSPD and mobile source emissions provided a comparison of impacts for these two source categories for the September 1993 episode. The results of these simulations indicated:

- Mobile source emissions contribute as much as 50 ppb to the simulated peak in the Houston area and as much as 10–15 ppb to the simulated peak ozone concentration in the Baton Rouge area.

OCSPD Impact Analysis for 1999

The meteorological and air quality inputs were fixed and the model was used as a forecasting tool to provide likely future ozone concentration estimates for a number of future-year (1999) onshore and OCSPD emission scenarios to assess the simulated impacts of OCSPD sources on the onshore nonattainment areas. Future-year modeling was performed for 1999 using projected emission inventory estimates for the onshore and offshore portions of the GMAQS domain. Uncertainties in the base-year (1993) onshore Houston inventory and the projected 1999 OCSPD inventory were incorporated into the analysis by performing OCSPD impact simulations using combinations of onshore and offshore emissions that bracketed the uncertainties. The use of adjusted emissions for the Houston area resulted in more realistic (expected) 1999 concentrations, given the small decreases from 1993 to 1999 in the projected emission inventory. Adjustments made to the 1999 Houston inventory that were similar to those made on the 1993 inventory, however, had little effect on simulated OCSPD impacts. The future-year (1999) modeling indicated:

- The maximum simulated ozone impacts for the August episode due to estimated 1999 OCSPD operations in the Houston area (southwest of the city) were 6–8 ppb at a time when the hourly average ozone concentrations calculated from all other emission sources were approximately 30–50 ppb. During periods and at locations where ozone concentrations were simulated to equal or exceed 125 ppb, the incremental ozone impacts due to OCSPD emissions were simulated to be less than 2 ppb.

- The maximum simulated ozone impacts for the August episode due to estimated 1999 OCSPD operations in the Beaumont/Port Arthur area were 6–8 ppb at a time when the hourly average ozone concentrations calculated from all other emission sources were approximately 40–60 ppb. During periods and at locations where ozone concentrations were simulated to equal or exceed 125 ppb, the incremental ozone impacts due to OCSPD emissions were simulated to be 2–4 ppb.

- For the Baton Rouge and Lake Charles nonattainment areas, the simulated incremental impacts from 1999 OCSPD emissions for the August episode, during the time of simulated maximum concentrations, were 0–2 ppb. Larger impacts from OCSPD emissions were simulated during the nighttime hours, and at locations along the Louisiana coastline and over the Gulf, well south of the Baton Rouge nonattainment area.

- When the OCSPD emissions were doubled for the August episode, the maximum simulated hourly incremental impacts increased to 18–20 ppb in the Houston area, 14–16 ppb in the Beaumont area, 10–12 ppb in the Lake Charles area, and 14–16 ppb in the Baton Rouge area. These maximum impacts occurred at times and locations when simulated concentrations were less than 124 ppb.

- The maximum simulated ozone impacts for the September episode due to estimated 1999 OCSPD operations in the Beaumont/Port Arthur area were 6–8 ppb along the coast during periods when ozone concentrations to the north were simulated to equal or exceed 125 ppb. In the area of the peak simulated concentration, the OCSPD impact was less than 2 ppb.

- For the Lake Charles nonattainment areas, the simulated incremental impacts from 1999 OCSPD emissions for the September episode during the nighttime hours were 6–8 ppb. During the afternoon hours, when peak concentrations were simulated, the maximum incremental increase was less than 2 ppb.

- For the Baton Rouge nonattainment area, the simulated incremental impacts from 1999 OCSPD emissions for the September episode during the nighttime hours were 4–6 ppb. During the afternoon hours, when peak concentrations are simulated, the maximum incremental increase was less than 2 ppb. Larger impacts from OCSPD emissions were simulated during other hours, and at locations along the Louisiana coastline and over the Gulf, well south of the Baton Rouge nonattainment area.

- When the OCSPD emissions were doubled for the September episode, the maximum simulated hourly incremental impacts increased to 16–18 ppb in the Houston area, 10–12 ppb in the Beaumont area, 10–12 ppb in the Lake Charles area, and 16–18 ppb in the Baton Rouge area. These maximum impacts occurred at times and locations when simulated concentrations were less than 124 ppb.

6.4 CONCLUDING REMARKS

Data analysis and modeling have been performed to assess and quantify the potential impacts of Gulf of Mexico OCSPD sources on observed ozone concentrations within the nonattainment areas of Texas and Louisiana. Maximum future-year onshore impacts from OCS operations in the Houston/Galveston nonattainment area vary according to meteorological episode, location, and time of day. Over the episodes, area, and time of day the simulated maximum onshore incremental impacts range from as high as 14 ppb

to less than 2 ppb. The highest incremental impacts are simulated to occur in the southern portions of the domain (closest to the Gulf) during times when the maximum simulated hourly ozone concentrations from all sources except OCSPD operations range between 30 to 80 ppb. In the vicinity of Houston (usually north and northwest of the downtown area) when maximum simulated ozone concentrations from all emissions categories except OCSPD are just below, equal to or in excess of 124 ppb, the maximum incremental impacts from OCSPD operations are 2-4 ppb.

Maximum future-year impacts in the Beaumont/Port Arthur area range from 8 to 10 ppb. The highest incremental impacts are simulated to occur along the coast. In the vicinity of the peak simulated concentration (northeast of Beaumont), the maximum incremental impacts from OCSPD operations are less than 2 ppb. For the Lake Charles/Calcasieu Parish and Baton Rouge areas, the maximum incremental impacts are 8-12 ppb. During the afternoon hours, when peak concentrations are simulated, the maximum incremental increase is 4-6 ppb.

These simulated estimates of impacts are similar to the qualitative conclusions reached from the analysis of the comprehensive field measurement program data (summarized above).

The magnitudes of the simulated incremental OCSPD ozone impacts for either episode, based on numerous sensitivity tests, do not appear to be sensitive to uncertainties in the base inventories used for the Houston subdomain. In other words, regardless of which future-year inventory is used (baseline or adjusted), the incremental impacts from OCSPD operations are very similar.

The magnitudes of the simulated incremental OCSPD ozone impacts are smaller than the model uncertainties, as estimated by comparing observed and simulated hourly ozone concentration. Depending on the day and region, the model tends to both overstate and understate the observed values, assuming there is no uncertainty in the observations. In the portions of the Houston subdomain where the simulated hourly ozone concentrations exceed 80 ppb, the estimated standard deviation (of the differences between simulated and observed values) is approximately 35 and 22 ppb, respectively, for 9 and 10 September, which may be compared with incremental OCSPD impacts that range between 0 and 4 ppb in that region on those days. In those portions of the domain where simulated hourly concentrations are less than 80 ppb, the estimated standard deviation is approximately 25 and 31 ppb, respectively, for 9 and 10 September, which may be compared with incremental OCSPD impacts that range between 0 and 14 ppb.

That the impacts attributed to OCSPD emissions are smaller than estimates of the standard deviations of observed and simulated hourly ozone concentration should not be interpreted, we believe, as evidence that the impacts are meaningless: UAM-V, irrespective of the uncertainty associated with estimating any specific, hourly ozone concentration, is most accurate when used to estimate relative impacts. Thus, while we are unable to state quantitatively what the accuracy of the simulated impacts are, we believe that they are considerably more accurate than what is suggested by the estimated standard deviations of ± 20 to 30 ppb.

The scope of this study did not permit a comprehensive assessment of the causes of model uncertainties. Qualitatively, it seems that uncertainties in daily emissions are particularly noticeable, but the other modeling inputs must also be involved. The methods for performing such an assessment that might be practical to decision makers and other users of the results reported here remain to be developed, and so must await further advancements in the analysis of air quality modeling results.

Nevertheless we can offer these speculations about the effect of bias on conclusions about corresponding biases in OCSPD impacts: when the simulated base-year concentrations show underestimation, we believe that the underestimation will not necessarily be reflected in a corresponding underestimation in simulated impacts. Further, we believe the converse is also true (i.e., when the model reveals a tendency to overstate observed concentrations in the base-year simulation, there is no tendency for the model to overstate incremental impacts). This belief is based on the finding that the incremental onshore OCSPD impacts appear to be independent of relatively large changes in the onshore inventory. In addition, this belief is also consistent with our current understanding of the nature of the chemistry of ozone formation and its treatment in the model.

7 RECOMMENDATIONS FOR FUTURE GULF OF MEXICO MEASUREMENT AND MODELING PROGRAMS

The 1993 GMAQS summer field measurement program collected a wealth of supplemental air quality and meteorological data, which have been analyzed and used in the meteorological and photochemical modeling analysis. This section presents a set of recommendations for conducting similar future studies for the Texas-Louisiana Gulf Coast area. The recommendations follow from the insights gained during this study concerning the mechanisms that influence ozone formation and transport in the area, and are meant to complement and extend the analyses performed to date. If undertaken, they may further refine the primary objective of this work—to quantify the ozone impacts of OCS petroleum development sources on onshore nonattainment areas of Texas and Louisiana.

The recommendations for future work fall into four categories: (1) additional field measurements, (2) data analysis, (3) emission inventory, and (4) meteorological and photochemical modeling.

ADDITIONAL FIELD MEASUREMENTS

Surface Air Quality Measurements

- Place additional surface monitors in rural areas, for example, north-northwest of Houston where the UAM-V is simulating higher ozone concentrations (see Figure 4-77). Possibly use mobile monitors to obtain data without having to set up fixed sites.

- Conduct air quality and meteorological measurements farther seaward, at the outer edge of the OCS, to better characterize boundary conditions (HC and NO_x).

- Repeat the continuously operating surface air quality and meteorological measurement components of both the 1993 GMAQS and existing agency networks. It is especially important to monitor ozone and NO_x at sites between Galveston Bay and Port Arthur, such as Smith Point and Gilchrist, where maximum ozone concentrations were measured during the September 1993 episode. It would be useful if these measurements were done every year, not just during special studies.

- Measure surface VOC and carbonyl concentrations in source-oriented locations, for use in emission inventory evaluations. Note that the 1993 surface VOC

measurements sponsored by TNRCC are likely to be invalidated, due to problems in sampling and in the laboratory. For the GMAQS aircraft VOC and carbonyl measurements, sampler and laboratory performance was demonstrated before the start of sampling. These measurements at some locations could be continuous gas chromatograms, rather than grab samples.

- Install at least two new VOC monitoring sites approximately 5 km north of the industrial areas of Texas City and Baytown, respectively, to measure VOC concentrations from daily fluctuations in local industrial emissions.

- Operate continuous gas chromatographs (GCs) at shoreline sites such as Gilchrist and Cocodrie to obtain many routine VOC signatures during all types of flow, including offshore and onshore flow. These continuous GC measurements of only about 50 species would supplement the more extensive VOC signatures from grab samples taken on intensive days.

Air Quality Measurements Aloft

- Obtain data to improve the spatial and temporal resolution of ozone concentrations aloft using either ozonesondes or ozone UV DIAL lidar. Note, however, that a complete validation of ozone UV DIAL lidar measurements is still needed before this method is used. Improved spatial resolution is needed in the daytime urban mixed layer and in locations where aircraft cannot fly near the surface (i.e., over the ship channel and over the developed portions of Houston). Improved temporal resolution is needed during the hours leading up to the maximum ozone concentration.

- Conduct additional aircraft measurements near large industrial complexes, to explore vertical transport of both NO_x and VOC pollutants, and near the land/gulf-breeze fronts, to examine vertical features.

- If logistics permit, collect more VOC speciation data aloft in populated and industrial areas, especially in the Houston/Beaumont/Galveston/Texas City area.

- Plan to expend a small amount of aircraft flight time and VOC/carbonyl sampling resources collecting data near several large platforms on nonintensive sampling days. In 1993, this was only done near the end of the intensive period, and for only two short flights.

- Perform high-altitude (to about 3,000 m) aircraft spirals at a second location in the southeast Texas area (this was done only at Houston-Hobby Airport during the 1993 GMAQS).

- Perform a multiple-tracer study involving both onshore and offshore releases. The results could quantify the relative contributions of onshore and offshore sources to pollutant concentrations arriving back onshore and at ozone exceedance sites. In general, tracers should be used not to monitor individual point source

contributions, but to characterize representative contributions from general source regions (e.g., Houston Ship Channel, northern Galveston Bay, southeastern Galveston Bay, downtown Houston, or differing distances offshore). Design of tracer experiments should be closely coupled with expected analyses, which should focus on trajectory analyses, and experiments should include sampling aloft in addition to surface sampling.

Meteorological Measurements

- Place additional wind and temperature monitoring sites between the coastline and Houston area population/industrial centers to more accurately characterize the gulf-breeze/land-breeze frontal passage during ozone episodes.

- Repeat offshore profiler measurements, but with one logistical change. The offshore systems during the 1993 GMAQS failed to report winds in the first one or two range gates because the cables between the antenna and the profiler electronics were too long (>200 ft, rather than "normal" lengths of about 100 ft), producing electronic interference that prevented the instruments from obtaining sufficient samples. This problem should be avoidable in the future.

- Make additional upper-air measurements (one or two stations) on the north side of Houston to better define the extent of the northward branch of flow reversal and the inland extent of transport once the gulf breeze is established. It is important to represent the airflow between the Houston metropolitan area and areas in which the highest ozone concentrations are observed.

- Make additional upper-air meteorological measurements to help characterize spatial and temporal gradients in mixing depth (e.g., add one or two stations on the shoreline and one or two inland; one station offshore is probably sufficient).

- Add several balloon soundings at each radar profiler site to support the QA objectives of the study. During episodes, perform some additional rawinsonde upper-air soundings at onshore locations between the shoreline and the locations of peak ozone, in order to better understand the role and structure of the gulf breeze. This would provide sufficient data to support the conversion of virtual temperature to temperature.

- Add additional upper-air measurements on the north side of Baton Rouge to collect more data regarding the southward flow that often develops in the morning during ozone exceedances.

- Measure water temperature in Galveston Bay for use in meteorological modeling analysis, and consider augmenting air-sea and air-land interface measurements in other locations to better characterize surface energy budgets that drive the gulf/land breeze.

- Perform additional wind and temperature measurements between the surface and the first altitude at which upper-air data might be reported (~125 m agl).

- Collect satellite imagery for use in data analysis and model evaluation in real time; we began this in mid-August and had to obtain the earlier images from the archives, which was more time consuming and more expensive.

DATA ANALYSES

- The additional measurements outlined above would allow closer analyses of the processes that affect ozone concentrations in the area, including mixing heights, temperature distribution aloft, VOC/NO_x ratios, land/gulf-breeze effects, vertical transport and carryover of precursors and ozone, and pollutant fluxes.

- Analyze vertical velocities, using the radar profiler and sodar data, to better understand the role of vertical mixing in ozone formation and pollutant transport.

- Develop and perform analysis of background pollutant concentrations entering the Gulf region from the south and east. During typical ozone episodes in the Baton Rouge/southeast Texas area, anticyclonic flow around a Bermuda High causes transport from the southeastern U.S. into the Gulf and back onshore in the southeast Texas area. Such a task would help evaluate the potential transport of pollutants into the GMAQS region and better quantify the amount of ozone and precursors added by offshore sources.

EMISSION INVENTORY

- Noninventoried sources or upset conditions at industrial facilities appear to be important in the Houston/Galveston and Beaumont/Port Arthur areas and may contribute to measured ozone concentrations during exceedance events. Day-specific variations in known sources are also likely to be significant, but little information is currently available to characterize them; for example, VOC excursions may last for days or for only a few hours. More information regarding noninventoried sources and upset conditions would be useful in determining the effects these emissions have on observed ozone concentrations.

- Speciation of hydrocarbons for some categories is still uncertain. For Baton Rouge and Houston area point sources, source-specific chemical speciation data may exist, but have not been incorporated into the inventory.

- The estimated emission factors and the effects of environmental conditions on plant transpiration/uptake are current topics of research. Advances continue to be made in the (1) quantification of multispecies emission factor estimates, (2) methodologies employed in canopy models, and (3) biogenic emission model input data (land use, crop acreage, biomass). Future biogenic emission inventories prepared for the area should take advantage of the recent research regarding emission factors, and should include updated locale-specific biomass and crop acreage data.

- Emissions associated with shipping-lane activity, now evenly distributed over all 24 hours of each day, should be more accurately allocated by using day-specific shipping-lane activity obtained from the harbormaster for the ports of Galveston and Houston.

- Fugitive emission estimation methods are often based on recorded leaks, but the leak reporting thresholds and record keeping are not standardized. For example, some facilities report leak concentrations to be zero if the recorded concentration falls below the reporting threshold when, in fact, there are actually non-zero emissions/concentrations.

- Estimates of OCSPD-related source activity/operations and corresponding emissions are somewhat uncertain. It is expected that information obtained in recent OCSPD emission surveys (e.g., Breton Sound) will be used to create an up-to-date emissions database of offshore sources.

- The emissions associated with lightering activity should be estimated more accurately. More detailed information is required regarding lightering activity (e.g., number of vessels, type, amount, length of operations, location).

- The onroad mobile emissions in the Houston area could be more accurately estimated by integrating information obtained for the transportation network from the TxDOT transportation model with the Direct Travel Impact Model (DTIM) model, which uses link-based VMT and road type information to estimate the magnitude and spatial and temporal allocation of mobile source emissions, a major component of the Houston area inventory.

METEOROLOGICAL AND PHOTOCHEMICAL MODELING

Meteorological Modeling

- Applying a prognostic meteorological model with added capabilities (e.g., true nested grid formulation, improved data-assimilation procedures, cloud physics, nonhydrostatic model dynamics) may improve characterization of the three-dimensional airflow patterns and pollutant transport associated with gulf breeze circulations.

- Increased horizontal resolution (e.g., 2 km) in the application of a meteorological model may improve representation of local-scale phenomena (e.g., bay breeze effects). Note that use of a finer grid spacing may require application of a nonhydrostatic meteorological model.

- While most ozone episodes in the Texas-Louisiana Gulf Coast area are characterized by relatively clear skies, the high temperatures and relatively moist conditions may give rise to convective activity (especially during the afternoon). Improved characterization of moist physics in the meteorological modeling may

improve representation of local-scale airflow features and vertical velocities. Simulated cloud-cover fields could also be used in the photochemical modeling.

- While standard approaches toward four-dimensional data assimilation (FDDA) do not include assimilation of surface temperature data, these data represent an important source of information. Recently researchers have suggested approaches to assimilation of surface temperature data that may improve representation of simulated surface temperatures and vertical temperature gradients.

- Further examination of the effects of vertical exchange coefficients on simulation results may improve the specification/diagnosis of this parameter (magnitude and vertical variation) from the meteorological model output.

Photochemical Modeling

- Increased vertical resolution may allow better representation of the distribution of point-source emissions and meteorological features.

- Plume heights for large point sources and associated area sources are probably important but poorly estimated, especially in regard to heat-island effects for area and fugitive sources in large industrial complexes.

- Model plume-height calculations should be evaluated against observed plume heights.

- Use of the plume-in-grid treatment for elevated point-source emissions within the Houston, Lake Charles, and Baton Rouge areas should be further examined.

- Several of the meteorological sensitivity simulations in this study should be repeated when improved emission inventories (e.g., updated 1993 inventory) for the Houston area become available. Deficiencies in the emissions may have inhibited the response of the photochemical model to changes in the meteorological inputs.

- Develop and perform a formal "process-oriented" model evaluation protocol. This would involve evaluating important physical and chemical processes within the model and would supplement standard model evaluations primarily based on observed pollutant concentrations (generally surface ozone). The measurements needed should be designed into the measurement program.

- Address the effects of performance and impacts of using an alternative chemical mechanism, particularly a mechanism that considers alternative aromatic chemistry, long-chain alkanes, and terpenes.

REFERENCES

AeroVironment Inc. 1994. "Quality assurance report for the Western and Central Gulf of Mexico Air Quality Study." Final report prepared for Systems Applications International by AeroVironment, Inc., Monrovia, CA, AV-FR-94/6012.

Allwine, K. J., and C. D. Whiteman. 1994. Single-station integral measures of atmospheric stagnation, recirculation, and ventilation. *Atmos. Environ.*, 28:713-721.

Anderson, J. A., and P. T. Roberts. 1994a. "The airborne air quality sampling program performed during the 1993 Coastal Oxidant Assessment Program for Southeast Texas (COAST)." Final report prepared for Texas Natural Resource Conservation Commission by Sonoma Technology, Inc., Santa Rosa, CA, STI-93310-1413-FR.

Anderson, J. A., and P. T. Roberts. 1994b. "The airborne air quality sampling program performed during the 1993 Gulf of Mexico Air Quality Study (GMAQS)." Draft final report prepared for Systems Applications International and Minerals Management Service by Sonoma Technology, Inc., Santa Rosa, CA, STI-92070-1412-DFR.

Anderson, J. A., B. M. Schoell, D. H. Hern, P. T. Roberts, and J. D. Prouty. 1993. "Data collected by the STI aircraft during the 1993 Coastal Oxidant Assessment Program for Southeast Texas (COAST)." Data volume prepared for Texas Natural Resource Conservation Commission by Sonoma Technology, Inc., Santa Rosa, CA, STI-93310-1390-DV.

Anderson, J. A., D. H. Hern, P. T. Roberts, J. D. Prouty, and B. M. Schoell. 1994. "Data collected by the STI aircraft during the 1993 Gulf of Mexico Air Quality Study (GMAQS)." Data volume prepared for Systems Applications International and Minerals Management Service by Sonoma Technology, Inc., Santa Rosa, CA, STI-92070-1403-DV.

AtmAA Inc. 1993. "Measurement of carbonyl compounds in the Gulf of Mexico Air Quality Study." Final report prepared for Sonoma Technology, Inc., by AtmAA, Inc., Chatsworth, CA.

Beyrich, F., and A. Weill. 1993. Some aspects of determining the stable boundary layer depth from sodar data. *Bound.-Layer Meteorol.*, 63:97-116.

Blumenthal, D. L., C. G. Lindsay, T. S. Dye, H. H. Main, M. E. Korc, P. T. Roberts, M. Arthur, and S. E. Ray. 1995. "Ozone Episodes in the Northeastern U.S.: Observations During 1994." Report prepared for Electric Power Research Institute by Sonoma Technology, Inc., Santa Rosa, California, STI-94362-1511-DFR.

Blumenthal, D. L., P. T. Roberts, F. W. Lurmann, C. G. Lindsey, T. S. Dye, S. Reynolds, and P. M. Roth. 1993. "Preliminary Scope for a Gulf Coast Ozone Study." Prepared for the American Petroleum Institute by Sonoma Technology, Inc., Santa Rosa, CA and Envair, San Rafael, CA, STI-92014-1202-FR.

Carter, W.P.L. 1991. "Development of ozone reactivity scales for volatile organic compounds." Report prepared for the U.S. Environmental Protection Agency, Research Triangle Park, NC, EPA-600/3-91-050.

Chang, J. C., and S. R. Hanna. 1995. "Representativeness of 1993 GMAQS ozone episodes and relations between ozone episodes and meteorological variables in the Gulf of Mexico." Report prepared for Systems Applications International by Earth Tech, Concord, MA, No. 1246.

DOC. 1990. *BEA Regional Projections to 2040, Volume I: States*. U.S. Department of Commerce, Bureau of Economic Analysis.

DOC. 1991. *1990 Census of Population and Housing: Summary Tape File 1 on CD-ROM*. U.S. Department of Commerce and Bureau of the Census.

DOI. 1990. *Land Use and Land Cover Digital Data from 1:250,000- and 1:100,000-Scale Maps: Data User's Guide*. Department of the Interior, U.S. Geological Survey, Reston, Virginia.

DOI. 1992. *Fugitive Hydrocarbon Emission from Pacific OCS Facilities*. U.S. Department of the Interior, Minerals Management Service, Camarillo, California (MMS 92-0043).

Douglas, S. G., R. C. Kessler, and E. L. Carr. 1990. *User's Guide for the Urban Airshed Model. Volume III: User's Guide for the Diagnostic Wind Model.* U.S. Environmental Protection Agency (EPA-450/4-90-007C).

Douglas, S. G., N. K. Lolk, and S. Mitsutomi. 1993. "Meteorological Modeling to Support Urban and Regional Photochemical Modeling of Los Angeles, Sacramento, and the Texas Louisiana Gulf Coast." In *Regional Photochemical Measurement & Modeling Studies Abstracts Book,* Session 17 (M4-II). Air & Waste Management Association, San Diego, California.

Douglas, S. G., N. Lolk, and M. Yocke. 1992. "Episode Selection Update." Memorandum to GMAQS Technical Review Committee from Systems Applications International, San Rafael, CA.

Douglas, S. G., S. B. Shepard, and J. L. Haney. 1993. "Photochemical Modeling of the Broader Sacramento Area: Base-Case Modeling Analysis." Systems Applications International, San Rafael, California (SYSAPP-93/056).

Douglas, S. G., C. K. Steiner, S. B. Shepard, A. B. Hudischewskyj, L. A. Gardner, N. K. Lolk, J. K. Morgan, and J. L. Haney. 1994. "Comparison of the UAM-IV and UAM-V Photochemical Models for Three Atlanta-Area Ozone Episodes." Systems Applications International, San Rafael, California (SYSAPP-94/106).

Dye, T. S., C. G. Lindsey, and J. A. Anderson. 1995. "Estimates of Mixing Depths from "Boundary Layer" Profilers." In *Preprints of the Ninth Symposium on Meteorological Observations and Instrumentation, Charlotte, NC, March 27-31.*

Dye, T. S., C. G. Lindsey, B. M. Schoell, J. N. Rosen, and C. M. Jones. 1994. "Upper Air Data Collected by 915 MHz Radar Wind Profilers and Radio Acoustic Sounding Systems During the 1993 Gulf of Mexico Air Quality Study and the Coastal Oxidant Assessment in Southeast Texas Study." Data volume prepared for Systems Applications International, Minerals Management Service and Texas Natural Resource Conservation Commission by Sonoma Technology, Inc., Santa Rosa, CA, STI-92084/93320-1408-DV.

EPA. 1991a. *Guideline for Regulatory Application of the Urban Airshed Model (UAM).* U.S. Environmental Protection Agency, Office of Air Quality Planning and Standards, Research Triangle Park, NC (EPA-450/4-91-013).

EPA. 1991b. *VOC/PM Speciation Data Base Management System (SPECIATE), Version 4.1.* U.S. Environmental Protection Agency Office of Air Quality Planning and Standards, Research Triangle Park, North Carolina (EPA 450/4-91-027).

EPA. 1992a. *Draft User's Guide to MOBILE5a.* U.S. EPA Office of Mobile Sources, Ann Arbor, Michigan.

EPA. 1992b. *Regional Oxidant Modeling - Emission Inventory Development and Emission Control Scenarios,* U.S. Environmental Protection Agency, Office of Air Quality Planning and Standards (EPA contract No. 68-D9-0168, work assignment No. 043).

EPA. 1992c. *Section 187 VMT Forecasting and Tracking Guidance.* U.S. Environmental Protection Agency.

EPA. 1992d. *User's Guide for the Urban Airshed Model, Volume IV: User's Manual for the Emissions Preprocessor System 2.0, Part A: Core Modules.* U.S. Environmental Protection Agency, Office of Air Quality Planning and Standards, Research Triangle Park, North Carolina (EPA-450/4-90-007D (R)).

EPA. 1993a. *Regional Interim Emission Inventories (1987-1991), Volume I: Development Methodologies*. U.S. Environmental Protection Agency, Office of Air Quality Planning and Standards, Research Triangle Park, North Carolina (EPA-454/R-93-021a).

EPA. 1993b. *Regional Oxidant Modeling of the 1990 Clean Air Act Amendments: Default Projection and Control Data* (draft), U.S. Environmental Protection Agency, Office of Air Quality Planning and Standards (EPA contract No. 68-D0-0120, work assignment No. II-60).

Federal Register. 1992. Inspection/Maintenance Program Requirements. *Federal Register, 40 CFR Part 51* [FRL-4531-6].

Fujita, E. M., B. E. Croes, C. L. Bennett, D. L. Lawson, F. W. Lurmann, and H. H. Main. 1992. Comparison of emission inventory and ambient concentration ratios of CO, NMOG, and NO_x in California's South Coast Air Basin. *J. Air Waste Manage. Assoc.*, 42:264-276.

Fujita, E. M., D. R. Goff, D. R. Lawson, A. Barnett, J. H. Price, J. Gibich, K. W. Rozacky, C. L. Martin, W. A. Lonneman, S. D. Hoyt, R. A. Rasmussen, W. L. Crow, and L. D. Ogle. 1994a. "Interlaboratory Comparison for Analysis of Hydrocarbons During the Coastal Oxidant Assessment for Southeast Texas (COAST) Project." Presented at Air & Waste Management Association Symposium on Measurement of Toxic and Related Air Pollutants, Durham, NC, May 3-6.

Fujita, E. M., J. G. Watson, J. C. Chow, and Z. Lu. 1994b. Validation of chemical mass balance receptor model applied to hydrocarbon source apportionment in the Southern California air quality study. *Environ. Sci. Technol.*, 28:1633-1649.

Fung, K. 1990. "Standard Operating Procedure. Analysis of Carbonyl Compounds in Air Samples Collected Using DNPH Impregnated Cartridges." Prepared for Sonoma Technology, Inc., by AtmAA, Inc., Chatsworth, CA.

GIT. 1993. *A Biogenic Hydrocarbon Emission Inventory for Baton Rouge, Louisiana Urban Airshed Domain*. Georgia Institute of Technology.

Goodin, W.R., G.J. McRae, J.H. Seinfeld. 1980. Objective analysis technique for constructing three-dimensional urban-scale wind fields. *J. Appl. Met.*, 19:98-108.

Harley, R. A., M. P. Hannigan, and G. R. Cass. 1992. Respeciation of organic gas emissions and the detection of excess unburned gasoline in the atmosphere. *Environ. Sci. Technol.*, 26:2395-2408.

Hess, S.L. 1959. *Introduction to Theoretical Meteorology*. Holt, Rinehart, New York.

HGAC. 1993. "HPMS Adjustment for All On-Road Mobile Source Emissions Inventories, August 1993." Houston-Galveston Area Council.

Holzworth, G. G. 1972. "Mixing Heights, Wind Speeds, and Potential for Urban Air Pollution Throughout the Contiguous United States." U.S. Environmental Protection Agency, Research Triangle Park, NC.

Jackson, R., and Z. Gram. 1994. Personal communication between R. Jackson, SAI and Zack Gram, Texas Department of Transportation (TexDOT) Modeling Head, (512) 465-7412, fax (512) 465-7921.

Jackson, R., and R. Kandalam. 1994. Personal communication between R. Jackson, SAI and Ranga Kandalam, Staff Engineer in the Transportation Department of the Houston-Galveston Area Council (HGAC), (713) 993-2417, fax (713) 993-4508.

Kearney, A. T. 1993. "Baseline Offshore Emissions from Marine Sources in the Gulf of Mexico." Alexandria, Virginia.

Kessler, R. C., and S. G. Douglas. 1991. A numerical study of mesoscale eddy development over the Santa Barbara Channel. *J. Applied Meteorol.*, 30(5).

Kessler, R. C., and S. G. Douglas. 1992. "User's Guide to the Systems Applications International Mesoscale Model (Version 3.0)." Systems Applications International, San Rafael, California (SYSAPP-92/072).

Lawson, D. R., N. Robinson, P. T. Roberts, et al. 1995. "1993 COAST Project, Including Data Management." Final report to be published by Desert Research Institute, Reno, NV.

LDEQ. 1993. *15% VOC Reduction Reasonable Further Progress Plan.* Louisiana Department of Environmental Quality.

Leadbetter, M. R., and L.-S. Huang. 1993. "Uncertainty Estimation for Emissions Inventories. Development and Simplification of Basic Methodology."

Lurmann, F. W., H. H. Main, K. T. Knapp, L. Stockburger, R. A. Rasmussen, and K. Fung. 1992. "Analysis of the Ambient VOC Data Collected in the Southern California Air Quality Study." Prepared for the California Air Resources Board by Sonoma Technology, Inc., Santa Rosa, CA, STI-99120-1161-FR.

Mahrer, Y., and R. A. Pielke. 1977. A numerical study of the air flow over irregular terrain. *Contr. Atmos. Phys.*, 50:98-113.

Mahrer, Y., and R. A. Pielke. 1978. A test of an upstream spline interpolation technique for the advective terms in a numerical mesoscale model. *Mon. Wea. Rev.*, 106:818-830.

MMS/EPA. 1993. *Preliminary Assessment of Gulf of Mexico OCS Contributions to Ozone Formation in Onshore Areas Using the Regional Oxidant Model.* Department of the Interior, Minerals Management Service, Gulf of Mexico OCS Region, New Orleans, Louisiana (MMS 93-0025).

Moore, G. E., J. P. Killus, and G. Z. Whitten. 1991. Composition of marine air offshore of the Western United States. *J. Appl. Meteorol.*, 30(5).

Morris, R. E., R. C. Kessler, S. G. Douglas, and L. R. Chinkin. 1990. "Preliminary Modeling for the San Joaquin Valley Air Quality Study." Systems Applications International, San Rafael, California (SYSAPP-90/106).

Myers, T. C. 1992. "Analyses of AIRS Ozone Data in Gulf Coast Region." Memorandum of September 1, 1992, Systems Applications International, San Rafael, California.

O'Brien, J. J. 1970. Alternative solutions to the classical vertical velocity profile. *J. Atmos. Sci.*, 39:2701-2711.

OGDEN. 1992. "Baton Rouge Summer 1992 Ozone Study." Final report prepared for Louisiana Department of Environmental Quality by OGDEN Environmental and Energy Services.

Olsen, R. J. 1980. *GEOECOLOGY: A County-Level Environmental Data Base for the Coterminous United States*. Environmental Sciences Division, Oak Ridge National Laboratory, Oak Ridge, Tennessee (Pub. No. 1537).

Pierce, T. E., B. K. Lamb, and A. R. Van Meter. 1990. "Development of a Biogenic Emission Inventory System for Regional Scale Air Pollution Models." Air and Waste Management Association 83rd Annual Meeting and Exhibition, Pittsburgh, Pennsylvania (June 24-29, 1990).

Randolph, R. 1993. "Economic Growth Analysis System: User's Guide." Prepared for U.S. Environmental Protection Agency by TRC Environmental Corporation, Chapel Hill, North Carolina (EPA-600/R-93-067b).

Rasmussen, R. 1994. "Standard Operating Procedures for Hydrocarbon Speciation." Prepared for Sonoma Technology by Oregon Graduate Institute, Beaverton, OR.

Richards, L. W., C. L. Blanchard, and D. L. Blumenthal. 1991. "Navajo Generating Station Visibility Study." Final report prepared for Salt River Project, Phoenix, AZ by Sonoma Technology, Inc., Santa Rosa, CA (STI-90200-1124-FR).

Roberts, P., D. Blumenthal, C. Lindsey, J. Anderson, M. Yocke, A. Barnett, R. Hamilton, M. Dybevick, and G. Zeigler. 1992. "Gulf of Mexico Air Quality Study Field Plan." Working draft no. 2 prepared for the Minerals Management Service by Sonoma Technology, Inc., Santa Rosa, CA (STI-92040-1212-WD2, Contract No. 1435000130604).

Roberts, P. T., and T. S. Dye. 1993. "Gulf of Mexico Air Quality Study Forecasting and Decision-Making Protocol." Draft report prepared for Systems Applications

International and Minerals Management Service by Sonoma Technology, Inc., Santa Rosa, CA (STI-92040-1361-DP, Contract No. 1435000130604).

Roberts, P. T., and H. H. Main. 1992. "Characterization of Three-Dimensional Air Quality During the SCAQS." In *Southern California Air Quality Study Data Analysis. Proceedings from SCAQS Data Analysis Conference, University of California, Los Angeles, CA, July 21-23.* Air & Waste Management Association, Pittsburgh, PA (STI-1223), VIP-26.

SAI. 1993. "Gulf of Mexico Air Quality Study Data Archival Protocol." Draft report prepared for Minerals Management Service by Systems Applications International, San Rafael, CA (SYSAPP-93/076).

SAI. 1994. "A Description of the Gulf of Mexico Air Quality Study Data Archive Files." Prepared for Minerals Management Service by Systems Applications International, San Rafael, CA.

Sailor, D. J., S. Douglas, and R. Kessler. 1992. "Analysis of Energy Efficiency and Air Quality Two-Dimensional Simulation Results." Draft Report Chapter 4.2. Deliverable #7 for CIEE Project AQ-91-02A.

Saricks, C. L., and A. D. Vyas. 1985. "Forecasting Transportation Activity and Emissions for the National Acid Precipitation Assessment Program." Center for Transportation Research, Argonne National Laboratory, Argonne, Illinois (NTIS-DE85018352).

Schoell, B. M., C. G. Lindsey, T. S. Dye, J. D. Prouty, and J. N. Rosen. 1994a. "Upper Air Data Collected by STI on Chevron's Garden Banks 236A Platform During the 2993 Gulf of Mexico Air Quality Study." Data volume prepared for Systems Applications International and Minerals Management Service by Sonoma Technology, Inc., Santa Rosa, CA (STI-92064-1407-DV).

Schoell, B. M., C. G. Lindsey, T. S. Dye, J. N. Rosen, J. D. Prouty, and M. W. Stoelting. 1994b. "Data Collected by a Network of Surface Meteorological Monitoring Stations During the 1993 Gulf of Mexico Air Quality Study." Data volume prepared for Systems Applications International and Minerals Management Service by Sonoma Technology, Santa Rosa, CA (STI-92084-1409-DV).

Schulhof, R. R., and S. G. Douglas. 1992. "User's Guide for the MM2UAM Software. Version 1.0." Systems Applications International, San Rafael, California.

Stauffer, D. R., and N. L. Seaman. 1990. Use of four-dimensional data assimilation in a limited-area mesoscale model. Part I: Experiments with synoptic-scale data. *Mon. Wea. Rev.*, 118:1250-1277.

Stauffer, D. R., N. L. Seaman, and F. S. Binkowski. 1991. Use of four-dimensional data assimilation in a limited-area mesoscale model. Part II: Effects of data assimilation within the planetary boundary layer. *Mon. Wea. Rev.*, 199:734-754.

Steiner, C.K.R., L. A. Gardner, M. C. Causley, M. A. Yocke, and W. L. Steorts. 1993. "Inventory Quality Issues Associated with the Development of an Emissions Inventory for the Minerals Management Service Gulf of Mexico Air Quality Study." Air and Waste Management Association Specialty Conference.

Steiner, C., and B. Steorts. 1994. Personal communication between C. Steiner, SAI, and B. Steorts, MMS.

Tingey, D. 1981. *Atmospheric Biogenic Hydrocarbons*. J. Bufalini and R. Arnts, eds., Ann Arbor Science Publication, Ann Arbor, Michigan, pp. 53-79.

Tingey, D., R. Evans, and M. Gumpertz. 1981. Effects of environmental conditions on isoprene emissions from live oak. *Planta,* 152:565.

Tingey, D., M. Manning, L. Grothaus, et al. 1980. Influence of light and temperature on monoterpene emission rates from slash pine. *Plant Physiol.*, 65:797.

TNRCC. 1994. Personal communication between R. Jackson, SAI, and Marty Boardman, Emission Inventory Division, Texas Natural Resource and Conservation Commission, (512) 239-1492, fax (512) 239-1515.

Ulrickson, B. L., and C. F. Mass. 1990. Numerical investigation of mesoscale circulations over the Los Angeles Basin. Part I: A verification study. *Mon. Wea. Rev.*, 118:2138-2161.

Wagner, K. K., and N.J.M. Wheeler. 1991. "An Investigation of Modeling Emission Inventory Bias with Urban Airshed Model Sensitivity Simulations." Presented at the AWMA Specialty Conference on Tropospheric Ozone, Atlanta, November.

Wesely, M. L. 1989. Parameterization of surface resistances to gaseous dry deposition in regional-scale numerical models. *Atmos. Environ.*, 23(6):1293-1304.

White, A. B. 1993. "Mixing Depth Detection Using 915 MHz Radar Reflectivity Data." *In Preprints of the Eighth American Meteorological Society Symposium on Meteorological Observations and Instruments, Anaheim, CA, January 17-22.*

Wyngaard, J. C., and M. A. LeMone. 1980. Behavior of the refractive index structure parameter in the entraining convective boundary layer. *J. Atmos. Sci.*, 37:1573-1585.

Zimmermann, P. 1979. *Determination of Emission Rates of Hydrocarbons from Indigenous Species of Vegetation in the Tampa Bay/Petersburg, Florida Area.* U.S. Environmental Protection Agency, Atlanta, Georgia (EPA-904/9-77-028).

The Department of the Interior Mission

As the Nation's principal conservation agency, the Department of the Interior has responsibility for most of our nationally owned public lands and natural resources. This includes fostering sound use of our land and water resources; protecting our fish, wildlife, and biological diversity; preserving the environmental and cultural values of our national parks and historical places; and providing for the enjoyment of life through outdoor recreation. The Department assesses our energy and mineral resources and works to ensure that their development is in the best interests of all our people by encouraging stewardship and citizen participation in their care. The Department also has a major responsibility for American Indian reservation communities and for people who live in island territories under U.S. administration.

The Minerals Management Service Mission

As a bureau of the Department of the Interior, the Minerals Management Service's (MMS) primary responsibilities are to manage the mineral resources located on the Nation's Outer Continental Shelf (OCS), collect revenue from the Federal OCS and onshore Federal and Indian lands, and distribute those revenues.

Moreover, in working to meet its responsibilities, the **Offshore Minerals Management Program** administers the OCS competitive leasing program and oversees the safe and environmentally sound exploration and production of our Nation's offshore natural gas, oil and other mineral resources. The MMS **Minerals Revenue Management** meets its responsibilities by ensuring the efficient, timely and accurate collection and disbursement of revenue from mineral leasing and production due to Indian tribes and allottees, States and the U.S. Treasury.

The MMS strives to fulfill its responsibilities through the general guiding principles of: (1) being responsive to the public's concerns and interests by maintaining a dialogue with all potentially affected parties and (2) carrying out its programs with an emphasis on working to enhance the quality of life for all Americans by lending MMS assistance and expertise to economic development and environmental protection.